Springer Tracts in Civil Engineering



Giandomenico Toniolo
Marco di Prisco

Reinforced Concrete Design to Eurocode 2

English Edition by Michele Win Tai Mak

Springer

Springer Tracts in Civil Engineering

Springer Tracts in Civil Engineering (STCE) publishes the latest developments in Civil Engineering—quickly, informally and in top quality. The series scope includes monographs, professional books, graduate textbooks and edited volumes, as well as outstanding Ph.D. theses. Its goal is to cover all the main branches of civil engineering, both theoretical and applied, including:

Construction and Structural Mechanics
Building Materials
Concrete, Steel and Timber Structures
Geotechnical Engineering
Earthquake Engineering
Coastal Engineering
Hydraulics, Hydrology and Water Resources Engineering
Environmental Engineering and Sustainability
Structural Health and Monitoring
Surveying and Geographical Information Systems
Heating, Ventilation and Air Conditioning (HVAC)
Transportation and Traffic
Risk Analysis
Safety and Security
To submit a proposal or request further information, please contact: Pierpaolo Riva at Pierpaolo.Riva@springer.com, or Li Shen at Li.Shen@springer.com

More information about this series at http://www.springer.com/series/15088

Giandomenico Toniolo · Marco di Prisco

Reinforced Concrete Design to Eurocode 2

English Edition by Michele Win Tai Mak

Springer

Giandomenico Toniolo
Department of Civil and Environmental Engineering
Politecnico di Milano
Milan
Italy

Marco di Prisco
Department of Civil and Environmental Engineering
Politecnico di Milano
Milan
Italy

Publisher and Authors acknowledge the role and contribution of Michele Win Tai Mak, in translating into English the Italian language work, authoring the foreword and providing/suggesting updates on the reference readings.

ISSN 2366-259X ISSN 2366-2603 (electronic)
Springer Tracts in Civil Engineering
ISBN 978-3-319-52032-2 ISBN 978-3-319-52033-9 (eBook)
DOI 10.1007/978-3-319-52033-9

Library of Congress Control Number: 2017930409

© Springer International Publishing AG 2017
This work is subject to copyright. All rights are reserved by the Publisher, whether the whole or part of the material is concerned, specifically the rights of translation, reprinting, reuse of illustrations, recitation, broadcasting, reproduction on microfilms or in any other physical way, and transmission or information storage and retrieval, electronic adaptation, computer software, or by similar or dissimilar methodology now known or hereafter developed.
The use of general descriptive names, registered names, trademarks, service marks, etc. in this publication does not imply, even in the absence of a specific statement, that such names are exempt from the relevant protective laws and regulations and therefore free for general use.
The publisher, the authors and the editors are safe to assume that the advice and information in this book are believed to be true and accurate at the date of publication. Neither the publisher nor the authors or the editors give a warranty, express or implied, with respect to the material contained herein or for any errors or omissions that may have been made. The publisher remains neutral with regard to jurisdictional claims in published maps and institutional affiliations.

Printed on acid-free paper

This Springer imprint is published by Springer Nature
The registered company is Springer International Publishing AG
The registered company address is: Gewerbestrasse 11, 6330 Cham, Switzerland

Foreword

This book on reinforced concrete design is unique for its comprehensive approach, as each topic is thoroughly analysed from more theoretical aspects, through the development of design formulas with their assumptions and justifications, and terminates with construction requirements and practical examples.

The textbook is primarily intended for undergraduate students and young practitioners. However, the strong link between theory and practical applications makes it a valuable handbook that experienced engineers would also find useful. As the complexity of projects increases, designers face progressively greater challenges, structural engineering deviates from standard solutions bringing the designers back to first principles; a thorough understanding of the theory and the structural fundamentals becomes extremely important to comprehend limits and worthiness of models.

The original book has been at the forefront of the development of the Limit State Design for the structural use of concrete in Italy and it has been a national reference for academics and practitioners for many years; since the first edition has been published, it has been continuously updated to incorporate the latest developments in reinforced concrete design. Because of its validity, the preface to the original edition has been kept as a general introduction to the work, with few updates by the authors.

The terminology, definitions and explanations of the original text are remarkably rigorous, in line with a cultural tradition that values consistency and preciseness, and this aspect of the book has been retained as much as possible. The need to make the English edition comply with a more practical nature of the industry made certain aspects of the translation particularly difficult, especially where theoretical rigour and preciseness had to be abandoned in favour of terms and expressions that are common in practice. Conversely, when deemed important, consistency and accuracy have been retained at the cost of less immediate clarity.

I would like to apologize to the reader for any errors or mistakes in the text that may have inadvertently been made, despite the countless reviews of a perfectionist who probably will never learn that “Better is Enemy of Good”.

Finally, I wish to thank the authors, Proff. Toniolo and di Prisco for giving me the opportunity to work on their book and bring it to a wider international audience, and for their continuous support and assistance.

Michele Win Tai Mak

Michele Win Tai Mak is a Structural Engineer at Ove Arup & Partners. His research and professional interests include the analysis and design of tall buildings, the assessment of existing reinforced concrete structures, seismic engineering, failure analysis and cementitious composites. He also undertakes project consultations and tutorials with engineering and architecture students in several universities in the United Kingdom. He holds a Master's degree from Politecnico di Milano and a Diplôme d'Ingénieur from École Spéciale des Travaux Publics, du Bâtiment et de l'Industrie de Paris.

Preface

The present work derives from the university textbook originally drafted within the cultural tradition of the Structural Engineering School of the Politenico di Milano. This English edition has been drafted following the publication of two fundamental documents:

- *Eurocode 2—Design of concrete structures*;
- *fib Model Code*,

as better specified in References. The first one represents the last amendment of the final version of the official EN design code collecting the consolidated principles and rules for concrete structures. The second document represents the new edition of the design code issued by the International Association of Concrete Structures, collecting the latest innovative developments of the research proposed for possible future updating of the official regulations.

With respect to the original edition, the text has therefore been revised and extended, incorporating the most important technological-scientific innovations, which are the basis of the two aforementioned documents, to present a complete set of limit state design criteria of the modern theory of reinforced concrete, saving its educational purposes.

First of all, the completeness typical of a general treatise has been abandoned, incorporating the topics considered of fundamental educational value but leaving out many further developments and alternatives. Specific references are reserved for those.

The intent has been to develop the textbook examining in depth methodological more than notional aspects of the presented topics, and focusing on the verification of assumptions, on the rigorousness of the analysis and on the consequent degree of reliability of results.

The textbook refers to part of the course of structural design and analysis for civil and building engineering students. Form and extent of arguments are mainly driven by teaching needs, as developed throughout the weeks of the academic year.

About its field of competence, the course of structural design and analysis is placed as a logical development after the course of structural mechanics. The fundamental models of structural behaviour are recalled from this discipline, fitting them out with the actual thicknesses due to the real construction materials. The specific properties of these materials and their complex structural arrangement bring up the problem of the reliability of the model: not just one unique solution results, but a domain of possible solutions characterized by different degrees of refinement can be obtained and in any case influenced by the randomness of the input data.

Structural design and analysis is limited to problems of verifications related to simple structures for which the extraction of a model is simple. The wider problem relative to the design choices and the analysis of real complex building arrangements is left to the subsequent specialized courses of the final academic year.

Information for Students and Instructors

The organization of teaching activities has weekly cycles of exercise sessions devoted to numerical applications of the topics already discussed from the theoretical point of view during the lessons. The structure of chapters in this text closely follows this organization. Each chapter develops an organic topic, which is eventually illustrated by examples in each final paragraph containing the relative numerical applications.

The application paragraphs altogether follow an overall plan with the development of the design of principal structural elements in a typical construction 'from roof, to foundations'. Other than being an opportunity for the application of single topics (e.g. beam in bending, column in compression, foundation footing, etc.), the overall subject shows the first examples of extraction of calculation models from a real structural context and eventually gives the complete building arrangement on which the fundamental verifications of overall stability are to be carried.

Specific appendices are also reported at the end of each chapter, to be used for practical design applications, containing data about materials, formulas for verifications and auxiliary tables, in line with the latest European regulations.

Milan, Italy

Giandomenico Toniolo
Marco di Prisco

Contents

1 General Concepts on Reinforced Concrete 1
1.1 Mechanical Characteristics of Concrete 1
1.1.1 Basic Properties of Concrete 2
1.1.2 Strength Parameters and Their Correlation 10
1.1.3 Failure Criteria of Concrete 18
1.2 Creep 22
1.2.1 Principles of Creep 23
1.2.2 Creep with Variable Stresses 26
1.2.3 Models of Linear Creep 28
1.3 Structural Effects of Creep 33
1.3.1 Resolution of the Integral Equation 35
1.3.2 General Method 37
1.3.3 Algebraic Methods 38
1.4 Behaviour of Reinforced Concrete Sections 40
1.4.1 Mechanical Characteristics of Reinforcement 41
1.4.2 Basic Assumptions for Resistance Calculation 46
1.4.3 Steel–Concrete Bond 52
Appendix: Characteristics of Materials 57

2 Centred Axial Force 83
2.1 Compression Elements 83
2.1.1 Elastic and Resistance Design 87
2.1.2 Effect of Confining Reinforcement 91
2.1.3 Effects of Viscous Deformations 96
2.2 Tension Elements 101
2.2.1 Verifications of Sections 102
2.2.2 Prestressed Tie Members 104
2.2.3 Cracking in Reinforced Concrete Ties 108

2.3 Cracking Calculations . . . 113
2.3.1 The Cracking Process . . . 114
2.3.2 Crack Width . . . 116
2.3.3 Verification Criteria . . . 120
2.4 Case A: RC Multi-storey Building . . . 124
2.4.1 Actions on Columns and Preliminary Verifications . . . 126
2.4.2 Notes on Reinforced Concrete Technology . . . 138
2.4.3 Durability Criteria of Reinforced Concrete Structures . . . 147
Appendix: General Aspects and Axial Force . . . 151

3 Bending Moment . . . 169
3.1 Analysis of Sections in Bending . . . 169
3.1.1 Elastic Design of Sections . . . 172
3.1.2 Resistance Design of Sections . . . 180
3.1.3 Prestressed Sections . . . 189
3.2 Flexural Cracking of Beams . . . 197
3.2.1 Crack Spacing . . . 198
3.2.2 Crack Width . . . 200
3.2.3 Verification Criteria . . . 202
3.3 Deformation of Sections in Bending . . . 204
3.3.1 Effects of Creep . . . 207
3.3.2 Moment-Curvature Diagrams . . . 220
3.3.3 Flexural Behaviour Parameters . . . 226
3.4 Case A: Design of Floors . . . 231
3.4.1 Analysis of Actions . . . 235
3.4.2 Service Verifications . . . 243
3.4.3 Resistance Verifications . . . 246
Appendix: Actions and Bending Moment . . . 252

4 Shear . . . 263
4.1 Behaviour of RC Beams in Shear . . . 263
4.1.1 Cracking of Beams . . . 265
4.1.2 Longitudinal Shear and Shear Reinforcement . . . 267
4.1.3 Mörsch Truss Model . . . 270
4.2 Beams Without Shear Reinforcement . . . 276
4.2.1 Analysis of Tooth Model . . . 278
4.2.2 Other Resistance Contributions . . . 283
4.2.3 Verification Calculations . . . 288
4.3 Beams with Shear Reinforcement . . . 295
4.3.1 The Modified Hyperstatic Truss Model . . . 298
4.3.2 The Variable Strut Inclination Truss Model . . . 302
4.3.3 Serviceability Verifications . . . 311

4.4 Case A: Beams Design . . . 315
4.4.1 Analysis of Actions . . . 320
4.4.2 Serviceability Verifications . . . 326
4.4.3 Resistance Verifications . . . 329
Appendix: Shear . . . 333

5 Beams in Bending . . . 341
5.1 Calculation Models of Beams in Bending . . . 341
5.1.1 Arch Behaviour . . . 345
5.1.2 Truss Model . . . 351
5.1.3 Standard Application Procedure . . . 355
5.2 Strut-and-Tie Balanced Schemes . . . 360
5.2.1 Support Details . . . 364
5.2.2 Corbels and Deep Beams . . . 374
5.2.3 Punching Shear in Slabs . . . 382
5.3 Flexural Deformations of Beams . . . 388
5.3.1 Curvature Integration . . . 391
5.3.2 Nonlinear Analysis of Hyperstatic Beams . . . 394
5.3.3 Collapse Behaviour of Hyperstatic Beams . . . 398
5.4 Case A: Shallow Rectangular Beam . . . 406
5.4.1 Serviceability Verifications . . . 409
5.4.2 Resistance Verifications . . . 413
5.4.3 Deflection Calculations . . . 418
Appendix: Elements in Bending . . . 421

6 Eccentric Axial Force . . . 429
6.1 Elastic Design of the Section . . . 429
6.1.1 Axial Compression Force with Small Eccentricity . . . 431
6.1.2 Compression and Tension with Uniaxial Bending . . . 436
6.1.3 Compression and Tension with Biaxial Bending . . . 440
6.2 Resistance Design of the Section . . . 444
6.2.1 Failure Mechanisms of the Section . . . 446
6.2.2 Resistance Verifications of the Section . . . 451
6.2.3 Design for Biaxial Bending . . . 462
6.3 Flexural Behaviour of Columns . . . 470
6.3.1 Design Models of Columns . . . 471
6.3.2 Moment-Curvature Diagrams . . . 476
6.3.3 Nonlinear Analysis of Frames . . . 483
6.4 Case A: Design of Columns . . . 493
6.4.1 Flexural Actions in Columns . . . 495
6.4.2 Serviceability Verifications . . . 499
6.4.3 Resistance Calculations . . . 503
Appendix: Eccentric Axial Force . . . 508

7 Instability Problems 531
7.1 Instability of Reinforced Concrete Columns 531
7.1.1 Analysis of Columns Under Eccentric Axial Force 535
7.1.2 Methods of Concentration of Equilibrium 539
7.1.3 Creep Effects 543
7.2 Second-Order Analysis of Frames 548
7.2.1 One-Storey Frames 550
7.2.2 Multistorey Frames 553
7.2.3 General Case of Frames 557
Appendix: Instability of Columns 559

8 Torsion 565
8.1 Beams Subject to Torsion 565
8.1.1 Peripheral Resisting Truss 571
8.1.2 Improvement and Application of the Model 578
8.1.3 Other Aspects of the Torsional Behaviour 586
8.2 Case A: Stability Core 590
8.2.1 Calculation of Internal Forces 592
8.2.2 Verifications of the Current Section 598
8.2.3 Verifications of Lintels and Stairs 607
Appendix: Torsion 612

9 Structural Elements for Foundations 621
9.1 Isolated Foundations 621
9.1.1 Massive Foundations 626
9.1.2 Footing Foundations 631
9.1.3 Pile Foundations 636
9.2 Continuous Foundations 640
9.2.1 Foundation Beams 644
9.2.2 Structure–Foundation Interaction 648
9.2.3 Foundation Grids and Rafts 652
9.3 Retaining Walls 656
9.3.1 Gravity Walls 662
9.3.2 Foundation Retaining Walls 667
9.3.3 Diaphragm Walls 669
9.4 Case A: Foundation Design 675
9.4.1 Verification of Footings 677
9.4.2 Design of the Retaining Wall 682
9.4.3 Design of the Corewall Foundation 689
Appendix: Data on Soils and Foundations 695

10 Prestressed Beams 711
10.1 Prestressing: Technological Aspects 711
10.1.1 Prestressing Systems 715

10.1.2 Instantaneous Losses 719
10.1.3 Long-Term Losses 724
10.2 Tendons Profile 728
10.2.1 Loads Equivalent to the Tendon 729
10.2.2 Available Moment and Limit Points 732
10.2.3 Hyperstatic Beams 737
10.3 Resistance Calculations 740
10.3.1 Verification of Prestressed Concrete Sections 742
10.3.2 Resistance Models of Prestressed Beams 748
10.3.3 Anchorage and Diffusion of Precompression. 758
10.4 Design Examples 770
10.4.1 Pretensioned Concrete Element 770
10.4.2 Post-tensioned Concrete Beam 785
10.4.3 Prestressed Concrete Flanged Beam 803
Appendix: Data on Prestressing 822

References 835

About the Authors

Giandomenico Toniolo was full professor of Structural Analysis and Design at Politecnico di Milano. Besides his academic tasks and a professional engagement as structural designer, he carried out a long activity in regulations and standards in Italy and Europe, participating in the National Commission for Technical Standards for Constructions and also in several committees of the European Committee for Standardization CEN such as CEN/TC250/SC2 for Eurocode 2 (concrete structures), CEN/TC250/SC8 for Eurocode 8 (seismic code), CEN/TC229 for precast concrete products. Within this latter committee he chaired for many years the WG1 on precast concrete structural products. He has been the coordinator of important European research projects on seismic design of concrete precast structures. He has also developed an extensive editorial activity by authoring many scientific works and a number of university text books. Amongst these is the text 'Cemento Armato: Calcolo agli Stati Limite', which he now publishes in its English version together with co-author Prof. Marco di Prisco.

Marco di Prisco is full Professor of Structural Analysis and Design at Politecnico di Milano, Italy. His research and consultant activity focuses on constitutive modelling for plain and fibre reinforced concrete, innovative materials, reinforced concrete interaction mechanisms, structural behavior of R/C and P/C elements, prefabricated and fibre reinforced concrete structures, infrastructures, structure retrofitting, soil-structure interaction, structural response at exceptional loads. At national level he is member of National Standard Committee of CNR (National Centre of Research) and participates to Technical Committees of the Infrastructures and Transport Ministry; at international level he is member of important advisory boards on concrete structures international conferences like FRAMCOS, PROTECT, BEFIB, CONSEC, honorary editor of European Journal of Environmental and Civil Engineering and member of the editorial board of Cement and Concrete Composites Journal. He is active member of ACI, fib and RILEM. Participating to national and international committees on fibre reinforced concrete, as a member of fib Presidium he was the responsible of the Model Code 2010 chapters on Fibre Reinforced Concrete and currently he is convener of the CEN TC250/SC2/Wg1/Tg2 to introduce FRC in EC2.

Symbols, Acronyms and Abbreviations

The attempt has been to adapt the notations in this textbook to the ones more commonly used internationally in the specific disciplinary sector. A significant step forward towards the unification of notation has been done within the standardization activity carried out by associations such as C.E.B. (now fib) and C.E.C.M. The English language gives the undisputed reference, overcoming the national ones (*y* for yield, *s* for steel, etc.), and even the noblest international languages such as French (*c* for concrete, instead of *b* of béton).

However, not everything is unified and there is room for the personal preferences of different authors. Finally, interferences are not completely solved with related disciplines such as computer-oriented structural analysis.

Lists of principal meaning of symbols are reported below. The mathematical ones are omitted, taken as granted, as well as the occasional ones that continuously occur in the text and that will rely on specific foregoing definitions.

Due to the high number of quantities to be treated, it is not possible to avoid repetitions and promiscuity of symbols. The context will clarify misunderstandings and, starting from the following tables, notations are divided in three different domains of application: the general one of safety criteria and actions definition for the semi-probabilistic method; the one of structural design for the analysis of frames and plates; the one relative to the construction materials and the design of relative elements.

Despite the size of tables, the following normalized codification of symbols covers a very limited area with respect to the extent of the subject.

Capital Roman Letters

	Actions and safety	Structural analysis	Member design
A	Accidental action	Cross-sectional area	Cross-sectional area
B	/	/	/
C	/	/	Resultant of compress
D	/	Diameter	Diameter
E	Effect of action	Long. elast. modulus	Long. elast. modulus
F	Action on structure	Concentrated couple	/
G	Permanent action	Tang. elast. modulus	Centre of gravity
H	/	Horizontal force	/
I	/	Second moment of area	Second moment of area
J	/	Torsional inertia	Torsional inertia
K	/	Section stiffness	Section stiffness
L	/	Total length	/
M	/	Bending moment	Bending moment
N	/	Axial force	Axial force
O	/	/	Pole, centre, origin
P	Prestressing	Concentrated load	Prestressing
Q	Variable action	Force or resultant	Longit. shear force
R	Resistance	Reaction or resultant	/
S	Internal force	First moment of area	First moment of area
T	Stress	Tors. mom. or temperature	Torsional moment
U	/	/	/
V	/	Shear force	Shear force
W	Weight of masses	Section modulus	Section modulus
X	/	Axis or unknown quantity	/
Y	/	Axis or unknown quantity	/
Z	/	Axis or unknown quantity	Resultant of tension

Small Roman Letters

	Actions and safety	Structural analysis	Member design
a	Random variab. action	Greater side dimension	/
b	/	Smaller side dimension	Cross-section width
c	Numerical coefficient	Numerical coefficient	Concrete cover
d	/	Flexibility	Effective depth
e	/	Eccentricity	Eccentricity
f	Probability function	Function	Material strength
g	Gravity acceleration	Function	Material density

(continued)

(continued)

	Actions and safety	Structural analysis	Member design
h	/	Height	Depth of section
i	/	Radius of gyration	/
j	/	/	Age in days
k	Probability coefficient	Stiffness	Coefficient
l	/	Length	Length, distance
m	/	Moment	/
n	Number of tests	/	/
o	(Not used)	(Not used)	(Not used)
p	Probability	Distributed load	/
q	Probability (1 − *p*)	Variable distributed load	Unity longit. shear
r	Random var. resistance	Force (or radius)	Relaxation function
s	Standard deviation	/	Spacing
t	/	Time	Thickness
u	/	Translation along *x*	Perimeter
v	/	translation along *y*	Creep function
w	/	Translation along *z*	Crack opening
x	generic random variab.	Coordinate	Neutral axis depth
y	/	Coordinate	Distance
z	/	Coordinate	Internal lever arm

Small Greek letters

	Actions and safety	Structural analysis	Member design
α	/	/	Angle (or coeff.)
β	/	Buckling coefficient	C/*bxfc* ratio
γ	Partial safety factor	Shear strain	Partial safety factor
δ	/	Translation	*d*/*h* ratio
ε	/	Strain	Strain
θ	/	Angle	Angle
ι	(Not used)	(Not used)	(Not used)
κ	/	Coefficient	Ratio (or coeff.)
λ	/	Slenderness ratio	Slenderness ratio
μ	/	Friction coefficient	Specific bend. mom.
ν	/	Poisson's ratio	Specific axial force
ξ	/	Coord. or translation	Ratio *x*/*h*
η	/	Coord. or translation	Ratio *y*/*h*
ζ	/	Coord. or translation	Ratio *z*/*h*
o	(Not used)	(Not used)	(Not used)
π	/	3,1415927…	/

(continued)

(continued)

	Actions and safety	Structural analysis	Member design
ρ	/	Generic stress	Relaxation coeff.
σ	/	Normal stress	Normal stress
τ	/	Shear stress	Shear stress
υ	/	/	Specific shear force
φ	/	Rotation	Creep coeff.
χ	/	Shear factor	Curvature ($1/r$)
ψ	Combination factor	Rotation	Angle
ω	/	Instability coeff.	Instability coeff.
ϕ	/	/	Rebar diameter

Subscripts

	Actions and safety	Structural analysis	Member design
a	Acting	/	/
b	/	/	Bolt or bond
c	/	Critic, collapse	Concrete
d	Design	/	Design
e	/	/	Elast., at elastic limit
f	Actions	/	/
g	Permanent actions	/	/
h	/	Horizontal	/
i	/	ith	/
j	/	jth	At day j
k	Characteristic	/	Characteristic
l	/	/	Longitudinal
m	Material	/	Mean
n	/	Normal	/
o	/	At the origin, reference	/
p	Prestressing	/	Prestressing
q	Variable actions	/	/
r	Resistant	/	Rupture
s	/	/	Steel
t	Time	Tangent	In tension
u	/	/	Ultimate of rupture
v	/	Vertical	Viscous
w	/	/	Web
x	/	Along or around x	/
y	/	Along or around y	Yield
z	/	Along or around z	/
ε	Geometric	/	/
θ	Thermal	/	Thermal

Frequently Used Symbols

Reinforced Concrete

R_c Concrete cubic compressive strength
f_c Concrete cylinder compressive strength
f_{ct} Concrete tensile strength
f_{ctf} Concrete flexural strength
f_b Bond strength
ε_{cs} Concrete shrinkage
ρ_s Geometrical reinforcement ratio (or percentage)
ψ_s Elastic reinforcement ratio (or percentage)
ω_s Mechanical reinforcement ratio (or percentage)

Steel

f_t Steel tensile strength
f_y Steel yield strength
f_{pt} Tensile strength of prestressing steel
$f_{p0,1}$ Stress at 0 and 1% residual elongation (proof stress)
$f_p(1)$ Stress at 1% elongation under loading (proof stress)
f_{py} Yield stress of prestressing steel
ε_t Steel failure strain
ε_u Ultimate strain (under maximum loading)
ε_{pt} Ultimate strain of prestressing steel

Others

l_o Buckling length ($=\beta_l$)
$\bar{\sigma}$, $\bar{\tau}$ Allowable stresses
γ_C Partial safety factor for concrete
γ_S Partial safety factor for steel
γ_F Partial safety factor for actions
γ_G Partial safety factor for permanent actions
γ_Q Partial safety factor for variable actions

Short Notes on Limit State Method

Safety Verifications

The content of the following chapters has been treated following the structural safety verification criteria of the *Limit States Method*. According to this method the safety verifications are done with the comparison between a *resistance parameter* and the corresponding *effect of the action*, both evaluated from the representative values of the quantities involved, that take into account their random variability.

Therefore, on the one side, the resistance parameter of concern (for example the resistance of a section) is deduced from the characteristic values R_{ki} of the *material strength* and from the nominal values of the concerned *geometrical dimensions*, based on a suitable mechanical *local model*. The value R_{ki} is represented by the 5% fractile of the statistical distribution of the strength of the ith material involved in the verification.

On the other side, the corresponding effect of *actions* is deduced from their characteristic values F_{kj} with an analysis of the *structural model* where nominal values of *geometrical quantities* are used. For the jth action, the value F_{kj} is represented by the 95% fractile of the statistical distribution of its intensity.

Safety verifications refer to the following:

- *ultimate limit states* (ULS) corresponding to the failure of the structure;
- *serviceability limit state* (SLS) for the functionality of the construction.

For what concerns the former, the text will hereafter mainly refer to the resistance against the local failure of the structural members. For what concerns the latter, service limits will be considered for stresses in materials, cracking in concrete and deflection of floors and beams.

The verification with respect to the resistance of ultimate limit state is obtained, applying *partial factors* of safety, with the comparison

$$R_{\mathrm{d}} \geq E_{\mathrm{d}}$$

where

R_{d} is the design resistance calculated with the *design values* $R_{\mathrm{d}i} = R_{ki}/\gamma_{\mathrm{M}i}$ of the strength of materials;

E_{d} is the design value of the effect of actions, calculated with the design values $F_{\mathrm{d}j} = \gamma F_j F_{kj}$ of actions;

Partial safety factors γ_{Mi} and γF_j, associated respectively to the ith material and jth action, cover the variability of respective values together with the incertitude relative to the geometrical tolerances and the reliability of the design model.

The verifications with respect to the serviceability limit states are done at the level of characteristic values with

$$E_k \leq E_{\mathrm{lim}}$$

where:

E_k is the value of the considered effect (stress in the material, crack opening or floor deflection) evaluated with the characteristic values of actions;

E_{lim} is the corresponding limit value which guarantees the functionality of the building.

Combination of Actions

For *permanent loads G*, which have a small random variation, the mean value is assumed as representative. *The self-weight of the structure* G_1, which can be defined with higher precision at design stage, is distinguished from the *dead loads of non-structural elements* G_2, being these latter defined with lower precision.

Variable actions, such as imposed loads on floors, snow loads and wind actions, are represented by their characteristic value Q_k, corresponding to the 95% fractile of the maximum values population. In order to account for the reduced probability that they would act at the same time with their maximum values, the actions are scaled down in the combination formulas with the pertinent *combination factors* whose values are reported in Chart 3.2. The factors, with reference to the relative (percent) duration of the different levels of intensity of the variable action, define the following combination values:

- *quasi-permanent* $\psi_{2j}\, Q_{kj}$: mean value of the time distribution of intensity;
- *frequent* $\psi_{1j}\, Q_{kj}$: value corresponding to the 95% fractile of the time distribution of intensity;

- *combination* $\psi_{0j}\ Q_{kj}$: value of small relative duration but still significant with respect to the possible concomitance with other variable actions.

For the different limit states' verifications the following combinations of actions are defined.

- *Fundamental combination*, used for ULS:

$$\gamma_{G1}G_1 + \gamma_{G2}G_2 + \gamma_{Q1}Q_{k1} + \gamma Q_2\psi_{02}Q_{k2} + \gamma_{Q3}\psi_{03}Q_{k3} + \cdots$$

- *Characteristic combination*, used for irreversible limit states (SLE):

$$G_1 + G_2 + Q_{k1} + \psi_{02}Q_{k2} + \psi_{03}Q_{k3} + \cdots$$

- *Frequent combination*, used for reversible serviceability limit state (SLE):

$$G_1 + G_2 + \psi_{11}Q_{k1} + \psi_{22}Q_{k2} + \psi_{23}Q_{k3} + \cdots$$

- *Quasi-permanent combination*, used for the long-term effects (SLE):

$$G_1 + G_2 + \psi_{21}Q_{k1} + \psi_{22}Q_{k2} + \psi_{23}Q_{k3} + \cdots$$

In those formulas, '+' implies 'to be combined with' and Q_{k1} represents the leading action for the concerned verification. Depending on the favourable or unfavourable effects for the verification, the partial safety factors have the following values respectively:

structural self-weight	γ_{G1} = 1 or 1.3
superimposed dead loads	γ_{G2} = 0 or 1.5
imposed loads	γ_{Q} = 0 or 1.5

What mentioned above refers to the verifications of the structure and foundation elements. For the verification of foundation soil, one can refer to Chap. 9 where a more comprehensive overall picture of the combination formulas is reported.

Chapter 1
General Concepts on Reinforced Concrete

Abstract This chapter presents the properties of the constitutive materials with their strength parameters and failure criteria. A special discourse is devoted to the creep of concrete and its structural effects. The behaviour of the composite reinforced concrete sections is finally presented with the related basic assumptions for resistance calculations.

1.1 Mechanical Characteristics of Concrete

Concrete is a composite material made of an *aggregate* of inert fillers (sand and gravel—or crushed stone—of different sizes), lumped together by the cement *paste*. The mechanical properties of this artificial conglomerate depend on those of its components (aggregate and cement paste) and on the *bond* at the interface between the two.

Chemical and technological aspects of concretes are not treated here: for these aspects one can refer to the relative disciplines. It is important to mention only the physical behaviour of the conglomerate leading to experimental results in terms of strength and deformation as measured by testing.

For a common concrete of normal weight, given that a good quality aggregate is used and correct technological and chemical production methodologies are followed, the mechanical properties mainly depend on the cement paste, which is the weakest component. Its theoretical strength, deductible from the relative molecular cohesion, is actually much higher than what measured experimentally. This phenomenon is explained by Griffith's theory of fracture mechanics, according to which the fracture depends on the presence of defects inside the material.

Defects mainly consist of *microcracks* that are formed in the cement paste and at the interface with the aggregate during setting and hardening, because of the shrinkage of the paste itself and the non-perfect adhesion between components. There are also *capillary pores* diffused in the cementitious matrix, even if well compacted, in a much lower percentage than in the aggregates. *Greater voids*

© Springer International Publishing AG 2017

G. Toniolo and M. di Prisco, *Reinforced Concrete Design to Eurocode 2*,
Springer Tracts in Civil Engineering, DOI 10.1007/978-3-319-52033-9_1

eventually remain in the concrete matrix due to non-perfect compaction of the fresh mixture.

The local strength of the matrix, limited by the presence of defects as mentioned above, determines one of the composite materials, to which the concept of homogeneity will further be extended on a macroscopic level. This means that the concrete strength is to be interpreted as a uniformly diffused property, as long as it refers to elements big enough with respect to the maximum aggregate size used.

1.1.1 Basic Properties of Concrete

The behaviour of concrete under loading is shown in the stress–strain diagrams as shown in Fig. 1.1.

From them the followings can be noted:

- high dissymmetry with much higher compression strength values than the ones in tension;
- nonlinear deformations starting from small stress values;
- very small ultimate fracture deformations with predominantly brittle failure;
- different initial elastic moduli for different material strength values;
- drop in stiffness much more rapid in tension than in compression.

In particular the decreasing part of the curves in Fig. 1.1 can be measured only with displacement-controlled tests. If otherwise it is the force to be progressively increased, when the peak strength is reached the specimen suddenly breaks with the instantaneous release of the potential elastic energy stored by the testing machine.

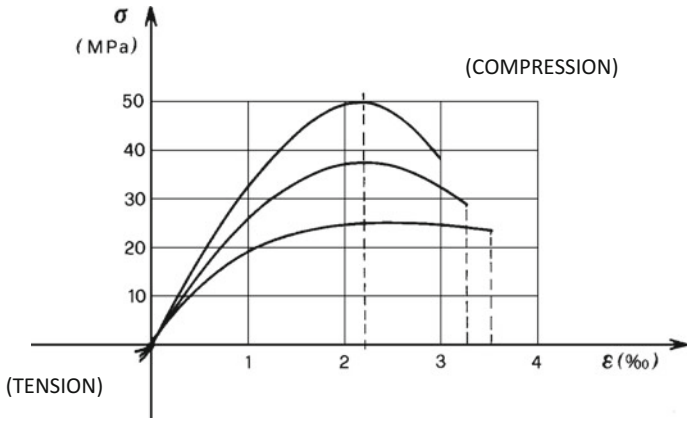


Fig. 1.1 Concrete stress–strain diagrams

Testing in tension is very difficult due to very small deformation values. The relative curves remain only approximately defined. Indicatively elongation values at rupture which are independent from the material strength would be noted.

Short-Term Strengths

With reference to the tests in compression, three stages are noticed as indicated in Fig. 1.2. A stage 'a' of low stresses is limited to about 0.4 times the failure strength, in which there is no significant microcracking propagation and the behaviour remains close to linear elastic. A stage 'b', in which the behaviour leaves the linearity because of the propagation of microcracks in the cement paste, stops in a new balanced and stable state. A stage 'c' of high stresses is greater than 0.8 times the ultimate strength, in which the propagation of microcracks becomes unstable, progressively leading the specimen to failure.

This leads to consider the duration of loads also. The solid line curve in Fig. 1.2 refers to the 'instantaneous' behaviour of the material, measured with tests of short duration. It ends with the sudden failure of the specimen, giving the strength f_c of the material. If, once a given stress value is reached, the specimen is kept under loading, increments of deformation ε can be measured along the time. Only after several years the deformation stabilizes on a final value (see dashed lines on Fig. 1.2). This is due to creep, a phenomenon that will be treated further on.

If the value σ exceeds 0.80 times the instantaneous strength f_c of concrete, the deformation does not reach the final stable value as the specimen fractures earlier. The dotted curve in Fig. 1.2 therefore indicates the *short-term strength* values obtained from the specimen, after a given duration of loading, because of the instable propagation of microcracks. The limit $\bar{f}_c$ represents the *long-term strength* of the material, to be relied upon for loads of long duration.

Ageing and Hardening

The mechanical properties of hardened concrete are gradually reached after a certain ageing period. Codes refer to the limit at 28 days for the evaluation of strength,

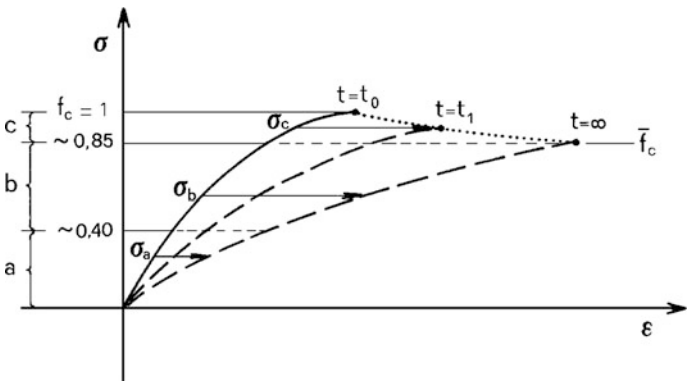


Fig. 1.2 Concrete stress–strain diagrams under long-term loading

but even after that limit further significant hardening of the material occurs. In Fig. 1.3 a hardening curve for normal ageing of concrete is indicated with a solid line. The strength measured at day j has been indicated with f_{cj}, with f_c the one representative of the class of the material measured at the normalized age of 28 days.

Based on the competent experimental results, the *hardening law* can be set as:

$$f_{cj} = e^{\beta(1-1/\sqrt{\tau})} f_c,$$

where $\tau = t/28$ is the ageing time over the 28-day limit and β is a coefficient related to the rate of strength development.

The value of β depends on the type of cement used (fast, normal or slow setting). For normal cements one can assume $\beta = 0.25$, which leads to final strength values

$$f_{c\infty} = 1.28 f_c$$

significantly higher than those at 28 days.

In terms of modulus of elasticity of the material, the hardening law can be expressed as

$$E_{cj} = \left[e^{\beta(1-1/\tau)}\right]^{0.3} E_c,$$

which shows smaller increments at late stages, against a more rapid development at shorter periods.

The temperature at which concrete is cured at the very early stages after casting has a significant influence on the hardening rate. This phenomenon is systematically used in prefabrication to attain high-strength values in short times, adopting *accelerated curing* methods consisting of appropriate heat treatments. The dashed curve in Fig. 1.3 shows the results of such treatment, which pays more rapid

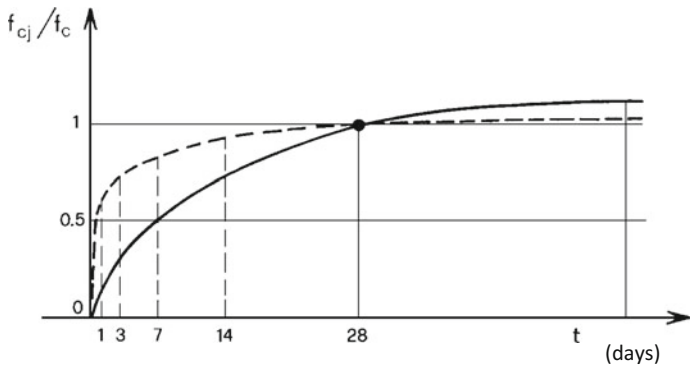


Fig. 1.3 Concrete-hardening curves

hardening and the subsequent possibility of demoulding the unit after a shorter time with a lower final concrete strength. The thermal treatment in fact, even if applied correctly, increases microcracking in the cementitious matrix.

Although not in a rigorous way, the curve relative to accelerated curing can be deduced from the already mentioned hardening law with $\beta = 0.08$.

Numerical data of hardening for cases of possible practical use are reported in Table 1.1.

Deformation Model

A mathematical model for the 'instantaneous' behaviour of concrete in compression is given by the Saenz formula:

$$\sigma = \frac{\kappa\eta - \eta^2}{1 + (\kappa - 2)\eta} f_c,$$

where $\eta = \varepsilon/\varepsilon_{c1}$ (see Fig. 1.4).

The coefficient

$$\kappa = \frac{\sigma^*}{f_c} \ (> 1)$$

represents the shape factor giving the degree of 'roundness' of curves: it is smaller for higher strength concrete with sharper σ–ε curves, and it is greater for lower strength concrete with more round σ–ε curves (see Fig. 1.1).

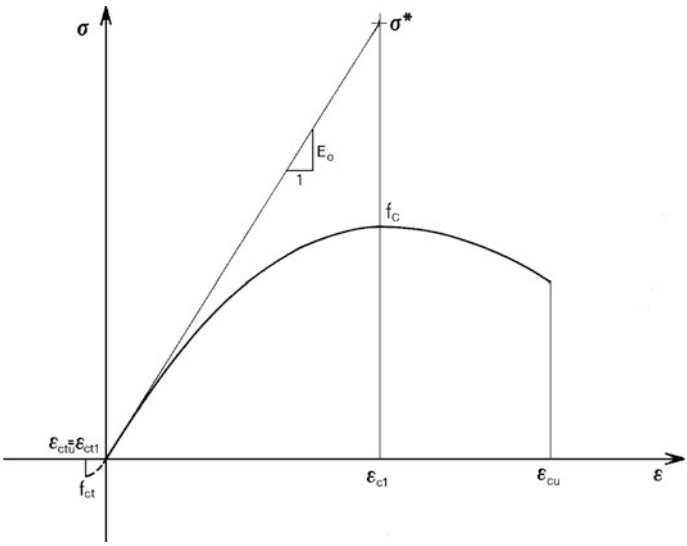


Fig. 1.4 Mathematical model for stress–strain curve

Its tangent at the origin E_o is needed for its determination, as (see Fig. 1.4)

$$\sigma^* = E_o\,\varepsilon_{c1}.$$

The test for the experimental evaluation of the modulus of elasticity E_c of concrete or the formulae that define it as a function of strength f_c give the secant instead (see also Fig. 1.10), as it will be specified further on. Therefore, it can be approximately set

$$E_o \approx 1.05\,E_c.$$

Still in an approximated way, for strength values $f_c \leq 50$ MPa other parameters of the equation can be set as

$$\varepsilon_{c1} \text{ from } 0.0019 \text{ to } 0.0024$$
$$\varepsilon_{cu} \approx 0.0035.$$

For high-strength concretes the values of ε_{c1} and ε_{cu} get closer and the decreasing part of the curve tends to disappear. More precise data are reported in Table 1.3.

In tension, because of the intrinsic difficulties of testing, a purely conventional forma can be assumed, represented by a cubic parabola that satisfies the conditions

$$\sigma = 0 \quad \frac{d\sigma}{d\varepsilon} = E_o \quad \text{for} \quad \varepsilon = 0$$
$$\sigma = f_{ct} \quad \frac{d\sigma}{d\varepsilon} = 0 \quad \text{for} \quad \varepsilon = \varepsilon_{ct1'}$$
$$\varepsilon_{ct1} = \varepsilon_{ctu} \approx 0.00015.$$

We would therefore have in tension

$$\sigma = \left[\kappa_t\,\eta_t - (2\kappa_t - 3)\eta_t^2 + (\kappa_t - 2)\eta_t^3\right] f_{ct}$$

for $0 < \eta_t < 1$, with

$$\eta_t = \frac{\varepsilon}{\varepsilon_{ct1}}; \quad \kappa_t = \frac{\sigma_t^*}{f_{ct}}; \quad \sigma_t^* = E_o \varepsilon_{ct1}.$$

A simplified schematization can also be assumed, in place of the cubic parabola, with a bilinear diagram such as

$$\sigma = E_o\,\varepsilon \qquad \text{for} \quad 0 < \sigma < 0.9 f_{ct}$$
$$\sigma = \left(1 - \frac{0.1}{\Delta\varepsilon_0}\varepsilon'\right) f_{ct} \quad \text{for} \quad 0.9 f_{ct} < \sigma < f_{ct},$$

where

$$\varepsilon' = \varepsilon_{ct1} - \varepsilon$$
$$\Delta\varepsilon_o = \varepsilon_{ct1} - 0.9 f_{ct}/E_o.$$

The parameters of deformation models for concrete presented here are reported for the different classes of strength in Table 1.3.

Shrinkage

Shrinkage is another property of concrete. During the first ageing periods the hardened concrete shrinks reducing its volume. This phenomenon has significant technological and mechanical effects in reinforced concrete structural elements.

The total deformation due to shrinkage is made of two components:

$$\varepsilon_{cs} = \varepsilon_{cd} + \varepsilon_{ca};$$

one due to drying, and the other of autogenous origin. *Drying shrinkage strain* ε_{cd} slowly develops after migration of water trapped in hardened concrete towards the outside. *Autogenous shrinkage strain* ε_{ca} develops during hardening of concrete itself during the first days after casting.

The *drying shrinkage law* can be represented by the following mathematical model (see Fig. 1.5):

$$\varepsilon_{cd}(t') = \varepsilon_{cd\infty} g_s(t')$$

where $\varepsilon_{cd\infty}$ is the final value of contraction and $g_s(t')$ is the function that expresses the increase of the phenomenon with time t' measured from its start.

The value of shrinkage is mainly influenced by the curing environment, the concrete thicknesses and its strength class. For normal Portland cement, with

$$h = \mathrm{RH}/100$$

the environment *relative humidity* ratio, with

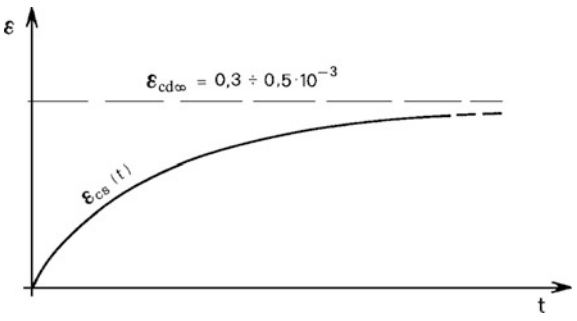


Fig. 1.5 Drying shrinkage curve

$$s = \frac{2A_c/u}{100}$$

the *equivalent thickness* of the element expressed in decimetre (A_c = concrete cross-sectional area, u = perimeter) and with

$$c = f_c/10$$

the *strength class* expressed in kN/cm^2, it can be set as

$$\varepsilon_{cd\infty} = k_s\, \varepsilon_{cdo},$$

where

$$k_s = 0.7 + 0.0094\,(5 - s)^{2.5} \qquad \text{for } s < 5$$
$$\varepsilon_{cdo} = 870 \times 10^{-6}\,(1 - h^3)e^{-0.12\,c.}$$

The law of growth can be set as

$$g_s = \frac{t'}{t' + 40\sqrt{s^3}} \quad (t' \text{ in days}).$$

The *autogenous shrinkage law* is given by

$$\varepsilon_{ca}(t) = \varepsilon_{ca\infty} g_a(t),$$

where

$$\varepsilon_{ca\infty} = 2.5 \times 10^{-6}\,(f_c - 18) \quad g_a(t) = 1 - e^{-0.2\sqrt{t}},$$

where t is the age of concrete expressed in days.

Shrinkage numerical data are reported in Tables 1.4 and 1.5 for cases of possible use. It is to be noted though that even using fine models as the ones presented here, a significant variance in the experimental results remains (≈0.30), in addition to the incertitude of the preventive evaluation of the parameters involved (especially the one relative to the humidity of the ageing environment). High precision previsions are usually not possible.

Design Nominal Values

For design applications, default previsions can be conventionally assumed considering an ageing in a medium environment ($h = 0.6$) based on reference situations.

For the evaluation of global effects on structures made of ordinary concrete with medium–low concrete classes, one obtains

$$\varepsilon_{cs\infty} = 0.36 \div 0.38 \cdot 10^{-3}.$$

For the evaluation of tension losses in pre-tensioned cables of precast elements with small thickness pre-stressed after one day of accelerated curing, with medium and high concrete classes, one obtains

$$\Delta\varepsilon_{cs\infty} = 0.34 \div 0.36 \cdot 10^{-3}.$$

For the calculation of tension losses in post-tensioned cables of elements with medium–small thickness, pre-stressed after 14 ageing days, with medium concrete classes, one obtains

$$\Delta\varepsilon_{cs\infty} = 0.32 \cdot 10^{-3}.$$

Unless more rigorous evaluations are needed, practical design calculation can be based on few nominal values corresponding to the principal conventional reference situations.

Other Properties

The main characteristic of fresh concrete is its *workability*, which is the possibility of pouring it in formworks with total filling, perfect conglobation of reinforcement and good compaction of the concrete itself. Better workability is obtained with fluid mixes. The measure of such property is done in mm of reduction of the Abrams' cone (see Fig. 1.6), called 'slump'.

It is to be noted that the increase of water content causes, together with higher fluidity of the fresh mixture, a strong strength reduction in the hardened concrete. As a matter of fact, all the water in excess to the stichometric water/cement ratio (≈0.35) remains inside pores that constitute defects. In order to improve workability without compromising the strength, appropriate additions have to be used.

The *classes of consistency*, codified according to ISO 4103, are four and distinguish fresh mixtures for technological production purposes based on their workability. They are specified in Table 1.6 together with a name (humid, plastic, semi-fluid, fluid) in order to facilitate the quotation in the technical documents.

It is eventually recalled that the coefficient of *thermal expansion* α_T of concrete is between 1.0 and 1.2 × 10^{-5} °C^{-1}. Its *volumic mass* varies between 2300 and 2400 kg/m^3 depending on the type of aggregates, whilst one of the reinforced concretes is assumed equal to 2500 kg/m^3 to take into account the higher weight of the reinforcement.

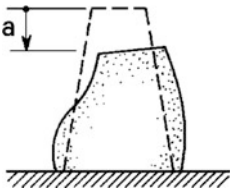


Fig. 1.6 Slump test

1.1.2 Strength Parameters and Their Correlation

Concrete strength is deducted from codified tests. The representativeness of the values obtained is strictly related to the correct testing procedures. First of all the size of the specimen has to be correlated to one of the aggregates used: $l \geq 5d_a$, where l is the minimum dimension of the specimen and d_a is the maximum aggregate size.

Compression tests are carried out loading specimens placed between the plates of a press up to failure. The quantity measured on cubic specimens is called *cubic strength* (in compression) and it is indicated with R_c. Failure usually occurs as indicated with dashed lines in Fig. 1.7, with lateral spalling of the material and the formation of a residual double-cone shape.

The stress state of a cubic specimen compressed between the plates of a press is influenced by the friction on the faces of the specimen itself. In addition to the longitudinal component of stresses, a transversal component is induced, in compression too, that opposes the transversal expansion and increases the strength.

To overcome the effect of friction, prismatic (or cylindrical) specimens have to be used that are slender enough. In this way, between the end portions roughly as long as the transverse dimension, where the effects caused by the friction are significant, an intermediate portion remains subject to a pure longitudinal stress flow. The strength measured on prismatic or cylindrical specimens whose length is at least 2.5 times the transverse dimension is called prismatic or cylinder strength (or more simply *compressive strength*) and indicated with f_c (see Fig. 1.7b).

The correlation between the two strength values defined above is given by the formula

$$f_c \approx 0.83\, R_c$$

largely verified experimentally. This allows to adopt, in the practice of reinforced concrete constructions, the test on the more manageable cubic specimens and to derive then from the results the prismatic strength required for structural design calculations.

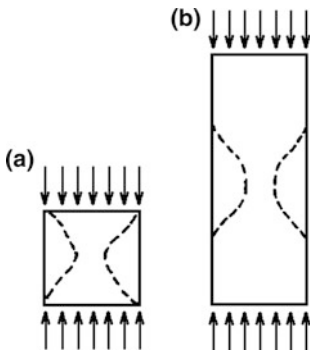


Fig. 1.7 Compression failure modes

Strength Classes

As better specified further on there are correlations between strength parameters that permit to identify the concrete class associating it to a unique quantity, the one corresponding to the lead parameter. The lead parameter is chosen as the compressive strength, the one that derives from the most elementary and direct test on the material.

The extent of the possible codified classes depends on the production technological capabilities: one starts from the lower bound with the lowest strength class compatible with the structural use of concrete; the upper limit is imposed by the level attained by the industrial production of the concrete itself.

The discretization introduced in identifying a finite number of classes within an upper and lower bound is based on the minimum step that would have a practical meaning on site in relation to the precision allowed by the calibration capabilities of the production itself.

The minimum strength for structural use is set around 8 MPa. The maximum one, achievable with modern industrial technologies, can be higher than 70 MPa. This limit does not take into account concretes aged in autoclaves, whose strength can be largely higher than 100 MPa. These concretes represent a different material not treated in this textbook. The minimum significant step is around 5 MPa.

Concrete normalized classes are indicated with the symbol *C* followed by the nominal values of cylinder and cubic strength. With these premises, the following strength groups can be codified, where the ones indicated as superior are currently admitted by national regulations only under some additional conditions for quality control.

Strength Classes

- very low C8/10–C12/15
- low C16/20–C20/25–C25/30
- medium C30/37–C35/43–C40/50–C45/55
- high C50/60–C55/67–C60/75–C70/85
- superior C80/95–C90/105

In the following section it is to be noted that a significant random variability of strength values is associated to every single production event. The values mentioned above have to be considered as the characteristic ones mentioned hereafter. With this clarification, the introduced classification shows

- *very low* strength classes, minimum for plain and lightly reinforced concrete structures;
- *low* strength classes, minimum for reinforced concrete structures;
- *medium* strength classes, minimum for pre-stressed concrete structures;
- *high*-strength classes, for which a special prior experimentation is required;
- *superior* strength classes, presently done only for experimental purposes.

The so-defined classes univocally identify the product according to its principal mechanical characteristics: compressive strength, tensile strength and modulus of elasticity. They do not identify other technological characteristics, such as workability of fresh concrete that, for the same strength, can be improved for example with the use of plasticizers, and the maximum aggregate size which relates to the elements' thicknesses and to the spacing between reinforcement bars. Those additional characteristics will have to be explicitly specified in the design documentation together with the strength class.

In Table 1.2 data relative to the three main mechanical parameters mentioned above are reported for all concrete classes.

Tensile Strength

Tensile tests are mainly carried the following two criteria. The first one leads to *direct strength* (in tension) f_{ct} measured inducing a field of pure longitudinal stresses in a specimen subject to tension between the clamps of a testing machine. Conventional prismatic or cylindrical specimens are used for this test, having glued with epoxy resin the metal articulated fixtures required for clamping device of the testing machine (see Fig. 1.8a). Glueing can be avoided using friction grips, directly applied at the ends of the specimens.

The relationship between tensile and compressive strength can be given by the formula

$$\begin{aligned} f_{ct} &= 0.27\sqrt[3]{f_c^2} && \text{for } f_c \leq 58 \text{ MPa} \\ f_{ct} &= 2.12\ \ln\left[1 + \tfrac{f_c}{10}\right] && \text{for } f_c > 58 \text{ MPa.} \end{aligned}$$

The *indirect strength* in tension f'_{ct} (splitting strength) is measured with the Brazilian test, which consists of inducing a linearly concentrated compression in the specimen (v. Fig. 1.8b, c). The diffusion of stresses in the specimen leads, in

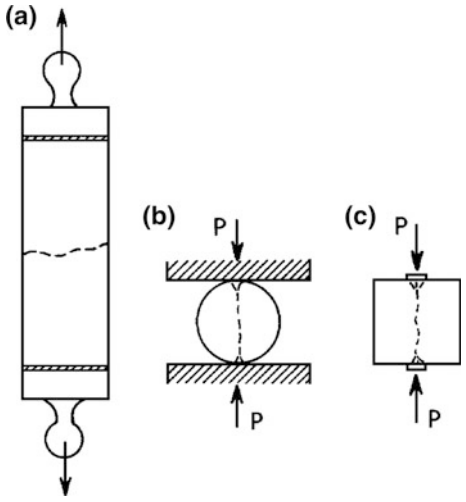


Fig. 1.8 Tests for tensile strength

addition to a flux of vertical compressive stresses, to a distribution of transversal tension stresses more or less constant throughout the intermediate part of the specimen.

Cylindrical specimen can be used, placed horizontally between the plane plates of a press, or more simply cubic specimens, same as the ones for the compressive test, having inserted loading strips to concentrate the load. Solving the problem of plane elasticity, the value of the transversal tensile component is obtained which, for the fracture load P, gives the strength value

$$f'_{ct} = \frac{2P}{\pi \Phi 1},$$

where l is the length of the specimen and Φ is its diameter ($\Phi = 1$ for cubic specimens). As it will be mentioned further on, the presence of the vertical compressive components does not influence significantly the tensile strength. The crack lines along which rupture occurs are indicated with dashed lines in Fig. 1.8.

The tensile strength measured indirectly with the Brazilian test coincides with the direct one; the correlation formula can therefore be

$$f'_{ct} \approx f_{ct}.$$

The standards give the conservative value $f_{ct} \approx 0.9f'_{ct}$.

The flexural test (see Fig. 1.9) gives another method for the indirect evaluation of the tensile strength. It consists of applying a bending load on a concrete beam in order to induce triangular distributions of normal stress σ, in tension at one side and in compression at the other side. Given the lower strength in tension of concrete, the part in tension will fail, from which the flexural strength f_{ctf} can be obtained.

The test has to be conducted with appropriate measures to isolate the central part of the beam outside the zones involved by stress concentrations due to loads and reactions and to avoid parasite stresses (due to torsion for example). Assuming a

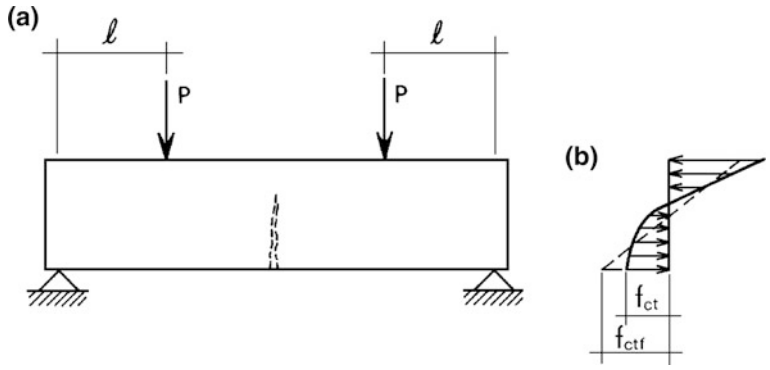


Fig. 1.9 Test for flexural strength

linear distribution of stresses, the strength value is obtained at the extreme fibre in the central part subject to tension under the failure bending moment $M = P\mathrm{l}$:

$$f_{\mathrm{ctf}} = \frac{6P1}{bh^2},$$

where b is the width and h is the depth of the rectangular section of the beam.

The *flexural strength* obtained is systematically higher than the tensile strength obtained directly. This is due to the fact that close to failure, the distribution of stresses σ in the section is not linear, as assumed the formula that interprets the test. The part in tension is outside the elastic range, with a distribution similar to the one indicated in Fig. 1.9b.

Very uncertain is the correlation with the direct tensile strength:

$$f_{\mathrm{ctf}} = \beta f_{\mathrm{ct}},$$

where very different values (β = 1.3–1.9) are proposed for β, whilst CEB–FIP Model Code 2010 sets it as a function of the beam depth h, deducing it from fracture theory as

$$\beta = \frac{25 + 1.5h^{0.7}}{1.5h^{0.7}} \quad (h \text{ in mm}),$$

with values between 1.1 and 1.7 indicatively.

Modulus of Elasticity

The test for the evaluation of concrete *modulus of elasticity* E_{c} is carried out on prismatic specimens subject to compression, measuring, for a given load, the contraction of the central part of the specimen itself. The loading is assumed equal to 0.4 times the predicted material strength f_{c}, and the measurement of shortening is done with four extensometers placed on the faces to compensate, with the mean value of readings, the possible eccentricity of the load itself (see Fig. 1.10a).

The following ratio is therefore evaluated

$$E_{\mathrm{c}} = \sigma_{\mathrm{p}}/\varepsilon_{\mathrm{p}}$$

that represents the secant modulus of elasticity (see Fig. 1.10b) and is a little smaller than the tangent E_{o} at the origin.

The correlation between modulus of elasticity and compressive strength can be set according to the formula

$$E_{\mathrm{c}} = 22000[f_{\mathrm{c}}/10]^{0.3}.$$

With this value the deformation parameters of the constitutive model as reported in Table 1.3 can be deducted.

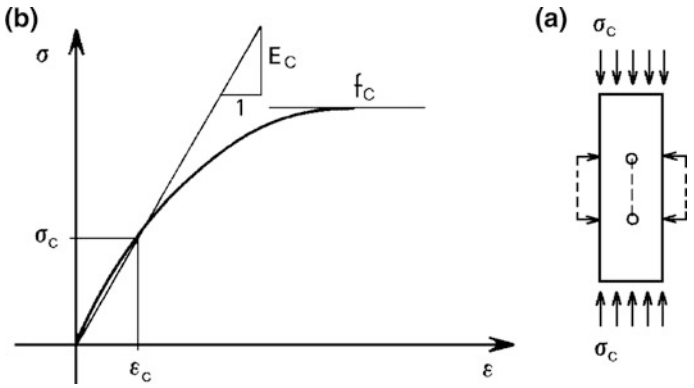


Fig. 1.10 Tests for the modulus of elasticity

The determination of the Poisson ratio ν (of *transversal contraction*) requires more complex testing procedures. Values between 0.16 and 0.20 are obtained for concrete. Those values are valid if high levels of compression are excluded, higher than 0.5 times the material strength, for which high increments of apparent transverse expansion are measured, because of the formation, when progressively approaching the rupture load, of macroscopic longitudinal cracks in the specimen.

The values of mechanical characteristics presented above are reported, for various concrete strength classes, in Table 1.2.

Mean and Characteristic Values

Tests, repeated on several specimens of the same concrete, show a dispersion of results, quite significant if related to the entire production cycle on site of a construction from foundation to the roof. If related to the continuous industrialized production of precast elements in industrial plants, given that the production procedures themselves are subject to an efficient system of quality control, the dispersion of results can be significantly smaller.

Extensive surveys have been conducted on construction sites and industrial plants. Analysing data, for example the ones relative to cubic strength R_c, with statistical procedure, *mean values* have been calculated:

$$R_{cm} = \frac{\sum_{i=1}^{n} R_{ci}}{n}$$

and standard deviations

$$s = \sqrt{\frac{\sum_{i=1}^{n} (R_{ci} - R_{cm})^2}{n-1}},$$

obtaining the *characteristic value*

$$R_{ck} = R_{cm} - ks$$

to be used in resistance verifications, which corresponds to the 5% probability of having a more unfavourable value. Using a suitable model of the distribution function, for a sufficient number of measurements ($n \geq 30$), the *deviation* was found as

$$\Delta R = R_{cm} - R_{ck} = ks$$

quite homogeneous across all controlled sites and plants, for which the following value can be assumed on average

$$\Delta R \approx 9.6 \text{ MPa}$$

independently from the concrete strength class.

Such fixed deviation penalizes less-resistant concretes more, as indicatively reported in the following table (values expressed in MPa):

R_{ck}	20	37	55	75
$\Delta R/R_{ck}$	0.48	0.26	0.17	0.13
R_{cm}/R_{ck}	1.48	1.26	1.17	1.13

If for example a cubic characteristic strength of 30 MPa is prescribed, the mix design of the relative concrete production will have to refer to a mean value R_{cm} = 30 + 9.6 ≈ 40 MPa about 1/3 higher than the characteristic one required. At the same time, such production can guarantee a characteristic strength equal to 0.75 times the mean value itself.

The model that fits in the best way to the random distribution of concrete strength throughout its site production is the lognormal expressed by (see Fig. 1.11)

$$f(x) = \frac{1}{(x - x_d)\sqrt{2\pi}\sigma} e^{\frac{-(\xi-\bar{\xi})^2}{2\sigma^2}},$$

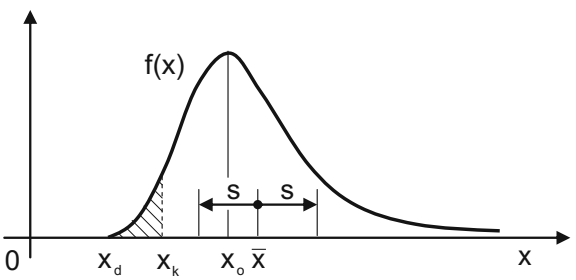


Fig. 1.11 Strength distribution curve

where $\xi = \ln(x - x_d)$ for $x \geq x_d$, and where $\bar{\xi}$ is the mean value of ξ and σ is its standard deviation. The lower bound value of the possible interval of random variability of the quantity x is indicated with x_d, calculated on the basis its mean $\bar{x}$ and its standard deviation s with

$$x_d = \bar{x} - \beta s.$$

For the reliability index, le regulations assume the value $\beta = 3.8$. The characteristic value $x_k = \bar{x} - ks$ corresponding to the 5% fractile is calculated with values of k that vary with the coefficient of variation $\delta = s/\bar{x}$:

$k = 1.579$	for	$\delta = 0.05$
$k = 1.514$	for	$\delta = 0.10$
$k = 1.451$	for	$\delta = 0.15$
$k = 1.390$	for	$\delta = 0.20$

If referred to prefabrication plants with an efficient quality control system, the deviation between mean and characteristic values of a given continuous concrete production is limited to

$$\Delta R \approx 6.0 \text{ MPa}.$$

The management cost of the control is therefore compensated by a reduction of cement quantity in the mix design, with less penalizing mean values. If for example a cubic characteristic strength equal to 55 MPa is prescribed, the mix can be designed for a mean value $R_{cm} = 55 + 6.0 \approx 61$ MPa about 11% higher than the characteristic one, whilst such production will be able to guarantee a characteristic strength equal to about 0.92 times the mean value itself.

If reported in terms of prismatic strength values ($\Delta f \approx 0.83 \Delta R$), such differences become

$$\Delta f = 8.0 \text{ MPa} \quad \text{and} \quad \Delta f = 5.0 \text{ MPa},$$

respectively, for ordinary and industrial controlled productions.

At the design stages, for calculations done according to the semi-probabilistic ultimate limit state method, previsions have to be based on the *characteristic value* f_{ck} of strength. Therefore, in order to deduct the other mechanical characteristics necessary for calculations, based on the type of ordinary or industrial production of the relative site or plant, the designer will have to estimate the mean value of compressive strength, respectively, with $f_{cm} = f_{ck} + 8$ or with $f_{cm} = f_{ck} + 5$ and on these values he can apply the correlation formulas reported in the previous pages.

The numerical values of related quantities are reported in Tables 1.2a and b for the two types of production, deduced from the mentioned correlations. In particular the characteristic (lower) values of tensile strength and modulus of elasticity are

calculated assuming their ratio to the corresponding mean values equal to 0.7 and 0.8, respectively, for ordinary and industrial productions. The mean value of cubic strength is reported as it is the most immediate reference for the tests that will be carried out during production, unless more articulated elaborations of results are required for acceptance verifications.

For the control of continuous concrete production-specific charts and diagrams can be used such as the ones reported in Table 1.11, where *shifting mean values* are used based on tests on the last three weeks of production.

1.1.3 Failure Criteria of Concrete

The one that better suits concrete is *Mohr's criterion*, or the criterion of internal friction, for which failure in shear occurs when the maximum shear stress reaches a limit which is the function of the average normal stress. Mohr assumes that those stresses τ_{max} and σ_{med} can be evaluated based on the two extreme principal stresses, whilst the intermediate one does not have a significant influence on rupture.

Indicating with σ_1, σ_2, σ_3 the three principal stresses representing the stress state in point of the material, given that

$$\sigma_1 \leq \sigma_2 \leq \sigma_3$$

failure would therefore depend on the component

$$\tau_{max} = \frac{\sigma_3 - \sigma_1}{2}$$

and would occur when this component reaches the value

$$\tau_r = F(\sigma_{med})$$

with

$$\sigma_{med} = \frac{\sigma_1 + \sigma_3}{2}$$

and F a given function, increasing towards higher compressions.

Mohr's Envelope Curve

A representation of the criterion is given by Mohr's envelope curve (see Fig. 1.12), which constitutes the envelope of all circles corresponding to failure limit situations. Ordinary tests on concrete give two limit circles: 'a', with $\sigma_1 = 0$ ($=\sigma_2$) and $\sigma_3 = f_{ct}$, deduced from tensile test; 'b', with $\sigma_1 = -f_c$ and $\sigma_3 = 0$ ($=\sigma_2$), deduced from compression test (as indicated respectively in Fig. 1.13a, b).

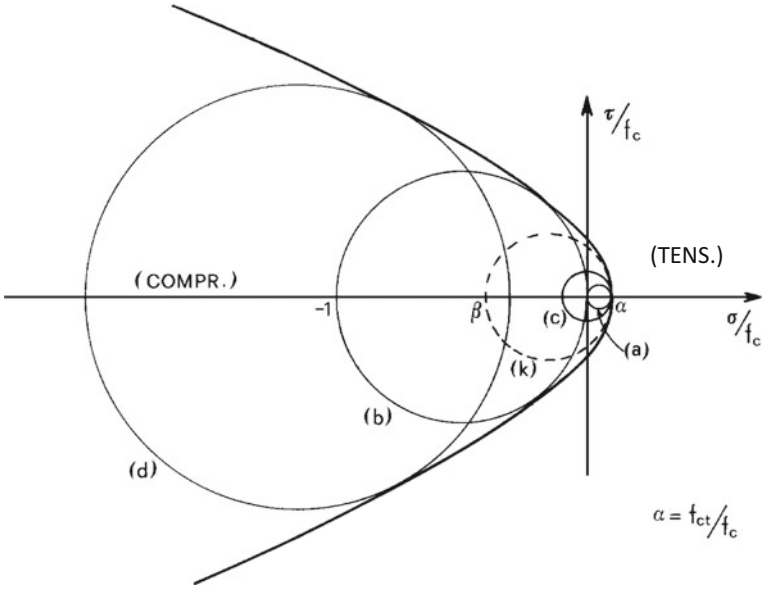


Fig. 1.12 Representation of Mohr's envelope curve for concrete failure

Circle 'c' corresponds to a state of pure shear stress $\tau = \sigma_3 = -\sigma_1$ (see Fig. 1.13c): failure occurs again for $\sigma_3 = f_{ct}$ (=τ), which leads to the equivalence between tensile strength and pure shear strength.

The circle 'k' of Fig. 1.12 is the last one tangent in α (=f_{ct}/f_c). It separates the states corresponding to the two failure modes: on the right for tension with cracking off occurring for the corresponding principal direction; and on the left, with $\sigma_1/f_c < \beta$, for inclined shear as observed in the compression test.

Tests of triaxial states, such as the one represented in Fig. 1.13d, are very difficult and complex. The function F of Mohr's criterion therefore remains not well defined.

In conclusion this criterion appears qualitatively correct, but contains significant approximations. The first one is to give infinite strength for 'hydrostatic' compressions with $\sigma_1 = \sigma_2 = \sigma_3$. The other ones come from neglecting the effect of the intermediate principal stress σ_2, which has a significant influence instead.

Models for Multiaxial States

For *biaxial stress states* σ_1, σ_2 (with $\sigma_3 \equiv 0$) curves such as the one represented in Fig. 1.14 have been defined experimentally.

The non-dependence of tensile strength from the other component remains confirmed with good approximation until it does not exceed the limit β approximately set at 0.4 times the compressive strength. In the compression domain the significant influence of the second component can be noted which increases the

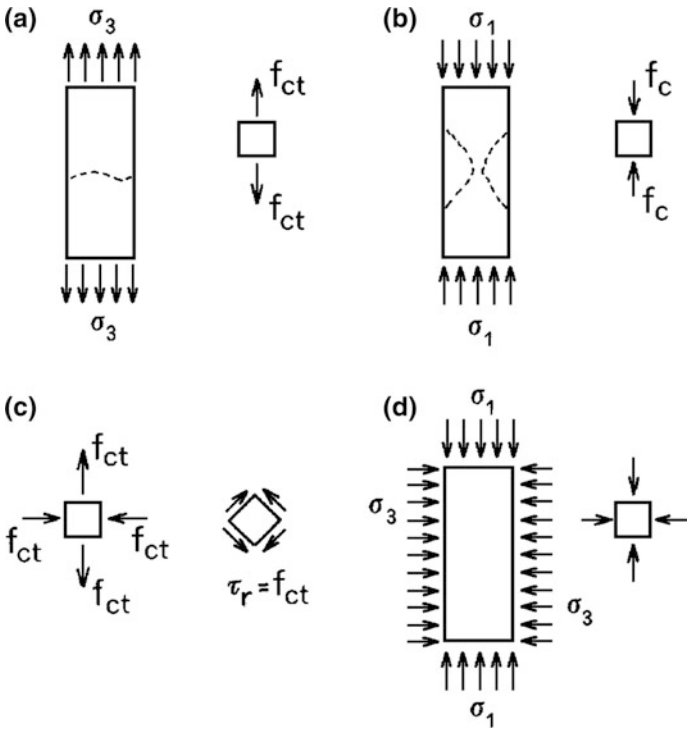


Fig. 1.13 Tests and failure limit situations

strength up to more than 1/4 times with respect to the monoaxial one, whilst Mohr's criterion would set it constant.

A good representation of the resistance limit curve is given, in the compression domain, by the elliptical formula:

$$\bar{\sigma}_1^2 - 1.26\bar{\sigma}_1\bar{\sigma}_2 + \bar{\sigma}_2^2 = 1 \quad (\text{with } \bar{\sigma}_3 \equiv 0),$$

where $\bar{\sigma}_i = \sigma_i / f_c$ are the specific principal stresses.

CEB–FIP MC 2010 gives a complete simplified model of the curve of Fig. 1.14 represented by the three formulas:

- *part A* (tension/tension with $\bar{\sigma}_2 \geq \bar{\sigma}_1 \geq 0$)

$$\bar{\sigma}_2 = \alpha \quad (\alpha = f_{ct}/f_c)$$

- *part B* (tension/compression with $\bar{\sigma}_2 > 0$ and $0 > \bar{\sigma}_1 > -0.96$)

$$\bar{\sigma}_2 = (1 + 0.8\bar{\sigma}_1)\,\alpha$$

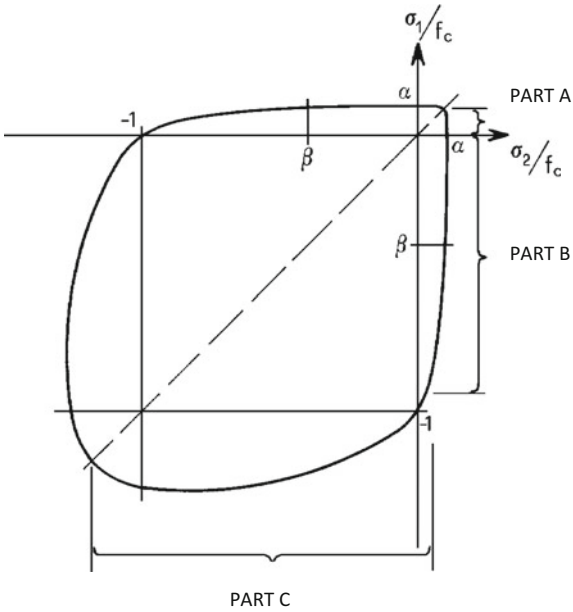


Fig. 1.14 Failure limit curve for biaxial stress states

- *part C* (compression/compression with $\bar{\sigma}_2 \geq \bar{\sigma}_1$ and $-0.96 > \bar{\sigma}_1$)

$$\bar{\sigma}_1 = \frac{(1+3.8\kappa)}{(1+\kappa)^2} \quad (\kappa = \bar{\sigma}_2/\bar{\sigma}_1).$$

The limited tensile strength of concrete is often completely neglected in the calculations of reinforced concrete capacity, allowing it to crack and tension stresses to convey into the steel bars that constitute the reinforcement. The models used in such calculations can therefore ignore the tension/tension states of concrete and reduce the ones of tension/compression to the monoaxial verification $\sigma_c < f_c$.

If neglecting the higher strength values of compression/compression states, even for them one can simply refer to the mentioned uniaxial verification. For biaxial states this simplification would lead to underestimate the resistance by up to 20%, as it can be deducted from the already discussed curve of Fig. 1.14. There are triaxial compression states specifically induced with appropriate confining reinforcement of concrete (see, for example, Sect. 2.1.2) that have to be correctly verified as they represent cases where the increase in resistance is essential for structural integrity and safety.

Several experimental researches have been carried on *triaxial stress states*, but the relevant difficulties of testing have not led to reliable results, with data very different according to different authors. However, it remains confirmed that the strength for 'hydrostatic' compressions, with $\sigma_1 = \sigma_2 = \sigma_3$, is much higher than the prismatic one. The type of diagrams obtained is shown in Fig. 1.15, represented

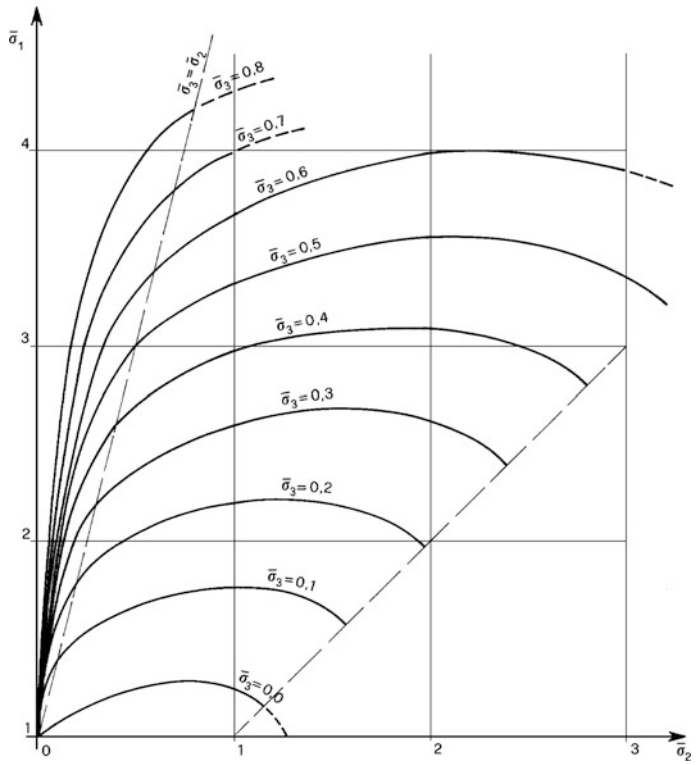


Fig. 1.15 Failure limit curves for triaxial stress states

with the 'level curves' σ_3 = const. of the limit strength boundary surface, only for the compression domain. For example for states characterized by $\bar{\sigma}_1 \ll \bar{\sigma}_2 = \bar{\sigma}_3$, the following curve could be deduced:

$$-\bar{\sigma}_1 \approx 1 - 4.0\,\bar{\sigma}_2 \quad (\text{for } 0 > \bar{\sigma}_2 > -1)$$

1.2 Creep

The components of the strain of concrete, as measured at a given time t, are given by

$$\varepsilon_c(t) = [\varepsilon_{cT}(t) + \varepsilon_{cs}(t')] + [\varepsilon_{ce}(t_o) + \varepsilon_{cv}(\tau, t_o)],$$

where

ε_c global strain at time t;
ε_{cT} thermal expansion due to the instantaneous temperature difference with respect to the initial one in concrete;

ε_{cs} progressive concrete shrinkage that increases with ageing t' measured from the beginning of the phenomenon;
ε_{ce} instantaneous elastic strain occurring at time t_o of application of loads;
ε_{cv} progressive creep strain that increases with the duration $\tau = t - t_o$ of loading itself.

The first two components of strain are independent from the stress state of concrete. The second two on the contrary are a consequence (respectively immediate and delayed) of the induced stress state and its history.

Among the four components of strain the last one due to creep is yet to be presented: it has significant effects on the behaviour of reinforced concrete structures, as shown in details in what follows.

1.2.1 Principles of Creep

Concrete under permanent loading exhibits delayed deformations in time that increase with decreasing rate up to stabilization after many years. The phenomenon is very important, so much that the slow delayed part of deformation normally exceeds the value of the elastic instantaneous part occurred at load application. The phenomenon is represented in Fig. 1.16a, as measurable experimentally on a prismatic concrete specimen subjected, starting from time t_o, to an uniaxial stress σ that remains unchanged along the time. The instantaneous elastic contraction is indicated with ε_e; the delayed contraction read at time t with ε_v. The total contraction is the summation of the two contributions: $\varepsilon = \varepsilon_e + \varepsilon_v$. After many years of measurements, the values of contractions stabilize on the final value $\varepsilon_e + \varepsilon_{v\infty}$.

The dual aspect of the same physical phenomenon, perceived above as creep measurement, is represented by relaxation (see Fig. 1.16b), for which the same prismatic concrete specimen, subjected to a permanent contraction ε, reacts with stresses σ that, starting from an initial elastic value σ_e, decrease progressively along the time until stabilization on a final value $\sigma_e - \sigma_{v\infty}$.

Linear Theory

The linear theory of creep, verified experimentally with good approximation as long as the stress state remains within about 0.45 times the concrete strength, expresses the part of the response due to creep as a simple proportion of the elastic one:

$$\varepsilon(t, t_o) = \varepsilon_e(t_o) + \varepsilon_v(t, t_o) = \varepsilon_e(t_o)\left[1 + \frac{\varepsilon_v(t, t_o)}{\varepsilon_e(t_o)}\right] = \frac{\sigma}{E_o}[1 + \varphi(t, t_o)]$$

having indicated with E_o the value of modulus of elasticity developed by the concrete at the time of load application. The *creep coefficient* $\varphi(t, t_o)$ expresses the ratio between the part due to creep measured at time t and the elastic part of the contraction under the constant stress σ, applied starting from time t_o.

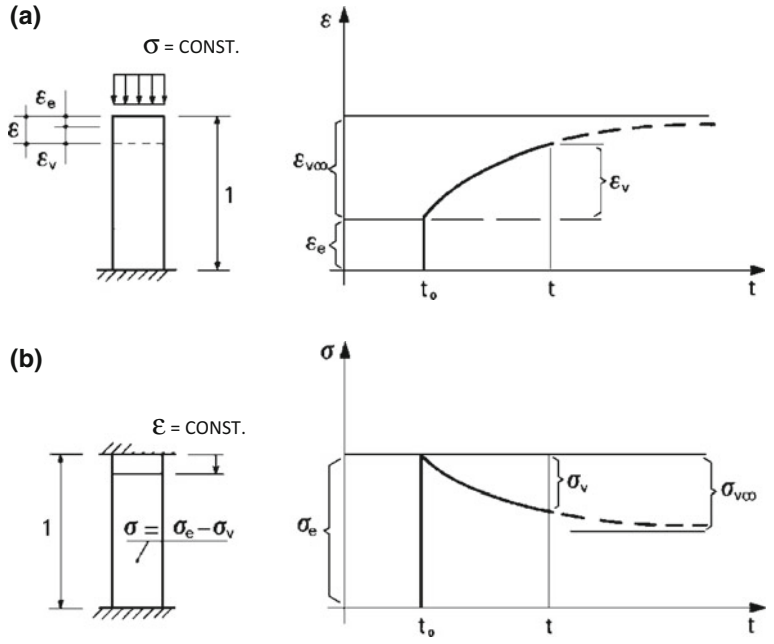


Fig. 1.16 Creep of concrete: creep (**a**) and relaxation (**b**)

In dual terms we have

$$\sigma(t,t_o) = \sigma_e(t_o) - \sigma_v(t,t_o) = \sigma_e(t_o)\left[1 - \frac{\sigma_v(t,t_o)}{\sigma_e(t_o)}\right] = E_o\,\varepsilon[1 - \rho(t,t_o)],$$

where the *relaxation coefficient* $\rho(t,\ t_o)$ expresses similarly the ratio between the relaxed part and the elastic part of stresses under the constant contraction ε.

Therefore, according to the linear theory, the viscoelastic behaviour of concrete is described by the *creep function*

$$v(t,t_o) = \frac{1}{E_o}[1 + \varphi(t,t_o)]$$

or by the relaxation function:

$$r(t,t_o) = E_o[1 - \rho(t,t_o)],$$

where the direct $\varepsilon = v\sigma$ and inverse $\sigma = r\varepsilon$ relationship is valid between stress and strain, the first one under the case of constant stresses, and the second under the case of constant strain.

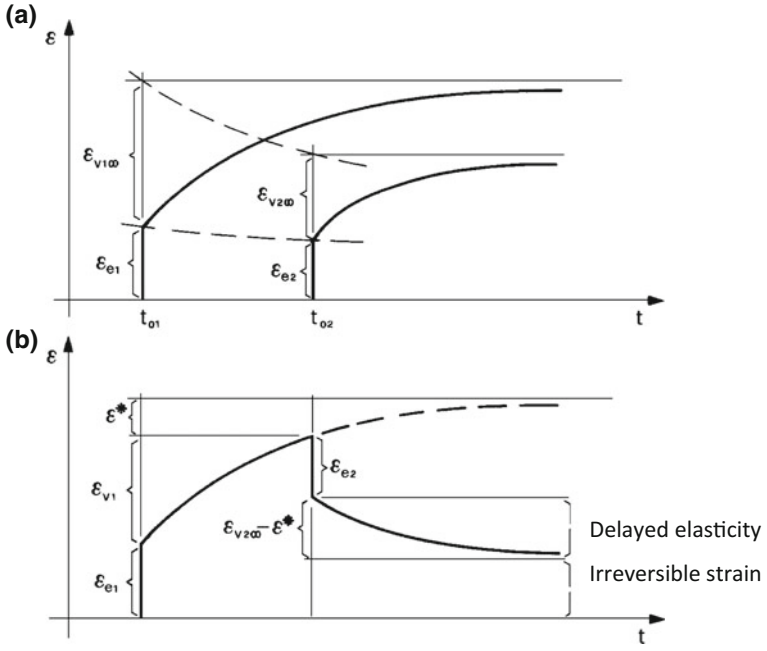


Fig. 1.17 Loading and unloading curves of concrete

The trend of those functions depends on the time t_o of loading application, which is the degree of maturity attained by the concrete. For example, two creep curves of the same concrete are represented in Fig. 1.17a when loaded starting from time t_{o1} or when loaded starting from time t_{o2}: both parameters ε_e and $\varepsilon_{v\infty}$, characteristic of the phenomenon, for the same imposed load, decrease until concrete has attained complete maturity. In the same way their ratio decreases with ageing

$$\varphi_\infty = \frac{\varepsilon_{v\infty}}{\varepsilon_e}.$$

Experiments eventually have indicated that, based on creep and relaxation functions, the *superposition principle* can be applied even for loads started at different times. In Fig. 1.17b for example the creep curve is plotted for a loading and unloading event, deduced for simple subtraction of curves in Fig. 1.17a. Two important aspects of the phenomenon can be noted: the *delayed elasticity*, as the strain that concrete slowly restores after unloading; the *irreversible strain* which represents the pure plastic part of the event. Experimental tests clearly give such results, where in particular for concretes loaded very early, the irreversible strain predominates over the delayed elasticity, for concretes loaded late the opposite is true.

1.2.2 Creep with Variable Stresses

The possibility of superposing effects assumed by the linear theory is used for the analysis of creep with variable stresses. A given loading history $\sigma = \sigma(t)$ can be applied to the concrete prism of Fig. 1.16a as represented in Fig. 1.18a. The contraction measured at time t is obtained superposing the effects of all loading increments $d\sigma$ to the effect of initial loading σ_o:

$$\varepsilon(t, t_o) = \sigma_o v(t, t_o) + \int_{t_0}^{t} \frac{d\sigma(\tau)}{d\tau} v(t, \tau) d\tau,$$

with $\sigma_o = \sigma(t_o)$. This relationship permits to evaluate the creep effects starting from a given loading history once the creep function is known; this can be done the resolution of an ordinary Riemann integral. Integrating per parts the same relationship one can obtain, in the case of E_c = const.,

$$\varepsilon(t, t_o) = \sigma_o v(t, t_o) + [\sigma(\tau) v(t, \tau)]_{t_o}^{t} - \int_{t_0}^{t} \sigma(\tau) \frac{\partial v(t, \tau)}{\partial \tau} d\tau$$

and being

$$v(t, t) = \frac{1}{E_c}.$$

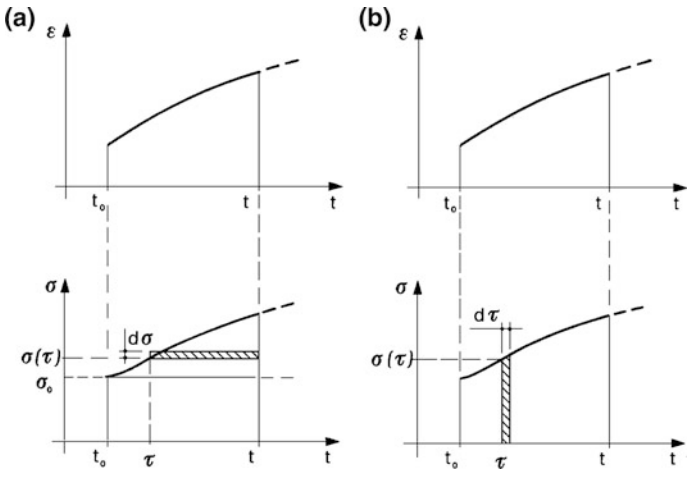


Fig. 1.18 Creep with variable stresses—superposition modes

The following relationship is obtained:

$$\varepsilon(t, t_o) = \frac{\sigma(t)}{E_c} + \int_{t_0}^{t} \frac{\sigma(\tau)}{E_c} \Phi(t, \tau) d\tau$$

with

$$\Phi(t, \tau) = -\frac{\partial \varphi(t, \tau)}{\partial \tau}$$

creep kernel of concrete. In this way the superposition is interpreted as summation of creep effects of many loading impulses $\sigma(\tau)d\tau$ (see Fig. 1.18b).

In dual terms, regarding relaxation one obtains

$$\sigma(t, t_o) = \varepsilon_o r(t, t_o) + \int_{t_0}^{t} \frac{d\varepsilon(\tau)}{d\tau} r(t, \tau) dt,$$

that is, for a modulus E_c = const.,

$$\sigma(t, t_o) = E_c \varepsilon(t) + \int_{t_0}^{t} E_c \varepsilon(\tau) \psi(t, \tau) d\tau$$

with

$$\psi(t, \tau) = -\frac{\partial \rho(t, \tau)}{\partial \tau}$$

relaxation kernel of concrete.

The choice of using creep relationships instead of relaxation relationships in the study of structural analysis problems depends on the adopted resolution method: compatibility equations based on balanced static unknowns (force method) or vice versa equilibrium equations based on compatibility geometrical unknown (displacement method).

Creep–Relaxation Relationship

Actually the necessary experimental data are available only for the creep function: applying a constant load in time and progressively measuring the deformations is relatively simple, whilst applying a constant deformation and progressively measuring forces is not so simple. The relaxation function can be deduced analytically, once the one for creep is known. One can think for example of expressing the constant unity strain state ε with both direct and dual relationships reported above. From the creep law for variable loading one has (with ε = 1)

$$1 = \sigma(t_o)v(t, t_o) + \int_{t_0}^{t} \frac{d\sigma(\tau)}{d\tau} v(t, \tau) d\tau.$$

From the relaxation law one has

$$\sigma(t, t_o) = r\,(t, t_o).$$

Substituting this in the previous relationship one obtains, being $r(t_o, t_o) = E_o$,

$$E_o v(t, t_o) + \int_{t_0}^{t} \frac{\partial r(\tau, t_o)}{\partial \tau} v(t, \tau) d\tau = 1.$$

This Volterra integral equation can be solved with appropriate numerical procedures.

1.2.3 Models of Linear Creep

For the study of the phenomenon of creep, models of theoretical mechanics have been initially applied. Starting from the basic ones consisting of Hooke's *spring* and Newton's *damper*, the former being transposed into the linear relationship between force and displacement, the latter into the linear relationship between force and velocity, the fundamental combinations have been used (the one *in series* by Maxwell and the one *in parallel* by Kelvin) in order to formulate composite schemes able to simulate the principal characteristics of the phenomenon. Hereditary models are for example quoted, derived from the scheme by Voigt or the one by Zerner (see Fig. 1.19a, b), which have the deformation law such as

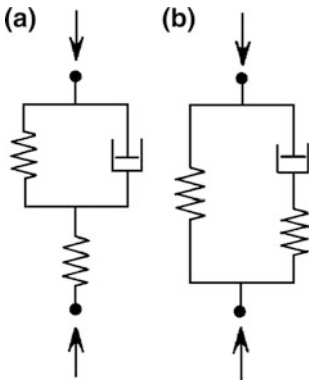


Fig. 1.19 Mechanical models for creep

$$\varepsilon(t, t_o) = \left\{ c_o + c_1 \left[1 - e^{-\beta(t-t_o)} \right] \right\},$$

where the constants c_o, c_1 and β depend on the characteristics of spring and damper.

The Extreme Theoretical Models

Mechanical models were not able to simulate certain important aspects of the phenomenon of creep, such as the ones related to ageing. Other theoretical models have been therefore formulated mathematically. Some, as the one by Dishinger presented hereafter, take into account the maturation of creep characteristics with the concrete ageing. Among these the two theoretical models that represent the extreme interpretations of the creep behaviour are further discussed.

A first model is deduced from the observation of how, for concrete at early stages, the trend of creep curves at a given instant, that is the speed of development, is significantly independent from the past duration of loading (see Fig. 1.20a). The slope of diagrams would therefore depend only on the time t of measurement and not on the time t_o of load application:

$$\frac{\partial \varphi(t, t_o)}{\partial t} = C(t).$$

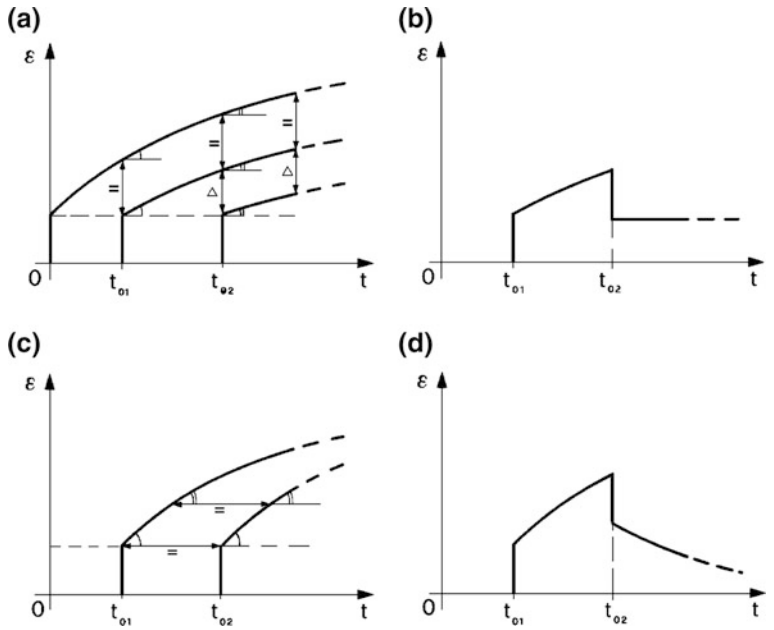


Fig. 1.20 Extreme theoretical models for creep

From this equation, integrating between t_o and t one obtains

$$\varphi(t, t_o) = c(t) - c(t_o).$$

In practice for $c(t)$, setting the origin of time at the minimum age at which the first loading of concrete is possible, an exponential law typical of exhaustion phenomena is assumed. Adding the elastic part, the creep function becomes

$$v(t, t_o) = \frac{1}{E_o}\left\{1 + \varphi_o\left[e^{-\beta t_o} - e^{-\beta t}\right]\right\},$$

where β is related to the fading speed of the phenomenon.

This model corresponds to the *extreme theory of ageing* by Dishinger–Whitney, according to which the final value φ_∞ of the creep coefficient decreases exponentially with the age of load application with respect to the one φ_o of the fist possible event:

$$\varphi_\infty = \varphi_o e^{-\beta t_o}.$$

It can also be noted how, applying the superposition principle for a loading and unloading event (see Fig. 1.20b), only the irreversible part of the strain remains after unloading. The Dishinger–Whitney model is therefore not able to represent the delayed elasticity.

A second model is deduced from the observation of how, for very aged concretes, the creep curves remain substantially the same for every successive event (see Fig. 1.20c). The deformation ε at time t of measurement would therefore depend only on the loading duration $t - t_o$ and the curves relative to events started and successive times would simply be translated along the x-axis, instead of along the y-axis as for the previous model. Assuming the usual exponential function and adding the elastic part one has

$$v(t, t_o) = \frac{1}{E_o}\left\{1 + \varphi_\infty\left[1 - e^{-\beta(t - t_o)}\right]\right\},$$

where the creep coefficient at infinite time remains the same for every successive loading event. This model corresponds to the *extreme hereditary theory* by Kelvin–Voigt. Applying the superposition principle for a loading and unloading event (see Fig. 1.19d), after unloading, one obtains the slow complete release of every strain. Kelvin–Voigt model is therefore capable of representing only the delayed elasticity and not the irreversible part of the residual strain.

Between the two extreme models, one of the *modified hereditary theories* can be proposed associating a coefficient $\varphi_\infty = \varphi_\infty(t_o)$ as a function of the loading time to the law expressed in terms of the duration $t - t_o$. It can be set, for example,

$$v(t,t_o)=\frac{1}{E_o}\left\{1+\varphi_o e^{-\alpha t_o}\left[1-e^{-\beta(t-t_o)}\right]\right\}.$$

According to such model, successive loading events have similar but reduced creep curves.

The interest of extreme or modified models, for the viscoelastic behaviour of concrete, lies in the simplicity of their analytical expression, which allows in several cases the formal integration of the solving equations of the studied problems. The approximations of related results are more or less technically acceptable, given also the incertitude related to the assumption on the correct values of the parameters E_c and φ_∞.

Empirical Models

Experimental results, as they became available, allowed to formulate *empirical models* capable of representing the various complex aspects of creep more accurately. It is to be noted that the relative experimentation is quite onerous. First of all it requires long durations, sometimes up to 30 years of loading. For a correct interpretation of results, it is necessary to adopt adequate measures in order to remove shrinkage deformation from the measurements and to distinguish different contributions. The study of the influence of ambient parameters for maturity and dimensional parameters for concrete shape presents relevant difficulties because of the number and the interdependence of the parameters themselves.

The one proposed by CEB–FIP MC 90 (see bull. CEB 213) can therefore be defined as a *modified hereditary model* since, with $\varphi_\infty = \varphi_\infty(t_o)$, a final amplitude decreasing with the concrete age at loading is associated to a hereditary function of growth in duration $g(t - t_o)$, as the ageing theory requires.

The creep law is therefore expressed with the coefficient

$$\varphi(t,t_o)=\varphi_\infty(t_o)\,g(t,t_o),$$

having in its two factors the main parameters that influence the phenomenon. The final value is further composed of three factors:

$$\varphi_\infty(t_o)=\beta_c\,\beta_{hs}\,\varphi_o,$$

where $\varphi_o = \varphi_o(t_o)$ is the *reference coefficient* which gives, as a function of the age t_o at loading, the values relative to a standard situation (strength f_c = 28 MPa, relative humidity RH = 80%, equivalent thickness $2A_c/u$ = 150 mm).

Defining also

$c = f_c/10$	index of concrete class (kN/cm^2)
$h = \mathrm{RH}/100$	relative humidity ratio
$s = (2A_c/u)/100$	index of equivalent thickness (dm)

the following formulas are given:

$$\beta_c = \frac{1.673}{\sqrt{c}} \qquad (= 1 \text{ for } c = 2.8)$$

$$\beta_{hs} = 0.725\left(1 + \frac{1-h}{0.46\sqrt[3]{s}}\right) \qquad (=1 \text{ for } h = 0.8 \text{ and } s = 1.5)$$

$$\varphi_o = \frac{4.37}{0.1 + t_o^{0.2}} \qquad (=\varphi_\infty \text{ for } \beta_c = \beta_{hs} = 1).$$

In Tables 1.12, 1.13 and 1.14, the numerical values of the above defined coefficients β_c, β_{hs} and φ_o are reported. In particular for the calculation of the reference coefficient φ_o a *nominal age* t_o of load application has to be assumed, correcting the *effective age* $\bar{t}_o$ based on the average temperature θ of concrete in the time frame. One therefore obtains

$$t_o = \beta_T \bar{t}_o \quad (\bar{t}_o = t_o \text{ for } \beta_T = 1)$$

for

$$\beta_T = e^{\left(13.65 - \frac{4000}{273+\theta}\right)} \quad (\beta_T = 1 \text{ for } \theta = 20\ ^\circ\text{C}).$$

This last formula (or the related Table 1.15) allows to take into account the effect of the accelerated maturation with a simple translation towards higher times of the loading age with which $\varphi_o = \varphi_o(t_o)$ is to be read.

The formulas reported above are given with fairly good reliability based on numerous experimental verifications that have been carried out (variance ≈ 0.20). Relevant incertitude remains in their application, related to the assumption at the design stage of the values of the parameters.

The calculations of creep effects are normally carried out in two extreme situations corresponding, respectively, to the initial stage with $\varphi = 0$ and the final stage with $\varphi = \varphi_\infty$. The first situation is analysed with elastic algorithms. The viscoelastic analysis in the final stage, or in the intermediate stages if required, requires the time function $g(t - t_o)$ on which the relative integrations are to be made. For such time law the available model is much less reliable than the others, especially at short terms.

The problem can be overcome if the approximations of a simplified analysis method are accepted, such as one of the effective moduli presented at the end of this paragraph. In this case it is not necessary to know the creep time law; the value of its final coefficient is sufficient.

The model proposed by CEB is anyway reported:

$$g(t - t_o) = \left[\frac{(t - t_o)}{\bar{t} + (t - t_o)}\right]^{0.3},$$

where the parameter

$$\bar{t} = 150\left[1 + (1.2\,h)^{18}\right]s + 250 \text{ (days)}$$

can be assumed equal to 500 for the most common environmental and structural situations.

Design Nominal Values

For application purposes, nominal estimations of the creep final coefficient can be assumed at the design stage, conventionally referred to some standard situations. Values of $\varphi_\infty(t_o)$ are reported hereafter for a nominal age of loading t_o = 14 Gg and for a relative humidity UR = 60%, considering three representative classes, respectively, of low, medium and high strength, combined with equivalent thickness values between small and medium.

	s = 1.0	s = 2.0	s = 3.0
C20/25	3.30	2.98	2.83
C35/43	2.66	2.41	2.28
C50/60	2.29	2.07	1.97

1.3 Structural Effects of Creep

The formulas previously shown refer to the local relationship between stress and strain. It is now analysed how the phenomenon of creep affects the behaviour of concrete sections and structures.

A first category of problems concerns sections and structures of *homogeneous material*. The linearity of the basic constitutive model is in this case extended from the point to sections and structures with integrations in which the creep function remains as a constant factor. Two fundamental results derive:

- in a homogeneous section or structure subject to *static actions* the stresses regime does not vary due to creep, whilst deformations have increments proportional to the creep coefficient; for example,

  $\chi(t, t_o) = \chi_e[1 + \varphi(t, t_o)]$ (see Fig. 1.21a)
  $u(t, t_o) = u_e[1 + \varphi(t, t_o)]$ (see Fig. 1.21b)

- in a homogeneous section or structure subject to *geometric actions* the deformation regime does not vary due to creep, whilst stresses have increments proportional to the relaxation coefficient; for example,

  $M(t, t_o) = M_e[1 - \rho(t, t_o)]$ (see Fig. 1.21c)
  $R(t, t_o) = R_e[1 - \rho(t, t_o)]$ (see Fig. 1.21d).

What mentioned above is valid as long as the structural behaviour remains within the first-order theory with irrelevant or negligible displacements relatively to the lying position of the forces.

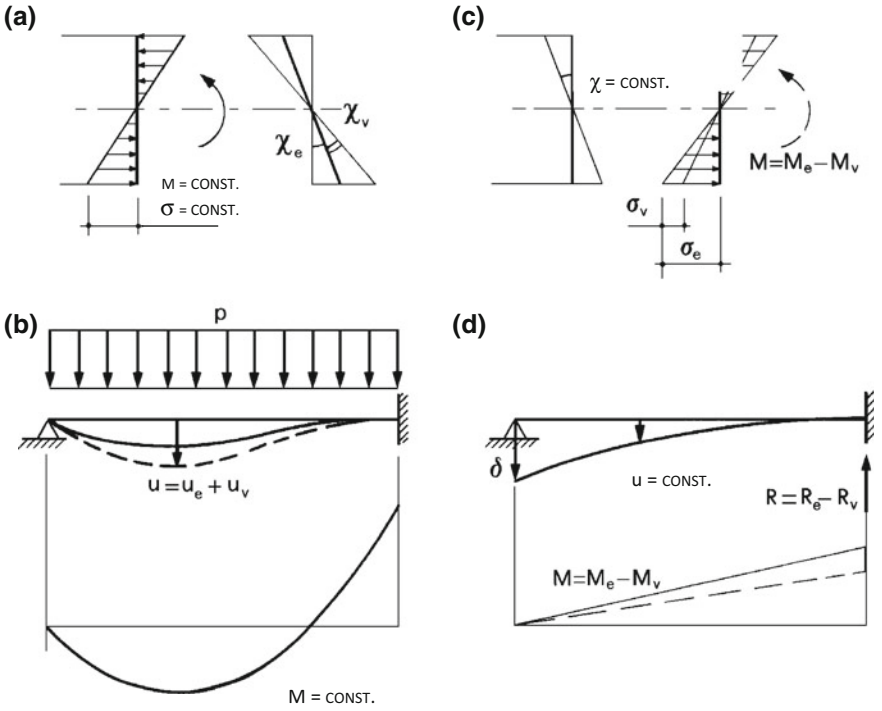


Fig. 1.21 Structural effects of creep

For *non-homogeneous* sections and structures, also remaining within a first-order behaviour, statically determined and undetermined cases have to be distinguished. In *statically determined cases* the static regime is not influenced by the deformation behaviour of the material, and therefore stresses do not change due to creep. Deformations have viscous increments locally proportional to the relative creep coefficients.

In *statically undetermined cases* on the contrary the non-homogeneity of the material causes the mutual influence of static and geometric regimes with respect to the effects of creep: both stresses and deformations, starting from the initial elastic configuration, have variations according to the global constitutive law of the structural problem.

The *second-order behaviour*, in which the stress regime is influenced by the displacements anyway, takes the problem again as for the statically undetermined cases, with the necessity of a global viscoelastic analysis for homogeneous and statically determined structures too. An important case of this category of problems is the instability of columns under combined compression and bending, discussed in Chap. 7.

1.3.1 Resolution of the Integral Equation

In order to show the computational aspects of the problem, one can first consider the algorithm that gives the response $\sigma = \sigma(\varepsilon)$ along the time, following a given deformation history $\varepsilon = \varepsilon(t)$, based on a known creep function $v(t, t_o)$. In order to obtain this, Volterra's integral equation is to be solved

$$\varepsilon(t) = \sigma_o v(t, t_o) + \int_{t_0}^{t} v(t, \tau) \mathrm{d}\sigma(\tau),$$

where $\sigma = \sigma(t)$ is the unknown function.

The solution is elaborated with an approximated numerical procedure which expresses the integral as a summation of finite contributions. The time interval $(t - t_o)$ is then subdivided in k increments (see Fig. 1.22), evaluating on one side the creep function for the chosen times:

$$v(t_k, t_i) \text{ with } i = 0, 1, \ldots, k,$$

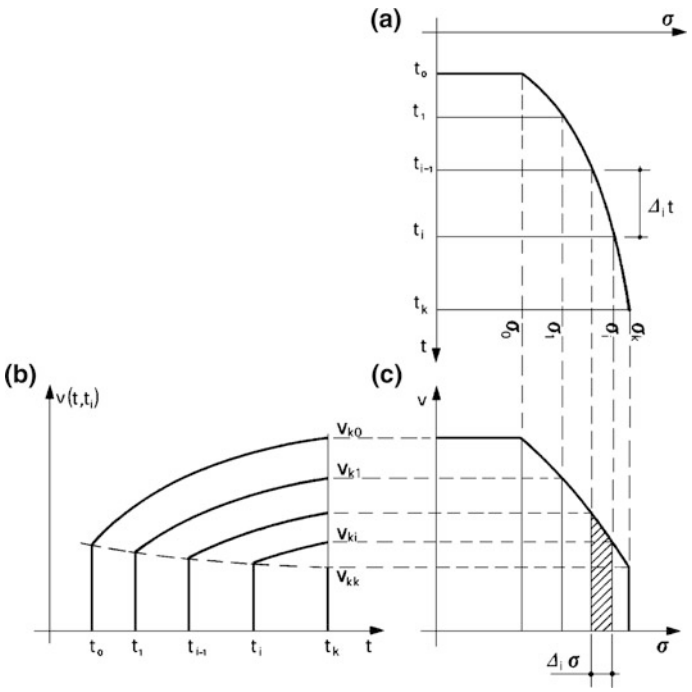


Fig. 1.22 Graphical representation of the numerical procedure

where t_k corresponds to the reading time t. Defining now through points, on the basis of a similar scansion of the curve $\sigma = \sigma(t)$, the function $v = v(\sigma)$ represented in Fig. 1.22c, the relevant equation, written for $t = t_k$, can be set as

$$\varepsilon_k \approx \sigma_o v(t_k, t_o) + \frac{1}{2}\sum_{i=1}^{k}[v(t_k, t_i) + v(t_k, t_{i-1})]\Delta_i\sigma$$

with $\varepsilon_k = \varepsilon(t_k)$ and having set

$$\Delta_i\sigma = \sigma_i - \sigma_{i-1}.$$

The area under the curve $v = v(\sigma)$ has therefore been expressed as summation of k trapezoids.

Such equation can be progressively re-written for increasing times and therefore with $k = 0, 1, 2, \ldots$. One will therefore have, with reference for example to the four intervals assumed in Fig. 1.22 and setting for brevity $v_{ki} = v(t_k, t_i)$,

$$\begin{aligned}
\varepsilon_0 &= v_{00}\sigma_0 \\
\varepsilon_1 &= v_{10}\sigma_0 + \frac{v_{11} + v_{10}}{2}\Delta_1\sigma \\
\varepsilon_2 &= v_{20}\sigma_0 + \frac{v_{21} + v_{20}}{2}\Delta_1\sigma + \frac{v_{22} + v_{21}}{2}\Delta_2\sigma \\
\varepsilon_3 &= v_{30}\sigma_0 + \frac{v_{31} + v_{30}}{2}\Delta_1\sigma + \frac{v_{32} + v_{31}}{2}\Delta_2\sigma + \frac{v_{33} + v_{32}}{2}\Delta_3\sigma \\
\varepsilon_4 &= v_{40}\sigma_0 + \frac{v_{41} + v_{40}}{2}\Delta_1\sigma + \frac{v_{42} + v_{41}}{2}\Delta_2\sigma + \frac{v_{43} + v_{42}}{2}\Delta_3\sigma + \frac{v_{44} + v_{43}}{2}\Delta_4\sigma.
\end{aligned}$$

All together the equations form an algebraic triangular linear system that can be solved with a simple forward substitution done in parallel to the generation of the coefficients. The unknowns σ_o, $\Delta_1\sigma$, $\Delta_2\sigma$, … are therefore progressively calculated and cumulated to give the response σ_1, σ_2, …, σ_i, …, σ_k.

In practice this procedure, automatically elaborated by electronic computation, is used to obtain the relaxation function setting $\varepsilon_o = \varepsilon_1 = \cdots = 1$ and extending it to infinite time. The accuracy of the elaborations depends on the time subdivision done in the integration interval. Optimum results are obtained with a constant subdivision in logarithmic scale:

$$\log(t_i) - \log(t_{i-1}) = \log a,$$

and assuming $a = 1.15$ and $\Delta_1 t = t_1 - t_o = 0.05$ days. This is proposed the C.E.B. Model Code that further suggests to extend the integration interval up to 10,000 days (≈30 years). Beyond such limit creep contributions are negligible.

1.3.2 General Method

In a statically undetermined non-homogeneous problem, where both functions $\sigma(t)$ and $\varepsilon(t)$ are unknown, the integral equation relative to the viscoelastic behaviour of the material has to be supplemented by the law that expresses the structural behaviour.

Let us consider the simple example of a reinforced concrete column subjected to an axial force N constant in time. Let A_c and A_s be the cross-sectional areas of concrete and reinforcement and let E_c and E_s be the elastic moduli of the two materials. Stated first the deformation compatibility with $\varepsilon_c = \varepsilon_s = \varepsilon$, the initial balanced elastic solution is obtained immediately from

$$\varepsilon_o = \frac{N}{E_c A_c (1 + \alpha_e \rho_s)}; \quad \sigma_{co} = E_c \varepsilon_o,$$

with $\rho_s = A_s/A_c$ and $\alpha_e = E_s/E_c$ (see point 2.1.1).

Following on, the migration of stresses from concrete to reinforcement steel has to fulfil the equilibrium relationship:

$$A_c \mathrm{d}\sigma_c + A_s \, \mathrm{d}\sigma_s = 0,$$

from which one obtains, being $\mathrm{d}\sigma_s = E_s \mathrm{d}\varepsilon$, the differential equation

$$\frac{\mathrm{d}\sigma_c}{\mathrm{d}\varepsilon} = -\rho_s E_s,$$

that, in the problem under consideration, supplements the Volterra's integral equation.

Transposing the equilibrium equation to finite differences, one has

$$\Delta_i \varepsilon = -\frac{\Delta_i \sigma_c}{\rho_s E_s},$$

and the procedure of numerical integration has to be modified as follows:

$$\begin{aligned}
&\Delta_1 \sigma_c = \frac{2(\varepsilon_1 - \nu_{10}\sigma_{co})}{\nu_{11} + \nu_{10}} && \varepsilon_1 = \varepsilon_0 \\
&\Delta_1 \varepsilon = -\frac{\Delta_1 \sigma_c}{\rho_s E_s} && \varepsilon_2 = \varepsilon_1 + \Delta_1 \varepsilon \\
&\Delta_2 \sigma_c = \frac{2(\varepsilon_2 - \nu_{20}\sigma_{co}) - (\nu_{21} + \nu_{20})\Delta_1 \sigma_c}{\nu_{22} + \nu_{21}} && \\
&\Delta_2 \varepsilon = -\frac{\Delta_2 \sigma_c}{\rho_s E_s} && \varepsilon_3 = \varepsilon_2 + \Delta_2 \varepsilon \\
&\Delta_3 \sigma_c = \ldots . &&
\end{aligned}$$

This corresponds to evaluate, in every single time interval $\Delta_i t$, the creep effects of relaxation as if they were due to a contraction ε_i of constant value and to elastically compensate at time t_i the consequent disequilibrium of stresses in the section with the additional contraction $\Delta_i \varepsilon$.

In the example presented, given that stresses σ_c are constant in the section and along the axis of the column, structural equilibrium can be imposed with one simple formula. But in general the equilibrium is expressed with integrals extended to the section and the structure. Consequent discretized numerical procedures, in addition to one of time integrations, lead to very onerous elaborations. From this onerousness comes the benefit of simplifying calculation, with respect to the general method presented above, with the approximated procedures reported below.

1.3.3 Algebraic Methods

Algebraic methods aim at the substitution of the integral in time, contemplated in the constitutive equation of viscoelasticity, with an algebraic equation, to avoid the discretized numerical procedure which follows step by step the history of the phenomenon. According to such methods, the actual continuous history of stress increments $\Delta\sigma(\tau) = \sigma(\tau) - \sigma_o$ following the first instantaneous load application can be substituted, in order to evaluate the creep effects at time t, with only one instantaneous increment $\Delta\sigma(t) = \sigma(t) - \sigma_o$ (see Fig. 1.23) applied from a given time t_1 conveniently chosen in an intermediate position between t_o and t:

$$\varepsilon(t, t_o) \approx \sigma_o v(t, t_o) + \Delta\sigma(t)\, v(t, t_1).$$

The Ageing Coefficient Method

A first method that gives very accurate results is the one called AAEMM (age-adjusted effective modulus method) or *ageing coefficient method*. According to this method it is set as

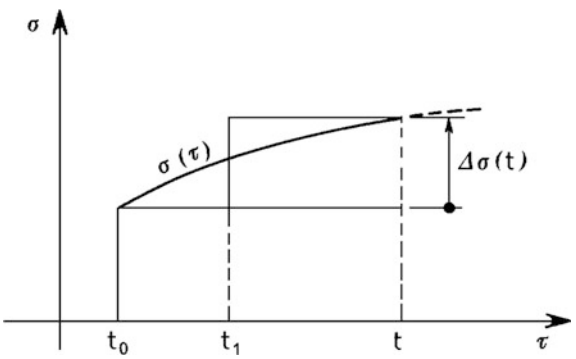


Fig. 1.23 Approximate representation of stress history

$$v(t,t_1) = \frac{1}{E_o}[1 + \chi(t,t_o)\,\varphi(t,t_o)],$$

where the function $\chi(t,\ t_o)$ is called ageing coefficient and is obtained from

$$\chi(t,t_o) = \frac{E_o}{E_o - r(t,t_o)} - \frac{1}{\varphi(t,t_o)}.$$

The evaluation of the relaxation function is therefore required. Practical applications, which are generally limited to the analysis of the final response for $t = \infty$, can rely on appropriate tables of $r(t,\ t_o)$. The solution is obtained elaborating first an instantaneous analysis of the structure at time t_o, evaluating the stresses relaxation at constant deformation with integrations on sections and structure with

$$\Delta\sigma(t) = \frac{\varepsilon_o - \sigma_o v(t,t_o)}{v(t,t_1)}$$

and eventually redistributing the resulting unbalanced forces with a further incremental analysis.

The necessary double-structural analysis and the integrations in between bring still too onerous computations. For this reason the ageing coefficient method, profitably used in simple analyses of single section, is not normally used in the analysis of complex frames.

The Effective Modulus Method

For a quicker analysis of frames, the bigger approximations of the method called EMM (effective modulus method) have to be accepted, which let time t_1 coincide with the instant t_o, as if the total stress $\sigma(t) = \sigma_o + \Delta\sigma(t)$ was applied with only one initial load step ($t_1 = t_o$):

$$\varepsilon(t) = \sigma(t)\,v(t,t_o).$$

This implies only one instantaneous analysis of the structure where the elastic modulus of concrete has been simply adjusted with

$$E^*(t) = \frac{E_o}{1 + \varphi(t,t_o)}.$$

Adopting this effective modulus the effects of creep are underestimated. The results have non-uniform approximations: bigger in configurations where creep effects highly influence the regime of redundancies, more limited in the opposite case. For statically determined cases or homogeneous configurations under static loads, even the effective modulus method gives exact results.

Eventually, in the case of successive iteration of permanent and instantaneous loads, a standard solution can be given to the problem, still in an approximated way.

For this more rigorous methods contemplate to follow the loading history, adding an instantaneous incremental analysis under accidental loads, to be cumulated to the previous viscoelastic response under permanent loads. The standard procedure on the contrary is limited to one only instantaneous analysis carried out with the weighted effective modulus:

$$E^*(t) = \frac{E_o}{1 + c\varphi(t, t_o)},$$

where c depends on the ratio between permanent loads and total loads. Acceptable results on an application level are obtained assuming for c the square of this ratio.

Technical Method
With an approximation that overestimates creep effects, certain technical solutions assume $t_1 = t$, evaluating the relaxation with

$$\Delta\sigma(t) = -\sigma_o\varphi(t, t_o),$$

that is, on the basis on a constant stress equal to the initial one. In this way for example the tension losses due to creep in pre-stressing cables are evaluated (see Sect. 10.1.3).

To conclude it is to be noted that, as it can be deduced from linear analyses of serviceability states and nonlinear analyses taken to the failure limit, in the domain of second-order behaviour with displacements that are no more negligible, creep plays a determining role with respect to the resistance of the structure. This is for example the case of the already mentioned instability of slender columns under combined compression and bending actions.

1.4 Behaviour of Reinforced Concrete Sections

The properties of *reinforced concrete*, which is of the composite material made of concrete with a reinforcement of steel bars conglobated within its mass, definitely deviate from those of the ideal isotropic, homogeneous, and perfectly elastic material assumed in the classic theory of the de Saint-Vénant's solid developed in *Structural mechanics*. The *homogeneity* is not valid because of the presence of two materials whose characteristics are significantly different, being steel much more rigid and resistant than concrete. The *isotropy* is not valid since the effectiveness of reinforcing bars mainly depends on their orientation. Also *elasticity* has to be intended according to particular criteria, even within limits of small internal forces with respect to the strength of the composite material, because of the non-symmetric behaviour of concrete in compression and tension. *Creep* eventually, discussed in the previous paragraphs, induces other significant alterations along the time on deformations and stresses.

So the behaviour of reinforced concrete is influenced by the properties of the two materials of which it is made of, beside the *bond* relationship that combines them. The quantity and layout of the *reinforcement* with respect to the element overall configuration also have an influence. These reinforcement bars have the main purpose of compensating the limited tensile strength of concrete, but they also have other important consequences such as reducing its *brittleness* in compression.

One particular aspect of reinforced concrete is *cracking*. It is in fact accepted that, even under common structural serviceability situations, concrete can crack as its tensile strength is exceeded in certain zones. The presence of reinforcing bars guarantees anyway the resistance.

This entails the other important aspect of *durability* which for reinforced concrete does not only involve chemical and technological problems (for example, protective painting of steel structures), but also and especially problems of pure structural design, such as the ones related to the evaluation of crack width and to the relative verifications to guarantee adequate protection of the steel reinforcement.

Cracking also forces to modify significantly the *design models* themselves. In several cases reinforced concrete elements are not considered as continuous and homogeneous solids any more (such as de Saint-Vénant's beam), but as complex frameworks made of concrete blocks and reinforcement bars, combined in different ways in the structural behaviour.

1.4.1 Mechanical Characteristics of Reinforcement

In normal reinforced concrete, steel products in *bars* or in *wires* are used as reinforcement; the former are provided in bundles of straight rods, usually of 12 m length and possibly bent in half to facilitate transportation; the latter are usually supplied wrapped in coils for considerable length.

Hot-rolled bars and wires can be left without further processing; their *natural hardness* steel is characterized by σ–ε diagrams similar to the one represented in Fig. 1.24a. These diagrams, deduced from tensile tests on pieces of bars or wires, exhibit

- linear elastic behaviour up to the yield limit f_y;
- elastic modulus E_s equal to, for all types of steel, 205,000 MPa;
- subsequent perfectly plastic behaviour with horizontal trend;
- restart, after a relevant elongation, of the increase of stresses due to the hardening of the material;
- attainment of the maximum resistance capacity f_t for considerable values of ultimate strain (uniform under maximum load) ε_u;
- decrease of the curve after the maximum loading due to necking of the specimen;
- considerably ductile rupture at a strain ε_t even greater;
- ductility parameters ε_u, ε_t generally smaller for steel higher strengths.

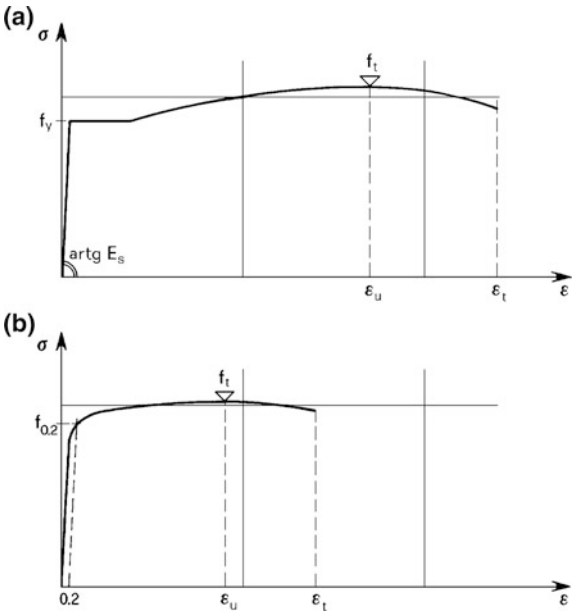


Fig. 1.24 Stress–strain curves of reinforcing steel

The behaviour in compression results substantially symmetric, apart from the stages near rupture.

The classification made with reference to the *mechanical characteristics* of steel is based on the following parameters:

f_t tensile strength
f_y yield stress
f_t/f_y hardening ratio
ε_u ultimate strain (under maximum loading).

Bars and wires for RC can also be produced by cold drawing. In this case the relative curves σ–ε do not show the horizontal plastic phase any more. Even the ultimate strain is reduced significantly. As a clear yield limit is not measurable experimentally, the value of $f_{0.2}$ is assumed as reference stress for strength calculations, equal to the stress corresponding to the residual elongation of 0.2% after unloading (see Fig. 1.24b).

With reference to the ultimate strain of the material, three *ductility classes* are distinguished:

- low ductility 'A'
  with $\varepsilon_{uk} \geq 2.5\%$ $(f_t/f_y)_k \geq 1.05$
- normal ductility 'B'
  with $\varepsilon_{uk} \geq 5.0\%$ $(f_t/f_y)_k \geq 1.08$
- high ductility 'C'
  with $\varepsilon_{uk} \geq 7.5\%$ $(f_t/f_y)_k \geq 1.15$.

For the calculations of *fatigue strength* the characteristic value of the limit range $\Delta\bar{\sigma}$ is to be provided, which leads to brittle rupture after 2×10^6 loading cycles. Such limit is measured experimentally applying to the specimen a tension force varying cyclically from a maximum of $\sigma_{max} = 0.6f_{vk}$ to a minimum $\sigma_{min} = \sigma_{max} - \Delta\bar{\sigma}$.

Technological characteristics of reinforcement basically consist of the degree of bond allowed by the surface finish of the product, of its bendability and weldability of the material itself.

About *bond* three types of finishes are distinguished:

- smooth 'E' with low bond
- indented 'I' with small teeth
- ribbed 'R' with improved bond.

In practice, apart from particular uses, only *ribbed bars* are used in reinforced concrete structures.

Bendability is assessed with a bending test to guarantee the possibility of shaping the bar without evident damage.

Welding can be used to connect the bars, without the risk of embrittlement of the material or decay of its mechanical characteristics, only for steel of proven *weldability*.

In reinforced pre-stressed concrete, high-strength hardened steel is used, such as *cold-deformed bars* (e.g. twisted) and *cold-drawn wires*. Thermally treated products are also used such as *tempered wires*, obtained with rapid cooling. The elative σ–ε diagrams are shown in Fig. 1.25. The classification done with respect to the mechanical characteristics of steel is based on the following parameters:

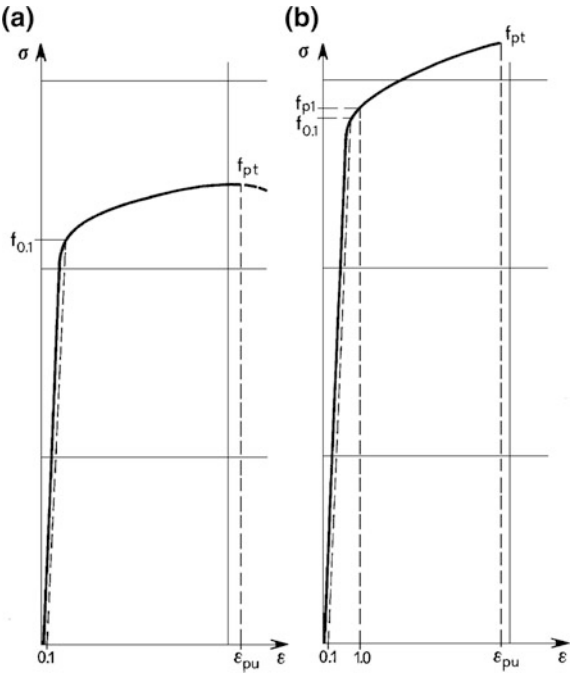


Fig. 1.25 Stress–strain curves of pre-stressing steel

f_{pt} tensile strength
$f_{0.1}$ stress at 0.1% residual elongation at unloading for wires
$f_{0.1}/f_{pt}$ hardening (inverse) ratio
$\varepsilon_{pt} \approx \varepsilon_{pu}$ ultimate rupture strain,

where sometimes in catalogues for strands $f_{0.1}$ is substituted by f_{p1} at 1% of elongation under loading. For that category of products, which is quite homogeneous, the two values are not much different.

High-strength hardened steel has always low ductility, with $\varepsilon_{uk} \geq 3.5\%$, $(f_{0.1}/f_{pt})_k \geq 0.8$ and it is not weldable. Among the technological properties of these products for P.C. *relaxation* and *susceptibility to stress corrosion* are also mentioned. Further discussion will be presented in Chap. 10.

It is recalled that steel density is equal to 7850 kg/m^3; its coefficient of thermal expansion is 1.0×10^{-5} °C^{-1}, close to one of the concretes. Thanks to the fact that these coefficients are very similar for steel and concrete, no self-induced stresses developed in the composite material.

Products for reinforced concrete reinforcement are as follows:

- bars
- wires
- welded mesh
- lattice girders.

The last two are obtained from the wire, by electric welding carried out in factory and delivered in plane panels the *welded mesh* and in straight truss beams the *lattice girders*. No further information is given about lattice girders, which use the same reinforcement as the welded mesh: for them one can refer to the catalogues for commercial shapes and sizes.

Among the many different products for RC available in the different countries, one can refer to those made of the following three types of steel named B450A, B450B and B450C, respectively, with low, medium and high ductility. They are produced in diameters from 6 to 40 mm. The nominal characteristic value of yield strength, expressed in MPa, is indicated after the symbol *B*. All these types of steel (see Fig. 1.26) are weldable and bendable.

Tendons for P.C. consist of

- bars
- wires
- strands.

In particular, stands can be obtained by combining 2 or 3 wires of small diameter (2.4 ÷ 3.5 mm) twisted around themselves, or 7 wires of even bigger diameter ($\leq$ 6 mm), with a straight central wire and six peripheral wires wrapped around it in spiral. The equivalent elastic modulus, deduced from tensile tests on pieces of strands, is a little lower than one of the single wires ($E_p \approx 195{,}000$ MPa) because of the geometrical effect of their straightening under loading.

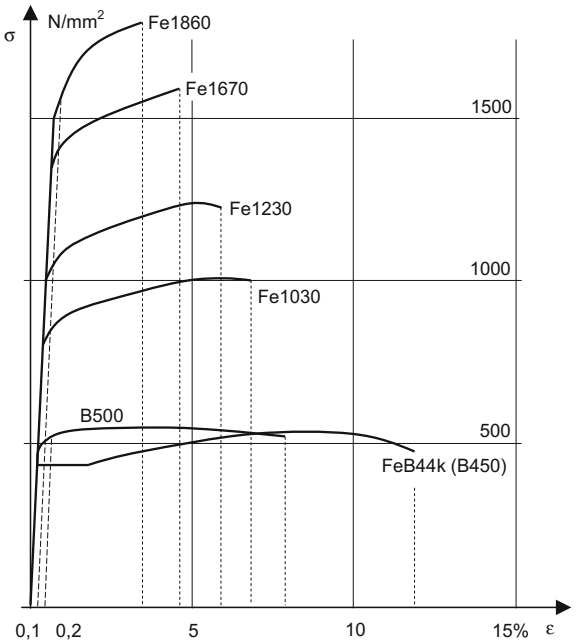


Fig. 1.26 Synoptic representation of different stress–strain curves

Among the great variety of available products for pre-stressing reinforcement only the most commonly used types are listed below (see Fig. 1.26):

- bars Fe1030 and Fe1230 in diameters from 20 to 50 mm;
- wire Fe1570, Fe1670, Fe1770, Fe1860 in diameters from 4 to 10 mm;
- strands 3W Fe1860, Fe1960, Fe2060 in diameters from 5.2 to 7.5 mm;
- strands 7W Fe1770, Fe1820, Fe1860 in diameters from 7.0 to 18.0 mm.

The type of steel is named with the symbol Fe followed by the characteristic tensile strength expressed in MPa. The class 1, 2 or 3 of relaxation of the product also has to be specified, according to what presented in Chap. 10. A *compacted* type of 7-wire strands exists and it is indicated with the letter 'C', made with trapezoidal wires instead of round, which do not leave voids inside the strand. The different strands are distinguished with the symbols 3 and 7W that indicate the number of elementary wires.

The European classification contemplates the following:

- Smooth 'E' or ribbed 'R' bars
  steel type Fe 1030 and Fe 1230
  with diameters between 20 and 50 mm
- Smooth 'E' or indented 'I' wires
  steel type Fe 1570, Fe 1670, Fe 1770 and Fe 1860
  with diameters between 4 and 10 mm
- Strands '3W' (3-wires)

steel type Fe 1860, Fe 1960 and Fe 2060
with nominal diameters between 5.2 and 7.5 mm
- Strands '7W' (7-wires)
steel type Fe 1770, Fe 1860 and Fe 2060
with nominal diameters between 7.0 and 18.0 mm
- Strands '7WC' (7-wires compacted)
steel type Fe 1770, Fe 1820 and Fe 1860
with nominal diameters between 12.7 and 18.0 mm.

The data relative to the type of products for R.C and P.C. mentioned above are reported in Tables 1.7, 1.8, 1.9, 1.10, 1.11, 1.12, 1.13, 1.14, 1.15, 1.16, 1.17, 1.18, 1.19, 1.20, 1.21.

It is to be noted that the quality of steel of the current industrial production is with good approximation constant and reliable, with a relative dispersion of representative values much smaller than what can be expected for concrete.

1.4.2 Basic Assumptions for Resistance Calculation

In reformulating the description of the behaviour of a structural beam element in reinforced concrete, the following assumptions are made. Reference is made to the current part of the beam, outside the end zones and the ones influenced by concentrated loads, with forces due to self-weight and applied surface pressures small with respect to the internal stress state. In this part the cross-sectional behaviour is basically independent from the specific load pattern and it depends only on the force resultant on the cross section itself.

As assumed in the problem of de Saint-Venant's solid, the first assumption, well verified in experimental results up to situations close to failure, is one of the *plane sections* (by Bernoulli): under the effect of applied forces, the sections displace and rotate remaining plane. Strain ε at a distance y from the beam axis, measured orthogonally to the neutral axis nn of no strain, is therefore given by (see Fig. 1.27)

$$\varepsilon = \varepsilon_o + \chi y,$$

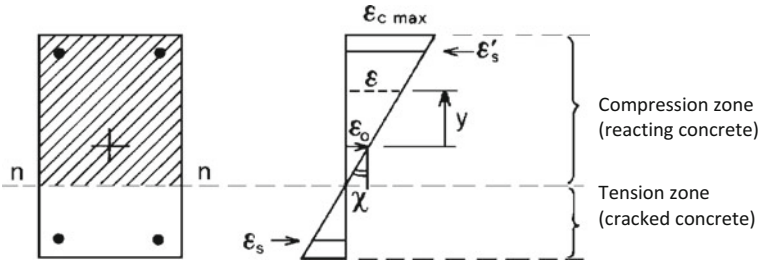


Fig. 1.27 Deformation model of RC section

where ε_o is the strain at the beam axis taken as reference ('design axis') and χ is a constant that represents the curvature of the beam at the considered section.

The second assumption concerns the *perfect bond* between concrete and reinforcement steel, basically verified as long as appropriate design rules are followed in reinforcement detailing. For the longitudinal rebars crossing the section of Fig. 1.27, this assumption leads to the equality

$$\varepsilon_s = \varepsilon_c,$$

between expansions (or contractions) of the two materials at their contact points.

The third assumption refers to both serviceability and strength calculations and leads to neglect completely the small tensile strength f_{ct} of concrete. This is equivalent to assume in the σ–ε diagram of this material:

$$E_{ct} \equiv 0.$$

A consequence is the so-called *partialization of the cross section* (see again Fig. 1.27), which is assumed to be cracked in the tension part of concrete. In opposition to the acting force, the *effective section* remains to resist, reduced in general with respect to the entire *geometrical section*, and consisting of the entire area of compression and tension rebars, and the only compression part of concrete. In the calculations of deformation and cracking, this assumption will have to be opportunely integrated.

The fourth assumption eventually refers to the behaviour of materials and it is expressed by the appropriate models that represent the *constitutive relationships* σ–ε. Two areas of application have to be distinguished: elastic analysis under moderate loads and nonlinear analysis as for ultimate limit states.

In the elastic analysis of cross sections, the elastic relationships represented by *Hooke's law* are assumed:

$$\sigma_c = E_c\varepsilon_c \quad \sigma_s = E_c\varepsilon_s;$$

the first one, relative to concrete, is only valid in compression. For the same strain $\varepsilon_c = \varepsilon_s = \varepsilon$ one has

$$\sigma_s = E_s\varepsilon = (E_s/E_c)\sigma_c = \alpha_e\sigma_c,$$

which means that, in the elastic range, steel is stressed α_e times more than the concrete around it, with α_e is equal to the ratio between the elastic moduli of the two materials.

In the nonlinear analysis of cross sections, appropriate analytical models suitable for numerical applications have to be defined to represent the real relationships σ–ε of the materials.

σ–ε Models for Concrete

The Saenz's model has already been discussed for concrete, which reproduces quite well the behaviour in compression under loads of small duration (see Fig. 1.4). For strength verifications such model could be used referring it to the design strength reduced by the partial safety factor $\gamma_C = 1.5$ of concrete

$$f_{cd} = f_{ck}/\gamma_C.$$

This strength value is to be further reduced to take into account the fraction of long-term loads.

Given that, in strength design of cross sections, magnitude and position of the resultant of compressions in concrete are to be calculated, it is possible to simplify the model with the assumption of simplified diagrams. It is sufficient to reproduce with good approximation the area and the centre of the surface covered by the diagram, without caring about the exact local slope of the curve. The three diagrams of Fig. 1.28 have been defined with these criteria: they represent the most widely used models.

The first model is the *parabola–rectangle* shown in Fig. 1.28a. The second one is the *triangle–rectangle* shown in Fig. 1.28b. The most simple is represented by the *stress block* shown in Fig. 1.28c. The values $\varepsilon_{c2} = 0.20\%$, $\alpha_{c3} = 0.15\%$, $\varepsilon_{c4} = 0.07\%$ and $\varepsilon_{cu} = 0.35\%$ are conventionally assumed for the three models, as a mean of the ones of the different strength classes up to C50/60. For the application of the semi-probabilistic limit state method, the *long-term design strength* is assumed equal to

$$f_{cd} = \alpha_{cc}\frac{f_{ck}}{\gamma_C} = \alpha_{cc}\frac{0.83\,R_{ck}}{\gamma_C},$$

where, starting from the characteristic value of the cubic strength experimentally determined, the value of the characteristic prismatic strength is obtained with the already mentioned correlation formula and from this value to the design value is obtained with the pertinent coefficient γ_C.

An appropriate cut of the short-term strengths is eventually applied, based on the duration features of the loading combination examined. In the case of permanent loads only, it can be assumed $\alpha_{cc} = 0.80$ (see Fig. 1.2). If the combination includes short-term loads, one can assume $\alpha_{cc} = 1.00$. Strictly speaking, the verifications

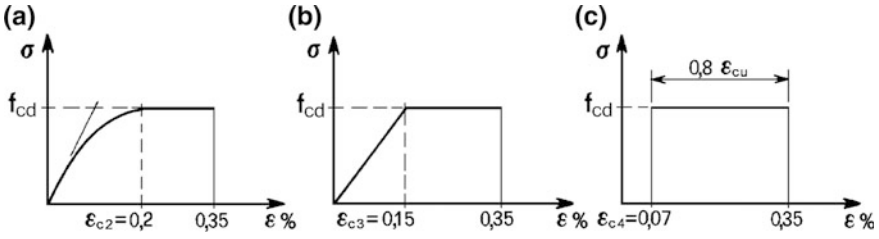


Fig. 1.28 Simplified σ–ε models for concrete in compression

under the two load combinations mentioned above should be repeated. Some regulations allow to take the average value $\alpha_{cc} = 0.85$ for a unique verification under a global loading combinations.

The extension of the models presented above the higher strength classes requires the adoption of modified values for the parameters ε_{c2}, ε_{c3}, ε_{c4} and ε_{cu} for which one can refer to Chart 1.22.

σ–ε Models for Steel

For steel, the *bilinear model* of Fig. 1.29 reproduces with good accuracy the behaviour of the material, straightening the plastic-hardening part after the yield point.

The analytical expression of the model is set with

$$\begin{aligned} \sigma &= E_o \varepsilon && \text{for } \varepsilon \leq \varepsilon_y \\ \sigma &= f_y + E_1 (\varepsilon - \varepsilon_y) && \text{for } \varepsilon > \varepsilon_y \end{aligned}$$

with

$$E_o = \frac{f_y}{\varepsilon_y} \quad E_1 = \frac{f_t - f_y}{\varepsilon_u - \varepsilon_y}.$$

For strength calculations of cross sections this *finite bilinear model with hardening* is used setting in the previous expressions (see Fig. 1.30a—model A):

$$\begin{aligned} f_y &= f_{yd} = \frac{f_{yk}}{\gamma_S} && \text{with } \gamma_S = 1.15 \\ f_t &= f_{td} = k f_{yd} && \text{with } k = 1.2 \\ \varepsilon_y &= \varepsilon_{yd} = \frac{f_{yd}}{E_s} \\ \varepsilon_u &= \varepsilon_{uk} \end{aligned}$$

and cutting it off at the limit

$$\varepsilon_{ud} = 0.9\, \varepsilon_{uk},$$

where one has

$$f'_{td} = f_y + E_1 (\varepsilon_{ud} - \varepsilon_y).$$

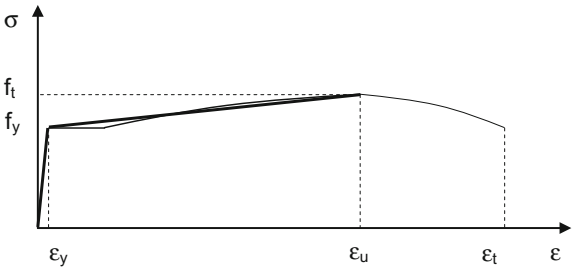


Fig. 1.29 Bilinear model for reinforcing steel

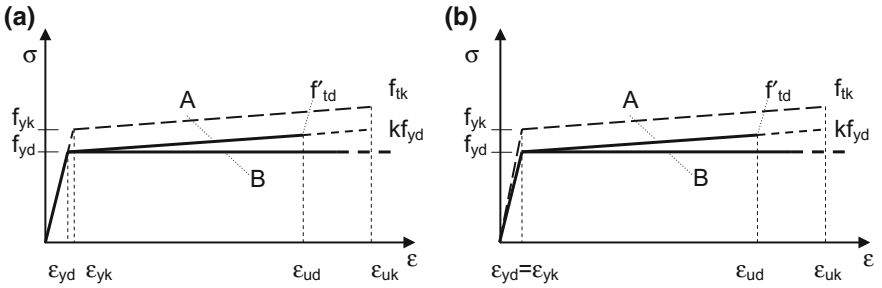


Fig. 1.30 Reinforcing steel σ–ε models for strength calculations

With a conservative approximation that leads to a simplification of the calculations, the *indefinite elastic–perfectly plastic* model can be adopted, setting $E_1 = 0$ and removing any limit to strains ε (see Fig. 1.30a—model B).

The alternative models of Fig. 1.30b are proposed by certain authors who see the elastic modulus E_s as a resisting characteristic of the material to be reduced with the pertinent coefficient γ_S ($E_{sd} = E_s/\gamma_S$). This model therefore sets the discontinuity of the bilinear curve in

$$\varepsilon_y = \varepsilon_{yk} = \frac{f_{yk}}{E_s}.$$

For pre-stressing steel a bilinear model can still be assumed as shown in Fig. 1.31, where the yield strength f_{py} (or $f_{p0.2}$) of the bars is substituted by the stresses $f_{p0.1}$ or f_{p1}, respectively, for wires and strands.

For strength calculations of cross sections, in the bilinear model relationships it is therefore set (v. Fig. 1.32a—model A):

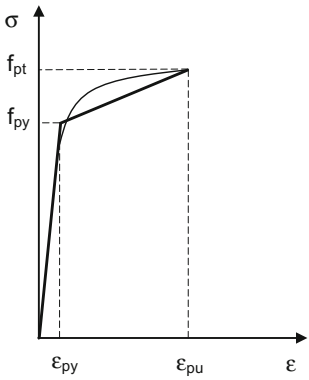


Fig. 1.31 Bilinear model for pre-stressing steel

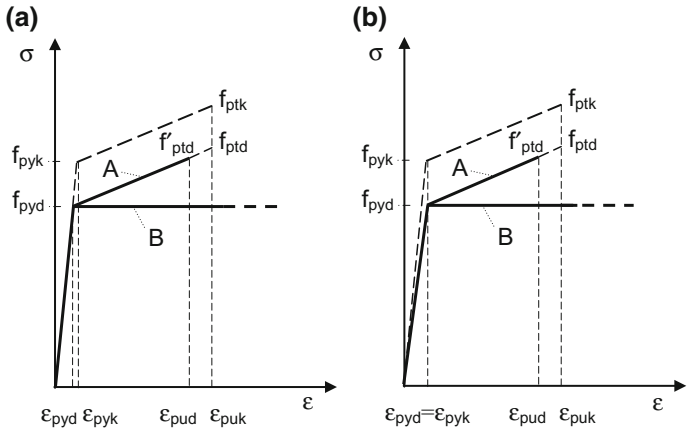


Fig. 1.32 Pre-stressing steel σ–ε models for strength calculations

$$\begin{aligned} f_t &= f_{ptd} = f_{ptk}/\gamma_S \qquad \text{con } \gamma_S = 1.15 \\ f_y &= f_{pyd} = \kappa f_{ptk} \qquad \text{con } \kappa = \left(f_{py}/f_{pt}\right)_k \\ \varepsilon_y &= \varepsilon_{pyd} = f_{pyd}/E_p \\ \varepsilon_u &= \varepsilon_{puk} \end{aligned}$$

and the model itself is cut off at the limit

$$\varepsilon_{pud} = 0.9\,\varepsilon_{puk},$$

where

$$f'_{ptd} = f_{pyd} + E_1\left(\varepsilon_{pud} - \varepsilon_{pyd}\right).$$

If more accurate values are not available, it can be conservatively assumed $\kappa = 0.9$ and $\varepsilon_{pdu} = 0.02$.

With a conservative approximation the model can be simplified setting $E_1 = 0$ and removing any limit to strains ε (see Fig. 1.32a—model B). Even for pre-stressing reinforcement the alternative model exists that penalizes the elastic modulus with $E_{pd} = E_p/\gamma_S$ (see Fig. 1.32) and that sets the discontinuity of the bilinear curve in

$$\varepsilon_{yk} = \varepsilon_{pyk} = \frac{f_{pyk}}{E_p}.$$

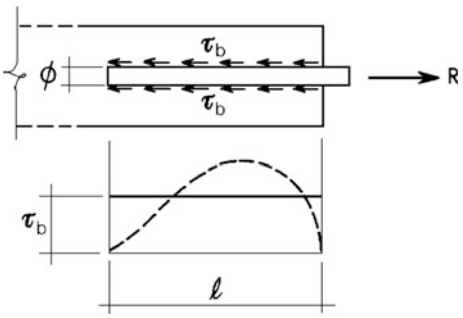


Fig. 1.33 Bond stresses on a steel bar

1.4.3 Steel–Concrete Bond

The union between steel and concrete in reinforced concrete elements is ensured with the proper anchorage of bars at their ends, as well as with the bond that develops along their entire length and that ensures the transfer of shear stresses between the two materials in each cross section. First of all, one can consider the basic example of pull-out of a steel bar of cross section A_s from a concrete block in which it is embedded for a length l (see Fig. 1.33). Bond stresses distributed on the contact surfaces oppose the force R which tends to cause slippage. Such stresses vary along the anchorage length with a certain profile but, in order to understand the global behaviour, a simplified constant value τ_b is here assumed. With this assumption, the equilibrium of the bar is therefore given by

$$R = \sigma_s A_s = \tau_b \, u \, 1,$$

with σ_s stress on its external section and u its bonding perimeter.

The failure of the system can either occur with the yielding of the steel or by slippage of the bar. Since both these possibilities would equally lead to failure, it can be assumed that, for an appropriate design of the structure, the possibility of slippage would not occur before yielding

$$\tau_{br} \, \pi \, \phi \, 1_o \geq f_y \, \phi^2 \frac{\pi}{4}.$$

having indicated the ultimate limit value of bond stress with τ_{br}. At the limit, putting the equality sign one therefore obtains

$$1_o = \frac{\phi f_y}{4 \, \tau_{br}},$$

which represents the *minimum anchorage length* according to the principle described above.

To ensure the full contribution of the steel reinforcement in a given section of reinforced concrete, before that cross section the steel has to be anchored in the concrete for a length equal to at least a given multiple of its diameter. Taking into account different values of partial safety factors, with $\gamma_C/\gamma_S = 1.5/1.15 \cong 1.3$, for a ribbed steel bar, with $f_v/\tau_{br} \cong 400/4.5 = 90$, one has

$$1_o \cong 90 \times 1.3/4 \cong 30\,\phi.$$

Such value is approximately valid for a proper coupling of the qualities of the two materials, for which higher steel strength shall be associated with a higher bond capacity. And this, as it will be shown later on, depends upon both the nature of the contact surface and the tensile strength of concrete.

The presence of hooks at the ends of the bars gives a different anchorage mechanism (see Fig. 1.34) and reduces the minimum required length l_o. Given the developed length of the hook needed for bending the bar itself, such reduction is significant for a smooth bar, little for a ribbed one. For the latter, a straight end of equal length is equally effective.

Types of Bond

Bond between steel and concrete is due to several phenomena of a different nature. The first one is *molecular chemical adhesion* that ensures a union without slippage, but that is limited to small strength values. There is then the *geometrical penetration* due to the roughness of the contact surfaces (see Fig. 1.35a). When forces increase effective contacts activate in a non-uniform way, thanks to small slippages that lead the surface irregularities to push one against the other. In order to enhance this phenomenon, actual interlocks can be obtained with *appropriate ribs* protruding from the reinforcing bars (see Fig. 1.35b).

Friction contributions due to possible *transverse compressions* (see Fig. 1.35c) can affect bond. These compressions occur to a small extent because of the concrete shrinkage. More significant is the self-anchoring phenomenon of pre-tensioned strands in pre-stressed concrete that, when released, tend to shorten exhibiting at the same time a transverse expansion. Furthermore, in certain zones direct actions can be applied, such as the flux of compressions that goes through the beams of a multi-storey frame at the columns location. There is eventually the contribution of

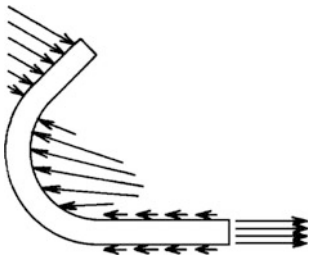


Fig. 1.34 End anchorage mechanism of a bar

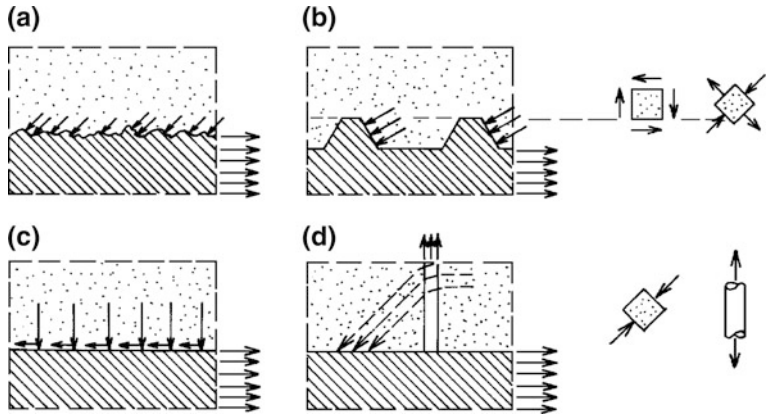


Fig. 1.35 Types of bond of steel bars

transverse confinement which also has the properties of friction and is provided by transverse reinforcement or hoops with a truss behaviour (see Fig. 1.35d).

In the two main bonding mechanisms described in Fig. 1.35a, b, the bar pull-out occurs with pure tension failure of the surrounding concrete. One can therefore set

$$1_{\mathrm{b}} = \frac{\phi f_{\mathrm{y}}}{4\,\beta_{\mathrm{b}} f_{\mathrm{ct}}} = \frac{\phi f_{\mathrm{y}}}{4 f_{\mathrm{b}}},$$

where $f_{\mathrm{b}} = \beta_{\mathrm{b}} f_{\mathrm{ct}}$ is the *equivalent strength* of bond and where β_{b} is the *effective contact ratio*. The values of this ratio for smooth bars are largely lower than 1, because of the limited extent of the effective contact zones with respect to the total surface. The ribs of the deformed bars increase the size of the concrete sleeve geometrically interlocked to the steel and this increases the equivalent bond strength.

Transverse compressions extend the effective contacts and at the same time they reduce, for the same longitudinal shear force, the principal tensile stress in concrete, increasing its resistance. Greater values of the ratio β_{b} are therefore observed, even greater than 1 for ribbed bars.

The *confinement* provided by transverse reinforcement leads to a different bond mechanism, establishing a resisting truss that, leaving the tensions to the steel reinforcement, stresses the concrete mainly with an inclined flux of compressions. When the transverse reinforcement is adequately proportioned and diffused, this leads to a much higher resistance, not related anymore to the pure tensile strength of concrete.

Several appropriate measures should be adopted in the detailing of reinforcement to ensure bond: First of all, an adequate *limitation of bars diameters* to avoid excessive anchorage lengths. As mentioned before, a *consistent combination of*

materials qualities also has to be ensured. One also has to take into account the negative effect of cracking, which causes detachments and damages of the surface of effective contact. It is preferable to *anchor the bars in compression zones* whenever possible. The proximity of reinforcing bars to the external concrete surface also reduces the bond strength, because of the reduced or null effectiveness of the surface layer. Therefore, bars normally have to be anchored *bending their ends inwards* or with appropriate shapes. It is eventually to be noted how the rebar lapping, that is their junction by simple superimposition, implies the transfer of stress flow through concrete. Such stresses are therefore to be accurately verified and appropriate *staggered laps* are required, not to concentrate the disturbance causing the possible excessive weakening of the concerned section.

The values of *equivalent bond strength* f_b required for the design are deduced from specific tests. The easiest one is the *pull-out test*, which consists of measuring the force required to extract the reinforcing bar from a cubic concrete specimen as shown in the scheme of Fig. 1.36a. More significant results, as they are more similar to the actual structural situations, are obtained from the *beam test* where the pull-out force is measured indirectly through the bending action of a beam as shown on the scheme in Fig. 1.36b.

From the tensile bond tests, with the appropriate measurement of the slippage δ, diagrams similar to the one described in Fig. 1.37 can be obtained. They are characterized by:

- stage OA without significant slippage up to the failure of the chemical adhesion;
- stage AB with progressive activation, thanks to initial slips, of the effective contacts and initiation of microcracking at the concrete interlocks;
- stage BC with progressive failure of the concrete interlocks up to failure limit of bond;
- stage CD measurable only with tests under displacement control, decreasing up to complete detachment of the steel bar.

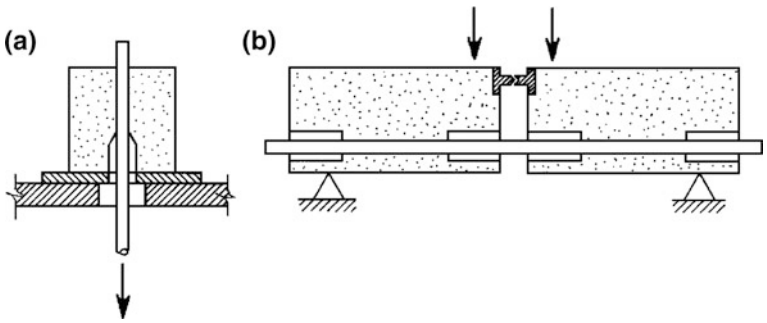


Fig. 1.36 Pull-out (**a**) and beam (**b**) tests for bond measurement

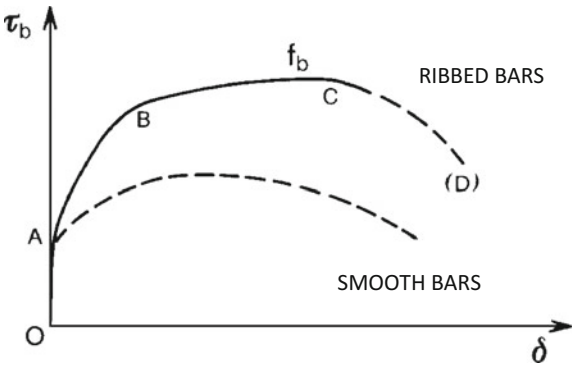


Fig. 1.37 Bond–slip experimental diagrams

For ribbed reinforcing bars the obtained values, expressed as a function of the characteristic strength of concrete, are given by

$$f_{bk} = 2.25 f_{ctk},$$

valid for diameters $\phi \leq 32$ mm. The design strength value is finally obtained from $f_{bd} = f_{bk}/\gamma_C$.

Appendix: Characteristics of Materials

Table 1.1: Hardening Curves of Concrete

The following table shows the values of the ratios f_{cj}/f_c between the strength at time t from casting and the strength at 28 days, where values deduced from the following formula:

$$\frac{f_{cj}}{f_c} = e^{\beta(1-1/\sqrt{\tau})},$$

and the values of the analogous ratio E_{cj}/E_c between elastic moduli, values deduced from the following formula:

$$\frac{E_{cj}}{E_c} = \left[e^{\beta(1-1/\sqrt{\tau})}\right]^{0.3} \quad \text{with } \tau = t/28,$$

where t is expressed in days (t = 0.58 corresponds to about 14 h of ageing, time of possible demoulding of precast elements).

Age	Strengths				Moduli			
	Accelerated curing (indicative values)	Concrete			Accelerated curing (indicative values)	Concrete		
		Fast setting	Normal setting	Slow setting		Fast setting	Normal setting	Slow setting
Days	β = 0.08	β = 0.20	β = 0.25	β = 0.38	β = 0.08	β = 0.20	β = 0.25	β = 0.38
0.58	0.62	0.30	0.23	0.10	0.87	0.70	0.64	0.51
1	0.71	0.42	0.34	0.20	0.90	0.77	0.72	0.61
2	0.80	0.58	0.50	0.35	0.94	0.85	0.81	0.73
3	0.85	0.66	0.60	0.46	0.95	0.88	0.86	0.79
4	0.88	0.72	0.66	0.54	0.96	0.91	0.88	0.83
5	0.90	0.76	0.71	0.59	0.97	0.92	0.90	0.86
6	0.91	0.79	0.75	0.64	0.97	0.93	0.92	0.88
7	0.92	0.82	0.78	0.68	0.98	0.94	0.93	0.89
10	0.95	0.87	0.85	0.77	0.98	0.96	0.95	0.93
14	0.97	0.92	0.90	0.85	0.99	0.98	0.97	0.95
21	0.99	0.97	0.96	0.94	1.00	0.99	0.99	0.98
28	1.00	1.00	1.00	1.00	1.00	1.00	1.00	1.00
60	1.03	1.07	1.08	1.13	1.01	1.02	1.02	1.04
90	1.04	1.09	1.12	1.18	1.01	1.03	1.03	1.05
180	1.05	1.13	1.16	1.26	1.01	1.04	1.05	1.07
365	1.06	1.16	1.20	1.32	1.02	1.04	1.06	1.09
∞	1.08	1.22	1.28	1.46	1.02	1.06	1.08	1.12

Table 1.2: Strength Classes of Concrete

The following tables show the strength and deformation parameters for different codified classes of concrete, of ordinary and controlled classes. Classes are characterized by characteristic values of cylinder and cubic strengths. Cylinder strength f_c, cubic strength R_c, tensile strength f_{ct} and elastic modulus E_c are reported in the consecutive columns, indicating the mean values with subscript m and the characteristic values with subscript k. Data are expressed in MPa and are calculated with the following formulas:

$$\begin{aligned} &R_{cm} = f_{cm}/0.83 \\ &f_{ctm} = 0.27\sqrt[3]{f_m^2} && \text{for } f_{cm} \le 58 \\ &f_{ctm} = 2.12\ \ln[1 + (f_{cm}/10)] && \text{for } f_{cm} > 58 \\ &E_{cm} = 22{,}000[f_{cm}/10]^{0.3} && \left(E^*_{cm} = E_{cm}/1000\right). \end{aligned}$$

In design previsions it is assumed $f_{cm} = f_k + \Delta f$, with $\Delta f = 8$ MPa for ordinary production (common construction sites) and with $\Delta f = 5$ MPa for controlled production (prefabrication plants). For the two types of production, it is assumed respectively $f_{ctk} = 0.7 f_{ctm}$ and $f_{ctk} = 0.8 f_{ctm}$.

Table 1.2a

Class	Ordinary production—$\Delta f = 8$ MPa						
	Class	f_{ck}	f_{cm}	R_{cm}	f_{ctm}	f_{ctk}	E^*_{cm}
Low	C16/20	16	24	29	2.2	1.6	29
	C20/25	20	28	34	2.5	1.7	30
	C25/30	25	33	40	2.8	1.9	31
Medium	C30/37	30	38	46	3.1	2.1	33
	C35/43	35	43	52	3.3	2.3	34
	C40/50	40	48	58	3.6	2.5	35
	C45/55	45	53	64	3.8	2.7	36

Table 1.2b

Class	Controlled production—$\Delta f = 5$ MPa						
	Class	f_{ck}	f_{cm}	R_{cm}	f_{ctm}	f_{ctk}	E^*_{cm}
Medium	C30/37	30	35	42	2.9	2.3	32
	C35/43	35	40	48	3.2	2.5	33
	C40/50	40	45	54	3.4	2.7	35
	C45/55	45	50	60	3.7	2.9	36
High	C50/60	50	55	66	3.9	3.1	37
	C55/67	55	60	72	4.1	3.3	38
	C60/75	60	65	78	4.3	3.4	39
	C70/85	70	75	90	4.5	3.6	40

Table 1.3: Deformation Parameters of Concretes

The following table shows the values of the main mechanical characteristics of concrete calculated as a function of the compressive strength with the formulas specified below:

$$
\begin{aligned}
&E_c = 22000[f_c/10]^{0.3} && \left(E_c^* = E_c/1000\right)\\
&\kappa = 1.05\,E_c\varepsilon_{c1}/f_c\\
&\varepsilon_{c1} = 0.7f_c^{0.31} \times 10^{-3} \le 2.8 \times 10^{-3} && \left(\varepsilon_{c1}^* = 1000\varepsilon_{c1}\right)\\
&\varepsilon_{cu} = \left\{2.8 + 27[(98 - f_c)/100]^4\right\}10^{-3} \le 3.5 \times 10^{-3} && \left(\varepsilon_{cu}^* = 1000\varepsilon_{cu}\right)\\
&f_{ct} = 0.27\sqrt[3]{f_c^2} && \text{for } f_c \le 58\\
&f_{ct} = 2.12\,\ln[1 + (f_c/10)] && \text{for } f_c > 58\\
&\alpha_t = f_{ct}/f_c\\
&\kappa_t = 1.05\,E_c\varepsilon_{ct1}/f_{ct} && (\varepsilon_{ct1} = 0.00015).
\end{aligned}
$$

Such values are to be used in the constitutive models σ–ε of concrete in compression and tension, respectively, expressed in the following form:

$$
\begin{aligned}
&\sigma = \frac{\kappa\eta - \eta^2}{1 + (\kappa - 2)\eta} f_c && (\eta = \varepsilon/\varepsilon_{c1})\\
&\sigma = \left[\kappa_t\eta_t - (2\kappa_t - 3)\eta_t^2 + (\kappa_t - 2)\eta_t^3\right]\alpha_t f_c && (\eta_t = \varepsilon/\varepsilon_{ct1}).
\end{aligned}
$$

Stresses and elastic moduli are expressed in MPa.

The other deformation characteristics are

- Poisson's raio $\nu = 0.20$
- coefficient of thermal expansion $\alpha_T = 1.0 \times 10^{-5}\,{}^\circ\mathrm{C}^{-1}$.

f_c	E_c^*	κ	ε_{c1}^*	ε_{cu}^*	f_{ct}	α_t	κ_t
24	28.6	2.35	1.90	3.50	2.25	0.094	2.01
28	30.0	2.21	2.00	3.50	2.49	0.089	1.90
33	31.5	2.07	2.10	3.50	2.78	0.084	1.78
38	32.8	1.96	2.20	3.50	3.05	0.080	1.69
43	34.1	1.87	2.20	3.50	3.31	0.077	1.62
48	35.2	1.79	2.30	3.50	3.57	0.074	1.56
53	36.3	1.72	2.40	3.50	3.81	0.072	1.50
35	32.0	2.03	2.10	3.50	2.89	0.083	1.75
40	33.3	1.92	2.20	3.50	3.16	0.079	1.66
45	34.5	1.84	2.30	3.50	3.42	0.076	1.59
50	35.7	1.76	2.40	3.50	3.66	0.073	1.53

(continued)

(continued)

f_c	E_c^*	κ	ε_{c1}^*	ε_{cu}^*	f_{ct}	α_t	κ_t
55	36.7	1.70	2.40	3.50	3.90	0.071	1.48
60	37.7	1.64	2.50	3.36	4.13	0.069	1.44
65	38.6	1.59	2.60	3.12	4.27	0.066	1.42
75	40.3	1.50	2.70	2.88	4.54	0.060	1.40

Table 1.4: Drying Shrinkage of Concrete

Drying shrinkage is given by

$$\varepsilon_{cd}(t') = \varepsilon_{cd\infty} g_s(t'),$$

where t' is time expressed in days and measured starting from the onset of the phenomenon.

The following tables show the final value of the drying shrinkage $\varepsilon_{cd\infty}$ for different relative humidities h of the ageing environment, for different strength classes c of concrete and for different equivalent thicknesses s. Values are deduced from the following formula:

$$\varepsilon_{cd\infty} = k_s \varepsilon_{cdo},$$

with

$$\begin{aligned} &k_s = 0.7 + 0.0094(5 - s)^{2.5} && \text{for } s < 5 \\ &k_s = 0.7 && \text{for } s < 5 \\ &\varepsilon_{do} = 870(1 - h^3)e^{-0.12c} \times 10^{-6}, \end{aligned}$$

where

$h = \mathrm{RH}/100$ relative humidity ratio;
$c = f_{cm}/10$ mean strength in $\mathrm{kN/cm^2}$;
$s = \frac{2A_c/u}{100}$ equivalent thickness in dm;

(A_c = cross-sectional area in $\mathrm{mm^2}$; u = perimeter of the section in mm).

The ones reported in the tables are mean values, for concrete of class N and for water/cement ratio ≤ 0.55, with coefficient of variation of about 0.30. For higher water/cement ratios, shrinkage is greater. For underwater ageing $\varepsilon_{cd\infty} = 0.00$ can be assumed.

Table 1.4a: Values of $\varepsilon^*_{cd\infty} = 1000 \cdot \varepsilon_{cd\infty}$ for RH = 50%

Class	f_{cm} (MPa)	Equivalent thicknesses in mm				
		50	100	150	300	≥ 500
C16/20	24	0.63	0.57	0.52	0.43	0.40
C20/25	28	0.60	0.54	0.50	0.41	0.38
C25/30	33	0.57	0.51	0.47	0.39	0.36
C30/37	38	0.53	0.48	0.44	0.36	0.34
C35/43	43	0.50	0.45	0.42	0.34	0.32
C40/50	48	0.47	0.43	0.39	0.32	0.30
C45/55	53	0.44	0.40	0.37	0.30	0.28
C30/37	35	0.55	0.50	0.46	0.38	0.35
C35/43	40	0.52	0.47	0.43	0.35	0.33
C40/50	45	0.49	0.44	0.41	0.33	0.31
C45/55	50	0.46	0.42	0.38	0.31	0.29
C50/60	55	0.43	0.39	0.36	0.30	0.28
C55/67	60	0.41	0.37	0.34	0.28	0.26
C60/75	65	0.39	0.35	0.32	0.26	0.24
C70/85	75	0.34	0.31	0.28	0.23	0.22

Table 1.4b: Values of $\varepsilon^*_{cd\infty} = 1000 \cdot \varepsilon_{cd\infty}$ for RH = 60%

Class	f_{cm} (MPa)	Equivalent thicknesses in mm				
		50	100	150	300	≥ 500
C16/20	24	0.56	0.51	0.47	0.39	0.36
C20/25	28	0.54	0.49	0.45	0.37	0.34
C25/30	33	0.51	0.46	0.42	0.35	0.32
C30/37	38	0.48	0.43	0.40	0.33	0.30
C35/43	43	0.45	0.41	0.37	0.31	0.28
C40/50	48	0.42	0.38	0.35	0.29	0.27
C45/55	53	0.40	0.36	0.33	0.27	0.25
C30/37	35	0.49	0.45	0.41	0.34	0.31
C35/43	40	0.47	0.42	0.39	0.32	0.30
C40/50	45	0.44	0.40	0.36	0.30	0.28
C45/55	50	0.41	0.37	0.34	0.28	0.26
C50/60	55	0.39	0.35	0.32	0.27	0.25
C55/67	60	0.37	0.33	0.30	0.25	0.23
C60/75	65	0.35	0.31	0.29	0.24	0.22
C70/85	75	0.31	0.28	0.25	0.21	0.19

Table 1.4c: Values of $\varepsilon^*_{cd\infty} = 1000 \cdot \varepsilon_{cd\infty}$ for RH = 70%

Class	f_{cm} (MPa)	Equivalent thicknesses in mm				
		50	100	150	300	≥ 500
C16/20	24	0.47	0.43	0.39	0.32	0.30
C20/25	28	0.45	0.41	0.37	0.31	0.29
C25/30	33	0.42	0.38	0.35	0.29	0.27
C30/37	38	0.40	0.36	0.33	0.27	0.25
C35/43	43	0.38	0.34	0.31	0.26	0.24
C40/50	48	0.35	0.32	0.29	0.24	0.22
C45/55	53	0.33	0.30	0.28	0.23	0.21
C30/37	35	0.41	0.38	0.34	0.28	0.26
C35/43	40	0.39	0.35	0.32	0.27	0.25
C40/50	45	0.37	0.33	0.30	0.25	0.23
C45/55	50	0.35	0.31	0.29	0.24	0.22
C50/60	55	0.33	0.30	0.27	0.22	0.21
C55/67	60	0.31	0.28	0.25	0.21	0.19
C60/75	65	0.29	0.26	0.24	0.20	0.18
C70/85	75	0.26	0.23	0.21	0.18	0.16

Table 1.4d: Values of $\varepsilon^*_{cd\infty} = 1000 \cdot \varepsilon_{cd\infty}$ for RH = 80%

Class	f_{cm} (MPa)	Equivalent thicknesses in mm				
		50	100	150	300	≥ 500
C16/20	24	0.35	0.32	0.29	0.24	0.22
C20/25	28	0.33	0.30	0.28	0.23	0.21
C25/30	33	0.32	0.29	0.26	0.22	0.20
C30/37	38	0.30	0.27	0.25	0.20	0.19
C35/43	43	0.28	0.25	0.23	0.19	0.18
C40/50	48	0.26	0.24	0.22	0.18	0.17
C45/55	53	0.25	0.22	0.21	0.17	0.16
C30/37	35	0.31	0.28	0.26	0.21	0.20
C35/43	40	0.29	0.26	0.24	0.20	0.18
C40/50	45	0.27	0.25	0.23	0.19	0.17
C45/55	50	0.26	0.23	0.21	0.18	0.16
C50/60	55	0.24	0.22	0.20	0.17	0.15
C55/67	60	0.23	0.21	0.19	0.16	0.14
C60/75	65	0.21	0.19	0.18	0.15	0.14
C70/85	75	0.19	0.17	0.16	0.13	0.12

Table 1.5: Drying Shrinkage Curves of Concrete

The following table shows the values of the function $g_s(t')$ which expresses the time law of drying shrinkage for different values of the equivalent thickness $2A_c/u$ (A_c = cross-sectional area of concrete; u = its perimeter).

Age	$2A_c/u$ (mm)				
	Small thickness	Medium–small	Medium thickness	Medium–large	Large thickness
Days	50	100	150	300	600
0.58	0.00	0.00	0.00	0.00	0.00
1	0.23	0.10	0.05	0.02	0.01
2	0.50	0.26	0.16	0.06	0.02
3	0.63	0.38	0.25	0.10	0.04
4	0.71	0.46	0.32	0.14	0.05
5	0.76	0.52	0.38	0.18	0.07
6	0.79	0.58	0.42	0.21	0.08
7	0.82	0.62	0.47	0.24	0.10
10	0.87	0.70	0.56	0.31	0.14
14	0.90	0.77	0.65	0.39	0.19
21	0.94	0.84	0.74	0.50	0.26
28	0.95	0.87	0.79	0.57	0.32
60	0.98	0.94	0.89	0.74	0.50
90	0.98	0.96	0.92	0.81	0.60
180	0.99	0.98	0.96	0.90	0.75
365	1.00	0.99	0.98	0.95	0.86
∞	1.00	1.00	1.00	1.00	1.00

The onset of the phenomenon is assumed at 14 h from casting ($t' = t - 0.58$). The values are calculated with the following formula:

$$g_s = \frac{t'}{t' + 4\sqrt{s^3}} \quad \text{with } s = \frac{2A_c/u}{100}.$$

For the calculation of shrinkage at time t it can be set as

$$\varepsilon_{cd} = \varepsilon_{cd\infty}\, g_s,$$

where $\varepsilon_{cd\infty}$ is deduced from Table 1.4.

Table 1.6: Autogenous Shrinkage of Concrete

Autogenous shrinkage is given by

$$\varepsilon_{ca}(t) = \varepsilon_{ca\infty}\, g_a(t),$$

where t is the concrete age expressed in days.

The following table shows the final value of autogenous shrinkage $\varepsilon_{ca\infty}$ for different mean strengths f_{cm} of concrete. The values are deduced from the following formula:

$$\varepsilon_{ca\infty} = 2.5(f_{cm} - 18) \cdot 10^{-6}$$

(in table $\varepsilon^*_{ca\infty} = 1000\varepsilon_{ca\infty}$).

Ordinary Class	f_{cm} (MPa)	$\varepsilon^*_{ca\infty}$
C16/20	24	0.02
C20/25	28	0.03
C25/30	33	0.04
C30/37	38	0.05
C35/43	43	0.06
C40/50	48	0.08
C45/55	53	0.09

Controlled Class	f_{cm} (MPa)	$\varepsilon^*_{ca\infty}$
C30/37	35	0.04
C35/43	40	0.06
C40/50	45	0.07
C45/55	50	0.08
C50/60	55	0.09
C55/67	60	0.11
C60/75	65	0.12
C70/85	75	0.14

Table 1.7: Autogenous Shrinkage Curves of Concrete

The following table shows the value of the function $g_a(t)$ that expresses the time law of autogenous shrinkage. The values are calculated with the following formula:

$$g_a = 1 - e^{-0.2\sqrt{t}},$$

where t is the concrete age expressed in days starting from casting.

Age	g_a
0.58	0.14
1	0.18
2	0.25
3	0.29
4	0.33
5	0.36
6	0.39
7	0.41
10	0.47
14	0.53
21	0.60
28	0.65
60	0.79
90	0.85
180	0.93
365	0.98
∞	1.00

Chart 1.8: Concrete Shrinkage and Nominal Values

Concrete shrinkage is given by

$$\varepsilon_{cs\infty} = \varepsilon_{cd} + \varepsilon_{ca},$$

where

ε_{cd} is the component of drying shrinkage (Tables 1.4 and 1.5)
ε_{ca} is the component of autogenous shrinkage (Tables 1.6 and 1.7).

The nominal values of final shrinkage for RH = 60% are reported below for the design of structures, in ordinary and pre-stressed reinforced concrete, as a function of thicknesses, concrete classes and effects to be evaluated.

Type/thickness	Class	Effect	1000 $\varepsilon_{cs\infty}$
Ordinary RC structures medium–big	Low	Global deformation	0.38
Ordinary RC structures medium–big	Medium	Global deformation	0.36
Pre-tensioned $(t_o \geq 14$ ore) small	High	Pre-stress losses	0.36
Pre-tensioned $(t_o \geq 14$ ore) medium–small	High	Pre-stress losses	0.32
Post-tensioned $(t_o \geq 14$ Gg) medium	High	Pre-stress losses	0.28

The time of application of pre-stressing is indicated t_o.

Table 1.9: Classes of Consistency of Fresh Concrete

Concerning workability and with reference to the subsidence a of Abrams cone (Slump test), the following classes of consistency of fresh concrete are distinguished.

Denomination	Humid	Plastic	Semi-fluid	Fluid
a (mm)	<50	50 ÷ 100	100 ÷ 150	>150
Class ISO 4103	S1	S2	S3	S4

Chart 1.10: Weight of Concrete Elements

With reference to concrete with normal aggregate, the specific weight of structural elements can be assumed equal to the following nominal values:

- plain concrete 24.0 kN/m^3
- reinforced concrete 25.0 kN/m^3

(coefficient of variation $\approx$ 0.06).

Table 1.11: Concrete Production Control

The control charts and the relative diagrams of a continuing concrete production in a given plant are reported below. The charts are to be used following the indications listed below:

- each chart should refer to a homogeneous type of mix constant in time;
- the mix should be named with the class and with a market specification of the final product;
- basic data should be added (content of cement, water/cement ratio, admixture content and aggregate size);
- the type of curing should be specified, also via the evaluation of β of the hardening law (see Table 1.1);
- it has to be specified whether strength measurements are referred to the reference age (28 days) f or at earlier ages f_j;
- 28-day tests should always be carried, tests at earlier ages only if required by early stages verifications;
- the chart is made of consecutive sheets, one for each solar month, where normally each row corresponds to a day;
- one concrete sample has to be taken every production day and cured in the same environment of casting;
- a sample consists of two specimens for 28-day tests, plus two specimens for earlier ages' tests if required;
- data, written on the row of the day of sampling, should start with the date of test;
- the strength measurements of the two specimens and the mean value should then be reported;
- if measured on cubic specimens, the strength value should be reduced with a factor of 0.83 to obtain the cylinder strength f_j;
- the mean value f_j should be corrected based on the age j of the specimen to deduce the reference (28 days) strength;
- the statistics should be calculated with the values of the set of n samples available in the last 21 solar days;
- for sets of $n < 6$ samples a conventional deviation of ks = 8 MPa should be assumed;
- for sets of $6 \leq n \leq 15$ samples the value of k should be taken from the table reported further on;
- for sets of $16 \leq n \leq 21$ samples the fixed value of $k = 1.48$ is assumed;
- for the n measurements available, the mean value f_m and the standard deviation s are then calculated;

- the current characteristic strength f_k is finally deduced, to be compared with one of the expected classes.

The formulas for the required calculations are (where R_1 and R_2 are the cubic strengths of the two cubic specimens and t is the concrete age in days at the time of testing):

$$f_j = 0.83\frac{R_1 + R_2}{2} \quad f = \frac{f_j}{e^{\beta(1-1/\tau)}} \quad \tau = t/28$$

$$f_m = \frac{\sum_{i=1}^{n} f_i}{n} \quad s = \frac{\sqrt{\sum_{i=1}^{n} (f_i - f_m)^2}}{n-1} \quad f_k = f_m - ks.$$

n	6	7	8	9	10	11	12	13	14	15
k	1.87	1.77	1.72	1.67	1.62	1.58	1.55	1.52	1.50	1.48

In any case the values of the variation coefficients s/f_m shall be less than 0.15. The following pages contain

- the template of control chart for data recording (with values shown as example);
- the diagram relative to the results of testing for the visualization of the production trend (with marks shown as example).

CONTROL CHART FOR CONTINUING CONCRETE PRODUCTION													
STANDARD ROOF ELEMENTS – CONCR. CLASS C35/43 – AGGR. ≤ 15mm									FACTORY				
MIX DESIGN: CEMENT 3,75 q/m^3 - W/C RATIO 0,40 – ADDITION 2,5%									PREFAB SYSTEM - MILAN				
ACCELERATED CURING (β=0,08) - TESTS AT: ~~28 DAYS~~ / DEMOULDING									OCTOBER 2014				p. 076
Sample	Test	specimens		mean	correlation to 28 days			for the set of samples of the last 21 solar days					
date	date	1	2	f_j	age	f_j/f	f	n	k	f_m	s	f_k	
1	2/10	30.5	30.0	25.1	0.67	0.65	38.6	15	1.48	41.5	2.37	38.0	
2	3/10	32.0	31.0	26.1	0.67	0.65	40.3	15	1.48	41.3	2.35	37.8	
3	6/10	39.0	39.5	32.6	3	0.85	38.3	15	1.48	41.2	2.46	37.6	
4													
5													
6	7/10	35.0	32.0	25.9	0.67	0.65	39.9	15	1.48	41.0	2.44	37.4	
7	8/10	31.0	31.5	25.9	0.67	0.65	39.9	15	1.48	40.8	2.40	37.2	
8	9/10	37.5	36.0	30.5	0.67	0.65	46.9	15	1.48	41.0	2.77	36.9	
9	10/10	34.0	34.5	28.4	0.67	0.65	43.7	15	1.48	40.9	2.66	37.0	
10	13/10	46.0	47.0	38.6	3	0.85	45.4	15	1.48	41.0	2.78	36.9	
11													
12													
13	14/10	33.5	34.0	28.0	0.67	0.65	43.0	15	1.48	41.1	2.82	36.9	
14	15/10	34.0	35.0	28.6	0.67	0.65	44.1	15	1.48	41.3	2.93	37.0	
15	16/10	33.0	34.5	28.0	0.67	0.65	43.0	15	1.48	41.3	2.93	37.0	
16	17/10	31.0	31.0	25.7	0.67	0.65	39.6	15	1.48	41.2	2.95	36.8	
17	21/10	42.0	43.5	35.5	4	0.88	40.3	15	1.48	41.3	2.91	37.0	
18													
19													
20													
21	22/10	35.0	35.0	29.0	0.67	0.65	44.7	14	1.50	41.9	2.76	37.8	
22	23/10	29.0	30.0	24.5	0.67	0.65	37.7	14	1.50	41.9	2.75	37.8	
23	24/10	30.0	30.5	25.1	0.67	0.65	38.6	14	1.50	41.8	2.96	37.4	
24	27/10	45.5	44.5	37.3	3	0.85	43.9	14	1.50	42.2	2.83	38.0	
25													
26													
27	28/10	33.0	34.0	27.8	0.67	0.65	42.7	14	1.50	42.4	2.75	38.3	
28	29/10	35.0	35.0	29.0	0.67	0.65	44.7	14	1.50	42.7	2.72	38.6	
29	30/10	35.0	35.5	29.3	0.67	0.65	44.9	14	1.50	42.6	2.52	38.8	
30	31/10	34.0	34.5	28.4	0.67	0.65	43.7	14	1.50	42.6	2.52	38.8	
31	3/11	47.0	47.0	39.0	3	0.85	44.7	14	1.50	42.5	2.28	39.1	

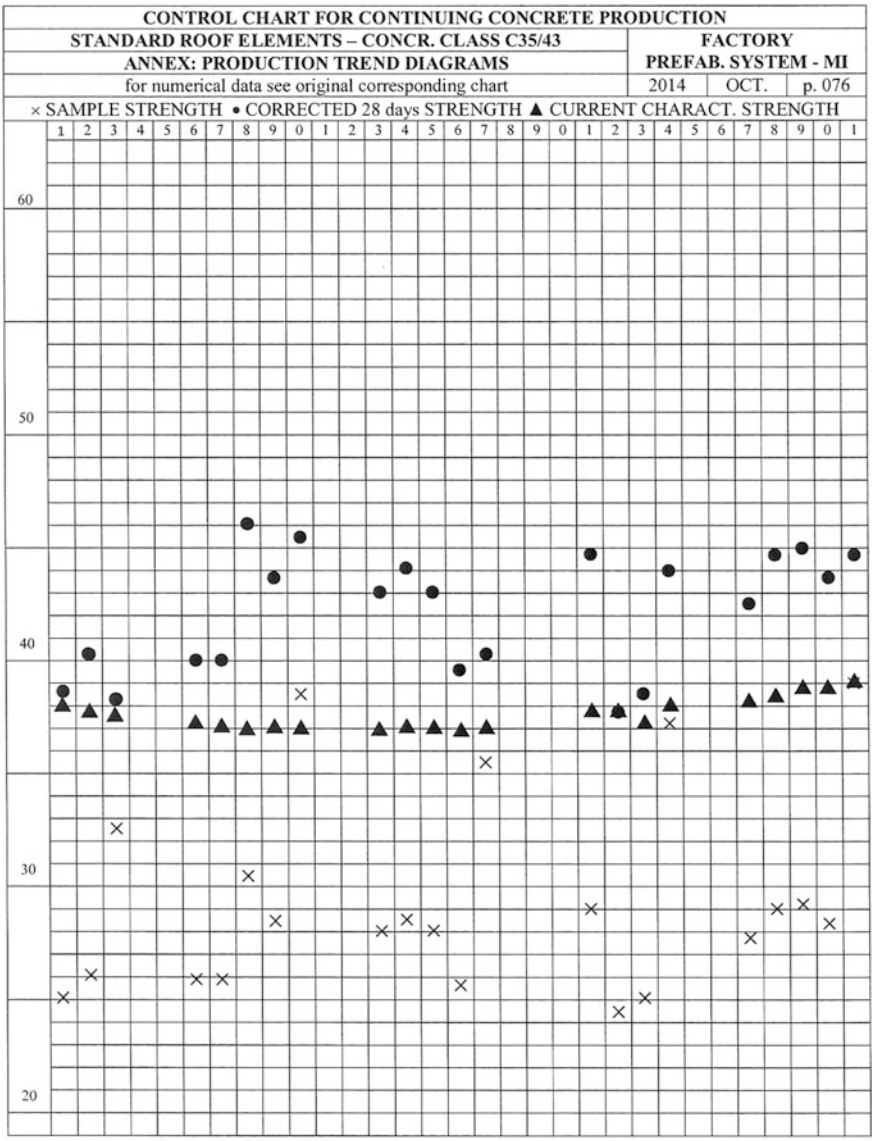

CONTROL CHART FOR CONTINUING CONCRETE PRODUCTION
STANDARD ROOF ELEMENTS – CONCR. CLASS C35/43
ANNEX: PRODUCTION TREND DIAGRAMS
for numerical data see original corresponding chart
FACTORY
PREFAB. SYSTEM - MI
2014 OCT. p. 076
× SAMPLE STRENGTH • CORRECTED 28 days STRENGTH ▲ CURRENT CHARACT. STRENGTH
1 2 3 4 5 6 7 8 9 0 1 2 3 4 5 6 7 8 9 0 1 2 3 4 5 6 7 8 9 0 1
60
50
40
30
20

Table 1.12: Creep: Class Coefficient

The following table shows, for the different strength classes of concrete, the value of the coefficient β_c of the formula:

$$\varphi_\infty = \beta_c \beta_{hs} \varphi_o$$

for the calculation of final concrete creep. The values are calculated with

$$\beta_c = \frac{1.673}{\sqrt{c}},$$

where $c = f_c/10$ is the class index and f_c is the mean strength in MPa.

For the other coefficients of the formulas, one can refer to Tables 1.13 and 1.14.

Ordinary Class	f_c (MPa)	β_c
C16/20	24	1.08
C20/25	28	1.00
C25/30	33	0.92
C30/37	38	0.86
C35/43	43	0.81
C40/50	48	0.76
C45/55	53	0.73

Controlled Class	f_c (MPa)	β_c
C30/37	35	0.89
C35/43	40	0.84
C40/50	45	0.79
C45/55	50	0.75
C50/60	55	0.71
C55/67	60	0.68
C60/75	65	0.66
C70/85	75	0.61

Table 1.13: Creep: Ambient Coefficient

The following table shows, for the different relative humidities RH of the ageing environment and for the different equivalent thicknesses $2A_c/u$, the values of the coefficient β_{hs} of the following formula:

$$\varphi_\infty = \beta_c \beta_{hs} \varphi_o$$

for the calculation of concrete final creep. The values are calculated with

$$\beta_{hs} = 0.725\left[1 + \frac{1-h}{0.46\sqrt[3]{s}}\right]$$

where h = HR/100 and $s = (2A_c/u)/100$ (A_c = cross-sectional area of concrete; u = its perimeter).

For the other coefficients of the formula, one can refer to Tables 1.12, 1.13, 1.14.

Relative humidity	$2A_c/u$ (mm)				
	Small thickness	Medium–small	Medium thickness	Medium–big	Big thickness
%	50	100	150	300	600
80	1.12	1.04	1.00	0.94	0.90
70	1.32	1.20	1.14	1.05	0.98
60	1.52	1.35	1.28	1.16	1.07
50	1.72	1.51	1.41	1.27	1.16

Table 1.14: Creep: Reference Coefficient

The following table shows, for the different concrete ages at loading, the values of the coefficient φ_o of the following formula:

$$\varphi_\infty = \beta_c \beta_{hs} \varphi_o,$$

for the calculation of final creep. The values are calculated with

$$\varphi_o = \frac{4.37}{0.1 + t_o^{0.2}} \quad (t_o \text{ in days}),$$

and should be assumed, with a coefficient of variation of about 0.20, for water/cement ratios ≤ 0.55. For higher ratios, the values are greater.

For the definition of t_o see Table 1.15; for the other coefficients of the formula, see Tables 1.12 and 1.13.

Age	φ_o
0.58	4.38
1	3.97
2	3.50
3	3.25
4	3.08
5	2.95
6	2.85
7	2.77
10	2.59
14	2.43
21	2.25
28	2.13
60	1.85
90	1.71
180	1.49
365	1.30

Table 1.15: Creep: Effect of Temperature

The following table shows, as a function of the average temperature θ of concrete in the time interval $0 - \bar{t}_o$, the value of the correction factor β_T with which the nominal age t_o can be deduced from the effective age $\bar{t}_o$ at loading:

$$t_o = \beta_T \bar{t}_o$$

This nominal age is used in the formula $\varphi_o = \varphi_o(t_o)$ of creep (see Table 1.14). The values are calculated with the following formula:

$$\beta_T = e^{\left(13.65 - \frac{4000}{273+\theta}\right)} \quad (\theta \text{ in } ^\circ\text{C})$$

θ	β_T
10	0.62
15	0.79
20	1.00
25	1.26
30	1.57

(continued)

(continued)

θ	β_T
35	1.34
40	2.39
45	2.92
50	3.55
55	4.28
60	5.14
65	6.15
70	7.30
75	8.63

Table 1.16: Creep: Nominal Coefficients

The nominal final values of creep coefficients are given below, for the design of ordinary and pre-stressed reinforced concrete, calculated in prevision of an environment with HR = 60% of relative humidity.

Type/thickness	Concrete class	Curing/age	Calculated effect	φ_∞
Ordinary RC struct. medium–big	Low	Natural $\bar{t}_o \geq 14$ days	Global deformation	3.1
Ordinary RC struct. medium–big	Medium	Natural $\bar{t}_o \geq 14$ days	Global deformation	2.5
Pre-tensioned small	High	Accelerated $\bar{t}_o \geq 14$ h	Pre-stress losses	3.1
Pre-tensioned medium–small	Medium	Accelerated $\bar{t}_o \geq 14$ h	Pre-stress losses	2.7
Post-tensioned medium	Medium	Natural $\bar{t}_o \geq 14$ days	Pre-stress losses	1.9

Table 1.17: Characteristics of Reinforcing Steel

B450C steel, used in reinforced concrete structures, is characterized by the following nominal values of characteristic yield strength f_{yo} and ultimate strength f_{to}

$$f_{yo} = 450 \text{ MPa}$$
$$f_{to} = 540 \text{ MPa}$$

The following table shows the requirements for the actual values of the main mechanical characteristics of B450C steel:

Characteristics	Symbol	Value
Characteristic yield strength (fractile 5%)	f_{yk}	≥ 450 MPa
Characteristic ultimate strength (fractile 5%)	f_{tk}	≥ 540 MPa
Uniform elongation (fractile 10%) ($=\varepsilon_{uk}$)	$(A_{gt})_k$	$\geq 7.5\%$
Strain-hardening ratio	$(f_t/f_y)_k$	
Minimum (fractile 10%)		≥ 1.15
Maximum (fractile 10%)		≤ 1.35
Overstrength ratio (fractile 10%)	$(f_t/f_{yo})_k$	≤ 1.25

Bars and wires made of B450C steel have to be bendable and weldable. Other characteristics common for all types of steel are

- specific weight (density) $g = 7850 \text{ kg/m}^3$
- longitudinal elastic modulus $E_s = 205000$ MPa
- coefficient of thermal expansion $\alpha_T = 1.0 \times 10^{-5} \text{ °C}^{-1}$.

Table 1.18: Bars and Wires: Commercial Diameters

ϕ (mm)	g (kg/m)	u (mm)	nA_s (mm^2)								
			1	2	3	4	5	6	7	8	9
6	0.222	18.9	28.3	56.5	84.8	113	141	170	198	226	254
8	0.395	25.1	50.5	101	151	201	251	302	352	402	452
10	0.617	31.4	79.0	157	236	314	393	471	550	628	707
12	0.888	37.7	113	226	339	452	566	679	791	905	1131
14	1.208	44.0	154	308	462	616	770	924	1078	1232	1385
16	1.578	50.3	201	402	603	804	1005	1206	1407	1608	1810
18*	1.998	56.6	254	509	763	1018	1272	1527	1781	2036	2290
20	2.466	62.8	314	628	942	1257	1571	1885	2199	2513	2827
22*	2.984	69.1	380	760	1140	1521	1901	2281	2661	3041	3421
24*	3.551	75.4	452	905	1357	1810	2262	2714	3167	3619	4072
25	3.853	78.5	491	982	1473	1963	2454	2945	3436	3927	4418

(continued)

(continued)

ϕ (mm)	g (kg/m)	u (mm)	nA_s (mm^2)								
			1	2	3	4	5	6	7	8	9
26*	4.168	81.7	531	1062	1593	2124	2655	3186	3717	4247	4778
28	*4.834*	*88.0*	*616*	*1232*	*1847*	*2463*	*3079*	*3695*	*4310*	*4926*	*5542*
30	*5.559*	*94.3*	*707*	*1414*	*2121*	*2827*	*3534*	*4241*	*4948*	*5655*	*6362*
32	*6.313*	*100.5*	*804*	*1608*	*2413*	*3218*	*4022*	*4827*	*5631*	*6436*	*7240*

Note Non-standard diameters are in italic; the diameters not normalized at European level (EN10080) are marked with a star

The table gives the weight g, the perimeter u and the cross-sectional area A_s for the commercial diameters ϕ of the hot-rolled ribbed wires and bars for reinforced concrete. Bars are supplied in 12-m-long bundles, wires up to diameters of 12 mm can be supplied in rolls.

Table 1.19: Bars for PC: Standard Diameters

The following table shows, for nominal diameters ϕ normalized by the European standard EN 10138/4, the values of

g	unit weight
u	perimeter of the equivalent bar
A_p	cross-sectional area
f_{ptk}	characteristic rupture strength
$f_{0.1k}$	characteristic strength at 0.1% residual elongation
$(f_{0.1}/f_{pt})_k$	hardening (reverse) ratio (=α_{rk})
ε_{uk}	indicative value of ultimate elongation
F_{ptk}	characteristic value of rupture load
$F_{0.1k}$	characteristic value of load at 0.1% residual elongation.

There are two types of steel Fe1030 and Fe1230 produced in hot-rolled bars subsequently subjected to cold-forming.

For the considered types of steel the following standard requirements are applied:

$$\varepsilon_{uk} \geq 3.5\% \quad \alpha_{rk} \geq 0.80.$$

The other general characteristics of the type of product are

- specific weight (density) $g = 7850\,\mathrm{kg/m^3}$
- longitudinal elastic modulus $E_p = 205000\,\mathrm{MPa}$
- coefficient of thermal expansion $\alpha_T = 1.0 \times 10^{-5}\,^{\circ}\mathrm{C}^{-1}$.

ϕ (mm)	g (kg/m)	u (mm)	A_p (mm^2)	f_{ptk} (MPa)	$f_{0.1k}$ (MPa)	α_{rk}	ε_{uk} (%)	F_{ptk} (kN)	$F_{0.1k}$ (kN)
20 *20*	2.47	62.8	314	1030 *1230*	830 *1080*	0.81 *0.88*	6.0 5.0	325 *385*	260 *340*
25 *25*	3.86	78.5	491	1030 *1230*	830 *1080*	0.81 *0.88*	6.0 5.0	505 *600*	416 *530*
26 *26*	4.17	81.7	531	1030 *1230*	830 *1080*	0.81 *0.88*	6.0 5.0	547 *653*	443 *575*
32 *32*	6.31	101	804	1030 *1230*	830 *1080*	0.81 *0.88*	6.0 5.0	830 *870*	670 *1109*
36 *36*	7.99	113	1018	1030 *1230*	830 *1080*	0.81 *0.88*	6.0 5.0	1050 *1100*	1208 *1400*
40 *40*	9.86	126	1257	1030 *1230*	830 *1080*	0.81 *0.88*	6.0 5.0	1295 *1357*	1050 *1732*
50	15.5	157	1960	1030	830	0.81	6.0	2020	1636

For the two types of steel in smooth and ribbed bars, the following table gives the values of

$\delta = 100(f_{ptm} - f_{ptk})/f_{ptm}$ percent deviation
$\Delta\bar{\sigma}$ fatigue limit range for 2×10^6 loading cycles.

Type	δ (%)	$\Delta\bar{\sigma}$ (MPa)	
Fe1030	≈7.5	200	Smooth
		180	Ribbed
Fe1230	≈6.0	200	Smooth
		180	Ribbed

Table 1.20: Cold-Drawn Wire: Standard Diameters

The following table shows, for the nominal diameters ϕ normalized by the European standard EN 10138/2, the values of

g unit weight
u perimeter of the equivalent bar
A_p cross-sectional area
f_{ptk} characteristic rupture strength
$f_{0.1k}$ characteristic strength at 0.1% residual elongation
$(f_{0.1}/f_{pt})_k$ hardening (reverse) ratio ($=\alpha_{rk}$)
ε_{uk} indicative value of ultimate elongation
F_{ptk} characteristic value of rupture load
$F_{0.1k}$ characteristic value of load at 0.1% residual elongation.

There are four types of steels, namely Fe1570, Fe1670, Fe1770 and Fe1870, produced in smooth or indented wires by cold drawing and stretching.

For the considered steels the following standard requirements are applied:

$$\varepsilon_{uk} \geq 3.5\% \quad \alpha_{rk} \geq 0.80.$$

The other general characteristics of the type of products are

- specific weight (density) $g = 7850\,\text{kg/m}^3$
- longitudinal elastic modulus $E_p = 205000\,\text{MPa}$
- coefficient of thermal expansion $\alpha_T = 1.0 \times 10^{-5}\,^{\circ}\text{C}^{-1}$.

The value of deviation $\delta = 100(f_{ptm} - f_{ptk})/f_{ptm}$ is for all types of steel $\delta \cong 7.5\%$.

The fatigue limit range for $2 \cdot 10^6$ loading cycles is

$$\Delta\bar{\sigma} = 200\,\text{MPa} \quad \text{for smooth wires}$$
$$\Delta\bar{\sigma} = 180\,\text{MPa} \quad \text{for indented wires.}$$

ϕ (mm)	g (kg/m)	u (mm)	A_p (mm^2)	f_{ptk} (MPa)	$f_{0.1k}$ (MPa)	α_{rk}	ε_{uk} (%)	F_{ptk} (kN)	$F_{0.1k}$ (kN)
4.0	0.989	12.6	12.6	1770	1520	0.86	4.2	22.3	19.2
4.0				*1860*	*1600*	*0.86*	4.0	*23.4*	*20.1*
5.0	0.154	15.7	19.6	1670	1440	0.86	4.6	32.7	28.1
5.0				*1770*	*1520*	*0.86*	4.2	*34.7*	*29.8*
6.0	0.222	18.9	28.3	1670	1440	0.86	4.6	47.3	40.7
6.0				*1770*	*1520*	*0.86*	4.2	*50.1*	*43.1*
7.0	0.302	22.0	38.5	1670	1440	0.86	4.6	64.3	55.3
7.5	*0.347*	*23.6*	*44.2*	*1670*	*1440*	*0.86*	4.6	*73.8*	*63.5*
8.0	0.395	25.1	50.3	1670	1440	0.86	4.6	84.0	72.2
9.4	*0.545*	*29.5*	*69.4*	*1570*	*1300*	*0.83*	5.0	*109.0*	*90.5*
10.0	0.616	31.4	78.5	1570	1300	0.83	5.0	123.0	102

Table 1.21: Strands: Standard Diameters

The following table shows, for the nominal diameters ϕ normalized by the European standard EN 10138/3, the values of

g	unit weight
u	perimeter of the equivalent bar
A_p	cross-sectional area
f_{ptk}	characteristic rupture strength

$f_{0.1k}$ characteristic strength at 0.1% residual elongation
$(f_{0.1}/f_{pt})_k$ hardening (reverse) ratio ($=\alpha_{rk}$)
ε_{uk} indicative value of ultimate elongation
F_{ptk} characteristic value of rupture load
$F_{0.1k}$ characteristic value of load at 0.1% residual elongation.

There are strands made of three wires 3W, seven wires 7W and compacted strands of seven wires 7WC obtained from cold-drawn wires of small diameters (2.4 ÷ 6.0 mm), in six types of steels, namely Fe1700, Fe1770, Fe1820, Fe1860, Fe1960 and Fe2060.

For the concerned steels there are the following standard requirements:

$$\varepsilon_{uk} \geq 3.5\% \quad \alpha_{rk} \geq 0.80$$

The other general characteristics of the type of products are

- specific weight (density) $g = 7850\,\text{kg/m}^3$
- longitudinal elastic modulus $E_p = 195000\,\text{MPa}$
- coefficient of thermal expansion $\alpha_T = 1.0 \times 10^{-5}\,^{\circ}\text{C}^{-1}$.

The value of deviation $\delta = 100(f_{ptm} - f_{ptk})/f_{ptm}$ is for all steels 7.5%.
The fatigue limit range for 2×10^6 loading cycles is

$$\Delta\bar{\sigma} = 190\,\text{MPa} \quad \text{for smooth wires}$$
$$\Delta\bar{\sigma} = 170\,\text{MPa} \quad \text{for indented wires.}$$

ϕ (mm)	g (kg/m)	u (mm)	A_p (mm^2)	f_{ptk} (MPa)	$f_{0.1k}$ (MPa)	α_{rk}	ε_{uk} (%)	F_{ptk} (kN)	$F_{0.1k}$ (kN)
Strand 3W									
5.2	0.107	16.3	13.6	1960	1670	0.85	4.6	26.7	22.7
5.2	*0.107*	*16.3*	*13.6*	*2060*	*1750*	*0.85*	4.2	*28.0*	*23.8*
6.5	0.166	20.4	21.2	1860	1580	0.85	4.6	39.4	33.5
6.5	*0.166*	*20.4*	*21.2*	*1960*	*1670*	*0.85*	4.6	*41.5*	*35.3*
6.8	*0.184*	*21.4*	*23.4*	*1860*	*1580*	*0.85*	4.6	*43.5*	*37.0*
7.5	0.228	23.6	29.0	1860	1580	0.85	4.6	53.9	45.8
Strand 7W									
7.0	*0.236*	*22.0*	*30.0*	*2060*	*1750*	*0.85*	4.6	*61.8*	*52.5*
9.0	0.393	28.3	50.0	1860	1580	0.85	5.0	93.0	79.0
11.0	*0.590*	*34.6*	*75.0*	*1860*	*1580*	*0.87*	5.0	*139*	*118*
12.5	0.730	39.3	93.0	1860	1580	0.85	5.0	173	147
13.0	*0.785*	*40.8*	*100*	*1860*	*1580*	*0.85*	5.0	*186*	*158*
15.2	1.090	47.8	139	1770	1500	0.85	5.0	246	209

(continued)

(continued)

ϕ (mm)	g (kg/m)	u (mm)	A_p (mm^2)	f_{ptk} (MPa)	$f_{0.1k}$ (MPa)	α_{rk}	ε_{uk} (%)	F_{ptk} (kN)	$F_{0.1k}$ (kN)
15.2	*1.090*	*47.8*	*139*	*1860*	*1580*	*0.85*	5.0	*258*	*219*
16.0	*1.180*	*50.3*	*150*	*1770*	*1500*	*0.85*	5.0	*265*	*225*
16.0	*1.180*	*50.3*	*150*	*1860*	*1580*	*0.85*	5.0	*279*	*237*
18.0	1.570	56.5	200	1770	1500	0.85	5.0	354	301
Compacted 7WC									
12.7	0.890	40.0	112	1860	1580	0.85	5.0	209	178
15.2	1.295	47.8	165	1820	1580	0.85	5.0	300	225
18.0	1.750	56.5	223	1700	1580	0.85	5.0	380	323

Chart 1.22: Concrete σ–ε Models

For the analysis of a section in reinforced or pre-stressed concrete at the ultimate limit state of rupture, one of the three models σ–ε for concrete described below can be adopted (see also Fig. 1.28).

Classes up to C50/60 ($f_{ck} \leq 50$ MPa)
For all models,

- ultimate compressive strain of the most stressed fibre $\varepsilon_{cu} = 0.35\%$
- mean ultimate strain of concrete in compression $\varepsilon_{c2} = 0.20\%$
- compressive strength of concrete $f_{cd} = \alpha_{cc} f_{ck}/\gamma_C$
- tensile strength of concrete $f_{ctd} = 0$.

Parabola–rectangle model

$$\begin{aligned} \sigma_c &= [1 - (1 - \varepsilon_c/\varepsilon_{c2})^2] f_{cd} && \text{for } 0 \leq \varepsilon_c < \varepsilon_{c2} \\ \sigma_c &= f_{cd} && \text{for } \varepsilon_{c2} \leq \varepsilon_c \leq \varepsilon_{cu} \end{aligned}$$

with $\varepsilon_{c2} = 0.2\%$.
Triangle–rectangle model

$$\begin{aligned} \sigma_c &= (\varepsilon_c/\varepsilon_{c3})\, f_{cd} && \text{for } 0 \leq \varepsilon_c < \varepsilon_{c3} \\ \sigma_c &= f_{cd} && \text{for } \varepsilon_{c3} \leq \varepsilon_c \leq \varepsilon_{cu} \end{aligned}$$

with $\varepsilon_{c3} = 0.15\%$.

Rectangular model

$$\begin{array}{ll} \sigma_c = (\varepsilon_c/\varepsilon_{c3}) f_{cd} & \text{for } 0 \le \varepsilon_c < \varepsilon_{c3} \\ \sigma_c = \mathrm{f}_{cd} & \text{for } \varepsilon_{c3} \le \varepsilon_c \le \varepsilon_{cu} \end{array}$$

with $\varepsilon_{c4} = 0.07\%(= 0.2\varepsilon_{cu})$.

Classes greater than C50/60 (f_{ck} > 50 MPa)
For all models,

- ultimate compressive strain of the most stressed fibre $\varepsilon_{cu} = 0.26 + 3.5[(90 - f_{ck})/100]^4\%$
- mean ultimate strain of concrete in compression $\varepsilon_{c2} = 0.20 + 0.0085(f_{ck} - 50)^{0.53}\%$
- compressive strength of concrete $f_{cd} = \alpha_{cc} f_{ck}/\gamma_C$
- tensile strength of concrete $f_{ctd} = 0$.

Parabola–rectangle model

$$\begin{array}{ll} \sigma_c = [1 - (1 - \varepsilon_c/\varepsilon_{c2})^n] f_{cd} & \text{for } 0 \le \varepsilon_c < \varepsilon_{cr} \\ \sigma_c = \mathrm{f}_{cd} & \text{for } \varepsilon_{cr} \le \varepsilon_c < \varepsilon_{cu} \end{array}$$

with $n = 1.4 + 23.4[(90 - f_{ck})/100]^4$.
Triangle–rectangle model

$$\begin{array}{ll} \sigma_c = \varepsilon_c/\varepsilon_{c3} f_{cd} & \text{for } 0 \le \varepsilon_c < \varepsilon_{c3} \\ \sigma_c = f_{cd} & \text{for } \varepsilon_{c3} \le \varepsilon_c \le \varepsilon_{cu} \end{array}$$

with $\varepsilon_{c3} = 0.15 + 0.55[(f_{ck} - 50)/400]$.
Rectangular model

$$\begin{array}{ll} \sigma_c = 0 & \text{for } 0 \le \varepsilon_c < \varepsilon_{c4} \\ \sigma_c = \eta f_{cd} & \text{for } \varepsilon_{c4} \le \varepsilon_c \le \varepsilon_{cu} \end{array}$$

with $\varepsilon_{c4} = \lambda \varepsilon_{cu}$ and

$$\eta = 1.0 - (f_{ck} - 50)/200$$
$$\lambda = 0.2 + (f_{ck} - 50)/400$$

Chapter 2
Centred Axial Force

Abstract This chapter presents the design methods of reinforced concrete elements subjected to axial action, starting from the columns under compression and proceeding with the tension members, for which in particular the criteria for cracking calculation are given. In the final section the structure of a multi-storey building is described, assumed as applicative example for the design calculations. The analysis of loads is developed and the complete design of a column is shown.

2.1 Compression Elements

Reinforced concrete columns have two types of reinforcement (see Fig. 2.1): longitudinal reinforcement consisting of bars at the corner and possibly also on the long sides; transverse reinforcement consisting of stirrups, which are bars of smaller diameter shaped to enclose the longitudinal reinforcement.

Under compression actions that are essentially centred, no tensile stresses arise in the columns. One could therefore think of not adopting any reinforcement at all, as concrete resists compression well. However, its brittleness requires a remedial. If massive works are excluded, for which any possible local brittle damage has a small impact on the global resistance, concrete elements always have to be encased in a sort of superficial steel cage. The size of such steel cage has to be related to the mass of concrete to be reinforced in order to introduce a significant increase in ductile resistance. This leads to *minimum reinforcement* requirements such as

$$A_s \geq \rho_o \, A_c$$

which imposes a minimum value ρ_o (e.g. =0.003) to the longitudinal *reinforcement geometrical ratio* $\rho_s = A_s/A_c$; or such as

$$A_s \geq v_0 \, N_{Ed}/f_{sd}$$

which imposes the possible increase in reinforcement based on a minimum ratio v_o (e.g. =0.10) of the expected load.

© Springer International Publishing AG 2017

G. Toniolo and M. di Prisco, *Reinforced Concrete Design to Eurocode 2*,
Springer Tracts in Civil Engineering, DOI 10.1007/978-3-319-52033-9_2

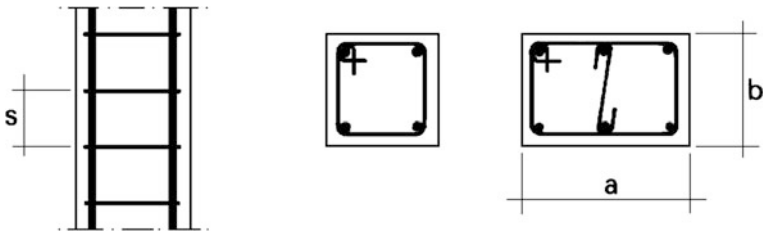


Fig. 2.1 Details of RC column—view and sections

Furthermore, an adequate distribution of reinforcement has to be guaranteed, imposing a *maximum spacing* of bars (e.g. ≤ 300 mm) and correlating the spacing of links to the column smaller side (e.g. $s \leq b$).

For reinforcement lower than the minimum values mentioned above, one can refer to the typology of *plain concrete* works (unreinforced or with light reinforcement), such as walls and other massive structures, designed according to specific criteria.

High reinforcement ratios, grater than a limit ρ_1 of about 4%, make the effective collaboration between the two materials uncertain because of bond problems. When the steel area is higher than the mentioned limit, one enters a range of a different type of composite material. One then refers to *composite structures*, where bond between steel and concrete should rely on special connecting devices and not only to surface adhesion.

The failure mode of a column in compression is indicated in Fig. 2.2a, with the development of the typical "hourglass" shape in the concrete and with buckling of

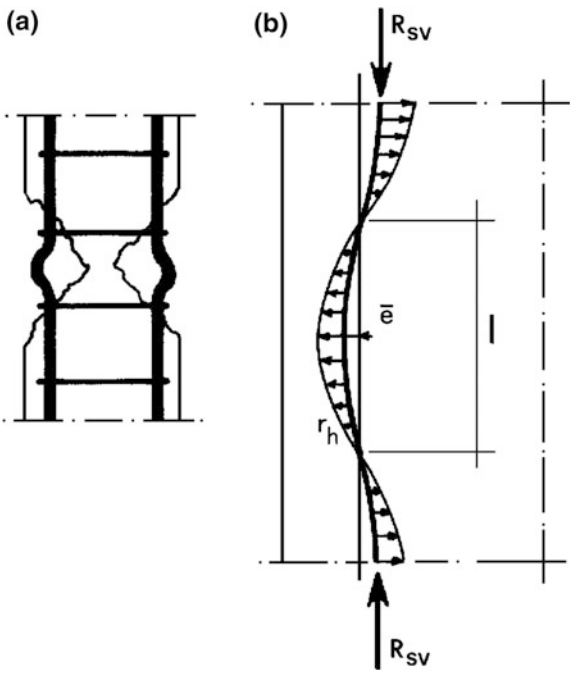


Fig. 2.2 Buckling of bars in compression

the longitudinal reinforcement. From this failure mode another important function of the stirrups is deduced, which is the limitation of the buckling length of the longitudinal bars, which otherwise would be too instable to offer a significant contribution to resistance. The *maximum spacing* of stirrups therefore has to be related to the diameter of the longitudinal bars with limitations such as

$$s \leq \kappa_o \, \phi$$

which, for example, with $\kappa_o = 12$, (being $i = \phi/4$ the radius of gyration and $s_o = 0.5$ s the buckling length), implicitly impose the limit

$$\lambda = s_o/i = 24$$

to the slenderness of the bars.

The stirrups have to be shaped and sized to guarantee an *effective restraint* towards the inside of the column, working in tension. Given that the transverse restraining force is proportional to the vertical one that runs inside the longitudinal bars (e.g. a few percent), the diameter of the stirrups has to be correlated to the one of the longitudinal reinforcement with limitations such as $\phi' \geq \phi/n$. The presence of longitudinal bars on the sides requires the addition of specific transverse connecting links.

The two *ends of the column* are the most critical zones, because of the possible disturbance created by the bars lapping (usually at the bottom), and because the bending moment reaches its maximum values there. It is good practice to reduce the stirrups spacing in those zones, for example halving it, in order to enhance their confining effect.

The reinforcement of elements with elongated cross section, such as *walls* (see Fig. 2.3a), requires the introduction of two sets of bars close to the external surfaces. The reinforcement consisting of horizontal straight bars of smaller diameter does not offer the through-link required to restrain the vertical bars with tensile forces only. For this, appropriate links (similar to the one shown with a dashed line in the figure) would be necessary, one for each pair of vertical bars, spaced vertically according to the same criteria described for stirrups.

Links are not necessary if the concrete layer covering the vertical bars can restrain them with transverse tensile stresses σ_h (see Fig. 2.3b). These tensile stresses should be low enough so that the concrete resistance to the vertical compressions is not significantly reduced. This leads to limitations for the diameter ϕ of the bars with respect to the concrete cover c. Only short notes are hereby given about the criterion that gives such limitations, as the numerical results are based on some parameters that are difficult to quantify.

Assuming a conventional model for the profile of the vertical bars to represent straightness tolerances of the bars, for example with the sinusoidal function (see Fig. 2.2b):

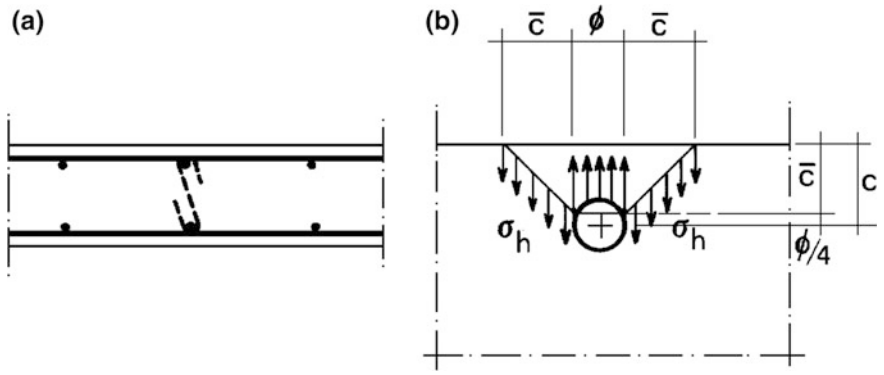


Fig. 2.3 **a** Transverse links and **b** restraint mechanism

$$e = \bar{e} \sin \frac{\pi}{1} x$$

under the action of the vertical force R_{sv} a transverse reaction is generated which varies according to the second-order derivative of the profile

$$r_h \cong R_{sv} e^{II}$$

This reaction is able of resisting the vertical force without relying on the bending stiffness of the bar. The maximum value of the horizontal force coincides with the point of maximum curvature $\bar{\chi}$ and can be expressed as in inversely proportional to the diameter. At the yield limit of the bar, one therefore has

$$\bar{r}_h = A_s f_y \bar{\chi} = \frac{\pi \phi^2}{4} f_y \frac{\kappa}{\phi}$$

The tensile stresses σ_h in the concrete cover oppose to the deviating action of the bar (see Fig. 2.3b), according to the equilibrium

$$\bar{r}_h = 2\bar{c}\sigma_{ct}/\sqrt{2}$$

Imposing the limit $\leq \beta f_{ct}$ (for example with $\beta = 0.20$) to such tension, it is eventually deduced

$$\bar{c} \geq 0.125\sqrt{2}\pi \frac{\kappa f_y}{\beta f_{ct}} \phi$$

where, with $f_y/f_{ct} \cong 250$, the tolerance κ has to be appropriately estimated. If, for example $\kappa = 1/400$ is assumed, the *minimum cover* is obtained with

$$c \geq \frac{\phi}{4} + \bar{c} \cong 2\phi$$

as a function of the diameter of the longitudinal bar, in order to rely on the full strength of the materials without the need for transverse confining links.

2.1.1 Elastic and Resistance Design

Given the reinforced concrete section of Fig. 2.4 subject to a centred compression force N, for the first design assumption the section translates remaining plane, exhibiting a constant contraction ε under load. For the second assumption of perfect bond between the two materials, it derives that steel is subject to the same deformation $\varepsilon_s = \varepsilon_c = \varepsilon$. The third assumption of concrete cracking in tension does not come into play, since only compression stresses occur: the resisting section in this case coincides with the geometrical section.

For an *elastic design*, stresses in the two materials are therefore obtained with the Hooke's law:

$$\sigma_c = E_c\, \varepsilon_c = E_c\, \varepsilon$$
$$\sigma_s = E_s\, \varepsilon_s = E_s\, \varepsilon$$

where in particular, for the equality of deformations ε, one has:

$$\frac{\sigma_c}{E_c} = \frac{\sigma_s}{E_s}$$

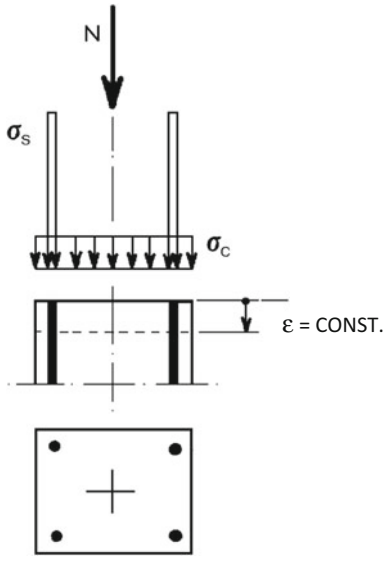


Fig. 2.4 Stresses on the section

which leads to

$$\sigma_s = \alpha_e \, \sigma_c$$

where $\alpha_e = E_s/E_c$ is the ratio between the elastic moduli of the two materials.

The equilibrium to translation of the cross section is therefore set with

$$\sigma_c A_c + \sigma_s A_s = N$$

having indicated with A_c and A_s the areas of concrete and steel, respectively, affected by stresses σ_c and σ_s. Introducing the above-mentioned relationship between these stresses, one eventually obtains:

$$\sigma_c (A_c + \alpha_e \, A_s) = \sigma_c A_i = N$$

having set

$$A_i = A_c + \alpha_e A_s$$

equivalent area of the section equalized to concrete. That is, in the elastic range, the steel area A_s should be amplified with the *homogenization coefficient* α_e to obtain a concrete area of the same capacity.

Indicating with ψ_s the *reinforcement elastic ratio*, evaluated weighing the areas of the two materials with the respective elastic modulus

$$\psi_s = \frac{E_s A_s}{E_c A_c} = \alpha_e \rho_s$$

one can express

$$A_i = A_c (1 + \psi_s)$$

where the amplification factor of the concrete area is enclosed in brackets.

The value of stresses under a given force N is therefore deduced as:

$$\sigma_c = \frac{N}{A_i}$$
$$\sigma_S = \alpha_e \, \sigma_c$$

Assuming the characteristic value of the force, these formulas are therefore used for serviceability verifications such as $\sigma_c < \bar{\sigma}_c$ (with $\bar{\sigma}_c = 0.45 f_{ck}$ for non-transient load situations).

For *resistance verification* (at the ultimate limit state) the assumption of elasticity should be replaced by the constitutive models σ–ε of the two materials (see Fig. 2.5). In addition to what mentioned in Sect. 1.4.2 about concrete models, it is to be noted that the ultimate strain ε_{cu} is reached under an imposed contractions.

If otherwise it is the load that increases, rupture occurs at the value ε_{c1} (see Fig. 1.4) suddenly developing with the uncontrolled failure of the specimen.

In concrete sections in bending, the variability of stresses provides a certain degree of redundancy to the system and therefore the less stressed fibres offer a control to the deformation of the more stressed ones. The beam edges in compression can therefore reach the limit ε_{cu}. On the contrary in concrete sections under axial compression there is no degree of redundancy, as all fibres are equally stressed. For this reason, the limit ε_{c1} shall be assumed as ultimate failure contraction.

The presence of steel reinforcement, if not already yielded, could provide in RC sections the deformations control to pass the limit ε_{c1}. This is valid up to the yield point of the reinforcement itself, at which any internal redundancy is lost. The problem does not have any practical relevance, as the viscous strain increment is to be added to the limit $\varepsilon_{c2} \cong \varepsilon_{c1} \cong 0.002$ and this always leads steel to yield, as it will be shown hereafter.

In the analysis of a section at the ultimate limit state, as indicated in Fig. 2.5, the parabola-rectangle model is assumed for concrete, where the ultimate failure contraction is approximated by the value ε_{c2}; moreover, the elastic-perfectly plastic model is assumed for steel, disregarding hardening which is negligible at the failure limit ε_{c2} of the section anyway.

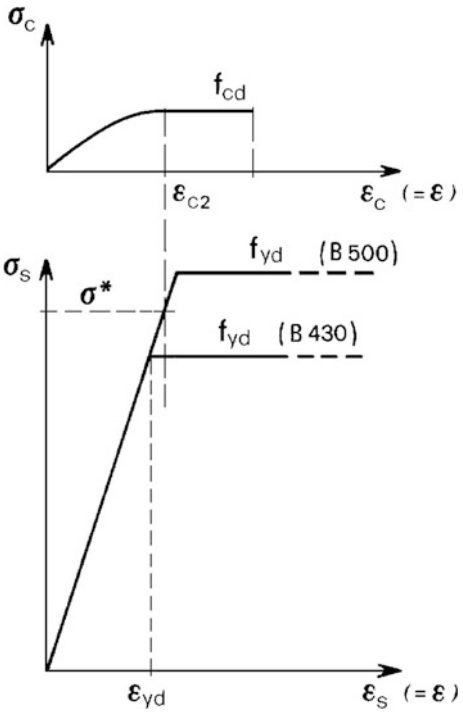


Fig. 2.5 Stress–strain diagrams of concrete and steel

Assuming for now an instantaneous load increment, at the mentioned failure limit ε_{c2} of the most brittle material, the equilibrium of the section is therefore set with the equation:

$$N_{Rd} = f_{cd}A_c + \sigma^* A_s$$

where it should be set $\sigma^* = E_s\varepsilon_{c2}$ if $\varepsilon_{yd} > \varepsilon_{c2}$, or $\sigma^* = f_{yd}$ if $\varepsilon_{yd} < \varepsilon_{c2}$.

Similarly to the elastic formula, this equation, for $\sigma^* = f_{yd}$, can be set as

$$N_{Rd} = f_{cd}\left(A_c + \frac{f_{yd}}{f_{cd}}A_s\right) = f_{cd}A_{ir}$$

where *the ideal area* equalized to concrete is

$$A_{ir} = A_c + \frac{f_{yd}}{f_{cd}}A_s = A_c(1 + \omega_s)$$

The homogenization coefficient of the steel area is here given by the ratio of the two strength values, whilst the dimensionless coefficient

$$\bar{\omega}_s = \frac{f_{yd}A_s}{f_{cd}A_c}$$

where the areas of the two materials are weighed with the respective strengths, is called *mechanical reinforcement ratio*. It indicates the relative contribution of the steel reinforcement to resistance.

In order to give the order of magnitude of such contribution, three situations are hereafter evaluated: a lower one corresponding to the minimum limit of 0.3% of geometric reinforcement ratio and to the association of steel B450C with the highest class of concrete; an upper one corresponding to the maximum limit of 4% of steel reinforcement ratio and the association of steel B450C with the lowest class of concrete; an intermediate one corresponding to a geometrical percentage of 0.8% and to a more balanced association of materials. Assuming, therefore $\gamma_S = 1.15$, $\gamma_C = 1.50$ and $\alpha_{cc} = 0.85$ one has:

$$\omega_s = 0.003\frac{450/1.15}{0.85 \times 70/1.50} \cong 0.03$$

$$\omega_s = 0.040\frac{450/1.15}{0.85 \times 16/1.50} \cong 1.73$$

$$\omega_s = 0.008\frac{450/1.15}{0.85 \times 30/1.50} \cong 0.21$$

It is noted how it is possible to go from low reinforcement elements with steel contribution practically negligible to situations, not frequent in reality, where the

reinforcement contribution is predominant. In common situations, the presence of reinforcement can increase the load capacity of columns approximately by 20% or 30%, this being on average the mechanical reinforcement percentage.

It is eventually to be noted that several design codes impose to take into account a minimum eccentricity of the axial force, for example with $e \geq 0.05$ h, where h is the depth of the section. The verification therefore refers to combined action of axial force and bending moment (see Chap. 6). Moreover, for moderate reinforcement ratios (approximately $\omega_s \leq 0.8$), such requirement remains implicitly fulfilled if, in the formula of verification of centred axial force, the concrete contribution is penalized attributing with $0.8f_{cd}$. In such case, fixing the value of mechanical reinforcement ratio, the formula deduced here becomes

$$N_{Rd} = f_{cd}A_c(0.8 + \omega_s)$$

2.1.2 *Effect of Confining Reinforcement*

The external cage made of stirrups and longitudinal bars provides a certain degree of confinement of concrete inside the column, counteracting the transverse expansion under loads and increasing the resistance. The effect in ordinary columns with stirrups is moderate because of the low density of the steel reinforcement mesh. As indicatively shown in Fig. 2.6, the low flexural stiffness of the straight portions of bars leaves the confining actions concentrated on the bends of the stirrups; such actions then diffuse on a limited internal portion of concrete.

In order to systematically take advantage of the effect described above, appropriate reinforcing hoops are adopted, much more closely spaced than in ordinary columns with stirrups. The *confined columns* therefore have a number of longitudinal bars (at least 6), closely distributed on a circular external perimeter and enclosed by a spiral bar (or circular links). The pitch of the spiral has to be properly limited with respect to the diameter, for example with $s \leq D/5$. In this way, an effective confinement of transverse expansions is obtained in the entire concrete cylindrical core delimited by the hoops (see Fig. 2.7).

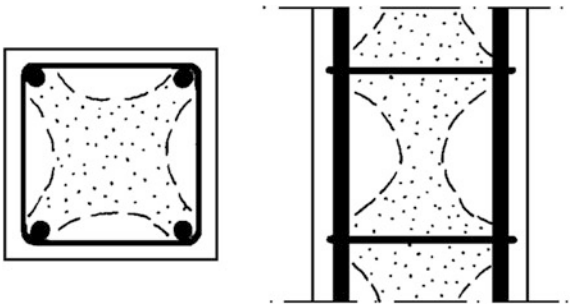


Fig. 2.6 Confining action on the concrete core

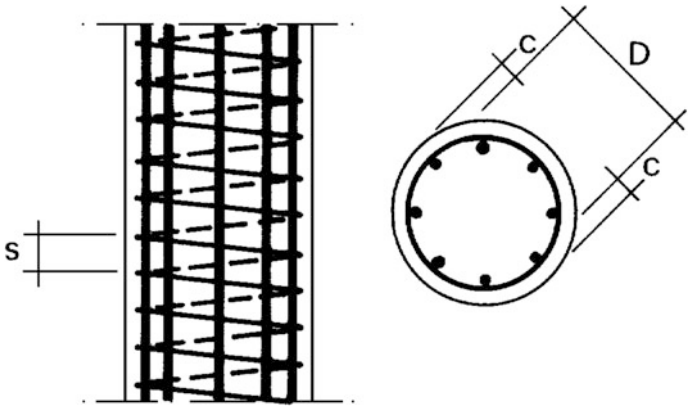


Fig. 2.7 Details of a confined column

In the elastic range, the effect of confinement on the stress distribution is very low, as shown hereafter.

Having defined $A_n = \pi D^2/4$ as the area of the core, A_l the area of the longitudinal reinforcement and $A_w = a_w \pi D/s$ the equivalent one of the spiral bar (of cross section a_w), the following relations are obtained. The isolated segment of the core of height s, subject to a vertical flux of stresses σ_v (see Fig. 2.8a) exhibits a shortening

$$\delta_{vo} = \frac{\sigma_v}{E_c} s$$

and, at the same time, an horizontal expansion

$$\delta_{ho} = -\nu \frac{\sigma_v}{E_c} D$$

The hoops oppose to such expansion with a horizontal stress σ_h (see Fig. 2.8b, c) which can be considered as the unknown of the problem. For the equilibrium of the semicircular piece of bar of Fig. 2.8c also the stress σ_w in the spiral can be expressed in terms of σ_h:

$$2\,\sigma_w\,a_w = \sigma_h\,Ds$$

whence

$$\sigma_w = \frac{Ds}{2a_w}\sigma_h = \frac{A_n}{\pi D^2/4}\frac{Ds}{2a_w}\sigma_h = 2\frac{A_n}{A_w}\sigma_h$$

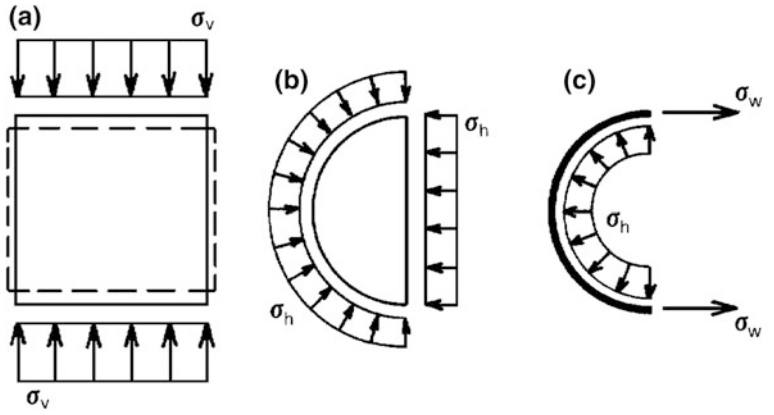


Fig. 2.8 Equilibrium conditions of concrete core and confining steel

The relative horizontal expansion between spiral and core due to the unknown σ_h is therefore obtained adding up the two deformation contributions of steel and concrete:

$$\delta_{hh}\sigma_h = D\left\{\frac{\sigma_w}{E_s} + \frac{1-\nu}{E_c}\sigma_h\right\} = D\left\{\frac{2A_n}{E_s A_w} + \frac{1-\nu}{E_c}\right\}\sigma_h$$

Eventually the compatibility of deformations is set between spiral and core:

$$\delta_{hh}\sigma_h + \delta_{ho} = 0$$

from which one obtains

$$\sigma_h = -\frac{\delta_{ho}}{\delta_{hh}} = \frac{\dfrac{\nu}{E_c}}{\dfrac{2A_n}{E_s A_w} + \dfrac{1-\nu}{E_c}}\sigma_v$$

that, with $\rho_w = A_w/A_n$, $\alpha_e = E_s/E_c$ and $\psi_w = \alpha_e\rho_w$, becomes:

$$\sigma_h = \frac{1}{\dfrac{2}{\psi_w} + \dfrac{1}{1-\nu} + 1}\frac{\nu}{1-\nu}\sigma_v$$

Without the spiral ($\psi_w = 0$) one has $\sigma_h \equiv 0$: it is the case of ordinary columns with stirrups. The maximum confining contribution is obtained instead at the limit situation of a spiral of so high size that it can be considered rigid with respect to concrete ($\psi_w = \infty$).

In this case one obtains

$$\sigma_h = \frac{\nu}{1-\nu}\sigma_v$$
$$(\sigma_h \cong 0.25\ \sigma_v \quad \text{for} \quad \nu \cong 0.20)$$

The vertical contraction of the confined column is therefore:

$$\varepsilon_v = \frac{1}{E_c}(\sigma_v - 2\nu\sigma_h) = \frac{\sigma_v}{E_c}\left(1 - \frac{2\nu^2}{1-\nu}\right)$$

lesser than the one of the ordinary column, as if concrete had an effective elastic modulus

$$E'_c = \frac{E_c}{1 - \dfrac{2\nu^2}{1-\nu}} = \frac{1-\nu}{(1+\nu)(1-2\nu)}E_c$$

With this effective elastic modulus, increased by about 10% with respect to the ordinary one as it can be deduced setting $\nu \cong 0.20$, the *elastic design* can be carried evaluating the stresses on the plane section of the column for a given axial force:

$$N = A_n\sigma_v + A_1\sigma_1 = \sigma_v\left(A_n + \alpha'_e\, A_1\right) = \sigma_v A'_i$$

being, with $\alpha'_e = E_s/E'_c \cong 0.9\alpha_e$ and with $\psi'_1 = \alpha'_e\rho_1$

$$A'_i = A_n\left(1 + \psi'_1\right)$$

the equivalent area. For longitudinal bars of about 1% with respect to the cross section of the core, with $6 \leq \alpha_e \leq 10$, values increased by about 1% are obtained for the stress σ_v in concrete, values decreased by about 9% are obtained for stress σ_1 in the longitudinal reinforcement.

Considering that the actual elastic deformability of the spiral further reduces this effect, which remains still limited to the concrete core excluding the external cover layer of thickness c, it can be seen how, in the elastic design, it can be neglected.

The *ultimate resistance* is instead significantly increased by the confinement as indicated in the following formulation which is based on the experimental results. First of all, the tests on confined columns exhibit early spalling outside the confining hoops. This occurs at level of the stresses close to the uniaxial strength f_c of concrete.

As the load N further increases, more significant transversal expansions of the core are observed, greatly increasing close to the ultimate limit, inducing tensions in the spiral reinforcement. If abnormal quantities of this reinforcement are excluded, the column failure occurs after the spiral yields. Failure itself, by crushing of the

concrete core, is characterized by high values of the contraction ε_v to which also corresponds the yielding of the longitudinal reinforcement. The stresses σ_{vr} of the concrete core measured at ultimate limit state are much higher than the uniaxial strength f_c. The increase in strength appears to depend linearly on the confining stress σ_{hr} given by the spiral:

$$\sigma_{vr} = f_c + \kappa\, \sigma_{hr}$$

Actually the different tests lead to significantly discordant values of κ: an estimate precise and reliable enough for such coefficient is still not available, with the consequence of the need to penalize the resisting effect of spirals with greater factors of safety.

Integrating therefore the assumptions with what results from the findings mentioned above, the equilibrium of the section at the ultimate limit state is:

$$N_r = A_n(f_{cd} + \kappa\sigma_{hr}) + A_1\sigma_{1r}$$

where the first term represents the contribution of the concrete core, the second one represents the contribution of the longitudinal reinforcement.

Since

$$\sigma_h = \frac{1}{2}\frac{A_w}{A_n}\sigma_w$$

setting $\sigma_{wr} = \sigma_{lr} = f_y$ and introducing the design values of the semi-probabilistic method, one eventually obtains

$$N_{Rd} = f_{cd}\left(A_n + \frac{f_{yd}}{f_{cd}}A_1 + \frac{\kappa f_{yd}}{2 f_{cd}}A_w\right) = f_{cd}A'_{ir}$$

where the homogenization coefficients of the two types of reinforcement (longitudinal and transverse) are distinguished by the factor $\kappa/2$. Assuming for example $\kappa = 4$ (see formula $\bar{\sigma}_1 = 1 + \bar{\sigma}_2$ of Sect. 1.1.3 for triaxial stress states with $\bar{\sigma}_1 \gg \bar{\sigma}_2 = \bar{\sigma}_3$), one obtains

$$N_{Rd} = f_{cd}A_n(1 + \omega_1 + 2\omega_w)$$

where it can be noted that, in terms of resistance contribution, the mechanical ratio $\omega_w = f_{sd}A_w/f_{cd}A_n$ of the confining reinforcement is weighed twice as much as the one of the longitudinal reinforcement. However, there is a limit $A_w \leq 2A_l$ for the confining reinforcement with respect to the longitudinal one, beyond which a failure by transverse shearing of the column occurs at lower load levels than the one deducible from the equation set above. The usual limitation to the longitudinal reinforcement ratio is to be eventually added, related to bond problems. Such limitation for confined columns can be set as $A'_{ir} \leq 2A_n$.

The comparison with the capacity of ordinary columns with stirrups can be deduced equating the contribution of reinforcement in the two cases:

$$\omega_1 = \omega_1 + 2\ \omega_w$$

which leads, for the same materials, to the relationship $A_s = (5/3)A_t$, having set $A_w = 2A_l$, having indicated with $A_t = A_l + A_w$ the total reinforcement of the confined column and with A_s the longitudinal reinforcement of the ordinary columns. Taking into account the additional presence of the stirrups, one can deduce that the circular arrangement allows to roughly halve the amount of reinforcement for the same capacity and the same size of concrete. This does not contemplate possible problems of shape, which is limited to the circle or the equilateral polygon for confined sections, nor economical problems which normally lead to prefer, where permitted, an increase in the area of concrete instead of the confining reinforcement.

In order to take into account a minimum load eccentricity, introducing for the confined columns the same reduction in concrete resistance as for the ordinary columns, one eventually obtains the (conservative) formula of the design resistance

$$N_{Rd} = f_{cd} A_n (0.8 + \omega_1 + 1.6\omega_w)$$

which reevaluates the contribution of longitudinal reinforcement with respect to concrete and its confining reinforcement.

2.1.3 *Effects of Viscous Deformations*

The formulas of elastic design presented before give the stresses for a short-term loading. Starting from these initial values, the permanence of loads leads to a slow redistribution of stresses between concrete and steel as a result of creep.

For an axial force N constant in time, the equilibrium of the section of Fig. 2.4 leads to equate the force increment that occurs in steel between time t and time $t + \mathrm{d}t$ to the decrement that simultaneously occurs in concrete:

$$A_s\ \mathrm{d}\sigma_s(t) = -A_c\ \mathrm{d}\sigma_c(t)$$

The compatibility formulated in the same time interval leads to equate the strain increments $d\varepsilon_s$ and $d\varepsilon_c$ of steel and concrete. The first one derives from the law of elasticity, the second one from the law of linear creep with variable stresses:

$$\varepsilon(t) = \frac{1}{E_c}\left\{\sigma(t) + \int_{t_0}^{t} \sigma(\tau)\Phi(t,\tau)\mathrm{d}\tau\right\}$$

where it is reminded that the creep kernel

$$\Phi(t,\tau) = -\frac{\partial\varphi(t,\tau)}{\partial\tau}$$

gives the elementary contribution of a load pulse $\sigma(\tau)\mathrm{d}\tau$ applied at the intermediate time τ (see Fig. 1.18b). If, for concrete loaded at an early age, an ageing model is assumed with:

$$\varphi(t,\tau) = c(t) - c(\tau)$$

one therefore obtains that each load pulse produces creep effects only within the interval of application contiguous to τ. These effects remain then unchanged:

$$\Phi(t,\tau) = -\frac{\partial\varphi(t,\tau)}{\partial\tau} = \Phi(\tau) = \left[\frac{\partial\varphi(t,\tau)}{\partial\tau}\right]_{t=\tau}$$

From the fundamental theorem of calculus one obtains in this case

$$\frac{\mathrm{d}}{\mathrm{d}t}\int_{t_0}^{t}\sigma(\tau)\Phi(\tau)\mathrm{d}\tau = \sigma(t)\Phi(t) = \sigma(t)\frac{\mathrm{d}\varphi(t)}{\mathrm{d}t}$$

which allows to eventually write the compatibility equation as

$$\frac{\mathrm{d}\sigma_\mathrm{s}(t)}{E_\mathrm{s}} = \frac{\mathrm{d}\sigma_\mathrm{c}(t)}{E_\mathrm{c}} + \frac{\sigma_\mathrm{c}(t)}{E_\mathrm{c}}\mathrm{d}\varphi(t)$$

Replacing now in this equation the value $\mathrm{d}\sigma_\mathrm{s} = -\mathrm{d}\sigma_\mathrm{c}/\rho_\mathrm{s}$ derived from the equilibrium, one has (with $\alpha_\mathrm{e} = E_\mathrm{s}/E_\mathrm{c}$ and $\psi_\mathrm{s} = \alpha_\mathrm{e}\rho_\mathrm{s}$):

$$-\left(1+\frac{1}{\psi_\mathrm{S}}\right)\mathrm{d}\sigma_\mathrm{c} = \sigma_\mathrm{c}\mathrm{d}\varphi$$

Setting for briefness

$$\beta = \frac{\psi_\mathrm{s}}{1+\psi_\mathrm{s}}$$

one obtains the differential equation

$$\frac{\mathrm{d}\sigma_\mathrm{c}}{\sigma_\mathrm{c}} = -\beta\mathrm{d}\varphi$$

with separation of variables which, integrated between t_o and t, leads to:

$$\ln \sigma_c(t) - \ln \sigma_{co} = -\beta\, \varphi(t)$$

with $\sigma_{co} = \sigma_c(t_o)$ and $\varphi(t_o) = 0$. Stresses in concrete therefore decrease, starting from an initial value

$$\sigma_{co} = \frac{N}{A_c + \alpha_e A_s} = \frac{N}{A_c(1+\psi_s)}$$

with an exponential rate:

$$\sigma_c(t) = \sigma_{co}\, e^{-\beta\varphi(t)}$$

down to stabilization on the final value

$$\sigma_{c\infty} = \sigma_{c0}\, e^{-\beta\varphi_\infty}$$

to which for equilibrium corresponds in steel the stress

$$\sigma_{s\infty} = \frac{N - A_c\sigma_{c\infty}}{A_s} = \frac{1+\psi_s - e^{-\beta\varphi_\infty}}{\rho_s}\sigma_{co}$$

The ratio between stresses in the two materials becomes:

$$\alpha_e^* = \frac{\sigma_{s\infty}}{\sigma_{c\infty}} = \alpha_e \frac{1+\psi_s - e^{-\beta\varphi_\infty}}{\psi_s - e^{-\beta\varphi_\infty}} = \alpha_e\left(\frac{e^{\beta\varphi_\infty}}{\beta} - \frac{1}{\psi_s}\right)$$

which allows to apply under viscoelastic conditions the same formulas of the elastic design where the *modified coefficient* α_e^* is to be introduced for the homogenization of steel areas, properly increased with respect to the elastic short-term one α_e. A *viscoelastic reinforcement ratio* can therefore be defined

$$\psi_S^* = \alpha_e^* \rho_s$$

with which one can estimate the final stresses

$$\sigma_{c\infty} = \frac{N}{A_c\left(1+\psi_s^*\right)}$$
$$\sigma_{s\infty} = \alpha_e^* \sigma_{c\infty}$$

In order to show the order of magnitude of creep effects in a reinforced concrete column, let us consider a section with $\rho_s = 0.008$, $\alpha_e = 6$ and $\varphi_\infty = 2.4$.

With those values one can deduce (with $\psi_s = 0.048$ and $\beta = 0.0458$):

$$\alpha_e^* = \left(\frac{e^{\beta\varphi_\infty}}{\beta} - \frac{1}{\psi_s}\right)\alpha_e = 3.54\alpha_e$$
$$\psi_e^* = \alpha_e^*\rho_s = 0.170$$
$$\sigma_{c\infty} = \frac{1+\psi_s}{1+\psi_s^*}\sigma_{co} = 0.896\sigma_{co}$$
$$\sigma_{s\infty} = \frac{\alpha_e^*\sigma_{c\infty}}{\alpha_e^*\sigma_{co}}\sigma_{so} \cong 3.17\sigma_{so}$$
$$\varepsilon_\infty = \frac{\sigma_\infty}{\sigma_{so}}\varepsilon_o \cong 3.17\varepsilon_o$$

It can be noted how, further to a limited reduction of stresses in concrete, stresses in steel can increase more than three times. Further significant increases are caused by the shrinkage as analysed in Sect. 2.2.1.

If one assumed the approximate technical method (see Sect. 1.3.3), evaluating creep effects on the basis of the initial stress in concrete, one would have:

$$\Delta\varepsilon = \frac{\sigma_{co}}{E_c}\varphi_\infty = 2.40\varepsilon_o$$
$$\Delta\sigma_s = E_s\Delta\varepsilon = \alpha_e\sigma_{co}\phi_\infty = 2.40\sigma_{so}$$
$$\Delta\sigma_c = -\rho_S\Delta\sigma_s = -\psi_s\sigma_{co}\phi_\infty = 0.115\sigma_{co}$$
$$\sigma_{c\infty} = \sigma_{co} - \Delta\sigma_c = 0.885\sigma_{co}$$
$$\sigma_{S\infty} = \sigma_{so} - \Delta\sigma_s = 3.40\sigma_{so}$$
$$\varepsilon_\infty = \varepsilon_o - \Delta\varepsilon = 3.40\varepsilon_o$$

with the overestimation of the effects.

Instead, if one assumed the effective modulus method (EMM of Sect. 1.3.3), evaluating the creep effects on the basis of the final stress in concrete, one would have:

$$E_c^* = \frac{E_c}{1+\phi} = \frac{E_c}{3.40}$$
$$\alpha_e^* = E_s/E_c^* = 3.40\alpha_e$$
$$\psi_s^* = \alpha_e\rho_s = 0.163$$
$$\sigma_{c\infty} = \frac{1+\psi_s}{1+\psi_s^*}\sigma_{co} = 0.901\sigma_{co}$$
$$\sigma_{s\infty} = 3.40 \times 0.90\ \sigma_{so} = 3.06\ \sigma_{so}$$
$$\varepsilon_\infty = 3.06\,\varepsilon_o$$

with the underestimation of the effects.

Effects on Strength

In order to evaluate the creep effects on the ultimate strength, the load history should be followed considering first the application of permanent actions, then the development of the consequent creep deformations with relative redistributions of stresses and eventually the final increase of variable loads up to failure. The conventional procedure starts from the characteristic values of permanent loads.

The σ–ε diagrams of the materials of Fig. 2.9 show an initial short-term segment *O-A* essentially linear also for concrete. The slow rearrangement of the section

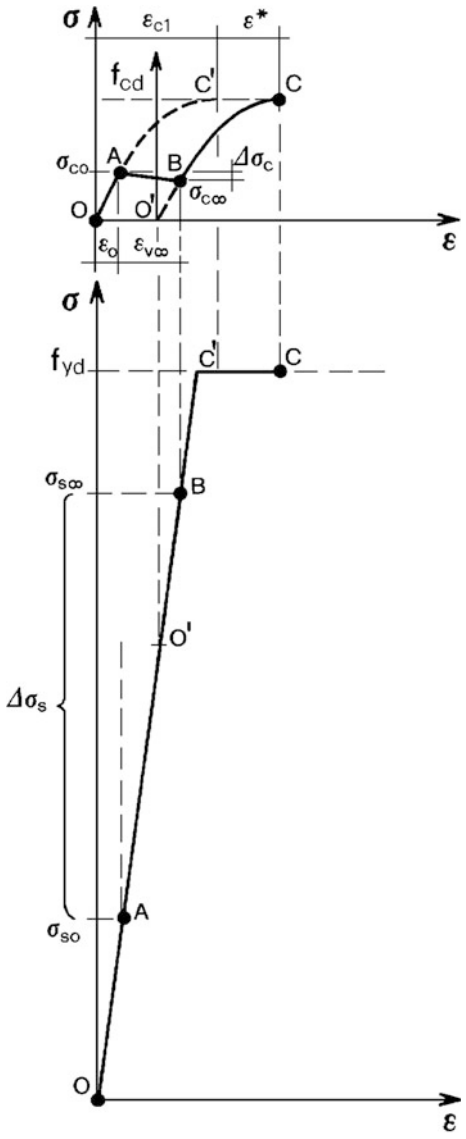


Fig. 2.9 Creep effects on stress–strain diagrams

follows (segment *A*-*B*) which shifts by $\varepsilon_{v\infty}$ in obedience to the laws of equilibrium and viscoelastic compatibility developed above.

The creep process led at its end to an increase $\Delta\sigma_s$ of the stress in steel and to a complementary relaxation $\Delta\sigma_c$ of the stress in concrete. Then a new instantaneous load follows the shifted σ_c-ε curve shown in the Fig. 2.9.

For example, in order to decompress concrete (segment *B*-*O'*) an expansion $\sigma_{c\infty}/E_c$ ($<\varepsilon_o$) would be necessary. At the same time steel would unload by $\alpha_e\sigma_{c\infty}$. At the new origin *O'* a residual stress $\sigma_{s\infty}$-$\alpha_e\sigma_{c\infty}$ would therefore remain in the reinforcement. The unloading of the external actions would lead to self-stresses $\sigma_c = \Delta\sigma_c$ in tension in concrete and $\sigma_s = \Delta\sigma_s = -\Delta\sigma_c/\rho_s$ in compression in steel, with a residual contraction of the column equal to $\Delta\sigma_s/E_s$.

If the load is increased from *B* up to failure, the point *C* of the shifted curve is reached, with a contraction greater by $\varepsilon^* = \varepsilon_{v\infty} - \Delta\sigma_c/E_c$ with respect to the contraction ε_{c1} of a short-time loading.

With respect to the model for the resistance verification of the section under short-term loading, valid for the initial stages, the one at t_∞ requires the simple translation of the diagram σ_c-ε by a segment

$$\varepsilon^* = \varepsilon_{v\infty} - \frac{\Delta\sigma_c}{E_c} = \frac{\Delta\sigma_s}{E_s}\left(1 - \alpha_e\frac{\Delta\sigma_c}{\Delta\sigma_s}\right) = \frac{\Delta\sigma_s}{E_s}(1+\psi_s)$$

The ultimate resistance basically does not change since the stress $\sigma_s = f_{yd}$ in steel remains constant from *C'* to *C*:

$$N_{Rd} = A_c f_{cd} + A_s f_{yd}$$

In the case of high-strength steel for which $\varepsilon_{c1} < \varepsilon_{yd}$, the accumulation $\varepsilon_{c1} + \varepsilon^*$ of the contractions at failure leads to a delayed yield of reinforcement and to a final resistance capacity that is given again by the formula shown above.

2.2 Tension Elements

With the section on reinforced concrete tie elements, the fundamental topic of cracking is introduced, which will be analysed again and developed hereafter with reference to elements in bending. The topic is very broad, involving static, chemical and technological aspects, and good levels of accuracy in the relative applicative calculations have not currently been achieved. Criteria and methods remain still subject to considerable refinements.

Further to the analyses of the cracking process, the topic of prestressing is introduced, considered as measure to keep cracking within appropriate service limits. On one hand therefore the possibility to satisfy, even for elements in tension, specific functional requirements; on the other hand the possibility of the full use of the resources of high-strength steel, as it will be better clarified hereafter.

Taken for granted the safety with respect to collapse, cracking has nevertheless three orders of consequences:

- the *loss of tightness*, generally not relevant, in some cases related to functional requirements (such as waterproofing of tanks), in other cases seriously detrimental with respect to durability (such as freeze/thaw phenomena that can progressively disintegrate concrete if exposed in climates with strong daily temperature ranges around zero);
- the *aesthetic decay* associated to the possible evidence of the cracking pattern and the sense of apparent static deficiency which make it unacceptable to users;
- the *damage of protection* against corrosion of the reinforcement, provided by the appropriate concrete cover, with uncertain durability of the resistance.

2.2.1 Verifications of Sections

If one assumes that concrete resists in tension, deforming elastically with a modulus E_{ct}, the calculation of stresses in the section of a RC tie subject to an axial tension force N leads to the same formula deduced for columns. With the usual assumptions related to the uncracked section, equilibrium leads to

$$\sigma_c = \frac{N}{A_c + \alpha_{et} A_S} \qquad \sigma_S = \alpha_{et}\sigma_c$$

where $\alpha_{et} = E_s/E_{ct}$ is the coefficient of homogenization of the reinforcement area.

Such formulas are used for *serviceability verifications* that do not concern the ultimate capacity of the structure. In particular with those formulas, given $\sigma_c = f_{ctk}$, the limit of cracks formation is defined, according to what is specified later on. With respect to collapse instead, the tensile strength of concrete is not proven to be reliable enough. Certain phenomena, commonly neglected in the normal resistance calculations, can in fact contribute to early cracking, to a degree which is often difficult to estimate.

Effects of Shrinkage

Tensile stresses occur in concrete, even before that the structure is subject to service loads, because of shrinkage. For the cross section of an element in RC, such effect can be estimated imposing equilibrium and compatibility at time t to which the value $\varepsilon_{CS}(t)$ of shrinkage corresponds, related to concrete only:

$$A_S\sigma_S(t) + A_c\sigma_c(t) = 0$$
$$\frac{\sigma_S(t)}{E_S} = \frac{\sigma_c(t)}{E_{ct}} + \varepsilon_{cs}(t)$$

From the first equation one obtains:

$$\sigma_S(t) = -\frac{1}{\rho_S}\sigma_c(t)$$

which, substituted in the second one, leads to

$$\sigma_c(t) = -\beta E_{ct}\varepsilon_{CS}(t)$$

where

$$\beta = \frac{\psi_{st}}{1+\psi_{st}}$$

with $\psi_{st} = \alpha_{et}\ \rho_s$.

Assuming for the contraction $\varepsilon_{cs}(t)$ the absolute value, the negative sign of the formula indicates a tensile stress $\sigma_c(t)$.

In order to give a qualitative indication about this phenomenon, one can consider the same cross section analysed at Sect. 2.1.3 with respect to the creep effects in the columns. Given that the limited level of tensile stresses allows to assume an elastic modulus $E_{ct} = E_c$, con $\rho_S = 0.008$ and $\alpha_{et} = 6$ ($E_c \cong 34{,}000$ N/mm^2), for a final value of shrinkage $\varepsilon_{cs\infty} = 0.00036$ one has (with $\psi_{st} = 0.048$ and $\beta = 0.0458$):

$$\sigma_{c\infty} = -0.56\ \text{N/mm}^2 \quad \text{(tension)}$$
$$\sigma_{s\infty} = +70.1\ \text{N/mm}^2 \quad \text{(compression)}$$

High reinforcement ratios increase tensile stresses in concrete, reducing compressions in steel to a lesser extent. Creep mitigates the phenomenon with time, same as for the common permanent actions. Neglecting the effects of simultaneous interaction between the two phenomena, the self-induced stresses due to shrinkage can be interpreted as instantaneous initial values followed by the slow viscous relaxation of stresses. This can be evaluated using the criteria defined in Sect. 2.1.3.

For the same cross section analysed above, following the criterion of the fictitious Modulus which underestimates the reduction of self-induced stresses, with $\varphi_\infty = 2.4$, for example one would therefore have:

$$E^*_{ct} = E_{ct}/(1+\varphi_\infty) = E_{ct}/3.40; \quad \alpha^*_{et} = E_s/E^*_{ct} = 3.4\alpha_{et}$$
$$\psi^*_{st} = \alpha^*_{et}\rho_S = 3.4\psi_{st};$$
$$\beta^* = \psi^*_{st}/\left(1+\psi^*_{st}\right) = 0.1403$$
$$\sigma'_{c\infty} = -\beta^* E^*_{ct}\varepsilon_{cs\infty} = -0.90\sigma_{c\infty}$$
$$\sigma'_{s\infty} = -\sigma'_{ct}/\rho_S = 0.90\sigma_{S\infty}$$

with a reduction of 10% of the effects with respect to the initial values.

Cracked Section
Therefore in the RC ties, the self-induced stresses due to shrinkage, added to stresses due to external loads, induce early concrete cracks. If now the assumption of cracked sections with $f_{ct} = 0$ is made, the resisting part of the tie is limited to the only reinforcement steel. The calculation is simply reduced to

$$\sigma_S = \frac{N}{A_S}$$

and, at the ultimate limit state, according to the elastic-perfectly plastic model, the capacity is given by

$$N_{Rd} = f_{yd} A_S$$

whilst according to the bilinear model with hardening, the capacity is given by

$$N_{Rd} = f'_{td} A_S$$

These formulas verify safety to failure of the tie; they do not give any indication about the cracking pattern under service loads. And the cracking verification, according to criteria shown hereafter, could give more restrictive limits to the design of the tie member.

2.2.2 Prestressed Tie Members

If cracking in service is to be avoided or limited, prestressing has to be applied to the tie. Naming σ_p the stress in the special cable centred in the section, pretensioned at a value ε_{po} of the strain before being locked with concrete, and with σ_s the stress in the ordinary passive reinforcement, the elastic compatibility of the section is imposed as:

$$\frac{\sigma_c}{E_c} = \frac{\sigma_S}{E_S} = \frac{\sigma_p}{E_p} - \varepsilon_{po}$$

from which one has

$$\sigma_S = \alpha_e \sigma_c$$
$$\sigma_p = \alpha_e \sigma_c + \sigma_{po}$$

having indicated with $\sigma_{po} = E_S \varepsilon_{po}$ the pretension in the cable at concrete decompression ($\sigma_c = 0$).

For the equilibrium of the section subject to an axial force N coming from external loads, with obvious meaning of the symbols one has:

$$N = \sigma_c A_c + \sigma_S A_S + \sigma_p A_p$$

from which by substitution one obtains:

$$N = \sigma_c (A_c + \alpha_e A_S + \alpha_e A_p) + N_{po}$$

with

$$N_{po} = \sigma_{po} A_p$$

prestressing force in the tie.

For the *verification of stresses* in service one therefore obtains:

$$\sigma_c = \frac{N}{A_i} - \frac{N_{po}}{A_i}$$

which shows the positive contribution of prestressing in controlling tensile stresses in concrete, being able to fulfil, for ties also, the limit $\sigma_c \leq 0$ which leads to $N \leq N_{po}$.

The equivalent area of the section equalized to concrete is given by

$$A_i = A_c\left(1 + \alpha_e \rho_S + \alpha_e \rho_p\right) = A_c(1 + \alpha_e \rho_t) = A_c(1 + \psi_t)$$

where the total area of reinforcement $A_t = A_s + A_p$ is equalized with the usual coefficient of homogenization $\alpha_e = E_s/E_c$, whilst in relative terms the increasing contribution is expressed in terms of the reinforcement elastic ratio $\psi_t = \alpha_e \rho_t = \psi_S + \psi_p$.

Imposing $N = 0$, the self-induced stresses due to prestressing, corresponding to the absence of external loads, are obtained as:

$$\sigma_c = -\frac{N_{po}}{A_i}; \quad \sigma_S = -\alpha_e \frac{N_{po}}{A_i}; \quad \sigma_p = \sigma_{po} - \alpha_e \frac{N_{po}}{A_i}$$

showing compressive stresses in concrete and passive reinforcement, tensile stresses in the pretensioned reinforcement. This situation is indicated by the dots in the diagrams of Fig. 2.10.

Under the assumption of *cracked section*, for $\sigma_c > 0$ (in tension), the equilibrium with the external force N is to be related to the steel part only of the section, both passive and pretensioned:

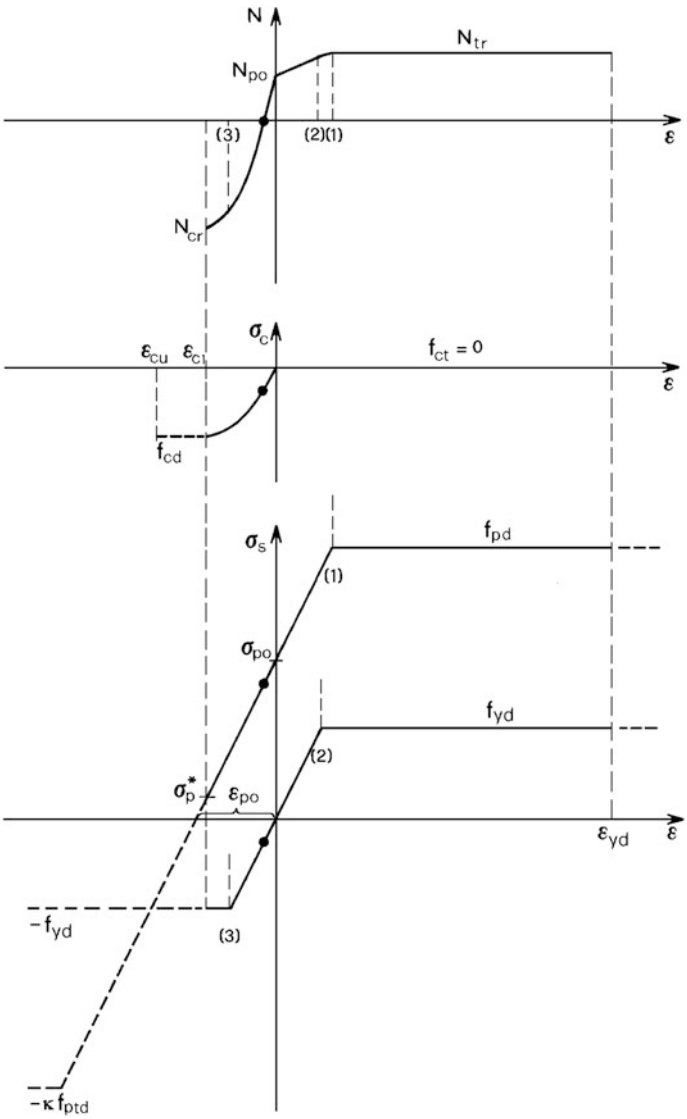


Fig. 2.10 Stress–strain diagrams of a prestressed tie

$$N = \sigma_s A_s + \sigma_p A_p$$

and with the addition of elastic compatibility which leads to $\sigma_p = \sigma_s + \sigma_{po}$ one obtains

$$\sigma_S = \frac{N}{A_t} - \frac{N_{po}}{A_t}$$
$$\sigma_p = \frac{N}{A_t} + \beta\frac{N_{po}}{A_t}$$

with $\beta = A_s/A_p$. If the elastic-perfectly plastic σ–ε model is adopted for both reinforcements, passive and pretensioned, the *ultimate resistance* in tension is defined by a value of the elongation to which the yielding of both reinforcements corresponds. In this case one therefore obtains

$$N_{Rd} = f_{yd}A_S + f_{yd}A_p$$

formula that does not depend on the initial stress σ_{po} in the cable. Prestressing therefore does not affect the ultimate capacity of the tie, whereas it has significant effects on the serviceability states where there is still an elastic behaviour of the materials.

Adopting the bilinear model with hardening, failure of the tie in tension is determined by the ultimate strain ε_{pud} of prestressing steel, which is the less ductile and was already subject pretensioning ε_{po} before being locked with concrete. At this ultimate limit, the passive steel has reached the strain

$$\varepsilon_S = \varepsilon_{pud} - \varepsilon_{po} < \varepsilon_{ud}$$

The ultimate capacity therefore becomes

$$N_{Rd} = \sigma_S A_S + f'_{ptd}A_p$$

with $\sigma_s = \sigma_s(\varepsilon_s)$. Having for common materials $\varepsilon_s > \varepsilon_{yd}$, one has

$$\sigma_S = f_{yd} + E_1(\varepsilon_S - \varepsilon_{yd})$$

In this case, prestressing ε_{po} affects directly the resistance of the tie by the reduction of the strain ε_s of passive reinforcement and therefore of its contribution to the rupture limit. The effect is small and, once again, prestressing remains determining for serviceability limit states.

Other than limiting tensile stresses in concrete and affecting the cracking pattern, prestressing affects the *stress ranges* under variable loads. In fact, if the prestressed tie is designed to remain uncracked (with $\sigma_c < f_{ctk}$), a variation ΔN of axial force induces in the reinforcement steel a variation

$$\Delta\sigma_S = \Delta\sigma_p = \alpha_e\frac{\Delta N}{A_i}$$

significantly lower than the one that would occur in the cracked section, where one would have

$$\Delta\sigma_S = \Delta\sigma_p = \frac{\Delta N}{A_t}$$

In relative terms, the range limitation is in the ratio of

$$\frac{\alpha_e A_t}{A_i} = \frac{\psi_t}{1+\psi_t}$$

Such effect is very important with respect to fatigue resistance of steel in structures subject to repeated loading cycles.

For external *compression* forces the prestressed tie obviously does not work well, as it can be deduced from the diagrams of Fig. 2.10. In service in fact the stresses σ_c in concrete become greater, whereas at ultimate failure limit the prestressing reinforcement is barely utilized or even counterproductive, as in the case of stresses σ_p^* that, at the limit strain ε_{c2} of the section, remain in tension.

2.2.3 Cracking in Reinforced Concrete Ties

In order to analyse the origin of the cracking process, let us consider the element of Fig. 2.11, made of concrete with one hypothetical reinforcing bar of diameter ϕ cast-in along its centreline. Let the element be initially completely uncracked and let us start loading it with a tension force N, of low magnitude, applied at the ends of the steel bar.

After the end segments of a length λ necessary for the diffusion of the force from steel to the entire section, a stress state is established in the entire internal segment of the element which can be calculated with the formulas obtained earlier:

$$\sigma_c = \frac{N}{A_c + \alpha_{et} A_S}; \quad \sigma_S = \alpha_{et}\sigma_c$$

which could be integrated with the contribution of shrinkage and creep. As long as the stress σ_c in concrete remains lower than its tensile strength, such stress state remains qualitatively unchanged, as indicated by the diagrams "a" of Fig. 2.11, where in particular it is to be noted how the bond stress τ_b is activated in the segments of incomplete stress diffusion.

Let us now imagine to increase the force N up to values of σ_c very close to the rupture values. At this point, in the internal segment of the element, where there is a complete distribution of stresses on the entire section, a first crack can arise, located where, due to the variability of the characteristic strength parameters, a section

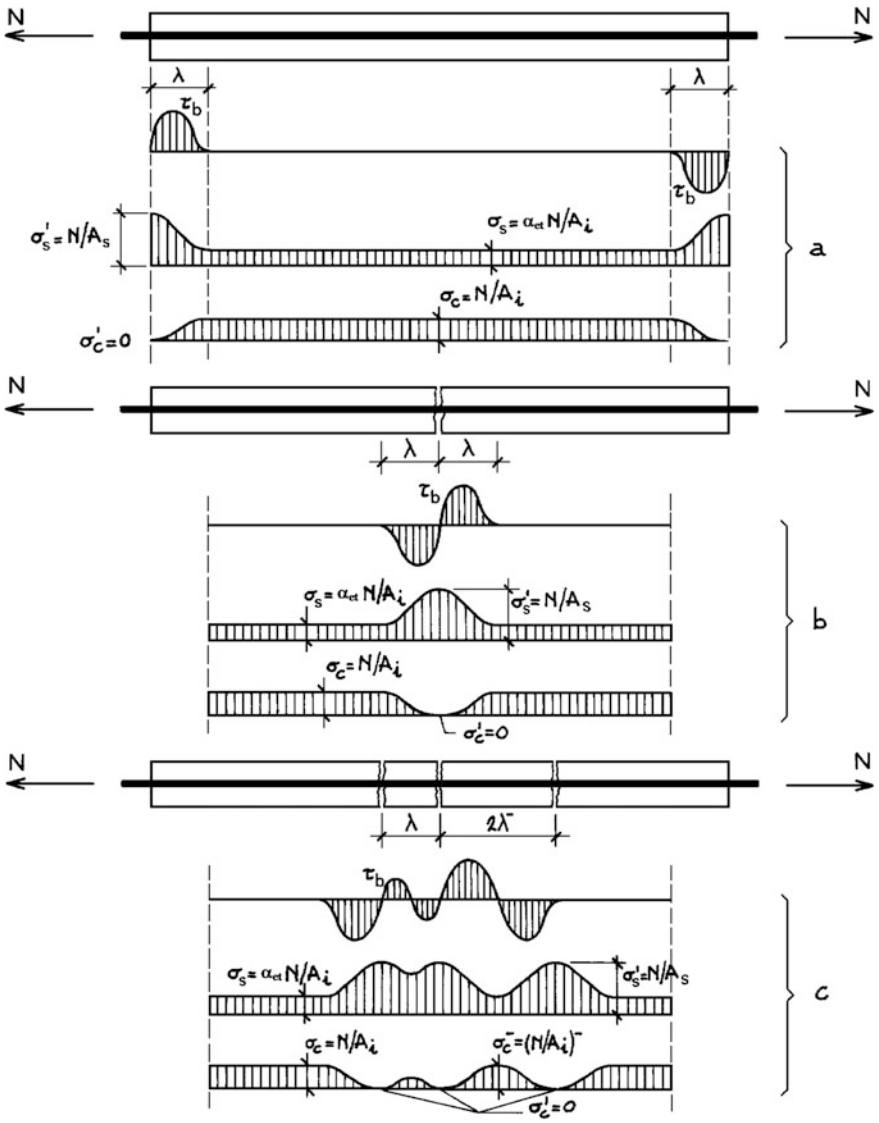


Fig. 2.11 Cracking process in a RC tie

weaker than the others is situated. A new stress state is therefore established, as described by the diagrams "b" of Fig. 2.11, with stresses in the rebar that vary from

$$\sigma'_{\mathrm{S}} = \frac{N}{A_{\mathrm{s}}}$$

at the crack location, to the value σ_S of segments with complete force diffusion, and with stresses in concrete that vary in parallel from 0 to σ_c.

When the force N increases up to overcome the tensile strength of concrete, cracking extends to the entire tie. The minimum distance of a possible subsequent crack from the first one is the parameter λ which characterizes the required length for the complete diffusion of stresses in the section, because only after such length the stress σ_c can reach its maximum value.

The process is qualitatively represented in the diagrams "c" of Fig. 2.11, with the lower and upper limits within which the actual crack spacing s can randomly vary

$$\lambda \leq s < 2\lambda$$

being $s = 2\lambda$ the first value of the distance which allows stress σ_c to reach its maximum value and therefore to introduce a new intermediate crack.

Further increments of N beyond the value of crack formation induce the progressive opening of already existing cracks. Few new cracks can still open in the middle of the longest segments; then the configuration stabilizes with crack widths progressively greater until, for high values of steel strain, bond itself fails.

Crack Spacing

In order to calculate the minimum distance λ between adjacent cracks let us consider the situation of Fig. 2.12 relative to a segment of a tie of length $2\ \lambda$. Given that the equilibrium of an infinitesimal segment of bar of length dx

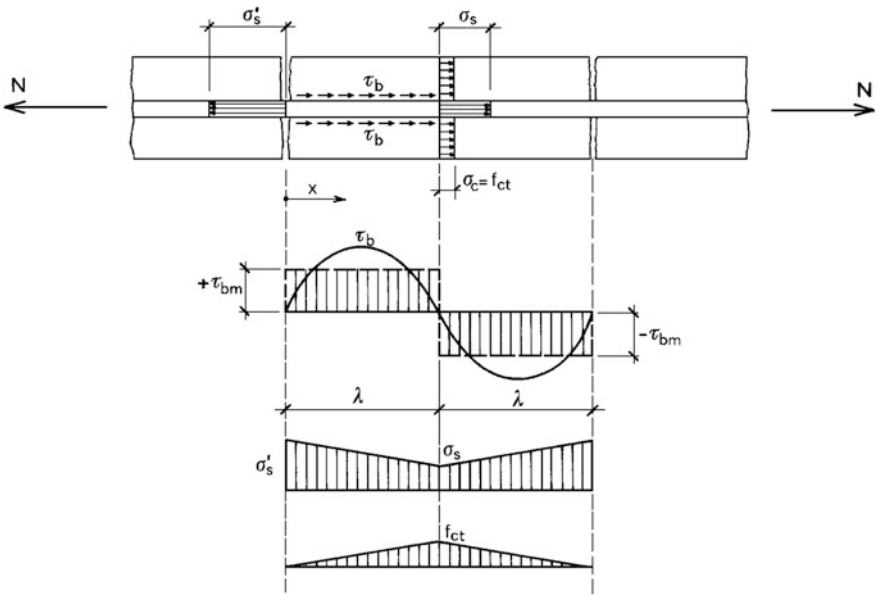


Fig. 2.12 Crasck spacing—equilibrium condition

$$A_s d\sigma_s(x) = \pi\phi\tau_b(x)dx$$

leads to express the bond stress in terms of the first derivative of the stress in the steel along the tie:

$$\tau_b(x) = \frac{\phi}{4}\frac{d\sigma_x(x)}{dx}$$

approximating the trend of bond stresses to the constant mean value τ_{bm}, a linear model follows for stresses variations $\sigma_s(x)$ as well as for the complementary stresses in concrete which vary along the centreline following the equilibrium $\sigma_s(x)$ $A_s + \sigma_c(x)A_c \equiv N$. These diagrams are shown in Fig. 2.12, where in particular, at the limit of crack formation, concrete maximum stress is equal to $\sigma_c = f_{ct}$.

For the equilibrium of half segment, one therefore has

$$N = \sigma'_s A_S = \sigma_S A_S + f_{ct} A_c$$

which leads to

$$\Delta\sigma_s = \sigma'_S - \sigma_S = \frac{1}{\rho_S} f_{ct}$$

The equilibrium of half part of the bar is therefore set as

$$A_s \Delta\sigma_s = \int_0^{\lambda} \pi\,\phi\,\tau_b(x)\,dx$$

which, with the constant model mentioned above, becomes

$$\frac{\pi\phi^2}{4}\Delta\sigma_s = \pi\,\phi\,\tau_{bm}\lambda$$

One therefore obtains

$$\lambda = \frac{\phi}{4}\frac{\Delta\sigma_s}{\tau_{bm}} = \frac{1}{4}\frac{\phi}{\rho_s}\frac{f_{ct}}{\tau_{bm}}$$

and, introducing for the bond stress the resisting value $f_b = \beta_b f_{ct}$ introduced in Sect. 1.4.3, one therefore has

$$\lambda = \frac{1}{4}\frac{\phi}{\rho_s}\frac{1}{\beta_b}$$

where β_b is the effective contact ratio.

The distance between adjacent cracks is greater for big bar diameters and for small reinforcement ratios. Even the bond parameter β_b has an influence on the spacing λ, which is smaller for ribbed bars with respect to the smooth ones.

In order to determine the crack width w, with a simplified formulation which assumes an elastic behaviour of the materials and approximates the diffusion of stresses according to the models presented above, one can calculate the difference between the elongation of the bar and the elongation of the concrete between two cracks that delimits the segment of Fig. 2.12. One therefore has, with obvious meaning of symbols:

$$w = 2(\Delta\lambda_s - \Delta\lambda_c)$$

with

$$\Delta\lambda_s = \int_0^{\lambda} \frac{\sigma_s(x)}{E_s} dx = \frac{\sigma'_s + \sigma_s}{2E_s}\lambda = \frac{2\sigma'_s - \Delta\sigma_s}{2E_s}\lambda$$

$$\Delta\lambda_c = \int_0^{\lambda} \frac{\sigma_c(x)}{E_c} dx = \frac{f_{ct}}{2E_c}\lambda$$

The second contribution is small, given the low mean value $f_{ct}/2$ of stresses and it is uncertain in relation to the actual distribution of stresses in the concrete segment. Therefore, neglecting the concrete strain, the crack with w_{om} relative to a segment of unit length is given by the mean value of the strain of the steel bar:

$$w_{om} = \varepsilon_{sm} = \frac{\Delta\lambda_s}{\lambda} = \frac{\sigma'_s}{E_s} - \frac{1}{2}\frac{\Delta\sigma'_s}{E_s} = \frac{\sigma'_s}{E_s} - \frac{f_{ct}}{2\rho_s E_s}$$

In this expression of strain, the first contribution represents the one of bare bar, the second contribution represents the stiffening effect of concrete in tension between the cracks ("tension stiffening").

It is to be noted that the summation of the widths of all cracks within a unit segment of a fully cracked tie does not depend on the crack spacing λ, but only on the stress in the bar calculated with the assumption of cracked sections, from the reinforcement ratio and from the tensile strength of concrete. Therefore, with the above-mentioned parameters unchanged, a greater crack spacing implies greater crack widths and vice versa.

In order to limit the crack *unit width* $w_{om} = \varepsilon_{sm}$, the stress in steel should be limited and concrete quality should be enhanced. In order to limit the *crack width*

$$w = w_{om} s$$

that is the width of individual cracks, ribbed bars and small diameters should also be used. The reinforcement ratio plays opposite roles: high ratio causes a greater but

more diffused cracking, with the diffusion effect prevailing which contributes to limit the width of individual cracks.

This formulation, based on much simplified theoretical assumptions, should be assumed as correct qualitative indication on the influence of the main parameters involved. It neglects certain important aspects of the phenomenon, such as the effects of the distribution of bars in the cross section. For a better quantification of the results, further deeper investigations should be carried, also with reference to the results of the experimental tests, as developed in the following chapter.

Eventually, the influence of other factor should be considered, such as the weakening of the sections in tension due to the stirrups, for which often the crack spacing corresponds to the spacing of the stirrups.

2.3 Cracking Calculations

With respect to the cracking verifications, structures can be in one of the following states:

- *cracked state in tension* if, even under a rare loading condition, the analysis of actions shows that the tensile concrete strength is exceeded;
- *uncracked state in tension* if this does not happen, not being able to exclude isolated cracks (e.g. due to shrinkage) which tend to open under tensile stresses, even if verified in the design under the tensile strength limit;
- *full compression state* (or, in less stringent terms, in low tension) where the absence of cracks is guaranteed.

The three states are defined by two limits:

- *the cracks formation limit* corresponding to the attainment of the tensile concrete strength ($\sigma_c = f_{ctk}$) in the uncracked section;
- *the decompression limit* corresponding to the zeroing of stresses ($\sigma_c = 0$) or, in less stringent terms, to the attainment of a very small tension limit (e.g. $\sigma_c = 0.25 f_{ctk}$) in the uncracked section.

In the cracked state, the resistance verifications shall be carried with the usual assumption of cracked sections, and the cracking verifications are addressed to the calculation of the width w according to the models specified hereafter for the full stabilized cracked stage of the tie. In the uncracked state in tension, the resistance verifications shall again be related to the cracked section, whereas the verifications of the crack width, where required, should be related to the possible isolated crack. In the full compression state the section remains uncracked while obviously no crack width verification is required.

With reference to their width w, one can indicatively distinguish:

- *capillary cracks* with $0.0 < w < 0.2$ mm (not visible to the naked eye, to be measured with special magnifying glasses);

- *small cracks* with $0.2 < w < 0.4$ mm (visible to the naked eye but not evident);
- *big cracks* with $0.4 < w < 0.8$ mm (evident if not covered by plaster or other coating).

Bigger cracks represent serious static damages. They should therefore be excluded in the design; if identified in existing structures, they should be verified, as they can indicate the beginning of the failure of bond or also the yielding of the reinforcement, and could require repairs, strengthening or remakings, or at least the application of protective coatings. At Sect. 2.3.3, after the description of the models for the calculation of the crack width, the relative verification criteria will be summarized in details.

2.3.1 The Cracking Process

When cracking arises, the reinforced concrete tie assumes the deformed shape indicated by the detail of Fig. 2.13. The fact that tensions reach zero value at the cracks locations generates an extensive unloading in concrete which, segment by segment, tends to shrink. At the same time the reinforcing bar, under the complementary increase in stresses, tends to lengthen more with respect to the previous configuration of uncracked cross sections. After an initial settlement δ corresponding

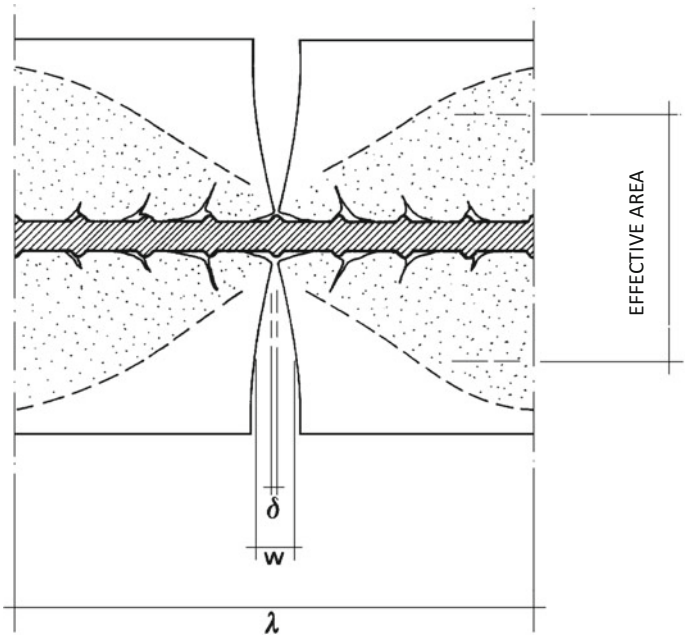


Fig. 2.13 Crack width

to the activation of the effective contacts, the relative slippage of the two materials is contrasted by bond. Thanks to this, part of the tensile force N in the tie, which is entirely concentrated in the reinforcing bar at the crack location, is diffused in the concrete segments as shown qualitatively with the dotted zones in Fig. 2.13. However, the gradual diffusion of stresses leaves concrete zones that are substantially unstressed, with a deformed shape of the segments which does not correspond anymore to plane sections. As indicated in Fig. 2.13, the crack itself is characterized by variable width, increasing with the distance from the reinforcement.

The phenomenon is approximated in the design, assuming an average behaviour through the segments, where the partial diffusion of stresses in concrete is represented by an effective area, reduced with respect to the actual area of the cross section, which depends on the position and distribution of the reinforcing bars. From these calculations a conventional value w of the crack width derives, on which verifications are empirically calibrated. However, these verifications are largely approximated because of the intrinsic difficulties of synthesizing in practical formulas the influence of numerous parameters in the various construction arrangements.

The overall behaviour of the tie, extended beyond the cracking limit, can be experimentally tested with the set-up of Fig. 2.14, measuring the elongation Δl. Correlating the values of the force N to the average elongation

$$\varepsilon_{sm} = \frac{\Delta 1}{1}$$

of the bar, diagrams similar to the one shown in Fig. 2.15 are obtained.

The curve of the experimental behaviour of the tie is therefore characterized by:

- segment OA uncracked up to the tensile failure limit of concrete, with a substantially linear trend that follows the straight line (with $\sigma_c = E_c\varepsilon$, $A_i = A_c + \alpha_e A_s$ *e* $\psi_s = \alpha_e A_s/A_c$):

$$N = \sigma_c A_i = \frac{1+\psi_s}{\psi_s} A_s E_s\ \varepsilon$$

- segment AB corresponding to the full cracking of the tie, with sudden reduction of the apparent stiffness due to the release of stresses in concrete and to the slippage of activation of bond contacts;

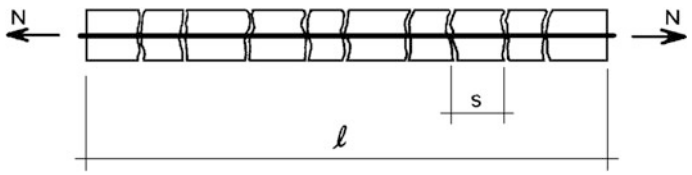


Fig. 2.14 RC tie—crack state

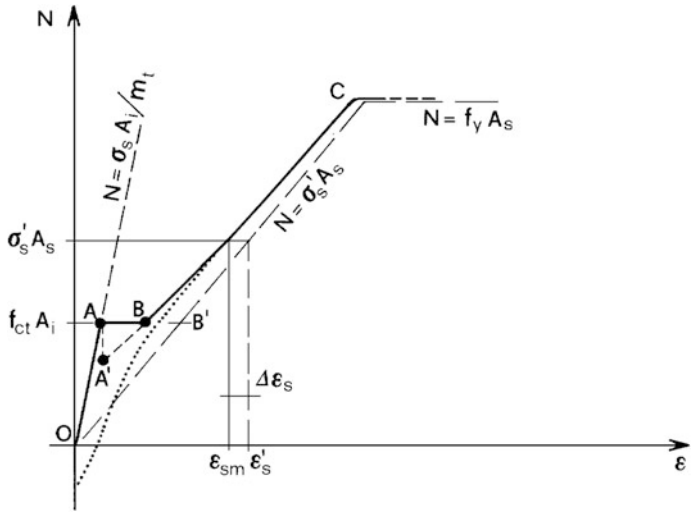


Fig. 2.15 Cracking of a RC tie—stress–strain diagram

- if the release of stresses in concrete was complete, the test would stabilize on the point B' of the line

$$N = \sigma'_S A_S = E_S A_S \varepsilon'_S$$

- whereas the segment BB' represents the tension stiffening, that is the stiffening effect given by the segments of concrete in tension between the cracks;
- if the test was performed under displacement control, the segment $AA'B$ would follow, with the relaxation of force instead of the increase of deformation;
- segment BC, with decreasing contribution of the concrete in tension due to cracking and slippage, up to steel yielding.

When the tie is unloaded, the behaviour follows the dotted segment of Fig. 2.15. Cracks gradually close up bringing their width value w to zero. However, friction prevents the complete recovery of slippage δ: for $N = 0$ steel remains in tension, concrete in compression on average. Just with the application of a compression force N it is possible to bring the strain ε_s to zero.

2.3.2 Crack Width

The average strain of steel reinforcement can be therefore read from the diagram of Fig. 2.15 as:

$$\varepsilon_{sm} = \varepsilon'_S - \Delta\varepsilon_S$$

where $\varepsilon'_s = \sigma'_s/E_s$ is the strain of the bare bar subject to the full force N, and $\Delta\varepsilon_s$ is the effect of tension stiffening that has been expressed from the theoretical point of view at Sect. 2.2.3 as $f_{ct}/(2\rho_s E_s)$. It can be observed experimentally that such effect is not constant, but decreases as the load increases: the *hyperbolic model* shows good fit with the measured data, decreasing with the stress σ'_s. With reference to the diagram of the behaviour transposed on the variable $\sigma'_s = N/A_s$ (see Fig. 1.16), where σ'_s and $\Delta\bar{\varepsilon}_s$ correspond to the point D of the theoretical cracks closure, one can therefore set:

$$\Delta\varepsilon_s = \frac{\bar{\sigma}'_s}{\sigma'_s}\Delta\bar{\varepsilon}_s$$

With this model one has:

$$\varepsilon_{sm} = \varepsilon'_s - \frac{\bar{\sigma}'_s}{\sigma'_s}\left(\bar{\varepsilon}'_s - \bar{\varepsilon}_{sm}\right)$$

which, with

$$\frac{\bar{\varepsilon}'_s}{\varepsilon'_s} = \frac{\bar{\sigma}'_s}{\sigma'_s}$$

leads to

$$\varepsilon_{sm} = \frac{\bar{\sigma}'_s}{\sigma'_s}\bar{\varepsilon}_{sm} + \varepsilon'_s\left[1 - \left(\frac{\bar{\sigma}'_s}{\sigma'_s}\right)^2\right]$$

If the first term is assumed to represent the average concrete strain ε_{cm}, decreasing as the force goes up because of the loss of bond (see Fig. 2.16), the second represents the average reinforcement strain related to the strain of concrete and therefore indicates the average unit crack width:

$$w_{om} = \varepsilon_{sm} - \varepsilon_{cm} = \frac{\sigma'_S}{E_S}\left[1 - \left(\frac{\bar{\sigma}'_s}{\sigma'_s}\right)^2\right]$$

With reference to the reinforcement stress calculated in the cracked section for the force corresponding to the tensile rupture of concrete:

$$\sigma'_{sr} = \frac{N_r}{A_s} = \frac{A_i f_{ct}}{A_s}$$

one can approximately set the origin of the hyperbolic model in:

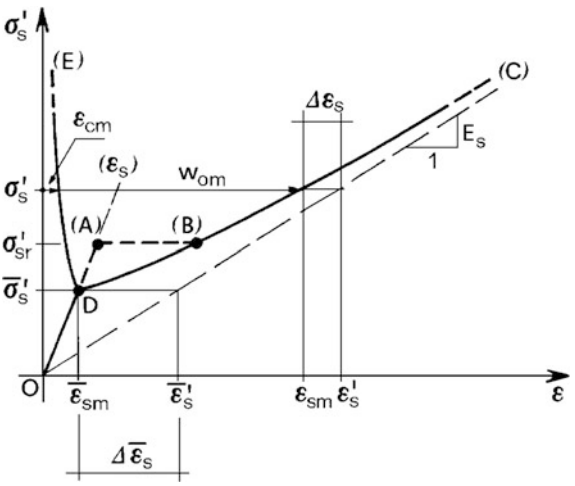


Fig. 2.16 Stress–strain cracking model

$$\bar{\sigma}'_{\mathrm{s}} \cong 0.7\sqrt{\beta^*}\sigma'_{\mathrm{sr}}$$

where the numerical coefficient represents the effect of the stress release in the concrete segments further to cracking and β^* synthesizes the influence of other main parameters:

$$\beta^* = \beta_{\mathrm{o}}\beta_1\beta_2$$

where $\beta_{\mathrm{o}}(\leq 1.0)$ indicates the effective reinforcement ratio that takes into account the distribution of the bars in the cross section, β_1 corresponds to the bond parameter already defined as the effective contact ratio (assumed here equal to 1.0 for ribbed bars, 0.5 for smooth bars), β_2 simulates the effects of duration and cycles of loads (=1.0 for the first load application, =0.5 for loads of long duration or repeated).

With those assumptions, the average unit crack width is given by

$$w_{\mathrm{om}} \cong \frac{\sigma'_{\mathrm{s}}}{E_{\mathrm{s}}}\left[1 - 0.5\beta_{\mathrm{o}}\beta_1\beta_2\left(\frac{\sigma'_{\mathrm{sr}}}{\sigma'_{\mathrm{s}}}\right)^2\right] \quad \text{for} \quad \sigma'_{\mathrm{S}} > \bar{\sigma}'_{\mathrm{S}}$$

$$w_{\mathrm{om}} = 0 \quad \text{for} \quad \sigma'_{\mathrm{S}} \leq \bar{\sigma}'_{\mathrm{S}}$$

It is to be noted that for prestressed ties, the average strain of reinforcement should be measured from the decompression of concrete. The stress σ'_{S} should therefore be replaced with the value $\sigma'_{\mathrm{p}} - \sigma_{\mathrm{po}}$.

Assuming now that the crack spacing varies between λ and 2λ, the crack width would therefore vary from

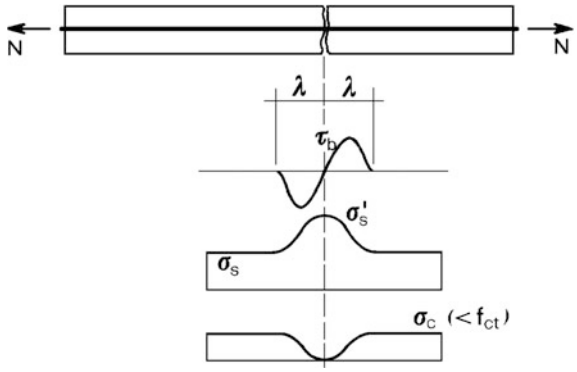


Fig. 2.17 Stress distribution around an isolated crack

$$w = \lambda w_{\text{om}} \quad \text{to} \quad w = 2\lambda w_{\text{om}}$$

In particular, for $\bar{\sigma}'_s < \sigma'_s < \sigma_{sr}$, the single crack width (see Fig. 2.17) is to be evaluated as

$$w = 2\lambda w_{\text{om}}$$

In Sect. 2.2.3 a formulation of λ has been given, with a simplified theoretical formulation, as a function of the bars diameter, the reinforcement ratio and the bond parameter. Experimental tests correct this expression with a binomial formula that also takes into account the edge distance c measured to the reinforcement centreline (see Fig. 2.18a):

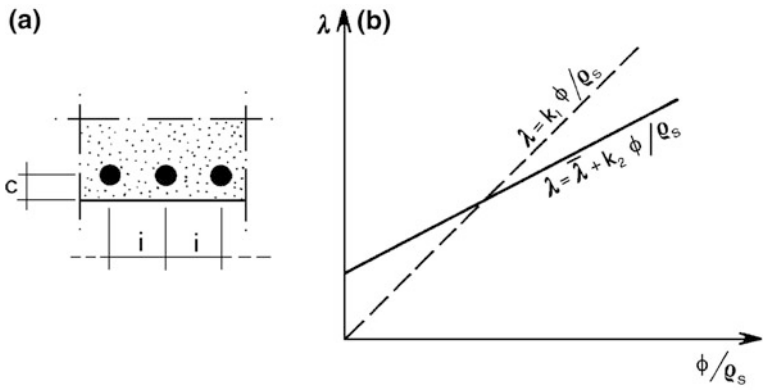


Fig. 2.18 Models for crack spacing

$$\lambda = c_o + \frac{0.1}{\beta_1}\left(\frac{\phi}{\rho_s}\right)$$

with $c_o = c - \phi/2$.

In this formula, the reinforcement ratio ρ_s should refer to the effective area consisting of a strip of thickness equal to $2.5c$. The two curves $\lambda = \lambda(\phi/\rho_s)$ are shown in Fig. 2.18b, the binomial empirical one with a solid line, the simplified theoretical one with a dashed line.

The formula of crack spacing shown above refers to the concrete layer surrounding the bar, with a width roughly equal to 5ϕ, which gives its protective cover against corrosion. When the spacing i between bars (see Fig. 2.18a) is largely greater than this value ($i \gg 5\phi$), in the intermediate portions a different cracking pattern occurs, characterized by a greater spacing, close to the transverse dimension of the element, and by a width of individual cracks proportionally greater. The concentration of width in few largely spaced cracks, even though it does not compromises the protection of reinforcement bars, can have negative aesthetic consequences because of the evidence of the phenomenon to the naked eye.

It is to be noted how the adopted model, with its point D (see Fig. 2.16), introduces a new limit state that is the one of (theoretical) *cracks re-closure*, which can be calculated equating stress $\sigma'_s = N/A_s$ to the value $\bar{\sigma}'_s$ defined above.

In Sect. 3.3 it will be also shown how, from the hyperbolic models of tension stiffening, a law of deformation of cracked sections can be deduced, with reference both to the axial deformations of ties and to the flexural curvatures of beams.

2.3.3 *Verification Criteria*

If well executed, respecting chemical requirements and technological prescriptions, concrete offers a good protection to reinforcement. The structural designer is responsible for the correct indication of the reinforcement position and the cracking verification.

The external concrete layer is subject to progressive carbonation along the time. This concerns indicatively a depth between 15 and 25 mm, beyond which the phenomenon is significantly reduced. Carbonation is the cause that triggers the oxidation process of steel. An adequate cover therefore has to be provided, otherwise oxidation starts and progressively extends, often with bulges, with consequent spalling and direct exposure of the reinforcement.

An excessive cracking opens the way for a deeper penetration of the phenomenon, whereas its speed of propagation is mainly related to three parameters:

- the *aggressiveness conditions* of the environment;
- the *percent duration* of exposure in the foreseen cracked state;
- the *sensitivity* of reinforcement to corrosion.

Apart from the more detailed indications of Table 2.1, the environments can be summarized into:

- *slightly aggressive*, ordinary environments with small humidity range (Classes: X0, XC1, XC2 and XC3 of Table 2.1);
- *moderately aggressive,* tidal, splash and spray zones or exposed to airborne salt (Classes: XD1 and XS1 of Table 2.1);
- *highly aggressive*, chlorides or sea waters (Classes: XD2, XD3, XS2 and XS3 of Table 2.1).

The percent duration of exposure is conventionally assumed in the different loads combinations:

- *rare*,
- *frequent*,
- *quasi-permanent.*

Concerning the propagation speed of the corrosion effects with respect to the initial strength, two types of reinforcement can be distinguished:

- *slightly sensitive*,
- *sensitive*,

the latter consisting in: small diameters ($\phi \leq 4$ mm), for which a given depth of oxidation has a high percent influence on the resisting cross section; tempered bars that exhibit surface microcracks, due to the thermal treatment undergone, open to a deeper penetration of corrosion; cold-hardened bars, in which surface microcracks open up under high tensile stresses ($\sigma_s > 390$ MPa).

Direct Analytical Criterion

The summary outline of the cracking verification criteria based on the calculation of crack width w can therefore be presented as indicated in the following table. The admissible limits of the width w_k correspond to $\bar{w}_1 = 0.2$ mm, $\bar{w}_2 = 0.3$ mm, $\bar{w}_3 = 0.4$ mm.

For the verification of crack openings according to the semi-probabilistic method, the conventional procedure is followed which assumes a characteristic value of the distance between cracks equal to

$$s_k = 2\lambda$$

and a characteristic value of the average unit width equal to

$$w_{ok} = kw_{om}$$

with $k = 1.7$.

The conventional width for the verifications is therefore obtained as:

$$w_k = s_k w_{ok}$$

and it shall be lower than the limit values $\bar{w}_i$ shown in the table.

Reinforce sensitivity	Environ. aggressive	State	Load combination	Verification	w_k
Slightly sensitive	Low	Cracked	Rare	–	–
			Frequent	Crack width	$\bar{w}_3$
			Quasi perm.	”	$\bar{w}_2$
	Medium	Cracked	Rare	–	–
			Frequent	Crack width	$\bar{w}_2$
			Quasi perm.	”	$\bar{w}_1$
	High	Cracked	Rare	–	–
			Frequent	Crack width	$\bar{w}_1$
			Quasi perm.	Re-closure	0
Sensitive	Low	Cracked	Rare	–	–
			Frequent	Crack width	$\bar{w}_2$
			Quasi perm.	”	$\bar{w}_1$
	Medium	Uncracked	Rare	Crack formation	–
			Frequent	Crack width	$\bar{w}_1^*$
			Quasi perm.	Re-closure	0*
	Medium	Uncracked	Rare	Crack formation	$\bar{w}_1^*$
			Frequent	Re-closure	0*
			Quasi perm.	Decompression	–

*Is referred to the width of the single isolated crack

Indirect Technical Criterion

The previous verification criterion, based on the analytical calculation of the crack width, appears to be conceptually correct. From the applicative point of view it is less effective because of the low accuracy of the formulas. Through the articulated verification workflow one arrives to an evaluation downgraded because of the modest precision of the elaborated data.

Currently, waiting for more reliable calculation models, the technical criterion that approximates certain parameters is in general preferable, which therefore also simplifies the verification of crack width, reducing it to a check of the stress level in the reinforcement.

The technical criterion is based on certain assumptions about the domain of validity and the limits of the concerned parameters:

- for the cracking unit width $w_{om} = \varepsilon'_S(1 - \kappa)$ with ribbed bars well distributed and under loads of long duration or repeated ($\beta_o = 1.0$, $\beta_1 = 1.0$ and $\beta_2 = 0.5$) a

variable stiffening contribution is assumed with σ'_{sr}/σ'_s indicatively from $\kappa \cong 0.25$ to $\kappa \cong 0.05$;

- requirements on the amount and distribution of reinforcement are imposed, for example with a distance between the bars $i \leq 5.0\phi$, to which a given empirical effective reinforcement ratio ρ^* corresponds;
- an average value of cover for longitudinal bars is assumed, for example with $c_o \cong 25$ mm.

Consequently, the cracks maximum spacing and the unit width are evaluated as a function of the bars diameter and the stress in steel (with $k = 1.7$):

$$s_k = 2\lambda = 2\left(c_o + \frac{0.1}{\beta_1}\frac{\phi}{\rho_s^*}\right) \cong 50 + 0.2\frac{\phi}{\rho_S^*}$$

$$w_{ok} = k\frac{\sigma'_s}{E_s}(1-\kappa) = \sigma'_s\left[1-\kappa(\sigma'_s)\right]/120000$$

Equating the expression of the crack width to the corresponding admissible limit value

$$w_k = s_k w_{ok} = \bar{w}_i$$

for the stress σ'_S calculated in the cracked section under the characteristic action of the pertinent load combination, the corresponding admissible value is eventually obtained with

$$\bar{\sigma}'_s = \sigma'_s(\bar{w}_i, \phi)$$

Based on these criteria, the tables of *admissible stresses* are given which, in the specified limits of applicability, implicitly satisfy the cracking width verifications.

For reinforcements sensitive to corrosion in environments mid or highly aggressive, the additional verifications for crack formation and decompression limit states are required under the appropriate loads combinations, whereas the verification of cracking re-closure is carried, still in terms of admissible stresses in steel, with $\sigma_s < \bar{\sigma}'_s$ (see Fig. 2.16).

The scheme of the verifications for ties according to the criteria mentioned above, in addition to the relative tables of admissible stresses, is shown in Chart 2.15 and Table 2.16.

Minimum Reinforcement

The cracking calculations presented here refers to the effects of static actions that are explicit tensile forces applied on the tie. Significant effects can also derive from geometrical actions such as shrinkage and thermal variations. The consequent self-induced stresses are added to the effects of external loads and, especially for redundant concrete sections, where the calculations lead to small reinforcement ratios, can cause excessive cracking.

Since self-induced stresses tend to extinguish when cracking arises, the adopted criterion consists of guaranteeing, independently from the external loads, a minimum amount of reinforcement capable of absorbing, at the yielding limit, the tensile force released by concrete when cracking:

$$A_s \geq A_c f_{ctm}/f_{yk}$$

With common materials this formula gives minimum reinforcement of about 0.7%.

2.4 Case A: RC Multi-storey Building

A first example of building on which numerical applications of the verification calculations are performed is represented by the multi-storey building whose typical plan and section are shown in Tables 1 and 2. It is a building of five storeys above ground with one basement level, with a rectangular plan, for residential use. The structural layout reflects a common typology, with some simplification of the layout with respect to the possible real configurations. This is with the aim of making easier the derivation of static schemes from the structural context.

A traditional cast in situ concrete building is assumed. The decks are made of clay blocks with interposed reinforced concrete ribs and a collaborating topping (see Fig. 2.20). The floor is spanning in the transverse direction with respect to the main side of the building and it is supported by three longitudinal beams, two edge beams within the floor thickness and a central deeper beam. There are transverse ribs to connect the main ones, in order to adequately distribute possible concentrate loads among them. At the two lateral edges the floors end with beams, more reinforced than the typical ribs, supporting the dead load of the cladding walls located there.

The edge beams consist of a solid strip of concrete, of the same thickness of the floor, containing the appropriate reinforcement. They sit on the corresponding row of columns, forming with these a supporting frame, resisting the actions coming from floors and the loads directly applied on the beams, such as the weight of the cladding walls. In the case under consideration the central beam is deeper than the floor, with a web that, together with the solid strip in the floor thickness, gives it the T shape. In addition to the internal row of columns, this beam sits on the walls of the staircase which, placed in a central position, splits it into two pieces, same as the edge beam of the inner façade.

The reinforced concrete walls of the staircase form a very rigid box structure. The lateral stability of the building relies on this central core to resist the expected horizontal forces. In Sect. 8.4 the analysis of the overall structural behaviour with respect to its global stability will be further developed. For now it is important to highlight how, with the horizontal elements connected to the central stability core, the individual vertical frames of the structure can be considered as non-sway frames: the small horizontal displacements allowed at different levels by the high

stiffness of the stability core have negligible effects on the other much flexible elements such as beams and columns.

From the synthetic description of works, it is clear that the multi-storey structure under analysis consists of a complex three-dimensional frame. In what follows the analysis of some elements of this frame will be performed, with approximated procedures based on the extraction of appropriate partial static schemes, mainly reduced to plane models of flexural behaviour. The global three-dimensional analysis would lead to an onerous calculation due to the high degree of redundancy of the structure. For a correct evaluation of internal forces, the variability of the structural configuration itself, further to the sequence of the execution stages of construction, should be taken into account. If set-up according to precise criteria that keep under control the degree of approximations introduced and their reliability limits with respect to safety, the simplified procedures give good technical solutions for the verification problems.

In the calculations that follow, reference is made to the European norm EN 1992-1-1:2004 "Eurocode 2: Design of Concrete Structures—Part 1: General rules and rules for buildings".

For the execution and functional purposes the structural layout is described in the *Design Documentation*, in which the structural designer transposes its work. This documentation consists of the *Construction Drawings* which will lead the execution on site and the *Design Report* which shows the analysis and the design calculations of the structures.

More details about the design report will be given in Sect. 3.4 of the following chapter. Certain general indications about the construction drawings are given here that should be considered only indicative since there can be significant variations based on the different structural typologies and the size of the works.

Usually, the basic reference is the overall design of the building described by *Drawings "A"* of the Architectural Design that give the *architectural arrangement* of the building, and by the relative *Drawings "B"* with the *construction details* of the works. For the structures, the competent designer should provide the *Drawings "C"* with indicated the general dimensions and the details of the concrete elements, as well as the *Drawings "D"* with the *reinforcement* detailing. For a building like the one examined in these pages, one can have, for example the following drawings (usually numbered in the order in which they are used on site according to the sequence of the works):

DRAWINGS "C" OF GENERAL ARRANGEMENT

DWG. C.1—Foundation Layout
DWG. C.2—Ground Floor Layout
DWG. C.3—Type Floor Layout
DWG. C.4—Roof Layout
DWG. C.5—General Sections

DRAWINGS "D" OF REINFORCEMENT

DWG. D.1—Foundation Details

DWG. D.2—Columns Tables
DWG. D.3—Ground Floor Slabs
DWG. D.4—Ground Floor Beams
DWG. D.5—Type Floor Slabs
DWG. D.6—Type Floor Beams
DWG. D.7—Roof Slabs
DWG. D.8—Roof Beams
DWG. D.9—Corewall
DWG. D10—Staircases Details

Sometimes, not for big constructions, the layout of the slabs reinforcement is directly incorporated in the General Arrangement drawing of the relative floor. Drawings of the type D.3, D.5 and D.7 can therefore be missing and the three concerned General Arrangement drawings can become:

DWG. CD.2—Ground Floor Layout and Slabs Reinforcement
DWG. CD.3—Type Floor Layout and Slabs Reinforcement
DWG. CD.4—Roof Layout and Slabs Reinforcement

Following the design applications, a few examples of construction drawings are shown in this volume, both for the General Arrangement (see Figs. 2.19, 2.20 and 12), and for the reinforcement (see Figs. 2.24, 3.48, 4.45, 5.50, 6.45, 8.25, 8.26, 8.31, 12, 13).

2.4.1 *Actions on Columns and Preliminary Verifications*

Analysis of Loads

For the analysis of loads applied on the bearing structure of the building, other than the dimensions of the structures themselves, finishes and occupancy as derived from the architectural design have to be considered. In these pages only a few construction elements are described, to show common examples of loads estimation. In Fig. 2.21 the different layers of the main types of walls are therefore indicated: the double external wall for the outer envelope of the building and the simple wall for internal partitions. Gravity loads are obviously evaluated as the product of volume and unit weight.

Double external wall

• external plaster	0.03×20	$= 0.60$	kN/m^2
• external hollow bricks	0.12×16	$\cong 1.90$	”
• rough plaster	0.02×20	$= 0.40$	”
• thermal insulation	0.03×1	$\cong 0.05$	”
• internal brickwork	0.06×11	$\cong 065$	”
• internal plaster	0.02×20	$= \underline{0.40}$	”
• tot per unit area of wall		$= 4.00$	kN/m^2

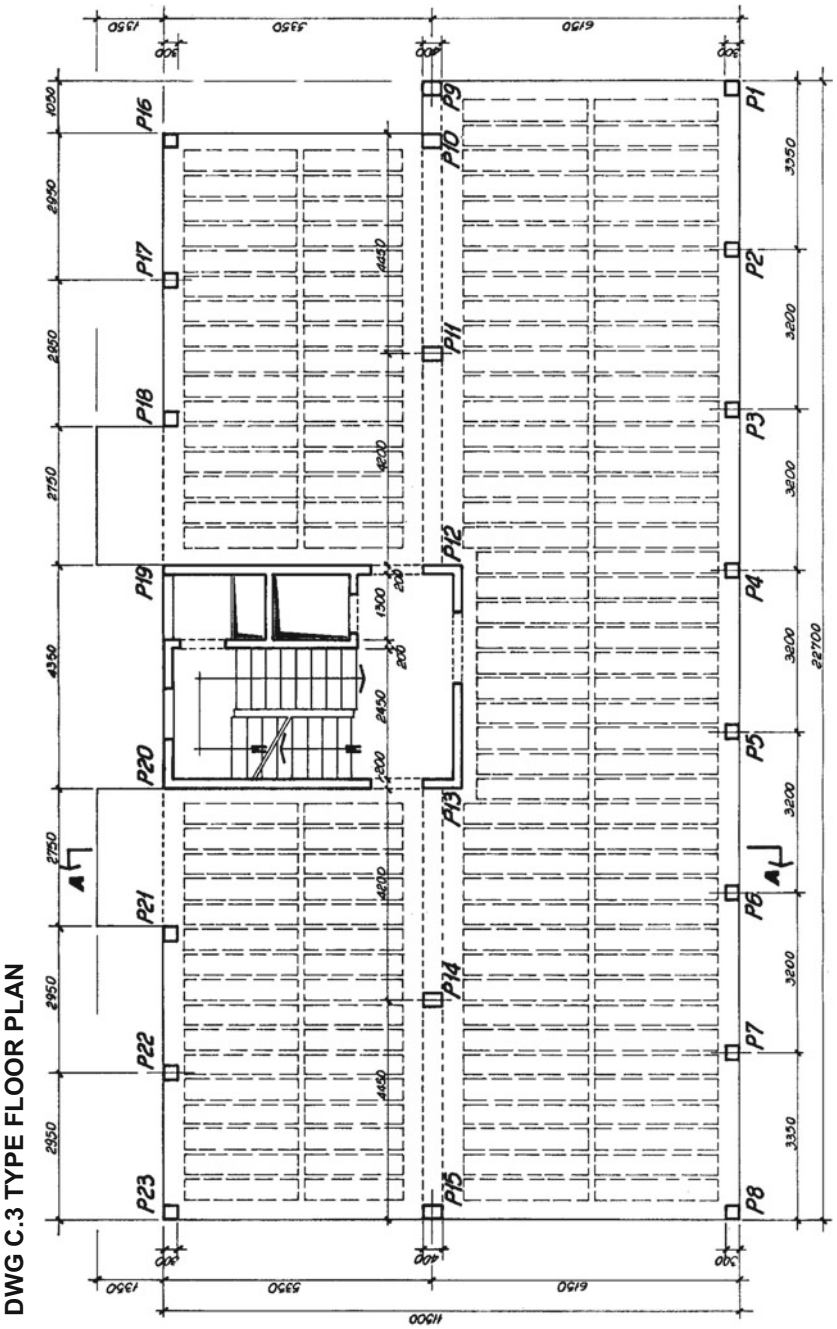


Fig. 2.19 Multistorey building—plan

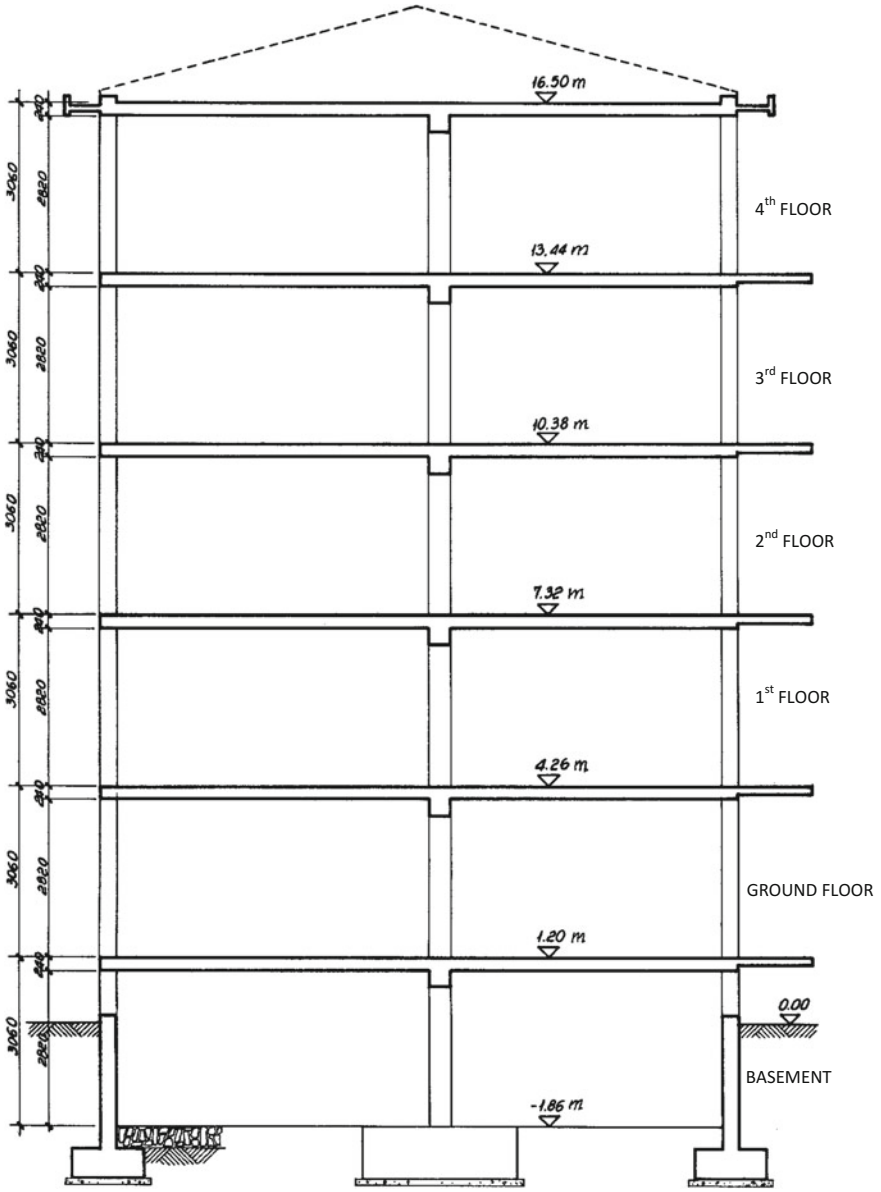


Fig. 2.20 Multistorey building—elevation

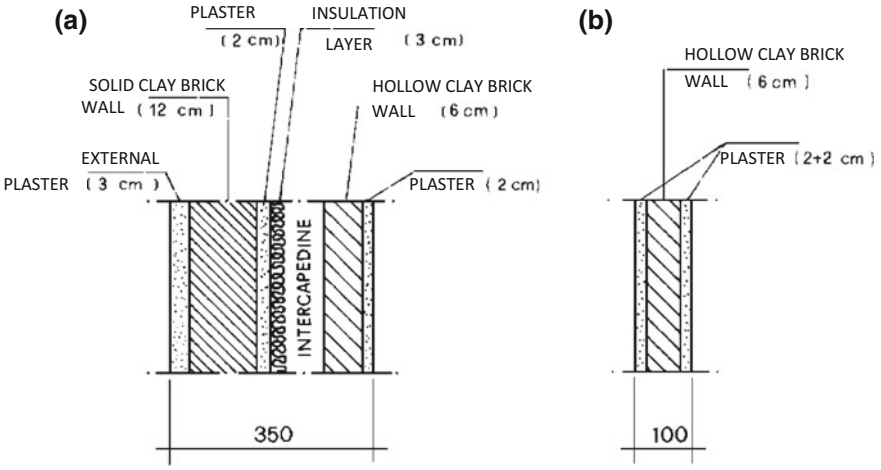


Fig. 2.21 Details of cladding (**a**) and partitioning (**b**) walls

Average dead load
(clear headroom 3.06 – 0.24 = 2.82 m)

• walls	2.82 × 4.00	≅ 11.30	kN/m
• openings incidence	−0.2 × 11.30	≅ −2.30	kN/m
at floor level per unit length of wall		= 9.00	kN/m

Simple partition

• plasters	2 × 0.02 × 20	= 0.80	kN/m^2
• brickwork	0.06 × 11	≅ 0.65	kN/m^2
tot per unit area of wall		= 1.45	kN/m^2
per unit length of wall	1.45 × 2.82	= 4.09	kN/m

Average dead load

• average load on plan 4.09/2.5	= 1.64	kN/m^2
• rounding	= 0.36	kN/m^2
tot per unit area of deck	= 2.00	kN/m^2

For what concerns the floors one can refer to the detail of Fig. 2.22 and to the dimensions of the deck shown in Fig. 2.19.

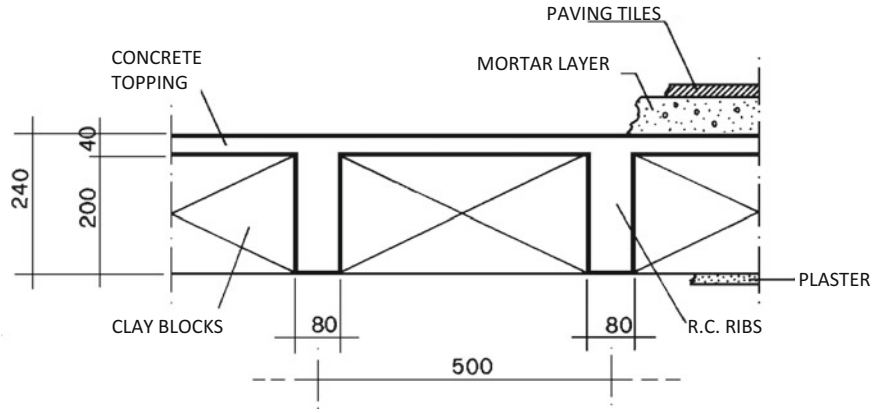


Fig. 2.22 Details of the floor

Type floor

• RC top slab	0.04 × 25	= 1.00	kN/m^2
• RC ribs	0.20 × 25 × 8/50	= 0.80	”
• hollow blocks	0.20 × 4*	= 0.80	”
tot per unit area of floor		= 2.60	kN/m^2

(*unit weight of hollow clay blocks ≅ 40 N/cm per square metre)
Average dead load

• current floor self weight		=2.60	kN/m^2
• incid. of solid ribs	(6.0 − 2.6) × 225/1150	≅0.65	”
• tot deck self weight		=3.25	kN/m^2
• flooring		=0.40	”
• screed (lightweight c.)	0.06 × 16	≅0.95	”
• plaster	0.02 × 20	=0.40	”
• distributed partitions		=2.00	”
tot permanent per unit area on plan		=7.00	kN/m^2

Variable loads

- live loads (residential) = 2.00 kN/m^2

For the roof a structure made of thin plates and bearing walls is assumed, sitting directly on the last horizontal floor, to form the slope of the pitched roof and an upper layer of common interlocking shingles.

Roof floor

• shingles	1.1^ × 0.60 ≅ 0.65	kN/m^2
• thin plates	1.1 × 0.35 ≅ 0.40	kN/m^2
• distributed bearing walls	1.5 × 0.65 ≅ 1.00	kN/m^2
• screed in lightweight concr.	0.08 × 16 ≅ 1.25	kN/m^2
• thermal insulation	0.03 × 1 ≅ 0.05	kN/m^2
• floor self-weight	= 3.25	kN/m^2
• plaster	0.02 × 20 = 0.04	kN/m^2
tot permanent per unit area on plan	= 7.00	kN/m^2

(^ projection of the pitched roof on plan)

Variable loads (snow)
(Zone 1, altitude $a_s < 200$ m, roof slope $\alpha < 30°$ with $\mu_d = 0.8$)

- variable load $0.8 \times 1.5 = 1.20$ kN/m^2

For the verification of column, variable loads at different floors of the building are assumed to occur with reduced intensity according to what is assumed in the characteristic combination***:

- top floor $1.0Q_o$
- lower floors $0.5Q_o + 1.0Q_1 + 0.7Q_2 + 0.7Q_3 + 0.7Q_4 \ldots$

with Q_o snow load on the roof and Q_1, Q_2, …, Q_i, … variable loads at residential floors numbered from top to bottom. In the case of concern one therefore has, with a unique load combination:

• roof	1.0 × 1.20	= 1.20	kN/m^2
• 4th floor	1.0 × 2.00–0.5 × 1.20	= 1.40	”
• lower floors	0.7 × 2.00	= 1.40	”

Actions on Columns

For the preliminary design of the columns, with reservation of farther verifications after more rigorous analyses of the frames, an approximated procedure can be followed based on the partition of the deck layout in *tributary areas*. This is obtained marking on such layout the mid-span lines of each individual span for slabs and beams in order to identify the loading areas to be attributed to each column (see Fig. 2.23). Apart from special situation, for example adjacent spans of very different length, it is possible to carry out an approximated evaluation of the effects of hyperstatic bending moments due to continuity of flexural elements, penalizing

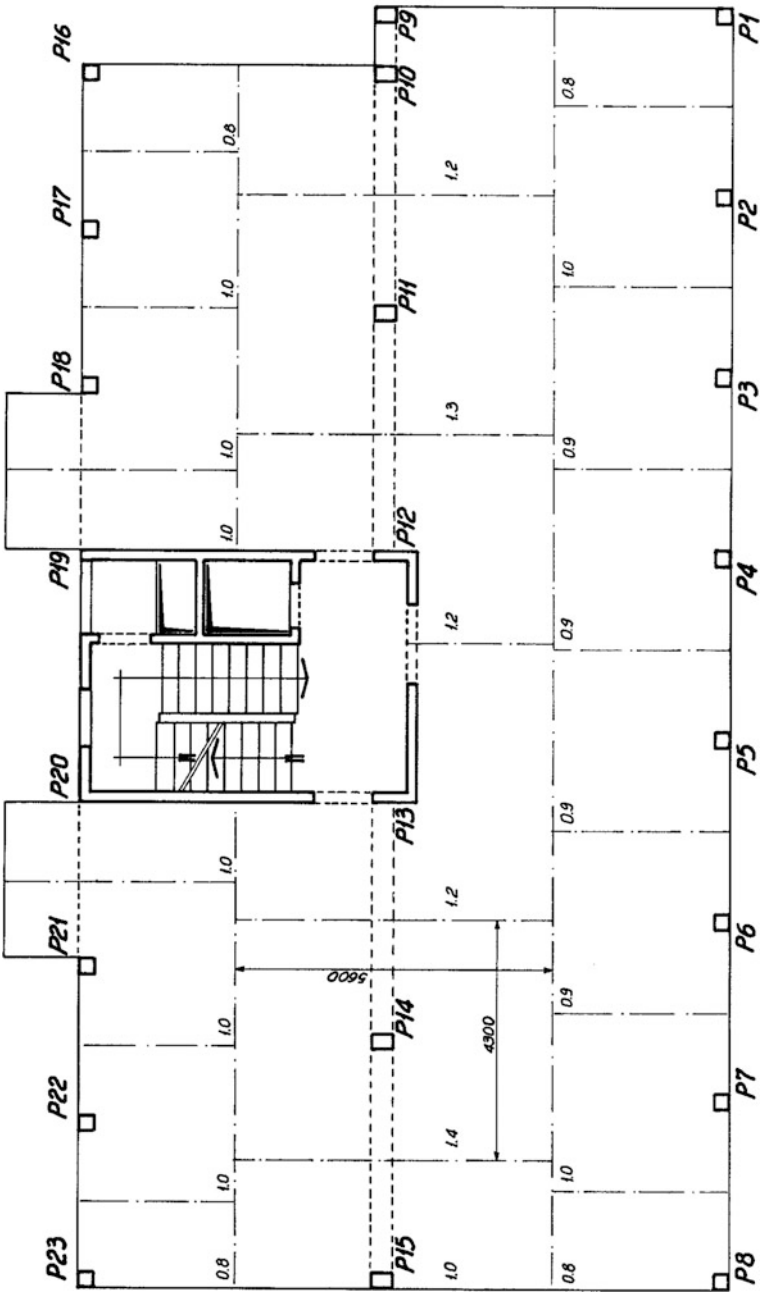


Fig. 2.23 Tributary areas of columns

certain areas with amplifying coefficients and reducing others at the same time. For the case under analysis this has been done with *weights* indicated inside each individual tributary area, where for example the increase of the floor reaction on the intermediate support given by the central beam has been estimated with 0.2, combining it with similar estimations on the orthogonal flexural behaviour of the beam.

After carrying out such partition, one can proceed with the estimation of loads for each individual column, or by groups of similar area, eventually summing up forces from the top to the bottom with the combination formula indicated above. The calculation is developed below with reference to one column only.

Colum P14

(tributary area	$1.4 \times 4.30 \times 5.60 \cong 33.7\ m^2$)		
• roof deck	33.7×7.00	$= 235.9$	kN
• beam	$1.2 \times 0.40 \times 0.30 \times 4.30 \times 25$	$= 15.5$	”
• column	$0.40 \times 0.30 \times 2.52'' \times 25$	$= \underline{7.6}$	”
total permanent loads on the roof		$= 259.0$	kN

(″ clear headroom underneath the beam = 2.52 m)

• type floor deck	33.7×7.00	$= 235.9$	kN
• beam	$1.2 \times 0.40 \times 0.30 \times 4.30 \times 25$	$= 15.5$	”
• column°	$0.40 \times 0.40 \times 2.52 \times 25$	$= \underline{10.1}$	”
tot. permanent loads on type floor		$= 261.5$	kN

(° average dimensions)

Roof

• permanent	$= 259.0$	kN
• variable 33.7×1.20	$= \underline{44.4}$	”
tot. roof	$= 299.4$	kN

4th floor

• permanent	$= 261.5$	kN
• variable 33.7×1.40	$= \underline{47.2}$	”
tot 4th floor	$= 308.7$	kN

lower floors

• permanent	= 261.5	kN
• variable	= 47.2	”
33.7 × 1.40		
tot lower floors	= 308.7	kN

After this preliminary analysis, the design calculations of sections and the service and ultimate limit state verifications can be neatly summarized as indicated in the following tables. The characteristics of materials assumed for the verifications are shown below.

Materials

Concrete (aggregate $d_a \leq 20$ mm)

• class C25/30 ordinary ($R_{cm} \cong 40$ N/mm^2)		
• characteristic strength	f_{ck}	= 25.0 N/mm^2
• design strength	$f_{cd} = 0.85 \times 25.0/1.5$	= 14.2 N/mm^2
• for centred axial force	$f'_{cd} = 0.80 \times 14.2$	= 11.3 N/mm^2
• allowable in service	$\bar{\sigma}_c = 0.45 \times 25.0$	= 11.2 N/mm^2
• for centred axial force	$\bar{\sigma}'_c = 0.70 \times 11.2$	= 7.8 N/mm^2

Steel (ribbed bars)

• type B450C with high ductility		
• characteristic strength	f_{tk}	= 540 N/mm^2
• yield stress	f_{yk}	= 450 N/mm^2
• design strength	$f_{yd} = 450/1.15$	= 391 N/mm^2
• allowable in service	$\bar{\sigma}_s$	= 0.80 × 450 = 360 N/mm^2

Homogenization coefficients

- for serviceability design $\alpha_e^* = 15$
- for ultimate design 391/11.3 = 34.6

It is to be noted that, as permitted by the codes, for the elastic design a conventional homogenization coefficient is assumed which takes into account the creep effects produced by the permanent quota of loads in an approximated way. Given that this quota corresponds on average to 0.7 of the total loads, with a creep coefficient $\varphi \cong 2.4$ and with reference to an average concrete with $\alpha_e \cong 7$, one obtains approximately:

$$\alpha_e^* \cong \left(1 + 0.70^2 \times 2.4\right) \cdot 7 \cong 15$$

This approximation does not affect significantly the evaluation of serviceability stresses in concrete, whereas it has no influence on the ultimate resistance of the sections.

Another approximation is made in the design of columns with the adoption of a global safety factor on actions, evaluated as the weighted mean between the factor $\gamma_{G1} = 1.30$ of structural dead loads and the one $\gamma_{G2} = \gamma_Q = 1.50$ of applied loads:

$$\gamma_F \cong 1.30 \times 0.35 + 1.50 \times 0.65 \cong 1.43$$

having estimated in 0.35 the incidence of structural dead loads on the total.

Verification Calculations

COLUMN P 14—SECTIONS DESIGN

	F_k (kN)	N_k (kN)	N_{Ed} (kN)	A_{co} (cm^2)	$a \times b$ (cm)	A_c (cm^2)	A_{so} (cm^2)	$n\phi$ (mm)	A_s (cm^2)
4°	299.4	299.4	428.1	379	30 × 40	1200	3.60	4ϕ12	4.52
3°	308.7	608.1	869.6	770	30 × 40	1200	3.60	4ϕ12	4.52
2°	308.7	916.8	1311.0	1160	30 × 40	1200	3.60	4ϕ12	4.52
1°	308.7	1225.5	1752.5	1551	40 × 40	1600	4.80	4ϕ14	6.16
PR	308.7	1534.2	2193.9	1942	50 × 40	2000	6.00	4ϕ14 + 2ϕ12	8.42
SI	308.7	1842.9	2635.3	2332	60 × 40	2400	7.20	6ϕ14	9.24

COLUMN P 14 SECTIONS VERIFICATION

	A_{ie} (cm^2)	σ_c (MPa)	A_{ir} (cm^2)	N_{Rd} (kN)	γ_r
4°	1268	2.4	1356	1532	3.58
3°	1268	4.8	1356	1532	1.76
2°	1268	7.2	1356	1532	1.17
1°	1692	7.4	1813	2049	1.17
PR	2008	7.6	2291	2589	1.18
SI	2539	7.3 ($\leq$ 7.8)	2720	3074	1.17 ($\geq$ 1.00)

In the first table, from the last floor to the basement, the values of the following parameters are shown:

- The load F_k coming from the upper floor of the column considered.
- The axial force N_k obtained progressively summing up the upper loads.
- The design value of the axial force N_{Ed} obtained amplifying by γ_F = 1.43 the previous force.
- The minimum theoretical concrete area $A_{co} = N_{Ed}/f'_{cd}$ necessary to resist the design force by itself.
- The actual dimensions $a \times b$ adopted for the column segment.
- The actual concrete area A_c.

- The theoretical minimum reinforcement area $A_{so} = 0.10 \times N_{Ed}/f_{yd}$ equal to at least to the 0.3% of the actual concrete section A_c.
- The adopted reinforcement for the column segment indicated with the number n of bars and their diameter ϕ.
- The area A_s of the actual steel reinforcement cross section.

In the second table, again from the top floors to the bottom, the values of the following parameters are shown:

- The equivalent area $A_{ie} = A_c + \alpha_e A_s$ referred to concrete with the conventional homogenization coefficient $\alpha_e = 15$ for the serviceability elastic design.
- The stress $\sigma_c = N_k/A_{ie}$ in concrete for the serviceability compression verification, to be compared with the value 7.8 indicated at the bottom of the table column.
- The equivalent area $A_{ir} = A_c + A_s f_{yd}/f'_{cd}$ referred to concrete with the coefficient for the ultimate design of the section.
- The resisting value $N_{Rd} = f'_{cd} A_{ir}$ of the axial force to be compared with the applied value N_{Ed}.
- The ratio $\gamma_r = N_{Rd}/N_{Ed}$ between resistance and action in the section for a uniform comparison of the situation, having to satisfy $\gamma_r \geq 1$.

The transition from the design carried in the previous pages to the construction drawings with member detailing does not require explanations other than some short notes on certain code requirements, such as the one about spacing s and diameter ϕ_o of stirrups ($s \leq 12\phi$, $\phi_o \leq \phi/4$, where ϕ is the diameter of the longitudinal reinforcement). The relative DWG D.2 (Fig. 2.24) shows the column elevation, from the foundations to the roof, with the reinforcement indicated. On the side, the longitudinal bars are shown for the necessary dimensions. The lapping of bars specified at each floor at the location of the construction joints is to be noted. The different sections are eventually shown at a greater scale with the position of bars and the detailing of stirrups. Concerning the bars lapping, the minimum anchorage length has been used:

$$l_b = \frac{\phi}{4} \frac{f_{yd}}{f_{bd}}$$

With

$$f_{yd} = 391\,\text{N/mm}^2$$

$$f_{ctk} = 1.95\,\text{N/mm}^2$$

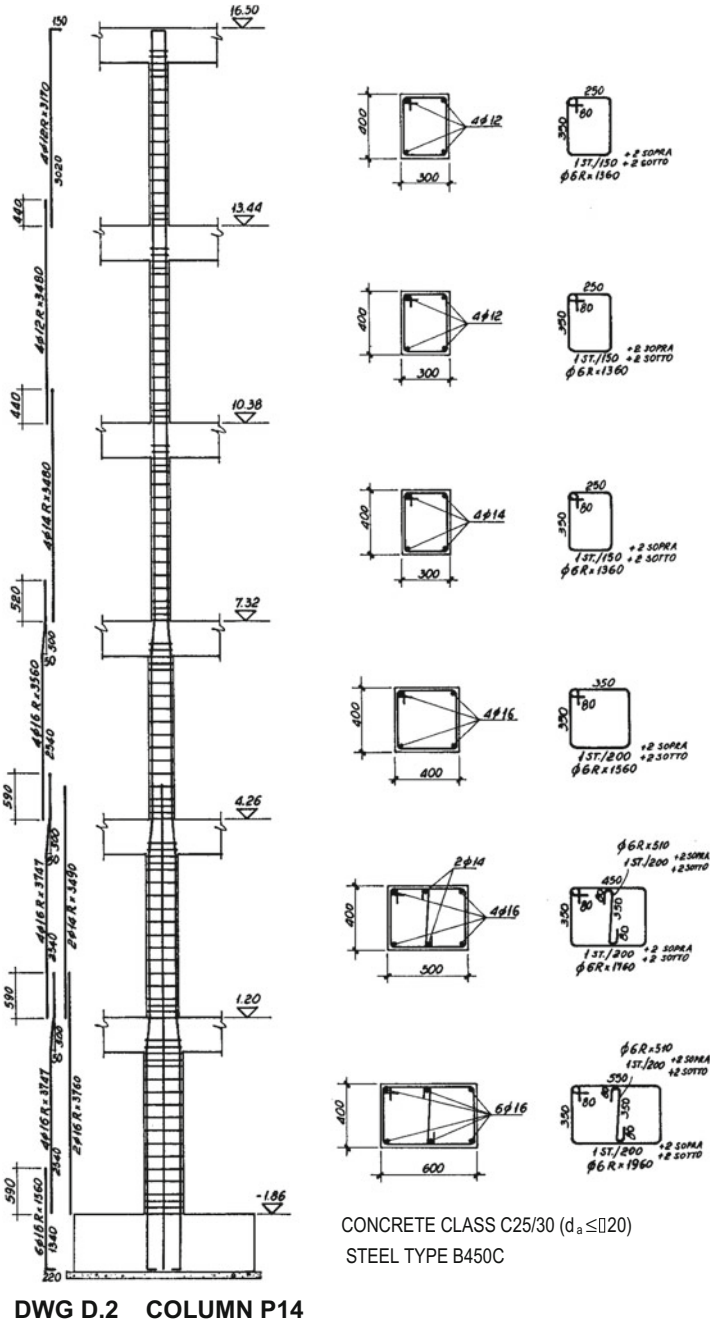


Fig. 2.24 Details of a column—elevation and sections

(see Table 1.7)

$$f_{ctd} = 1.95/1.5 = 1.30\,\text{N/mm}^2$$

$$f_{bd} = 2.25 \times 1.30 = 2.92\,\text{N/mm}^2$$

one obtains

$$l_b = \frac{\phi}{4}\frac{391}{2.92} \cong 33\phi$$

2.4.2 Notes on Reinforced Concrete Technology

Several construction requirements are shown as follows for the correct design of reinforced concrete structures. They are not exact compulsory rules; however, their general compliance is necessary to ensure that the models assumed in the design can actually occur in the behaviour of the real structure.

Minimum Thicknesses

A first aspect concerns the minimum thicknesses to be assigned to elements in order to guarantee sufficient *homogeneity of the concrete*, also with respect to the relevance of the static function of the considered part. Such minimum thicknesses should be directly related to the maximum size d_a of the aggregate used that can vary for common structures between 12 and 25 mm. With the aim of ensuring a good distribution of grains up to $0.8d_a$ close to the maximum aggregate size, the following values can be indicated.

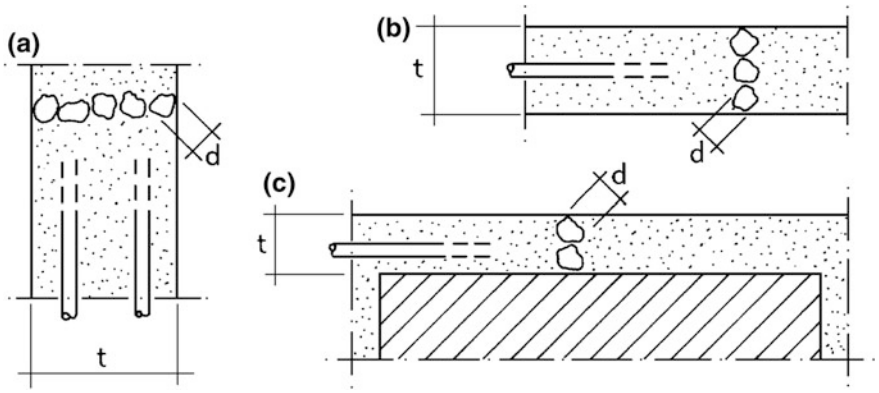


Fig. 2.25 Aggregate size and minimum thicknesses

- Structural elements reinforced on both faces (see Fig. 2.25a):

$$t \geq 0.8 \times 5d_a = 4.0d_a \quad (50-100\,\text{mm})$$

- Slabs and ribs with one layer of reinforcement (see Fig. 2.25b):

$$t \geq 0.8 \times 3d_a = 2.4d_a \quad (30-60\,\text{mm})$$

- Concrete collaborating toppings on permanent blocks (see Fig. 2.25c):

$$t \geq 0.8 \times 2d_a = 1.6d_a \quad (20-40\,\text{mm})$$

Given that the minimum size for a complete homogeneity of the material is equal to $5d_a$, in the structural parts with $t < 5d_a$ the characteristic concrete strength should be adequately reduced for design, for example with

$$f_{ck}^{*} = \left(0.5 + 0.1\frac{t}{d_a}\right) f_{ck}$$

For plain (unreinforced) concrete elements the minimum thickness should be $t \geq 5.0d_a$.

In any case, an absolute minimum thickness value should be assigned, which derives from the type of material considered and from its processing technologies, in order to guarantee a *sufficient compact mass* to structural elements, for example with:

• components for extruded or vibrocompacted floors	t ≥ 30 mm
• ordinary cast in situ floor components	t ≥ 40 mm
• main structural elements	t ≥ 50 mm
• wall panels and plain concrete	t ≥ 80 mm

Bars Position

The position of bars in the cross section should respect minimum dimensions for spacing and edge distance. This is to allow aggregates to go through, to ensure a good concrete enclosure of the bars for bond purposes and also to ensure protection of the reinforcement against corrosion. The values given below to the *concrete cover c* and to the *bar spacing* i_h horizontal and i_v, vertical are measured to the centrelines of the bars (see Fig. 2.26); the *net cover* $c_o = c - \phi/2$ and the *net spacing* $i_o = i - \phi$ refer to the corresponding net thicknesses of concrete.

With the usual principle of allowing all (or almost) aggregate to go through, the following minimum dimensions can be indicated:

• Minimum net spacing:	horizontal i_{oh}	vertical i_{ov}
passive bars (see Fig. 2.26a)	1.0 d_a	0.8 d_a
prestressed strands (see Fig. 2.26b)	1.2 d_a	1.0 d_a

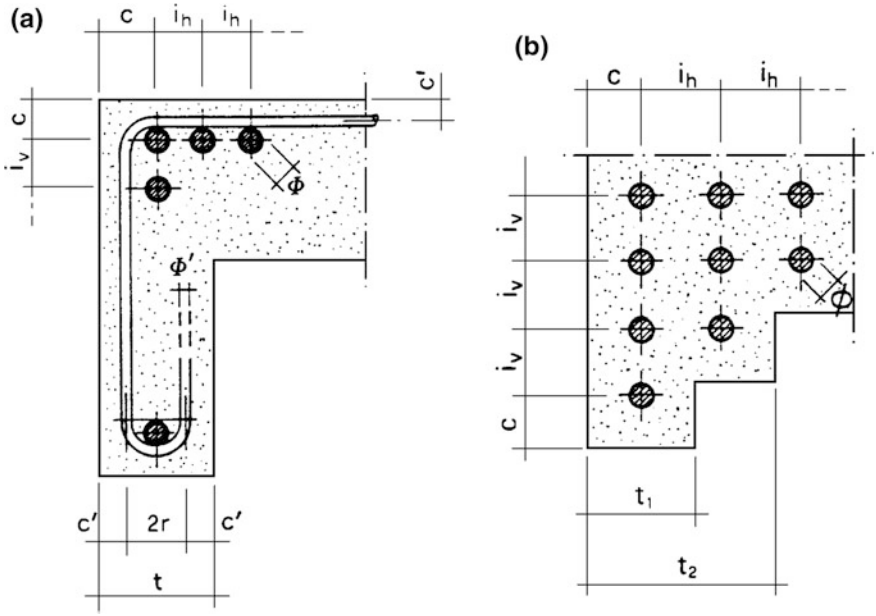


Fig. 2.26 Bar positioning—cover and spacing

• Minimum net cover:	c'_o	c_o
stirrups and links (see Fig. 2.26a)	0.8 d_a	–
passive reinforcement (see Fig. 2.26a)	–	1.0 d_a
prestressed reinforc. (see Fig. 2.26b)	–	1.0 d_a

With the principle of ensuring a *good concrete enclosure of bars*, for a full bond due to a compact concrete layer around them, the following minimum dimensions can be indicated:

• Minimum values	spacing i_o	cover c_o
passive reinforcement (see Fig. 2.26a)	1.0 ϕ	1.0 ϕ
prestressed reinforc. (see Fig. 2.26b)	2.0 ϕ	1.5 ϕ

With these values for example the thicknesses t_1 and t_2 of the prestressed element with adherent pretensioned strands indicated in Fig. 2.26b can be deduced. For strands of respectively 12.5 mm (0.5″) and 15.2 mm (0.6″), one therefore has the following dimensions expressed in mm:

ϕ	i_o	c_o	$t_1 = 4\phi$	$t_2 = 7\phi$
12.5	25	19	50	88
15.2	30	23	61	106

In particular the thicknesses t_1 and t_2 shown here are compatible respectively with aggregates of $d_a \leq 12$, $d_a \leq 16$, $d_a \leq 20$ and $d_a \leq 25$ mm, except for possible increases due to the bending diameter of stirrups.

Concerning the cover necessary to ensure the *protection of reinforcement* against corrosion, one can refer to the following Sect. 2.4.3 where the problem of durability of reinforced concrete structures is discussed in more details.

It is implied that the greatest among the three requirements mentioned above has to be satisfied. An additional and more stringent cover requirement can be added when, because of the use conditions of the building, a particular *fire resistance* of structures is required. Moreover, it is to be kept in mind that an excessive cover causes problems with respect to cracking control. For values greater than the indicative value $c_o \cong 40$ mm, the addition of a *skin reinforcement* is generally required, not taken into account for resistance purposes, placed as protection of the outer layer for the normal service of structures.

Reinforcement Tolerances

The tolerances of execution and installation, related to the common production technology, lead to significant variability of dimensions with respect to the nominal values indicated in the design and therefore the minimum values shown above should be taken with due caution.

In particular, with reference to the *effects on structural safety*, the partial factors γ_M given by the codes already take into account the variability of resisting dimensions of the cross sections due to reinforcement tolerances. These tolerances are shown in Chart 2.5 of the Appendix.

With reference to the *effects on durability*, the tolerances of the concrete cover matter. This concrete cover has to be ensured with the use of adequate *spacers*, applied to the external bars of the reinforcement cage in order to impose the offset from the contiguous surface of the formwork. Table 2.17 of the Appendix takes into account such tolerances in giving the minimum values of cover for the different classes of exposure and resistance.

Bars Bending

In the design of sections and the reinforcement detailing, *bending radius* of bars also has to be taken into account, whose minimum value is related to the diameter of the bars in order to avoid microcracks during manufacturing. The value (see Fig. 2.27a)

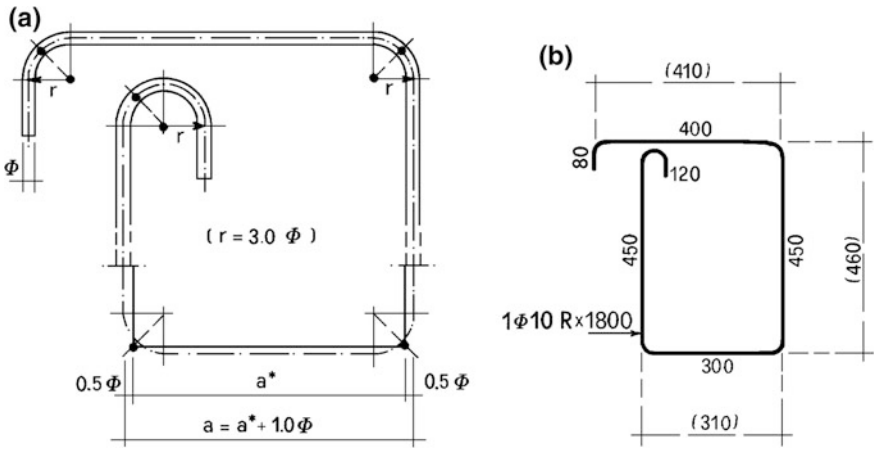


Fig. 2.27 Details of bar shaping

$$r \cong 3.0\phi$$

refers to ribbed bars that are nowadays commonly used. Such value defines to the axial circle; the internal bending diameter of the bar, corresponding to the one of the mandrel to be used, is equal to 5ϕ.

What mentioned above refers to the bending of longitudinal bars in order to obtain end hooks and also to the shaping of stirrups. For bent bars of beams, used as shear reinforcement in tension (see Chap. 5), the problem of possible cracking of concrete arises, caused by the compressions acting towards the inner part of the bend. In this case bending radii should be used that are roughly doubled.

In the *construction details drawings* the indications of radii are normally omitted (see Fig. 2.27b), limiting on giving the length of the axial polygon line of the bars, obviously in addition to their diameter and few additional dimensions if necessary. As indicated in details in Fig. 2.27a, the nominal side length a^* indicated in the drawing, equal to the development from end to end of the actual axial polygon line of the bar, is 1.0ϕ smaller than the actual dimension a of the bar.

It is to be noted that, in order to be inserted in the tool for bending, the end hook of a bar needs a certain extension beyond the circular bend. For the minimum length u, measured from the last end of the axial polygon line, the following values can be assumed in the detail drawings (see Fig. 2.27b):

• open (bend) at 90°	$u = 8\phi$
• semi-closed (hook) at 135°	$u = 10\phi$
• closed (loop) at 180°	$u = 12\phi$

The minimum thickness of a rib to be provided with stirrups as the one shown in Fig. 2.22a can now be deduced in the following way:

$$t \geq 2(c'_o + r) = 1.6d_a + 7\phi'$$

which, with the minimum commercial diameter of 6 mm, leads to 61 and 68 mm, respectively for aggregate sizes d_a equal to 12 and 16 mm. For bigger aggregates the limitation $t \geq 4.0d_a$ is the limiting one.

Reinforcement Anchorage

A very important aspect is the one related to the end anchorage of bars. As already mentioned at Sect. 1.4.3, in order to ensure the collaboration of the steel reinforcement in a given section it is necessary that the reinforcement be extended by a segment equal to the necessary *anchorage length*. According to the principle that ensures the full possible use of the resistance resources of steel everywhere, such length is obtained from

$$l_b = \frac{\phi f_{sd}}{4f_{bd}}$$

with $f_{bd} = \beta_b f_{ctd}$ and $\beta_b = 2.25$ for ribbed bars, $\beta_b \cong 1{,}0$ for smooth bars.

If instead one wants to refer to the actual stress acting in the bar, with a calculation repeated for each different situation, a reduced anchorage length can be attributed l'_b, estimated with the ratio between the required steel area and the one actually present:

$$l'_b = l_b A'_s / A_s$$

Such value refers to a bar in tension anchored inside a compact concrete zone. The same length can be conservatively assumed for the anchorage of bars in compression.

Bars interrupted in tensile zones and close to the external surface with the cover layer essentially ineffective for bond, would require a double anchorage length. They should be avoided, unless adequate confinement is provided with closely spaced transverse stirrups.

Reinforcement Joints

The problem of bars joints presents very similar problems. Excluding special techniques that are not very common, such as welding (allowed for steels explicitly indicated as weldable) or the use of couplers (threaded or sleeved), the reinforcement joint is obtained by simple *lapping* of the bars, adequately extended to ensure the anchorage of each of them.

Other than presenting once again the calculation of the anchorage length l_b recalled above, this joint requires the transfer of stresses from one bar to the other through the concrete around. The *bars distance* therefore has an influence on the lapping, according to what is indicated in Fig. 2.28a, whereas in Fig. 2.24b it is

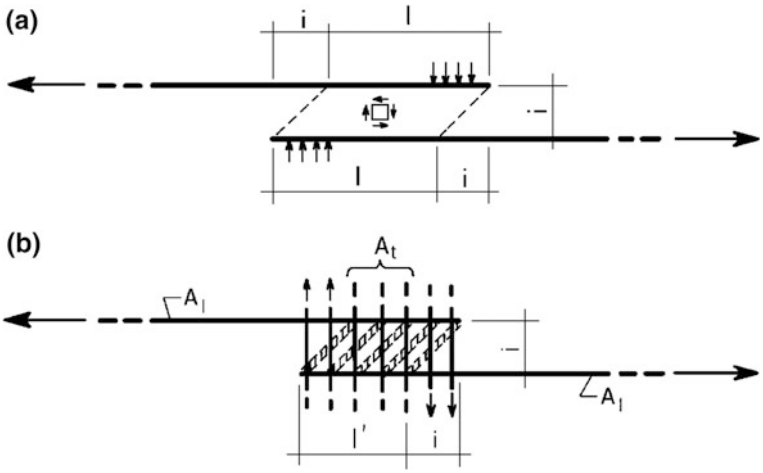


Fig. 2.28 Force transmission in bars overlapping zone

recalled how a good transverse confinement, with a total area of stirrups A_t equal to the one A_l of the reinforcement to be lapped, improves significantly the behaviour of the joint, letting concrete work only in compression in the resisting truss.

Transverse forces are also shown in Fig. 2.28, which are necessary to balance the offset tensions transferred between the longitudinal bars. Such forces are taken by the transverse stirrups in the case of Fig. 2.28b, whereas in the case of Fig. 2.28a

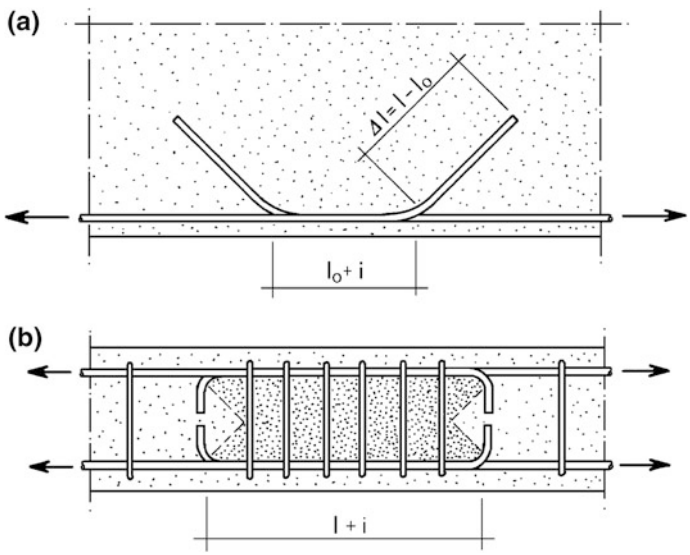


Fig. 2.29 Bars overlapping tension zones of beams (**a**) and ties (**b**)

they lead to tensions in the concrete in between. If not adequately designed, this type of joint can therefore lead to *longitudinal cracks* with opening of the joint.

The effectiveness of the anchorage, as already said, is reduced by the proximity of the reinforcement to the external surface and by the possible cracking state of concrete. Therefore, joints in tension zones are normally to be avoided and, when necessary, they should be staggered and provided with a segment $i + l_o$ of straight overlapping equal to at least $i + 20\phi$, followed by an end segment bent inwards, towards the compression zone (see Fig. 2.29a). The latter would have the extension Δl necessary to complete the required anchorage length l_b of the bar. In the design, the bond strength of the surface overlapping straight segment is to be halved.

For ties with section fully in tension, lapping, when necessary, are to be designed with caution, evaluating the anchorage length with a halved bond strength and ending bars with additional hooks. The stirrups spacing should also be reduced locally, for a good *confinement of the joint*, creating a truss mechanism centred on the compression core of concrete (see Fig. 2.29b).

To conclude, it is to be noted how *fatigue phenomena* deriving from repeated loads can weaken bond, especially if under actions of alternate sign. This directly affects the effectiveness of anchorages and reinforcement joints.

Reinforcement Layout

A last aspect to be mentioned in these last pages refers to the reinforcement layout. In reinforced concrete, the steel bars have to resist axial forces mainly in tension. Their limited flexural stiffness, small with respect to the one of the composite element, causes that every *bar deviation* from the straight configuration concentrates transverse forces in concrete at the bending location.

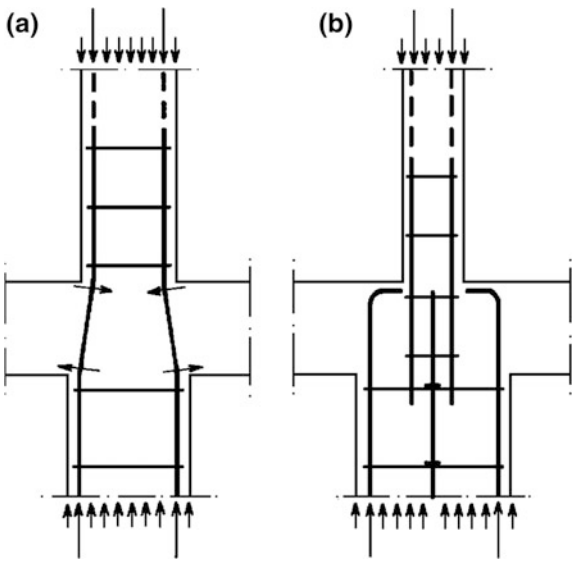


Fig. 2.30 Details of bars overlapping in column joints

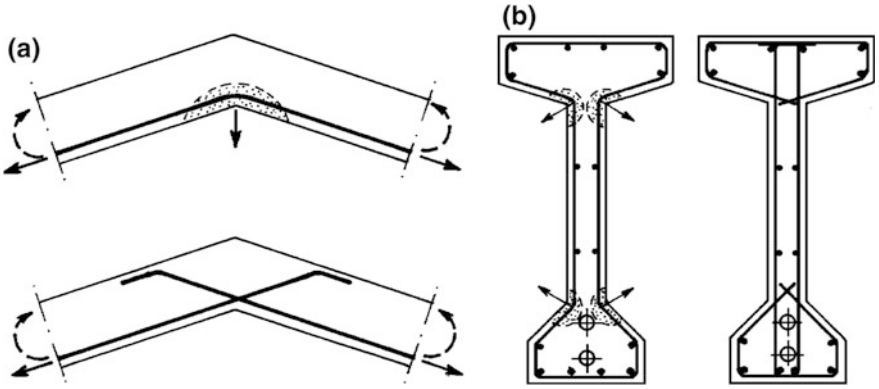


Fig. 2.31 Bad and good reinforcement details: knee beam (**a**) and PC section (**b**)

The case of elements in compression causes fewer concerns as the integrity of concrete allows the control of the diverging actions. As said before, the slenderness of the bars in compression should be limited with appropriate transverse bars (such as stirrups in column) to limit the tendency to buckle towards the outside, with possible spalling of concrete.

Figure 2.30a, b show instead the case of joints of superimposed segments of columns with different dimensions. Given that the sections are always fully in compression, if the angle of bending is small it is possible to redirect the longitudinal bars coming from the lower portion to insert them within the reduced area of the upper portion, allowing limited transverse forces contained within the deck thickness. Greater dimensional deviations require instead the interruption of the lower reinforcement and the start of the upper one with appropriate inner starter bars.

For reinforcement in tension, the problem is more delicate as it concerns zones of mostly cracked concrete, not capable of containing transverse diverging forces. In Fig. 2.31 two typical situations are described for example.

The first one refers to a folded beam in bending: in the incorrect solution shown on top, the transverse action of reinforcement in tension is indicated, which causes the spalling the concrete bottom; in the lower solution instead the reinforcement is correctly shaped, with straight extensions up to the compression zone and separate anchorages without transverse diverging forces.

Figure 2.31b refers to the I-section typical of precast beams in prestressed concrete. For the case of stirrups in tension, the incorrect solution which concentrates disruptive forces at the internal corners is indicated on the left side, the correct one that subdivides stirrups in three pieces and has every end side properly anchored with straight extensions on the right side.

2.4.3 Durability Criteria of Reinforced Concrete Structures

The durability aspects, which are discussed in the following pages, refer to structural elements in plain, reinforced and prestressed concrete. Only structures of common buildings, with residential, commercial or industrial use, as well as certain other civil construction, are considered.

The durability requirements refer to the resistance and serviceability of the structures as defined by the relative limit states in the appropriate structural verifications. Fire resistance is not considered; neither are other aspects such as insulation, appearance, etc….

In the following provisions, it has been assumed that fitting-out works and services be correctly executed and maintained in a good efficiency state, so to preserve structures from unexpected situations (water stagnation, overheating, damage of cover, leakage of aggressive materials, etc…).

Metallic inserts, even if connected or partially embedded in concrete elements, should be considered separately, with different criteria.

Service Life

The *expected service life* T_s is the period during which the structure is expected to maintain an adequate level of safety and functionality, without requiring excessive unexpected obligations for maintenance and repairs.

The capability of concrete structures to satisfy durability requirements is estimated through:

- the definition of the environmental conditions;
- the design provisions for materials and structures;
- the provisions for the execution and controls;
- the instructions for use and maintenance.

Apart from different provisions, explicitly indicated in the documentation of the design and contract, for common residential buildings the expected service life, exempt from excessive maintenance obligations, is assumed equal to 50 years.

Deterioration Processes

The following aggressive actions are considered:

- high presence of humidity;
- washout waters;
- marine environment;
- effects of freezing/thawing;
- chemical emissions.

Mechanical effects due to high stresses in materials are prevented with the verification of the specific serviceability limit states, such as the one of maximum compressions against progressive propagation of microcracking in concrete.

The physical deterioration due to abrasion is prevented with appropriate hard layers, such as the ones for carriage pavements.

The *presence of water* or humidity is the determining factor, which is directly connected to certain chemical reactions, facilitates the flow of the other aggressive substances on the structures and determines their penetration inside concrete pores.

Under the actions listed above, the following deterioration processes are to be considered:

- the *corrosion of reinforcement* and of prestressing steel if directly exposed to oxidant agents or if exposed because of damages to the protective layer made of passive oxide when reached by carbonation of concrete cover, corrosion that develops with the progressive oxidation of steel, with expansions and spalling of concrete layers;
- the attack of concrete surface due to the direct *washout action* of rain or pure waters, possibly with carbon dioxide, which causes the dissolution of free unbonded lime and the progressive consumption of the material, or due to other surface processes of deterioration such as the expansion actions of sulphatic waters;
- chemical actions of *marine environment*, due to the high concentration of salts in environments submerged in water or in the saturated atmosphere of coastal areas, actions that develop with the surface dissolution caused by the expansion effects and that are increased in the splash zones because of the mechanical erosion of waves;
- the *freezing/thawing* effects due to the repeated formation of ice and increased by the use of antifreeze substances, effects that develop with the degradation of concrete caused by internal pressures of trapped water when freezes, and by spalling of the surface concrete caused by the high thermal gradient under the external antifreeze agents;
- other *chemical attacks* due to aggressive solids, liquids or gases, possibly facilitated by the presence of humidity.

Materials Properties

It is taken for granted that a correct technology is applied for the production of materials in order to avoid chemical instabilities, such as the alkali-aggregate reaction in concrete or the strain-age embrittlement of steel.

Concrete

With respect to durability a concrete of good quality is necessary in order to obtain:

- a *low permeability* to water penetration;
- a *well compacted* solid mass without enclosed voids;
- a homogeneous material of *high class* of resistance;
- a skin *without damages* with appropriate surface finishing.

For freeze-resistant concretes, a minimum air content (per unit mass of concrete) can be specified through the appropriate dosage of an air entraining admixture, to ensure a uniform distribution of micropores in which freezing water can freely expand.

Steel
The durability properties of steels for ordinary and prestressed reinforced concrete are related to the surface exposed per unit mass of the material, to the presence of surface cracks and their width.

These properties are given through a *sensitivity index* to corrosion that increases with

- small diameters of bars or strands;
- hardening processes of the material;
- high levels of tension in service states.

Reinforced concrete
Certain design criteria should be satisfied in order to obtain durable structures; first of all for any type of concrete structures the design should assume and explicitly indicate:

- the maximum size of the aggregate used in relation to the element thicknesses for a good homogeneity of the material and its consequent full strength;
- the minimum absolute value of thicknesses in order to ensure a overall sufficient mass of the elements;
- a proportioned choice of shapes and dimensions in order to avoid damages caused by early cracking due to shrinkage and thermal effects.

For reinforced concrete works, the design should add appropriate specifications regarding:

- the maximum aggregate size in relation to the free spaces between bars, and between bars and formwork in order to allow a complete compact cast of works;
- a minimum value of spacing between bars with reference to their diameters for a full bond resistance with concrete without damages at the interface;
- a minimum cover of reinforcement in relation to the concrete class and other factors that have an influence on steel corrosion.

Performances of Structures
The performances of the structures with respect to durability depend on the *service state* of the elements, which is related to the level of tensile stresses in concrete and which is distinguished in:

- *cracked state* when, under a rare load combination, the maximum tensile stress in concrete exceeds the characteristic strength βf_{ctk};

- *uncracked tension state* when, under the condition indicated above, the maximum tension, even if significant, does not exceed the characteristic value of the concrete strength βf_{ctk};
- *compression state* when, under the most unfavourable rare load combination, the concrete section remains entirely in compression.

The latter can be substituted by a less stringent one that limits the maximum tensile stress in concrete to a very conservative allowable value (for example $0.25\beta f_{ctk}$).

In the strength βf_{ctk} mentioned above it has to be assumed $\beta = 1$ for a constant distribution of tensions, $\beta = 1.3$ if referred to the extreme value of a triangular flexural distribution of stresses.

Also the type of *surface finishing* of elements should be considered distinguishing the cases of:

- elements with *exposed surfaces*, without any protection;
- *typical finishing*, such as plaster, tiling, …;
- *special finishing*, with protective characteristics, such as waterproof barriers (membranes, water-repelling varnish, paints, …);

where, for cracked states, varnish, paints or the other types of adherent coatings should be applied with special measures in order to preserve their integrity when the foreseen concrete cracking occurs.

Minimum Requirements

For *durable structures* certain minimum values of the relevant parameters should be fulfilled. In addition to the thicknesses of elements and the reinforcement spacing already mentioned in the previous paragraph, an additional geometric parameter relates to the different slenderness of the parts of an element: an excessive dimensional dissimilarity causes shrinkage and thermal effects that are highly differential, with the possibility of early cracking.

The following indicative prescription refers to the ratio between the equivalent thicknesses of the connected parts of the same concrete section:

Minimum shape ratio of the section:

$$\frac{s_1}{s_2} \geq \frac{1}{8} \quad (s_2 \geq s_1)$$

with $s_i = 2A_i/u_i$, where A_i is the area and u_i is the perimeter of the single homogeneous part of the cross section.

The main parameter related to the protection of reinforcement against corrosion is the concrete cover which can be given as a function of the aggressiveness of the environment and the material strength. The minimum values of cover are given in the table below, expressed in mm. They refer to constructions with a nominal life of 50 years. For constructions with a nominal life of 100 years (for example important bridges) they should be increased by 10 mm. For classes of resistance lower than

C_{min} they should be increased by 5 mm. For plate elements exposed to only one side they can be reduced by 5 mm.

Concrete classes		Environment	Bars for RC other elements		Strands other elements	
C_{min}	C_o	Aggressiveness	$C \geq C_o$	$C_{min} \leq C \leq C_o$	$C \geq C_o$	$C_{min} \leq C \leq C_o$
C25/30	C35/45	Low	20	25	20	25
C28/35	C40/50	Medium	30	35	30	35
C35/45	C45/55	High	40	45	40	45

The values of the table refer to actual built dimensions. In order to obtain the nominal values to be specified in the design, such values of cover should be increased by tolerances of reinforcement positioning assumed equal to ±10 mm for ordinary workmanship, equal to ±5 mm for controlled production. In any case it is implied that for the correct positioning, adequately distributed spacers are used. The indicative number is 4 per m^2 of formwork.

Appendix: General Aspects and Axial Force

Table 2.1: Environmental Conditions: Exposure Classes

The following table, reproduced in a summarized form, is extracted from the European Norm EN 206-1 "Concrete specification, performance, production and conformity". Classes XC, XD and XS refer to corrosion of reinforcement, classes XF and XA refer to the surface attack of concrete.

Minimum concrete covers for the protection of reinforcement against corrosion for different degrees of aggressiveness are given in Table 2.17.

Class	Description	Examples
1. *No risk of corrosion or attack*		
X0	Plain concrete without attacks Reinf. concrete in very dry environ	Concrete inside buildings with very low air humidity
2. *Corrosion induced by carbonation*		
XC1	Dry or permanently wet	Concrete inside buildings
XC2	Wet, rarely dry	Many foundations
XC3	Moderate humidity	External concrete sheltered
XC4	Cyclic wet and dry	Structures in water line
2. *Corrosion induced by chlorides*		
XD1	Moderate humidity	Airborne salt
XD2	Wet, rarely dry	Swimming pools
XD3	Cyclic wet and dry	Bridges, outdoor pavements

(continued)

(continued)

Class	Description	Examples
3. *Corrosion induced by chlorides from sea water*		
XS1	Exposed to airborne salt	Structures near to the coast
XS2	Permanently submerged	Parts of marine structures
XS3	Tidal, splash and spray zones	Parts of marine structures
4. *Freeze/thaw attack*		
XF1	Wet surfaces, without de-icing agents	Vertical surf. exposed to rain
XF2	Wet surfaces, with de-icing agents	Vertical surfaces of bridges
XF3	Soaked surf. without de-icing agents	Horiz. surfaces open to rain
XF4	Soaked surf. with de-icing agents	Horiz. surfaces of bridges
5. *Chemical attack*		
XA1	Slightly aggressive chemical environ.	Natural soils-groundwater
XA2	Moderate aggressive chem. environ.	Natural soils-groundwater
XA3	Highly aggressive chemical environ.	Natural soils-groundwater

For design applications, with reference to corrosion of reinforcement, the exposure classes can be grouped as follows:

Aggressiveness	Exposure classes
Low	X0, XC1, XC2, XC3
Medium	XC4, XD1, XS1
High	XD2, XD3, XS2, XS3

With reference to freeze/thaw attack or chemical attack (classes XF and XA) an adequate concrete mix design should be adopted.

Chart 2.2: Concrete: Design Strength

In the resistance verifications (ultimate limit states) the following values (in MPa) are adopted:

$$f_{cd} = \alpha_{cc} \frac{f_{ck}}{\gamma_C} \quad \text{design compressive strength}$$

with α_{cc} = 1.00 for short term loads and α_{cc} = 0.85 for ordinary loads.

$$f_{c2} = 0.6\left(1.0 - \frac{f_{ck}}{250}\right) f_{cd} \cong 0.50 f_{cd} \quad \text{reduced design strength}$$

$$f_{ctd} = \frac{f_{ctk}}{\gamma_C} \quad \text{tensile design strength}$$

where the partial safety factor should be assumed equal to:

$\gamma_C = 1.5$ for concrete of ordinary production
$\gamma_C = 1.4$ for concrete of controlled production with $\delta \leq 0.10$

(δ coefficient of variation = ratio of the standard deviation to the mean value).

In the verifications of stresses (serviceability limit state) the following values are adopted for concrete:

$\bar{\sigma}_c = 0.45 f_{ck}$ allowable tensile stress for quasi-permanent combination
$\bar{\sigma}_{cj} = 0.60 f_{ckj}$ allowable tensile stress for characteristic combination
$\bar{\sigma}'_{cj} = 0.70 f_{ckj}$ allowable tensile stress at prestressing.

The value of the ultimate tensile stress $\bar{\sigma}'_{ct} = \beta f_{ctk}$ refers to the limit of crack formation, with:

$\beta = 1.0$ for constant distribution
$\beta = 1.3$ for triangular distribution.

For parts with a thickness $t < 5d_a$, where d_a is the maximum aggregate size, all values of resistance and allowable stresses should be reduced by the factor $(0.5 + 0.1t/d_a)$.

Chart 2.3: Steel: Design Strength

In the resistance verifications (ultimate limit states) the values indicated below are adopted for steel of reinforced and prestressed concrete.

For passive reinforcement

$$f_{yd} = \frac{f_{yk}}{\gamma_S} \quad \text{design value of yield stress}$$

$$f_{td} = \frac{f_{tk}}{\gamma_S} (= k f_{yd}) \quad \text{design strength } (k = 1.20)$$

For prestressing reinforcement

$$f_{ptd} = \frac{f_{ptk}}{\gamma_S} \quad \text{design strength for prestressing strands}$$

$$f_{ypd} = 0.9 f_{ptd} \quad \text{design value of the yield stress}$$

The partial safety factor for all reinforcements should be assumed equal to $\gamma_S = 1.15$.

In the verification of stresses (serviceability limit state) the values indicated as follows are adopted for steel.

For passive reinforcement

$$\bar{\sigma}_s = 0.80 f_{yk} \quad \text{allowable stress of passive reinforcement}$$

For prestressing reinforcement

$\bar{\sigma}_p = 0.80 f_{pyk}$ allowable stress after losses
$\bar{\sigma}_{pi} = 0.85 f_{pyk} \leq 0.75 f_{ptk}$ initial admis. stress in post-tensioned tendons
$\bar{\sigma}_{pi} = 0.90 f_{pyk} \leq 0.80 f_{ptk}$ initial admis. stress in pre-tensioned tendons

where f_{py} is to be substituted by $f_{p0.1}$ or f_{p1}, respectively for wires and strands.

In the calculations of stresses in service, the viscoelastic effects can be approximated with the assumption in the elastic formulas of

$$\alpha_e = \frac{E_s}{E_c} = 15$$

as homogeneizaton coefficient of the steel areas in the resisting section.

For tensile stresses in the reinforcement, the allowable limits given by Table 2.16 are also to be considered, for the cracking verifications.

Chart 2.4: Reinforcement: Shaping and Detailing

The schemes of the present chart refer to the bending of steel bars for reinforced concrete with a diameter $\phi \leq 24$ mm, unless noted otherwise.

- *Bending radius (at the axis)* for end hooks and stirrups:

$$r \geq 3.0\,\phi$$

- *Mandrel diameter*

$$d_o = 2r - \phi \quad (\geq 5\phi)$$

- *Bending radius (at the axis)* for bent bars and continuous reinforcement

$$r' = 2r \quad (d'_o \geq 11\phi)$$

- *Developed length of the end hook* for $r = 3\phi$ with $\alpha = 90° \div 135° \div 180°$ for bent bars and continuous reinforcement

$$u \geq 8\phi,\ 10\phi \text{ and } 12\phi$$

- *Detailing* referred to the rectified axial polygon line (with a^* nominal sides dimensioned in the reinforcement drawings)

$$a = a^* + 1.0\phi \quad \text{actual dimensions for } r = 5\phi$$

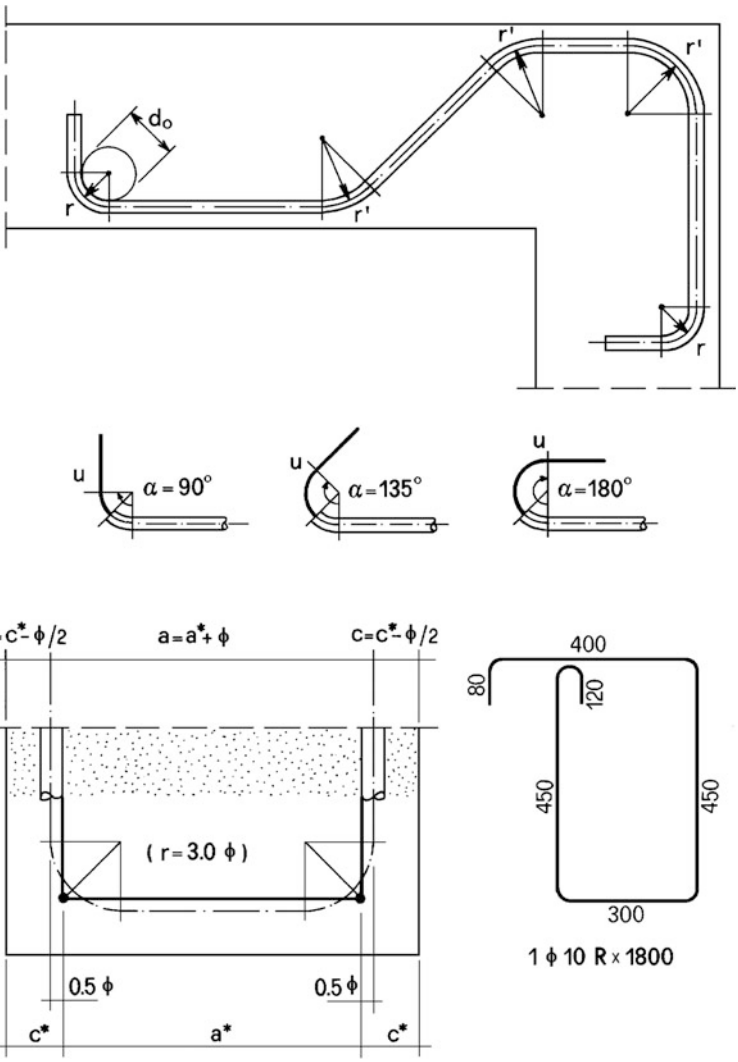


Chart 2.5: Reinforcement: Positioning Tolerances

The following deviations δ from the nominal dimensions shown in the design refer to the position of the longitudinal bars (passive bars or pretensioned strands) in the cross section. The relevant dimension (height or width) of the section is indicating with l.

$\pm\bar{\delta} = 0.04\ l\ (\geq 5\ \text{mm})$ for $l < 500$ mm
$\pm\bar{\delta} = 15 + 0.01\ l\ (\leq 30\ \text{mm})$ for $l > 500$ mm

The partial safety factors already take into account such tolerances in the resistance verifications.

For the values of cover, given that spacers adequately distributed on the formwork surfaces are used, it can be assumed:

$$\pm\delta = 10\ \text{mm}$$

The above-mentioned positioning tolerances can be halved in the case of industrial production in which the verification of bars positioning is part of the quality control system. In this case the tolerance of the cover becomes

$$\delta = -0 \quad \text{and} \quad \delta = +5\ \text{mm}$$

Table 2.6: Bond: Design Strength

The following table shows, for different codified classes of concrete and for the design of end anchorages of the bars, the following values:

f_{bk} characteristic bond strength
l_b anchorage length

Ordinary production $\Delta f = 8$ MPa			Controlled production $\Delta f = 5$ MPa		
Concrete class	f_{bk}	l_b/ϕ	Concrete class	f_{bk}	l_b/ϕ
			C30/37	5.2	28
C16/20	3.6	41	C35/43	5.6	26
C20/25	3.8	38	C40/50	6.1	24
C25/30	4.3	34	C45/55	6.5	22
C30/37	4.7	31	C50/60	7.0	21
C35/43	5.2	28	C55/67	7.4	20
C40/50	5.6	26	C60/75	7.6	19
C45/55	6.1	24	C70/85	8.1	18

The values are expressed in MPa and are deduced from the formulas:

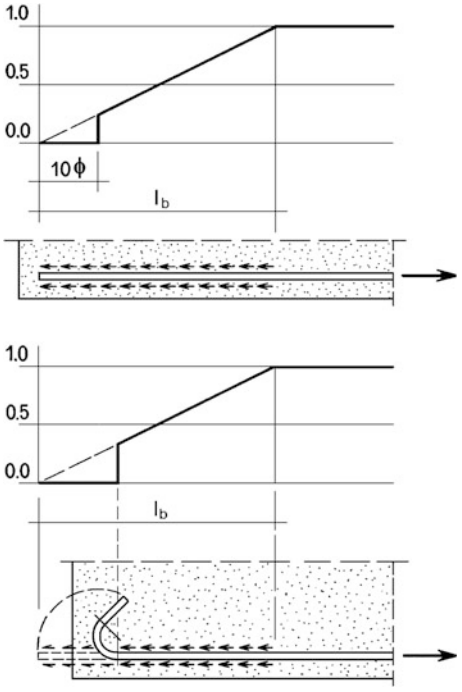
$f_{bk} = \beta_b f_{ctk}$ (see Table 1.2)
$\beta_b = 2.25$ for ribbed bars

$$l_b = \frac{\phi}{4}\frac{f_{yd}}{f_{bd}} \quad (f_{yd} = f_{yk}/\gamma_S; f_{bd} = f_{bk}/\gamma_C)$$

In particular, the anchorage length refers to the ribbed bars in steel of the type B450C, with $\gamma_S = 1.15$ and $\gamma_C = 1.5$ and it is expressed as a ratio to the diameter ϕ of the bar (l_b/ϕ). For anchorages in surface zones in tension, the bond strength should be halved.

Chart 2.7: Reinforcement: Anchorages and Overlaps

It can be assumed that bond stresses at the end of a bar in tension are distributed along the anchorage length l_b with a constant value and that the effectiveness of the bar in tension increases linearly starting from its end up to the full value (=1.0) of its capacity, reached at the distance l_b. The first segment equal to 10ϕ is to be considered ineffective. For the anchorage, hooks are to be calculated with reference to their developed length and they are to be considered ineffective up to the tangent point. The following scheme refers to an end anchorage in uncracked zone.



The overlapping on the tension side corresponds to a double end anchorage of the consecutive bars and it should be done with a segment $l_b < (20\phi + i)$ of straight overlapping, where i is the distance between bars to be joint, plus an end segment of length $u \geq 10\phi$ bent inwards, towards the compression zone. For bond, the effectiveness of the surface straight segment l_{ob} should be halved; the full capacity of the bar is therefore reached at:

$$l_{ob} = 2(l_b - u)$$

with l_b defined in Table 2.6. The following scheme gives the complementary growth of the effectiveness of the two joint bars. The capacity of the joint, indicated by the dotted line, can be enhanced increasing the overlapping.

Reinforcement joints in tie elements should be done with a full confinement, introducing transverse stirrups in the segment of bars overlapping, commensurate to the axial force to be transferred.

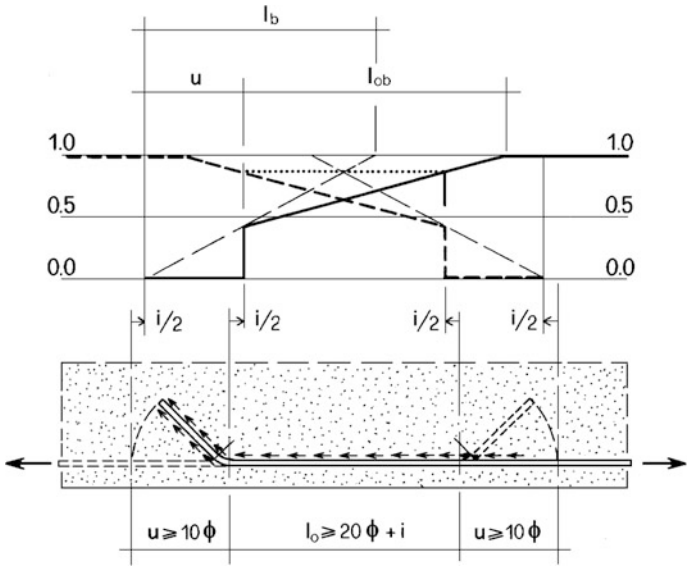


Chart 2.8: Concrete Structures: Minimum Dimensions

Structural elements in plain, reinforced and prestressed concrete should be designed with the minimum dimensions given by the most restrictive minimum values of the following cases:

Absolute Minimum Thicknesses
Technological limits to ensure a *sufficient compact mass*:

components for extruded or vibrocompacted floors	$t \geq 30$ mm
components for cast in situ floors	$t \geq 40$ mm
parts of main structural elements	$t \geq 50$ mm
wall panels and plain concrete	$t \geq 80$ mm

Relative Minimum Thicknesses
Requirement of good *homogeneity of concrete* for a uniform strength (d_a = maximum aggregate size):

• walls in plain concrete (unreinforced)	$t \geq 5.0\ d_a$
• structural elements reinforced on both sides	$t \geq 4.0\ d_a$
• slabs and ribs reinforced on one layer	$t \geq 2.4\ d_a$
• reinforced toppings sitting on permanent blocks	$t \geq 1.6\ d_a$

Minimum Bar Spacing (Concrete)
Guarantee of the passage of aggregates for good compaction of concrete (d_a = maximum aggregate size):

	Spacing		Cover
	Horizontal i_{oh}	Vertical i_{ov}	c_o
• stirrups and links	$\geq 1.6\ d_a$	$\geq 1.6\ d_a$	$\geq 0.8\ d_a$
• passive reinforcement	$\geq 1.0\ d_a$	$\geq 0.8\ d_a$	$\geq 1.0\ d_a$
• pretensioned reinforc.	$\geq 1.2\ d_a$	$\geq 1.0\ d_a$	$\geq 1.0\ d_a$

Minimum Bar Spacing (Steel)
Requirement of *good encasing* of bars for effective bond (ϕ reinforcement diameter):

	Spacing i_o	Cover c_o
• passive reinforcement	$\geq 1.0\ \phi$	$\geq 1.0\ \phi$
• pretensioned reinforc.	$\geq 2.0\ \phi$	$\geq 1.5\ \phi$

For cover see also Table 2.17.

Chart 2.9: Ordinary Columns: Formulas and Construction Rules

Reinforced concrete sections subject to compression axial force.

Symbols

N_{Ek}	characteristic axial force
N_{Ed}	design axial force
b	smaller side dimesion of section
ϕ	diameter of longitudinal bars
ϕ'	stirrups diameter
i	centre-to-centre distance of longitudinal bars
s	stirrups spacing (current part)
s'	stirrups spacing (column ends)
A_c	concrete area
A_s	area of longitudinal reinforcement
$\rho_s = A_s/A_c$	geometrical reinforcement ratio
$\alpha_e = E_s/E_c$	elastic moduli ratio (see Chart 2.3)
$\psi_s = \alpha_e\ \rho_s$	elastic reinforcement ratio
f_{cd}	concrete design strength
f_{yd}	reinforcement design strength
$r_s = f_{yd}/f_{cd}$	design strength ratio
$\omega_s = r_s\ \rho_s$	mechanical reinforcement ratio
σ_c	concrete stress
σ_s	steel stress
$\bar{\sigma}_c$	concrete allowable stress (see Chart 2.2)
N_{Rd}	design resisting axial force

Verifications

Service

$$\sigma_c = \frac{N_{Ed}}{A_c(1+\psi_s)} \leq 0.7\bar{\sigma}_c \quad (\sigma_s = \alpha_e\sigma_c)$$

Resistance

$$N_{Rd} = f_{cd}A_c(0.8+\bar{\omega}_s)$$

Construction requirements

$b \geq 200\ mm$	(≥ 150 mm in prefabrication)
$A_s \geq 0.10\ N_{Ed}/f_{yd}$	i $\leq$ 300 mm
$\rho_s \geq 0.003$	s $\leq$ b
$\rho_s \leq 0.04$	s $\leq$ 300 mm

$\phi \geq 12$ mm $\qquad$ $s \leq 12\,\phi$
$\phi' \geq \phi / 4$ $\qquad$ $s' \leq 0.6\,s$

Chart 2.10: Confined Columns: Formulas and Construction Requirements

Symbols

D	diameter of spiral
n	number longitudinal bars
s	pitch of spiral or spacing of hoops
a_w	area of spiral or hoops
$A_n = \pi D^2/4$	area of confined core
$A_w = a_w\,\pi D/s$	equivalent area of spiral or hoops
$\omega_1 = r_s\,A_1/A_n$	longitudinal mechanical reinforcement ratio
$\omega_w = r_s\,A_w/A_n$	spiral or hoops mechanical reinforcement ratio

See also Chart 2.9.

Verifications

Service

$$\sigma_c = \frac{N_{Ed}}{A_c(1+\psi_s)} \leq \bar{\sigma}_c \quad (\sigma_s = \alpha_e \sigma_c)$$

Resistance

$$N_{Rd} = f_{cd} A_c (0.8 + \omega_1 + 1.6\omega_w) \geq N_{Ed}$$

Construction Requirements

$n \geq 6$
$s \leq D/5$
$0.8 + \omega_1 + 1.6\,\omega_s \leq 2$
$A_1 \geq A_w/2$
Data of Chart 2.9 are also valid except s'.

Chart 2.11: RC Walls: Construction Requirements

Walls reinforced on both sides with internal vertical bars and external horizontal bars.

Symbols

t wall thickness
ϕ diameter of vertical bars
ϕ' diameter of horizontal bars
i centre-to-centre distance between vertical bars
s spacing of horizontal bars
c edge axis distance
a_v area of vertical reinforcement per unit length
a_h area of horizontal reinforcement per unit height

Construction requirements

$a_v \geq 0.0030\ t$ (total on both sides)
$a_v \leq 0.04\ t$ (total on both sides)
$a_h \geq 0.0015\ t$ (total on both sides)
$i \leq 300$ mm
$\phi \geq 8$ mm
$i \leq 2\ t$
$\phi' \geq \phi/3$
$s \leq 300$ mm
$c \geq 2\ \phi$
$s \leq 25\ \phi$

The end parts of the walls are to be reinforced with longitudinal (vertical) and transverse bars according to the requirements for ϕ, ϕ' and s of Chart 2.9.

The requirements above are to be applied if the vertical reinforcement is taken into account in the calculation of the capacity of the wall according to the verification formulas of Chart 2.9.

Table 2.12: Creep in Columns: Stress Redistribution

The following table shows, for different elastic reinforcement rations and for the three nominal coefficients of final creep given for RC in Table 1.16, the stress variation ratios with respect to the initial elastic values:

ψ_s	$\varphi_\infty = 1.9$			$\varphi_\infty = 2.5$			$\varphi_\infty = 3.1$		
	α_e^*	σ_c^*	σ_s^*	α_e^*	σ_c^*	σ_s^*	α_e^*	σ_c^*	σ_s^*
0.00	*2.90*	*1.00*	*2.90*	*3.50*	*1.00*	*3,50*	*4.10*	*1.00*	*4.10*
0.02	2.94	0.96	2.83	3.56	0.95	3.39	4.20	0.94	3.95
0.04	2.97	0.93	2.76	3.62	0.91	3.29	4.29	0.89	3.81
0.06	3.01	0.90	2.70	3.69	0.87	3.20	4.39	0.84	3.68
0.08	3.04	0.87	2.64	3.75	0.83	3.11	4.48	0.79	3.56
0.10	3.07	0.84	2.59	3.81	0.80	3.03	4.58	0.75	3.46
0.12	3.11	0.82	2.53	3.87	0.77	2.96	4.68	0.72	3.36
0.14	3.14	0.79	2.49	3.93	0.74	2.89	4.77	0.68	3.26
0.16	3.17	0.77	2.44	3.99	0.71	2.82	4.87	0.65	3.17

(continued)

(continued)

ψ_s	$\varphi_\infty = 1.9$			$\varphi_\infty = 2.5$			$\varphi_\infty = 3.1$		
	α_e^*	σ_c^*	σ_s^*	α_e^*	σ_c^*	σ_s^*	α_e^*	σ_c^*	σ_s^*
0.18	3.20	0.75	2.40	4.04	0.68	2.76	4.96	0.62	3.09
0.20	3.24	0.73	2.36	4.10	0.66	2.70	5.06	0.60	3.02
0.22	3.27	0.71	2.32	4.16	0.64	2.65	5.15	0.57	2.95
0.24	3.30	0.69	2.28	4.22	0.62	2.60	5.25	0.55	2.88
0.26	3.33	0.68	2.25	4.27	0.60	2.55	5.34	0.53	2.82
0.28	3.36	0.66	2.21	4.33	0.58	2.50	5.44	0.51	2.76
0.30	3.38	0.65	2.18	4.38	0.56	2.46	5.53	0.49	2.70
0.32	3.41	0.63	2.15	4.44	0.55	2.42	5.62	0.47	2.65
0.34	3.44	0.62	2.13	4.49	0.53	2.38	5.71	0.46	2.60
0.36	3.47	0.60	2.10	4.54	0.52	2.34	5.80	0.44	2.56
0.38	3.50	0.59	2.07	4.60	0.50	2.31	5.90	0.43	2.51
0.40	3.52	0.58	2.05	4.65	0.49	2.28	5.99	0.41	2.47

$\alpha_e^* = \alpha_{e\infty}/\alpha_e$ homogeneization coefficient of reinforcement
$\sigma_c^* = \sigma_{c\infty}/\sigma_{co}$ final stress in concrete
$\sigma_s^* = \sigma_{s\infty}/\sigma_{so}$ final stress in steel $(=\varepsilon_\infty/\varepsilon_o)$

where the stresses σ_{co}, σ_{so} in the materials are intended to be calculated with the service verification formula of Chart 2.9 based on the actual ratio $\alpha_e = E_s/E_c$ of elastic moduli.

The values of the table are calculated with the formulas:

$$\alpha_e^* = \frac{e^{\beta\phi_\infty}}{\beta} - \frac{1}{\psi_s} \quad \text{with } \beta = \frac{\psi_s}{1+\psi_s}$$

$$\sigma_c^* = e^{-\beta\phi\infty}$$

$$\sigma_s^* = \alpha_e^* \sigma_c^*$$

valid for concrete loaded at an early stage (extreme ageing theory).

Table 2.13: Shrinkage in RC: Stress Effects

The following table shows, for the different elastic reinforcement ratios $\psi_s = \alpha_e \rho_s$, the coefficients

$$\beta = \frac{\psi_s}{1+\psi_s} \quad \beta' = \frac{1}{1+\psi_s}$$

for the calculation of shrinkage self-induced stresses in concrete and steel

$$\sigma_{cs} = \beta\sigma_{ce} \quad \sigma_{ss} = -\beta'\sigma_{se}$$

with

$$\sigma_{ce} = E_c\varepsilon_{cs} \quad \sigma_{se} = E_s\varepsilon_{cs}$$

in the doubly symmetric RC sections (ε_{cs} = concrete shrinkage).

ψ_s	β	β'	ψ_s	β	β'
0.00	*0.00*	*1.00*			
0.02	0.02	0.98	0.22	0.18	0.82
0.04	0.04	0.96	0.24	0.19	0.81
0.06	0.06	0.94	0.26	0.21	0.79
0.08	0.07	0.93	0.28	0.22	0.78
0.10	0.09	0.91	0.30	0.23	0.77
0.12	0.11	0.89	0.32	0.25	0.76
0.14	0.12	0.88	0.34	0.25	0.75
0.16	0.14	0.86	0.36	0.26	0.74
0.18	0.15	0.85	0.38	0.28	0.72
0.20	0.17	0.83	0.40	0.29	0.71
			∞	*1.00*	*0.00*

Chart 2.14: Ties in Reinforced and Prestressed Concrete

Reinforced concrete sections subject to axial tension force with possible centred precompression.

Symbols

A_p	area of prestressing reinforcement
$\rho_p = A_p/A_c$	geometric prestressing reinforcement ratio
$\psi_p = \alpha_e\ \rho_p$	prestressing elastic reinforcement ratio
$A_t = A_s + A_p$	total area of passive plus active reinforcement
$\psi_t = \psi_s + \psi_p$	total elastic reinforcement ratio
$\alpha = A_s/A_p$	passive to active reinforcement ratio
σ_{po}	prestressing stress in the tendon
$N_{po} = \sigma_{po}\ A_p$	prestressing force in the tendon

See also Charts 2.2, 2.3 and 2.9.

Verifications

Service

- *Uncracked section*

$$\sigma_c = \frac{N_{ak} - N_{po}}{A_c(1 + \psi_t)}$$
$$\sigma_s = \alpha_e \sigma_c \quad \sigma_p = \alpha_e \sigma_c + \sigma_{po}$$

Verification of decompression of concrete $\sigma_c \leq 0$
Verification of cracks formation $\sigma_c \leq \bar{\sigma}'_{ct}$

- *Cracked section*

$\sigma_s = \frac{N_{ak} - N_{po}}{A_t} \leq \bar{\sigma}_s$ (see also Table 2.16)
$\sigma_p = \frac{N_{ak} - \alpha N_{po}}{A_t} \leq \bar{\sigma}_s$ (see also Table 2.16)

Resistance

$$N_{Rd} = f_{sd} A_s + f_{pd} A_p \geq N_{ad}$$

Minimum reinforcement

$$A_s \geq A_c f_{ctm} / f_{yk}$$

For technological data see Chart 2.15.

Chart 2.15: Cracking in RC and PC: Verification Scheme

The following scheme shows the verifications required in the different service conditions of the elements in reinforced and prestressed concrete. The symbols are defined here under:

σ'_s stress in passive reinforcement calculated in the cracked section;
σ_c stress in concrete in tension calculated in the uncracked section;
$\sigma^*_P = \sigma'_p - \sigma_{po}$ stress increment in the pretensioned reinforcement calculated in the cracked section with respect to the decompression of concrete;

Type of reinforce	Load combinations	Environment aggressiveness		
		Low	Medium	High
Passive	Rare	–	–	–
	Frequent	$\sigma'_s \leq \bar{\sigma}'_{s3}$	$\sigma'_s \leq \bar{\sigma}'_{s2}$	$\sigma'_s \leq \bar{\sigma}'_{s1}$
	Quasi perman.	$\sigma'_s \leq \bar{\sigma}'_{s2}$	$\sigma'_s \leq \bar{\sigma}'_{s1}$	$\sigma'_s \leq \bar{\sigma}'_s$
Pretensioned	Rare	–	$\sigma_C < \beta f_{ctk}$	$\sigma_C < \beta f_{ctk}$
	Frequent	$\sigma^*_p \leq \bar{\sigma}'_{s2}$	$\sigma^*_p \leq \bar{\sigma}'_{s1}$	$\sigma^*_p \leq \bar{\sigma}'_s$
	Quasi perman.	$\sigma^*_p \leq \bar{\sigma}'_{s1}$	$\sigma^*_p \leq \bar{\sigma}'_s$	$\sigma_C \leq 0$

For the allowable stresses $\bar{\sigma}'_{s1}$, $\bar{\sigma}'_{s2}$, $\bar{\sigma}'_{s3}$, see Table 2.16. The passive reinforcement is made of ribbed bars; the pretensioned reinforcement is made of adherent smooth or indented wires or strands. For the classification of environments see Table 2.1.

$\bar{\sigma}'_s = 0.5\sigma'sr$ with σ'_{sr} stress corresponding to cracking of the section ($\bar{\sigma}_{sr} = (A_c + \alpha_e A_s) f_{ctk}/A_s$ for ties);

$\beta f'_{ctk}$ characteristic tensile strength of concrete (with $\beta = 1.0$ for constant distribution and $\beta = 1.3$ for triangular distribution of stresses);

$\sigma^*_D = \sigma'_D - \sigma_{DO}$ increment of tension in pretensioned reinforcement calculated in the cracked section with respect to decompression in concrete.

Table 2.16: Cracking in RC and PC: Allowable Stresses

The following table shows, for different values of the diameter ϕ, the allowable stresses in passive and pretensioned reinforcement to be used in cracking verifications of Chart 2.15. Stresses $\bar{\sigma}'_{s1}$, $\bar{\sigma}'_{s2}$, $\bar{\sigma}'_{s3}$ correspond respectively to crack widths $\bar{w}_1 = 0.2$ mm, $\bar{w}_2 = 0.3$ mm, $\bar{w}_3 = 0.4$ mm.

The values are expressed in MPa and refer to longitudinal reinforcement with ribbed bars distributed along the edges in tension of the section, with a centre-to-centre distance

$i \leq 5\phi$ for pure tension (ties)
$i \leq 8\phi$ for pure bending (beams)

and to alternate or long duration loads.

Pure tension (Ties)			ϕ (mm)	Pure bending (beams)		
$\bar{\sigma}'_{s1}$	$\bar{\sigma}'_{s2}$	$\bar{\sigma}'_{s3}$		$\bar{\sigma}'_{s1}$	$\bar{\sigma}'_{s2}$	$\bar{\sigma}'_{s3}$
240	320	360	8	280	360	400
225	280	320	10	260	320	360
210	250	290	12	240	280	320
195	235	295	14	220	260	300
180	220	260	16	200	240	280
165	205	235	18	190	230	260
150	190	210	20	180	220	240
140	175	190	22	170	210	230
130	165	180	24	160	200	220

This table is deduced from the analogous table of the standard EN 1992-1-1:2004 with adequate adaptations.

Table 2.17: Durability: Minimum Cover of Reinforcement

The following tables give, for the different combination of environmental aggressiveness (see Table 2.1), the values of minimum reinforcement cover for the protection against corrosion. The values of the table are expressed in mm and refers to the actual concrete cover required for constructions of a nominal life of 50 years. The nominal values of cover to be shown in the drawings would have to be increased by the positioning tolerances of reinforcement assumed equal to ±10 mm for ordinary production, equal to ±5 mm for controlled production.

Concrete classes		Environment	Bars for plate elements		Bars for other elements	
C_{min}	C_o	Aggressiv.	$C \geq C_o$	$C_{min} \leq C < C_o$	$C \geq C_o$	$C_{min} \leq C < C_o$
C25/30	C35/45	Low	15	20	20	25
C30/37	C40/50	Medium	25	30	30	35
C35/45	C45/55	High	35	40	40	45

Concrete classes		Environment	Strands for plate elements		Strands for other elements	
C_{min}	C_o	Aggressiv.	$C \geq C_o$	$C_{min} \leq C < C_o$	$C \geq C_o$	$C_{min} \leq C < C_o$
C25/30	C35/45	Low	25	30	30	35
C30/37	C40/50	Medium	35	40	40	45
C35/45	C45/55	High	45	50	50	50

For constructions with a nominal life of 100 years, the values of the table should be increased by 10 mm. For strength classes lower than C_{min}, such values are to be increased by 5 mm. For elements of controlled production they can be reduced by 5 mm.

Chapter 3
Bending Moment

Abstract This chapter presents the design methods of reinforced and prestressed concrete sections subjected to bending moment. The criteria for cracking calculation are here extended to beams in flexure, for which the analysis of deformation is shown including creep effects. In the final section after the specific analysis of loads, the design of floors is shown with the pertinent serviceability and resistance verifications.

3.1 Analysis of Sections in Bending

In a beam as the one in reinforced concrete outlined in Fig. 3.1a, sections react to bending moment produced by external loads with a distribution of normal stresses σ partially in tension and partially in compression. The simultaneous presence of shear actions is not considered for now; it will be largely discussed in Chap. 4. Because of one of the assumptions of reinforced concrete design, the one that assumes the tensile strength of concrete equals to zero, the section of the beam cracks remaining, as resisting part for resistance calculations, the zone of concrete in compression plus all the steel reinforcement in tension and compression. The reinforcement will therefore be mainly placed on the beam side in tension in order to constitute its *tension chord*, collaborating with the *compression chord* given by the concrete. The part of concrete in tension does not contribute to this resistance; it only ensures the connection between the two chords, as it will be better specified further on.

The actual behaviour of concrete sections in bending undergoes several phases according to the force level (see Fig. 3.1b):

- *phase I* of low force levels with still an elastic behaviour of both materials and a "butterfly" elastic distribution of stresses in concrete on the uncracked section;
- *phase IA* with stresses at the concrete side in tension close to its tensile strength and behaviour still linear elastic for the part in compression, nonlinear for the one in tension; this phase is often approximated to the linear one of phase I amplifying fictitiously the concrete tensile strength in the design (see the

© Springer International Publishing AG 2017

G. Toniolo and M. di Prisco, *Reinforced Concrete Design to Eurocode 2*,
Springer Tracts in Civil Engineering, DOI 10.1007/978-3-319-52033-9_3

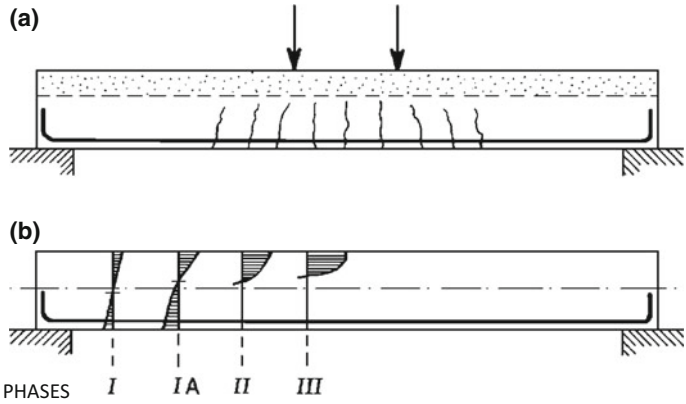


Fig. 3.1 Behaviour phases of a beam in bending

bending test described at Sect. 1.1.2), or a lower elastic modulus is assumed in tension with respect to the one in compression (e.g. with $E_{ct} = E_c/2$);

- *phase II* where, once the concrete tensile strength is attained, cracking is initiated, which extends instantaneously up to a level close to the neutral axis, transferring the entire tension force in the steel reinforcement; concrete in compression and reinforcement can still be within the nearly linear elastic behaviour;
- *phase III* with internal forces close to the ultimate flexural capacity of the section where the behaviour of materials definitely goes beyond the linear elastic range.

Phases I and II are contemplated in the service verifications, and phase III for the resistance verification.

It is to be noted that the neutral axis, centred with respect to the resisting section in pure bending, moves when the force level varies. A distinction should therefore be made between design axis of the beam, that is the one assumed in the analysis of the frame for the definition of diagrams of the internal forces and coinciding in general with the centroid of the geometrical section of concrete only, and the centroids of the resisting sections that vary, also for beams with constant cross section shape, with the level and type of force, other than for possible changes of reinforcement.

In the following, the above-mentioned assumptions of plane sections and deformation compatibility will be applied. For elastic calculations, Hooke's law will be added, sometimes alongside with the assumption of cracked section. Through the appropriate equilibrium conditions of the section, the verification formulas of stresses produced by the bending moment will therefore be deduced, where, in particular, the centroidal moment of inertia of the resisting section remains the main parameter of the structural behaviour.

In the resistance design, given the three assumptions of plane sections, deformation compatibility and cracked sections, the one on elasticity based on Hooke's law should be substituted by a more complete σ–ε model of the material, extended up to the ultimate values of deformations corresponding to rupture limits.

For concrete, the three models parabola–rectangle, bilinear and rectangular of Fig. 1.28 have been introduced at Sect. 1.4.2. Given the linearity of contractions in concrete, which for sections in bending vary from 0 on the neutral axis *nn* to the maximum value ε_c on the extreme fibre, the distribution of stresses on such part will reproduce the constitutive model itself, fully or partially, depending whether the maximum contraction ε_c has attained the ultimate limit ε_{cu} (see Fig. 3.2).

Therefore, in the resistance calculations, the resultant force of compressions in concrete is to be evaluated:

$$C = \int_0^x \sigma\, b\, \mathrm{d}y$$

and its contribution in terms of bending moment:

$$M_c = \int_0^x y\, \sigma\, b\, \mathrm{d}y$$

with $\sigma = \sigma(\varepsilon)$ given by the constitutive model and $\varepsilon = y\varepsilon_c/x$ expressed on the basis of the linearity of deformations.

For rectangular sections, with b = cost., these formulas simply translate into the evaluation of the area under the stress diagram and in the identification of its centroid. If for example the rupture ultimate contraction $\varepsilon_c = \varepsilon_{cu}$ is attained, the three different models proposed for the concrete constitutive law, through elementary geometrical calculations, lead to a resulting force of compressions:

$$C = \beta_o b\, x f_{cd}$$

set at a distance $\kappa_o x$ from the edge of the section in compression (see Fig. 3.3), with

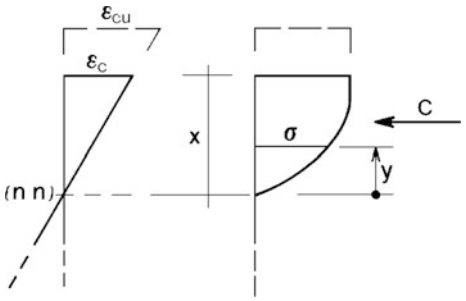


Fig. 3.2 Distribution of strains and stresses in the section

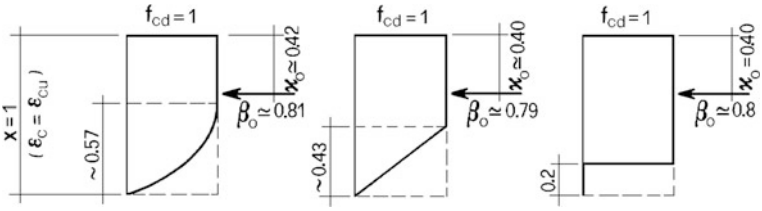


Fig. 3.3 Models of stresses in compression zone

$$\beta_o \cong 0.8 \quad \kappa_o \cong 0.4.$$

The coefficient β_o represents the ratio between the area under the actual diagram and one of the circumscribed rectangles; the coefficient κ_o defines the position of the centroid with respect to the extent x of the diagram itself.

For a maximum compressive strain ε_c of concrete lesser than the ultimate value ε_{cu} (see Fig. 3.4), such coefficients are well approximated by the following expressions:

$$\beta = \beta(\bar{\varepsilon}_c) = (1.6 - 0.8\bar{\varepsilon}_c)\bar{\varepsilon}_c$$
$$\kappa = \kappa(\bar{\varepsilon}_c) = 0.33 + 0.07\bar{\varepsilon}_c,$$

which link the behaviour from $\varepsilon_c = \varepsilon_c/\varepsilon_{cu} = 1$ (with $\beta = \beta_o \cong 0.8$ and $\kappa = \kappa_o \cong 0.4$) up to $\varepsilon_c \to 0$ (with $\beta \to 0$ and $\kappa \to 1/3$).

3.1.1 Elastic Design of Sections

Uncracked Section

For an elastic calculation on an uncracked section, corresponding to the behaviour of phase I, what deduced in structural mechanics for the de Saint-Vénant's beam is valid: it suffices to homogenize the reinforcement areas with the coefficient $\alpha_e = E_s/E_c$ and use the consequent equivalent characteristic I_i of the section.

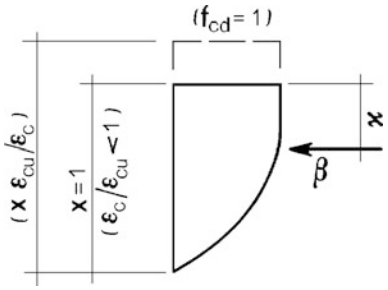


Fig. 3.4 Reduced model of stresses in compression zone

Referring to the section with double reinforcement described in Fig. 3.5, one therefore has

$$\sigma_c = -\frac{M}{I_i} y_c \quad \text{(in compression)}$$
$$\sigma'_c = \frac{M}{I_i} y'_c \quad \text{(in tension)}$$
$$\sigma_s = \alpha_e \frac{M}{I_i} y_s \quad \text{(in tension)}$$
$$\sigma'_s = -\alpha_e \frac{M}{I_i} y'_s \quad \text{(in compression)},$$

where the moment of inertia I_i is obtained from the formulas of the Geometry of Masses:

$$I_i = hb\left[\frac{h^2}{12} + \left(y_c - \frac{h}{2}\right)^2\right] + \alpha_e A_s y_s^2 + \alpha_e A'_s y'^2_s$$
$$y_c = \frac{S'_i}{A_i} \quad y'_c = h - y_c \quad y_s = y'_c - c \quad y'_s = y_c - c'$$
$$S'_i = \frac{h^2 b}{2} + \alpha_e A_s (h - c) + \alpha_e A'_s c'$$
$$A_i = hb + \alpha_e A_s + \alpha_e A'_s.$$

The classic assumptions of Bernoulli and elasticity have been used above, in addition to one of the compatibilities between the deformations of the two materials.

Cracked Section

For an elastic behaviour on cracked sections of phase II, the analysis of the section with single reinforcement of Fig. 3.6 starts from the usual assumptions of the reinforced concrete design:

- Bernoulli's assumption leads to a linear diagram of strains ε, where in particular the position x of the neutral axis will have to be defined through a first condition of equilibrium of the section;

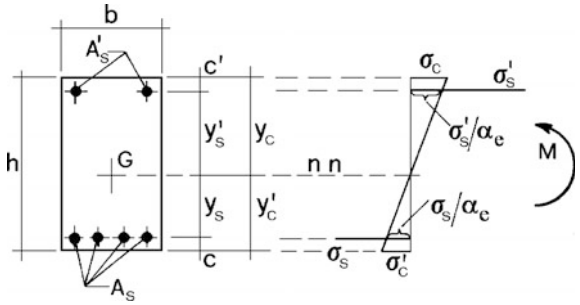


Fig. 3.5 Stress distribution in an uncracked section

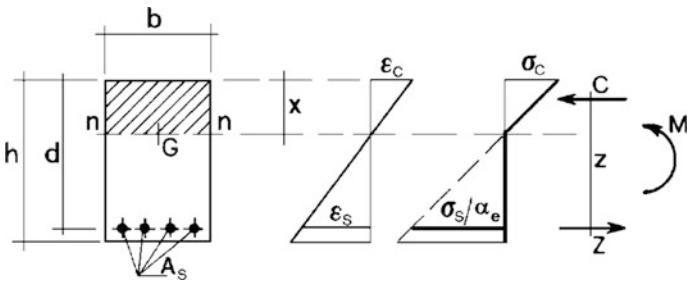


Fig. 3.6 Strain and stress distribution in a cracked section

- the assumption of compatibility leads to identify within the same diagram, the strain of the ε_s of the reinforcement;
- the assumption of cracked sections leads to defining only the concrete part in compression as resisting (the dashed one in the figure) plus the section A_s of the steel reinforcement;
- finally, the assumption of elasticity allows the transition to the diagram of stresses σ, still linear, where in particular the stress in compression at the upper edge of concrete is indicated with $\sigma_c = E_c\varepsilon_c$, the stress in tension of the reinforcement with $\sigma_s = E_s\varepsilon_s$.

The concrete under the neutral axis *nn* does not contribute; the dashed straight segment, shown in Fig. 3.6 as the continuation of the diagram of stresses σ in the zone of concrete in compression, allows to intercept the ordinate σ_s/α_e at the level of the reinforcement, with $\alpha_e = E_s/E_c$ equal to the usual homogenization coefficient.

Indicating with C the resultant force of compressions and with Z the resultant force of tensions, both assumed positive, the equilibrium to translation of the section is written as

$$Z - C = 0.$$

For the rectangular section with simple reinforcement under study, such resultant forces are simply equal to

$$C = \frac{1}{2}\sigma_c bx \quad Z = \sigma_s A_s,$$

and one therefore has

$$\frac{1}{2}\sigma_c bx - \sigma_s A_s = 0,$$

having assumed positive the tensile stresses in the steel reinforcement and compressive stresses in concrete. Writing now the equality that links, in the diagram of stresses, the two values σ_c and σ_s, one has (see Fig. 3.6)

$$\frac{\sigma_s/\alpha_e}{d-x} = \frac{\sigma_c}{x}$$

from which one derives

$$\sigma_s = \alpha_e \sigma_c \frac{d-x}{x},$$

which, substituted in the previous equation, gives

$$\frac{1}{2}\sigma_c b x - \alpha_e \sigma_c \frac{d-x}{x} A_s = 0.$$

Simplifying σ_c, which is definitely not equal to 0 for $M \neq 0$, and properly reorganizing the terms, one eventually has

$$x^2 + \frac{2\alpha_e A_s}{b} x - \frac{2\alpha_e A_s}{b} d = 0.$$

2° degree algebraic equation in x, which gives the position of the neutral axis:

$$x = \frac{\alpha_e A_s}{b}\left\{-1 + \sqrt{1 + \frac{2bd}{\alpha_e A_s}}\right\}.$$

The negative square root which does not have physical meaning is discarded, corresponding to a neutral axis outside the section.

Having then defined the extent of the resisting section, the verification of stresses produced by the bending moment M on the section is obtained from the rotational equilibrium which equates such moment to one of the internal couples. Setting therefore (see Fig. 3.6)

$$z = d - \frac{x}{3}$$

as lever arm of the internal couple, with reference to the centre of tensions, one can write

$$C\,z = M,$$

from which

$$\sigma_c = \frac{2M}{z\,b\,x} \quad \text{(compression)}$$

and with reference to the centre of compressions one can write

$$Z\,z = M,$$

from which

$$\sigma_s = \frac{M}{zA_s} \quad \text{(tension)}.$$

Introducing the *elastic reinforcement ratio* defined as

$$\psi_s = \frac{\alpha_e A_s}{bd} = \alpha_e \rho_s,$$

the same formulas of definition of the resisting section become

$$x = \psi_s \left\{ -1 + \sqrt{1 + \frac{2}{\psi_s}} \right\} d = \xi d$$
$$z = \left(1 - \frac{\xi}{3}\right) d = \zeta d,$$

where the positions of the neutral axis and the lever arm of the internal couple are given by the non-dimensional quantities ξ and ζ as a function of the effective depth d of the section.

For a rectangular section with double reinforcement, with a similar procedure, given $A_t = A_s + A'_s$ and $\psi_t = \alpha_e A_t / bd$, one obtains (see Fig. 3.7)

$$x = \psi_t \left\{ -1 + \sqrt{1 + \frac{2\delta}{\psi_t}} \right\} d$$

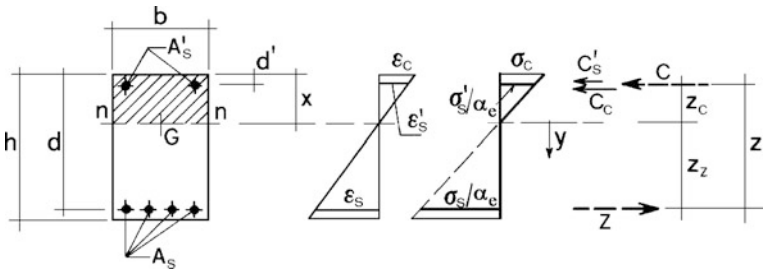


Fig. 3.7 Strain and stress distribution in a section with double reinforcement

with

$$\delta = \frac{\mathrm{d}A_\mathrm{s} + \mathrm{d}'A'_\mathrm{s}}{A_\mathrm{t}} \frac{1}{d},$$

and by consequence

$$\sigma_\mathrm{c} = \frac{M}{I_i} x \quad \text{(compression)}$$
$$\sigma_\mathrm{s} = \alpha_\mathrm{e} \frac{M}{I_i} (d - x) \quad \text{(tension)}$$
$$\sigma'_\mathrm{s} = -\alpha_\mathrm{e} \frac{M}{I_i} (x - d') \quad \text{(compression)}$$

with

$$I_i = \frac{bx^3}{3} + \alpha_\mathrm{e} A_\mathrm{s} (d - x)^2 + \alpha_\mathrm{e} A'_\mathrm{s} (x - d')^2.$$

It is reminded that, in order to evaluate the lever arm z of the internal couple, given (see Fig. 3.7)

$$z = z_\mathrm{c} + z_z,$$

and taking into account the linearity $\sigma(y) = cy$ of the stress diagram, one has

$$z = \frac{\int_0^x y\,\sigma\,\mathrm{d}y}{\int_0^x \sigma\,\mathrm{d}y} + \frac{\int_0^{d-x} y\,\sigma\,\mathrm{d}y}{\int_0^{d-x} \sigma\,\mathrm{d}y} = \frac{\int_0^x y^2 \mathrm{d}y}{\int_0^x y\,\mathrm{d}y} + \frac{\int_0^{d-x} y^2 \mathrm{d}y}{\int_0^{d-x} y\,\mathrm{d}y},$$

where one can note the centroidal static moments and moments of inertia of the two halves of the resisting section separated by the centroidal axis itself:

$$z = \frac{I_\mathrm{c}}{S_\mathrm{c}} + \frac{I_z}{S_z}.$$

Having, for the property of the centroid $S_\mathrm{c} = S_z (= S_i)$, one eventually has (with $I_i = I_\mathrm{c} + I_z$)

$$z = \frac{I_i}{S_i},$$

where, for the particular case of the section under analysis, one has

$$S_i = \frac{bx^2}{2} + \alpha_e A'_s (x - d') + \alpha_e A_s (d - x).$$

Other cases of practical interest, such as one of the T-sections, can be treated with identical procedures. A more complete formulary is shown in Chart 3.3 of the Appendix. For sections of any other shape, the equilibrium conditions should be applied through appropriate discretized numerical procedures.

Biaxial Bending

For uncracked sections, biaxial bending is treated simply superimposing the effects of the two principal orthogonal bending moments in which it can be decomposed, with the caution of homogenizing the reinforcement areas to the concrete with the usual coefficient. Considering also the axial action *N,* one therefore has formulas of the following type:

$$\sigma_c = \frac{N}{A_i} \pm \frac{M_y}{I_{yi}} z_c \pm \frac{M_z}{I_{zi}} y_c$$

$$\sigma_s = \alpha_e \left\{ \frac{N}{A_i} \pm \frac{M_y}{I_{yi}} z_s \pm \frac{M_z}{I_{zi}} y_s \right\},$$

being y and z the two principal axes of inertia of the section.

For cracked sections, the resisting part should be defined in advance. The analysis is therefore based on setting the adequate equilibrium conditions, where among the unknowns appear the geometrical parameters necessary to identify the neutral axis that separates the resisting compression part of concrete from the cracked part in tension. We limit for now to the simple case in which the concrete zone in compression has a triangular shape, leaving more complex cases to a subsequent description (see Sect. 6.2.3) that analyses the combined biaxial bending with axial force through a single algorithm of general validity.

Therefore, referring to the section of Fig. 3.8, the following three conditions are set:

- translational equilibrium along the beam axis;
- rotational equilibrium within the plane *ss* of the applied forces;
- rotational equilibrium within an orthogonal plane.

The unknowns are

- the two intersection points x and b necessary to define the position of the neutral axis *nn*;
- the stress in a point, for example the maximum σ_c at the extreme vertex of concrete, the others being deducible from the linearity of the diagram.

On concrete such diagram identifies a tetrahedron with the centroid on the coordinates $b/4$ and $x/4$ from the vertex and a volume equal to $\sigma_c bx/6$ (see also Fig. 3.9).

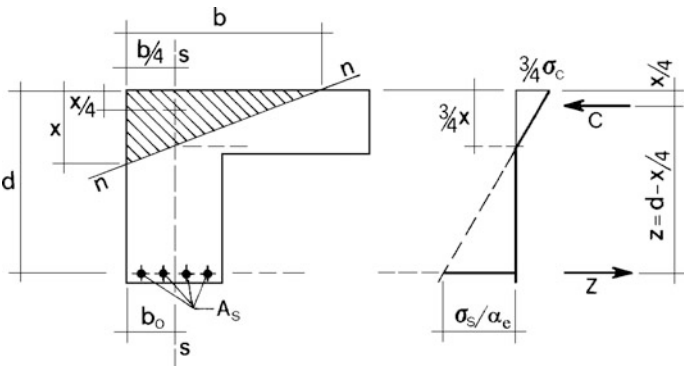


Fig. 3.8 Section under biaxial bending

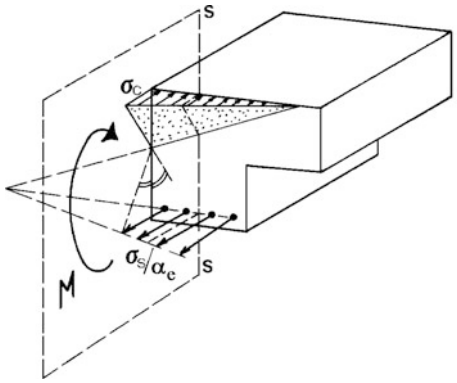


Fig. 3.9 Stress distribution—section under biaxial bending

Therefore, applying the last condition of rotational equilibrium and assuming that the reinforcement area A_s is distributed on a relatively limited portion with respect to the other involved dimensions, so that resultant force Z can be concentrated at the centroid of the bars, one has

$$Z\,b_o = C\,b/4,$$

which, with $Z = C$, leads to

$$b = 4\,b_o.$$

The other intersection point of the neutral axis is defined on the basis of the already mentioned translational equilibrium condition:

$$\sigma_c \frac{bx}{6} - \sigma_s A_s = 0.$$

From this, taking into account the linearity of the diagram of σ, one obtains

$$\frac{bx}{6} - \alpha_e \frac{d - 3x/4}{x} A_s = 0,$$

which leads to the positive root

$$x = \frac{9\alpha_e A_s}{4b} \left\{ -1 + \sqrt{1 + \frac{32bd}{27\alpha_e A_s}} \right\}.$$

Eventually, with the rotational equilibrium within the plane of applied forces, one obtains

$$\sigma_c = \frac{6M}{z\,b\,x} \quad \sigma_s = \frac{M}{zA_s},$$

with

$$z = d - \frac{x}{4}$$

lever arm of the internal couple.

This description refers to a beam free from lateral restraints. If instead the beam is connected to a slab that provides a continuous lateral restraint, the inflexion is kept in the vertical plane *ss* with different distributions of stresses (see 6.1.3).

3.1.2 *Resistance Design of Sections*

At the ultimate limit of the phase III of the flexural behaviour, a reinforced concrete section is in the situation corresponding to the attainment of the ultimate deformation of one of the two materials: either the strain ε_{ud} of the reinforcement in tension or the maximum strain ε_{cu} at the edge of the concrete in compression (see Figs. 1.28 and 1.30).

The case of a rectangular section with single reinforcement is represented in Fig. 3.10, with the possible failure modes showed. Three different fields are indicated as follows:

- *field "a" of low reinforcements* characterized by the failure of the steel reinforcement, with $\varepsilon_s = \varepsilon_{ud}$, whereas at the compression concrete edge the contraction does not attain the ultimate limit ($\varepsilon_c < \varepsilon_{cu}$);
- *field "b" of medium reinforcements* characterized by the failure of the concrete at the compression edge ($\varepsilon_c = \varepsilon_{cu}$) with steel already yielded ($\varepsilon_{ud} > \varepsilon_s > \varepsilon_{yd}$);

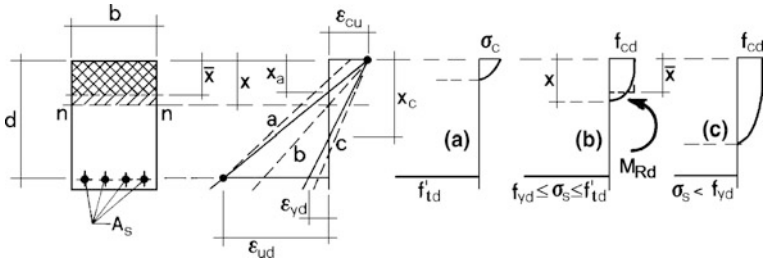


Fig. 3.10 Stain and stress distributions at the ultimate limit state

- *field "c" of high reinforcements* still characterized by the failure of concrete by attainment of ultimate contraction $\varepsilon_c = \varepsilon_{cu}$ with steel still in the elastic range ($\varepsilon_s < \varepsilon_{yd}$).

Indefinite Elastoplastic Model

With the indefinite elastoplastic B model of Fig. 1.30, the field "*a*" disappears and in field "*b*" the translational equilibrium $Z - C = 0$ of the section is set with

$$Z = A_s f_{yd} \quad (= \text{cost.})$$
$$C = \beta_o b x f_{cd},$$

from which the position of the neutral axis is deduced

$$x = \frac{A_s f_{yd}}{\beta_o b f_{cd}} = \frac{1}{\beta_o} \omega_s d = \xi d,$$

having indicated with

$$\omega_s = \frac{A_s f_{yd}}{b\, d f_{cd}},$$

the *mechanical reinforcement ratio* and with

$$\xi = \frac{\omega_s}{\beta_o},$$

the non-dimensional position of the neutral axis ($\xi = x/d$).

The extreme situation at the boundary of field "*c*" is characterized by the following equation:

$$\frac{\varepsilon_{cu}}{x_c} = \frac{\varepsilon_{yd} + \varepsilon_{cu}}{d},$$

which leads to

$$x_c = \frac{\varepsilon_{cu}}{\varepsilon_{yd} + \varepsilon_{cu}} d = \xi_c d.$$

The limit depends on yield ε_{yd} which varies with the resistance of steel itself. The corresponding mechanical ratio

$$\omega_{sc} = \beta_o \, \xi_c$$

gives the *limit reinforcement* which separates the concerned two fields "*b*" and "*c*".

To give an order of magnitude of those ratios, one can assume a type B450C of steel for which one has

$$f_{yd} = f_{yk}/\gamma_S = 450/1.15 = 391\,\mathrm{N/mm^2}$$
$$\varepsilon_{yd} = f_{yd}/E_s = 391/205000 \cong 0.0019,$$

with $\varepsilon_{cu} = 0.0035$ and $\beta_o = 0.8$, one therefore obtains

$$\xi_c \cong 0.65 \quad \omega_{sc} \cong 0.52.$$

If associated with a good concrete, for which

$$f_{yd}/f_{cd} \cong 25,$$

one has the following geometric reinforcement ratio:

$$\rho_{sc} = 0.021.$$

For the limit situation examined, one has a lever arm of the internal couple

$$z = d - \kappa_o x = (1 - \kappa_o \, \xi) d = \zeta \, d,$$

which, in a non-dimensional form and with $\kappa_o = 0.4$, assumes the value

$$\zeta_c \cong 0.74,$$

which shows a low utilization of the effective depth d of the section for the flexural capacity. For low reinforcement instead, one would have lever arms of the internal couple slightly smaller than the effective depth of the section ($\zeta > 0.90$).

The calculation of the flexural resistance M_{Rd} for the verification with respect to the applied moment M_{Ed},

$$M_{\mathrm{Rd}} > M_{\mathrm{Ed}}$$

at the ultimate limit state of the section, is carried with the usual equilibrium conditions to translation and rotation. Translational equilibrium, already written at the previous paragraph, therefore leads to identifying the neutral axis:

$$\xi = \frac{\omega_{\mathrm{s}}}{\beta_{\mathrm{o}}},$$

with ω_{s} evaluated on the basis of the geometrical characteristics b, d, A_{s} of the section and the strength of materials f_{cd}, f_{yd}. Therefore, having verified that

$$\xi \leq \xi_{\mathrm{c}},$$

the resisting moment is immediately obtained from the rotational equilibrium

$$M_{\mathrm{Rd}} = Z\, z = f_{\mathrm{yd}}\, A_{\mathrm{s}}\, \zeta\, d,$$

with $\zeta = 1 - \kappa_{\mathrm{o}}\xi$.

It is to be noted that the mechanical reinforcement ratio, as calculated on the basis of the geometry of the section and the strength of materials

$$\omega_{\mathrm{s}} = \frac{A_{\mathrm{s}} f_{\mathrm{yd}}}{b\, d\, f_{\mathrm{cd}}},$$

corresponds, apart from the effective depth d, to the extent of the constant diagram of compressions of the rectangular model (see Fig. 3.10b):

$$\bar{x} = \omega_{\mathrm{s}} d \quad (= \beta_{\mathrm{o}} x).$$

Such model, which assumes a reduced zone of concrete in compression loaded uniformly, results completely equivalent to the previous one with respect to the equilibrium equations written for the section. Placing the resultant force C at the mid-depth of the compression zone, once again one obtains the lever arm

$$z = d - \bar{x}/2 = (1 - \omega_{\mathrm{s}}/2)d,$$

which leads to the same value of the resisting moment.

The constant model results very convenient when applied in an approximate way to sections of complex shape. With reference for example to the T-section of Fig. 3.11, given that, calculated with the formula of the rectangular section, it results in

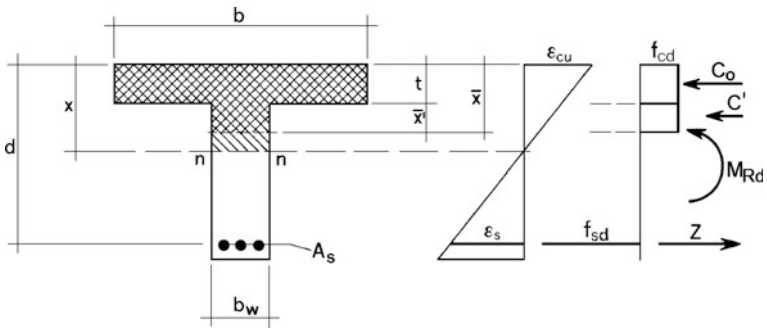


Fig. 3.11 T-section at ultimate limit state of bending

$$\bar{x} > t$$

translational equilibrium $Z - C_o - C' = 0$ can be immediately rewritten as

$$A_s f_{yd} - b t f_{cd} - b_w \bar{x}' f_{cd} = 0,$$

from which one obtains

$$\bar{x}' = \frac{A_s f_{yd}}{b_w f_{cd}} - \frac{b\,t}{b_w}.$$

Choosing the centre of the reinforcement in tension for the calculation of the moment of the internal couple, one has

$$M_{Rd} = C_0(d - t/2) + C'(d - t - \bar{x}'/2)$$

with

$$C_o = b\,t f_{cd} \quad C' = b_w \bar{x}' f_{cd}.$$

The calculation of the strains on the section, instead, would always have to be referred to the actual neutral axis. Setting it, in an approximated way, equal to $x = \bar{x}/\beta_o = (t + x')/0.8$ same as the rectangular section, one has for example

$$\varepsilon_s = \frac{d - x}{x}\varepsilon_{cu},$$

for the verification $\varepsilon_{yd} \leq \varepsilon_s$ of being within field "*b*" of medium reinforcement.

For very small reinforcement with respect to the width b of the resisting concrete, the height $x = \xi d$ of the compression zone is reduced so much that its value is not reliable with respect to the geometric tolerances. It is therefore good practice not

to assume values higher than $\zeta = 0.96$ in the calculation for the evaluation of the lever arm $z = \zeta d$ of the internal couple.

σ–ε Model with Hardening

If the bilinear model with hardening is assumed (see Fig. 1.30—model A), the field "*a*" of low reinforcements is also defined, whose limit is given by the equation (see Fig. 3.10)

$$\frac{\varepsilon_{cu}}{x_a} = \frac{\varepsilon_{ud} + \varepsilon_{cu}}{d},$$

which leads to

$$x_a = \frac{\varepsilon_{cu}}{\varepsilon_{ud} + \varepsilon_{cu}} d = \xi_a d.$$

The limit depends on the reinforcement ductility. For B450C steel (see Table 1.17) with $\varepsilon_{uk} = 7.5\%$ and $f_{td} = 1.2 f_{yd}$ one has

$$\begin{aligned}
&\varepsilon_{ud} = 0.9\varepsilon_{uk} = 6.75\% \\
&E_1 = (f_{td} - f_{yd})/(\varepsilon_{uk} - \varepsilon_{yd}) = 2.736 f_{yd} = 1068\,\mathrm{N/mm^2} \\
&f'_{td} = f_{yd} + E_1(\varepsilon_{ud} - \varepsilon_{yd}) = 1.18 f_{yd} = 461\,\mathrm{N/mm^2}.
\end{aligned}$$

From the equation written above one therefore obtains

$$\xi_a = 0.049,$$

whereas from the equilibrium

$$\beta_o\, b\, x_a f_{cd} = A_s f'_{td},$$

one obtains

$$\omega_{sa} = \frac{A_s f_{yd}}{b\, d\, f_{cd}} = \xi_a \beta_o / 1.18 = 0.033.$$

This is a very low mechanical reinforcement ratio which is made inadmissible by other minimum reinforcement requirements. The field "*a*" of low reinforcement characterized by ratios $\omega_s < \omega_{sa}$ is therefore not good practice and it is not discussed here.

• Field "*b*"

Given $\omega_{sa} < \omega_s \leq \omega_{sc}$ and that we are in the field of medium reinforcement, the translational equilibrium of the section can be set as

$$\beta_o\, b\, x f_{cd} - A_s\, \sigma_s = 0,$$

with

$$\sigma_s = f_{yd} + E1\,(\varepsilon_s - \varepsilon_{yd}) \quad \text{for } \varepsilon_s \geq \varepsilon_{yd}.$$

From the similarity of the diagram of deformations

$$\frac{\varepsilon_{cu}}{x} = \frac{\varepsilon_s}{d-x},$$

the strain of reinforcement can be expressed in terms of position of the neutral axis:

$$\varepsilon_s = \frac{d-x}{x}\varepsilon_{cu} = \frac{1-\xi}{\xi}\varepsilon_{cu},$$

with $\xi = x/d$. The stress in the reinforcement is therefore expressed as

$$\sigma_s = f_{yd} + E_1\left(\frac{1-\xi}{\xi}\varepsilon_{cu} - \varepsilon_{yd}\right) = f_{yd} + E_1\varepsilon_{yd}\left(\frac{1-\xi}{\xi}\alpha_o - 1\right),$$

with $\alpha_o = \varepsilon_{cu}/\varepsilon_{yd}$ and also

$$\sigma_S = f_{yd}\left[1 + \alpha\left(\frac{1-\xi}{\xi}\alpha_o - 1\right)\right],$$

with $\alpha = E_1/E_s$ and $f_{yd} = E_s\varepsilon_{yd}$.

Substituting this expression in the equilibrium equation, one has

$$\beta_o b\,d f_{cd}\,\xi - A_s f_{yd}\left[1 + \alpha\left(\frac{1-\xi}{\xi}\alpha_o - 1\right)\right] = 0.$$

Rationalizing and rearranging

$$\beta_o b\,d f_{cd}\,\xi^2 - A_s f_{yd}[1 - \alpha(1+\alpha_o)]\xi - A_s f_{yd}\alpha\alpha_o = 0,$$

one eventually obtains the second-degree equation

$$\xi^2 - \frac{\omega_s}{\beta_o}[1 - \alpha(1+\alpha)]\xi - \frac{\omega_s}{\beta_o}\alpha\alpha_o = 0,$$

which leads to the positive root

$$\xi = \frac{1}{2}\frac{\omega_s}{\beta_o}[1 - \alpha(1+\alpha_o)]\left\{1 + \sqrt{1 + 4\beta_o^2\frac{\alpha\,\alpha_o}{\omega_s}/[1 - \alpha(1+\alpha_o)]^2}\right\}.$$

For B450C steel, with

$$\alpha_o = \frac{\varepsilon_{cu}}{\varepsilon_{yd}} = \frac{0.35}{0.19} = 1.84 \quad \alpha = \frac{E_1}{E_s} = \frac{1068}{205000} = 0.0052$$

and $\beta_o = 0.8$, one obtains

$$\xi = 0.6185\omega_s\left\{1 + \sqrt{1 + 0.0315/\omega_s}\right\}$$

for $0.033 \leq \omega_s \leq 0.52$.

The rotational equilibrium finally leads to the definition of the resisting moment:

$$M_{Rd} = \sigma_s A_s z = f_{yd}\left[1 + \alpha\left(\frac{1-\xi}{\xi} - 1\right)\right]A_s(1 - \kappa_o\xi)d,$$

that is

$$M_{Rd} = \beta_o f_{cd} b\, x\, z = \beta_o f_{cd} b\, \xi\,(1 - \kappa_o\xi)d^2,$$

with $\kappa_o = 0.4$. The good practice of setting an upper limit to the lever arm of the internal couple is reminded, with

$$\xi = 1 - \kappa_o\xi \leq 0.96,$$

which corresponds to $\xi \geq 0.10$.

- *Field* "*c*"

In the zone of high reinforcement, with $\omega_s > \omega_{sc}$, the reinforcing steel is still within the elastic range with $\sigma_s = E_s\varepsilon_s$. Setting also

$$\frac{\varepsilon_{cu}}{x} = \frac{\varepsilon_s}{d - x},$$

from which one has

$$\varepsilon_s = \frac{d - x}{x}\varepsilon_{cu} = \frac{1 - \xi}{\xi}\varepsilon_{cu},$$

the stress in steel can be written as

$$\sigma_s = E_s\varepsilon_s = f_{yd}\frac{1 - \xi}{\xi}\alpha_o,$$

with $\alpha_o = \varepsilon_{cu}/\varepsilon_{yd}$. With this expression, the translational equilibrium

$$\beta_o\, b\, x f_{cd} - A_s\, \sigma_s = 0$$

after obvious steps becomes

$$\beta_o\, \xi^2 + \omega_s\, \alpha_o \xi - \omega_s\, \alpha_o = 0,$$

from which the positive root is deduced

$$\xi = \frac{\omega_s \alpha_o}{2\beta_o} \left\{ -1 + \sqrt{1 + \frac{4\beta_o}{\alpha_o \omega_s}} \right\},$$

which gives the position of the neutral axis.

The usual rotational equilibrium gives finally the resisting moment:

$$M_{Rd} = \sigma_s A_s \zeta\, d = f_{yd} \frac{1-\xi}{\xi} \alpha_o A_s (1 - \kappa_o \xi) d,$$

or, with respect to the centre of tensions:

$$M_{Rd} = \beta_o f_{cd}\, b\, \xi\, (1 - \kappa_o \xi)\, d^2.$$

It is to be noted how the case of highly reinforced sections, to be calculated with these last formulas, is not frequent. In effect, such sections have a brittle behaviour which is good practice to avoid. When it is not possible to increase the sizes of concrete, a remedial to the brittleness can be given using reinforcement also in the compression zone.

Sections with Double Reinforcement

The case of the sections with double reinforcement is described with the indefinite elastoplastic σ–ε model. The section under analysis is therefore represented in Fig. 3.12. Its resistance is derived with the usual method, first of all deducing the resisting concrete part in compression from the translational equilibrium of the section itself. Assuming to be within the field "*b*" and with reinforcement in compression also yielded, one therefore has

$$A_s f_{yd} - A'_s f_{yd} - b\, \bar{x} f_{cd} = 0,$$

from which one immediately obtains

$$\bar{x} = (\omega_S - \omega'_S) d$$

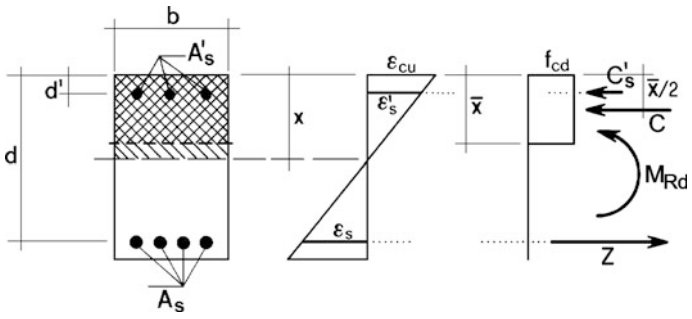


Fig. 3.12 Section with double reinforcement at ultimate limit state of bending

having indicated with

$$\omega_s = \frac{A_s f_{yd}}{bdf_{cd}} \quad \omega'_s = \frac{A'_s f_{yd}}{bdf_{cd}},$$

the mechanical steel ratios in tension and compression. The neutral axis ($x = \bar{x}/\beta_o$) therefore moves upwards, away from the limit situation of high reinforcement.

Having verified the yield condition of reinforcement

$$\varepsilon_s = \frac{d-x}{x}\varepsilon_{cu} \geq \varepsilon_{yd} \quad \varepsilon'_s = \frac{x-d'}{x}\varepsilon_{cu} \geq \varepsilon_{yd},$$

the resisting moment is eventually deduced from the rotational equilibrium of the section:

$$M_{Rd} = A_s f_{yd}(d - \bar{x}/2) + A'_s f_{yd}(\bar{x}/2 - d').$$

3.1.3 Prestressed Sections

If the beam is prestressed with a tendon of area A_p placed with an eccentricity e from the centroid of the homogenized section (towards the side in tension), naming $N_{po} = \sigma_{po} A_p$ the prestressing force measured at the decompression of concrete, from the formula of combined uniaxial bending and compression in the elastic range and uncracked section, same as the one mentioned at Sect. 6.1, one has (see Fig. 3.13)

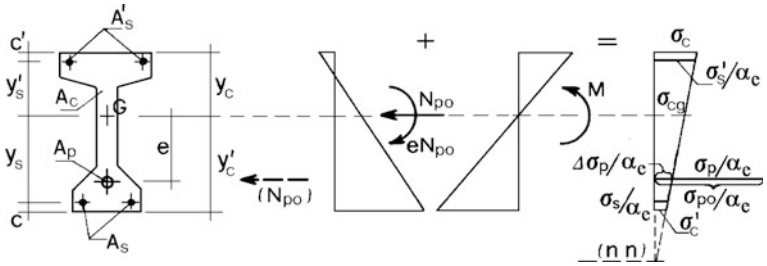


Fig. 3.13 Stress distribution in a prestressed section

$$\sigma_c = -\frac{N_{po}}{A_i} + \frac{N_{po}e}{W_{ic}} - \frac{M}{W_{ic}}$$

$$\sigma_{cG} = -\frac{N_{po}}{A_i}$$

$$\sigma'_c = -\frac{N_{po}}{A_i} - \frac{N_{po}e}{W'_{ic}} + \frac{M}{W'_{ic}}$$

$$\sigma_s = \alpha_e\left\{-\frac{N_{po}}{A_i} - \frac{N_{po}e}{W_{is}} + \frac{M}{W_{is}}\right\}$$

$$\sigma_p = \sigma_{po} + \alpha_e\left\{-\frac{N_{po}}{A_i} - \frac{N_{po}e}{W_{ip}} + \frac{M}{W_{ip}}\right\}$$

$$\sigma'_s = \alpha_e\left\{-\frac{N_{po}}{A_i} + \frac{N_{po}e}{W'_{is}} - \frac{M}{W'_{is}}\right\},$$

with positive stresses in tension and where

$$W_{ic} = I_i/y_c; \quad W'_{ic} = I_i/y'_c; \quad W_{is} = I_i/y_s; \quad W'_{is} = I_i/y'_s; \quad W_{ip} = I_i/e.$$

The geometric characteristics of the equivalent section, equalized to concrete with the usual homogenization coefficient $\alpha_e = E_s/E_c$, are again obtained from formulas such as

$$A_i = A_c + \alpha_e(A_s + A'_s) + \alpha_e A_p.$$

Similar to what deduced at Sect. 2.2.2 for the uncracked prestressed tie, the verification formulas show the superposition of the effects of prestressing and external loads, with an axial component N_{po} and a bending component $M - N_{po}e$.

Cracked Section

For an elastic behaviour with cracked sections typical of phase II, the analysis of the prestressed section of Fig. 3.14 starts from the same assumptions mentioned for the normal reinforced concrete section. In this case, setting $Z_p = N_{po} + \Delta Z_p$, the equilibrium of the section is given by the equations

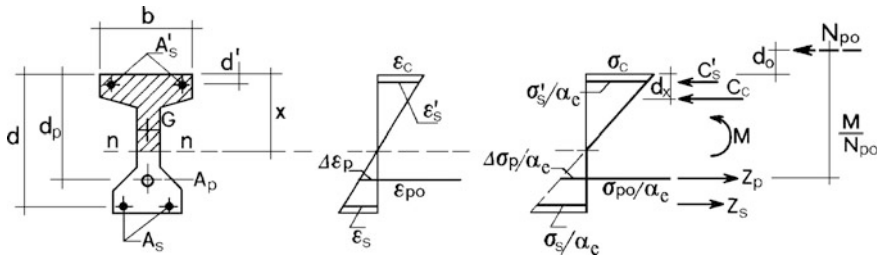


Fig. 3.14 Prestressed section in cracked phase

$$\begin{cases} C_c + C'_s - Z_s - \Delta Z_p = N_{po} \\ C_c(d_o + d_x) + C'_s(d_o + d') - Z_s(d_o + d) - \Delta Z_p(d_o + d_p) = 0, \end{cases}$$

with

$$d_o = \frac{M}{N_{po}} - d_p \quad N_{po} = \sigma_{po} A_p,$$

where the first equation refers to the translation along the axis of the beam and the second refers to the rotation of the section. In particular to express the moment, as any pivot point can be arbitrarily chosen for such system of forces with resultant equal to zero, the centre of the translated prestressing force is used, in order to remove its contribution from the second equation, together with one of the external moments to which it has been summed.

Setting now

$$\begin{aligned} C_c &= \sigma_c V_{cx} \\ C'_s &= \sigma'_s A'_s \\ Z_s &= \sigma_s A_s \\ \Delta Z_p &= \Delta\sigma_p A_p \end{aligned}$$

where V_{cx} is the function of x which represents the volume of the solid of compressions in concrete for its unit height, one obtains

$$\sigma_c V_{cx}(d_o + d_x) + \sigma'_s A'_s(d_o + d') + \sigma_s A_s(d_o + d) + \Delta\sigma_p A_p(d_o + d_p) = 0.$$

Using again the similarities of the diagram of stresses (see Fig. 3.14)

$$\sigma'_s = \alpha_e \sigma_c \frac{x - d'}{x}$$
$$\sigma_s = \alpha_e \sigma_c \frac{d - x}{x}$$
$$\Delta\sigma_p = \alpha_e \sigma_c \frac{d_p - x}{x},$$

the equation is reduced to the only unknown x:

$$V_{cx}(d_o + d_x) + \sigma_e \frac{x - d'}{x} A'_s (d_o + d') - \alpha_e \frac{d - x}{x} A_s (d_o + d) - \alpha_e \frac{d_p - x}{x} A_p (d_o + d_p) = 0.$$

The complexity of this equation depends on the shape of the section on which the functions V_{cx} and d_x relative to concrete in compression are expressed. For a rectangular section, one has for example

$$V_{cx} = \frac{1}{2} bx$$
$$d_x = \frac{1}{3} x,$$

which lead to the third-degree algebraic equation (with $d_s = d_o + d$, $d'_s = d_o + d'$, $d'_p = d_o + d_p$):

$$x^3 + 3d_o x^2 + \frac{6\alpha_e}{b}(A_s d_d + A'_s d'_s + A_p d'_p)x - \frac{6\alpha_e}{b}(A_s d_s d + A'_s d'_s d' + A_p d'_p d_p) = 0,$$

which is identical to the one that will be derived at Sect. 6.1.2 for sections in combined axial compression and bending in reinforced concrete. So, the formulas adopted as follows will also be identical, for the calculation of stresses, through the translational equilibrium

$$\sigma_c = \frac{N_{po} x}{\frac{bx^2}{2} + \alpha_e (x - d') A'_s - \alpha_e (d - x) A_s - \alpha_e (d_p - x) A_p}.$$

The bending moment applied to a prestressed section is therefore treated, also in the elastic range with cracked section, as a case of combined axial compression and bending.

Resistance Design

In order to show the resistance design of a section in prestressed concrete, we refer to the simple case of a rectangular shape with only pretensioned reinforcement (see Fig. 3.15). Sections with a complex shape and several layers of passive and active reinforcement will be discussed under the more general topic of combined axial

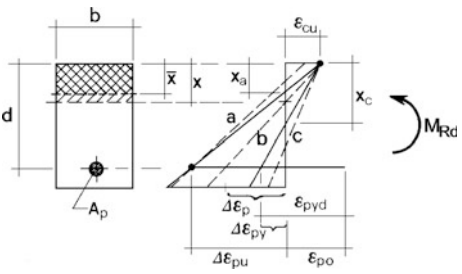


Fig. 3.15 Strain distribution at ultimate limit state of bending

force and bending, requiring appropriate algorithms of numerical calculus for the integration of stresses.

Therefore, with the premise that, also for prestressing steel, the simplified constitutive model that neglects hardening (model B of Fig. 1.32) is assumed, the description of the previous paragraph is repeated, bearing in mind that, beyond the decompression state of concrete, the reinforcement presents a pretension ε_{po} (see also Fig. 3.15).

Having written the translational equilibrium of the section under the assumption of yielded reinforcement and concrete at the failure limit:

$$\beta_o b x f_{cd} - A_p f_{pyd} = 0,$$

one also obtains $x = \xi d$ with

$$\xi = \frac{1}{\beta_o}\frac{A_p f_{yd}}{b d f_{cd}} = \frac{1}{\beta_o}\omega_p,$$

having indicated with ω_p the mechanical prestressing reinforcement ratio.

The extreme situation at the boundary of field "*c*", read on the diagram of strains ε, gives the relation

$$x_c = \frac{\varepsilon_{cu}}{\Delta\varepsilon_p - \varepsilon_{cu}} d = \xi_c d,$$

which depends on the pretension in the tendon, having

$$\Delta\varepsilon_{py} = \varepsilon_{pyd} - \varepsilon_{po}.$$

Given that, for the limits set by the verifications in service, the yield point is roughly similar to one of the passive reinforcements, assuming the same value $\Delta\varepsilon_p \cong 0.0019$ of the numerical example of Sect. 3.1.2, one also has

$$\xi_c \cong 0.65$$
$$\omega_{pc} \cong 0.52.$$

With a ratio

$$f_{\mathrm{pyd}}/f_{\mathrm{cd}} \cong 60$$

consistently with the high strength of steels used in prestressing, one has

$$\rho_{\mathrm{pc}} \cong 0.0087.$$

It can be noted that, other parameters being substantially equal, the geometrical reinforcement limit ratios are significantly smaller than the ones for ordinary reinforced concrete.

Therefore, for a given section, verified that it belongs to the field "*b*" of medium reinforcements with $\xi \leq \xi_{\mathrm{c}}$ the calculation of the resisting moment is simply carried with

$$M_{\mathrm{Rd}} = f_{\mathrm{pd}} A_{\mathrm{p}} \zeta d$$

where $\zeta = 1 - \kappa_{\mathrm{o}} x$.

Also for the prestressed section the limitation on the lever arm of the internal couple is imposed $\zeta \leq 0.96$. With the constant model of compressions in concrete, one therefore has

$$\begin{aligned} &\bar{x} = \omega_{\mathrm{p}} d \quad (x = \bar{x}/\beta_{\mathrm{o}}) \\ &z = d - \bar{x}/2 \quad (\leq 0.96d) \\ &M_{\mathrm{Rd}} = f_{\mathrm{pd}} A_{\mathrm{p}} z \quad (\geq M_{\mathrm{Ed}}), \end{aligned}$$

with equal reliability of verifications.

In *field* "*c*" of high reinforcements, with $\omega_{\mathrm{s}} > \omega_{\mathrm{sc}}$ the translational equilibrium

$$\beta_{\mathrm{o}}\, bx f_{\mathrm{cd}} - A_{\mathrm{p}} \sigma_{\mathrm{p}} = 0,$$

with $\sigma_{\mathrm{p}} = \sigma_{\mathrm{po}} + \Delta\sigma_{\mathrm{p}}$ and with

$$\Delta\sigma_{\mathrm{p}} = E_{\mathrm{s}} \frac{1-\xi}{\xi} \varepsilon_{\mathrm{cu}} = f_{\mathrm{yd}} \frac{1-\xi}{\xi} \alpha_{\mathrm{o}}$$

leads to the second-degree equation:

$$\beta_{\mathrm{o}}\, \xi^2 + \omega_{\mathrm{p}}\, \xi(\alpha_{\mathrm{o}} - \beta_{\mathrm{p}}) - \alpha_{\mathrm{o}}\, \omega_{\mathrm{p}} = 0$$

where, once again, it has been set $\alpha_{\mathrm{o}} = \varepsilon_{\mathrm{cu}}/\varepsilon_{\mathrm{pyd}}$ and the coefficient of partial pre-compression is introduced

$$\beta_p = \frac{\sigma_{po}}{f_{pyd}}$$

as the ratio between the pretension applied to the tendon and the yield strength of steel. Therefore, derived the position of the neutral axis with,

$$\xi = \frac{\omega_p(\alpha_0 - \beta_p)}{2\beta_0}\left\{-1 + \sqrt{1 + \frac{4\beta_0}{\omega_p(\alpha_0 - \beta_p)^2}}\right\}$$

one eventually obtains

$$M_{Rd} = \sigma_p A_p \zeta d = f_{yd}\left(\beta_p + \frac{1-\xi}{\xi}\alpha_o\right)A_p(1 - \kappa_o\xi)d,$$

or

$$M_{Rd} = \beta_0 f_{cd}\, b\, \xi(1 - \kappa_o\, \xi)d^2.$$

For prestressed sections as well, the case of high reinforcement with brittle failure is not frequent. Therefore, the formulas of field "*b*" are applied in general. The simultaneous presence of passive reinforcement, not pretensioned, is instead frequent. In this case, from the usual equilibrium conditions (see Fig. 3.16), one obtains

$$\bar{x} = (\omega_p + \omega_s - \omega'_s)d \quad (x = \bar{x}/\beta_o)$$
$$M_{Rd} = A_p f_{pyd}(d_p - \bar{x}/2) + A_s f_{yd}(d_p - \bar{x}/2) + A'_s f_{yd}(\bar{x}/2 - d'),$$

with the conditions

$$\varepsilon_p = \varepsilon_{po} + \frac{d_p - x}{x}\varepsilon_{cu} \geq \varepsilon_{pyd}$$
$$\varepsilon_s = \frac{d - x}{x}\varepsilon_{cu} \geq \varepsilon_{yd}$$
$$\varepsilon'_s = \frac{x - d'}{x}\varepsilon_{cu} \geq \varepsilon_{yd}.$$

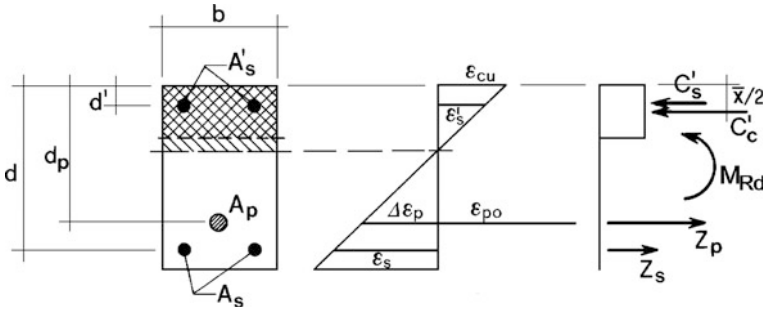


Fig. 3.16 Section with double reinforcement

It is to be noted how, in the resistance formulas of field "*b*", the pretensioning of the tendons is forgotten: at the ultimate limit state of the section, when all the reinforcement yielded, only the strengths of materials count. This is opposite to what happens in the elastic range, cracked or uncracked, where precompression plays a dominant role in determining the stress state.

Field a

Given instead $\omega < \omega_{pa}$ and therefore assuming to be in the field of low reinforcement, the similarity deduced from the diagram of deformations can be written as

$$\frac{\varepsilon_c}{x} = \frac{\Delta\varepsilon_{pu}}{d-x}$$

with $\Delta\varepsilon_{pu} = \varepsilon_{pu} - \varepsilon_{po}$ and the strain at the compression edge of concrete can be expressed in terms of position x of the neutral axis

$$\bar{\varepsilon}_c = \frac{\varepsilon_c}{\varepsilon_{cu}} = \frac{x}{d-x}\frac{\varepsilon_{pu} - \varepsilon_{po}}{\varepsilon_{cu}} = \frac{\xi}{1-\xi}(\alpha_1 - \alpha_2),$$

with $\xi = x/d, \alpha_1 = \varepsilon_{pud}/\varepsilon_{cu}$ and with $\alpha_2 = \varepsilon_{po}/\varepsilon_{cu}$.

Using now the approximated formulations for the necessary coefficients $\beta = \beta(\bar{\varepsilon}_c)$ and $\kappa = \kappa(\bar{\varepsilon}_c)$, one obtains, after obvious steps,

$$\beta = (1.6 - 0.8\bar{\varepsilon}_c)\bar{\varepsilon}_c = \frac{a_o - a_1\xi}{(1-\xi)^2}\xi$$
$$\kappa = 0.33 + 0.07\,\bar{\varepsilon}_c = \frac{c_o - c_1\xi}{1-\xi},$$

with

$$a_o = 1.6(\alpha_1 - \alpha_2) \quad a_1 = 0.8(\alpha_1 - \alpha_2)[2 + (\alpha_1 + \alpha_2)]$$
$$c_o \cong 0.33 \quad c_1 \cong 0.33 - 0.07(\alpha_1 - \alpha_2).$$

The translational equilibrium of the section

$$\beta\, b\, x f_{cd} - A_p f'_{ptd} = 0$$

can rely on the above-mentioned approximated formulation of $\beta = \beta(\xi)$ and give

$$(a_o - a_1\xi)\xi^2 b\, d f_{cd} - (1-\xi)^2 A_p f'_{ptd} = 0$$

which, appropriately rearranged, leads to the third-degree algebraic equation

$$-a_1\xi^3 + (a_o - \omega'_p)\xi^2 + 2\omega'_p\,\xi - \omega'_p = 0$$

to be resolved in $0 < \xi < \xi_a$. For practical applications, good accuracy is given in the interval $0.050 < \omega'_p < 0.10$ from the approximated solution

$$\xi \cong 0.066 + 0.924\,\omega'_p.$$

The rotational equilibrium is eventually set, from which one immediately obtains

$$M_{Rd} = f'_{ptd} A_s\,\zeta\,d,$$

with $\zeta = 1 - \kappa\xi$ deduced from the above-mentioned approximated formulation of the second coefficient $\kappa = \kappa(\xi)$.

3.2 Flexural Cracking of Beams

The topic of cracking described in Chap. 2 with reference to the reinforced concrete tie is discussed again in this section. All verification criteria discussed in that chapter are also valid for the beams in bending without substantial modifications. Regarding the influence of the reinforcement distribution in the section, which is approximated for ties in the appropriate quantification of the effective area, only the systematic direct or indirect contribution in the verification formulas of the concrete cover with respect to the depth of the section is to be added.

First in fact, the variation $\Delta\sigma_s$ of the stress in the reinforcement between cracked and uncracked sections, on which the cracks spacing λ directly depends, is not related to the reinforcement ratio ρ_s only, but also to the lever arm of the internal couple and to its different arrangements assumed in the cracked and uncracked sections. Second, the crack width w which for ties was conventionally assumed constant on the section (see Fig. 2.13) shows a systematic increase towards the edge in tension of the section.

Conventionally assuming a linear variation from the neutral axis of the cracked section (see Fig. 3.17), with respect to the value w' calculated at the level of the reinforcement, the maximum value w at the edge in tension increases for larger, in relative terms, concrete covers

$$w = w'\frac{h - x'}{d - x'} = w'\left(1 + \frac{c/d}{1 - \xi'}\right),$$

with $h = d + c$ and $\xi' = x'/d$. For deep beams with low reinforcements, this amplification is small:

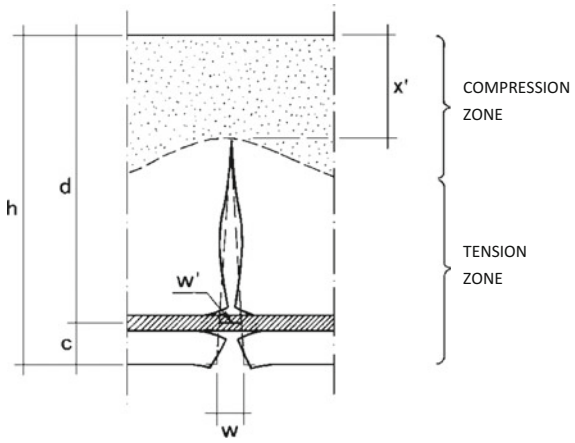


Fig. 3.17 Crack profile

$$w \cong w' \left(1 + \frac{0.05}{0.80}\right) = 1.06\, w'.$$

For shallow beams with high reinforcements, the width amplification is very large:

$$w \cong w' \left(1 + \frac{0.20}{0.50}\right) = 1.40\, w'.$$

3.2.1 Crack Spacing

Similar to what has been described at Sect. 2.2.3 for the tie, one can consider an isolated beam segment between two subsequent cracks (see Fig. 3.18). Let 2λ be its length, with λ equal to the minimum cracking distance. As a moment M has to be transferred through the segment under analysis, the stress configurations described in the already mentioned figure will occur at its ends and in the middle. The first situation can be deduced from the formulas of the cracked section presented at Sect. 3.1.1; the second situation can be deduced from the ones of the uncracked section presented in the same section. For the equilibrium of half of the segment one would therefore have

$$M = \sigma'_s A_s z' = \sigma_s A_s z_s + \frac{1}{2}\sigma_c b(h - x) z_c,$$

where the meaning of symbols is indicated in Fig. 3.18. Setting $\sigma_c = f_{ctf}$,

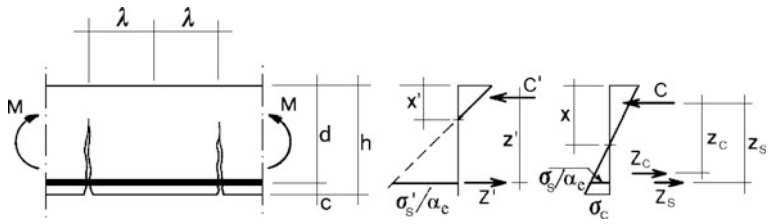


Fig. 3.18 Equilibrium conditions along the beam

$$\sigma'_s = \left\{ \frac{1}{2} f_{ctf} b(h-x) z_c + \sigma_s A_s z_s \right\} \frac{1}{A_s z'},$$

and the variation $\Delta\sigma_s = \sigma'_s - \sigma_s$ is therefore obtained as

$$\Delta\sigma_s = \left\{ \frac{1}{2} \frac{z_c}{z'} - \sigma_e \rho^*_s \frac{d-x}{h-x} \left(1 - \frac{z_s}{z'} \right) \right\} \frac{f_{ctf}}{\rho^*_s} = \gamma \frac{f_{ctf}}{\rho^*_s},$$

having set

$$\sigma_s = \alpha_e \sigma_c \frac{d-x}{h-x},$$

and having indicated with

$$\rho^*_s = \frac{A_s}{b(h-x)},$$

the reinforcement ratio referred to the zone in tension of the uncracked section.

Writing now the equilibrium of the bars between the crack and the section in the middle of the segment, with the assumption of a constant bond stress ($(\tau_b = \tau_{bm} = \text{const.})$ and assuming n bars of the same diameter ϕ:

$$n \frac{\pi \phi^2}{4} \Delta\sigma_s = n \, \pi \phi \tau_{bm} \lambda,$$

from which one eventually obtains

$$\lambda = \gamma \frac{\phi}{4\rho^*_s} \frac{f_{ctf}}{\tau_{bm}} = \gamma \frac{\phi}{4\rho^*_s} \frac{\beta}{\beta_b},$$

having set $f_{ctf} = \beta f_{ct}$ and $\tau_{bm} = \beta_b f_{ct}$.

Such formulation of the minimum cracking distance coincides with the one obtained through the analogous theoretical model of the tie, apart from the coefficient

$$\gamma\beta = \left\{\frac{1}{2}\frac{z_c}{z'} - \alpha_e\rho_s^*\frac{d-x}{h-x}\left(1-\frac{z_s}{z'}\right)\right\}\beta,$$

which summarizes the flexural characteristics of the section in the cracked and uncracked phase.

Similar to what specified at Sect. 2.3.2, the theoretical formulation of the distance λ is to be modified empirically to take into account the experimental results, especially for what concerns the influence of the distribution of bars in the section. One therefore has

$$\lambda = c_o + \gamma\,\beta\frac{0.1\,\phi}{\beta_1\rho_s},$$

where $c_o = c - \phi/2$ is the clear concrete cover, β_1 is equal to 1.0 for ribbed bars and ρ_s is the geometrical reinforcement ratio referred to the effective area consisting of a strip of thickness equal to $2.5c \leq (h-x)/3$. In such formulation, assuming in an approximated way $z' \cong z_s \cong \beta z_c$, it can be set as

$$\gamma\beta \cong \frac{1}{2},$$

staying within the tolerances relative to the other uncertainties of the model.

It is to be noted how in the beams in bending, other factors being equal, the cracking distance is definitely smaller than for ties, with the positive effect of limiting the width of single cracks.

3.2.2 Crack Width

The behaviour of the beam in bending, measured with tests beyond the cracking limit, is described in Fig. 3.19 where the diagram of the applied moment M is shown as function of the measured curvature χ. The test is carried inducing a constant distribution of bending moment on a central segment of the beam of sufficient length and deducing the average curvature as ratio between the relative rotation of its ends and their distance.

Similar to the diagram $N = N(\varepsilon)$ obtained for the tie, the curve $M = M(\chi)$ of the beam in bending is characterized by

- segment OA uncracked up to the failure limit of the concrete edge in tension, essentially linear, that follows the line

$$M = E_c\,I_i\,\chi$$

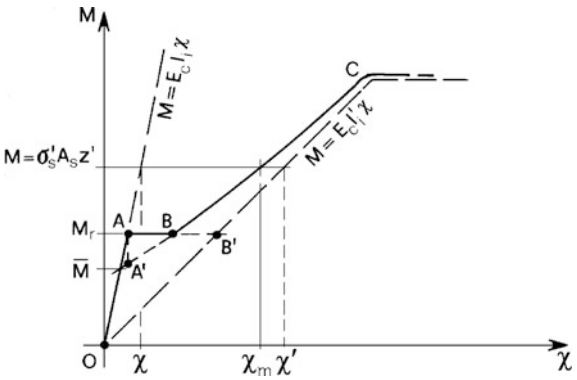


Fig. 3.19 Moment-curvature cracking model

with I_i moment of inertia of the uncracked section homogenized to concrete;

- segment AB corresponding to the complete cracking of the beam, with sudden reduction of the flexural stiffness due to the release of tensile stresses in concrete and to activation slippages of bond contacts;
- if the unloading of tensile stresses in concrete was total, the situation would stabilize on point B' of the line

$$M = E_c I_i' \chi$$

with I_i' moment of inertia of the cracked section homogenized to concrete; the segment BB' represents the stiffening effect still given by the segments of concrete in tension between the cracks (tension stiffening);

- if the test were carried in displacement control, it would follow the segment $AA'B$ exhibiting the internal force relaxation, instead of the increase in deformation;
- segment BC, with decreasing contribution of concrete in tension due to the increase of cracking and slippages, up to the yield point of steel.

As for the tie under axial tension force, the diagram can be transposed for the beam in bending as well, substituting the variable M with the corresponding stress

$$\sigma_s' = \alpha_e \frac{M}{I_i'} y_s' \quad (y_s' = d - x')$$

calculated in the cracked section; the variable χ can be again substituted with the strain $\varepsilon = \chi y_s'$, obtaining a diagram similar to the one of Fig. 2.16.

For the average deformation of steel in the cracked phase

$$\varepsilon_{sm} = \frac{\sigma_{s'}}{E_s} - \Delta\varepsilon_s,$$

the hyperbolic model of tension stiffening can be assumed for the beam in bending as well:

$$\Delta\varepsilon_s = \frac{\bar{\sigma}'_s}{\sigma'_s}\Delta\bar{\varepsilon}_s \quad (\text{per } \sigma'_s \geq \bar{\sigma}'_s).$$

One arrives again to the formulation of the average unit cracking width at the level of the reinforcement:

$$w'_{om} = \varepsilon_{sm} - \varepsilon_{cm} = \frac{\sigma'_s}{E_s}\left[1 - 0.5\beta_0\beta_1\beta_2\left(\frac{\sigma'_{sr}}{\sigma'_s}\right)^2\right],$$

where σ'_{sr} is the stress in steel corresponding to the cracking moment $M_r = f_{ctf}I_i/(h-x)$, evaluated on the cracked section ($\sigma'_{sr} = M_r y'_s/I'_i$).

At the extreme edge of the beam the width increases, as already mentioned, according to the relation,

$$w_{om}\left(1 + \frac{c/d}{1-\xi'}\right)w'_{om}.$$

It is to be noted that for prestressed beams, for the cracking calculations described here, the average deformation of the reinforcement is to be measured starting from the decompression of concrete. The value $\sigma'_p - \sigma_{po}$ therefore has to be substituted to the stress σ'_s.

3.2.3 Verification Criteria

The verification, according to the *direct analytical criterion*, is carried calculating the conventional value of the width of the single crack with

$$w_k = s_k w_{ok},$$

where the characteristic distance is assumed equal to

$$s_k = 2\lambda,$$

and the characteristic unit width is given by

$$w_{ok} = k w_{om},$$

with the same value of k = 1.7 given at Sect. 2.2.3 for ties.

As already mentioned, the accuracy of the direct analytical calculation of the cracking width is unsatisfactory.

Especially the point D of theoretical re-closure of cracks (see Fig. 2.16), from which the model starts, remains uncertain. With reference to the diagram of Fig. 3.19, the uncertainty is in the determination of the moment $\overline{M}$, with the result of introducing significant errors in the evaluation of tension stiffening.

But other than for the formula of the cracking unit width w'_{om}, the algorithm remains inaccurate also for the uncertain evaluation of the cracking distance λ. For beams in bending, such distance is given by the formula

$$\lambda = c_o + \frac{0.05\,\phi}{\beta_1\,\rho_s}.$$

The reinforcement ratio ρ_s evaluated on the effective area of the part of concrete in tension should be introduced. For the evaluation of such effective area, an indication similar to one of the ties is given, with a height

$$2.5(h-d) \quad (\leq (h-x)/3)$$

from the edge of the section in tension.

The *indirect technical criterion* is proposed as an alternative to the previous verification method, also for beams in bending, which consists of imposing an upper limit, as a function of the diameter of the bars, to the tensile stress in the reinforcement evaluated on the cracked section. This criterion is described in detail at Sect. 2.3.3, whereas in Tables 2.15 and 2.16 the verifications and relative allowable stresses are summarized.

The criterion for the definition of the minimum reinforcement that guarantees a cracking control even at an early onset, anticipated by the effects of shrinkage and thermal variations, is eventually to be presented. Assuming that the reinforcement is capable of absorbing at the yield limit the moment released by the concrete when cracking occurs (see Fig. 3.18):

$$A_s f_{yk} z' \geq \frac{1}{2}(h-x) b f_{ctf} z_c,$$

one obtains with the appropriate simplifications

$$A_s \geq \frac{1}{2}(h-x) b f_{ctm}/f_{yk},$$

which, for common materials, indicates a minimum reinforcement of about 0.25% if referred to the tension side, of about 0.15% if referred to the entire concrete section.

3.3 Deformation of Sections in Bending

The hyperbolic model of tension stiffening presented at Sect. 2.3.2 for ties and extended to beams in bending at Sect. 3.2.2 gives the average strain ε_{sm} of the reinforcement in tension, as summation of the average strain ε_{cm} of concrete and the unit crack width w'_{om}, at the level of the reinforcement (see Fig. 2.16)

$$\varepsilon_{sm} = \varepsilon_{cm} + w'_{om} = \frac{\bar{\sigma}'_s}{\sigma'_s}\bar{\varepsilon}_{sm} + \left[1 - \left(\frac{\bar{\sigma}'_s}{\sigma'_s}\right)^2\right]\varepsilon'_s,$$

where the first term decreases with the stress level σ'_s, the second increases. Setting now (with $\sigma_s = \sigma'_s$)

$$\bar{\varepsilon}_{sm} = \frac{\bar{\sigma}'_s}{\sigma'_s}\varepsilon_s,$$

one can write

$$\varepsilon_{sm} = \left(\frac{\bar{\sigma}'_s}{\sigma'_s}\right)^2 \varepsilon_s + \left[1 - \left(\frac{\bar{\sigma}'_s}{\sigma'_s}\right)^2\right]\varepsilon'_s = \eta\varepsilon_s + (1-\eta)\varepsilon'_s,$$

where

$$\eta = \left(\frac{\bar{\sigma}'_s}{\sigma'_s}\right)^2 \cong 0.5\ \beta_0\beta_1\beta_2\left(\frac{\sigma'_{sr}}{\sigma'_s}\right)^2$$

is the function related to the model assumed.

For the tie, the strains ε_s and ε'_s are therefore to be evaluated, the first one with reference to the uncracked section:

$$\varepsilon_s = \frac{N}{E_c A_i},$$

the second with reference to the cracked section:

$$\varepsilon'_c = \frac{N}{E_c A_s} = \frac{N}{E_c \alpha_e A_s} = \frac{N}{E_c A'_i},$$

where with $A_i = A_c + \alpha_e A_s$ and $A'_i = \alpha_e A_s$ the homogenized areas in the two cases have been indicated.

The average strain of the tie in the cracked state is therefore obtained from

$$\varepsilon_{\mathrm{m}} = \eta \frac{N}{E_{\mathrm{c}} A_i} + (1-\eta)\frac{N}{E_{\mathrm{c}} A_i'} = \frac{N}{E_{\mathrm{c}} A_{\mathrm{m}}(\eta)},$$

with

$$A_{\mathrm{m}}(\eta) = \frac{A_i A_i'}{\eta A_i' + (1-\eta) A_i},$$

equivalent area of the section, decreasing as the stress level increases according to the function

$$\eta = 0.5\beta_0\beta_1\beta_2 + \left(\frac{N_{\mathrm{r}}}{N}\right)^2.$$

Extending now in an approximated way the same model to curvatures (see Fig. 3.20), for the beam in bending one has

$$\chi_{\mathrm{m}} = \eta\,\chi + (1-\eta)\chi',$$

where the curvature $\chi = \varepsilon_y / y_{\mathrm{s}}$ is evaluated with reference to the uncracked section:

$$\chi = \frac{M}{E_{\mathrm{c}} I_i},$$

whereas $\chi' = \varepsilon_y' / y_{\mathrm{s}}'$ is evaluated with reference to the cracked section:

$$\chi' = \frac{M}{E_{\mathrm{c}} I_i'}.$$

The average curvature of the beam in the cracked state is similarly obtained as

$$\chi_{\mathrm{m}} = \frac{M}{E_{\mathrm{c}} I_{\mathrm{m}}(\eta)},$$

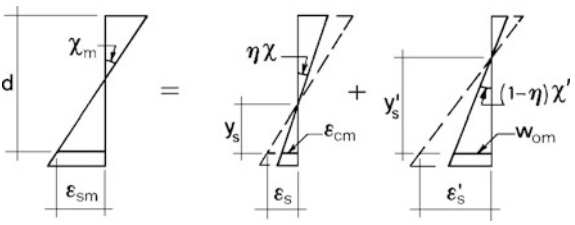


Fig. 3.20 Deduction of the average curvature

with

$$I_{\mathrm{m}}(\eta) = \frac{I_i I_i'}{\eta I_i' + (1-\eta) I_i}$$

equivalent moment of inertia of the section, decreasing when the stress increases, based on the function

$$\eta = 0.5\, \beta_0 \beta_l \beta_2 \left(\frac{M_{\mathrm{r}}}{M}\right)^2.$$

Such formulation can be used in the calculation of the deformations of the beams in bending, where integrations on the curvatures are required, for a more precise evaluation than the one deducible from the linear elastic models. These elastic models usually refer to the geometrical section of concrete, neglecting the contribution of the reinforcement and the influence of cracking of sections beyond the cracking limit.

Instead, the deformation model presented here leads to the definition of the moment-curvature model of the section in bending, correcting the law of linear elastic behaviour of materials beyond the cracking limit of the section itself. It can be applied for calculations in service under limited load levels, for which concrete in compression is substantially still in the linear range and steel has not yielded.

The diagrams $M = M(\chi)$ that derive mainly depend on the ratio

$$\psi = \frac{I_i'}{I_i}$$

between the moment of inertia of the cracked section and one of the uncracked sections. On such ratio the *diversion* is measured between the two lines $M = EI_i\chi$ and $M = EI_i'\chi$ relative to the elastic behaviour of the section within and beyond the cracking limit, whereas the type of connection between them is determined by the hyperbolic law already mentioned.

Some of these diagrams are shown in Fig. 3.21 in a non-dimensional form, having set

$$\frac{\chi}{\chi_{\mathrm{r}}} = \frac{M/E_{\mathrm{c}} I_{\mathrm{m}}(\eta)}{M_{\mathrm{r}}/E_{\mathrm{c}} I_i} = \frac{M}{M_{\mathrm{r}}} \frac{\eta I_i' + (1-\eta) I_i}{I_i'} = \frac{M}{M_{\mathrm{r}}} \frac{1-\eta(1-\psi)}{\psi},$$

and having assumed $\beta_0 = \beta_l = \beta_2 = 1$ with

$$\eta = \left(\frac{M_{\mathrm{r}}}{M}\right)^2.$$

The three values $\psi = 0.2 \div 0.4 \div 0.6$ of the ratio between the moments of inertia correspond to increasing steel ratios which, for rectangular sections with single

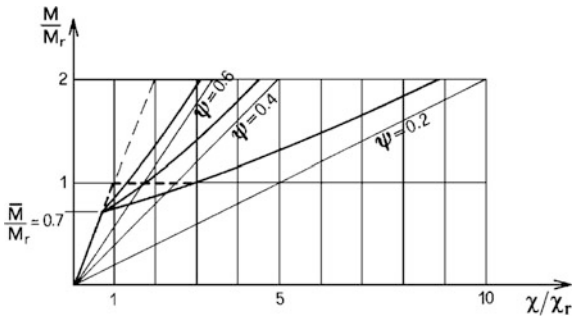


Fig. 3.21 Adimensional moment-curvature diagrams

reinforcement, can be indicated approximately in $\rho_s = 0.005 \div 0.010 \div 0.020$. The dashed part of the diagrams of Fig. 3.21 refers to the first load cycle that reaches the cracking limit, whereas for the following cycles the diversion of the behaviour occurs without discontinuities starting from the moment $\overline{M} \cong 0.7M_r$ of theoretical re-closure of cracks. Such limit, which cannot be precisely quantified as mentioned before, can vary for different values of the ratio β_0 of effective area depending on the distribution of the reinforcement on the part of the section in tension, for different values of the coefficient β_1 related to the type of bond or for different values of the coefficient β_2 related to duration and repetitiveness of loads.

3.3.1 *Effects of Creep*

Similar to what has been done at Sect. 2.1.3 with reference to the section under centred axial compression, the effects of creep of concrete on the behaviour of sections in bending are now analysed. A section with double reinforcement is shown in Fig. 3.22, with the necessary geometrical dimensions. In particular, it is assumed that G is the centroid of the composite section, homogenized with the elastic coefficient $\alpha_e = E_s/E_c$, G_c is the centroid of the concrete and G_s is one of the steel reinforcements.

The initial situation corresponding to the instantaneous application of bending moment is indicated with $\varepsilon_o = \chi_o y$. Under this bending moment, the section continues to deform with increments ε_{vt} due to creep, for which the total strain measured at time t is

$$\varepsilon_t = \varepsilon_0 + \varepsilon_{vt} = \varepsilon_{Gt} + \chi_t\, y,$$

where ε_{Gt} is strain that progressively occurs on the initial centroidal fibre G and χ_t is the total curvature increasing with time.

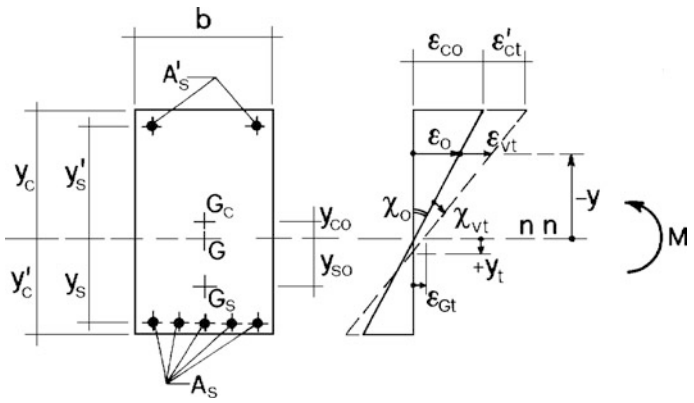


Fig. 3.22 Elastic and viscous components of flexural deformation

The creep coefficient $\varphi = \varphi(t-\tau)$ of the extreme ageing theory is again assumed, which allows a simplification of the formal elaborations required by the theory. Referring therefore to the effects produced in the elementary time interval between t and $t + \mathrm{d}t$, the variation of the deformation is obtained differentiating the compatibility law written above:

$$\mathrm{d}\varepsilon_t = \mathrm{d}\varepsilon_{vt} = \mathrm{d}\varepsilon_{Gt} + y\mathrm{d}\chi_t.$$

The constitutive laws reproduce the perfect elasticity for steel, with

$$\mathrm{d}\sigma_{st} = E_s\,\mathrm{d}\varepsilon_{st} = E_s(\mathrm{d}\varepsilon_{Gt} + y_s\,\mathrm{d}\chi_t)$$
$$\mathrm{d}\sigma'_{st} = E_s\,\mathrm{d}\varepsilon'_{st} = E_s(\mathrm{d}\varepsilon_{Gt} - y'_s\,\mathrm{d}\chi_t),$$

as well as the linear viscoelasticity with variable stresses for concrete, with

$$\mathrm{d}\varepsilon_t = \frac{1}{E_c}(\mathrm{d}\sigma_{ct} + \sigma_{ct}\mathrm{d}\varphi_t),$$

from which

$$\mathrm{d}\sigma_{ct} = E_c\,\mathrm{d}\varepsilon_{ct} - \sigma_{ct}\mathrm{d}\varphi_t = E_c(\mathrm{d}\varepsilon_{Gt} + y\,\mathrm{d}\chi_t) - \sigma_{ct}\,\mathrm{d}\varphi_t.$$

Uncracked Section

The equilibrium of the section of Fig. 3.22, considered as uncracked, under the action of the bending moment M constant in time, can be written setting the invariance of the axial and flexural components of the internal reaction

$$\mathrm{d}N_\mathrm{t} = A_\mathrm{s}\mathrm{d}\sigma_\mathrm{st} + A'_\mathrm{s}\mathrm{d}\sigma'_\mathrm{st} + \int_{-y_\mathrm{c}}^{+y'_\mathrm{c}} b\mathrm{d}\sigma_\mathrm{ct}\mathrm{d}y = 0$$

$$\mathrm{d}M_\mathrm{Gt} = y_\mathrm{s}A_\mathrm{s}\mathrm{d}\sigma_\mathrm{st} - y'_\mathrm{s}A'_\mathrm{s}\mathrm{d}\sigma'_\mathrm{st} + \int_{-y_\mathrm{c}}^{+y'_\mathrm{c}} yb d\sigma_\mathrm{ct}\mathrm{d}y = 0.$$

Substituting in these equations the constitutive models defined before, one obtains

$$\left[E_\mathrm{s}(A_\mathrm{s} + A'_\mathrm{s}) + E_\mathrm{c}\int_{+y_\mathrm{c}}^{-y'_\mathrm{c}} b\,\mathrm{d}y\right]\mathrm{d}\varepsilon_\mathrm{Gt} + \left[E_\mathrm{s}(y_\mathrm{s}A_\mathrm{s} - y'_\mathrm{s}A'_\mathrm{s}) + E_\mathrm{c}\int_{-y_\mathrm{c}}^{+y_\mathrm{c}} yb\,\mathrm{d}y\right]\mathrm{d}\chi_\mathrm{t} =$$
$$= \left[\int_{-y_\mathrm{c}}^{+y'_\mathrm{c}} \sigma_\mathrm{ct}b\,\mathrm{d}y\right]\mathrm{d}\varphi_\mathrm{t}$$
$$\left[E_\mathrm{s}(y_\mathrm{s}A_\mathrm{s} - y'_\mathrm{s}A'_\mathrm{s}) + E_\mathrm{c}\int_{-y_\mathrm{c}}^{+y_\mathrm{c}} y_\mathrm{b}\mathrm{d}y\right]\mathrm{d}\varepsilon_\mathrm{Gt} + \left[E_\mathrm{s}(y_\mathrm{s}^2A_\mathrm{s} + y_\mathrm{s}'^2A'_\mathrm{s}) + E_\mathrm{c}\int_{-y_\mathrm{c}}^{+y'_\mathrm{c}} y^2b\mathrm{d}y\right]\mathrm{d}\chi_\mathrm{t} =$$
$$= \left[\int_{-y_\mathrm{c}}^{+y_\mathrm{c}} y\sigma_\mathrm{ct}b\,\mathrm{d}y\right]\mathrm{d}\varphi_\mathrm{t},$$

having grouped the coefficient of the single unknown $\mathrm{d}\varepsilon_\mathrm{Gt}$ and $\mathrm{d}\varphi_\mathrm{t}$.

In such coefficient, the expressions of areas, static moments and moments of inertia of steel and concrete can be noted, as well as, at the right side of the equality, the ones of the axial and bending component of the resultant of stresses in concrete. With obvious symbology, one can write more synthetically (considering now for $A = A'_\mathrm{s} + A''_\mathrm{s}$ the total reinforcement area):

$$E_\mathrm{c}(\alpha_\mathrm{e}A_\mathrm{s} + A_\mathrm{c})\,\mathrm{d}\varepsilon_\mathrm{Gt} + E_\mathrm{c}(\alpha_\mathrm{e}S_\mathrm{sG} + S_\mathrm{cG})\mathrm{d}\chi_\mathrm{t} = N_\mathrm{ct}\,\mathrm{d}\varphi_\mathrm{t}$$
$$E_\mathrm{c}(\alpha_\mathrm{e}S_\mathrm{sG} + S_\mathrm{cG})\,\mathrm{d}\varepsilon_\mathrm{Gt} + E_\mathrm{c}(\alpha_\mathrm{e}I_\mathrm{sG} + I_\mathrm{cG})\mathrm{d}\chi_\mathrm{t} = M_\mathrm{cGt}\mathrm{d}\varphi_\mathrm{t}.$$

Having, for the property of the centroid G of the homogenized section,

$$S_{i\mathrm{G}} = \alpha_\mathrm{e}S_\mathrm{sG} + S_\mathrm{cG} = 0,$$

the equilibrium system is reduced to

$$E_c A_i \, d\varepsilon_{Gt} = N_{ct} \, d\varphi_t$$
$$E_c I_{iG} \, d\chi_t = M_{cGt} d\varphi_t,$$

that is to two concatenated differential equations, being

$$N_{ct} = N_{ct}(\varepsilon_{Gt}, \chi_t)$$
$$M_{cGt} = M_{cGt}(\varepsilon_{Gt}, \chi_t).$$

Therefore, in the general case, deduced the unknown with

$$d\varepsilon_{Gt} = \frac{N_{ct}}{E_c A_i} d\varphi_t$$
$$d\chi_t = \frac{M_{cGt}}{E_c I_{iG}} d\varphi_t$$

and expressed the variations of the components of the reaction of concrete:

$$dN_{ct} = E_c A_c \, d\varepsilon_{Gt} + E_c S_{cG} d\chi_t - N_{ct} \, d\varphi_t$$
$$dM_{cGt} = E_c S_{cG} d\varepsilon_{Gt} + E_c I_{cG} d\chi_t - M_{cGt} d\varphi_t,$$

as immediately deducible extracting the competent terms from the equilibrium system set at the beginning, substituting the first ones into the second ones and separating variables one has

$$\frac{dN_{ct}}{\beta N_{ct} - \frac{S_{cG}}{I_{iG}} M_{cGt}} = -d\varphi_t$$
$$\frac{dM_{cGt}}{\alpha M_{cGt} - \frac{S_{cG}}{A_i} N_{ct}} = -d\varphi_t,$$

with

$$\beta = \frac{\alpha_e \rho_s}{1 + \alpha_e \rho_s} \quad \rho_s = \frac{A_S}{A_c}$$
$$\alpha = \frac{\alpha_e \mu_s}{1 + \alpha_e \mu_s} \quad \mu_s = \frac{I_{sG}}{I_{cG}}.$$

The integration of the differential algorithm deduced above can be easily conduced in the elementary case of a symmetric section in which the centroids of concrete and reinforcement coincide ($y_{co} = y_{so} = 0$ in Fig. 3.22).

As indicated in Fig. 3.23, in such case the axial component of the resultant of stresses in concrete depends only on the strain ε_{Gt}, whereas the flexural component

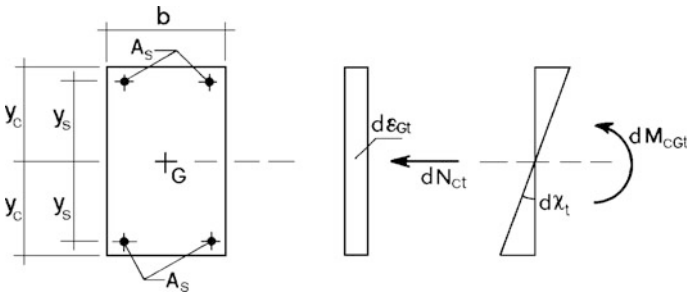


Fig. 3.23 Elementary deformation contributions

depends only on the curvature χ_t. Therefore, in terms of variations in the elementary time interval, one has the following relations:

$$\begin{aligned} \mathrm{d}N_{\mathrm{ct}} &= E_{\mathrm{c}}A_{\mathrm{c}}\,\mathrm{d}\varepsilon_{\mathrm{Gt}} - N_{\mathrm{ct}}\mathrm{d}\varphi_{\mathrm{t}} \\ \mathrm{d}M_{\mathrm{cGt}} &= E_{\mathrm{c}}I_{\mathrm{cG}}\mathrm{d}\chi_{\mathrm{t}} - M_{\mathrm{cGt}}\mathrm{d}\varphi_{\mathrm{t}}, \end{aligned}$$

deduced from the more general ones of the non-symmetrical section, having removed the terms with $S_{\mathrm{cG}} = 0$.

Substituting in these the expressions of $\mathrm{d}\varepsilon_{\mathrm{Gt}}$ and $\mathrm{d}\chi_{\mathrm{t}}$, one has

$$\begin{aligned} \mathrm{d}N_{\mathrm{ct}} &= -\left(1 - \frac{A_{\mathrm{c}}}{A_i}\right)N_{\mathrm{ct}}\mathrm{d}\varphi_{\mathrm{t}} \\ \mathrm{d}M_{\mathrm{cGt}} &= -\left(1 - \frac{I_{\mathrm{cG}}}{I_{i\mathrm{G}}}\right)M_{\mathrm{cGt}}\mathrm{d}\varphi_{\mathrm{t}} \end{aligned}$$

and, separating variables, the two independent and formally identical differential equations are eventually obtained:

$$\begin{aligned} \frac{\mathrm{d}N_{\mathrm{ct}}}{N_{\mathrm{ct}}} &= -\beta\mathrm{d}\varphi_{\mathrm{t}} \\ \frac{\mathrm{d}M_{\mathrm{cGt}}}{M_{\mathrm{cGt}}} &= -\alpha\mathrm{d}\varphi_{\mathrm{t}}, \end{aligned}$$

which, integrated between t_{o} and t, lead to the functions

$$\begin{aligned} N_{\mathrm{ct}} &= N_{\mathrm{co}}\mathrm{e}^{-\beta\varphi(t-t_0)} \\ M_{\mathrm{cGt}} &= M_{\mathrm{cGo}}\mathrm{e}^{-\alpha\varphi(t-t_0)}. \end{aligned}$$

The first one was already obtained at Sect. 2.1.3 with reference to columns; the second one differs only by the coefficient

$$\alpha = \frac{\alpha_e \mu_s}{1 + \alpha_e \mu_s} \quad \text{with} \quad \mu_s = \frac{I_{sG}}{I_{cG}},$$

evaluated on the ratio of moments of inertia, instead of the ratio ρ_s of areas. As for the axial behaviour of columns, a fictitious homogenization coefficient was defined

$$\alpha_e^* = \alpha_e \left(\frac{e^{\beta \varphi_\infty}}{\beta} - \frac{1}{\alpha_e \rho_s} \right)$$

to evaluate with the same elastic formulas the final viscoelastic situation, so for the section in bending one can assume the coefficient

$$\alpha_e^* = \alpha_e \left(\frac{e^{\alpha \varphi_\infty}}{\alpha} - \frac{1}{\alpha_e \mu_s} \right)$$

and apply with this the competent elastic formulas. Being μ_s usually equal to 2 or 3 times ρ_s, the new fictitious coefficient of homogenization is higher than the one to be used in the calculations of columns in compression.

In the elastic phase of uncracked sections, high stress redistributions can therefore occur due to the creep effects under the action of a permanent bending moment, similar to what quantified at Sect. 2.1.3 with reference to the case of axial compression. Data relative to the creep stress redistribution under bending moment are shown in Table 3.18, just for the case of double symmetrical reinforcement analysed here.

Cracked Section

The analysis of creep effects in a reinforced concrete section in bending in the cracked phase becomes more complicated because the resisting section varies in time. In Fig. 3.24 the initial elastic position of the neutral axis is indicated with x_o, whereas the unknown

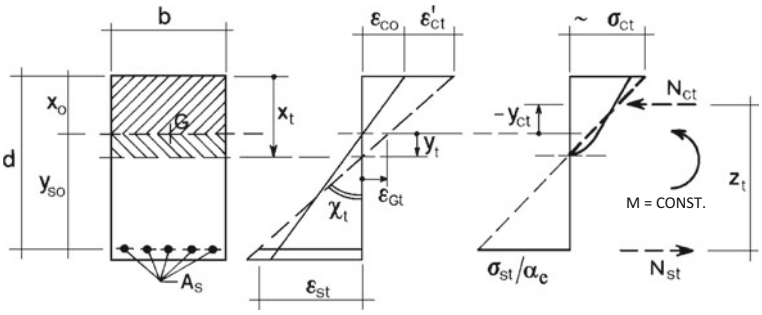


Fig. 3.24 Creep effects on the section in bending

$$y_t = \frac{\varepsilon_{Gt}}{\chi_t}$$

measures its progressive lowering under the constant moment M.

For the calculation of the resultant N_{ct} of stresses on the resisting part of concrete (in compression), in addition to a limit of integration $x_t = x_o + y_t$ variable with the time t of measurement, one also has a beginning of the viscoelastic effects differentiated for the different fibres concerned by the phenomenon. In fact, on the upper fibres between 0 and x_o the initial time t coincides with the one t_o of application of the action M, on the lower fibres between x_o and x_t, the origin instead is progressively deferred: from t_o on the initial neutral axis to t on the current neutral axis. The consequent diagram of stresses on concrete will be linear on the upper part and curve on the lower one, as indicated by the solid line of Fig. 3.24.

All this complicates the analytical algorithm so that it requires, for a correct solution of the problem, the application of a discretized numerical procedure of the same type of the one presented at Sect. 1.3.2. For the qualitative indication of the main parameters that affect the flexural behaviour of a reinforced concrete section in the cracked state, certain approximations can be introduced that allow a formal elaboration of the algorithms, although more complex than the one elaborated at the previous paragraph.

Therefore first, in order to uniform at time t_o the origin of stresses on all fibres concerned at time t, one can consider that, up to the first application of the bending moment M, the resisting section is extended to the entire depth x_t of concrete, with initial stresses partially in compression and partially in tension. Further in the development of the process, up to the current time t, the area $A_{io} = A_{ct} + \alpha_e A_s$, its centroid G and the moment of inertia $I_{iGo} = I_{cGt} + \alpha_e I_{Gst}$ remain unchanged, whereas the static moment S_{iGo} remains equal to zero. From this simplifying assumption it derives, given the linearity of the following laws of viscoelastic behaviour, still a triangular diagram of stresses on concrete, as indicated with a dashed line on the graphic of Fig. 3.24, where in particular the maximum compression at time t on the edge of the section has been indicated with σ_{ct}.

Therefore, differentiating the function $y_t = -\varepsilon_{Gt}/\chi_t$,

$$dy_t = -\frac{\chi_t d\varepsilon_{Gt} - \varepsilon_{Gt} d\chi_t}{\chi_t^2} = -\frac{d\varepsilon_{Gt} + y_t d\chi_t}{\chi_t}$$

and rewriting the formulations of $d\varepsilon_{Gt}$ and of $d\chi_t$, already deduced for the uncracked section, with reference now to the cracked section

$$d\varepsilon_{Gt} = \frac{N_{ct}}{E_c A_{io}} d\varphi_t$$

$$d\chi_t = \frac{M_{cGt}}{E_c I_{iGo}} d\varphi_t,$$

the differential equation is obtained by substitution:

$$\mathrm{d}y_\mathrm{t} = -\left\{\frac{N_\mathrm{ct}}{A_{i\mathrm{o}}} + \frac{M_\mathrm{cGt}}{I_{i\mathrm{Go}}} y_\mathrm{t}\right\} \frac{1}{E_\mathrm{c}} \frac{\mathrm{d}\varphi_\mathrm{t}}{\chi_\mathrm{t}}.$$

In order to express now the components N_so and M_cGt as a function of the unknown y_t, the equilibrium relations are considered as

$$N_\mathrm{ct} = -N_\mathrm{st} = -A_\mathrm{s}\, E_\mathrm{s}\, \varepsilon_\mathrm{st} = -A_\mathrm{s}\, E_\mathrm{s}\, (y_\mathrm{so} - y_\mathrm{t})\, \chi_\mathrm{t}$$
$$M_\mathrm{cGt} = y_\mathrm{ct}\, N_\mathrm{ct} = -y_\mathrm{ct}\, A_\mathrm{s}\, E_\mathrm{s}\, (y_\mathrm{so} - y_\mathrm{t})\, \chi_\mathrm{t},$$

where y_ct is the lever arm of the resultant N_ct relative to the centroid G assumed for the evaluation of moments. In particular, for the rectangular section of Fig. 3.24,

$$y_\mathrm{ct} = \frac{x_\mathrm{t}}{3} - x_\mathrm{o} = -\frac{1}{3}(2x_\mathrm{o} - y_\mathrm{t}).$$

With such formulations of the components, one eventually has

$$\mathrm{d}y_\mathrm{t} = \left\{\frac{1}{A_{i\mathrm{o}}} + \frac{1}{I_{i\mathrm{Go}}} y_\mathrm{ct} y_\mathrm{t}\right\} A_\mathrm{s} \frac{E_\mathrm{s}}{E_\mathrm{c}} (y_\mathrm{so} - y_\mathrm{t}) \mathrm{d}\varphi_\mathrm{t}$$
$$= \frac{\beta}{3i_0^2} \left\{3i_0^2 - (2x_\mathrm{o} - y_\mathrm{t}) y_\mathrm{t}\right\} (y_\mathrm{so} - y_\mathrm{t}) \mathrm{d}\varphi_\mathrm{t},$$

with

$$\beta = \frac{\alpha_\mathrm{e} \rho_\mathrm{s}^*}{1 + \alpha_\mathrm{e} \rho_\mathrm{s}^*} \qquad \rho_\mathrm{s}^* = \frac{A_\mathrm{s}}{A_\mathrm{ct}} = \frac{A_\mathrm{s}}{b x_\mathrm{t}},$$

and with

$$i_\mathrm{o}^2 = \frac{I_{i\mathrm{Go}}}{A_{i\mathrm{o}}},$$

square of the radius of gyration of the resisting section at the time t of measurement.

Expressed in the form

$$\frac{\mathrm{d}y_\mathrm{t}}{(y_\mathrm{t}^2 - 2x_\mathrm{o} y_\mathrm{t} + 3i_\mathrm{o}^2)(y_\mathrm{so} - y_\mathrm{t})} = \frac{\beta}{3i_\mathrm{o}^2} \mathrm{d}\varphi_\mathrm{t};$$

the equation can be integrated by separation of variables between t_o and t, obtaining

$$F(y_\mathrm{t}; x_\mathrm{o}) = -\frac{\beta}{3i_\mathrm{o}^2} \varphi(t - t_\mathrm{o}),$$

with

$$F(y_t;x_o)=\frac{1}{y_{so}^2-2x_oy_{so}+3i_o^2}\left\{\ln\frac{y_{so}-y_t}{y_{so}}-\frac{1}{2}\ln\frac{y_t^2-2x_oy_t+3i_o^2}{3i_o^2}\right.$$
$$\left.-\frac{y_{so}-x_o}{\sqrt{3i_o^2-x_o^2}}\left[\operatorname{arctg}\frac{x_o}{\sqrt{3i_o^2-x_o^2}}-\operatorname{arctg}\frac{(x_o-y_t)}{\sqrt{3i_o^2-x_o^2}}\right]\right\},$$

where, for the rectangular section with single reinforcement of Fig. 3.24, set $\eta_t=y_t/d$ and $\rho_s=A_s/bd$, one has

$$x_o=\alpha_e\rho_s\left\{-1+\sqrt{1+\frac{2}{\alpha_e\rho_s}\left(1+\frac{\eta_t^2}{2\alpha_e\rho_s}\right)}\right\}d=\xi_o d$$
$$y_{so}=d-x_o=(1-\xi_o)d=\eta_{so}\,d,$$

whilst i_o^2 can be calculated accordingly.

A transcendent equation is therefore obtained where, limiting to the final response for $t=\infty$, the solution y_∞ can be obtained numerically. It depends on the two parameters: $\alpha_e\,\rho_s=\alpha_eA_s/bd=\xi_o\,\rho_s^*$ that can be defined as the *elastic reinforcement ratio*; φ_∞ which represents the creep coefficient of concrete. In Fig. 3.25 the results are plot, expressed in terms of $\eta_\infty=y_\infty/d$. Given the approximations introduced and the small deviation from x_o, such lowering of the neutral axis can be considered as measured from the position x relative to the initial cracked section.

Therefore, referring to situations very sensitive to the effects of viscosity, with $\eta_\infty\cong 0.15$, and assuming an initial elastic configuration with $x\cong 0.3d$, for the equilibrium one has

$$M=\sigma_\infty A_s\,z_\infty=\sigma_{so}\,A_s\,z,$$

which, being $z=d-x/3\cong 0.90d$ and $z_\infty=d-x_\infty/3\cong 0.85d$, leads to a final stress increased with respect to the initial one by the inverse ratio of the respective lever arms of the internal couple:

$$\sigma_{s\infty}=\frac{z}{z_\infty}\sigma_{so}=1.06\sigma_{so}.$$

Similarly for concrete one has

$$\frac{1}{2}\sigma_{c\infty}bx_\infty z_\infty=\frac{1}{2}\sigma_{co}bxz,$$

from which

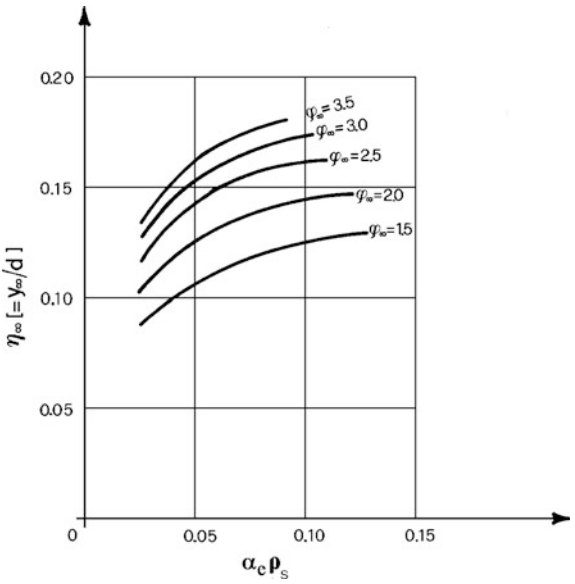


Fig. 3.25 Lowering of the neutral axis

$$\sigma_{c\infty} = \frac{x}{x_\infty}\frac{z}{z_\infty}\sigma_{co} = 0.67 \times 1.06\sigma_{co} \cong 0.71\sigma_{co},$$

where it can be noted, in addition to the amplifying factor due to the smaller lever arm of the internal couple, the reducing one due to the greater extent of the concrete area in compression.

The effective homogenization coefficient α_e^*, for the application of the elastic formulas to the final viscoelastic situation, is read through the usual similarity on the diagram of stresses:

$$\alpha_e^* = -\frac{x_\infty}{d - x_\infty}\frac{\sigma_{s\infty}}{\sigma_{c\infty}} = -\frac{\xi_\infty}{1 - \xi_\infty}\frac{\xi_\infty}{\xi}\frac{\sigma_{so}}{\sigma_{co}},$$

which, with

$$\alpha_e = -\frac{\xi}{1 - \xi}\frac{\sigma_{so}}{\sigma_{co}},$$

leads to

$$\alpha_e^* = \frac{1 - \xi}{1 - \xi_\infty}\frac{\xi_\infty^2}{\xi^2}\alpha_e.$$

In the case under examination, with $\xi = 0.30$ and $\xi_\infty = 0.45$, one has

$$\alpha_e^* \cong 2.86\,\alpha_e.$$

It can be noted from the numerical example shown how creep, despite what happens for columns in compression or for uncracked sections in bending, leads to very limited increments of stresses in steel for cracked sections in bending. This is due to the situation of internal almost isostaticity, held by the equilibrium $M = N_s z$, which is not heavily affected by the lever arm z of the particular constitutive law of the material.

If the shape of the section were an *ideal* T (see Fig. 3.26), with a compression flange of small thickness t with respect to the affective depth d and with a web of negligible size, without significant error, one could consider the resultant C of compressions always applied at the mid-depth of the flange. This would lead to a lever arm of the internal couple

$$z = d - t/2$$

constant in time; in this case creep would not have any effect on the stresses variation of the section, which would be fixed in

$$\sigma_c = -\frac{M/z}{b\,t} = \text{cost.}$$
$$\sigma_s = \frac{M/z}{A_s} = \text{cost.}$$

Only curvature would vary, with increments in time that could be evaluated with the formula

$$\chi_{vt} = \chi_o(1 + \varphi_t x/d)$$

typical of an isostatic situation.

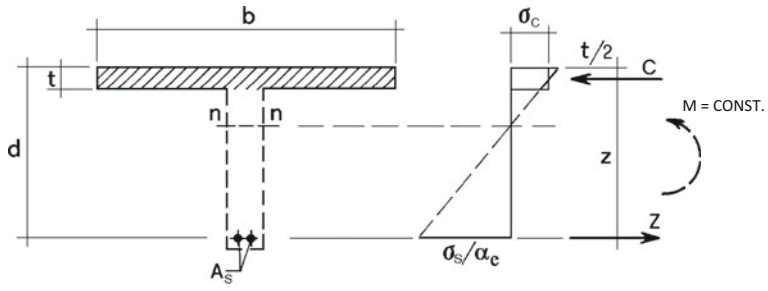


Fig. 3.26 Equilibrium condition of the ideal T-section

Influence on Ultimate Resistance

In order to evaluate the effects of creep on the ultimate capacity of the section in bending, the load history should be followed from the initial application of permanent loads, to the subsequent development of creep effects, eventually followed by the instantaneous increase of loads up to failure. In Fig. 3.27 this load history is described in terms of stresses and deformations.

Contrary to the situation of Fig. 2.9 which referred to a section under uniform compression, the case under analysis shows a variation of strain along the depth of the section. The strain ε_c at the edge in compression of the section is shown in the abscissas. The stress σ_c on the same edge of concrete is directly related to this, and the upper diagram of Fig. 3.27 therefore reproduces the constitutive law of this material (the one used for the resistance calculations). The lower diagram instead refers to the

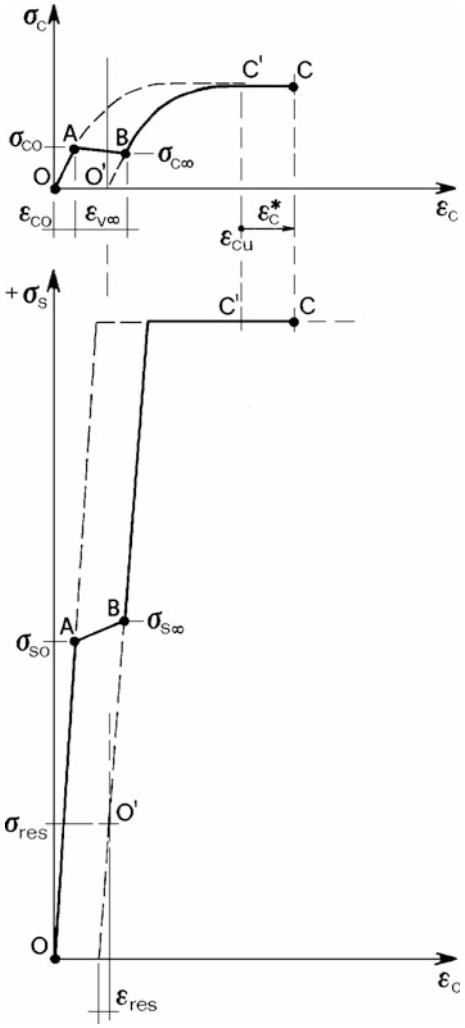


Fig. 3.27 Creep effects on stress–strain diagrams

reinforcement in tension at a distance d from the top edge. The constitutive law of steel will therefore be related to the parameter ε_c through the similarity on the strains of the section. The elastic portion for example will be given by

$$\sigma_s = E_s \varepsilon_s = -E_s \frac{1-\xi}{\xi} \varepsilon_c,$$

and will remain linear only for a given position $\xi = x/d$ of the neutral axis.

Except for the initial segment of the instantaneous elastic behaviour, in which the position of the neutral axis is indeed fixed, the subsequent segments of the diagrams under consideration are just indicative, as deviated from the straight line outlined in the figure because of the alternate changes in position of the neutral axis itself.

Further to these clarifications it is to be noted how, in the diagrams of Fig. 3.27, after the first segment *O–A* corresponding to the instantaneous application of the permanent fraction of loads, the segment *A–B* of progressive viscoelastic rearrangement of the section follows. At the end of the process, according to what elaborated in the previous pages, a limited increase $\Delta\sigma_s = \sigma_{s\infty} - \sigma_{so}$ of the stress in the reinforcement occurs, together with a decrease $\Delta\sigma_c = \sigma_{c\infty} - \sigma_{co}$ of the stress on the edge of concrete in compression. On the same edge, the contraction stabilizes on the value $\varepsilon_{c\infty} = \varepsilon_{co} + \varepsilon_{v\infty}$. At this point a new instantaneous load follows the curve σ_c–ε_c shifted in the figure with the new origin in O'.

Self-induced stresses are neglected here, as they would remain distributed on the section when the bending moment is instantly removed; however, it is just noted how, on the new origin corresponding to the decompression of the external edge of concrete, a value different from zero of the residual stress remains in the steel, according to the global translational equilibrium of the section. On the ultimate limit state, such residual stress has the same effects of pretension. Therefore, it does not affect the ultimate value of the moment in the domain of medium reinforcements where, with yielded steel, the translational equilibrium of the section remains

$$\beta_0 bx f_{cd} - A_s f_{yd} = 0$$

and leads to the definition of the position of the neutral axis with

$$\xi = \frac{1}{\beta_0} \omega_s,$$

which is not affected by the initial coaction existing at the origin O'. Only the limit with the high reinforcements changes:

$$x_c = \frac{\varepsilon_{cu}}{\Delta\varepsilon_s + \varepsilon_{cu}} d = \xi_c d,$$

with $\Delta\varepsilon_s = \varepsilon_{yd} - \varepsilon_{res}$, in the sense of reducing their extent. Given the small value of ε_{res} for common structural situations and on the conservative side, such effect is usually neglected, and as a result the resisting moment of the section is underestimated for high reinforcements.

3.3.2 Moment-Curvature Diagrams

At the beginning of Sect. 3.3, moment-curvature diagrams deduced by the hyperbolic tension stiffening model have already been presented. They can be applied, even in the cracked phase, within the service limit of the section in bending for action of small duration. In a non-dimensional form, such diagrams depended on two parameters: the *diversion ratio* $\psi = I_i'/I_i$ and the *limit of theoretical re-closure* of cracks $\overline{M}/M_r$ (see Fig. 3.21).

For section with medium reinforcements, it is possible to complete those diagrams with an end segment beyond the yield point of the reinforcement, should the analysis have to be extended up to situations close to failure. Such segment is shown in Fig. 3.28 expressed by the line

$$\chi_m = \chi_{ym} + \frac{\chi_u' - \chi_y'}{M_u - M_y}(M - M_y) \quad \text{for } M_y < M < M_u,$$

where the limit moments are evaluated on the cracked section (see Fig. 3.29)

$$M_y = \frac{I_i'}{y_s'} f_y \quad \chi_y' = \frac{f_y/E_s}{y_s'}$$
$$M_u = f_y A_s z_u' \quad \chi_u' = \frac{\varepsilon_{cu}}{x_u'},$$

with

$$z_u' = (1 - \omega_s/2)d \quad x_u' = \omega_s\, d/0.8.$$

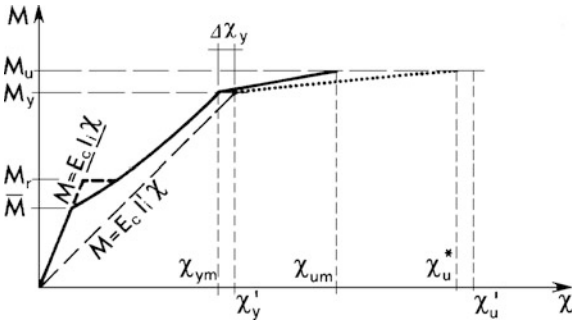


Fig. 3.28 Moment-curvature model

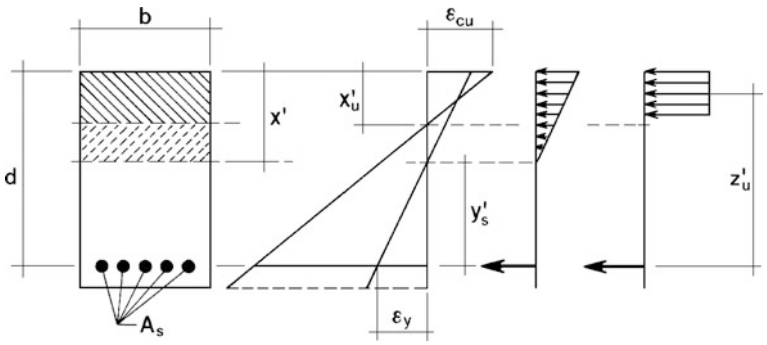


Fig. 3.29 Equilibrium conditions of the section

The beginning of the straight segment is translated on the curvature

$$\chi_{\mathrm{ym}} = \chi'_y - \Delta\chi_y,$$

where the tension stiffening of concrete in tension appears at the level of steel yielding:

$$\Delta\chi_y = 0.5\beta_0\beta_1\beta_2\left(\frac{M_{\mathrm{r}}}{M_y}\right)^2.$$

For the typical sections of beams, the average deformability in the yielded phase is significantly reduced so that the end segment is cut at

$$\chi_{\mathrm{um}} = \chi_{\mathrm{ym}} + \left(\chi'_{\mathrm{u}} - \chi'_y\right)/2.$$

For the critical sections that determine the beam failure, a concentration of plastic rotations occurs. These can be evaluated, along the dotted line of Fig. 3.28 which ends in

$$\chi^*_{\mathrm{u}} = \chi'_{\mathrm{u}} - \Delta\chi_y.$$

When applied for the calculation of the capacity of the beams, the limits M_y and M_{u} of the end segment of the curves should be calculated with the material strengths f_y and f_{c} reduced with respect to the characteristic values with the appropriate factors γ_M.

Integration of Stresses Over the Section

In the general case, with nonlinear constitutive laws σ–ε of materials and for actions at the ultimate limit of the section, the diagram $M = M(\chi)$ cannot be formally

represented with a mathematical model, but it should be calculated with appropriate numerical integrations of stresses over the section.

With reference to the generic section of Fig. 3.30, for a given deformed status defined by the strain ε_o on the design axis and by the curvature χ, the numerical integrations for the evaluation of axial N and flexural M components of actions can be set as

$$N \cong \sum_{i=1}^{n} b(y)\sigma_c(\varepsilon)\Delta y + \sum_{j=1}^{m} A_{sj}\sigma_s(\varepsilon_{sj})$$

$$M \cong \sum_{i=1}^{n} yb(y)\sigma_c(\varepsilon)\Delta y + \sum_{j=1}^{m} y_{sj}A_{sj}\sigma(\varepsilon_{sj}),$$

with

$$y = \left(i - \frac{1}{2}\right)\Delta y - y_c$$

$$\varepsilon = \varepsilon_o + \chi y.$$

The concrete section has been divided into n strips of depth $\Delta y = h/n$, numbered from top to bottom, and the material stresses σ_c and σ_s have been derived from the appropriate constitutive laws.

In order to obtain a point M, χ of the diagram, with $N \equiv 0$, these numerical integrations should be repeated modifying, with tries oriented according to the sign of the last value obtained for N, the strain at the axis ε_o, until the new N is with good approximation equal to zero. In the domain of positive moments, the procedure should be resumed with values of the curvature χ progressively increased from 0 to χ_u, the latter corresponding to the ultimate compressive strain ε_{cu} at the concrete edge in compression or the ultimate tensile strain ε_u of the lower reinforcement of the section.

The issues of numerical calculation in such analysis are omitted here, as the ones relative to the good convergence of the iterations or the ones relative to the adequate density of calculation points to obtain the main characteristics of the curves.

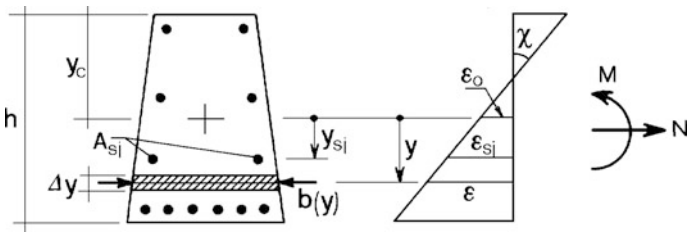


Fig. 3.30 Integration of the stresses over the section

Diagrams for Deformation Calculations

The obtained diagrams can be related to a deformation calculation; in this case the characteristic values f_{ck} and f_{yk} should be assumed for the materials, and more refined σ–ε models are used. In particular for concrete the rational fractional formula by Saenz is used in compression and the conventional cubic parabola in tension, as described at Sect. 1.1.1 (see Fig. 1.4).

In order to take the tension stiffening into account, the segment in tension can be fictitiously extended beyond the ultimate limit ε_{ctu}, with the hyperbolic decreasing curve (see Fig. 3.31):

$$\sigma(\varepsilon) = \frac{\bar{\varepsilon}}{\varepsilon}\bar{\sigma},$$

where

$$\bar{\sigma} = \sigma(\bar{\varepsilon})$$

corresponds to the limit

$$\bar{\varepsilon} \cong 0.7\sqrt{\beta^*}\,\varepsilon_{ctu}$$

of theoretical re-closure of cracks, as specified at Sect. 2.3.2 ($\beta^* = \beta_0\beta_1\beta_2$). The dashed segment in Fig. 3.31 refers to load cycles after the first one.

Several typical configurations of diagrams obtained from the numerical integrations described here will be shown in the next paragraph.

Effects of Creep on Curvatures

An exact calculation of moment-curvature diagrams, which takes into account the viscoelastic behaviour of concrete under long-term loads, should be carried with two orders of numerical integrations, one in time and the other along the depth of the section, in order to follow the evolution in time of the phenomenon and adjust at each time step the viscoelastic equilibrium of the section. Such calculation would be extremely complex and onerous, and therefore simplified methods are followed

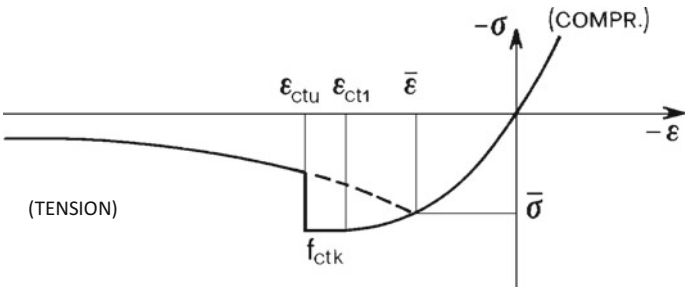


Fig. 3.31 Stress–strain model in tension

which permit to treat the problem with algebraic algorithms, in line with what described at Sect. 1.3 especially devoted to viscosity in concrete.

According to the criteria of the effective modulus method EMM described at Sect. 1.3.3, the effect of creep can be simulated with the amplification, by $1 + c\varphi$ of the diagram σ–ε along the abscissas. In this case the Saenz's model defined for short-term loads should be reduced and cut-off to take into account the long-term strengths, as described in Fig. 3.32. One should remind that c is the square of the ratio of the permanent part to the total load.

With such method, from the integrations of stresses $M = M(\chi)$ diagrams are obtained that are stretched along the abscissas. Their use can avoid the integrations along the time in the analysis of the viscoelastic behaviour of sections, even though the drawback of the simplification is a much lower accuracy of the results of the relative structural applications.

The mathematical formulations of the moment-curvature diagrams derived from the hyperbolic model of tension stiffening can also be adapted for the long-term actions with viscoelastic effects. In order to do so, it suffices to use the effective concrete modulus instead of the elastic one in the relative formulas. Such effective modulus can be given by

$$E_c^* = \frac{E_c}{1 + c\varphi},$$

according to the above-mentioned method EMM or by more refined formulations, again of the type

$$E_c^* = \frac{E_c}{\alpha_e^*},$$

with α_e^* evaluated according to what developed for the section in bending at Sect. 3.3.1.

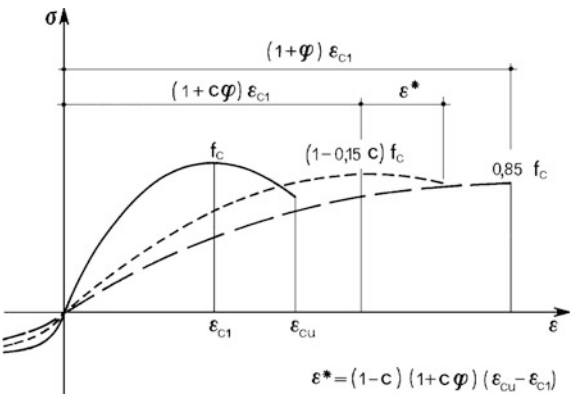


Fig. 3.32 Creep effects on stress–strain diagram

Of course the effective modulus also modifies the homogenization ratio of the steel areas in the evaluations of the geometrical characteristics I_i' and I_i of the cracked and uncracked section.

Diagrams for Resistance Calculations

The diagrams obtained with the numerical integrations along the depths of the section can refer to a resistance calculation; in this case the design values f_{cd} and f_{yd} are introduced and the appropriate σ–ε diagrams of materials are used, already described at Sect. 1.4.2 (for example, the parabola–rectangle model in compression and zero resistance in tension for concrete).

In the next paragraph several typical configurations of the obtained diagrams will be shown, which refer exclusively to the local behaviour of sections and cannot be used to deduce the global deformed shape of beams. They give information on such local behaviour very important for design, as the one on the ductile resources of sections.

The parabola–rectangle law can also be fictitiously modified, in order to take into account the creep effects, with an amplification along the abscissas by $1 + c\varphi$ (see Fig. 3.33). In such law, which refers to resistance calculations, the quota of the short-term strengths was already removed with $f_{cd} = \alpha_{cc} f_{ck}/\gamma_C$ and therefore no additional reduction of the ordinates should be done. Instead, the ending part of the curve should be cut-off, similar to what is done for the rational fractional law used in the deformation calculations (see Fig. 3.32).

The moment-curvature diagrams that are obtained with such modification of the constitutive concrete law are also stretched along the abscissas. These diagrams $M^*(\chi; \varphi)$ can be used for the solution of structural problems as the elementary one described in Fig. 3.34 where it has been assumed to find, through the intersection of the respective curves, the curvature consequent to a given moment $\overline{M}$.

As shown by the diagrams of the above-mentioned figure, the solution χ^* obtained from the equivalent modified diagram is though much less accurate than the one χ given by the exact method, which accurately follows the load history, as indicated by the segment *O–A–B* of the dashed curves of the same figure. In fact, the conventional approximation of the diagrams leads, with smaller angles of

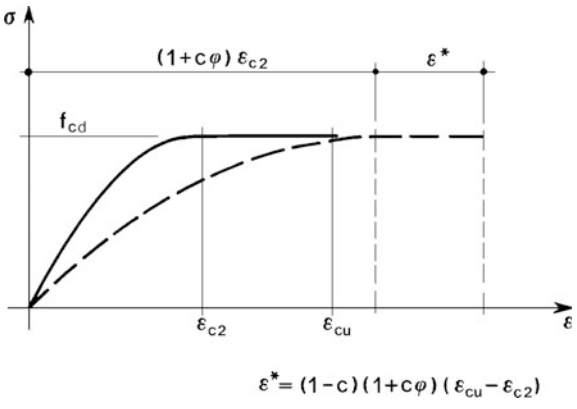


Fig. 3.33 Parabola–rectangle σ–ε with creep effects

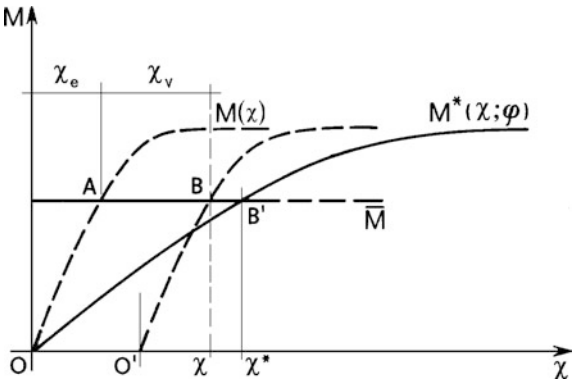


Fig. 3.34 "Exact" and approximate solutions of curvature

intersection, to solutions with a more uncertain numerical definition and much more sensitive to the errors of evaluation of the relevant parameters.

3.3.3 Flexural Behaviour Parameters

With the exemplification of M–χ diagrams carried hereafter, we intend to highlight few significant parameters of the flexural behaviour of sections. With reference to the rectangular section with double reinforcement of Fig. 3.35, the following *non-dimensional values* of the relevant parameters are preliminarily defined:

$$\delta = \frac{d}{h} \qquad \delta' = \frac{d'}{h}$$

$$\omega_s = \frac{A_s f_{yd}}{bhf_{cd}} \qquad \omega'_s = \frac{A'_s f_{yd}}{bhf_{cd}}$$

$$\omega_t = \omega_s + \omega'_s \qquad \alpha = \omega'_s/\omega_s = A'_s/A_s$$

$$v = \frac{N}{bhf_{cd}} \qquad \mu = \frac{M}{bh^2 f_{cd}}$$

$$\bar{\chi} = \chi h.$$

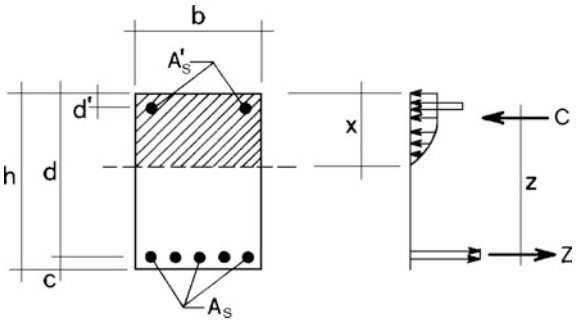


Fig. 3.35 Equilibrium condition of the cracked section

If one is only interested in the resistance of the section, without any reference to the behaviour in service where the contribution of the zone in tension counts, the concrete cover c in the tension zone can be neglected setting $d = h$ ($\delta = 1$). Already in Sect. 3.2 the non-dimensional variables were used

$$\xi = \frac{x}{d} \quad \zeta = \frac{z}{d},$$

related to the resistance calculations of the section in bending.

The order of magnitude of the non-dimensional variables defined above can be indicatively deduced from the following evaluations. Given that the *concrete cover* varies from 3 to 5 cm, for sections of normal depths its non-dimensional value can be set as

$$c/h = \delta' = 0.05 = \cdots = 0.20,$$

and consequently *the effective depth*:

$$\delta = 1 - \delta' = 0.95 = \cdots = 0.80.$$

The *mechanical reinforcement ratio* in tension, going from the domain of low to high reinforcement (see Sect. 3.2.1), can be equal to

$$\omega_s = 0.10 = \cdots = 0.60,$$

whereas the *compression reinforcement ratio*, from the single reinforcement to the double symmetric one, is equal to

$$\alpha = 0.00 = \cdots = 1.00.$$

The *axial force* is not relevant to the current description, which refers to simple bending. Nonetheless its non-dimensional value is calculated with reference to the resisting value relative to concrete only, and it is therefore limited (see Sect. 3.1.1) to

$$\nu \leq 1 + \omega_t = 1 + \omega_s(1 + \alpha).$$

The non-dimensional value of the *bending moment* reaches values that, for single reinforcement, can be set as

$$\mu \leq \frac{\beta f_{cd} b x z}{f_{cd} b h^2} = \beta \xi \zeta \delta^2,$$

and go for low and high reinforcement from

$$0.8 \times 0.25 \times 0.8 \times 0.9^2 \cong 0.13$$

to

$$0.8 \times 0.50 \times 0.7 \times 0.9^2 \cong 0.23.$$

The non-dimensional value of the maximum *curvature* is defined by the ultimate strain limits of the materials

$$\bar{\chi} = \frac{\varepsilon_{cu} + \varepsilon_{sh}}{d} h = \frac{\varepsilon_{cu} + \varepsilon_{sd}}{\delta} \cong \frac{0.0675}{0.9} = 0.075.$$

The diagrams of Fig. 3.36 have been obtained with the *resistance constitutive laws* and with values of ω_s belonging to the domain of low reinforcements for the curve "*a*", medium reinforcements for the curve "*b*" and high reinforcements for the curve "*c*". The curvatures $\bar{\chi}_y$ and $\bar{\chi}_u$ at the steel yield limit and at the ultimate limit of the section are highlighted. The curve "*c*", in particular, shows a brittle early rupture without yielding.

An important parameter of the flexural behaviour of the section, related to the plastic adaptation capacity for static actions beyond the yield limit and to the possibility of energy dissipation under seismic actions, is the *coefficient of plastic adaptation*:

$$c_p = \frac{\bar{\chi}_u}{\bar{\chi}_y},$$

which decreases when the mechanical steel ratio increases, until it becomes equal or lesser than 1 for brittle sections.

The presence of reinforcement in the compression zone has the effect of increasing the ductility of sections, without significantly modifying, except for high reinforcements, the value of the ultimate capacity.

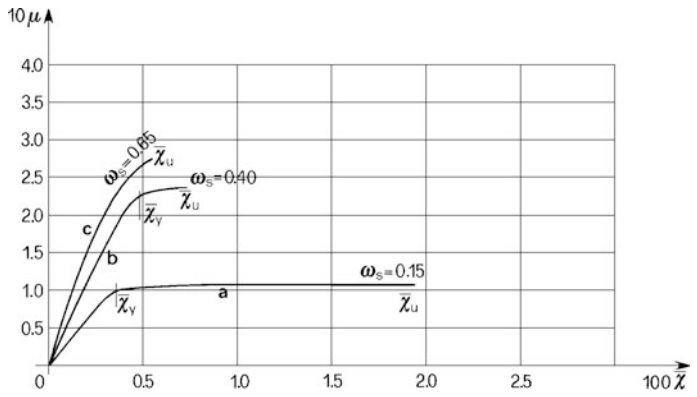


Fig. 3.36 Resistance constitutive lows

Re-elaborated for the same sections with the *deformation constitutive laws* and therefore for calculations in service, the diagrams appear as indicated in Fig. 3.37.

The first phase of uncracked section, the cracking threshold showed by the sudden drop of stiffness, the following phase of cracked section with tension stiffening progressively decreasing and eventually the last phase of ductile behaviour and yielded steel are to be noted.

Given that the characteristic values f_{ck} and f_{yk} of the strengths have been used, and the non-dimensional values of parameters have been expressed with respect to the design strength f_{cd} of concrete, the ultimate moments are greater than the ones attained in the resistance diagrams, approximately by γ_C for high reinforcements, and by γ_S for other situations. The ductility parameters are also modified according to the different ratios between strengths of concrete and steel ($\gamma_C/\gamma_S > 1$).

The points corresponding to the value $\varepsilon_s = 0.001$ of the average strain of reinforcement are indicated with an asterisk in the curves of Fig. 3.37. These value are conventionally assumed as the limit related to the crack width, and roughly corresponding to the unit characteristic crack width w_{ok} which, for a characteristic distance equal to $s_k = 100$ mm, leads to a width $w_k = 0.1$ mm of the single crack. Such points give the conventional limits of the serviceability verifications.

Choice of Precompression

The typical moment-curvature curve of deformation of a section in bending is shown in Fig. 3.38, having in particular removed the cracking threshold relative to the first load cycle. Starting from the zero value of the action (point 0), the curve increases up to the limit of theoretical re-closure of cracks (point 1) beyond which it exhibits a sudden drop of stiffness. It then reaches the limit related to the cracking verification (point 2) corresponding for example to the conventional crack width w_k, and then increases again up to the ultimate limit evaluated with a resistance calculation (point 3), beyond which the difference due to the factor γ_M remains (=1 for deformation calculation, >1 for resistance calculation).

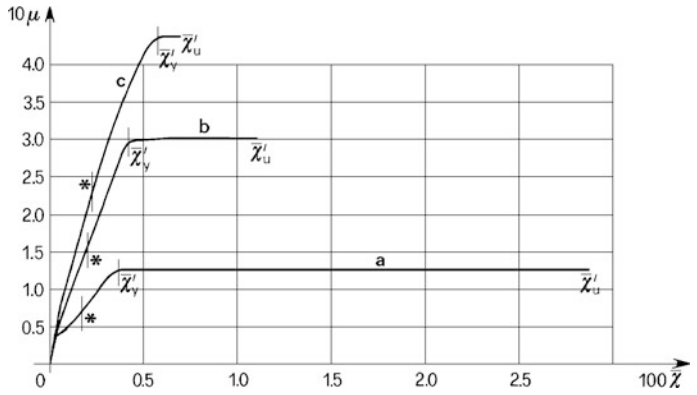


Fig. 3.37 Deformation constitutive lows

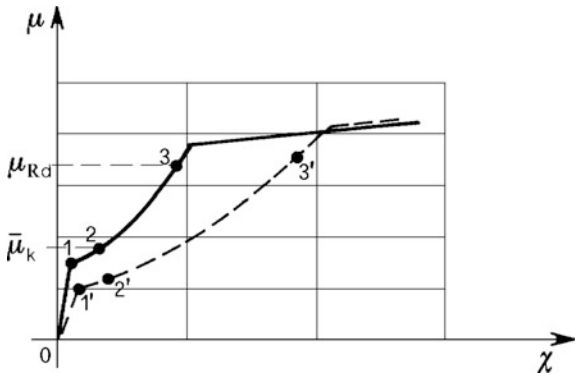


Fig. 3.38 Moment-curvature deformation diagrams

Given that, at the ultimate limit, the actions should be amplified by γ_F (=1.30 or 1.50), whereas at the cracking limit state their characteristic values are applied, possibly partially reduced with the concurrence coefficients ψ_i related to the percent duration of loads, one has a balanced design of the section when

$$\frac{\mu_{Rd}}{\bar{\mu}_k} \cong \frac{\gamma_F}{\psi},$$

where μ_{Rd} is the design resisting moment, $\bar{\mu}_k$ is the allowable moment in service corresponding to the limit imposed by the cracking verification and ψ is the global average value of the concurrence coefficient in the load combination. If

$$\bar{\mu}_k \ll \frac{\psi}{\gamma_F}\mu_{Rd},$$

the ultimate resistance of materials cannot be fully utilized because of an inadequate behaviour in service.

The use of high-strength steels leads, for a given ω_s, to curves similar to the dashed one in Fig. 3.38. The ultimate resistance does not change significantly, whereas the allowable moment in service is considerably reduced. The curve is also shifted on the abscissas, showing a reduction in stiffness of the section which, beyond the cracking limits, can lead to an excessive deformability of the beam. Therefore, for those steels, the limits set by the serviceability conditions would not allow to fully utilize their resources for strength.

In order to conveniently use high-strength steels, one should prestress them so that the cracking limits are increased, stiffening at the same time the section. The moment-curvature curves are shown in Fig. 3.39a, b, for resistance and deformation, respectively, repeated for different levels of precompression. The *coefficient of partial precompression* is indicated with c_p, which is the ratio between the actual applied pretension σ_{po} and the maximum one allowed by the tendon (e.g. 0.75 f_{ptk} in service). The three curves of each diagram therefore refer to the section without

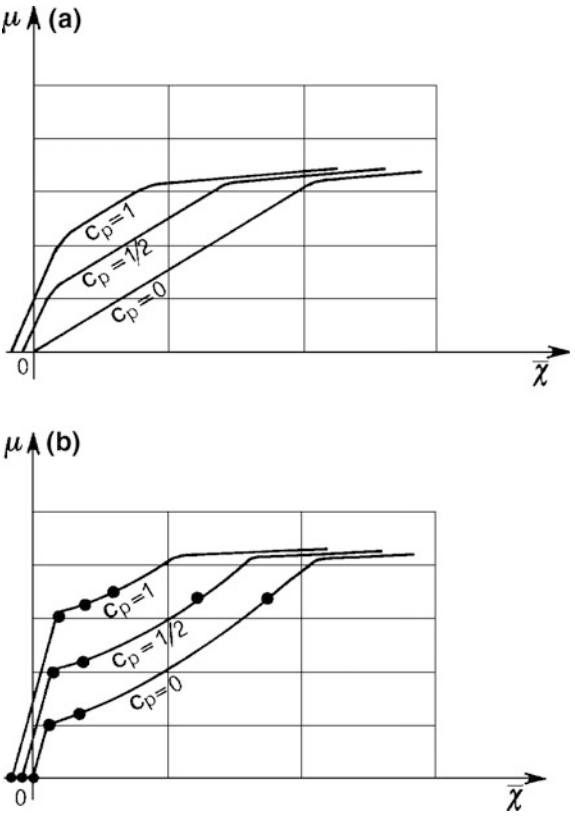


Fig. 3.39 Resistance (**a**) and deformation (**b**) diagrams with precompression

precompression (the lower one), half precompression (intermediate one) and total precompression (upper one).

It is to be noted how the use of increasing levels of precompression does not lead, for a given ω_s, to significant variations of the final resistance; the behaviour in intermediate situations, prior to yielding of steel, is instead significantly stiffened. In particular, in the deformation diagrams it is to be noted the big increase in cracking moments up to values close to the resistance itself. In the section with high precompression, one can therefore have an ultimate failure limit of the section very close to the allowable one in service.

3.4 Case A: Design of Floors

The calculation of actions on floors is carried with reference to strips of modular width, related to the spacing of ribs, on partial static schemes of continuous beams appropriately defined for the different zones of the deck. Such schemes interpret in

an approximate way the real structural behaviour where the floor ribs are supported by the main beams with elastic rotational and translational (vertical) flexible end supports. The degree of flexibility of these constraints depends on the flexibility of the beams and the flexibility of the other connected elements such as columns. It varies along the beams, from a minimum value at the columns locations, to the maximum value around the mid-span of the beams. Other uncertainties derive from the transverse discontinuities due to adjacent strips with different span or structural walls.

Therefore, in order to take into account the peculiarity of the structural layout, appropriate modifications will have to be applied to the simple schemes of continuous beam as the ones shown in Fig. 3.40 with reference to the four types of strips that can be derived from the deck of Fig. 2.19. If for example it is possible to neglect the degree of rotational constraint on the internal supports, as not significantly involved by the almost balanced arrangement of the opposite spans, the same assumption cannot be made at the extreme supports where the flexural stiffness of the vertical elements (columns or walls) induces a fixed-end moment, perhaps of low magnitude, but not equal to zero as the simplified model assumes.

Also, it is eventually reminded how certain loads acting on the floor have to be represented by simplified schemes, as referred to configurations that are not predictable with accuracy. It is the case of live loads and certain superimposed

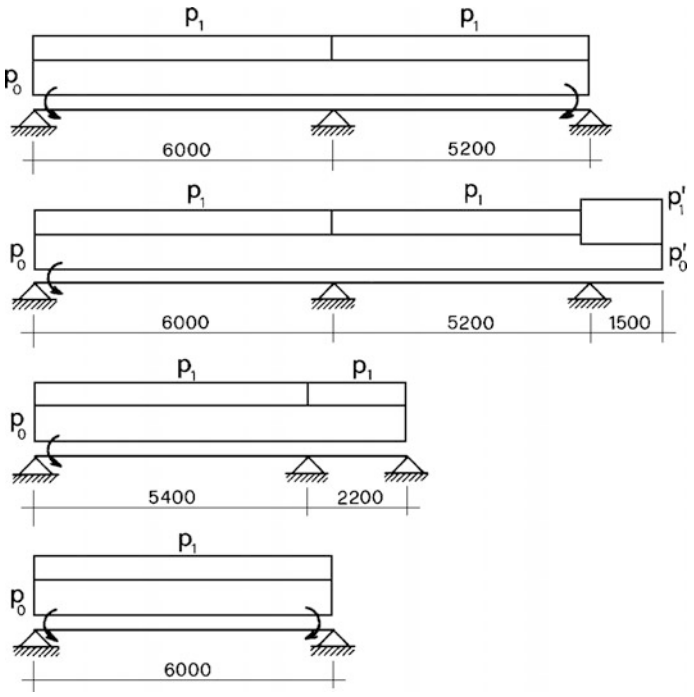


Fig. 3.40 Calculation schemes of the different floor strips

permanent loads, as the weight of partitions, whose layout can vary with respect to the initial design assumptions. For such loads a conventional scheme of uniform distribution is assumed, relying on the appropriate transverse mid-span ribs to distribute the load discontinuities, the same that allow to reduce the transverse discontinuities of behaviour due to the diversity of the structural layouts.

In the following paragraphs, the design of one type of strip is developed, limited to flexural verifications. A method to approximately evaluate the end moments of the strip is also given. The results are eventually translated in the competent construction drawing, containing the construction details of the reinforcement.

The outcome of the design calculations, together with the relative synthetic summary of the elaborations, is presented in a specific report, in order to show the analyses, the design and the verifications carried. A possible scheme of such report is shown hereafter:

Design Report

1 General

- 1.1 Description of works
- 1.2 Analysis of loads
- 1.3 Materials

2 Design of Columns

- 2.1 Actions on columns
- 2.2 Design and verifications
- 2.3 Particular calculations

3 Design of Floors

- 3.1 Analysis of actions
- 3.2 Serviceability verifications
- 3.3 Resistance verifications

4 Design of Beams

- 4.1 Analysis of actions
- 4.2 Serviceability verifications
- 4.3 Resistance verifications

5 Overall Stability

- 5.1 Analysis of actions
- 5.2 Verification of lateral stability elements
- 5.3 Additional calculations

6 Design of Foundations

- 6.1 Verifications of footings
- 6.2 Calculations of walls and beams
- 6.3 Particular calculations

The list of content shown above is obviously only indicative and variations may be applied. It starts with a chapter devoted to the general aspects of the overall structural system. Its first section can contain a synthetic description of the building, similar to what has been done at the beginning of Sect. 2.4 of this volume. The following one presents the analysis of the weights of the main elements as anticipated at Sect. 2.4.1 (double wall, simple partition, typical floor, …). Eventually, the characteristics of materials are given (concrete and steel) assumed for the structure under analysis, as already done after the corresponding section in the above-mentioned Sect. 2.4.1.

The second chapter presents the design of columns that can be based on the division of the decks in *tributary areas* (see Fig. 2.23) and on the analysis of actions as the one described before for the column P14. The calculations for the design and the verification of the column segments at the different floors can be summarized in the competent tables already described at Sect. 2.4.1.

The following chapters are related to the elements of the deck in bending (floors and beams) for which few calculation examples will follow. Their typical stages of analysis, service and resistance can be developed in more detail, as indicated below for beams:

4.1 Analysis of actions

- 4.1.1 Load conditions
- 4.1.2 Load combinations
- 4.1.3 Proportioning of reinforcement

4.2 Serviceability verifications

- 4.2.1 Bending moment
- 4.2.2 Shear force
- 4.2.3 Deformation verifications

4.3 Resistance verifications

- 4.3.1 Flexural resistance
- 4.3.2 Shear resistance
- 4.3.3 Verifications of joints

The analysis of actions is repeated for the individual partial static schemes as the ones shown in Fig. 3.40. A convenient procedure to determine the different verification situations can consist of elaborating the situations for single *elementary conditions*, loading separately span by span. The verification situations will then be deduced with the *weighed combinations* of the single solutions.

With reservation of re-elaborating these combinations for the resistance verifications with the different weights due to the relevant safety factors, the characteristic values of loads are used at first, typical of the serviceability verifications. For the *proportioning of reinforcement*, carried with reference to resistance, the global safety factor $\gamma_F \cong 1.43$ can be approximately used, already assumed in Sect. 2.4.1 for the verification of columns, with a simple proportional amplification of forces.

The next section of the serviceability limit states refers to the verifications of stresses produced by bending moment and shear in concrete and in the reinforcement, the latter including the cracking limits according to the criteria recalled in Sect. 3.2.3. Certain deformation calculations can be added, with the evaluation of the viscoelastic flexural deflections of the floor spans under service loads.

The section of ultimate limit states eventually verifies the resistance of the critical sections both of maximum moment and maximum shear, adding possible local verifications at the supports, necessary to complete the design with the details of the joints of the structure.

In this section, as already mentioned, only flexural calculations will be presented. One can refer to Sect. 4.4 of the following chapter for the completion of shear verification of the analysed floor.

3.4.1 Analysis of Actions

Reference is made to the zone of the floor with two consecutive spans, respectively, equal to 6.00 and 5.20 m, comprised between columns P6–P8–P21–P23 of Fig. 2.19. The analysis of loads has already been developed in Sect. 2.4.1, defining the load per m^2 of floor with 3.25 kN/m^2 of structural self-weight, 3.75 kN/m^2 of superimposed dead loads due to finishing and 2.00 kN/m^2 of live loads. In that instance, with respect to the design of columns, only the total maximum load was relevant. The maximum negative and positive forces now have to be evaluated on the different sections, as they result from the possible different load combinations.

To this end, in addition to the live loads, the part of superimposed dead load has to be identified that can vary along the beam length with respect to the maximum value assumed in the already mentioned analysis of loads. It is mainly the case of the self-weight of partitions, which can be missing in large floor areas (for example where living rooms are positioned) and the self-weight of finishing that can be significantly lower (as for wood flooring). In the analysis of the flexural actions in the continuous beam of Fig. 3.41 the following loads have therefore been assumed, referred to a floor strip with a width of 1.0 m containing two ribs of the ones dimensioned in Fig. 2.22.

Elements that might be missing

• distributed partitions	2.00	kN/m^2
• substituted finishing	0.40	”
• new lightweight flooring	−0.10	”
	2.30	kN/m

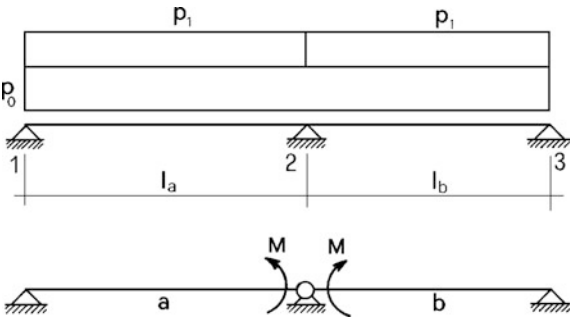


Fig. 3.41 Calculation schemes of the continuous beam

For a strip with b = 1.0 m

• structural self-weight	3.25	kN/m
• superimposed dead load	1.45	”
tot. permanent loads	p_o = 4.70	kN/m
• variable elements	2.30	kN/m
• live loads	2.00	”
tot. variable loads	p_1 = 4.30	kN/m

Load Conditions

In the static scheme of Fig. 3.41 the two beams are assumed to have constant cross section (EI = cost.), neglecting the higher stiffness of the segments with solid section at the supports with respect to the typical T-shaped section. The compatibility equation according to the force (Flexibility) method is set:

$$M_2\phi_{22} + \phi_{20} = 0,$$

with

$$\phi_{22} = \frac{1_a}{3EI} + \frac{1_b}{3EI}.$$

The two elementary load conditions are the ones indicated with “A” and ”B” in Fig. 3.42. For these conditions, with the values defined above for loads and with l_a = 6.00 m and l_b = 5.20 m, the moments M_2 at the intermediate support and M_a, M_b at the two mid-spans are therefore obtained.

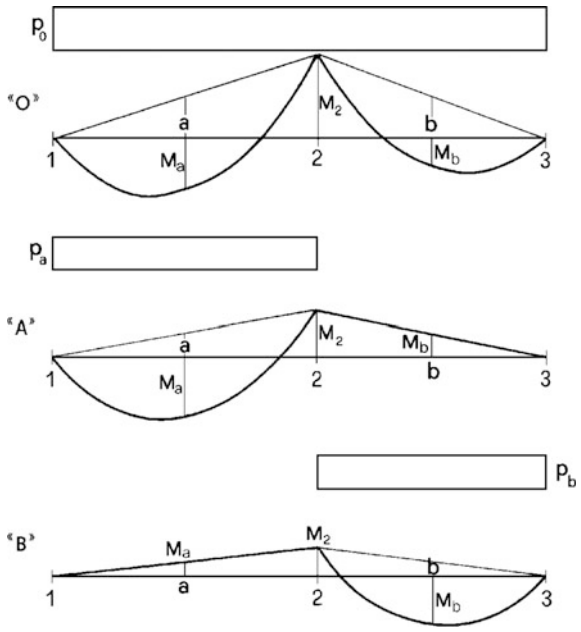


Fig. 3.42 Permanent "O" and variable elementary "A", "B" load conditions

- Condition "A" ($p_a = p_1$ on span a)

$$\phi_{20} = \frac{p_a l_a^3}{24EI}$$
$$M_2 = -2.411 p_a = -10.366\,\text{kNm}$$
$$M_a = \frac{p_a l_a^2}{8} + \frac{M_2}{2} = 4.500 p_a - 1.205 p_a = 3.295 p_a = 14.167\,\text{kNm}$$
$$M_b = \frac{M_2}{2} = -1.205 p_a = -5.183\,\text{kNm}.$$

- Condition "B" ($p_b = p_1$ on span b)

$$\phi_{20} = \frac{p_b l_b^3}{24EI}$$
$$M_2 = -1.569 p_b = -6.748\,\text{kNm}$$
$$M_a = \frac{M_2}{2} = -0.785 p_b = -3.374\,\text{kNm}$$
$$M_b = \frac{p_b l_b^2}{8} + \frac{M_2}{2} = 3.380 p_b - 0.785 p_b = 2.595 p_b = 11.160\,\text{kNm}.$$

The basic situation of permanent load, indicated with "O" in Fig. 3.42, is obtained from the condition A + B with $p_b = p_a = p_o$:

- Condition "O" (p_o on both spans)

$$M_2 = -2.411 p_o - 1,569 p_o = -18.706\,\text{kNm}$$
$$M_a = 3.295 p_o - 0.785 p_o = 11.797\,\text{kNm}$$
$$M_b = -1.205 p_o + 2.595 p_o = 6.533\,\text{kNm}.$$

Loads Combinations

The three load conditions lead to the diagrams of bending moment of Fig. 3.42. Showing now on the same graph the four possible combinations O, O + A, O + B and O + A + B between these diagrams, the envelope diagram of Fig. 3.43 is obtained which gives on the entire continuous beam the maximum and minimum values of the bending moment. The maximum positive moments M'_a and M'_b on the two spans are obtained, respectively, from the combinations O + A and O + B with $(p_o + p_1)$.

- Combination "O + A"

$$R_1 = \frac{p 1_a}{2} + \frac{M_2}{1_a} = \frac{900 \times 6.0}{2} - \frac{29.072}{6.0} = 22.155\,\text{kN}$$
$$x_1 = \frac{R_1}{p} = \frac{22.155}{9.00} = 2.46\,\text{m}$$
$$M'_a = R_1 x_1 - p\,\frac{x_1^2}{2} = 22.155 \times 2.46 - 9.00\,\frac{2.46^2}{2} = +27.269\,\text{kNm}.$$

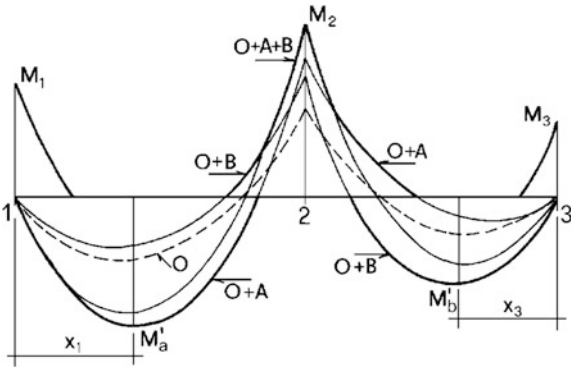


Fig. 3.43 Envelope diagram of bending moment

- Combination "O + B"

$$R_3 = \frac{pl_b}{2} + \frac{M_2}{l_b} = \frac{900 \times 5.2}{2} - \frac{25.454}{5.2} = 18.505\,\text{kN}$$
$$x_3 = \frac{R_3}{p} = \frac{18.505}{9.00} = 2.06\,\text{m}$$
$$M'_b = R_3 x_3 - p\frac{x_3^2}{2} = 18.505 \times 2.06 - 9.00\frac{2.06^2}{2} = +19.024\,\text{kNm}.$$

The maximum negative moment at the internal support is eventually obtained from the combination O + A + B (also with $p = p_o + p_1$)

- Combination "O + A + B"

$$M_2 = -18.706 - 10.366 - 6.748 = -35.820\,\text{kNm}.$$

Scheme for the End Supports

In order to evaluate the fixed-end moments at the ends 1 and 3 of the floor strip, one can refer to the static scheme of Fig. 3.44, where a full degree of fixity is assumed between the floor itself and the columns located at the ends. Within the significant approximations of this scheme, the columns are assumed as pinned at the mid-height in order to take into account the combined action of the upper and lower floors.

The moment of inertia of the floor section with a width of 1.0 m, with reference to the dimensions shown in Fig. 2.22, is therefore obtained from the following calculations:

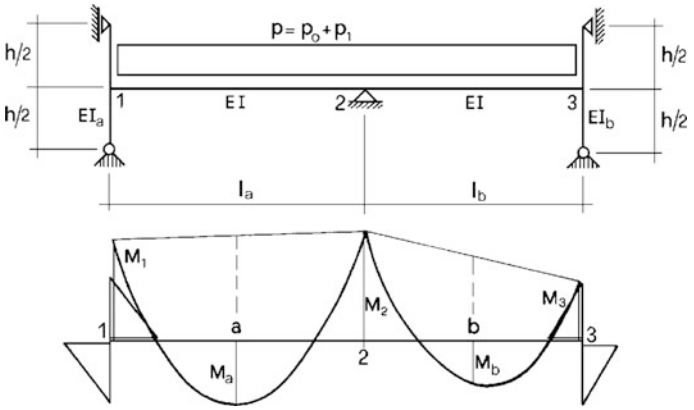


Fig. 3.44 Calculation scheme for the end moments

$$\begin{aligned} 100 \times 4 = 400 \times 2 \quad &= \quad 800 \\ 16 \times 20 = \underline{320} \times 14 = \quad &\underline{4480} \\ A = 720\,\mathrm{cm}^2 \quad &5280\ \mathrm{cm}^3 \end{aligned}$$

$$y_G = 5280/720 = 7.3\,\mathrm{cm}$$

$$\begin{aligned} 400\left(5.3^2 + 4^2/12\right) &= 11769\,\mathrm{cm}^4 \\ 320\left(6.7^2 + 20^2/12\right) &= \underline{25031}\,\mathrm{cm}^4 \\ I &= 36800\,\mathrm{cm}^4. \end{aligned}$$

For the maximum section 45 × 30 cm of the column one obtains

$$I_o = 45 \times 30^3/12 = 101250\ \ \mathrm{cm}^4.$$

This moment of inertia should be related to the width of the floor strip on the basis of the columns spacing:

$$\begin{aligned} I_a &= 101250 \times 1.00/3.20 \cong 32000 \cong 0.85\,I \\ I_b &= 101250 \times 1.00/2.95 \cong 34000 \cong 0.90\,I. \end{aligned}$$

Solving now the frame scheme under consideration with the displacements (Stiffness) method, one has

$$\begin{cases} m_{11}\phi_1 + m_{12}\phi_2 + \qquad\quad m_{10} = 0 \\ m_{21}\phi_1 + m_{22}\phi_2 + m_{23}\phi_2 + m_{20} = 0 \\ \qquad\quad m_{32}\phi_2 + m_{33}\phi_3 + m_{30} = 0, \end{cases}$$

where the three unknowns ϕ_1, ϕ_2, ϕ_3 represent the rotations at the joints and where, with h = 3.06 m, the coefficients are equal to

$$\begin{aligned} m_{11} &= 2\frac{3EI_a}{h/2} + \frac{4EI}{l_a} = 4.00\,EI \\ m_{12} = m_{21} &= \frac{2EI}{l_a} = 0.333\,EI \\ m_{22} &= \frac{4EI}{l_a} + \frac{4EI}{l_b} = 1.436\,EI \\ m_{23} = m_{32} &= \frac{2EI}{l_b} = 0.385\,EI \\ m_{33} &= \frac{4EI}{l_b} + 2\frac{3EI_b}{h/2} = 4.299\,EI \\ m_{10} &= -\frac{pl_a^2}{12} = -27.00\,\mathrm{kNm} \\ m_{20} &= +\frac{pl_a^2}{12} - \frac{pl_b^2}{12} = 6.720\,\mathrm{kNm} \\ m_{30} &= +\frac{pl_b^2}{12} = +20.280\,\mathrm{kNm}. \end{aligned}$$

The solution of the equilibrium system leads to

$$\phi_1 = +7.183/EI$$
$$\phi_2 = -5.206/EI$$
$$\phi_3 = -4.251/EI,$$

and the moments are consequently obtained as (see Fig. 3.44)

$$M_1 = -\frac{pl_a^2}{12} + \frac{4EI}{l_a}\phi_1 + \frac{2EI}{l_a}\phi_2 = -23.95\,\text{kNm}$$
$$M_2 = -\frac{pl_a^2}{12} - \frac{2EI}{l_a}\phi_1 - \frac{4EI}{l_a}\phi_2 = -25.92\,\text{kNm}$$
$$M_3 = -\frac{pl_b^2}{12} - \frac{2EI}{l_b}\phi_2 - \frac{4EI}{l_b}\phi_3 = -15.01\,\text{kNm}$$
$$M_a = +\frac{pl_a^2}{8} + \frac{M_1 + M_2}{2} = +15.57\,\text{kNm}$$
$$M_b = +\frac{pl_b^2}{8} + \frac{M_2 + M_3}{2} = +9.96\,\text{kNm}.$$

The two end parts of the relative diagram are used to complete the envelope of Fig. 3.43 with the moments M_1 and M_3 which represent the maximum negative on the end supports of the floor.

Design of Reinforcement

First, we refer to the diagram of Fig. 3.43 drawn with the characteristic values of loads, increasing the moments proportionally to the global safety factor $\gamma_F = 1.43$ (weighed average between $\gamma_G = 1.30$ and $\gamma_Q = 1.5$—see Sect. 2.4.1).

For the design of reinforcement the approximate formula is used that, at the ultimate limit state of failure, assumes the steel yielded, excluding the zone "*c*" of high reinforcements, and approximates the lever arm of the internal couple to 0.9 times the effective depth of the section. With the strength values specified at Sect. 2.4.1 ($f_{yd} = 391\ \text{N/mm}^2$) one therefore has the following reinforcements referred to the three cases of Fig. 3.45:

- *Section "a"* ($M = 27269$ Nm, $d = 21.0$ cm)

$$A_s = \frac{2726900 \times 1.43}{0.9 \times 21 \times 39100} = 5.28\,\text{cm}^2.$$

  $2 \times 2\phi 14$ are assumed with $6.16\ \text{cm}^2$
- *Section "2"* ($M = 35820$ Nm, $d = 21.0$ cm)

$$A_s = \frac{3582000 \times 1.43}{0.9 \times 21 \times 39100} = 6.93\,\text{cm}^2.$$

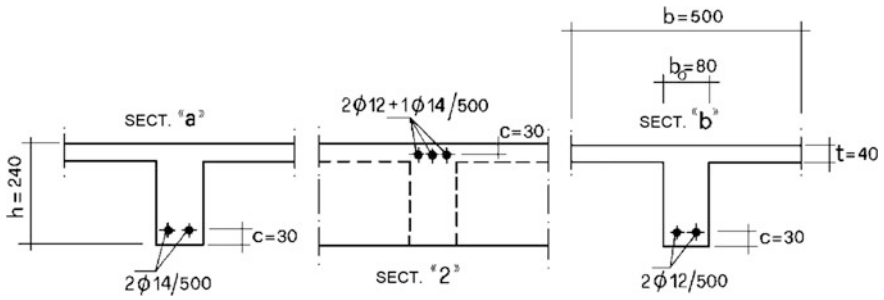


Fig. 3.45 Mid-span *left*, *central* support and mid-span *right* sections

$2 \times (1\phi 14 + 2\phi 12)$ area assumed with 7.60 cm^2

- *Section "b"* (M = 19024 Nm, d = 21.0 cm)

$$A_s = \frac{1902400 \times 1.43}{0.9 \times 21 \times 39100} = 3.72\,\text{cm}^2.$$

$2 \times 2\phi 12$ are assumed with 4.52 cm^2

- *Section "1"* (M = 23950 Nm, d = 21.0 cm)

$$A_s = \frac{2395000 \times 1.43}{0.9 \times 21 \times 39100} = 4.63\,\text{cm}^2.$$

$2 \times (2\phi 10 + 1\phi 12)$ are assumed with 5.40 cm^2

- *Section "3"* (M = 15010 Nm, d = 21.0 cm)

$$A_s = \frac{1501000 \times 1.43}{0.9 \times 21 \times 39100} = 2.90\,\text{cm}^2.$$

$2 \times (1\phi 10 + 1\phi 12)$ are assumed with 3.84 cm^2.

The layout of the bars is shown in Fig. 3.46 according to these calculations, with reference to one floor rib.

A more precise proportioning procedure starts from the rotational equilibrium of the section (see Fig. 3.10b):

$$M_{Ed} = f_{cd} b \bar{x}(d - \bar{x}/2).$$

For the given applied moment M_{Ed}, this condition leads to a second-degree equation in $\bar{x}$:

$$f_{cd} b \bar{x}^2/2 - f_{cd} b \bar{x} + M_{Ed} = 0,$$

which gives, for $2M_{Ed} < f_{cd} b d^2$, to the root

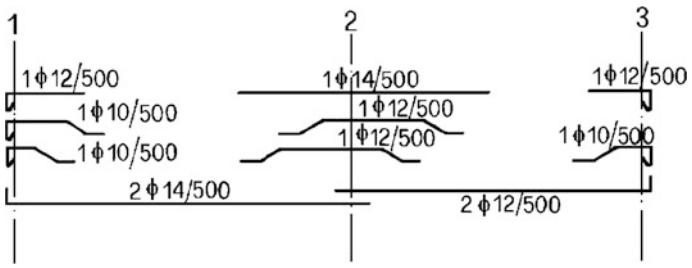


Fig. 3.46 General layout of reinforcing bars

$$\bar{x} = d\left\{1 - \sqrt{1 - \frac{2M_{\mathrm{Ed}}}{bd^2 f_{\mathrm{cd}}}}\right\}.$$

This allows to precisely evaluate the lever arm of the internal couple with $z = d - \bar{x}/2$, instead of approximating it to $z \cong 0.9d$.

3.4.2 Service Verifications

With respect to the verifications, there are three types of sections. At the mid-spans there is the T-shaped section subject to a positive moment with the upper flange in compression of a width equal to b. For this section, given the small thickness of the slab, the strength of the flange has to be reduced with the coefficient

$$0.5 + 0.1\frac{t}{d_{\mathrm{a}}} = 0.5 + 0.1\frac{4.0}{2.0} = 0.7,$$

where the thickness of the flange is t = 4.0 cm and the maximum dimension of the aggregate is d_{a} = 2.0 cm. With a weighted average, the conventional resistance of the entire part in compression is obtained, which is adjusted, with respect to the basic value corresponding to the concrete class adopted, with the coefficient:

$$\frac{0.7 \times 42 + 1.0 \times 8}{50} \cong 0.75.$$

There is then the solid rectangular section subject to a negative moment with concrete in compression at the lower edge. This situation occurs at the supports where, according to the scheme of Fig. 3.46, there is a double reinforcement. Given the absence of stirrups adequate to confine the bars in compression, the lower reinforcement is neglected in the resistance verifications. There are eventually the T-shaped sections subject to a negative moment located at the edges of the solid floor strips close to the supports. In these sections the effective width of concrete in compression corresponds to the width b_{o} of the web.

For the verifications of the ultimate limit state of compressions in concrete at service, one can refer to the allowable value of the stress (see Sect. 2.4.1);

$$\bar{\sigma}_c = 11.2\,\mathrm{N/mm^2},$$

for sections with negative moment, to the value

$$\bar{\sigma}_c^* = 0.75 \times 11.2 = 8.4\,\mathrm{N/mm^2},$$

for sections with positive moment.

With reference to the cracking verifications, a slightly aggressive environment is assumed as defined in Table 2.1. On the conservative side with respect to what shown in Table 2.15, the characteristic (rare) combination of actions is applied with a cracking width limited to w_2 = 0.3 mm (see Chart 2.15).

The allowable value of tensile stresses in steel, for 14 mm bars as the one used, becomes (see Table 2.16)

$$\bar{\sigma}'_{s2} = 260\,\mathrm{N/mm^2} \quad (< 0.8 f_{yk} = 360\,\mathrm{N/mm^2}).$$

Flexural Actions

With reference only to the most critical situations, one has the following elastic verifications (with α_e = 15).

- *Section "2"*

(M = 35820 Nm, d = 21.0 cm, b = 100 cm, d' = 3.0 cm, A_s = 7.60 cm^2, A'_s = 4.52 cm^2 neglected)

$$\rho_s = \frac{7.60}{21.0 \times 100} = 0.003610$$

$$15\rho_s = 0.05428$$

$$x = 0.05428\left\{1 - \sqrt{1 - \frac{2}{0.05428}}\right\}21.0 = 0.2796 \times 21.0 = 5.9\,\mathrm{cm}$$

$$z = \left(1 - \frac{0.2796}{3}\right)21.0 = 0.907 \times 21.0 = 19.0\,\mathrm{cm}$$

$$\sigma_c = \frac{2 \times 3582000}{19.0 \times 59 \times 1000} = 6.4\,\mathrm{N/mm^2} \quad (< \bar{\sigma}_c)$$

$$\sigma_s = \frac{2 \times 3582000}{19.0 \times 760} = 248\,\mathrm{N/mm^2} \quad (< \bar{\sigma}'_s).$$

- *Section "a"*

(M = 27269 Nm, d = 21.0 cm, b = 100 cm, t = 4 cm, b_o = 16.0 cm, A_s = 6.16 cm^2, $A'_s = 0$)

The formula for T-shaped sections is applied with $x > t$, here written for double reinforcement:

$$x = \frac{\alpha_e A_t + at}{b_o}\left\{-1 + \sqrt{1 + \frac{at^2 + 2\alpha_e(\mathrm{d}A_s + d'A'_s)}{(\alpha_e A_t + at)^2} b_o}\right\},$$

where $A_t = A_s + A'_s$ and $a = b - b_o$, which leads, with $A'_s = 0$, and a = 84 cm, to

$$x = 26.77\left\{-1 + \sqrt{1 + \frac{326.6}{26.77^2}}\right\} = 5.5\,\mathrm{cm}.$$

One therefore obtains

$$\begin{aligned} I_i &= \frac{1}{3}\left(bx^3 - ay^3\right) + \alpha_e A_s (d-x)^2 + \alpha_e A'_s (x-d')^2 \\ &= \frac{1}{3}(16638 - 284) + 22199 = 27650\,\mathrm{cm}^4 \\ \sigma_c &= \frac{27269}{27650} 5.5 = 5.4\,\mathrm{N/mm^2} \quad \left(< \bar{\sigma}_c^*\right) \\ \sigma_s &= 15\frac{27269}{27650} 16.0 = 237\,\mathrm{N/mm^2} \quad (< \bar{\sigma}'_{s2}) \\ z &= \frac{I_i}{\alpha_e A_s (d-x)} = \frac{27650}{1478} = 18.7\,\mathrm{cm} \quad (\cong 0.89d). \end{aligned}$$

- *Section "2"* (60 cm from the support 2)

$$\begin{aligned} R'_2 &= \frac{9.00 \times 5.2}{2} + \frac{35.820}{5.2} = 30.288\,\mathrm{kN} \\ M'_2 &= -35.820 + 30.288 \times 0.60 - 9.00\frac{0.60^2}{2} = -19.267\,\mathrm{kNm} \end{aligned}$$

(d = 21.0 cm, b = 16 cm, b = 100 cm, d' = 3.0 cm, A_s = 5.34 cm^2, A'_s = 4.52 cm^2)

$$\begin{aligned} \rho_t &= \frac{9.86}{21.0 \times 16} = 0.0293 \\ 15\rho_t &= 0.44018 \\ \delta &= \frac{21.0 \times 5.34 + 3.0 \times 4.52}{21.0 \times 9.86} = 0.607 \end{aligned}$$

$$x = 0.44018\left\{-1+\sqrt{1+\frac{2\times 0.607}{0.44018}}\right\}21.5 = 8.7\,\text{cm}$$

$$I_i = \frac{1}{3}16\times 8.7^3 + 15\times 5.34\times 12.8^2 + 15\times 4.52\times 6.2^2 = 19242\,\text{cm}^4$$

$$\sigma_c = \frac{19267}{19242}\times 8.7 = 8.7\,\text{N/mm}^2 \quad (<\bar{\sigma}_c)$$

$$\sigma_s = 15\frac{19267}{19242}12.8 = 193\,\text{N/mm}^2 \quad (<\bar{\sigma}'_{s2})$$

$$z = \frac{19242}{15\times 5.34\times 12.8} = 18.8\,\text{cm} \quad (\cong 0.87d).$$

3.4.3 Resistance Verifications

For the verifications at the ultimate limit state of failure of sections, the resisting moments should be evaluated with the formulas deduced in Sect. 3.1.2. For the material strength of Sect. 2.4.1 one has

$$f_{cd} = 14.2\,\text{N/mm}^2$$
$$f_{yd} = 391\,\text{N/mm}^2$$
$$r = f_{yd}/f_{cd} = 27.5,$$

and for $f^*_{cd} = 0.75 f_{cd}$ in T-shape section with flange in compression,

$$f_{yd}/f^*_{cd} = 27.5/0.75 = 36.7.$$

With $\varepsilon_{cu} = 0,35\%$ and $\varepsilon_{yd} = 391/2050 = 0.19\%$ ($\alpha_o = 0.19/0.35 = 0.543$), the limit towards high reinforcement is given by

$$\omega_{sc} = 0.8\frac{0.35}{0.19+0.35} = 0.8\times 0.65 = 0.5185.$$

For the application of safety factors of actions, one can distinguish the structural self-weight

$$g_1 = 3.25\,\text{kN/m} \quad (\gamma_{G1} = 1.00 \div 1.30),$$

the superimposed dead loads

$$g_2 = 3.75\,\text{kN/m} \quad (\gamma_{G2} = 0.00 \div 1.50),$$

and the live loads

$$q = 2.00\,\text{kN/m} \quad (\gamma_Q = 0.00 \div 1.50).$$

The design values M_{ad} of the acting moment are deduced combining the corresponding moments of the elementary load conditions defined in Sect. 3.4.1, weighed with the relative safety factors.

- *Section "2"*
  (combination $\gamma_{G1} g_1 O + \gamma_{G2} g_2 O + \gamma_Q q O$)

$$\begin{aligned} 3.25 \times 1.30 &= 4.225 \\ 3.75 \times 1.50 &= 5.625 \\ 2.00 \times 1.50 &= \underline{3.000} \\ p &= 12.850\,\text{kN/m} \end{aligned}$$

$$M_{2d} = 12.850 \times 3.980 = 51.143\,\text{kNm}$$

(d = 21.0 cm, b = 100 cm, A_s = 7.60 cm^2)

$$\omega_s = \frac{7.60}{21.0 \times 100} 27.50 = 0.0036 \times 27.5 = 0.0995 \quad (< \omega_{sc})$$
$$z = (1 - \omega_s/2)d = 0.950 \times 21.0 = 19.9\,\text{cm}$$
$$M_{Rd} = 7.60 \times 39.40 \times 0.199 = 59.589\,\text{kNm} \quad (> M_{2d}).$$

- *Section "a"*
  (combination $\gamma_{G1} g_1 A + g_1 B + \gamma_{G2} g_2 A + \gamma_Q q A$)

$$\begin{aligned} 3.25 \times 1.30 &= 4.225 & \times 2.411 &= 10.186 \\ 3.25 \times 1.00 & & \times 1.569 &= 5.099 \\ 3.75 \times 1.50 &= 5.625 & \times 2.411 &= 13.562 \\ 2.00 \times 1.50 &= \underline{3.000} & \times 2.411 &= \underline{7.233} \\ p_a &= 12.850\,\text{kN/m} & -M_2 &= 36.080\,\text{kNm} \end{aligned}$$

$$R_1 = \frac{12.850 \times 6.0}{2} - \frac{36.080}{6.0} = 32.537\,\text{kN}$$
$$x_1 = \frac{32.537}{12.850} = 2.53\,\text{m}$$
$$M_{ad} = 32.537 \times 2.53 - 12.850 \times 2.53^2/2 = 41.193\,\text{kNm}$$

(d = 21.0 cm, b = 100 cm, t = 4 cm, A_s = 6.16 cm^2)

$$\omega_S = \frac{6.16}{21.0 \times 100} 36.7 = 0.0029 \times 36.7 = 0.1077$$
$$x = 0.1077 \times 21.0/0.8 = 2.8\,\text{cm} \quad (<t)$$
$$z = (1 - 0.1077/2)21.0 = 0.9461 \times 21.0 = 19.9\,\text{cm}$$
$$M_{Rd} = 6.16 \times 39.10 \times 0.199 = 47.930\,\text{kNm} \quad (> M_{ad}).$$

- *Section "b"*
(combination $g_1 A + \gamma_{G1} g_1 B + \gamma_{G2} g_2 B + \gamma_Q q B$)

$$3.25 \times 1.00 \quad \times 2.411 = 7.836.$$

$$\begin{array}{lll} 3.25 \times 1.30 = & 4.225 & \times 1.569 = \quad 6.6290 \\ 3.75 \times 1.50 = & 5.625 & \times 1.559 = \quad 8.826 \\ 2.00 \times 1.50 = & \underline{3.000} & \times 1.559 = \quad \underline{4.707} \\ & p_b = 12.850\,\text{kN/m} & -M_2 = 27.998\,\text{kNm} \end{array}$$

$$R_3 = \frac{12.850 \times 5.20}{2} - \frac{27.998}{5.20} = 28.026\,\text{kN}$$
$$x_1 = \frac{28.026}{12.850} = 2.18\,\text{m}$$
$$M_{bd} = 28.026 \times 2.18 - 12.850 \times 2.18^2/2 = 30.5625\,\text{kNm}$$

(d = 21.0 cm, b = 100 cm, t = 4 cm, A_s = 4.52 cm^2)

$$\omega_s = \frac{4.52}{21.0 \times 100} 36.7 = 0.0022 \times 36.7 = 0.0790$$
$$x = 0.0790 \times 21.0/0.8 = 2.1\text{cm} \quad (<t)$$
$$z = (1 - 0.0790/2)21.0 = 0.9605 \times 21.0 = 20.2\,\text{cm}$$
$$M_{Rd} = 4.52 \times 39.10 \times 0.202 = 35.700\,\text{kNm} \quad (> M_{bd}).$$

- *Section "1"*
(dedicated solution)

$$M_{1d} = \gamma_F M_{1k} = 1.43 \times 23.95 = 34.20\,\text{kNm}$$

(d = 21.0 cm, b = 100 cm, A_s = 5.40 cm^2)

$$\omega_S = \frac{5.40}{21.0 \times 100} 27.5 = 0.0026 \times 27.5 = 0.0707 \quad (<0.08)$$
$$z = 0.96 \times 21.0 = 20.2\,\text{cm}$$
$$M_{Rd} = 5.40 \times 39.10 \times 0.202 = 42.650\,\text{kNm} \quad (> M_{1d})$$

- *Section "3"*
  (dedicated solution)

$$M_{3d} = 1.43 \times 15.010 = 21.43\,\text{kNm}$$

(d = 21.0 cm, b = 100 cm, A_s = 3.84 cm^2)

$$\omega_S = \frac{3.84}{21.0 \times 100} 27.5 = 0.0018 \times 27.5 = 0.0503 \quad (<0.08)$$
$$z = 0.96 \times 21.0 = 20.2\,\text{cm}$$
$$M_{Rd} = 3.84 \times 39.10 \times 0.202 = 30.329\,\text{kNm} \quad (> M_{3d}).$$

- *Section 2'* (60 cm from the support 2)
  (same as for section 2)

$$R'_2 = \frac{12.850 \times 5.20}{2} + \frac{51.143}{5.20} = 43.245\,\text{kN}$$
$$M'_2 = 51.143 - 43.245 \times 0.60 + 12.850 \frac{0.60^2}{2} = 27.509\,\text{kNm}$$

(d = 21.0 cm, b = 16 cm, A_s = 5.34 cm^2)

$$\omega_S = \frac{5.34}{21.0 \times 16} 27.5 = 0.00160 \times 27.5 = 0.4371 \quad (<\omega_{sc})$$
$$z = (1 - 0.4371/2) \times 21.0 = 16.4\,\text{cm}$$
$$M_{Rd} = 5.34 \times 39.10 \times 0.164 = 34.242\,\text{kNm} \quad (> M_{2d}).$$

- *Section 1'* (30 cm from the support 1)
  (same as for section 1)

$$R_{1k} = \frac{9.00 \times 6.00}{2} - \frac{25.92 - 23.95}{6.00} = 26.677\,\text{kN}$$
$$R_{1d} = 26.677 \times 12.850/9.00 = 38.089\,\text{kN}$$
$$M'_{1d} = 34.20 - 38.089 \times 0,30 + 12.850 \frac{0.30^2}{2} = 22.77\,\text{kNm}$$

(d = 21.0 cm, b = 16 cm, A_s = 3.83 cm^2)

$$\omega_s = \frac{3.83}{21.0 \times 16} 27.5 = 0.0114 \times 27.5 = 0.3135 \quad (<\omega_{sc})$$
$$z = (1 - \omega_s/2) \times d = 0.843 \times 21.0 = 17.7\,\text{cm}$$
$$M_{Rd} = 3.83 \times 39.10 \times 0.176 = 26.51\,\text{kNm} \quad \left(> M'_{1d}\right).$$

- *Section 3′* (30 cm from the support 3)
  (same as for section 3)

$$R_{3k} = \frac{9.00 \times 5.20}{2} - \frac{25.92 - 15.01}{5.20} = 21.302\,\text{kN}$$
$$R_{3d} = 21.302 \times 12.850/9.00 = 30.414\,\text{kN}$$
$$M'_{3d} = 21.43 - 30.414 \times 0.30 + 12.850\frac{0.30^2}{2} = 12.88\,\text{kNm}$$

(d = 21.0 cm, b = 16 cm, A_s = 2.26 cm^2)

$$\omega_s = \frac{2.26}{21.0 \times 16.0}27.5 = 0.0067 \times 27.5 = 0.1850 \quad (<\omega_{sc})$$
$$z = (1 - \omega_s/2) \times d = 0.907 \times 21.0 = 19.1\,\text{cm}$$
$$M_{Rd} = 2.26 \times 39.10 \times 0.191 = 16.88\,\text{kNm} \quad (> M'_{3d}).$$

Layout of Reinforcement

The last verifications described above refer to safety against the failure of the critical sections of the examined floor strip. Once the overall reinforcement layout is defined, consistently with the indications of such calculations, the verifications are to be extended to the entire length of the floor. This is obtained according to what indicated in Fig. 3.48, where the diagram of the resisting moment has been overlaid with the envelope diagram of the applied moment obtained from Fig. 3.43, further to the amplification of the ordinates for the appropriate γ_F. The overall reinforcement layout is correct if this last diagram remains everywhere external to one of the acting moments (Fig. 3.37).

In order to define with completeness the diagram of the resisting moment, few calculations are missing in addition to the ones developed for the critical sections. They are shown hereafter.

- *T-shaped section with flange in tension*

  (assumed reinforcement with 2 × 1ϕ14, with A_s = 3.08 cm^2)

$$\omega_s = \frac{3.08}{21.0 \times 16.0}27.5 = 0.0092 \times 27.5 = 0.2521 \quad (<\omega_{sc})$$
$$z = (1 - \omega_s/2) \times d = 0.874 \times 21.0 = 18.4\,\text{cm}$$
$$M_{Rd} = 3.08 \times 39.10 \times 0.184 = 22.2\,\text{kNm}.$$

On the different floor segments, the positive and negative resisting moments are therefore shown in DWG. 5, as calculated in the previous pages based on the different shapes and different reinforcements of the sections. The different parts of

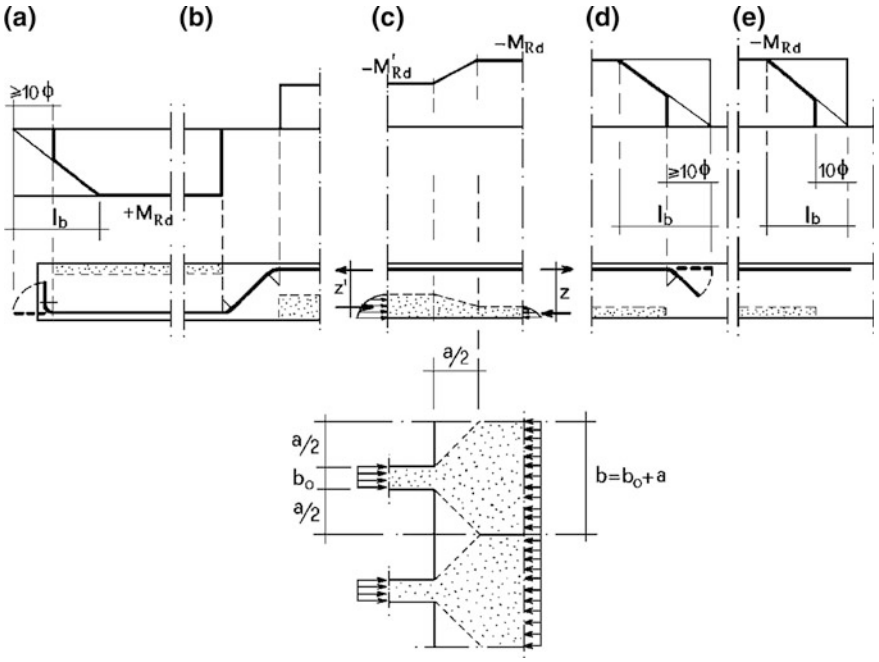


Fig. 3.47 End and internal discontinuity zones of the floor rib

the diagram of constant value are connected at the ends and at the internal discontinuities, according to the criteria described in Fig. 3.47, where the minimum anchorage length is indicated with $l_b = n\phi$. In particular, for the materials adopted in the case under analysis, $l_b = 35\phi$ results with reference to an anchorage in a zone of compact concrete (see Sect. 2.4.1).

The end anchorage of a bar at the edge of a floor is shown in Fig. 3.47a: it is assumed that, starting from the limit of complete anchorage of the bar, the resisting moment decreases linearly stopping at the tangent of the bending arc. The case of a bent bar that goes from the lower face to the upper one of the floor is shown in Fig. 3.47b: the resisting moment consequently changes sign after reaching zero value between the two horizontal tangents. Figure 3.47c refers to a sudden change of section: assuming a diffusion of compression in concrete at 45° a starting from the smallest effective width b_o up to the larger b corresponding to the ribs spacing (as indicated in plan in detail in the lower part of Fig. 4.47), a linear connection can be drawn between the two values of resisting moment. Figure 3.47d refers to an end anchorage in the tension zone with the bar bent towards the inside of the floor. The end anchorage with an extended straight bar in the compression zone is eventually shown in Fig. 3.47e.

Appendix: Actions and Bending Moment

Table 3.1: Partial Safety Factors For Actions

In the resistance verifications (ultimate limit states) the design values

$$F_d = \gamma_F F_k$$

are adopted for actions, obtained with the pertinent *partial safety factors*. The factors shown in the following table are to be applied to the nominal values of actions deducible from the competent design codes (representative of F_k). The values are taken from Eurocode EN 1990. They refer to the resistance limit state of the structure "STR" including the foundation elements. For the verifications of the equilibrium ultimate limit state as rigid body "EQU" and the limit state of the resistance of the ground "GEO", one can refer to Chart 9.6.

Usually thermal variations (Q_ε) are not taken into account in the resistance verifications. The snow load is included in the variable actions Q. In the absence of more accurate analyses, the wind load W can be treated similar to the variable actions. For prestressing P the nominal value (specified in the design) is assumed.

The partial factors in the table are given for the *analysis of actions* to be carried with a linear elastic design, for structural situations with negligible second order effects, within the semi-probabilistic limit states method, assuming the safety factors of materials of Charts 2.2 and 2.3 for the subsequent resistance verification. In such analysis, the single load units should be distinguished, each one to be multiplied with the minimum or maximum value of the relative partial factor, depending whether it is favourable or unfavourable to the resistance for the verification under consideration.

Action (nominal value)		Factor	Min.	Max.
Structural self-weight (permanent actions)	G_1	γ_{G1}	1.00	1.30
Superimposed dead load (permanent actions)	G_2	γ_{G2}	0.00	1.50
Live loads (variable actions)	Q	γ_Q	0.00	1.50
Internal action (prestressing)	P	γ_P	1.00	1.20[a]

[a]Refers to local actions (e.g. on anchorages) with prestressing represented by a force

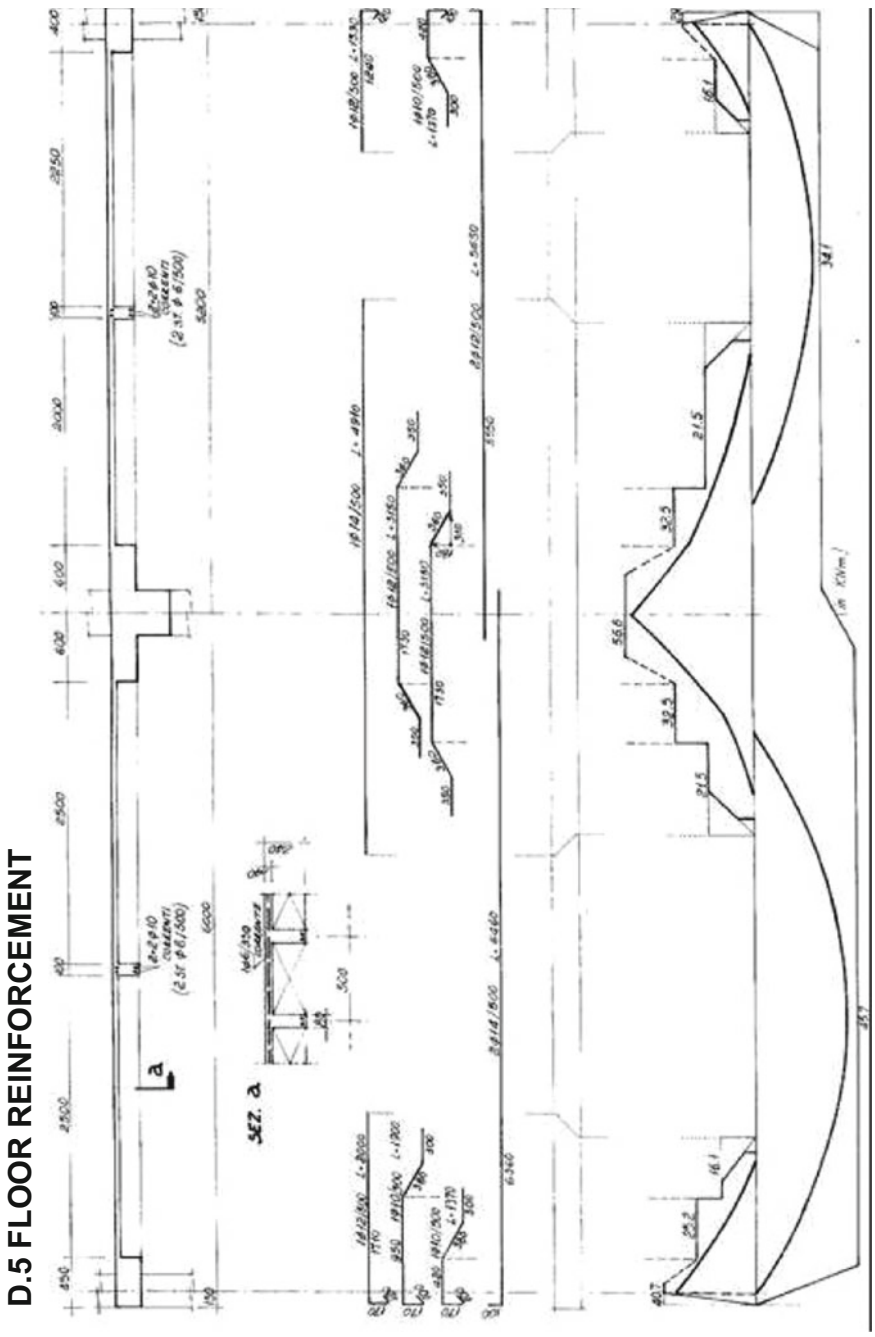


Fig. 3.48 Floor reinforcement layout and action/resistance diagrams

Chart 3.2: Formulas of Action Combination

The single load units, assumed with the respective design value F_d or with the respective nominal value F_k (see Table 3.1), should be used in the model for the structural analysis according to the combinations specified hereafter. Formulas and factors are deduced from the Eurocode 0 EN 1990 (Q_1 = most critical load for the verification under consideration). For the meaning of symbols see Table 3.1.

Resistance Verifications (ULS)

$$F_d = \gamma_{G1}G_1 + \gamma_{G2}G_2 + \gamma_P P + \gamma_Q Q_1 + \gamma_Q\{\psi_{02}Q_2 + \psi_{03}Q_3 + \cdots\}.$$

Serviceability Verifications (SLS)

- characteristic combination (rare)

$$F_k = G_1 + G_2 + \psi_{0\varepsilon}Q_\varepsilon + P + Q_1 + \psi_{02}Q_2 + \psi_{03}Q_3 + \cdots$$

- frequent combination

$$F_k = G_1 + G_2 + \psi_{1\varepsilon}Q_\varepsilon + P + \psi_{11}Q_1 + \psi_{22}Q_2 + \psi_{23}Q_3 + \cdots$$

- quasi-permanent combination

$$F_k = G_1 + G_2 + \psi_{2\varepsilon}Q_\varepsilon + P + \psi_{21}Q_1 + \psi_{22}Q_2 + \psi_{23}Q_3 + \cdots$$

Combination Factors

In the combination formulas shown above, the following values of the factors ψ_0, ψ_1 and ψ_2 can be used.

Category/variable action	Ψ_{0j}	Ψ_{1j}	Ψ_{2j}
Category A: domestic, residential areas	0.7	0.5	0.3
Category B: office areas	0.7	0.5	0.3
Category C: congregation areas	0.7	0.7	0.6
Category D: shopping areas	0.7	0.7	0.6
Category E: storage areas	1.0	0.9	0.8
Category F: traffic area, vehicle weight $\leq$ 30 kN	0.7	0.7	0.6
Category G: traffic area, 30 kN < vehicle weight $\leq$ 160 kN	0.7	0.5	0.3
Category H: roofs	0.0	0.0	0.0

(continued)

(continued)

Category/variable action	Ψ_{0j}	Ψ_{1j}	Ψ_{2j}
Wind	0.6	0.2	0.0
Snow (altitude $\leq$ 1000 m a.s.l)	0.5	0.2	0.0
Snow (altitude > 1000 m a.s.l.)	0.7	0.5	0.2
Temperature	0.6	0.5	0.0

In the combinations at the SLS it is implied that the loads Q_i that give a favourable contribution with respect to the verifications are omitted.

For the allowable stresses of materials see Charts 2.2, 2.3–2.15 and Table 2.16.

Chart 3.3: Section in Bending: Elastic Design—Formulas

RC sections subject to pure uniaxial bending.

Symbols

M_{Ek}	characteristic value of the applied moment
A_{s}	area of the reinforcement in tension
A'_{s}	area of the reinforcement in compression
$A_{\mathrm{t}} = A_{\mathrm{s}} + A'_{\mathrm{s}}$	total reinforcement area
b	width of the edge in compression
d	effective depth (see figures)
d'	concrete cover of the reinforcement in compression
$\rho_{\mathrm{s}} = A_{\mathrm{s}}/bd$	geometric reinforcement ratio in tension
$\rho'_{\mathrm{s}} = A'_{\mathrm{s}}/bd$	geometric reinforcement ratio in compression
$\alpha_{\mathrm{e}} = E_{\mathrm{s}}/E_{\mathrm{c}}$	ratio of elastic moduli (see Chart 2.3)
$\psi_{\mathrm{s}} = \alpha_{\mathrm{e}}\rho_{\mathrm{s}}$	elastic reinforcement ratio in tension
$\psi'_{\mathrm{s}} = \alpha_{\mathrm{e}}\rho'_{\mathrm{s}}$	elastic reinforcement ratio in compression
$\psi_{\mathrm{t}} = \psi_{\mathrm{s}} + \psi'_{\mathrm{s}}$	total elastic reinforcement ratio
σ_{c}	maximum compressive stress in concrete
σ'_{c}	maximum tensile stress in concrete
σ_{s}	stress in the reinforcement in tension

See also Charts 2.2 and 2.3.

Serviceability Verifications in Phase I

(Uncracked section—see figure)

$$\sigma'_{\mathrm{c}} = \frac{M_{\mathrm{Ek}}}{I_{\mathrm{c}}} y'_{\mathrm{c}} \quad \left(\sigma_{\mathrm{S}} = \alpha_{\mathrm{e}} \frac{M_{\mathrm{Ek}}}{I_{\mathrm{c}}} y_{\mathrm{S}}\right),$$

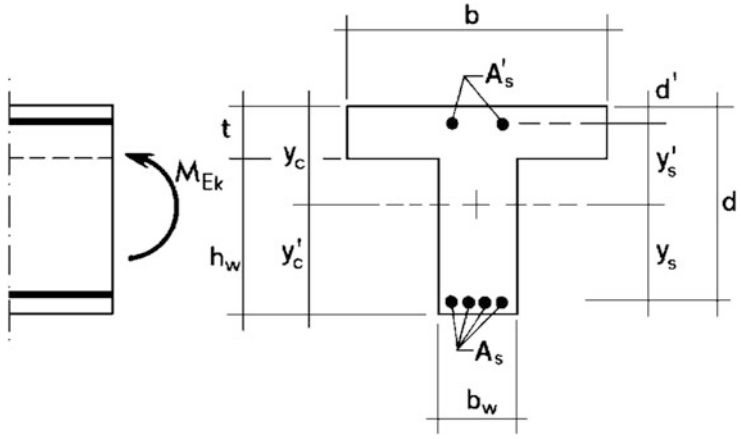
with

$$Ab = bt \quad A_w = b_w h_w \quad h_w = h - t$$
$$A_i = A_b + A_w + \alpha_e A_s + \alpha_e A'_s$$
$$S_i = A_b t/2 + A_w(t + h/2) + \alpha_e A_s d + \alpha_e A'_s d'$$
$$y_c = S_i/A_i \quad y'_c = h - y_c$$
$$y_s = d - y_c \quad y'_s = y_c - d'$$
$$y_b = y_c - t/2 \quad y_w = t + h_w/2 - y_c$$
$$I_i = A_b(t^2/12 + y_b^2) + A_W(h_W^2/12 + y_W^2) + \alpha_e A_S y_W^2 + \alpha_e A'_S y'^2_S,$$

for the verifications

at the decompression limit	$\sigma'_c \le 0$
at the limit of cracks formation	$\sigma'_c \le \bar{\sigma}'_{ct}$.

(for the rectangular section, set $t = h$).



Serviceability Verifications in Phase II
(Cracked section—see figures)
Rectangular section—single reinforcement

$$\sigma_c = \frac{2M_{Ek}}{zbx} \le \bar{\sigma}_c; \quad \sigma_S = \frac{M_{Ek}}{zA_S} \le \bar{\sigma}_S \text{ (see also Table 2.16)}$$

with

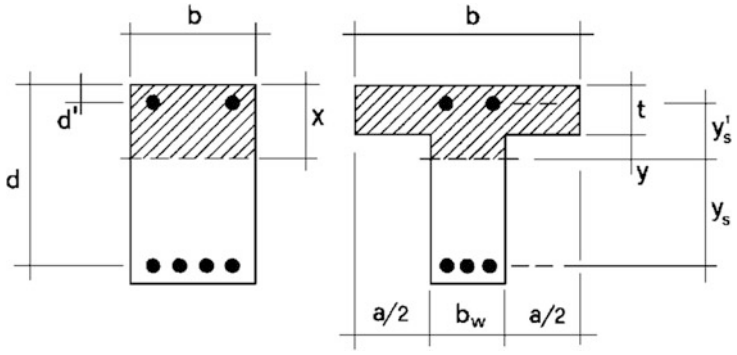
$$x = \psi_S\left\{-1 + \sqrt{1 + 2/\psi_s}\right\}d$$
$$z = d - x/3.$$

Rectangular section—double reinforcement

$$\sigma_c = \frac{M_{Ek}}{I_i}x \le \bar{\sigma}_c; \quad \sigma_S = \alpha_e \frac{M_{Ek}}{I_i} y_S \le \bar{\sigma}_S \text{ (see also Table 2.16)}$$

with

$$x = \psi_t\{-1 + \sqrt{1 + 2\delta/\psi_t}\}d$$
$$\delta = (dA_S + d'A'_S)/(dA_t)$$
$$I_i = bx^3/3 + \alpha_e A_S y_S^2 + \alpha_e A'_S y'^2_2$$
$$y_s = d - x \quad y'_s = x - d'.$$



T-shape section—single reinforcement

$$\sigma_c = \frac{M_{Ek}}{I_i}x \le \bar{\sigma}_c; \quad \sigma_S = \alpha_e \frac{M_{Ek}}{I_i} y_S \le \bar{\sigma}_S \text{ (see also Table 2.16)}$$

with $(a = b - b_w)$

$$x = \frac{at + \alpha_e A_S}{b_w}\left\{-1 + \sqrt{1 + \frac{at^2 + 2\alpha_e A_s d}{(at + \alpha_e A_S)^2} b_w}\right\} \quad (> t)$$
$$I_i = (bx^3 - ay^3)/3 + \alpha_e A_S y_S^2 \quad (y = x - t).$$

T-shaped section—double reinforcement

$$\sigma_c = \frac{M_{Ek}}{I_i}x \le \bar{\sigma}_c; \quad \sigma_S = \alpha_e \frac{M_{Ek}}{I_i} y_S \le \bar{\sigma}_S \text{ (see also Table 2.16)}$$

with $(a = b - b_w)$

$$x = \frac{at + \alpha_e A_t}{b_w}\left\{-1 + \sqrt{1 + \frac{at^2 + 2\alpha_e\left(A_s d + A'_s d'\right)}{(at + \alpha_e A_t)^2} b_w}\right\} \quad (> t)$$
$$I_i = (bx^3 - ay^3)/3 + \alpha_e A_S y_S^2 + \alpha_e A'_S y'^2_S \quad (y = x - t).$$

Chart 3.4: Section in Bending: Resistance Design—Formulas

Symbols

M_{Ed}	design value of the applied moment
M_{Rd}	design value of the resisting moment
$r = f_{yd}/f_{cd}$	design strengths ratio
$\omega_s = r\rho_s$	mechanical reinforcement ratio in tension
$\omega'_s = r\rho'_s$	mechanical reinforcement ratio in compression
$\omega_t = \omega_s + \omega'_s$	total mechanical reinforcement ratio
$\varepsilon_{yd} = f_{yd}/E_s$	yield strain of steel

See also Charts 2.2, 2.3 and 3.3.

Resistance Verifications in Phase III
(Cracked section—see figure Chart 3.3)
Rectangular section—single reinforcement

$$M_{Rd} = A_s f_{yd}\, z \geq M_{Ed}$$

with

$$\bar{x} = \omega_S d$$
$$z = d - 0.5\,\bar{x}$$
$$\xi = \omega_s/0.8$$
$$\varepsilon_s = \varepsilon_{cu}(1-\xi)/\xi \geq \varepsilon_{yd}.$$

Rectangular section—double reinforcement (*case* $\sigma'_s = f_{yd}$)

$$M_{Rd} = A_s f_{yd}\, z_s + A'_s f_{yd}\, z'_s \geq M_{Ed}$$

with

$$\bar{x} = (\omega_s - \omega'_s)d$$
$$z_s = d - 0.5\,\bar{x}$$
$$z'_s = 0.5\,\bar{x} - d'$$
$$\xi = (\omega_s - \omega'_s)/0.8$$
$$\varepsilon_s = \varepsilon_{cu}(1-\xi)/\xi \geq \varepsilon_{yd}$$
$$\varepsilon'_s = \varepsilon_{cu}(\xi - \delta')/\xi \geq \varepsilon_{yd}.$$

Rectangular section—double reinforcement (*case* $\sigma'_s < f_{sd}$)

$$M_{Rd} = A_s f_{yd}\, z_s - A'_s\, \sigma'_s\, z'_s \geq M_{Ed}$$

with $\varepsilon_{cu} = 0.0035$, $\alpha_o = \varepsilon_{yd}/\varepsilon_{cu}$, $\delta' = d'/d$ and with

$$\bar{\xi} = \frac{1}{2}\left\{ \left(\omega_s - \omega'_s/\alpha_o\right) + \sqrt{\left(\omega_s - \omega'_s/\alpha_o\right)^2 + 3.2\delta'\omega'_s/\alpha_o} \right\}$$
$$\bar{x} = \bar{\xi}\, d$$
$$z_s = d - 0.5\,\bar{x}$$
$$z'_s = 0.5\,\bar{x} - d'$$
$$\xi = \bar{\xi}/0.8$$
$$\varepsilon_s = \varepsilon_{cu}(1-\xi)/\xi \geq \varepsilon_{yd}$$
$$\varepsilon'_s = \varepsilon_{cu}(\xi - \delta')/\xi < \varepsilon_{yd}$$
$$\sigma'_s = \varepsilon'_s E_s.$$

T-shaped section—single reinforcement

$$M_{Rd} = f_{cd} bt(d - t/2) + f_{cd} b_w y(y_s - y/2) \geq M_{Ed}$$

with $a = b - b_w$ and with

$$\bar{x} = (rA_a - at)/b_w \quad (> t)$$
$$y = \bar{x} - t\ (>0) \quad y_s = d - \bar{x}$$
$$x = \bar{x}/0.8$$
$$\varepsilon_s = \varepsilon_{cu}(d - x)/x \geq \varepsilon_{yd}.$$

T-shaped section—double reinforcement (*case* $\sigma'_s = f_{yd}$)

$$M_{Rd} = f_{cd} bt(d - t/2) + f_{cd} b_w y(y_s - y/2) + f_{yd} A'_s(d - d') \geq M_{Ed}$$

with $a = b - b_w$ and with

$$\bar{x} = (rA_s - rA'_s - at)/b_w \quad (> t)$$
$$y = \bar{x} - t\ (>0)$$
$$y_s = d - \bar{x}$$
$$x = \bar{x}/0.8$$
$$\varepsilon_s = \varepsilon_{cu}(d - x)/x \geq \varepsilon_{yd}$$
$$\varepsilon'_s = \varepsilon_{cu}(x - d')/x \geq \varepsilon_{yd}.$$

T-shaped section—double reinforcement (*case* $\sigma'_s < f_{sd}$)

$$M_{Rd} = f_{cd} bt(d - t/2) + f_{cd} b_w y(y_s - y/2) + \sigma'_s A'_s(d - d') \geq M_{Ed}$$

with $\alpha_o = \varepsilon_{cu}/\varepsilon_{yd}, a = b - b_w$ and with

$$\bar{x} = \frac{1}{2b_w}\left\{(rA_s - at - rA'_s\alpha_o) + \sqrt{(rA_s - at - rA'_s\alpha_o)^2 + 3.2d'b_w rA'_s\alpha_o}\right\}$$
$$y = \bar{x} - t(>0) \quad y_s = d - \bar{x}$$
$$x = \bar{x}/0.8$$
$$\varepsilon_s = \varepsilon_{cu}(d - x)/x \geq \varepsilon_{yd}$$
$$\varepsilon'_s = \varepsilon_{cu}(x - d')/x < \varepsilon_{yd}$$
$$\sigma'_s = \varepsilon'_s E_s.$$

Table 3.5: Section in Bending: Viscous Redistribution of Stresses

For a section in reinforced concrete, symmetric for shape and reinforcement, subject to uniaxial bending in the uncracked phase I, the following table shows, for different ratios $\kappa_s = E_s I_s/E_c I_c$ between the elastic stiffnesses of reinforcement and concrete and for three nominal coefficients ϕ_∞ of final viscosity, the following variation ratios with respect to the initial elastic values:

$$\alpha^*_e = \alpha_{e\infty}/\alpha_e \quad \text{homogenization coefficient of reinforcement}$$
$$\sigma^*_c = \sigma_{c\infty}/\sigma_{co} \quad \text{final stress in concrete}$$
$$\sigma^*_s = \sigma_{s\infty}/\sigma_{so} \quad \text{final stress in steel } (=\chi_\infty/\chi_o),$$

where stresses $\sigma_{c\infty}$ and σ_{so} in the materials are assumed calculated with the competent formulas of serviceability verification of Chart 3.3 based on the actual value $\alpha_e = E_s/E_c$ of the elastic moduli. The variation ratio of stresses in steel coincides with the one χ_∞/χ_o between final and initial curvatures of the section in bending.

The use of the table requires the calculation of the centroidal moments of inertia of the steel area I_s and of one of the concretes I_c in order to deduce, from their ratio $\mu_s = I_s/I_c$, the parameter

$$\kappa_s = \mu_s \alpha_e.$$

The values of the table have been calculated with the following formulas:

$$\alpha^* = \frac{e^{\beta\phi}_\infty}{\beta} - \frac{1}{\kappa_s} \quad \text{with } \beta = \frac{\kappa_s}{1 + \kappa_s}$$
$$\sigma^*_c = e^{-\beta\phi_\infty} \qquad \sigma^*_s = \alpha^*_e \sigma^*_c,$$

valid for concretes loaded at early stages (extreme ageing theory).

χ_s	$\phi_\infty = 2.4$			$\phi_\infty = 2.9$			$\phi_\infty = 3.4$		
	α_e^*	σ_c^*	σ_s^*	α_e^*	σ_c^*	σ_s^*	α_e^*	σ_c^*	σ_s^*
0.00	3.40	1.00	3.40	3.90	1.00	3.90	4.40	1.00	4.40
0.05	3.54	0.89	3.16	4.11	0.87	3.58	4.69	0.85	3.99
0.10	3.68	0.80	2.96	4.32	0.77	3.32	4.98	0.73	3.66
0.15	3.82	0.73	2.79	4.52	0.69	3.10	5.28	0.64	3.39
0.20	3.95	0.67	2.65	4.73	0.62	2.92	5.57	0.57	3.16
0.25	4.08	0.62	2.52	4.93	0.56	2.76	5.87	0.51	2.97
0.30	4.21	0.57	2.42	5.13	0.51	2.63	6.16	0.46	2.81
0.35	4.33	0.54	2.32	5.32	0.47	2.51	6.46	0.41	2.67
0.40	4.45	0.50	2.24	5.52	0.44	2.41	6.75	0.38	2.55
0.45	4.56	0.47	2.17	5.70	0.41	2.32	7.03	0.35	2.45
0.50	4.68	0.45	2.10	5.89	0.38	2.24	7.32	0.32	2.36
0.55	4.79	0.43	2.04	6.07	0.36	2.17	7.60	0.30	2.27
0.60	4.89	0.41	1.99	6.24	0.34	2.10	7.88	0.28	2.20
0.65	5.00	0.39	1.94	6.42	0.32	2.05	8.15	0.26	2.14
0.70	5.10	0.37	1.90	6.59	0.30	2.00	8.42	0.25	2.08
0.75	5.19	0.36	1.86	6.75	0.29	1.95	8.69	0.23	2.02
0.80	5.29	0.34	1.82	6.91	0.28	1.91	8.95	0.22	1.97
0.85	5.38	0.33	1.79	7.07	0.26	1.87	9.20	0.21	1.93
0.90	5.47	0.32	1.75	7.23	0.25	1.83	9.46	0.20	1.89
0.95	5.56	0.31	1.73	7.38	0.24	1.80	9.70	0.19	1.85
1.00	5.64	0.30	1.70	7.53	0.23	1.77	9.95	0.18	1.82

Chart 3.6: Section in Bending: Additional Formulas

Reinforced concrete sections subject to uniaxial bending.

Symbols

M_{ok} characteristic value of the cracking moment
M_{od} design value of the cracking moment

See also Charts 2.2, 3.3 and 3.4.

Cracking Moment
Serviceability verifications

$$M_{ok} = \bar{\sigma}'_{ct} I_i / y'_{ct} \leq M_{Ek} \quad (\bar{\sigma}'_{ct} = \beta f_{ctk})$$

(for f_{ctk} see Table 1.2a, b)

Resistance verifications

$$M_{\mathrm{od}} = \beta f_{\mathrm{ctd}} I_i / y'_{\mathrm{c}} \leq M_{\mathrm{Ed}} \quad (\beta = 1.3)$$

(for I_i, y'_{c} see Chart 3.3 with figure).

Minimum Reinforcement

For the longitudinal reinforcement at the edge of the beam in tension, a minimum area is to be set so that the force released by the concrete in tension when cracking occurs can be resisted by that reinforcement at the characteristic yield stress f_{yk}. This force should be conventionally calculated based on the triangular distribution of stresses with a maximum at the edge in tension equal to the mean value f_{ctm} of the concrete tensile strength.

For T-shape sections or similar, it can be set for example:

$$A_{\mathrm{s}} \geq \frac{1}{2} y'_{\mathrm{c}} b_{\mathrm{w}} f_{\mathrm{ctm}} / f_{\mathrm{yk}}$$

(see figure Chart 3.3).

Chapter 4
Shear

Abstract This chapter presents the design methods of reinforced concrete elements subjected to shear action. The basic resistance mechanisms are described and the related models are deduced, that is the tooth model for beams without shear reinforcement and the truss model for beams with shear reinforcement, with their more recent improvements. In the final section, after the completion of the floor design with the pertinent shear verifications, a complete design of a beam is developed, starting from the stress analysis and following with the serviceability and resistance verifications, both for bending moment and for shear.

4.1 Behaviour of RC Beams in Shear

For shear force, the behaviour of beams in reinforced concrete exhibits the greatest differences with respect to the one of the de Saint-Vénant solid. As it will be shown further on, more articulated models are used in the design, among which the fundamental ones are since now mentioned here such as the Mörsch truss model, the tooth model, the arch behaviour e and the strut-and-tie models.

The equilibrium equation that relates shear to the variation in bending moment is once again reminded. The two force components go together with mutual influences and they are sometimes inseparably joined in one unique combined behaviour.

In relation to what mentioned for the bending moment, firstly the well-known Jourawski formula is applied

$$\tau = \frac{VS}{Ib}$$

deduced for the Saint-Vénant solid; this formula gives the shear stress τ on a chord of width b of the plane section, due to a shear V, where S is the centroidal static moment of one of the parts separated by the chord itself and I is the centroidal moment of inertia of the entire section.

Within the elastic behaviour, the section is to be homogenized with the same coefficient $\alpha_e = E_s/E_c$ and the equivalent parameters I_i and S_i equalized to concrete

© Springer International Publishing AG 2017

G. Toniolo and M. di Prisco, *Reinforced Concrete Design to Eurocode 2*,
Springer Tracts in Civil Engineering, DOI 10.1007/978-3-319-52033-9_4

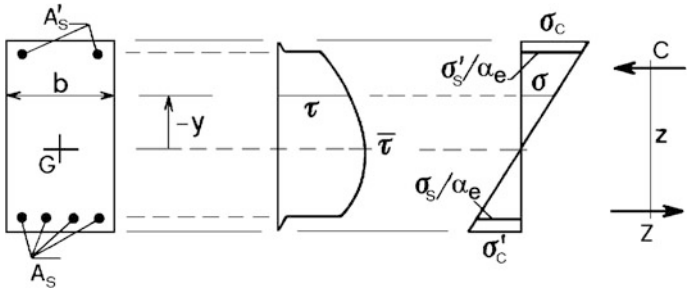


Fig. 4.1 Uncracked section—stresses distribution for shear and moment

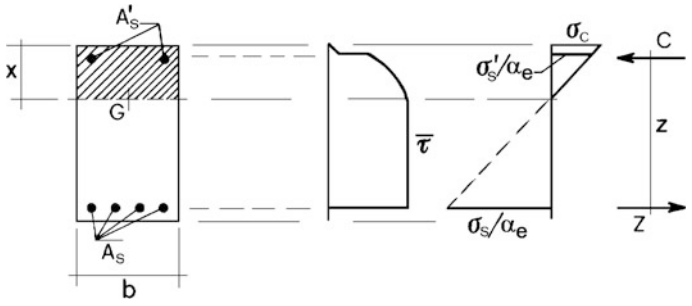


Fig. 4.2 Cracked section—stresses distribution for shear and moment

are to be used. If the section is in the uncracked Phase I with respect to the bending moment, diagrams $\tau = \tau(y)$ similar to the one shown in Fig. 4.1 will be deduced from the given formula. The maximum value is normally reached on the centroidal chord, for which

$$\bar{\tau} = \frac{V\bar{S}_i}{I_i b} = \frac{V}{zb},$$

where $z = I_i/\bar{S}_i$ is the lever arm of the internal couple.

If instead the section, with respect to the bending moment, is in the cracked Phase II, the same Jourawski's formula, referred to the cracked resisting section, leads to diagrams $\tau = \tau(y)$ similar to the one shown in Fig. 4.2, where it can be noted how the shear stress remains constant on the entire concrete cracked zone, fixed to the maximum value:

$$\bar{\tau} = \frac{V}{zb}$$

4.1.1 Cracking of Beams

The discussion carried up to this point has significant inconsistencies. The most evident one is that, if the tensile strength of concrete is neglected, the presence of pure tensile stresses is not possible either (see Figs. 1.12 and 1.13c).

In order to clarify the problem, let us consider the behaviour of the beam of Fig. 4.3 subject to a progressively increasing magnitude of the load. As long as the maximum principal tensile stresses, which can be calculated with the assumption of uncracked section, do not exceed the rupture limit, the configuration of the isostatic lines remains similar to the one indicated in the left side of the beam of Fig. 4.3c. At the neutral axis, which is centroidal for uniaxial bending, where only the shear stress $\bar{\tau}$ is present, a cross flux oriented at 45° occurs, consisting of compressions that rise and tensions that go down towards the mid-span of the beam. The isostatic lines then converge horizontally towards the edges of the beam, where the shear stresses are equal to zero, whereas the normal stresses reach their maximum value.

The first crack occurs when, increasing the load, the rupture limit of the principal tensile stress is reached at a certain point of the beam. If this happens in the central zone where the flexural component of the internal force predominates, the crack starts from the concrete edge in tension and extends vertically. If the rupture limit is reached in the end parts where the shear component predominates, the cracks starts at the level of the centroid at 45°, that is orthogonally to the maximum tensile stresses. In the intermediate zones where, in addition to shear, a significant flexural component is present, the cracks can start from the bottom side, produced by the latter component, and extend in an inclined direction on the web of the beam. The possible cracking pattern, when eventually extended to the entire beam, is shown in Fig. 4.3b.

When cracking occurs, the beam configuration adjusts to what is foreseen by the cracked section assumption, for which a constant distribution of pure shear stresses (see Fig. 4.4) occurs in the zone of concrete in tension. Following this assumption the isostatic lines would arrange themselves as indicated in the right half of the beam of Fig. 4.3c. However, it is clear that, through the cracked section, all stresses should converge in the two chords of the beam, the one of the concrete in compression delimited by the neutral axis and the one in tension of the steel reinforcement.

The cross flux of stresses disposed at 45° cannot in fact uniformly diffuse in the part of the beam in tension. The one indicated in the mentioned figure is therefore to be intended as conventionally representative of the average behaviour of the material, through the segments isolated by the cracks, for the global equilibrium with the applied shear force.

However, more complex models are necessary for the correct analysis of the beam in the cracked phase, especially when, being in the Phase III of the flexural behaviour, one wants to evaluate the ultimate shear resistance.

Two possible shear failure modes of the beam are eventually indicated in Fig. 4.3d. Failure can occur, as represented on the right, by shearing off of the web

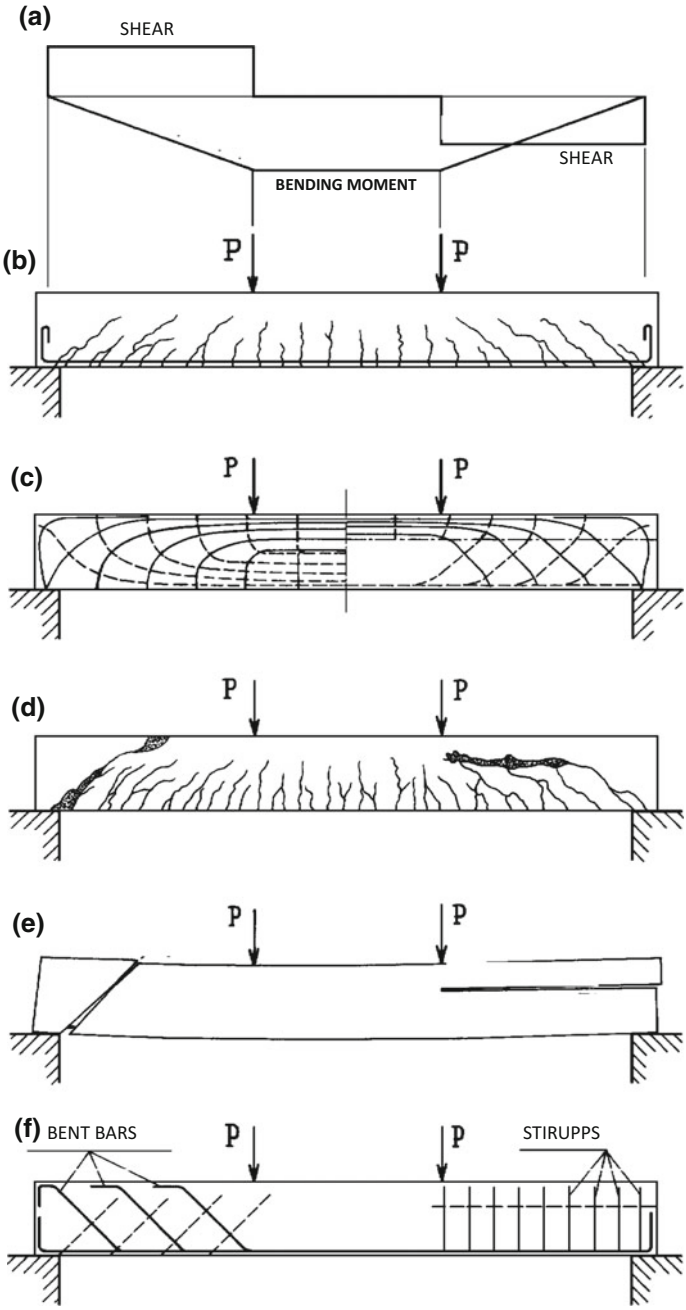


Fig. 4.3 Cracking process and shear failure mechanisms

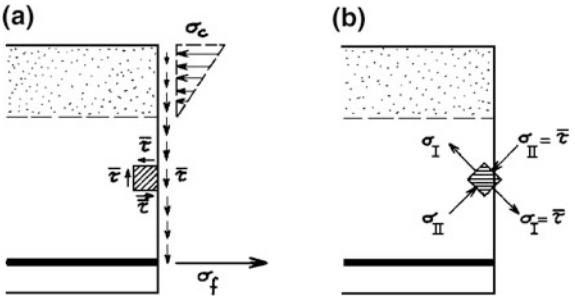


Fig. 4.4 Cracked section—theoretical distribution of stresses

segments at their fixed connection to the compression chord, with longitudinal sliding of one part of the beam with respect to the other. Otherwise the end shear crack can extend in the transverse direction at 45° on the compression chord, with the complete detachment of the beam, as represented on the left. The longitudinal 'sliding section' and the transverse 'detachment section' are outlined in Fig. 4.3e.

The behaviour of the two types of shear reinforcement can already be guessed on such failure modes, obviously having to carry out further more rigorous analyses. *Stirrups* and *bent bars* are placed as indicated in Fig. 4.3f: they cross the depth of the beam, linking its top and bottom fibres and therefore opposing to the horizontal shearing or providing a hanging support against the detachment of the beam segments.

4.1.2 Longitudinal Shear and Shear Reinforcement

Let us consider an infinitesimal element of beam subject to a moment M and a shear force V. The well-known equilibrium relationship (to rotation) is valid between the moment variation and the shear force

$$\frac{\mathrm{d}M}{\mathrm{d}x} = V,$$

whereas, for cracked sections, the stresses due to the mentioned force components are distributed as indicated in Fig. 4.5a.

Let us now assume to cut the concerned element at the level of the centroidal axis (see Fig. 4.5b). The equilibrium to the longitudinal translation of one of the two parts highlights the force $q\mathrm{d}x$ exchanged with the other part:

$$q\mathrm{d}x = C' - C = Z' - Z = \frac{\mathrm{d}M}{z} = \frac{V}{z}\mathrm{d}x,$$

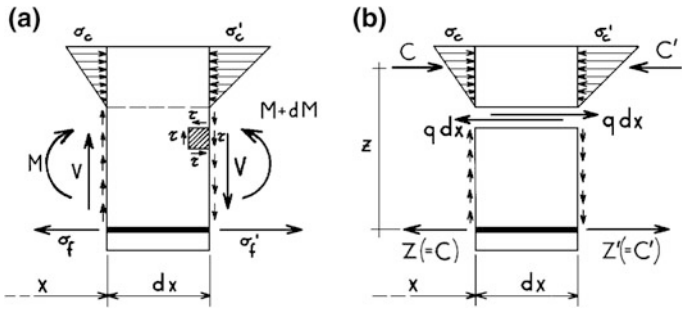
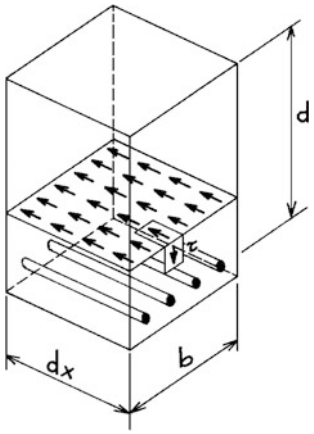


Fig. 4.5 Equilibrium condition of a beam segment

Fig. 4.6 Longitudinal shear stresses



where z is the lever arm of the internal couple. The quantity q, which refers to the unit length, is called *longitudinal shear unit force*. The same force can be interpreted as the resultant of the shear stresses τ on the horizontal surface (see Fig. 4.6):

$$q\mathrm{d}x = \tau\, b\mathrm{d}x = \frac{VS}{Ib}\, b\, \mathrm{d}x,$$

which, at the level of the maximum stress $\bar{\tau}$ (with $I/\bar{S} = z$), again leads to

$$q = \frac{V}{z}.$$

The shear reinforcement—stirrups and bent bars as already described in the previous Fig. 4.3f—are distributed with a given spacing along the beam. Each of them refers to a segment of finite length (see Fig. 4.7a, b) to which a share of the *longitudinal shear force* corresponds, defined by

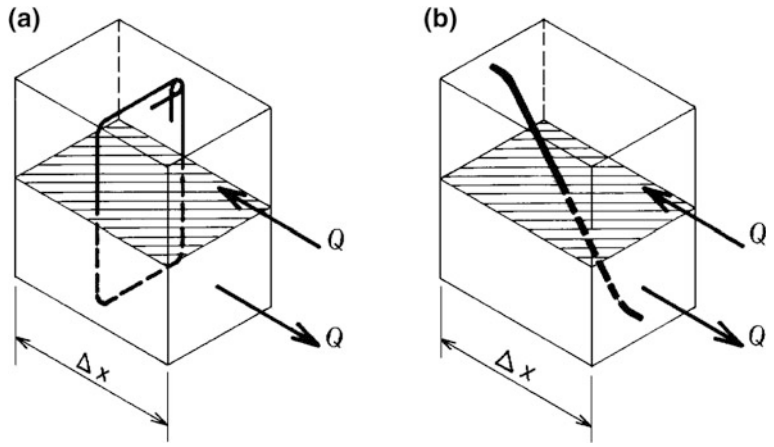


Fig. 4.7 Shear reinforcement—stirrup (**a**) and bent bar (**b**)

$$Q = \int_{x}^{x+\Delta x} q\mathrm{d}x = \int_{x}^{x+\Delta x} (V/z)\mathrm{d}x$$

The calculation of the action therefore consists of evaluating portions of area of the diagram of the unit longitudinal shear force q or, for $z \cong$ cost., portions of area of the shear diagram, as indicated in Fig. 4.8, for which one has, between x_1 and x_2:

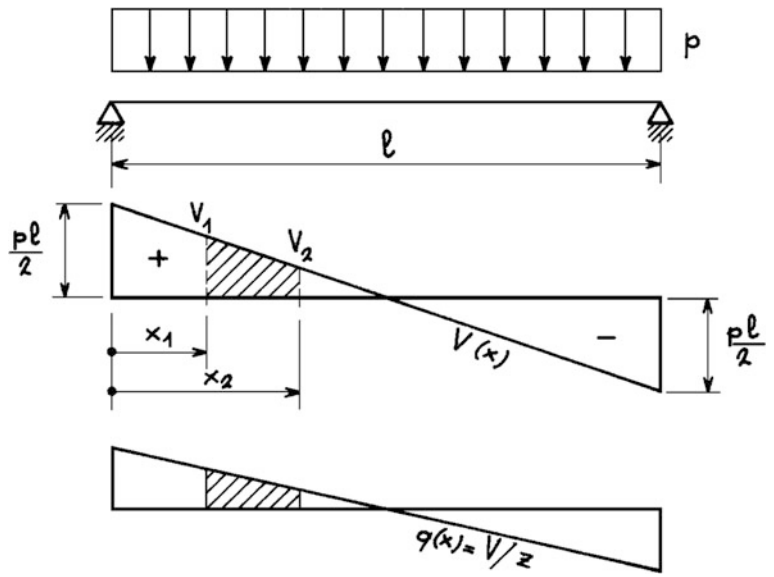


Fig. 4.8 Shear and unit longitudinal shear diagrams

$$Q = \frac{(x_1 - x_2)(V_1 - V_2)/2}{z}$$

It is to be noted that the presence of shear transverse reinforcement does not affect significantly the behaviour of the beam in the Phase I, in which the stress state can be deduced, as mentioned at the beginning this chapter, with the common formulas referred to the uncracked sections. In the cracked phase instead, such reinforcement is activated according to the changed resisting mechanisms.

4.1.3 Mörsch Truss Model

The fundamental model of shear resistance of the reinforced concrete beam has been deduced from its cracking behaviour and considers the beam as a truss structure consisting of a compression chord (the concrete resisting in bending, possibly with the reinforcement included), a tension chord (the longitudinal steel reinforcement resisting in bending) and web members. The latter are made of concrete segments in compression isolated by the cracks oriented at 45° and the transverse reinforcement in tension (stirrups or bent bars) distributed along the beam to connect its chords.

In the Mörsch truss model, the different elements of the described scheme are intended as strut/ties with pinned ends, in order to work with axial force only. Modularizing the model, which in reality is more closely spaced, one therefore has, for the same beam of Fig. 4.3, the mechanism described in Fig. 4.9. Its central part corresponds to the beam segment with no shear force and constant moment, where the connecting web members between chords are not mobilized.

With reference to a single transverse reinforcement bar, the calculation is carried on the model of Fig. 4.10, where the longitudinal shear force Q of the concerned segment (of length Δx), that derives from the variation of tensile stresses in the tension chord between the two extremes of the segment, is highlighted. In the more

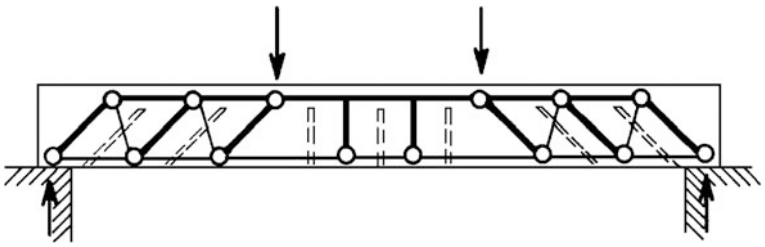


Fig. 4.9 Mörsch truss model

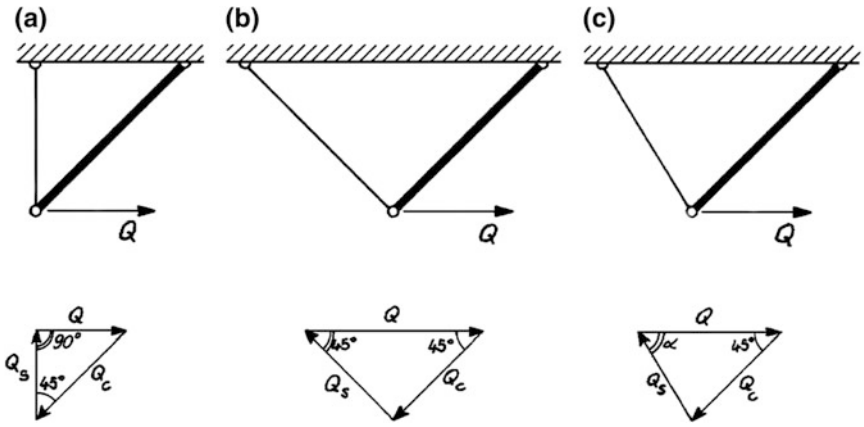


Fig. 4.10 Equilibrium conditions for a single transverse reinforcement

general case of inclination α of the considered bar (see Fig. 4.10c), the equilibrium at the bottom node leads to:

$$\begin{cases} Q_s \cos\alpha + Q_c/\sqrt{2} = Q \\ Q_s \sin\alpha - Q_c/\sqrt{2} = 0 \end{cases},$$

where Q_s is the tensile force in the steel and Q_c is the compression force in the concrete.

One therefore derives:

$$Q_s = \frac{1}{\cos\alpha + \sin\alpha} Q$$
$$Q_c = \frac{\sqrt{2}\sin\alpha}{\cos\alpha + \sin\alpha} Q$$

For vertical stirrups, with $\alpha = 90°$ (see Fig. 4.10a), one has:

$$Q_s = Q$$
$$Q_c = \sqrt{2}Q$$

The optimum arrangement for the bent bars, that is the one that, for a given action Q, minimizes the internal forces, is at 45°, for which one has (see Fig. 4.10b):

$$Q_S = Q_c = Q/\sqrt{2}$$

It is to be noted that vertical stirrups have an equal behaviour if, changing the sign of shear, the direction of the shear force Q is inverted and by consequence also

the orientation of the concrete struts. It is not the case for the bent bars, whose inclination should be directed according to the sign of the shear force.

Resistance Verifications

The *Mörsch truss* represents the isostatic model that allows to verify the shear resistance of beams with appropriate reinforcement without relying on the tensile strength of concrete. It leads to the evaluation of tensile stresses acting on the transverse reinforcement (of cross section A_{st}) with

$$\sigma_s = \frac{Q_s}{A_{st}}$$

as well as of the compressive stresses acting on the concrete web (of width b) with

$$\sigma_c = \frac{Q_c}{b\Delta x/\sqrt{2}} = \frac{\sqrt{2}q_c}{b}$$

(see Fig. 4.11).

Vice versa, the capacity of the beam segment in terms of resisting shear can be evaluated based on the strength of materials. A *tension–shear* is therefore obtained as the ultimate shear compatible with the resistance of the transverse reinforcement:

$$V_{yd} = \frac{zQ}{\Delta x} = \frac{zQ_s}{\Delta x}(\cos\alpha + \sin\alpha)$$

which, with $\sigma_s = f_{yd}$ ($Q_s = A_s f_{yd}$), leads to

$$V_{yd} = za_s f_{yd}(\cos\alpha + \sin\alpha),$$

where $a_s = A_s/\Delta x$ indicates the steel area per unit length of the beam. A *compression–shear* is also obtained as the ultimate shear compatible with the resistance of the concrete of the web:

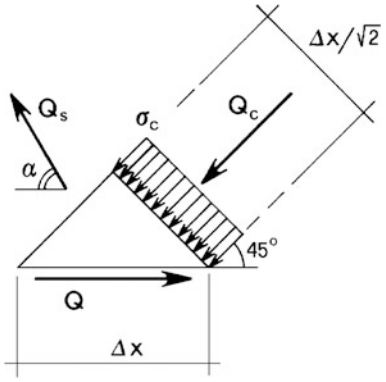


Fig. 4.11 Tensile steel and compressive concrete stresses

$$V_{cd} = \frac{zQ}{\Delta x} = \frac{zQ_c}{\Delta x}(1 + c\,tg\,\alpha)/\sqrt{2}$$

which, with $\sigma_c = f_{c2}$ ($Q_c = f_{c2} b\ \Delta x/\sqrt{2}$), leads to

$$V_{cd} = zbf_{c2}(1 + c\,tg\,\alpha)/2,$$

where $f_{c2} = 0.50 f_{cd}$ indicates the *reduced strength* (see Chart 2.2) to be attributed to concrete, having a uniform distribution of compressive stresses in a cracked field disturbed by the tensile stresses coming from the transverse reinforcement.

In the *isostatic truss* model, the capacity is the one corresponding to its weakest element, therefore one has

$$V_{Rd} = \min\left(V_{yd}, V_{cd}\right)$$

as the *resisting shear* of the beam segment examined. In general, except rare situations with very thin and highly reinforced webs, steel is the weakest element that gives the limit

$$V_{Rd} = V_{yd}$$

These formulas are significantly approximated on the conservative side, because they neglect certain relevant contributions that will be discussed in the following paragraphs. But first other important aspects are to be highlighted about the shear behaviour of beams with shear reinforcement and in general of the truss mechanisms which ensure their resistance.

Node Connections

Similarly to the actual steel trusses (see Fig. 4.12a) where the bearing capacity is ensured both by the resistance of the single members of the truss and by the resistance of the elements (bolted or welded) which constitute their connections at the nodes, also the truss mechanism of Fig. 4.9, which gives the bearing capacity of the reinforced concrete beams, is based both on the resistance of the web members and on the resistance of their *node connections*.

The truss chords, the one of concrete in compression and the one of steel reinforcement in tension, are verified in terms of bending moment according to the criteria presented at Sect. 3.1.2; the web members, the ones of the concrete in compression and the ones of stirrups or bent bars in tension, are verified in terms of shear force according to the criteria exposed above (with the improvements given further on).

The resistance at the connections, equally determinant for the capacity of the beam, should be ensured through the correct reinforcement detailing, to allow the transfer of forces between the different parts of the mechanism: the longitudinal shear force Q, for example, shall be transmitted between the web members and the

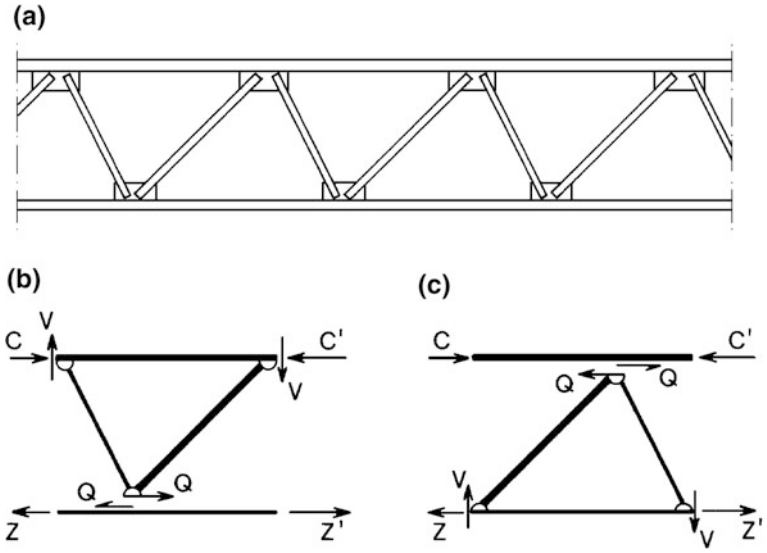


Fig. 4.12 Joint connections of the truss model

longitudinal reinforcement (see Fig. 4.12b); the same force Q, at the opposite edge, shall be transmitted between the web members and the concrete chord in compression (see Fig. 4.12c).

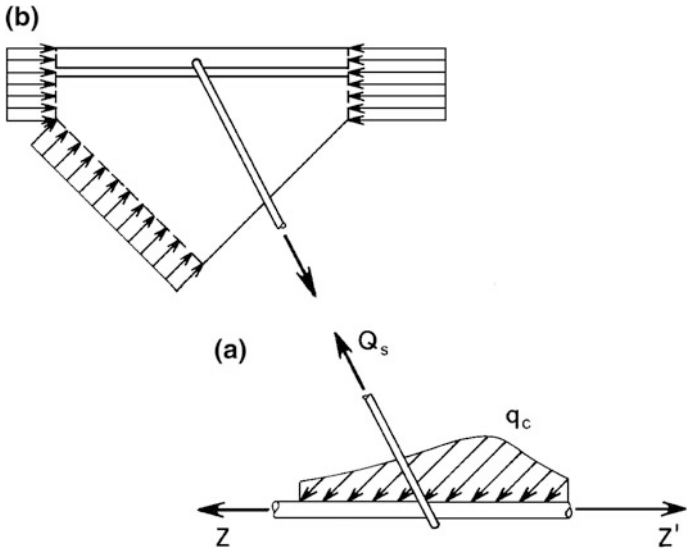


Fig. 4.13 Anchorages of stirrups

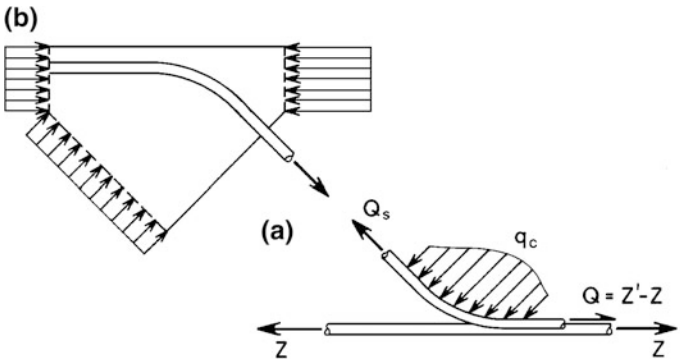


Fig. 4.14 An chorages of bent bars

The anchorage of stirrups at the tension chord should be done hooking them to the longitudinal bars, on which the inclined compressions push, as indicated in Fig. 4.13a. The transfer of the longitudinal shear force to the current bars occurs through the bond which involves the internal half-surface of the bars and which is enhanced by friction thanks to the transverse compressive stresses.

In the compression chord, at the opposite face, the stirrups require an adequate anchorage length, also obtained with end hooks; the anchorage is significantly increased by the presence of the longitudinal bars (hangers) which allow a more diffused transfer of pressures to the concrete around. In this way, the rising flow of compressive stresses can be diverted towards the longitudinal chord, as indicated in Fig. 4.13b.

The behaviour of bent bars is rather different. As indicated in Fig. 4.14a, the decrease $Z'-Z = Q$ of the force in the tension chord occurs directly as the bent bar itself carries part of the force Q. At the deviation, the bar exchanges pressures with the concrete of the web and this type of force transfer between elements in tension and compression of the truss is less effective. Pressures localized along the bar bend can in fact lead to concrete shearing off, with early failure of the resisting mechanism.

At the compression edge, the bar has an opposed bend, with analogous problems of localized pressures. The end anchorage requires an adequate length for the transfer of the force Q by bond to the concrete chord, so that the equilibrium at the node indicated in Fig. 4.14b can be ensured.

For the reasons mentioned above, in the calculation of the resistance to tension–shear, it is good practice to penalize the bent bars (for example with a reduction coefficient equal to 0.8) with respect to the stirrups that, encasing the longitudinal bars, have a more effective anchorage at the nodes of the truss.

4.2 Beams Without Shear Reinforcement

In the previous section, an introduction of the problem of the shear behaviour of beams in reinforced concrete has been given, following the classic path of the traditional theory that wants to keep the assumption of concrete tensile strength equal to zero. The integral adoption of this assumption leads to two conclusions:

- there cannot be shear resistance without appropriate transverse reinforcement;
- the design of such reinforcement is based on the isostatic model of Mörsch truss.

Both these conclusions are superseded by the more recent developments of the theory. Elements in bending (slabs for example) without shear reinforcement have been used since a long time; more recent experimentation also demonstrated that the isostatic model leads to significant overdimensioning of the reinforcement.

To sum up what has been presented so far, the beam in bending shown in Fig. 4.3 can be considered in the following phases.

Phase I—Uncracked
Stresses are calculated with reference to the uncracked section (see Paragraph 3.1.1 and 4.1):

$$\text{due to moment} \qquad \sigma'_c = \frac{M}{I_i} y'_c \qquad (< f_{ctf})$$

$$\text{due to shear} \qquad \bar{\tau}_c = \frac{V}{zb} \qquad (= \sigma_I < f_{ct})$$

The limit of this phase correspond either to $\sigma'_c = f_{ctf}$ or $\sigma_I = f_{ct}$:

$$\text{due to moment} \quad M_o = I_i f_{ctf} / y'_{ct}$$

$$\text{due to shear} \quad V_o = zbf_{ct}$$

Cracking of Beam
The cracking can occur with the patterns indicated in Fig. 4.15:

$$a-\text{due to moment} \quad M > M_o \quad \text{with } V \cong 0$$

$$b-\text{due to shear} \quad V > V_o \quad \text{with } M \cong 0$$

$$c-\text{due to moment} \quad M > M_o \quad \text{with } V > 0$$

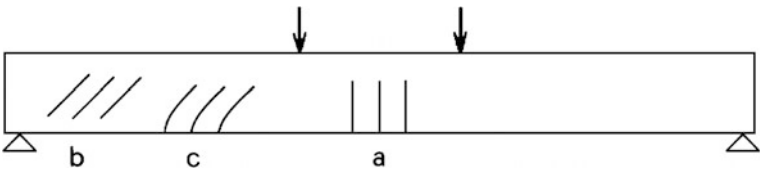


Fig. 4.15 Possible cracking patterns of the beam

Because of the presence of reinforcement (longitudinal and transverse) a different resisting mechanism is established, consisting of steel bars in tension and concrete compression elements.

Phase II—Cracked
In the cracked elastic phase, longitudinal stresses on the plane section (see Paragraph 3.1.1) are calculated with

$$\text{due to moment} \quad \sigma_c = \frac{2M}{zbx} \quad \sigma_c = \frac{2M}{zA_s},$$

whereas in the web, with Mörsch truss one has (see Sect. 4.1.3):

$$\text{due to shear} \quad \sigma_c = \frac{2V}{zb}\frac{\sin\alpha}{\cos\alpha + \sin\alpha}$$
$$\sigma_s = \frac{V}{za_s}\frac{1}{\cos\alpha + \sin\alpha}.$$

The limit for this phase, based on the steel yield point, corresponds to $\sigma_s = f_y$:

$$\text{due to moment} \quad M_y = zA_s f_y$$
$$\text{due to shear} \quad V_y = za_s f_y(\cos\alpha + \sin\alpha)$$

Phase III—Up to Rupture
It extends beyond the yield limit only if there are hyperstatic resources (see Paragraph 3.1.2):

$$\text{due to moment} \quad M_R = z_r A_s f_y \quad (z_r > z),$$

whereas for the isostatic truss model one would have:

$$\text{due to shear} \quad V_R = V_y$$

As already mentioned, this last result is proven to be wrong by facts, which additionally show how there can be a cracked Phase II also for beams without shear reinforcement.

Experimental Results
Experimental tests on the shear behaviour of reinforced concrete beams, despite the difficulties of interpretation due to the number of factors that affect the results and to their complex interferences, give certain clear indications that are reported hereafter.

- Also beams without shear reinforcement show a systematic non negligible resistance.
- Such resistance mainly derives from the tensile strength of concrete, but it is also influenced by other factors.

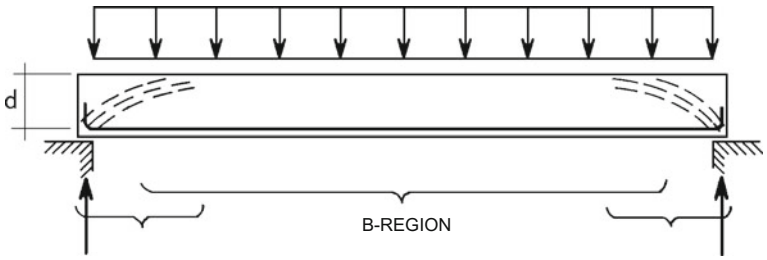


Fig. 4.16 Current "B" flexural behaviour and discontinuity "D" regions

- Without shear reinforcement, the cracking onset in the web because the tensile strength is exceeded by the maximum principal tensile stress is immediately followed by the complete rupture of the beam.
- The presence of cracks due to bending moment on the contrary does not annul the shear resistance, thanks to a *tooth* resisting mechanism, whose capacity is lower than the one of the uncracked beam, but still capable of balancing limited shear actions.
- The onset of shear cracking in beams with appropriate transverse reinforcement activates the *truss* resisting mechanism, whose higher capacity is based on the compression resistance of the concrete of the web and on the tension resistance of the transverse reinforcement.
- The tensile strength of concrete and the other factors contributes, also in the beams with shear reinforcement, in enhancing the resisting mechanism with respect to the elementary Mörsch truss.
- The refined resistance models, with or without shear reinforcement, result reliable in the beam parts with current shear behaviour, away from the zones of application of reactions or concentrated loads.
- In these latter zones, other diffusion mechanisms arise, such as the arch effect, as better described hereafter.

In this chapter, the flexural behaviour of beams is discussed, analysing its different resistance contributions for a correct verification in shear of the typical sections, called *B-regions* because Bernoulli's assumption is valid, outside the zones of arch behaviour, called *D-regions* because corresponding to discontinuities, as indicatively described in Fig. 4.16.

4.2.1 Analysis of Tooth Model

For a beam without shear reinforcement assumed to be cracked due to bending moment, consistently with the cracking pattern observed experimentally, a behaviour

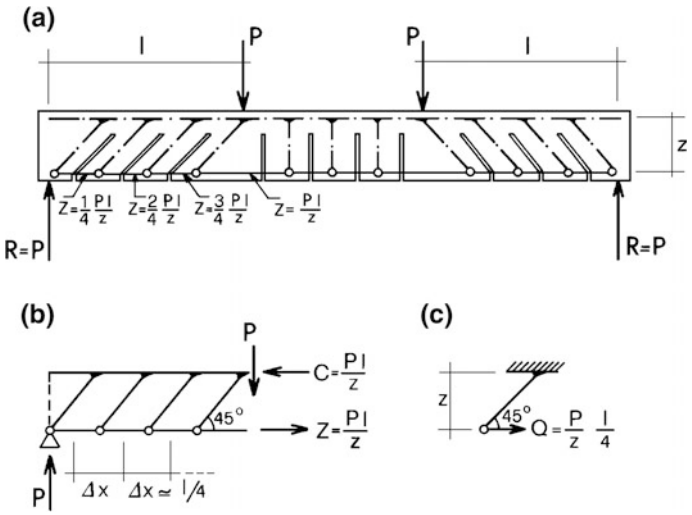


Fig. 4.17 Tooth model for beams without shear reinforcement

mechanism similar to the one described in Fig. 4.17 can be adopted where, in the lateral parts subject to shear $V = P$, the formation of a number of ideal web members is foreseen, inclined at 45° according to the cracks orientation. Excluding the first one, which is subject to the arch effect due to the concentrated reaction $R = P$, the following web members are only subject to the longitudinal shear force Q, which represents the increase of the tensile force Z in the longitudinal reinforcement.

The single segment of length a, together with its thicknesses, is shown in Fig. 4.18. Only the increase Q of the longitudinal forces in the tension and compression chords is highlighted, balanced by the shear V according to the relation:

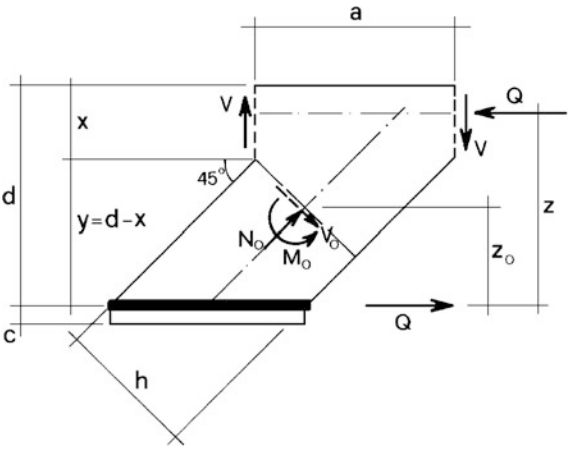


Fig. 4.18 Equilibrium condition of a beam segment

$$Q\,z = V\,a.$$

The equilibrium written above relies on the resistance of the two critical sections of the *tooth behaviour*:

- the fixed end of the inclined segment to the compression chord, subject to the components N_o and M_o of the action (in addition to V_o);
- the one of the compression chord through which, at the crack location, the shear force V has to be transferred, together with the longitudinal force $C = M/z$ that increases by $Q = Va/z$ between the left and the right edge of the considered segment.

This latter section is assumed as already verified in the flexural design, which only takes into account normal stresses σ due to the bending moment neglecting the shear stresses τ due to the shear force.

The possibility to transfer the longitudinal shear force from the reinforcement in tension to the compression chord depends on the resistance of the single tooth at the fixed end, that is the possibility that the variable flexural action actually concerns the entire effective depth d of the beam.

Analysing the inclined segment in an approximated way with the verification formulas of the beams in bending, one has (also see Fig. 4.18):

$$M_o = Qz_o \qquad N_o = Q/\sqrt{2}$$

and the maximum tensile stress at the edge in tension of the critical fixed end section becomes:

$$\sigma_s = \frac{M_o}{bh^2/6} - \frac{N_o}{bh}$$

which, with $h = a/\sqrt{2}$ and $z_o = y - a/4$, leads to

$$\sigma_s = \frac{Q}{ba} 4\left(3\frac{y}{a} - 1\right)$$

At the ultimate failure limit, with $\sigma = f_{ctf} = \beta f_{ct}$, one therefore obtains:

$$V_{Rd} = \frac{Q_{Rd}}{a} z = \beta f_{ctd} bz \frac{1/4}{3y/a - 1},$$

which depends primarily on the ratio y/a between penetration and spacing of cracks. Calibrating the value of this ratio on the basis of the experimental results, it could be assumed

$$a \cong 1.25y \qquad (\approx d \quad \text{for} \quad y \approx 0.8d),$$

which would give a distance from the initial crack comparable to the effective depth of the beam, necessary for the diffusion of stresses on the entire effective depth d. Setting also, within the big approximations already made, $\beta \cong 1.6$, it is eventually obtained:

$$V_{\text{ctd}} \cong 0.28zbf_{\text{ctd}}.$$

Given that for normal amounts of longitudinal reinforcement the lever arm of the internal couple in the cracked phase is on average equal to

$$z \cong 0.9d,$$

the formula becomes

$$V_{\text{ctd}} \cong 0.25dbf_{\text{ctd}}.$$

The comparison with the uncracked section for which, with

$$z \cong 0.7d$$

one has a resistance (see Phase I),

$$V_{\text{od}} \cong 0.7dbf_{\text{ctd}}$$

shows a reduction of the shear capacity of the beam by a factor of almost three. This reduction appears to be smaller when other resistance contributions, that will be discussed further on, become significant.

It is to be noted that for non-rectangular sections, the width b of the formulas used here should be substituted with the one b_{w} of the web.

The description reported above, although approximated, reflects well the experimental results, giving a qualitatively correct interpretation of the resisting mechanism.

The described tooth behaviour gives the ultimate shear resistance resource of beams without transverse reinforcement, thanks to the tensile strength of concrete that constitutes its inclined teeth. Moreover, the shear resistance in the cracked phase finds another limitation which becomes determinant when the section of the compression chord fails. This occurs in beams where the compression zone of concrete is small with respect to the effective depth (small x/d), as it can occur for excessively reduced reinforcement ratios ρ_{s} in tension or in the case of combined tension axial force and bending moment.

Given that for T-shaped sections an effective width $b' > b_{\text{w}}$ (see Fig. 4.19) should be assumed, having to take into account the diffusion of shear stresses that rise from the web, the minimum resultant C of compressions at the end of the

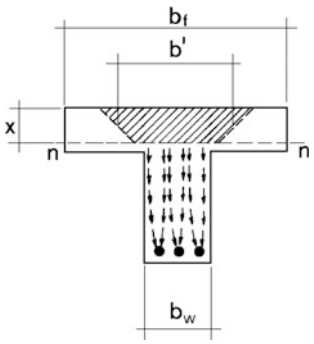


Fig. 4.19 Diffusion of shear stresses in a T section

B-region, at the connection node with the first inclined segment that receives the support reaction R (see Fig. 4.17), is equal to

$$C = R = V$$

The stresses in the competent section of the compression chord can therefore be evaluated in an approximated way with:

$$\sigma_c \cong \frac{C}{b'x} = \frac{V}{b'x}$$
$$\tau_c \cong \frac{V}{b'x} \cong \sigma_c$$

Being $(\tau_c/\sigma_c)^2 \cong 1$, the principal tensile stress becomes:

$$\sigma_I = \frac{\sigma_c}{2}\left\{-1 + \sqrt{1 + 4\left(\frac{\tau_c}{\sigma_c}\right)^2}\right\} \cong 0.62\sigma_c$$

from which one obtains, at the limit of the resistance $\sigma_I = f_{ctd}$:

$$V_{Rd} \cong \frac{b'x}{0.62} f_{ctd} \cong 1.6b'xf_{ctd}$$

This rupture mechanism of the compression chord occurs simultaneously to the one of the inclined segment when:

$$0.28bzf_{ctd} = 1.6b'xf_{ctd}$$

and therefore, for rectangular sections with $b' = b$, setting $z \cong d - 0.5x$, when:

$$\frac{x}{d} \cong 0.16.$$

With values of $\xi = x/d < 0.16$ rupture therefore occur by failure of the compression chord, with greater values it occurs by failure of the web members, as indicated with the sliding and detachment sections in Fig. 4.3d, e. For T-shaped sections with $b' > b_w$ the limit value decreases; for example with $b'/b = 2$ it becomes $x/d \cong 0.08$ showing how, for this type of sections, the field of ruptures by transverse detachment is much narrower than the one by longitudinal sliding.

The resistance formulas relative to the two different rupture modes can be summarized in the single expression:

$$V_{ctd} = 1.6b'xf_{ctd} = 0.28zb_w f_{ctd}\frac{1.6b'x}{0.28zb_w} = 0.28b_w z f_{ctd}\delta,$$

that is

$$V_{ctd} = 0.25b_w d f_{ctd}\delta \qquad \text{for } z \cong 0.9d$$

With

$$\delta = \frac{1.6b'x}{0.28zb_w}\frac{b'}{b_w} = \frac{5.71\xi}{1-0.5\xi} \leq 1$$

coefficient that takes into account situations of low longitudinal reinforcement in tension, or combined axial tension force and bending moment. In particular, in the case of combined tension and bending with entirely cracked section ($\xi = 0$, $\delta = 0$) the shear resistance V_{ctd} given by the formula is annulled and the introduction of the transverse reinforcement becomes necessary to be integrated with the longitudinal ones and with the transverse concrete struts in a truss behaviour equal to the one described at Paragraph 4.1.3.

4.2.2 *Other Resistance Contributions*

Other important contributions to the shear resistance of reinforced concrete beams have been highlighted by the experimentation and indicated as contribution of *axial compression*, *dowel action* and *aggregate interlock*.

Axial Compression

The contribution of an axial component of the force occurs, when in compression, thanks to the higher consistency of the resisting uncracked part of concrete. In fact, the position of the neutral axis of a section under combined compression and bending is lower than what foreseen in Fig. 4.18: the depth x of the upper chord increases and the measure y of cracks penetration simultaneously decreases. This

increases the resistance of both components of the tooth behaviour: the longitudinal backbone which is thicker and the transverse teeth that are stockier.

The enhancement of the resisting mechanism is well represented by the ratio

$$\frac{M_{\mathrm{Ro}}}{M_{\mathrm{Ed}}}.$$

Between the decompression moment $M_{\mathrm{Ro}} = N_{\mathrm{Ed}} I_i / y'_c A_i$, corresponding to the value 0 of the stress at the edge in tension of the section still uncracked, and the moment M_{Ed} induced by the design actions under analysis. In particular, for ordinary reinforced concrete sections subject to uniaxial bending, such ratio is always zero. It increases instead with the presence of an axial component of the external force or of a pre-compression. The maximum value should be limited to 1, which corresponds to the section entirely in compression without cracks.

Using the same symbol δ, adopted for beams under combined tension and bending within the domain $0 \leq \delta < 1$, the contribution of the axial compression can therefore be evaluated with the coefficient:

$$\delta = 1 + \frac{M_{\mathrm{Ro}}}{M_{\mathrm{Ed}}} \qquad (1 \leq d \leq 2).$$

To be used in the same verification formula deduced in the previous paragraph. Such empirical calculation procedure therefore introduces a proportional increase of the resistance based on the actual flexural cracking state of the beam segment examined.

Dowel Action

The second effect concerns the contribution given by the longitudinal reinforcement which crosses the cracked zone in tension of the beam. The exact evaluation is difficult, depending on many factors, such as the diameter and the distribution of the bars. The following approximated analysis, with adjusted geometrical parameters based on the experimental results, tends to give a qualitatively correct interpretation of the phenomenon.

The contribution V^* indicated in Fig. 4.20a is not limited by the shear resistance of the bars, which are moreover subject to tension due to the bending moment, but by the resistance of the surrounding concrete subject to the stresses σ^* indicated in Fig. 4.20b. Such contribution V^* can be calculated in an approximated way on the basis of the resistance to spalling of the concrete cover.

Assuming that the flexural stiffness of the bars allow to distribute the pressures σ^* along a segment l^* roughly equal to 5ϕ and that the minimum net bar spacing is ϕ (where ϕ is the diameter of the bars), one has

$$V^* = n l^* \phi \sigma^* = \frac{20}{\pi} \left(n \frac{\pi \phi^2}{4} \right) \sigma^*,$$

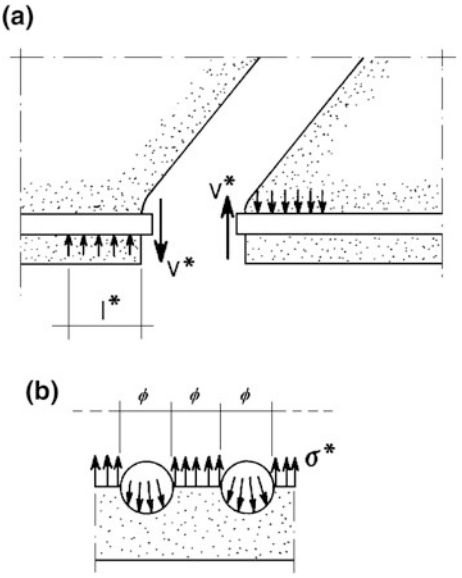


Fig. 4.20 Details of the dowel action

where n is the number of the bars. At the limit $\sigma^* = f_{ctd}$ of the tensile strength of concrete, indicating with $A_s = n\pi\phi^2/4$ the longitudinal reinforcement area, one has:

$$V^* \cong 6.5\, A_s f_{ctd}.$$

On the segment of Fig. 4.21, at the level of the reinforcement, a balancing couple V^*a is opposed to the flexural action Qz_o of the shear. The moment at the fixed end of the segment is therefore equal to

$$M_o = Qz_o - V^* a$$

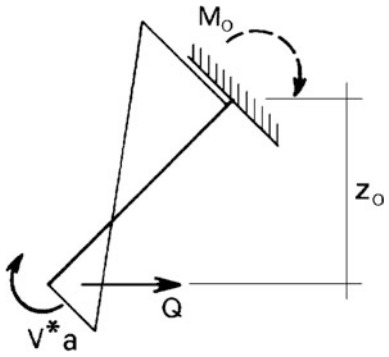


Fig. 4.21 Equilibrium condition of the inclined segment

and, introduced in the same verification formula of the combined compression and bending

$$\sigma = \frac{M_o}{bh^2/6} - \frac{N}{bh} = f_{ctd}$$

adopted at Paragraph 4.2.1, leads to

$$V_{ctd} = \frac{Q_{Rd}}{a} z = \frac{\beta f_{ctd} b z}{4(3y/a - 1)} \left[1 + \frac{78 A_s}{\beta b a}\right]$$

where, with respect to the base value of the resistance already deduced for the tooth behaviour, the amplifying contribution of the dowel action of the longitudinal reinforcement appears in the square brackets.

With the same assumptions $\beta \cong 1.6$ and $a \cong d$ one obtains:

$$V_{ctd} \cong 0.28 b z f_{ctd} (1 + 50\rho_s)\delta,$$

that is

$$V_{ctd} \cong 0.28 b z f_{ctd} (1 + 50\rho_s)\delta \qquad \text{for } z \cong 0.9d,$$

where

$$\rho_s = \frac{A_s}{bd}$$

indicates the geometrical reinforcement ratio in tension on the concrete effective section bd, and $b = b_w$ is the width of the web of the section.

The maximum contribution of the dowel action should be limited with $(1 + 50\rho_s) \leq 2$ and therefore within the limit $V^* a = Q z_o/2$ for which the two end sections of the inclined segment (see Fig. 4.21) are subject to equally stressed.

Aggregate Interlock

The aggregate interlock occurs with contact pressures between the adjacent surfaces separated by a crack, when the segments tend to slide relatively to each other because of the shear force (see Fig. 4.22). A condition for the shear balancing component R_t of such pressures to occur is the presence of a normal component R_n, which prevents the increase of the crack width and ensures that the aggregate interlocks remain when the stress increases up to the rupture limit. Between the two components the friction law can be assumed

$$R_t = \mu R_n,$$

where μ increases with the coarseness of the cracking surface and therefore practically with the size of the aggregate used.

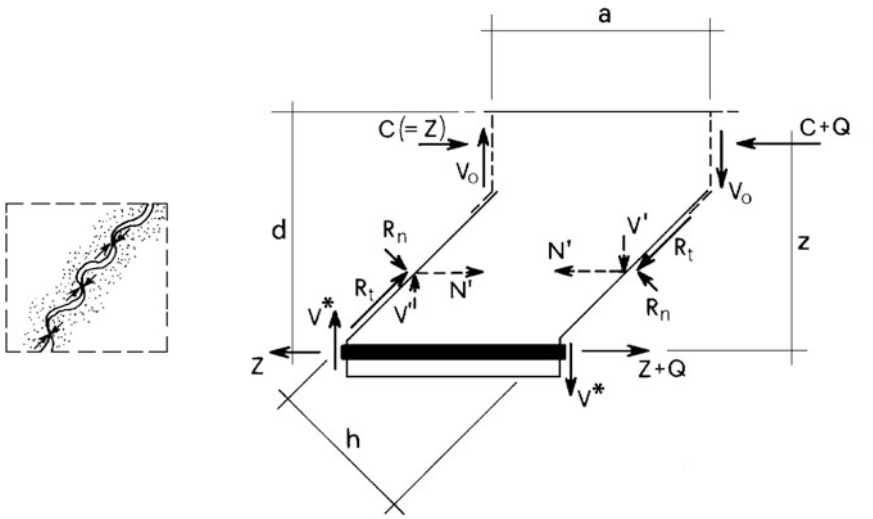


Fig. 4.22 Aggregate interlock in the concrete web

For an inclination of the cracks at 45°, the resultant of pressures can be decomposed in its axial N' and shear V' components:

$$N' = (R_t + R_n)/\sqrt{2} = (\mu + 1)R_n/\sqrt{2}$$
$$V' = (R_t - R_n)/\sqrt{2} = (\mu - 1)R_n/\sqrt{2},$$

from which the contribution is obtained

$$V' = \frac{\mu - 1}{\mu + 1} N' \qquad (V' > 0 \,\text{per}\, \mu > 1)$$

which gives the balancing couple $V'a$ to be introduced in the fixed end moment of the segment:

$$M_o = Qz_o - V^* a - V' a$$

in addition to the contribution of the dowel effect.

It can be noted that the effect of aggregate interlock has a significant contribution only with a cracking surface significantly coarse with $\mu > 1$: normal friction is not sufficient, a proper interlock of aggregates is instead necessary. It is also necessary that a compression axial reaction N' arises. This can be given, in the case under consideration of beams without shear reinforcement, by the upper and lower chords that cross the cracks. But their effect is reduced with the distance, more rapidly if the prominences of the surface roughness given by the aggregates are less evident.

The measure of such decrease can be therefore related to the ratio between the effective depth of the beam, from which the distance between the tension and compression chords depends, and the maximum aggregate size. In more simple terms, given that usually this size is fixed (≅20 mm), the effective depth of the beam can be assumed as the only parameter for the measurement of the phenomenon.

Quantitative indications are deduced from experimental tests which show how, for beams with a depth greater than 0.6 m, the contribution of aggregate interlock remains essentially negligible and how, for shallower beams there is a linear enhancement of the resistance that can be approximately evaluated with the coefficient

$$\kappa = 1.6 - d \qquad (\geq 1, \text{ with } d \text{ expressed in meters}).$$

One eventually arrives to the formula

$$V_{\text{ctd}} = 0.28bzf_{\text{ctd}}\kappa(1 + 50\rho_{\text{s}})\delta,$$

which summarizes the different contributions to shear resistance of beams without transverse reinforcement.

If on one hand, for common structural situations such simple combination of effects appears to be adequately reliable, it is also true that there are significant interactions between the different coefficients, whose correct analysis would require further in-depth analysis. Therefore, in the following chapter an alternative formula is also given, deduced in a purely empirical way, which does not refer to a precise mechanical resistance model.

4.2.3 Verification Calculations

For beams without shear reinforcement, the resistance formula corresponding to the tooth behaviour has therefore been deduced, which is here recalled with the approximation $z \cong 0.9d$ and with the limitation $V_{\text{ctd}} \leq V_{\text{od}}$:

$$V_{\text{ctd}} = 0.25bdf_{\text{ctd}}\kappa(1 + 50\rho_{\text{s}})\delta \qquad (\leq 0.7bdf_{\text{ctd}}),$$

where the meaning of the variables is recalled:

d	effective depth of the section
$b = b_{\text{w}}$	minimum width of the web
$\kappa = 1.6 - d \geq 1$	(d in m) amplification for shallow beams
$\rho_{\text{s}} = A_{\text{s}}/bd \leq 0.02$	geometrical reinforcement ratio in tension
$\delta = 1 + M_{\text{Ro}}/M_{\text{Ed}}$	($1 < \delta \leq 2$) for beams in combined compression and bending or prestressed

$\delta = 1$ for beams in bending with $\xi \geq 0.16\beta'$ ($\beta' = b'/b_w$)
$\delta = 5.71\xi\beta'/(1 - 0.5\xi)$ ($0 \leq \delta \leq 1$) for beams in bending and combined tension and bending with $\xi < 0.16/\beta'$

or more simply $\delta = 0$ for beams in combined tension and bending.

The zero value of δ should also be assumed when alternate loads would induce the reversal of the sign of the shear force at significant levels, with the possibility of crossed cracks in the concrete of the web and consequent rupture of its inclined teeth. Therefore, the introduction of transverse reinforcement is also necessary for such situations, as for beams under combined tension and bending.

More recent design codes give a different formula deduced in a purely empirical way based on the results of countless experimental tests:

$$V_{ctd} = 0.18bd\kappa(100\rho_s f_{ck})^{1/3}/\gamma_C + 0.15bd\sigma_c$$

with a minimum

$$V_{ctd} \geq bdv_{min} + 0.15bd\sigma_c,$$

where d, b and ρ_s are the same as defined above, whereas

$\kappa = 1 + \sqrt{200/d} \leq 2.0$ (d expressed in mm)
$\sigma_c = N_{Ed}/A_c$ (A_c area of the section)
$v_{min} = 0.035\kappa^{3/2} f_{ck}^{1/2}$.

The drawback of the better agreement with the experimental results is the less physical evidence of the rupture mechanism, where for example the tensile concrete strength does not appear directly, which instead represents the main resistance parameter. According to an alternative approximated procedure, the increase of shear resistance due to compression is instead introduced in the formula with an additional constant term that depends only on the axial force present in the load condition under analysis.

It is reminded that the resistance calculated with these formulae constitutes an ultimate resource in the case of a prior presence of cracking due to bending moment. The limit of formation of shear cracks, corresponding to $\sigma_I = f_{ctd}$, generally remains higher and for sections of ordinary reinforced concrete subject to uniaxial bending, where $\sigma_I = \tau$, gives as already mentioned (in the uncracked Phase I) a value

$$V_{od} = bzf_{ctd},$$

that is

$$V_{od} = 0.7bdf_{ctd} \qquad \text{for } z \cong 0.7d$$

that exceeds the resistance of the tooth model (with $\delta = 1$) in the indicative ratio of about 2.7 for deep beams ($\kappa = 1$) and with low reinforcement ($\rho_s < 0.1\%$). For shallow beams with high reinforcement (e.g. $d = 0.2$ m and $\rho_s = 2.0\%$) the two resistances remain substantially equal thanks to the mentioned enhancing contributions of aggregate interlock and dowel action.

With the presence of an axial compression, the limit of shear cracks formation is given by

$$\sigma_1 \frac{\sigma_c}{2} \left\{ -1 + \sqrt{1 + 4\left(\frac{\tau_c}{\sigma_c}\right)^2} \right\} = f_{ctd},$$

which leads to

$$\tau_c = f_{ctd} \sqrt{1 + \frac{\sigma_c}{f_{ctd}}}$$

and eventually to

$$V_{od} = bz\tau_c = bzf_{ctd} \sqrt{1 + \frac{\sigma_c}{f_{ctd}}}$$

Moment Shift Rule

The tooth model behaviour assumed for the verification at the ultimate limit state of the beam in flexure has a consequence also on the distribution of stresses due to bending moment. Consistently with the inclination at 45° of the teeth through which the longitudinal shear force Q is transferred, the decrease of flexural tensile stresses in the reinforcement occurs with a delay of z with respect to the parallel decrease of compressions in the concrete chord. This is described in Fig. 4.23, where it can be noted how, for the curtailment of the bars, the force $Z = M/z$ to be used for the verification of the reinforcement should be shifted by z with respect to the section with moment M.

The resisting moment calculated on the basis of the reinforcement of the different sections should therefore be compared, not to the diagram of the original bending moment (e.g. the one indicated by the dashed line in Fig. 4.23), but to the diagram obtained shifting properly the former one. On each beam segment the direction of the shifting is given by the corresponding sign of the shear force on which the orientation of the inclined cracks depends. In particular it can be noted how, on the end support with no moment, without other appropriate reinforcement as bent bars, an amount of flexural reinforcement should be provided commensurate with the support reaction R itself, as this is the force $Z = M/z$ calculated on the basis of the moment $M \cong Rz$ of the shifted section.

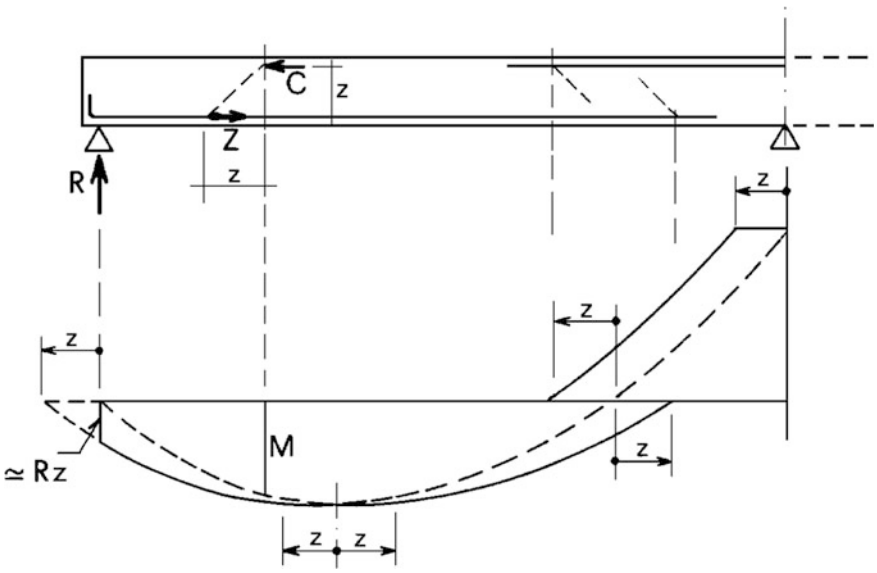


Fig. 4.23 Beam without shear reinforcement—"moment shifting" effect

Uncracked Segments

In the modern theory of reinforced concrete, which tends to take into account the tensile strength of concrete in the verifications, consistently to the fact that it is allowed to calculate the shear capacity of beams without shear reinforcement on the basis of the parameter f_{ctd}, also for bending it is possible to evaluate a cracking limit

$$M_{od} = \beta I_i f_{ctd} / y_c' \qquad (\beta = 1.3)$$

with which zones with flexural cracks (with $M_{Ed} > M_{od}$), where the shear capacity is given by the tooth behaviour, can be distinguished from zones without flexural cracks, where the higher shear capacity is ensured by the behaviour as an uncracked beam.

This criterion is indicated in Fig. 4.24, where for example a segment without flexural cracks can be noted close to the support up to the section of moment $M_{Ed} = M_{od}$. Therefore, for the shear verification a first zone can be identified, extended by $z/2$ beyond such limit section, where the formula of the uncracked beam is to be applied:

$$V_{Ed} < 0.7bdf_{ctd} \qquad \text{for } z \cong 0.7d,$$

a subsequent mid-span zone can be identified with high moments where the formula of the tooth behaviour is to be applied:

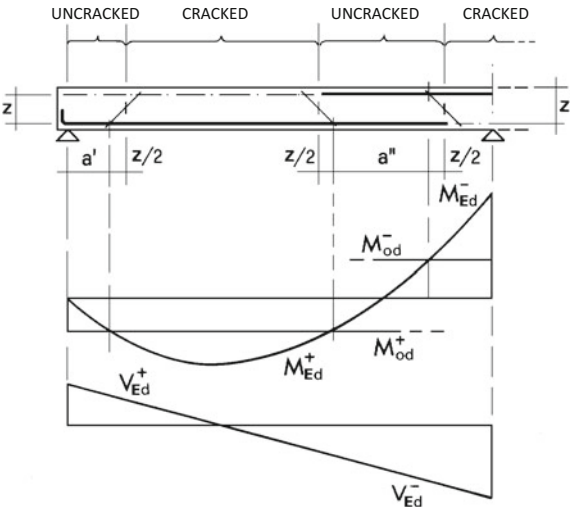


Fig. 4.24 Cracked and uncracked regions

$$V_{\mathrm{Ed}} < 0.25 b d f_{\mathrm{ctd}} \kappa (1 + 50\rho_{\mathrm{s}}) \qquad (\delta = 1)$$

and so forth.

In the case of a compression axial force N_{Ed}, the flexural cracking limit becomes

$$M_{\mathrm{Ed}} = \frac{I_i}{y' c}\left(\frac{N_{\mathrm{Ed}}}{A_{\mathrm{i}}} + \beta f_{\mathrm{ctd}}\right)$$

and the shear resistance of the uncracked zone remains (with $z \cong 0.7d$)

$$V_{\mathrm{od}} = 0.7 b d f_{\mathrm{ctd}} \sqrt{1 + \frac{\sigma_{\mathrm{c}}}{f_{\mathrm{ctd}}}}$$

Moment–Shear Interaction

A continuous beam is represented in Fig. 4.25a, indicating the possible flexural cracking pattern consistent with the stress state. The theoretical tooth model of the same beam is reported in Fig. 4.25b, on which the longitudinal spine of the compression chord is highlighted which, from the top edge in the mid-span, moves to the bottom one around the internal support. Without transverse reinforcement, the shear force has to be transferred through the longitudinal spine, apart from the contribution given by the dowel action, which is limited by the resistance to spalling of the concrete cover layer of the reinforcement.

On the left side support the beam undergoes the deviation of the reaction R on an inclined flux of compressions R_{c} which crosses the web involving the effective depth of the beam, providing the couple $C + Z$ with the lever arm z of the flexural behaviour. The equilibrium relations on which this diffusion mechanism is based

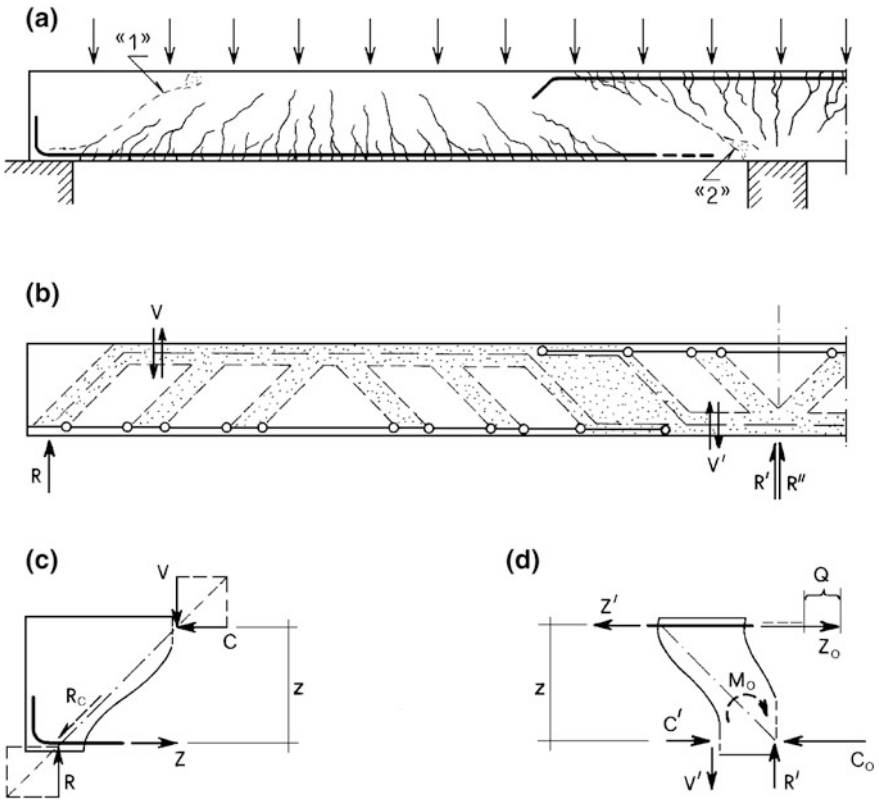


Fig. 4.25 Cracking pattern, tooth model and critical regions

are shown in Fig. 4.25c, highlighting the force $Z = R$ of the longitudinal reinforcement shifted on the support according to what already shown in Fig. 4.23.

At the upper node the component V of the force R_c is transferred along the chord together with the component C, as assumed for the calculation of the shear resistance at Paragraph 4.2.1. The resistance of such chord, with respect to a possible type '1' failure indicated with a dashed line in Fig. 4.25a, is implicitly ensured by the verification of the tooth behaviour with the coefficient δ (≤ 1) presented at the mentioned paragraph.

On the intermediate support instead, a diffusion mechanism of actions oriented from the compression edge of the beam to the in tension edge occurs. Therefore, apart from the dowel action effect, the reaction R' is divided in two at the lower node, transferring the shear force V' directly to the spinal chord and the longitudinal shear $Q = C_o - C'$ to the inclined tooth (see Fig. 4.25d). This latter, with its flexural resistance, brings the force to the upper chord, involving the entire depth z of the beam.

For the intermediate support the behaviour described above reproduces the normal tooth behaviour, without singular teeth with the presence of compressions only. The resistance formula, with the aim of preventing the possible type '2' failure indicated with the dashed line in Fig. 4.25a, consequently remains unchanged, with the only remark concerning the critical section of the spinal chord. In the description developed at Paragraph 4.2.1, the minimum compression $C = R = V$ was assumed in the section, in addition to the shear component V. For its low magnitude, the component C in fact increases the resistance, as for a given V the principal tensile stress is reduced.

On the intermediate support instead, high compressions in the chord are to be expected due to the peak of the bending moment. In this situation the compressive strength of concrete is crucial, whereas the simultaneous presence of shear has an adverse effect as it increases the principal compression stress. For the levels of shear allowed by the tooth behaviour, with shear stresses in the chord of the same order of the tensile strength of concrete, this interaction is limited and allows to apply also, as for any other case of bending, the verification formulas of shear and bending moment separately from each other.

Behaviour in Service

In beams without shear reinforcement, the ultimate resistance verification according to the tooth model imposes a limit to the stress lower than the one of shear cracks formation. The latter is therefore excluded as incompatible with the resistance itself. The possible presence at the bottom face of flexural cracks recalls the competent verification formulas presented at Paragraph 3.2.

However, the concentration of longitudinal reinforcement on the lower layer leaves the beam web without any effective restraint against the excessive opening of flexural cracks due to the simultaneous presence of shear. The use of beams without adequate stirrups should therefore be excluded in all cases of relatively slender webs.

Plate elements of significant width, slabs and common types of floors remain, for which the extent itself acts against the lateral exposure of the web cracks. These elements can therefore be designed without shear reinforcement according to the criteria of the previous section, as long as appropriate measures are taken to protect the free lateral sides. Appropriate stirrups can be placed for example (see Fig. 4.26a), unless the edge, as it often happens, already houses a beam or curb with its own stirrups (see Fig. 4.26b).

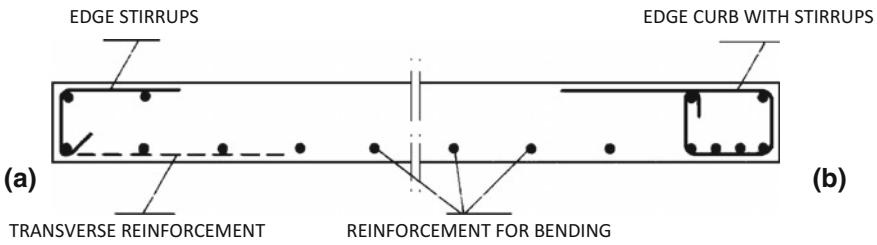


Fig. 4.26 Plate element and edge reinforcement

Beams with Minimum Shear Reinforcement

For beams with slender web, for which the presence of stirrups is necessary to contrast the cracks opening, the design criterion will be presented at Paragraph 4.3.3. A minimum amount of stirrups is deduced as a function of the width b_w of the web and the ratio f_{ct}/f_y of the material's strengths.

For the shear verification of the beam, if the resistance of the tooth behaviour, which neglects the presence of minimum reinforcement, is sufficient, it is possible not to add other verifications related to such stirrups, as the actual truss mechanism is certainly more resistant.

Calculations can therefore include the resistance verifications of the beam without shear reinforcement, whereas for the service verifications the minimum stirrups required will be calculated independently from the action.

4.3 Beams with Shear Reinforcement

We shall now refer to Paragraph 4.1.3 where the elementary model of the isostatic truss was presented for the design in shear of beams with transverse shear reinforcement. This model is represented in Fig. 4.27, shown with respect to the actual diffuse configuration of the truss.

Moment Shifting

It should be noted how, also for the truss behaviour, a *rule of moment shifting* is valid, analogous to the one presented for the tooth behaviour of beams without shear reinforcement. The magnitude a_1 of the shifting depends on the inclination α of the bar, as the compressions in the web remain directed at 45°, and can be deduced by the simplified scheme of Fig. 4.28 which refers to a module of length z $(1 + ctg\alpha)$.

For the equilibrium of the two top nodes involved, one has:

$$Q' = Vctg\alpha$$
$$Q'' = V$$

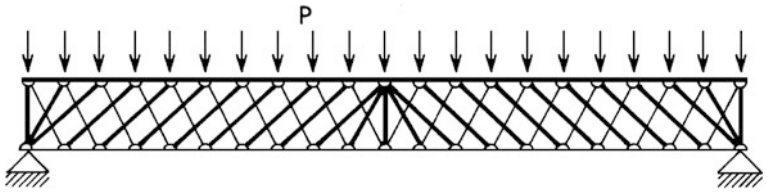


Fig. 4.27 Diffuse truss model

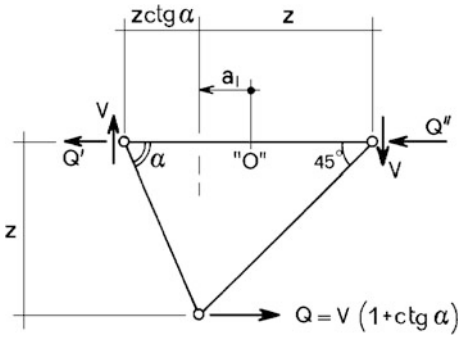


Fig. 4.28 Equilibrium conditions of a modular segment

Considering now the actual structural continuity, the global longitudinal shear force $Q = Q' + Q'' = V(1 + ctg\alpha)$ can be referred to the mid-point O of the upper chord, therefore obtaining

$$a_1 = \frac{1}{2}z(1 + ctg\alpha) - zctg\alpha = \frac{1}{2}z(1 - ctg\alpha).$$

For stirrups, with $\alpha = 90°$ the value $a_1 = z/2$ is halved with respect to the beams without shear reinforcement. For bars bent at 45° the shifting is reduced to 0. With angles $\alpha < 45°$ an opposed shifting ($a_1 < 0$) would derive. Nevertheless, the codes prescribe for the shifting of moment a minimum value (e.g. with $a_1 \geq 0$). It is to be noted that with this diffused model there is a simultaneous shifting of compressions on the opposite chord, equal and reverse to the one of the tensions in the steel reinforcement.

Bars Spacing

In order to ensure the correct behaviour of beams designed according to the Mörsch truss model, appropriate detailing rules are to be followed in the positioning of bars, which would allow the actual formation in the beam of the resisting mechanisms assumed in the design. First, as already mentioned at Paragraph 4.1.3, the transverse reinforcement should be bent taking care of their adequate anchorage in order to ensure the transfer of the tension forces they are subject to.

Moreover, the truss behaviour requires to limit the spacing between reinforcements within $z(1 + ctg\alpha)$, so that they can accommodate at the node the flux of compressions coming from the strut inclined at 45°. As indicated in Fig. 4.29a, the spacing s between vertical stirrups should consequently be limited to the value z equal to the lever arm of the internal couple. For bars bent at 45° such maximum value can be brought to $2z$ (see Fig. 4.29b).

Bars bent at 45° over the support are very effective to contain stresses at the fixed end or continuity sections of the beams. Here the simultaneous presence of high bending moment induces nearly vertical cracks, and such closely spaced reinforcement add a truss configured as described in Fig. 4.29c to the other resisting mechanisms anchored to the upper longitudinal reinforcement.

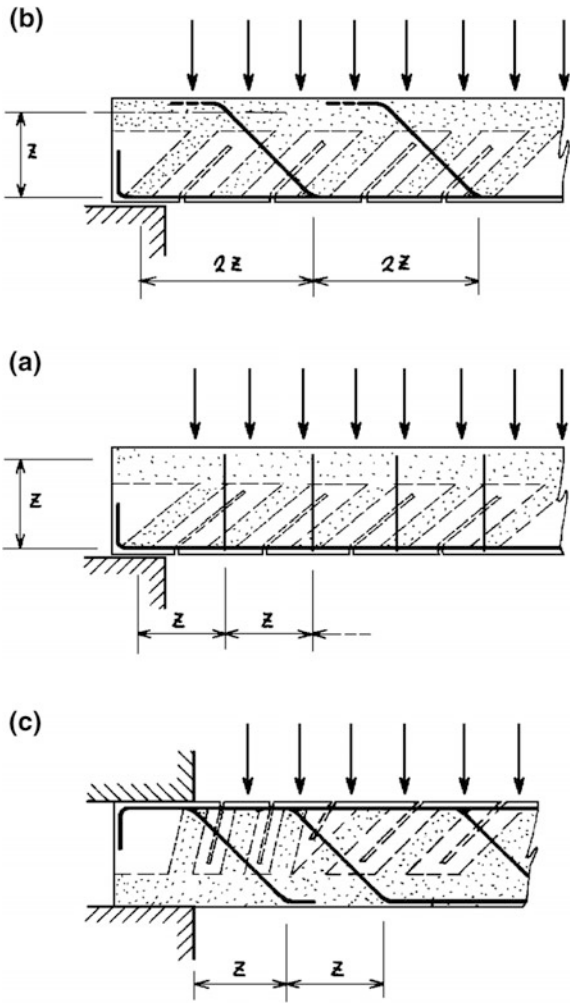


Fig. 4.29 Bars maximum spacing

Complementary Effects

With reference to the isostatic elementary truss again, certain particular effects are mentioned hereafter which lead to modifications of the model itself with respect to what has been presented so far.

The first effect concerns the level of application of loads on the beam and considers the ones applied on the top face as favourable for the actions on the transverse reinforcement; *hung loads* instead (see Fig. 4.30a) should be hold up with an adequate integration of the stirrups, adding the intensity of the load to the internal force due to shear:

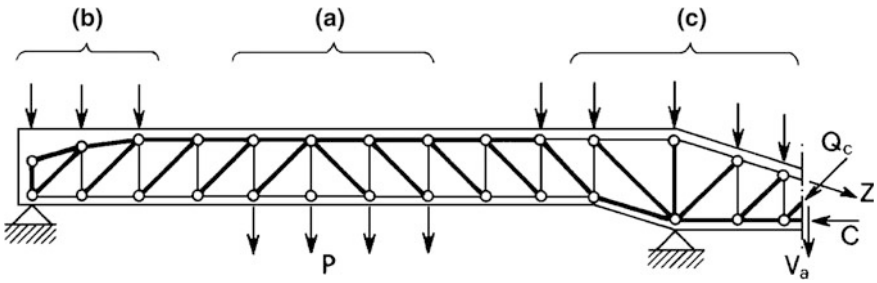


Fig. 4.30 Hung loads (**a**), inclined compressions (**b**), variable depth (**c**)

$$q_s = \frac{V}{z} + p \qquad (\text{for } \alpha = 90^\circ).$$

A second effect concerns the contribution of a *decreasing trajectory* of compressions in the concrete chord, deviated with respect to the horizontal direction of the upper edge of concrete. Such effect, which has been well highlighted by experimentation, can be taken into account with an appropriate adaptation of the truss model (see Fig. 4.30b).

The inclination of the resultant of the longitudinal stresses in the chords also gives a contribution to shear resistance which becomes important in the case of beams of *variable depth* (see Fig. 4.30c). In the calculation of forces in the web members, the vertical components of the forces C and Z of the compression and tension chords can be subtracted from the shear force V_{Ed}:

$$V_{wd} = V_{Ed} - V_{Cd} - V_{Zd},$$

where the contributions V_{Cd} and V_{Zd} can also be negative for certain unfavourable configurations of the structural layout.

The significant contribution in the prestressed beams given by the presence of *curved tendons* is eventually mentioned, where the layout is deviated with respect to the axis of the beams consistently with the shear action, as shown in details in Chap. 10 devoted to prestressed beams.

4.3.1 The Modified Hyperstatic Truss Model

As already mentioned in Paragraph 4.1.3, Mörsch isostatic truss is significantly conservatively approximated and leads to an overproportioning of the transverse reinforcement. The design model should therefore be refined and the first spontaneous modification appears to be the one of introducing the contribution of the

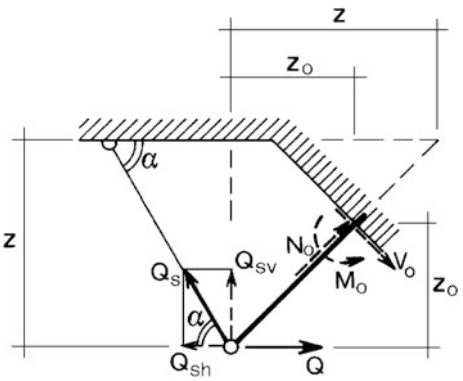


Fig. 4.31 Hyperstatic truss model

tensile strength of concrete in the web, as already done for the beams without shear reinforcement.

For beams with transverse reinforcement, the shear resistance can therefore be calculated on a model that reproduces the Mörsch truss superimposed to the tooth mechanism, with appropriate corrections deduced by the results of the specific experiments. Such modified truss is represented in Fig. 4.31.

The scheme is hyperstatic but, with the appropriate assumptions of the behaviour of materials at the ultimate limit situation, it can be analysed with simple equilibrium relations of forces. Firstly it is in fact observed that failure can occur either by the rupture of the concrete of the inclined strut in compression or by the failure of the reinforcement tension tie.

Compression–Shear

The first case is indicated as *compression–shear* and contemplates a brittle failure with small deformations. Without significant displacements of its node, the resisting truss of Fig. 4.31 works with predominant axial forces: the hyperstatic moment M_o in this case can be neglected and the resistance itself is equivalent to the one of the original Mörsch truss. As deduced at Paragraph 4.1.3, one therefore has:

$$V_{cd} = zbf_{c2}(1 + ctg\alpha)/2,$$

which can be written as

$$V_{cd} = 0.45bdf_{c2}(1 + ctg\alpha)$$

for $z \cong 0.9d$.

This formula gives the shear resistance of the beam with transverse reinforcement when relying on the compressive strength of the concrete of the web. In particular the factor due to the inclination of the transverse reinforcement is grouped in parentheses: for vertical stirrups (with $\alpha = 90°$) such factor is equal to 1, doubling for an angle $\alpha = 45°$. Codes generally limit to such value 2 the factor under consideration.

Tension–Shear

In the case where the failure of the resisting mechanism begins with the yielding of the transverse reinforcement, the significant deformations subsequent to the ductility of the steel are to be expected at rupture. The significant displacements of the node induce significant flexural forces in the strut of the resisting truss of Fig. 4.31, with a fixed end moment M_o which increases up to rupture. The maximum tensile stresses in the tooth will therefore limit the resistance, under the action of the longitudinal shear Q and with the balancing contribution Q_s of the yielded steel.

The mechanism described above is indicated as *tension–shear* and it relies on the following equilibrium. Also with reference to Fig. 4.31, given

$$Q_{sh} = Q_s \cos \alpha$$
$$Q_{sv} = Q_s \sin \alpha$$

one has:

$$N_o = \frac{Q}{\sqrt{2}} + \frac{Q_{sv} - Q_{sh}}{\sqrt{2}} = \frac{1}{\sqrt{2}} \{Q + Q_s(\sin \alpha - \cos \alpha)\}$$
$$M_o = Qz_o - (Q_{sv} - Q_{sh})z_o = \{Q - Q_s(\sin \alpha - \cos \alpha)\}z_o,$$

therefore the flexural verification of the fixed end section

$$\sigma = \frac{M_o}{bh^2/6} - \frac{N_o}{bh} = f_{ctd}$$

becomes, with $h = \Delta x/\sqrt{2}$

$$f_{ctf} = \frac{Q}{b\Delta x} \left\{ \frac{12}{\Delta x/z_o} - 1 \right\} -$$
$$- \frac{Q_s}{b\Delta x} \left\{ \frac{12}{\Delta x/z_o} (\sin \alpha + \cos \alpha) + (\sin \alpha - \cos \alpha) \right\}.$$

The fist term reproduces the tooth behaviour as deduced at Paragraph 4.2.1. In the current case of beams with shear reinforcement the crack distance has a different arrangement. It is also revealed from experimentation how difficult it is to directly correlate the resistance results to the actual reduced dimensions of the segments ($\Delta x/z_o \ll 1$). The higher measured resistance would depend on a systematic contribution of aggregate interlock, not reduced anymore by the beam depth but related to the amount of transverse reinforcement and due to the contrast given by the reinforcement itself against the uncontrolled opening of shear cracks.

The second term represents the resistance contribution of the transverse reinforcement, deriving from the force Q_s evaluated at steel yielding, having related its area A_s to the length Δx of the segment starting from the spacing s of bars:

$$Q_s = f_{yd} A_s \frac{\Delta x}{s} = f_{yd} a_s \Delta x,$$

where $a_s = A_s/s$ is the area of the transverse reinforcement per unit length. It is noted that the flexural term of such contribution is always favourable, whereas the second, which gives the axial component on the concrete element, can be unfavourable to the resistance: for bars inclinations α lesser than 45°, such term changes sign indicating an axial force that becomes in tension.

The formula now discussed is to be modified empirically, as the actual resisting mechanism observed from the experimental tests is more complex than the elementary one assumed in the description and gives systematically higher results than the theoretical ones. First, the verification formula of the inclined element, within the relevant approximations of the interpretative analysis, can be simplified removing the terms corresponding to the axial forces that are usually favourable and in any case of secondary magnitude:

$$f_{ctf} = \frac{Q}{b\Delta x} \frac{12}{\Delta x/z_o} - \frac{Q_s}{b\Delta x} \frac{12}{\Delta x/z_o} (\sin\alpha + \cos\alpha).$$

From here the resisting value of shear can be deduced with:

$$V_{sd} = V'_{ctd} + V_{yd} = \frac{Q_{Rd}}{\Delta x} z = \beta f_{ctd} b z \frac{\Delta x/z_o}{12} + f_{yd} a_s z (\sin\alpha + \cos\alpha).$$

For the coefficient $\beta\Delta x/12z_o$, not representing only the aspect ratio of the elements isolated by the cracks anymore, but including in a global sense different resisting effects, among which the fixed contribution of the aggregate interlock ensured firstly by the tying effect of stirrups, the experimentation would indicate the value 0.6. Introducing the factor δ of combined tension or compression and bending, one eventually obtains:

$$V_{sd} = V'_{ctd} + V_{yd} \cong 0.60 b z f_{ctd} \delta + a_s z f_{yd} (\sin\alpha + \cos\alpha),$$

that is

$$V_{sd} = V'_{ctd} + V_{yd} \cong 0.54 b d f_{ctd} \delta + 0.90 a_s d f_{yd} (\sin\alpha + \cos\alpha)$$

for $z \cong 0.9d$. The two other factors assumed for beams without shear reinforcement and related to small depths and dowel action have basically no influence, whereas it is recalled, with $\delta = 0$, that concrete is not effective in tension in the case of beams under combined tension and bending, or with shear of alternate sign.

In the resistance formula for tension–shear, with $V'_{ctd} > V_{ctd}$, the higher contribution of the concrete resistance in tension can be noted with respect to what calculated for the tooth behaviour of beams without shear reinforcement. This is

due to the effect of the aggregate interlock which brings this contribution to values close to the shear resistance V_{od} of the uncracked beam for all depths.

However, in order to rely on such higher effectiveness of the concrete of the web, a minimum amount of transverse and well-distributed reinforcement is necessary. Codes also prescribe resistance reductions for bent bars, as already mentioned, because of the concentrations of stresses at the bars bends and the consequent risk of longitudinal cracking of concrete, assigning them a reduction factor equal to 0.8.

Resistance Verifications

For the verification of the ultimate limit state, after evaluating the resistance values for compression–shear and tension–shear with the formulae reported above, the lesser of the two is assumed for the comparison with the applied shear:

$$V_{Rd} = \min(V_{cd}, V_{sd}) > V_{Ed}.$$

It is to be noted that certain codes, in the formula of tension–shear, substitute the contribution V'_{ctd} of concrete in tension with the resistance V_{ctd} of the tooth behaviour:

$$V_{sd} = V_{ctd} + V_{yd}.$$

Such approximation, which is nevertheless conservative, does not appear to be conceptually justified because it leaves a determining influence of the dowel action of the longitudinal reinforcement, which cannot coexist with a truss mechanism and because introduces an aggregate interlock effect which is variable with the depth, whereas it is in fact substantially independent. Such approximation penalizes in particular the deep beams.

4.3.2 The Variable Strut Inclination Truss Model

The formula of tension–shear presented above introduces an additional resistance contribution, in addition to the one of the transverse reinforcement, expressing it as a function of the concrete tensile strength. This is because reference has been made to the tooth behaviour, where the fixed end section of the tooth (see Fig. 4.32a) is subject to combined compression and bending and its resistance is limited by the maximum stress at the edge in tension.

As already mentioned, such model is not accurately confirmed by the experimental results, which highlight a closely spaced cracking with thin concrete segments of little flexural stiffness. In order to justify the greater values of the experimental results, the previous analysis introduces an approximate numerical coefficient, incorporating in a global sense various resisting effects. However, the incorrect proportional reference to the concrete tensile strength remains.

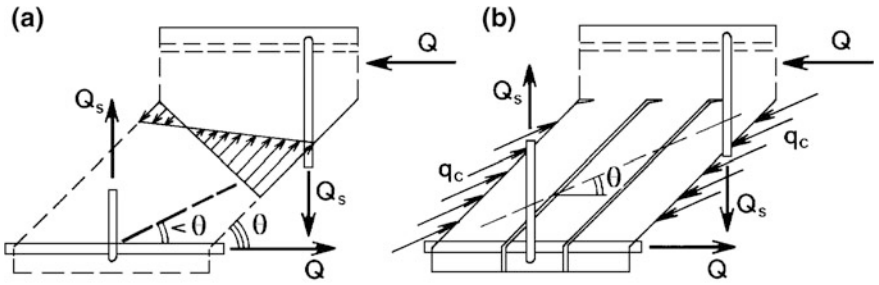


Fig. 4.32 Original (**a**) and improved (**b**) models of stress diffusion

As already mentioned, the aggregate interlock is the main effect, which gives a contribution to shear resistance even greater than the flexural one of the fixed end tooth. Especially for high level of forces, for which the cracking extent progressively reduces the flexural stiffness of the teeth until it affects their fixed end, the contribution of aggregate interlock becomes dominant.

Instead of giving an incorrect approximate representation in terms of the secondary parameter f_{ct}, the effect under consideration can be directly represented with an orientation θ of the flux q_c of compressions in the web appropriately reduced with respect to the direction θ_I ($\cong 45°$) of the initial cracking (see Fig. 4.32b), relying on the aggregate interlock for the transfer of forces through the cracks.

A beam segment subject to bending moment and shear (M, V) is represented in Fig. 4.33 where the resisting mechanism is highlighted. This consists of the two chords involved by the longitudinal forces $C = Z = M/z$ due to the bending moment; it also consists of the web members where tension and compression forces (Q_s, q_c) intersect to balance the applied shear V.

The equilibrium relations at the node of Fig. 4.10 are to be revised for the new inclination $\theta < 45°$ of compressions, as indicated in Fig. 4.34a, and are traduced in the equations:

$$\begin{cases} Q_s \cos\alpha + Q_c \cos\theta = Q \\ Q_s \sin\alpha - Q_c \sin\theta = 0 \end{cases},$$

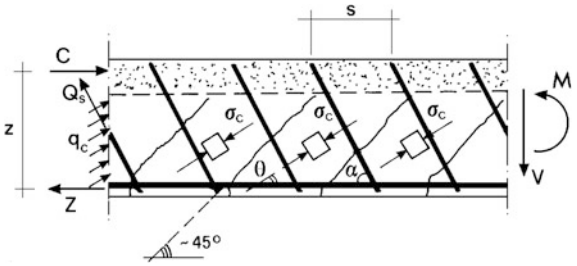


Fig. 4.33 Variable strut inclination model

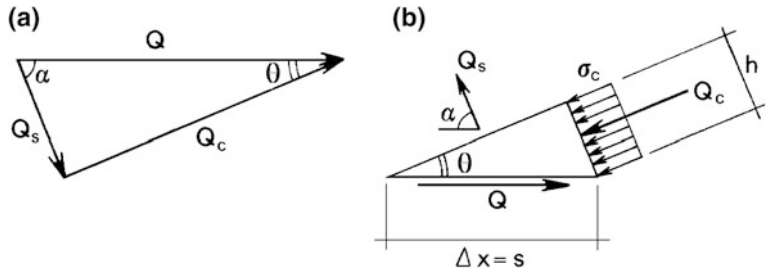


Fig. 4.34 Equilibrium conditions of the web truss

from which one obtains

$$Q = Q_s \cos\alpha(ctg\alpha + ctg\theta)$$
$$Q = Q_c \sin\theta(ctg\alpha + ctg\theta).$$

From the first relationship, with $Q_s = A_s f_{ys}$ and $a_s = A_s/s$ ($s = \Delta x$), the resistance to *tension–shear* is obtained:

$$V_{sd} = \frac{Qz}{\Delta x} = a_s z f_{yd} \sin\alpha(ctg\alpha + ctg\theta)$$

From the second, with $Q_c = \sigma_c bh = bsf_{c2}\sin\theta$ (see Fig. 4.34b), the resistance to *compression–shear* is obtained:

$$V_{cd} = \frac{Qz}{\Delta x} = bzf_{c2} \sin^2\theta(ctg\alpha + ctg\theta)$$

According to the variable inclination truss model, the prevalence of one on the other depends on the orientation θ assumed for compressions in the web. In order to show how such resistances vary, the parameters are adimesionalized with

$$\upsilon_{sd} = \frac{V_{sd}}{bzf_{c2}}$$
$$\upsilon_{cd} = \frac{V_{cd}}{bzf_{c2}}.$$

Defining then the *web mechanical reinforcement ratio b*:

$$\omega_w = \frac{a_s f_{yd}}{bf_{c2}} \sin\alpha$$

and setting for brevity $\lambda_s = ctg\alpha$ and $\lambda_s = ctg\theta$ one obtains:

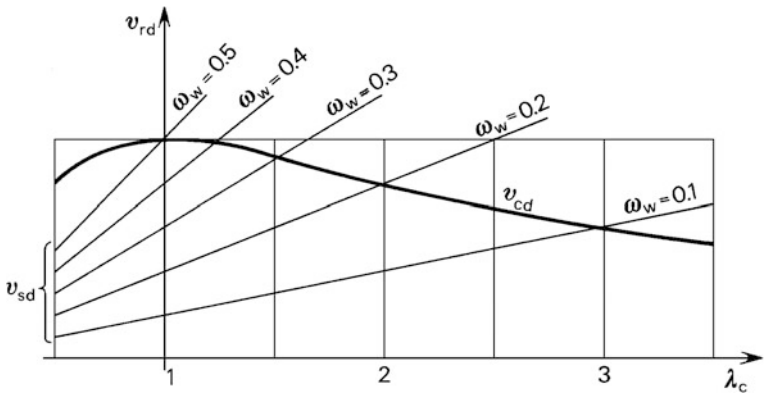


Fig. 4.35 Adimentional compression and tensile shear strengths

$$\upsilon_{sd} = \omega_w(\lambda_s + \lambda_c)$$
$$\upsilon_{cd} = (\lambda_s + \lambda_c)/\left(1 + \lambda_c^2\right)$$

which in particular, for vertical stirrups with $\alpha = 90°$, become:

$$\upsilon_{sd} = \omega_w \lambda_c$$
$$\upsilon_{cd} = \lambda_c/\left(1 + \lambda_c^2\right)$$

The two curves $\upsilon_{sd} = \upsilon_{sd}(\lambda_c; \omega_w)$ and $\upsilon_{cd} = \upsilon_{cd}(\lambda_c)$ are shown in Fig. 4.35, the latter being referred to vertical stirrups and some values of the web mechanical reinforcement ratio ($\omega_w = 0.1 \div 0.2 \div \cdots \div 0.5$).

For the resistance verification, the specific value $\lambda_c = \lambda_r$ of the inclination of compressions in the web, for which the ultimate limit state of the shear force is reached, is yet to be defined. This value is deduced, with reference to the diagram of Fig. 4.36, considering how, for a given reinforcement, the situation evolves beyond the cracking limit of the beam.

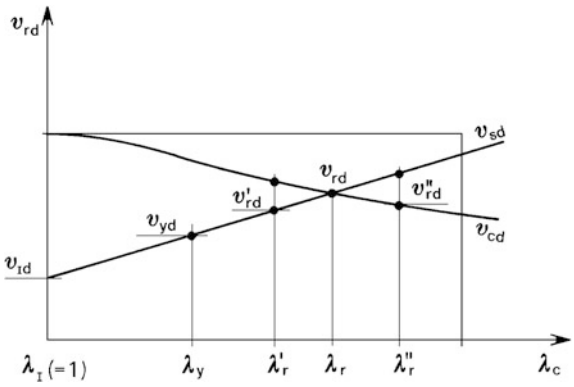


Fig. 4.36 Ultimate limit state of shear resistance

The *initial cracking* appears to be oriented in the direction of the isostatic lines in the previous situation of uncracked beam:

$$ctg\theta_{\mathrm{I}} = \lambda_{\mathrm{I}} = \frac{\tau}{\sigma_{\mathrm{I}}},$$

where the principal tensile stress is equal to

$$\sigma_{\mathrm{I}} = \frac{1}{2}\left\{\sqrt{\sigma^2 + 4\tau^2}\right\}$$

and the normal σ and shear τ components refer to the centroidal fibre of the cross section, assuming negative the ones in compression. In particular for uniaxial bending with $\sigma = 0$ ($\sigma_{\mathrm{I}} = \tau$), one obtains:

$$\lambda_{\mathrm{I}} = 1 \qquad (\theta_{\mathrm{I}} = 45^{\circ}).$$

For a proportional growth of the two normal and shear components of the stress with $\tau/\sigma = c$ = cost., one obtains:

$$\lambda_{|} = \frac{\pm 2c}{\pm 1 + \sqrt{1 + 4c^2}}.$$

Assuming + for σ in tension and − for σ in compression. For a constant compression value of the normal stress with $\sigma_{\mathrm{o}} = -\sigma$ = cost., at the cracking limit

$$\sigma_{|} = \frac{1}{2}\left\{-\sigma_0 + \sqrt{\sigma_0^2 + 4\tau^2}\right\} = f_{\mathrm{ct}},$$

from which

$$\tau^2 = f_{\mathrm{ct}}^2 + f_{\mathrm{ct}}\sigma_0,$$

one obtains:

$$\lambda_{|} = \frac{2\sqrt{f_{\mathrm{ct}}^2 + f_{\mathrm{ct}}\sigma_0}}{-\sigma_0 + \sqrt{\sigma_0^2 + 4\left(f_{\mathrm{ct}}^2 + f_{\mathrm{ct}}\sigma_0\right)}}$$

According to the Mörsch *isostatic model*, the resistance would correspond to such cracking pattern, referred to the yielding limit of the transverse reinforcement and given by

$$\upsilon_{\mathrm{Id}} = \omega_{\mathrm{w}}(\lambda_{\mathrm{s}} + \lambda_{\mathrm{I}}),$$

that is

$$\upsilon_{Id} = \omega_w$$

for uniaxial bending ($\lambda_I = 1$) with vertical stirrups ($\lambda_s = 0$).

Actually (see Fig. 4.36) the *reinforcement yielding* is reached for a significantly higher value υ_{yd} of the shear because, after the initial cracking and the subsequent activation of the tensile stresses, the hyperstatic effects are also immediately activated, mainly the ones of interlock, which unload the transverse reinforcement as if the flux of compressions was oriented in a more inclined direction:

$$\lambda_y > \lambda_I$$

The hyperstatic effects remain beyond the yield point of the reinforcement and allow the further increase of shear, thanks to the *plastic redistribution* which compensates the increase with a greater contribution of the concrete due to a further lower inclination of the compressions in the web.

The ultimate resistance resource is reached when, with $\lambda_c = \lambda_r$, *rupture of concrete* also occurs, having at that limit (see Fig. 4.36):

$$\upsilon_{rd} = \upsilon_{sd} = \upsilon_{cd}.$$

Such ultimate situation can be reached if the *ductility resources*, represented by the ultimate elongation ε_u of steel, are sufficient to avoid its early rupture when the plastic deformation increases beyond the yield point.

Figure 4.36 also shows how, estimating an *approximate inclination* as the rupture limit and assuming the lower of the corresponding tension–shear and compression–shear in the resistance verification, safety is nevertheless ensured even more; in particular an underestimation λ'_r brings the tension–shear to the resistance role ($\upsilon'_{rd} = \upsilon'_{sd} < \upsilon_{sd} < \upsilon'_{cd}$); an overestimation λ''_r brings the compression–shear to the role of resistance ($\upsilon''_{rd} = \upsilon''_{cd} < \upsilon_{rd} < \upsilon''_{sd}$).

A *lower limit* for the rupture inclination is given by the orientation of the initial cracking

$$\lambda_r \geq \lambda_I$$

as the hyperstatic resources of the web members derive from the predominant deformations of its ties and are always oriented towards a lower inclination θ of its fibres in compression.

An *upper limit* eventually for the rupture inclination is given, relatively to the one of initial cracking, based on the ductility resources of steel, with expressions of the following type

$$\lambda_r \leq \lambda_{max} = \lambda_I + \Delta\lambda,$$

for example with $\Delta\lambda = 1$ for steel of normal ductility. The codes for ductile steel type B450C assume $\Delta\lambda = 1.5$.

Resistance Verification

The value of the inclination λ_r at the ultimate limit state is therefore obtained equating the resistance in tension–shear υ_{sd} and the resistance in compression–shear υ_{cd}:

$$\omega_w(\lambda_s + \lambda_c) = (\lambda_s + \lambda_c)/\left(1 + \lambda_c^2\right),$$

from which it is obtained

$$\lambda_c = \lambda_r = \sqrt{\frac{1 - \omega_w}{\omega_w}},$$

that is a value increasing with the smaller reinforcements. Such value is to be compared with the limits indicated before.

Field "b" of reinforcements

If $\lambda_I \leq \lambda_r \leq \lambda_{max}$, the calculated inclination is compatible with an ultimate situation of an yielded steel not early broken. Choosing the shorter expression of tension–shear for the calculation of the resistance, in this field of medium reinforcements one obtains

$$V_{Rd} = a_s z f_{yd} \sin\alpha(\lambda_s + \lambda_r),$$

that is

$$V_{Rd} = 0.9 a_s d f_{yd} \lambda_r$$

for $z \cong 0.9d$ and vertical stirrups ($\alpha = 90°$). In this last case the resistance, expressed in an adimesional form, becomes

$$\upsilon_{rd} = \sqrt{\omega_w(1 - \omega_w)}.$$

Field "a" of low reinforcements

If $\lambda_r > \lambda_{max}$, the inclination should be set equal to the upper limit $\lambda_c = \lambda_{max}$. In this field of low reinforcements the resistance is given by the tension–shear with:

$$V_{Rd} = a_s z f_{yd} \sin\alpha(\lambda_s + \lambda_{max}),$$

that is

$$V_{Rd} = 0.90 a_s d f_{yd} \lambda_{max}$$

for $z \cong 0.9d$ and vertical stirrups ($\alpha = 90°$). In this last case the resistance, expressed in an adimesional form, becomes:

$$\upsilon_{rd} = \omega_w \lambda_{max}$$

Field "c" of high reinforcements

If $\lambda_r < \lambda_I$, the inclination should be set equal to the lower limit $\lambda_c = \lambda_I$. In this case of high reinforcements, the resistance is given by the compression–shear with:

$$V_{Rd} = b z f_{c2} (\lambda_S + \lambda_I) / \left(1 + \lambda_I^2\right),$$

that is

$$V_{Rd} = 0.9 b d f_{c2} \lambda_I / \left(1 + \lambda_I^2\right)$$

for $z \cong 0.9$d and vertical stirrups ($\alpha = 90°$). In this last case the resistance, expressed in an adimesional form, becomes:

$$\upsilon_{rd} = \omega_w \lambda_I / \left(1 + \lambda_I^2\right)$$

Minimum and Maximum Reinforcements

For *uniaxial bending* with $\lambda_I = 1$ and $\lambda_{max} = 2$, the two limits towards the low and high reinforcements are obtained from the relationship ($\upsilon_{sd} = \upsilon_{cd}$):

$$\omega_w = 1 / \left(1 + \lambda_c^2\right)$$

With $\lambda_c = \lambda_{max} = 2$ the *minimum reinforcement* is obtained:

$$\omega_{wa} = 0.20$$

With $\lambda_c = \lambda_I = 1$ the *maximum reinforcement* is obtained:

$$\omega_{wc} = 0.50$$

The entire resistance curve is shown in Fig. 4.37 in adimensional form through the three fields, according to the formulae (with $\lambda_I = 1$, $\lambda_{max} = 2$ and $\lambda_s = 0$):

- field 'a' ($\omega_s < 0.2$):

$$V_{Rd} = 1.8 a_s d f_{yd} \qquad (\upsilon_{rd} = 2\omega_w)$$

- field 'b' ($0.2 \leq \omega_s \leq 0.5$):

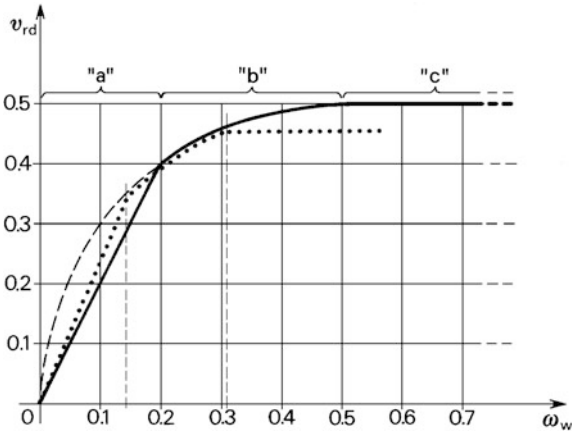


Fig. 4.37 Fields of low (**a**), medium (**b**) and high (**c**) reinforcement ratios

$$V_{Rd} = 0.9 a_s d f_{yd} \sqrt{(1-\omega_w)/\omega_w} \left(\upsilon_{rd}\left(\sqrt{\omega_w(1-\omega_w)}\right)\right)$$

- field 'c' ($\omega_s > 0.5$):

$$V_{Rd} = 0.45 b d f_{c2} \qquad (\upsilon_{rd} = 0.50).$$

For a *prestressed section* with a non-zero centred axial force (in compression with $\sigma < 0$), assuming for example, with $\sigma_I < \tau$, an orientation of the initial cracking equal to

$$\lambda_I = \frac{\tau}{\sigma_I} = 1.5 \quad (\theta \cong 34^\circ)$$

and an upper limit brought to

$$\lambda_{max} = \lambda_I + 1.0 = 2.5,$$

the following minimum and maximum reinforcements would be obtained

$$\omega_w = 0.14 \qquad \omega_{wc} = 0.31$$

and the resistance curve would be modified as indicated by the dotted line of Fig. 4.37, with enhancement of ductile resistances (towards the low reinforcements) and significant reduction of the brittle resistances (towards high reinforcements).

Moment Shift Rule

With respect to what presented at the beginning of this paragraph with reference to Mörsch model with struts inclined at 45°, only the inclination angle θ changes for the new model. The length of the module represented in Fig. 4.28 becomes

$$z(ctg\alpha + ctg\theta) = z(\lambda_s + \lambda_c)$$

and, with the same diffused interpretation of forces, the following shifting is obtained

$$a_1 = \frac{1}{2}z(\lambda_s + \lambda_c) - z\lambda_s = \frac{1}{2}z(\lambda_c - \lambda_s)$$

to be limited with $a_1 \geq 0$ and where it can be assumed $z \cong 0.9d$. Such shifting is to be attributed, with respect to the section where the moment is calculated, both to the tensions in the longitudinal reinforcement, and in the reverse sense to the compressions in the opposite concrete chord.

4.3.3 Serviceability Verifications

The experimental behaviour in shear of reinforced concrete beams can be observed on configurations similar to the one assumed in Fig. 4.3, applying on the lateral parts with constant shear $V = P$ the appropriate instrumentation for the measurement of the shear deformation γ. This instrumentation consists of couples of orthogonal extensometers, rotated at 45° with respect to the axis of the beam, applied to the surface of the web at the level of the centroid. Measuring (with mechanical or electrical instruments) the two orthogonal strains, the required shear deformation can be deduced from their halved difference.

From such experimentation curves $V = V(\gamma)$ similar to the one shown in Fig. 4.38 are obtained, where it can be noted:

- segment OA uncracked up to the tensile strength of the concrete of the web, with very small deformations and with a substantially linear trend that follows the straight line

$$V = G_c A_i^* \gamma,$$

  where $A_i^* = bz$ is evaluated for the uncracked section;
- segment AB corresponding to cracking in the web, with a limited sudden reduction of the stiffness due to the release of tensile stresses in concrete;
- if there were not other stiffening contributions and the release of stresses in concrete were complete, the test would stabilize on the point B' of the line

$$V = E_s A' \gamma,$$

- where A' can be evaluated on the basis of the characteristics of the Mörsch isostatic truss model; the segment BB' is not given as much by the limited tension stiffening effect of the concrete elements crossed by the transverse reinforcement, but rather by the hyperstatic contributions of the resisting truss

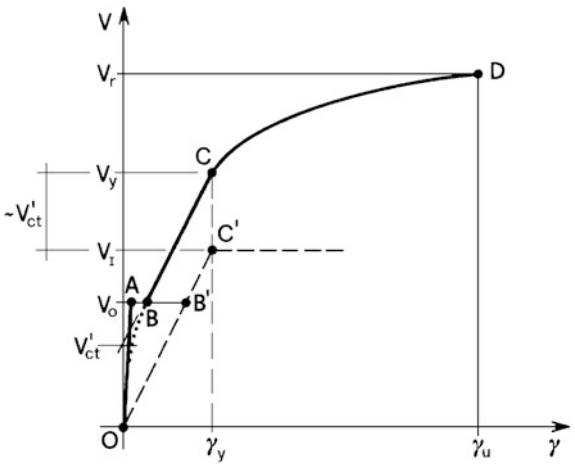


Fig. 4.38 Experimental resistance curve

that significantly reduce the stresses in its ties independently from their bond to concrete;

- if the concerned beam zone exhibited previous cracking due to shear (or bending moment), the diagram threshold *A* would be smoothed as indicated by the dotted line of Fig. 4.38;
- segment *BC*, with substantially constant hyperstatic contributions, up to the steel yield point, which occurs at a level V_y much higher than the one V_I that can be calculated on the isostatic truss;
- final segment *CD* with significant plastic strain of the transverse reinforcement, up to compressive rupture of concrete; the ultimate value V_r of shear corresponds to what is obtained by the resistance formulae of the variable inclination truss.

It is to be noted that, although the ultimate resistance V_r is predicted with good accuracy by the formulae of the variable inclination truss with reference to an elementary and well defined condition of plastic equilibrium, this is not the case in service situations of equilibrium in cracked state where the enhancing contribution, evaluated on the basis of the tensile strength of concrete (see Paragraph 4.3.1) at the fixed level of $V'_{ct} \cong 0.77V_o$, is not confirmed by the experimentation with the same accuracy. By consequence the serviceability verifications of the maximum stresses in the materials and the cracking verifications do not have the same reliability as the resistance and should be appropriately integrated with construction requirements, which have a qualitative theoretical justification, but are quantified empirically on the basis of the long practical experience.

Concerning the deformations due to shear, that are also calculated not with great accuracy, it is to be observed that they have little influence on the deflections of

beams, that are predominantly determinate by the bending moment. The problem does not appear to be relevant for practical applications.

Verification of Stresses

The calculation of the stress state in service of the web elements in the cracked state can be based on the truss model, with compression struts oriented on the direction θ_I of the initial cracking, but assuming for the calculation of the tensile stresses in the reinforcement a value of shear $V_{Ek} - V'_{ctk}$ without hyperstatic contributions of concrete. With this criterion it can therefore be set:

$$\begin{aligned}\sigma_s &= \frac{V_{Ek} - V'_{ctk}}{za_s}\frac{1}{\sin\alpha(ctg\alpha + ctg\theta_I)} = \frac{V_{Ek} - V'_{ctk}}{za_s}\frac{\sqrt{1+\lambda_s^2}}{\lambda_s + \lambda_I} \le \bar{\sigma}_s \\ \sigma_c &= \frac{V_{Ek}}{zb}\frac{1}{\sin^2\theta_I(ctg\alpha + ctg\theta_I)} = \frac{V_{Ek}}{zb}\frac{1+\lambda_I^2}{\lambda_s + \lambda_I} \le 0.6\bar{\sigma}_c\end{aligned},$$

where in particular the allowable compressive stress in the concrete of the web has been reduced with the same ratio of the strengths f_{c2}/f_{cd}. For uniaxial bending ($\lambda_I = 1$) with vertical stirrups ($\lambda_s = 0$) the formulae are simplified in:

$$\begin{aligned}\sigma_s &= \frac{V_{Ek} - V'_{ctk}}{za_s} \cong \frac{V_{Ek} - V'_{ctk}}{0.9da_s} \le \bar{\sigma}_s \\ \sigma_c &= \frac{2V_{Ek}}{zb} \cong \frac{V_{Ek}}{0.9db} \le 0.6\bar{\sigma}_c\end{aligned}.$$

It is reminded that the contribution of concrete in tension can be evaluated with (see Paragraph 4.3.1):

$$V'_{ctk} = 0.60bzf_{ctk}\delta,$$

that is

$$V'_{ctk} = 0.54bdf_{ctk}$$

for uniaxial bending (δ = 1) with $z \cong 0.9d$.

Construction Requirements

In addition to the ones presented at the beginning of this paragraph and aimed at ensuring the actual formation of the ultimate resisting mechanism, appropriate reinforcement criteria should be added in relation to the serviceability requirements. The aim is to contain the cracking due to shear, for which reliable verification algorithms are not available, as the ones for the calculation of the crack width presented at Paragraph 3.2.2 for beams in bending. Certain design criteria are instead used which have been empirically calibrated on experience, although they have a clear qualitative justification.

First the low effectiveness of bent bars is to be noted, as too isolated and too internal to oppose to the shear crack opening near the surfaces of the web. A minimum amount of peripheral stirrups is therefore necessary, which can be defined according to the criterion presented below. For a given total amount, smaller crack widths are obtained using stirrups with smaller diameters and more closely spaced. For high forces, when the shear action leads to reinforcements significantly higher than the minimum mentioned above, an effective measure for containing cracks consists of limiting the use of bent bars with respect to the total required reinforcement. Therefore, certain design codes require to allocate at least 50% of the longitudinal shear force to peripheral stirrups, and control their spacing with limits similar to $s \leq 0.8d$ ($\leq$300 mm).

Minimum Shear Reinforcement

A minimum peripheral amount of stirrups can be imposed, independently from the value of the shear force, with the principle of ensuring the resistance of the stirrups themselves, at their yield point, for the shear released by the cracking of the concrete of the web. It can therefore be set

$$V_{\mathrm{om}} - V_{\mathrm{ctm}} = V_{\mathrm{yk}}$$

which, for uniaxial bending and vertical stirrups, with the formulas of tension–shear presented at Paragraph 4.3.1 and with the approximation $z \cong 0.9d$, becomes

$$0.7dbf_{\mathrm{ctm}} - 0.54bdf_{\mathrm{ctm}} = 0.9a_{\mathrm{s}}df_{\mathrm{yk}}.$$

Consequently, rounded within the design approximations, the following limitation is obtained

$$a_{\mathrm{s}} \geq 0.2bf_{\mathrm{ctm}}/f_{\mathrm{yk}}.$$

With the common materials, minimum reinforcement ratios of peripheral stirrups of the order of $\bar{\rho}_{\mathrm{s}} = 100a_{\mathrm{s}}/b \cong 0.13\%$ are therefore imposed.

Cracking Verification

The *decompression limit* state cannot be verified for beams subject to bending and shear, without adopting systems of bidirectional prestressing (longitudinal e transverse). Such technique is rather impractical; its application is limited to few long-span cantilever bridges. With a less restrictive interpretation, a reduced limit to the maximum principal tensile stress can be set:

$$\sigma_{\mathrm{I}} \leq \bar{\sigma}_{\mathrm{ct}},$$

where σ_{I} is evaluated on the basis of the characteristic values of the stresses σ and τ in the centroidal fibre for the uncracked section. Similarly, the verification at the limit state of *cracks formation* is set with:

$$\sigma_I < f_{ctk}.$$

In particular it is reminded that, in sections in ordinary reinforced concrete in uniaxial bending, one has $\sigma_I = \tau = V_{Ek}/bz$ with $z \cong 0.7d$.

For the limit of *cracks opening*, without a reliable algorithm for the direct calculation and for the subsequent verification $w_k \leq \bar{w}_i$, an approximate method is proposed that sets a limit to the stress in the stirrups in relation to their spacing. Such *indirect technical criterion* is set empirically and leads to the verification

$$\sigma_s \leq \bar{\sigma}'_s \qquad \text{with } \bar{\sigma}'_s = \bar{\sigma}'_s(s),$$

generally more stringent than the one given above for the common verification of tensile stresses in the stirrups, having on average $\bar{\sigma}'_s < \bar{\sigma}_s$ ($=0.8f_{yk}$). In Table 4.4 admissible stresses is shown, specifying that values are provisional, not yet adequately proven by the experience.

4.4 Case A: Beams Design

The calculations of a beam of the typical deck of the multi-storey building described in Figs. 2.19 and 2.20 will be presented further on in the current section. But the design of the floor examined at Paragraph 3.4 has to be completed first. The analysis of forces was then presented, followed by the serviceability and resistance verifications only for flexural aspects relative to bending moment. Integrations relative to shear force are now given, to complete the set of verifications. Despite what usually happens for solid slabs, for the type of ribbed slab under consideration, the shear behaviour represents an important aspect. The reduced thickness of the web of the T-shaped section relative to each rib leads in fact to a limited shear resistance, if relying on tensile stresses in concrete. Sometimes transverse reinforcement is required, such as the bent bars assumed in Fig. 3.48. With reference therefore to the structural layout already fully defined in such drawing, the competent resistance verifications are reported.

Analysis of Actions

With reference to the solutions elaborated at Paragraph 3.4.1 and the combinations considered at Paragraph 3.4.3, one has the following diagrams of the shear force (with $p_d = 12.362$ kN/m).

Section 2′
(combination p_dO)

$$-V'_{2d} = \frac{p_d 1_a}{2} + \frac{|M_{2d}|}{1_a}$$
$$= \frac{12.850 \times 6.00}{2} + \frac{51.143}{6.00} = 47.074 \text{ kN}$$
$$x'_2 = 47.074/12.850 = 3.66 \text{ m}$$

Section 2″
(combination $p_d O$)

$$V'_{2d} = \frac{p_d 1_b}{2} + \frac{|M_{2d}|}{1_b} =$$
$$= \frac{12.850 \times 5.20}{2} + \frac{51.143}{5.20} = 43.245 \text{ kN}$$
$$x'_2 = 43.245/12.850 = 3.37 \text{ m}$$

Section '1'
(dedicated solution)

$$V_{1d} = \frac{p_d 1_a}{2} + \frac{|M_{2d}| - |M_{1d}|}{1_a} =$$
$$= \frac{12.850 \times 6.00}{2} + \frac{37.07 - 34.20}{6.00} = 38.07 \text{ kN}$$
$$x'_2 = 38.07/12.850 = 2.96 \text{ m}$$

with $M_{2d} = \gamma_F M_{2k} = -1.43 \times 25.92 = -37.07$ kN
Section '3'
(dedicated solution)

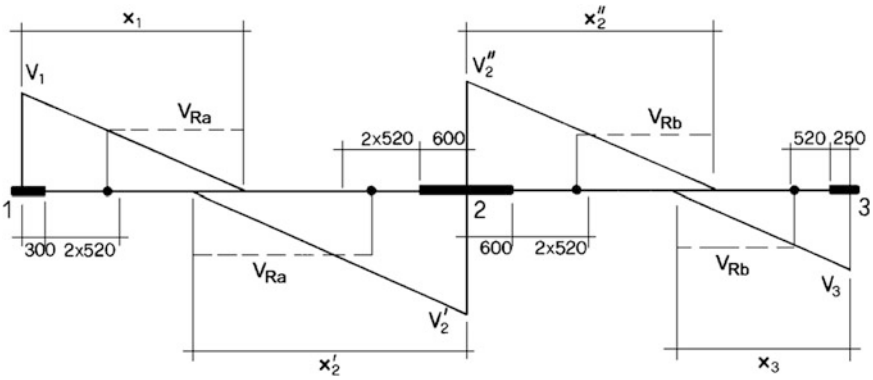


Fig. 4.39 Shear diagram along a floor strip

$$-V_{3d} = \frac{p_d 1_b}{2} - \frac{|M_{2d}| - |M_{3d}|}{1_b} =$$
$$= \frac{12.850 \times 5.20}{2} + \frac{37.07 - 21.43}{5.20} = 30.40 \text{ kN}$$
$$x_3 = 30.40/12.850 = 2.37 \text{ m}.$$

The diagrams defined in this way are shown in Fig. 4.39 which, for each beam segment, refer to the most critical situation (for load pattern and interpretation of constraints).

Resistance Without Shear Reinforcement
(Class C25/30 ordinary, f_{ctk} = 1.9 N/mm^2, f_{ctd} = 1.9/1.5 = 1.27 N/mm^2)

With reference to the 1 m-wide floor strip, the web thickness is equal to

$$b_w = 2 \times 8.0 = 16.0 \text{ cm}$$

One also has (d = 21.0 cm):

$$\kappa = 1.6 - d = 1.39(\text{m})$$

Span a
(d = 21.0 cm, A_s = 6.16 cm^2)

$$\kappa = 1.6 - d = 1.39(\text{m})$$
$$\rho_s = \frac{6.16}{16.0 \times 21.0} = 0.0183$$
$$(1 + 50\rho_s) = 1.915$$
$$V_{Ra} = 0.25 b_w d \kappa (1 + 50\rho_s) f_{ctd} = 28.42 \text{ kN/m}.$$

With the code formula one would have (ρ_s = 0.0183):

$$\kappa = 1 + \sqrt{200/d} = 1.976 \qquad (d \text{ in mm})$$
$$(100\rho_s f_{ck})^{1/3} = 3.572$$
$$V_{Ra} = 0.18 b_w d \kappa (100\rho_s f_{ck})^{1/3}/\gamma_c = 28.46 \text{ kN/m}.$$

Span b
(d = 21.0 cm, A_s = 4.52 cm^2)

$$\kappa = 1.6 - d = 1.39(\text{m})$$
$$\rho_s = \frac{4.52}{16.0 \times 21.0} = 0.0135$$
$$(1 + 50\rho_s) = 1.67$$
$$V_{Rb} = 0.25 b_w d \kappa (1 + 50\rho_s) f_{ctd} = 24.76 \text{ kN/m}.$$

With the code formula one would have (ρ_s = 0.0135):

$$\kappa = 1 + \sqrt{200/d} = 1.976 \qquad (d \text{ in mm})$$
$$(100\rho_s f_{ck})^{1/3} = 3.228$$
$$V_{Rb} = 0.18 b_w d \kappa (100\rho_s f_{ck})^{1/3} / \gamma_c = 25.72 \text{ kN/m}.$$

These resisting values, referred to the zones with positive moment, are indicated with a dashed line in Fig. 4.39.

From the diagrams in the figure, even without repeating the calculation for the zones with negative moment, it can be noted how the end segments are not covered by the current resistance of the T-shaped section. Once diffused within the solid strips with b_w = 100 cm, forces find a much higher resistance, even without taking into account (with $\rho_s = 0$) the contribution of the longitudinal tension reinforcement:

$$V_R = 0.25 \times 1000 \times 210 \times 1.39 \times 1.27/1000 = 92.68 \text{ kN/m}.$$

According to the reinforcement layout assumed in Fig. 3.48, bent bars at $\alpha = 30°$ from the horizontal are placed in the portions under consideration which, with $z \cong 18.9$ cm and $ctg\alpha = \sqrt{3}$, can cover (with $\theta = 45°$ and $ctg\theta = 1$) a segment whose length is equal to:

$$\Delta x = 18.9\left(1 + \sqrt{3}\right) \cong 52 \text{ cm}.$$

Having bent bars localized at the ends of the ribs, instead of stirrups continuously distributed along their length, a transverse mechanical reinforcement ratio cannot be clearly defined. For the verification of the segments Δx with bent bars both resistances in tension–shear and compression–shear are evaluated:

$$V_{Rs} = 0.8 A_s z f_{yd} \sin\alpha (\lambda_s + \lambda_c)/\Delta x$$
$$V_{Rc} = b_w z f_{c2} (\lambda_s + \lambda_c)/\left(1 + \lambda_c^2\right)$$

based on an approximated estimation of the inclination $\lambda_c (= ctg\theta)$ of compressions at the failure limit. The 0.8 factor of the first formula represents the resistance reduction to be attributed to bent bars (with respect to stirrups) for their lower effectiveness (see Paragraph 4.1.3).

It is therefore set

$$\lambda_c = 2.0$$

which, with $\sin \alpha = 0.5$, $\lambda_s = ctg\,\alpha = \sqrt{3}$, $f_{c2} = 0.5 \times 14.2 = 7.1$ N/mm^2, $z \cong 0.9d = 18.9$ cm, leads to the following resistances.

- Segment with $2 \times 1\phi 10$
  ($A_s = 1.57$ cm^2)

$$V_{Rs} = 0.8 \times 157 \times 189 \times 391 \times 0.5\left(\sqrt{3} + 2.0\right)/(520 \times 1000) =$$
$$= 33.31 \text{ kN}$$
$$V_{Rc} = 160 \times 189 \times 7.1 \times \left(\sqrt{3} + 2.0\right)/\left[\left(1 + 2.0^2\right) \times 1000\right] =$$
$$= 160.26 \text{ kN} (\gg V_{Rs})$$

- Segment with $2 \times 1\phi 12$
  ($A_s = 2.26$ cm^2)

$$V_{Rs} = 0.8 \times 226 \times 189 \times 391 \times 0.5\left(\sqrt{3} + 2.0\right)/(520 \times 1000) =$$
$$= 47.95 \text{ kN}$$
$$V_{Rc} = 160.26 \text{ kN} (\gg V_{Rs}).$$

The resistance verifications are therefore carried with reference to the shear force acting in the middle of the most stressed segments.

- *Section 2′* with $2 \times 1\phi 12$
  ($x = 60.0 + 52.0/2 = 86$ cm)

$$V_{Ed} = 47.074 - 12.850 \times 0.86 = 36.02 \text{ kN} \quad (< V_{Rs})$$

- *Section 1* with $2 \times 1\phi 10$
  ($x = 30.0 + 52.0/2 = 56$ cm)

$$V_{Ed} = 38.07 - 12.850 \times 0.56 = 30.87 \text{ kN} \qquad (< V_{Rs}).$$

With this verifications, the construction layout of the floor already fully described in Fig. 3.48 is therefore confirmed.

4.4.1 Analysis of Actions

The case relative to the reinforced concrete multi-storey building is resumed with the design of a beam of the type floor. With reference to the numbering shown in Fig. 2.19, the central beam that runs between columns P13-P14-P15 is examined. The analysis of loads carried in the previous chapters gives a total load on the floor equal to 9.00 kN/m^2, divided into 4.70 kN/m^2 of permanent loads and 4.30 kN/m^2 of variable loads. Approximately, taking into account the effect of the hyperstatic continuity moment of the floor and the self-weight of the dropped beam, one therefore obtains:

$$\begin{aligned} 1.2 \times 5.60 \times 4.70 &= 31.6 \\ 0.40 \times 0.30 \times 25 &= \underline{3.0} \\ p_o &= 34.6 \text{ kNm} \\ 1.2 \times 5.60 \times 4.30 &= \underline{28.9} \\ p_1 &= 28.9 \text{ kNm} \end{aligned}$$

The static scheme shows two equal spans of l = 4.30 m connected, through the columns, to the entire multi-storey frame, as indicated in Fig. 4.40. Partial models for the design of the beam under consideration can be extracted according to the criteria illustrated in the same figure. The continuity with the central column can be

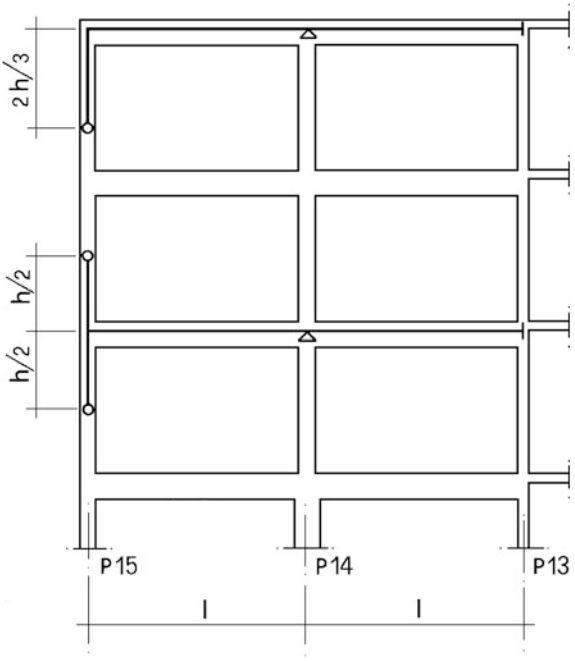


Fig. 4.40 Calculation schemes taken from the multi-storey frame

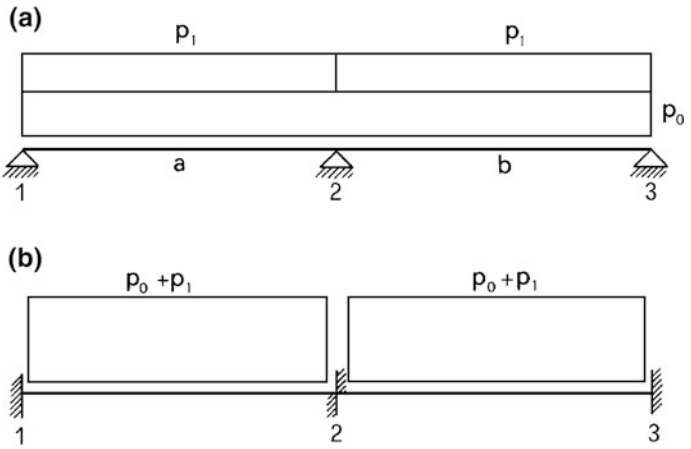


Fig. 4.41 Partial calculation schemes

neglected given the almost balanced arrangement around such constraint. The degree of rotational fixity at the end support of the beam can be represented with good accuracy by the pinned vertical elements, rigidly connected to the beam itself, estimating properly their height with respect to the combined behaviour with the other floors. The representation of the rotational restraint at the opposite end (P13) is more difficult, where the connection not aligned with the walls of the staircase makes the behaviour more complex.

The simplified procedure has been chosen here based on the partial static scheme of continuous beam doubled for limit interpretations of the rotational restraints at the ends of the beam itself. The highest forces will be conservatively assumed, which derive, on each beam segment, from the two different models. The greater simplicity of the relative calculations has the drawback of a higher reinforcement.

Therefore, with such criterion the beam of Fig. 4.41a is analysed with simple supports for the three load conditions examined below, expecting from the appropriate combinations the maximum positive values within the spans and the maximum negative value on the intermediate support for the bending moment. From the scheme with fixed ends of Fig. 4.41b the maximum negative value of the moment is instead expected at the end of the beam.

Load Conditions

- *Condition 'O'* (p_o on both spans)

$$M_2 = \frac{p_o 1^2}{8} = -2.311 p_o = -79.97 \text{ kNm}$$
$$M_a = \frac{p_o 1^2}{8} + \frac{M_2}{2} = +1.156 p_o = +39.98 \text{ kNm}$$
$$M_b = +1.156 p_o = +39.98 \text{ kNm}$$
$$V_1 = \frac{p_o 1}{2} + \frac{M_2}{2} = 1.612\, p_o = 55.79 \text{ kN}$$
$$-V_2' = \frac{p_o 1}{2} - \frac{M_2}{2} = 2.687\, p_o = 92.99 \text{ kN}$$
$$V_2'' = 92.99 \text{ kN}$$
$$-V_3 = 55.79 \text{ kN}$$

- *Condition 'A'* (p_1 on the span a)

$$M_2 = \frac{p_1 1^2}{16} = -1.156 p_1 = -33.40 \text{ kNm}$$
$$M_a = \frac{p_o 1^2}{8} + \frac{M_2}{2} = +1.733 p_1 = +50.10 \text{ kNm}$$
$$M_b = \frac{M_2}{2} = -0.578 p_1 = -16.70 \text{ kNm}$$
$$V_1 = \frac{p_1 1}{2} + \frac{M_2}{2} = 1.881\, p_1 = 54.37 \text{ kN}$$
$$-V_2' = \frac{p_1 1}{2} - \frac{M_2}{2} = 2.419\, p_1 = 69.90 \text{ kN}$$
$$V_b = -\frac{M_2}{1} = 0.269 p_1 = 7.77 \text{ kN}$$

- *Condition 'B'* (p_1 on the span b)

$$M_2 = 33.40 \text{ kNm}$$
$$M_a = -16.70 \text{ kNm}$$
$$M_b = +50.10 \text{ kNm}$$
$$-V_a = 7.77 \text{ kN}$$
$$-V_2'' = 69.90 \text{ kN}$$
$$-V_3 = 54.37 \text{ kN}$$

Load Combinations

- *Condition 'O + A + B'*

$$
\begin{aligned}
M_2 &= -79.97 - 33.40 - 33.40 = -146.77 \text{ kNm} \\
M_a = M_b &= +39.98 + 50.10 + 16.70 = 73.38 \text{ kNm} \\
+V_1 &= -V_3 = 55.79 + 54.37 - 7.77 = 102.394 \text{ kN} \\
-V_2' &= +V_2'' = 92.99 + 69.90 + 7.77 = 170.66 \text{ kN} \\
x_2' &= x_2'' = 170.66/63.5 = 2.69 \text{ m}
\end{aligned}
$$

- *Condition 'O + A' (symmetric of 'O + B')*

$$
\begin{aligned}
M_2 &= -79.97 - 33.40 = -113.37 \text{ kNm} \\
M_a &= +39.98 + 50.10 = +90.08 \text{ kNm} \\
M_b &= +39.98 - 16.70 = +23.28 \text{ kNm} \\
V_1 &= 55.79 + 54.37 = 110.16 \text{ kN} \\
-V_2' &= 92.99 + 69.90 = 162.89 \text{ kN} \\
V_2'' &= 92.99 + 7.77 = 100.76 \text{ kN} \\
-V_3 &= 55.79 - 7.77 = 48.02 \text{ kN}.
\end{aligned}
$$

Scheme for End Constraints

- *Situation of double fixed ends* (see Fig. 4.41b)

$$(p = p_o + p_1 = 63.5 \text{ kN/m})$$

$$
\begin{aligned}
M_1 = M_2 = M_3 &= -\frac{p1^2}{12} = -1.541\,p = -97.84 \text{ kNm} \\
M_a = M_b &= \frac{p1^2}{24} = +0.770\,p = +48.92 \text{ kNm} \\
+V_1 = -V_2' &= +V_2'' = -V_3 = \frac{p1}{2} = 2.15p = 136.52 \text{ kN} \\
x_1 = x_3 &= 1/2 = 2.15 \text{ m}.
\end{aligned}
$$

The consequent diagrams of internal forces are shown in Fig. 4.42 with the identification of the maximum positive and negative values. In particular the most stressed section with positive moment is defined with reference to the combination $O + A$:

$$
\begin{aligned}
R_1 &= V_1 = 110.16 \text{ kN} \\
\bar{x}_1 &= \frac{110.16}{63.5} = 1.73 \text{ m} \\
M_a'(=Mb) &= 110.16 \times 1.73 - 63.5 \times 1.73^2/2 = +95.55 \text{ kNm}.
\end{aligned}
$$

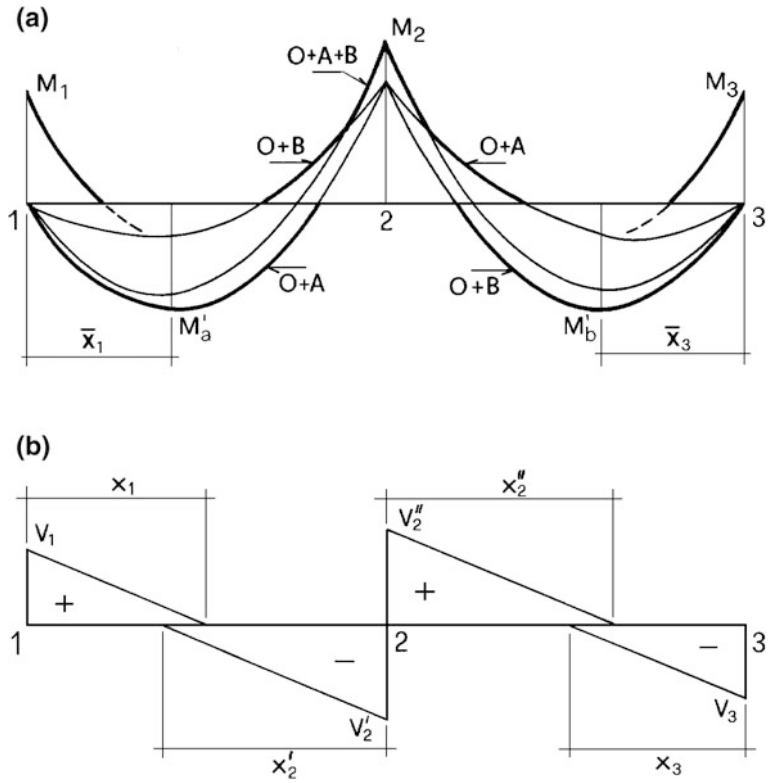


Fig. 4.42 Envelope diagrams for moment (**a**) and shear (**b**)

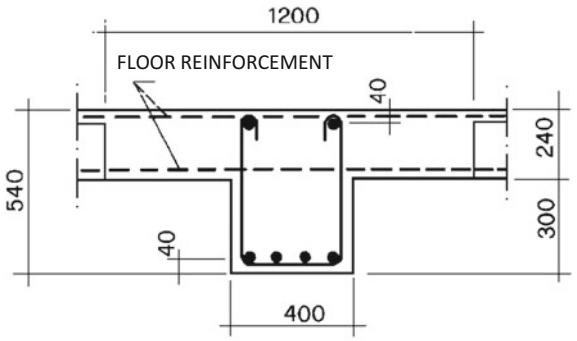


Fig. 4.43 Section of the beam

Proportioning of Longitudinal Reinforcement

With reference to the type 1 section of the beam represented in Fig. 4.43, the calculations for the proportioning of the reinforcement are now carried based on the maximum positive and negative values of the bending moment defined above. The approximate formula is used, similarly to what has been done for the floor at Paragraph 3.4.1 and a global coefficient $\gamma_F \cong 1.43$ is assumed for the amplification of actions. With $f_{yd} = 391$ N/mm^2 one therefore has:

- *Section 'I'* ($M = 97{,}840$ Nm, $d = 50$ cm)

$$A_s = \frac{9{,}784{,}000 \times 1.43}{0.9 \times 50 \times 39{,}100} = 7.95 \text{ cm}^2$$

  $4\phi16$ are assumed for 8.04 cm^2
- *Section 'a'* ($M = 95{,}550$ Nm, d = 50 cm)

$$A_s = \frac{9{,}555{,}000 \times 1.43}{0.9 \times 50 \times 39{,}100} = 7.77 \text{ cm}^2$$

  $4\phi16$ are assumed for 8.04 cm^2
- *Section '2'* ($M = 146{,}770$ Nm, $d = 50$ cm)

$$A_s = \frac{14{,}677{,}000 \times 1.43}{0.9 \times 50 \times 39{,}100} = 11.93 \text{ cm}^2$$

  $6\phi16$ are assumed for 12.06 cm^2.

The scheme of the bars positioning is shown in Fig. 4.44 according to this calculation.

Proportioning of Transverse Reinforcement

Assuming the trial value $\lambda_c = 2$, also with $z \cong 0.9d = 45$ cm and for vertical stirrups ($ctg\alpha = 0$), the proportioning of the transverse reinforcement is now carried. We

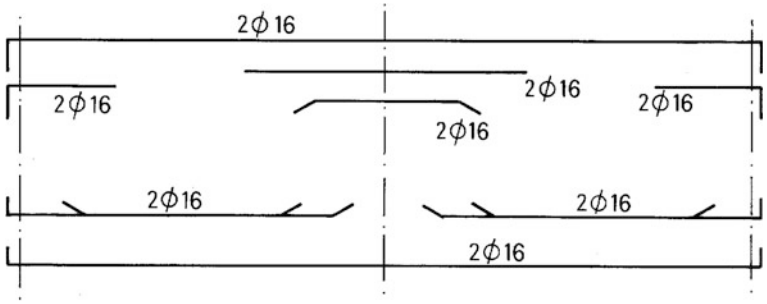


Fig. 4.44 General layout of the reinforcement bars

refer to the value of shear force calculated in the middle of the end segments of the spans, assuming for such segments an approximate reduced length $\Delta x = z = 45$ cm. The distance of such sections from the axis of the column (of side $a = 30$ cm) is:

$$x \cong \frac{a}{2} + \frac{\Delta x}{2} = 37.5 \text{ cm}$$

The minimum amount of stirrups required based on the web width is:

$$\bar{a}_s = 0.2 b_w f_{ctm}/f_{yk} = 20 \times 40 \times 2.8/450 = 4.98 \text{ cm}^2/\text{m}$$

- *End '1'*

$$V_{Ed} = 1.43(136.52 - 63.5 \times 0.375) = 161.17 \text{ kN}$$
$$a_s = \frac{V_{Ed}}{0.9 d f_{yd} \lambda_c} = \frac{16{,}117{,}000}{45 \times 39{,}100 \times 2} = 4.58 \text{ cm}^2/\text{m}$$

1 st. ϕ8/200 is assumed for 5.03 cm^2/m.

- *End '2'*

$$V_{Ed} = 1.43(170.66 - 63.5 \times 0.375) = 209.99 \text{ kN}$$
$$a_s = \frac{V_{Ed}}{0.9 d f_{yd} \lambda_c} = \frac{20{,}999{,}000}{45 \times 39{,}100 \times 2} = 5.97 \text{ cm}^2/\text{m}$$

1 st. ϕ8/150 is assumed for 6.71 cm^2/m.

4.4.2 Serviceability Verifications

With reference to the structural layout described in Fig. 4.45, deduced by the design calculations of the reinforcement carried at the previous paragraph, the verifications of stresses in the materials under service are now reported.

Flexural Actions

For the verifications of the serviceability limit state of compression in concrete, one should refer to the allowable value of the stress (see Paragraph 2.4.1):

$$\bar{\sigma}_c = 11.2 \text{ N/mm}^2.$$

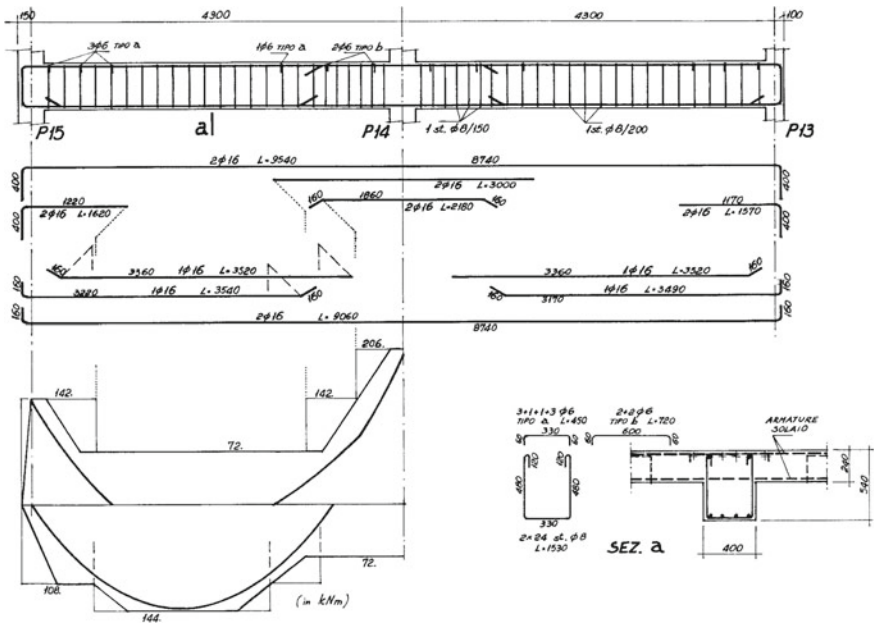


Fig. 4.45 Reinforcement details of the beam

With reference to the verification of cracks width for slightly aggressive environment, the admissible value of tensile stresses in steel, for rebars of diameter ϕ 16 mm as the ones used in the beam, is (see Tables 2.15 and 2.16):

$$\bar{\sigma}'_s = 280\,\mathrm{N/mm^2} \qquad (<0.8 f_{yk} = 360\,\mathrm{N/mm^2}).$$

We conservatively refer to the rare combination.

- *Section '1'*
  (M = 97,840 Nm, d = 50.0 cm, b = 40 cm, d' = 4 cm, A_s = 8.04 cm^2, A'_s = 6.03 cm^2)

$$\rho_t = \frac{8.04 + 6.03}{40 \times 50} = 0.0070$$
$$\psi_t = 15 \times 0.0070 = 0.1055$$
$$\delta = \frac{8.04 \times 50 + 6.03 \times 4}{14.07 \times 50} = 0.606$$
$$x = 0.1055\left\{-1 + \sqrt{1 + \frac{2 \times 0.606}{0.1055}}\right\}50.0 = 0.267 \times 50 = 13.4 \text{ cm}$$
$$I_i = 40 \times 13.4^3/3 + 15 \times 8.04 \times 36.6^2 + 15 \times 6.03 \times 9.4^2 =$$
$$= 32,081 + 161,551 + 7992 = 201,624 \text{ cm}^4$$
$$\sigma_c = \frac{97{,}840}{201{,}624}13.4 = 6.5 \text{ N/mm}^2 \qquad (<\overline{\sigma}_c)$$
$$\sigma_s = 15\frac{97{,}840}{201{,}624}36.6 = 266 \text{ N/mm}^2 \qquad \left(<\overline{\sigma}'_s\right)$$

- *Section 'a'*
  (M = 95,550 Nm, d = 50.0 cm, b = 120 cm, d' = 4 cm, A_s = 8.04 cm^2, A'_s = 4.02 cm^2)

$$\rho_t = \frac{8.04 + 4.02}{120 \times 50} = 0.0020$$
$$\psi_t = 15 \times 0.0020 = 0.0300$$
$$\delta = \frac{8.04 \times 50 + 4.02 \times 4}{12.06 \times 50} = 0.693$$
$$x = 0.0300\left\{-1 + \sqrt{1 + \frac{2 \times 0.693}{0.0300}}\right\}50.0 = 0.176 \times 50 = 8.8 \text{ cm}$$
$$I_i = 120 \times 8.8^3/3 + 15 \times 8.04 \times 41.2^2 + 15 \times 4.02 \times 4.8^2 =$$
$$= 27,259 + 204,711 + 1389 = 233,359 \text{ cm}^4$$
$$\sigma_c = \frac{95{,}550}{233{,}359}8.8 = 3.6 \text{ N/mm}^2 \qquad (<\overline{\sigma}_c)$$
$$\sigma_s = 15\frac{95{,}550}{233{,}359}41.2 = 253 \text{ N/mm}^2 \qquad \left(<\overline{\sigma}'_s\right)$$

- *Section '2'*
  (M = 146,770 Nm, d = 50.0 cm, b = 40 cm, d' = 4 cm, A_s = 12.06 cm^2, A'_s = 4.02 cm^2)

$$\rho_t = \frac{12.06 + 4.02}{40 \times 50} = 0.0080$$
$$\psi_t = 15 \times 0.0080 = 0.12000$$
$$\delta = \frac{12.06 \times 50 + 4.02 \times 4}{16.08 \times 50} = 0.770$$
$$x = 0.1200\left\{-1 + \sqrt{1 + \frac{2 \times 0.770}{0.1200}}\right\}50.0 = 0.326 \times 50 = 16.3 \text{ cm}$$
$$I_i = 40 \times 16.3^3/3 + 15 \times 12.06 \times 33.7^2 + 15 \times 4.02 \times 12.3^2 =$$
$$= 57{,}743 + 205{,}446 + 9123 = 272{,}312 \text{ cm}^4$$
$$\sigma_c = \frac{146{,}770}{272{,}312}16.3 = 8.8 \text{ N/mm}^2 \qquad (<\overline{\sigma}_c)$$
$$\sigma_s = 15\frac{146{,}770}{272{,}312}33.7 = 272 \text{ N/mm}^2 \qquad \left(<\overline{\sigma}'_s\right).$$

4.4.3 Resistance Verifications

For the resistance verifications the load combinations should be reformulated with the application of the appropriate amplifying coefficients for actions. To this end, one can distinguish the structural self weight (with γ_G = 1.00 ÷ 1.30):

$$g_1 = 1.2 \times 3.25 \times 5.60 + 0.40 \times 0.30 \times 25 = 24.8 \text{ kN/m}$$

the superimposed dead loads (with γ_{G2} = 0.00 ÷ 1.50):

$$g_2 = 1.2 \times 3.75 \times 5.60 = 25.2 \text{ kN/m}$$

and the live loads (with γ_Q = 0.00 ÷ 1.50):

$$q = 1.2 \times 2.00 \times 5.60 = 13.5 \text{ kN/m}$$

The combinations use the elementary load conditions developed at Paragraph 4.4.1.

Flexural Resistance
The values of the material strengths used in the following verifications are recalled:

$$f_{cd} = 14.2 \text{ N/mm}^2$$
$$f_{yd} = 391 \text{ N/mm}^2$$
$$r = f_{yd}/f_{cd} = 27.7.$$

The limit towards the high reinforcements remains $\omega_{sc} = 0.52$ and will always be definitely higher than the ones of the design sections examined. Towards the low reinforcements, for $\omega_s < 0.08$, it is assumed $z = 0.96d$.

- *Section '2'*
  (combination $\gamma_{G1}g_1O + \gamma_{G1}g_2O + \gamma_Q qO$)

$$\begin{aligned} 24.8 \times 1.30 &= 32.24 \\ 25.2 \times 1.50 &= 37.30 \\ 13.5 \times 1.50 &= \underline{20.25} \\ p &= 90.29 \text{ kN/m} \\ M_{Ed} &= 90.29 \times 2.311 = 208.66 \text{ kNm} \end{aligned}$$

  (d = 50.0 cm, b = 40 cm, A_s = 12.06 cm^2, $A'_s \cong 0$)

$$\begin{aligned} \omega_s &= \frac{12.06}{50.0 \times 40} 27.50 = 0.0060 \times 27.5 = 0.1650 \\ z &= (1 - \omega_s/2)d = 0.917 \times 50.0 = 45.8 \text{ cm} \\ M_{Rd} &= 12.06 \times 39.10 \times 0.458 = 216.0 \text{ kNm} \quad (> M_{Ed}) \end{aligned}$$

- *Section 'a'*
  (combination $\gamma_{G1}g_1A + g_1B + \gamma_{G2}g_2A + \gamma_Q qA$)

$$\begin{aligned} 24.8 \times 1.30 &= 32.24 \times 1.156 = 37.27 \\ 24.8 \times 1.00 &= 24.80 \times 1.156 = 28.67 \\ 25.2 \times 1.50 &= 37.80 \times 1.156 = 43.70 \\ 13.5 \times 1.50 &= \underline{20.25} \times 1.156 = \underline{23.41} \\ p_a &= 90.29 \text{ kN/m } M_2 = 133.05 \text{ kNm} \\ R_1 &= \frac{90.29 \times 4.30}{2} - \frac{133.05}{4.3} = 163.18 \text{ kN} \\ x_1 &= \frac{163.18}{90.29} = 1.81 \text{ m} \\ M_{Ed} &= 163.18 \times 1.81 - 90.29 \times 1.81^2/2 = 147.46 \text{ kNm} \end{aligned}$$

  (d = 50.0 cm, b = 120 cm, A_s = 8.04 cm^2, $A'_s \cong 0$)

$$\omega_s = \frac{8.04}{50.0 \times 120} 27.50 = 0.0013 \times 27.5 = 0.0357 \qquad (<0.08)$$
$$z = 0.96 \times 50.0 = 48.0 \text{ cm}$$
$$M_{Rd} = 8.04 \times 39.1 \times 0.480 = 152.05 \text{ kNm} \qquad (> M_{Ed})$$

- *Section '1'*
  (dedicated solution)

$$M_{Ed} = 1.541 \times 90.29 = 139.14 \text{ kNm}$$
$$\omega_s = \frac{8.04}{50.0 \times 40.0} 27.5 = 0.0040 \times 27.5 = 0.1105$$
$$z = (1 - \omega_s/2)d = 0.945 \times 50.0 = 47.2 \text{ cm}$$
$$M_{Rd} = 8.04 \times 39.10 \times 0.472 = 148.38 \text{ kNm} \qquad (> M_{Ed}).$$

In order to complete the diagram of the resisting moment shown in Table 6, the remaining sections are calculated:

- with $2\phi16$ (b = 40 cm, A_s = 4.02 cm^2, $A'_s \cong 0$)

$$\omega_s = \frac{4.02}{50.0 \times 40.0} 27.5 = 0.0020 \times 27.5 = 0.0553 \qquad (<0.08)$$
$$z = 0.96 \times 50.0 = 48.0 \text{ cm}$$
$$M_{Rd} = 4.02 \times 39.10 \times 480 = 75.45 \text{ kNm}$$

- with $2\phi16$ (b = 120 cm, A_s = 4.02 cm^2, $A'_s \cong 0$)

$$\omega_s \ll 0.08$$
$$M_{Rd} = 4.02 \times 39.10 \times 0.480 = 75.45 \text{ kNm}$$

- with $3\phi16$ (b = 120 cm, A_s = 6.03 cm^2, $A'_s \cong 0$)

$$\omega_s \ll 0.08$$
$$M_{Rd} = 6.03 \times 39.10 \times 0.480 = 113.17 \text{ kNm}.$$

Shear Resistance

The values of the materials strengths used in the following verifications are recalled

$$f_{c2} = 7.1 \text{ N/mm}^2$$
$$f_{yd} = 391 \text{ N/mm}^2$$
$$r = f_{yd}/f_{c2} = 55.1.$$

Assuming conservatively $\lambda_{max} = 2$, the minimum reinforcement is given by ω_{wa} = 0.20.

- *Extremity '1'* (d = 50.0 cm, b_w = 40.0 cm, a_s = 5.03 cm^2/m)

$$\omega_w = \frac{0.0503}{40.0} 55.1 = 0.00126 \times 55.1 = 0.0693 \qquad (< \omega_{sa})$$
$$\lambda_r = 2$$
$$V_{Rd} = 0.9 \times 5.03 \times 50.0 \times 391 \times 2/1000 = 177.01 \text{ kN}$$

(dedicated solution)

$$R_1 = 2.15 \times 90.29 = 194.12 \text{ kN}$$
$$x = 7.5 + z\lambda_r/2 = 52.5 \text{ cm}$$
$$V_{Ed} = 194.12 - 90.29 \times 0.525 = 146.72 \text{ kN} \qquad (< V_{Rd})$$

- *Extremity '2'* (d = 50.0 cm, b_w = 40.0 cm, a_s = 6.71 cm^2/m)

$$\omega_w = \frac{0.0671}{40.0} 55.1 = 0.00168 \times 55.1 = 0.0924 \qquad (< \omega_{sa})$$
$$\lambda_r = 2$$
$$V_{Rd} = 0.9 \times 6.71 \times 50.0 \times 391 \times 2/1000 = 236.12 \text{ kN}$$

(combination pO)

$$R'_2 = 2.687 \times 90.29 = 242.61 \text{ kN}$$
$$x = 7.5 + z\lambda_r/2 = 52.5 \text{ cm}$$
$$V_{Ed} = 242.61 - 90.29 \times 0.525 = 195.21 \text{ kN} \qquad (< V_{Rd}).$$

With $\lambda_r = \lambda_c = 2$ assumed for the verifications of shear resistance, the translation of moments to cover the diagrams of the bending action becomes (see DWG. 6)

$$a_1 = z\lambda_c/2 = 45.0 \text{ cm}$$

Appendix: Shear

Chart 4.1: Beams Without Shear Reinforcement: Formulas

RC elements in bending without transverse shear reinforcement.

Symbols

V_{Ek}	characteristic value of the shear force
V_{Ed}	design value of the shear force
V_{od}	design resistance to shear cracking
V_{ctd}	design resistance without shear reinforcement
b_w	minimum web width
$\overline{z}$	lever arm of the internal couple (uncracked section)
z	lever arm of the internal couple (cracked section)
d	effective depth (flexural) of the section
$\rho_l = A_s/db_w$	longitudinal geometric reinforcement ratio
a_l	shifting of the longitudinal reinforcement on the beam axis

See also Charts 2.2, 2.3, 2.9, 3.3, 3.10, 3.18.

Serviceability Verifications

Uncracked section

(zones with $M_{Ek} < M_{ok}$—see Chart 3.18)

$$\sigma_I = \frac{1}{2}\left(-\sigma + \sqrt{\sigma^2 + 4\tau^2}\right)$$

with

$$\tau = \frac{V_{Ek}}{\overline{z}b_w}$$

$$\sigma = \frac{N_{Ek}}{A_i} \quad > 0 \text{ for compression,}$$

that is

$$\sigma_I = \frac{V_{Ek}}{\overline{z}b_w} \quad \text{for uniaxial bending } (N_{Ek} = 0),$$

where (see also Chart 3.3):

$$\overline{z} = Ii/\bar{S}_i$$

$$\bar{S}_i = b_w y_c'^2/2 + \alpha_e A_s y_s,$$

that is

$$\overline{z} \cong 0.7d \quad \text{for rectangular section}$$

for the verification

at the shear cracking limit $\sigma_I \leq f_{ctk}$

Cracked section

(zones with $M_{Ek} > M_{ok}$—see Chart 3.18)

For plate elements: no verification

(beams within floor depth, plates, slabs, …—with protected lateral edges).

For beam elements: minimum stirrups (see Chart 4.5)

(with exposed webs).

Resistance Verifications

Uncracked section

(zones with $M_{Ed} < M_{od}$—see Chart 3.18)

$$V_{od} = \overline{z} b_w f_{ctd}\, \delta \geq V_{Ed},$$

with

$$\overline{z} \cong 0.7d$$

$$\delta = \sqrt{1 - \sigma / f_{ctd}}$$

$\sigma = N_{Ed}/A_i > 0$ for compression

(δ = 1 for uniaxial bending).

Cracked section

(zones with $M_{Ed} > M_{ok}$—see Chart 3.18)

$$V_{ctd} = 0.25 d b_w f_{ctd} \kappa r \delta \geq V_{Ed}$$

($V_{ctd} \leq V_{od}$) with

κ = 1.6 – $d \geq 1$	(d expressed in m)
$r = 1.0 + 50\rho_1 \leq 2$	
$\delta = 1 + M_{Ro}/M_{Ed} \leq 2$	for combined compression and bending
$M_{Ro} = \sigma I_i / y'_c$	$\sigma = N_{Ed}/A_i > 0$ for compression
δ = 1	for uniaxial bending
δ = 0	for combined tension and bending

Zero value V_{ctd} = 0 should be set also for relevant alternated shear forces with inverted signs.

Alternatively, according to more recent codes, it can be set:

$$V_{ctd} = 0.18 d b_w \kappa (100 \rho_l f_{ck})^{1/3} / \gamma_C + 0.15 b_w d \sigma_c$$
$$\geq b_w d v_{min} + 0.15 b_w d \sigma_c$$
$$V_{ctd} \geq V_{Ed},$$

where

$\kappa = 1 + \sqrt{200/d} \leq 2.0$	(d in mm)
$\sigma_c = N_{Ed}/A_c \geq 0$	in compression
A_c	area of the section
$v_{min} = 0.035\ \kappa^{3/2}\sqrt{f_{ck}}$	(f_{ck} in N/mm^2).

Construction Requirements
The longitudinal reinforcement at the face of the beam in tension, calculated based on the bending moment, should be shifted in increase by

$$a_1 = z \cong 0.9d$$

Chart 4.2: Resistance of Beams with Shear Reinforcement: Formulas

RC beams with transverse shear reinforcement.

Symbols

V_{cd}	design resistance for compression–shear
V_{sd}	design resistance per tension–shear
V_{Rd}	design value of the resistance with shear reinforcement
A_w	area of web transverse reinforcement
s	spacing of transverse shear reinforcement
$a_w = A_w/s$	unit area of transverse reinforcement
α	angle of transverse bar on the beam axis
$\rho_w = a_w \sin\alpha / b_w$	geometrical web reinforcement ratio
$\omega_w = \rho_w f_{yd}/f_{c2}$	mechanical web reinforcement ratio
θ_I	angle of initial shear cracking
θ	angle of web compressions on the beam axis
$\lambda_s = ctg\ \alpha$	inclination of transverse shear reinforcement
$\lambda_I = ctg\ \theta_I$	inclination of initial shear cracking
$\lambda_c = ctg\ \theta$	inclination of web transverse compressions

(see also Charts 2.2, 2.3, 2.9, 3.3, 3.10, 3.18, 4.1).

Resistance with Assigned Truss
Assumed λ_c in the interval $\lambda_I \leq \lambda_c \leq \lambda_{max}$, it is set

$$V_{Rd} = \min(V_{cd}, V_{sd}) \geq V_{Ed}$$

with V_{Ed} evaluated in the middle of the considered segment and

$\lambda_I = \tau/\sigma_I$ (=1 for uniaxial bending)
$\lambda_{max} = \lambda_I + 1.5$ (=2.5 for uniaxial bending)

(for τ and σ_I see Chart 4.1)
Tension–shear (z ≅ 0.9*d*)

$V'_{sd} = a_w z f_{yd} \sin\alpha(\lambda_s + \lambda_c)$ stirrups with $\alpha < 90°$
$V'_{sd} = a_w z f_{yd} \lambda_c$ stirrups with $\alpha = 90°$
$V''_{sd} = 0.8 A_w z f_{yd} \sin\alpha(\lambda_s + \lambda_c)/s$ bent bar
$V_{sd} = V'_{sd} + V''_{sd}$ for a given λ_c

Compression–shear ($z \cong 0.9d$)

$V_{cd} = z b_w f_{c2}(\lambda_s + \lambda_c)/(1 + \lambda_c^2)$ stirrups with $\alpha < 90°$
$V_{cd} = z b_w f_{c2} \lambda_c/(1 + \lambda_c^2)$ stirrups with $\alpha = 90°$

with stirrups orthogonal to the axis and bent bars:

$$V_{cd} = z b_w f_{c2}(\alpha'' \lambda_s + \lambda_c)/(1 + \lambda_c^2) \quad \alpha'' = V''_{sd}/V_{sd}.$$

Resistance with Calculated Truss
$\omega_{wa} = 1/(1 + \lambda_{max}^2)$ (=0.138 for uniaxial bending)
$\omega_{wc} = 1/(1 + \lambda_I^2)$ (=0.5 for uniaxial bending)

Low reinforcement ($\omega_w \leq \omega_{wa}$)

$\lambda_c = \lambda_{max}$ ($z \cong 0.9d$)
$V_{Rd} = a_w z f_{yd} \lambda_c$ stirrups with $\alpha = 90°$
$V_{Rd} = 2.5 a_w z f_{yd}$ for uniaxial bending

Medium reinforcements ($\omega_{wa} < \omega_w < \omega_{wc}$)

$\lambda_c = \sqrt{(1 - \omega_w)/\omega_w}$ ($z \cong 0.9d$)
$V_{Rd} = a_w z f_{yd} \lambda_c$ stirrups with $\alpha = 90°$

High reinforcements ($\omega_w \geq \omega_{wc}$)

$\lambda_c = \lambda_I$ ($z \cong 0.9d$)
$V_{Rd} = z b_w f_{c2} \lambda_c/(1 - \lambda_c^2)$ stirrups with $\alpha = 90°$
$V_{Rd} = z b_w f_{c2}/2$ for uniaxial bending.

Complementary Indications
Verification sections
The first verification section is usually located at

$$z(\lambda_s + \lambda_c)/2 \qquad (z \cong 0.9d)$$

from the contiguous support. The resistance related to the shear reinforcement can be referred to beam segments of finite length, not greater than 1/4 of the span, to be compared to the mean value of shear applied on the same segment.

Hung loads

In the case of loads applied on the lower part of the beam, an area of stirrups (orthogonal to the axis) should be added equal to

$$p_d/f_{yd} \qquad (\text{per unit length}),$$

where p_d is the design value of hung distributed load.

Variable depth

In the case of beams with variable depth, for the verification of the web members a reduced value of the applied shear should be assumed with

$$V_{Ed} - V_{Cd} - V_{Zd},$$

where

V_{Cd} transverse component of the force in the compression chord
V_{Zd} transverse component of the force in the tension chord.

Such components can be positive or negative based on their direction (and therefore favourable or unfavourable for the resistance of the web mechanism) and should be calculated with the design value of the bending moment applied on the considered section.

Chart 4.3: Beams with Shear Reinforcement: Service Conditions and Construction Rules

RC beams with transverse shear reinforcement.

Symbols

V'_{ctk} tension contribution of the concrete of the web
σ_w tensile stress in stirrups
σ_c compression stress in the concrete of the web

see also Charts 2.2, 2.3, 4.1, 4.2.

Serviceability Verifications

Uncracked zones

The zones of the beam that, with uncracked sections, satisfy the cracking verification of Chart 4.1, do not require further verifications.

Cracked zones—stirrups

$$\sigma_w = \frac{V_{Ek} - V'_{ctk}}{z a_w \sin\alpha} \frac{1}{\lambda_s + \lambda_I} \le \overline{\sigma}_w \quad \text{stirrups with } \alpha < 90^\circ$$

$$\sigma_w = \frac{V_{Ek} - V'_{ctk}}{z a_w \lambda_I} \le \overline{\sigma}_w \quad \text{stirrups with } \alpha < 90^\circ$$

With stirrups orthogonal to the axis of unit area a_w and bent bars with equivalent area $a^*_w = A_w \sin\alpha(\lambda_s + \lambda_I)/s$

$$\sigma_w = \frac{\alpha'\left(V_{Ek} - V'_{ctk}\right)}{z a_w \lambda_I} \le \overline{\sigma}_w \quad \alpha' = a_w/\left(a_w + a^*_w\right) \le 0.5,$$

with

$$V'_{ctk} = 0.60 b_w z f_{ctk} \delta \qquad (z \cong 0.9\,d)$$

and where

$\delta = 1 + M_{ro}/M_{Ek} \le 2$	combined compression and bending
$M_{ro} = \sigma I_i / y'_c$	$\sigma = N_{Ek}/A_i \ge 0$ in compression
$\delta = 1$	in uniaxial bending
$\delta = 0$	in combined tension and bending

A zero value of δ (with $V'_{ctk} = 0$) should be also set in the case of relevant alternate shear forces with inverted sign.

It should be assumed (see Chart 4.1):

$$\lambda_I = \tau/\sigma_I \qquad (= 1.0 \text{ for uniaxial bending}),$$

whereas for the allowable stress $\bar{\sigma}_w$ one should refer to Chart 4.6.

Cracked zones—concrete

$$\sigma_c = \frac{V_{Ek}}{z b_w} \frac{1 + \lambda_I^2}{\lambda_s + \lambda_I} \le 0.6\overline{\sigma}_c \qquad \text{stirrups with } \alpha < 90^\circ$$

$$\sigma_c = \frac{V_{Ek}}{z b_w} \frac{1 + \lambda_I^2}{\lambda_I} \le 0.6\overline{\sigma}_c \qquad \text{stirrups with } \alpha < 90^\circ.$$

With stirrups orthogonal to the axis and bent bars (as before):

$$\sigma_c = \frac{V_{Ek}}{z b_w} \frac{(\alpha'\lambda_s + \lambda_I)\left(1 + \lambda_I^2\right)}{\lambda_I(\lambda_s + \lambda_I)} \le 0.6\overline{\sigma}_c \qquad \alpha' \ge 0.5,$$

again with $z \cong 0.9d$ e $\lambda_I = \tau/\sigma_I$.
'Standard' cracked zones
(uniaxial bending and orthogonal stirrups)

$$\sigma_w = \frac{V_{Ek} - V'_{ctk}}{z a_w} \leq \overline{\sigma}_w \qquad \text{with } V'_{ctk} = 0.60\, b_w z f_{ctk}$$

$$\sigma_c = \frac{2V_{Ek}}{z b_w} \leq 0.6\overline{\sigma}_c \qquad \text{with } z \cong 0.9d.$$

Construction Data
Shifting of moments
The longitudinal reinforcement at the edge of the beam in tension, calculated based on the bending moment, should be shifted in increase by

$$a_1 = z(\lambda_c - \lambda_s)/2 \geq 0 \qquad \text{with } z \cong 0.9d$$

Spacing of stirrups
The spacing of stirrups orthogonal to the beam axis ($\alpha = 90°$) should be limited with

$$s \leq 0.8d \qquad (\leq 300\,\text{mm})$$

Minimum Stirrups
The minimum amount of peripheral stirrups close to the lateral faces of the web and encasing the longitudinal reinforcement, should be limited with

$$a_w \geq 0.2 b_w f_{ctm}/f_{yk}$$

Bent bars
In any case a quota of the shear force not less than 0.5 should be assigned to stirrups:

$$V'_{sd} \geq 0.50 V_{sd}$$

The remaining shear force is to be resisted by the bent bars.
Flat beams
For large beams with $b_w \gg d$ the stirrups of each of the free lateral faces should be limited with

$$a'_w \geq 0.1 d f_{ctm}/f_{yk},$$

whereas the total amount of transverse reinforcement should be uniformly distributed on the width resisting to shear with a spacing of links $s \leq 1.2d$.

Flat beams with protected lateral faces can be reinforced with bent bars only; in this case in the resistance verifications it is assumed $\lambda_c = \lambda_I$ (=1 for uniaxial bending).

Table 4.4: Shear Cracking: Allowable Stresses in Stirrups

The following table shows, for different values of the longitudinal spacing *s* of stirrups, the allowable stresses $\bar{\sigma}_w$ to be used in the serviceability verifications of the cracked zones as per Chart 4.3.

The values are expressed in MPa and refer to the peripheral stirrups close to the lateral faces of the web and bent so that they include the longitudinal reinforcement.

Allowable stresses of this table are given in an *experimental way.*

s (mm)	50	100	150	200	250	300
$\bar{\sigma}_w$	*200*	*150*	*100*	*75*	*60*	*50*

Chapter 5
Beams in Bending

Abstract This chapter presents the application of the basic tooth, truss and arch models to overall beam systems, showing the practical design procedure. The strut and ties balanced schemes are then applied to the resistance calculations of bearings, corbels, deep beams and slabs in punching shear. The criteria of nonlinear and collapse analysis are also presented. In the final section, the same beam examined in Chap. 4 is repeated with the different choice of flat shallow section.

5.1 Calculation Models of Beams in Bending

Although deduced from global models of beams in bending (see Figs. 4.9, 4.17 and 4.27), the analysis of the shear behaviour in Chap. 4 was referred to elementary modules (see Figs. 4.10, 4.18, 4.31 and 4.32) corresponding to beam segments with constant characteristics. We now extend the same analysis to the entire beam, therefore to its global model.

For beams without transverse reinforcement, the fundamental model for the calculation of the resistance is the *tooth model* which refers to a configuration already cracked due to the bending moment. Therefore, for the continuous beam of Fig. 5.1 the configuration of the resistance scheme is the one indicated in Fig. 5.2a.

The model consists of beam segments with uniform behaviour subject to shear with constant sign. These segments are separated by transition zones with no shear, through which the orientation of the inclined segments in the web changes: following the different inclination of the principal tensile stress due to shear, cracks orientate themselves with a rising or descending inclination consistently with the clockwise or counterclockwise direction of shear.

Type 'a' sections are located in the centre of the transition zones, characterized by stationary moment (see Fig. 5.1). For these sections, the equilibrium is set as

$$Zz = M$$

© Springer International Publishing AG 2017

G. Toniolo and M. di Prisco, *Reinforced Concrete Design to Eurocode 2*,
Springer Tracts in Civil Engineering, DOI 10.1007/978-3-319-52033-9_5

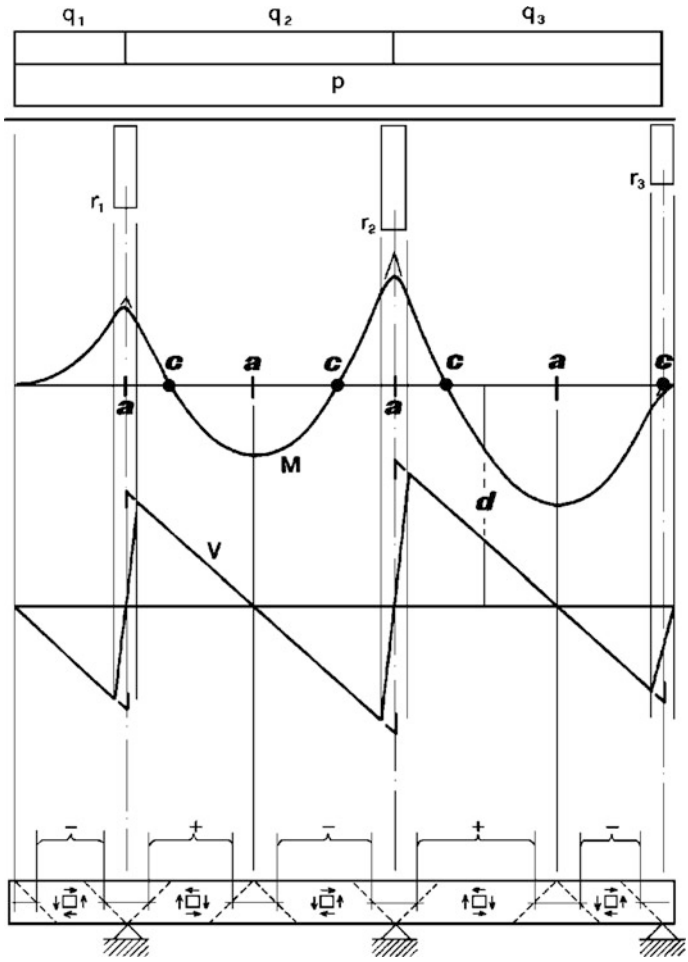


Fig. 5.1 Global model of a beam in bending

or

$$Cz = M$$

with reference, respectively, to the force of the chord in tension or one of the chord in compression (see Fig. 5.2b, c).

Each individual beam segment with constant orientation of the inclined web members is typically subject to variable bending. The *type* '*b*' *section* can be set at its most stressed end under shear, interface with the contiguous transition zone (see Fig. 5.2a). In this section the equilibrium is set as:

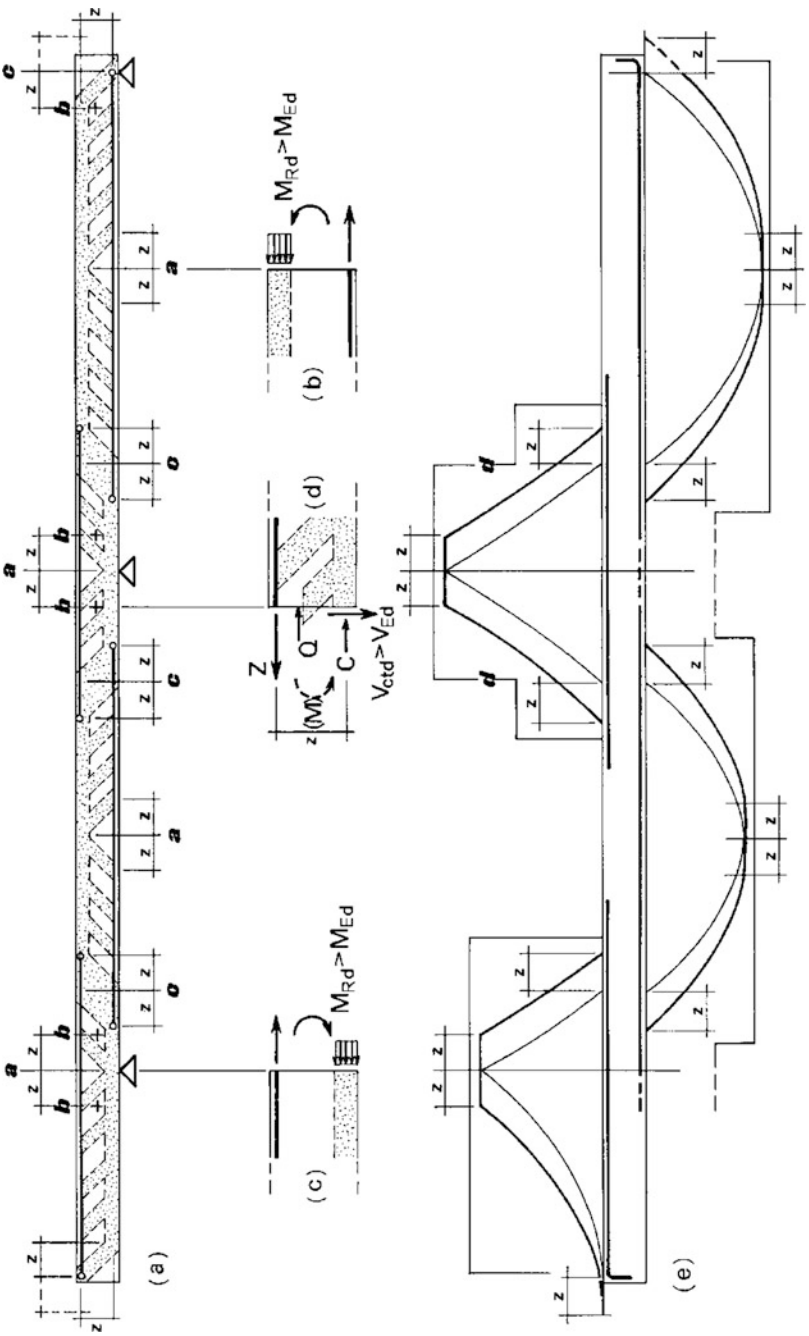


Fig. 5.2 Resistance scheme of a beam without shear reinforcement

$$qz = V$$

with reference to the unit longitudinal shear force in the concrete web (see Fig. 5.2d).

There are also the *type* '*c*' *sections* at the centre of the zones, where moment changes sign. The role of the chords is here inverted, which swap tensions and compressions with a superposition $2z$ of tensions that depends on the 45° inclination of the web members (see Figs. 5.1 and 5.2a). The equilibrium in these sections with no moment is set as

$$Z = V$$

with reference to the tension force in both chords of the continuity zones, or the only chord brought to the end support of the beam.

Within the segments with current behaviour there are the generic *type* '*d*' *sections* with non-zero moment and not maximum shear. For these sections, the equilibrium relationships, based on the longitudinal forces of the tension and compression chords and on the longitudinal shear, are set as

$$Z = \frac{M}{z} + V$$
$$C = \frac{M}{z}$$
$$q = \frac{V}{z}$$

These formulas include, as particular cases with $M = 0$ or $V = 0$, all the previous ones and they can give a meaningful synthesis of the resistance verifications with:

$$Z_{\mathrm{Ed}} = \frac{M_{\mathrm{Ed}}}{z} + V_{\mathrm{Ed}} < A_{\mathrm{S}} f_{\mathrm{yd}}$$
$$C_{\mathrm{Ed}} = \frac{M_{\mathrm{Ed}}}{z} < b\,\bar{x} f_{\mathrm{cd}}$$
$$q_{\mathrm{Ed}} = \frac{V_{\mathrm{Ed}}}{z} < 0.28 b_{\mathrm{W}} f_{\mathrm{ctd}} c$$

where the factors enhancing the shear resistance typical of the tooth behaviour have been included in the coefficient c (see Sect. 4.2.2).

Such formulas treat the calculation model as isostatic, based on the three elementary equilibrium equations. In reality the resisting mechanism has a hypestaticity in the evaluation of the geometrical parameters z and $\bar{x}$, which requires the additional condition

$$A_S f_{yd} = b\bar{x} f_{cd}$$

written here for sections 'a' of maximum moment with $V_{Ed} = 0$. With the solution

$$\bar{x} = A_S f_{yd}/\mathrm{bf}_{c1}$$
$$z = d - \bar{x}/2$$

the geometry of the model is eventually defined with completeness.

If one wants to use the elementary equilibrium equations written above for the structural design, for example for the evaluation of the necessary reinforcement in the most stressed sections, an approximated estimation of the geometry has to be given, for example with $z \cong 0.9d$:

$$A_S \cong \frac{M_{Ed}}{0.9 d f_{yd}}$$

subject to a more rigorous calculation afterwards.

In the final verifications, then, the equivalent formulas can be used

$$M_{Ed} < M_{Rd} \quad \text{for sections } 'a'$$
$$V_{Ed} < V_{ctd} \quad \text{for sections } 'b'$$

deduced in the previous Chapters (see Fig. 5.2b–d), with the addition of the moment shift rule presented at Sect. 4.2.3 and recalled in Fig. 5.2e. The application of this rule automatically fixes the superposition of reinforcement on sections 'c'. Naturally for each section 'd', where a change in shape or reinforcement occurs, both verifications of moment and shear should be repeated.

5.1.1 Arch Behaviour

In addition to the longitudinal shear behaviour discussed in the previous pages based on the tooth model, another fundamental type of model for the analysis is the arch model. As already mentioned, such behaviour is typical of the beam zones involved by diffusion phenomena of concentrated forces, but it can be further extended with a deviation if the actions on a flux of compressions directly oriented on the support, as shown in the following description.

Flexural Behaviour of Beams

In order to introduce this phenomenon with the main parameters that affect it, we refer to the elementary example of Fig. 5.3, where a simply supported beam is assumed, subject to symmetric point loads of magnitude P at a distance l from the respective adjacent supports. On such beam, which is assumed to have constant

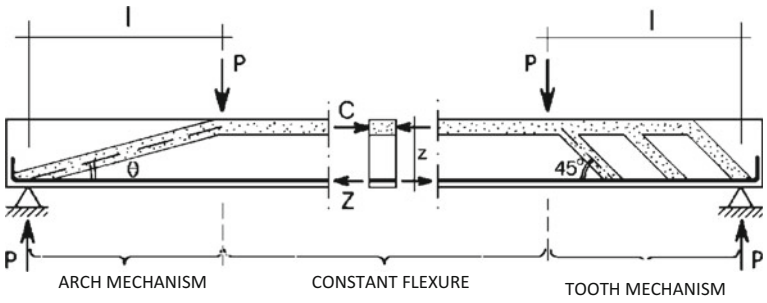


Fig. 5.3 Arch (*left*) and tooth (*right*) mechanisms

cross section, constant longitudinal reinforcement and no transverse reinforcement, the maximum internal forces are:

$$M = Pl$$
$$V = P$$

Assuming to increase the load beyond the resistance limit of the beam, one of the following three failure mechanisms can be observed:

- rupture by bending moment of a section of the central part according to the corresponding mechanism described at Sect. 3.1.2;
- rupture by longitudinal shear of a lateral beam part according to the corresponding mechanism described at Sect. 4.2;
- rupture with an arch behaviour of a lateral section under the overall force according to what is going to be presented here.

Therefore, in the first case the limit state of collapse of the beam, setting $\bar{x} \cong 0.2d$, $z \cong 0.9d$ and $\rho_s = A_s/db$, is defined by the resisting moment:

$$M_R \cong 0.2d\, b f_c z = \rho_s d b f_y z$$

of its section; in the second case instead, with $b_w = b$, the same limit state is defined by the resisting shear:

$$V_R \cong 0.25d\, b f_{ct}(1 + 50\rho_s)$$

where the two other factors κ and δ of the longitudinal shear behaviour are assumed equal to one.

The prevalence of a rupture mechanism on the other mainly depends on the aspect ratio of the beam and therefore on the slenderness (see Fig. 5.3):

$$\lambda = \frac{I}{z} = \operatorname{ctg}\theta = \frac{M}{V\,z}$$

The reinforcement ratio ρ_s also has an influence, which modifies the boundary limit values between the different behaviours.

Therefore, in order to analyze these aspects, one can correlate the rupture situations to the above-mentioned slenderness λ. The adimensional value of the moment P_Rl is chosen to represent the rupture situations, corresponding to the collapse load P_R, divided by the resisting moment M_R of the section.

As represented by the line '*a*' of Fig. 5.4, the first type of rupture, the one due to bending moment, is in this way characterized by the constant unit value:

$$\mu = \frac{M_R}{M_R} = 1$$

The rupture by longitudinal shear gives:

$$\mu = \frac{V_R l}{M_R} = \frac{0.25 d b f_{ct}(1 + 50\rho_s) l}{\rho_s d\, b f_y z}$$

which with $f_y/f_{ct} \cong 250$, becomes:

$$\mu = 0.0001 \frac{1 + 50\rho_s}{\rho_s} \lambda$$

showing a linear dependence on the slenderness λ, with a coefficient that decreases when the reinforcement ratio increases, as indicated in Fig. 5.4 by the set of lines '*b*' coming the origin.

The two mechanisms analyzed above remain uncoupled: for the resistance of the beam, the integrity of the tension and compression chords subject to the couple of

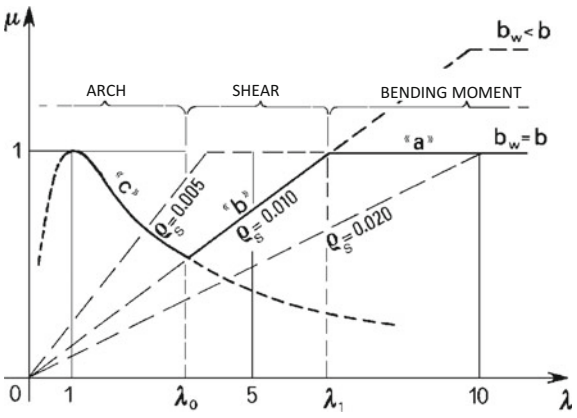


Fig. 5.4 Different domains of rupture of the beam

the bending moment is necessary, as well as the integrity of the web elements subject to longitudinal shear. It is, therefore, clear that the weaker between the two gives the limit of resistance of the beam itself. In the diagram of Fig. 5.4 the lower values should therefore be assumed; in this way two different domains of rupture behaviour are highlighted, separated by the limit slenderness λ_1: one of beams with smaller slenderness ($\lambda < \lambda_1$) where the resistance is related to shear; one of beams with greater slenderness ($\lambda > \lambda_1$) where the resistance is related to bending moment.

When the reinforcement increases, the flexural resistance of the section increases more rapidly than the shear resistance contribution due to the dowel action. Therefore, for higher reinforcements the domain '*b*' limited by the shear resistance is extended.

The rupture by arch behaviour can be related to the failure of the concrete strut where the compressions coming from the prints of application of the concentrated load *P* converge. In the left side of the beam of Fig. 5.3 the resisting scheme under consideration is described, where the inclination of the strut is indicated with θ. The longitudinal steel reinforcement completes the scheme, providing the tie that resists the horizontal component of the force at the support.

On the simplified model of Fig. 5.5, where the geometrical parameters have been adjusted on the basis of the experimental results, it is therefore obtained:

$$R_c = P/\sin\theta$$

which, with

$$R_{cR} = h\,b f_c = a\,b f_c \sin\theta \quad (a \approx 2\bar{x} \approx 0.4d)$$

leads to

$$P_R = a\,b f_c \sin^2\theta \cong 0.4d\,b f_c \sin^2\theta$$

Carrying out the same adimesionalization with M_R and setting $\sin^2\theta = 1/(1+\lambda^2)$, it is therefore obtained:

$$\mu = \frac{P_R 1}{M_R} = \frac{0.4d\,b f_c 1\ \sin^2\theta}{0.2d\,b f_c z} = 2\frac{\lambda}{1+\lambda^2}$$

This relation is represented by the curve '*c*' of Fig. 5.4. This curve refers to an overall resistance mechanism which occurs in stocky beams (with $\lambda < \lambda_o$) in place of the previous one, increasing the resistance with respect to the shear behaviour, when the arch mechanism is more effective.

It is to be noted that, referred to the equally necessary resistance of the tie (see Fig. 5.5):

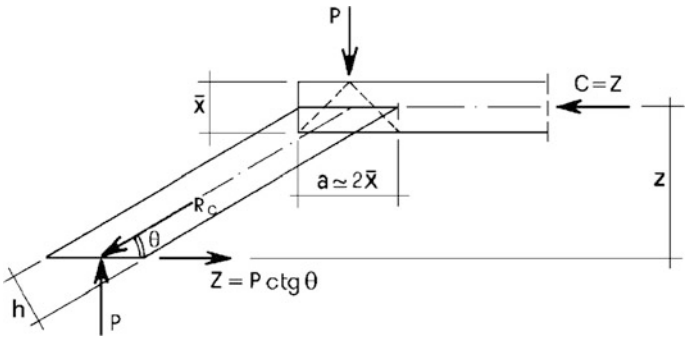


Fig. 5.5 Simplified model on arch mechanism

$$Z_{\mathrm{R}} = A_{\mathrm{s}} f_y = \rho_{\mathrm{s}} d\, b f_y = P_{\mathrm{R}}\, \lambda$$

the arch mechanism gives a higher constant value:

$$\mu = \frac{P_{\mathrm{R}} 1}{M_{\mathrm{R}}} = \frac{\rho_{\mathrm{S}} d\, b f_y 1/\lambda}{\rho_{\mathrm{S}} d\, b f_y z} = 1$$

corresponding to the flexural one, of which in fact it represents an alternative way to satisfy the same equilibrium of forces. The force demand in the reinforcement therefore does not change, except for the fact that in the flexural *l* shear behaviour it decreases from the maximum value $Z = Pl/z$ to zero value towards the supports, whereas in the arch behaviour it remains constant on the entire length of the beam.

What presented in this paragraph gives the indications on the rupture behaviour of reinforced concrete beams, valid from a qualitative point of view. The actual evaluation of the resistance should be based on the competent formulas, as deduced in the previous pages. In particular the geometrical parameters of the resisting section will have to be calculated, here approximated with $z \cong 0.9$ d, and the data on the material strengths should be duly considered. The diagrams of Fig. 5.4, shown for $\omega_{\mathrm{s}} \cong 0.20$ ($\rho_{\mathrm{s}} \cong 0.008$ with $f_{\mathrm{yd}}/f_{\mathrm{cd}} \cong 25$), would be significantly altered in their dimensions if they were referred to T-shaped sections with $b/b_{\mathrm{w}} > 1$ (see dashed segments in Fig. 5.4).

Simple and Combined Arches

For beams without shear reinforcement one can, therefore, rely on the arch behaviour within certain limits of the beam slenderness (see Fig. 5.6a, b). The need to extend the longitudinal reinforcement without reductions on the entire length of the beam is recalled.

In the simply supported configuration with the load intensity *p* uniformly distributed along the entire span *L* of the beam (see Fig. 5.6a), the arch behaviour gives, with $P = pL/2 = V$ and $\lambda = (L/4)/z$, a capacity of the concrete of the web:

$$V_{Rd} = 0.4d\, b_w f_{Cd} / \left(1 + \lambda^2\right)$$

expressed in terms of maximum shear at the supports, or

$$p_{Rd} = 2V_{Rd}/L$$

expressed in terms of distributed load.

The capacity of the reinforcement, with M = PL/4 and $P = Z/\lambda$, is given by

$$M_{Rd} = A_S f_{yd}\, z$$

which corresponds to the common flexural verification of the section at the mid-span with $M = pl^2/8$. The only difference is the need to extend the reinforcement without reductions up to the supports and to provide here the adequate anchorage to collect the compression force coming from the concrete.

An analogous model leads, for the cantilever of Fig. 5.6b, to the resistance verification (with λ = (L/2)/z):

$$V_{Rd} = 0.4d\, b_w f_{Cd} / \left(1 + \lambda^2\right) = p_{Rd} L$$

whereas the flexural verification remains

$$M_{Rd} = A_S f_{yd}\, z = p_{Rd}\, L^2/2$$

For continuous beams with inversion of the bending moment, one can have schemes with combined arches similar to the ones described in Fig. 5.6c, where the need for transverse reinforcement at their connections can be noted in order to ensure that the supported arches are hung. This hanger can consist of bent bars, traditionally used for slabs and floors, or less common stirrups concentrated in the zones where moment changes sign.

Given its higher resistance for low slenderness values, the design based on the arch behaviour can be advantageous in terms of concrete, with respect to the tooth behaviour. However, one has to pay attention to the geometrical compatibility of the assumed schemes. These in fact, as for the case represented in Fig. 5.6d, can constitute a valid resisting mechanism at the ultimate limit state of the beam, but without any restraint to cracking in service. Therefore, the competent flexural verifications should always be associated, also for the zones on the continuity supports, and the design criteria already discussed for cracking should be adopted. This leads to the addition of top reinforcement over the continuity supports, not considered in the resistance calculations but necessary to smear cracking into many cracks of small width.

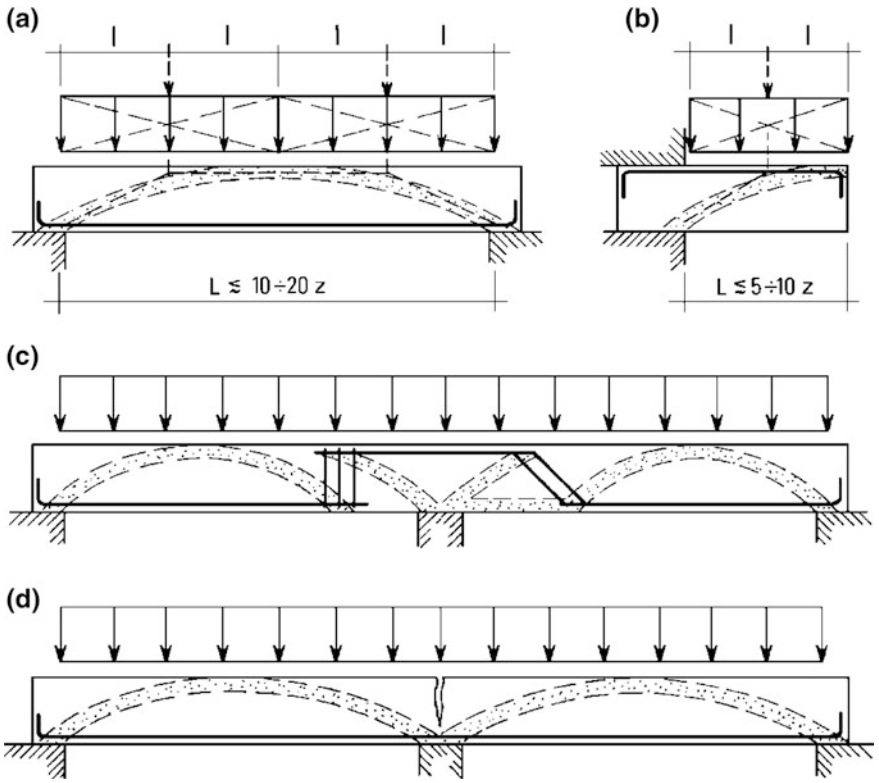


Fig. 5.6 Arch mechanisms for different beam arrangements

5.1.2 Truss Model

For the same beam of Fig. 5.1, assumed now to have transverse shear reinforcement, the resisting scheme according to the truss model consists of two longitudinal tension and compression chords, plus connecting web members between them made of concrete diagonal struts in compression and steel bars in tension.

The composition of this model is indicated in Fig. 5.7, divided in several parts based on the sign of shear: certain parts have rising compression struts, others have decreasing compression struts. The extract of a segment of positive shear (clockwise) is described more in detail in Fig. 5.8.

At the locations of maximum moment, the different parts are separated by transition zones where the compressions in the web are fan shaped. The *type* '*a*' *sections* are located at the centre of these zones, characterized by stationary moment.

Every single beam part, where the web members keep a constant orientation, has a typical variable flexural behaviour. Its ends, at the limit with the fan-shaped zones,

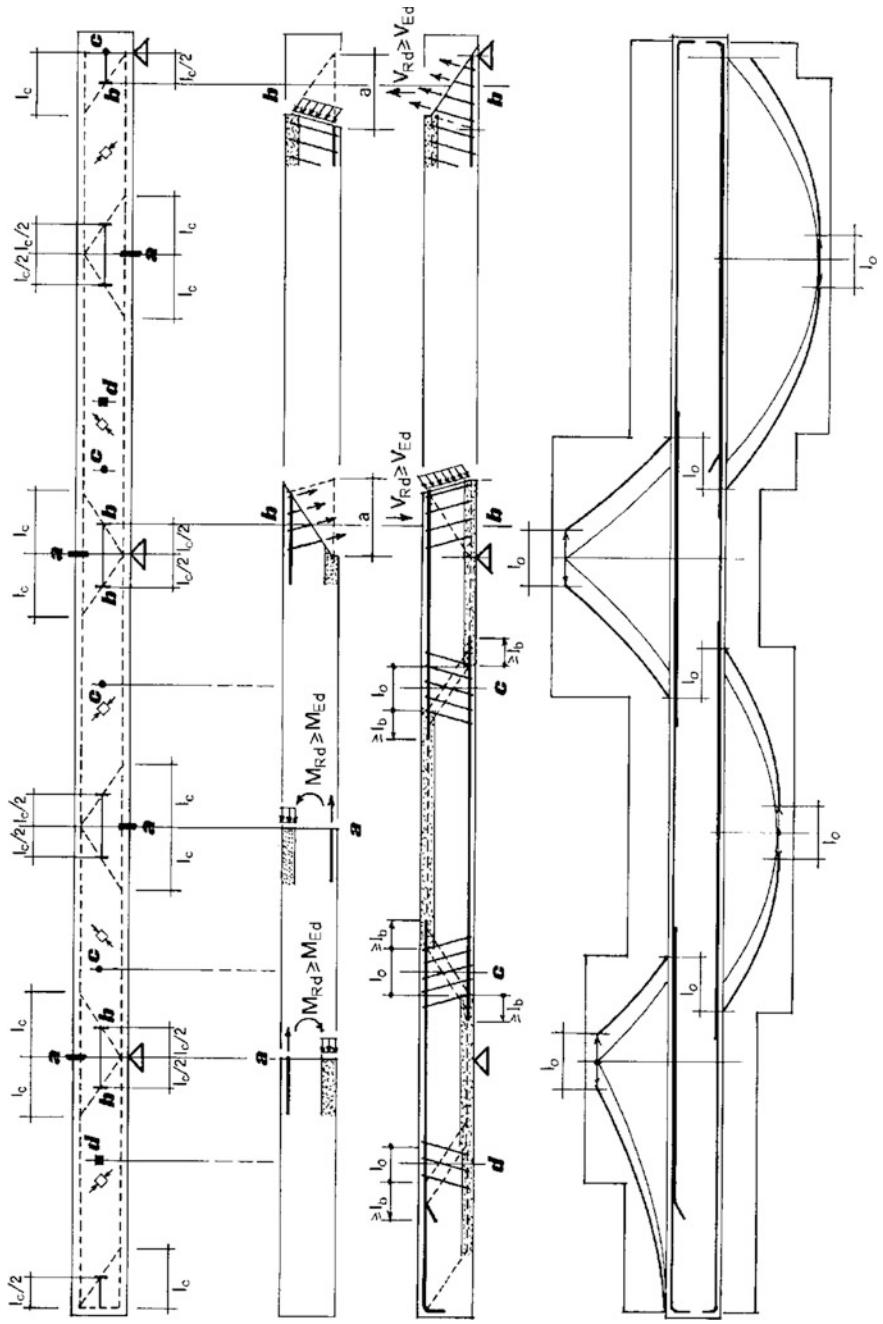


Fig. 5.7 Resistance scheme of a beam with shear reinforcement

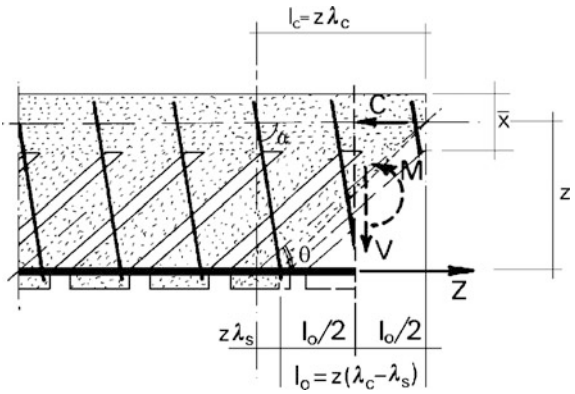


Fig. 5.8 Details of the resistance model

correspond to *type* '*b*' *sections* where the first verifications of the web members can be done, obviously limiting to the side of the maximum shear force.

Regarding the two chords of the resisting model, there are then the *type* '*c*' *sections*, at the centre of the zones where moment changes sign. The role of the chords is here inverted, which swap tensions and compressions with a superposition l_o of tensions that depend on the inclination of the web elements.

Eventually, along the beam there can be *type* '*d*' *sections* corresponding to a discontinuity of shape or reinforcement, where the verifications for moment and shear or both should be repeated, as shown in Fig. 5.7.

In the detail of Fig. 5.8 the main geometrical parameters of the model are also indicated: the distance z between chords, the inclination α of the tension bars and the inclination θ of the compression struts. From these inclinations derives also the length

$$1_c = z \operatorname{ctg} \theta = z\lambda_c$$

of one module of compression diagonal, as well as the length

$$1_0 = z(\operatorname{ctg} \theta - \operatorname{ctg} \alpha) = z(\lambda_c - \lambda_S)$$

of overlapping of the chords, related to the shifting $a_l = l_o/2$ of the moment (see last item of Sect. 4.3.2).

In Fig. 5.9, we eventually represented an elementary module of length

$$1_V = z(\operatorname{ctg} \theta + \operatorname{ctg} \alpha) = z(\lambda_c + \lambda_S)$$

which includes a tension bar and the concatenated compression strut. Such length is related to the maximum spacing between the transverse shear reinforcement bars.

Elementary Equilibrium Equations of the Model

Similarly to what has been presented in the introduction to this Sect. 5.1 for the tooth model of beams without shear reinforcement, elementary equilibriums can be

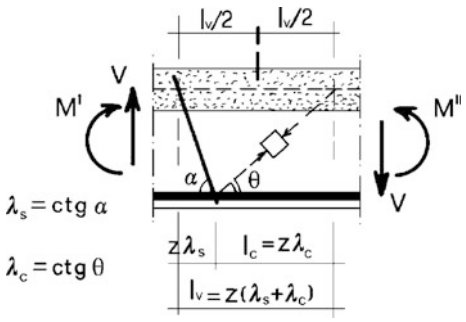


Fig. 5.9 Elementary module of the resistance mechanism

set also for the truss model, for the calculation of forces in the four types of elements that constitute it.

- *Tension chord*

$$Z_{\mathrm{Ed}} = \frac{M_{\mathrm{Ed}}}{z} + \frac{V_{\mathrm{Ed}}}{2}(\operatorname{ctg}\theta - \operatorname{ctg}\alpha) < A_{\mathrm{S}} f_{\mathrm{yd}}$$

- *Compression chord*

$$C_{\mathrm{Ed}} = \frac{M_{\mathrm{Ed}}}{z} - \frac{V_{\mathrm{Ed}}}{2}(\operatorname{ctg}\theta - \operatorname{ctg}\alpha) < b\bar{x} f_{\mathrm{Cd}} + A'_{\mathrm{S}} f_{\mathrm{yd}}$$

- *Diagonals in tension*
  (on a unit segment)

$$q'_{\mathrm{Ed}} = \frac{V_{\mathrm{Ed}}}{z} \frac{1}{(\operatorname{ctg}\theta + \operatorname{ctg}\alpha)\sin\alpha} < a_{\mathrm{w}} f_{\mathrm{yd}}$$

- *Diagonals in compression*
  (on a unit segment)

$$q''_{\mathrm{Ed}} = \frac{V_{\mathrm{Ed}}}{z} \frac{1}{(\operatorname{ctg}\theta + \operatorname{ctg}\alpha)\sin\theta} < b_{\mathrm{w}} f_{c2} \sin\theta$$

In the formulas written above, the components M_{Ed} and V_{Ed} of the applied force are expressed as absolute values. The other symbols are used with the usual meaning:

$b\bar{x}$	width and depth of the compression chord
b_{w}	web thickness
A_{s}	area of the longitudinal reinforcement in tension
A'_{s}	area of the longitudinal reinforcement in compression
$a_{\mathrm{w}} = A_{\mathrm{w}}/s$	unit area of the transverse reinforcement

having again indicated the competent material strengths with f_{yd}, f_{cd}, f_{c2}.

The calculation model is actually not isostatic and the geometric parameters $\overline{x}$, z and θ should be defined with the appropriate additional conditions:

$$A_S f_{yd} = b\overline{x} f_{cd} + A'_S f_{yd}$$

$$a_W f_{yd} \sin\alpha = b_W f_{c2} / \left(1 + \mathrm{ctg}^2\theta\right)$$

From these it is obtained for example (with $A'_s = 0$):

$$\overline{x} = A_S f_{yd} / b f_{cd}$$
$$z = d - \overline{x}/2$$
$$\mathrm{ctg}\,\theta = \sqrt{\frac{b_W f_{c2}}{a_W f_{yd} \sin\alpha} - 1}$$

If the elementary equilibrium relations written above are adopted for the structural design, an approximated estimation of the geometry is to be given, for example with

$$z \cong 0.9d$$
$$\overline{x} \cong 0.2d$$
$$\mathrm{ctg}\,\theta = \lambda_{max} = 2$$

subject to more rigorous further calculations.

In the final verifications, carried on the defined structural layout, the equivalent formulas can be directly used

$$M_{Ed} < M_{Rd} \quad \text{for sections } 'a'$$
$$V_{Ed} < V_{Rd} \quad \text{for sections } 'b'$$

as deduced in the previous chapters, with the additional rule of moment shifting, as described in Fig. 5.7. The application of this rule automatically fixes the superposition of reinforcement on sections '*c*', whereas for sections '*d*' with a change of shape or reinforcement, the same verifications on moment or shear or both should be repeated.

5.1.3 Standard Application Procedure

First, it is to be noted that the presence of transverse shear reinforcement highly enhances the shear behaviour of beams, reducing at the same time the benefit of the possible arch behaviour. Therefore, in this case there is no interest in a design

systematically based on a model similar to the one presented at Sect. 5.1.1 for beams without shear reinforcement. At most, certain local verifications might have to be added at the supports to the common verifications of the typical shear beam parts, according to what presented at Sect. 5.2.1.

Following the same criteria of the mentioned Sect. 5.1.1 on the arch behaviour, one can think of expressing in a adimesionalized form the shear resistance with (see Fig. 5.3):

$$\mu = \frac{V_{\mathrm{Rd}} 1}{M_{\mathrm{Rd}}}$$

In a situation of low reinforcement with $\lambda_r = \lambda_{max} = 2$, for the resistance in compression of the concrete of the web one obtains (with $b_w = b$)

$$V_{\mathrm{Rd}} = V_{\mathrm{cd}} = b\, z f_{c2}\, \lambda_r / \left(1 + \lambda_r^2\right) \cong 0.36 b\, d f_{c2}$$

which, with $f_{c2}/f_{cd} = 0.6$, leads to

$$\mu = \frac{0.36 b\, d f_{c2} 1}{0.2 b\, d f_{cd} z} = 1.08\lambda$$

This formula shows that even from $\lambda = 1$, therefore from the end of the first square beam segment, the compression-shear resistance is higher than the flexural one.

If calculated on the basis of the resistance of the stirrups, the capacity in tension-shear of the web members, with a reinforcement $a_w = 0.0015$b approximately corresponding to the minimum allowed by the criterion of non-brittleness (see Sect. 4.3.3), becomes

$$V_{\mathrm{Rd}} = V_{\mathrm{sd}} = a_{\mathrm{W}} \mathrm{z} f_{\mathrm{yd}} \lambda_r = 0.0027 b\, d f_{\mathrm{yd}}$$

which leads to

$$\mu = \frac{0.0027 b\, d f_{\mathrm{yd}} 1}{\rho_s b\, d f_{\mathrm{yd}} z} = \frac{0.0027}{\rho_s} \lambda$$

This formula shows an adimensional resistance increasing with the slenderness λ of the beam, with a gradient that decreases when the longitudinal reinforcement increases as indicated by the set of lines '*b*' of Fig. 5.10. In the same figure the intersection λ_I with the line '*a*' separates the domain of the high slenderness $(\lambda > \lambda_1)$, characterized by rupture due to bending moment, from the domain of the medium slenderness $(\lambda < \lambda_1)$, characterized by rupture due to tension-shear.

Concerning the arch behaviour, first it is noted that the capacity $\mu = 2\lambda/(1 + \lambda^2)$, deduced at Sect. 5.1.1 with reference to the scheme of Fig. 5.5, refers to the beams without transverse shear reinforcement. For those beams, the

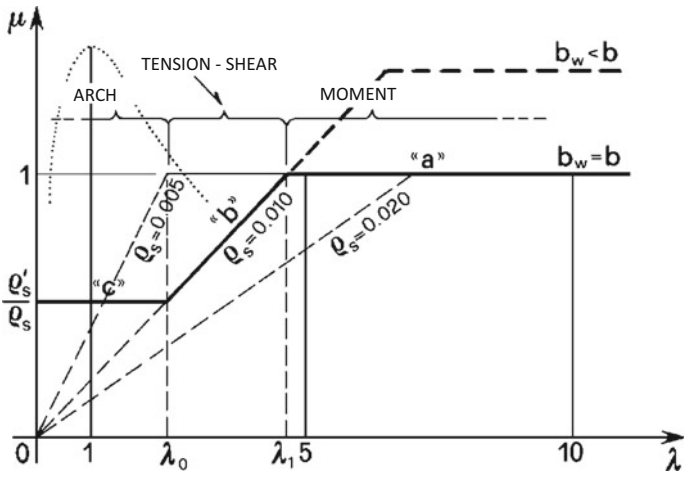


Fig. 5.10 Different domains of rupture of the beam

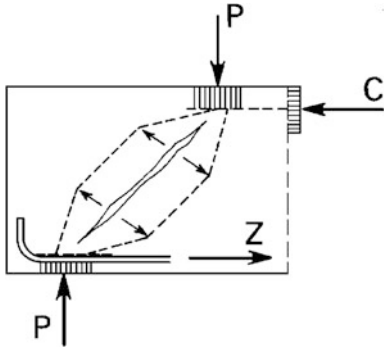


Fig. 5.11 Possible rupture mode of the end strut

compression resistance of the inclined strut is reduced by transverse tensions induced by the concentrated forces P in their diffusion on the beam web (see Fig. 5.11).

If adequate confining stirrups are present in the concrete web close to the support, opposing to the already mentioned transverse tensile stresses and to the possible inclined crack indicated in the scheme of Fig. 5.11, the resistance of the compression strut increases up to

$$\mu = c\frac{2\lambda}{1+\lambda^2}$$

with a coefficient which is experimentally quantified in $c \cong 1.5$.

The dotted curve of Fig. 5.10 indicates how high such resistance is and therefore how the lower capacity given by the resistance Z_R of the longitudinal tie is the limiting one in the arch behaviour.

If the flexural reinforcement of the beam was entirely brought up over the support, this latter capacity in the diagram of Fig. 5.10 would be given by the line $\mu = 1$ as extension of the segment '*a*'. One would therefore have continuity from the flexural behaviour of high slenderness values, up to one of tie-archs, which is the equivalent for low slenderness, excluding the shear behaviour.

If, as for the most common structural situations, just a quota of the longitudinal reinforcement is brought up over the support, with $\rho'_s/\rho_s < 1$ the local capacity of the tie-arch decreases to the level indicated in the same Fig. 5.10 by the segment '*c*'. Two domains are then distinguished: a domain $\lambda < \lambda_o$ of low slenderness, where the resistance of the tie is the limiting parameter, and a domain $\lambda_o < \lambda < \lambda_1$ of medium slenderness, where the resistance of the transverse shear reinforcement is the limiting parameter. The diagram eventually shows how, for T-shaped sections with $b_w < b$, the domain of tension-shear could be extended towards higher slenderness. At the beam ends, zones with tie-arch behaviour still remain, whose extent depends, as already mentioned, by the amount of longitudinal reinforcement brought to the support.

What anticipated above gives the qualitative indications about the failure behaviour of beams with shear reinforcement. The actual evaluation of the resistance, for both bending moment and shear, should be carried on the basis of the competent formulas, as deduced in the previous chapters. The arch behaviour is excluded from the *verifications of typical zones* '*B*' and reserved to the diffusion zones '*D*' close to the supports. This latter phenomenon, otherwise called 'effect of the decreasing inclination of longitudinal compressions' (see introduction to Sect. 4.3), can be implicitly taken into account *shifting the first section* '*b*' of shear verification, as described in details in Fig. 5.12. The amount of such shift, which actually depends on the ratio between transverse and longitudinal reinforcement, in the *standard procedure* is approximated to the inclination λ_c of the web struts.

Design Sections

With these specifications, the order of calculations in the practical design applications can be summarized as follows:

S*ections* '*a*'

of maximum moment for the proportioning of the longitudinal reinforcement and for the main bending moment verifications;

S*ections* '*b*'

of maximum shear and for the proportioning of the transverse reinforcement and for the main shear verifications;

S*ections* '*c*'

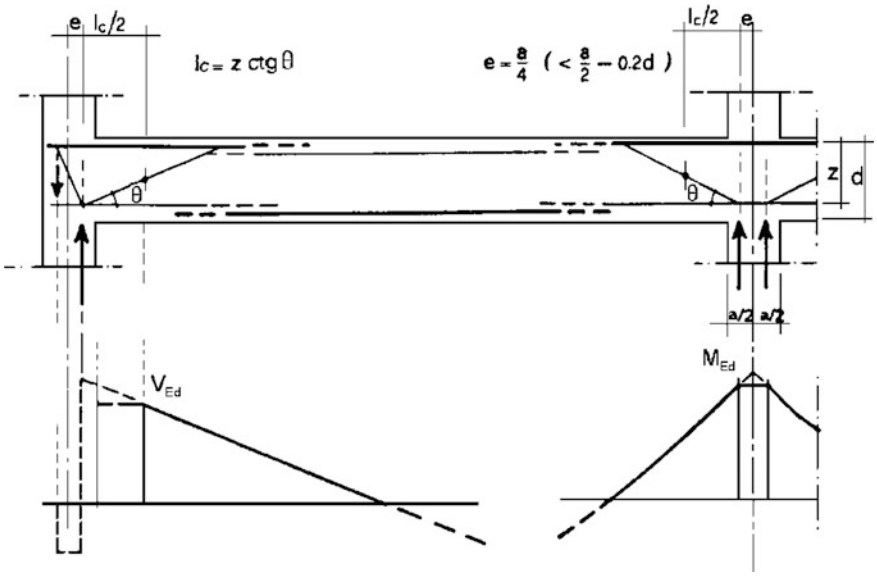


Fig. 5.12 Location of the critical sections for shear (*left*) and moment (*right*)

of zero moment for the definition of the lapping of the opposed longitudinal reinforcements or for the anchorage of bars at the simply supported ends;

S*ections* '*d*'

of discontinuity for the repetition of competent verifications and the anchorage of interrupted bars.

Steps of Proportioning and Verification

As already mentioned, the analysis of the sections '*c*' can simply be substituted by the usual *shifting of moments* showed in the traditional representation of Fig. 5.7 (bottom). For other types of sections, the design can be systematically carried in three coordinated steps:

Step 1: proportioning of the reinforcement with the approximate assumption of the necessary geometrical parameters ($z \cong 0.9d$ and $\lambda_c = 2$);
Step 2: verification with a more rigorous formula of the resistance as deduced from the proportioning carried before;
Step 3: additional calculation of stresses in the materials under serviceability loads for the necessary verifications of durability and cracking.

The *local verifications of details at the nodes* are to be added to the calculations listed above, equally important to ensure the safety of the structure.

5.2 Strut-and-Tie Balanced Schemes

The tooth and truss models presented in the previous section interpret with adequate reliability the behaviour of the current parts of the beam. Diffusion phenomena occur at the nodes, whose exact analysis would require the elaboration of complex algorithms. For a resistance calculation, such analysis can be substituted with the elementary one of isostatic mechanisms, consisting of concrete struts and steel ties, identified in the concerned zones according to appropriate criteria.

Figure 5.13 shows how in particular, for connection nodes of structural beam elements, two types of diffusion zones D can be identified:

- *transition zones* D_1

  through which one goes from the linear de Saint-Vénant behaviour 'M, V, N', to a bi-dimensional (or three-dimensional) diffusion behaviour;

- *discontinuity zones* D_2

  in which the stress diffusion involves a bi-dimensional (or three-dimensional) domain without predominant dimensions.

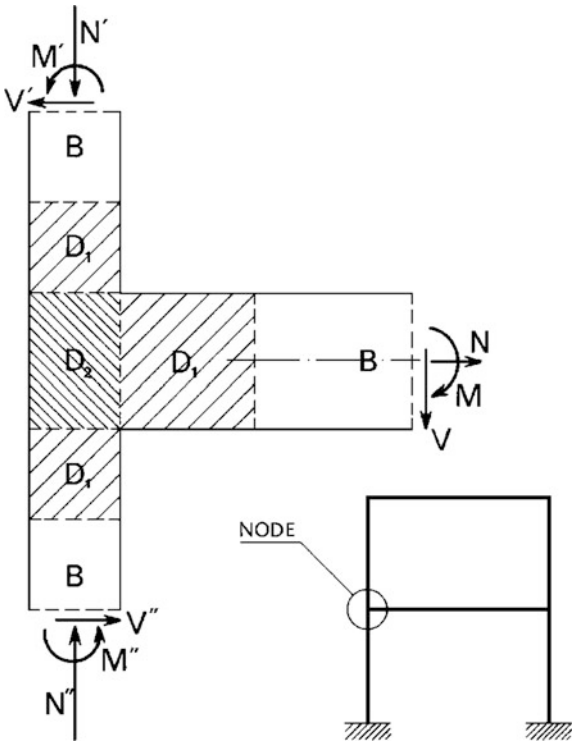


Fig. 5.13 Transition (D_1) and discontinuity (D_2) zones

The resistance of both types of zones can be verified on balanced schemes. In zone D_2 the web struts and ties arrange in a particular way based on each single case examined. In zone D_1 the web elements are already arranged towards the configuration of the current model of the relative slender element that comes from the node itself.

The three fundamental conditions to apply such procedure are as follows:

- the bars of the balanced scheme should be oriented with good approximation according to the *actual load paths* of the last elastic situations;
- steel should have *enough ductility* to allow, with its plastic strains, the adaptation of the real resisting mechanism towards the one assumed in the design scheme;
- concrete struts in compression should have a higher resistance than steel ties, so that the latter can yield without early brittle rupture of concrete.

An onerous bi- or three-dimensional analysis of the concerned node in order to derive the orientation to be given to the elements of the simplified model is obviously not possible. Therefore, the procedure can be effectively applied only to those common and recurrent cases of nodes, for which the type of structural behaviour and the plausible load paths are already known.

Under the above-mentioned conditions of load path, ductility and over-resistance, the possibility to *superimpose different and simultaneous mechanisms* is also valid, meaning that the capacity of the node can be evaluated with an appropriate summation of one of the single resisting mechanisms acting in parallel.

In the following paragraph, various examples of the application of the simplified procedure described above will be shown which, as already mentioned, respects the equilibrium in the resisting ultimate situation. However, no information is given on the deformation compatibility in the situations in service, for which the procedure itself should be integrated with appropriate construction requirements, especially in order to ensure an effective resistance against the possible concrete cracking.

Effective Dimensions

Another important aspect of the diffusion problem in beams concerns the diffusion of stresses within the concrete starting from the section with zero moment. The case of ribs in bending is shown in Fig. 5.14, which, together with the top compression flange, form beams with a T-section.

The diffusion of the end reaction of a rib is schematically shown in the mentioned figure, first in the web and then in the flange. It is clear how every calculation that involves the diffusion of compressions in the concrete of the web should refer to a resisting width $b = b_w$ corresponding to the width of the web itself. Starting from the onset at the top flange, an orthogonal diffusion of compressions also occurs, involving up to the entire available width $b = b_f$ of the flange. Beyond the limit of complete diffusion of stresses, the verifications (e.g. for bending moment) can therefore be referred to the entire T-shaped section.

A *conventional model of diffusion* which assumes a 1/1 slope (45° angle) is indicated in Fig. 5.15. Starting from the point O, where, according to the

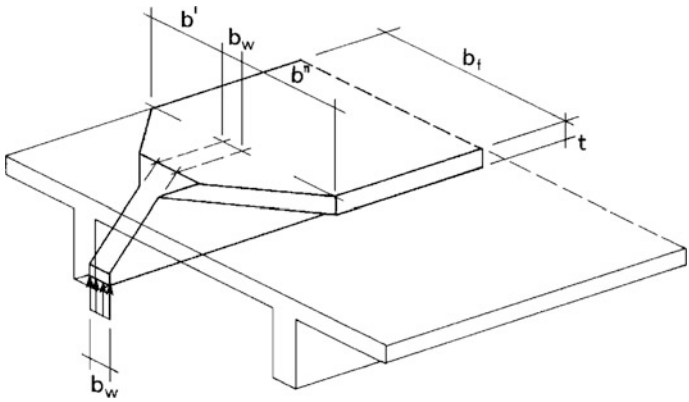


Fig. 5.14 Diffusion of stresses on web and flange

mechanisms further analyzed later on, the support reaction is deviated in the web, the resisting depth d_x increases linearly with the distance x from the support, whereas the width remains fixed in b_w. Section *1* located at y (=$d - t$) from the support is the last one with a rectangular shape; from there the diffusion in the flange starts and the shape becomes a T with variable flange width b_x and thickness t_x.

The section *2* located at the distance d from the support is the first one affected by the stresses for the entire height: it corresponds approximately to the beginning of the current beam part to be verified under the components M, V, N of the internal force. Its *effective dimensions* are:

$$\begin{aligned} d_x &= d && \text{effective depth} \\ b_x &= b_w + 2t && \text{effective width} \end{aligned}$$

Beyond section *2*, the effective width of the flange keeps increasing with

$$b_x = b_W + 2(x - y)$$

up to its maximum value equal to

$$b_x = b_f = b' + b_W + b''$$

where b', b'' correspond to either the distance from the free edge or the half distance from the adjacent beam. Section *3* is therefore the first one with a complete T-shape which, in the model of Fig. 5.15, remains constant up to the opposite deviation of the web compressions.

The model is obviously approximated and it should be adapted in terms of dimensions to the specific geometry of every single case, especially in order to follow the design resisting schemes of Figs. 5.2e and 5.7. Traditionally, it is also a common practice to adopt certain conservative criteria, such as limiting the extent

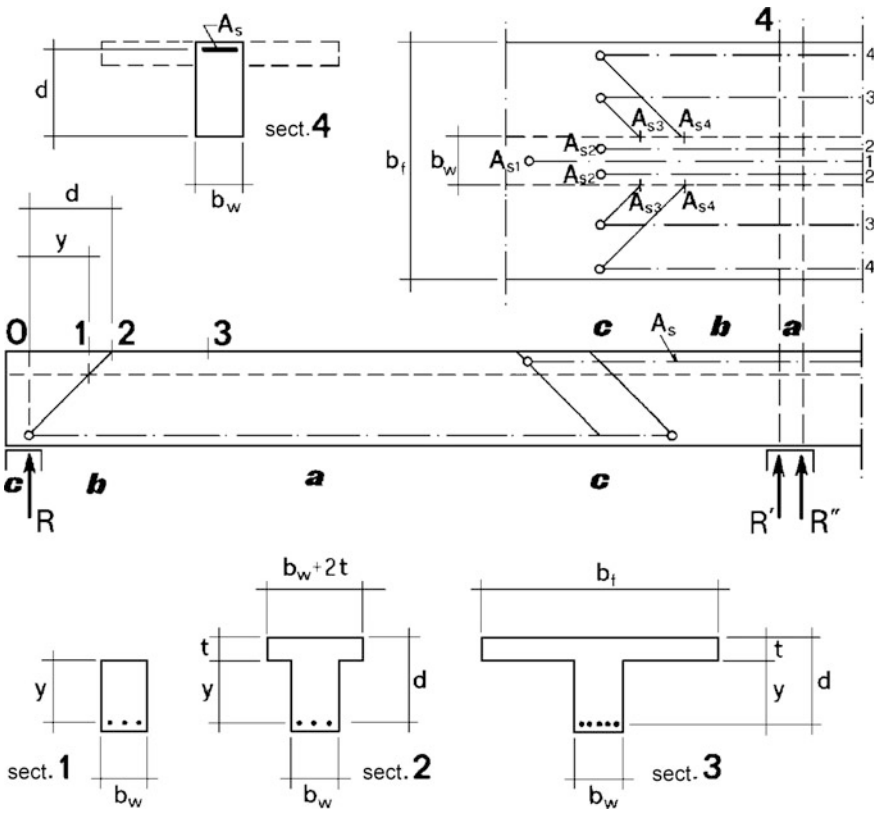


Fig. 5.15 Conventional model of stress diffusion

of the effective flange as a function of the thickness of the flange itself (for example with $b' \leq 5t$, $b'' \leq 5t$).

Again in Fig. 5.15 the diffusion model for positive moments terminates in the subsequent section '*c*' with null moment, symmetrically with respect to the section '*a*' of maximum moment. It has been assumed that the second section '*c*' is located within the relative span of the continuous beam. At its location, tensions and compressions of the chords exchange position and the upper flange of the beam becomes in tension.

In the detail in plan of the concerned figure, it is indicated how a diffusion mechanism also occurs for possible tension reinforcement located outside the web. With the same 1/1 inclination adopted for compressions, the length of the bars in the flange should be increased by an extent equal to their distance to the web. This in addition to what derives from the rule of moment shifting for the reinforcement located within the web thickness.

The diffusion model of the effective dimensions described above neglects several effects, such as the ones related to the amount and inclination of transverse

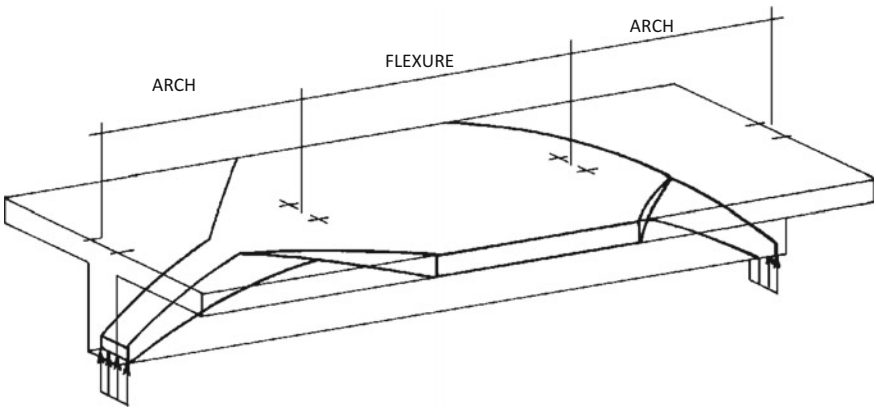


Fig. 5.16 Lateral arch behaviour in the beam web

reinforcement. However, it can constitute a valid reference, although approximated, provided that integrative appropriate design criteria are observed. For the diffusion of stresses in the flange, for example, a good transverse confinement of the concrete should be ensured, either with appropriate transverse reinforcement or with a global restraint of the slab with continuous peripheral ties. For the case of flanges without reinforcement, appropriate modifications should be assumed with more conservative estimations of the parameter of the model. A smaller diffusion angle could be assumed for example, with an inclination brought to 2/3 (= 34°).

Eventually it is to be noted that the arch behaviour, extended to the entire spans of the beam, similar to the ones represented in Fig. 5.6, is not compatible with the collaboration of protruding flanges. One can only rely on the arch behaviour of the lateral segments close to the supports, leaving a central part with full depth current behaviour of the beam, whose extent is sufficient for the diffusion of compression in the flange (see Fig. 5.16).

5.2.1 Support Details

Within the domain of beams in bending described in the current chapter, the main node is represented by the zones located on the supports. It can be the case of simple end or continuity supports or supports that offer also a degree of rotational restraint.

Beams Without Shear Reinforcement

We refer to the tooth model described in Fig. 5.2, for which it is implied that the current parts are designed according to the methods previously recalled. Local verifications are to be added for zones D_1, which in the model are identified in the

first 'square' segment of length z equal to the lever arm of the internal couple ($\cong 0.9d$).

Leaving out the arch behaviour, for which the end segments are also included in its global behaviour, the first web strut, where the support reaction is diverted, is inclined at 45° similar to the teeth of the contiguous tooth behaviour. The difference consists in the force mainly in compression, whereas the teeth of the current part are mainly under bending (by longitudinal shear).

Normally there are not particular problems for the verification of the first concrete segment, thanks to its good compressive strength, whereas the contiguous internal segment has to relay on the lower tensile strength of concrete. The analysis of the support is needed mainly to verify the resistance of the longitudinal reinforcement that reaches it, as well as its adequate anchorage beyond the axis of the support itself. Here, in fact the longitudinal tie and the inclined strut of the web have to exchange stresses by bond.

Three possible solutions are shown in Fig. 5.17. The first one corresponds to what follows, without bent bars, from the rule of moment shifting, where the reaction R is balanced by a tension force $Z = R$ in the longitudinal bars and by a compression force $S_c = \sqrt{2}R$ in the web strut (see Fig. 5.17a). With the formula of the arch behaviour, to the latter force (with $\theta = 45°$) corresponds a capacity:

$$R_{Rc} = 0.4b\,d\,f_{cd}\sin^2\theta = 0.2b\,d\,f_{cd}$$

whereas based on the reinforcement resistance one has

$$R_{Rs} = A_s f_{yd}/\mathrm{ctg}\,\theta = A_s f_{yd}$$

For the local verification at the support, one should have

$$R_{Rs} \geq R_{Ed} \quad R_{Rc} \geq \gamma_R R_{Rs}$$

where γ_R is the factor that covers the possible higher steel strength with respect to the nominal value used in the design.

The alternative solution described in Fig. 5.17c contemplates the use of the bent bars right on the support. In this case the equilibrium with the reaction R, brought to the upper node by $S_c = R$, gives a tension force $S_s = R/\sin\alpha = \sqrt{2}R$ in the bar and a compression force $C = R\mathrm{ctg}\,\alpha = R$ in the concrete chord. Based on the resistance of the latter, one therefore has a capacity

$$R_{Rc} \cong 0.2d\,b f_{cd}$$

corresponding to the flexural capacity of the section with moment $M = Rz$, whereas based on the resistance of the vertical strut, conventionally applying the same formula of the arch behaviour with $\sin^2\theta = 1(\theta = 90°)$, a value $0.4\mathrm{dbf}_{cd}$ doubled with respect to the previous one would be obtained. With reference to the resistance of the bent bar, one has instead

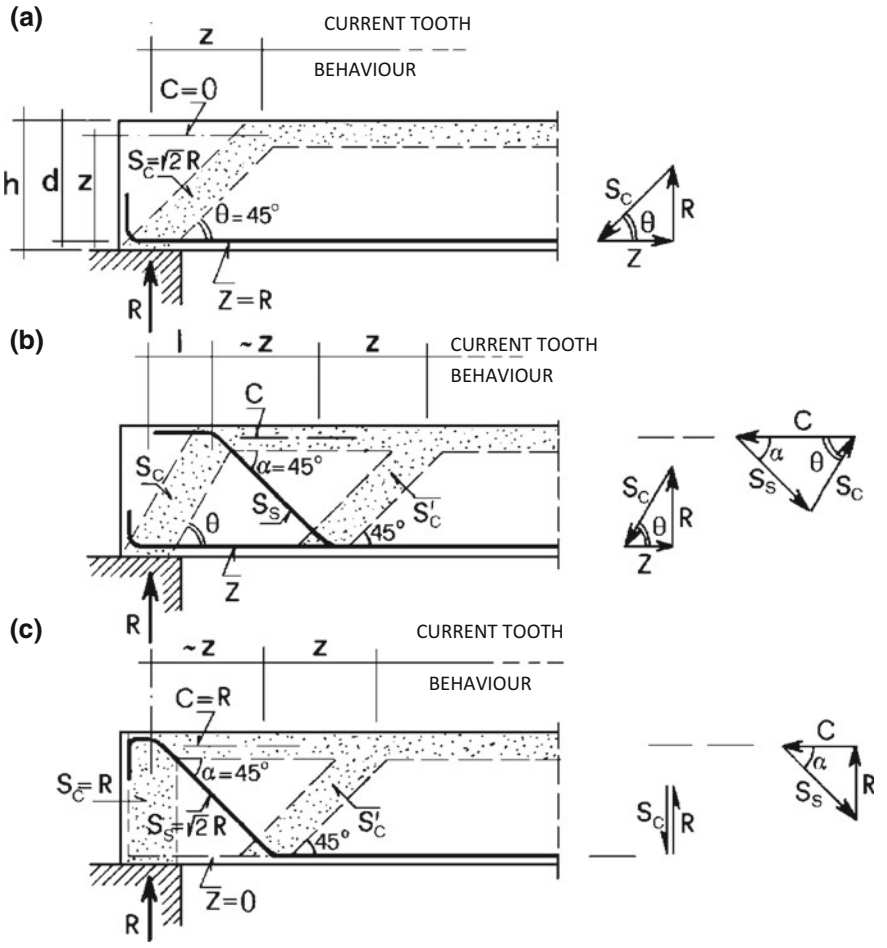


Fig. 5.17 Possible different details over the end support

$$R_{\mathrm{Rs}} = A_{\mathrm{s}} f_{\mathrm{yd}} \sin\alpha \quad \left(= A_{\mathrm{s}} f_{\mathrm{yd}} \Big/ \sqrt{2} \,\mathrm{per}\, \alpha = 45^{\circ}\right)$$

For the local verification, one should also have

$$R_{\mathrm{Rs}} \geq R_{\mathrm{Ed}} \quad R_{\mathrm{Rc}} \geq \gamma_{\mathrm{R}} R_{\mathrm{Rs}}$$

From the mentioned Fig. 5.17c it can be noted how, with the use of the bent bar, the beginning of the current tooth behaviour is shifted inwards, where the value of the shear force is somewhat decreased. Such solution can therefore be used to extend the end zone with web concrete in compression, and to enhance in this way the overall shear resistance of the beam.

For a good behaviour in service, the edge in tension of the last beam segment cannot be left without longitudinal reinforcement, even though the force Z in the ultimate resisting mechanism is equal to zero. Therefore, the solution of Fig. 5.17c should always be integrated with the one of Fig. 5.17a.

For combined mechanisms with longitudinal reinforcement and bent bars, the resistance can be calculated adding up the elementary contributions mentioned above. Indicating for example with A_{sl} the area of the longitudinal reinforcement and with A_{st} the one of the bent bars over the support, the resisting value of the reaction becomes:

$$R_{Rd} = R'_{Rs} + R''_{Rs} = A_{sl} f_{yd} + A_{st} f_{yd} \Big/ \sqrt{2}$$

For the web strut it should result:

$$R'_{Rc} = 0.2 d\, b f_{cd} \geq \gamma_R R'_{Rs}$$

while for the compression chord it should result:

$$R''_{Rc} = 0.2 d\, b f_{cd} \geq \gamma_R R''_{Rs}$$

It can be noted that the combined solution also allows to share the force on the concrete between web and chord, increasing in this way the capacity of the support. Conservative rules limit the use of bent bars, for example with $R'_{Rs} \geq 0.5 R_{Rd}$.

A further shifting of the beginning of the current tooth behaviour inwards is obtained with the intermediate solution of Fig. 5.17b, which leaves the bent bar at a distance $l < z$ from the support. The equilibrium at the bottom node leads to a tension force $Z = R\lambda$ in the longitudinal reinforcement, with $\lambda = l/z$, and to a compression force $S_c = R/\sin\theta$ in the strut of the web. With the same formulas of the arch behaviour, the following capacity values correspond to those forces:

$$R'_{Rs} = A_{sl} f_{yd} / \lambda$$
$$R'_{Rc} = 0.4 d\, b f_{cd} \sin^2\theta = 0.4 d\, b f_{cd} / \left(1 + \lambda^2\right)$$

Brought to the upper node, the force S_c gives a tension force $S_s = R/\sin\alpha = \sqrt{2}R$ in the bent bar and a compression $C = (\mathrm{ctg}\,\alpha + \mathrm{ctg}\,\theta)R = (1+\lambda)R$ in the concrete chord. Based on the resistance of the bent bar and the concrete compression chord, one has the capacity values:

$$R''_{Rs} = A_{st} f_{yd} \sin\alpha \quad \left(= A_{st} f_{yd} \Big/ \sqrt{2} \text{ per } \alpha = 45^\circ\right)$$
$$R''_{Rc} = 0.2 d\, b f_{cd} / (1 + \lambda)$$

It can be noted how this intermediate solution allows, similar to the combined one, to increase the capacity of the support. The verification of its resistance will therefore be

$$R'_{Rs} \geq R_{Ed} \quad R'_{Rc} \geq \gamma_R R'_{Rs}$$
$$R''_{Rs} \geq R_{Ed} \quad R''_{Rc} \geq \gamma_R R''_{Rs}$$

Similar resisting schemes occur at the continuity support, as shown in Fig. 5.18. With reference to the beam web, the same formulas for the resistance verification are used, referred to the segment on the left side (with R'_{Ed}) as well as to the one on the right side (with R''_{Ed}), with the respective thicknesses b and reinforcement A_s. Concerning the tension and compression chords, their verification is already included in the one for bending moment that they are committed to transfer.

Half Joints

A common type of support consists of the so-called *half joints* (see Fig. 5.19), which are kept within the current depth of a beam supported by the cantilevering part of a main beam. The construction details of the node are similar to the one of the support of Fig. 5.17, with the necessary adjustments for the force transfer from the zone of discontinuity of reduced depth to the transitional one of full depth.

Therefore, in the first solution (see Fig. 5.19a) the reaction R is taken by the horizontal tension force Z' in the reinforcement A'_s and by the inclined compression

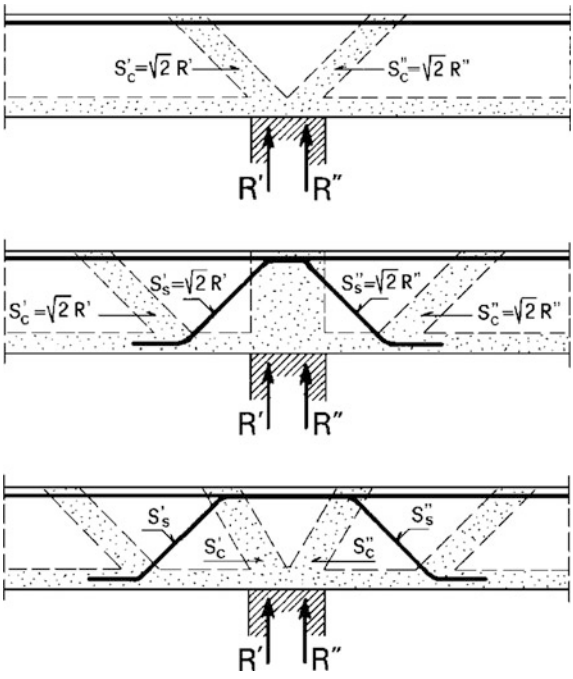


Fig. 5.18 Possible different details over the internal support

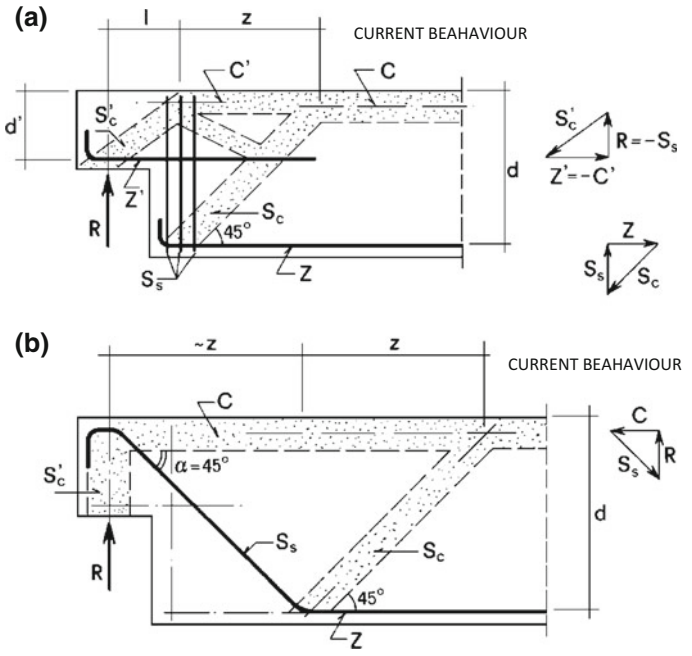


Fig. 5.19 Possible different details of half joints

S'_c in the concrete. The inclination $\lambda = l/z'$ of the latter depends on the geometry of the node. When reaching the top face, the compression itself is deviated to the horizontal direction thanks to the hanging force S_s of the vertical reinforcement A_v. At the bottom face this reinforcement resists the inclined flux S_c of web compressions, balanced by the horizontal force Z of the main tension reinforcement A_s of the beam.

In the second solution, the reaction R is brought to the top and it is balanced by the compression C of the concrete chord and by the tension S_s of the bent bar. The latter brings the force directly to the full depth behaviour of the beam. Similar to the previous one, Fig. 5.19b also includes the triangle of forces of the relative equilibrium.

For a good behaviour in service it is not possible to leave the bottom faces of the joint without reinforcement. The solution of Fig. 5.19b will, therefore, always have to be integrated with one of Fig. 5.19a, to which a quota at least equal to 0.50 of the total reaction should be assigned.

The verifications are therefore set with the formulas:

Solution a $(\lambda = l/0.9d')$

$$R'_{\mathrm{Rs}} = A'_{\mathrm{s}} f_{\mathrm{yd}} / \lambda \geq R_{\mathrm{Ed}}$$
$$R'_{\mathrm{Rc}} = 0.4\mathrm{bd}' f_{\mathrm{cd}} / \left(1 + \lambda^2\right) \geq \gamma_R R'_{\mathrm{Rs}}$$
$$R''_{\mathrm{Rs}} = \min\left(A_V f_{\mathrm{yd}}, A_{\mathrm{S}} f_{\mathrm{yd}}\right)$$
$$R_{\mathrm{Rc}} = 0.2 b\, d\, f_{\mathrm{cd}} \geq \gamma_{\mathrm{R}} R'_{\mathrm{Rs}}$$

Solution b (with $\alpha = 45^{\circ}$)

$$R_{\mathrm{Rs}} = A_{\mathrm{s}} f_{\mathrm{yd}} / \sqrt{2}$$
$$R_{\mathrm{Rc}} = 0.2 b\, d\, f_{\mathrm{cd}} \geq \gamma_R R_{\mathrm{Rs}}$$

or, with the ones of the combined solution, obtained with the appropriate superposition of capacities, similar to what done for the combination of mechanisms of Fig. 5.17a–c.

Beams with Shear Reinforcement

The presence of stirrups, other than confining the concrete of the web enhancing its resistance, allows a more rapid diffusion of stresses over the depth of the beam. An end support is shown in Fig. 5.20a similar to the one of Fig. 5.17a. From the footprint of the support, the reaction diffuses with fan-shaped compression lines inside the web of the beam. At the end of the transition zone the orientation stabilizes according to the inclination λ_c = ctg θ proper of the current behaviour of the internal part of the beam.

For the calculation of the capacity of the support, the same equilibrium of forces of the case without stirrups of Fig. 5.17a can be set, based on an average inclination of compressions in the web. With $\lambda_o = \lambda_c/2$ one obtains

$$R_{\mathrm{Rs}} = A_{\mathrm{s}} f_{\mathrm{yd}} / \lambda_{\mathrm{o}} \geq R_{\mathrm{Ed}}$$
$$R_{\mathrm{Rc}} = 0.6 b\, d\, f_{\mathrm{cd}} / \left(1 + \lambda_{\mathrm{o}}^2\right) \geq \gamma_{\mathrm{R}} R_{\mathrm{Rs}}$$

The enhancing factor c = 1.5 due to the confinement of stirrups has already been included in the numerical coefficient of the formula related to the resistance of the concrete of the web. The formula related to the resistance of the longitudinal reinforcement coincides with what is expected by the rule of moment shifting of Sect. 4.3.2 (with vertical stirrups: $\lambda_s = 0$).

Given that the inclination of compressions in the contiguous current beam part depends on the amount of transverse shear reinforcement, with $\lambda_c = \sqrt{(1 - \omega_{\mathrm{W}})/\omega_{\mathrm{W}}}$ within the limits $\lambda_I < \lambda_c < \lambda_{max}$, the design of stirrups affects the capacity of the support. Within the domain of low shear reinforcement with $\lambda_c = \lambda_{max} = 2.5$ one has for example:

$$R_{\mathrm{Rs}} = A_{\mathrm{s}} f_{\mathrm{yd}} \geq R_{\mathrm{Ed}}$$
$$R_{\mathrm{Rc}} = 0.23 b\, d f_{\mathrm{cd}} \geq \gamma_{\mathrm{R}} R_{\mathrm{Rs}}$$

Within the domain of high reinforcement with $\lambda_{\mathrm{c}} = \lambda_{\mathrm{I}} = 1$ one has:

$$R_{\mathrm{Rs}} = 2A_{\mathrm{s}} f_{\mathrm{yd}} \geq R_{\mathrm{Ed}}$$
$$R_{\mathrm{Rc}} = 0.48 b\, d f_{\mathrm{cd}} \geq \gamma_{\mathrm{R}} R_{\mathrm{Rs}}$$

The resistance of stirrups is, however, calculated with the appropriate shear verification of the section '*b*' located at the limit $l_c/2$ of the transition zone.

The use of bent bars within the zone $0 \leq l < l_c/2$ (v. Figure 5.20b) leads to formulas similar to the ones of the case of Fig. 5.17b. However, being the case of beams with shear reinforcement, stirrups are always also present. The capacity of the support should, therefore, be calculated with the superposition of two mechanisms in parallel, one that starts with a strut inclined by $\lambda = l/z$ on the bent bar, the other that starts with a strut inclined by $\lambda_{\mathrm{o}} = \lambda_{\mathrm{c}}/2$ on the first stirrups of the beam.

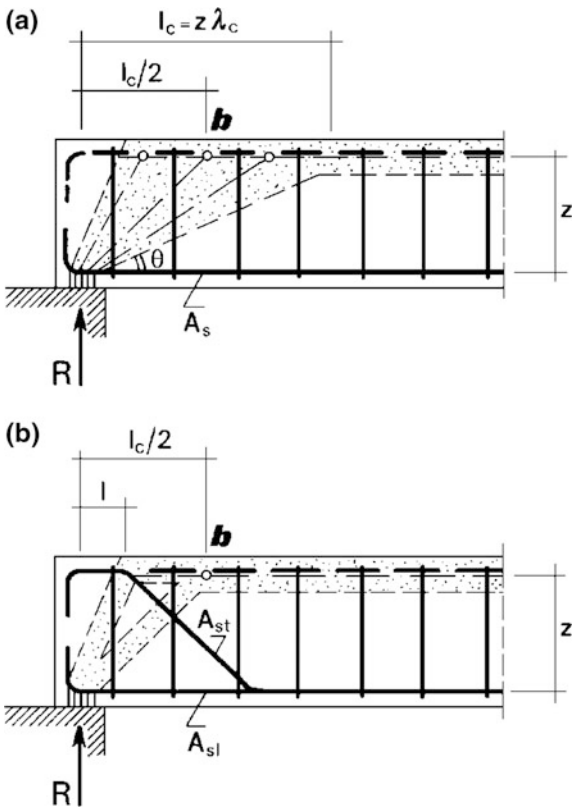


Fig. 5.20 Possible different details over the end support

For this calculation, a criterion can be adopted that assigns the quota of the reaction compatible with the resistance of the bent bar A_{st} (also limited to $0.5R_{Ed}$) to the first mechanism:

$$R'_{Rs} = A_{st} f_{yd} \sin \alpha \quad \left(= A_{st} f_{yd} \Big/ \sqrt{2} \text{ per } \alpha = 45^\circ \right)$$

and reserve the remaining action

$$R_{od} = R_{Ed} - R'_{Rs} \quad (\geq 0.5 R_{Ed})$$

to the second mechanism based on the resistance of the stirrups. For the other bars of the model, that is, for the concrete of the web and the longitudinal reinforcement A_{sl}, a resistance calculation can be carried weighting the effects of the two different inclinations with

$$\alpha_o = R_{od}/R_{Ed}$$
$$\alpha' = 1 - \alpha_o$$

For the verification one can therefore set:

$$R_{Rs} = \frac{A_{sl} f_{yd}}{\alpha_o \lambda_o + \alpha' \lambda} \geq R_{Ed}$$
$$R_{Rc} \approx \frac{0.6 b\, d\, f_{cd}}{\alpha_o \left(1 + \lambda_o^2\right) + \alpha' \left(1 + \lambda^2\right)} \geq \gamma_R R_{Rs}$$

with approximation of summing up algebraically in the web compressions that are not parallel.

The same formulas for the verification of the web of the beam (concrete struts and possible bent bars) are also used for the diffusion zones of the beam at the sides of the continuity supports, with the respective part of the reaction, similar to what indicated in Fig. 5.18. The tension and compression chords are instead verified on the type '*a*' section with reference to the maximum moment (negative) that they have to transfer.

Indirect Supports

The case of indirect supports of secondary beams on the main beam that transfers the loads to the vertical supports is shown in Fig. 5.21. The position of the action transferred to the contiguous discontinuity zone of the main beams depends on the type of solution adopted in the transition zone of the secondary beam (see Fig. 5.21a). The solution 1, with bent bars designed for the entire support reaction, allows to place the action on the top of the main beam. From there the action can diffuse with fan-shaped lines of compressions and then return to the current behaviour of the truss mechanism.

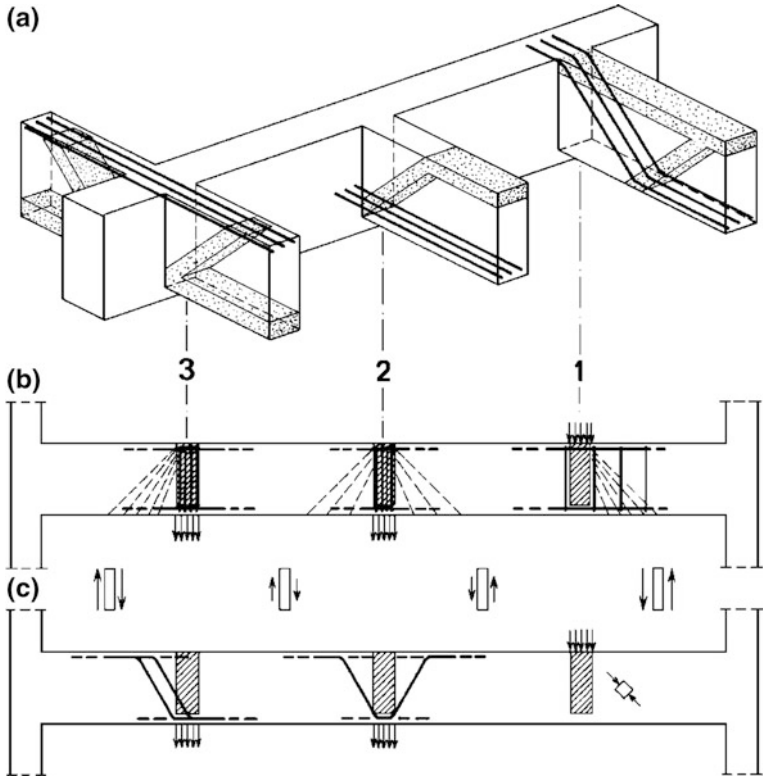


Fig. 5.21 Details of indirect supports

In the supports that do not make use of bent bars instead, the reaction concentrates in the inclined concrete strut of the secondary beam. In this case the vertical action on the main beam is applied at its bottom and has to be hung with appropriate reinforcement. Closely spaced stirrups can be used that, bringing the load to the top of the main beam, allow the subsequent fan-shaped diffusion of the compressions on the resisting mechanism (see Fig. 5.21b). Bent bars that receive the support action of the secondary beam from below can also be used (see Fig. 5.21c).

Bent bars shall be placed on the side where the bearing action of the main beam comes from. For the support 3 for example, where the shear is oriented clockwise, the bars should be placed on the left side. For the mid-span support 2, corresponding to the change of shear orientation (from clockwise to counterclockwise) the support of the action comes from both sides and the hangers should be placed symmetrically.

5.2.2 Corbels and Deep Beams

The problem of *corbels*, where the resisting mechanisms can be analyzed with the formulas deduced for the arch behaviour, is similar to the one of the support details of beams discussed at the previous paragraph. Figure 5.22a shows the scheme with longitudinal tie and inclined strut for which one has, with $\lambda = l/z$ and $z \cong 0.9d$, a resisting force:

$$P_{Rs} = A_s f_{yd} \frac{1}{\lambda}$$

if related to the longitudinal reinforcement, one has a resisting force:

$$P_{Rc} \cong 0.4 d\, b f_{cd} \frac{c}{1+\lambda^2}$$

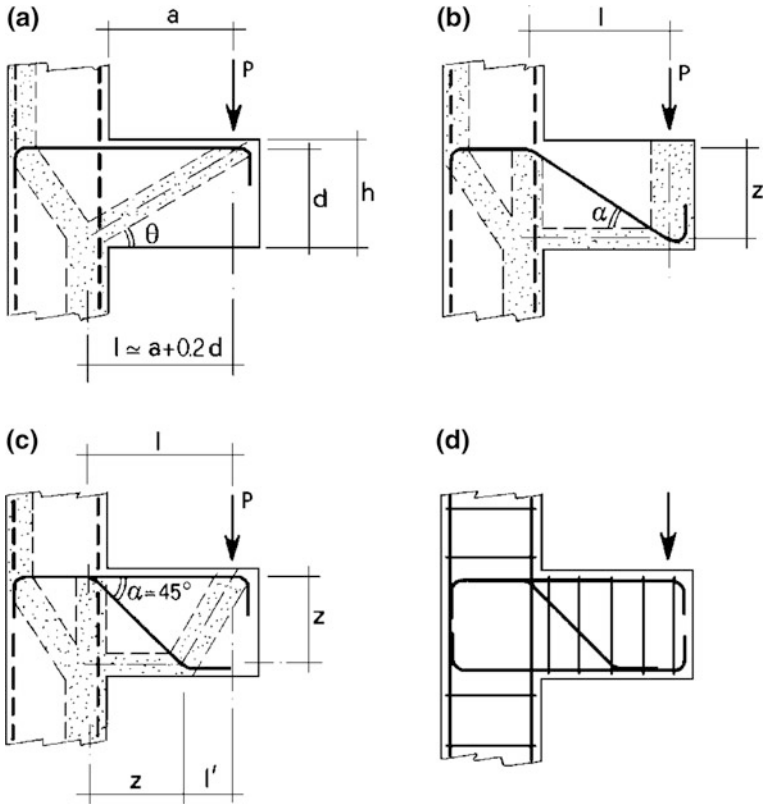


Fig. 5.22 Possible different details of corbels

if related to the web concrete of the corbel. In the latter formula one shall assume c = 1 for cantilevering slabs without stirrups, c = 1.5 for cantilevering beams which have at least a minimum shear reinforcement.

The solution that uses a bent bar at an angle α on the horizontal is shown in Fig. 5.22b. With $\lambda = l/z = \text{ctg}\,\alpha$, one has a resisting force:

$$P_{\text{Rs}} = A_{\text{st}} f_{\text{yd}} \sin\alpha = A_{\text{st}} f_{\text{yd}} \frac{1}{\sqrt{1+\lambda^2}}$$

if related to the bent bar, one has a resisting force:

$$P_{\text{Rc}} \cong 0.2 d\, b f_{\text{cd}} \frac{1}{\lambda}$$

if related to the concrete chord. It is to be noted that, similar to the overturned detail of Fig. 5.17c, this solution should necessarily be integrated with the previous one to which at least 0.5 of the total load should be assigned.

For the solution of Fig. 5.22c, with $l' < z$ and $\lambda' = l'/z$, the resisting force is eventually given by the lesser of the two values that, respectively, refer to the resistance of the longitudinal reinforcement and the resistance of the bent bar:

$$P'_{\text{Rs}} = A_{\text{s}1} f_{\text{yd}} \frac{1}{\lambda'} \quad P''_{\text{Rs}} = A_{\text{st}} f_{\text{yd}} \frac{1}{\sqrt{2}}$$
$$P_{\text{Rs}} = \min\left(P'_{\text{Rs}}, P''_{\text{Rs}}\right) \geq R_{\text{Ed}}$$

where it should also result

$$P_{\text{Rc}} \cong 0.2 d\, b f_{\text{cd}} \frac{1}{\lambda} \geq \gamma_{\text{R}} R_{\text{Rs}} \quad (\text{con } \lambda = 1/z)$$

The verification of the isostatic truss scheme made of struts and ties refers to the ultimate resistance of the corbel. The reinforcement will have to be further supplemented for the service behaviour with the addition of stirrups and the relative longitudinal hanger bars in the compression zone, necessary to complete the steel cage (see Fig. 5.22d). The stirrups, added to the longitudinal reinforcement, also offer a resistance contribution, enhancing the one of the concrete of the web.

Lintels

Another important case of deep beams concerns the lintels of the corewalls of buildings. Following a common structural solution, the box wall system of the staircase, present in multi-storey buildings, is used to resist horizontal actions such as wind or seismic actions. The need for openings for doors or windows through such walls weakens their resistance and requires, in order to rely on the collaboration of the stud walls with the resisting actions distributed along the entire effective width L (see Fig. 5.23), the use of connecting lintels for the transfer of the longitudinal shear force Q form one side of the system to the other. Magnitude and

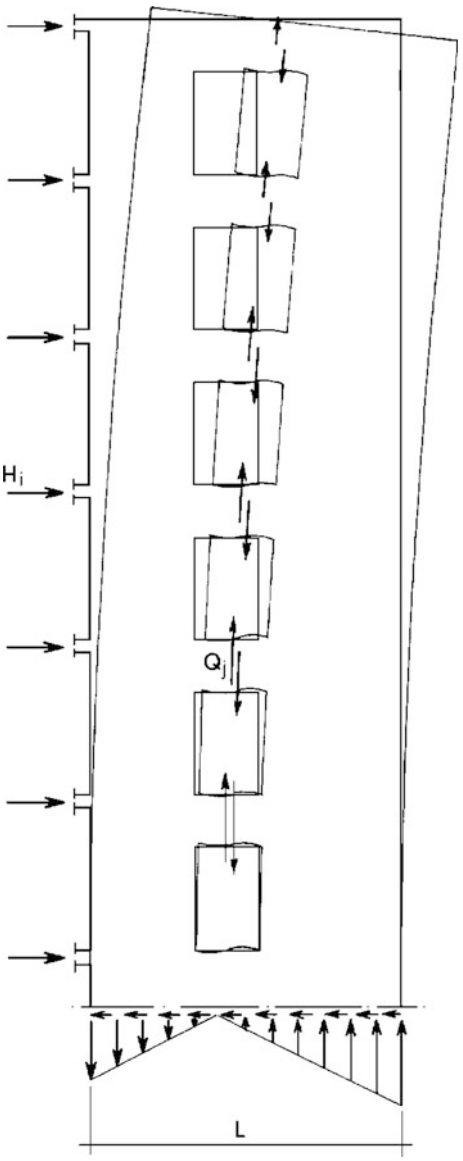


Fig. 5.23 Behaviour of the corewall of a multi-storey building

position of shear forces Q_j in the lintels depend, other than the applied forces H_i, also on the relative stiffnesses of the different parts of the structural system.

Let us therefore assume that the action on the examined lintel consists of the force Q located at a distance e from the mid-span. Figure 5.24 shows this force and the approximations with which one can assume the main geometrical parameters related to the resistance of the lintel, such as the lever arm z and the distance l between constraining points.

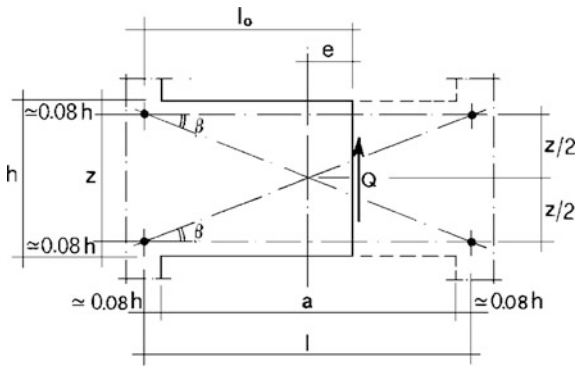


Fig. 5.24 Geometrical parameters of the lintel model

The possible resisting schemes are represented in Fig. 5.25. The first one is based on the longitudinal reinforcement to resist the tension forces S'_s and S''_s. The equilibrium is completed by the flux of compressions Q_c that crosses the concrete web with an inclination β.

One has three equilibrium equations (see Fig. 5.25a):

$$\begin{cases} S_{ch} - S'_s - S''_s = 0 \\ S_{cv} = Q \qquad (S_{ch} = \lambda S_{cv} = \lambda Q) \\ S'_s \dfrac{z}{2} - S''_s \dfrac{z}{2} = -\mathrm{Qe} \end{cases}$$

with

$$\lambda = \operatorname{ctg} \beta = l/z$$

from which one can derive:

$$S'_s = \left(\frac{\lambda}{2} - \frac{e}{z}\right) Q$$

$$S''_s = \left(\frac{\lambda}{2} + \frac{e}{z}\right) Q$$

For the particular cases of $e = 0$ and $e = l/2$ one has respectively:

$$S'_s = S''_s = \frac{\lambda}{2} Q$$

and

$$S'_s = 0 \quad S''_s = \lambda Q$$

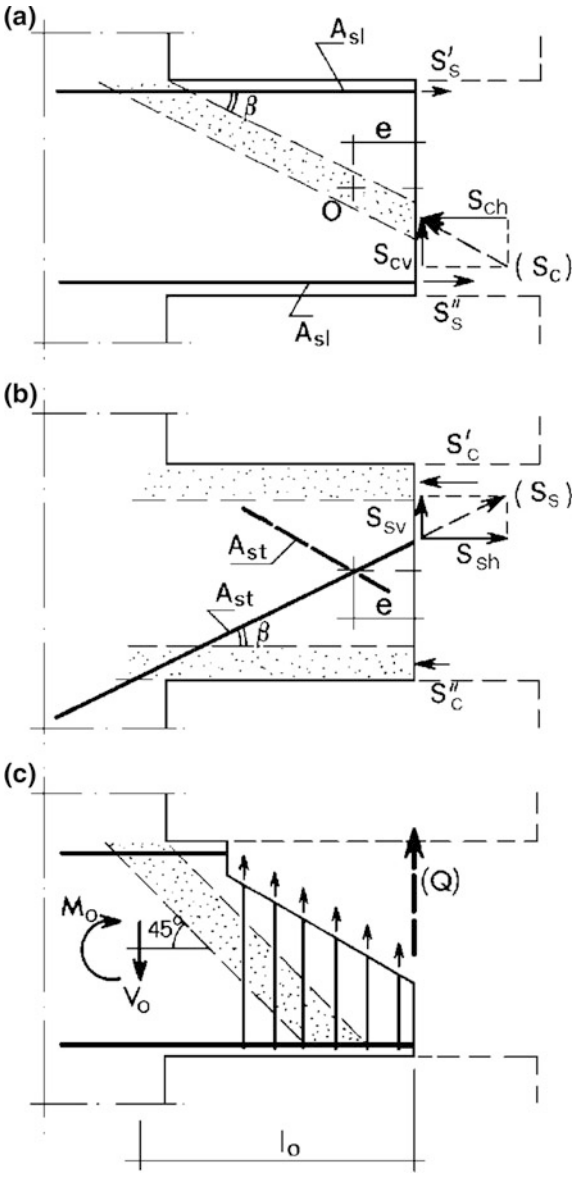


Fig. 5.25 Resisting schemes of the lintel

which correspond to the antisymmetric situation of Fig. 5.26a with lateral walls of the same stiffness and to the situation of fix and pinned ends of Fig. 5.26b with a much lower stiffness of the second stud.

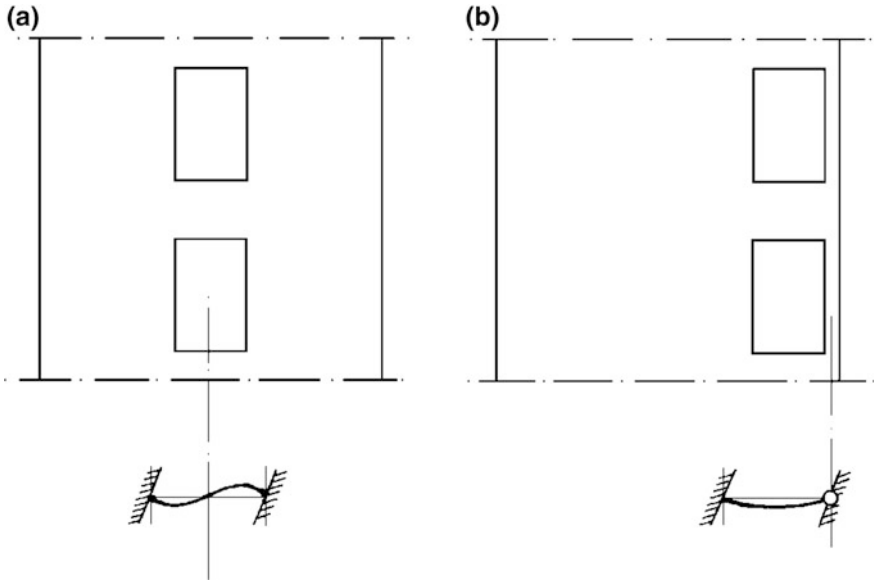


Fig. 5.26 Different structural situations of the lintel

The flux of compressions in the strut of the web of the lintel remains equal to:

$$S_c = Q\frac{1}{\sin\beta} = Q\sqrt{1+\lambda^2}$$

and leads, according to the formulas of the arch behaviour of beams with shear reinforcement with $d \cong 0.92h$, to the stress

$$\sigma_c \cong \frac{Q}{0.55hb}\left(1+\lambda^2\right)$$

Setting at the resistance limit $S''_s = A_{sl}f_{yd}$ and $\sigma_c = f_{cd}$, one obtains the capacities

$$Q_{Rc} = 0.55h\,b f_{cd}/\left(1+\lambda^2\right)$$
$$Q_{Rs} = A_{sl}f_{yd}z/(1/2+e)$$

for the verification

$$Q_{Rs} \geq Q_{Ed} \quad Q_{Rc} \geq \gamma_R Q_{Rs}$$

What presented above requires the presence of a minimum amount of shear reinforcement and obviously it is valid when, reversing the direction of the action Q, the roles of the reinforcement are exchanged and the web strut with ascending inclination is activated instead of the one with descending inclination.

In order to enhance the resistance of the concrete of the web in slender lintels with $\lambda \gg 1$ a high shear reinforcement can be adopted (see Fig. 5.25c)

$$a_s \geq 0.50 b f_{c2} / f_{yd}$$

which, with $\lambda_R = 1$ and $z \cong 0.84h$, leads to a resistance (see Sect. 4.3.2)

$$Q_{Rc} = V_{cd} = 0.42 b\, h f_{c2}$$

whereas the one related to longitudinal reinforcement remains unchanged.

The dual solution of the resisting scheme for the lintel contemplates the use of diagonal rebars as indicated in Fig. 5.25b. The resistance relies on the same equilibrium relations of the previous solution, where the function of the two materials, and correspondingly the sign of the forces, are exchanged. Not taking into account the contribution of the descending bar, one has:

$$S'_c = \left(\frac{\lambda}{2} + \frac{e}{z}\right) Q$$
$$S''_c = \left(\frac{\lambda}{2} - \frac{e}{z}\right) Q$$

One also has, for the two particular cases of Fig. 5.26a, b with $e = 0$ and $e = l/2$, respectively, the forces:

$$S'_c = S''_c = \frac{\lambda}{2} Q$$

and

$$S'_c = 0 \quad S''_c = \lambda Q$$

whereas the force in the diagonal bar remains in any case equal to:

$$S_S = Q\sqrt{1 + \lambda^2}$$

Setting at the resistance limit $S'_c = 0.16 hbf_{cd}$ and $S_s = A_{st} f_{yd}$, one obtains the capacities

$$Q_{Rc} = 0.16 h\, b f_{cd}\, z/(1/2 + e)$$
$$Q_{Rs} = A_{st} f_{yd} \Big/ \sqrt{1 + \lambda^2}$$

The reinforcement with diagonal bars can only supplement the one with longitudinal bars, which should be designed for at least 0.5 of the total action. The combined use of the two types of reinforcement with longitudinal and diagonal bars

allows to split the internal force in the concrete dividing it between web and chords. The global capacity can be evaluated summing up the two contributions of the reinforcement:

$$Q_{\mathrm{Rd}} = Q'_{\mathrm{Rs}} + Q''_{\mathrm{Rs}} = \frac{A_{\mathrm{s1}} f_{\mathrm{yd}} z}{1/2 + e} + \frac{A_{\mathrm{st}} f_{\mathrm{yd}}}{\sqrt{1+\lambda^2}} > Q_{\mathrm{Ed}}$$

For the resistance of the concrete of the web one should has:

$$Q'_{\mathrm{Rc}} \approx \frac{0.55 h\, b f_{\mathrm{cd}}}{\left(1+\lambda^2\right)} \geq \gamma_{\mathrm{R}} Q'_{\mathrm{Rs}}$$

Dividing then the action in two parts, proportional to the capacity of the two mechanisms with

$$\alpha' = \frac{Q'_{\mathrm{Rs}}}{Q_{\mathrm{Rd}}} \quad (\alpha^o = 1 - \alpha')$$

the resistance of the concrete chords, taking into account the tension in the first mechanism, is:

$$Q''_{\mathrm{Rc}} \cong \frac{0.16 b\, h f_{\mathrm{cd}} z}{1/2 + e} \geq \gamma_{\mathrm{R}} Q''_{\mathrm{Rs}} - \alpha' Q'_{\mathrm{Ed}}$$

The overall reinforcement layout is eventually indicated in Fig. 5.27, placed symmetrically due to the possible inversion of the shear force further to the alternation of the horizontal actions on the building (e.g. wind from left and right sides). The appropriate end anchorages of the reinforcement bars are obviously to be ensured. For significant depth of the lintel, it is appropriate to introduce additional longitudinal bars along the web, for technological construction purposes of having a

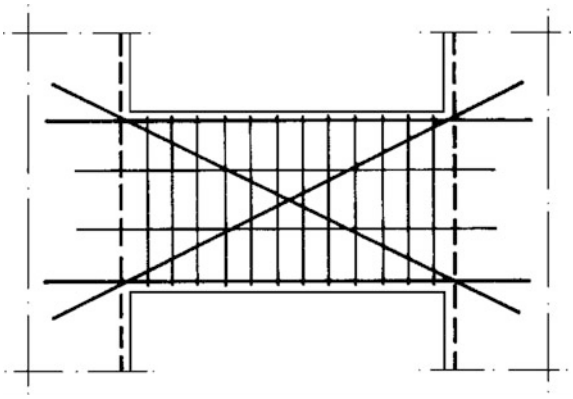


Fig. 5.27 Overall reinforcement layout of the lintel

stable steel cage, as well as enhancing contribution with respect to the cracking behaviour.

5.2.3 *Punching Shear in Slabs*

The supports of plate elements on columns constitute a problem of bi-directional bending. It is about analyzing how the fluxes of stresses, diffused on the extent of the plate, can concentrate within the reduced dimensions of the supports. The term *punching shear* is associated with such calculation, with reference to the possibility of a rupture by perforation of the plate due to its reduced thickness in relation to the magnitude of the localized reaction and to the reduced dimensions of the area on which the reaction itself is distributed. For continuity supports, two sets of orthogonal cracks are to be expected on the upper face of the concerned plate zone, due to the peaks of moments M_x and M_y.

Despite the high number of tests carried on such type of structural node, the problem has not reached an exhaustive and final formulation. Codes propose a conventional calculation based on the same formulas deduced for the unidirectional shear of beams, with the definition of a *critical perimeter* along which the resistance is to be distributed. Such perimeter corresponds to the one that delimits (as an upper bound) the rupture surface as shown by the experimentation.

Slabs Without Transverse Reinforcement

A scheme indicating the rupture surface is shown in Fig. 5.28, which takes the shape of a truncated cone, with the sides $a \times b$ of the smaller base coinciding with the perimeter of the supporting column and the sides $A \times B$ of the bigger base significantly longer. For slabs without transverse shear reinforcement, the

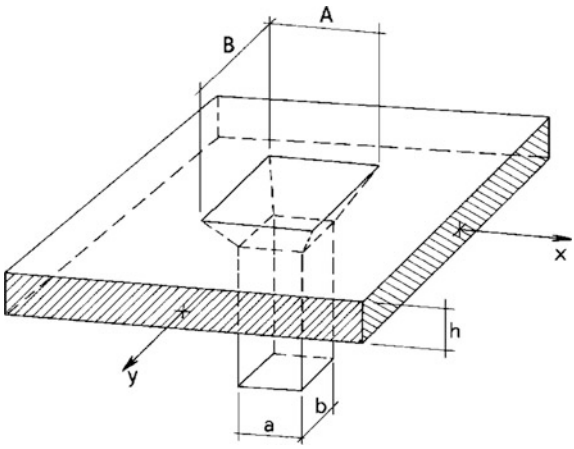


Fig. 5.28 Scheme of the resisting surface in punching shear

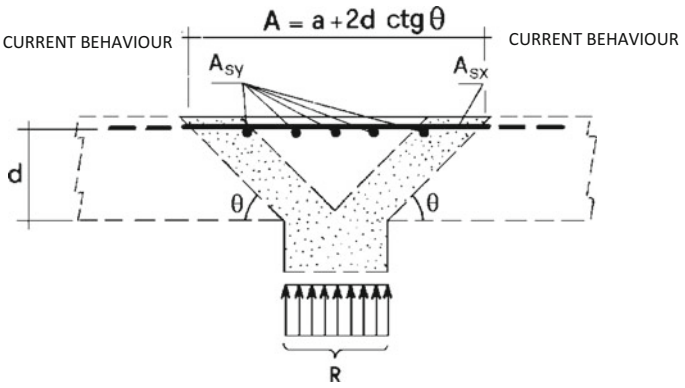


Fig. 5.29 Detail of the diffusion zone

experimentation shows an inclination of the rupture surfaces (see Fig. 5.29) equal to about

$$\lambda = \text{ctg}\,\theta = 3/2 \quad (\theta \cong 34^\circ)$$

Therefore, a diffusion zone with fan-shaped compressions could be identified, whose sides are

$$A = a + 2d\lambda \cong a + 3d$$
$$B = b + 2d\lambda \cong b + 3d$$

with the bevels at the corners indicated in Fig. 5.30. Outside the perimeter of the diffusion zone we go back to the current behaviour of slabs in bending. In the model presented above the effective depth is assumed equal to the mean one

$$d = (d_x + d_y)/2$$

and it is implied that the plate is subject to distributed loads directed downwards.

In the case of double symmetry of the flexural behaviour around the support, the resistance verifications can be referred to an uniform constant distribution of stresses along the concerned perimeter. More precisely one has:

- *verification of the support*

  ($u_o = 2a + 2b$ perimeter affected by the compressions)

$$R_{Rc} = 0.4 d u_o f_{cd} \frac{1}{1+\lambda^2} = 0.123 d u_o f_{cd}$$

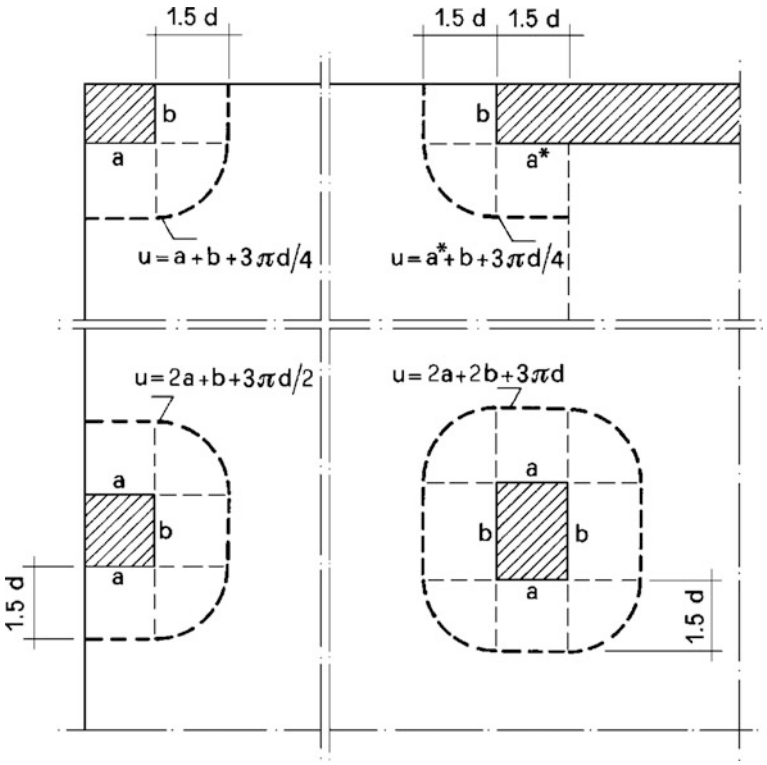


Fig. 5.30 Perimeter of the diffusion zone for the different positions

- *verification of the critical perimeter*

  ($u = 2a + 2b + 3\pi d$ concerned critical perimeter)

$$V_{\text{ctd}} = R_{\text{Rd}} = 0.25\text{d}u f_{\text{ctd}} \kappa (1 + 50\rho_{\text{s}})$$

with

$\kappa = 1.6 - d \geq 1$	(d in m) increase for thin slabs
$\rho_{\text{s}} = \sqrt{\rho_{\text{sx}} \rho_{\text{sy}}} \leq 0.020$	geometric reinforcement ratio in tension
$\rho_{\text{sx}} = A_{\text{SX}}/\text{Bd}$	A_{sx} area of bars within B
$\rho_{\text{sy}} = \text{A}_{\text{sy}}/\text{Ad}$	A_{sy} area of bars within A

More recent codes give a different formula empirically deduced:

$$V_{\text{ctd}} = 0.18\text{ud}\kappa (100\rho_{\text{s}} f_{\text{ck}})^{1/3}/\gamma_c \geq \text{ud}\text{v}_{\text{min}}$$

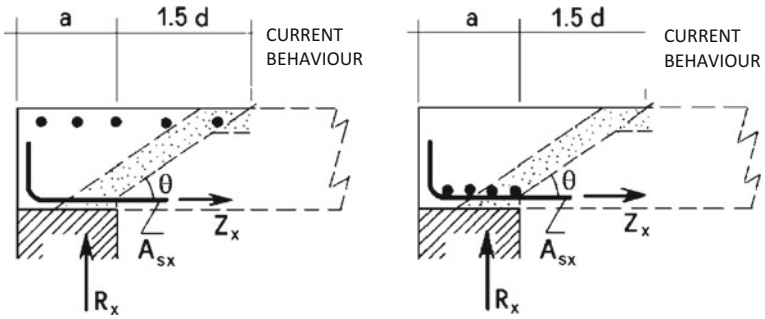


Fig. 5.31 Details on edge (*left*) and corner (*right*) supports

with the same expressions given to κ and $v_{\min}$ in 4.2.3 for the corresponding shear formula.

Regarding the flexural reinforcement A_{sx}, A_{sy}, they should be designed on the basis of the moments M_x, M_y at the support in the two corresponding directions, as deduced from the analysis of the plate, and referred, respectively, to the widths B, A previously defined. The rule of the moment shifting is also to be taken into account, for which the reinforcement calculated at the support should be extended, without reduction, by a length equal to about $1.5d$ (on each side).

On an end support, corresponding to the edge or the corner of the plate, where the bending moment is equal to zero in one or both the directions (see Fig. 5.31), an amount of bottom reinforcement shall be brought capable to resist the force Z for the equilibrium at the node:

$$Z_x = R_x\lambda \quad (R_x = \alpha_x R)$$

With $\lambda = 3/2$ the bearing capacity verification is

$$R_{xd} = 0.667 A_{sx} f_{yd} > \alpha_x R_{Ed}$$

where the quota of the reaction that concerns the side of the support under consideration can be evaluated for the edge or corner situations, respectively, with

$$\alpha_x \cong b/(2a)$$
$$\alpha_x \cong b/a$$

This is obviously valid for substantially symmetric situations, otherwise the quota of the reaction that concerns each side of the support should be deduced from the correct analysis of stresses over the plate.

Slabs with Bent Bars

Similarly to what described in Figs. 5.17 and 5.18 for the cases of unidirectional bending, similar transverse reinforcement can be adopted to enhance the capacity of the support also in the case of bi-directional bending of slabs.

Reinforcement for punching shear normally consists of two orthogonal sets of bent bars placed above the column. Their use allows enhancing the capacity locally utilizing the higher compression resistance resources of concrete. The rupture surface, where its tensile resistance is again crucial, is moved away to a peripheral contour where the peak forces are reduced. One therefore enters again in the zones of typical flexural behaviour for which the normal verification formulas are valid.

The typical reinforcement layout is shown in Fig. 5.32. For the verifications, the formulas of the following type are to be applied on each of the four sides:

$$R'_{\mathrm{xd}} = A_{\mathrm{tx}} f_{\mathrm{yd}} \sin\alpha > \alpha'_x R_{\mathrm{Ed}}$$

or, with $\lambda_x = l_x/0.9d_x$:

$$R'_{\mathrm{Xd}} = 0.4b\, d_{\mathrm{X}} f_{\mathrm{cd}}/(1 + \lambda_{\mathrm{X}}^2) > \alpha'_{\mathrm{X}} R_{\mathrm{Ed}}$$

similar to the ones presented with reference to supports of unidirectional beams. For doubly symmetric configurations of actions and resistance, the verification can be carried in terms of global reaction:

$$R_{\mathrm{Rs}} = A_{\mathrm{t}} f_{\mathrm{yd}} \sin\alpha > R_{\mathrm{Ed}} \qquad \left(A_{\mathrm{t}} = 2A_{\mathrm{tx}} + 2A_{\mathrm{ty}}\right)$$

$$R_{\mathrm{Rc}} = 0.4\mathrm{du}_{\mathrm{o}} f_{\mathrm{cd}} \frac{1}{1+\lambda_{\mathrm{o}}^2} > R_{\mathrm{Ed}} \quad \left(\lambda_{\mathrm{o}} \cong \lambda_x \cong \lambda_y\right)$$

In the case of edge or corner supports with zero moment, for the lower longitudinal reinforcement of the plate the same verification formula $Z_x = R_x\lambda$ before reported is valid, with the substitution of $\lambda(= 1.5)$ with the value defined above. In particular, with bent bars placed above the axis of the support $(l_x = 0)$ the force Z_x of the longitudinal reinforcement is equal to zero; however, a minimum amount of this reinforcement is yet necessary, similar to what mentioned for the supports of the beams.

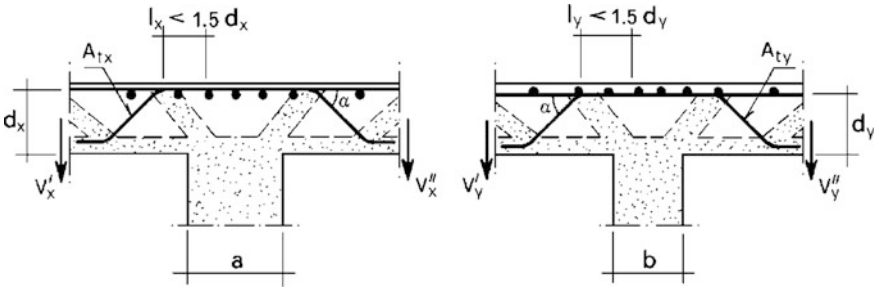


Fig. 5.32 Reinforcement layout over an internal column

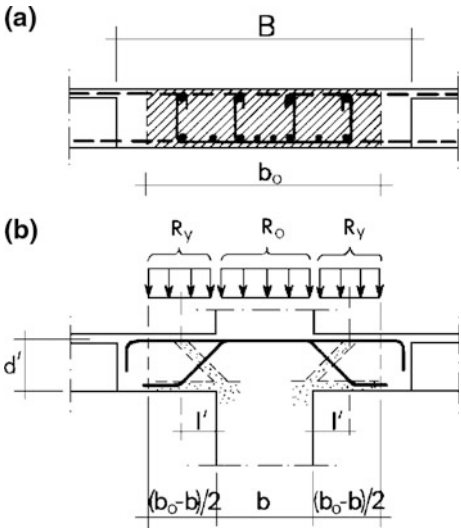


Fig. 5.33 Reinforcement layout for a shallow beam

Shallow Beams

A frequent case of verification to punching shear is the one relative to beams cast within the floor depth (see Fig. 5.33). It is the case of substantially unidirectional bending in a flat element with large width, supported by columns with much smaller dimensions.

The beam is designed with appropriate stirrups to resist shear according to the truss model of Fig. 5.2. Sometimes the width of concrete in the resistance model is undefined, as the actual one remains, for different construction reasons, excessive with respect to the shear requirements and stirrups are not provided on the entire width.

Therefore, in the case under consideration, the design is carried in two steps: the first one consists of a normal verification of *beam in bending* in the longitudinal direction; the second one consists of a local verification of *corbels* cantilevering out from columns in the transverse direction.

In the longitudinal direction, the shear verification is carried in the section type '*b*' close to the support. Having a significant web width available, a low shear reinforcement ratio is expected. With $\lambda_c = \lambda_{max} = 2.5$ the distance from the support of the first verification section in shear is equal to

$$x_o = \frac{l_c}{2} = \frac{1}{2}\lambda_c z \cong 1.1d$$

The effective width b_o of the concrete is defined as the minimum compatible with the resistance in compression-shear:

$$0.9b_o\, d f_{c2} \lambda_c/(1+\lambda_c^2) = V_{Ed}$$

where the force V_{Ed} is evaluated in the section of abscissa x_o. With $\lambda_c = 2.5$ one therefore derives:

$$b_o = 3.22\ V_{Ed}/d f_{c2}$$

Obviously if b_o calculated this way were greater than the actual width B of the beam, one should set $b_o = B$, then designing the required stirrups in the medium-reinforcement domain (with $\lambda_c = 2.5$). The links should be distributed on the resisting width b_o with the spacing limits indicated in the Chart 4.5.

In the transverse direction on the supports, the design is carried assigning a quota of the shear to the protrusions, proportional to their extent. In terms of reaction one therefore has (see Fig. 5.33b):

$$R_y = \frac{b_o - b}{2b_o} R$$

where b is the side of the column. This force is localized at a distance

$$l' = (b_o - b)/4$$

from the edge, for a verification of stocky cantilever according to the criteria exposed at Sect. 5.2.2.

It often occurs that, with $b_o < b$, the column width is enough for the resistance without taking into account the contribution of the lateral protrusions of the plate. In this case no additional transverse reinforcement would be necessary over the column. According to a conservative criterion, shear is, however, distributed along the width actually reinforced to shear.

5.3 Flexural Deformations of Beams

The deformation calculations of beams in reinforced concrete, for the evaluation of hyperstatics or of certain parameters of the deformation itself such as vertical deflections, are generally based on the elastic flexural characteristics of the geometrical concrete sections. For limited load levels this leads to good results, where the only significant uncertainty derives from the difficulty of a correct evaluation of the elastic modulus E_c. The value of this modulus affects in an inversely proportional measure the deformations; it affects in general much less the hyperstatics as they depend on the ratios between the stiffnesses of the different members of the frame and not on their absolute value.

For levels of actions beyond the cracking limit, the elastic assumptions referred to the geometrical section of concrete lead to more significant errors. Deformations

are in fact heavily influenced by the divergence of the behaviour of the cracked section which, even if helped by the tension stiffening, exhibits a sudden drop of its flexural stiffness. The deviation from the initial linear behaviour of the uncracked section is quantified mainly by the reinforcement ratio. In general, the effects of cracking on the hyperstatics are less significant, especially if cracking is diffused uniformly on the different members of the frame.

For load levels towards the failure limit of the sections, the distribution of hyperstatic stresses depends more and more from the reinforcement proportioning of the sections. If such proportioning has been carried with reference to the elastic diagrams of the stresses in service, the same ratios between moments are found at the ultimate limit state of collapse of the frame. If instead the reinforcement distribution is different, the configuration of the hyperstatics tends to adapt to it with a redistribution of forces from the section that yield first towards the ones that are less stressed. The limited ductility resources of the reinforced concrete sections reduce the possibility of plastic adaptation of the structure. The use of high reinforcement ratios with consequent brittle behaviour of the sections excludes it completely.

Few basic examples of nonlinear analysis are shown hereafter, for the evaluation of deformations of isostatic beams, for the calculation of stresses in hyperstatic beams and for the evaluation of their collapse load. With this occasion, mention will be made to the problems of the numerical calculation required by the solving algorithms.

The elementary algorithm of the problems of nonlinear calculation discussed in this section is the one of the deformation analysis of the simply supported beam in bending (see Fig. 5.34a). Excluding the case of stocky beams for which the contributions of shear deformation are significant and remaining within the theory of first order valid for absence of axial forces, the elementary algorithm consists of the following *integrations of curvatures*:

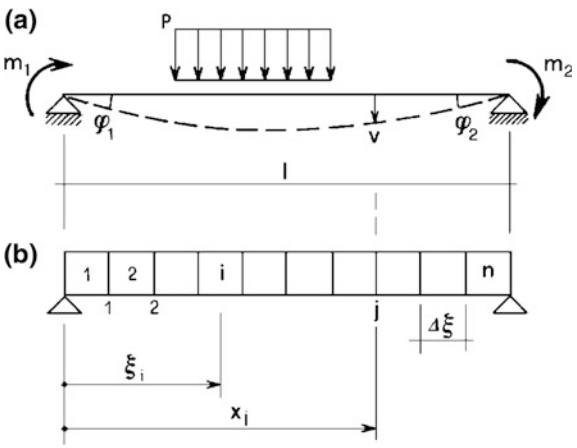


Fig. 5.34 Discretized model for deformation calculation

$$\phi_1 = \int_0^1 \chi(\xi)\,\frac{1-\xi}{1}\,\mathrm{d}\xi$$

$$\phi_2 = \int_0^1 \chi(\xi)\,\frac{\xi}{1}\,\mathrm{d}\xi$$

$$\mathrm{v} = \phi_1 x - \int_0^1 (x-\xi)\chi(\xi)\mathrm{d}\xi$$

having indicated with

$$\chi = \chi(M)$$

the curvature caused by the bending moment M in the section of abscissa ξ.

On the isostatic configuration of the elementary situation of the beam of Fig. 5.34a, the bending moment $M(\xi)$ can be directly expressed as a function of the loads p and the hyperstatics m_1, m_2. Therefore the curvature χ, which in the linear elastic case remained proportional to the bending moment with $\chi = M/\mathrm{El}(\mathrm{El} = \mathrm{cost})$, in the nonlinear analysis is to be read in the diagrams $M = \mathrm{M}(\chi)$ expressly defined (see Fig. 5.35).

The moment-curvature diagrams can be defined with mathematical models which lead to analytical closed-form expressions, or they can be defined numerically and therefore represented by sets of point values. For this calculation one can refer to Sect. 3.3.2.

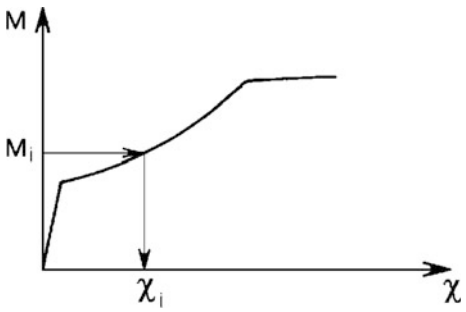


Fig. 5.35 Curvature read from $M(\chi)$ diagram

5.3.1 Curvature Integration

With reference to the simply supported beam represented in Fig. 5.34, the numerical algorithm relative to the integration of curvatures for the calculation of the end rotations and of the flexural deformation line, can be set as:

$$\phi_1 \cong \sum_{i=1}^{n} \chi_i \frac{1-\xi_i}{1} \Delta\xi$$

$$\phi_2 \cong \sum_{i=1}^{n} \chi_i \frac{\xi_i}{1} \Delta\xi$$

$$v(x) \cong \phi_1 x_j - \sum_{i=1}^{j} (x_i - \xi_i)\chi_i \Delta\xi \quad \text{with } j = 1, 2, \ldots, n-1$$

where, having discretized the beam in n segments of length $\Delta\xi = l/n$ (see Fig. 5.34b), one has:

$$\xi_i = \left(i - \frac{1}{2}\right)\Delta\xi \quad x_j = j\Delta\xi$$

An example of elaboration of these algorithms is shown below with reference to the prestressed beam of Fig. 5.36. The results are summarized in the subsequent figures.

The curves of the increment of deflection at the mid-span of the beam are shown in Fig. 5.37 for three different ratios of partial prestress (curve '*a*' with no prestress, curve '*b*' with half prestress, curve '*c*' with total prestress). The significantly different stiffnesses in the cracked and uncracked phases of the sections can be noted, as well as the contribution of prestress with respect to the limitation of the deformation of the beam. The $\sigma-\varepsilon$ deformation diagrams for the materials have obviously been used, with non-zero concrete resistance in tension and hyperbolic tension stiffening model beyond the cracking limit.

Given that a total load 960 kN is assumed (equal to about 96.5 kN/m), in the case of total prestress a deflection of about 6 mm is read which, added to the precamber corresponding to the absence of load, leads to a range of about 12 mm. Such value can be calculated with good approximation with the elastic formula

$$v = \frac{5}{384}\frac{pl^4}{EI}$$

referred to the current geometrical section of concrete. Instead, for the half prestress case a deflection of 26.5 mm would be read which, added to the corresponding initial precamber, would bring the total range to about 29.0 mm. The creep effects under permanent loads have not been taken into account in what mentioned above.

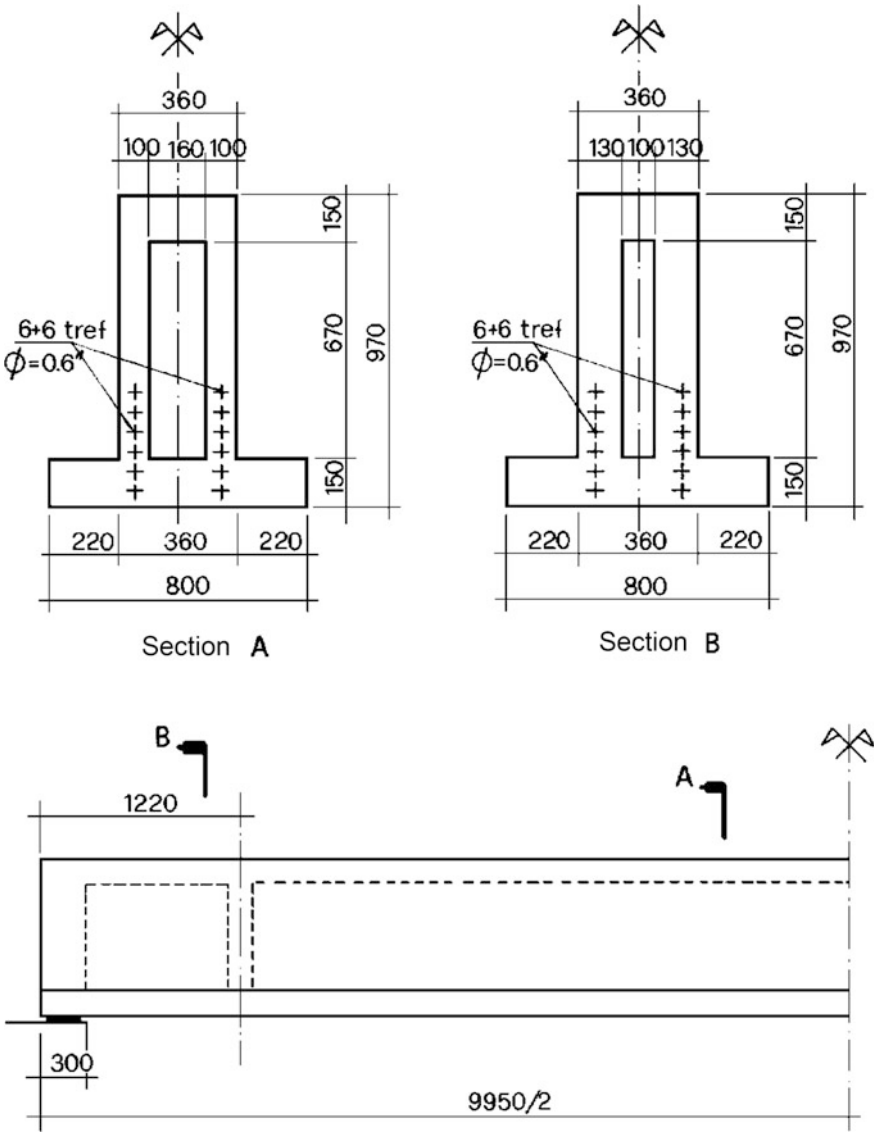


Fig. 5.36 Example of prestressed beam

The deformed shapes of the beam in relation to the increase of the load are eventually shown in Fig. 5.38, only for the case of total prestress.

It is to be noted that, for the correct evaluation of the flexural deformations of beams, the creep effects play a determining role. The exact method would require an integration on time, in addition to the one set above on the beam length, according to the criteria of the procedure described at Sect. 1.3.2. In the practical

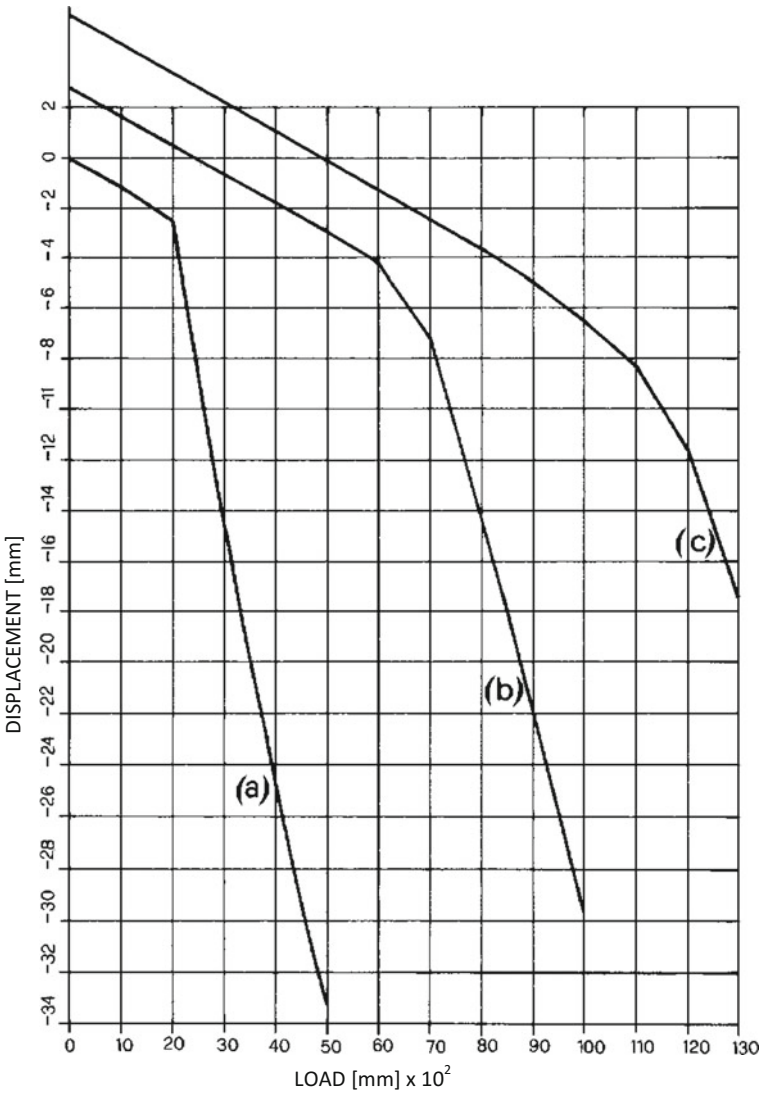


Fig. 5.37 Mid-span deflection curves

applications, the approximations of the algebraic methods are acceptable, such as the one that uses, in the numerical definition of the moment-curvature diagrams, the constitutive models $\sigma-\varepsilon$ amplified on the abscissas by $1+c\phi$, as described at Sect. 3.3.2 (see Fig. 3.32). More drastic approximations are expected if one moves the amplification after the integrations of curvatures, with expressions similar to

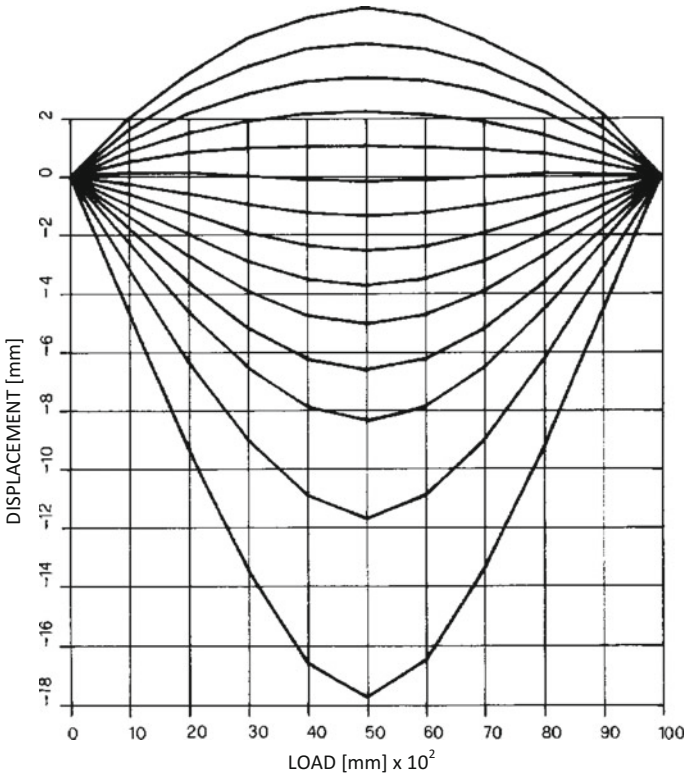


Fig. 5.38 Beam deformation for increasing loads

$$v_\infty = v_o(1 + c\phi_\infty)$$

5.3.2 *Nonlinear Analysis of Hyperstatic Beams*

Let 'us consider the fixed-end beam of Fig. 5.39 subject to static forces (for ex. the loads p, P and F) and to geometrical actions (for example the settlements η_1, ϕ_{10}, η_2 e ϕ_{20}) as indicated in the figure. Setting the solution according to the force method, the beam is made isostatic removing the rotational constraints at its ends and applying the hyperstatics m_1 and m_2. A linear elastic calculation based on the characteristics of the geometrical section of concrete would lead to the values m_{10} and m_{20}; for example to

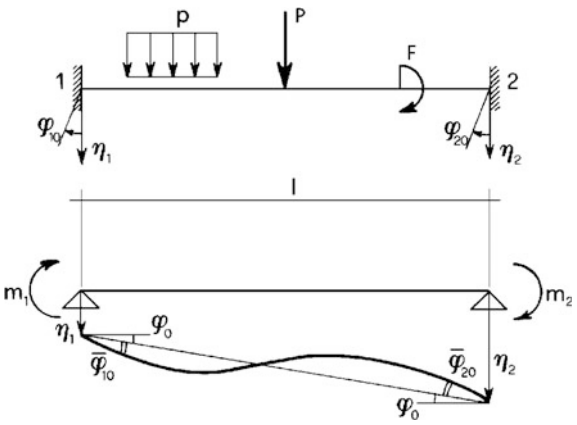


Fig. 5.39 Nonlinear calculation model for hyperstatic beam

$$m_{10} = -\frac{pl^2}{12} + \frac{E_c I_c}{l}(4\phi_{10} + 2\phi_{20}) - \frac{6E_c I_c}{l^2}(\eta_2 - \eta_1)$$
$$m_{20} = +\frac{pl^2}{12} + \frac{E_c I_c}{l}(2\phi_{10} + 4\phi_{20}) - \frac{6E_c I_c}{l^2}(\eta_2 - \eta_1)$$

in the case of $E_c I_c$ = cost and only one load p distributed uniformly on the beam.

Within the domain of nonlinear behaviour of sections, integrating curvatures according to the procedures described at the previous paragraph, two flexural rotations $\bar{\phi}_1$ e $\bar{\phi}_2$ at the ends are obtained which, added to the rigid one $\phi_0 = (\eta_2 - \eta_1)/l$ of the beam, lead to values

$$\phi_1 = \bar{\phi}_1 + \phi_0 \qquad \phi_2 = \bar{\phi}_2 + \phi_0$$

that generally do not respect compatibility

$$\phi_1 \neq \phi_{10} \qquad \phi_2 \neq \phi_{20}$$

Therefore, in order to re-establish compatibility, the value of the hyperstatics should be modified, starting form m_{10} and m_{20}, with attempts properly directed, until it results from the same integrations of the new curvatures:

$$\phi_1 \cong \phi_{10}$$
$$\phi_2 \cong \phi_{20}$$

With such iterative procedure, the balanced and compatible solution can be reached, which follows the nonlinear constitutive model expressed in terms of moment-curvature relationship of the sections.

An example of convergence of the nonlinear calculation of the hyperstatics of a fixed-end beam with constant section and reinforcement is shown in the table of

N	ROT1	RAPP.MOM1	ROT2	RAPP.MOM2
1	0.56469	1.00000	−0.56469	1.00000
2	0.30354	1.00000	0.38232	0.80000
3	−1.81210	0.80000	1.81210	0.80000
4	−1.39225	0.80000	1.25937	0.84000
5	−0.99695	0.80000	0.77021	0.88000
6	−0.49320	0.80000	0.03929	0.92000
7	−0.43726	0.80000	−0.13047	0.96000
8	−0.30656	0.84000	−0.18595	0.96000
9	−0.08386	0.88000	−0.24221	0.96000
10	0.18546	0.92000	−0.29903	0.96000
11	0.17465	0.92000	−0.26465	0.95200
12	0.16390	0.92000	−0.23064	0.94440
13	0.15322	0.92000	−0.19750	0.93600
14	0.14257	0.92000	−0.16470	0.92800
15	0.13191	0.92000	−0.13191	0.92000
16	0.12100	0.92000	−0.08885	0.91200
17	0.10972	0.92000	−0.03157	0.90400
18	0.09838	0.92000	0.02586	0.89600
19	0.05338	0.91200	0.03757	0.89600
20	−0.04150	0.90400	0.04967	0.89600
21	−0.00172	0.90400	0.03813	0.89760
22	0.00071	0.90400	0.02660	0.89920
23	0.00314	0.90400	0.01507	0.90080
24	0.00557	0.90400	0.00354	0.90240
25	0.00800	0.90400	−0.00800	0.90400
26	−0.00354	0.90240	−0.00556	0.90400
27	−0.00402	0.90240	−0.00326	0.90368
28	−0.00451	0.90240	−0.00095	0.90336
29	−0.00499	0.90240	0.00135	0.90304
30	−0.00269	0.90272	0.00087	0.90304
31	0.00038	0.90304	0.00038	0.90304

Fig. 5.40 Convergence of the nonlinear calculation

Fig. 5.40, for a load uniformly distributed along its entire length. The steps of the subsequent iterations are indicated with '*N*', the rotations calculated at both ends of the beam with 'ROT1' and 'ROT2', the tentative values of the two hyperstatic moments referred to the elastic ones $pl^2/12$ with 'RAPP.MOM1' and 'RAPP. MOM2'. The M-χ deformation diagrams have been used.

The optimal convergence achieved by the numerical procedure can be noted. In particular, having assumed in the example a load level higher than the cracking limit of the most highly stressed sections (at the fixed ends), a redistribution of moments resulted of about 10% towards the uncracked mid-span of the beam.

The nonlinear analysis of continuous beams, as well as the more general one of frames in reinforced concrete, can be carried according to the criteria of the

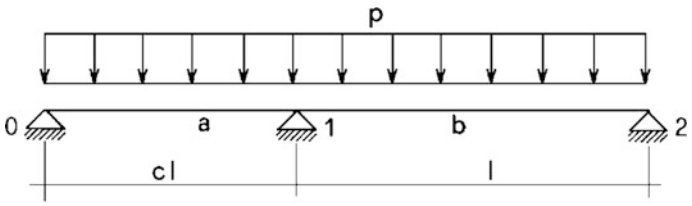


Fig. 5.41 Example of continuous beam

displacement method, therefore assuming as compatible unknowns the node displacements and setting the equilibrium conditions at the nodes. We now limit the description to few notions on the articulation of the relative algorithms, leaving out the manifold numerical problems that such calculation implies.

The algorithm therefore develops through three orders of interlocked iterations: an internal one aiming at the numerical definition of the diagram M-χ of sections; an intermediate one consisting of the analysis of the individual beam repeated by trial and error up to the definition of the nonlinear moments corresponding to the assigned values of the nodal displacements; an external one on the structure consisting of subsequent linear elastic solutions of the equilibrium system progressively adjusted in its terms.

For the continuous beams the definition of the diagrams M-χ can be carried in advance once and for all, or rather substituted by the assigned functions of the competent mathematical models of deformation of the sections.

With reference for example to the continuous beam of Fig. 5.41, according to the criteria of the displacement method the rotation ϕ_1 of the node 1 is assumed as unknown. The elastic equilibrium condition is then set which gives

$$\phi_{10} = \frac{\overline{m}_{10}}{3\mathrm{EI}/1} \frac{c}{1+c}$$

with

$$\overline{m}_{10} = \frac{\mathrm{pl}^2}{8}(1-c^2)$$

This represents the initial linear elastic solution which leads to

$$M_{10} = \frac{\mathrm{p1}^2}{8}[1-(1-c)c]$$

$$M_{\mathrm{a}}(x) = \frac{\mathrm{pcl}}{2}x\left(1-\frac{x}{\mathrm{cl}}\right) + M_{10}\frac{x}{\mathrm{cl}}$$

$$M_b(x) = \frac{\mathrm{pl}}{2}x\left(1-\frac{x}{\mathrm{cl}}\right) + M_{10}\left(1-\frac{x}{l}\right)$$

For each individual element we now proceed with the integration of curvatures read on the competent diagrams M-χ; such integrations are repeated modifying the moment at the node 1 starting from M_{10} until $\phi_1 \cong \phi_{10}$ results. Two moments M_{a1} and M_{b1} result that generally do not comply with the equilibrium at the node:

$$M_{b1} - M_{a1} = r1 \neq 0$$

where r_1 represents the unbalanced residual.

Such residual is, therefore, redistributed elastically on the members with the same algorithm:

$$\Delta\phi_1 = \frac{-r_1}{3EI/l} \frac{c}{1+c}$$

obtaining the increment $\Delta\phi_1$ that re-establishes equilibrium and brings the solution to

$$\phi_{11} = \phi_{10} + \Delta\phi_1$$

with

$$M_{11} = M_{b1} + \frac{3EI}{1}\Delta\phi_1 = M_{a1} - \frac{3EI}{1}\Delta\phi_1$$

At this point the cycle resumes with the integration of curvatures on the individual members, with the evaluation of the new unbalanced residual r_2 and with the elaboration of the new incremental elastic solution $\Delta\phi_2$ which leads to $\phi_{12} = {}_{11} + \Delta\phi_2$. The procedure is finally stopped when the residual r_i and the subsequent incremental solution $\Delta\phi_i$ become negligible.

Given the amount of required elaborations, it follows that such procedure needs the use of automatic calculation. In the analysis of continuous beams the axial force is equal to zero. A further complication in the calculation of frames derives instead from the presence of axial force and from its dependence from the values of hyperstatic moments. Since the axial force affects the diagrams M-χ of the sections as it will be specified in Chap. 6, the procedure of the automatic calculation for the nonlinear analysis of frames should contemplate the numerical redefinition of such diagrams at each step of the external iterative cycle, that is when the forces in the members are adjusted, after the new modifying elastic solution.

5.3.3 *Collapse Behaviour of Hyperstatic Beams*

The example of continuous beam of Fig. 5.42 presents again the topic of the influence of nonlinear behaviour of sections on the value of the hyperstatics. In particular, repeating the calculation for progressively increasing loads up to the

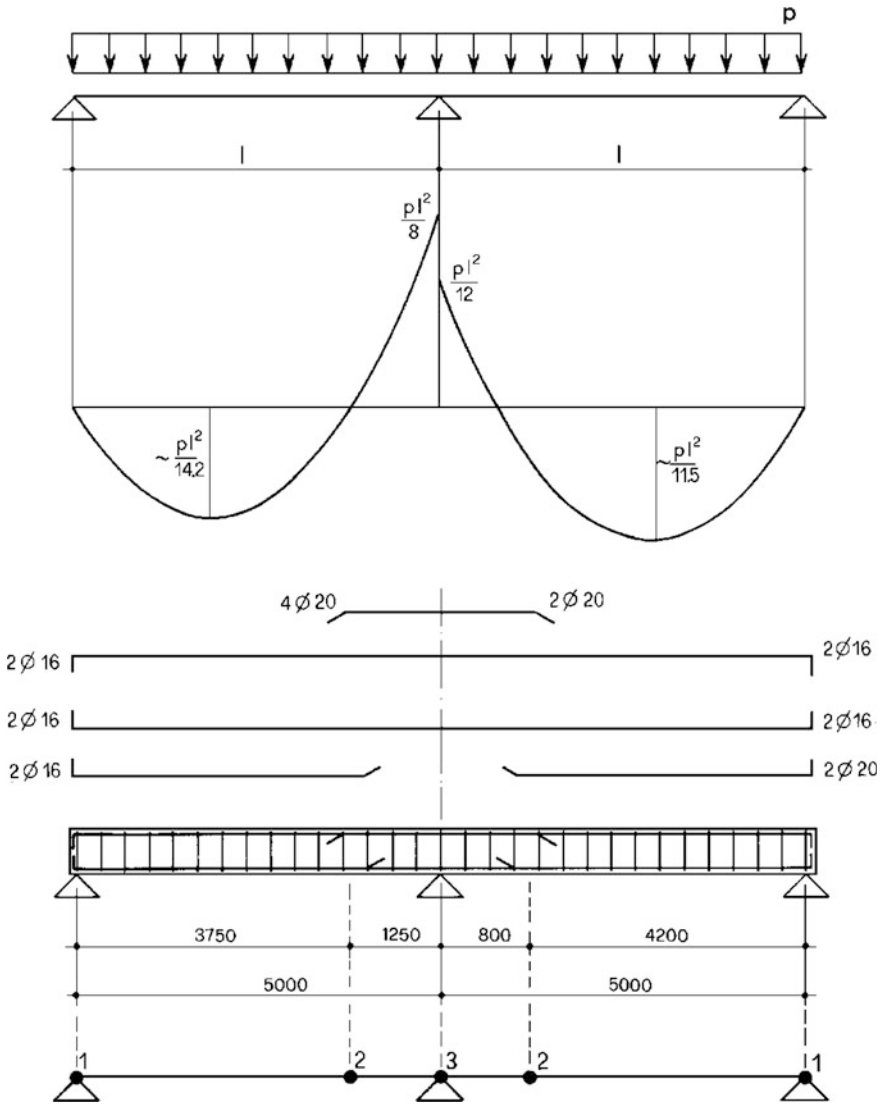


Fig. 5.42 Example of nonlinear calculation up to collapse

collapse limit of the beam, the effect of the reinforcement proportioning on the force distribution and on the ultimate value of the load is shown.

Given the symmetric configuration of the beam, only one span has been analyzed, representing with a fixed-end the effect of continuity on the intermediate support. The only hyperstatic is therefore the moment on such fixed-end, whose value is to be modified by trial and error, starting from the elastic value $pl^2/8$, until the corresponding rotation results equal to zero with good approximation.

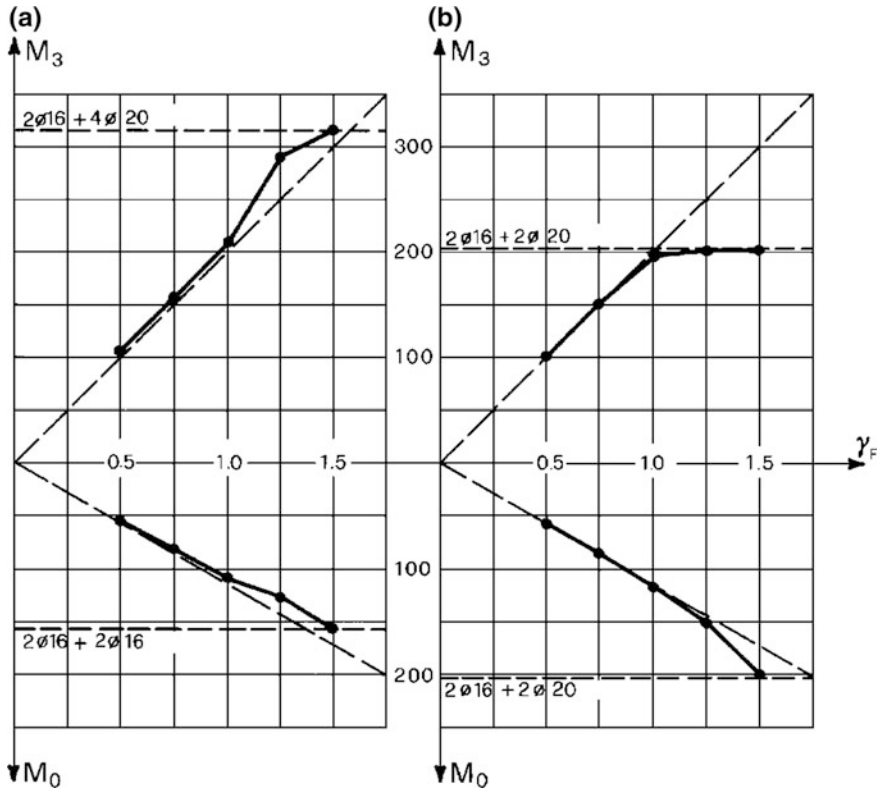


Fig. 5.43 Ways to collapse for consistent (**a**) and redistributed (**b**) steel proportioning

An initial proportioning of the reinforcement has been carried consistently with the elastic distribution of moments, as indicated on the left half of Fig. 5.42. A second proportioning has then been carried assuming a value of the moment at the intermediate support reduced to two-thirds of the elastic one, and increasing the positive moments on the span accordingly, complying with the equilibrium with the load p, as indicated in the right half of Fig. 5.42. On each of the two configurations the calculation has been carried according to the same procedure described above and repeated for different levels $\gamma_F p$ of the load.

The analysis, carried with the same iterative procedure described at the previous paragraph, led to the results summarized in the diagrams of Fig. 5.43a, b. The first figure shows the behaviour of the beam when the load increases ($\gamma_F = 0.50 \div 0.75 \div 1.00 \div \ldots$) in the case of the consistent proportioning of the reinforcement. The second figure similarly shows the behaviour of the beam in the case of the redistributed proportioning of the reinforcement, again in terms of increase of the moments M_o on the span and M_3 on the internal continuity support of the beam.

The substantially linear behaviour can be noted in both cases up to the serviceability levels ($\gamma_F = 1$) of the load. Beyond this limit the behaviour deviates from linearity because of concrete cracking and then reinforcement yielding. However, for the consistent proportioning the near-contemporaneity of the yielding of the two critical sections keeps the rupture point close to the linear behaviour. For the redistributed proportioning instead, the early yielding (with $\gamma_F \cong 1.00$) of the continuity section brings the behaviour far away from the linear one, redistributing every subsequent load increment onto the section on the span. Thanks to the significant plastic rotational capacity of the first section, the same value of the collapse load has been attained ($\gamma_F \cong 1.50$)). At this point, with the yielding of the second critical section too, the beam is transformed into a hypostatic mechanism with consequent loss of equilibrium.

One can refer to Chap. 6 for a more complete discussion of the problems of nonlinear analysis similar to the one here introduced. At this moment we are only interested in deducing certain design criteria of the hyperstatic beams.

Plastic Design

Expecting a collapse similar to the one of the example of Figs. 5.42 and 5.43, that is caused by the loss of equilibrium by transformation of the beam into an hypostatic mechanism, the criteria of the *plastic design* could be directly applied without going through the onerous elaboration of the nonlinear analyses repeated for values progressively increasing of the load.

One can in fact assume to identify the collapse of the beam in the mechanism of Fig. 5.44, where the first plastic hinge is located at the section of maximum negative moment M_3, whereas the second one is located approximately in the zone of possible maximum positive moment M_o.

Giving to the above-mentioned moments the plastic values consequent to the given proportioning

$$M_o = M_{ro} + A_{sq} f_{yd} z'$$
$$M_3 = M_{r3} + A_{s3} f_{yd} z''$$

the equilibrium limit situation can be calculated under the collapse load

$$p_c = \gamma p_e$$

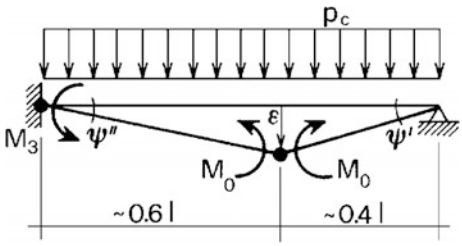


Fig. 5.44 Plastic hinges calculation

where p_e is the serviceability value of the load. Through the Principle of Virtual Work (see Fig. 5.44) one has:

$$p_c 1 \frac{\varepsilon}{2} = M_o \psi' + (M_o + M_3)\psi''$$

where

$$\psi' \cong \frac{\varepsilon}{0.4 \times 1} \quad \psi'' \cong \frac{\varepsilon}{0.6 \times 1}$$

Setting now

$$M_o = c_o M_e \quad M_3 = c_3 M_e$$

with

$$M_e = \frac{p_e l^2}{8}$$

maximum elastic moment at the continuity support under the serviceability load, after the appropriate substitutions and simplifications one obtains

$$\gamma = \frac{1}{4}\left\{\frac{c_o}{0.4} + \frac{c_o + c_3}{0.6}\right\} = \frac{5c_o + 2c_3}{4.8}$$

Assuming M_e the one corresponding to the reinforcement of $2\phi16 + 2\phi20$ of the section, in the two cases of consistent and redistributed proportioning of Fig. 5.43a–b, the following values of the *collapse multiplier* γ are respectively obtained:

$$2\phi16 + 2\phi16 \quad c_o \cong 0.78 \quad (\text{at the mid} - \text{span})$$
$$2\phi16 + 4\phi20 \quad c_3 \cong 1.61 \quad (\text{at the support})$$
$$\gamma = \frac{5 \times 0.78 + 2 \times 1.16}{4.8} \cong 1.48$$

or

$$2\phi16 + 2\phi20 \quad c_o \cong 1.00 \quad (\text{at the mid-span})$$
$$2\phi16 + 2\phi20 \quad c_3 \cong 1.00 \quad (\text{at the support})$$
$$\gamma = \frac{5 \times 1.00 + 2 \times 1.00}{4.8} \cong 1.46$$

Within the approximation of the data assumed above, the same results elaborated with the complex nonlinear analysis described previously are immediately obtained. However, it is to be noted that, if in the case of consistent proportioning the plastic

moments are proportional to the elastic linear ones and the near-contemporary formation of the two plastic hinges does not require big deformations of the sections, in the case of redistributed proportioning big plastic deformations are required at the first plastic hinge before the second hinge can be formed. If the plastic rotational capacities are not sufficient, for example because of an excessive reinforcement, early rupture can occur, localized in the continuity section, before the transformation of the beam into a mechanism.

Linear Analysis with Redistribution

From these considerations, the following consequences result:

- for the structural safety of the hyperstatic beams it is always possible, in the structural design, to refer to forces deduced from a *linear analysis* that use the elastic characteristics of the sections;
- it is also possible to refer the structural design to different stress diagrams, obtained with a *redistribution of hyperstatic moments* that keeps the equilibrium with the external loads, as long as they are close enough to the linear elastic one.

The moment redistribution shown in Fig. 5.45 can be arbitrary but limited, as mentioned above, within the plastic rotation capacities of the under-designed critical sections. In this way, for example the reduction ΔM_3 of the moment M_3, with respect to the value M_e deduced from the linear analysis on the section *3*, should be compared with the rotational capacities of the same section, which depend on its ductility characteristics.

In the nonlinear analysis, such limit is implicitly set with the appropriate ultimate value χ_u of the curvature of the section included in the relative diagrams M-χ. If instead one starts from a linear analysis, a limit can be set to the moment reduction, quantified on the basis of the mechanical reinforcement ratio (see Fig. 3.36), or rather based on the adimentionalized position of the neutral axis which is directly related to it:

$$\xi = x/d = (\omega_s - \omega'_s)/0.8$$

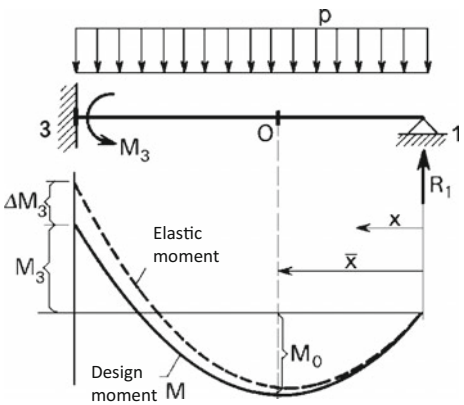


Fig. 5.45 Example of moment redistribution

In the CEB-FIP Model Code 2010, for the choice of the redistribution in the under-designed critical section, a design moment is indicated

$$M_{\mathrm{d}} = \delta M_{\mathrm{e}}$$

where for average and high-ductility steels, the reduction coefficient should be conservatively limited with

$$\delta \geq 0.44 + 1.25\xi \geq 0.7 \quad \text{for } f_{\mathrm{ck}} \leq 50\,\mathrm{MPa}$$

and with higher limits for $f_{\mathrm{ck}} > 50\,\mathrm{MPa}$.

In order to clarify the reinforcement design method based on the redistributed diagram of the moment, one can consider the graphic of Fig. 5.46. With reference to the beam of Fig. 5.45, the linear analysis of forces would lead to the following elastic values of moments.

$$M_{3\mathrm{e}} = \frac{\mathrm{pl}^2}{8} \qquad \text{at the fixed end}$$

$$M_{\mathrm{oe}} = \frac{\mathrm{pl}^2}{14.2} \qquad \text{on the span}$$

Such values correspond to the abscissa $\delta = 1$ of the graphic under consideration.

A consistent proportioning of the reinforcement in the two sections, which gives them the resistance values $\overline{M}_{3e}$ and $\overline{M}_{oe}$ in the same ratio $c = 14.2/8 = 1.78$, would lead to the capacity

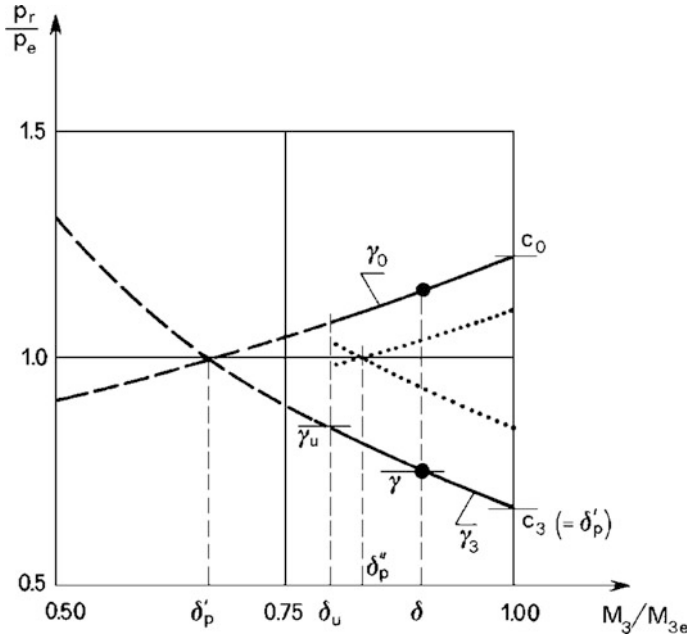


Fig. 5.46 Collapse factor γ for different moment redistributions

$$p_e = 8\overline{M}_{3e}/1^2 = 14.2\overline{M}_{oe}/1^2$$

which corresponds to the ordinate $\gamma = 1$ of the diagram of Fig. 5.46.

Instead, one can now assume to have proportioned the reinforcement in the section *3* (similarly to the example of Fig. 5.42 on the right side), with a reduction of its resistance to

$$\overline{M}_3 = c_3\overline{M}_{3e} = 0.70\overline{M}_{3e} \quad (\Delta M_{3e} = -0.30M_{3e})$$

For the equilibrium, the corresponding increase of the moments on the span should be

$$\Delta M_o = -\Delta M_3 x/1$$

and, placing approximately the maximum moment in

$$\overline{x} = 0.4 \times 1$$

the new enhanced proportioning of the section O leads to a resistance

$$\overline{M}_o = \overline{M}_{oe} - 0.4\Delta M_3 = (1 + 0.4 \times 0.30 \times 1.78)\overline{M}_{oe}$$

,that is

$$\overline{M}_o = c_o\overline{M}_{oe} = 1.21\overline{M}_{oe}$$

The actual configuration of the stresses in the hyperstatic beam under analysis depends on the level of forces. In the serviceability elastic phases, one has a linear behaviour with $M_3 = M_{3e}(\delta = 1)$. Once the resistance $\overline{M}_3$ of the under-proportioned critical section is attained, the redistribution starts with $\delta < 1$. For the generic balanced situation with

$$M_3 = \delta M_{3e} = \delta pl^2/8$$
$$M_o \cong M_{oe} + 0.4(1 - \delta)M_{3e} = [1 + 0.4(1 - \delta)c]pl^2/14.2$$

the capacity p_r is deduced by the comparison of acting moments with the respective resistances

$$\frac{\delta pl^2}{8} \le \overline{M}_3 \qquad (= c_3\overline{M}_{3e})$$
$$\frac{1 + 0.4(1 - \delta)c}{14.2} pl^2 \le \overline{M}_o \qquad (= c_o\overline{M}_{oe})$$

from which, con $\overline{M}_{3e} = p_e l^2/8$ and $\overline{M}_{oe} = p_e l^2/14.2$, the following values are obtained:

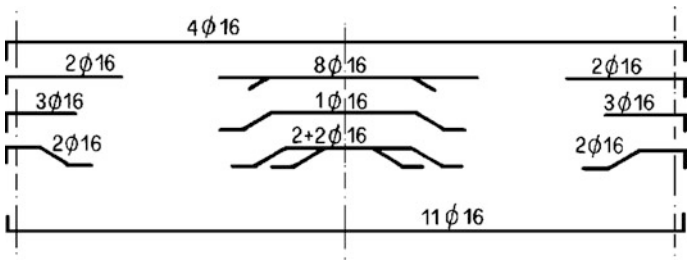


Fig. 5.47 General layout of longitudinal reinforcement

$$p_{3r} = \frac{c_3}{\delta} p_e = \gamma_3 p_e$$
$$p_{or} = \frac{c_o}{1 + 0.4(1 - \delta)c} p_e = \gamma_o p_e$$

From the curves of Fig. 5.46, it can be noted that the capacity based on the resistance of the fixed-end increases when δ decreases, the one based on the resistance of the span section decreases instead.

A plastic design would identify the collapse ultimate situation in point δ'_p of intersection of the curves, with the full utilization $(\gamma = 1)$ of the structural design.

The limited plastic rotational capacity of section *3* can instead lead to its early failure at point $\delta_{u'}$ with a capacity limited to γ_u, and the exuberant proportioning of the span section *O* would remain unutilized.

Any arbitrary value of the reduction coefficient δ, included in the compatible interval $\delta_u < \delta < 1$ and followed by the calculation of the corresponding moments in the critical sections, leads to a conservative safety verification with $\gamma < \gamma_u$.

A design carried within the limits $\delta_u < \delta''_p < 1$ of the compatible redistribution, such as the one indicated with dotted lines in the graph of Fig. 5.46, with $\gamma = 1$ leads to a full utilization of the structural design (Fig. 5.47).

5.4 Case A: Shallow Rectangular Beam

The design of the beam already analyzed at Sect. 4.4.1 is now repeated, assuming a different solution, which is a flat shallow beam within the floor depth (see Fig. 5.48), relying on the relevant width of the solid strip necessary for the transverse ribs of the floor. The consequences of the better architectural functionality are the higher reinforcement and the higher flexibility of the beam in bending. For static aspects, punching shear verifications will have to be added due to the limited dimensions of columns where the shear stresses are concentrated as already described in details at Sect. 5.2.3.

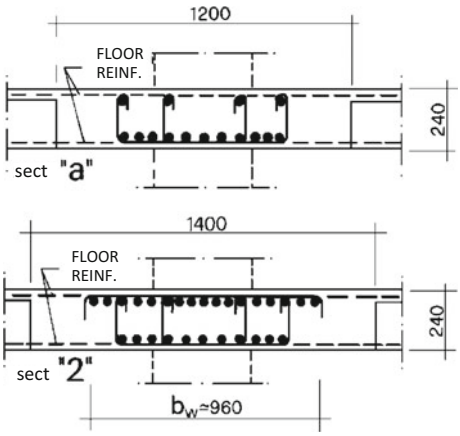


Fig. 5.48 Shallow beam sections at mid-span "a" and central support "2"

The stress analysis under the loads a little reduced due to the lower self-weight of the beam (po = 31.6 kN/m instead of 34.6 kN/m) is not repeated. Assuming therefore the same values of forces calculated at Sect. 4.4.1, one has (with $\gamma_F \cong 1.43$) the following proportioning.

Longitudinal Reinforcement

Section '1' (M = 97,840 Nm, d = 20 cm)

$$A_s = \frac{9{,}784{,}000 \times 1.43}{0.9 \times 20 \times 39{,}100} = 19.88\,\text{cm}^2$$

$11\phi16$ are assumed for 22.12 cm^2
Section 'a' (M = 95,550 Nm, d = 20 cm)

$$A_s = \frac{9{,}555{,}000 \times 1.43}{0.9 \times 20 \times 39{,}100} = 19.41\,\text{cm}^2$$

$11\phi16$ are assumed for 22.12 cm^2
Section '2' (M = 146,770 Nm, d = 20 cm)

$$A_s = \frac{14{,}677{,}000 \times 1.43}{0.9 \times 20 \times 39{,}100} = 29.82\,\text{cm}^2$$

$17\phi16$ are assumed for 34.18 cm^2.
A layout of the longitudinal reinforcement, to be subject to further verifications, is assumed as indicated in Fig. 5.47.

Transverse Reinforcement

Assuming a tentative value $\lambda_c = 2$, with $z \cong 0.9d = 18$ cm, the distance of the first design section from the column axis ($e = a/2 - 0.2d$) is evaluated:

$$x = e + \frac{z}{2}\lambda_c = 11 + 18 = 29 \text{ cm}$$

having indicated with a = 30 cm the side of the column.

It is decided to proportion current stirrups the beam with reference to half of the shear acting on the most stressed end 2′:

$$V^*_{\text{Ed}} = 1.43(170.66 - 63.5 \times 0.29) = 217.71\,\text{kN}$$

$$a_{\text{s}} = \frac{V_{\text{Ed}}/2}{\text{zf}_{\text{yd}}\lambda_{\text{c}}} = \frac{217{,}710/2}{18 \times 391 \times 2} = 7.73\,\text{cm}^2/\text{m}$$

With a spacing limited to s $\leq$ 0.8d = 160 mm, 1 + 1ϕ6/140 are assumed for 8.07 cm^2/m.

The following resisting shear force corresponds to the current stirrups distribution proportioned this way (see Fig. 5.48):

$$V'_{\text{Rd}} = 8.07 \times 18 \times 391 \times 2/1000 = 113.59\,\text{kN}$$

which, with $p_{\text{d}} = 1.43 \times 63.5 = 90.8$ kNm, leaves uncovered the following portions of longitudinal shear Q (see Fig. 5.49).

• *End* ‘1’ ($V_{1\text{d}} = 1.43 \times 136.52 = 195.22$ kN)

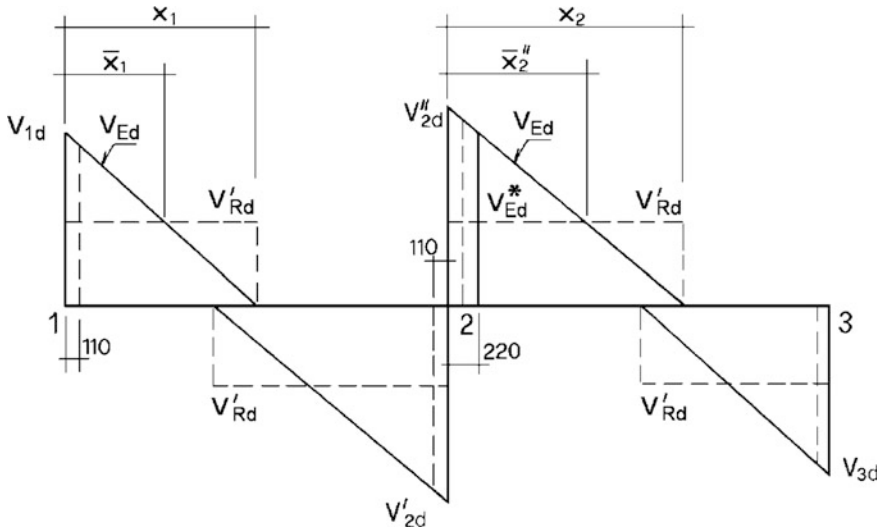


Fig. 5.49 Diagrams of acting and resisting shear

$$\bar{x}_1 = \frac{195.22 - 113.59}{90.8} = \frac{81.63}{90.8} = 0.90 \text{ m}$$

$$Q''_{Ed} \cong \frac{1}{2} 81.63 \times 90/18 = 204.07 \text{ kN}$$

with bent bars at $\alpha = 30°(\sin\alpha = 0.50\ \lambda_s = 1.73)$ one has

$$A_s = \frac{Q''_{Ed}}{0.8 f_{yd} \sin\alpha(\lambda_c + \lambda_s)} = \frac{204{,}070}{0.8 \times 39{,}100 \times 0.5 \times 3.73} = 3.50 \text{ cm}^2$$

$2\phi 16$ are assumed for 4.02 cm^2.
End 2' (V'_{2d} = 1.43 × 170.66 = 244.04 kN)

$$\bar{x}'_2 = \frac{244.04 - 113.59}{90.8} = \frac{130.45}{90.8} = 1.44 \text{ m}$$

$$Q''_{Ed} \cong \frac{1}{2} 130.45 \times 144/18 = 521.80 \text{ kN}$$

with bent bars at $\alpha = 30\,(\sin\alpha = 0.50\ \lambda_s = 1.73)$ one has

$$A_s = \frac{521{,}800}{0.8 \times 39{,}100 \times 0.5 \times 3.73} = 8.94 \text{ cm}^2$$

$5\phi 16$ are assumed for 10.05 cm^2.

5.4.1 Serviceability Verifications

With reference to the structural layout described in Fig. 5.50, deduced from the proportioning calculations of the reinforcement carried in the previous pages, the verifications of stresses in the materials under service loads are now reported.

Flexural Forces
For the verifications of the maximum compressions in concrete, one can refer to the allowable stress value (see Sect. 2.4.1):

$$\bar{\sigma}_c = 11.2 \text{ N/mm}^2$$

The allowable value of tensile stresses in steel, for rebar diameters $\phi \leq 16$ mm such as the ones used in the beam under analysis, becomes (see Table 2.16):

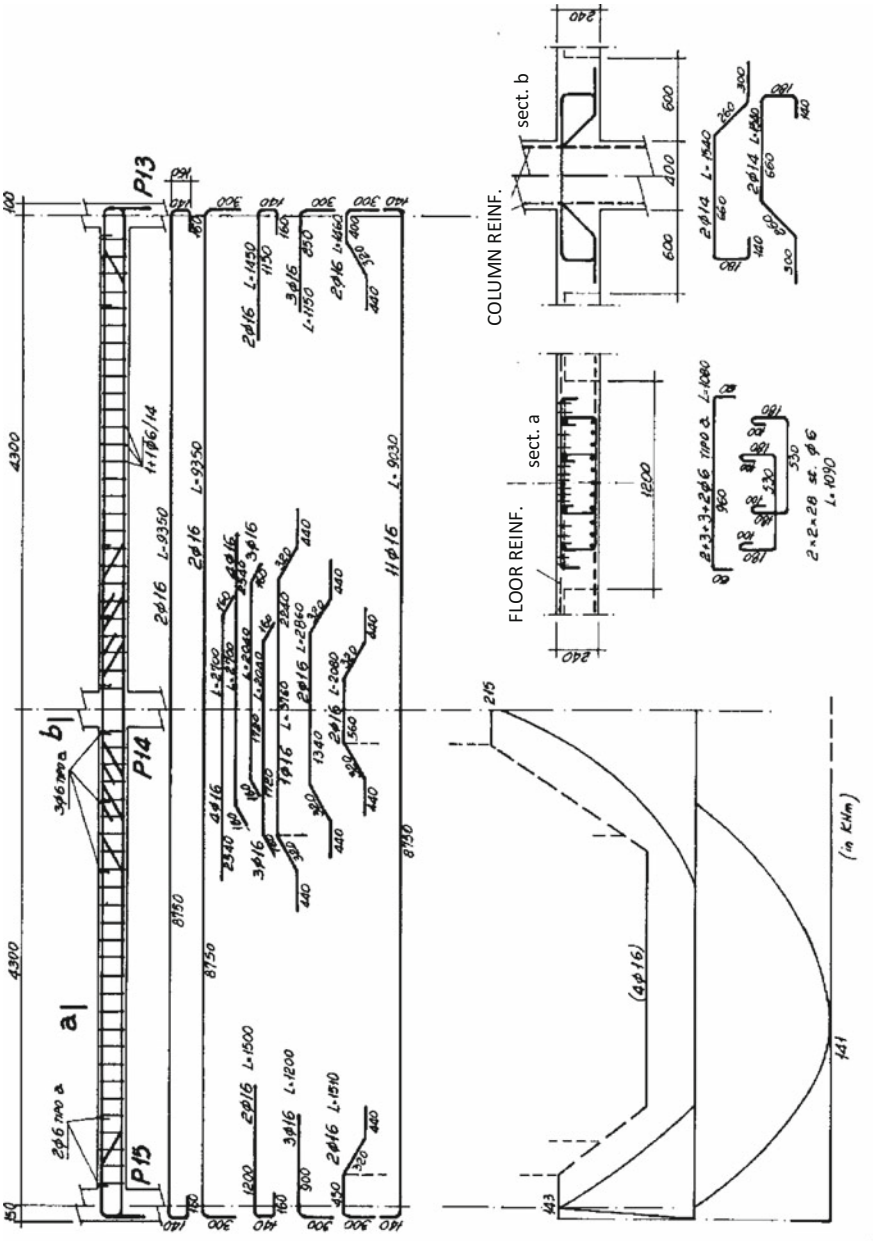


Fig. 5.50 Reinforcement details of the beam

$$\bar{\sigma}'_{\mathrm{s}} = 280\,\mathrm{N/mm^2} \quad \left(< 0.8 f_{\mathrm{yk}} = 360\,\mathrm{N/mm^2}\right)$$

and it refers to the cracking verification. We conservatively refer again to the rare combination of actions.

In order to identify the effective width of the concrete in compression, a 45° distribution of stresses is assumed at the end 1 starting from the free edge of the column from which the fixed-end moment comes from. Setting the first verification section at the internal edge of the same column, one has an effective width

$$b_{\mathrm{f}} = b + 2\mathrm{a} = 40 + 2 \times 30 = 100\,\mathrm{cm}$$

where a, b are the sides of the cross section of the column.

No significant bending action comes to the continuity of section *2* from the internal column, but only the vertical reaction localized within the column footprint. It is assumed that the unidirectional analysis of stresses, assumed constant on the effective width b_{f}, can be approximately be extended to two segments equal to a maximum of $3d$. One therefore has

$$b_{\mathrm{f}} \leq b + 2 \times 3\mathrm{d} = 40 + 6 \times 20 = 160\,\mathrm{cm}$$

Actually the solid concrete strip has been brought to b_{f} = 140 cm on the beam part corresponding to the central column, whereas it has been limited to b_{f} = 120 cm on the central part of the span. The section 'a' can therefore rely on the latter effective width, neglecting the contribution of the topping (t = 4 cm) which further extends on the floor.

Section '1'
(M = 97840 Nm, d = 20 cm, b = 100 cm, d' = 4 cm, A_{s} = 22.12 cm^2, A'_{s} = 22.12 cm^2)

$$\rho_{\mathrm{t}} = \frac{22.12 + 22.12}{100 \times 20} = \frac{44.24}{2000} = 0.0221$$

$$\psi_{\mathrm{t}} = 15 \times 0.0221 = 0.3318$$

$$\delta = \frac{22.12 \times 20 + 22.12 \times 4}{44.24 \times 20} = 0.600$$

$$x = 0.3318\left\{-1 + \sqrt{1 + \frac{2 \times 0.600}{0.3318}}\right\}20 = 0.3811 \times 20 = 7.62\,\mathrm{cm}$$

$$I_i = 100 \times 7.62^3/3 + 15 \times 22.12 \times 12.38^2 + 15 \times 22.12 \times 3.62^2$$
$$= 147{,}400 + 50{,}853 + 4384 = 69{,}950\,\mathrm{cm^4}$$

$$\sigma_{\mathrm{c}} = \frac{97{,}840}{69{,}950}7.62 = 10.7\,\mathrm{N/mm^2} \quad (< \bar{\sigma}_{\mathrm{c}})$$

$$\sigma_{\mathrm{s}} = 15\frac{97{,}840}{69{,}950}12.38 = 260\,\mathrm{N/mm^2} \quad (< \bar{\sigma}'_{\mathrm{s}})$$

Section '*a*'
(M = 95550 Nm, d = 20 cm, b = 120 cm, d' = 4 cm, A_s = 22.12 cm^2, A'_s = 8.04 cm^2)

$$\rho_t = \frac{22.12 + 8.04}{120 \times 20} = \frac{30.16}{2400} = 0.0126$$
$$\psi_t = 15 \times 0.0126 = 0.1885$$
$$\delta = \frac{22.12 \times 20 + 8.04 \times 4}{30.16 \times 20} = 0.787$$
$$x = 0.1885\left\{-1 + \sqrt{1 + \frac{2 \times 0.787}{0.1885}}\right\}20 = 0.3878 \times 20 = 7.76\,\text{cm}$$
$$I_i = 120 \times 7.76^3/3 + 15 \times 22.12 \times 12.24^2 + 15 \times 8.04 \times 3.76^2$$
$$= 18{,}692 + 49{,}709 + 1705 = 70{,}106\text{cm}^4$$
$$\sigma_c = \frac{95{,}550}{70{,}106}7.76 = 10.6\,\text{N/mm}^2 \quad (< \bar{\sigma}_c)$$
$$\sigma_s = 15\frac{95{,}550}{70{,}106}12.24 = 250\,\text{N/mm}^2 \quad (< \bar{\sigma}'_s)$$

Section '2'
(M = 146,770 Nm, d = 20 cm, b = 140 cm, d' = 4 cm, A_s = 34.18 cm^2, A'_s = 22.12 cm^2)

$$\rho_t = \frac{34.18 + 22.12}{140 \times 20} = \frac{56.30}{2800} = 0.0201$$
$$\psi_t = 15 \times 0.0201 = 0.3016$$
$$\delta = \frac{34.18 \times 20 + 22.12 \times 4}{56.30 \times 20} = 0.686$$
$$x = 0.3016\left\{-1 + \sqrt{1 + \frac{2 \times 0.686}{0,3016}}\right\}20 = 0.4087 \times 20 = 8.17\,\text{cm}$$
$$I_i = 140 \times 8.17^3/3 + 15 \times 34.18 \times 11.83^2 + 15 \times 22.12 \times 4.17^2$$
$$= 25{,}449 + 71{,}752 + 5770 = 102{,}971\text{cm}^4$$
$$\sigma_c = \frac{146{,}770}{102{,}971}8.17 = 11.6\,\text{N/mm}^2 \quad (< \bar{\sigma}_c)$$
$$\sigma_s = 15\frac{146{,}770}{102{,}971}11.83 = 253\,\text{N/mm}^2 \quad (< \bar{\sigma}'_s)$$

Shear Forces
Being the case of flat beam with protected lateral edges, no serviceability shear verification is necessary.

5.4.2 Resistance Verifications

We refer to the same load combinations elaborated at Sect. 4.4.3 for the solution of dropped beam. The values of material strengths are taken from the same paragraph.

Flexural Resistance

$$f_{yd} = 391\ \text{N/mm}^2 \quad \varepsilon_{yd} = 391/2050 = 0.191\%$$
$$f_{cd} = 14.2\ \text{N/mm}^2 \quad \varepsilon_{cu} = 0.35\%$$
$$r = f_{yd}/f_{cd} = 27.5 \quad \alpha = \varepsilon_{cu}/\varepsilon_{yd} = 1.832$$

Section '1'
(d = 20 cm, b = 100 cm, d' = 4 cm, $\delta' = d'/d = 0.200$, A_s = 22.12 cm^2, A'_s = 22.12 cm^2)

$$\omega_s = \frac{22.12}{100 \times 20} 27.5 = 0.304$$
$$\omega'_s = \frac{22.12}{100 \times 20} 27.5 = 0.304$$

reinforcement in compression in the elastic range

$$\omega_s - \omega'_s \alpha_o = -0.2529$$
$$\overline{x} = \frac{1}{2}\left\{ \left(\omega_s - \omega'_s \alpha_o\right) + \sqrt{\left(\omega_s - \omega'_s \alpha_o\right)^2 + 3.2\delta' \omega'_s \alpha_o} \right\} d$$
$$= 0.1977 \times 20 = 3.95\ \text{cm}$$
$$x = \overline{x}/0.8 = 4.94\ \text{cm}$$
$$\varepsilon'_s = \frac{\text{x} - \text{d}'}{x} \varepsilon_{cu} = 0.067\% \quad \left(< \varepsilon_{yd}\right)$$
$$z_s = \text{d} - 0.5\overline{x} = 18.02\ \text{cm}$$
$$z'_s = 0.5\overline{x} - d' = -2.02\ \text{cm}$$
$$\sigma'_s = \varepsilon'_s E_s = 0.00067 \times 205{,}000 = 137\ \text{N/mm}^2$$
$$M_{Rd} = A_s f_{yd} z_s - A'_s \sigma'_s z'_s = 157.58 - 6.09 = 151.49\ \text{kNm}$$
$$M_{Ed} = 139.14\ \text{kNm} \quad \left(< M_{Rd}\right)$$

Section '*a*'
(d = 20 cm, b = 120 cm, d' = 4 cm, $\delta' = d'/d = 0.200$, A_s = 22.12 cm^2, A'_s = 8.04 cm^2)

$$\omega_s = \frac{22.12}{120 \times 20} 27.5 = 0.253$$
$$\omega'_s = \frac{8.04}{120 \times 20} 27.3 = 0.0921$$

reinforcement in compression in the elastic range

$$\omega_s - \omega'_s \alpha_o = +0.0843$$
$$\bar{x} = \frac{1}{2}\left\{0.0843 + \sqrt{0.0843^2 + 3.2 \times 0.200 \times 0.0921 \times 1.832}\right\} 20$$
$$= 0.2236 \times 20 = 4.47\,\text{cm}$$
$$x = 4.47/0.8 = 5.59\,\text{cm}$$
$$\varepsilon'_s = \frac{5.59-4}{5.59} 0.35 = 0.100\% \quad (< \varepsilon_{yd})$$
$$z_s = 20 - 0.5 \times 4.47 = 17.76\,\text{cm}$$
$$z'_s = 0.5 \times 4.47 - 4 = -1.76\,\text{cm}$$
$$\sigma'_s = 0.0001 \times 205{,}000 = 205\,\text{N/mm}^2$$
$$M_{Rd} = A_s f_{yd} z_s - A'_s \sigma'_s z'_s = 153.60 - 2.90 = 150.70\,\text{kNm}$$
$$M_{Ed} = 147.46\,\text{kNm} \quad (< M_{Rd})$$

Section '2'
(d = 20 cm, b = 140 cm, d' = 4 cm, δ' = d'/d = 0.200, A_s = 34.18 cm^2, A'_s = 22.12 cm^2)

$$\omega_s = \frac{34.18}{140 \times 20} 27.5 = 0.3357$$
$$\omega'_s = \frac{22.12}{140 \times 20} 27.5 = 0.2173$$

reinforcement in compression in the elastic range

$$\omega_s - \omega'_s\alpha_o = -0.0624$$

$$\bar{x} = \frac{1}{2}\left\{-0.0624 + \sqrt{0.0624^2 + 3.2 \times 0.200 \times 0.2173 \times 1.832}\right\}20$$

$$= 0.2231 \times 20 = 4.46\,\text{cm}$$

$$x = 4.46/0.8 = 5.58\,\text{cm}$$

$$\varepsilon'_s = \frac{5.58-4}{5.58}0.35 = 0.099\% \quad (<\varepsilon_{yd})$$

$$z_s = 20 - 0.5 \times 4.46 = 17.77\,\text{cm}$$

$$z'_s = 0.5 \times 4.46 - 4 = -1.77\,\text{cm}$$

$$\sigma'_s = 0.000990 \times 205{,}000 = 203\,\text{N/mm}^2$$

$$M_{Rd} = A_s f_{yd} z_s - A'_s \sigma'_s z'_s = 237.48 - 7.95 = 229.53\,\text{kNm}$$

$$M_{Ed} = 208.66\,\text{kNm} \quad (<M_{Rd})$$

Shear Resistance

$$f_{yd} = 391\,N/\text{mm}^2$$

$$f_{c2} = 7.1\,N/\text{mm}^2$$

$$r = f_{yd}/f_{c2} = 55.1$$

It is conservatively assumed

$$\lambda_c = \lambda_{max} = 2 \quad (\omega_w \le \omega_{wa} = 0.20)$$

Effective width
(Section 2′ of maximum shear, x = 29 cm)

$$V_{2d} = 242.61\,\text{kN} \quad p_d = 90.29\,\text{kN/m}$$

$$V_{Ed} = 242.61 - 90.29 \times 0.29 = 216.43\,\text{kN}$$

$$b_o = \frac{1+\lambda_c^2}{0.9\lambda_c}\frac{V_{Ed}}{df_{c2}} = 2.78\frac{216{,}430}{20 \times 710} = 42\,\text{cm}$$

$$b_o \cong 40\ \text{cm} \quad (\text{column side})$$

Even though the column width is sufficient for the resistance, the maximum value is assumed for b_w compatible with the presence of stirrups with 4 links:

$$b_w \cong 4 \times 1.2 \times d = 96\,\text{cm}$$

which corresponds to the dimension necessary for a good distribution of longitudinal reinforcement (see Fig. 5.48). With $b_w \gg b_o$, the situation of low web reinforcement and the conservative verification value $\lambda_c = \lambda_{max} = 2$ remain. The current shear resistance, corresponding to 8.07 cm^2/m of vertical stirrups, is the one already calculated when proportioning the reinforcement:

$$V'_{Rd} = 114.46\,\text{kN}$$

More precise verifications of bent bars added at the span ends are shown below. For these verifications the longitudinal shear force corresponding to the uncovered part of the shear is evaluated. As indicated in Fig. 5.51, such portion consists of a rectangular portion that extends from the centre 'e' of the support reaction up to the first verification section 'x', plus a triangular part that extends from the latter section up to the one '$\bar{x}$' of current resistance.

End '1'

(z = 18 cm, $\sin\alpha = 0.5$, $\lambda_s = 1.73$, A_s = 4.02 cm^2)

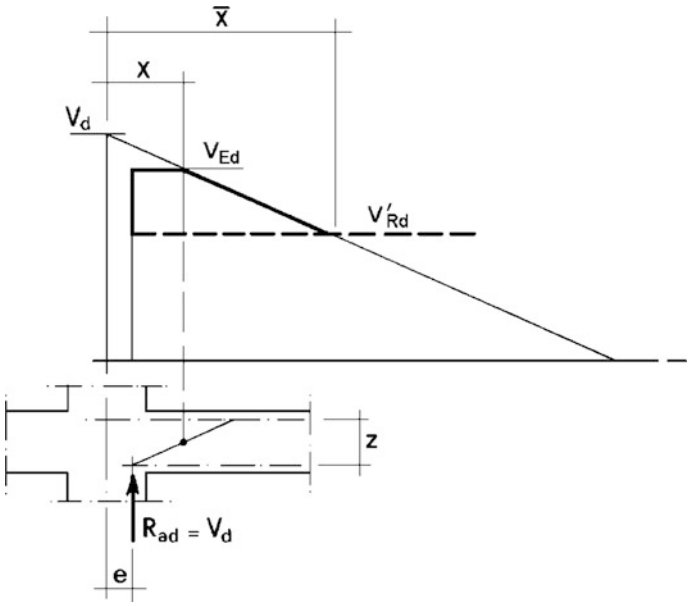


Fig. 5.51 Distribution of shear action between stirrups and bent bars

$$V_{1d} = 195.22\,\text{kN} \quad p_d = 90.8\,\text{kN/m}$$
$$e = 11\ \text{cm} \qquad x = 29\ \text{cm}$$
$$V_{Ed} = 195.22 - 90.8 \times 0.29 = 168.89\,\text{kN}$$
$$\bar{x}_1 = \frac{195.22 - 113.59}{90.8} = \frac{81.63}{90.8} = 0.90\,\text{m}$$
$$(29 - 11) \times 81,63 \quad = 1469$$
$$(88 - 29) \times 81,63/2 \quad = 2408 \quad Q''_{Ed} = 3877/18 = 215.39\ \text{kN}$$
$$Q''_{Rd} = 0.8 A_s f_{yd} \sin\alpha(\lambda_c + \lambda_s)$$
$$= 0.8 \times 4.02 \times 39.1 \times 0.5 \times 3.73 = 234.52\,\text{kN} \quad \left(> Q''_{Ed}\right)$$

End '2'
(z = 18 cm, $\sin\alpha = 0.5$, $\lambda_s = 1.73$, A_s = 10.05 cm^2)

$$V'_{2d} = 244.04\,\text{kN} \quad p_a = 90.8\,\text{kN/m}$$
$$e = 11\ \text{cm} \qquad x = 29\ \text{cm}$$
$$V_{Ed} = 244.04 - 90.8 \times 0.29 = 217.71\,\text{kN}$$
$$\bar{x}_2 = \frac{244.04 - 113.59}{90.8} = \frac{130.45}{90.8} = 1.44\,\text{m}$$
$$(29 - 11) \times 130.45 = 2348$$
$$(142 - 29) \times 130.45/2 = 7370$$
$$Q''_{Ed} = 9718/18 = 540\ \text{kN}$$
$$Q''_{Rd} = 0.8 \times 10.05 \times 39.1 \times 0.5 \times 3.73 = 586\,\text{kN} \quad \left(> Q''_{Ed}\right)$$

Punching Shear

The verification of the beam support on the column is now shown, only for the most stressed end 2. The resisting value of the reaction is to be calculated, on the basis of the inclined compressions that go inside the column, both from the front edge of width b = 40 cm, and from the two lateral sides of length $a/2$ = 15 cm each.

Being the case of a beam with shear reinforcement, is assumed $\lambda_o = \lambda_c/2 = 1$ is assumed, obtaining the resistance (with $u_o = a/2 + b + a/2$ = 70 cm):

$$R'_{Rd} = 0.6 u_o d f_{cd} / \left(1 + \lambda_0^2\right) = 0.6 \times 70 \times 20 \times 1.42/2 = 596.40\,\text{kN}$$

whereas the applied force is equal to:

$$R'_{Ed} = 242.61\,\text{kN} \quad \left(\ll R'_{Rd}\right)$$

Having assumed a resisting width of the web b_w = 96 cm, a force comes from the contiguous protrusion on each lateral edge of the column which is equal to

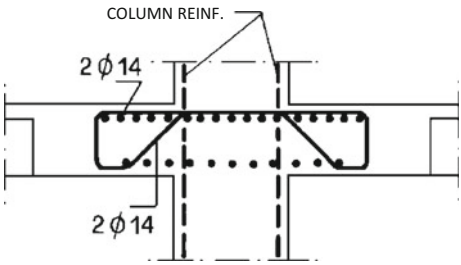


Fig. 5.52 Transverse reinforcement above the column

$$R'_{\mathrm{E}} = \frac{96 - 40}{96}\frac{242.61}{2} = 70.76\,\mathrm{kN}$$

Summing up the one coming from the opposed (symmetric) span, one has in total

$$R_{\mathrm{E}} = R'_{\mathrm{E}} + R''_{\mathrm{E}} = 141.52\,\mathrm{kN}$$

It is decided to resist such action with:

- $2\phi14$ straight for 3.08 cm^2 ($\mathrm{l_s}$ = 28 cm)
- $2\phi14$ bent for 3.08 cm^2 ($\alpha = 45°$)

arranged above the column across the beam (see Fig. 5.52). The resistance is therefore equal to (with $\lambda_s = \mathrm{l_s}/z = 28/18 = 1.56$):

$$\begin{aligned} 3.08 \times 39.1/1.56 &= 77.20 \\ 3.08 \times 39.1/\sqrt{2} &= \underline{85.41} \\ \mathrm{R_r} &= 162.61\ \mathrm{kN} \quad (> R_{\mathrm{E}}) \end{aligned}$$

It can be noted on the mentioned Fig. 5.52 how both reinforcements pick up the inclined flux of compressions in the web at the bottom face of the beam.

Regarding the column at the end 1, being an end edge of the floor there is certainly an adequately reinforced edge beam, which is a beam transverse to the main one with longitudinal reinforcement and stirrups. Therefore, its design includes, in addition to directly applied loads (such as the weight of the cladding walls), also the lateral actions transferred by the protrusions of the main beam.

5.4.3 *Deflection Calculations*

Finally, a brief deformation calculation is shown under the linear pseudoelastic assumption referred to the geometrical concrete section. From this calculation a functional indication useful for the type of construction under study is expected. Excessive deformability of the elements in bending of the decks (floors and beams)

could be incompatible with the integrity of the non-structural walls and cause their extensive cracking. Other issues might arise, such as for example the spalling of floors made of hollow bricks and concrete.

For the evaluation of deformations, the analysis of loads carried at Sects. 2.4.1 and 3.4.1 is recalled with

• permanent loads with fixed pattern	4.70	kN/m^2
• permanent loads with variable pattern	2.30	kN/m^2
• variable accidental loads	2.00	kN/m^2

which led to evaluate on the beam under consideration the actions listed at Sect. 4.4.1:

$$\begin{aligned} p_o &= 34.6 \quad kN/m \quad \text{permanent fixed} \\ p'_1 &= 15.5 \quad kN/m \quad \text{permanent with variable pattern} \\ p''_1 &= 13.4 \quad kN/m \quad \text{accidental} \end{aligned}$$

Such distinction is required to establish the load combination in the calculation of the span deflection, assuming the one '*O*' with loads on both spans (of the layout of Fig. 4.41a) for permanent fixed, assuming the one with loads on the concerned span only for the variable pattern part. The following deflections correspond to these two conditions respectively:

$$v \cong \frac{1}{200} \frac{p1^4}{EI}$$

or

$$v \cong \frac{1}{120} \frac{p1^4}{EI}$$

The parameter that measures the *flexural deformability* for the functional verifications mentioned above is the ratio *v*/l between the maximum span deflection and the span length of the concerned element. Indicatively the following limit values can be given:

$\frac{1}{200} < \frac{v}{1}$	Excessive deformations for any type of structural element
$\frac{1}{400} < \frac{v}{1} < \frac{1}{200}$	Significant deformations acceptable for roofs and without non-structural walls
$\frac{1}{800} < \frac{v}{1} < \frac{1}{400}$	Average deformations allowable except for specific requirements
$\frac{v}{1} < \frac{1}{800}$	Small deformations required for specific functional requirements

It is to be noted that the concerned functional verifications should refer to the maximum range of the deflection that the element to be protected is supposed to withstand. In the case under examination for example, being the case of the

integrity of non-structural walls, instantaneous deformations due to structural self-weight and permanent loads including the self-weight of the partitions, should not be considered. The increase in deflection subsequent to the completion of walls shall be computed, therefore adding up:

- the viscous part $\phi_\infty v_g$ of the deformation due to permanent loads p_o e p'_1;
- the total deformation $(1 + \phi_\infty)v'_q$ due to the quasi-permanent part
- $\psi_2 p''_1$ of variable loads (with $\psi_2 = 0.3$ from Chart 3.2);
- the elastic deformation v''_q due to the remaining part $(1 - \psi_2)p''_1$ of variable loads.

The following distinction also has to be made:

$$\begin{aligned} \psi_2 p''_1 &= 0.3 \times 13.4 = 9.4\,\text{kN/m} \\ (1-\psi_2)p''_1 &= 0.7 \times 13.4 = 9.4\,\text{kN/m} \end{aligned}$$

It is assumed, with $f_{ck} = 25$ N/mm^2, and $f_{cm} = f_{ck} + 8 = 33$ N/mm^2, an elastic modulus (see Table 1.2a):

$$E = E_{cm} = 2200[f_{cm}/10]^{0.3} \cong 31{,}000\,\text{N/mm}^2$$

and a creep coefficient (see Table 1.16):

$\phi_\infty = 3.1$ (low class, medium dry environment)

The moment of inertia of the typical section is equal to:

$$I = I_c = 120 \times 24^3/12 \cong 138{,}000\,\text{cm}^4$$

One therefore has

$$\begin{aligned} (0+3.1)\ 34.6/200 &= 0.536 \\ (0+3.1)\ 15.5/120 &= 0.400 \\ (1+3.1)\ 4.0/120 &= 0.137 \\ (1+0.0)\ 9.4/120 &= 0.078 \\ &\quad 1.151\,\text{N/mm} \end{aligned}$$

$$\frac{I^4}{E_c I_c} = \frac{4.30^4 \times 10^{10}}{310 \times 13.8 \times 10^8} = 7.99\,\text{mm}^2/\text{N}$$

$$v = 7.99 \times 1.151 = 9.09\,\text{mm}$$

and in relation to the span length one has the value

$$\frac{v}{l} = \frac{9.09}{4300} = \frac{1}{473} \quad \left(< \frac{1}{400}\right)$$

close to the allowable limit. It can be noted how the solution of flat beam can lead to problems of excessive deformability.

For the dropped beam solution (see Fig. 4.43) one would have:

$$120 \times 24 = 2880 \times 12 = 34560$$
$$40 \times 30 = \underline{1200} \times 39 = \underline{46800}$$
$$A_c = 4080\,\text{cm}^2 \quad S_c = 81360\,\text{cm}^3$$

$$y_c = 81360/4080 = 19.9\text{cm}$$
$$19.9 - 12.0 = 7.9\,\text{cm} \quad 19.9 - 39.9 = -20\,\text{cm}$$

$$2880\left(24^2/12 + 7.9^2\right) \cong 318000$$
$$1200\left(30^2/12 + 19.1^2\right) \cong \underline{528000}$$
$$I_c = 846000\,\text{cm}^4$$

$$v = 9.09 \times 138{,}000/846{,}000 = 1.48\,\text{mm}$$
$$\frac{v}{I} = \frac{1.48}{4300} = \frac{1}{2900}$$

which shows a very small deformability.

For the calculation of deformations more rigorous methods can surely be adopted than the one based on the use of approximated formulas, as deduced from an estimation of the effectiveness of rotational constraints at the ends of the beam span examined. For example the solution of the partial hyperstatic frame of Fig. 4.40 can be developed under the competent loads conditions. Further to a more rigorous solution, it is also possible to introduce the effects of cracking as indicated at Sects. 3.3 and 5.3.1.

Appendix: Elements in Bending

Chart 5.1: Arch Behaviour: Formulas

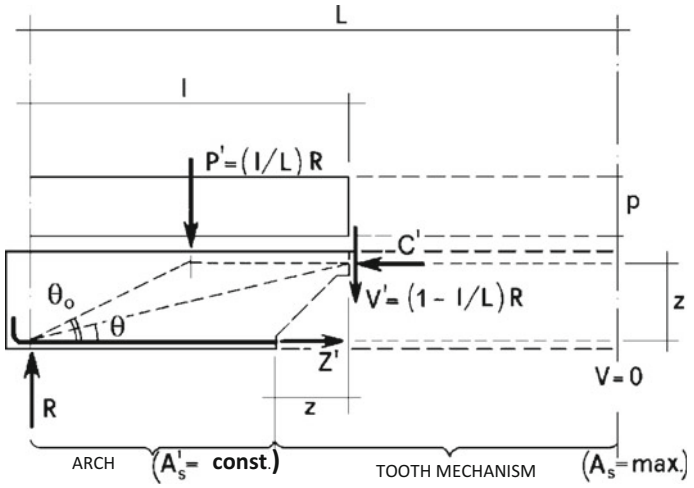
RC elements in bending without transverse shear reinforcement.

Symbols (see figure)

p_{Ed}	design value of the applied distributed load
L	distance of the section of maximum moment
$R_{Ed} = p_{Ed}\,L$	design action on the support
R_{Rd}	design value of the resistance at the support
d	effective depth (flexural) of the element
z ($\cong 0.9d$)	lever arm of the internal couple

l	length of the arch behaviour ($z \leq l \leq L$)
$\lambda = l/z$	inclination of the lower strut (= ctg θ)
$\lambda_o = \lambda/2$	inclination of the upper strut (= ctg θ_o)
b_w	minimum web thickness of the element
A'_s	longitudinal reinforcement of the arch behaviour

see also Charts 2.2 and 2.3.



Resistance Verification

$$R_{Rs} = \frac{A'_s f_{yd}}{\lambda} \frac{2L}{2L-1}$$

$$R_{Rc} = 0.4 d\, b_w f_{cd} \frac{4L}{8L-31}$$

$$R_{Rd} = \min(R_{Rs}, R_{Rc}) \geq R_{Ed}$$

Chart 5.2: Bearing Details: Formulas

RC elements in bending

Symbols

R_{Ed}	design action at the support
R_{Rd}	design value of the resistance at the support
A_{sl}	area of the longitudinal reinforcement at the support

A_{st}	area of the bent bars at the support
α	bending angle of the bars on the horizontal
l	bending distance from the support
d	effective depth (flexural) of the element
$z(\cong 0.9d)$	lever arm of the internal couple
b_w	minimum web thickness of the element
θ	angle of the compressions in the web at the limit of shear resistance
$\lambda_c = \text{ctg } \theta$	inclination of the transverse compressions in the web
$\lambda_o = \lambda_c/2$	mean inclination of compressions at the support
$\gamma_R = 1.25$	reliability coefficient of the model

see also Charts 2.2, 2.3, 4.1 and 4.2.

Elements Without Stirrups

$$
\begin{aligned}
R'_{Rs} &= A_{s1} f_{yd} \quad \left(\geq R''_{rs}\right) \\
R''_{Rs} &= A_{st} f_{yd} \sin\alpha \quad (1 \leq z/2) \\
R_{Rs} &= R'_{Rs} + R''_{Rs} \geq R_{Ed} \\
R_{Rc} &= 0.2\, d\, b_w f_{cd} R_{Ed} / R'_{Rs} \geq \gamma_R R'_{Rs}
\end{aligned}
$$

Elements with Stirrups

$$
\begin{aligned}
R'_{Rs} &= A_{s1} f_{yd} / \lambda_o \qquad \left(\geq R''_{Rs}\right) \\
R''_{Rs} &= A_{st} f_{yd} \sin\alpha \qquad (1 \leq z/2) \\
R_{Rs} &= R'_{Rs} + R''_{Rs} \geq R_{Ed} \\
R_{Rc} &= 0.6\, d\, b_w f_{cd} R_{Rs} / \left[R'_{Rs}\left(1 + \lambda_0^2\right)\right] \geq \gamma_R R'_{Rs}
\end{aligned}
$$

For minimum stirrups see Chart 4.5.

Chart 5.3: Corbels: Formulas

RC elements in bending

Symbols

P_{Ed}	design value of the applied load on the corbel
P_{Rd}	design value of the resistance
l ($\leq 2z$)	distance of the load from the fixed-end (or of the resultant)
A_{sl}	area of the longitudinal reinforcement of the corbel
A_{st}	area of bent bars
α	bending angle of bars on the horizontal
d	effective depth (flexural) of the cantilever

z ($\cong 0.9d$)	lever arm of the internal couple
b_w	minimum web thickness of the cantilever
$\lambda = l/z$	inclination of transverse compressions in the web
b	width of the compression flange
$\gamma_R = 1.25$	reliability coefficient of the model

see also Charts 2.2, 2., 4.1 and 4.2.

Resistance Verification

$$P'_{Rs} = A_{s1} f_{yd} / \lambda \quad \left(\geq P''_{Rs}\right)$$
$$P''_{Rs} = A_{st} f_{yd} \sin \alpha$$
$$P_{Rs} = P'_{Rs} + P''_{Rs} \geq P_{Ed}$$
$$P''_{Rc} = 0.2 d\, b f_{cd} P_{Rs} / \left[\lambda P''_{Rs}\right] \geq \gamma_R P''_{Rs}$$

- *Corbels without stirrups*

$$P'_{Rc} = 0.4 d b_w f_{cd} P_{Ed} / \left[P'_{Rs}\left(1 + \lambda^2\right)\right] \geq \gamma_R P'_{Rs}$$

- *Corbels with stirrups*

$$P'_{Rc} = 0.6 d b_w f_{cd} P_{Ed} / \left[P'_{Rs}\left(1 + \lambda^2\right)\right] \geq \gamma_R P'_{Rs}$$

For the minimum stirrups see Chart 4.5.

Chart 5.4: Punching Shear in Slabs: Formulas

RC bidimesional elements, without transverse reinforcement, in bending in both directions x and y.

Symbols

R_{Ed}	design action on the column
R_{Rd}	design value of the punching shear resistance
a, b	sides of the column along x and y
d_x, d_y	effective depths (flexural) of the plate along x and y
A_x, A_y	concerned flexural reinforcements along x and y
u_o	perimeter of the column affected by stresses
u	critical perimeter of the diffusion zone of the plate
A, B	dimensions of the diffusion zone along x and y

see also Charts 2.2 and 2.3.

Resistance Verification

$$R_{\mathrm{Rc}} = 0.123d\,u_{\mathrm{o}}f_{\mathrm{cd}}$$
$$R_{ct} = 0.25d\,u f_{\mathrm{ctd}}\kappa\, r$$
$$R_{\mathrm{Rd}} = \min(R_{\mathrm{Rc}}, \mathrm{R_{ct}}) \geq R_{\mathrm{Ed}}$$

with

$$d = \left(d_x + d_y\right)/2$$
$$\kappa = 1.6 - d \geq 1 \quad (d \text{ expressed in } m)$$
$$R = 1.0 + 50\rho_{\mathrm{s}} \leq 2$$
$$\rho_{\mathrm{s}} = \sqrt{\rho_{\mathrm{sx}}\rho_{\mathrm{sy}}}$$
$$\rho_{\mathrm{sx}} = A_{\mathrm{sx}}/\mathrm{Bd} \quad A_{\mathrm{sx}} \text{ area of bars included in } B$$
$$\rho_{\mathrm{sy}} = A_{\mathrm{sy}}/\mathrm{Ad} \quad A_{\mathrm{sy}} \text{ area of bars included in } A$$

Alternatively, according to more recent codes, it can be set

$$R_{\mathrm{Rd}} = \min(R_{\mathrm{Rc}}, \mathrm{R_{ct}}) \geq R_{\mathrm{Ed}}$$
$$R_{\mathrm{ct}} = 0.18\mathrm{du}\kappa(100\rho_{\mathrm{s}}f_{\mathrm{ck}})^{1/3}\Big/\gamma_{\mathrm{C}} \geq \mathrm{duv_{min}}$$

with

$$\kappa = 1 + \sqrt{200/d} \leq 2.0 \quad (d \text{ expressed in mm})$$
$$v_{\mathrm{min}} = 0.035\kappa^{3/2}\sqrt{f_{\mathrm{ck}}}$$

(For the definition of d, ρ_{s} and R_{Rs} see above).

Shear Perimeters

For substantially symmetric arrangements of forces around the column, with constant uniform distribution of stresses along the shear perimeters, the following cases are possible.

- *Internal column*

$$u_{\mathrm{o}} = 2a + 2b$$
$$A = a + 3d \quad B = b + 3\mathrm{d}$$
$$u = 2a + 2b + 3\pi d$$

- *Edge column*

$$u_o = 2a + b \quad \text{(one side } b \text{ on the edge)}$$
$$A = a + 1.5d \quad B = b + 3\text{d}$$
$$u = 2a + b + 1.5\pi d$$

- *Corner column*

$$u_o = a + b$$
$$A = a + 1.5d \quad B = b + 1.5d$$
$$u = a + b + 0.75\pi d$$

Chart 5.5: Coefficients for Moment Redistribution

Within the *Linear analysis* with redistribution of hyperstatic moments of RC beams, the following values of the reduction coefficients δ of the elastic moments of critical sections can be adopted. It is implied that the bending moments of the other sections along the spans are to be modified accordingly, complying with the equilibrium with the applied load.

Symbols

M_{ed}	design value of the hyperstatic moment of the linear elastic analysis
$M_{Ed} = \delta M_{ed}$	deduced value of the moment for the design of reinforcement
$\xi = x/d$	adimensionalized position of the neutral axis of the section

see also Chart 3.10.

Reduction Coefficients

High-ductility steels

(as defined in Table 1.17)

$\delta \geq 0.44 + 1.25\xi$ for concrete classes from C16/20 to C50/60

$\delta \geq 0.56 + k\xi$ for concrete classes from C50/60 to C70/75

where

$$k = 1.25(0.6 + 0.0014/\varepsilon_{cu})$$
$$\varepsilon_{cu} = 0.0031; 0.0029; 0.0027 \text{ for } C55/60\,; C60/65; C70/75$$

in the limits $0.70 \leq \delta \leq 1.00$.

NOTE: Concrete classes are the ones shown in Table 1.2a, b.

Chart 5.6: Allowable Deformations of elements in Bending

In the calculations of deformations with the appropriate serviceability load combinations, for RC and prestressed elements in bending of the decks of common buildings, one can make reference to the following allowable values indicating the ratio *v*/l between the maximum deflection and the span length.

$\frac{v}{l} \leq \frac{1}{200}$ for any type of structural element
$\frac{v^*}{l} \leq \frac{1}{400}$ for decks with non-structural walls
$\frac{v}{l} \leq \frac{1}{800}$ for particular requirements of high stiffness

The viscous effects developed at the time of the verification should be included in the deflection v. The value v^* refers to the maximum range of the viscoelastic deflection that non-structural walls have to accommodate.

Chapter 6
Eccentric Axial Force

Abstract This chapter presents the design methods of reinforced concrete sections subjected to eccentric axial force with their serviceability and resistance verifications. Specific design models are shown for columns and the criteria for nonlinear analysis of frames are presented. In the final section a complete design of an edge column is developed, starting from the stress analysis and following with the pertinent verifications of the critical sections.

6.1 Elastic Design of the Section

The problem of combined axial farce and bending on reinforced concrete sections represents the natural extension of the one relative to simple bending. Starting from the same assumptions and with the same criteria adopted in the previous chapters, the cases of combined compression/tension and bending will be analyzed, within the elastic range or at the resistance ultimate limit state, in cracked or uncracked sections.

First it should be recalled that, within the phase I of uncracked section, the elastic calculation of stresses for the serviceability verifications can rely on the superposition of effects such as

$$\sigma_c = \pm\frac{N}{A_i} - \frac{M}{I_i}y_c$$

$$\sigma_s = \alpha_e\left[\pm\frac{N}{A_i} + \frac{M}{I_i}y_s\right]$$

with $\alpha_e = E_s/E_c$, where the symbols refer to Fig. 6.1 and stresses are assumed positive in tension. It is implied that the moments M are to be evaluated with respect to the centroidal axis of the homogenized section, whereas the neutral axis is shifted

© Springer International Publishing AG 2017

G. Toniolo and M. di Prisco, *Reinforced Concrete Design to Eurocode 2*,
Springer Tracts in Civil Engineering, DOI 10.1007/978-3-319-52033-9_6

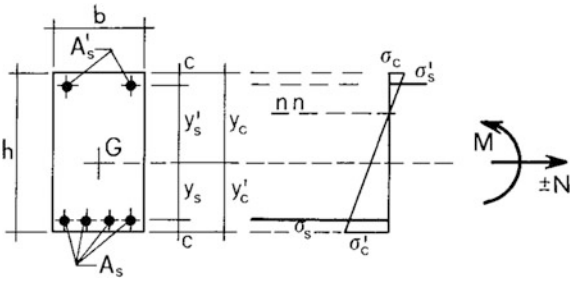


Fig. 6.1 Stress distribution in elastic uncracked section

from the centroidal position, towards the fibers in tension if the component N is in compression, towards the ones in compression if the component N is in tension.

Further to what was mentioned above, the classic assumptions of Bernoulli and elasticity are used, in addition to the one of compatibility between the deformations of the two materials. The same formulas based on the superposition of effects are to be applied also when, foreseeing a behaviour in phase II where the concrete tensile strength is neglected, section cracking does not occur due to the presence of a combined bending and compression axial force with small eccentricity of the resultant.

For example, with reference to the symmetric section of Fig. 6.2, the section remains uncracked with the neutral axis which does not intersect it as long as the resultant is within the central core of inertia:

$$e < u$$

The dimension u of the core is evaluated with

$$u = \frac{i^2}{h/2}$$

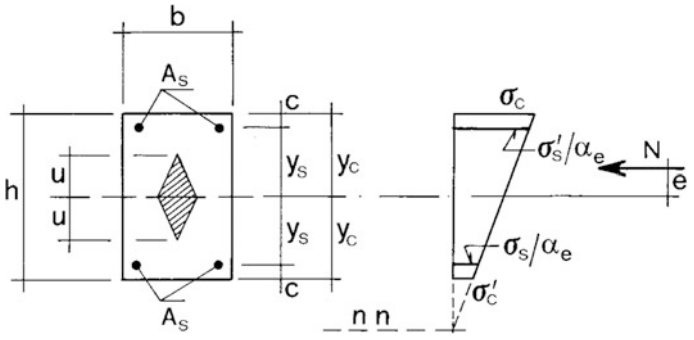


Fig. 6.2 Stress distribution in an entirely compressed section

where

$$i^2 = \frac{I_i}{A_i}$$

and the geometrical characteristics are referred to the homogenized section:

$$A_c = hb \quad A_t = 2A_s$$
$$A_i = A_c + \alpha_e A_t$$
$$I_i = A_c \frac{h^2}{12} + \alpha_e A_t y_s^2$$

6.1.1 Axial Compression Force with Small Eccentricity

The following description refers to homogeneous sections of a material with no tensile strength such as walls made of bricks, blocks, stones or unreinforced concrete. In all these cases, the assumption of homogeneity has to be intended from the macroscopic point of view with reference to the global behaviour of the element.

The cases of increasing eccentricity of the resultant of compressions are shown in Fig. 6.3. The problem is bounded within the limit $e < a/2$ as, with the resultant outside the section, there cannot be equilibrium without tensile resistance. Therefore for $e > a/2$ the element overturns.

The case of Fig. 6.3a refers to a centred compression and simply leads to:

$$\sigma = \frac{N}{ab} = cost.$$

The case of a center of compressions within the core ($e < a/6$) is shown in Fig. 6.3b, for which the maximum value σ of compressions is calculated with the superposition of effects:

$$\sigma = \frac{N}{ab} + \frac{Ne}{a^3 b/12}\frac{a}{2} = \frac{N}{ab}\left(1 + \frac{6e}{a}\right)$$

The case of Fig. 6.3c is at the limit of the previous one with $e = a/6$ and with the neutral axis that, located on the edge of the section, still leaves it uncracked:

$$\sigma = \frac{N}{ab}\left(1 + \frac{6a/6}{a}\right) = \frac{2N}{ab}$$

On the triangular diagram of compressions the rotational and translational equilibriums of the section are immediately evident; the first one makes the point of application of the external force coincide with the centroid of the reactions distributed on the section:

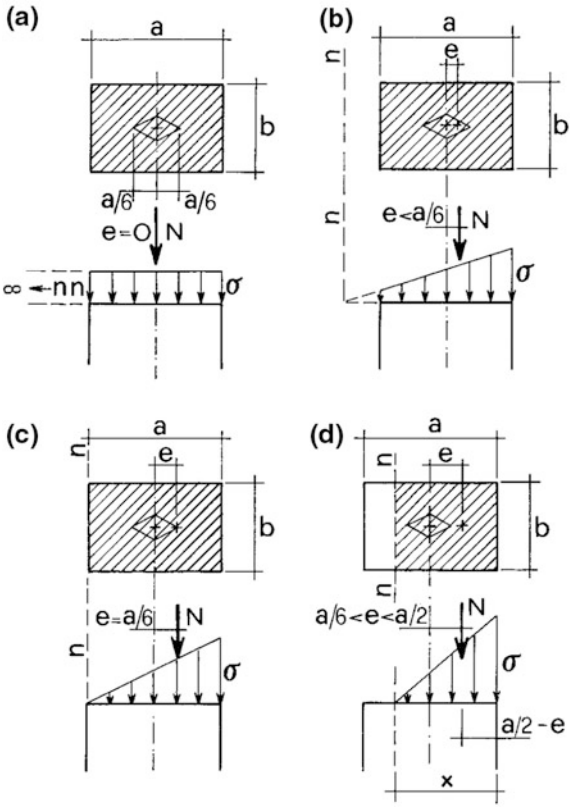


Fig. 6.3 Stress distribution in an unreinforced section

$$\frac{a}{2} - e = \frac{a}{3}$$

in the second one the action itself is equal to the resultant of the reactions:

$$N = \frac{1}{2} ab\sigma$$

The last case described in Fig. 6.3d refers to a center of compressions outside the core of the geometrical section ($e > a/6$). In this case the neutral axis intersects the section and this latter cracks. The extent x of the resisting part is deduced from the same equilibrium equations mentioned for the previous case. For the rotational equilibrium about the edge with higher compressions one has:

$$\frac{a}{2} - e = \frac{x}{3}$$

from which it is obtained:

$$x = 3\left(\frac{a}{2} - e\right)$$

Once the height x of the resisting section is known, the translational equilibrium leads to:

$$\sigma = \frac{2N}{xb}$$

As e tends to $a/2$, with $x \to 0$, the maximum compression σ tends to infinity, highlighting the threshold of equilibrium beyond which, as already mentioned, overturning occurs.

Combined Compression and Biaxial Bending

For the same sections analyzed here, which are made of a material with no tensile strength, the possible cases of combined compression and biaxial bending are shown in Fig. 6.4a–b–c.

The first case refers to a center of compressions within the central core of inertia of the section, for which one has:

$$\frac{e_y}{a} + \frac{e_z}{b} \leq \frac{1}{6}$$

In this case the section remains uncracked and the maximum stress on the corner O is evaluated with:

$$\sigma = \frac{N}{ab} + \frac{Ne_y}{a^3b/12}\frac{a}{2} + \frac{Ne_z}{ab^3/12}\frac{b}{2} = \frac{N}{ab}\left(1 + \frac{6e_y}{a} + \frac{6e_z}{b}\right)$$

When instead one has

$$\frac{e_y}{a} + \frac{e_z}{b} > \frac{1}{6}$$

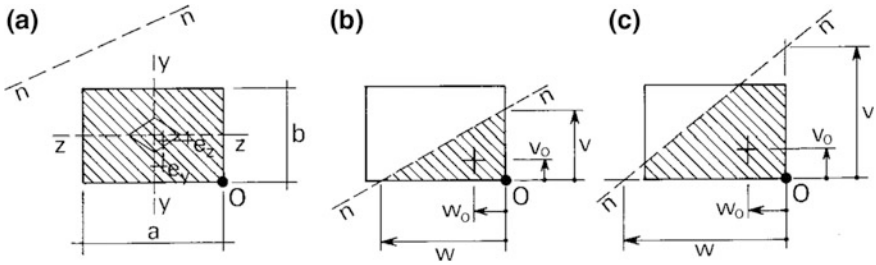


Fig. 6.4 Section with combined compression and biaxial bending

the section cracks. The simplest case is represented in Fig. 6.4b with a neutral axis that intersects the edges of the section adjacent to the corner O of maximum stress. With $v \leq b$ and $w \leq a$, the portion of the material in compression has a triangular shape on which the diagram of stresses forms a right tetrahedron.

Given

$$w_o = \frac{a}{2} - e_y \qquad v_o = \frac{b}{2} - e_z$$

for the rotational equilibrium about the edges of the section, the center of compressions shall coincide with the center of mass of such tetrahedron. The intersections with the neutral axis are therefore immediately deduced with:

$$w = 4\, w_o \quad v = 4 v_o$$

For the translational equilibrium, eventually, the volume of the stress solid is equal to the applied axial force:

$$\frac{1}{6}\sigma v w = N$$

from which the maximum compression stress on the corner O is obtained:

$$\sigma = \frac{6N}{vw}$$

In the general case, when one or both intersections are out of the sides ($v > b$, $w > a$), the problem becomes more complicated for geometrical reasons. On the portion of the material in compression of Fig. 6.4c, the stress solid, bounded by the plane that rises from the zero value on the neutral axis nn up to the peak value σ on the corner O of the section, has a more complicated configuration. It can be evaluated as a global tetrahedron of sides v and w and height σ, from which the smaller tetrahedrons indicated in Fig. 6.5 are to be subtracted.

One therefore has, with $\alpha = a/w$ and $\beta = b/v$, the following characteristics:

- Volume (for $\sigma = 1$)

$$V = \frac{vw}{6} - \frac{v(w-a)^3}{6w^2} - \frac{w(v-b)^3}{6v^2} = \frac{vw}{6}\Theta(\alpha, \beta)$$

with $\Theta(\alpha, \beta) = 1 - (1-\alpha)^3 - (1-\beta)^3$

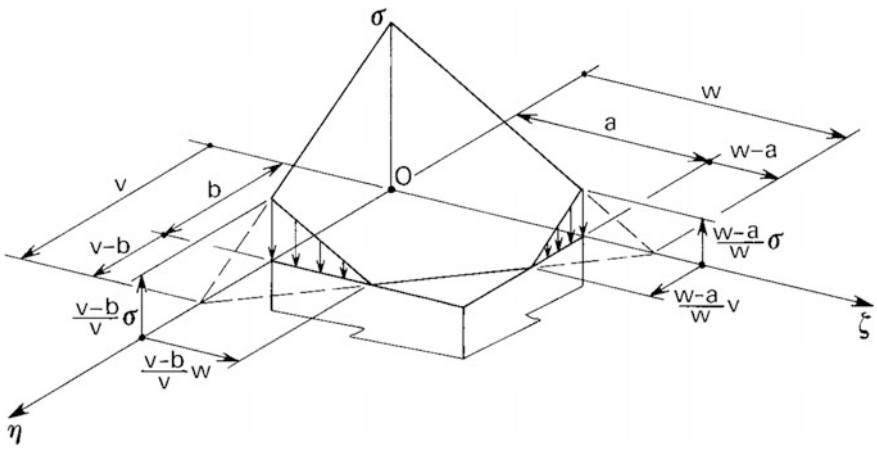


Fig. 6.5 Stress distribution in a cracked section

- Static moment about η (for $\sigma = 1$)

$$S_\eta = \frac{vw}{6}\frac{v}{4} - \frac{v(w-a)^3}{6w^2}\left(a + \frac{w-a}{4}\right) - \frac{w(v-b)^3}{6v^2}\frac{(v-b)}{4v} = \\ = \frac{vw^2}{24}\Phi(\alpha,\beta)$$

with $\Phi(\alpha,\beta) = 1 - (1+3\alpha)(1-\alpha)^3(1-\beta)^4$

- Static moment about ζ (for $\sigma = 1$)

$$S_\zeta = \frac{vw}{6}\frac{v}{4} - \frac{v(w-a)^3}{6w^2}\frac{v(w-a)}{4w} - \frac{w(v-b)^3}{6v^2}\left(b + \frac{v-b}{4}\right) = \\ = \frac{v^2w}{24}\psi(\alpha,\beta)$$

with $\psi(\alpha,\beta) = 1 - (1-\alpha)^4 - (1+3\beta)(1-\beta)^3$

In the equations shown above, the second two terms are to be calculated only if $\alpha < 1$ and $\beta < 1$ respectively.

For the rotational equilibrium about the axes η and ζ one has:

$$\frac{S_\eta}{V} = w_o \quad \frac{S_\zeta}{V} = v_o$$

where v_o and w_o are the coordinates of the point of application of the axial force. The nonlinear system is therefore obtained as follows:

$$w\frac{\phi(\alpha,\beta)}{\theta(\alpha,\beta)} = 4w_o \quad v\frac{\psi(\alpha,\beta)}{\theta(\alpha,\beta)} = 4v_o$$

and it is to be solved with the appropriate iterative numerical procedures.

Once the intersections w and v with the neutral axis are obtained, from the translational equilibrium of the section

$$\sigma V = N$$

the maximum stress value is obtained:

$$\sigma = \frac{6N}{vw}\frac{1}{\theta(\alpha,\beta)}$$

Such procedure can be integrated in the more general one presented at Sect. 6.1.3 with reference to sections with reinforcement.

6.1.2 Compression and Tension with Uniaxial Bending

The analysis of stresses in the section under combined compression and bending of Fig. 6.6, assumed in the cracked elastic phase, is carried with the usual equilibrium equations of the section. It is more convenient to write the rotational equilibrium about the point O first, so that the intensity N of the external force does not appear:

$$C_c\left(d_o + \frac{x}{3}\right) + C'_s d'_s - Z d_s = 0$$

having set $d_o = e - y_c, d'_s = d_o + d'e\, d_s = d_o + d$.

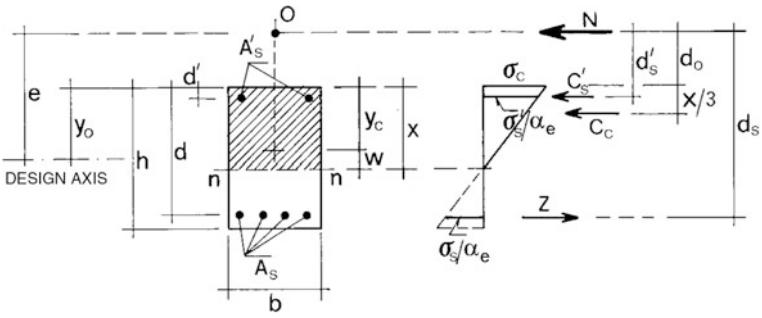


Fig. 6.6 Cracked section under compression and uniaxial bending

For the rectangular section with double reinforcement under examination, the resultants of compressions and tensions in the two materials are equal to:

$$C_c = \frac{1}{2}\sigma_c bx \qquad C'_s = \sigma'_s A'_s \qquad Z = \sigma_s A_s$$

for which, with the usual similarities that relate the values σ_c, σ'_s and σ_s in the linear diagram of stresses:

$$\sigma'_s = \alpha_e \frac{x - d'}{x}\sigma_c \qquad \sigma_s = \alpha_e \frac{d - x}{x}\sigma_c$$

one obtains:

$$\frac{1}{2}\sigma_c bx\left(d_o + \frac{x}{3}\right) + \alpha_e \frac{x - d'}{x}\sigma_c A'_s d'_s - \alpha_e \frac{d - x}{x}\sigma_c A_s d_s = 0$$

Simplifying σ_c and appropriately grouping the terms, the cubic equation is eventually obtained:

$$x^3 + 3d_o x^2 + \frac{6\alpha_e}{b}\left(A_s d_s + A'_s d'_s\right)x - \frac{6\alpha_e}{b}\left(A_s d_s d + A'_s d'_s d'\right) = 0$$

The solution bounded between $\bar{x}$ (position of the neutral axis for uniaxial bending) and h (for which the section is uncracked), therefore, gives the extent of the compression zone (resisting) of concrete.

Once the x is known, the value of stresses σ_c, σ'_s and σ_s in the materials is obtained from the translational equilibrium of the section:

$$C_c + C'_s - Z = -N$$

which, with the pertinent substitutions, becomes:

$$\frac{1}{2}\sigma_c bx + \alpha_e \frac{x - d'}{x}\sigma_c A'_s - \alpha_e \frac{d - x}{x}\sigma_c A_s = N$$

from which it is eventually obtained:

$$\sigma_c = \frac{N}{\dfrac{bx}{2} + \alpha_e \dfrac{x - d'}{x}A'_s - \alpha_e \dfrac{d - x}{x}A_s} = \frac{N}{S_i}x$$

In this equation

$$S_i = \frac{bx^2}{2} + \alpha_e A'_s(x - d') - \alpha_e A_s(d - x) \quad (> 0)$$

indicates the static moment about the neutral axis of the resisting section homogenized with respect to concrete. The stresses in the tension and compression reinforcement are consequently calculated with the equations indicated previously.

With $d_o \to \infty$, and therefore at the limit of simple bending, the equation deduced here fails as it tends to the undetermined expression 0/0. For a generally applicable formula, therefore valid for cracked sections under simple bending or combined compression/tension and bending, the superposition of effects can be set with reference to the resisting section ($y_c = x - w$):

$$\sigma_c = \frac{N}{A_i} + \frac{M_G}{I_i} y_c \qquad \text{in compression}$$
$$\sigma'_s = \alpha_e \left[\frac{N}{A_i} + \frac{M_G}{I_i} (y_c - d') \right] \qquad \text{in compression}$$
$$\sigma_s = \alpha_e \left[\frac{N}{A_i} - \frac{M_G}{I_i} (d - y_c) \right] \qquad \text{in tension}$$

having set:

$$A_i = bx + \alpha_e A'_s + \alpha_e A_s$$

The flexural contribution refers to the centroid G whose distance from the neutral axis nn (see Fig. 6.6) is:

$$w = \frac{S_i}{A_i}$$

With reference to the centroidal axis one therefore has:

$$M_G = N(d_o + y_c)$$
$$I_i = bx \left[\frac{x^2}{12} + \left(y_c - \frac{x}{2} \right)^2 \right] + \alpha_e A'_s (y_c - d')^2 + \alpha_e A_s (d - y_c)^2$$

Introducing, with $\alpha_e = E_s/E_c$, the elastic reinforcement ratios defined as

$$\psi_s = \frac{\alpha_e A_s}{bh} \qquad \psi'_s = \frac{\alpha_e A'_s}{bh}$$

the resolving equation of combined compression and bending becomes

$$\xi^3 + 3\delta_o \xi^2 + 6\left(\psi_s \delta_s + \psi'_s \delta'_s\right)\xi - 6\left(\psi_s \delta_s \delta + \psi'_s \delta'_s \delta'\right) = 0$$

having set

$$\xi = x/h \qquad \delta = d/h \qquad \delta' = d'/h$$
$$\delta_o = d_o/h \qquad \delta_s = d_s/h \qquad \delta'_s = d'_s/h$$

as adimensional geometrical parameters of the section.

Section Under Combined Tension and Bending

For tensile forces N with small eccentricity, the section fully cracks: only the steel reinforcement remains to resist. This occurs as long as the center of tensions remains within the central core of inertia of the resisting steel section with respect to the concrete outline. With reference to the centroid G of the reinforcement defined by

$$y_s = \frac{A'_s}{A_s + A'_s} y_t \quad y'_s = \frac{A_s}{A_s + A'_s} y_t$$

(see Fig. 6.7), the dimensions of the core are:

$$u = \frac{i^2}{y_c} \qquad u' = \frac{i^2}{y'_c}$$

with

$$i^2 = \frac{A_s y_s^2 + A'_s y'^2_s}{A_s + A'_s}$$

Therefore, given that the eccentricity e of the axial force is small enough to keep it within the core, the equilibrium of the steel resisting section simply leads to dividing the action between the two reinforcements in an inversely proportion to their respective distances:

$$Z = \frac{d'_s}{y_t} N \quad (\sigma_s = Z/A_s)$$
$$Z' = \frac{d_s}{y_t} N \quad (\sigma'_s = Z'/A'_s)$$

For greater eccentricities, the section cracks leaving a concrete portion in compression. The configuration of this resisting section is indicated in Fig. 6.8.

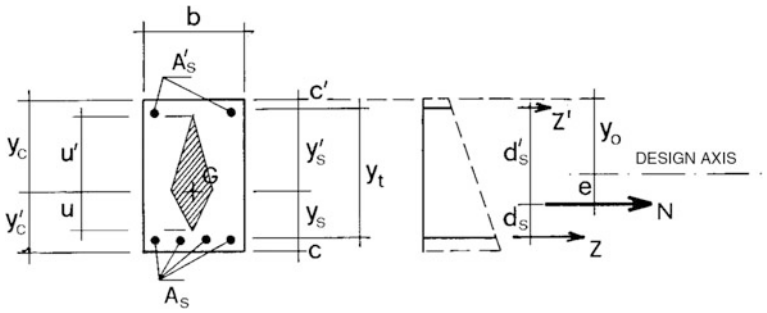


Fig. 6.7 Entirely cracked section under tension and uniaxial bending

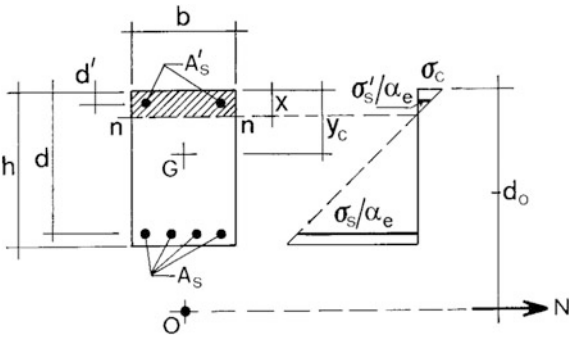


Fig. 6.8 Cracked section under tension and uniaxial bending

For the definition of the position x of the neutral axis, an identical equation is obtained with the same equilibrium equations previously set for the analysis of combined compression and bending:

$$x^3 + 3d_o x^2 + \frac{6\alpha_e}{b}\left(A_s d_s + A'_s d'_s\right)x - \frac{6\alpha_e}{b}\left(A_s d_s d + A'_s d'_s d\right) = 0$$

that is

$$\xi^3 + 3\delta_o \xi^2 + 6\left(\psi_s \delta_s + \psi'_s \delta'_s\right)\xi - 6\left(\psi_s \delta_s \delta + \psi'_s \delta'_s \delta'\right) = 0$$

in an adimensional form, where d_o is assumed negative and consequently the dimensions $d_s = d_o + d$ *e* $d'_s = d_o + d'$ are negative as well. The solution of this equation is to be calculated between 0 (section entirely cracked) and $\bar{x}$ (position of the neutral axis for simple bending).

The stresses σ_c, σ'_s and σ_s in the materials are also evaluated with the formulas deduced previously, where in particular it results $S_i < 0$.

6.1.3 Compression and Tension with Biaxial Bending

For uncracked sections, the elastic calculation of stresses under combined axial force and biaxial bending utilizes the formulas of superposition of effect already presented at Sect. 3.1.1. With the algorithms of the Geometry of masses, the orientation of the principal axes of inertia of the homogenized section is to be defined in advance and the bending moment is to be decomposed along these axes in its two components of uniaxial bending.

For cracked sections it is not possible to carry out this decomposition in advance. The resisting section depends on the characteristics of the applied forces and the relative central ellipse of inertia with its related parameters is therefore initially unknown. The cases of biaxial bending, simple or combined with an axial force, generally occur when the action plane does not coincide with an axis of symmetry

of the section, or when the geometrical section does not have any axis of symmetry. In the latter case, uniaxial bending represents a singular case that is difficult to identify in advance and therefore can be treated with the same general algorithms of the biaxial bending. If, in the solution obtained in this way, the neutral axis is orthogonal to the axis of the applied force, it could then be said that this is a case of uniaxial bending.

For the analysis of combined axial force with biaxial bending in cracked sections, similarly to what has been done for the specific case at Sect. 3.1.1, three equilibrium equations are set, one for the translation along the beam axis, and the others for rotations about two orthogonal axes appropriately chosen based on the geometrical regularities of the section. From the solution of such system, the three unknowns of the problem are deduced: two geometrical parameters necessary for the definition of the orientation of the neutral axis in the plane of the section, and the third one consisting of the stress value in a particular point of the section (for example the maximum compression on the farthest concrete corner from the neutral axis). The equations of plane deformations, the compatibility between the materials deformations and cracked section conditions complete the algorithm. For the elastic calculation, the usual linear relationship between stresses and strains is eventually added.

This type of analysis is applied hereafter to rectangular sections with reinforcement, subject to generic combined system of axial forces and bending moments. A frequent case of biaxial bending is to be mentioned, which is solved in a simpler way based on the equilibrium equations on the vertical bending plane only. The horizontal equilibrium remains granted by the presence of an additional structural constraint.

It is the case of decks edge beams, similar to the ones represented in Fig. 6.9. Contrary to the one of Fig. 3.8, which assumed not having any restraints along the span, could bend freely out of the vertical plane of the applied forces, the beams under analysis are rigidly connected with the floor and this, with its great in-plane stiffness, prevents any significant horizontal component of their flexural deformation. Forced to move within the vertical plane parallel to the direction of external loads, the sections of the beams have to rotate about horizontal neutral axes, as indicated in Fig. 6.9.

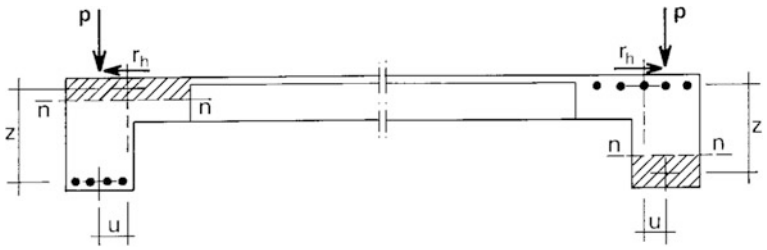


Fig. 6.9 Sections with horizontally restrained deformation

The non-symmetric layout of the resisting section therefore leads to two components of the internal couple: one $Zz = Cz$ that acts in the vertical plane for the direct equilibrium with the bending action p; the second one $Zu = Cu$ that acts in the horizontal plane for the equilibrium with the reaction r_h provided by the floor constraint. The verification calculations usually analyze the main vertical component of uniaxial bending only, leaving undetermined the force with which the floor provides the secondary horizontal component.

Analytical Verification Method

The three equilibrium conditions now applied to the rectangular reinforced concrete section of Fig. 6.10, one for the translation along the axis of the beam, and others for the rotations about the two axes η and ζ, lead to the system:

$$\begin{cases} \sigma_c V_c + \sum_i \sigma_{si} A_{si} = N \\ \sigma_c S_{c\eta} + \sum_i \sigma_{si} A_{si} \zeta_i = M_\eta \quad (= N w_o) \\ \sigma_c S_{c\zeta} + \sum_i \sigma_{si} A_{si} \eta_i = M_\zeta \quad (= N v_o) \end{cases}$$

where σ_c is the maximum stress in the concrete corner O, V_c is the volume of the solid of compression on the resisting area of concrete for a unit height, whereas $S_{c\eta}$ and $S_{c\zeta}$ are the static moments of such solid with respect to the axes η and ζ. The expressions of the parameters V_c, $S_{c\eta}$ and $S_{c\zeta}$ have already been defined at Sect. 6.1.1 as a function of the intersections v and w of the neutral axis with the axes η and ζ:

$$\begin{aligned} V_c &= \frac{vw}{6}\Theta(\alpha,\beta) &&= \frac{vw}{6}\left[1-(1-\alpha)^3-(1-\beta)^3\right] \\ S_{c\eta} &= \frac{vw^2}{24}\Phi(\alpha,\beta) &&= \frac{vw^2}{24}\left[1-(1+3\alpha)(1-\alpha)^3-(1-\beta)^4\right] \\ S_{c\zeta} &= \frac{v^2w}{24}\psi(\alpha,\beta) &&= \frac{v^2w}{24}\left[1-(1-\alpha)^4-(1+3\beta)(1-\beta)^3\right] \end{aligned}$$

with $\alpha = a/w \leq 1$ and $\beta = b/v \leq 1$.

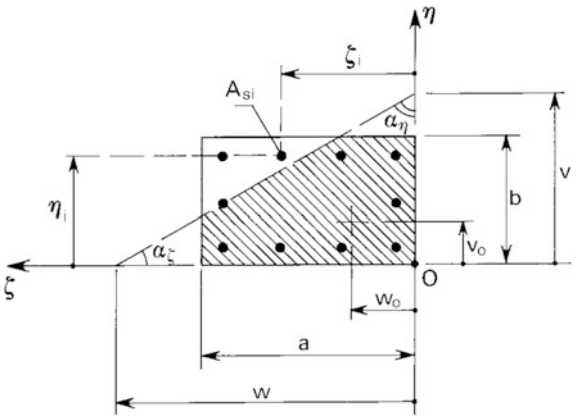


Fig. 6.10 Cracked section under axial force and biaxial bending

The stresses σ_{si} on the individual reinforcement bars are deduced from the equation of the inclined plane passing through the neutral axis:

$$\sigma_{si} = \alpha_e \sigma_c \left(1 - \frac{\zeta_i}{w} - \frac{\eta_i}{v}\right)$$

The equation is written here in a parametric form as a function of the intersections w and v.

Substituting this equation in the equilibrium system, one obtains:

$$\begin{cases} \sigma_c V_c + \alpha_e \sigma_c \left(\sum_i A_{si} - \dfrac{1}{w}\sum_i A_{si}\zeta_i - \dfrac{1}{v}\sum_i A_{si}\eta_i\right) = N \\ \sigma_c S_{c\eta} + \alpha_e \sigma_c \left(\sum_i A_{si}\zeta_i - \dfrac{1}{w}\sum_i A_{si}\zeta_i^2 - \dfrac{1}{v}\sum_i A_{si}\zeta_i\eta_i\right) = M_\eta \\ \sigma_c S_{c\zeta} + \alpha_e \sigma_c \left(\sum_i A_{si}\eta_i - \dfrac{1}{w}\sum_i A_{si}\zeta_i\eta_i - \dfrac{1}{v}\sum_i A_{si}\eta_i^2\right) = M_\zeta \end{cases}$$

Setting now:

$$\begin{array}{ll} A_t = \Sigma_i A_{si} & \text{(total area of reinforcement)} \\ S_{s\eta} = \Sigma_i A_{si}\zeta_i & \text{(its static moment about } \eta) \\ S_{s\zeta} = \Sigma_i A_{si}\eta_i & \text{(its static moment about } \zeta) \\ I_{s\zeta} = \Sigma_i A_{si}\zeta_i^2 & \text{(its second moment of area about } \eta) \\ I_{s\eta} = \Sigma_i A_{si}\eta_i^2 & \text{(its second moment of area about } \zeta) \\ I_{\eta\zeta} = \Sigma_i A_{si}\zeta_i\eta_i & \text{(its centrifugal moment about } \eta, \zeta) \end{array}$$

and grouping the terms appropriately, one eventually obtains:

$$\begin{cases} N\dfrac{1}{\sigma_c} + \alpha_e S_{s\eta}\dfrac{1}{w} + \alpha_e S_{s\zeta}\dfrac{1}{v} = V_c + \alpha_e A_t \\ M_\eta \frac{1}{\sigma_c} + \alpha_e I_{s\eta}\dfrac{1}{w} + \alpha_e I_{h\zeta}\dfrac{1}{v} = S_{c\eta} + \alpha_e S_{s\eta} \\ M_\zeta \dfrac{1}{\sigma_c} + \alpha_e I_{\eta\zeta}\dfrac{1}{w} + \alpha_e I_{s\zeta}\dfrac{1}{v} = S_{c\zeta} + \alpha_e S_{s\zeta} \end{cases}.$$

This is a pseudolinear system with the unknowns $1/\sigma_c$, $1/w$, $1/v$. In the left-side terms the parameters V_c, $S_{c\eta}$ and $S_{c\zeta}$, relative to the stress response of concrete, remain function of the intersections w and v with the main axes.

An appropriate iterative numerical procedure is adopted in order to calculate the solution. The tangent method, which requires the previous formal elaboration of the first derivatives with respect to $1/w$ and $1/v$ of the mentioned functions, ensures a quick convergence. The solution corresponding to the uncracked section, which is calculated with the well-known closed-form expressions typical to the superposition of effects, can be assumed as the first trial one from which the iterative process can start.

The algorithm presented here is of general applicability, aimed at the elastic design of cracked rectangular sections, whatever is the layout of the reinforcement and subject to simple uniaxial or biaxial bending, or combined compression/tension force

with uniaxial or biaxial bending. The cases of combined compression and bending with small eccentricity, which leave the section uncracked, are solved stopping the procedure at the initial attempt. For cases of combined tension and bending close to complete cracking of the section, with w and v close to zero, numerical indeterminateness can occur. In this case, it is worthwhile assuming the unknowns σ_c, v and α_η or σ_c, w and α_ζ depending if the component M_ζ or M_η of the bending moment predominates (see Fig. 6.10). The domain of combined tension and bending with entirely cracked section concerns the steel reinforcement only and the solution can be calculated with the closed-form expressions based on the same characteristics A_t, $S_{s\eta}$, …, $I_{s\zeta}$, $I_{\eta\zeta}$ used for the coefficients of the general equilibrium system.

For sections of any shape, saving the formal definition of the algorithm, the calculation of the parameters V_c, $S_{c\eta}$ and $S_{c\zeta}$ relative to the stress behaviour of concrete requires more complex articulations of the procedure.

6.2 Resistance Design of the Section

It is recalled how, in the design of a reinforced concrete section at the failure ultimate limit state, the appropriate σ–ε models of the material behaviour should be added to the three assumptions of plane sections, compatibility between materials and cracked sections. Such models include, in terms of deformations, the limit values that define the failure of the section. Therefore, in particular, as specified at Sect. 1.4.2, ultimate limit state can be determined by the failure of concrete by reaching its maximum compressive strain ε_{cu} (see Fig. 1.28), or by the failure of the steel reinforcement by reaching its maximum tensile strain ε_{ud} for ordinary reinforcement (see Fig. 1.30) or ε_{pud} for prestressing reinforcement (see Fig. 1.32). The more restrictive limit ε_{c1} to the uniform compressive strain, assumed for centred compression at Sect. 2.1.1, should be referred in the present case to the average value along the depth of the section.

The possible failure mechanisms of the section are, therefore, deduced completing the diagram already drawn in Fig. 3.10 for simple bending. In addition to the extension of the diagram in the domains of sections entirely in tension and in compression, the new pivot point C is to be added which defines the failure in the domain of combined compression and bending with small eccentricity (see Fig. 6.11). In particular the distance $\bar{y} = \bar{\eta}h$ of the center C from the mostly stressed edge in compression is derived from

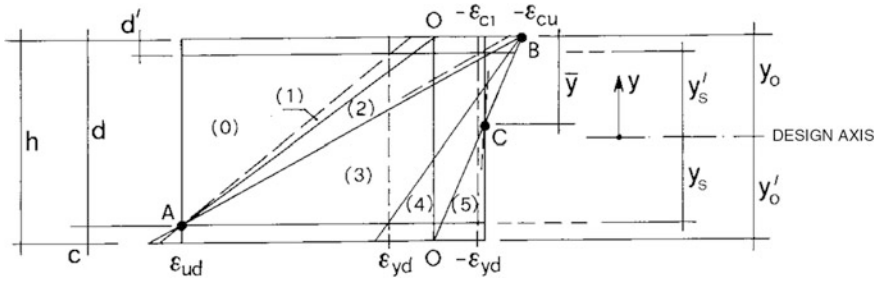


Fig. 6.11 Resistance ultimate states of the section

$$\bar{y} = \frac{\varepsilon_{cu} - \varepsilon_{c1}}{\varepsilon_{cu}} h$$

which, for $\varepsilon_{cu} = 0.35\%$ and $\varepsilon_{c1} = 0.20\%$, leads to $\bar{\eta} \cong 0.43$.

The evaluation of the resultant of compressions in concrete and its moment with respect to the design axis requires the execution of integrals such as:

$$\int \sigma_c(\varepsilon) b \, dy \qquad \int \sigma_c(\varepsilon) b y \, dy$$

extended to the resisting part in compression of the section. It is reminded that for rectangular sections such integrals lead to expressions such as:

$$\beta b x f_{cd} \qquad \beta b x f_{cd}(y_o - \kappa x)$$

As already mentioned at Sect. 3.2, the coefficients β and κ of these expressions are evaluated with:

- for $\bar{\varepsilon}_c = \varepsilon_c/\varepsilon_{cu} < 1$ (domain 2 with pivot *A*)

$$\left.\begin{aligned} \beta &\cong (1.6 - 0.8\bar{\varepsilon}_c)\bar{\varepsilon}_c \\ \kappa &\cong 0.33 + 0.07\bar{\varepsilon}_c \end{aligned}\right]$$

- for $\varepsilon_c = \varepsilon_{cu}$ (domains 3 and 4 with pivot *B*)

$$\begin{aligned} \beta &\cong 0.8 \\ \kappa &\cong 0.4 \end{aligned}$$

Eventually in the domain 5 of uncracked sections (with pivot *C*), with reference to the symbols of Fig. 6.12 it can be set:

$$\begin{aligned} \int_C \sigma_c b \, dy &= \beta^* b h f_{cd} \\ \int_C \sigma_c b y \, dy &= \beta^* b h f_{cd}(y_o - \kappa^* h) \end{aligned}$$

where, setting $\xi = x/h$ (>1) and $\bar{\eta} = \bar{y}/h (\cong 0.43)$, one has:

$$\begin{aligned} \beta^* &= 1 - \frac{(1-\bar{\eta})^3}{3(\xi - \bar{\eta})^2} \\ \kappa &= \frac{1}{2}\left[1 - \frac{(1-\bar{\eta})^3}{6(\xi - \bar{\eta})^2}(3 + \bar{\eta})\right]\frac{1}{\beta^*} \end{aligned}$$

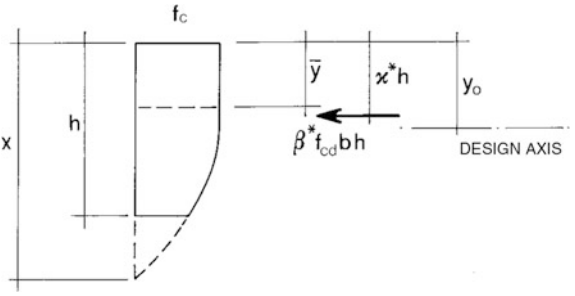


Fig. 6.12 Stress distribution in an entirely compressed section

6.2.1 Failure Mechanisms of the Section

The possible domains of rupture, indicated in the diagram of Fig. 6.11 for the section with double reinforcement are described hereafter where the formulas refer to a finite elastoplastic model of steel (model *A* of Fig. 1.30 with $f'_{td} = f_{yd}$). If one wanted to take into account the over-resistance of steel with $f'_{td} > f_{yd}$, the parameter f_{yd} should be replaced with the appropriate function $\sigma_s(\varepsilon)$. In the above mentioned formulas, the axial forces N in tension and the moments that put the lower reinforcement A_s in tension have been assumed positive. Therefore compressive stresses $\sigma_c(\varepsilon)$ are to be assumed as negative.

- Domain 0 (pivot *A*)
  section entirely cracked, reinforcement in tension yielded with undetermined deformation which always gives the internal forces:

$$N = f'_{td}A_s + f_{yd}A'_s$$
$$M = f'_{td}A_s y_s - f_{yd}A'_s y'_s$$

- Domain 1 (pivot *A*)
  section entirely cracked, lower reinforcement in tension at failure, upper reinforcement in tension in the elastic range with $\varepsilon_{yd} > \varepsilon'_s > \varepsilon_{ud}d'/d$; the resisting internal forces are equal to:

$$N = f'_{td}A_s + E_s\varepsilon'_s A'_s$$
$$M = f'_{td}A_s y_s - E_s\varepsilon'_s A'_s y'_s$$

- Domain 2′ (pivot *A*)
  cracked section, lower reinforcement in tension at failure, upper reinforcement in the elastic range with $\varepsilon_{ud}d'/d > \varepsilon'_s > -\varepsilon_{yd}$; the internal forces are:

$$N = f'_{\mathrm{td}} A_{\mathrm{s}} + E_{\mathrm{s}} \varepsilon'_{\mathrm{s}} A'_{\mathrm{s}} + \int_{\mathrm{A}} \sigma_{\mathrm{c}}(\varepsilon) b \, \mathrm{d}y$$

$$M = f'_{\mathrm{td}} A_{\mathrm{s}} y_{\mathrm{s}} - E_{\mathrm{s}} \varepsilon'_{\mathrm{s}} A'_{\mathrm{s}} y'_{\mathrm{s}} - \int_{\mathrm{A}} \sigma_{\mathrm{c}}(\varepsilon) b y \, \mathrm{d}y$$

- Domain 2″ (pivot *A*)
  cracked section, lower reinforcement in tension at failure, upper reinforcement in compression yielded; the internal forces are:

$$N = f'_{\mathrm{td}} A_{\mathrm{s}} - f_{\mathrm{yd}} A'_{\mathrm{s}} + \int_{\mathrm{A}} \sigma_{\mathrm{c}}(\varepsilon) b \, \mathrm{d}y$$

$$M = f_{\mathrm{yd}} A_{\mathrm{s}} y_{\mathrm{s}} + f_{\mathrm{yd}} A'_{\mathrm{s}} y'_{\mathrm{s}} - \int_{\mathrm{A}} \sigma_{\mathrm{c}}(\varepsilon) b y \, \mathrm{d}y$$

- Domain 3 (pivot *B*)
  cracked section with concrete at failure, lower reinforcement in tension yielded, upper reinforcement in compression yielded; the internal forces are:

$$N = f_{\mathrm{yd}} A_{\mathrm{s}} - f_{\mathrm{yd}} A'_{\mathrm{s}} + \int_{\mathrm{B}} \sigma_{\mathrm{c}}(\varepsilon) b \, \mathrm{d}y$$

$$M = f_{\mathrm{yd}} A_{\mathrm{s}} y_{\mathrm{s}} + f_{\mathrm{yd}} A'_{\mathrm{s}} y'_{\mathrm{s}} - \int_{\mathrm{B}} \sigma_{\mathrm{c}}(\varepsilon) b y \, \mathrm{d}y$$

- Domain 4 (pivot *B*)
  cracked section with concrete at failure, upper reinforcement in compression yielded, lower reinforcement in the elastic range with $\varepsilon_{yd} > \varepsilon_{\mathrm{s}} > \varepsilon_{\mathrm{cu}} c/h$; the internal forces are:

$$N = E_{\mathrm{s}} \varepsilon_{\mathrm{s}} A_{\mathrm{s}} - f_{\mathrm{yd}} A'_{\mathrm{s}} + \int_{\mathrm{B}} \sigma_{\mathrm{c}}(\varepsilon) b \, \mathrm{d}y$$

$$M = E_{\mathrm{s}} \varepsilon_{\mathrm{s}} A_{\mathrm{s}} y_{\mathrm{s}} + f_{\mathrm{yd}} A'_{\mathrm{s}} y'_{\mathrm{s}} - \int_{\mathrm{B}} \sigma_{\mathrm{c}}(\varepsilon) b y \, \mathrm{d}y$$

- Domain 5′ (pivot *C*)
  uncracked section with concrete at failure, upper reinforcement in compression yielded, lower reinforcement in compression in the elastic range with $\varepsilon_{\mathrm{cu}} c/h > \varepsilon_{\mathrm{s}} > -\varepsilon_{\mathrm{yd}}$; the internal forces are:

$$N = E_{\mathrm{s}} \varepsilon_{\mathrm{s}} A_{\mathrm{s}} - f_{\mathrm{yd}} A'_{\mathrm{s}} + \int_{\mathrm{C}} \sigma_{\mathrm{c}}(\varepsilon) b \, \mathrm{d}y$$

$$M = E_{\mathrm{s}} \varepsilon_{\mathrm{s}} A_{\mathrm{s}} y_{\mathrm{s}} + f_{\mathrm{yd}} A'_{\mathrm{s}} y'_{\mathrm{s}} - \int_{\mathrm{C}} \sigma_{\mathrm{c}}(\varepsilon) b y \, \mathrm{d}y$$

- Domain 5″ (pivot *C*)
  uncracked section with concrete at failure, reinforcement in compression yielded; the internal forces are:

$$N = -f_{yd}A_s - f_{yd}A'_s + \int_C \sigma_c(\varepsilon) b \, dy$$
$$M = -f_{yd}A_s y_s + f_{yd}A'_s y'_s - \int_C \sigma_c(\varepsilon) b y \, dy$$

It is to be noted that the situation with upper reinforcement in compression at yield limit, instead at the boundary of the domain 2, for higher values of concrete cover d'/d can be within the domain 3. In this case this latter will be divided into a sub-domain 3′, with upper reinforcement in compression in the elastic range, and a sub-domain 3″, with upper reinforcement in compression yielded.

For rectangular section the evaluation of the resultant of compressions in concrete and its moment with respect to the design axis can rely on the coefficients β and κ already mentioned. Repeating the calculations contemplated by the previous formulas for different arrangements of the section, rotated about the pivots *A*, *B* or *C*, the interaction curve *N*–*M* is defined point by point, which corresponds to the failure boundary of the section itself. For the verification the point N_{Ed}, M_{Ed} representing the applied forces should remain within such boundary.

Interaction Diagrams

An example of numerical calculation of the failure boundary is shown for a rectangular section with symmetric double reinforcement. The adimensionalized values of the axial and flexural components of the resisting forces are calculated:

$$\nu = \frac{N_{Rd}}{f_{cd} b h}$$
$$\mu = \frac{M_{Rd}}{f_{cd} b h^2}$$

based on the following data (see Fig. 6.13):

$c = d' = 0,10\,h$	$(\delta' = 0.10, \delta = 0.90)$
$\omega_s = 0.10$	$\left(\omega_s = A_s f_{yd}/bhf_{cd}\right)$
$\omega'_s = \omega_s = 0.10$	$\left(\omega_t = \omega_s + \omega'_s = 0.20\right)$
$y_o = h/2$	$(\eta_o = y_o/h = 0.50)$
$y_s = y'_s = 0.40\,h$	$(\eta_s = \eta'_s = 0.40)$
$f_{yd} = 450/1.15 = 394\,\mathrm{N/mm^2}$	$\left(\varepsilon_{yd} = f_{yd}/E_s = 0.0018\right)$
$\varepsilon_{cu} = 0.0035$	
$\varepsilon_{c1} = 0.0020$	

For the steel a conventional failure strain is also assumed with ε_{sd} = 0.010.

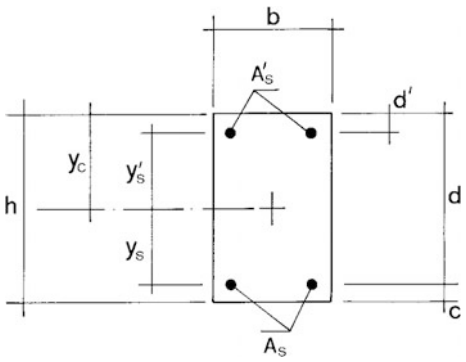


Fig. 6.13 Case of rectangular section with symmetric reinforcement

- Point "1" (domain 0)

$$v = v_t + 0 = \frac{f_{yd} A_t}{f_{cd} bh} = \omega_t = 0.200$$
$$\mu = v_s \eta_s - v'_s \eta'_s + 0 = \omega_s \eta_s - \omega'_s \eta'_s = 0.000$$

- Point "2" (domain 2 with $\varepsilon'_s = 0$)

$$\xi = \delta' = 0.10$$
$$\varepsilon_c = \frac{\xi}{\delta - \xi} \varepsilon_s = 0.125\, \varepsilon_{sd}$$
$$\bar{\varepsilon}_c = \varepsilon_c / \varepsilon_{cu} = 0.357$$
$$\beta = (1.6 - 0.8\bar{\varepsilon}_c)\bar{\varepsilon}_c = 0.469$$
$$\kappa = 0.33 + 0.07\bar{\varepsilon}_c = 0.355$$
$$v = v_s - v_c = \omega_s - \frac{\beta f_{cd} bx}{f_{cd} bh} = \omega_s - \beta\xi = 0.100 - 0.047 = 0.053$$
$$\mu = v_s \eta_s - v_c(\eta_o - \kappa\xi) = 0.040 + 0.022 = 0.062$$

- Point "3" (limit scenario between domains 2 and 3)

$$x = \frac{\varepsilon_{cu}}{\varepsilon_{sd} + \varepsilon_{cu}} d = 0.233h \quad \left(\xi = \frac{x}{h} = 0.233\right)$$

$$\varepsilon'_s = -\frac{\xi - \delta'}{\xi}\varepsilon_{cu} = 0.571\varepsilon_{cu} = 0.0020 \quad (> \varepsilon_{yd})$$
$$\nu = \nu_s + \nu'_s - \nu_c = \omega_s - \omega'_s - \beta_o\xi = 0 - 0.186 = -0.186$$
$$\mu = \nu_s\eta_s - \nu'_s\eta'_s + \nu_c(\eta_o - \kappa_o\xi) = 0.040 + 0.040 + 0.076 = 0.156$$

- Point "4" (limit scenario between domains 3 and 4)

$$x = \frac{\varepsilon_{cu}}{\varepsilon_{yd} - \varepsilon_{cu}}d = 0.583h \quad \left(\xi = \frac{x}{h} = 0.583\right)$$

$$\nu = \omega_s - \omega'_s - \beta_o\xi = 0 - 0.467 = -0.467$$
$$\mu = \omega_s\eta_s + \omega'_s\eta'_s + \beta_o\xi(\eta_o - \kappa_o\xi) = 0.040 + 0.040 + 0.124 = 0.204$$

- Point "5" (domain 4 with $\varepsilon_s = 0$)

$$\xi = \delta = 0.90$$
$$\nu = -\omega'_s - \beta_o\xi = -0.100 - 0.720 = -0.820$$
$$\mu = \omega'_s\eta'_s + \beta_o\xi(\eta_o - \kappa_o\xi) = 0.040 + 0.101 = 0.141$$

- Point "6" (limit scenario domain 5)

$$\nu = -\omega_t - 1.000 = -1.200 \quad (= \nu_{min})$$
$$\mu = -\omega_s\eta_s + \omega'_s\eta'_s - \nu_c(\eta_o - 0.5) = 0.000$$

The interaction curve obtained in this way is shown in Fig. 6.14. For a more detailed description it suffices to evaluate other intermediate situations. For the verification in simple compression, with $\gamma'_s = 1.25\gamma_C$, the curve is cut-off at the abscissa:

$$\nu_o = -\omega_t - 0.8 = -1.000$$

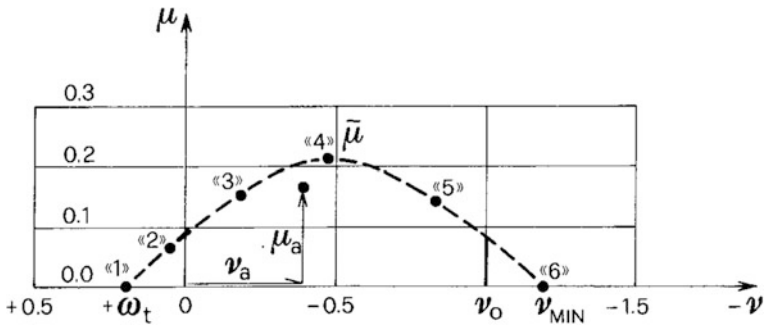


Fig. 6.14 Interaction limit curve

6.2.2 *Resistance Verifications of the Section*

Having an interaction curve as the one in Fig. 6.14, for the verification of the section of concern the point v_E, μ_E representing the applied force is set in the same scale of the diagram, as indicated in the mentioned figure. The verification is satisfied if such point is within the failure boundary. It can be noted how in the case of symmetric reinforcement, approximately up to the value $v = -0.5$ the presence of a compression axial component increases the flexural resistance of the section.

For practical purposes it is convenient to use families of curves, with the same adimensionalized variables for a more general validity. An example of the entire family of curves with $\omega_t = 0.0–0.1–0.2–\ldots–1.0$ is shown in Fig. 6.15, always evaluated for a symmetric reinforcement $\left(\omega'_s = \omega_s = \omega_t/2\right)$. A family of curves for non-symmetric reinforcement with $\alpha = A'_s/A_s = 0.5$ is instead shown in Fig. 6.16, where the different shape of the failure boundaries for positive and negative

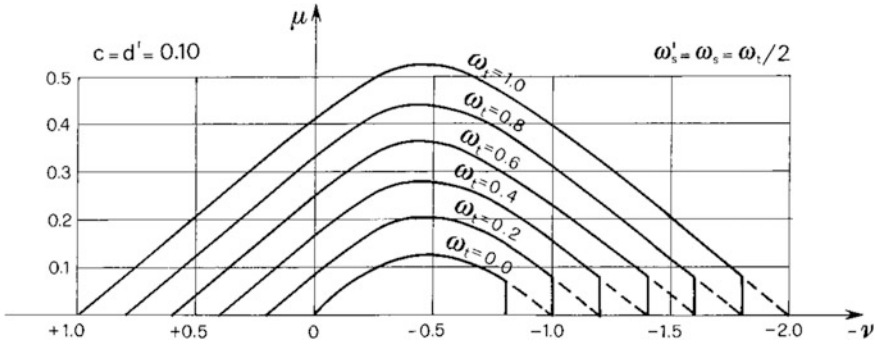


Fig. 6.15 Family of interaction curves for symmetric section

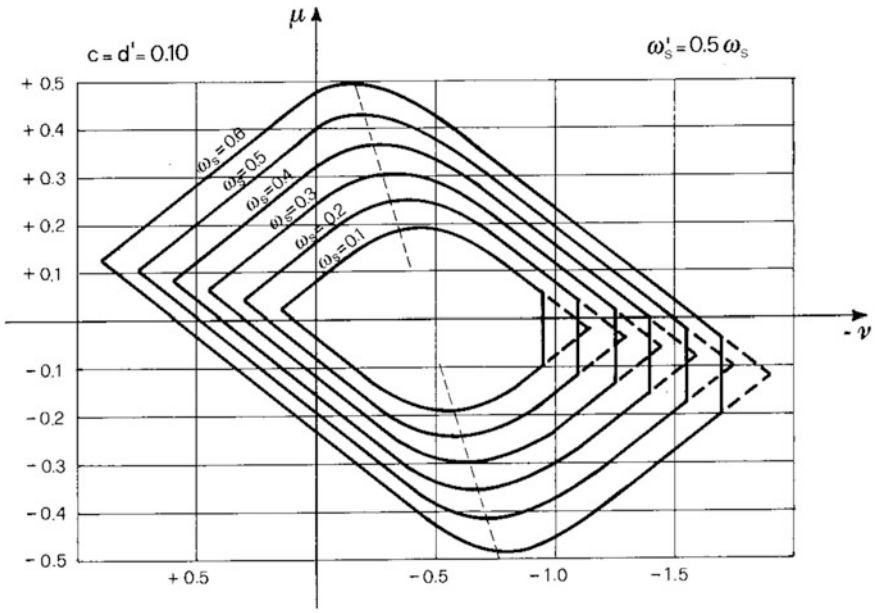


Fig. 6.16 Family of interaction curves for non-symmetric section

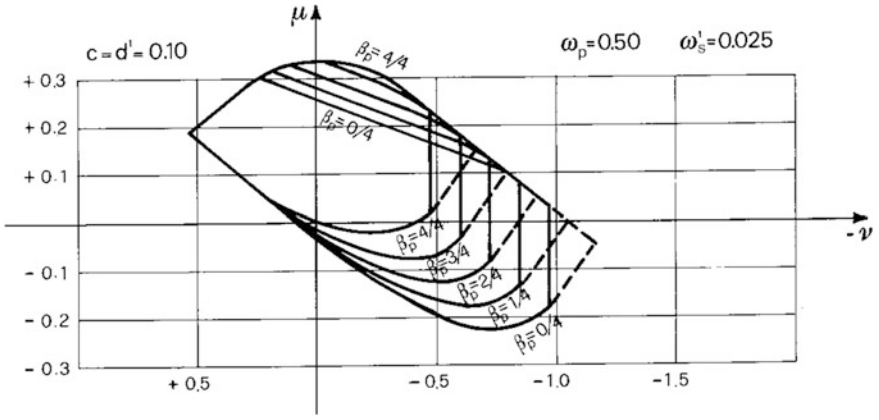


Fig. 6.17 Prestressing effects on the interaction curves

moments can be noted, with points of maximum flexural resistance shifted backward or forward for the high reinforcement ratios.

Figure 6.17 eventually shows the effect of the pretensioning of the reinforcement. For the same rectangular section of Fig. 6.13 with $c = d' = 0.10\ h$, an upper passive reinforcement equal to $\omega'_s = 0.025$ has been provided and a lower pretensioned reinforcement equal to $\omega_p = 0.50$ (with $f_{pyd} = f_{ptd} = 1600/1.15 = 1391\ \text{N/mm}^2$,

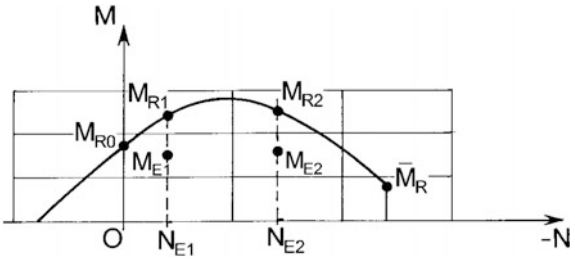


Fig. 6.18 Representation of analytical verification

$\varepsilon_{yd} = 0.00675$). The five curves shown in the figure correspond to the values $\beta_p = 0.00–0.25–0.50–0.75–1.00$ of the coefficient of partial prestressing ($\beta_p = \sigma_{po}/f_{pyd}$).

Analytical Verification

The graphical verification that utilizes the diagrams with the resistance adimensionalized curves can be substituted by analytical procedures that lead directly to a numerical verification of the section under combined compression and bending. Such procedures lead to a comparison of bending moments, applied and resisting, as shown in Fig. 6.18.

The verification therefore coincides with the one for uniaxial bending presented at Sect. 3.1.2, with the difference that for combined compression and bending the resisting moment is a function of the axial force:

$$M_{Ed} < M_{Rd}(N_{Ed})$$

The axial force is therefore interpreted as an internal characteristic of the section, similarly to the geometrical ones related to its dimensions or the static ones related to the strength of materials. Uniaxial bending represents a particular case with zero value of the axial force, as indicated by the point M_{R0} of Fig. 6.18.

The verifications by vertical lines represented in the figure shall be obviously carried after the introduction of the partial safety factors, to reduce the strength of materials on one side, and amplify the intensity of loads on the other. It is to be noted that the axial force N_E can have a decreasing or increasing effect on the flexural resistance and should consequently be amplified or not with the coefficient γ_F depending on the cases.

Further to what has been mentioned above, the possible interdependence of actions should obviously be taken into account. If for example the two axial and flexural actions derive from one single load, as represented in Fig. 6.19a, their amplification goes together and the two limit situations of verification will be

$$\gamma_F M_{Ek} < M_R(\gamma_F N_{Ek})$$
$$M_{Ek} < M_R(N_{Ek})$$

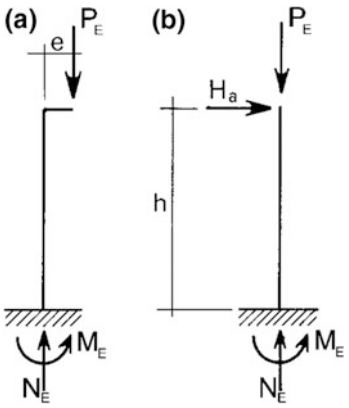


Fig. 6.19 Interdependent (**a**) and independent (**b**) flexural and axial actions

If instead the flexural force is independent from the axial force, as indicated in Fig. 6.19b, the two limit situations of verification can be

$$\gamma_F M_{E,max} < M_R\left(\gamma_F N_{E,max}\right)$$
$$\gamma_F M_{E,max} < M_R\left(N_{E,min}\right)$$

On this matter, the code requirements refer more generally to verifications repeated for all possible load combinations.

A simple algorithm is presented for the verification of the section in reinforced concrete under combined compression and bending, described hereafter for the case of rectangular section with double reinforcement with:

- cracked section with $x < d$,
- reinforcements in tension and compression yielded,
- concrete edge in compression at failure limit.

A constant distribution $\sigma_c = f_{cd}$ of compressions in concrete is assumed, extended up to $\bar{x} = \beta_o x \cong 0.8x$.

Such limit situation is represented in Fig. 6.20. The equilibrium of the section is set with the equations

$$\begin{cases} C + C'_s - Z = N_o \\ C(y_o - \bar{x}/2) + C'_s y'_s + Z y_s = M_{Rd} \end{cases}$$

and therefore with

$$\begin{cases} f_{cd} b\bar{x} + f_{yd} A'_s - f_{yd} A_s = N_o \\ f_{cd} b\bar{x}(y_o - \bar{x}/2) + f_{yd} A'_s y'_s + f_{yd} A_s y_s = M_{Rd} \end{cases}$$

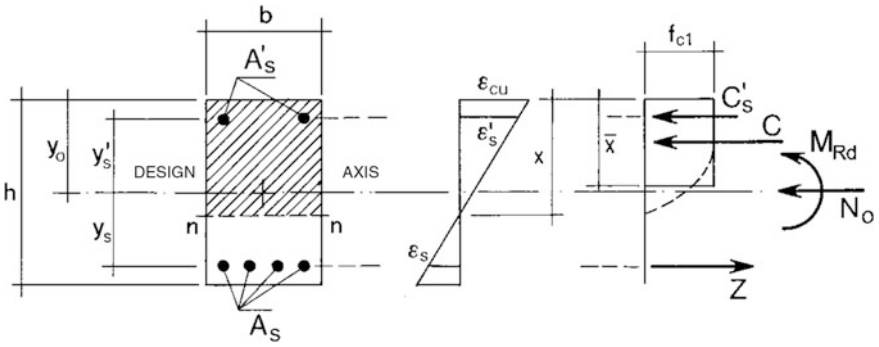


Fig. 6.20 Resistance limit state under compression and uniaxial bending

where the absolute value of the axial force has been indicated with

$$N_o = |N_{Ed}|$$

intended as an internal resisting characteristic. The position of the neutral axis is obtained from the first equation

$$\bar{x} = \frac{N_o + f_{yd}A_s - f_{yd}A'_s}{f_{cd}b}$$

and the second equation below eventually gives the value of the resisting moment

$$M_{Rd} = M_{Rd}(N_o) = f_{cd}b\bar{x}(y_o - \bar{x}/2) + f_{yd}A'_s y'_s + f_{yd}A_s y_s$$

In the case where a value

$$x = \bar{x}/\beta_o > \frac{\alpha_o}{1+\alpha_o}d \quad (\alpha_o = \varepsilon_{cu}/\varepsilon_{yd})$$

shows, with $\varepsilon_s < \varepsilon_{yd}$, the incompatibility of the solution with the yielding of the reinforcement in tension, in the previous equilibrium equations the term $f_{yd}A_s$ shall be substituted with $\sigma_s A_s$. Therefore setting

$$\sigma_s = E_s\varepsilon_s = E_s\frac{d-x}{x}\varepsilon_{cu}$$

and after the appropriate substitutions, the first equation becomes:

$$\beta_o f_{cd}bx^2 + \left[f_{yd}A'_s + \alpha_o f_{yd}A_s - N_o\right]x - \alpha_o f_{yd}A_s d = 0$$

that, adimensionalized with $f_{cd}bh^2$, becomes:

$$\beta_o\xi^2 - \left(\nu_o - \alpha_o\omega_s - \omega'_s\right)\xi - \alpha_o\omega_s\delta = 0$$

The position of the neutral axis is therefore given by

$$\xi = \frac{1}{2\beta_o}\left\{\left(\nu_o - \alpha_o\omega_s - \omega'_s\right) + \sqrt{\left(\nu_o - \alpha_o\omega_s - \omega'_s\right)^2 + 4\beta_o\alpha_o\omega_s\delta}\right\}$$

With $\bar{x} = \beta_o\xi h \cong 0.8x$, the resisting moment is given by

$$M_{Rd} = M_{Rd}(N_o) = f_{cd}b\,\bar{x}(y_o - \bar{x}/2) + f_{yd}A'_s y'_s + \sigma_s A_s y_s$$

where

$$\sigma_s = f_{yd}\frac{\delta - \xi}{\xi}\alpha_o \qquad \left(< f_{yd}\right)$$

Unreinforced Section

The cracked section under combined compression and bending analyzed before is shown in Fig. 6.21a, as the section of a reinforced concrete column. Figure 6.21d shows the corresponding situation of an unreinforced section. For this latter section, the translational equilibrium $C = N_o$ leads to

$$\bar{x} = \frac{N_o}{f_{cd}b}$$

and consequently to the resisting moment

$$M_{Rd}(N_o) = N_o e = f_{cd}b\,\bar{x}(y_o - \bar{x}/2)$$

Figure 6.21b–e refer to the limit situation $x = h$ with uncracked section for which one has:

$$\bar{C} \cong 0.8 f_{cd}bh$$

Without reinforcement the following resisting moment corresponds

$$\bar{M}_{Rd} = 0.8 f_{cd}bh(y_o - 0.4h)$$

which for a rectangular section with $y_o = h/2$, becomes

$$\bar{M}_{Rd} = 0.8 f_{cd}bh^2$$

Taking into account that the resisting axial force is limited to the value (see Fig. 6.21f)

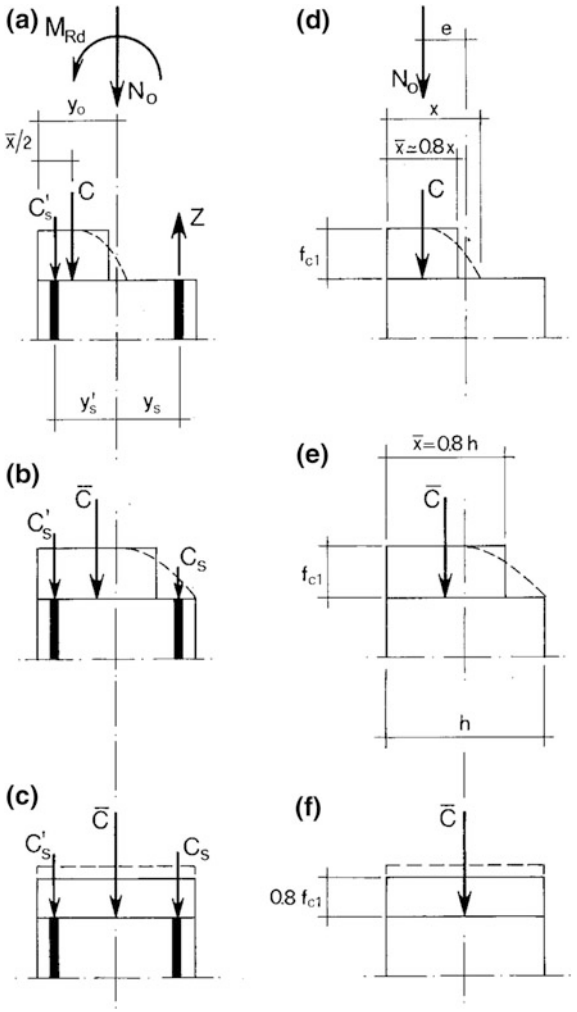


Fig. 6.21 Compression and uniaxial bending in an unreinforced section

$$N_{\mathrm{Rd}} = 0.8 f_{\mathrm{cd}} bh = \bar{C}$$

the corresponding resisting moment is the minimum that can be attributed to a highly compressed section:

$$\bar{M}_{\mathrm{Rd}} = M_{\mathrm{Rd}}(N_{\mathrm{Rd}}) = 0.08 f_{\mathrm{cd}} bh^2 = \min.$$

This moment is the one that corresponds to the interaction diagram $\omega_t = 0.0$ cut-off of Fig. 6.15.

For reinforced sections (see Fig. 6.21c), the contributions of the reinforcement should be added. If it is symmetric with $C'_s y'_s = C_s y_s$, as it is often the case for

reinforced concrete columns, one has the same minimum value of the resisting moment, as it can be observed in all cut-off curves of Fig. 6.15 (with ω_t = 0.2 0.4 ÷…). For non-symmetric reinforcements instead (see Fig. 6.16) the curves cut-off towards the high compressions leave a different value of the resisting moment, varying with the mechanical reinforcement ratio.

Reduced Effective Depth

A particular interpretation of the behaviour of the section at the ultimate limit state of combined compression and bending can be given to highlight how, when the axial force increases, the available part of the pure flexural capacity is reduced. In addition to giving a clear physical evidence to the interaction of the two axial and flexural components, such interpretation also gives the model to evaluate the effects on the combined behaviour with shear.

If divided respectively by $f_{cd}bh$ *e* $f_{cd}bh^2$, the two equilibrium equations written above lead to the adimensional expressions:

$$\begin{cases} \bar{\xi} = \nu_o - \omega'_s + \omega_s \\ \mu_{Rd} = \bar{\xi}(\eta_o - \bar{\xi}/2) + \omega'_s\eta'_s + \omega_s\eta_s \end{cases}$$

respectively for the translation along the axis and for the rotation of the section.

In Fig. 6.22 the internal reactions of the section, which appear in these expressions, have been decomposed in two parts: a part given by

$$C'_s + C_o = N_o$$

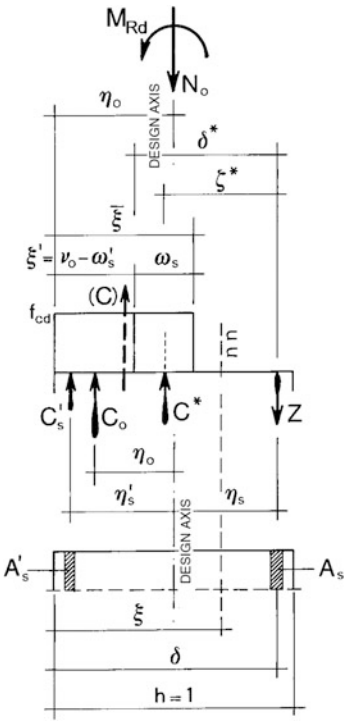


Fig. 6.22 Deduction of the reduced effective depth δ^*

to balance the given axial force; another part, with null resultant, given by the couple

$$C^* = Z \qquad (C_o + C^* = C)$$

Assigning the first contribution to the edge part of the section in compression, for equilibrium a portion of concrete is to be reserved to it (see Fig. 6.22) equal to:

$$x' = \frac{N_o - f_{yd}A'_s}{f_{cd}b} = \left(v_o - \omega'_s\right)h = \xi' h$$

a *reduced effective depth* remains

$$d^* = d - x' = \left(\delta - v_o + \omega'_s\right)h = \delta^* h$$

to give the pure flexural response

$$M^* = Zz^*$$

which relies on a portion

$$\bar{x}^* = \frac{f_{yd}A_s}{f_{cd}b} = \omega_s h$$

of concrete in compression. With the conservative approximation of placing the resultant C^* in the middle of such portion, the lever arm of the internal couple becomes

$$z^* = d^* - \bar{x}^*/2 = (\delta^* - \omega_s/2)h = \zeta^* h$$

In total, therefore, the resisting moment, expressed with reference to the design axis, consists of two components: one of *eccentric compression*

$$M'_{Rd} = N_o y'$$

where y' is the distance from the mentioned centroidal axis of the two reactions C'_s and C_o; plus a *pure flexural component*

$$M''_{Rd} = f_{yd}A_s z^*$$

which uses the reduced effective depth of the section. This reduced portion of the section also offers the residual shear resistance, with the truss mechanism already described at Sect. 4.3.2, which is to be verified in the cases where high values of the axial, flexural and shear components coexist, as it will be discussed in more detail at Sect. 6.3.1.

What mentioned above is valid also in the case of reinforcement in tension not yielded, provided that $\sigma_s A_s$ is set in place of $f_{yd} A_s$ as mentioned before.

σ–ε Model with Hardening If the finite bilinear model with hardening is assumed (see Fig. 1.30—model A), assuming that both reinforcements in tension and compression are yielded, the translational equilibrium condition of the section under combined compression and bending at the ultimate limit state of its resistance is written as

$$\beta_o b x f_{cd} + A'_s \sigma'_s - A_s \sigma_s = N$$

where it has been assumed that, with $\varepsilon_c = \varepsilon_{cu}$, the concrete is at its failure limit, the value of the axial force corresponds to the applied design force ($N = N_{Ed}$) and the stresses in the reinforcement are expressed based on the mentioned model

$$\sigma'_s = f_{yd} + E_1 \left(\varepsilon'_s - \varepsilon_{yd} \right)$$
$$\sigma_s = f_{yd} + E_1 \left(\varepsilon_s - \varepsilon_{yd} \right)$$

From the linearity of the strains ε on the section one obtains for the reinforcement:

$$\varepsilon'_s = \frac{x - d'}{x} \varepsilon_{cu} = \frac{\xi - \delta'}{\xi} \varepsilon_{cu}$$
$$\varepsilon_s = \frac{d - x}{x} \varepsilon_{cu} = \frac{\delta - \xi}{\xi} \varepsilon_{cu}$$

with $\delta' = d'/h$, $\delta = d/h$ and $\xi = x/h$. Substituting these expressions in the previous formulas one therefore has:

$$\sigma'_s = f_{yd} + E_1 \left(\frac{\xi - \delta'}{\xi} \varepsilon_{cu} - \varepsilon_{yd} \right) = f_{yd} + E_1 \varepsilon_{yd} \left(\frac{\xi - \delta'}{\xi} \alpha_o - 1 \right)$$
$$\sigma_s = f_{yd} + E_1 \left(\frac{\delta - \xi}{\xi} \varepsilon_{cu} - \varepsilon_{yd} \right) = f_{yd} + E_1 \varepsilon_{yd} \left(\frac{\delta - \xi}{\xi} \alpha_o - 1 \right)$$

with $\alpha_o = \varepsilon_{cu}/\varepsilon_{yd}$. Grouping now f_{yd} (con $f_{yd} = E_s \varepsilon_{yd}$) one obtains:

$$\sigma'_s = f_{yd} \left[1 + \alpha \left(\frac{\xi - \delta'}{\xi} \alpha_o - 1 \right) \right]$$
$$\sigma_s = f_{yd} \left[1 + \alpha \left(\frac{\delta - \xi}{\xi} \alpha_o - 1 \right) \right]$$

with $\alpha = E_1/E_s$. Replaced in the original equilibrium equation, these expressions lead to

$$\beta_o bhf_{cd}\xi + A'_s f_{yd}\left[1+\alpha\left(\frac{\xi-\delta'}{\xi}\alpha_o - 1\right)\right] + \\ - A_s f_{yd}\left[1+\alpha\left(\frac{\delta-\xi}{\xi}\alpha_o - 1\right)\right] = N$$

which, rearranged, becomes

$$\beta_o bhf_{cd}\xi^2 + \left\{A'_s f_{yd}[1+\alpha(\alpha_o-1)] - A_s f_{yd}[1-\alpha(\alpha_o+1)] - N\right\}\xi + \\ - \left(A'_s f_{yd}\alpha\alpha_o\delta' + A_s f_{yd}\alpha\alpha_o\delta\right) = 0$$

Dividing everything by $\beta_o bhf_{cd}$ one finally has

$$\xi^2 - \frac{1}{\beta_o}\left\{\omega_s[1-\alpha(1+\alpha_o)] - \omega'_s[1-\alpha(1-\alpha_o)] + v\right\}\xi - \frac{\alpha\alpha_o}{\beta_o}\left(\omega_s\delta + \omega'_s\delta'\right) = 0$$

second degree equation which leads to the positive real root:

$$\xi = \frac{1}{2}c\left\{1+\sqrt{1+4a/c^2}\right\}$$

with

$$c = \frac{1}{\beta_o}\left\{\omega_s[1-\alpha(1+\alpha_o)] - \omega'_s[1-\alpha(1-\alpha_o)] + v\right\}$$
$$a = \frac{\alpha\alpha_o}{\beta_o}\left(\omega_s\delta + \omega'_s\delta'\right)$$
$$\omega_s = \frac{A_s f_{yd}}{bhf_{cd}} \qquad \omega'_s = \frac{A'_s f_{yd}}{bhf_{cd}} \qquad v = \frac{N_{Ed}}{bhf_{cd}}$$

The resisting moment is therefore calculated with

$$M_{Rd} = \beta_o bxf_{cd}(y_o - \kappa_o x) + A'_s f_{yd}\left[1+\alpha\left(\frac{x-d'}{x}\alpha_o - 1\right)\right](y_o - d') + \\ + A_s f_{yd}\left[1+\alpha\left(\frac{d-x}{x}\alpha_o - 1\right)\right](d - y_o)$$

where $\beta_o = 0.8$, $\kappa_o = 0.4$, $x = \xi h$ and y_o is the distance of the design axis from the edge in compression of the section.

6.2.3 Design for Biaxial Bending

For the design of a section at the ultimate limit state, subject to the three combined components N, M_y and M_z, the corresponding failure boundary is to be evaluated. This is represented by the surface:

$$F\left(N, M_y, M_z\right) = 0$$

which, in the three-dimensional space of the examined combined actions, corresponds to situations for which, in the furthest points from the neutral axis, the maximum compressive strain ε_{cu} in the concrete or the maximum tensile strain ε_{ud} in the reinforcement is reached.

For each possible inclination of the neutral axis, the appropriate integrations of stresses, which lead to the evaluation of the three corresponding internal components, are set with the usual assumptions of calculation. In the following descriptions, with reference to the symbols shown in Fig. 6.23, the application of the mentioned criteria is shown in details, assuming again to refer the geometrical parameters of the section to a couple of orthogonal axes η, ζ chosen based on its regularity in shape.

Once the inclination of the neutral axis nn is fixed by the intersection with the axes v and w, the resisting area of the concrete in compression is consequently set

$$A'_c = A'_c(v, w)$$

according to the assumption of cracked section.

The assumptions of plane section and compatibility lead to the expression of the deformation plane

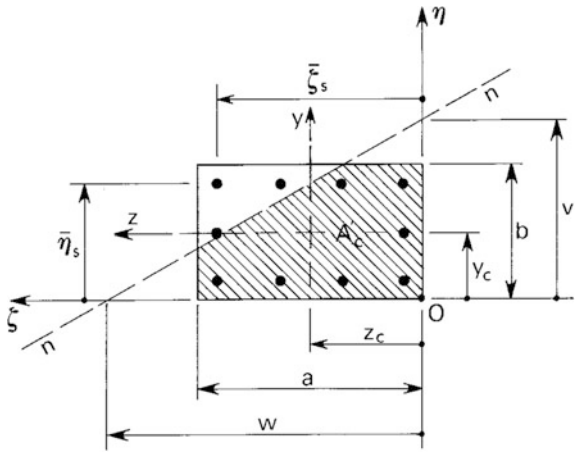


Fig. 6.23 Cracked section under axial action and biaxial bending

$$\varepsilon = \varepsilon_c \left(1 - \frac{\zeta}{w} - \frac{\eta}{v}\right)$$

as a function of the intersections with the main axes v and w.

The definition of the ultimate limit state fixes the value of the parameter ε_c referred to the origin O. Chosen on the furthest corner of the perimeter from the neutral axis, it has to correspond with the maximum compressive strain in the concrete. It is therefore set

$$\varepsilon_c = \varepsilon_{cu}$$

or

$$\varepsilon_c = \frac{\varepsilon_{ud}}{1 - \frac{\bar{\zeta}_s}{w} - \frac{\bar{\eta}_s}{v}} \qquad (\text{if} < \varepsilon_{cu})$$

where the first case indicates the failure of concrete in compression, the second indicates the earlier failure of the reinforcement in tension.

Once the strains ε on the section are defined, it is possible to evaluate the corresponding stress in each point using the usual material models $\sigma = \sigma(\varepsilon)$.

The three resisting internal components for the considered situation are therefore evaluated with:

$$N = \int_{A_c'} \sigma_c(\varepsilon) dA + \sum\nolimits_i \sigma_s(\varepsilon_{si}) A_{si}$$

$$M_\eta = \int_{A_c'} \zeta \sigma_c(\varepsilon) dA + \sum\nolimits_i \zeta_i \sigma_s(\varepsilon_{si}) A_{si}$$

$$M_\zeta = \int_{A_c'} \eta \sigma_c(\varepsilon) dA + \sum\nolimits_i \eta_i \sigma_s(\varepsilon_{si}) A_{si}$$

The possible change of the reference system on the design axes y, z, assumed here for translation only, is finally set (see Fig. 6.23):

$$M_y = M_\eta - N z_c$$
$$M_z = M_\zeta - N y_c$$

Repeating this procedure for the different possible positions of the neutral axis, the failure boundary is defined. Figure 6.24 shows such boundary for a doubly symmetric section.

For practical applications, the isolines N = cost. are calculated, with appropriate procedures of numerical integration, showing them in an adimensionalized form in the radial diagrams as the one shown in Fig. 6.25, which refers to the doubly symmetric section of Fig. 6.26.

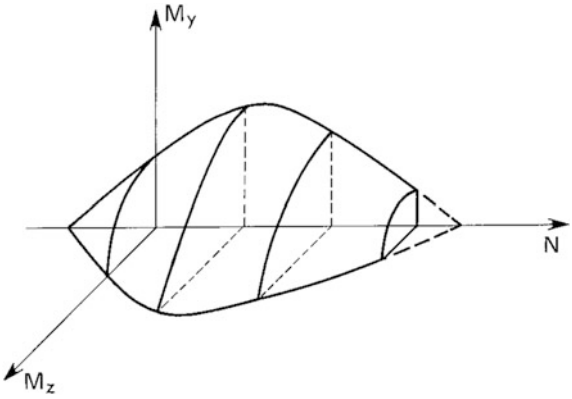


Fig. 6.24 Interaction limit surface for doubly symmetric section

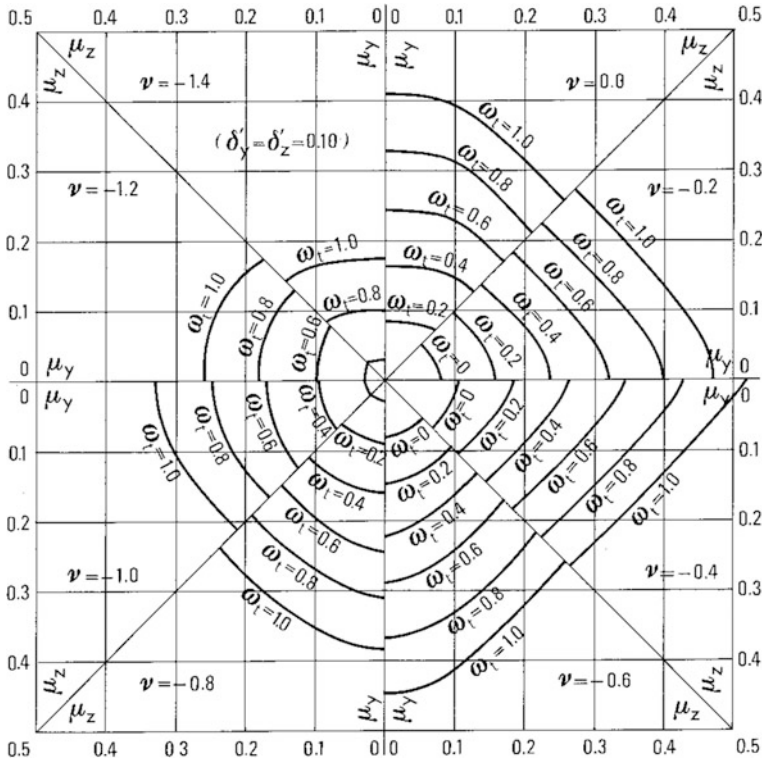


Fig. 6.25 Plane representation of the interaction surface with isolines

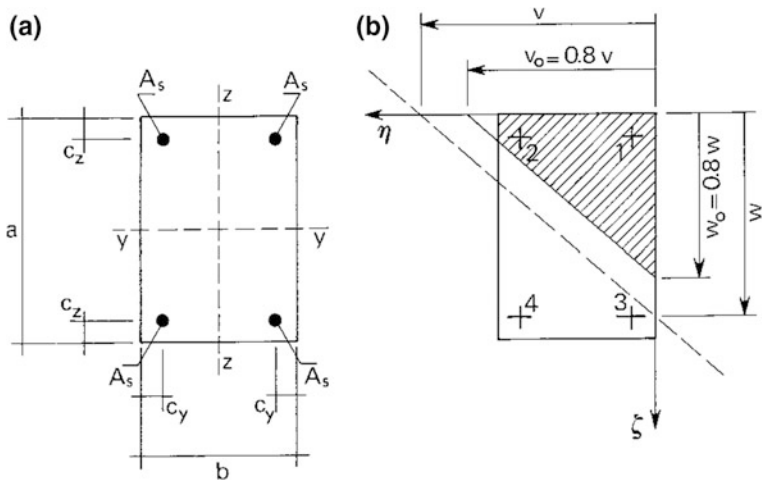


Fig. 6.26 Case of rectangular section with doubly symmetric reinforcement

The adimensionalized values of the three internal forces are defined by:

$$v = \frac{N_{rd}}{f_{cd} b a}$$
$$\mu_y = \frac{M_{yd}}{f_{cd} b a^2}$$
$$\mu_z = \frac{M_{zd}}{f_{cd} b^2 a}$$

whereas the other parameters that are required in the calculation, again in the case of double symmetry of Fig. 6.26, are:

$$\omega_t = \frac{f_{yd} A_t}{f_{cd} b a} \quad (\text{con } A_t = 4A_s)$$
$$\delta'_z = \frac{c_z}{a} \qquad \delta'_y = \frac{c_y}{b}$$

$$\alpha_o = \frac{\varepsilon_{cu}}{\varepsilon_{yd}} = \frac{0.35}{0.19} = 1.842$$

A manual elaboration of the algorithms can be carried if the stress-block constitutive law described in Fig. 1.28c is assumed for concrete. The lower accuracy of such relationship with constant stress is to be noted when applied on compression deviated portions of concrete, with respect to what is instead obtained on regular rectangular portions. However, it allows to evaluate in a very simple way the resultant of stresses on the resisting concrete.

In order to show an example of such calculation, one can consider the situation of Fig. 6.26b, characterized by the following data:

$$\omega_t = 0.40 \qquad (= 4\omega_s)$$
$$\delta'_y = 0.15 \qquad \delta'_z = 0.10$$
$$1/\alpha_o = 1/1.842 = 0.543$$

The resisting internal components are to be defined for the position of the neutral axis corresponding to the intersections

$$v = 1.5b$$
$$w = 0.9a$$

Given

$$\varepsilon_c = \varepsilon_{cu} (= 0.0035)$$

the tensile strain in the reinforcement, assumed positive in tension, are consequently obtained with

$$\varepsilon_{si} = -\left(1 - \frac{\zeta_i}{w} - \frac{\eta_i}{v}\right)\varepsilon_{cu}$$

On the four bars one therefore has:

$$\varepsilon_{s1} = -\left(1 - \frac{0.10}{0.90} - \frac{0.15}{1.50}\right)\varepsilon_{cu} = -0.7889\varepsilon_{cu} \quad (< -0.19\varepsilon_{cu} \quad \text{bar yielded})$$
$$\varepsilon_{s2} = -\left(1 - \frac{0.10}{0.90} - \frac{0.85}{1.50}\right)\varepsilon_{cu} = -0.3222\varepsilon_{cu} \quad (> -0.19\varepsilon_{cu} \quad \text{bar yielded})$$
$$\varepsilon_{s3} = -\left(1 - \frac{0.90}{0.90} - \frac{0.15}{1.50}\right)\varepsilon_{cu} = +0.1000\varepsilon_{cu} \quad (< +0.19\varepsilon_{cu} \quad \text{bar elastic})$$
$$\varepsilon_{s4} = -\left(1 - \frac{0.90}{0.90} - \frac{0.85}{1.50}\right)\varepsilon_{cu} = +0.5667\varepsilon_{cu} \quad (> +0.19\varepsilon_{cu} \quad \text{bar yielded})$$

The shape of the concrete in compression which resists with a constant stress f_{cd} consists of a triangle with sides

$$v_o = 0.8 \times 1.5b = 1.20b$$
$$w_o = 0.8 \times 0.9a = 0.72a$$

from which the smaller triangle with sides

$$v_o - b = 0.20b$$

$$\frac{0.72a}{1.20b}0.20b = 0.12a$$

is to be removed.

With this premises, the resultant of stresses in the section is evaluated in an adimensionalized form (with $\omega_{si} = 0.10$).

$$\begin{aligned}
-1.20 \times 0.72/2 &= -0.4320\\
+0.20 \times 0.12/2 &= +0.0120\\
-0.10 &= -0.1000\\
-0.10 \times 0.3222 \times 1.842 &= -0.0593\\
+0.10 \times 0.1000 \times 1.842 &= +0.0184\\
+0.10 &= \underline{+0.1000}\\
v &= -0.4609
\end{aligned}$$

The moments about the axes η, and ζ are equal to:

$$\begin{aligned}
-0.4320 \times 0.72/3 &= -0.1037\\
+0.0120 \times 0.12/3 &= +0.0005\\
-0.1000 \times 0.10 &= -0.0100\\
-0.0593 \times 0.10 &= -0.0059\\
+0.0184 \times 0.90 &= +0.0166\\
+0.1000 \times 0.90 &= \underline{+0.0900}\\
\mu_\eta &= -0.0133
\end{aligned}$$

$$\begin{aligned}
-0.4320 \times 1.20/3 &= -0.1728\\
+0.0120 \times (1 + 0.20/3) &= +0.0128\\
-0.1000 \times 0.15 &= -0.0150\\
-0.0593 \times 0.85 &= -0.0504\\
+0.0184 \times 0.15 &= +0.0028\\
+0.1000 \times 0.85 &= \underline{+0.0850}\\
\mu_\zeta &= -0.1376
\end{aligned}$$

The change on the design axes eventually leads to:

$$\begin{aligned}
\mu_y &= -0.0133 + 0.4609 \times 0.5 = +0.221\\
\mu_z &= -0.1376 + 0.4609 \times 0.5 = +0.093
\end{aligned}$$

Obviously, in order to draw an isoline by points with $v = \bar{v} =$ cost. (for example with $\bar{v} = -0.40$), the position of the neutral axis is to be modified by trial and error until the calculated axial component satisfies with good approximation that value. The two values μ_y, μ_z corresponding to a point of the curve will follow. After

modifying the direction of the neutral axis, the procedure is to be started again from the beginning.

The graphical verification of the resistance of the section under combined compression and biaxial bending will consist of plotting in the due scale the point μ_y, μ_z corresponding to the action in the corresponding sector of the diagram. For the verification, this point will have to be covered by the curve segment that represents the resistance.

Analytical Verification

The verification of the section subject to combined compression and biaxial bending can be carried numerically based on an approximated analytical representation of the local sector concerned by the failure boundary. For sections with both symmetric shape and reinforcement it can therefore be set

$$\left(\frac{M_y}{M_{\mathrm{Ryd}}}\right)^{\alpha} + \left(\frac{M_z}{M_{\mathrm{Rzd}}}\right)^{\alpha} = 1$$

which represents the failure boundary for $N = N_{\mathrm{Ed}} = \text{cost}$. The two moment components about the principal axes of inertia of the section (axes of symmetry) have been indicated with M_y, M_z; the corresponding resisting values in uniaxial bending have been indicated with M_{Ryd}, M_{Rzd} (functions of N).

The exponent α represents the degree of rounding of the curve in the plane of the two orthogonal coordinates M_y, M_z. For $\alpha = 1$, the curve sets into the straight line that connects the two points (M_{Ryd}, 0) and (0, M_{Rzd}) and that represents the extreme conservative approximation. For $\alpha = 2$, the curve corresponds to a circular arc. For $\alpha \to \infty$, the curve degenerates in two orthogonal straight segments that would correspond to the reciprocal independence of the two uniaxial bending resistances.

The numerical definition of the exponent α is done by a parametric comparison between the results of the approximated expression and the ones of the correct numerical analysis, with the optimized criterion of minimizing the deviations between the two curves. The obtained values for a given geometry, depend on two parameters

$$\nu = \frac{N_{\mathrm{Ed}}}{abf_{\mathrm{cd}}} \quad \text{dimentionalized axial force}$$

$$\omega_{\mathrm{s}} = \frac{A_{\mathrm{s}} f_{\mathrm{yd}}}{abf_{\mathrm{cd}}} \quad \text{total mechanical reinforcement ratio}$$

where a, b are the sides of the rectangular section. The tabulations of the exponent α for two typical geometrical configurations of the section are given in Table 6.10.

For square sections, with symmetrical reinforcement also with respect to the diagonals, a purely analytical procedure can be followed again based on the previous calculation of the resisting moments in combined compression and uniaxial bending. In this case the resisting moment about the median axis of the section,

which is the same in the two directions ($M_o = M_{Ryd} = M_{Rzd}$), and the resisting moment about the diagonal, which is also the same in the two directions ($M_{Rk} = M_{R\eta d} = M_{R\xi d}$ where η and ξ are the diagonal axes of the section), are needed. The two components of the latter resisting moment are equal to each other:

$$M_k = M_{yk} = M_{zd} = M_{Rk}/\sqrt{2}$$

Accepting a lower accuracy with respect to the optimized criterion mentioned before, the exponent α can be estimated setting that the curve, in addition to the extreme points of coordinates (M_o, 0) and (0, M_o), runs through the intermediate point of coordinates (M_k, M_k). One therefore has the equation

$$\left(\frac{M_k}{M_o}\right)^{\alpha} + \left(\frac{M_k}{M_o}\right)^{\alpha} = 2\left(\frac{M_k}{M_o}\right)^{\alpha} = 1$$

which leads to

$$\lg\left(\frac{M_k}{M_o}\right)^{\alpha} = \lg\frac{1}{2}$$

that is

$$\alpha \lg\left(\frac{M_k}{M_o}\right) = -\lg 2$$

from which one eventually obtains

$$\alpha = -\frac{\lg 2}{\lg(M_k/M_o)}$$

For the large category of columns with square section this formula allows a purely analytical calculation without the need for tabulations.

For the verification of combined compression and biaxial bending it should therefore be set:

$$\left(\frac{M_{Eyd}}{M_{Ryd}}\right)^{\alpha} + \left(\frac{M_{Ezd}}{M_{Rzd}}\right)^{\alpha} \leq 1$$

having indicated the two orthogonal components of uniaxial bending of the applied moment with M_{Eyd}, M_{Ezd}, α being deduced from tabulations or analytically as mentioned before.

6.3 Flexural Behaviour of Columns

An overall summary is given for the design of the typical structural elements subject to combined compression and bending: the columns. For these elements, similarly to what has been presented for beams, the following operations should be carried, aimed mainly at ensuring, with the appropriate construction details, the actual behaviour according to the models assumed in calculation, aimed again at verifying on such models the adequacy of the dimensions for both serviceability and safety against collapse.

Construction Details
The data presented at Sect. 2.1 for columns in compression and summarized in Chart 2.9 are valid, in addition to the general ones on reinforcement anchorage and minimum dimensions shown in Charts 2.7 and 2.8.

Serviceability Verifications
The principal verifications concern the stress state as it can be deduced by the elastic formulas presented at Sect. 6.1, which neglect the concrete tensile strength. It is reminded that the *verifications of stresses* concern the conservation of the mechanical integrity of materials and, excluding transient situations, assume the following allowable values:

$\bar{\sigma}_c = 0.45 f_{ck}$ for maximum compressions in concrete
$0.7\bar{\sigma}_c$ for the average compression (centroidal)
$\bar{\sigma}_s = 0.80 f_{yk}$ for the maximum tensions in steel

For the verification of *cracks opening*, as contemplated in Chart 2.15, the maximum tension in the reinforcement, calculated as mentioned above with the cracked section assumption, should again be compared to the limits $\bar{\sigma}'_{s1}, \bar{\sigma}'_{s2}$ or $\bar{\sigma}'_{s3}$ shown in Table 2.16.

For the *cracking verifications* contemplated in Chart 2.15 the elastic design of the uncracked section can be required, in order to evaluate the maximum tensile stresses in the concrete. The allowable values of such stresses are here recalled:

$\bar{\sigma}_{ct} = 0$ limit of decompression
$\bar{\sigma}'_{ct} = \beta f_{ctk}$ limit of cracking formation

with $\beta = 1.3$ for triangular stress distributions. All the cracking verifications concern the durability of reinforced concrete, as discussed in details at Sect. 2.3.3.

Resistance Verifications
These verifications concern the critical and most highly stressed sections of columns and are carried with the algorithms presented at Sect. 6.2. Moreover, a global model of the column subject to shear and variable combined compression and bending is presented in the next section.

6.3.1 Design Models of Columns

Similarly to what has been done for beams at Sect. 5.1, a global model for the design of columns under combined compression and bending is now presented. A typical situation of a column belonging to a reinforced concrete frame is represented in Fig. 6.27a. The actions S come from the beams connected at its ends which translate into a constant axial compression N_o, a shear force V also constant and a bending moment M varying linearly along the height l, starting from the value

$$M_a = N_o e_1 \qquad \text{at the bottom}$$

up to the value

$$M_b = N_o e_2 \qquad \text{at the top}$$

The critical sections of such column with respect to the resistance to combined compression and bending are the ones at the ends where, for the same axial force, the maximum values of the bending moment are attained. The column itself is divided in three different segments: the central one with a small eccentricity of the axial force and uncracked sections, as a tensile stress in concrete lower than the corresponding design strength results from the elastic calculation

$$\sigma'_c = -\frac{N_o}{A_i} + \frac{M}{I_i} y'_c < \beta f_{ctd} \quad (\beta = 1.3)$$

and two end segments where the greater eccentricities lead to concrete cracking.

Cracked Segments

For these end segments a model consisting of two mechanisms in parallel can be set: one corresponding to the direct transmission of the compression force between the two extreme compression portions of the critical sections of the column (see Fig. 6.27b); another truss mechanism placed in the residual portion, not concerned by such compression force, and corresponding to variable pure bending along the axis (see Fig. 6.27c). Such mechanism extends up to where, with the decrease of the eccentricity of the axial force, the part of the section in tension reduces as far as to disappear in the central uncracked segment.

This composite model is intended to be applied for resistance calculations, including shear, referred to critical sections located at the ends of the column. Its extent is therefore not so important as its configuration is close to the critical sections. At the ultimate limit state of the column, these sections are assumed to be subject to the resisting values of bending moment and shear whereas the axial force is kept at the level $N_o = N_{Ed}$ of the applied external action.

Certain approximations will be done, such as neglecting the reduction effect of the shear component V' on the resistance of the concrete part subject to axial force

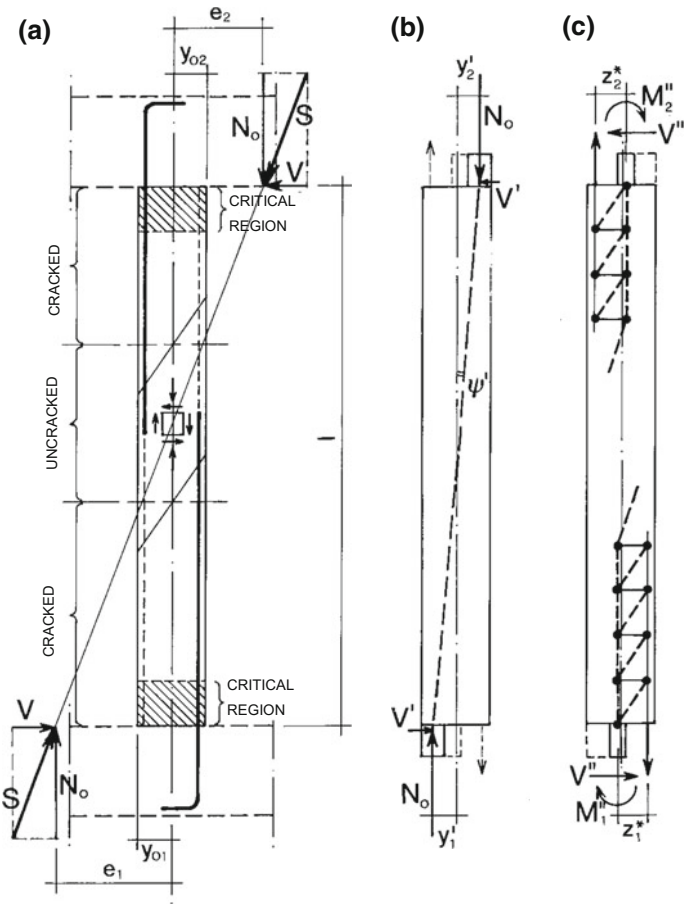


Fig. 6.27 Typical column (**a**) and its model with two mechanisms (**b**) + (**c**)

N_o, and neglecting at the same time the enhancing effect of the inclined trajectory of stresses in the compression chord of the truss on the resistance V''_{Rd} of its web members. Such chord has been drawn vertical in Fig. 6.25c, parallel to the tension chord constituted by the reinforcement.

Therefore, having defined the extent of the part in compression reserved to the force N_o (see Fig. 6.22):

$$x' = \frac{N_o - f_{yd}A'_s}{f_{cd}b}$$

based on what has already been mentioned at Sect. 6.2.2, the extreme position of the action itself is subsequently deduced with

$$M'_{\mathrm{Rd}} = f_{\mathrm{cd}} b x' (y_{\mathrm{c}} - \bar{x}/2) + f_{\mathrm{yd}} A'_{\mathrm{s}} y'_{\mathrm{s}}$$
$$y' = M'_{\mathrm{Rd}} / N_{\mathrm{o}}$$

Such eccentricities, calculated for the two end sections of the column, are indicated with y'_1 and y'_2 in Fig. 6.27. This contemplates that both sections be stressed to their resistance limit.

A transverse component corresponds to the direct transmission of the compression force, deviated between the two extreme sections

$$V'_{\mathrm{Rd}} = N_{\mathrm{o}} tg\, \psi' = N_{\mathrm{o}} \frac{y'_1 + y'_2}{1}$$

which gives a first contribution to shear resistance.

For very different levels of the bending actions in the two end sections, it is possible that one of them has not reached the resistance limit state. It is the case of columns fixed at the bottom end and pinned at the beams at the top. For these situations the eccentricity y'_2 of the load will correspond to the one of the bearing positions of the beams. If for example the supports of two contiguous and equal beams are located symmetrically with respect to the axis of the column, one will have $y'_2 = 0$ with

$$V'_{\mathrm{Rd}} = N_{\mathrm{o}} \frac{y'_1}{1}$$

Obviously, it is always possible to neglect (with $V'_{\mathrm{Rd}} = 0$) the resisting contribution due to the deviated transmission of the compression force and proportion the other resisting (truss) mechanism for the entire applied shear force. In any case, the resistance of such truss mechanism should be referred to the reduced effective depth of the section (see Fig. 6.22)

$$d^* = d - x'$$

With a compression chord whose depth is

$$\bar{x}^* = \frac{\sigma_{\mathrm{s}} A_{\mathrm{s}}}{f_{\mathrm{cd}} b}$$

the reduced section can rely on a lever arm

$$z^* \cong d^* - \bar{x}^*/2$$

of the internal couple (with $M''_{\mathrm{Rd}} = \sigma_s A_{\mathrm{s}} z^*$).

The shear resistance can eventually be evaluated with the criteria presented at Sect. 4.3.2 and therefore assuming the lesser

$$V''_{\mathrm{Rd}} = \min(V_{\mathrm{sd}}, V_{\mathrm{cd}})$$

between the tension-shear given by the stirrups

$$V_{\mathrm{sd}} = a_{\mathrm{w}} z^* f_{\mathrm{yd}} \lambda_{\mathrm{c}}$$

and the compression-shear given by the concrete of the web

$$V_{\mathrm{cd}} = z^* b f_{\mathrm{c2}} \lambda_{\mathrm{c}} / \left(1 + \lambda_{\mathrm{c}}^2\right)$$

with

$$\lambda_{\mathrm{I}} \leq \lambda_{\mathrm{c}} \leq \lambda_{\max}$$

The limits within which the inclination λ_{c} of the compressions in the web are to be assumed, with $\lambda_{\mathrm{c}}^2 = (1 - \omega_{\mathrm{w}})/\omega_{\mathrm{w}}$, are

$$\lambda_{\mathrm{I}} = \tau / \sigma_{\mathrm{I}}$$
$$\lambda_{\max} = \lambda_{\mathrm{I}} + \Delta\lambda \quad (\text{see } 4.3.2)$$

having set

$$\tau \cong \frac{V_{\mathrm{Ek}}}{0.7\,\mathrm{db}} \qquad \sigma = \frac{N_{\mathrm{Ek}}}{A_i}$$
$$\sigma_{\mathrm{I}} = \frac{1}{2}\left(-\sigma + \sqrt{\sigma^2 + 4\tau^2}\right)$$

For the critical sections of the column of Fig. 6.27a the following the verifications have to be fulfilled:

$$M_{\mathrm{Ed}} < M_{\mathrm{Rd}}(N_{\mathrm{o}}) = M'_{\mathrm{Rd}} + M''_{\mathrm{Rd}} \quad (\text{compression and bending})$$
$$V_{\mathrm{Ed}} < V_{\mathrm{Rd}}(N_{\mathrm{o}}) = V'_{\mathrm{Rd}} + V''_{\mathrm{Rd}} \quad (\text{shear})$$

It is to be noted that the interaction between the axial and shear components is included in the verification formula, with a greater limit inclination λ_{I} of the web members, and with a lower effective depth d^* of the resisting part of the section. For low compressions the first effect can predominate with an initial increase of the shear resistance. For progressively higher compressions the second effect predominates and leads to a significant reduction of the residual spare resources of shear resistance. Extreme situations with compression levels close to the pure axial resistance of the column are not compatible with the truss model described here. They fall under the following case of uncracked segments with small axial force eccentricity.

The interaction of the bending moment with the axial force has already been described at Sect. 6.2.2 (see for example the diagrams of Fig. 6.15). A note is to be

added about the interaction with shear that, in the cracked portions calculated with the truss model, is given by the rule of translation of moments already presented at Sect. 4.3. With stirrups orthogonal to the axis of the column, this rule leads to extending the reinforcement in tension, beyond the design section, for a length

$$a_1 = z^* \lambda_c / 2$$

Uncracked Segments

For situations such as the one of the column of Fig. 6.27a, the sections of the uncracked central part cannot be in states close to the ultimate axial resistance. A distribution of normal stresses σ much lower than the limit f_{cd} is to be expected, that can be calculated with the elastic formulas. The presence of a concurrent shear component adds the shear stress τ, that can also be calculated with the elastic formula.

A conservative criterion of the resistance verification for these situations is to limit the principal stresses acting at the centroidal axis of the column. The absolute value of such stresses is

$$\sigma_I = \frac{1}{2}\left(-\sigma + \sqrt{\sigma^2 + 4\tau^2}\right) \quad \text{(in tension)}$$
$$\sigma_{II} = \frac{1}{2}\left(+\sigma + \sqrt{\sigma^2 + 4\tau^2}\right) \quad \text{(in compression)}$$

and depend on the axial and shear force with

$$\sigma = \frac{N_o}{A_i} \qquad \tau = \frac{V_{Ed}}{b\bar{z}}$$

(with $\bar{z} = I_i/S_i' \cong 2h/3$). One therefore has the following verifications.

For low compressions ($\sigma_{II} \leq f_{c1}/3$), which do not affect the tensile strength of the material:

$$\sigma_I < f_{ctd}$$

For high compressions ($f_{cd}/3 < \sigma_{II} < f_{cd}$), which significantly reduce the tensile strength of the material:

$$\sigma_I < f_{ctd}\frac{3}{2}\left(1 - \frac{\sigma_{II}}{f_{cd}}\right)$$

In terms of forces in the section, these verifications become

$$V_{Ed} < V_{Rd}$$

with

$$V_{\mathrm{Rd}} = \bar{z} b \sqrt{\bar{\sigma}_{\mathrm{td}} (\bar{\sigma}_{\mathrm{td}} + \sigma)}$$

where it can be set approximately

$$\begin{aligned} \bar{\sigma}_{\mathrm{td}} &= f_{\mathrm{ctd}} && \text{for } \sigma \le f_{\mathrm{c1}}/3 \\ \bar{\sigma}_{\mathrm{td}} &= f_{\mathrm{ctd}} \frac{3}{2} \left(1 - \frac{\sigma}{f_{\mathrm{cd}}} \right) && \text{for } \sigma > f_{\mathrm{cd}}/3 \end{aligned}$$

It can be noted that the interaction formulas presented here remove any spare capacity of shear resistance when the normal stress approaches the compressive strength of the concrete. In any case the following verification is to be added

$$N_{\mathrm{Ed}} = N_{\mathrm{o}} < 0.8 f_{\mathrm{cd}} A_{\mathrm{c}} + f_{\mathrm{yd}} \left(A_{\mathrm{s}} + A'_{\mathrm{s}} \right)$$

which limits the value of the axial force component independently from the other flexural and shear components.

6.3.2 Moment-Curvature Diagrams

In the deformation calculations, including the ones necessary for the cracking verifications, the appropriate curves $M = M(\chi)$ are to be calculated. In the case of combined axial force and bending, the moment-curvature relationship is also affected by the axial force N on the section. One therefore has a surface

$$\Phi(M, \chi, N) = 0$$

of which, based on the requirements, a curve should be assumed that results from the intersection with a specific plane

$$aN + bM = c$$

In the case of uniaxial bending described at Sect. 3.3, the curves $M = M(\chi)$ represented the intersection with the plane $N = 0$. In that case, in addition to the numerical integration procedure of stresses, generally applicable with nonlinear constitutive σ–ε laws of materials and extended up to the failure limit of the sections, an analytical expression for the cracked behaviour in service could be formulated, based on the ratio $\psi = I'_i / I_i$ between moments of inertia of the cracked and uncracked section, and on the hyperbolic tension stiffening model (see Fig. 3.21).

For sections subject to combined axial force and bending, the type of interdependence between flexural and axial force is to be specified first, as already shown with reference to the load cases of Fig. 6.19.

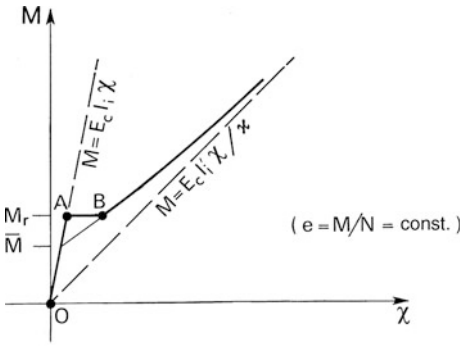


Fig. 6.28 Moment-curvature diagram for e = const

Constant Eccentricity

The first case of Fig. 6.19a refers to combined compression and bending with constant eccentricity ($M/N = e$ = cost.); for this type of interaction the section deforms in bending within the elastic range according to the two laws (see Fig. 6.28):

$$M = E_c I_i \chi$$
$$M' = E_c I_i' \chi$$

Indicating with $M = Ne$, the moment with respect to the centroidal axis of the homogenized uncracked section and with $M' = Ne'$ the moment with respect to the new centroidal axis of the cracked section (see Fig. 6.29). In Fig. 6.28 the ordinates refer to the fixed design axis, which coincides with the first centroidal axis; therefore in the second law the following substitution is to be done

$$M' = Ne' = Ne(e'/e) = M\kappa$$

where $\kappa = e'/e$ is the ratio between the eccentricities in the cracked and uncracked section. The second law therefore becomes

$$M = E_c I_i' \chi / \kappa$$

For the deformation analysis beyond the cracking limit, it is possible to link the two lines with the same hyperbolic tension stiffening model adopted for simple

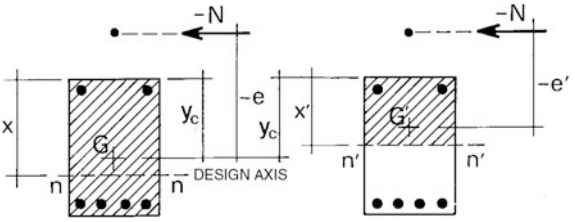


Fig. 6.29 Uncracked and cracked sections

bending at Sect. 3.3, with the same weighed average of the curvatures represented in Fig. 3.20. In the case under examination one therefore obtains:

$$\chi_{\mathrm{m}} = \eta \frac{M}{E_{\mathrm{c}} I_{\mathrm{i}}} + (1-\eta) \frac{M}{E_{\mathrm{c}} I'_{\mathrm{c}}} \kappa = \frac{M}{E_{\mathrm{c}}} \frac{\eta I'_{\mathrm{i}} + (1-\eta)\kappa I_i}{I_i I'_i}$$

which leads to expressing the average curvature with the pseudolinear formula

$$\chi_{\mathrm{m}} = \frac{M}{E_{\mathrm{c}} I_{\mathrm{m}}(\eta)}$$

where the equivalent moment of inertia of the section

$$I_{\mathrm{m}}(\eta) = \frac{I_{\mathrm{i}} I'_{\mathrm{i}}}{\eta I'_i + (1-\eta)\kappa I_i}$$

varies with the level of forces according to the function

$$\eta = 0.5 \beta_{\mathrm{o}} \beta_1 \beta_2 \left(\frac{M_{\mathrm{r}}}{M} \right)^2$$

where the coefficients β_{o}, β_1, β_2 are the same defined at Sect. 2.3.2.

The effect of the axial force is included in the coefficient κ, in addition to the different *diversion ratio* $\psi = I'_i/I_i$ between the two extreme lines that limit the model. For combined compression and bending, the effect consists of a higher stiffness of the cracked section with respect to the simple bending and a postponed drop of the tension stiffening.

A similar description can be proposed for combined tension and bending, for which in particular the moment of first cracking M_{r} is lower and the diversion ψ higher. Therefore, in this case the effect of the axial force is to reduce the stiffness of the section in the cracked state and anticipate the drop of the tension stiffening.

Constant Axial Force

The curves $M = M(\chi)$ drawn for $N = \bar{N} = \text{cost.}$ are the ones indicated in Fig. 6.30 with reference to the domain of combined compression and bending. In this case the eccentricity $e = M/\bar{N}$ increases with the moment M. The neutral axis of the resisting section in the cracked state consequently moves.

The deformation initially follows the line

$$M = E_{\mathrm{c}} I_{\mathrm{i}} \chi$$

of the uncracked section. The point D of Fig. 6.30 represents the decompression limit, beyond which the section, assumed in the phase II with $f_{\mathrm{ct}} = 0$, starts to crack progressively reducing its flexural stiffness. When the moment increases, the curve relative to the cracked section tends to the line:

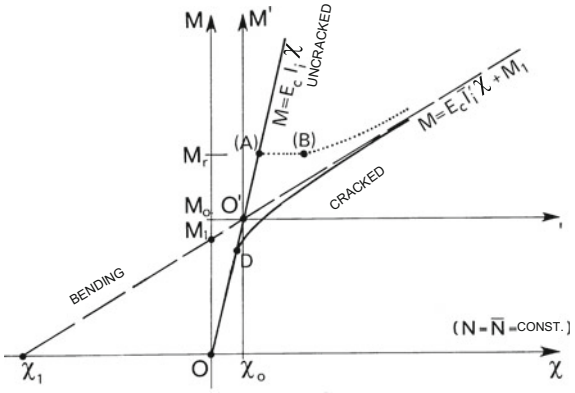


Fig. 6.30 Moment-curvature diagram for N = const

$$M = E_c \bar{I}_i' \chi + M_1$$

where I_i' refers to the resisting section of simple bending and

$$M_1 = \bar{N}(y_c - \bar{x}')$$

is the transport moment of the resultant on the new centroid G' (see Fig. 6.31).

For this type of behaviour, the correct linking of the two curves according to the hyperbolic model of tension stiffening is more problematic. In an approximated way, with significant errors in the portion with medium eccentricities, it is possible to assume the asymptotic line of the cracked section under simple bending, in place of the actual curve that starts from the point D, and refer the mentioned hyperbolic model to its intersection O' with the line of uncracked section.

Such model is indicated in Fig. 6.30 by the dashed line that starts from the point A corresponding to the moment of first cracking. The same formulas of the previous case can therefore be applied, where the variables are to be substituted with (see Fig. 6.30):

$$\chi = \chi' + \chi_o$$
$$M = M' + M_o$$

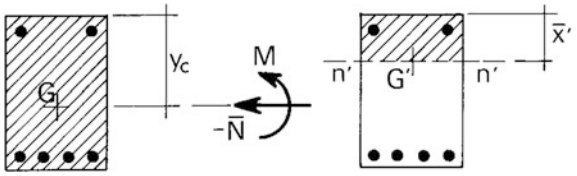


Fig. 6.31 Uncracked section and cracked section in simple bending

obtaining for the two lines of uncracked state and simple bending, respectively, the equations:

$$M' = E_c I_i \chi'$$
$$M' = E_c \bar{I}_i' \chi'$$

For what presented above, the coordinates of the new origin are

$$M_o = \frac{M_1}{1-\psi}$$
$$\chi_o = \frac{M_o}{EI_i} = \frac{M_1}{EI_i(1-\psi)}$$

with $\psi = \bar{I}_i'/I_i$.

The average curvature is obtained with the weighted mean:

$$\chi_m = \eta' \frac{M'}{E_c I_i} + (1-\eta') \frac{M'}{E_c \bar{I}_i'} + \chi_o =$$
$$= \frac{1}{E_c} \frac{M\left[\eta' \bar{I}_i' + (1-\eta') I_i\right] - M_1 I_i (1-\eta')}{I_i \bar{I}_i'}$$

which, setting

$$\mu = \frac{M}{M_1}$$

can be expressed in the pseudolinear form

$$\chi_m = \frac{M}{E_c I_m(\mu)}$$

with an equivalent moment of inertia of the section

$$I_m(\eta, \mu) = \frac{\mu I_i \bar{I}_i'}{\mu \eta' \bar{I}_i' + (\mu - 1)(1-\eta') I_i}$$

which varies with the level μ of the action with

$$\eta' = 0.5 \beta_o \beta_1 \beta_2 \left(\frac{M_r'}{M'}\right)^2 = 0.5 \beta_o \beta_1 \beta_2 \left(\frac{\mu_r (1-\psi) - 1}{\mu (1-\psi) - 1}\right)^2$$

The limit of first cracking

$$\mu_r = \frac{M_r}{M_1} = \frac{M'_r + M_o}{M_1}$$

is evaluated for the uncracked section under combined compression and bending with

$$M_r = \left(\beta f_{ct} - \frac{\bar{N}}{A_i}\right)\frac{I_i}{y'_c} \qquad (\beta = 1.3)$$

whereas the coefficients β_o, β_1, β_2 are again the ones already defined at Sect. 2.3.2.

A similar description can be proposed in the domain of combined tension and bending, where in particular the moment M_1 would be negative and the intersection

$$\chi_1 = -\frac{M_1}{E_c \bar{I}'_i}$$

(see Fig. 6.30) would be in the domain of positive curvatures.

The model presented here, as already mentioned, is not very accurate in the segment of medium eccentricities. The more significant influence of creep effects is to be added to the lower reliability of the analytical model. Under the axial force due to permanent loads, these effects induce eccentricities with respect to the initial centroid, eccentricities that are greater for a dissymmetric arrangement of the reinforcement in the concrete section. For these reasons, a correct evaluation of the curves would require the numerical procedure of integration applied according to the same criteria exposed at Sect. 3.3.2.

Typical Diagrams

Two sets of curves with $N = \bar{N}$ = cost. are shown in an adimensionalized form (with $\bar{\chi} = \chi h$) in Figs. 6.32 and 6.33, calculated numerically up to the failure limit of the section. The first set refers to the σ–ε laws for resistance, the second to the deformation σ–ε laws for deformation, both for the same rectangular section of Fig. 6.13 with $\omega_t = 0.4$. In particular it can be noted how the value of the axial compression force, other than the level of the ultimate moment, affects the ductility characteristics of the section. High values of the axial force ν make its behaviour more brittle, with early failures of the concrete in compression.

Given that, for the curves of Fig. 6.33, the characteristic values f_{ck} and f_{yk} of the strength have been used and that the parameters

$$\nu = \frac{N}{f_{cd} b h}$$

$$\mu = \frac{M}{f_{cd} b h^2}$$

have been adimensionalized again with the design resistance $f_{cd} = 0.85 f_{ck}/\gamma_C$ of concrete, the ultimate moments of these diagrams are higher than the ones reached by the previous diagrams of Fig. 6.32, which instead utilize the strengths reduced

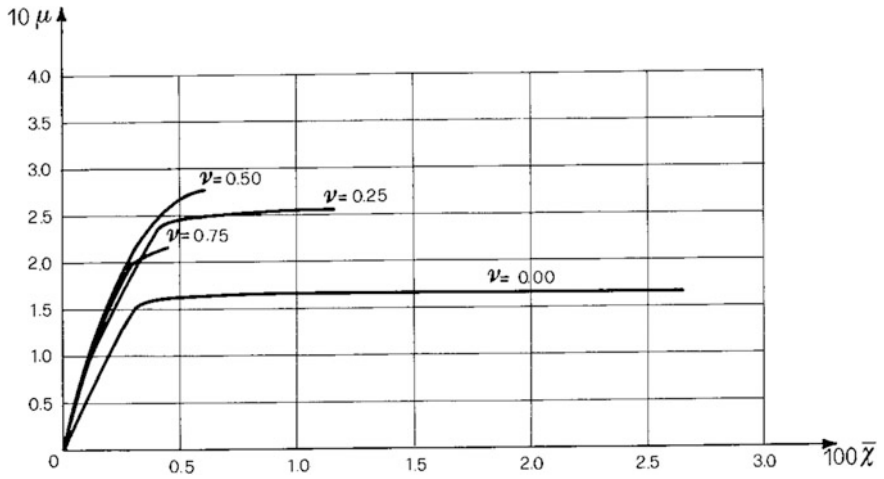


Fig. 6.32 Resistance moment-curvature curves

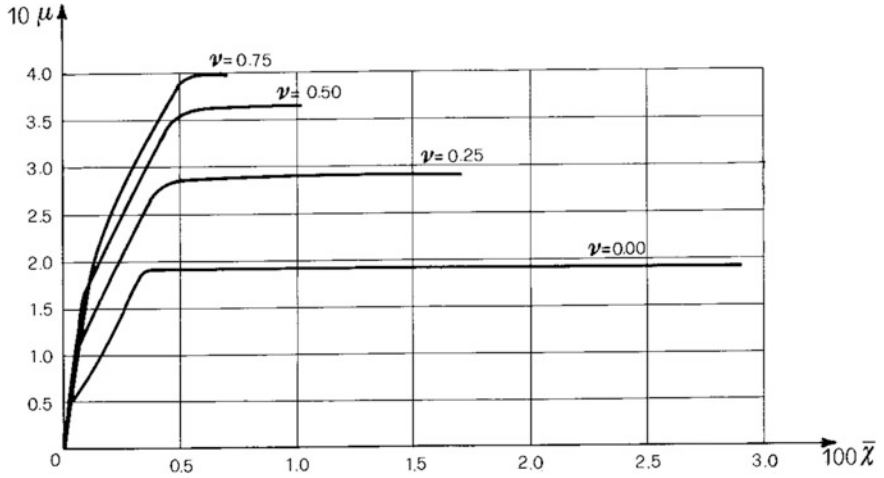


Fig. 6.33 Deformation moment-curvature curves

by the competent coefficients γ_M. The ductility parameters of the sections are also modified consequently to the different ratio between the resistance of concrete and steel ($\gamma_C/\gamma_S > 1$).

6.3.3 Nonlinear Analysis of Frames

The topic follows Sect. 5.3.2, where the nonlinear analysis of hyperstatic beams was presented. The extension of those algorithms to frames implies the addition of the effects of axial forces, which are of two types: *mechanical effects* consisting of the alteration of the moment-curvature diagrams of the sections, as shown in Sect. 6.3.2; *geometrical effects* consisting of the second order moments produced by the axial forces in the deformed configuration of the elements.

The evaluation of the second-order geometrical effects will be discussed in Sect. 7.2.3. For now it is taken for granted that the algorithm for the second-order analysis of single elements is available, in order to evaluate the rotations at the ends of each element subject to axial force and bending moments. If there were no slender elements in the frame, with high axial compressions, for the evaluation of the end rotations the first-order analysis according to the numerical procedure presented at Sect. 5.3.1 (see Fig. 5.34) could be carried, with the only change of the $M = M(\chi)$ diagrams due to the presence of the axial force.

Applicability Domain

Further to these premises, the applicability domain of a general algorithm for the nonlinear analysis of frames can be defined, foreseeing an automated calculation procedure prepared for its elaboration. A manual calculation is indeed not possible due to the amount of numerical operations.

Only plane frames are discussed, made of linear elements with straight axis; deep beams and therefore issues related to finite dimensions of joints and eccentricities of the connected members are excluded.

Based on the appropriate assignment of the topological, geometrical and mechanical data, which give the complete description of the structural model, the procedure will have to follow the mentioned analysis and give a response in terms of forces and displacements in all critical sections, under any given load condition.

No possibility of automatic design is foreseen, therefore the procedure can only refer to the final safety verification of the structural as defined at the end of prior design stages.

For the analysis of this type of frames, the ordinary displacement method is applied, which contemplates three equilibrium equations for each node: two translational equilibrium equations along the axes x, y and one rotational equilibrium equation about the axis z of the global system of orthogonal coordinates. The unknown are the corresponding geometrical parameters δ_x, δ_y, ϕ_z which define the displacement of a node in the plane.

As already mentioned at Sect. 5.3.2, the nonlinear analysis is carried with the iterative repetition of linear solutions of the frame appropriately directed. For these linear elastic solutions, certain simplifying assumptions are made:

- the members have constant cross section (e.g.: the entire geometrical section of the concrete only);

- only flexural actions are applied along the bars, so that the axial force is constant along each individual member;
- loads in any direction can be obviously concentrated on the nodes.

In the nonlinear evaluation of the flexural response of a member, only the deformations due to bending moment are taken into account; the deformations due to shear are neglected.

Both mechanical and geometrical effects of the axial force are taken into account: that is the influence on the moment-curvature relationship of the section and the second order contributions on the bending moment.

For the axial behaviour of members, the approximation of the simple elastic evaluation $N = EA\varepsilon$ through all subsequent steps of the nonlinear analysis is accepted.

For the flexural behaviour of beams, the appropriate numerical integration of the moment-curvature relation will be performed in order to calculate the exact values of the two end rotations, as described at Sects. 5.3.1 and 7.2.3.

The general scheme of the procedure is developed in three concatenated closed cycles:

- an *external cycle*, referred to the *structure*, for the iterative repetition of the solution of the equilibrium linear elastic system, progressively modified in its terms;
- an *intermediate cycle*, referred to the individual *element*, for the repetition by trial and error of its numerical analysis aimed at the correct nonlinear evaluation of the end moments corresponding to the given values of the end rotations;
- an *internal cycle*, referred to each individual *section*, with the numerical definition by points of the moment-curvature diagrams to be used for the analysis of the elements, repeated correcting of the value of the axial force based on the last elaborated solution.

The inner cycle of the numerical analysis of the section can be avoided if an appropriate analytical model for the moment-curvature law is assumed.

Numerical Solution of Nonlinear Systems

A brief presentation of the possible numerical methods to solve systems of nonlinear equations is necessary. In structural analysis a nonlinear problem can be set in the pseudolinear form

$$K(Y, Q)Y = \overline{F}(Y, Q)$$

This expression represents the system of equilibrium conditions typical of the displacement method, where K is the stiffness matrix, Y is the vector of unknown nodal displacements, $\overline{F}$ is the vector of known terms that contains the perfectly fixed end forces due to the loads.

For a nonlinear problem the coefficients K and the known terms $\bar{F}$ are not constant, but are function of the nodal displacement and the loads on the elements, as shown for the bidimensional case in Fig. 6.34b. If only forces concentrated at the nodes are present, the equilibrium system becomes

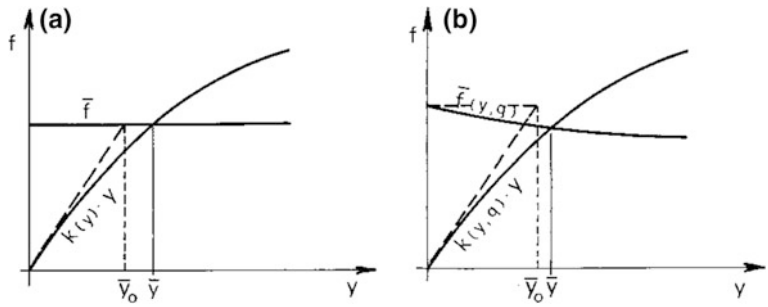


Fig. 6.34 Representation of nonlinear equilibrium equations

$$K(Y)Y = \overline{F}$$

and its bidimensional representation is modified to the one of Fig. 6.34a, where the right-side term referred to loads and becomes constant.

In Fig. 6.34, the intersection of the dashed lines gives the linear solution $\bar{y}_o$ calculated with the initial value k_o of the stiffness. The correct nonlinear solution $\bar{y}$ is shifted sideways under the intersection of the real response curve of the structure.

Let us consider for simplicity only the case of loads concentrated at the nodes. Figure 6.35a shows the left-side term

$$f(y) = k(y)y$$

which represents the structural response at the node as a function of its displacement y. For this curve the tangent at the point i is given by

$$f_i' = k_i + k_i' y_i$$

where k_i is the *variable stiffness* and k_i' is its first derivative (see Fig. 6.35b–c).

It is noted that the tangent to the response curve can be calculated only when the analytical expression of the stiffness $k(y)$ in terms of a continuous (derivable) function is known. It is not the case of reinforced concrete beams for which only a discretized numerical evaluation is possible.

The absence of the derivative makes inapplicable the *Step-by-Step Method* (by Euler–Cauchy) and also the *Tangent Method* (by Raphson–Newton) described respectively in Fig. 6.36a, b. In particular the step-by-step procedure, applied with the secant instead of the tangent, converges to a different curve than the assigned one, in each point of which the tangent is equal to the secant of the latter.

For the reinforced concrete beams instead the variable stiffness k_i can be calculated with the appropriate numerical elaborations based on the discretization in segments of the beam itself. This allows to define the line $k_i y$ secant in the point i of the response curve (see Fig. 6.35d).

For the solution of the nonlinear equilibrium system it is therefore possible to apply the *Secant Method* (see Fig. 6.37a). This consists of a repetition of linear

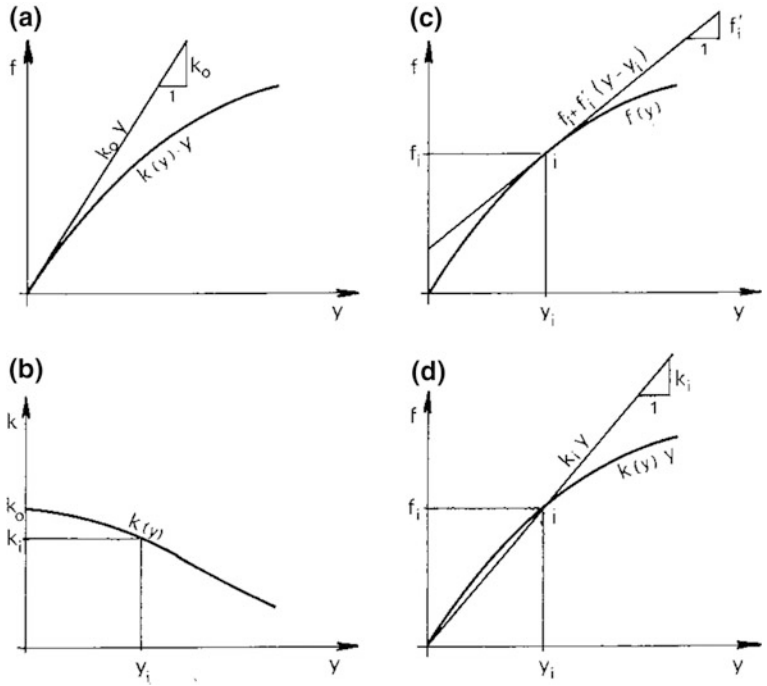


Fig. 6.35 Initial (**a**), variable (**b**), tangent (**c**) and secant (**d**) stiffness

solutions where the stiffness coefficients are replaced each time by new values that come from the previous solution. The process can be stopped when the residuals r_i, which represent the unbalanced part of the nodal force still present in the last calculated solution, become small enough.

However, for practical applications it is simpler to carry out the direct numerical calculation of the global response f_i, instead of the individual stiffness coefficients k_i of which it consists. This leads to the *Method of redistribution of residuals* (see Fig. 6.37b) and gives the most convenient way to elaborate the numerical solution of the nonlinear structural analysis.

This method consists of a repetition of linear incremental solutions, all done with the same stiffness coefficients, where the known terms of the equations are substituted each time with the residuals due to the quota of the nodal force not yet balanced, as results from the last value of the accumulated structural response. This procedure is also used, with only one repetition, to enhance the accuracy of the solution in a big linear system, where the residuals correspond to the numerical errors of the first calculated solution.

The use of constant coefficients reduces the calculations, given that the most onerous operation of inversion of the relative matrix can be done once and for all. On the other hand, the not adjusted orientation of the subsequent linear solutions leads to a greater number of iterations.

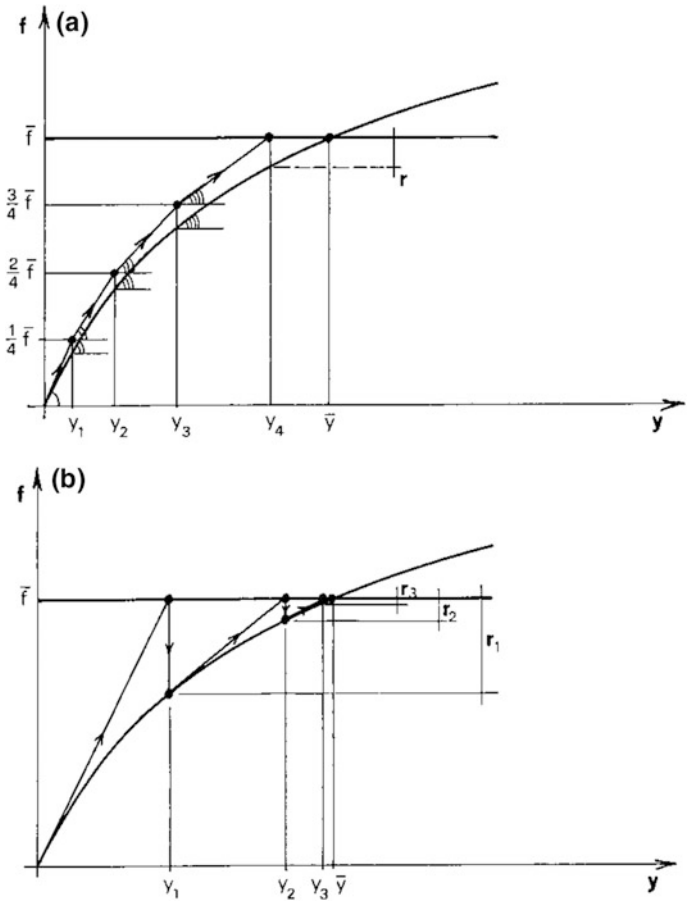


Fig. 6.36 Representations of step-by-step (**a**) and tangent (**b**) methods

Example

An application of nonlinear calculation is shown hereafter with reference to the portal frame described in Fig. 6.38. The numerical elaborations are referred to a concrete with strength R_{ck} = 35 N/mm^2 and a steel type FeB44 k (B450H). The assumed loads are described in Fig. 6.39a with the characteristic values:

$$\begin{aligned} g &= 33.0\,\text{kN/m} \quad \text{(permanent)} \\ q &= 15.0\,\text{kN/m} \quad \text{(variable)} \\ P &= 25.0\,\text{kN} \quad \text{(permanent)} \end{aligned}$$

We limit here to an analysis under the forces

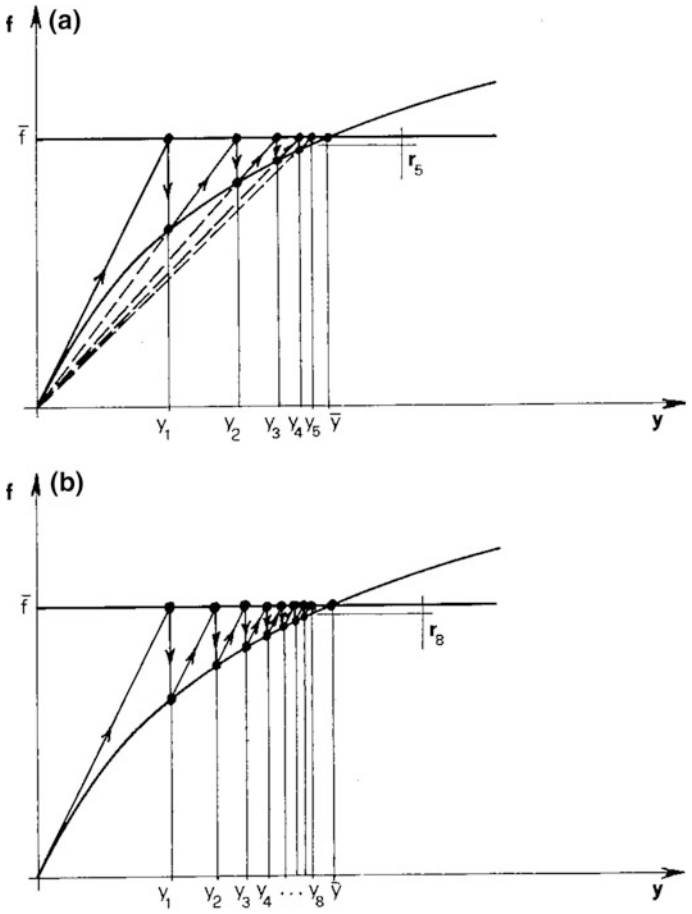


Fig. 6.37 Secant (**a**) and residual redistribution (**b**) methods

$$p = 33.0 + 15.0/3 = 38.0\,\text{kN/m}$$
$$P = 25.0\,\text{kN}$$

$$H = 0.07 \times (38.0 \times 4.0 + 25.0) \cong 12.4\,\text{kN}$$

In addition to the solution with all the loads amplified by $\gamma_F = \gamma'_F = 1.5$ aimed at the definition of the forces for a resistance verification of the sections according to the criteria of the semi-probabilistic method at the ultimate limit states, the analysis is repeated with the same vertical loads ($\gamma_F \equiv 1.5$) progressively increasing the

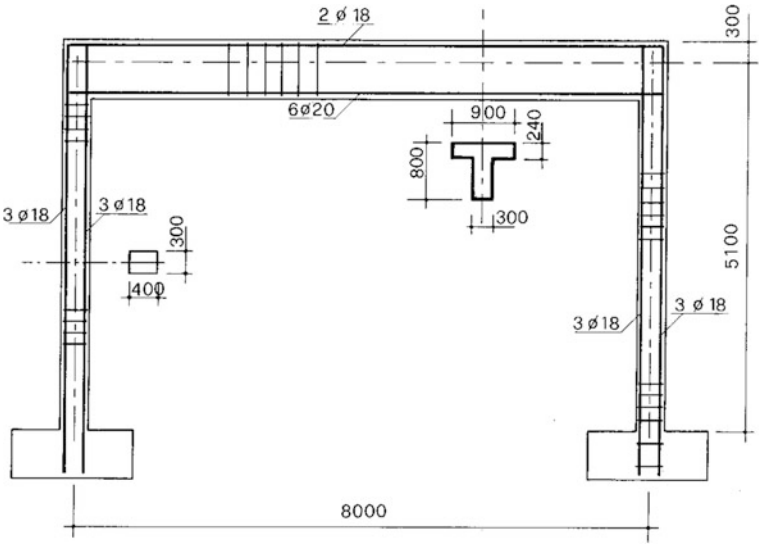


Fig. 6.38 Example of reinforced concrete frame

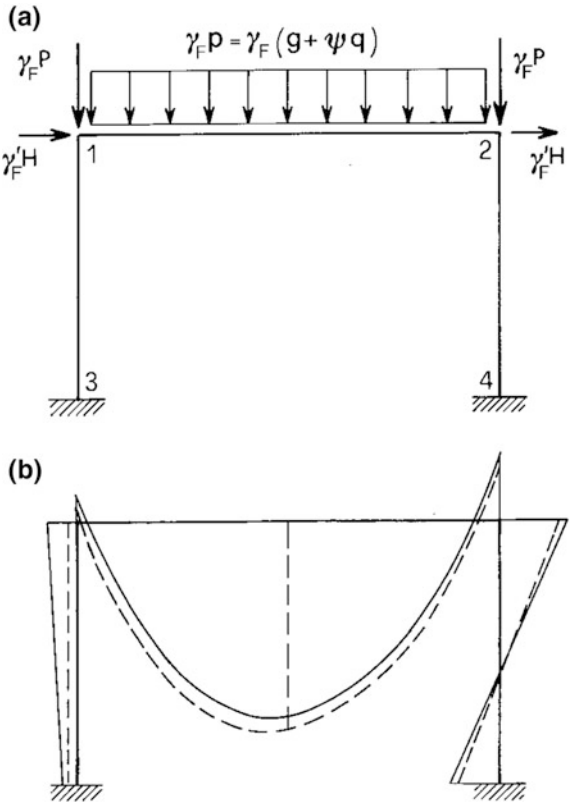


Fig. 6.39 Static scheme (**a**) and moment distribution (**b**)

horizontal load with $\gamma'_F = 0.00 \div 0.25 \div 0.50 \div \ldots$ up to the collapse of the structure. For these calculations the resistance constitutive laws of materials have been used.

The diagrams of the bending moment only for the solution with $\gamma_F = \gamma'_F = 1.5$ are shown in Fig. 6.39b, the one from the linear elastic analysis with the dashed line, the one from the nonlinear analysis with the continuous line. The significant redistribution of moments consequent to the higher cracking of the column with higher flexural actions can be noted.

An extract of the printout obtained from the execution of the automated calculation program is shown as follows, limited to the topological input data and to the results of the first and the last (15th) steps of the iterative process.

```
NODO          COORDINATE              VINCOLI

 N.           X          Y          TRAX TRAY ROTZ

  1           0.        5100.         0    0    0
  2        8000.        5100.         0    0    0
  3           0.           0.         1    1    1
  4        8000.           0.         1    1    1

ASTA INCIDENZE CORRELAZIONI

 N.    N1    N2     SEZ. MAT.

  1     1     2       1    1
  2     3     1       2    1
  3     4     2       2    1

CARATTERISTICHE

ASTA        A            J            E            L            C            S

  1 .3997E+06 .2346E+11 .2909E+05      5000.      1.0000      0.0000
  2 .1305E+06 .1869E+10 .2909E+05      5100.      0.0000      1.0000
  3 .1305E+06 .1869E+10 .2909E+05      5100.      0.0000      1.0000

                DESCRIZIONE CARICHI

CARICHI NODALI

NODO        PX           PY

  1      13600.      -37500.
  2      13600.      -37500.

CARICHI DISTRIBUITI SULLE ASTE

ASTA      CARICO

  1        -37.00
  2          0.00
  3          0.00
```

SOLUZIONE NON LINEARE - ITERAZIONE 1

ASTA	ROTAZIONI ASSEGNATE	ROTAZIONI CALCOLATE
1	0.1517E-02-0.1335E-02-0.2812E-01-0.1254E-02	
2	-0.7901E-03 0.7304E-03-0.7900E-03 0.7303E-03	
3	-0.7877E-03-0.2119E-02-0.7876E-03-0.2120E-02	

NODO	SPOST -X	SPOST -Y	ROTAZIONE
1	0.4029E+01	-.3411E+00	0.1520E-02
2	0.4017E+01	-.3722E+00	-.1331E-02

ASTA N.	N (N)	T1 (N)	T2 (N)	M1 (NAM)	MO (NAM)	M2 (NAM)
1	-17852.	216395.	-239606.	-14300.	395278.	-107144.
2	-253895.	748.	748.	-18116.	-16208.	-14300.
3	-277105.	36452.	36452.	-78761.	14191.	107144.

SFORZI EFFETTIVI NON LINEARI

ASTA N.	N (N)	T1 (N)	T2 (N)	M1 (NAM)	MO (NAM)	M2 (NAM)
1	-17852.	253610.	-203390.	-247840.	310598.	-42963.
2	-253895.	730.	780.	-18868.	-16880.	-14891.
3	-277105.	29535.	29535.	-66655.	8659.	83972.

SOLUZIONE NON LINEARE - ITERAZIONE 15

ASTA	ROTAZIONI ASSEGNATE	ROTAZIONI CALCOLATE
1	0.3729E-02-0.3423E-02	0.3725E-02-0.3423E-02
2	-0.1602E-02 0.2130E-02-0.1602E-02	0.2130E-02
3	-0.1599E-02-0.5019E-02-0.1597E-02-0.5025E-02	

NODO	SPOST -X	SPOST -Y	ROTAZIONE
1	0.8171E+01	-.3450E+00	0.3732E-02
2	0.8154E+01	-.3683E+00	-.3420E-02

ASTA N.	N (N)	T1 (N)	T2 (N)	M1 (NAM)	MO (NAM)	M2 (NAM)
1	-24269.	219304.	-236696.	-53382.	367833.	-122951.
2	-256804.	-5668.	-5668.	-24474.	-38928.	-53382.
3	-274196.	42869.	42869.	-95679.	13636.	122951.

SFORZI EFFETTIVI NON LINEARI

ASTA N.	N (N)	T1 (N)	T2 (N)	M1 (NAM)	MO (NAM)	M2 (NAM)
1	-24269.	219262.	-236738.	-54454.	366592.	-124362.
2	-256804.	-5663.	-5663.	-24462.	-38903.	-53345.
3	-274196.	42677.	42677.	-95259.	13566.	122392.

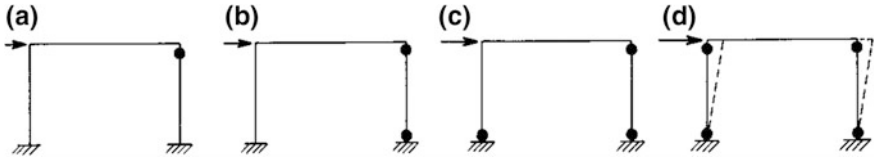


Fig. 6.40 Progressive formation of plastic hinges

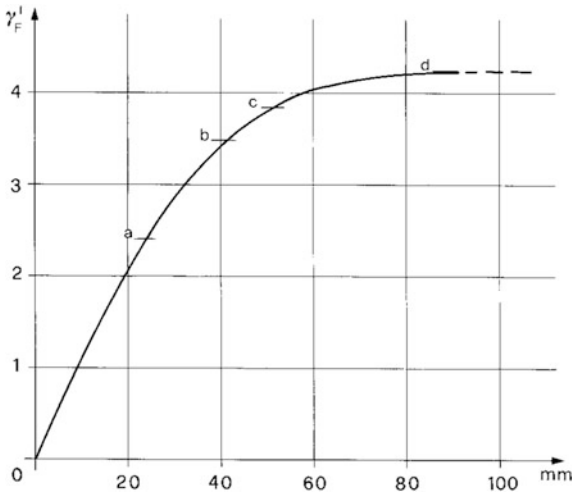


Fig. 6.41 Nonlinear growth of top displacement

This solution gives the values of internal forces for the resistance verifications of sections, but it does not give any information on the reserve of the structure with respect to the ultimate capacity to collapse. Figure 6.40 shows how the three degrees of hyperstaticity can progressively utilize their resources during the progressive plastic failure of the most stressed sections. If we limit the calculation only to the verification under the design values of the loads (with $\gamma_F = \gamma'_F = 1.5$) we stop at the first step of the formation of the collapse mechanism, that is the situation of Fig. 6.40a.

Repeated therefore for progressively increasing values of the horizontal force (for the same vertical loads), the analysis gives the solutions that have been summarized in the two following figures. The trend of the horizontal displacement of the beam when the force $\gamma'_F H$ increases is shown in Fig. 6.41. The progressive loss of stiffness of the frame follows the subsequent yielding of the critical sections reached at the points *a*, *b*, *c*, *d* indicated in the figure. The last one corresponds to the collapse limit of the mechanism of Fig. 6.40d.

The diagrams of growth of the bending moment in the four critical sections (at the top and bottom of the two columns) when the horizontal force increases are

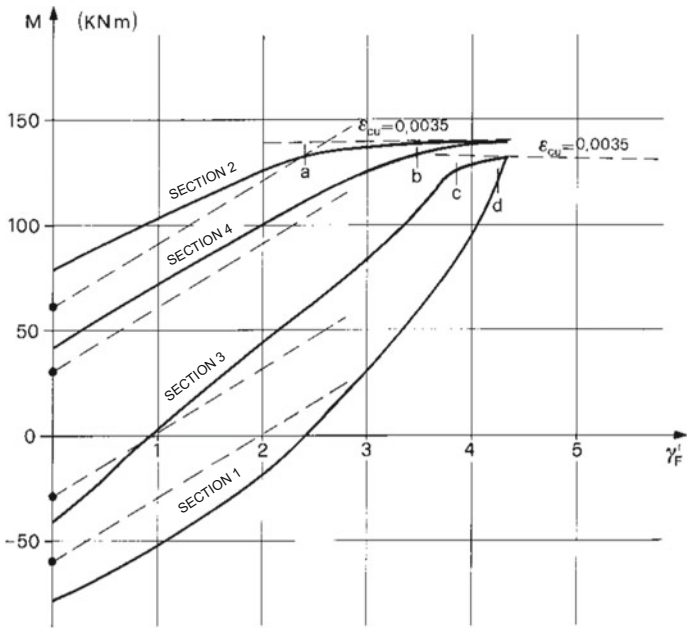


Fig. 6.42 Growth of bending moments up to collapse

eventually shown in Fig. 6.42. The linear elastic behaviour is indicated by the dashed lines. It can be noted that basically the collapse mechanism (situation *d*) is reached for $\gamma'_F = 4.25$, without an early localized brittle failure. The good capability of plastic redistribution of moments shown by the analysis is a consequence of the limited mechanical reinforcement ratio of the sections and the limited value of the relative axial force in the columns ($\nu \cong 0.15$).

6.4 Case A: Design of Columns

We refer to the column P15 of the multi-storey building in reinforced concrete described in Figs. 2.19 and 2.20. In Fig. 2.23 the relative tributary area is defined with an associated weight 1,0 for the effects of hyperstatic moments.

For the analysis of loads the data elaborated at Sect. 2.4.1 are recalled:

Permanent loads deck	=7.00 kN/m^2
Variable loads roof	=1.20 kN/m^2
Variable loads type floor	=2.00 kN/m^2
Current weight of cladding wall	=11.30 kN/m

Column P15
(tributary area 1.0 × 2.30 × 5.60 ≅ 12.9 mq)

Deck	12.9 × 7.00	= 90.3 kN
Beam	0.9 × 0.40 × 0.30 × 2.30 × 25	= 6.2 kN
Column	0.40 × 0.30 × 2.52 × 25	= 7.6 kN
Total permanent loads of roof		= 104.1 kN
Cladding wall	1.2 × 11.30 × 5.20	= 70.5 kN
Total permanent loads of type floor		= 174.6 kN

Roof

Permanent loads		=104.1 kN
Variable loads	12.9 × 1.20	=15.5 kN
Total loads of roof		=119.6 kN

Fourth floor

Permanent loads		=174,6 kN
Variable loads	12.9 × 1.40	=18.1 kN
Total loads of fourth floor		=192.7 kN

Lower floors

Permanent loads		=174.6 kN
Variable loads	12.9 × 1.40	=18.1 kN
Total loads third floor		=192.7 kN

Ground floor

Permanent loads		=174.6 kN
Variable loads	12.9 × 1.40	=18.1 kN
Wall	0.30 × 3.22 × 5.20 × 25	=125.6 kN
Total loads of ground floor		=318.3 kN

The following table reproduces the calculation of the axial forces at the bottom of the different portions of the column under analysis and the relative minimum proportioning, which will then have to be verified with the addition of the bending moment.

In this table, the first column contains the vertical loads of the decks; the second shows the progressive sum for the evaluation of the characteristic axial forces; the third one gives the design values with the amplification by $\gamma_F = 1.43$; the forth column shows the minimum concrete section $A_{co} = N_{Ed}/f'_{cd}$ based on the only axial

force (with f'_{cd} = 11.3 N/mm^2). The subsequent columns show the data of geometrical design of the columns.

Column P 15—Design of Sections

	F_k	N_k	N_{Ed}	A_{co}	$a \times b$	A_c	A_{so}	$n\phi$	A_s
	(kN)	(kN)	(kN)	(cm^2)	(cm)	(cm^2)	(cm^2)	(mm)	(cm^2)
4°	119.6	119.6	171	151	30 × 40	1200	3.60	4ϕ12	4.52
3°	192.7	312.3	447	396	30 × 40	1200	3.60	4ϕ12	4.52
2°	192.7	505.0	722	639	30 × 40	1200	3.60	4ϕ12	4.52
1°	192.7	697.7	998	883	30 × 40	1200	3.60	4ϕ12	4.52
PR	192.7	890.4	1273	1127	30 × 40	1200	3.60	4ϕ12	4.52
SI	318.3	1208.7	1728		(wall)				

In the next section, the bending moments are evaluated based on a partial static scheme only for the load configuration assumed previously. The analysis will be repeated for the two solutions of dropped and flat floor beam. The different stiffness ratios between beams and columns will lead to very different values of the moments in the two cases. It is to be noted how, concerning the bending moments in the beams, the two limit schemes assumed in Sect. 4.4.1 (see Figs. 4.41 and 4.42) will cover the differences of the diagrams obtained here at the various floors (see Fig. 6.43).

6.4.1 *Flexural Actions in Columns*

For the calculation of the bending moment on the various portions of the column P15 we refer to the partial static scheme of Fig. 6.43a. Such scheme includes the column from the foundation to the roof, connected at the various floors with the adjacent beam span. Given the balanced configuration of the beam on its intermediate support (P14), a fixed-end constraint has been set on this support. It is reminded that the building is stabilized laterally by the staircase corewall that, with its high stiffness, prevents any significant horizontal displacements of the floors.

The data of the fixed nodes frame of Fig. 6.43a are the following:

$$l = 4.30\,\text{m}$$
$$h = 3.06\,\text{m}$$
$$h_o = 3.46\,\text{m}$$
$$I_p = 40 \times 30^3/12 = 90{,}000\,\text{cm}^4$$
$$I_o = 0.5 \times 560 \times 30^3/12 = 630{,}000\,\text{cm}^4 \quad (0.5\,\text{for partial diffusion})$$
$$I_t = 845{,}750\,\text{cm}^4\,(\text{dropped beam---see Sect. 4.4.1})$$
$$I_t = 138{,}240\,\text{cm}^4\,(\text{flat beam---see Sect. 5.4})$$

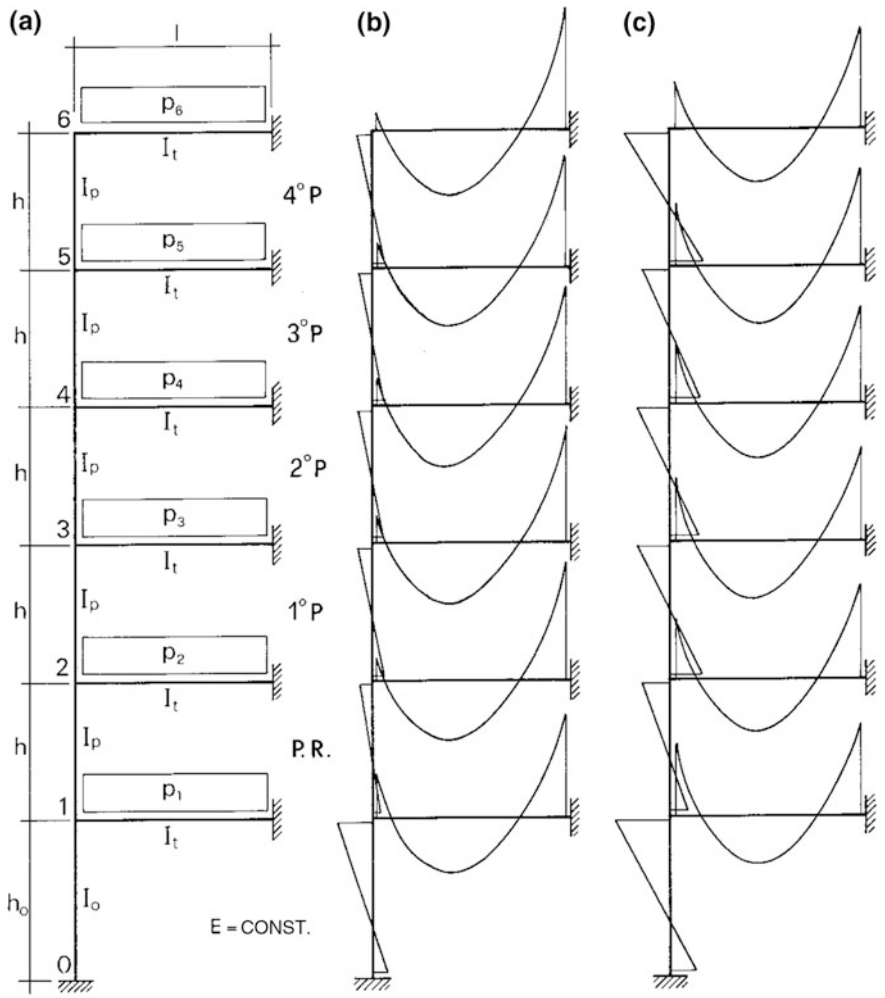


Fig. 6.43 Static scheme (**a**) and moment distribution (**b**) and (**c**)

- Permanent loads

$$\begin{aligned} 1.2 \times 7.00 \times \quad 5.60 &= 47.04 \\ 0.40 \times 0.30 \times \quad 25 &= \underline{3.00} \\ p_o &= 50.04 \quad \text{kN/m} \end{aligned}$$

- Total loads at floor levels

$$\begin{aligned} 1.2 \times 1.20 \times \quad 5.60 &= \quad 8.06 \\ &\underline{\quad\quad 50.04} \\ p_6 &= 58.10 \quad \text{kN/m} \end{aligned}$$

$$\begin{aligned} 1.2 \times 1.40 \times \quad 5.60 &= \quad 9.41 \\ &\underline{\quad\quad 50.04} \\ p_5 &= 59.45 \quad \text{kN/m} \end{aligned}$$

$$\begin{aligned} 1.2 \times 1.40 \times \quad 5.60 &= \quad 9.41 \\ &\underline{\quad\quad 50.04} \\ p_4 = p_3 = p_2 = p_1 &= 59.45 \quad \text{kN/m} \end{aligned}$$

In view of a solution with the displacement method, the perfectly fixed-end moments are equal to:

$$\begin{aligned} 4.30^2/12 &= 1.54 \\ m_{60} &= -1.54 \times 58.10 = -89.47\,\text{kNm} \\ m_{50} &= -1.54 \times 59.45 = -91.55\,\text{kNm} \\ m_{40} &= -1.54 \times 59.45 = -91.55\,\text{kNm} \quad = m_{30} = m_{20} = m_{10} \end{aligned}$$

The stiffnesses of the beam are calculated on the basis of the following ratios:

$$\begin{aligned} k_\text{p} &= 90{,}000/306 \cong 294\,\text{cm}^3 \\ k_\text{o} &= 630{,}000/346 \cong 1820\,\text{cm}^3 \\ k_\text{t} &= 846{,}000/430 \cong 1967\,\text{cm}^3 \qquad \text{(dropped beam)} \\ k_\text{t} &= 138{,}000/430 \cong 321\,\text{cm}^3 \qquad \text{(flat beam)} \end{aligned}$$

The rotational equilibrium conditions of the nodes lead to the following equations:

$$\begin{cases} 4(k_\text{t}+k_\text{p})\phi_6 + 2k_\text{p}\phi_5 = -m_{60}/E \\ 2k_\text{p}\phi_6 + 4(k_\text{t}+2k_\text{p})\phi_5 + 2k_\text{p}\phi_4 = -m_{50}/E \\ 2k_\text{p}\phi_5 + 4(k_\text{t}+2k_\text{p})\phi_4 + 2k_\text{p}\phi_3 = -m_{40}/E \\ 2k_\text{p}\phi_4 + 4(k_\text{t}+2k_\text{p})\phi_3 + 2k_\text{p}\phi_2 = -m_{30}/E \\ 2k_\text{p}\phi_3 + 4(k_\text{t}+2k_\text{p})\phi_2 + 2k_\text{p}\phi_1 = -m_{20}/E \\ 2k_\text{p}\phi_2 + 4(k_\text{t}+k_\text{p}+k_\text{o})\phi_1 = -m_{10}/E \end{cases}$$

In the two cases under analysis of dropped and flat beam, dividing all terms of the equations by 2, one has the following coefficient matrices:

$$\begin{vmatrix} 4522. & 294. & 0. & 0. & 0. & 0, \\ 294. & 5110. & 294. & 0. & 0. & 0. \\ 0. & 294. & 5110. & 294. & 0. & 0. \\ 0. & 0. & 294. & 5110. & 294. & 0. \\ 0. & 0. & 0. & 294. & 5110. & 294. \\ 0. & 0. & 0. & 0. & 294. & 8162. \end{vmatrix}$$

$$\begin{vmatrix} 1230. & 294. & 0. & 0. & 0. & 0. \\ 294. & 1818. & 294. & 0. & 0. & 0. \\ 0. & 294. & 1818. & 294. & 0. & 0. \\ 0. & 0. & 294. & 1818. & 294. & 0. \\ 0. & 0. & 0. & 294. & 1818. & 294. \\ 0. & 0. & 0. & 0. & 294. & 4870. \end{vmatrix}$$

which, with the same known terms b_i, lead to the solutions

$$\begin{array}{lll} b_6 = 4474/\mathrm{E} & \phi_6 = 0.9377/\mathrm{E} & \phi_6 = 3.2357/\mathrm{E} \\ b_5 = 4578/\mathrm{E} & \phi_5 = 0.7957/E & \phi_5 = 1.6804/\mathrm{E} \\ b_4 = 4578/\mathrm{E} & \phi_4 = 0.8039/\mathrm{E} & \phi_4 = 2.9445/\mathrm{E} \\ b_3 = 4578/\mathrm{E} & \phi_3 = 0.8025/\mathrm{E} & \phi_3 = 1.8666/\mathrm{E} \\ b_2 = 4578/\mathrm{E} & \phi_2 = 0.8191/\mathrm{E} & \phi_2 = 2.0846/\mathrm{E} \\ b_1 = 4578/\mathrm{E} & \phi_1 = 0.5314/\mathrm{E} & \phi_1 = 0.8142/\mathrm{E} \end{array}$$

The bending moments at the bottom and at the top of each portion of column are eventually evaluated with:

$$M_{ij} = Ek_{\mathrm{p}}\left(4\phi_i + 2\phi_j\right)$$

and the ones in the end section of the beam are evaluated with

$$M_i = Ek_{\mathrm{t}} \cdot 4\phi_i + m_{\mathrm{io}}$$

obtaining, in the two cases under examination of dropped and flat beam, the values of the following table.

The diagrams shown in Fig. 6.43b–c correspond respectively to the two solutions.

Column P15—Bending Moments in kNm

Node	Columns	Beam	Columns	Beam
6	+15.7	−15.7	+47.9	−47.9
5	+14.9 +14.1	−29.0	+38.8 +31.2	−70.0
4	+14.1 +14.2	−28.3	+32.7 +33.8	−66.5
3	+14.2 +14.3	−28.5	+33.4 +34.2	−67.6
2	+14.4 +12.8	−27.2	+35.5 +29.3	−64.8
1	+11.1 +38.7	−49.8	+21.8 +59.3	−81.1
0	+19.3	(found)	+29.6	(found)

6.4.2 *Serviceability Verifications*

The serviceability verifications of few sections of the column under analysis are developed as follows. The cross section of the column is shown in Fig. 6.44, which is assumed constant for all the storeys of the building above ground.

Solution with Dropped Beam

The maximum bending moment occurs at the top section of the column at the last floor, together with the lowest axial force. The geometrical characteristics of this section, assumed as uncracked, are obtained homogenizing with $\alpha_e = 15$ the area of the reinforcement ($2 + 2\phi 12$).

- *Column at 4th Floor—Top section*

$$A_i = 30 \times 40 + 15 \times 4.52 = 1200 + 67.8 \cong 1268\,\text{cm}^2$$
$$I_i = 1200 \times 30^2/12 + 67.8 \times 11^2 = 90{,}000 + 8204 = 98{,}204\,\text{cm}^4$$
$$i^2 = 98{,}204/1268 = 77.45\,\text{cm}^2$$
$$u = 77.45/15.0 = 5.2\,\text{cm}$$

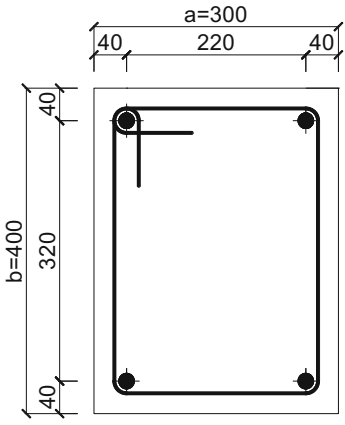


Fig. 6.44 Cross section of the column

For the case under analysis with dropped beam one has

$$\begin{aligned} N &= 119.6 - 7.6 = 112.0\,\text{kN} \\ M &= 15.7\,\text{kNm} \\ e &= 1570/112.0 = 14.0\,\text{cm} \quad (> u) \end{aligned}$$

The section therefore cracks. As indicated in Sect. 6.1.2, for an elastic behaviour of materials, the position of the neutral axis is given by the equation:

$$x^3 + 3d_o x^2 + \frac{6\alpha_e}{b}\left(A_s d_s + A'_s d'_s\right)x - \frac{6\alpha_e}{b}\left(A_s d_s d + A'_s d'_s d'\right) = 0$$

In the case under analysis, with $A_s = A'_s = 2.26\ \text{cm}^2$, one has the following coefficients:

$$\begin{aligned} d_o &= e - a/2 = 14.0 - 15.0 = -1.0\,\text{cm} \\ d_s &= d_o + d = -1.0 + 26.0 = 25.0\,\text{cm} \\ d'_s &= d_o + d' = -1.0 + 4.0 = 3.0\,\text{cm} \\ 6\alpha_e/b &= 6 \times 15/40 = 2.25\,\text{cm}^{-1} \end{aligned}$$

which lead to

$$x^3 - 3.0x^2 + 142.4x - 3366 = 0$$

with the solution

$$x = 12.7\,\text{cm}$$

Setting

$$\begin{aligned} S_i &= \frac{bx^2}{2} + \alpha_e A'_s(x - d') - \alpha_e A_s(d - x) = 3125 + 288 - 458 = \\ &= 3070\,\text{cm}^3 \end{aligned}$$

the stresses are eventually evaluated:

$$\begin{aligned} \sigma_c &= \frac{N}{S_i}x = \frac{1120}{3070}12.7 = 4.6\,\text{N/mm}^2 \\ \sigma_s &= \alpha_e \frac{d - x}{x}\sigma_c = 15\frac{13.3}{12.7}4.6 = 72\,\text{N/mm}^2 \end{aligned}$$

The verifications of the maximum stresses in the materials are satisfied, having (see Sect. 2.4.1):

$$\sigma_c < \bar{\sigma}_c = 11.2\,\mathrm{N/mm^2}$$
$$\sigma_s < \bar{\sigma}_s = 360\,\mathrm{N/mm^2}$$

- *Column at Ground Floor*

On the column portion at the ground floor, the axial force predominates. On the top and bottom sections, the forces are:

$$N = 890.4 - 7.6 = 882.2\,\mathrm{kN} \quad M = 12.8\,\mathrm{kNm}$$
$$N = 890.4\,\mathrm{kN} \quad M = 11.1\,\mathrm{kNm}$$

with eccentricity respectively equal to

$$\mathrm{e} = 1280/882.2 = 1.5\,\mathrm{cm}$$
$$\mathrm{e} = 1110/890.4 = 1.4\,\mathrm{cm}$$

which leave the sections uncracked. With 2 + 2ϕ20 as longitudinal reinforcement, one has:

$$A_i = 30 \times 40 + 15 \times 4.52 = 1200 + 68 = 1268\,\mathrm{cm^2}$$
$$I_i = 1200 \times 30^2/12 + 68 \times 11^2 = 98{,}228\,\mathrm{cm^4}$$

At the most highly stressed concrete edge, in the two sections respectively, one has:

$$\sigma_c = \frac{8822}{1268} + \frac{12{,}800}{98{,}228}15.0 = 6.96 + 1.95 = 8.9\,\mathrm{N/mm^2}$$
$$\sigma_c = \frac{8904}{1268} + \frac{11{,}100}{98{,}228}15.0 = 7.02 + 1.70 = 8.7\,\mathrm{N/mm^2}$$

remaining within the limit $\bar{\sigma}_c$ = 11.2 N/mm^2. For the uniform compression in the most highly stressed section (see Sect. 2.4.1) one has:

$$\sigma_{co} = 7.02 < \bar{\sigma}'_c = 7.8\,\mathrm{N/mm^2}$$

Solution with Flat Beam

The solution with flat beam, as deduced at the previous Sect. 6.4.1, leads to higher bending moments in the columns, so that an increase in the reinforcement is required at the top floor.

- *Column at 4th floor—Top section*

$$N = 112.0\,\text{kN}$$
$$M = 47.9\,\text{kNm}$$
$$e = 4790/112.0 = 42.8\,\text{cm}$$

with $2\phi 20 + 2\phi 12$ in tension and $2\phi 12$ in compression (see Table 8) one has:

$$A_s = 8.54\,\text{cm}^2$$
$$A'_s = 2.26\,\text{cm}^2$$
$$d_o = 42.8 - 15.0 = 27.8\,\text{cm}$$
$$d_s = 27.8 + 26.0 = 53.8\,\text{cm}$$
$$d'_s = 27.8 + 4.0 = 31.8\,\text{cm}$$

and the equation becomes

$$x^3 + 83.4x^2 + 1195x - 27{,}529 = 0$$

from which the neutral axis results:

$$x = 11.8\,\text{cm}$$

After calculating the static moment

$$S_i = 11.8^2 \times 40/2 + 15 \times 7.8 \times 2.26 - 15 \times 14.2 \times 8.54 =$$
$$= 2785 + 264 - 1819 = 1230\,\text{cm}^3$$

one obtains the stresses

$$\sigma_c = \frac{1120}{1230} 11.8 = 10.7\,\text{N/mm}^2 \quad \left(< \bar{\sigma}_c = 11.2\,\text{N/mm}^2\right)$$
$$\sigma_s = 15 \frac{14.2}{11.8} 10.7 = 193\,\text{N/mm}^2 \quad \left(< \bar{\sigma}'_{s3} = 240\,\text{N/mm}^2 \text{per } \phi 20\right)$$

(see Table 2.16)

- *Column at 4th Floor—Bottom section*

$$N = 119.6\,\text{kN}$$
$$M = 38.8\,\text{kNm}$$
$$e = 3880/119.6 = 32.4\,\text{cm}$$

With $2\phi14 + 2\phi12$ in tension and $2\phi12$ in compression one has

$$\begin{aligned} A_s &= 5.34\,\text{cm}^2 \\ A'_s &= 2.26\,\text{cm}^2 \\ d_o &= 32.4 - 15.0 = 17.4\,\text{cm} \\ d_s &= 17.4 + 26.0 = 43.4\,\text{cm} \\ d'_s &= 17.4 + 4.0 = 21.4\,\text{cm} \end{aligned}$$

and the equation becomes:

$$x^3 + 52.2x^2 + 630.3x - 13{,}993 = 0$$

with the solution

$$x = 10.7\,\text{cm}$$

One therefore obtains:

$$\begin{aligned} S_i &= 10.7^2 \times 40/2 + 15 \times 6.7 \times 2.26 - 15 \times 15.3 \times 5.34 = \\ &= 2290 + 227 - 1226 = 1291\,\text{cm}^3 \end{aligned}$$

and the stresses eventually become

$$\sigma_c = \frac{1196}{1291}10.7 = 9.9\,\text{N/mm}^2 \quad \left(< \bar{\sigma}_c = 11.2\,\text{N/mm}^2\right)$$

$$\sigma_s = 15\frac{15.3}{10.7}9.9 = 213\,\text{N/mm}^2 \quad \left(< \bar{\sigma}'_{s3} = 300\,\text{N/mm}^2 \text{per } \phi14\right)$$

(see Table 2.16).

The verifications at the lower floors are here omitted, which are within the allowable limits without modifications to the reinforcement.

6.4.3 Resistance Calculations

The characteristics of materials that concern the resistance verifications of the critical sections of columns subject to combined compression and bending are first recalled (see Sect. 2.4.1):

$$\begin{aligned} f_{cd} &= 14.2\,\text{N/mm}^2 \quad \text{combined compression and bending} \\ f'_{cd} &= 11.3\,\text{N/mm}^2 \quad \text{centered compression} \\ f_{yd} &= 391\,\text{N/mm}^2 \\ \varepsilon_{yd} &= 0.0019 \end{aligned}$$

In the calculations, the applied forces evaluated under the global serviceability combination quantified at Sect. 6.4.1 will be amplified by $\gamma_F = 1.43$. Given that bending moments and axial forces are substantially proportional, for the flexural verifications of the sections the maximum values of both forces will be assumed.

Other parameters related to the σ–ε material models are:

$$\begin{aligned}\beta_o &= C/f_{cd}bx = 0.8\\ \alpha_o &= \varepsilon_{cu}/\varepsilon_{yd} = 0.35/0.19 = 1.84\\ r &= f_{yd}/f_{cd} = 27.5\\ r' &= f_{yd}/f'_{cd} = 34.6\end{aligned}$$

In the case under analysis, the same concrete section (30 cm × 40 cm) is on all portions of the column, with:

$$\begin{aligned}N_{co} &= f_{cd}ab = 14.2 \times 120 = 1704\,\text{N}\\ M_{co} &= f_{cd}a^2b = 1704 \times 0.30 = 511.2\,\text{kNm}\\ \delta &= 26/30 = 0.8667 \quad \text{position reinforcement in tension}\\ \delta' &= 4/30 = 0.1333 \quad \text{position reinforcement in compression}\\ \eta_c &= 15/30 = 0.5000 \quad \text{position design axis}\\ \eta_s &= \delta - \eta_c = 0.3667 \quad \text{lever arm of } \omega_s\\ \eta'_s &= \eta_c - \delta' = 0.3667 \quad \text{lever arm of } \omega'_s\end{aligned}$$

The yield limits

$$\begin{aligned}\varepsilon_s &= \varepsilon_{yd} \quad \text{in tension}\\ \varepsilon'_s &= \varepsilon_{yd} \quad \text{in compression}\end{aligned}$$

of the reinforcement correspond respectively to

$$\begin{aligned}\bar{\xi} &= \beta_o\xi \le \beta_o\delta\alpha_o/(\alpha_o + 1) = 0.4494 = \bar{\xi}_{sup}\\ \bar{\xi} &= \beta_o\xi \le \beta_o\delta'\alpha_o/(\alpha_o - 1) = 0.2336 = \bar{\xi}_{inf}\end{aligned}$$

where $\bar{\xi}$ is the extent of the constant diagram of compressions $\sigma_c = f_{cd}$ in concrete.

The calculations of the resisting moment

$$M_{Rd} = M_{Rd}(N_{Ed})$$

for all critical sections are grouped in the following tables where:

- Two rows are associated to each storey, one for the top section, one for the bottom section.

- The axial forces $N_{Ed} = \gamma_F N_{Ek}$ are shown in the first column, expressed in kN, different between top and bottom based on the self-weight of the column.
- The adimensionalized axial force $v_o = N_{Ed}/N_{co}$ is shown in the second column.
- The mechanical reinforcement $\omega_s = f_{sd}A_s/N_{co}$ and $\omega'_s = f_{sd}\,A'_s/N_{co}$. are shown in the two following columns.
- The compression zone in the concrete is shown in the fifth column, calculated with

$$\bar{\xi} = v_o + \omega_s - \omega'_s \quad \text{for } \bar{\xi}_{inf} \le \bar{\xi} \le \bar{\xi}_{sup}$$

- For $\bar{\xi} \le \bar{\xi}_{inf}$ the reinforcement in compression in neglected setting

$$\bar{\xi} = v_o + \omega_s$$

- For $\bar{\xi} > \bar{\xi}_{sup}$ the compression zone is calculated with

$$\bar{\xi} = \left\{ \left(v_o - \alpha_o\omega_s - \omega'_s\right) + \sqrt{\left(v_o - \alpha_o\omega_s - \omega'_s\right)^2 + 4\beta_o\alpha_o\omega_s\delta} \right\}/2$$

- The lever arm of the resultant of compressions $\eta_o = \eta_c - \xi/2$ is shown in the sixth column
- The following ratios are shown in the next two rows

$$\begin{aligned}
&\alpha_s = \sigma_s/f_{yd} = \left(\beta_o\delta - \bar{\xi}\right)\alpha_o/\bar{\xi} && \text{for } \bar{\xi} > \bar{\xi}_{sup}\\
&\alpha_s = \sigma_s/f_{yd} = 1 && \text{for } \bar{\xi} \le \bar{\xi}_{sup}\\
&\alpha'_s = \sigma'_s/f_{yd} = 1 && \text{for } \bar{\xi} \ge \bar{\xi}_{inf}\\
&\alpha'_s = \sigma'_s/f_{yd} = 0 && \text{for } \bar{\xi} < \bar{\xi}_{inf}
\end{aligned}$$

- The last row contains the resisting moments of the sections expressed in kNm and calculated with

$$M_{Rd} = \left(\bar{\xi}\eta_o + \alpha_s\omega_s\eta_s + \alpha'_s\omega'_s\eta'_s\right)M_{co}$$

The first table refers to the solution with a dropped beam. Of the second table, relative to the solution with a flat beam, only the first two rows are different, corresponding to the 4th floor, where the reinforcement has been increased. The reinforcement at different storeys is the one defined previously.

Based on the calculated resisting moments, the verifications are eventually carried as summarized in the two following tables. The superabundant flexural resistance can be noted, due to the modest magnitude of the applied moments with respect to the sections, which are proportioned following technological requirements and minimum dimensions prescribed for columns in compression. Resistance values are closer to the flexural applied action only for the last storey of the solution with flat beam, for which the reinforcement had to be increased.

Concerning the resisting axial force, we limit to evaluate it in the most stressed section at the base of the ground floor:

$$N_{\mathrm{Rd}} = f'_{\mathrm{cd}} A_{\mathrm{c}} + f_{\mathrm{yd}} A_{\mathrm{t}} = 11.3 \times 120 + 391 \times 0.452 =$$
$$= 1356 + 177 = 1533\,\mathrm{kN}$$
$$\gamma_{\mathrm{r}} = N_{\mathrm{Rd}} / N_{\mathrm{Ed}} = 1533/1273 = 1.20 \quad (> 1.00)$$

Column P15—Calculation of Resisting Moments (Dropped Beam) (Fig. 6.45)

	N_{Ed}	ν_{o}	ω_{s}	ω'_{s}	$\bar{\xi}$	η_{o}	α_{s}	α'_{s}	M_{Rd}
4th	160	0.0939	0.0516	0.0516	0.1455	0.4272	1.0000	0.0000	41.4
	171	0.1004	0.0516	0.0516	0.1520	0.4240	1.0000	0.0000	42.6
3rd	436	0.2559	0.0516	0.0516	0.2559	0.3720	1.0000	1.0000	68.0
	447	0.2623	0.0516	0.0516	0.2623	0.3688	1.0000	1.0000	68.8
2nd	711	0.4173	0.0516	0.0516	0.4173	0.2913	1.0000	1.0000	81.5
	722	0.4237	0.0516	0.0516	0.4237	0.2881	1.0000	1.0000	83.7
1st	987	0.5792	0.0516	0.0516	0.5520	0.2240	0.4712	1.0000	82.0
	998	0.5857	0.0516	0.0516	0.5006	0.2197	0.4365	1.0000	76.9
GF	1262	0.7406	0.0516	0.0516	0.6896	0.1552	0.0100	1.0000	72.3
	1273	0.7471	0.0516	0.0516	0.6953	0.1523	−0.0051	1.0000	63.8

Column P15—Calculation of Resisting Moments (Flat Beam)

	N_{Ed}	ν_{o}	ω_{s}	ω'_{s}	$\bar{\xi}$	η_{o}	α_{s}	α'_{s}	M_{Rd}
4th	160	0.0939	0.1960	0.0516	0.2383	0.3808	1.0000	1.0000	94.0
	171	0.1004	0.1225	0.0516	0.1713	0.4143	1.0000	0.0000	59.2
3rd	436	0.2559	0.0516	0.0516	0.2559	0.3720	1.0000	1.0000	68.0
	447	0.2623	0.0516	0.0516	0.2629	0.3688	1.0000	1.0000	68.8
2nd	711	0.4173	0.0516	0.0516	0.4173	0.2913	1.0000	1.0000	81.5
	722	0.4237	0.0516	0.0516	0.4237	0.2881	1.0000	1.0000	83.7
1st	987	0.5792	0.0516	0.0516	0.5520	0.2240	0.4712	1.0000	82.0
	998	0.5857	0.0516	0.0516	0.5686	0.2197	0.4305	1.0000	79.9
GF	1262	0.7406	0.0516	0.0516	0.6896	0.1552	0.0100	1.0000	72.3
	1273	0.7471	0.0516	0.0516	0.6953	0.1523	−0.0051	1.0000	63.8

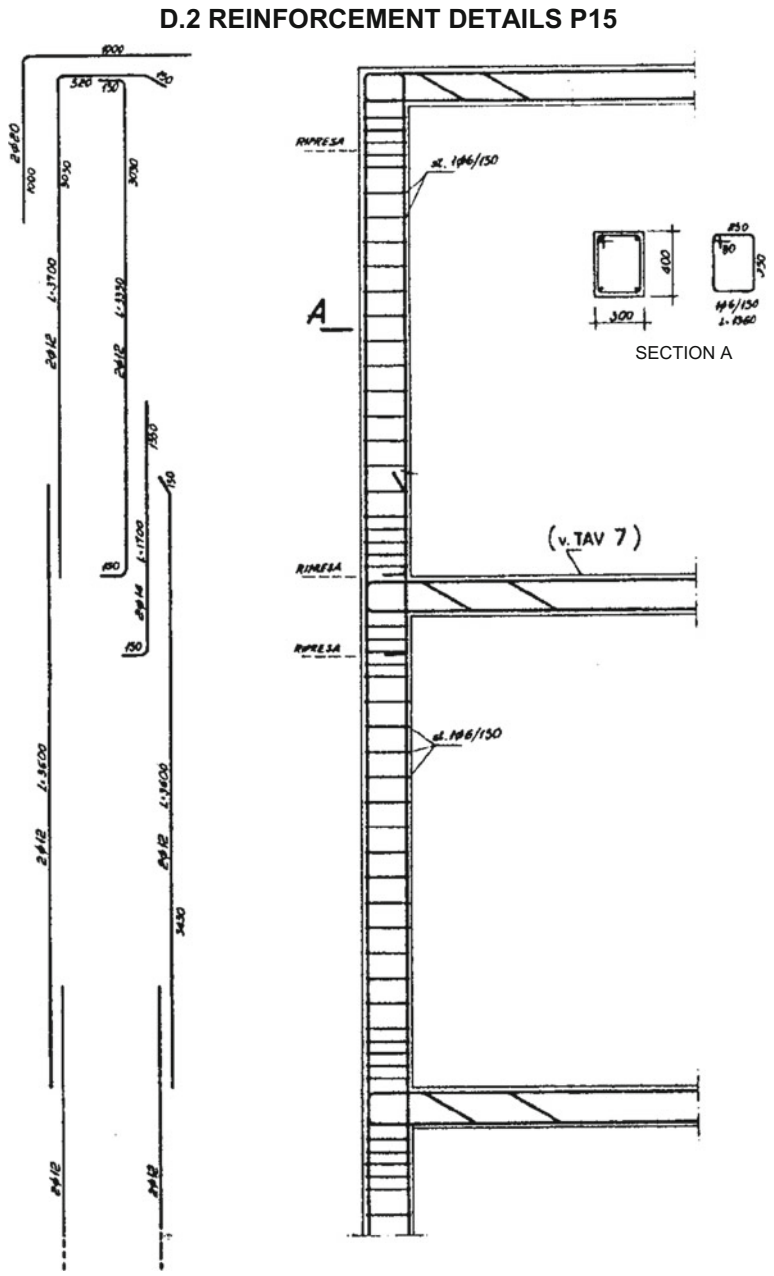


Fig. 6.45 Reinforcement details of edge column

Column P15—Resistance Verifications

Dropped beam				Flat beam			
	M_{Rd} (kNm)	M_{Ed} (kNm)	γ_r		M_{Rd} (kNm)	M_{Ed} (kNm)	γ_r
4th	41.4 42.6	22.5 20.9	1.84 2.04	4°	94.0 59.2	68.5 55.5	1.37 1.07
3rd	68.0 68.8	20.2 20.2	3.37 3.41	3°	68.0 68.8	44.6 46.8	1.52 1.47
2nd	81.5 83.7	20.3 20.3	4.01 4.12	2°	81.5 83.7	48.3 46.8	1.69 1.79
1st	82.0 79.9	20.4 20.6	4.02 3.88	1°	82.0 76.9	48.9 50.8	1.68 1.51
GF	72.3 63.8	18.3 15.9	3.95 4.01	GF	72.3 63.8	41.9 31.2	1.73 2.04
			(≥ 1.00)				(≥ 1.00)

Appendix: Eccentric Axial Force

Chart 6.1: Eccentric Axial Force: Elastic Design—Formulas

RC Sections subject to combined tension/compression and uniaxial bending.

Symbols

N_{Ek}	characteristic value of the applied axial force (positive in compression)
M_{Ek}	characteristic value of applied bending moment
A_s	area of the reinforcement in tension
A'_s	area of the reinforcement in compression
$A_t = A_s + A'_s$	total reinforcement area
y_o	position of the design axis
b	width of the edge in compression
h	total depth of the section (see figures)
d	effective depth
d'	concrete cover of the reinforcement in compression
$\rho_s = A_s/(bh)$	geometric reinforcement ratio in tension
$\rho'_s = A'_s/bd$	geometric reinforcement ratio in compression
$\alpha_e = E_s/E_c$	ratio of elastic moduli (see Chart 2.3)
$\psi_s = \alpha_e \rho_s$	elastic reinforcement ratio in tension
$\psi'_s = \alpha_e \rho'_s$	elastic reinforcement ratio in compression
$\psi_t = \psi_s + \psi'_s$	total elastic reinforcement ratio

σ_c maximum compressive stress in concrete
σ'_c maximum tensile stress in concrete
σ_s stress in the reinforcement in tension

see also Charts 2.2 and 2.3.

Serviceability Verifications in Phase I
(uncracked section—see figure)

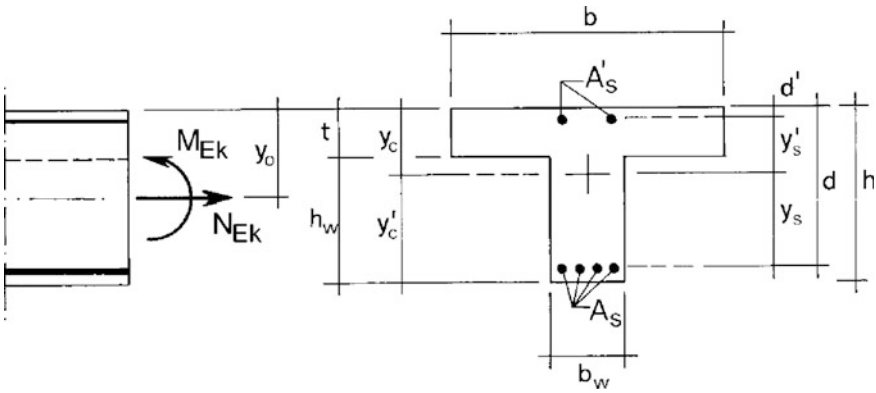
Compression with small eccentricity

$$\sigma_c = \frac{N_{Ek}}{A_i} + \frac{M'_{Ek}}{I_i} y_c \le \bar{\sigma}_c$$
$$\sigma_G = \frac{N_{Ek}}{A_i} \le 0.7\bar{\sigma}_c$$

with

$$A_b = bt \qquad A_w = b_w h_w \qquad h_w = h - t$$

$$A_i = A_b + A_w + \alpha_e A_s + \alpha_e A'_s$$
$$S_i = A_b t/2 + A_w(t + h_w/2) + \alpha_e A_s d + \alpha_e A'_s d'$$
$$y_c = S_i/A_i \qquad y'_c = h - y_c$$
$$y_s = d - y_c \qquad y'_s = y_c - d'$$
$$y_b = y_c - t/2 \qquad y_w = t + h_w/2 - y_c$$
$$I_i = A_b(t^2/12 + y_b^2) + A_w(h_w^2/12 + y_w^2) + \alpha_e A_s y_s^2 + \alpha_e A'_s y'^2_s$$
$$M'_{Ek} = M_{Ek} - N_{Ek}(y_o - y_c)$$



(for the rectangular section, set $t = h$)

Generic combined axial force and bending

$$\sigma'_c = \frac{N_{Ek}}{A_i} + \frac{M'_{Ek}}{I_i} y'_c \quad \text{(positive in tension)}$$

$$\left(\sigma_s = -\alpha_e \frac{N_{Ek}}{A_i} + \alpha_e \frac{M_{Ek}}{I_i} y_s\right)$$

for the verification at the cracking limit:

$$\sigma'_c \le 1.3 f_{ctk} \quad \left(= \bar{\sigma}'_{ct} \text{ with } \beta = 1.3\text{---see Chart 2.2}\right)$$

Serviceability Verifications in Phase II
(cracked section under combined compression and bending)

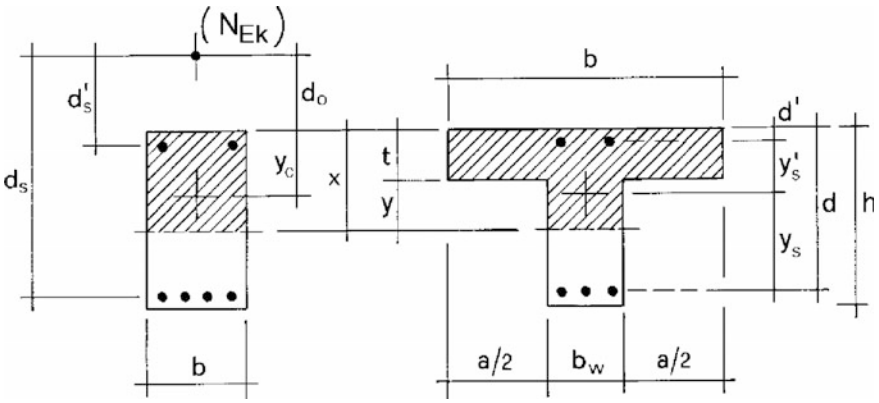
Rectangular unreinforced section

$$e = M_{Ek}/N_{Ek} \quad (h/6 \le e < h/2)$$

$$\sigma_c = \frac{2N_{Ek}}{bx} \le \bar{\sigma}_c$$

with

$$x = 3(y_o - e)$$



Rectangular section—double reinforcement
(see figure)

$$\sigma_c = \frac{N_{Ek}}{A_i} + \frac{M'_{Ek}}{I_i} y_c \le \bar{\sigma}_c \quad \text{(compression)}$$

$$\sigma_s = -\alpha_e \frac{N_{Ek}}{A_i} + \alpha_e \frac{M'_{Ek}}{I_i} y_s \le \bar{\sigma}_s \quad \text{(tension see also Table 2.16)}$$

with

$$\begin{aligned} A_i &= bx + \alpha_e A_s + \alpha_e A'_s \\ S_i &= bx^2/2 + \alpha_e A_s d + \alpha_e A'_s d' \\ y_c &= S_i/A_i \\ y_s &= d - y_c \quad y'_s = y_c - d' \\ I_i &= bx\left[\frac{x^2}{12} + \left(y_c - \frac{x}{2}\right)^2\right] + \alpha_e A_s y_s^2 + \alpha_e A'_s y_s'^2 \\ M'_{Ek} &= M_{Ek} - N_{Ek}(y_o - y_c) \end{aligned}$$

whereas the neutral axis can be deduced from the equation

$$\xi^3 + 3\delta_o\xi^2 + 6\left(\psi_s\delta_s + \psi'_s\delta'_s\right)\xi - 6\left(\psi_s\delta_s\delta + \psi'_s\delta'_s\delta'\right) = 0$$

where it has been set:

$$\begin{array}{ll} x = \xi h & (<h) \\ d_o = e - y_o & e = M_{Ek}/N_{Ek} \\ \delta_o = d_o/h & \delta' = d'/h \\ \delta_s = \delta + \delta_o & \delta'_s = \delta' + \delta_o \end{array}$$

T-Section—double reinforcement
(see figure)

$$\sigma_c = \frac{N_{Ek}}{A_i} + \frac{M'_{Ek}}{I_i} y_c \le \bar{\sigma}_c \quad \text{compression}$$

$$\sigma_s = \alpha_e \frac{N_{Ek}}{A_i} + \alpha_e \frac{M'_{Ek}}{I_i} y_s \le \bar{\sigma}_s \quad \text{(tension see also Table 2.16)}$$

with (a = b − b_w, y = x − t):

$$\begin{aligned} A_i &= b_w x + at + \alpha_e A_s + \alpha_e A'_s \\ S_i &= b_w x^2/2 + at^2/2 + \alpha_e A_s d - \alpha_e A'_s d' \\ y_c &= S_i/A_i \\ y_x &= y_c - x/2 \quad y_t = y_c - t/2 \\ y_s &= d - y_c \quad y'_s = y_c - d' \\ I_i &= bx\left(x^2/12 + y_x^2\right) + at\left(t^2/12 + y_t^2\right) + \alpha_e A_s y_s^2 + \alpha_e A'_s y_s'^2 \\ M'_{Ek} &= M_{Ek} - N_{Ek}(y_o - y_c) = N_{Ek}(d_o + y_c) \end{aligned}$$

whereas the neutral axis can be deduced from the equation

$$\xi^3 - 3\delta_o\xi^2 + \frac{3}{\beta}\left[\alpha\tau(2\delta_o + \tau) + 2\left(\psi_s\delta_s + \psi'_s\delta'_s\right)\right]\xi + \\ - \frac{1}{\beta}\left[\alpha\tau^2(3\delta_o + 2\tau) + 6\left(\psi_s\delta_s\delta + \psi'_s\delta'_s\delta'\right)\right] = 0$$

where it has been set ($t < x < h$):

$$\begin{array}{ll} x = \xi h & \tau = t/d \\ \beta = b_w/b & \alpha = 1 - \beta \\ d_o = e - y_o & e = M_{Ek}/N_{Ek} \\ \delta_o = d_o/h & \delta' = d'/h \quad \delta = d/h \\ \delta_s = \delta + \delta_o & \delta'_s = \delta' + \delta_o \end{array}$$

Combined Tension and Bending in Phase II

(cracked section—N_{Ek} positive in tension)

Entirely cracked section

$$\sigma_s = \frac{1}{y_t A_s}\left[N_{Ek}d'_s + M_{Ek}\right] \le \bar{\sigma}_s \quad \text{(tension see also Table 2.16)}$$

$$\left(\sigma'_s = \frac{1}{y_t A'_s}\left[N_{Ek}d_s - M_{Ek}\right]\right)$$

with

$$y_s = \frac{A'_s}{A_s + A'_s}y_t \quad y'_s = \frac{A_s}{A_s + A'_s}y_t$$
$$y_t = d - d'$$
$$d_s = d - y_o \quad d'_s = y_o - d'$$

Rectangular cracked section

(see figure)

$$\sigma_c = \frac{N_{Ek}}{A_i} + \frac{M'_{Ek}}{I_i}y_c \le \bar{\sigma}_c \quad \text{compression}$$

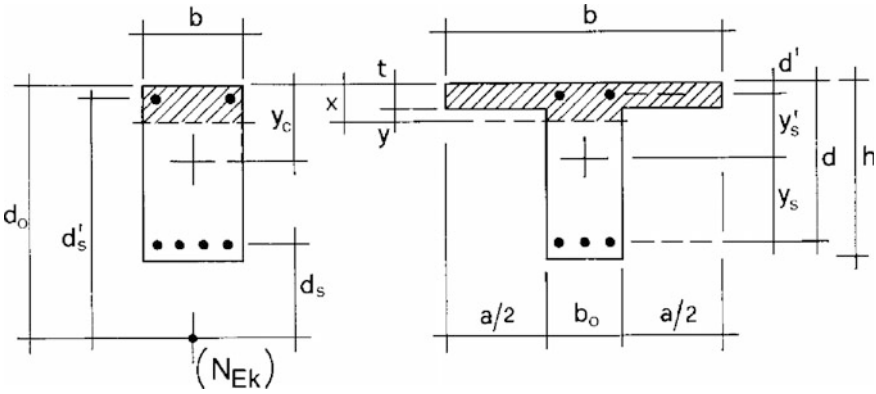
$$\sigma_s = -\alpha_e\frac{N_{ak}}{A_i} + \alpha_e\frac{M'_{ak}}{I_i}y_s \le \bar{\sigma}_s \quad \text{(tension see also Table 2.16)}$$

with A_i, I_i, y_c, y_s, M'_{Ek} calculated similarly to the corresponding section under combined compression and bending, whereas the neutral axis is deduced from the equation

$$\xi^3 - 3\delta_o\xi^2 - 6\left(\psi_s\delta_s + \psi'_s\delta'_s\right)\xi + 6\left(\psi_s\delta_s\delta + \psi'_s\delta'_s\delta'\right) = 0$$

where it has been set:

$$\begin{array}{ll} x = \xi h & (>0) \\ d_o = e + y_o & e = M_{Ek}/N_{Ek} \\ \delta_o = d_o/h & \delta' = d'/h \quad \delta = d/h \\ \delta_s = \delta_o - \delta & \delta'_s = \delta_o - \delta' \end{array}$$



T-shaped cracked section
(see figure)

$$\sigma_c = \frac{N_{Ek}}{A_i} + \frac{M'_{Ek}}{I_i} y_c \le \bar{\sigma}_c \quad \text{(compression)}$$

$$\sigma_s = -\alpha_e \frac{N_{Ek}}{A_i} + \alpha_e \frac{M'_{Ek}}{I_i} y_s \le \bar{\sigma}_s \quad \text{(tension see also Table 2.16)}$$

with A_i, I_i, y_c, y_s, M'_{Ek} calculated similarly to the corresponding section under combined compression and bending, whereas the neutral axis is deduced from the equation

$$\xi^3 - 3\delta_o \xi^2 - \frac{3}{\beta}\left[\alpha\tau(2\delta_o - \tau) + 2\left(\psi_s \delta_s + \psi'_s \delta'_s\right)\right]\xi + \\ + \frac{1}{\beta}\left[\alpha\tau^2(3\delta_o - 2\tau) + 6\left(\psi_s \delta_s \delta + \psi'_s \delta'_s \delta\right)\right] = 0$$

where it has been set ($t < x < h$):

$$\begin{array}{ll} x = \xi h & \tau = t/h \\ \alpha = a/b & \beta = b_w/b \\ d_o = e + y_o & e = M_{Ek}/N_{Ek} \\ \delta_o = d_o/h & \delta' = d'/h \quad \delta = d/h \\ \delta_s = \delta_o - \delta & \delta'_s = \delta_o - \delta' \end{array}$$

Chart 6.2: Combined Axial Force and Uniaxial Bending: Resistance Design—Formulas

RC sections subject to combined compression/tension and uniaxial bending. Unless stated otherwise, the indefinite elastic-perfectly plastic σ–ε model has been assumed (model of Fig. 1.30a) for the reinforcement steel.

Symbols

N_{Ed}	design value of the applied axial force
M_{Ed}	design value of the applied bending moment
M_{Rd}	design value of the resisting bending moment
$r = f_{yd}/f_{cd}$	strength ratio
$\omega_s = r\rho_s$	mechanical reinforcement ratio in tension
$\omega'_s = r\rho'_s$	mechanical reinforcement ratio in compression
$\varepsilon_{yd} = f_{yd}/E_s$	steel yield strain

see also Charts 2.2, 2.3 and 6.1.

Combined Compression and Bending in Phase III
(cracked section with N_{Ek} positive in compression)

Unreinforced rectangular section

$$N_{Ed} \le 0.8 f_{cd} bh$$
$$M_{Rd} = N_{Ed} e \ge M_{Ed}$$

with

$$e = y_o - \bar{x}/2$$
$$\bar{x} = N_{Ed}/f_{cd} b$$

Rectangular section—double reinforcement
(case with $\sigma_s = f_{yd}$ in tension and $\sigma'_s = f_{yd}$ in compression)

$$M_{Rd} = f_{cd} b\bar{x}(y_o - \bar{x}/2) + f_{yd} A_s y_s + f_{yd} A'_s y'_s \ge M_{Ed}$$

with

$$\bar{x} = \left(N_{\mathrm{Ed}} + f_{\mathrm{yd}}A_s - f_{\mathrm{yd}}A'_{\mathrm{s}}\right)/f_{\mathrm{cd}}b$$
$$y_{\mathrm{s}} = d - y_{\mathrm{o}} \quad y'_{\mathrm{s}} = y_{\mathrm{o}} - d'$$

Rectangular section—double reinforcement
(case with $\sigma_{\mathrm{s}} < f_{yd}$ in tension and $\sigma'_{\mathrm{s}} = f_{yd}$ in compression)

$$M_{\mathrm{Rd}} = f_{\mathrm{cd}}b\bar{x}(y_{\mathrm{o}} - \bar{x}/2) + \sigma_s A_{\mathrm{s}}y_{\mathrm{s}} + f_{\mathrm{yd}}A'_{\mathrm{s}}y'_{\mathrm{s}} \geq M_{\mathrm{Ed}}$$
$$\left(N_{\mathrm{Ed}} \leq 0.8f_{\mathrm{cd}}bh + f_{\mathrm{yd}}A_{\mathrm{s}} + f_{\mathrm{yd}}A'_{\mathrm{s}}\right)$$

with ($\varepsilon_{\mathrm{cu}} = 0.0035$):

$$\bar{x} = \frac{h}{2}\left\{\left(v_{\mathrm{o}} - \alpha_{\mathrm{o}}\omega_{\mathrm{s}} - \omega'_{\mathrm{s}}\right) + \sqrt{\left(v_{\mathrm{o}} - \alpha_{\mathrm{o}}\omega_{\mathrm{s}} - \omega'_{\mathrm{s}}\right)^2 + 3.2\alpha_{\mathrm{o}}\omega_{\mathrm{s}}\delta}\right\}$$
$$\alpha_{\mathrm{o}} = \varepsilon_{\mathrm{cu}}/\varepsilon_{\mathrm{yd}} \quad v_o = N_{\mathrm{Ed}}/(f_{\mathrm{cd}}bh)$$
$$\sigma_{\mathrm{s}} = E_{\mathrm{s}}\frac{0.8d - \bar{x}}{\bar{x}}\varepsilon_{\mathrm{cu}} \leq f_{\mathrm{yd}} \quad \text{di tension}$$

Rectangular section—double reinforcement
(case with $\sigma_{\mathrm{s}} = f_{\mathrm{yd}}$ in tension and $\sigma'_s < f_{\mathrm{yd}}$ in compression)

$$M_{\mathrm{Rd}} = f_{\mathrm{cd}}b\bar{x}(y_{\mathrm{o}} - \bar{x}/2) + f_{\mathrm{yd}}A_{\mathrm{s}}y_{\mathrm{s}} - \sigma'_{\mathrm{s}}A'_{\mathrm{s}}y'_{\mathrm{s}} \geq M_{\mathrm{Ed}}$$

with ($\varepsilon_{\mathrm{cu}} = 0.0035$ and $\delta' = d'/h$):

$$\bar{x} = \frac{h}{2}\left\{\left(v_{\mathrm{o}} - \omega_{\mathrm{s}} - \alpha_{\mathrm{o}}\omega'_{\mathrm{s}}\right) + \sqrt{\left(v_{\mathrm{o}} - \omega_{\mathrm{s}} - \alpha_{\mathrm{o}}\omega'_{\mathrm{s}}\right)^2 + 3.2\alpha_{\mathrm{o}}\omega'_{\mathrm{s}}\delta'}\right\}$$
$$\alpha_{\mathrm{o}} = \varepsilon_{\mathrm{cu}}/\varepsilon_{\mathrm{yd}} \quad v_{\mathrm{o}} = \frac{N_{\mathrm{Ed}}}{bhf_{\mathrm{cd}}}$$
$$\sigma'_{\mathrm{s}} = E_{\mathrm{s}}\frac{\bar{x} - 0.8d'}{\bar{x}}\varepsilon_{\mathrm{cu}} \leq f_{\mathrm{yd}} \quad \text{in compression}$$

T-shaped section—double reinforcement
(case with $\sigma_{\mathrm{s}} = f_{\mathrm{yd}}$ in tension and $\sigma'_{\mathrm{s}} = f_{\mathrm{yd}}$ in compression)

$$M_{\mathrm{Rd}} = f_{\mathrm{cd}}bt(y_{\mathrm{o}} - t/2) + f_{\mathrm{cd}}b_{\mathrm{w}}\bar{y}(y_{\mathrm{o}} - t - \bar{y}/2) + f_{\mathrm{yd}}A_{\mathrm{s}}y_{\mathrm{s}} + f_{\mathrm{yd}}A'_{\mathrm{s}}y'_{\mathrm{s}} \geq M_{\mathrm{Ed}}$$

with

$$\bar{\mathrm{y}} = \frac{N_{\mathrm{Ed}} + \mathrm{f_{yd}A_s} - \mathrm{f_{yd}A'_s}}{\mathrm{f_{cd}b_w}} - \frac{\mathrm{t}}{\beta}(\geq 0)$$
$$\beta = b_{\mathrm{w}}/b \quad (\bar{x} = t + \bar{y})$$

T-shaped section—double reinforcement
(case with $\sigma_{\mathrm{s}} < f_{\mathrm{yd}}$ in tension and $\sigma'_{\mathrm{s}} = f_{\mathrm{yd}}$ in compression)

$$M_{Rd} = f_{cd} bt(y_o - t/2) + f_{cd} b_w \bar{y}(y_o - t - \bar{y}/2) + \sigma_s A_s y_s + f_{yd} A'_s y'_s \geq M_{Ed}$$

with (ε_{cu} = 0.0035 and $\delta = d/h$):

$$\bar{x} = \frac{h}{2\beta}\left\{(v_o - \alpha_o \omega_s - \omega'_s - \alpha\tau) + \right.$$
$$\left. + \sqrt{(v_o - \alpha_o \omega_s - \omega'_s - \alpha\tau)^2 + 3.2\alpha_o \beta \omega_s \delta}\right\}$$

$$\alpha_o = \varepsilon_{cu}/\varepsilon_{yd} \qquad v_o = \frac{N_{Ed}}{bhf_{cd}}$$
$$\beta = b_w/b \qquad \alpha = 1 - \beta$$
$$\bar{y} = \bar{x} - t \quad (>0) \qquad \tau = t/h$$

Rectangular section—double reinforcement
Finite bilinear model with hardening (Fig. 1.30—model A):

$$\varepsilon_{ud} = 0.9\varepsilon_{uk} \quad \varepsilon_{yd} = f_{yd}/E_s$$
$$E_1 = (f_{td} - f_{yd})/(\varepsilon_{uk} - \varepsilon_{yd})$$
$$f'_{td} = f_{yd} + E_1/(\varepsilon_{uk} - \varepsilon_{yd})$$

For B450C steel (see Table 1.17)

$$\varepsilon_{ud} = 6.75\% \qquad \varepsilon_{yd} = 0.19\%$$
$$E_1 = 1068\,\text{N/mm}^2 \quad f'_{td} = 461\,\text{N/mm}^2$$

with $f_{yd} \leq \sigma_s \leq f'_{td}$ and $f_{yd} \leq \sigma'_s \leq f'_{td}$

$$M_{Rd} = f_{cd} b\bar{x}(y_o - \bar{x}/2) + A'_s f_{yd}\left[1 + \alpha\left(\frac{\bar{x} - \beta_o d'}{\bar{x}}\alpha_o - 1\right)\right](y_o - d') +$$
$$+ A_s f_{yd}\left[1 + \alpha\left(\frac{\beta_o d - \bar{x}}{\bar{x}}\alpha_o - 1\right)\right](d - y_o)$$

$$\bar{x} = \frac{h}{2}c\left\{1 + \sqrt{1 + 4a\beta_o/c^2}\right\} \qquad \beta_o = 0.8$$
$$a = \alpha\alpha_o(\omega_s d/h + \omega'_s d'/h)$$
$$c = \omega_s[1 - \alpha(1 + \alpha_o)] - \omega'_s[1 - \alpha(1 - \alpha_o)] + v_o$$
$$v_o = \frac{N_{Ed}}{bhf_{cd}} \qquad \alpha_o = \varepsilon_{cu}/\varepsilon_{yd} \qquad \alpha = E_1/E_s$$

Combined Tension and Bending in Phase III
(cracked section—double reinforcement with N_{Ed} positive in tension)

Entirely cracked section
(with $\sigma_s = f_{yd}$ in tension and $\sigma'_s < f_{yd}$ in tension)

$$M_{Rd} = f_{yd}A_s y_s - \sigma'_s A'_s y'_s \geq M_{Ed}$$

with

$$\sigma'_s = \frac{N_{Ed} - f_{yd}A_s}{A'_s} \quad \text{in tension}$$

$$y_s = d - y_o \quad y'_s = y_o - d'$$

Rectangular cracked section
(case with $\sigma_s = f_{yd}$ in tension and $\sigma'_s < f_{yd}$ in compression)

$$M_{Rd} = f_{cd}b\bar{x}(y_o - \bar{x}/2) \; + \; f_{yd}A_s y_s + f_{yd}A'_s y'_s \geq M_{Ed}$$

with

$$\bar{x} = \left(f_{yd}A_s - f_{yd}A'_s - N_{Ed}\right)/f_{cd}b$$

Rectangular cracked section
(case with $\sigma_s = f_{yd}$ in tension and $\sigma'_s < f_{yd}$ in compression)

$$M_{Rd} = f_{cd}b\bar{x}(y_o - \bar{x}/2) + f_{yd}A_s y_s + \sigma'_s A'_s y'_s \geq M_{Ed}$$

with ($\varepsilon_{cu} = 0.0035$ and $\delta' = d'/h$):

$$\bar{x} = \frac{h}{2}\left\{\left(\omega_s - \alpha_o\omega'_s - v_o\right) + \sqrt{\left(\omega_s - \alpha_o\omega'_s - v_o\right)^2 + 3.2\alpha_o\omega'_s\delta'}\right\}$$

$$\alpha_o = \varepsilon_{cu}/\varepsilon_{yd} \quad v_o = \frac{N_{Ed}}{bhf_{cd}}$$

$$\sigma'_s = \frac{\bar{x} - 0.8d'}{\bar{x}}\varepsilon_{cu} \leq f_{yd} \quad \text{in compression}$$

T-shaped section—double reinforcement
(case with $\sigma_s = f_{yd}$ in tension and $\sigma'_s = f_{yd}$ in compression)

$$M_{Rd} = f_{cd}bt(y_o - t/2) \; + \; f_{cd}b_w\bar{y}(y_o - t - \bar{y}/2) + f_{yd}A_s y_s + f_{yd}A'_s y'_s \geq M_{Ed}$$

with

$$\bar{y} = \frac{f_{yd}A_s - f_{yd}A'_s - N_{Ed}}{f_{cd}b_w} - \frac{t}{\beta} \quad (\geq 0)$$

$$\beta = b_w/b \quad (\bar{x} = t + \bar{y})$$

T-shaped section—double reinforcement
(case with $\sigma_s = f_{yd}$ in tension and $\sigma'_s < f_{yd}$ in compression)

$$M_{\mathrm{Rd}} = f_{\mathrm{cd}} bt(y_{\mathrm{o}} - t/2) + f_{\mathrm{cd}} b_{\mathrm{w}} \bar{y}(y_{\mathrm{o}} - t - \bar{y}/2) + f_{\mathrm{yd}} A_{\mathrm{s}} y_{\mathrm{s}} + \sigma'_{\mathrm{s}} A'_{\mathrm{s}} y'_{\mathrm{s}} \geq M_{\mathrm{Ed}}$$

with ($\varepsilon_{\mathrm{cu}}$ = 0.0035 and $\delta' = d'/h$):

$$\bar{x} = \frac{h}{2\beta}\left\{(\omega_{\mathrm{s}} - \alpha_{\mathrm{o}}\omega'_{\mathrm{s}} - v_{\mathrm{o}} - \alpha\tau) + \right.$$
$$\left. + \sqrt{(\omega_{\mathrm{s}} - \alpha_{\mathrm{o}}\omega'_{\mathrm{s}} - v_{\mathrm{o}} - \alpha\tau)^2 + 3.2\alpha_{\mathrm{o}}\beta\omega'_{\mathrm{s}}\delta'}\right\}$$

$$\alpha_{\mathrm{o}} = \varepsilon_{\mathrm{cu}}/\varepsilon_{\mathrm{yd}} \quad v_{\mathrm{o}} = \frac{N_{\mathrm{Ed}}}{bhf_{\mathrm{cd}}}$$
$$\beta = b_{\mathrm{w}}/b \quad \alpha = 1 - \beta$$
$$\bar{y} = \bar{x} - t \quad (> 0) \qquad \tau = t/h$$

Chart 6.3: Columns Under Combined Compression and Bending: Shear Resistance

RC columns subject to shear and combined compression with variable bending.

Symbols

$N_{\mathrm{o}} = N_{\mathrm{Ed}}$	design value of the axial force (in compression)
$e = M_{\mathrm{Ed}}/N_{\mathrm{o}}$	eccentricity of the axial force
V_{Ed}	design value of the applied shear force
V_{Rd}	design value of the resisting shear force
b_{w}	column web width
a_{w}	unit area of the web reinforcement (orthogonal stirrups)
$\rho_{\mathrm{w}} = a_{\mathrm{w}}/b_{\mathrm{w}}$	geometric reinforcement ratio of the web
$\omega_{\mathrm{w}} = \rho_{\mathrm{w}} f_{\mathrm{yd}}/f_{\mathrm{c2}}$	mechanical reinforcement ratio of the web
λ_{I}	inclination of initial shear cracking
λ_{c}	inclination of web transverse compressions

see also Charts 2.2, 2.3, 6.1, 6.2.

Cracked Segments

Where one has, for the stress calculated at the concrete edge in tension, the value

$$\sigma'_{\mathrm{c}} = -\frac{N_{\mathrm{o}}}{A_i} + \frac{N_{\mathrm{o}} e}{I_i} y'_{\mathrm{c}} > \beta f_{\mathrm{ctd}} \quad (\beta = 1.3)$$

the shear resistance is to be calculated with reference to the reduced effective depth:

$$d^* = d - \left(N_{\mathrm{o}} - f_{\mathrm{yd}} A'_{\mathrm{s}}\right)/f_{\mathrm{cd}} b$$

with

$$V_{\mathrm{Rd}} = \min(V_{\mathrm{sd}}, V_{\mathrm{cd}}) \geq V_{\mathrm{Ed}}$$

where

$$V_{\mathrm{sd}} = 0.9 d^{*} a_{\mathrm{w}} f_{\mathrm{sd}} \lambda_{\mathrm{c}}$$
$$V_{\mathrm{cd}} = 0.9 d^{*} b_{\mathrm{w}} f_{\mathrm{c2}} \lambda_{\mathrm{c}} / \left(1 + \lambda_{\mathrm{c}}^{2}\right)$$

The inclination λ_{c} should be assumed within the limits

$$\lambda_{\mathrm{I}} \leq \lambda_{\mathrm{c}} \leq \lambda_{\max}$$

with

$$\lambda_{\mathrm{I}} = \tau / \sigma_{\mathrm{I}} \quad \lambda_{\max} = \lambda_{\mathrm{I}} + 1.5$$

where

$$\tau \cong \frac{V_{\mathrm{Ek}}}{0.7\, \mathrm{db_w}} \qquad \sigma = \frac{N_{\mathrm{Ek}}}{A_i} \quad (<0)$$

$$\sigma_{\mathrm{I}} = \frac{1}{2}\left(\sigma + \sqrt{\sigma^2 + 4\tau^2}\right)$$

(see also Chart 4.2 with d^{*} in place of d)

Uncracked Segments

Where, for the stress calculated at the concrete edge in tension, one has the value

$$\sigma_{\mathrm{c}}' = -\frac{N_{\mathrm{o}}}{A_i} + \frac{N_{\mathrm{o}} e}{I_i} y_{\mathrm{c}}' \leq \beta f_{\mathrm{ctd}} \quad (\beta = 1.3)$$

the shear resistance can be calculated with

$$V_{\mathrm{Rd}} = 0.7\, \mathrm{db_w} \sqrt{\bar{\sigma}_{\mathrm{td}} (\bar{\sigma}_{\mathrm{td}} + \sigma)} \leq V_{\mathrm{Ed}}$$

with

$$\sigma = \frac{\mathrm{N_o}}{A_i} \quad (>0)$$

and with

$$\bar{\sigma}_{\mathrm{td}} = f_{\mathrm{ctd}} \qquad \text{for } \sigma \leq f_{\mathrm{cd}}/3$$
$$\bar{\sigma}_{\mathrm{td}} = 1.5(1 - \sigma/f_{\mathrm{cd}}) f_{\mathrm{ctd}} \qquad \text{for } \sigma > f_{\mathrm{cd}}/3$$

It shall always be

$$N_{Ed} = N_o < 0.8 f_{cd} A_c + f_{yd} A_t$$

where A_t is the total area of the longitudinal reinforcement.

Chart 6.4: Combined Axial Force and Uniaxial Bending: Supplementary Formulas

RC sections subject to combined compression/tension and uniaxial bending.

Symbols

M_{ok} characteristic value of the cracking moment
M_{od} design value of the cracking moment

see also Charts 2.2, 6.1, 6.2.

Cracking Moment

Serviceability verifications

$$M_{ok} = \left(\bar{\sigma}'_{ct} - N_{Ek}/A_i\right) I_i / y'_c \geq M_{Ek} \quad \left(\bar{\sigma}'_{ct} = \beta f_{ctk}\right)$$

(for f_{ctk} see Table 1.2)

Resistance verifications

$$M_{od} = (\beta f_{ctd} - N_{Ed}/A_i) I_i / y'_c \geq M_{Ed} \quad (\beta = 1.3)$$

(for A_i, I_i, y'_c see Chart 6.1 with figure).

Minimum Reinforcement

For the longitudinal reinforcement at the beam edge in tension a minimum reinforcement should be provided to resist the force released by the concrete in tension when cracking occurs, at the characteristic yield limit f_{yk}. Such force is to be conventionally calculated based on a triangular distribution of stresses with a maximum at the edge in tension equal to the mean value f_{ctm} of the concrete tensile strength.

For T-shaped sections or similar, it can be set for example:

$$A_s \geq \frac{1}{2} \left(y'_c + w\right) b_w f_{ctm} / f_{yk}$$

with

$$w = \frac{I_i}{A_i e'} \qquad e' = e + (y_o - y_c)$$

where

$$e = \frac{M_{Ek}}{N_{Ek}}$$

is the maximum positive (for $N_{Ek} > 0$) or negative (for $N_{Ek} < 0$) eccentricity foreseen in the use of the structure (see Chart 6.1 and figure).

Columns Under Combined Compression and Bending
For the construction requirements what reported in Chart 2.9 is also valid.

Chart 6.5: Combined Compression and Biaxial Bending—Section with 4 Bars

The following graph shows the resistance curves of RC rectangular sections as the one in the figure. The section is assumed to be subject to biaxial bending referred to the axes *yy* and *zz*. The curves have been obtained with $\varepsilon_{yd} = 0.2\%$, $\varepsilon_{cu} = 0.35\%$ and with concrete covers $c_y = 0.1a$, $c_z = 0.1b$. The definitions are:

$$v = N_{ED}/abf_{cd} \quad \text{centred adimentional axial force}$$

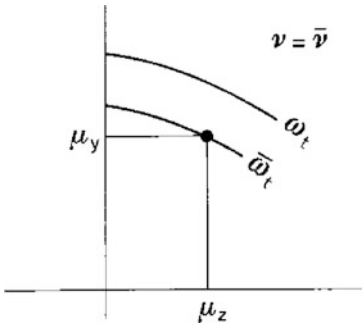
$$M_{yd} = \mu_y a^2 b f_{cd} \quad \text{applied moment about } yy$$

$$M_{zd} = \mu_z a b^2 f_{cd} \quad \text{applied moment about } zz$$

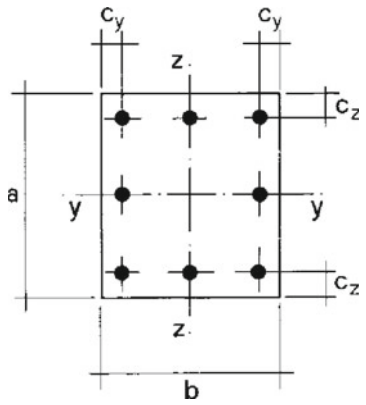
$$\omega_t = A_t f_{yd}/(abf_{cd}) \quad \text{total mechanical reinforcement ratio}$$

see also Charts 2.2, 2.3 and 6.12 and Note on Chart 6.8.

How to Read the Graph
Use the sector relative to the given axial force v. Insert to scale the point of coordinates μ_y, μ_z corresponding to the given moments. Identify the curve $\bar{\omega}_t$ passing through this point (see below). It shall be $\omega_t > \bar{\omega}_t$. In the graphs with eight sectors (for doubly symmetric sections) choose the axes y and z so that $\mu_y \geq \mu_z$.



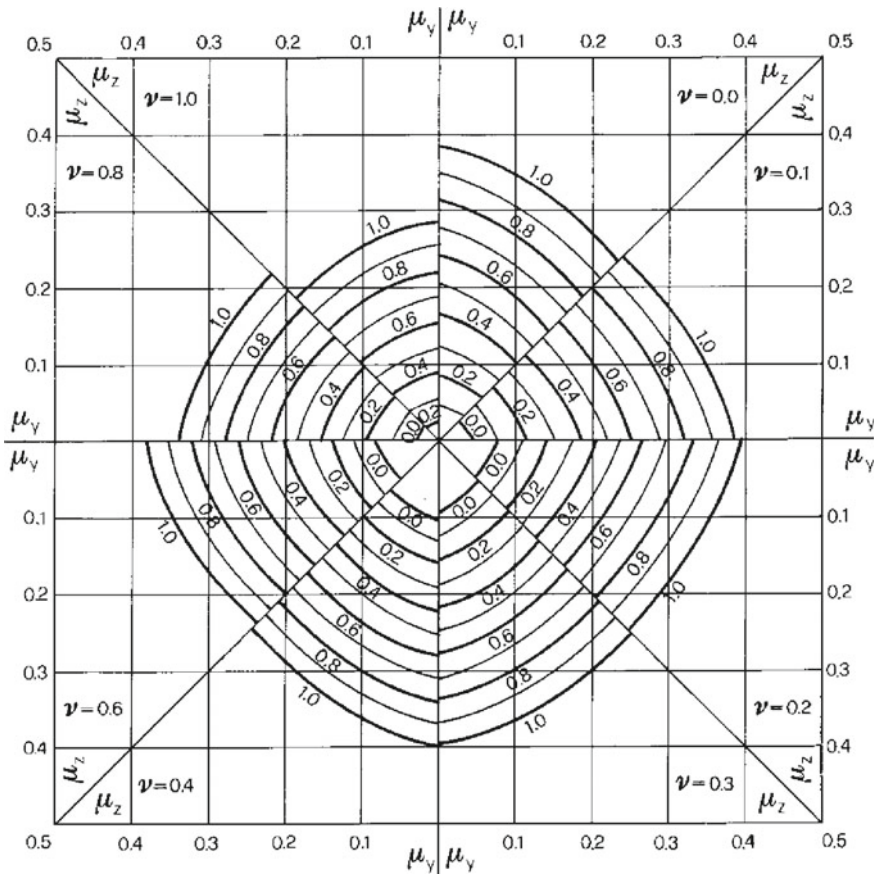
Graph 6.6: Combined Biaxial Bending—Section with 8 Bars



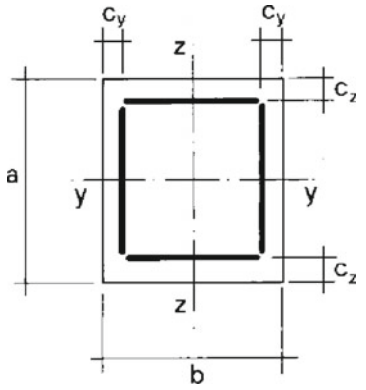
See also Graph 6.5

$$A_t = 8A_s$$

$$\omega_t = 0,0 - 0,2 - .... - 1,0$$



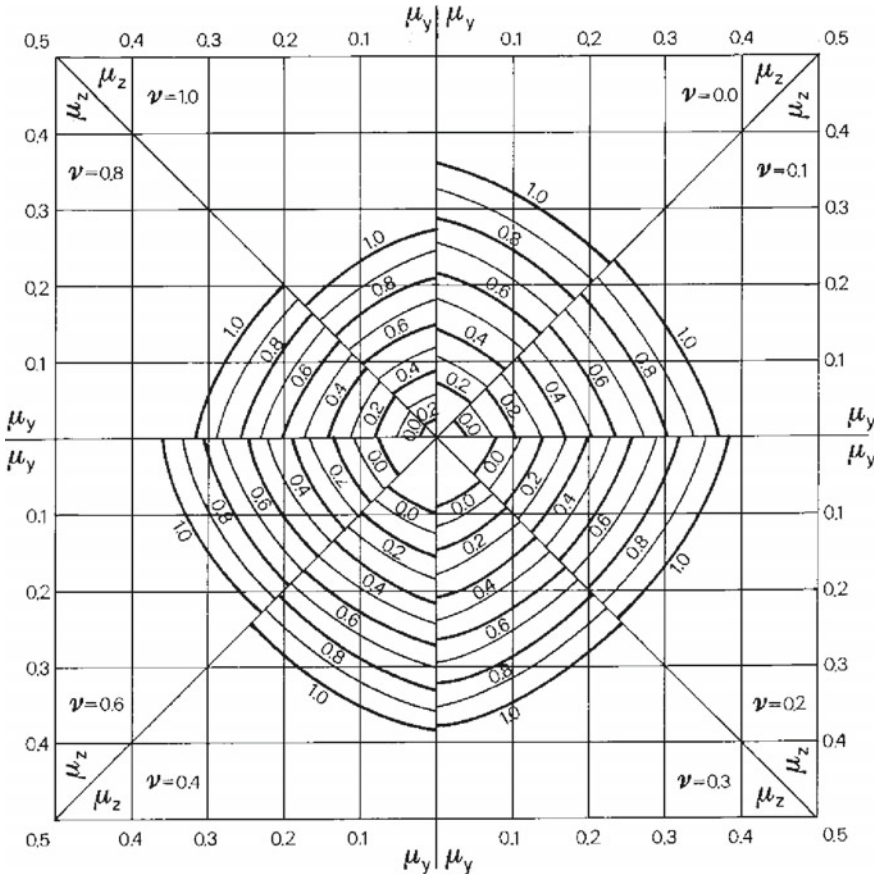
Graph 6.7: Combined Biaxial Bending–Peripheral Reinforcement



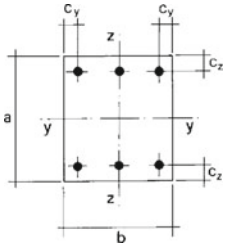
See also Graph 6.5

$$A_t = 4A_s$$

$$\omega_t = 0,0 - 0,2 - .... - 1,0$$



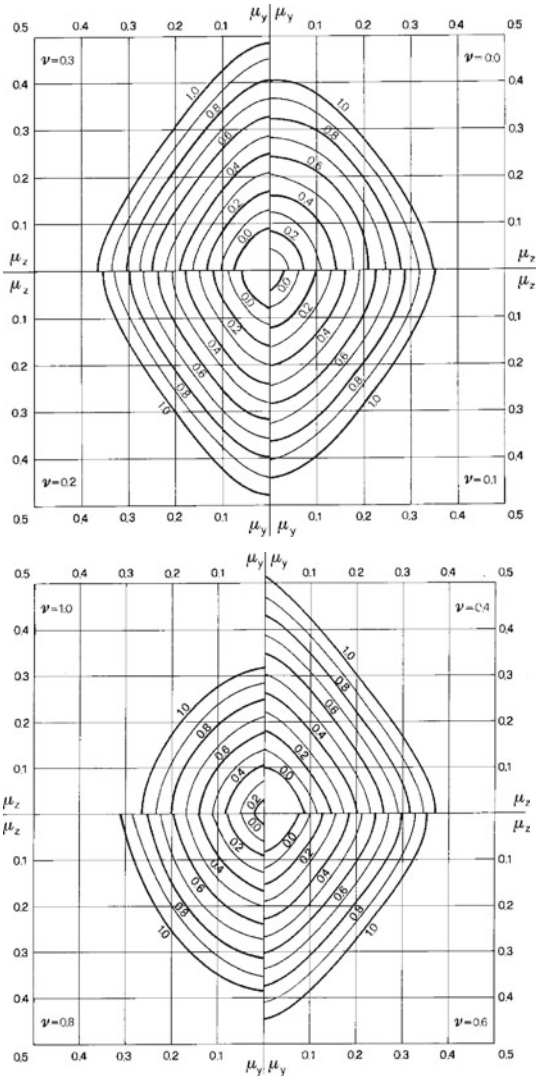
Graph 6.8: Combined Biaxial Bending—Section with 6 Bars



See also Graph 6.5

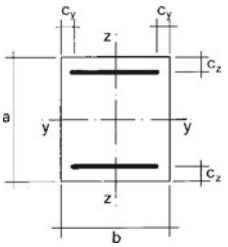
$$A_t = 6A_s$$

$$\omega_t = 0,0 - 0,2 - .... - 1,0$$



Note: Given that a constant distribution ('stress block') for the compressions in concrete has been assumed, a precautionary coefficient $\gamma_o \geq 1$ has been added to compensate the approximations of the model at the high levels of axial force ($v \geq 0.4$). With respect to the exact values, the ones read in the diagrams are therefore reduced by 5–10% depending on the different situations.

Graph 6.9: Combined Biaxial Bending—2 Sides Reinforcement



See also Graph 6.5

$A_t = 2A_s$

$\omega_t = 0,0 - 0,2 - .... - 1,0$

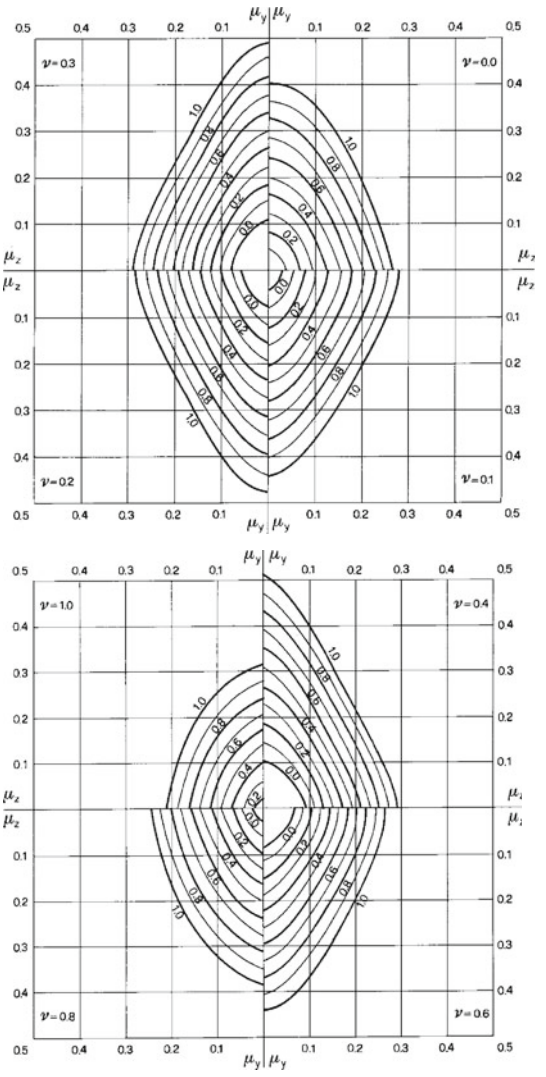

μ_y μ_y
$\nu=0.3$
$\nu=0.0$
$\nu=0.2$
$\nu=0.1$
μ_z
μ_z
$\nu=1.0$
$\nu=0.4$
$\nu=0.8$
$\nu=0.6$

Table 6.10 Combined Biaxial Bending—Analytical Verification

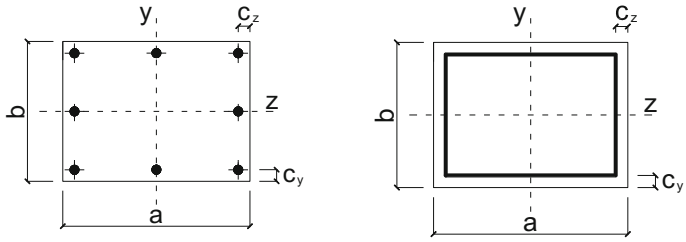
Doubly symmetric reinforced concrete section subject to combined compression and biaxial bending.

Symbols

N_{Ed} design value of the applied axial force
M_{Eyd} design value of the applied moment about y
M_{Ezd} design value of the applied moment about z
y, z principal axes of inertia (of symmetry) of the section
M_{Ryd} resisting moment in uniaxial bending about y
M_{Rzd} resisting moment in uniaxial bending about z

Resistance Verification

$$\left(\frac{M_{Eyd}}{M_{Ryd}}\right)^{\alpha} + \left(\frac{M_{Ezd}}{M_{Rzd}}\right)^{\alpha} \leq 1$$



For the rectangular sections described above, the exponents α are given in the tables as a function of the following parameters:

$$v = \frac{N_{Ed}}{(abf_{cd})} \quad \text{adimentional axial force}$$

$$\omega = \frac{A_s f_{yd}}{abf_{cd}} \quad \text{total mechanical reinforcement ratio}$$

$$\kappa_y = c_y/a \quad \kappa_z = c_z/a \quad \text{adimentional concrete covers}$$

ν − ω	0.00	0.10	0.20	0.30	0.40	0.50	0.60	0.70	0.80	0.90	1.00
0.00		2.846	2.126	1.875	1.714	1.578	1.499	1.430	1.379	1.335	1.304
0.05	3.503	2.284	1.930	1.728	1.578	1.491	1.420	1.363	1.323	1.303	1.292
0.10	2.620	2.023	1.752	1.589	1.488	1.407	1.352	1.326	1.312	1.299	1.286
0.15	2.198	1.819	1.616	1.486	1.403	1.365	1.342	1.320	1.303	1.289	1.277
0.20	1.978	1.670	1.508	1.435	1.387	1.354	1.325	1.311	1.290	1.272	1.258
0.25	1.829	1.593	1.477	1.405	1.365	1.328	1.300	1.278	1.259	1.245	1.232
0.30	1.728	1.529	1.430	1.366	1.322	1.290	1.266	1.247	1.232	1.219	1.208
0.35	1.652	1.478	1.385	1.326	1.287	1.258	1.237	1.220	1.207	1.196	1.187
0.40	1.599	1.437	1.350	1.296	1.259	1.233	1.214	1.198	1.186	1.176	1.168
0.45	1.566	1.414	1.324	1.269	1.236	1.211	1.192	1.181	1.173	1.165	1.157
0.50	1.549	1.443	1.365	1.310	1.272	1.244	1.223	1.206	1.193	1.183	1.175
0.55	1.544	1.467	1.399	1.346	1.305	1.274	1.249	1.230	1.215	1.204	1.194
0.60	1.556	1.492	1.432	1.382	1.339	1.305	1.278	1.256	1.238	1.224	1.213
0.65	1.582	1.519	1.462	1.416	1.373	1.337	1.307	1.283	1.264	1.247	1.233
0.70	1.627	1.553	1.494	1.446	1.407	1.369	1.337	1.311	1.288	1.269	1.254
0.75	1.698	1.597	1.532	1.478	1.441	1.401	1.368	1.339	1.314	1.293	1.275

Values of α for the section with 8 bars and with $\kappa_y = \kappa_z = \kappa = 0.10$ ($\delta_{max} = 2.1\%$).

$\nu - \omega$	0.00	0.10	0.20	0.30	0.40	0.50	0.60	0.70	0.80	0.90	1.00
0.00		2.540	2.072	1.848	1.730	1.644	1.590	1.543	1.509	1.484	1.463
0.05	3.501	2.225	1.901	1.750	1.652	1.588	1.538	1.504	1.477	1.456	1.444
0.10	2.619	2.002	1.781	1.668	1.587	1.533	1.498	1.470	1.453	1.434	1.419
0.15	2.198	1.841	1.690	1.592	1.533	1.493	1.467	1.443	1.424	1.408	1.395
0.20	1.978	1.730	1.608	1.536	1.492	1.458	1.432	1.412	1.396	1.384	1.374
0.25	1.830	1.641	1.543	1.488	1.449	1.421	1.401	1.384	1.372	1.361	1.352
0.30	1.729	1.570	1.493	1.445	1.412	1.389	1.371	1.358	1.348	1.340	1.333
0.35	1.652	1.517	1.448	1.406	1.378	1.359	1.345	1.334	1.326	1.319	1.314
0.40	1.599	1.473	1.407	1.370	1.346	1.330	1.319	1.311	1.304	1.299	1.296
0.45	1.566	1.441	1.377	1.341	1.320	1.305	1.296	1.289	1.284	1.281	1.278
0.50	1.549	1.453	1.386	1.340	1.310	1.289	1.273	1.268	1.265	1.263	1.261
0.55	1.544	1.477	1.420	1.376	1.342	1.317	1.299	1.285	1.275	1.267	1.260
0.60	1.556	1.501	1.451	1.408	1.374	1.347	1.327	1.310	1.297	1.286	1.278
0.65	1.582	1.527	1.479	1.439	1.405	1.376	1.352	1.334	1.319	1.308	1.297
0.70	1.627	1.560	1.509	1.470	1.434	1.404	1.379	1.358	1.342	1.327	1.315
0.75	1.698	1.602	1.543	1.498	1.463	1.431	1.405	1.383	1.365	1.348	1.335

Values of α with peripheral reinforcement and with $\kappa_y = \kappa_z = \kappa = 0.05$ ($\delta_{max} = 2.2\%$).

With a square section symmetric also about the diagonals, set

$M_o = M_{Ryd} = M_{Rzd}$ resisting moment in uniaxial bending about a median axisy or z.

$M_{Rk} = M_{R\eta d} = M_{R\xi d}$ resisting moment in uniaxial bending about a diagonal axis η or ξ.

one has

$$\alpha = -\frac{\log 2}{\lg(M_k/M_o)}$$

with

$$M_k = M_{Rk}/\sqrt{2}$$

Chapter 7
Instability Problems

Abstract This chapter deals with the design criteria of instability verification of slender-reinforced concrete columns under eccentric compression loads. The general approach of second-order analysis of such columns is presented, together with the simplified methods based on equilibrium concentration and the important effects of creep are shown. The second-order analysis of frames is finally discussed.

7.1 Instability of Reinforced Concrete Columns

Euler's formula

$$P_{\mathrm{E}} = \frac{\pi^2 EI}{l_0^2}$$

gives the value of the critical load of a column subject to axial compression under the assumption of elastic behaviour of the material. It is valid as long as the corresponding stress

$$\sigma_{\mathrm{E}} = \frac{P_{\mathrm{E}}}{A} = \frac{\pi^2 E}{\lambda^2} \qquad (\text{with } \lambda = l_0/i, i^2 = I/A)$$

remains within the proportionality limit.

In the case of reinforced concrete, such formula should be referred to a section of composite material (concrete plus steel). According to the criteria repeated several times for the elastic design of such material, one therefore has:

$$P_{\mathrm{E}} = \frac{\pi^2 E_c I_i}{l_0^2}$$

© Springer International Publishing AG 2017

G. Toniolo and M. di Prisco, *Reinforced Concrete Design to Eurocode 2*,
Springer Tracts in Civil Engineering, DOI 10.1007/978-3-319-52033-9_7

or

$$\sigma_{\mathrm{E}} = \frac{P_{\mathrm{E}}}{A_i} = \frac{\pi^2 E_{\mathrm{c}}}{\lambda^2},$$

where the geometrical characteristics I_i and A_i are evaluated for the homogenized section, obtained by increasing the steel areas of the reinforcement by the factor $\alpha_{\mathrm{e}} = E_{\mathrm{s}}/E_{\mathrm{c}}$.

The limits of applicability of these formulas first derive from the fact that concrete leaves the linear elastic behaviour early. Therefore, up to moderate slenderness values, the flexural stiffness of the section is lower than what can be calculated with the elastic modulus E_{c} of concrete, and the homogenization coefficient between steel and concrete is altered.

There is also great influence of the concrete creep with its different effects. The first one concerns the redistribution of stresses under permanent axial loads with compressions in steel progressively brought to high levels. Therefore, in the instantaneous buckling of the column, the flexural increase of stresses starts from an initial altered situation, with minor residual resources of the reinforcement in compression. And then, under permanent actions of combined compression and bending, a progressive viscous increase of the flexural deformations occurs, with consequent amplification of the second-order instability effects. Along the time, the situation progressively approaches the critical configuration, losing its resistance resources.

A more rigorous procedure will be further described at Sect. 7.1.1 with reference to columns under combined compression and bending. In these introduction notes, an approximated verification method of the axial load is recalled based on the assumption of a simplified model of the elastoplastic behaviour of concrete. This method is applicable with good reliability when the absence of significant flexural actions under the permanent loads guarantees against the instability effects of viscous deformation.

Omega Method for Columns in Compression

The curves $P_{\mathrm{cr}} = P_{\mathrm{cr}}(l)$ are shown in Fig. 7.1 as it can be experimentally deduced by testing, on the same configuration of pinned end supports, reinforced concrete columns made with the same materials and with the same section, varying their height l. A first portion is noted with $0 < l < l_1$, where rupture occurs by crushing of concrete without significant lateral buckling. The capacity in this interval is simply given by:

$$N_{\mathrm{r}} = f_{\mathrm{c}} A_{\mathrm{c}} + f_{\mathrm{y}} A_{\mathrm{s}}$$

A last portion is noted with $l > l_2$, where the elastic unstable collapse by sudden lateral buckling of the column occurs. The capacity in this interval, if limited to tests of small duration, is well represented by the Euler's elastic formula referred, as mentioned before, to the homogenized section:

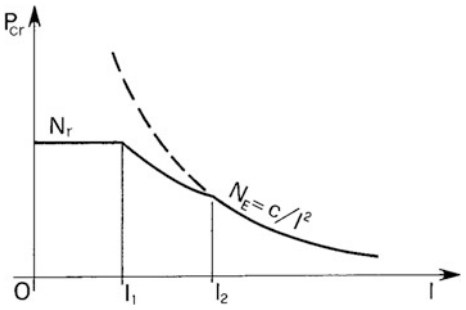


Fig. 7.1 Experimental curve of critical load

$$N_{\mathrm{E}} = \frac{\pi^2 E_{\mathrm{c}} I_i}{l^2}$$

In the central portion with $l_1 < l < l_2$, an intermediate of elastoplastic instability is observed with lateral buckling and rupture of the section under combined compression and bending. The trend in this interval shows a link between the two curves mentioned above:

$$\begin{aligned} P_{\mathrm{cr}} &= N_{\mathrm{r}} = \mathrm{cost.} \quad \text{for } 0 < l < l_1 \\ P_{\mathrm{cr}} &= N_E = c/l^2 \quad \text{for } l_2 < l \end{aligned}$$

In order to generalize the results of the experimental tests, the curves $\sigma_{\mathrm{cr}} = \sigma_{\mathrm{cr}}(\lambda)$ are to be deduced. With reference to the interval of great slenderness values with elastic behaviour of materials, it is therefore assumed

$$\sigma_{\mathrm{cr}} = \frac{N_{\mathrm{E}}}{A_i} = \frac{\pi^2 E_{\mathrm{c}}}{\lambda^2}$$

having correctly homogenized the section with the coefficient $\alpha_{\mathrm{e}} = E_{\mathrm{s}}/E_{\mathrm{c}}$. Extending this definition to the domain of medium and low slenderness values, an approximation is introduced deriving from the fact that the homogenization ratio based on the elastic moduli is no more representative of the ratio between stresses nor of the ratio between the stiffnesses of the two materials. Therefore, the contribution of the steel reinforcement is not correctly taken into account at the ultimate limit state of collapse, with variable errors depending on the reinforcement ratio itself.

The lower reliability of the curves is indicatively shown in Fig. 7.2, where the magnitude of the possible error increases with lower slenderness values and greater reinforcement ratios. Naturally for stocky elements with prismatic rupture the problem is of no interest as, for the calculation of the capacity, there is no need for an elastic homogenization of the section. For elements with medium slenderness instead, the calculation of the capacity is affected by the reliability limits of the

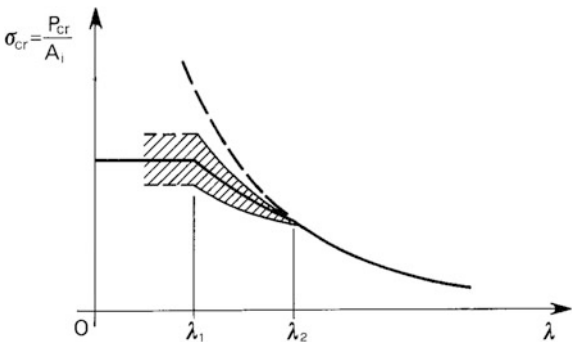


Fig. 7.2 Critical stress curve

formulas based on the deformation models referred to concrete only, as the one presented below.

With an empirical interpretation of the results obtained from the tests, in the domain of medium slenderness it can be set

$$\sigma_{cr} \cong \frac{1.25 f_c}{1 + 0.0001\lambda^2}$$

rather conservative formula that Ritter proposes for $\lambda_1 < \lambda < \lambda_2$ with $\lambda_1 \cong 50$ and $\lambda_2 \cong 100$. Other empirical formulas, less penalizing, have been proposed, such as the one

$$\sigma_{cr} \cong \frac{f_c}{1 + 0.00025(\lambda - 50)^2}$$

used in old codes.

The instability verification of reinforced columns in compression can in this way be based on the evaluation of the stress acting in the concrete, evaluated with the elastic formula:

$$\sigma_c = \frac{N}{A_c + \alpha_e A_s} = \frac{N}{A_i}$$

The comparison with the resisting critical stress follows, with the appropriate global safety factor:

$$\sigma_c < \sigma_{cr}(\lambda)/\gamma,$$

where $\sigma_{cr}(\lambda)$ is to be evaluated with Ritter's formula for $\lambda_1 < \lambda < \lambda_2$.

Using the appropriate tabulations (see Table 7.1) which give the coefficient

$$\omega(\lambda) = \frac{f_c}{\sigma_{cr}(\lambda)}$$

the *stability verification* is therefore written, in the logic of an approximated method of allowable stresses, as:

$$\sigma_c = \frac{N_k}{A_i} < \frac{\bar{\sigma}}{\omega(\lambda)},$$

where it should conservatively be set (with $\gamma_F \cong 1.43$):

$$\bar{\sigma} = 0.8 f_{cd}/\gamma_F \cong 0.56 f_{ck}/\gamma_C$$

The extension of such method to the domain of high slenderness values, with $\lambda > \lambda_2$ and $\sigma_{cr} = \pi E_c/\lambda^2$, leads to insufficient reliability. The more general and rigorous verification criteria described below are to be used.

7.1.1 Analysis of Columns Under Eccentric Axial Force

The second-order analysis for the beam under combined compression and bending in the elastic range is governed by the well-known indefinite equilibrium equation

$$EIv'' = -M_1(x) - Pv,$$

where the first term represents the pullback moment with which the generic section at the abscissa x reacts, the second term adds the second-order moment due to the axial load to the one due to flexural loads (first-order contribution). With reference, for example, to the column of Fig. 7.3, one has

$$M_1 = F + Hx$$

In the general case of reinforced concrete sections, the pullback moment cannot be expressed as a linear function of the curvature v'' with a flexural stiffness $EI = \cos t$. It will have to be read in the competent diagram

$$M = M(\chi)$$

with $\chi = -v''$. This diagram is drawn as already mentioned at Sects. 3.2.2 and 6.3.2. Assuming the curvature $\chi = \chi(x)$ as unknown function, one therefore has:

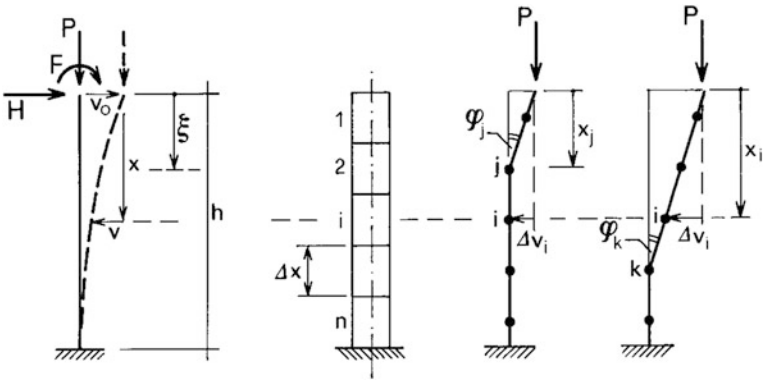


Fig. 7.3 Column deflection and discretization procedure

$$M(\chi) = M_1(\chi) + Pv,$$

where v can be expressed as

$$v = \int_0^x \xi\chi(\xi)\mathrm{d}\xi + \int_x^h x\chi(\xi)\mathrm{d}\xi$$

The numerical solution of this equation contemplates the subdivision of the column in n segments of length $\Delta x = h/n$ and the substitution of the function $\chi(x)$ with n variables $\chi_1, \chi_2, \ldots, \chi_n$ representing the curvature in the middle of the respective segments.

Having therefore set (see also Fig. 7.3):

$$\begin{aligned} M_i &= M_i(\chi_i) \\ M_{1\mathrm{i}} &= M_1(x_i) = F + H\,x_i \\ \phi_i &= \chi_i \Delta x \\ x_i &= (i - 1/2)\Delta x \end{aligned}$$

one has

$$v_i \cong \sum_{j=1}^{i} x_j \phi_j + \sum_{k=i+1}^{n} x_i \phi_k$$

and the equilibrium of moments in the section i is written in the discretized form:

$$M_i = M_{1i} + P\left[\sum_{j=1}^{i} x_j \phi_j + \sum_{k=i+1}^{n} x_k \phi_k\right]$$

General Method

According to the discretized procedure described above, for the considered n sections one has, appropriately rearranging the terms, the pseudolinear system:

$$\begin{cases} 1\chi_1 + 1\chi_2 + 1\chi_3 + \ldots \quad \ldots + 1\chi_n & = 2(M_1 - M_{11})/(P\Delta x^2) \\ 1\chi_1 + 3\chi_2 + 3\chi_3 + \ldots \quad \ldots + 3\chi_n & = 2(M_2 - M_{12})/(P\Delta x^2) \\ 1\chi_1 + 3\chi_2 + 5\chi_3 + \ldots \quad \ldots + 5\chi_n & = 2(M_3 - M_{13})/(P\Delta x^2) \\ \quad \ldots \quad \ldots \quad \ldots \quad \ldots \quad \ldots \quad \ldots & = \quad \ldots \\ 1\chi_1 + 3\chi_2 + 5\chi_3 + \ldots + (2n-1)\chi_n & = 2(M_n - M_{1n})/(P\Delta x^2) \end{cases}$$

where on the second term, the total moments M_i remain function of the respective unknown χ_i.

For the elaboration of the system an iterative procedure can be followed, according to a method that ensures convergence and recalculates the next solution $\chi_1, \chi_2, \ldots, \chi_n$ based on the moments $M_1, M_2, \ldots, M_n$ obtained with the values $\chi_1', \chi_2', \ldots, \chi_n'$ of the previous solution.

A good convergence is ensured by the method where the total moment $M_i = M_i(\chi_i)$ is expressed as the sum of a linear contribution and a variable deviation s_i (see Fig. 7.4):

$$M_i = k_i \chi_i - s_i$$

In particular, for k_i the elastic value $E_c I_i$ of the flexural stiffness is assumed which, if correctly calculated, corresponds to the initial tangent of the actual response curve $M_i(\chi_i)$ of the section. Substituting these expressions in the system, equations of the following type are obtained:

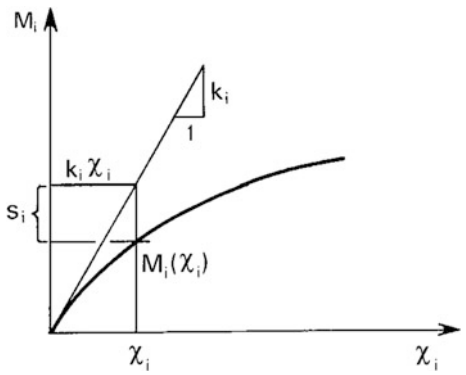


Fig. 7.4 Moment-curvature representation

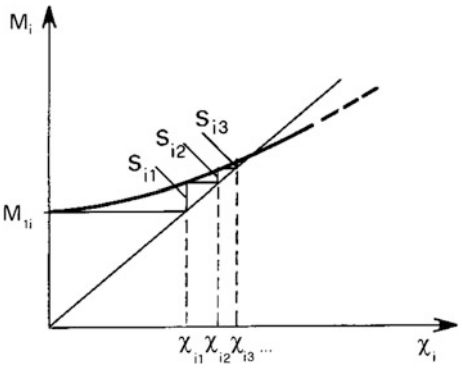


Fig. 7.5 Iterative procedure

$$-c\chi_1 - 3c\chi_2 - \ldots + [k_i - (2i-1)c]\chi_i - \ldots - (2i-1)c\chi_n = M_{\mathrm{li}} + s_i,$$

where $c = P\Delta x^2/2$ has been set. On the first term one has the elastic response "weakened" by the second-order effect; on the second term the first-order constant term of the flexural loads is corrected by the deviation s_i of the actual nonlinear response of the section.

The iterative procedure for the solution of the system can start from zero values $s_{io} = 0$ of the deviations. The linear solution χ_{i1} that derives (see Fig. 7.5) corresponds to the second-order elastic behaviour. The subsequent values $M_{i1} = M_i(\chi_{\mathrm{i1}})$ of the response curve of the sections give the deviations

$$s_{\mathrm{i1}} = k_i\chi_{i1} - M_{i1}$$

that are the unbalanced residuals of the actual nonlinear equations. One then resumes with a new cycle setting on the second term the known values $M_{1i} + s_{i1}$ in place of the previous ones M_{1i}, elaborating the corresponding solution χ_{i2} and evaluating the subsequent deviations s_{i2}. The procedure is stopped when the magnitude of the residual deviations obtained from the last linear solution is negligible and when at the same time the solution coincides with the previous one with good approximation.

It is to be noted that, being the case of a displacements calculation, the curves M-χ to be used are the ones in deformation and that they also depend on the axial force $P = \mathrm{cos}t.$ (see Sect. 6.3.2). Since in the instability calculation, the flexural stiffness of the section directly affects the ultimate resistance of the structure, such curves are to be calculated with the design values $f_{\mathrm{cd}} = f_{\mathrm{ck}}/\gamma_{\mathrm{C}}$ and $f_{\mathrm{yd}} = f_{\mathrm{yk}}/\gamma_S$ of the materials strengths. Their maximum ordinates therefore coincide approximately with the ones of the resistance diagrams, whereas they differ in the rest because of the effects of tension stiffening, concrete tensile strength and the more precise modelling of its tangent modulus. A more detailed description on the topic will be given at Sect. 7.2.

The calculations required by the general method described here above are onerous, therefore the procedures of concentration of equilibrium described at the following section are often used instead.

7.1.2 Methods of Concentration of Equilibrium

The criteria of the *General method* for the second-order analysis of columns under combined compression and bending have been discussed at Sect. 7.1.1, based on a discretized procedure of numerical integration. When the second-order analysis is to be carried, not for individual columns, but for frame structures such as the one shown in Fig. 7.15, the numerical procedure of integration typical of the general method should be repeated countless times for the different elements of the frame and through the solving iterative algorithms of the entire structure. A significant reduction of operations can be obtained if such integrations are avoided, and therefore if the equilibrium is ensured, not with continuity along the elements, but only in certain critical sections.

For the sway frames, for which the second-order unstabilizing effects are more significant, usually bending moments diagrams with maximum values at the ends of the columns are expected. The sections at the bottom and at the top of the single columns are therefore the most stressed.

Based on these considerations, a procedure can be adopted that just ensures the nonlinear equilibrium of the critical sections at the ends of each column and approximates the behaviour of columns with a type function that represents their flexural deformed shape according to a continuous analytical model.

In the following sections, only the practical details of such approximated calculation criterion will be further analyzed with reference to few simple cases. The first case concerns the so-called model column and refers again to one single column. The method will be subsequently refined with the choice of a more complete model for the type function. The application of these models on few common structural schemes will be shown, before presenting the more general method for the analysis of complex frames at the end of the entire chapter.

The Model Column

Among the methods of concentration of equilibrium, the most elementary one refers again to a single column fixed at the base, as the one already analyzed at Sect. 7.1.1 (see Fig. 7.3). This method, called of the *model column*, assumes a *sinusoidal* deformed shape of the axis of the type:

$$v = v_o \sin \frac{\pi}{l} x$$

with $l = 2\ h$ and with $v_o = v(h)$, equal to the displacement of the top of the column. The variable v_o is therefore the only geometrical parameter necessary to define quantitatively the flexural deformed shape of the column.

From the model assumed, it follows that the curvature is given by:

$$\chi(x) = -v'' = v_o \frac{\pi^2}{l^2} \sin \frac{\pi}{l} x$$

and, in the critical section at the bottom of the column where the maximum moment is expected, such curvature is equal to (with $x = l/2$):

$$\chi_o = \frac{\pi^2}{l^2} v_o$$

which depends linearly on the displacement v_o. Concentrating the equilibrium in the bottom section one therefore has

$$M(\chi_o) = M_1(h) + P\, v_o$$

and therefore, with obvious substitutions:

$$M_o = F + Hh + P \frac{l^2}{\pi^2} \chi_o$$

The solution can therefore be obtained plotting the moment-curvature diagram $M = M(\chi;P)$ for the considered section and superimposing the line of the second term of the equilibrium equation written above. The value of this line at the origin $\chi_o = 0$ is equal to the first-order moment $M_{10} = F + Hh$ with a slope proportional to the axial load with the constant l^2/π^2. The intersection of the two curves represents the equilibrium situation of the bottom section (see Fig. 7.6).

In order to show the approximation of the method, let us assume it applied to an elastic behaviour with

$$M_o = EI\chi_o = EI \frac{\pi^2}{l^2} v_o$$

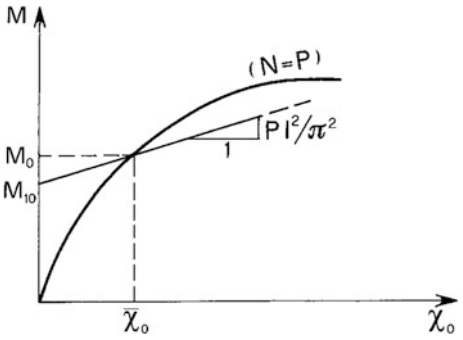


Fig. 7.6 Model column solution

One therefore has

$$EI\frac{\pi^2}{l^2}v_o = F + Hh + Pv_o$$

from which it is obtained

$$v_o = \frac{F + Hh}{\pi^2 EI/l^2 - P} \quad (\text{with } l = 2h)$$

The approximation of the formula can be noted which, for $P = 0$ (with $\pi^2 \cong 10$), leads to:

$$v_o = \frac{2Fh^2}{5EI} + \frac{2Hh^3}{5EI} = 0.8\frac{Fh^2}{2EI} + 1.2\frac{Hh^3}{3EI}$$

underestimating the contribution of the couple F by 20% and overestimating the one of the force H by the same amount with respect to the correct values.

The moment at the bottom of the column, having set $\nu = P/P_E$ with $P_E = \pi^2 EI/l^2$, is:

$$M_o = \frac{1}{1-\nu}F + \frac{1}{1-\nu}Hh,$$

where it can be noted that the amplifying coefficient of the first-order contributions is the same for the two different types of load, being related to the sinusoidal diagram of the bending moment deriving from the model assumed. The correct solution, still within the elastic range, would instead lead to different deformed shapes for the couple F and for the force H, with amplifying coefficients expressed by different functions of the ratio $\nu = P/P_E$:

$$M_o = \frac{1}{\cos\frac{\pi}{2}\sqrt{\nu}}F + \frac{tg\frac{\pi}{2}\sqrt{\nu}}{\frac{\pi}{2}\sqrt{\nu}}Hh$$

Finite Elements

According to the classic finite elements analysis the shape function, assumed to represent the flexural deformed shape of a beam element (beam or column), is a cubic parabola. The four constant of such function can be defined in terms of displacements and rotations at the two ends of the element with the pertinent geometrical conditions. In the linear elastic domain, the cubic parabola model leads to the known expressions of the rotational and translational stiffnesses such as $4EI/h$, $6EI/h^2$ and $12EI/h^3$.

With an approximated application, the same model can be extended to the second-order analysis as well, concentrating the deviatoric effects of loads at the nodes. Applying this procedure to the same cantilevering column previously analyzed with

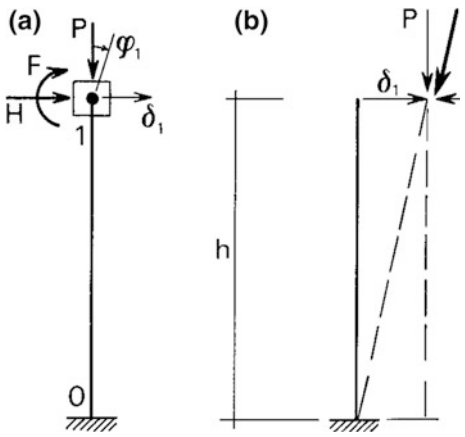


Fig. 7.7 Second-order solution of the cantilever column

the sinusoidal curve of the model column, the solving system typical of the direct displacement method can be set on the scheme of Fig. 7.7a, with the addition of the second-order deviatoric effect evaluated on the mechanism of Fig. 7.7b:

$$\begin{cases} \dfrac{4EI}{h}\phi_1 - \dfrac{6EI}{h^2}\delta_1 = F \\ -\dfrac{6EI}{h^2}\phi_1 + \dfrac{12EI}{h^3}\delta_1 = H + \dfrac{P}{h}\delta_1 \end{cases}$$

The first equation expresses the rotational equilibrium of the node 1, the second one expresses the translational equilibrium including the second-order effect of P.

The solution of the system eventually leads to

$$\delta_1 = \frac{3F/2 + Hh}{\frac{3EI}{h^2} - P}$$

which complies with the first-order solution with $P = 0$:

$$\delta_1 = \frac{Fh^2}{2EI} + \frac{Hh^3}{3EI}$$

and which, with

$$\frac{3EI}{h^2} = 0.3\frac{10EI}{(l/2)^2} = 1.2\frac{10EI}{(l)^2} \cong \frac{6}{5}P_{\mathrm{E}}$$

keeps the amplifying coefficients of the moments for the two types of loads separated:

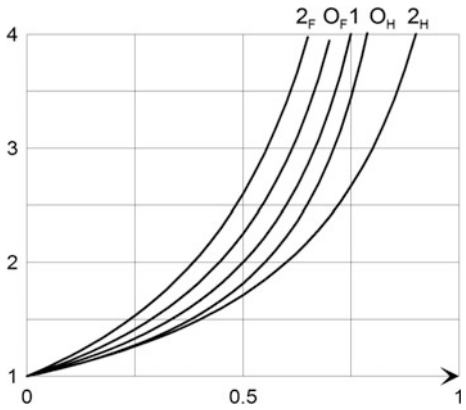


Fig. 7.8 Moment amplifying coefficients for the different models

$$M_o = F + Hh + P\delta_1 = \frac{1 + 3\nu/5}{1 - 5\nu/6}F + \frac{1}{1 - 5\nu/6}Hh \quad \nu = P/PE$$

The curves 2_F and 2_H representing such coefficients are shown in Fig. 7.8 as a function of ν (in abscissa), compared to the curve 1 relative to the model column and to the curves O_F and O_H, relative to the correct solution, where the subscripts obviously refer to the couple F and the force H respectively. It can be noted how the cubic parabola model, when applied to the second-order analysis, leads to significant differences with respect to the correct solution. The model column remains more inaccurate.

For a calculation that takes into account the mechanical nonlinearity of the material, the rotational equilibrium of the bottom section can be set.

$$M(\chi_o) = F + Hh + P\delta_1$$

being able to evaluate the corresponding curvature

$$\chi_o = -\frac{2}{h}\phi_1 + \frac{6}{h^2}\delta_1$$

according to the model assumed.

The problem of the elaboration of the equilibrium nonlinear system is not further discussed here, as the simple column with fixed end at the bottom represents a particular case of the more general algorithm discussed further on.

7.1.3 Creep Effects

One can represent for a given section, for example, the most stressed one at the bottom of the column of Fig. 7.3, the rotational equilibrium with the equation

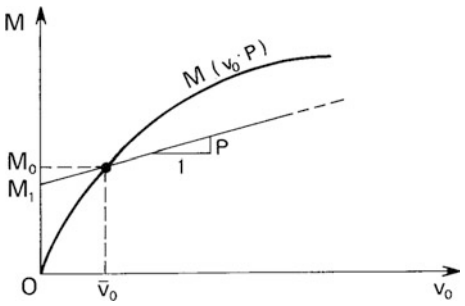


Fig. 7.9 Representation of the second-order solution

$$M(\chi_o) = M_1 + P\nu_o \quad (\nu_o = \delta_1),$$

where $\nu_o = v(h)$ is the displacement at the top of the column. In a plane $M-\nu_o$ (see Fig. 7.9), the second term is represented by the line with the value $M_1 = F+Hh$ at the origin and slope P. On the first term, the response curve M is expressed as a function of the curvature χ (and of the load P).

It is recalled how the *sinusoidal model* of the deformed shape of the column axis led to a curvature value proportional to the displacement at the top (see Sect. 7.1.2):

$$\chi_o = \frac{\pi^2}{l^2}\nu_o \cong \frac{2.5}{h^2}\nu_o$$

Also with the *cubic parabola model*, the following type of expression would be obtained

$$\chi = \frac{c}{h^2}\nu_o,$$

where, for example, one would have $c = 3$ for $F = 0$ and $H \neq 0$. The relationship would remain substantially linear even if deduced exactly with the general method.

The curve deduced from the moment-curvature diagram of the section can therefore be superimposed in an approximated way to the line of the second term of the equilibrium equation after the transformation of the abscissa with the coefficient c/h^2. The solution is subsequently obtained at the intersection M_o, $\bar{\nu}_o$ indicated in Fig. 7.9.

A resistance verification of the considered section to combined compression and bending is consequently carried with the moment M_o evaluated this way.

Limit situations similar to the ones represented in Fig. 7.10 correspond instead to the collapse of the column due to buckling; the first one by combined compression and bending, the second one by centred compression. Therefore one should first verify that the intersection exists; second proceed with the resistance verification of the section with M_o and P.

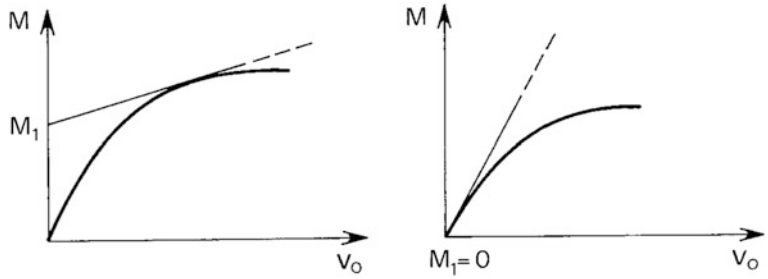


Fig. 7.10 Limit collapse situations for eccentric and centred axial compression

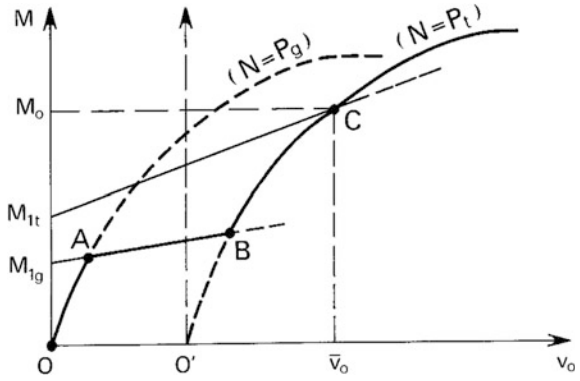


Fig. 7.11 Representation of creep effects on second-order behaviour

Based on the same type of graphical representation, the destabilizing effects of creep can be deduced from the diagram of Fig. 7.11, where it has been assumed to initially apply the permanent portion of loads instantaneously, wait for the end of creep increases of the deformation and eventually apply the remaining instantaneous portion of the loads.

The translation of the final response curve under total loads, due to the creep deformations *A*–*B*, leads to a significant increase of the total moment M_o, together with the increase of deformations, with the possibility of delayed failure of the section. Such effect can also lead to a delayed instability, due to reduced residual resistance to the instantaneous load increments (see Fig. 7.12a) or even due to the collapse under permanent loads (see Fig. 7.12b).

In order to closely follow the load curve as described above, one should apply the general method described at Sect. 1.3.2 also for the integration of the constitutive creep equations. In order to simplify the required calculations, one could use the algebraic method of the effective module (EMM—see Sect. 1.3.3) for which the diagrams $M = M(\chi)$ are used, plotted with a σ-ε concrete law modified based on the ratio $(1 + c\varphi)$ (see Fig. 7.13) and under a single global load condition.

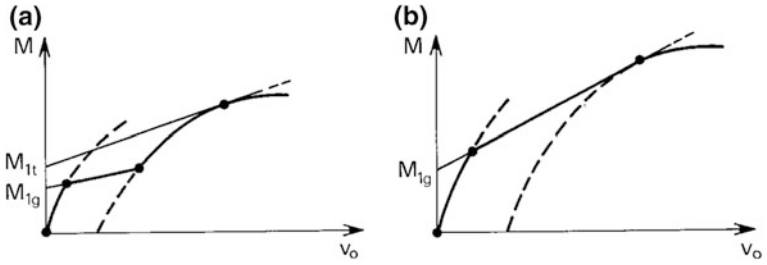


Fig. 7.12 Delayed instability cases due to creep

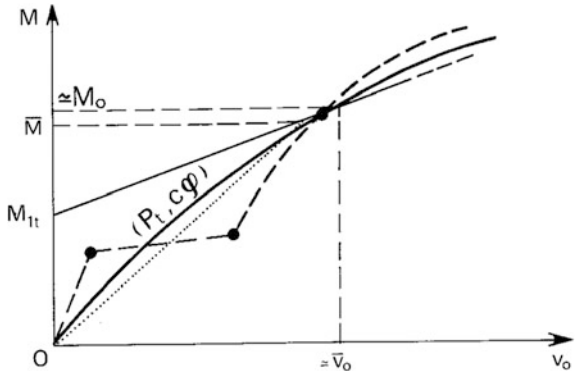


Fig. 7.13 Pseudoelastic solution with effective modulus

The lower accuracy of the *simplified procedure* imposes specific conditions, both with a conservative assumption of the creep coefficient φ, and with a correct evaluation of the quadratic ratio c between the permanent portion and the total bending action.

Within the approximation of the method EMM a *pseudoelastic verification procedure* can be set, which linearizes the response (see dotted line of Fig. 7.13) of the section under combined compression and bending. One has to evaluate the maximum moment $\overline{M}$ with a second-order elastic analysis, using the *effective modulus* in such analysis (see also Sect. 1.3.3)

$$E_{\mathrm{c}}^{*} = \frac{E_{\mathrm{c}}}{1 + c\varphi},$$

where E_{c} is the elastic modulus of concrete (see Sect. 1.1.2) and c, φ are the coefficients defined above. In order to take into account the cracking of the section, a moment of inertia I' appropriately reduced will be used. With the components

$$N \cong P$$
$$M \cong \overline{M}$$

calculated in this way, the resistance verification of the section under combined compression and bending is eventually to be carried.

Unless a more rigorous evaluation is done, given that for common reinforced concrete structures under gravity loads one has $c \cong 0.7^2$ and $\varphi \cong 3.6$, it can be set

$$E^* = \frac{E_c}{1 + 0.7^2 \times 3.6} \cong 0.36 E_c$$

In order to take into account the cracking of the section under combined compression and bending, the moment of inertia of the geometrical concrete section can be further reduced with

$$I' = 0.5\, I$$

arriving to a flexural stiffness reduced with

$$EI \cong 0.18\, E_c I_c$$

Such approximated evaluation can be applied when the bending moments in the columns are caused by gravity loads, as it would be excessively penalizing in other cases. When the bending moments in the columns are caused by horizontal actions such wind, with $c = 0$ it can be set $E^* = E_c$.

Applying these criteria of second-order elastic design for the cantilevering column of Fig. 7.3, one obtains directly

$$\overline{M} = M_o = \frac{1}{\cos \alpha h} F + \frac{tg \alpha h}{\alpha h} Hh \quad \text{with } \alpha = \sqrt{\frac{P}{EI}}$$

For the stability of the column, the resistance verification of its bottom section subject to $N = P$ and $M = \overline{M}$ should consequently be carried.

Within the domain of the limit states method for the elastic modulus E_c a design value will be used

$$E_{cd} = E_{cm} / \gamma'_c,$$

where E_{cm} is the mean value of the elastic modulus (see Table 1.2) and γ'_c is equal to 1.2.

7.2 Second-Order Analysis of Frames

The verification procedure of the stability of reinforced concrete frames with slender elements, of the type represented in Fig. 7.14, in the general case can be based on the following criteria.

Safety verification

- Also for instability problems, the safety verification method based on the comparison of the effects of the applied forces with the calculated resistance of the critical sections (see Fig. 7.15) is followed.

Calculation of the resistance

- On one side, the resistance values of the materials should be initially reduced with the competent coefficients γ_C and γ_S (see Charts 2.2 and 2.3) that include the incertitude of the model, referred to the possible local situation of the *critical sections*.
- The analysis of the section is carried with the ordinary geometrical assumptions and the appropriate constitutive laws of the material strengths (see Chart 6.12).
- The calculated resistance is then expressed in terms of the bending moment $M_{Rd} = M_{Rd}(N_{Ed})$ in the critical sections.

Analysis of actions effects

- On the other side, the external are amplified with the competent coefficients γ_F and combined with the appropriate coefficients ψ_o (see Charts 3.1 and 3.2).

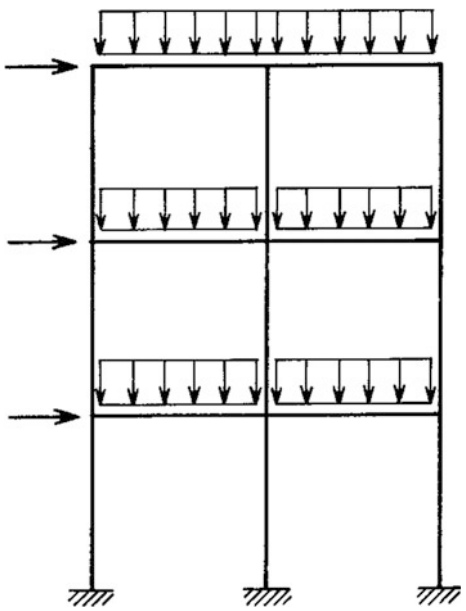


Fig. 7.14 RC multistorey frame with slender columns

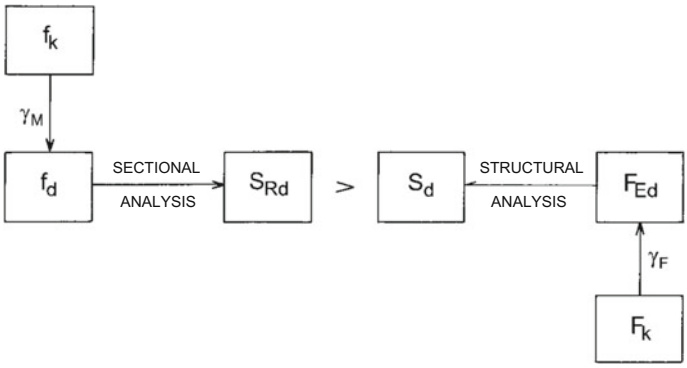


Fig. 7.15 Verification procedure of the stability of RC frames

- The analysis of the structure is carried on the structural model taking into account both nonlinearities, mechanical and geometrical, due to the non-elasticity of materials and the non-negligible magnitude of deflections.
- The necessary constitutive laws, to be used in the elaboration of the structural model for the flexural behaviour of the elements, should be defined with the characteristic strengths f_{ck}, f_{yk} of the materials, applying them to the *current section* of the elements.
- The less penalized characteristics of the current section of the elements give their deformation behaviour that can be integrated to determine the structural response to the applied actions in terms of the diagrams of the bending moments.

This procedure can be summarized in the block-diagram of Fig. 7.15.

The route on the left side corresponds to the calculation of the resistance S_{Rd} of the section starting from the strength f_d of the materials. It is carried with the known assumptions of plane sections ($\varepsilon = \varepsilon_o + \chi y$) and compatibility ($\varepsilon_s = \varepsilon_c$), neglecting the concrete tensile strength ($f_{ct} = 0$) and adopting the appropriate constitutive models (σ-ε) of materials including the failure limit ($\varepsilon_{max} = \varepsilon_u$).

The route on the right side leads to the evaluation of the internal actions S_{Ed} starting from the loads F_{Ed}. For this analysis the strength f_k of the materials is adopted, from which the moment-curvature diagrams $\chi = \chi(M)$ of the sections can be deduced with the same assumptions of plane sections and strain compatibility, but with deformation constitutive models σ-ε that include the concrete tensile strength and the tension stiffening model beyond the cracking limit (see Sects. 3.3 and 6.3.2).

What mentioned above leads to the equilibrium system $KY = \overline{F}$, with its geometrical and mechanical nonlinearities, to be solved with the appropriate methods of numerical calculation. After this solution, the verification of in the critical sections $S_{Rd} > S_{Ed}$ is eventually performed in terms of bending moments.

The numerical algorithm of elaboration of the nonlinear equilibrium system is significantly onerous and requires automated calculation. The relative procedure are described at Sect. 6.3.3, recalling Sect. 5.3.2, and with the integrations recalled at Sect. 7.2.3.

For the ordinary design calculations, in order to avoid the excessively onerous general method described above, one can think of following the pseudoelastic procedure of the reduced flexural stiffness, approximately set as

$$EI \simeq \frac{0.3}{1+0.5\varphi} E_{cd} I_c$$

A second-order elastic analysis of the frame is therefore to be elaborated, avoiding the numerous numerical integrations related to the mechanical nonlinearity.

It is reminded that for sway frames, which are more sensitive to the instability effects and therefore constitute the principal domain of applications of the algorithm under consideration, in the second-order elastic analysis the linearized stiffnesses can be assumed with good accuracy such as

$$k_\nu = \frac{12 E_c^* I}{l^3}(1+\nu)$$

and similar ones. Moreover, with appropriate estimations of the axial forces N that allow the preventive approximated evaluation for the columns of $\nu = N/N_E$, the solving system is brought back to linearity.

For what mentioned above, as anticipated at Sect. 7.1.3, a conservative quantification of the main parameter is to be done, assuming

$$E_{cd} = E_{cm}/\gamma_c' \quad (\text{con } \gamma_c' = 1.2)$$

7.2.1 One-Storey Frames

We initially refer to one-storey frames similar to the one shown in Fig. 7.16a. For their second-order analysis, one can think of applying the direct displacement method assuming the geometrical unknown ξ and setting the translational equilibrium equation of the beam (see Fig. 7.16b):

$$\sum r_j = H,$$

where r_j indicates the shear force in the column jth, whereas H is the horizontal force applied on the beam.

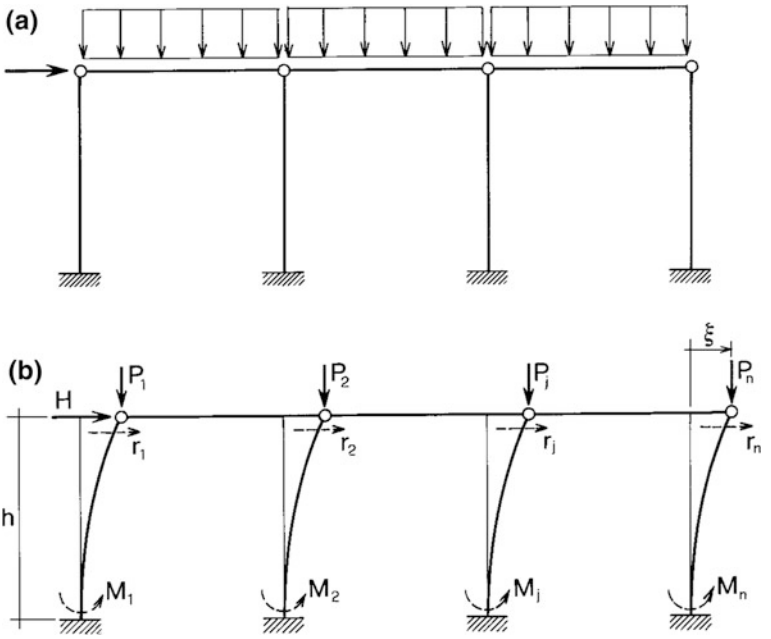


Fig. 7.16 Second-order analysis of one-storey precast frame

Neglecting the axial deformation of beams, the translation at the top is the same for all columns and equal to the assumed unknown ($v_o = \xi$). For the generic column one can set

$$r_j = \frac{M_j}{h} - \frac{P_j}{h}\xi$$

from which the following equation is obtained

$$M - P\xi = Hh$$

with

$$M = \sum M_j$$
$$P = \sum P_j$$

respectively, equal to the sum of the moments at the bottom of the columns and to the sum of the vertical loads acting on the same columns.

The moments at the bottom of the columns remain function of the curvature and the axial force:

$$M_j = M_j(\chi; P_j)$$

With reference to a possible mathematical model of flexural deformation, the curvature is expressed as a function of the displacement ξ:

$$\chi = \frac{c}{h^2} v_o \quad (v_o = \xi)$$

(with $c = 2.5$ for the sinusoidal model, $c = 3.0$ for the cubic model) and it can therefore be set

$$M(\xi) - P\xi = Hh$$

nonlinear equation from which the unknown ξ is to be derived, with the appropriate numerical procedure. Graphically such solution is again represented by the intersection of the curves of Fig. 7.9, where M and P are the sums of the moments and loads defined above.

From this solution, the moments for each column are eventually obtained

$$M_j = M_j(\chi; P_j) \quad \text{with } \chi = c\xi/h^2$$

with which the respective bottom sections are to be verified.

Pseudoelastic Procedure

Within the simplified procedure that assumes the reduced flexural stiffness EI as mentioned above, the second-order analysis of the frame of Fig. 7.16 is based on the linear expressions

$$M_j = \frac{3EI_j}{h^2} G'_m(P_j)\xi = k'_{mj}\xi$$
$$r_j = \frac{3EI_j}{h^3} G'_v(P_j)\xi = k_{vj}\xi$$

of the moment at the bottom and the shear in the columns, that use the appropriate corrective functions G'_m and G'_v to insert the second-order effects in the stiffnesses. The translational equilibrium equation therefore becomes

$$K_v\xi = H$$

with

$$K_v = \sum k'_{vj}$$

and leads to the solution

$$\xi = \frac{H}{K_v}$$

from which one obtains for each column

$$M_j = \frac{k'_{mj}}{K_v} H$$

It is reminded that, being the case of translational behaviour, the linearized expressions as summarized in Chart 7.2 can be used for the stiffnesses. The solving formulas of certain common types of multiple frames are eventually shown in Chart 7.3.

7.2.2 *Multistorey Frames*

We now refer to multistorey frames in reinforced concrete with n floors and m columns as the one described in Fig. 7.17. It is a scheme that allows certain simplifications of the solving algorithm and that refers to a structural layout which

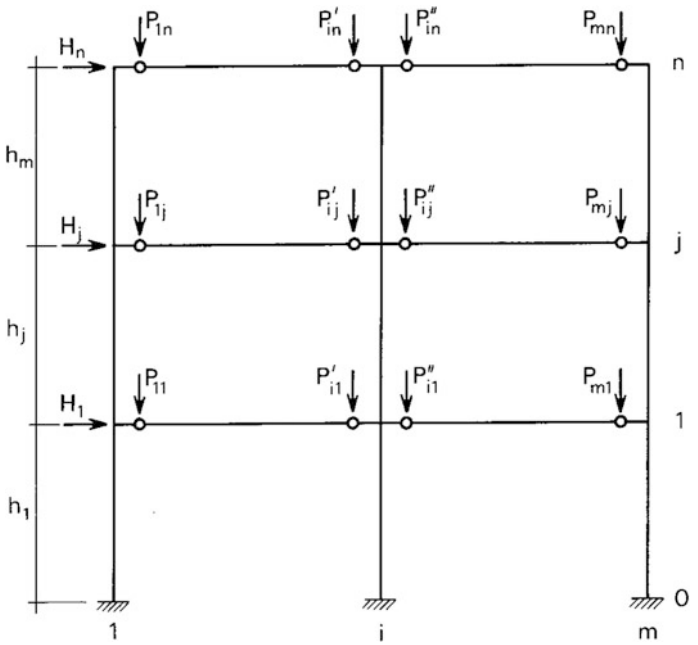


Fig. 7.17 Multistorey precast frame

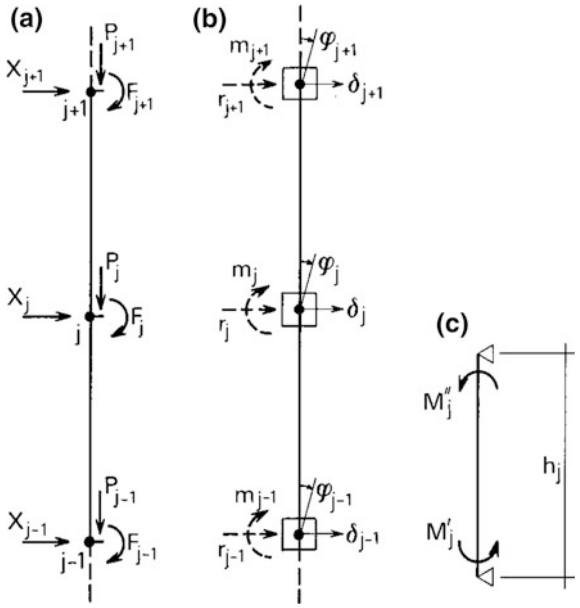


Fig. 7.18 Details of the stiffness analysis

is fairly common in precast buildings, with dominant problems due to instability, given the significant slenderness of columns.

A generic portion of the *i*th column is shown in Fig. 7.18a. Similarly to the method described previously for the isolated column, the geometrical unknowns ϕ_j and δ_j at the nodes can be assumed and the rotational and translational equilibrium equations can be set on the nodes (see Fig. 7.19b):

$$\begin{cases} m_j = -F_j \\ r_j = X_j + N_j \frac{\delta_j^*}{h_j} - N_{j+1} \frac{\delta_{j+1}^*}{h_{j+1}} \end{cases}$$

with

$$N_j = \sum_{k=j}^{n} P_k$$
$$\delta_j^* = \delta_j - \delta_{j-1}$$
$$m_j = M_j'' + M_{j+1}''$$

For a nonlinear response of the section, the internal moments M_j are to be read in the relative moment-curvature diagrams:

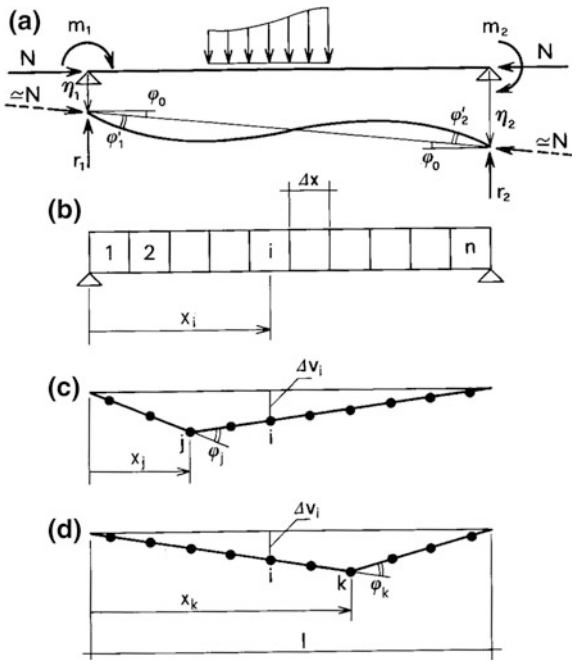


Fig. 7.19 Discretized procedure for second analysis

$$\begin{aligned} M'_j &= M_j(\chi'_j; N_j) \\ M''_j &= M_j(\chi''_j; N_j) \end{aligned},$$

where the curves derive from the assumed deformation model, as function of the nodal translations and rotations:

$$\chi'_j = -\frac{2}{h_j}\phi_j + \frac{6}{h_j^2}\delta_j^* - \frac{4}{h_j}\phi_{j-1}$$

$$\chi''_j = \frac{4}{h_j}\phi_j + \frac{6}{h_j^2}\delta_j^* - \frac{2}{h_j}\phi_{j-1}$$

The translational force r_j eventually derives from the equilibrium of the elements (see Fig. 7.19c):

$$r_j = \frac{M'_j + M''_j}{h_j} - \frac{M'_{j+1} + M''_{j+1}}{h_{j+1}}$$

For the entire frame, assuming that the axial deformations of the beams are negligible, the translational equations at the floors can be summed, obtaining:

$$\sum_{i=1}^{m} r_{ij} = H_j + \sum_{i=1}^{m} N_{ij} \frac{\delta_j^*}{h_j} - \sum_{i=1}^{m} N_{ij+1} \frac{\delta_{j+1}^*}{h_{j+1}}$$

Therefore the $m \cdot n$ rotational equilibrium equations in the unknowns ϕ_{ij} remain, plus n equations of global translational equilibrium of the beams in the unknowns δ_j.

The method, similarly to the model column, requires the moment-curvature diagrams $M_j = M_j(\chi_j;N_j)$ with $N_j = \cos t$ for the sections of all the column portions.

For the solution of the nonlinear system, an iterative procedure of redistribution of residuals can be followed. The internal moment of the sections is initially expressed as the difference between a linear term and a deviation as already done for the elaboration of the general method at Sect. 7.1.1 (see Fig. 7.4):

$$\begin{aligned} M_j' &= k_j \chi_j' - s_j' \\ M_j'' &= k_j \chi_j'' - s_j'' \end{aligned},$$

where the constant k_j is the elastic stiffness EI_j of the section, calculated based on its moment of inertia and the elastic modulus of the material.

Rearranging the terms, the equilibrium equations become:

$$\begin{aligned} &\frac{2EI_j}{h_j}\phi_{j-1} + \left(\frac{4EI_j}{h_j} + \frac{4EI_{j+1}}{h_{j+1}}\right)\phi_j + \frac{2EI_j}{h_{j+1}} + \\ &- \frac{6EI_j}{h_j^2}(\delta_j - \delta_{j-1}) - \frac{6EI_{j+1}}{h_{j+1}^2}(\delta_{j+1} - \delta_j) = F_j - s_j'' - s_{j+1}' \\ &- \frac{6EI_j}{h_j^2}(\phi_{j-1} + \phi_j) + \frac{6EI_{j+1}}{h_{j+1}^2}(\phi_j + \phi_{j+1}) + \left(\frac{12EI_j}{h_j^3} - \frac{N_j}{h_j}\right)(\delta_j - \delta_{j-1}) + \\ &- \left(\frac{12EI_{j+1}}{h_{j+1}^3} - \frac{N_{j+1}}{h_{j+1}}\right)(\delta_{j+1} - \delta_j) = X_j + \frac{s_j' + s_j''}{h_j} - \frac{s_{j+1}' + s_{j+1}''}{h_{j+1}} \end{aligned}$$

where the latter, as mentioned before, is to be summed for all the nodes of the floor j.

Set in a pseudolinear form, the system can be solved with successive linear analyses, starting from zero values of the deviations s, and then progressively redefining them based on the elaborated tentative solution:

$$s_j = k_j \chi_j - M(\chi_j)$$

The first linear solution obtained with $s_j = 0$ corresponds to the second-order elastic analysis.

7.2.3 General Case of Frames

The method of the linear analysis of reinforced concrete frames has been presented in details at Sect. 6.3.3. When there are significant axial forces applied on slender columns, the calculation procedures should be integrated with the algorithms aimed at introducing the second-order effects in their behaviour.

Besides the remaining parts of the procedure, one has to substitute the definition of curvatures in the calculations of the flexural deformations of the elements (see Figs. 5.34 and 5.35), such definition in the first-order analysis resulted directly from the curves $M = M(\chi)$ on the isostatic configuration of the moments along the element.

One can therefore think of subdividing a generic bar in n segments (see Fig. 7.19b) similarly to what has been done for the column of Fig. 7.3. This time the configuration is that of a simply supported beam with its applied loads and the hyperstatic moments at the ends (see Fig. 7.19a).

In the equilibrium equation of the current section at the abscissa x

$$M(\chi) = M_1(x) + Nv(x),$$

which adds the second-order contribution given by the axial force N to the first-order moment M_1, the deflection v can be expressed as a function of the curvature χ with

$$v(x) = \frac{1}{l}\int_0^x \xi(l-x)\chi(\xi)d\xi + \frac{1}{l}\int_x^1 (l-\xi)x\chi(\xi)d\xi$$

Assuming the curvatures χ_1, χ_2, …, χ_n of the centerlines of the segments, in a discretized form it can be set:

$$v_i \cong \frac{1}{l}\sum_{j=1}^{i} x_j(l-x_i)\phi_j + \frac{1}{l}\sum_{k=i+1}^{n} (l-x_k)x_i\phi_k,$$

where

$$\begin{aligned} l &= n\Delta x \\ \phi_i &= \chi_i \Delta x \\ x_i &= (i-1/2)\Delta x \end{aligned}$$

and the equilibrium of moments in the section i becomes

$$M_i = M_{1i} + \frac{N}{l}\left[\sum_{j=1}^{i} x_j(l - x_i)\phi_j + \sum_{k=i+1}^{i} (l - x_k)x_i\phi_k\right]$$

Rewriting the equation for all the n segments, the pseudolinear system is therefore obtained:

$$\begin{cases} 1(2n-1)\chi_1 + 1(2n-3)\chi_2 + 1(2n-5)\chi_3 + \ldots + 1\cdot 1\chi_n & = 4n(M_1 - M_{11})/(N\Delta x^2) \\ 1(2n-3)\chi_1 + 3(2n-3)\chi_2 + 3(2n-5)\chi_3 + \ldots + 3\cdot l\chi_n & = 4n(M_2 - M_{12})/(N\Delta x^2) \\ 1(2n-5)\chi_1 + 3(2n-5)\chi_2 + 5(2n-5)\chi_3 + \ldots + 5\cdot l\chi_n & = 4n(M_3 - M_{13})/(N\Delta x^2) \\ \quad \ldots \quad \ldots \quad \ldots \quad \ldots \quad \ldots & = \quad \ldots \\ 1\cdot l\chi_1 + 3\cdot l\chi_2 + 5\cdot l\chi_3 \ + \ \ldots \ + \ (2n-1)\cdot l\chi_n & = 4n(M_n - M_{1n})/(N\Delta x^2) \end{cases}$$

where on the right-side term the variables $M_i = M_i(\chi_i)$ are again function of the pivotal unknown.

For the solution of the system, the iterative procedure already presented with reference to the general method of Sect. 7.1.1 can be used.

With the calculated values of the curvatures χ_1, χ_2, … χ_n, the numerical integrations can be elaborated for the calculation of the rotations at the ends of the element (see Sect. 5.3.1):

$$\phi_1' \cong \sum_{i=1}^{n} \chi_i \frac{l - x_i}{l}\Delta x$$

$$\phi_2' = \sum_{i=1}^{n} \chi_i \frac{x_i}{l}\Delta x$$

And then one can proceed to the correction of the hyperstatic moments as described at Sect. 5.3.2 and to the subsequent evaluation of transverse reactions:

$$\begin{aligned} r_1 &= -\frac{m_1 + m_2}{l} - N\frac{\eta_2 - \eta_1}{l} + r_{10} \\ r_2 &= +\frac{m_1 + m_2}{l} + N\frac{\eta_2 - \eta_1}{l} + r_{20} \end{aligned},$$

(where r_{10} and r_{20} are the contributions of the loads applied on the bar).

Moments and reactions of all the elements of the frame are eventually to be summed at the nodes to impose their equilibrium, according to the procedure described at Sect. 6.3.3.

As already noted, such general method is significantly onerous. Settling for the simplified procedure with a second-order analysis of the frame with the deformation parameters *EI* appropriately reduced, it is possible to avoid the discretizations of the elements and to summarize their behaviour in the global stiffnesses of the end sections. In Chart 7.2 a summary is shown with the most recurrent formulas of such second-order stiffnesses.

Appendix: Instability of Columns

Table 7.1: Instability Verification of Columns in Compression

The following table shows the values of the coefficient ω for the stability verification of reinforced concrete columns subject to centred axial compression.

Symbols

ω = 1 + $(\lambda-50)^2$/ 4000 reduction coefficient for resistance
λ = l_o/i column slenderness in the plane of lowest stiffness
i = I_i/A_i radius of gyration in the same plane
l_o buckling length in the same plane

see also Chart 2.9.

Verification

$$\sigma_c = \frac{N_{ak}}{A_c + \alpha_e A_s} < \frac{\bar{\sigma}^*}{\omega(\lambda)}$$

with

$$\bar{\sigma}^* = 0.48 f_{ck}/\gamma_C$$

(see Chart 2.2)
valid for $50 \leq \lambda \leq 100$.

λ	50	55	60	65	70	75	80	85	90	95	100
ω	1.00	1.01	1.03	1.06	1.10	1.16	1.23	1.31	1.40	1.51	1.63

Chart 7.2: Second Order Analysis of Frames

For the stability verifications, the stress analysis in reinforced concrete frames can be carried with the displacement method, where *modified stiffnesses* are used with the second-order contributions. For such linear pseudoelastic analysis an *effective module* is assumed

$$E^* = 0.36E_{cm}/\gamma'_c$$

for bending moments induced by gravity loads and

$$E^* = E_{cm}/\gamma'_c$$

for bending moments induced by horizontal loads such as wind, with $\gamma'_c = 1.2$, where E_{cm} is deduced by the Table 1.2.

Loads are to be introduced in the fundamental combination with their *design values* $F_d = \gamma_F F_k$.

In the hyperstatic configurations, the axial forces N_{Ed} necessary for the calculation of the *corrective functions* $G(\nu)$ of the stiffnesses, when it cannot be deduced by approximated evaluations, can be calculated through an initial first-order analysis (setting $G(\nu) = 1$ for the first time). In the predominantly sway behaviour of the frame, for the second-order modified stiffnesses of straight elements with constant cross section, the linearized expressions listed hereafter can be assumed.

Element with fixed ends (see Fig. 7.20a).

$k_1 = k_{10}G(\nu) = \frac{4E^*I}{l}(1 - \nu/3)$ direct rotational stiffness
$k_i = k_{io}G_i(\nu) = \frac{2E^*I}{l}(1 + \nu/6)$ indirect rotational stiffness
$k_m = k_{mo}G_m(\nu) = \frac{6E^*I}{l^2}(1 - \nu/6)$ indirect translational stiffness
$k_v = k_{vo}G_v(\nu) = \frac{12E^*I}{l^3}(1 - \nu)$ direct translational stiffness

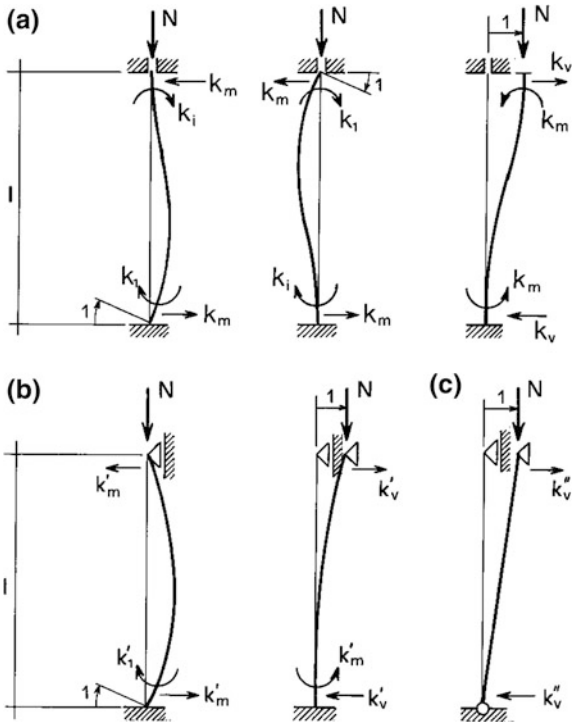


Fig. 7.20 .

Element with one fixed end and one pinned end (see Fig. 7.20b)

$k'_1 = k'_{10} G'_1(\nu) = \frac{3E^*I}{l}(1 - 2\nu/3)$ direct rotational stiffness
$k'_i = 0$ indirect rotational stiffness
$k'_m = k'_{mo} G'_m(\nu) = \frac{3E^*I}{l^2}(1 - 2\nu/3)$ indirect translational stiffness
$k'_v = k'_{vo} G'_v(\nu) = \frac{3E^*I}{l^3}(1 - 4\nu)$ direct translational stiffness

Doubly pinned element (see Fig. 7.20c)

$k'_l = k''_i = k''_m = 0$ any other stiffness
$k''_v = k''_{vo} G''_v(\nu) = \frac{E^*I}{l^3}(-10\nu)$ direct translational stiffness

(in k''_{vo} any value for E^*I can be assumed, but the same as in ν).
In what listed above, it has been set

$$\nu = N/N_E$$
$$N = N_{\mathrm{Ed}} \quad (\text{positive in compression})$$
$$N_{\mathrm{E}} = \pi^2 E^* I/l^2 \quad (\pi^2 \cong 10)$$

I is the moment of inertia of the section referred to concrete with $\alpha_e = 15$ (see Chart 2.3).

For beams that are not subject to significant axial forces it can usually be assumed $G(\nu) = 1$.

Based on the calculated forces, the resistance verifications of the critical sections of the frame are eventually to be performed as specified in Chart 6.12 and 6.21.

Chart 7.3: One-Storey Frames

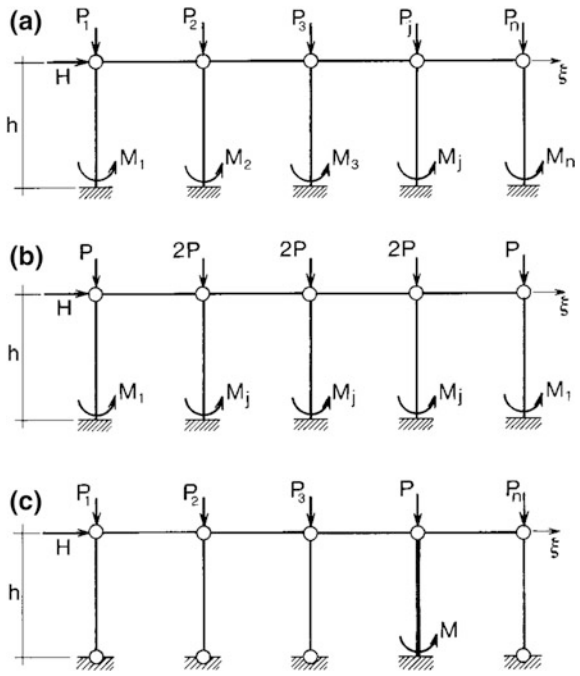
For the type of one-storey frame of Fig. 7.21a, the translational equilibrium equation of the beam is set as:

$$k_{\mathrm{v}} \xi = r_{\mathrm{o}},$$

where

$$k_{\mathrm{v}} = k'_{\mathrm{v}1} + k'_{\mathrm{v}2} + \ldots + k'_{\mathrm{v}n}$$

Fig. 7.21 .



is the total translational stiffness of the frame and r_o is the sum of explicit horizontal forces H plus the translational effects of vertical loads P due to the possible positioning eccentricities of the beams and the competent construction tolerances.

The translation of the beam si then calculated with

$$\xi = r_o/k_v$$

from which one can obtain the horizontal actions (shear forces) in the columns:

$$\begin{aligned} V_1 &= r_o k'_{v1}/k_v \\ V_2 &= r_o k'_{v2}/k_v \\ &\cdots \\ V_n &= r_o k'_{vn}/k_v \end{aligned}$$

as well as the bending moments at the bottom:

$$\begin{aligned} M_1 &= r_o k'_{ml}/k_v \\ M_2 &= r_o k'_{m2}/k_v \\ &\cdots \\ M_n &= r_o k'_{mn}/k_v \end{aligned}$$

For columns that are all equal one has

$$M_1 = r_o h\, G'_{\mathrm{ml}} / \sum G'_{\mathrm{vj}}$$
$$M_2 = r_{\mathrm{o}} h\, G'_{\mathrm{m2}} / \sum G'_{\mathrm{vj}}$$
$$\ldots$$
$$M_{\mathrm{n}} = r_{\mathrm{o}} h\, G'_{\mathrm{m}n} / \sum G'_{\mathrm{vj}}$$

For the stiffnesses and the relative corrective functions, the expressions shown in Chart 7.2 are assumed, with

$$\nu_j = P_j / P_{\mathrm{E}} \quad (P_{\mathrm{E}} = \pi^2 E^* I_{\mathrm{j}} / h^2)$$

Uniform Distribution of Loads and Stiffnesses

In the case of the multiple frame of Fig. 7.21b consisting of n columns with the same cross section and with doubled load on the internal columns, the moments at the bottom are calculated with:

$$M_1 = \frac{r_{\mathrm{o}} h}{n} \kappa_1 \text{for the 2 external columns}$$
$$M_j = \frac{r_{\mathrm{o}} h}{n} \kappa_2 \text{for the } n-2 \text{ external columns}$$

where (with $\nu = P/P_{\mathrm{E}}$):

$$\kappa_1 = \frac{n(1 - 2\nu/3)}{2(1 - 4\nu) + (n-2)(1 - 8\nu)} \quad (\text{for } n \geq 2)$$
$$\kappa_j = \frac{n(1 - 4\nu/3)}{2(1 - 4\nu) + (n-2)(1 - 8\nu)} \quad (\text{for } n \geq 2)$$

For example, a row of $n = 5$ columns, with the external ones loaded at $\nu = 0.05$ and the internal ones at $2\nu = 0.10$, will have the following moments at the bottom:

$$M_1 = \frac{5(1 - 0.1/3)}{2(1 - 0.2) + 3(1 - 0.4)} \frac{r_{\mathrm{o}} h}{5} = 1.422 M_{\mathrm{o}}$$

$$M_j = \frac{5(1 - 0.2/3)}{2(1 - 0.2) + 3(1 - 0.4)} \frac{r_{\mathrm{o}} h}{5} = 1.373 M_{\mathrm{o}},$$

where $M_{\mathrm{o}} = r_{\mathrm{o}} h/5$ is the value from a first-order analysis. The corrected second-order values of the bending moments written above should therefore be used, together with the corresponding axial force $N_1 = P$ or $N_{\mathrm{j}} = 2P$, in the verification of the bottom section of the columns.

Frames with One Stability Element

In the case of the one-storey frame of Fig. 7.21c consisting of n columns, where only one of them has the required constraints to resist the horizontal actions, assuming the axial force on the stability element $P = cP_{\text{tot}}$, its moment at the bottom becomes:

$$M = r_0 h \kappa,$$

where (with $\nu = P/P_{\text{E}}$):

$$\kappa = \frac{3(1 - 2\nu/3)}{3(1 - 4\nu) - 10\nu/c}$$

and where $P_E = \pi^2 E^* I/h^2$ refers to the same stability element.

For example, in a simple portal frame with only two columns with a load $P = P_{\text{tot}}/2$ acting on the stabilizing one ($c = 1/2$), assuming an axial force $\nu = 0.025$ the moment at its base is equal to

$$M = \frac{3 - 0.05}{3 - 0.30 - 0.50} r_{\text{o}} h = 1.341 M_{\text{o}},$$

where $M_{\text{o}} = r_{\text{o}} h$ is the value from a first-order analysis.

In a row of 5 columns with a load $P = P_{\text{tot}}/8$ on the stabilizing one ($c = 1/8$), assuming again an axial force $\nu = 0.025$ the moment at the base is equal to

$$M = \frac{3 - 0.05}{3 - 0.30 - 2.00} r_{\text{o}} h = 4.214 M_{\text{o}}$$

These corrected second-order values should be used, together with the axial force $N = P$, for the verification of the bottom section of the stabilizing column.

Chapter 8
Torsion

Abstract This chapter presents the design methods of RC elements subjected to torsion. After an introductory note on the stress distribution in beam elements as deduced from the basic structural mechanics, the peripheral truss model is described, with its more recent improvements, for the torsional resistance calculations of RC beams. The interaction of torsion with the other internal force components of bending moment, shear and axial action is treated for the actual design applications. In the final section, with reference to the overall stability of the building examined in the previous chapters, the calculation of the corewall system is developed under the pertinent horizontal actions.

8.1 Beams Subject to Torsion

Similarly to what was done in the previous chapters for the design of the structural elements of the reinforced concrete multi-storey building, the analysis of forces is often carried on partial static schemes reduced to plane models (see for example Figs. 4.40 and 6.43). In reality each structure develops in a three-dimensional space and receives combined actions also outside the plane of the model, because of the continuity of transverse elements and the eccentricity of loads and constraints. This leads, other than the cases of biaxial bending discussed at Sect. 3.1.1 and more generally at Sects. 6.1.3 and 6.2.3, to the presence of torsion.

Significant levels of torsion arise for example in beam grids that constitute all traditional decks in reinforced concrete, where the bending moments in beams along one direction generate, through fixed supports at the nodes, torsion on the orthogonal beams. However, the use of simplified plane models can be justified in many cases where torsion does not play a determining role.

For this reason different codes distinguish between two types of torsion:

- *secondary or compatibility torsion*, not necessary for the resistance of the structure (see Fig. 8.1a);
- *primary or equilibrium torsion*, necessary for the resistance of the structure (see Fig. 8.1b).

© Springer International Publishing AG 2017

G. Toniolo and M. di Prisco, *Reinforced Concrete Design to Eurocode 2*,
Springer Tracts in Civil Engineering, DOI 10.1007/978-3-319-52033-9_8

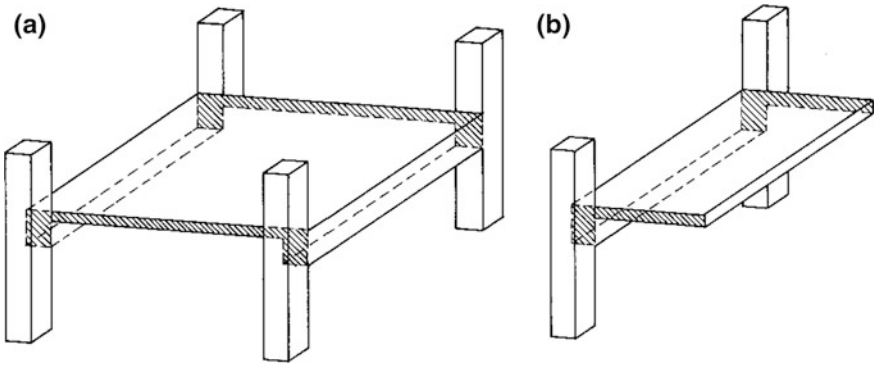


Fig. 8.1 Example of compatibility (**a**) and equilibrium (**b**) torsion

In the first case it is possible to omit the torsional verifications in the beam design, provided that in the design of the transverse elements the stabilizing effect of that torsion is at the same time neglected. This criterion is illustrated in Fig. 8.2a where, neglecting the torsional stiffness of beams, the slab supported by them finds equilibrium in the limit situation of simple supports for which it should be designed. The design of beams by uniaxial bending should still lead to the introduction of adequate stirrups related to shear that give cracking control in service and the necessary degree of ductility against early rupture, also towards torsion.

For the situation of Fig. 8.2b instead, the equilibrium of the cantilevering slab is only ensured by the fixed-end support that the torsional resistance of the beam gives. Therefore, in this case a complete flexural and torsional verification of the beam is necessary.

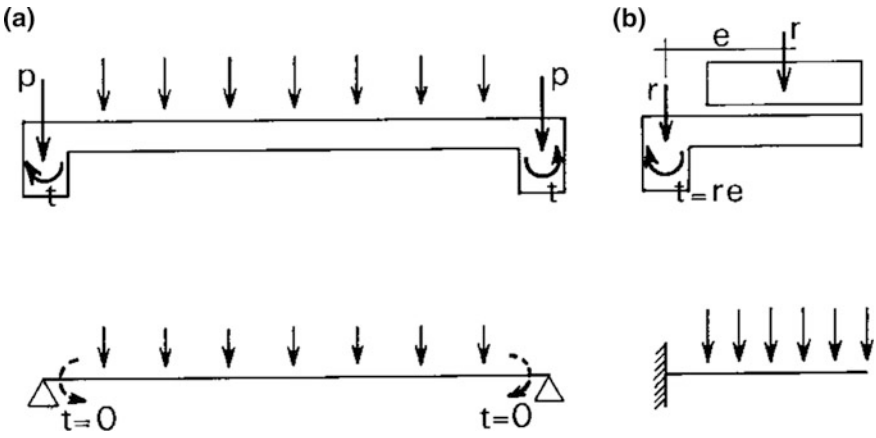


Fig. 8.2 Calculation schemes for compatibility (**a**) and equilibrium (**b**) torsion

Circulatory Torsion

Before introducing the models for the resistance calculations of beams in reinforced concrete, some results of the torsional analysis of beams made of homogeneous isotropic material are recalled.

The classical theory of the de Saint-Vénant solid leads to simple results only in the case of circular sections (or circular hollow sections). Under an applied torque T, in such sections a circulatory closed flow of shear stresses develops, whose magnitude increases linearly in the elastic range from the centroid towards the external edge of the section (see Fig. 8.3a). The maximum value is obtained with:

$$\tau = \frac{T}{W_t}$$

where the torsional resisting modulus is equal to:

$$W_t = \frac{\pi r^3}{2}$$

The two end sections of an elementary beam segment of length dx rotate relatively around the centroidal axis, remaining planes, with:

$$d\phi = \frac{T}{GJ} dx$$

where G is the shear modulus and J is the torsional moment of inertia that coincides, in the case under analysis, with the polar moment of inertia of the section:

$$J = \frac{\pi r^4}{2}$$

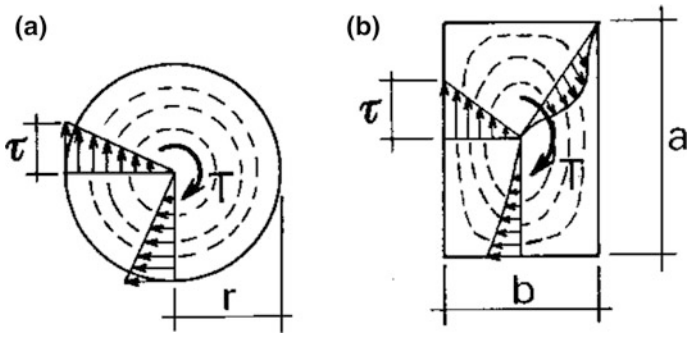


Fig. 8.3 Stress distribution in circular (**a**) and rectangular (**b**) sections

For sections with a generic shape, the problem of *circulatory torsion* is more complicated. In the case of rectangular sections, frequent in reinforced concrete, the competent formulation based on the theory of elasticity leads again to formulas of the following type:

$$\tau = \frac{T}{W_t} \quad d\phi = \frac{T}{GJ}dx$$

with

$$W_t = k_1 ab^2 \quad J = k_2 ab^3$$

where, setting $\beta = b/a$ (≤ 1), it can be written:

$$k_1 \cong \frac{1}{3 + 1.8\beta}$$
$$k_2 \cong \frac{1}{3 + 4.1\sqrt{\beta^3}}$$

The closed flow of shear stresses develops on lines that follow the outline of the section, as indicated in Fig. 8.3b, linking the discontinuities. The stress reaches its maximum value at the ends of the shorter median, and it is equal to zero at the corners. The section, other than rotating around the centroidal axis, warps.

For sections made of rectangles, after evaluating the single torsional inertias with the same formula

$$J_i = k_{2i} a_i b_i^3$$

the global one is obtained as their sum:

$$J = \sum_i J_i$$

and gives the common rotation

$$d\phi = \frac{T}{GJ}dx$$

The analysis of stresses can be carried decomposing the torque on the different rectangles based on the relative inertia:

$$T_i = \frac{J_i}{J}T$$

and then applying for each one the same formula:

$$\tau_i = \frac{T_i}{W_{ti}}$$

With

$$W_{ti} = k_{1i} a_i b_i^2$$

It should be reminded how, for complex shapes, the torsional analysis in the elastic range can rely on the criterion of analogy with *Prandtl's membrane*, then extended for the plastic design with the criterion of analogy of *Nadia's mound of sand*. The surface along which an inflated membrane restrained along the contour arranges itself, or the natural slope of a mound of sand placed on the section gives, with the isolines and the transverse slopes, the flux lines of stresses and their values, except for a volumetric constant related to the value of the torsional moment.

Bredt's Formula

A particular case, also important for the models presented in the following paragraphs, is the *thin-walled hollow sections* (see Fig. 8.4a). For such sections, provided that the magnitude τ of the shear stress can be assumed constant along the thickness t for its small value with respect to the global dimensions of the section, the equilibrium with the torque is written as:

$$T = \oint \tau t r \, \mathrm{d}s$$

Since the flux

$$q = \tau t$$

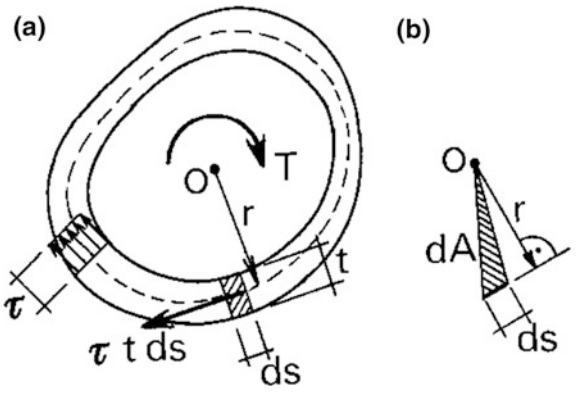


Fig. 8.4 Stress distribution in thin-walled hollow section

has to be constant along the entire perimeter due to the local equilibrium of each element ds, it is obtained (see Fig. 8.4b):

$$T = \tau t \oint r \, \mathrm{d}s = 2q \int_A \mathrm{d}A = 2qA$$

which leads to *Bredt's formula*

$$q = \frac{T}{2A}$$

where A is the area enclosed by the middle fiber of the hollow section.

The maximum shear stress is given by

$$\tau = \frac{T}{W_\mathrm{t}}$$

with

$$W_\mathrm{t} = 2At_\mathrm{o}$$

where t_o is the minimum thickness. The torsional rotation is calculated with the integral

$$\mathrm{d}\phi = \frac{T\mathrm{d}x}{4GA^2} \oint \frac{\mathrm{d}s}{t} = \frac{T}{GJ}\mathrm{d}x$$

where the torsional moment of inertia is defined by

$$J = \frac{4A^2}{\oint \frac{\mathrm{d}s}{t}}$$

For hollow sections with constant thickness this formula becomes

$$J = \frac{4A^2 t}{L}$$

where L is the length of the developed middle fiber, whereas for sections with n segments with constant thickness it becomes

$$J = \frac{4A^2}{\sum_{i=1}^{n} l_i/t_i}$$

where l_i and t_i are the length and thickness of the ith segment.

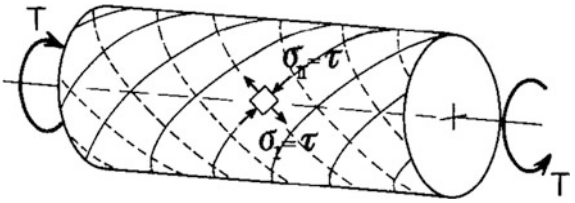


Fig. 8.5 Orientation of principal stresses under pure torsion

To conclude it is noted how in a beam subject to pure torsion, the principal stresses are oriented according to helical isostatic lines that are directed in each point at 45° with respect to the axis of the beam (see Fig. 8.5).

8.1.1 Peripheral Resisting Truss

The behaviour of a beam in reinforced concrete subject to pure torsion can be deduced by the experimental diagram of Fig. 8.6, where the value of the torque applied at the ends of the tested beam is indicated with T and the mean value of the torsional curvature with χ, calculated as the ratio between the relative rotation measured between the ends and their distance.

The curve $T = T(\chi)$ is therefore characterized by:

- uncracked segment *O–A* up to the rupture limit by tension in concrete, substantially linear that follows the line:

$$T = G_c J \chi$$

where J can be calculated, with the formulas presented before, with reference to the geometrical concrete section, since the reinforcement has a small influence;

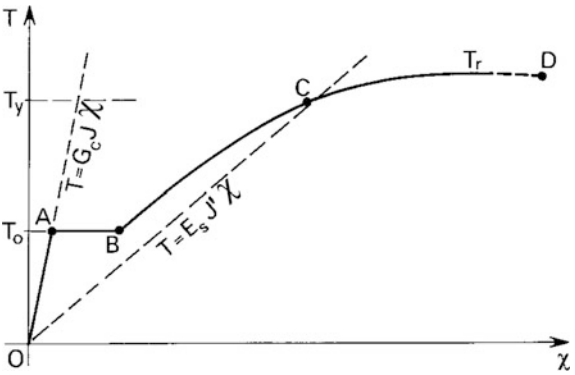


Fig. 8.6 Experimental behaviour of a RC beam under pure torsion

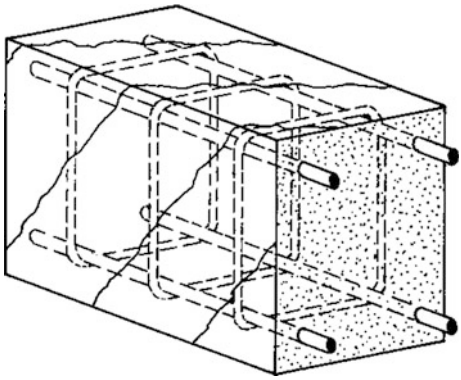


Fig. 8.7 Torsional cracks pattern of the RC beam

- in the absence of the appropriate reinforcement, the limit T_o corresponding to the point A represents the ultimate resistance of the beam;
- for beams with adequate reinforcement, beyond the limit A the beam cracks as indicatively shown in Fig. 8.7, stabilizing on a different resisting mechanism where tensions in the bars develop, whereas inclined fields of compressions develop in the concrete segments;
- the drop in torsional stiffness highlighted by the segment A–B is on average more significant than the analogous drop in flexural stiffness exhibited by beams in bending;
- segment B–C with positive slope that can be approximated to an elastic linear behaviour of the type

$$T = E_S J' \chi$$

  deduced on the model of the new resisting mechanism, where the deformation contribution of the steel reinforcement is predominant, even if other stiffening effects related to concrete have a significant influence;
- final segment C–D with yielding of the reinforcing bars, measurable only up to the resistance ultimate limit T_r in the tests under load-control;
- the extent of the diagram on the subsequent segments of the torsional behaviour depends on the reinforcement ratio and the corresponding ductile or brittle failure modes.

Rausch's Model

Consistent with the cracking pattern observed in the beam (see Fig. 8.7) and starting from the fundamental Ritter–Mörsh truss model developed for shear in beams, the resisting mechanism in torsion is modeled as a spatial arrangement of the truss itself. The beam in reinforced concrete can therefore be schematically represented by a truss of steel bars in tension and concrete in compression developed within the peripheral portion of the section containing the reinforcement (see Fig. 8.8).

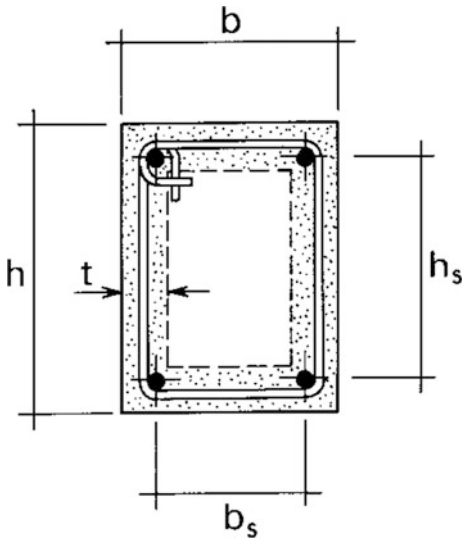


Fig. 8.8 Peripheral position of the resisting mechanism

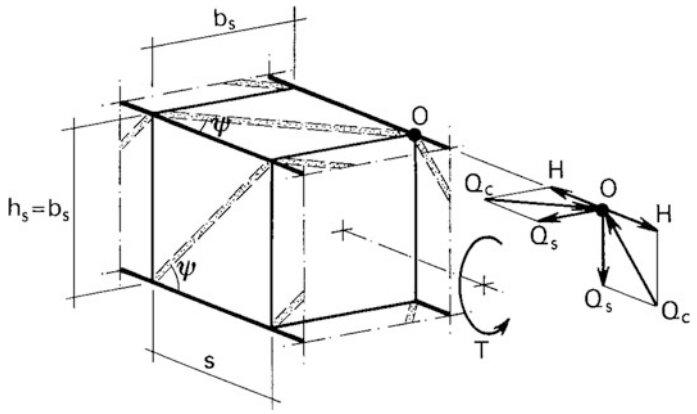


Fig. 8.9 Model of the resisting peripheral truss

Rausch's *resisting peripheral truss* is shown in Fig. 8.9 for the case of a square section, for which it can be drawn in a discretized way. Assuming that all the four vertical links are subject to a constant tensile force Q_s and that the struts of concrete in compression are oriented on each side at $\theta = 45°$ consistent with the cracking pattern observed in the experimental tests, the equilibrium in each node of the truss leads to:

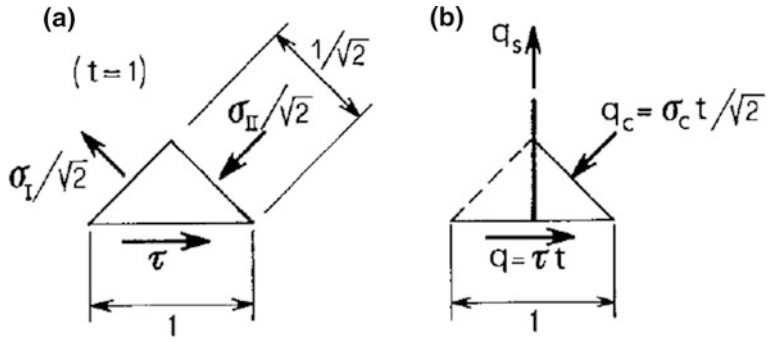


Fig. 8.10 Stress equilibrium before (**a**) and after (**b**) cracking

$$Q_s = Q_c/\sqrt{2}$$

Due to the rotational and translational equilibrium of the section, one again has

$$4H - 4Q_c/\sqrt{2} = 0$$
$$T = 2b_s Q_c/\sqrt{2} = 2b_s Q_s = 2b_s H$$

In order to extend the formulation to rectangular sections, the truss should be uniformly distributed along the axis of the beam according to the following criterion. Assuming that in the uncracked stage the local equilibrium with the applied stress τ relies on the relationships (see Fig. 8.10a):

$$\sigma_I = \sigma_{II} = \tau$$

the principal tensile stress σ_I is lost beyond the cracking limit and the equilibrium, brought into the thickness t of the resisting peripheral shell, is ensured by the flux q_s of the transverse tensile stresses that develops in the stirrups (see Fig. 8.10b):

$$q_s = Q_s/s = q_c/\sqrt{2}$$

having indicated with s the spacing of the stirrups. For the rectangular section, reinforced as indicated in Fig. 8.9 where it should be set $s \neq h_s \neq b_s$, the torsion is given by the sum of the contributions of the two couples indicated in Fig. 8.11:

$$T = \frac{q_c b_s}{\sqrt{2}} h_s + \frac{q_c h_s}{\sqrt{2}} b_s = 2b_s h_s \frac{q_c}{\sqrt{2}}$$

Assuming $A = b_s h_s$, the inclined flux of compressions can be therefore calculated with

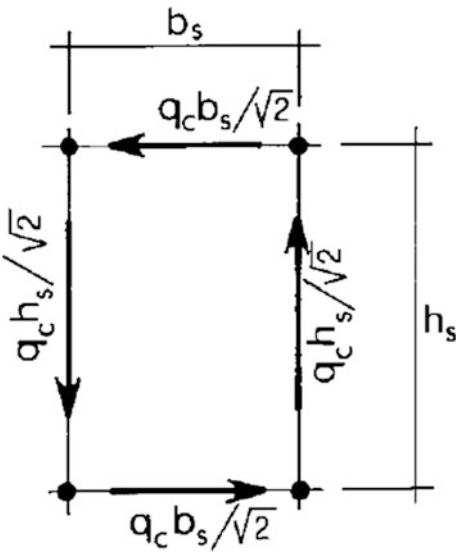


Fig. 8.11 Equilibrium details of the internal forces

$$q_c = \frac{T}{2A}\sqrt{2} = q\sqrt{2}$$

which highlights the Bredt's formula of hollow sections. The tensile force distributed in the stirrups is derived with

$$q_s = q_c/\sqrt{2} = q$$

Thanks to the global translational equilibrium of the section along the axis of the beam it is eventually obtained

$$Q_l = \sum_i H_i = (2b_s + 2h_s)q_c/\sqrt{2})$$

that is

$$Q_l = u\,q$$

where u is the perimeter of the closed profile of the resisting truss. Thanks to symmetry of the section, in the case of the reinforcement of Fig. 8.9, the tensile force on each of the four longitudinal bars can be defined with

$$H = Q_l/4$$

Torsional Resistance

From this formulation one can deduce the torsional resistance of a beam with stirrups $a_s = A_s/s$ (cm^2/m) and with longitudinal reinforcement $a_l = A_l/u$ (cm^2/m). On the truss model the resistance of the stirrups leads to:

$$T_{sd} = 2Aq_{sd} = 2A\frac{A_s}{s}f_{yd} = 2Aa_s f_{yd}$$

The resistance of the longitudinal bars leads to:

$$T_{ld} = \frac{2A}{u}Q_l = 2A\frac{A_l}{u}f_{yd} = 2Aa_l f_{yd}$$

The resistance of the concrete in compression eventually leads to:

$$T_{cd} = \frac{2A}{\sqrt{2}}q_c$$

which, with $q_c = \sigma_c t\sqrt{2}$, leads to

$$T_{cd} = Atf_{c2}$$

where with

$$f_{c2} = 0.50f_{cd}$$

the *reduced resistance* has been indicated, the same used for the calculation of the compression-shear (see Sect. 4.1.3).

The lesser between the values T_{sd} and T_{ld} gives the *tension-torsion* resistance, typical of beams with medium reinforcement, the value T_{cd} gives the resistance to *compression-torsion* typical of highly reinforced beams. Low reinforcements lead eventually to a torsional resistance corresponding to the cracking limit of the concrete section, with

$$T_{Rd} = W_t\tau_{rd} = W_t f_{ctd}$$

independent from the reinforcement.

For the validity of Rausch's Model based on the resisting peripheral truss, certain design requirements are to be followed in the reinforcement layout. For the longitudinal bars one has that:

- their dislocation in the section does not have a significant influence on the resistance, such that even internal prestressing strands are able to ensure the longitudinal translational equilibrium of the section;
- the presence of bars at the corners of the beam is fundamental to ensure the deviation of inclined fluxes of compressions within the peripheral concrete shell

and the diameter of the same bars needs to be sufficiently big with respect to the spacing of the stirrups around them;
- the adequate end anchorage of the bars is eventually important to ensure their full capacity in tension.

For the stirrups:

- they should be effectively closed to ensure the transfer of the continuous circulatory flux of tensile stresses on the entire perimeter;
- for the ultimate resistance, the spacing between stirrups should be limited to $s < b_s$, which allows the development of the resisting truss;
- for the serviceability behaviour, better performances are obtained with stirrups of smaller diameters and more closely spaced, because they lead to smaller crack widths;
- the minimum amount of shear reinforcement, according to the criterion of non-brittleness, remains the one already defined for shear at Sect. 4.3.3.

According to the isostatic model presented here, it is to be noted eventually that it is convenient to equally share the reinforcement between stirrups and longitudinal bars with

$$A_s u = A_l s \quad \text{that is} \quad a_s = a_l$$

because any excess on one type of reinforcement with respect to the other could not be utilized for the resistance. In reality, in this case hyperstatic effects develop that enhance the resistance, as explained later in more details.

Spiral Reinforcement

The type of torsional reinforcement described above is the one generally adopted for reinforced concrete beams. A different type exists, theoretically more effective because it allows to reduce the tensions in steel and limits at the same time the compressions in the concrete. It is the case of spiral-shaped bent bars with branches on each side inclined at 45° according to the inclination of the isostatic lines in tension. The equilibrium of this different truss (see Fig. 8.12a, b) relies on the relationships:

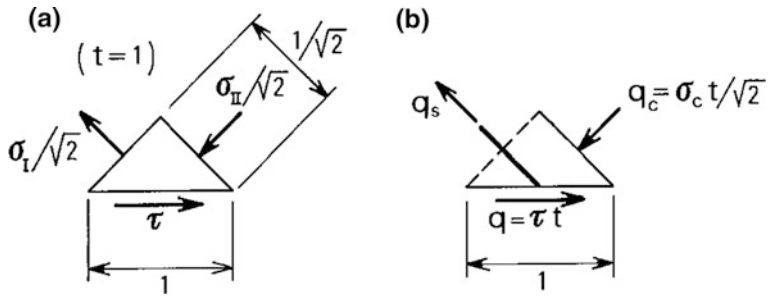


Fig. 8.12 Stress equilibrium before (**a**) and after (**b**) torsional cracking

$$q_s = q_c = q/\sqrt{2}$$

which lead to a tension-torsion resistance equal to

$$T_{sd} = 2Aq_{sd}\sqrt{2} = 2Aa_s f_{yd}\sqrt{2}$$

and to a compression-torsion resistance equal to

$$T_{cd} = 2Aq_{cd}\sqrt{2} = 2Atf_{c2}$$

without the need for longitudinal bars.

In reality, the longitudinal bars at the corners of the beam are always needed, required for the deviation of fluxes of inclined compressions that flow within the peripheral shell of the concrete. Contrary to the previous one, the layout of this type of reinforcement depends on the direction of the torsional moment. It therefore cannot be used where the torsional moment alternates in sign. If the higher complexity of manufacturing necessary for the spiral is considered, one can understand how the torsional reinforcement with such spiral bent bars is not common in practical applications.

8.1.2 Improvement and Application of the Model

The theory of torsion in reinforced concrete beams, based on the resisting peripheral truss, had good experimental confirmations with numerous tests. In particular the followings can be noted:

- experimentation largely covers the domain of medium reinforcements where the resistance is limited by the capacity of the longitudinal bars or the stirrups; moreover, such domain is the one of greater practical interest;
- in the cases of pure torsion, the isostatic model of the resisting peripheral truss leads to resistance values that match very well the experimental ones;
- a level of uncertainty arises on the correct determination of the geometrical characteristics of the resisting section b_s, h_s and t; for these dimensions the following values can be assumed (see Fig. 8.13):

  $$t = A_c/u_c \geq 1.5c$$

  where $A_c = bh$ and $u_c = 2b + 2h$, from which

  $$b_s = b - t \quad h_s = h - t$$
  $$A = b_s h_s \quad u = 2(b_s + h_s)$$

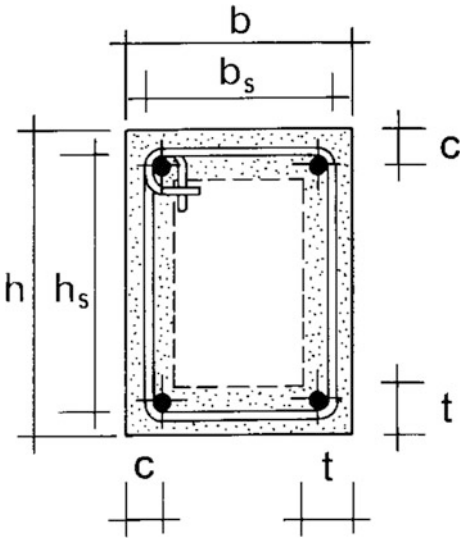


Fig. 8.13 Nominal dimensions of the resisting mechanism

it can be noted how the definition of t results less precise and therefore leads to less reliable values of the resistance by compression-torsion;

- for prestressed beams, experimental tests confirm that pre-tensioning does not significantly affects the ultimate resistance by tension-torsion: its effect remains to increase the cracking limit of the beams;
- other refined theories introduce the effects of aggregate interlocking and dowel action of the reinforcement in the resisting peripheral truss, which are significant when $A_s u \neq A_l s$;
- in reality, thanks to such effects, the resisting mechanism by tension-torsion has a certain degree of hyperstaticity when the capacity of the stirrups and the longitudinal bars are significantly different: failure does not occur with the yielding of the weaker reinforcement, allowing the internal force to increase, up to an ultimate value included within the two limits T_{sd} and T_{ld} defined before;
- in order to take those hyperstatic resources into account, the truss model can be refined, considering the new orientation of the inclined flux of compressions beyond the yielding point of the weaker reinforcement, assuming an inclination of the concrete struts $\theta \neq 45°$, similar to what was done with the variable inclination truss for shear (see Sect. 4.3.2).

Variable Inclination Truss

With reference to the model of Fig. 8.9, the equilibrium equations written at Sect. 8.1.1 are therefore reproposed in the more general case of $\theta \neq 45°$:

$$
\begin{aligned}
Q_{\mathrm{s}} &= Q_{\mathrm{c}} \sin\theta \quad \text{(transverse)} \\
4H &= 4Q_{\mathrm{c}} \cos\theta \quad \text{(longitudinal)} \\
T &= 2b_{\mathrm{s}}Q_{\mathrm{c}} \sin\theta = 2b_{\mathrm{s}}Q_{\mathrm{s}} = 2b_{\mathrm{s}}H\, tg\theta
\end{aligned}
$$

Setting (with $Q_l = 4H$):

$$
\begin{aligned}
q_{\mathrm{s}} &= \frac{Q_{\mathrm{s}}}{s} \quad \text{(along the beam axis)} \\
q_{\mathrm{c}} &= \frac{Q_{\mathrm{c}}}{s} \quad \text{(along the beam axis)} \\
q_{\mathrm{u}} &= \frac{Q_{\mathrm{c}}}{b_{\mathrm{s}}} = q_{\mathrm{c}} ctg\theta \quad \text{(along the perimeter)}
\end{aligned}
$$

one has

$$
\begin{aligned}
q_{\mathrm{s}} &= q_{\mathrm{c}} \sin\theta = q_{\mathrm{u}} \sin\theta\, tg\theta \\
Q_l &= \oint q_{\mathrm{u}} \cos\theta \mathrm{d}u = u q_{\mathrm{u}} \cos\theta
\end{aligned}
$$

where $u = 2(b_{\mathrm{s}} + h_{\mathrm{s}})$ is the perimeter of the resisting shell.

And eventually the torsional moment is obtained with

$$
T = 2b_{\mathrm{s}}h_{\mathrm{s}}q_{\mathrm{u}} \sin\theta = 2Aq_{\mathrm{u}} \sin\theta
$$

which leads, with the appropriate substitutions, to the three formulas:

$$
\begin{aligned}
T_{\mathrm{cd}} &= 2Aq_{\mathrm{c}} \cos\theta \\
T_{\mathrm{sd}} &= 2Aq_{\mathrm{s}} ctg\theta \\
\mathrm{T}_{l\mathrm{d}} &= 2Aq_l tg\theta
\end{aligned}
$$

At the resistance limit of the materials

$$
\begin{aligned}
q_{\mathrm{c}} &= f_{\mathrm{c}2} t \sin\theta \\
q_{\mathrm{s}} &= f_{\mathrm{yd}} A_{\mathrm{s}} / s \\
q_l &= f_{\mathrm{yd}} A_l / u
\end{aligned}
$$

one therefore has (with $\lambda_{\mathrm{c}} = ctg\theta$):

$$
\begin{aligned}
T_{\mathrm{cd}} &= 2Atf_{\mathrm{c}2} \sin\theta \cos\theta = 2\mathrm{A}tf_{\mathrm{c}2}\lambda_{\mathrm{c}}/(1+\lambda_{\mathrm{c}}^2) \\
T_{\mathrm{sd}} &= 2A\frac{A_{\mathrm{s}}}{s} f_{\mathrm{yd}} ctg\theta \quad = 2Aa_{\mathrm{s}} f_{\mathrm{yd}} \lambda_{\mathrm{c}} \\
T_{l\mathrm{d}} &= 2A\frac{A_l}{s} f_{\mathrm{yd}} tg\theta \quad = 2Aa_l f_{\mathrm{yd}} / \lambda_{\mathrm{c}}
\end{aligned}
$$

where the first formula refers to compression-torsion, the two subsequent refer to tension-torsion, respectively, for stirrups and longitudinal bars. For the verification one should obtain

$$T_{\mathrm{Rd}} = \min(T_{\mathrm{cd}}, T_{\mathrm{sd}}, T_{\mathrm{ld}}) \geq T_{\mathrm{Ed}}$$

Any value of λ_{c} around the one λ_{I} of initial cracking can be assumed, if within the domain $\lambda_{\min} \leq \lambda_{\mathrm{c}} \leq \lambda_{\max}$ of the capabilities of plastic adaptation of the reinforcement steel. For ductile steel one can set $\lambda_{\min} = \lambda_{\mathrm{I}}/2.5$ and $\lambda_{\max} = 2.5\lambda_{\mathrm{I}}$. At the yielding limit of both reinforcements one has

$$T_{\mathrm{sd}} = T_{\mathrm{ld}}$$

which leads to the definition of the ultimate orientation of the compressions:

$$\lambda_{\mathrm{c}} = \lambda_{\mathrm{r}} = \sqrt{a_l/a_{\mathrm{s}}}$$

with

$$a_l = A_l/u \quad a_{\mathrm{s}} = A_{\mathrm{s}}/s$$

Interaction Problems

In real structural situations, simple torsion rarely occurs. In general, in beams and columns the torsional moment T coexists with the other internal forces M, V, N.

In the uncracked elastic phase, the simultaneous presence of torsion and other forces is treated by simple superposition of effects. In order to evaluate the cracking limit, the principal tensile stress deduced from the normal σ and shear τ stresses in the mostly stressed points has to be compared with the parameter f_{ctk} of concrete tensile resistance.

At the ultimate limit state, the capacity of a reinforced concrete beam under the combined action of the different internal forces can be deduced on the same truss model presented with reference to simple torsion. Figure 8.14 refers for example to the case of a rectangular section of a beam subject also to bending moment and shear.

Considering its symmetries, in the above-mentioned figure the tensile forces in the two reinforcement bottom chords have been indicated with H', the ones in the top chords with H''. The inclined flux of compressions in the horizontal sides of the peripheral resisting concrete shell has been indicated with q_{c} and the ones in the vertical sides, where the effect of shear V modifies the values, has been indicated with q'_{c}, q''_{c}. On this model the following local equilibrium conditions with the transverse tensions in the stirrups are valid. For simplicity these equilibrium conditions are written below for the case of $\theta = 45°$ ($\lambda_{\mathrm{c}} = 1$):

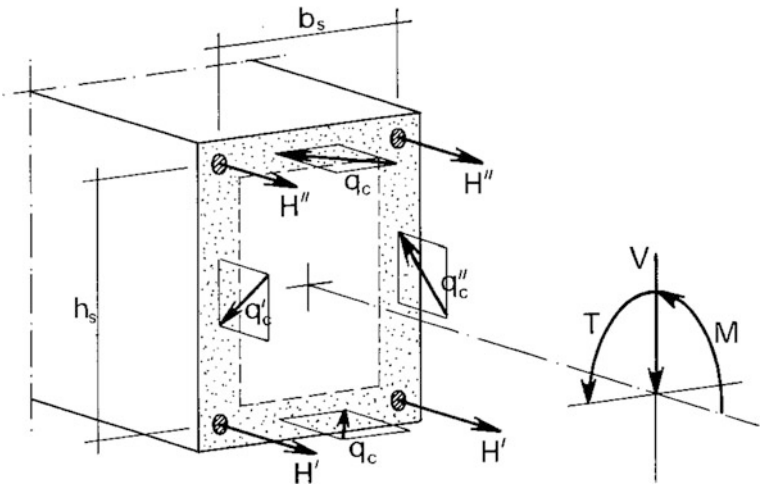


Fig. 8.14 Stress distribution under M, V, T interaction

$$q_s = q_c/\sqrt{2}$$
$$q'_s = q'_c/\sqrt{2}$$
$$q''_s = q''_c/\sqrt{2}$$

The equilibrium conditions of the closed flux in the resisting shell are:

$$q_c = \frac{q'_c + q''_c}{2} \quad q_s = \frac{q'_s + q''_s}{2}$$

With these conditions, the equilibrium of the section of Fig. 8.14 is set with the equations:

$$2H' + 2H'' = 2b_s \frac{q_c}{\sqrt{2}} + \frac{q'_c + q''_c}{\sqrt{2}} h_s = u \frac{q_c}{\sqrt{2}}$$
$$T = b_s h_s \frac{q_c}{\sqrt{2}} + \frac{q'_c + q''_c}{\sqrt{2}} h_s \frac{b_s}{2} = 2A \frac{q_c}{\sqrt{2}}$$
$$M = 2H' \frac{h_s}{2} - 2H'' \frac{h_s}{2}$$
$$V = \frac{q'_c}{\sqrt{2}} h_s - \frac{q''_c}{\sqrt{2}} h_s$$

In particular in the first equation, which expresses the longitudinal translational equilibrium, the possible term N of the axial force is to be added, if present.

With reference therefore to the resistance of the longitudinal bars of the beam, the interaction between *torsional and bending moment* is obtained combining the translational equilibrium mentioned above:

$$\frac{q_c}{\sqrt{2}} = \frac{2H' + 2H''}{u}$$

with the competent rotational ones

$$2H' + 2H'' = \frac{T}{2A}u$$
$$2H' - 2H'' = \frac{2M}{h_s}$$

where it can be noted how, if the following average value of tensions in the longitudinal reinforcement chords is associated to the torsional moment

$$H = \frac{2H' + 2H''}{4} \quad (= Q_l/4)$$

the semi-difference is associated to the bending moment

$$2\Delta H = \frac{2H' - 2H''}{2}$$

according to what indicated in Fig. 8.15.

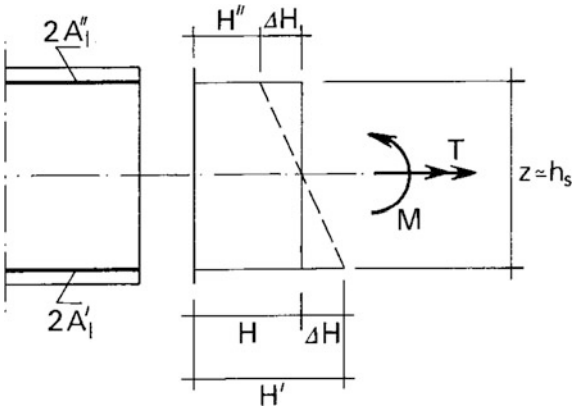


Fig. 8.15 Bending moment and torsion interaction

On the two reinforcement levels, lower and upper, one therefore has the forces:

$$2H' = \frac{T/2}{2A/u} + \frac{M}{h_s}$$
$$2H'' = \frac{T/2}{2A/u} - \frac{M}{h_s}$$

which, at the resistance limit, can be, respectively, equal to

$$2H' = 2A'_l f_{yd}$$
$$2H'' = 2A''_l f_{yd}$$

The simple linear superposition of effects can be noted.

Having defined with

$$M_{Rd} = 2A'_l f_{yd} h_s$$
$$T_{Rd} = 4A''_l f_{yd} 2A/u$$

the resisting ultimate values for the uncoupled actions of bending moment and torsional moment, in a dimensional form is therefore obtained:

$$1 = \frac{T}{T_{Rd}} \frac{A''_l}{A'_l} + \frac{M}{M_{Rd}}$$
$$\frac{A''_l}{A'_l} = \frac{T}{T_{Rd}} \frac{A''_l}{A'_l} - \frac{M}{M_{Rd}}$$

that is, with $\kappa = A'_l/A''_l$:

$$\frac{T}{T_{Rd}} = \kappa - \kappa \frac{M}{M_{Rd}}$$
$$\frac{T}{T_{Rd}} = 1 + \kappa \frac{M}{M_{Rd}}$$

The first relationship, which implies the yielding of the lower reinforcement chords, is crucial when the bending component predominates; the second relationship, which implies the yielding of the top reinforcement chords, is instead crucial when the torsional component predominates; both depend on the ratio κ between the reinforcement levels, as indicated in Fig. 8.16.

What mentioned above shows simple linear interaction formulas which allow to *superimpose the effects* of torsion and bending on the isostatic truss model. One therefore has that:

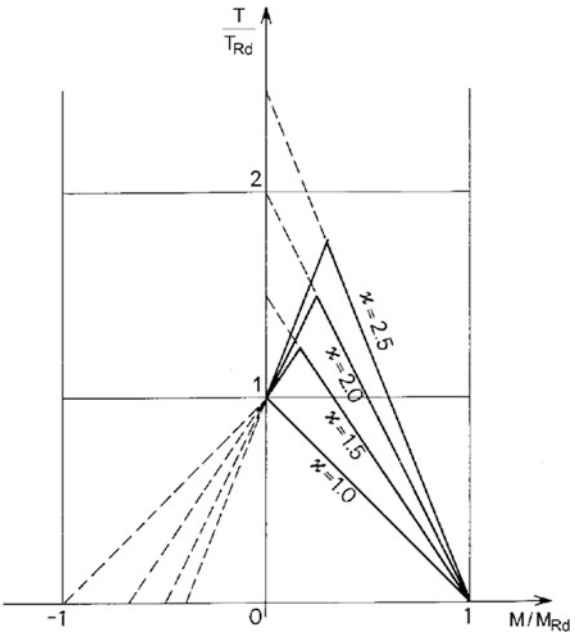


Fig. 8.16 Resistance limit curves for *M–T* interaction

- at the edge of the beam in tension under the bending moment the longitudinal reinforcement designed on the basis of the torsional moment is to be added to the one required by the bending moment;
- at the edge in compression under the bending moment, if the tension force due to the torsional moment does not exceed the one in compression due to the bending moment, no longitudinal reinforcement is required.

In the interaction between *torsion and shear,* when limited by the transverse stirrups, the resistance of the reinforced concrete beam is obtained by combining the equilibrium equation of the torsional moment:

$$T = b_s h_s q_s + \frac{q'_s + q''_s}{2} h_s b_s = (q'_s + q''_s)A$$

with the one of shear:

$$V = (q'_s - q''_s) \cdot h_s$$

written here for $\theta = 45°$. From these equations two relationships are obtained:

$$q'_s = \frac{T}{2A} + \frac{V}{2h_s}$$
$$q''_s = \frac{T}{2A} - \frac{V}{2h_s}$$

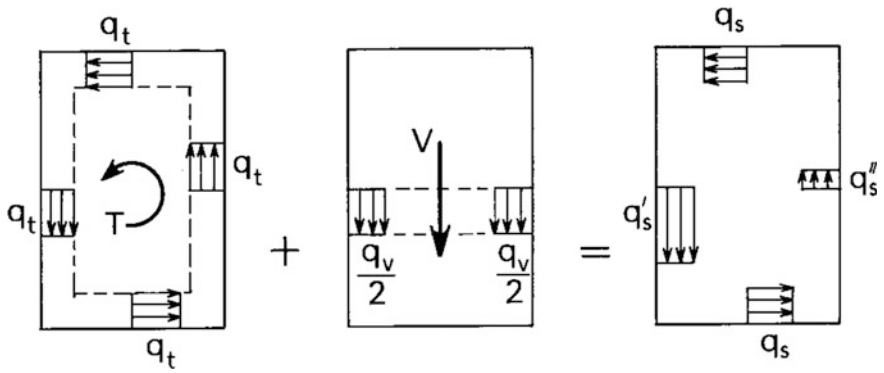


Fig. 8.17 Sum of fluxes in *V–T* interaction

similar to the ones of the longitudinal reinforcement, which also show again a linear combination of effects based on the *sum of fluxes* shown in Fig. 8.17: on each side of the section the stirrups should be verified with the relative longitudinal shear force q_s, q'_s or q''_s, calculating it with the algebraic sum of the two contributions of shear and torsion on the basis of the chosen inclination $\lambda_c = ctg\theta$ of the compressions.

8.1.3 Other Aspects of the Torsional Behaviour

The interaction formulas for bending-torsion and shear-torsion, derived with reference to the truss model and referred to the resistance of the reinforcement, are well confirmed by the experimental tests.

However, there are situations where the resistance is limited by the *compressions in concrete*. For example, in sections with big bending moments, the resistance of the compression chord can be significantly reduced by the simultaneous presence of the flux q of shear stresses due to torsion. Similarly, on the worse side of highly stressed webs under shear, di addition of the flux of compressions due to torsion can lead to the failure of concrete.

It is the case of highly reinforced sections, indeed not very frequent in common structures, for which the following empirical formulas have been proposed

$$\left(\frac{M_{Ed}}{M_{Rd}}\right)^2 + \left(\frac{T_{Ed}}{T_{cd}}\right)^2 < 1$$

$$\left(\frac{V_{Ed}}{V_{cd}}\right)^2 + \left(\frac{T_{Ed}}{T_{cd}}\right)^2 < 1$$

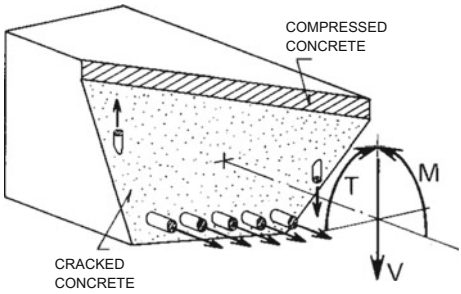


Fig. 8.18 Model of the skew section

For these formulas the correspondence with experimental results is less precise, although their approximations are generally conservative. A different interpretation of the interaction problems has been proposed with the *Theory of the skew section* (see Fig. 8.18), which, however, with respect to the resistance of the reinforcement, leads to results substantially identical to the ones given by the truss model.

The deformation behaviour of beams subject to torsion is related to a torsional stiffness k_t which in the uncracked state can be evaluated with

$$k_t = G_c J$$

according to the formulas presented at the beginning of this chapter and referred to the geometrical section of the concrete.

In the cracked state the torsional stiffness can be evaluated with reference to the truss model. Neglecting the axial deformability of the concrete struts in comparison to the one of the steel reinforcement, the torsional rotation ϕ between two sections at a distance s can be evaluated for example with the Principle of Virtual Work. On the beam segment subject to a unit torsional moment, one has the following stresses in the stirrups and in the longitudinal bars (with $\theta = 45°$):

$$\bar{\sigma}_s = \frac{1}{2A}\frac{s}{A_s}$$
$$\bar{\sigma}_l = \frac{1}{2A}\frac{u}{A_l}$$

On the beam segment subject to the moment T, for the same bars one has the deformations:

$$\varepsilon_s = \frac{\bar{\sigma}_s T}{E_s}$$
$$\varepsilon_l = \frac{\bar{\sigma}_l T}{E_s}$$

Therefore, setting the external work equal to the internal work one obtains:

$$1\phi = \int \bar{\sigma}\varepsilon \, \mathrm{dv}$$

which leads to

$$\phi = \bar{\sigma}_\mathrm{s}\varepsilon_\mathrm{s}A_\mathrm{s}\frac{u}{\mathrm{s}} + \bar{\sigma}_l\varepsilon_l A_l = u\frac{\frac{s}{A_\mathrm{s}} + \frac{u}{A_l}}{4A^2E_\mathrm{s}}T$$

A torsional stiffness is then deduced equal to

$$k_\mathrm{t} = \frac{T}{\phi} = E_\mathrm{s}\frac{4A^2A_\mathrm{s}A_l}{(sA_l + uA_\mathrm{s})u} = E_\mathrm{s}J'$$

As indicatively shown in Fig. 8.6, this estimation of the torsional stiffness of reinforced concrete beams in the cracked state is rather restrictive. The effects of tension stiffening related to tensions resisted by the concrete are in fact neglected, which are initially significant and decrease with the increase of the forces, similar to what happens in the deformation behaviour of beams in bending.

Non-uniform Torsion

What presented here refers to circulatory (or uniform) torsion characterized by closed fluxes of stresses, also in the case of non-circular sections when the constraints allow the warping of the sections. If instead the constraints prevent warping, a second contribution of *warping torsion* arises in addition to the first one.

However, this additional contribution remains negligible in the cases of compact sections, very frequent for beams in reinforced concrete, as for square and rectangular sections (see Fig. 8.19a), and for T or L-shaped sections (see Fig. 8.19b). The contribution of non-uniform torsion for I or C-shaped sections (see Fig. 8.19c) can instead be significant, thanks to the bi-flexural behaviour of the flanges when they are adequately constrained by the beam supports.

The bi- or multi-flexural behaviour becomes determining in the case of coupled beams (see Fig. 8.20a), where the torsion due to the eccentricity of the flexural load is balanced by a variable distribution of the load itself on the different beams: each beam is subsequently designed for simple bending. If instead the same beams are enclosed in a hollow section, with one or more voids (see Fig. 8.20b), the contribution of circulatory torsion is predominant, as it is the case in all closed sections with a Bredt behaviour.

Eventually, the particular case of folded plates is worth mentioning, consisting of a number of thin plates connected to each other forming cross sections that deform significantly under the applied loads (see Fig. 8.21). For this type of structures the beam behaviour is complicated due to the complex warping of the sections and the

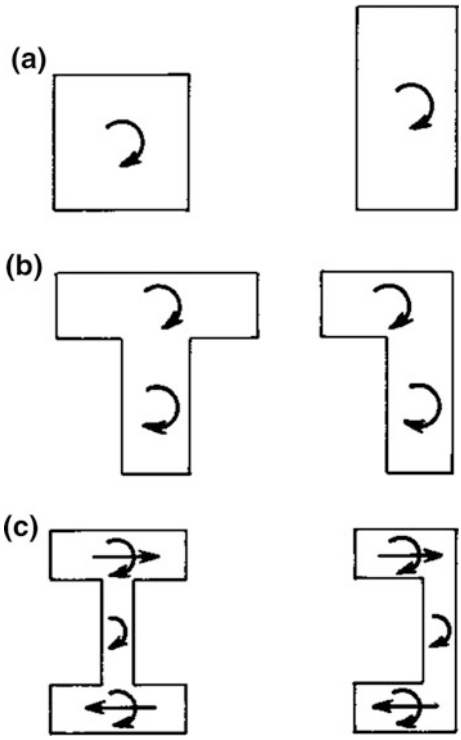


Fig. 8.19 Cases of circulatory (**a** and **b**) and warping (**c**) torsion

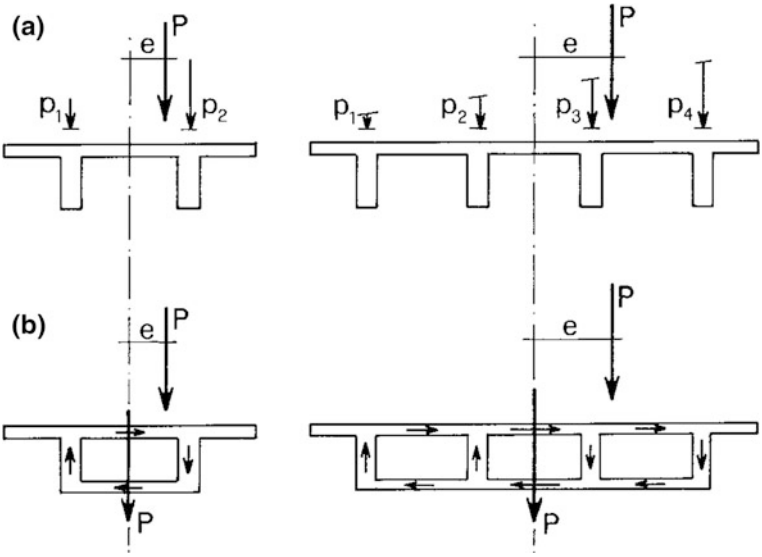


Fig. 8.20 Multiflexural (**a**) and circulatory (**b**) behaviour of a multi-rib deck

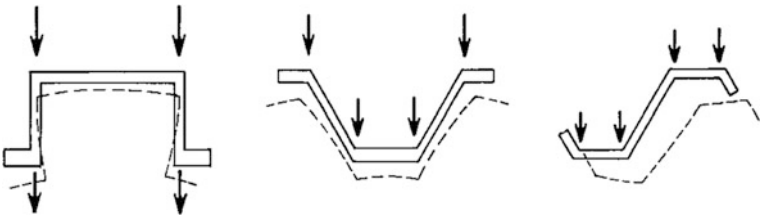


Fig. 8.21 Deformation warping effects in folded plates systems

fundamental contribution of transverse bending transferred between plates. Their design is therefore based on analysis methods substantially different from the ones described in this chapter.

8.2 Case A: Stability Core

In this section, the fundamental verifications relative to the overall stability of the multi-storey building described in Fig. 2.19 will be carried out. The main aspect to be evaluated is the resistance against horizontal forces. Assuming that the building is not located in a seismic zone and therefore that dynamic undulatory actions due to the vibration of its masses are not to be expected, the horizontal actions to be considered in the verifications are reduced to:

- *wind load* due to the kinetic pressure acting in the transverse or longitudinal direction of the building;
- *nominal force*, equal to a fraction of the weights, to approximately represent the sway horizontal effects due to the flexural actions on the columns, the systematic and unintentional eccentricities of loads and possibly the second order effects deriving from the floor drifts.

Wind Load

Reference will be made to Eurocode 1 and to the related Italian National Annex for the specific aspects of the considered site. The reference *kinetic pressure* on a plane obstacle is given by

$$q_b = \rho\, v_b^2/2 = v_b^2/1.6$$

having set ρ = 1.25 kg/m^3 the air density and having indicated with v_b the *reference wind speed* measured at ground level. The latter is given based on the location of the site and its altitude a_s by

$$v_b = v_{bo} + k_a(a_s - a_o) \geq v_{bo}$$

Assuming that the site is located in *Zone 1* (for example Lombardy) one has $v_{bo} = 25$ m/s, $k_a = 0.01$ and $a_o = 1000$ m. For a site located in flat land with $a_s < a_o$ one therefore obtains

$$v_b = v_{bo} = 25 \text{ m/s} \quad q_b = 391 \text{ N/m}^2$$

The *pressure* applied on the walls of the building is therefore calculated as

$$p = q_b c_e c_p c_d$$

where c_d is a *dynamic coefficient* (set = 1 for normal configurations), c_p is the *shape coefficient* (set = +0.8 for the windward pressure, = −0.4 for the downwind suction) and c_e is the *exposure coefficient,* function of the height z of the element concerned from ground level:

$$c_e = k_r^2 c_t \ln(z/z_o)[7 + c_t \ln(z/z_o)] \geq c_e(z_{min})$$

where c_t is the *topographic coefficient* (set here = 1 excluding locations on hills or dales). For a *rugosity Class B* (built suburban area) in the hinterland of Zone 1 an *exposure category IV* is deduced, for which one has $k_r = 0.22$, $z_o = 0.3$ m and $z_{min} = 8$ m.

At 18.0 m from the ground level (height of the building—see Fig. 8.22), one therefore has $c_e = 2.20$. A constant distribution of pressures and suctions is here assumed along the entire height with an intensity equal to the maximum value

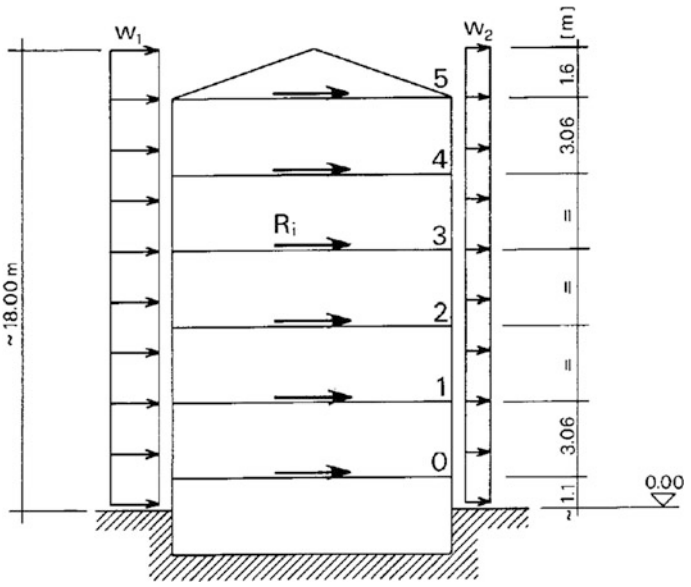


Fig. 8.22 Scheme of wind pressure on the building

calculated at 18 m, neglecting the reduction that, at the level z_{min} = 8 m, would lead to a coefficient c_e = 1.63:

$$p_1 = +391 \times 2.20 \times 0.8 = 688\,\text{N/m}^2$$
$$p_2 = -391 \times 2.20 \times 0.4 = -344\,\text{N/m}^2$$

Therefore in total the overturning action is equal to

$$p_1 - p_2 = 1032\ \text{N/m}^2$$

distributed along the entire height of the building.

Nominal Force
In addition to the wind action, the nominal one should be considered represented by a system of forces R concentrated at the floors and evaluated on the basis of the weights of the relative decks with

$$R_i = k(G_i + \psi_o Q_i)$$

where G_i are the permanent loads, Q_i the variable loads, ψ_o is their combination coefficient and k = 0.01 is the push coefficient. For the evaluation of the loads one can refer to Sect. 2.4.1.

As already mentioned at Sect. 2.4, the horizontal forces described above are concentrated, through the diaphragms consisting of the decks at the different floors, on the *stability core* made of the walls of the staircase.

8.2.1 Calculation of Internal Forces

The analysis for the evaluation of the forces in the corewall under the horizontal actions described above are shown below.

Conventional Force
For the calculation of the masses of the building, a further analysis of loads is carried in addition to the one shown at Sect. 2.4.1.

Average load for the type floor

Deck and other permanent loads	= 7.00 kN/m^2
Dropped beams	≅ 0.50 kN/m^2
Internal columns	≅ 0.25 kN/m^2
Live loads	= 1.40 kN/m^2
Total	= 9.15 kN/m^2

(also extended to the roof level)

Average load for areas with solid slab

Slab (including stairs ramps)	0.15 × 25	= 3.75 kN/m^2
Plaster	0.02 × 20	= 0.40 kN/m^2
Screed	0.06 × 20	= 1.20 kN/m^2
Flooring		= 0.40 kN/m^2
Parapet walls, rises, …		= 0.25 kN/m^2
Live loads (as internal areas)		= 1.40 kN/m^2
		= 7.40 kN/m^2

(difference with typical floor 7.40 – 9.15 = −1.75 kN/m^2)

Average load for external walls (also extended to roof level)

Typical masonry	= 11.30 kN/m
Windows	≅ −2.25 kN/m
Columns 0.1 × (7.50 − 3.00) × 2.82	≅ 1.25 kN/m
Total	= 10.30 kN/m

Stairs corewall loads (RC wall + plaster on both sides)

$$(0.20 \times 25 + 0.04 \times 20) \times 2.82 \times 20.0 \cong 327 \text{ kN}$$

The necessary calculations to evaluate the weight of a deck and its centre of gravity are shown in the following table (see Fig. 8.23).

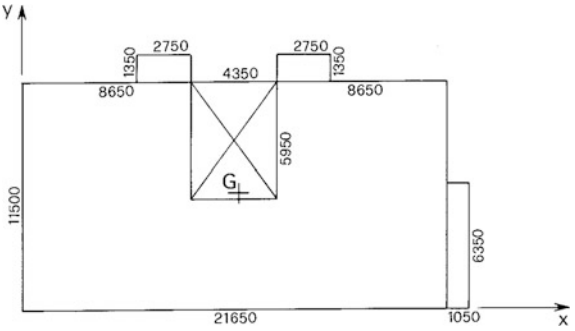


Fig. 8.23 Overall dimensions of the type floor

Loads on one floor								
a_i (m)	b_i (m)	A_i (m^2)	p (kNm)	r_i (kN)	x_i (m)	m_{yi} (kNm)	y_i (m)	m_{xi} (kNm)
21.65	11.50	249.0	9.15	2278	10.82	24,651	5.75	13,098
1.05	6.35	6.7	9.15	61	22.17	1359	3.17	193
5.50	1.35	7.4	7.40	55	10.82	593	12.17	666
4.35	5.95	25.9	−1.75	−45	10.82	−490	8.52	−383
21.65	…	…	10.30	223	10.82	2413	0.15	33
2.10	…	…	10.30	22	22.17	488	3.17	70
17.30	…	…	10.30	178	10.82	1926	11.35	2020
…	10.90	…	10.30	112	0.15	17	5.75	644
…	5.75	…	10.30	59	22.55	1330	3.17	187
…	5.15	…	10.30	53	21.50	1139	8.62	457
…	…	…	…	327	10.82	3538	8.52	2786
				3323		36,964		19,771

$$x_G = 36964/3323 = 11.12 \text{ m}$$
$$y_G = 19771/3323 = 5.95 \text{ m}$$

The resistance centre of the stability element can be assumed to be located on the centreline of the corewall, schematically represented by the rectangular outline of the perimeter walls (see Fig. 8.24). The coordinates of such centre are equal to:

$$x_o = 10.82 \text{ m}$$
$$y_o = 8.52 \text{ m}$$

For forces acting in the two directions x and y one therefore has the following eccentricities:

$$-e_y = -5.95 + 8.52 = 2.57 \text{ m}$$
$$e_x = 11.12 - 10.82 = 0.30 \text{ m}$$

whereas the conventional horizontal force for each floor, to be considered acting either in the direction x or in the direction y, is equal to:

$$R_i = 0.01 \times 3323 = 33.2 \text{ kN}$$

The following table shows the calculation of shear, bending and torsion forces on the stability core. The subsequent columns refer to:

- the serial number i of the deck, from the roof to the first floor;
- the conventional horizontal force R_i relative to each deck to be considered acting either in the x or y direction;

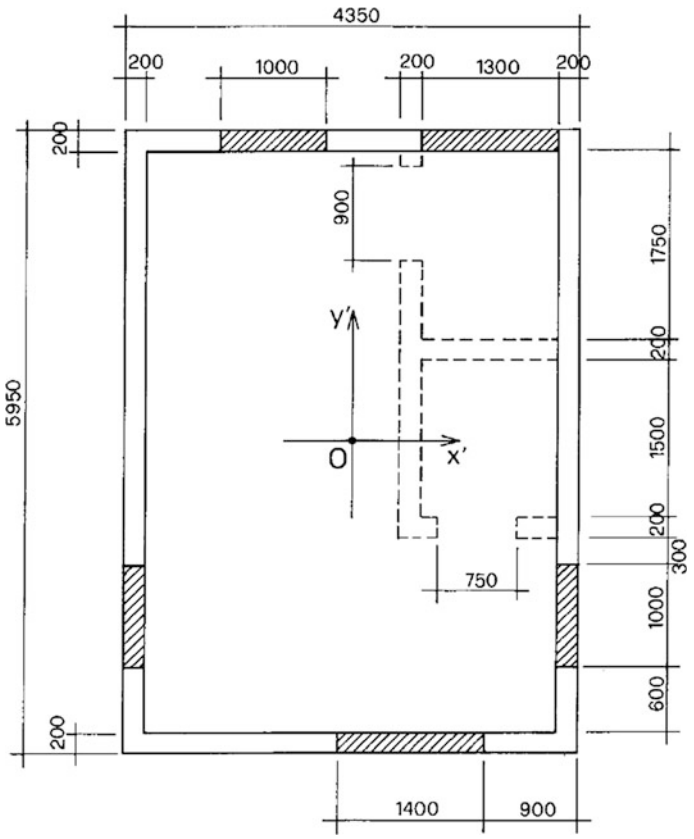


Fig. 8.24 Section of the stability core

- the shear force $V_i = R_i + V_{i+1}$, constant in the segment under the concerned deck and equal for actions along x or y;
- the height h_i of the storey below;
- the moment $M_i = V_i h_i + M_{i+1}$ at the bottom of the segment underneath and equal for action along x or y;
- the eccentricity e_{yi} of the force $R_{xi} = R_i$;
- the torsion $T_{xi} = V_i e_{yi}$ due to action along x, constant on the segment underneath;
- the eccentricity e_{xi} of the force $R_{yi} = R_i$;
- the torsion $T_{vi} = V_i e_{xi}$ due to action along y, constant on the segment underneath.

i	R_i (kN)	V_i (kN)	h_i (m)	M_i (kNm)	e_{yi} (m)	T_{xi} (kNm)	e_{xi} (m)	T_{yi} (kNm)
5	33.2	33.2	3.06	102	2.58	85.7	0.30	10.0
4	33.2	66.4	3.06	305	2.58	171.3	0.30	19.9
3	33.2	99.6	3.06	610	2.58	257.0	0.30	29.9
2	33.2	132.8	3.06	1016	2.58	342.6	0.30	39.8
1	33.2	166.0	3.06	1524	2.58	428.3	0.30	49.8

The analysis ends at the upper side of the deck "0" at the raised ground floor as the basement below consist of a box system of reinforced concrete walls extended to the entire perimeter of the building. The critical cross section of the corewall is therefore the one at level +1.10 m (see Fig. 8.22).

Wind Load

Regarding the wind loads, the following forces act at each floor:

$$W_{xi} = 1.032 \times 11.50 \times 3.06 \cong 36.3 \text{ kN} \quad \text{in the } x\text{-direction}$$

where $e'_{yi} = -5.75 + 8.52 = 2.77$ m

$$W_{yi} = 1.032 \times 22.70 \times 3.06 \cong 71.7 \text{ kN} \quad \text{in the } y\text{-direction}$$

where $e'_{xi} = 11.35 - 10.82 = 0.53$ m.

The following tables, similar to the previous one, contain the calculations of the forces on the stability core due to the actions specified above.

The global forces are obtained adding the effects of the conventional force to the ones due to wind:

Force along x						
i	W_i (kN)	V_i (kN)	h_i (m)	M_i (kNm)	e_i (m)	T_i (kNm)
5	36.3	36.3	3.06	111	2.77	100.6
4	36.3	72.6	3.06	333	2.77	201.1
3	36.3	108.9	3.06	666	2.77	301.7
2	36.3	145.2	3.06	1111	2.77	402.2
1	36.3	181.6	3.06	1666	2.77	503.0

Force along y						
i	W_i (kN)	V_i (kN)	h_i (m)	M_i (kNm)	e_i (m)	T_i (kNm)
5	71.7	71.7	3.06	219	0.53	38.0
4	71.7	143.4	3.06	658	0.53	76.0
3	71.7	215.1	3.06	1316	0.53	114.0

(continued)

(continued)

Force along y						
i	W_i (kN)	V_i (kN)	h_i (m)	M_i (kNm)	e_i (m)	T_i (kNm)
2	71.7	286.8	3.06	2194	0.53	152.0
1	71.7	358.5	3.06	3291	0.53	190.0

Force along x				Force along y		
i	M_i (kNm)	V_i (kN)	T_i (kNm)	M_i (kNm)	V_i (kN)	T_i (kNm)
5	213	69.5	186.3	321	104.9	48.0
4	638	139.0	372.4	963	209.8	95.9
3	1276	208.5	558.7	1926	314.7	143.9
2	2127	278.0	744.8	3210	419.6	191.8
1	3190	347.6	931.3	4815	524.5	239.8

Vertical Actions

Together with horizontal ones, there are vertical forces relative to the portion of loads that each floor transfers to the staircase walls. With reference to Fig. 2.23, the weights relative to the tributary areas of columns P12, P13, P19 and P20 are to be calculated, in addition to the ones of the staircase core itself. One can refer to the same analysis of loads carried here for the estimation of the loads of the type floor, removing the contribution of the internal columns.

- Loads on corewall and P12, P13, P19, P20

$2 \times 1.38 \times 1.35 \times 1.0$	$= 3.73 \times 7.40$	$= 28$ kN
$2 \times 1.38 \times 2.75 \times 1.0$	$= 7.59 \times 8.90$	$= 68$ kN
$2 \times 2.05 \times 5.60 \times 1.2$	$= 27.55 \times 8.90$	$= 245$ kN
$1 \times 4.35 \times 2.40 \times 1.2$	$= 12.53 \times 8.90$	$= 112$ kN
$1 \times 4.35 \times 5.95 \times 1.0$	$= 25.88 \times 7.40$	$= \underline{192 \text{ kN}}$
Total deck		$= 645$ kN
Deck		$= 645$ kN
Partitions	$2 \times 1.38 \times 10.30$	$= 28$ kN
Corewall		$= \underline{327 \text{ kN}}$
Total floor		$= 1000$ kN

Axial force on corewall		
i	F_i (kN)	N_i (kN)
5	1000	1000
4	1000	2000
3	1000	3000
2	1000	4000
1	1000	5000
0	1000	6000

The diagrams of the internal forces in the corewall, in its behaviour as a vertical cantilever fixed at the bottom, are shown on Fig. 8.25. Bending and torsional moments are to be considered with either sign, consistently with the possible inversion of the horizontal forces. Axial forces are deduced from the previous table.

8.2.2 *Verifications of the Current Section*

The exact analysis of the stress distribution in the corewalls, taking into account its irregularities in shape due for example to the presence of door or window openings, or the ones related to the articulated layout of the walls themselves, requires the elaboration of complex calculation algorithms. In a simplified way, the problem can be treated with the beam formulas, considering the cross section of the corewall as the one of a slender solid subject to the same internal forces considered in the classical de Saint-Vénant's theory. The first serviceability and resistance verifications can therefore be performed, which will hereby be carried under one global load condition. Local effects due to the above-mentioned irregularities can also be treated with simplified approximations and additional verifications to ensure equilibrium, according to the procedures described in the followings.

With reference to Fig. 8.24, firstly the resistance parameters of the current section of the corewall are calculated. In the bending parameter, the contribution of the internal walls will be neglected and one of the perimeter walls will be approximately modified as the openings were uniformly distributed along their length.

- *Area*

$2 \times 3.95 \times 0.20$	$= 1.58$
$2 \times 5.95 \times 0.20$	$= \underline{2.38}$
	$3.96\ \text{m}^2$
$-3 \times 1.00 \times 0.20$	$= -0.60$
$-1 \times 1.30 \times 0.20$	$= -0.26$
$-1 \times 1.40 \times 0.20$	$= \underline{-0.28}$
	$-1.14\ \text{m}^2$

Total perimeter walls = $2.82\ \text{m}^2$

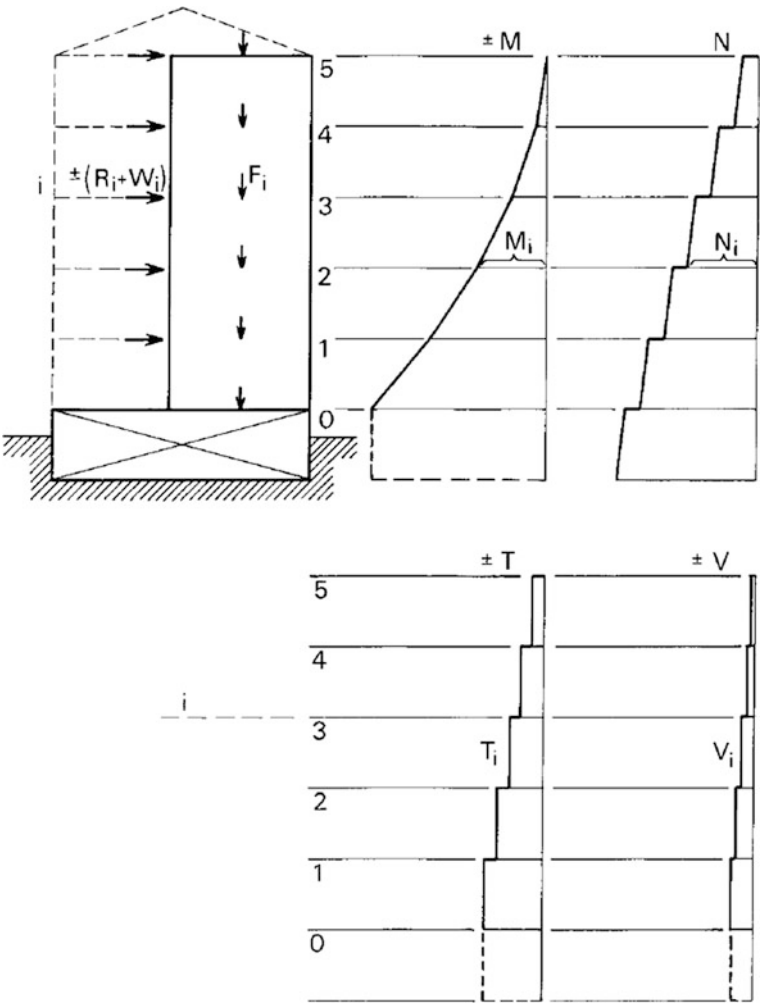


Fig. 8.25 Internal forces distribution in the corewall

2.75 × 0.20	= 0.55
1.85 × 0.20	= 0.37
	0.92

Total corewalls = 3.74 m^2
(2.82/3.96 ≅ 0.71)

- *Moments of inertia*

$1.58 \times 5.75^2/4$	$= 13.06$
$2.38 \times 5.95^2/12$	$= \underline{7.02}$
	$I_{x'} \cong 20.08 \times 0.71 = 14.26\ m^4$
$1.58 \times 3.85^2/12$	$= 2.05$
$2.38 \times 4.15^2/4$	$= \underline{10.25}$
	$I_{y'} \cong 12.30 \times 0.71 = 8.73\ m^4$

- *Torsional resistance*

$$2A_t = 2 \times 4.15 \times 5.75 = 47.72\ m^2$$

Maximum Stresses in Service

The serviceability verification of the bottom section of the raised ground floor therefore leads to the following values of stresses:

$$\sigma_0 = \frac{-5000}{3740} = -1.34\ N/mm^2$$
$$(\text{average compression})$$

Force along x ($e_x = 3190/5000 = 0.64$ m)

$$\Delta\sigma \cong \pm\frac{3190}{8730}2.175 = \pm 0.79\ N/mm^2 \quad (\text{due to moment})$$
$$\sigma_{min} = -1.34 - 0.79 = -2.13\ N/mm^2 \quad (\text{maximum compression})$$
$$\sigma_{max} = -1.34 + 0.79 = -0.55\ N/mm^2 \quad (\text{minimum compression})$$
$$\tau_v \cong \frac{1}{0.71}\frac{311.2}{0.8 \times 4.35 \times 400} = 0.31\ N/mm^2 \quad (\text{due to shear})$$
$$\tau_t = \frac{1}{0.71}\frac{931.3}{47.72 \times 200} = 0.14\ N/mm^2 \quad (\text{due to torsion})$$
$$\tau_{max} = 0.31 + 0.14 = 0.45\ N/mm^2$$

With conservative assumptions one obtains following principal stresses (maximum compression at one side and maximum tension at the other side):

$$\sigma_{II} \cong -\frac{1}{2}\left[2.13+\sqrt{2.13^2+4\times 0.45^2}\right] = -\frac{1}{2}(2.13+2.31) = -2.22\,\text{N/mm}^2$$

$$\sigma_{I} \cong +\frac{1}{2}\left[-0.55+\sqrt{0.55^2+4\times 0.45^2}\right] = +\frac{1}{2}(-0.55+1.05) = +0.25\,\text{N/mm}^2$$

Force along y $(e_y = 4815/5000 = 0.96\ \text{m})$

$$\Delta\sigma \cong \pm\frac{4815}{14260}2.975 = \pm 1.00\,\text{N/mm}^2 \quad \text{(due to moment)}$$

$$\sigma_{\min} = -1.34 - 1.00 = -2.34\,\text{N/mm}^2 \quad \text{(maximum compression)}$$

$$\sigma_{\max} = -1.34 + 1.00 = -0.34\,\text{N/mm}^2 \quad \text{(minimum compression)}$$

$$\tau_v \cong \frac{1}{0.71}\frac{524.5}{0.8\times 5.95\times 400} = 0.39\,\text{N/mm}^2 \quad \text{(due to shear)}$$

$$\tau_t = \frac{1}{0.71}\frac{239.8}{47.72\times 200} = 0.04\,\text{N/mm}^2 \quad \text{(due to torsion)}$$

$$\tau_{\max} = 0.39 + 0.04 = 0.43\,\text{N/mm}^2$$

With conservative assumptions one has the following principal stresses (maximum compression at one side and maximum tension at the other side):

$$\sigma_{II} \cong -\frac{1}{2}\left[2.34+\sqrt{2.34^2+4\times 0.43^2}\right] = -\frac{1}{2}(2.34+2.49) = -2.42\ \text{N/mm}^2$$

$$\sigma_{I} \cong +\frac{1}{2}\left[-0.34+\sqrt{0.34^2+4\times 0.43^2}\right] = +\frac{1}{2}(0.34+0.92) = +0.29\ \text{N/mm}^2$$

Verifications

These calculations, although within the relevant approximations made, show a stress level largely within the allowable limits (see Sect. 2.4.1):

- maximum principal stress in compression

$$2.42 < \bar{\sigma}_c \quad (= 11.2\,\text{N/mm}^2)$$

- maximum principal stress in tension

$$0.29 < f_{ctk} \quad (= 1.95\ \text{N/mm}^2)$$

However, an adequate reinforcement is to be provided, calculated as indicated further on.

Resistance Verifications—Normal Forces

For the resistance verifications, the superposition formulas deduced at Sect. 8.1.2 are initially applied. For the forces normal to the corewall section one therefore has, on the two windward and leeward chords, an overall longitudinal force equal to

$$2H = \pm\frac{M}{a} + \frac{T/2}{2A_t/u} - \frac{N}{2}$$

having indicated the longitudinal force on each of the four corners of the corewall with H. The perimeter of the resisting section is equal to:

$$u = 2(4.15 + 5.75) = 19.80 \text{ m}$$

with $2A_t/u$ = 47.72/19.80 = 2.41 m. The resistance in compression of one of the four corners is equal on average (without considering the reinforcement):

$$\bar{H}_{Rd} \cong 0.71 f'_{cd} t\, u/4 = 0.71 \times 1.13 \times 20 \times 1980/4 = 7240 \text{ kN}$$

However, the particular layout of openings in the walls isolates a corner with smaller dimensions (see Fig. 8.24), with

$$H_R \cong 1.13 \times 20 \times (90 + 60) = 3390 \text{ kN}$$

According to this procedure, it can therefore be noted how the resistance is concentrated on the four corners of the box wall system, how the axial force N (vertical) is equally divided, how the bending moment M is simply decomposed into the couple of compressions on the windward corners and tensions on the leeward corners with the lever arm a to be calculated in an approximated way and eventually how the contribution of longitudinal tensions due to the torsional moment is added. The latter contribution is exchanged between reinforcement in tension and the concrete web diagonals in compression in Rausch's spatial truss model and it is to be calculated for the behaviour in the cracked state. In the uncracked state the effect of the torsional moment remains the flux $q = \tau_t$ of shear stresses in a closed circuit. However, the presence of openings in the perimeter walls significantly modifies such behaviour.

Force along x (assumed $a \cong 0.8 \times 4.15 = 3.32$ m).

$$\frac{M}{a} = \frac{3190}{3.32} = 961 \text{ kN}$$

$$\frac{T/2}{2A_t/u} = \frac{931.3}{2 \times 2.41} = 193 \text{ kN}$$

$$\frac{N}{2} = \frac{5000}{2} = 2500 \text{ kN}$$

$$2H' = +961 + 193 - 2500 = -1346 \text{ kN (corners with lower compression)}$$

The section remains uncracked.

$$2H'' = -961 - 2500 = -1346 \text{ kN (corners with higher compression)}.$$

Therefore, on a leeward corner one has, with $\gamma_F = 1.5$, a design value of the applied force equal to

$$H''_{Ed} = 1.5 \times 3461/2 = 2596 \text{ kN} \quad (< H_{Rd})$$

Force along y (assumed $a \cong 0.8 \times 5.75 = 4.60$ m)

$$\frac{M}{a} = \frac{4815}{4.60} = 1047 \text{ kN}$$
$$\frac{T/2}{2A_t/u} = \frac{2398}{2 \times 2.41} = 50 \text{ kN}$$
$$\frac{N}{2} = \frac{5000}{2} = 2500 \text{ kN}$$
$$2H' = +1047 + 50 - 2500 = -1403 \text{ kN (corners with lower compression)}$$

The section remains uncracked.

$$2H'' = -1047 - 2500 = -3547 \text{ kN (corners with higher compression)}.$$

Therefore, on a leeward corner one has, again with $\gamma_F = 1.5$, a force equal to

$$-H''_{Ed} = 1.5 \times 3547/2 = 2660 \text{ kN} \quad (< H_{Rd})$$

The small eccentricity of the axial load with respect to the dimensions of the corewall does not require the contribution of the longitudinal bars for the resistance. In any case, a minimum amount of longitudinal bars has to be provided according to the reinforcement criteria of columns, and to resist local actions due to shape irregularities.

Reinforcement Design

The reinforcement layout of the corewalls are shown in Figs. 8.26 and 8.27.

The longitudinal bars, designed as mentioned above, are placed mainly at the corners of the core and at the edges of the openings, and stirrups are to be provided similar to common columns.

The reinforcement can be eventually completed on the current portions of the walls with two sets of orthogonal layers, designing the vertical bars on the minimum value (see Chart 2.11):

$$a_s = 0.0030 \text{ t} = 0.30 \times 20 = 6.0 \text{ cm}^2/\text{m}$$

which corresponds to 1 + 1ϕ10/250 (6.29 cm^2/m).

Designing the horizontal ones with reference to the minimum value (see also Chart 2.11):

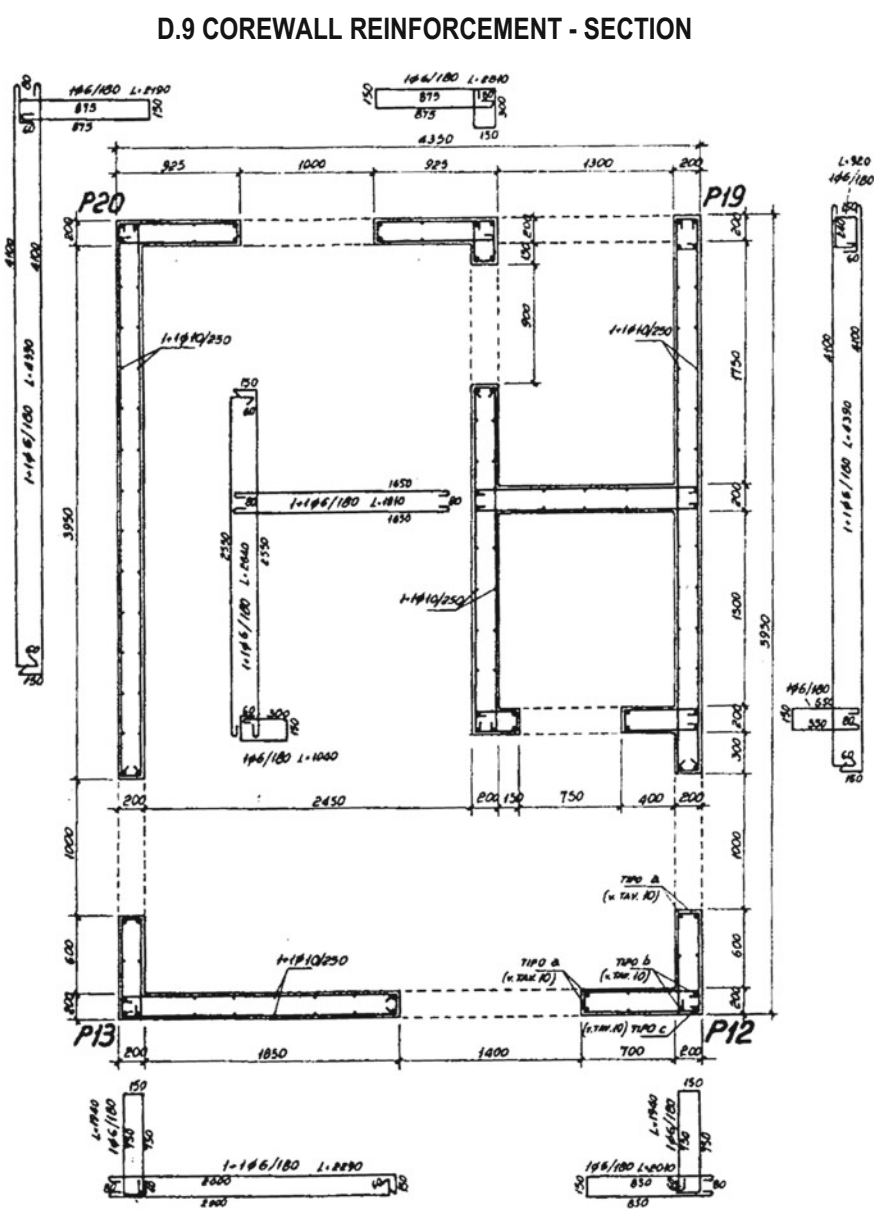


Fig. 8.26 Corewall reinforcement—section

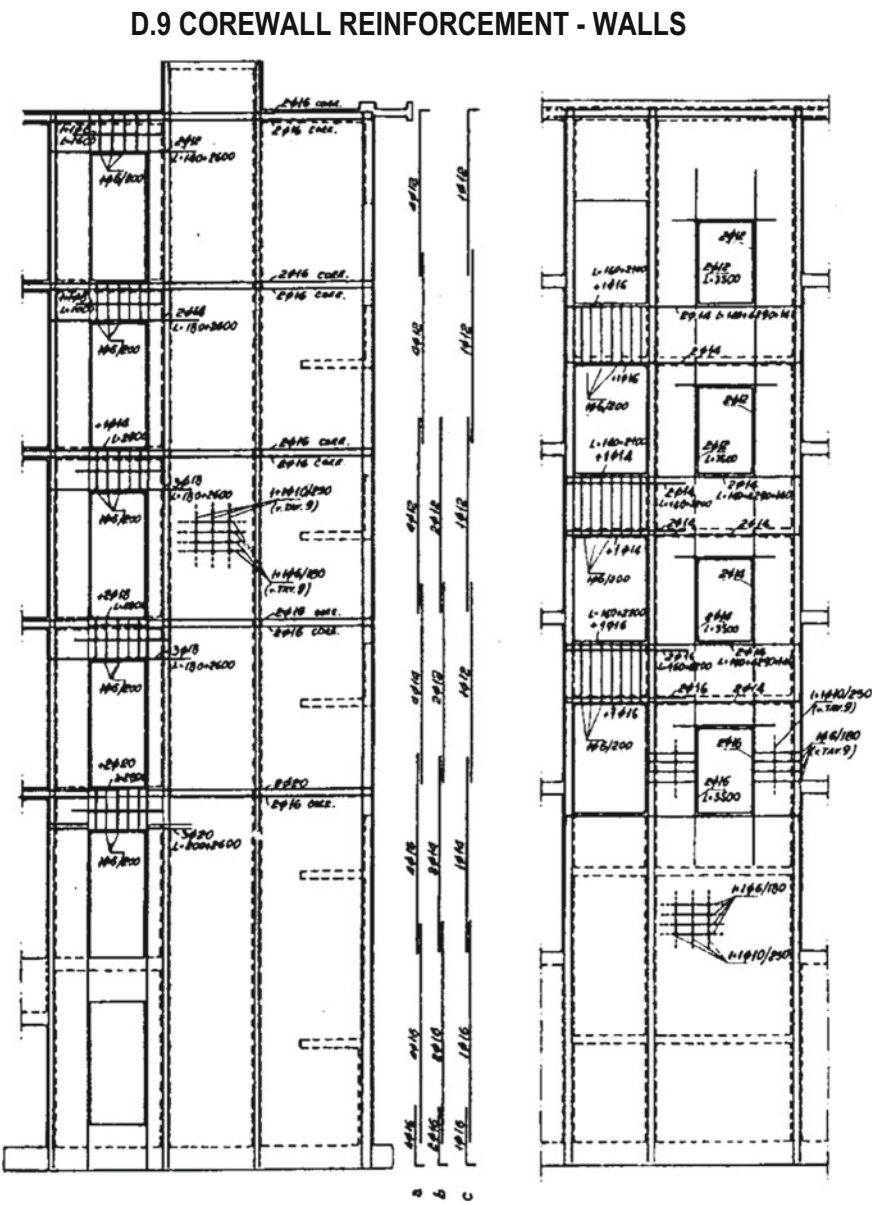


Fig. 8.27 Corewall reinforcement—walls

$$a_h = 0.0015\ t = 0.15 \times 20 = 3.0\ cm^2/m$$

which corresponds to 1 + 1ϕ6/180 (3.17 cm^2/m).

For the horizontal reinforcement, the value calculated above is to be verified and possibly increased on the basis of the shear forces on the walls due to shear and torsion. For an isostatic distribution of forces, the shear forces at the different storeys that relate to the two sets of shear walls (the ones oriented along x and the ones oriented along y) with the summations

$$V' = \frac{V}{2} + \frac{T}{2A_t}a_x \quad V'' = \frac{V}{2} - \frac{T}{2A_t}a_y$$

In the two directions one has, respectively,

$$2A_t/a_x = 47.72/4.15 = 11.50\ m$$
$$2A_t/a_y = 47.72/5.75 = 8.30\ m$$

The shear forces in the walls are taken from the competent table of the previous section:

i	Along x		P13–P12	P20–P19
	$V_i/2$	$T_i a_x/2A_t$	V'_{xi}	V''_{xi}
	(kN)	(kN)	(kN)	(kN)
5	34.7	16.2	50.9	18.5
4	69.5	32.4	101.9	37.1
3	104.3	48.6	152.9	55.7
2	139.0	64.8	203.8	74.2
1	173.8	81.0	254.8	92.8

i	Along y		P12–P19	P13–P10
	$V_i/2$	$T_i a_y/2A_t$	V'_{yi}	V''_{yi}
	(kN)	(kN)	(kN)	(kN)
5	52.4	5.8	58.2	46.6
4	104.9	11.6	116.5	93.3
3	157.3	17.3	174.6	140.0
2	209.8	23.1	232.9	186.7
1	262.2	28.9	291.1	233.3

Only the design of the shear wall between the columns P_{12} and P_{13} is here reported, for which at the lower storey, with $\gamma_F = 1.5$, one has a force equal to

$$V_{\mathrm{Ed}} = 1.5 \times 254.8 = 382 \text{ kN}$$

With an effective depth reduced by the opening present in the wall, one has

$$z \cong 0.8(4.15 - 1.40) = 2.20 \text{ m}$$

from which, assuming $\lambda_c = 2.0$, one obtains, with $1 + 1\phi 6/180$, a resistance in tension-shear equal to:

$$V_{\mathrm{sd}} \cong a_{\mathrm{h}} z f_{\mathrm{yd}} \lambda_{\mathrm{c}} = 3.17 \times 2.20 \times 39.1 \times 2.0 = 545 \text{ kN} > V_{\mathrm{Ed}} = 382 \text{ kN}$$

The minimum reinforcement is therefore adequate. The resistance in compression-shear remains higher

$$V_{\mathrm{cd}} = z b_{\mathrm{w}} f_{\mathrm{c2}} \lambda_{\mathrm{c}} / \left(1 + \lambda_{\mathrm{c}}^2\right) = 2.20 \times 200 \times 7.1 \times 2/5 = 1250 \text{ kN}$$

What mentioned above does not take into account the local flexural effects in the two wall posts separated by the opening.

8.2.3 *Verifications of Lintels and Stairs*

In order to ensure a combined action between the different parts of the corewall, as it has been assumed in the calculations carried in the previous paragraph, the lintels of the wall openings, working as coupling beams, should be able to transfer the longitudinal shear forces due to shear and torsion. The openings can also isolate slender wall panels that have a prevalent flexural behaviour in the resistance to horizontal actions.

Coupling Beam

We start with the design of the lintel in the walls directed along y, assuming the shear force V'_{yi} calculated in the previous paragraph. For the verifications one can refer to what presented at Sect. 5.2.2. With reference to the symbols used in Fig. 5.24, the geometrical characteristic of the lintel are (see Fig. 8.28):

$$h = 80 \text{ cm} \quad a = 100 \text{ cm} \quad b = 20 \text{ cm}$$
$$z \cong 0.84\, h = 67 \text{ cm} \quad l \cong a + 0.16\, h \cong 113 \text{ cm}$$

An eccentricity of the longitudinal shear force Q is also assumed, equal to

$$e \cong l/6 \cong 19 \text{ cm}$$

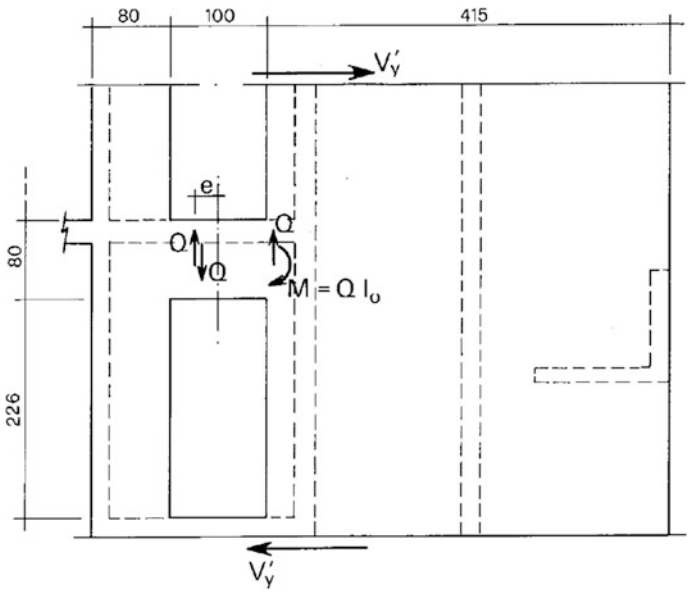


Fig. 8.28 Action acting on lintels

It is therefore obtained:

$$\lambda = \frac{1}{z} = 1.69 \qquad 1 + \lambda^2 = 3.86$$
$$\frac{\lambda}{2} + \frac{e}{z} = 1.13 \quad l_o = 1.13 \times 0.67 = 0.76 \text{ m}$$

The calculations are summarized in the following table where the different columns indicate:

- the serial number i of the floor, from the roof to the first floor;
- the shear force V'_{yi} at each floor for forces along y taken from the previous table;
- the longitudinal shear force $Q_{Ed} = \gamma_F V'_{yi} h_i / z_i$ transferred by the coupling beam, with $h_i (= 3.06 \text{ m})$ the floor height, $z_i (\cong 4.60 \text{ m})$ the estimated value of the resisting lever arm of the wall and $\gamma_F = 1.5$;
- the resistance $Q_{Rd} = 0.55 hbf_{cd}/(1 + \lambda^2)$ calculated on the basis of the web strut, replaced by the greater resistance of an increased stirrup quantity where necessary;
- the necessary longitudinal reinforcement $A_{lo} = Q_{Ed}(\lambda/2 + e/z)/f_{vd}$ on each of the chords, top and bottom, of the lintel;
- the actual reinforcement $n\phi$ determined for the lower edge (the top one already has the current reinforcement of the floor beam);
- the corresponding actual area A_l;
- the actual stirrups ϕ/s present in the coupling beam;

- the corresponding actual unit area a_s.

In particular the resisting value of the longitudinal shear force that does not take into account the reinforcement is

$$Q_{\mathrm{Rd}} = 0.55 \times 80 \times 20 \times 1.42/3.86 = 324 \text{ kN}$$

whilst the minimum amount of stirrups required based on the criterion on non-brittle failure (see QDR. 4.5) remains:

$$a_{\mathrm{s}} = 0.2 b f_{\mathrm{ctm}}/f_{\mathrm{yk}} = 0.2 \times 2000 \times 2.78/450 = 2.47 \text{ cm}^2/\text{m}$$

i	V'_{yi} (kN)	Q_{Ed} (kN)	Q_{Rd} (kN)	A_{lo} (cm^2)	l. bars (nΦ)	A_l (cm^2)	Stirrups (ϕ/s)	a_{s} (cm^2/m)
5	58.2	58.2	324	1.68	2ϕ12	2.26	1ϕ6/200	2.83
4	116.5	116.2	324	3.36	2ϕ14	3.39	1ϕ6/200	2.83
3	174.6	174.2	324	5.05	2ϕ18	5.09	1ϕ6/200	2.83
2	232.9	232.4	324	6.72	3ϕ18	7.63	1ϕ6/200	2.83
1	291.1	290.5	324	8.40	3ϕ20	9.42	1ϕ6/200	2.83

Stair Flight

The current section, dedicated to the design of the stability core of the multi-storey building in reinforced concrete analyzed in the previous chapters, is now concluded. Only few calculations, carried according to approximated procedures, have been presented.

In addition the design of the stairs with cantilevering steps is also briefly presented (see Fig. 8.29). The analysis of loads, carried in the horizontal plan, leads to the following values.

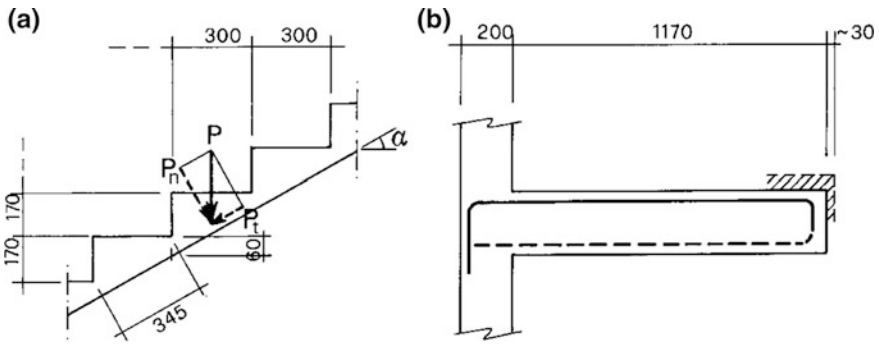


Fig. 8.29 Geometric details of stairs

Stairs loads

RC structure	$25 \times (0.23 + 0.06)/2$	$\cong$ 3.60 kN/m^2
Plaster	$1.1 \times 0.02 \times 20$	= 0.44 kN/m^2
Screed	$1.6 \times 0.04 \times 20$	= 1.28 kN/m^2
Flooring and risers	1.7×0.40	= 0.68 kN/m^2
Total permanent		= 6.00 kN/m^2
Live		= 4.00 kN/m^2
Total distributed		= 10.00 kN/m^2
Steel railing		= 0.60 kN/m

The bending component p_n perpendicular to the plate is obtained with:

$$\cos \alpha = \frac{30.0}{34.5} = 0.87$$

and therefore for the cantilever of Fig. 8.27b, assuming a design span equal to:

$$l \cong 1.05 \times 1.20 = 1.26 \text{ m}$$

the following fixed-end moment is obtained for a single step:

$$10.00 \times 1.26^2/2 = 7.94$$
$$0.60 \times 1.26 = 0.76$$
$$M_{\text{Ek}} = 8.70 \times 0.30 \times 0.87 = 2.27 \text{ kNm}$$

For the bending resistance verification, one has (see Fig. 8.30):

$$M_{\text{Ed}} = \gamma_{\text{F}} M_{\text{Ek}} = 1.43 \times 2270 = 3246 \text{ Nm}$$

and, with

$$\text{b} = 34.5 \text{ cm} \quad \text{d} \cong 14.0 \text{ cm}$$
$$A_{\text{s}} = 0.79 \text{ cm}^2 \quad (1\phi 10/\text{step})$$

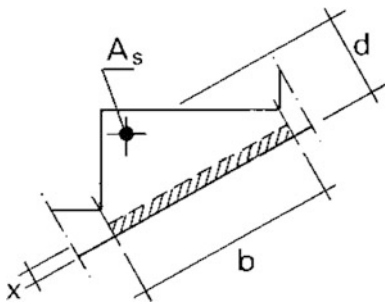


Fig. 8.30 Moment resisting section of a step

one obtains, neglecting the reinforcement in compression:

$$\omega_s = \frac{0.79 \times 391}{34.5 \times 14.0 \times 14.2} = 0.0450 \quad (\ll \omega_{sa})$$
$$z = 0.96 \times 14.0 = 13.4 \text{ cm}$$
$$M_{Rd} = 391 \times 79 \times 0.134 = 4139 \quad (> M_{Ed})$$

The reinforcement details of a ramp are shown in Fig. 8.31.

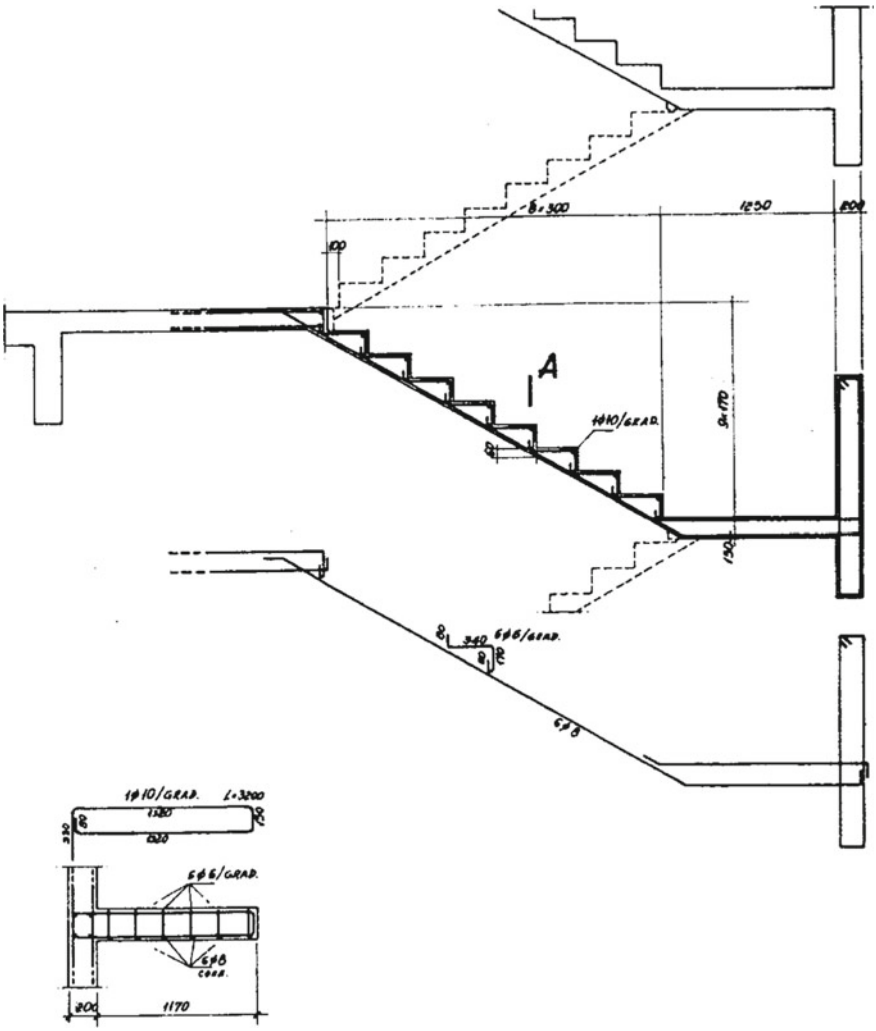


Fig. 8.31 Stair reinforcement

Appendix: Torsion

Table 8.1: Torsion: Elastic Design—Formulas

Reinforced concrete elements subject to circulatory torsion.

Symbols

T	Torsional moment
W	Resisting torsional module of the section
J	Torsional moment of inertia of the section
τ	Maximum shear stress
G	Elastic shear modulus
χ	Torsional curvature
h_s	Depth of resisting section
b_s	Width of resisting section
$A = h_s b_s$	Area enclosed by the resisting perimeter reinforcement
A_s	Sectional area of a closed stirrup
s	Spacing of stirrups
$a_s = A_s/s$	Unit area of stirrups
A_l	Total area of longitudinal bars
$u = 2(h_s + b_s)$	Perimeter of resisting peripheral reinforcement
$a_l = A_l/u$	Unit area of longitudinal reinforcement

Uncracked Section

- *Circular section* (r = radius of the section)

$$J = \frac{\pi r^4}{2} \quad \chi = \frac{T}{GJ}$$
$$W = \frac{\pi r^3}{2} \quad \tau = \frac{T}{W}$$

- *Circluar hollow section* (r_e, r_i = external and internal radii)

$$J = \frac{\pi}{2}(r_e^4 - r_i^4) \quad \chi = \frac{T}{GJ}$$
$$W = \frac{J}{r_e} \qquad \tau = \frac{T}{W}$$

- *Rectangular section* (h, b = longer and shorter sides)

$$J = k_2 h b^3 \qquad \chi = \frac{T}{GJ}$$
$$W = k_1 h b^2 \qquad \tau = \frac{T}{W}$$
$$k_1 = \frac{1}{3 + 1.8\beta} \quad k_2 = \frac{1}{3 + 4.1\sqrt{\beta^3}}$$

with $\beta = b/h \leq 1$.

Section composed of rectangles (h_i, b_i = sides of the i-th rectangle)

$$J_i = k_{2i} h_i b_i^3$$
$$J = \sum J_i \quad \chi = \frac{T}{GJ}$$
$$T_i = \frac{J_i}{J} T$$
$$W_i = k_{1i} h_i b_i^2 \quad \tau = \frac{T}{W_i}$$

Thin hollow section (t, t_o = current and minimum thicknesses)

$$J = 4A^2 / \oint \frac{dl}{t} \quad \chi = \frac{T}{GJ}$$

where A is the area enclosed by the mid-fiber and l is the abscissa along the mid-fiber

$$W = 2At_o \quad \tau = \frac{T}{W}$$

In particular for a thickness t = const.:

$$J = 4A^2 t / L \quad L = \text{perimeter on the mid-fiber}$$

For sides with thickness t_i = cost.:

$$J = 4A^2 / \sum L_i / t_i \quad L_i = \text{length of the } i\text{-th side.}$$

Rectangular Cracked Section

RC straight beam with constant cross section, subject to simple torsion in the cracked elastic stage, reinforced with longitudinal bars and transverse stirrups.

Stress in stirrups

$$\sigma_s = \frac{T}{2Aa_s} \quad \text{circulatory tension}$$

Stress in longitudinal bars

$$\sigma_l = \frac{T}{2Aa_l} \quad \text{longitudinal tension}$$

Peripheral concrete stress

$$\sigma_c = \frac{T}{At} \quad \text{compression inclined at } 45^\circ$$

with

$$A_c = bh \quad u_c = 2b + 2h$$
$$t = A_c/u_c \geq 1.5c$$
$$b_s = b - t \quad h_s = h - t$$
$$A = b_s h_s$$

where b and h are the longer and shorter sides of the section and c is the concrete cover at the axis of the bar placed at the corners.

Chart 8.2: Torsion: Resistance Design—Formulas

Reinforced concrete straight elements with constant cross section, subject to circulatory torsion, at the resisting ultimate limit state of the cracked phase, reinforced with longitudinal bars and transverse stirrups.

Symbols

T_{Ed}	Design value of torsion
T_{Rd}	Design value of torsional resistance
T_{sd}	Torsional resistance from stirrups
T_{ld}	Torsional resistance from longitudinal bars
T_{cd}	Torsional resistance from concrete
θ_{I}	Angle of initial cracking due to torsion
θ	Angle of peripheral compressions on the beam axis
$\lambda_{\mathrm{I}} = ctg\theta_{\mathrm{I}}$	Inclination of initial cracking due to torsion
$\lambda_{\mathrm{c}} = ctg\theta$	Inclination of peripheral compressions in concrete
σ_{I}	Tensile principal stress corresponding to τ

see also Charts 2.2, 2.3, 8.1.

Resistance with Isostatic Truss

With $\lambda_{\mathrm{I}} = \lambda_{\mathrm{c}} = 1$ it is set

$$T_{\mathrm{Rd}} = \min(T_{\mathrm{sd}}, T_{ld}, T_{\mathrm{cd}}) \geq T_{\mathrm{ad}}$$

where

$$T_{\mathrm{sd}} = 2Aa_{\mathrm{s}} f_{\mathrm{yd}} \quad \text{tension-torsion from stirrups}$$
$$T_{ld} = 2Aa_l f_{\mathrm{yd}} \quad \text{tension-torsion from longitudinal bars}$$
$$T_{\mathrm{cd}} = Atf_{\mathrm{c2}} \quad \text{compression-torsion from concrete}$$

Resistance with Given Truss

Assumed λ_c in the interval $\lambda_{min} \leq \lambda_c \leq \lambda_{max}$, one can set

$$T_{Rd} = \min(T_{sd}, T_{ld}, T_{cd}) \geq T_{Ed}$$

where

$$\begin{aligned} T_{sd} &= 2Aa_s f_{yd}\lambda_c \quad \text{tension-torsion from stirrups} \\ T_{ld} &= 2Aa_l f_{yd}/\lambda_c \quad \text{tension-torsion from longitudinal bars} \\ T_{cd} &= 2Atf_{c2}\lambda_c/\left(1+\lambda_c^2\right) \quad \text{compression-torsion from concrete} \end{aligned}$$

and where for simple torsion one has:

$$\begin{aligned} \lambda_I &= \tau/\sigma_I = 1.0 \\ \lambda_{min} &= \lambda_I/2.5 = 0.4 \\ \lambda_{max} &= 2.5\,\lambda_I = 2.5 \end{aligned}$$

Resistance with Calculated Truss

$$\lambda_r = \sqrt{a_l/a_s}$$

- *High shear reinforcement ratio* $(\lambda_r < \lambda_{min})$

$$T_{Rd} = \min(T_{ld}, T_{cd}) \geq T_{Ed}$$

where

$$\begin{aligned} T_{ld} &= 2Aa_l f_{yd}/\lambda_{min} = 5Aa_l f_{yd} \quad (< T_{sd}) \\ T_{cd} &= 2Atf_{c2}\lambda_{min}/\left(1+\lambda_{min}^2\right) = 0.69Atf_{c2} \end{aligned}$$

- *Balanced reinforcement* $(\lambda_{min} \leq \lambda_c \leq \lambda_{max})$

$$T_{Rd} = \min(T_{sd}, T_{cd}) \geq T_{Ed}$$

where

$$\begin{aligned} T_{sd} &= 2Aa_s f_{yd}\lambda_r \quad (= T_{ld}) \\ T_{cd} &= 2Atf_{c2}\lambda_r/\left(1+\lambda_r^2\right) \end{aligned}$$

- *Low shear reinforcement ratio* $(\lambda_r > \lambda_{max})$

$$T_{Rd} = \min(T_{sd}, T_{cd})$$

where

$$T_{sd} = 2Aa_s f_{yd}\lambda_{max} = 5Aa_s f_{yd} \quad (< T_{ld})$$
$$T_{cd} = 2Atf_{c2}\lambda_{max}/\left(1+\lambda_{max}^2\right) = 0.69Atf_{c2}$$

Chart 8.3: Torsion: Interaction Formulas

Reinforced concrete elements subject to torsion, uniaxial bending, shear and axial force.

Symbols

N_{Ed}	Design value of applied axial force
M_{Ed}	Design value of applied bending moment
M_{Rd}	Design value of resisting bending moment
V_{Ed}	Design value of applied shear force
V_{cd}	Design value of resistance by compression-shear
z	Distance between tension and compression chords
y_s	Distance between tension chord and axial force axis
y_c	Distance between compression chord and axial force axis
λ_c'	Inclination of higher compressions
λ_c''	Inclination of lower compressions
λ_c	Mean inclination of web compressions
A_s	Area of longitudinal reinforcement in tension under M_{Ed}
A_s'	Area of longitudinal reinforcement in compression under M_{Ed}
a_s'	Unit area of stirrups on the side under higher tension
a_s''	Unit area of stirrups on the side under lower tension
$\bar{x}$	Depth of compression chord
b	Width of compression chord
b_w	Width of web

see also Charts 2.2, 2.3, 3.11, 4.2, 6.12, 8.1 and 8.2.

Notes on Truss Model

In the following interaction formulas M_{Ed}, V_{Ed}, T_{Ed} are assumed with the absolute value, whereas N_{Ed} is intended positive in tension and of small magnitude ($M_{\mathrm{Ed}} \gg |N_{\mathrm{Ed}}|z$). The inclination λ_c'' is assumed positive if rising like λ_c', negative if falling.

For the elements of the truss model the resistance verifications are therefore set as shown hereby.

- *Tension chord* (due to M_{Ed})

$$Z_{\mathrm{Ed}} = N_{\mathrm{Ed}} \frac{y_{\mathrm{c}}}{z} + M_{\mathrm{Ed}} \frac{1}{z} + V_{\mathrm{Ed}} \frac{\lambda_{\mathrm{c}}}{2} + T_{\mathrm{Ed}} \frac{\lambda_{\mathrm{c}}}{4A} < A_{\mathrm{s}} f_{\mathrm{yd}}$$

- *Compression chord* (due to M_{Ed})

$$C_{\mathrm{Ed}} = +N_{\mathrm{Ed}} \frac{y_{\mathrm{s}}}{z} - M_{\mathrm{Ed}} \frac{1}{z} + V_{\mathrm{Ed}} \frac{\lambda_{\mathrm{c}}}{2} + T_{\mathrm{Ed}} \frac{\lambda_{\mathrm{c}}}{4A} < A_{\mathrm{s}}' f_{\mathrm{yd}}$$

  if from the formula above one obtains $C_{\mathrm{Ed}} < 0$, it is set:

$$(*) C_{\mathrm{Ed}} = -N_{\mathrm{Ed}} \frac{y_{\mathrm{s}}}{z} + M_{\mathrm{Ed}} \frac{1}{z} - V_{\mathrm{Ed}} \frac{\lambda_{\mathrm{c}}}{2} < b\bar{x} f_{\mathrm{cd}} + A_{\mathrm{s}}' f_{\mathrm{yd}}$$

- *Transverse stirrup* (side with higher tension)

$$q_{\mathrm{sd}}' = \left[V_{\mathrm{Ed}} \frac{1}{2z} + T_{\mathrm{Ed}} \frac{1}{2A} \right] \frac{1}{\lambda_{\mathrm{c}}'} < a_{\mathrm{s}}' f_{\mathrm{yd}}$$

- *Transverse stirrup* (side with lower tension)

$$q_{\mathrm{sd}}'' = \left[V_{\mathrm{Ed}} \frac{1}{2z} - T_{\mathrm{Ed}} \frac{1}{2A} \right] \frac{1}{\lambda_{\mathrm{c}}''} < a_{\mathrm{s}}'' f_{\mathrm{yd}}$$

- *Diagonal in compression* (more stressed side)

$$(*) \bar{q}_{\mathrm{cd}}' = \left[V_{\mathrm{Ed}} \frac{1}{2z} + T_{\mathrm{Ed}} \frac{1}{2A} \right] \frac{1 + \lambda_{\mathrm{c}}'^2}{\lambda_{\mathrm{c}}'} < t f_{\mathrm{c2}}$$

- *Diagonal in compression* (least stressed side)

$$(*) \bar{q}_{\mathrm{cd}}'' = \left[V_{\mathrm{Ed}} \frac{1}{2z} - T_{\mathrm{Ed}} \frac{1}{2A} \right] \frac{1 + \lambda_{\mathrm{c}}''^2}{\lambda_{\mathrm{c}}''} < t f_{\mathrm{c2}}$$

Based on what mentioned above, the suggested values are

$$
\begin{aligned}
&1.0 \le \lambda'_c \le 2.5 \\
&\quad + \lambda'_c/2 \le \lambda''_c \le + \lambda'_c \quad \text{if} \quad V_{Ed}/2z > T_{Ed}/2A \\
&\quad - \lambda'_c \le \lambda''_c \le - \lambda'_c/2 \quad \text{if} \quad V_{Ed}/2z < T_{Ed}/2A \\
&\lambda_c = (\lambda'_c + \lambda''_c)/2
\end{aligned}
$$

The formulas indicated with (*) can be substituted by the more reliable empirical ones of the next section. In the verification of the chords the term $V_{Ed}\lambda_c/2$ introduces the rule of translation of moments already shown in the construction requirements of Chart 4.3.

Application to the Project

For the interaction formulas reported above, the following practical interpretations are given.

Reinforcement in tension

The necessary longitudinal reinforcement can be designed separately for bending moment (see Chart 3.11) including the possible axial force (see Chart 6.12), and for torsion (see Chart 8.2) placing along the tension side of the beam all the flexural reinforcement plus half of the torsional reinforcement.

If on the edge in compression due to the bending moment, the effect of torsion is predominant, a longitudinal reinforcement designed for the residual tension is introduced, equal to half of the global torsional one minus the flexural compression.

On the contrary, if the effect of bending is predominant, no torsional reinforcement is to be added on the edge in compression, whereas the effect of the circulatory flux of shear stresses on its resistance limit can be evaluated with the empirical formula shown below.

The orthogonal stirrups necessary on each of the two sides of the section can be designed separately for half of the shear force (see Chart 4.2) and for torsion (see Chart 8.2), again for a given inclination λ'_c *o* λ''_c of the web compressions; the two sets of stirrups are therefore to be added or deduced, depending on whether it is the case of the side with higher or lower stresses.

Concrete in compression

For compressions in concrete, the bending-torsion and shear-torsion in traction of beams with no significant axial forces can be evaluated, respectively, with the following empirical formulas of resistance verification:

$$\left(\frac{M_{Ed}}{M_{Rd}}\right)^2 + \left(\frac{T_{Ed}}{T_{cd}}\right)^2 \le 1 \qquad \left(\frac{V_{Ed}}{V_{cd}}\right)^2 + \left(\frac{T_{Ed}}{T_{cd}}\right)^2 \le 1.$$

Chart 8.4: Torsion: Construction Requirements

For the symbols see Chart 8.1.

Stirrups

Stirrups should be bent to follow, without outward pressures, the entire resisting peripheral perimeter of the section.

Stirrups should be closed, with adequate anchorages to ensure an effective circulatory continuity.

The stirrups spacing should be limited, other than with what shown for shear in Chart 4.5, also with $s \leq u/8$.

For the minimum amount of stirrups, one can follow what mentioned for shear in the mentioned Chart 4.5.

Longitudinal bars

The longitudinal bars should be effectively continuous, well anchored at the ends and enclosed in the stirrups.

At each stirrup bending there should be a longitudinal bar, whose diameter should be sufficient, with respect to the stirrup spacing, to deviate the flux of compressions in the concrete.

Along the resisting peripheral perimeter there should be at least one longitudinal bar every 350 mm.

For the minimum longitudinal reinforcement one can follow what mentioned for beams in bending in Chart 3.19.

Chapter 9
Structural Elements for Foundations

Abstract This chapter presents the design methods of the foundations starting from the basic soil models and following with the verification of the isolated footings and foundation piles. The analysis of continuous foundation beams, grids and rafts together with then problems of structure–foundation interaction are the examined. The calculation of retaining walls is treated with the models of earth pressure and the pertinent verifications of stability. Finally the diaphragm walls, possibly provided with anchoring prestressed tendons, are presented. The final section shows the application of the design procedures to the different foundation elements of the same multi-storey building treated in the preceeding chapters.

9.1 Isolated Foundations

In this chapter, the analysis of structural elements for foundations is presented, only for few typical cases and on the basis of simplified theoretical models, in order to highlight the design problems of such elements. The topics related to the *Analysis and design of foundations* are much broader. Also the complex problems of *Geotechnics* are not discussed except few quotations. Only the evaluation of the soil response on the foundation structures is discussed in order to define the internal forces necessary to the service and resistance verifications, without discussing comprehensively the stability and bearing capacity of the soils.

One can refer to the already mentioned specific disciplines for further information, as well as for the analysis of the reliability of the theoretical models adopted here in relation to the actual behaviour and the complex interactions of the buildings with the soils on which they are founded.

Resisting System

The resisting system of a building (see Fig. 9.1) consists of the *structure* and the *soil* strata affected by the forces. The requirements of resistance and stability (ultimate limit states) and the ones of functionality (serviceability limit states) should obviously be referred to the entire *resisting system*.

© Springer International Publishing AG 2017

G. Toniolo and M. di Prisco, *Reinforced Concrete Design to Eurocode 2*,
Springer Tracts in Civil Engineering, DOI 10.1007/978-3-319-52033-9_9

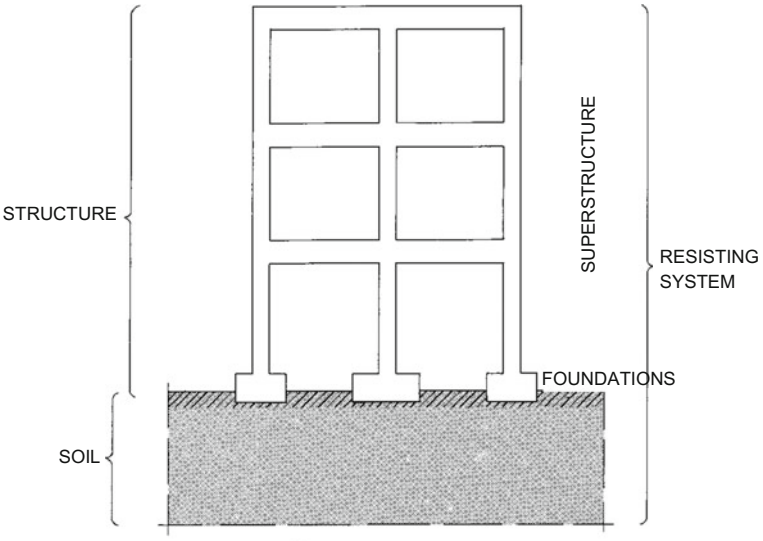


Fig. 9.1 Resisting system of the building

As already mentioned, the problems of *soil capacity* are not fully discussed here, nor are the ones related to the calculation of its *short-term and delayed deformations*. Concerning the rest, the resistance and service calculations of the elements (such as beams and columns) that constitute the *superstructure* have been extensively discussed in the previous chapters. The description is eventually completed in this chapter, presenting the issues related to the design of *foundations*.

The function of foundations is primarily to distribute vertical forces coming from the superstructure onto a ground surface big enough to ensure the resistance (see Fig. 9.2a); their self-weight can also be used, in the case of very eccentric loads, to bring the resultant force within the footprint (see Fig. 9.2b); through friction on the bottom surface, foundations can eventually transfer horizontal forces to the ground.

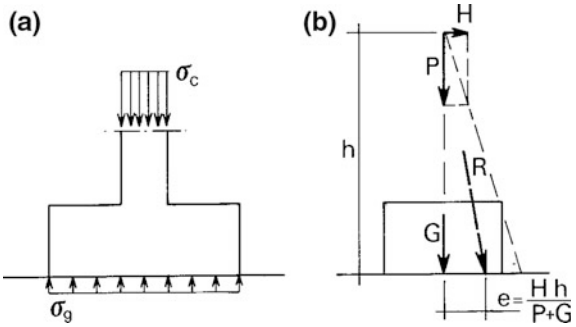


Fig. 9.2 Equilibrium conditions under centred (**a**) and eccentric (**b**) loads

In particular, those last aspects lead to the verifications of *overturning* and *sliding*, of which several examples will be given in Sect. 9.3.

Resistance Verifications

A summary of the criteria of resistance verifications following the ultimate limit state method is presented below, also including the soil behaviour. Three types of verification can be distinguished, based on three possible failure modes, identified respectively with the symbols EQU, STR and GEO.

EQU or loss of static equilibrium of the structure considered as a rigid body: concerns the possible overturning or sliding of the structure when the resistance and deformability of the soil and the structural materials are not involved. They are therefore stability verification in flotation conditions or with a high strength rock, for on one can assume an overturning about the edge of the support base.

STR or local or global failure of the structure including foundations: concerns the resisting mechanisms discussed in the previous chapters for the different structural elements such as columns and beams, and presented in this chapter for the foundation elements. The soils is assumed to be very resistant, capable of a reaction substantially elastic ('strong soil and weak structure' assumption).

GEO or local or global failure of the foundation soil: concerns the failure modes of soil or an excessive deformation according to the classical theories of soil mechanics. Overturning and sliding are included when the deformability and resistance of the soil are involved. The structure is considered very resistant, capable of transferring the forces to the soil with a substantially elastic behaviour ('strong structure and weak soil' assumption).

In reality the ultimate limit state of the structural system could correspond to a combined failure mode of simultaneous failure of structure and soil. However, the analysis of such mechanism would be very complex, and only the two extreme conditions mentioned under STR and GEO are analysed, carrying out both verifications with the appropriate values of partial safety factors.

For the geotechnical verifications of soil resistance, less reliable models are used. In order to cover these higher uncertainties, a model coefficient γ_R is introduced in the verification

$$E_d \leq \frac{1}{\gamma_R} R_d,$$

where

R_d is the design value of the resistance based on the design values $X_{di} = X_{ki}/\gamma_i$ of the pertinent mechanical parameters of the soil;

E_d is the design value of the effect of actions, based on the design values $F_{dj} = \gamma_{Fj} F_{kj}$ of forces

The following table shows the values of the partial safety factors for the three types of verifications, both for action and resistance. It is implied that, between minimum and maximum values, the one that reduces the resistance should be adopted.

The weight of soil supported by the structures (i.e. roof gardens) should be considered as a variable action. The partial factor γ_φ should be applied as the divisor of the tangent of the internal friction angle of soil.

		EQU	STR	GEO
Actions–loads				
Structural self-weight	γ_{G1}	0.9 ÷ 1.1	1.0 ÷ 1.3	1.0
Other permanent	γ_{G2}	0.0 ÷ 1.5	0.0 ÷ 1.5	0.0 ÷ 1.3
Variable actions	γ_Q	0.0 ÷ 1.5	0.0 ÷ 1.5	0.0 ÷ 1.3
Lateral earth pressure				
Angle of internal friction	γ_φ	1.25	1.25	1.25
Cohesion	γ_c	1.25	1.25	1.25
Soil weight	γ_γ	1.0	1.0	1.0
Model partial factors				
Soil resistance	γ_R	1.0	–	1.8
Sliding	γ'_R	1.1	–	1.1
Materials resistance				
Concrete	γ_C	–	1.5	–
Reinforcement	γ_S	–	1.15	–
Soil resistance				
Angle of internal friction	γ_φ	–	–	1.25
Cohesion	γ_c	–	–	1.25
Soil weight	γ_γ	–	–	1.0

Soil Models

In order to evaluate the actions transferred between foundation and soil through their contact surfaces, assumptions of an elastic behaviour will be used. The limitations on the validity of the elastic assumptions referred to reinforced concrete elements have already been discussed in several instances in the previous chapters. This type of assumption is much less reliable if referred to the soil, due to the evident immediate plastic deformations and the subsequent relevant long-term settlements that occur under the foundations.

In any case, the soil response to the actions coming from the structures above, evaluated with the elastic models in terms of contact pressures on the foundations, gives in general an acceptable solution based on which the appropriate design calculations of structures can be carried. As shown later on, in addition one can refer to the extreme upper and lower bound quantifications of the parameters characterizing the soil behaviour, in order to cover, in between the two corresponding elastic evaluations of the responses, the uncertainties deriving from the model and from the inaccurate quantification of the parameters.

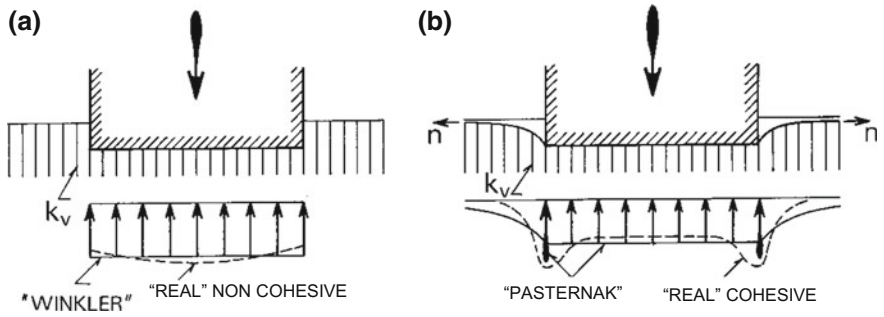


Fig. 9.3 Soil models of Winkler (**a**) and Pasternak (**b**)

Winkler Soil

The basic elastic model representing the behaviour of the soil under foundations is the Winkler model. This model represents the soil as a series of distributed and independent springs and neglects the effect of cohesion, significant at the perimeter edges of the foundation. At this location, the Winkler model would imply a sharp discontinuity of the soil surface in the deformed configuration (see Fig. 9.3a); due to cohesion instead, the adjacent zones of soil not directly loaded are dragged in the deformation. The effects are reduced rapidly with the distance and give an additional reaction distributed linearly along the edges of the foundation.

Pasternak Soil

A model that takes into account the effect of cohesion is Pasternak's model, according to which the springs of the elastic behaviour of the soil are connected by a membrane, subject to a flux n of tensions. The intensity of these tensions is related to the cohesion of the soil. The type of response from Pasternak's model is shown in Fig. 9.3b.

Boussinesq Soil

The two previous ones are surface models referred to the base level of the foundations. The elastic constants representing the deformation behaviour of the soil are given in a global form, inclusive of the integration along the depth of the involved strata.

In Boussinesq's model, instead the third dimension is considered and the soil is seen as a continuous and homogeneous semi-space where the integrations are to be extended following the constitutive laws of elasticity. Despite the higher accuracy of the results, especially in terms of deformations, the complexity of the algorithms makes this model less suitable for practical applications of the foundation design.

A Winkler soil is assumed from now on, neglecting in the analysis the localized effects along the edges of the foundations due to cohesion. This contribution is not significant for foundations with large dimensions, and the approximations related to its omission are acceptable. The approximations of the elastic behaviour are much more significant, given the actual behaviour of soils characterized by substantial

plastic components of the instantaneous deformation and subsequent long-term progressive settlements.

Soil Response
The linear relationship

$$\sigma = k\delta$$

Between the *contact pressure* σ and the corresponding *elastic settlement* δ of the foundation is expressed through an elastic constant k referred to the soil, which mainly depends on the characteristics of the soil, but is also related to the dimensions of the foundation itself.

Expressed in N/mm^3, la constant k is called *subgrade coefficient* and in the most common models it is assumed as linear function of the depth ξ

$$k = k_1 \xi$$

for non-cohesive soils, or in the binomial form

$$k = k_o + k_1 \xi$$

for cohesive soils.

9.1.1 Massive Foundations

The first case concerns solid concrete blocks, directly casts in the ground to fill the trench dug with the correct size, in order not to alter significantly the characteristics of the soil. Such type of element is used, for example, for the foundation of antennas (see Fig. 9.4).

For the analysis of massive foundations one can initially assume an elastic behaviour of soil, characterized by a coefficient of horizontal response k_h and a subgrade coefficient (vertical) k_v.

The first one is defined as the ratio between the pressure σ_h applied on the vertical face of the soil and the consequent displacement of the point of application; it is assumed as varying linearly with the depth ξ and therefore, to a horizontal translation δ_h of the block, a resisting triangular diagram (see Fig. 9.5a) corresponds, with $k_h = k_1\xi$, being k_1 expressed in N/mm^4.

A constant distribution of pressures $\sigma_v = k_v\delta_v$ corresponds instead to a vertical translation of the block (see Fig. 9.5b) being k_v expressed in N/mm^3 and keeping in mind that, for δ_v with opposite sign (directed upwards), no reaction is given by the ground.

Friction between foundation and soil and the subsequent shear forces are neglected.

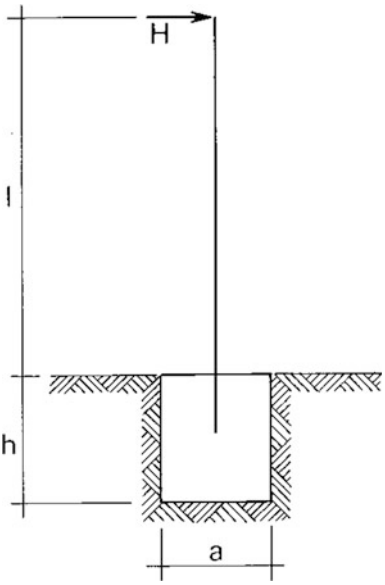


Fig. 9.4 Scheme of massive foundation

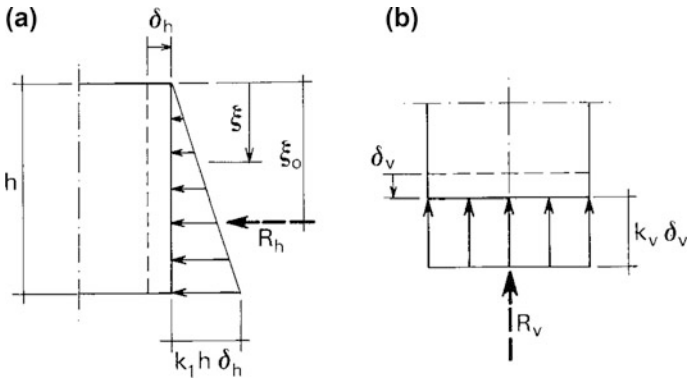


Fig. 9.5 Soil pressure response for horizontal (**a**) and vertical (**b**) displacements

Assuming a prismatic shape of the block, the actions H, P and F are expressed, including the self-weight, with reference to the point O of Fig. 9.6, whose distance from the top edge is $\xi_o = 2h/3$, where one has (see Fig. 9.4)

$$F = H\ (l + 2h/3)$$

The three geometrical unknowns, corresponding to the actions mentioned above, are the horizontal δ_h and vertical δ_v translations, and the rotation ϕ.

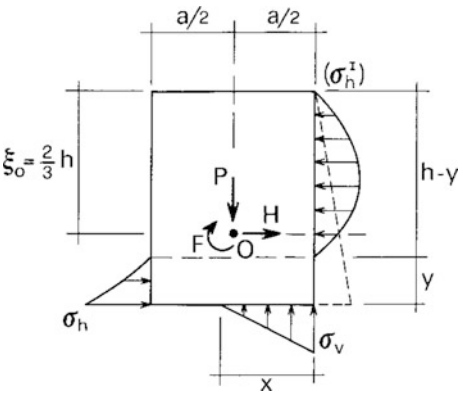


Fig. 9.6 Distribution of pressure on the massive foundation

The reactions on the *vertical faces* of the block, orthogonal to the plane of application, are evaluated as described below.

- For a horizontal translation $\delta_h = 1$

$$R_h = \int_0^h k_h b \, d\xi = k_1 b \int_0^h \xi \, d\xi = \frac{1}{2} k_1 b h^2$$

$$R_v = 0$$

$$M_\phi = \int_0^h (\xi_o - \xi) k_h b \, d\xi = 0 \quad (\text{per } \xi_o = 2h/3)$$

- For a vertical translation $\delta_v = 1$

$$R_h = R_v = M_\phi = 0$$

- For a rotation $\phi = 1$

$$R_h = \int_0^h k_h (\xi_o - \xi) b \, d\xi = 0 \quad (\text{per } \xi_o = 2h/3)$$

$$R_v = 0$$

$$M_\phi = \int_0^h k_h (\xi_o - \xi)^2 b \, d\xi = k_1 b \int_0^h (\xi_o - \xi)^2 \xi \, d\xi = \frac{1}{36} k_1 b h^4$$

The reactions on the *base of the block*, under the assumption of a surface entirely in compression ($x \geq a$), have the following values.

- For a horizontal translation $\delta_\mathrm{h} = 1$

$$R_\mathrm{h} = 0$$

- For a vertical translation $\delta_\mathrm{v} = 1$

$$\begin{aligned} R_\mathrm{h} &= 0 \\ R_\mathrm{v} &= k_\mathrm{v} ba \\ M_\phi &= 0 \end{aligned}$$

- For a rotation $\phi = 1$

$$\begin{aligned} R_\mathrm{h} &= 0 \\ R_\mathrm{v} &= 0 \\ M_\phi &= \frac{1}{12} k_\mathrm{v} ba^3 \end{aligned}$$

The equilibrium system

$$\begin{cases} \dfrac{1}{2} k_1 bh^2 \delta_h = H \\ k_\mathrm{v} ba \delta_\mathrm{v} = P \\ \left(\dfrac{1}{36} k_1 bh^4 + \dfrac{1}{12} k_\mathrm{v} ba^3 \right) \phi = F \end{cases}$$

gives

$$\begin{aligned} \delta_\mathrm{h} &= \frac{2H}{k_1 bh^2} \\ \delta_\mathrm{v} &= \frac{P}{k_\mathrm{v} ba} \\ \phi &= \frac{36F}{k_1 bh^4 + 3k_\mathrm{v} ba^3} \end{aligned}$$

which, for example, with $k_1 h = k_\mathrm{v}$, lead to

$$\begin{aligned} \sigma_\mathrm{v} &= k_\mathrm{v} \left(\delta_\mathrm{v} + \phi \frac{a}{2} \right) = \frac{P}{ba} + \frac{18F}{ba^2 (3 + \alpha^3)} \\ \sigma_\mathrm{h} &= k_1 h \left(\phi \frac{h}{3} - \delta_\mathrm{h} \right) = \frac{12F}{bh^2 (1 + 3/\alpha^3)} - \frac{1H}{bh} \\ \sigma_\mathrm{h}^\mathrm{I} &= k_1 \delta_\mathrm{h} + k_1 \xi_\mathrm{o} \phi = \frac{2H}{bh^2} + \frac{24F}{bh^3 (1 + 3/\alpha^3)} \end{aligned}$$

having set $\alpha = h/a$, and having indicated with $\sigma_{\mathrm{h}}^{\mathrm{I}}$ the initial slope of the diagram of horizontal pressures.

The position of the neutral axis is given by

$$x = \frac{a}{2} + \frac{\delta_{\mathrm{v}}}{\phi}$$

When

$$\frac{\delta_{\mathrm{v}}}{\phi} < \frac{a}{2}$$

the base of the block is not entirely in compression and the algorithm has to be modified. For a section not entirely in compression, the reactions at the base become

$$R_{\mathrm{v}} = \frac{1}{2} k_{\mathrm{v}} b x^2 \phi$$
$$M_{\phi} = \frac{1}{2} k_{\mathrm{v}} b x^2 \phi \left(\frac{a}{2} - \frac{x}{3}\right)$$

The equilibrium system becomes

$$\begin{cases} \frac{1}{2} k_1 b h^2 \delta_h = H \\ \frac{1}{2} k_v b x^2 \phi = P \\ \frac{1}{2} k_{\mathrm{v}} b x^2 \phi \left(\frac{a}{2} - \frac{x}{3}\right) + \frac{1}{36} k_1 b h^4 \phi = F \end{cases}$$

The first equation gives

$$\delta_{\mathrm{h}} = \frac{2H}{\mathrm{k}_1 b h^2}$$

From the subsequent ones, one obtains respectively

$$\phi = \frac{2P}{k_{\mathrm{v}} b x^2}$$
$$P\left(\frac{a}{2} - \frac{x}{3}\right) + \frac{k_1 h^4 P}{18 k_{\mathrm{v}} x^2} = F$$

and, for $k_{\mathrm{v}} = k_1 h$, one has the third degree algebraic equation in the unknown x

$$-6P\mathrm{x}^3 + 9(Pa - 2F)x^2 + Ph^3 = 0$$

Having resolved it, one obtains

$$\delta_{\mathrm{v}} = \left(x - \frac{\mathrm{a}}{2}\right)\phi = \left(x - \frac{a}{2}\right)\frac{P}{k_{\mathrm{v}} b x^2}$$

and the pressures are eventually calculated with

$$\sigma_{\mathrm{v}} = k_{\mathrm{v}} x \phi = \frac{2P}{bx}$$

$$\sigma_{\mathrm{h}} = k_1 h\left(\phi\frac{h}{3} - \delta_{\mathrm{h}}\right) = \frac{2Ph}{3bx^2} - \frac{2H}{bh}$$

$$\sigma_{\mathrm{h}}^{\mathrm{I}} = k_1 \delta_{\mathrm{h}} + k_1 \xi_{\mathrm{O}} \phi = \frac{2H}{bh^2} + \frac{4P}{3bx^2}$$

9.1.2 Footing Foundations

Footings (see Fig. 9.7) are commonly used as columns foundations. They are cast on a blinding layer of lean mix concrete within the formwork shutters, after having placed the appropriate steel reinforcement.

The soil used to backfill the voids of the trench remains soft and does not give any contribution to the lateral resistance. Forces are therefore transferred to the ground through the base of the footing.

For the calculation of the pressures transferred to the soil (see Fig. 9.8), in the general case of centred or eccentric forces, assuming an elastic behaviour of the soil, one can refer to Sect. 6.1. Only the criteria for the reinforcement and the resistance verifications of the footings are presented, considering the footings as stocky elements in reinforced concrete, assuming the mentioned diagrams of pressures as external forces, balanced with the ones coming from the column and the self-weight of the footing.

For non-sway frames, the vertical forces from the columns are basically centred; with a footing centred on the column one obtains constant distributions of pressures on the soil (see Fig. 9.8a). The hyperstatic moments of the frame can alter the situation, with diagrams varying linearly such as the one of Fig. 9.8b. For sway

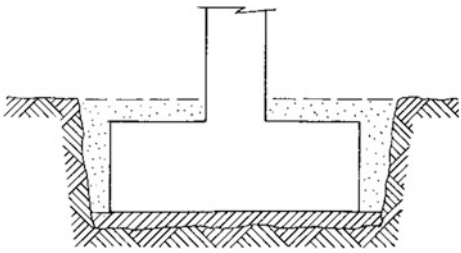


Fig. 9.7 Footing foundation

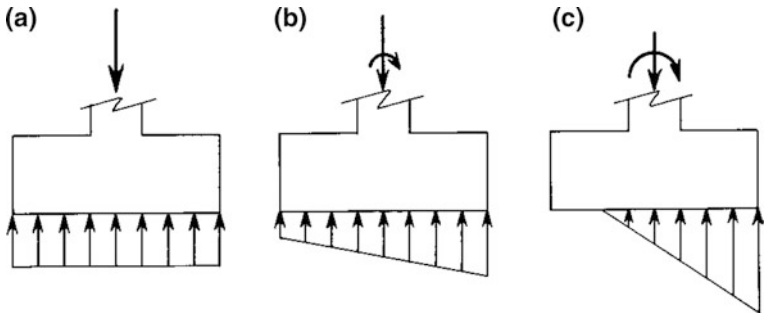
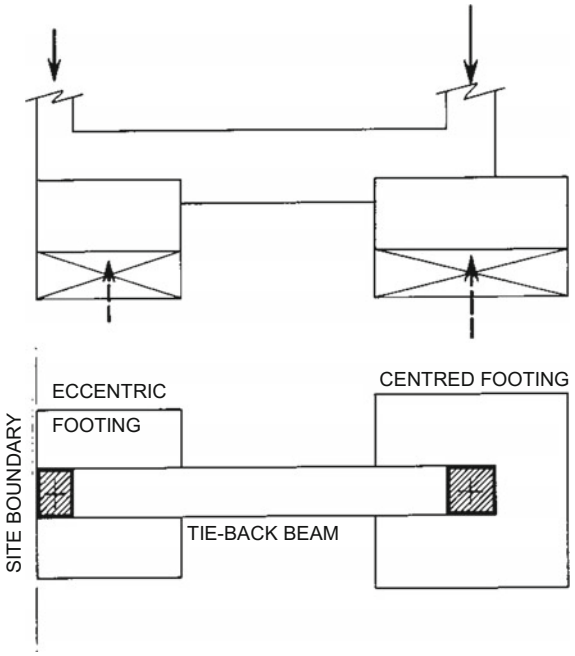


Fig. 9.8 Pressure distributions rendered by the soil

frames instead, horizontal actions generally induce significant bending moments on the columns which lead to greater eccentricities of the force, with the possibility of having the base of the footing not entirely in compression (see Fig. 9.8c).

There are also particular situations that do not allow the footing to be centred on the column, such as the one of a foundation on the site boundary. In those cases, in order to avoid the issues related to the great eccentricity of the base with respect to the column, a *tie-back beam* connected to the adjacent internal footing is introduced to recentre the load on the foundation with its flexural stiffness (see Fig. 9.9).

Fig. 9.9 Tie-back beam



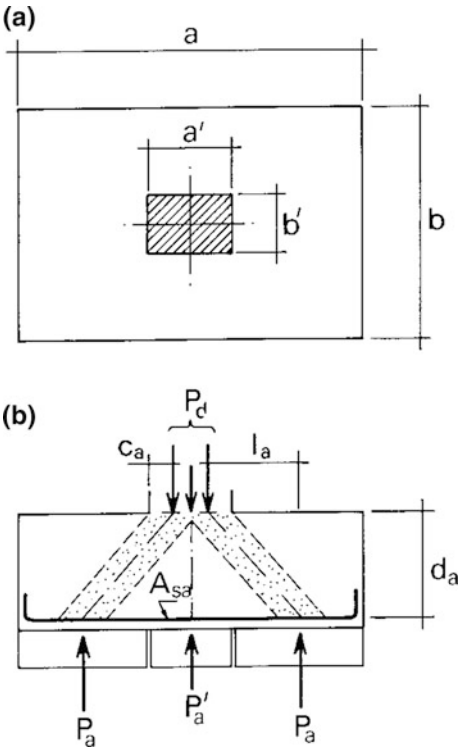


Fig. 9.10 Resisting model of isolated footing

Design of Footings

With reference to the doubly symmetric case of Fig. 9.10, the footing can be designed as an inverted double cantilever bent upwards by the soil reaction in the two orthogonal directions. Similar to what has been presented on Sect. 5.2 for stocky cantilevers, two orthogonal resisting schemes can be assumed which are able, with a combined functioning, to bring back the reaction distributed on the base within the column footprint.

One therefore has, in the direction of the side a, with c_a = min (0.2d$_a$, a'/4)

$$2P_a = \frac{a - a'}{a} P_d \quad P'_a = \frac{a'}{a} P_d$$

$$l_a \cong \frac{a - a'}{4} + c_a \quad \lambda_a = \frac{l_a}{d_a}$$

$$P_{rs} = P'_a + 2A_{sa} f_{yd} \frac{1}{\lambda_a} \quad (> P_d)$$

and similarly in the direction of the side b, with c_b = min (0.2d_b, b/4)

$$2P_b = \frac{b - b'}{b} P_d \quad P'_b = \frac{b'}{b} P_d$$
$$l_b \cong \frac{b - b'}{4} + C_b \quad \lambda_b = \frac{l_b}{d_b}$$
$$P_{rs} = P'_b + 2A_{sb} f_{yd} \frac{1}{\lambda_b} \quad (> P_d)$$

From the concrete resistance, one has

$$P_{rc} \cong P_o + 2 \times 0.4 d_a b' f_{cd} \frac{1}{1 + \lambda_a^2} + 2 \times 0.4 d_b a' f_{cd} \frac{1}{1 + \lambda_b^2}$$

with

$$P_o \cong \frac{a'b'}{ab} P_d$$

for the verification $P_{rc} > P_d$.

The two set of reinforcement A_{sa} and A_{sb} are therefore to be positioned in the two orthogonal directions as indicated in Fig. 9.11.

In the case of an eccentric load, the capacity of the resisting scheme should be calculated on the basis of the actual resultant of pressures on each of the four protrusions of the footing.

Other similar resisting schemes are proposed by different authors with very similar results, as the scheme with cantilevers in bending for the design of the reinforcement, with

$$M_a = \sigma_v b l_a^2 / 2 \quad A_{sa} \geq \frac{M_a}{f_{yd} 0.9 d_a},$$
$$M_b = \sigma_v a l_b^2 / 2 \quad A_{sb} \geq \frac{M_b}{f_{yd} 0.9 d_b},$$

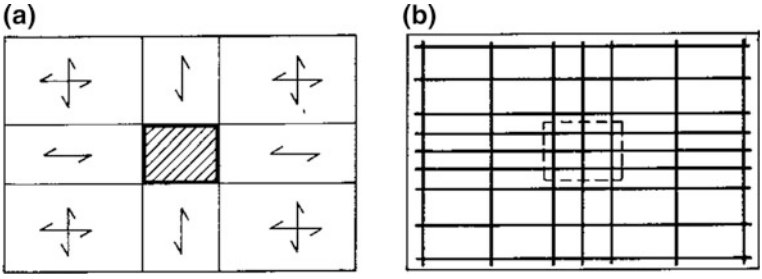


Fig. 9.11 Base reinforcement of the footing

where, for a centred vertical load P_d, one has

$$\sigma_v = \frac{P_d}{ab} \quad l_a = \frac{a - a'}{2} \quad l_b = \frac{b - b'}{2}$$

Verification of Punching Shear

For not very thick footings (see Fig. 9.12a), in addition to the bending verifications of the fixed end section in both directions, which can take into account the entire width of the pad (b for M_a, a for M_b) for the compressions in the concrete, the verification of punching shear is necessary. This verification is carried according to the same criteria presented at Sect. 5.2.3, evaluating the capacity on the *critical perimeter*

$$P'_r = 0.25 u d f_{ctd} \kappa (1 + 50\rho_s)$$

and another one within the perimeter of the column

$$P''_r = 0.4 u_o d f_{cd} / \left(1 + \lambda^2\right),$$

where for the meaning of symbols one can refer to the above-mentioned Sect. 5.2.3.

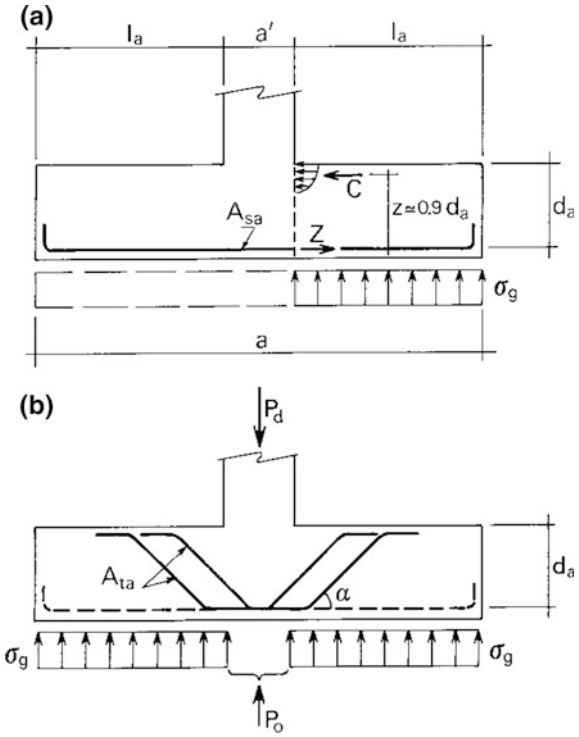


Fig. 9.12 Slender footing—bending (**a**) and) and punching shear (**b**) reinforcement

Assuming for the resistance

$$P_r = \min\left(P'_r, P''_r\right)$$

for the verification one should obtain

$$P_r > P_d - P_o$$

If necessary, the appropriate transverse reinforcement is introduced consisting of two orthogonal sets of bent bars as indicated in Fig. 9.12b. The capacity of this reinforcement, as already mentioned at Sect. 5.2.3, is evaluated with

$$P_{rs} = 2(A_{ta} + A_{tb}) f_{sd} \sin \alpha$$

For non-slender footings verified with strut-and-tie schemes (see Fig. 9.10) the punching shear verification is implicitly included in the relative formulas presented before.

9.1.3 Pile Foundations

When the upper soil strata do not have the adequate capacity, *deep foundations* are to be adopted which bring the actions down to deeper strata with the use of piles.

The most common types of deep foundations are driven piles and bored piles.

Driven piles (see Fig. 9.13a) consist of precast concrete elements, appropriately reinforced both for the transient stages of lifting, transportation and installation, and for the permanent behaviour. They have a circular cross section, tapered along the length, and they are installed in the ground with a driving machine. During driving, measuring the penetration, it is possible to verify the actual capacity of the pile. Once installed, a top segment of concrete is usually demolished to expose the reinforcement and to anchor it in the cast in situ foundation element above.

Bored piles (see Fig. 9.13b) are built after driving in the ground a cylindrical metallic formwork and removing the soil inside it. Concrete is then cast and vibrated, while the metallic formwork is progressively extracted from the ground. A cage of longitudinal bars and transverse circular hoops is introduced in these piles too, at least on a top part long enough to cover the zone where significant bending actions can arise. Starter bars are left on the top for the necessary anchorage in the concrete element above.

Piles Bearing Capacity

The bearing capacity of the pile is given by two contributions (see Fig. 9.13): *skin friction* and *end bearing*, to be calculated with reference to the concerned surfaces, with the appropriate formulas of soil mechanics, based on the characteristics of the

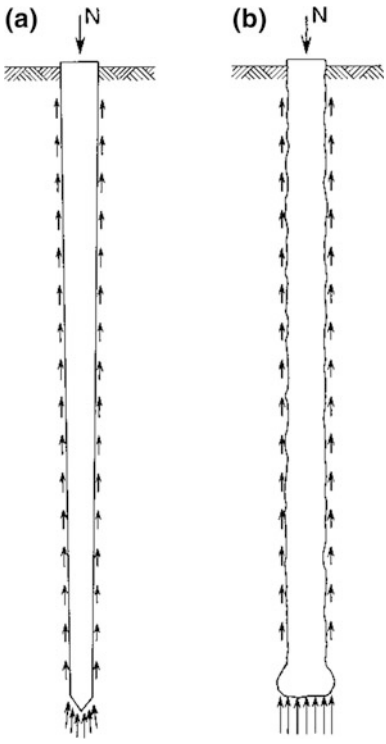


Fig. 9.13 Driven (**a**) and bored (**b**) piles

soil strata. Usually, given the load capacity at the top on the basis of the pile cross section, its length is calculated to obtain the same capacity on the basis of the specific properties of the soil.

If big diameters are excluded, which constitute actually a continuation of the structural element above, the piles are used in groups to support each individual foundation element (see Fig. 9.14), and they are arranged not to require any flexural resistance for the equilibrium with the vertical possibly eccentric actions. So, at least three non-aligned piles are to be placed under each isolated footing (see Fig. 9.14a), otherwise appropriate coupling beams are to be introduced (see Fig. 9.14c).

In order not to interfere too much on the relative capacity, the distance between piles should be indicatively equal to three times their diameter. For groups of a significant number of piles, the *group capacity* should also be verified calculating the contribution of skin friction with reference to the envelope perimeter surface of the group.

Even though the self-weight of the foundation is directly transferred on the soil underneath during casting, all loads are subsequently transferred almost entirely to the piles, due to the long term settlements of the superficial soil and the much higher stiffness of the piles. The pad is therefore effectively founded on localized supports.

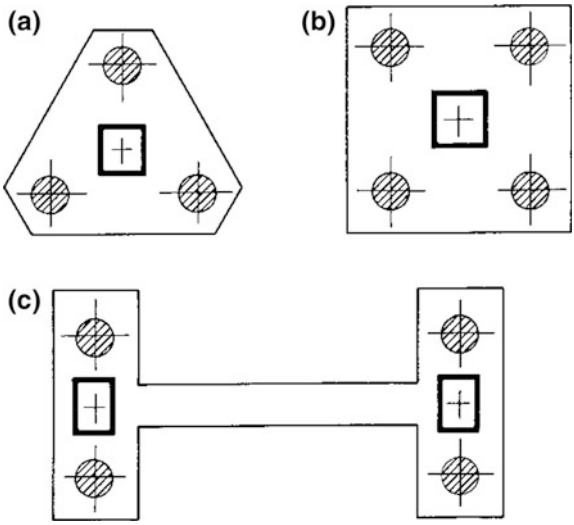


Fig. 9.14 Positioning of piles under the footing

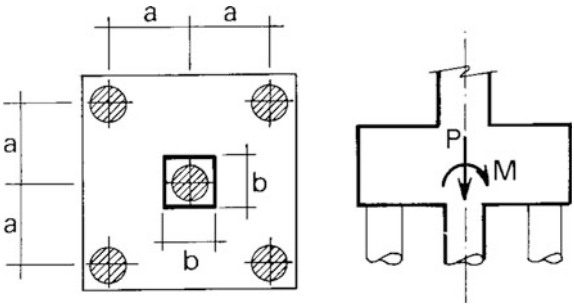


Fig. 9.15 Action applied on the piles

The distribution of forces on the piles of a foundation element can be calculated, neglecting the flexibility of the footing and assuming the elastic reactions concentrated on the pile centres. This leads to formulas similar to the ones of combined compression and bending in a beam section. With reference to the case of Fig. 9.15, one has, for example, on the most stressed piles

$$N = \frac{P}{A^*} + \frac{M}{I^*}a$$

with $A^* = 5$ and $I^* = 4a^2$.

Design of the Footing

The verification of the footing is then carried on the same resisting schemes of stocky cantilevers previously discussed. If, for example, the reinforcement is arranged along the diagonals (see Fig. 9.17a), one has for each pile (see Fig. 9.16)

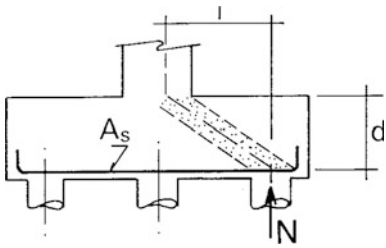


Fig. 9.16 Resisting model of the footing

$$N_{rs} = A_s f_{yd} \frac{1}{\lambda}$$

$$N_{rc} = 0.4\, db^* f_{cd} \frac{1}{1+\lambda^2}$$

with

$$\lambda = \frac{l}{d} \quad l \cong \sqrt{2}(a - b/2 + c)$$

$$b^* \cong \sqrt{2b} \quad c = \min(b/4, 0.2d)$$

If the reinforcement is arranged along the four sides (see Fig. 9.17b), the decomposition of the tension force leads to two orthogonal sets of reinforcement, each one equal to

$$A_s \geq \frac{N}{\sqrt{2} f_{yd}} \lambda$$

The two choices shown on Fig. 9.17 both require additional bars to complete the reinforcement cage. They are substantially equivalent being

$$\left(\frac{N}{f_{yd}}\right)\left(\sqrt{2}a\right) = \left(\frac{N}{\sqrt{2} f_{yd}}\right)(2a)$$

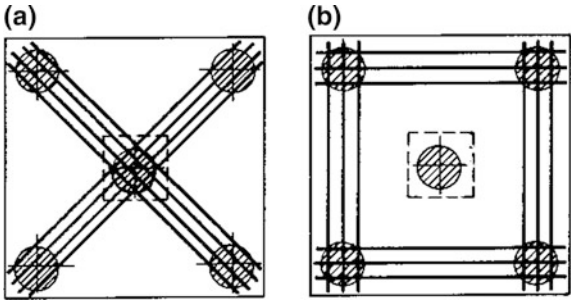


Fig. 9.17 Possible layouts of reinforcement

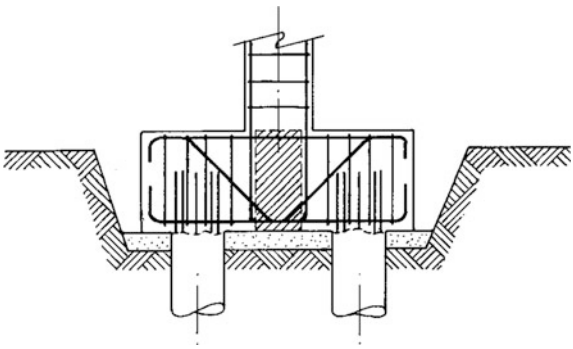


Fig. 9.18 Reinforcement details of a double cantilever

The possible adoption of bent bars leads to the use of the same formulas seen for stocky cantilevers. An example of reinforcement of a reversed double cantilever, used as foundation of a column (similar to the ones of Fig. 9.14c), is shown in Fig. 9.18. The detail is similar to the one presented in Fig. 5.22d for a stocky cantilever and it can be designed with the same verification formulas shown in the above-mentioned section.

9.2 Continuous Foundations

The analysis of continuous foundation beams similar to the one shown in Fig. 9.19 can be performed on the basis of the same elastic model of the soil behaviour assumed in the previous section. A Winkler soil is therefore assumed in the following, neglecting in the analysis the possible forces concentrated along the edges of the foundation due to the soil cohesion.

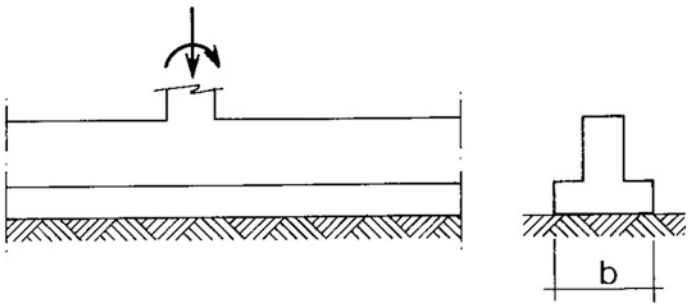


Fig. 9.19 Continuous foundation beam

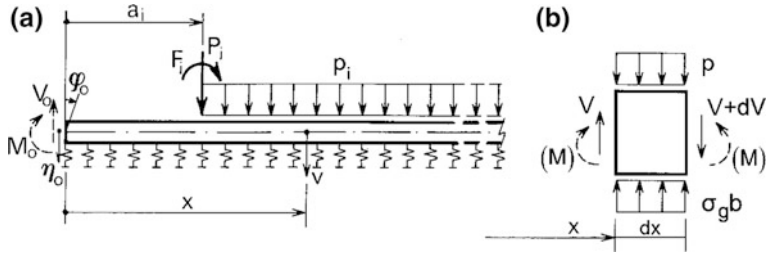


Fig. 9.20 Beam on elastic soil—model (**a**) and equilibrium of beam segment (**b**)

Beam on Elastic Soil

Within the approximations of Winkler's model, the equilibrium indefinite equation of the beam of Fig. 9.20, assumed with a constant cross section, is deduced from the vertical translational equilibrium of the generic segment of infinitesimal length dx

$$\mathrm{V} - (V + \mathrm{d}V) + \sigma_{\mathrm{g}} b \mathrm{d}x - p \mathrm{d}x = 0,$$

where the ground pressure σ_{g} is proportional to the vertical translation v through the subgrade constant k

$$\sigma_{\mathrm{g}} = kv$$

And the shear V can be expressed with the equation of the elastic line

$$V = \frac{\mathrm{d}M}{\mathrm{d}x} = -EI \frac{\mathrm{d}^3 v}{\mathrm{d}x^3}$$

Dividing all terms of the equation by dx, reducing and substituting, one obtains

$$EI\, v^{\mathrm{IV}} + bkv = p,$$

where the first term represents the elastic reaction force of the section, which corresponds to the variation of shear; the second term represents the soil reaction based on the above-mentioned elastic model; the third one expresses the intensity of the distributed load, in terms of force per unit length.

Set in the following form:

$$v^{\mathrm{IV}} + 4\beta^4 \mathrm{v} = \frac{p}{EI}$$

with

$$\beta^4 = \frac{bk}{4EI}$$

and where b is the width of the base, EI is the flexural stiffness of the section, such equation gives the integral

$$\begin{aligned} v(x) &= v_{\mathrm{o}}(x) + v_{\mathrm{p}}(x) = \\ &= C_1 ch\beta x \cos \beta x + C_2 ch\beta x \sin \beta x + \\ &+ \ C_3 sh\beta x \cos \beta x + C_4 sh\beta x \sin \beta x + v_{\mathrm{p}}(x) \end{aligned}$$

valid under the assumption of v always positive, which means that there are no local uplifts of the base.

The elastic line can be re-written assuming as constants the four *state parameters* of the initial section of the beam. These parameters are defined by (see Fig. 9.20):

$$\begin{aligned} \eta_{\mathrm{o}} &= v(0) \\ \phi_{\mathrm{o}} &= v^{\mathrm{I}}(0) \\ M_{\mathrm{o}} &= -EIv^{\mathrm{II}}(0) \\ V_{\mathrm{o}} &= -EIv^{\mathrm{III}}(0) \end{aligned}$$

arriving to the expression

$$\begin{aligned} v_{\mathrm{o}}(x) = \eta_{\mathrm{o}} ch\beta x \cos \beta x + \frac{\phi_{\mathrm{o}}}{2\beta}(ch\beta x \sin \beta x + sh\beta x \cos \beta x) + \\ - \frac{M_{\mathrm{o}}}{2\beta^2 EI} sh\beta x \sin \beta x - \frac{V_{\mathrm{o}}}{4\beta^3 EI}(ch\beta x \sin \beta x - sh\beta x \cos \beta x) \end{aligned}$$

For loads similar to the ones described in Fig. 9.20, the particular integral becomes

$$\begin{aligned} v_{\mathrm{p}}(x) = -\sum_{\mathrm{i}} \frac{F_{\mathrm{i}}}{2\beta^2 EI} sh\beta z_{\mathrm{i}} \sin \beta z_{\mathrm{i}} u(z_{\mathrm{i}}) + \sum_{\mathrm{i}} \frac{P_{\mathrm{i}}}{4\beta^3 EI}(ch\beta z_{\mathrm{i}} \sin \beta z_{\mathrm{i}} + \\ - sh\beta z_{\mathrm{i}} \cos \beta z_{\mathrm{i}}) u(z_{\mathrm{i}}) + \sum_{\mathrm{i}} \frac{p_{\mathrm{i}}}{4\beta^4 EI}(1 - ch\beta z_{\mathrm{i}} \cos \beta z_{\mathrm{i}}) u(z_{\mathrm{i}}) \end{aligned}$$

having set $z_i = x - a_i$ and indicating with $u(z_i)$ the step function, which is equal to 0 for $z_i < 0$, and 1 for $z_i > 0$.

Such expression of the elastic line is particularly convenient for the necessary numerical calculations. First, two out of the four integration constants are in fact immediately defined based on the restraint conditions at the first beam end. For a free end, for example, one has $M_{\mathrm{o}} = V_{\mathrm{o}} = 0$. The two other constants are defined

with the simple solution of the system of two equations that express the restraint conditions at the second end of the beam.

In addition, the expressions of the elastic line $v(x)$ and the functions $\phi(x)$, $M(x)$ and $V(x)$ remain based on five recurrent functions, obtained from it by subsequent derivations

$$
\begin{aligned}
g_1(\zeta) &= ch\zeta\ \cos\zeta \\
g_2(\zeta) &= \frac{1}{2}(ch\zeta\ \sin\zeta + sh\zeta\ \cos\zeta) \\
g_3(\zeta) &= \frac{1}{2}sh\zeta\ \sin\zeta \\
g_4(\zeta) &= \frac{1}{4}(ch\zeta\ \sin\zeta + sh\zeta\ \cos\zeta) \\
g_5(\zeta) &= \frac{1}{4}(1 - ch\zeta\ \cos\zeta)
\end{aligned}
$$

having

$$
\begin{aligned}
v(x) &= g_1(\beta x)\eta_{\mathrm{o}} + \frac{1}{\beta}g_2(\beta x)\phi_{\mathrm{o}} - \frac{1}{\beta^2 EI}g_3(\beta x)M_{\mathrm{o}} - \frac{1}{\beta^3 EI}g_4(\beta x)V_o + \\
&\quad + \sum_i \left\{\frac{-1}{\beta^2 EI}g_3(\beta z_i)F_i + \frac{1}{\beta^3 EI}g_4(\beta z_i)P_i + \frac{1}{\beta^4 EI}g_5(\beta z_i)p_i\right\}u(z_i) \\
\phi(x) &= -4\,\beta g_4(\beta x)\eta_{\mathrm{o}} + g_1(\beta x)\phi_o - \frac{1}{\beta EI}g_2(\beta x)M_{\mathrm{o}} - \frac{1}{\beta^2 EI}g_3(\beta x)V_{\mathrm{o}} + \\
&\quad + \sum_i \left\{\frac{-1}{\beta EI}g_2(\beta z_i)F_i - \frac{1}{\beta^2 EI}g_3(\beta z_i)P_{\mathrm{i}} + \frac{1}{\beta^3 EI}g_4(\beta z_i)p_i\right\}u(z_i) \\
M(x) &= 4\beta^2 EIg_3(\beta x)\eta_o + 4\beta EIg_4(\beta x)\phi_o + g_1(\beta x)M_o + \frac{1}{\beta}g_2(\beta x)V_{\mathrm{o}} + \\
&\quad + \sum_i \left\{g_1(\beta z_{\mathrm{i}})F_i - \frac{1}{\beta}g_2(\beta z_i)P_i - \frac{1}{\beta^2}g_3(\beta z_i)p_i\right\}u(z_i) \\
V(x) &= 4\beta^3 EIg_2(\beta x)\eta_o + 4\beta^2 EIg_3(\beta x)\phi_o - 4\beta g_4(\beta x)M_o + g_1(\beta x)V_{\mathrm{o}} + \\
&\quad + \sum_i \left\{-4\beta g_4(\beta z_i)F_i - g_1(\beta z_i)P_i - \frac{1}{\beta}g_2(\beta z_i)p_i\right\}u(z_i)
\end{aligned}
$$

The results calculated with these formulas are significantly influenced by the constant

$$\beta = 4\sqrt{\frac{bk}{4EI}}$$

that is the ratio between the elastic stiffness of the foundation soil and the one of the beam. On the other hand, the precise evaluation of the subgrade constant k is quite

difficult, as it depends on the dimensions of the foundation other than the characteristics of the soil. At the design stage, one has usually a lacking knowledge of these characteristics.

9.2.1 Foundation Beams

For the stress analysis of the foundation beams, with the algorithms presented above, it is good practice to repeat the calculation for two limit values of the constant k: a first upper bound value with the most favourable assumptions on the soil resistance; a second lower bound value, for example 6 or 8 times lower than the previous one, to cover the uncertainties of the assumption and the effects of plastic deformations and long-term soil settlements.

With reference, for example, to the continuous foundation beam of Fig. 9.21, the diagrams of the ground pressures $\sigma_g = kv$ and the internal forces M and V in the beam are shown in the subsequent Fig. 9.23.

The vertical loads of the edge columns and the internal ones, coming from the multi-storey overlying reinforced concrete structure, have been respectively assumed equal to

$$P' = 400 \text{ kN} \quad P = 650 \text{ kN}$$

For the section of the beam described in Fig. 9.22, assuming a concrete with a characteristic strength f_{ck} = 20 N/mm^2, one has

$$E_{cm} \cong 22000[(20+8)/10]^{0.3} \cong 30000 \text{ N/mm}^2$$
$$A = 0.53 \text{ m}^2$$
$$p_o = 0.53 \times 25 = 13.25 \text{ kN/m}$$
$$I = 0.0451 \text{ m}^4$$
$$E_{cm}I \cong 30000 \times 0.0451 \times 10^6 = 1353 \times 10^6 \text{ Nm}^2$$

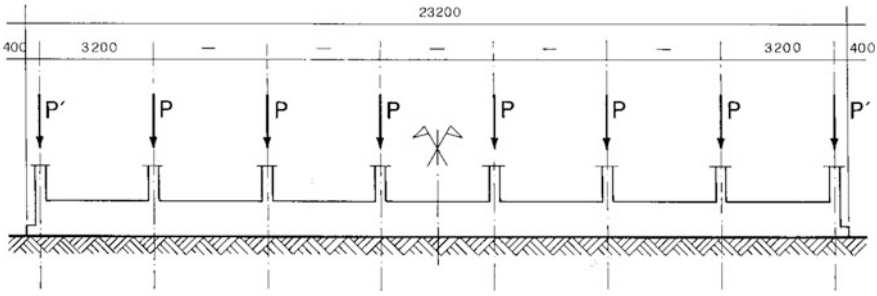


Fig. 9.21 Example of continuous foundation beam

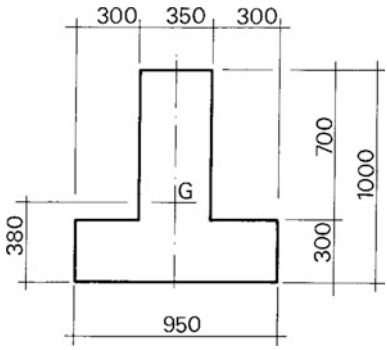


Fig. 9.22 Cross section of the foundation beam

Having eventually estimated a subgrade constant

$$k = 0.140 \text{ N/mm}^3$$

with b = 0.95 m one has

$$\beta = \sqrt[4]{\frac{140 \times 0.95}{4 \times 1353}} \cong 0.40 \text{ m}^{-1}$$

With k' = k/7 one eventually has

$$\beta' = \sqrt[4]{\frac{20 \times 0.95}{4 \times 1353}} \cong 0.24 \text{ m}^{-1}$$

From the diagrams of Fig. 9.23 it can be noted how, for the two limit cases, the values of ground pressures do not change much, whereas the differences of the internal forces in the beam are significant. These calculations have been carried without introducing the self-weight of the beam, as it does not induce flexural forces because it is balanced by the soil reaction in each section. Adding the pressure due to the self-weight to the one due to loads P, one obtains

$$\sigma_g \cong 0.213 + \frac{13.25}{950} \cong 0.227 \text{ N/mm}^2$$

and consequently the soil settlements in the two limit cases are respectively

$$\delta \cong 0.227/0.140 \cong 1.6 \text{ mm}$$
$$\delta\prime \cong 0.227/0.020 \cong 11.4 \text{ mm}$$

Approximated Models

Sometimes in the predesign stage, the general algorithm based on the model of the elastic beam on elastic soil presented above is not elaborated. A simpler hand

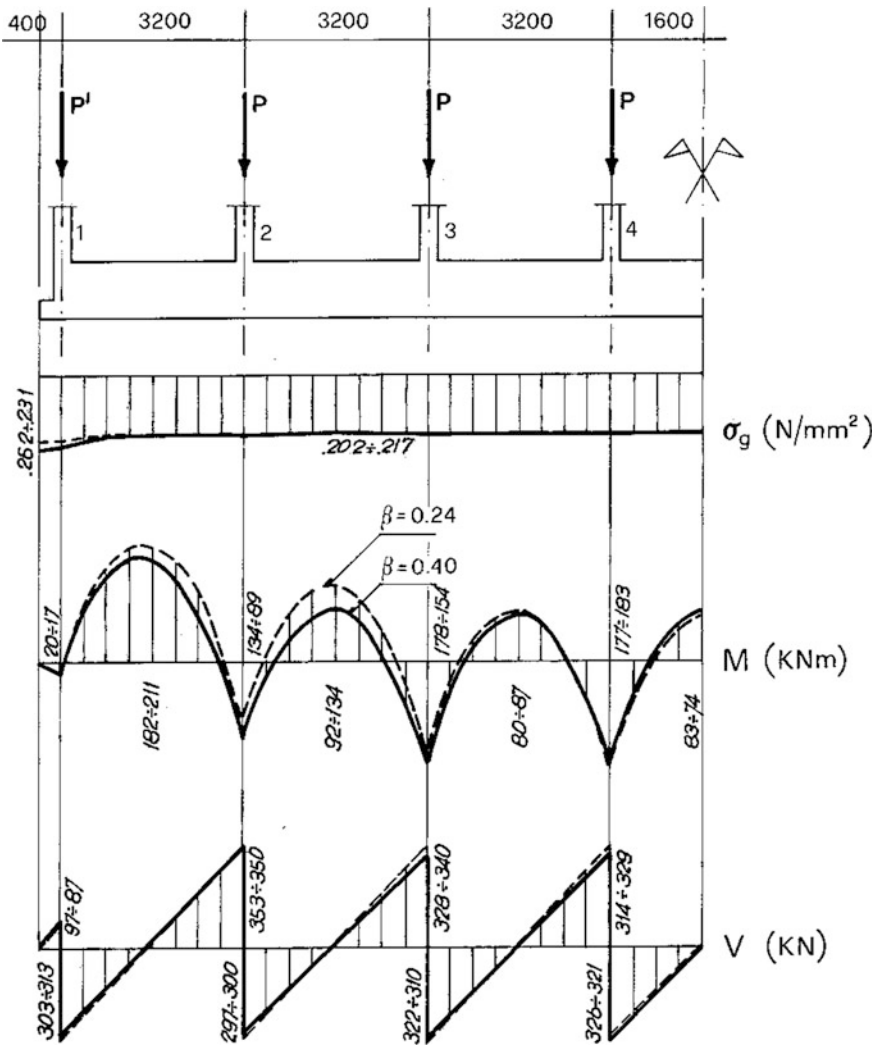


Fig. 9.23 Distributions of soil pressure and internal forces

calculation can be carried with approximated models, which are not very reliable, as shown hereafter.

If the ground pressure is calculated assuming that its distribution along the beam varies linearly, as if the beam were perfectly rigid, an estimation that globally satisfies the equilibrium with the applied forces can be simply done with the basic equations of statics. For example, with reference to the symmetric case of Fig. 9.21, a constant distribution is immediately obtained

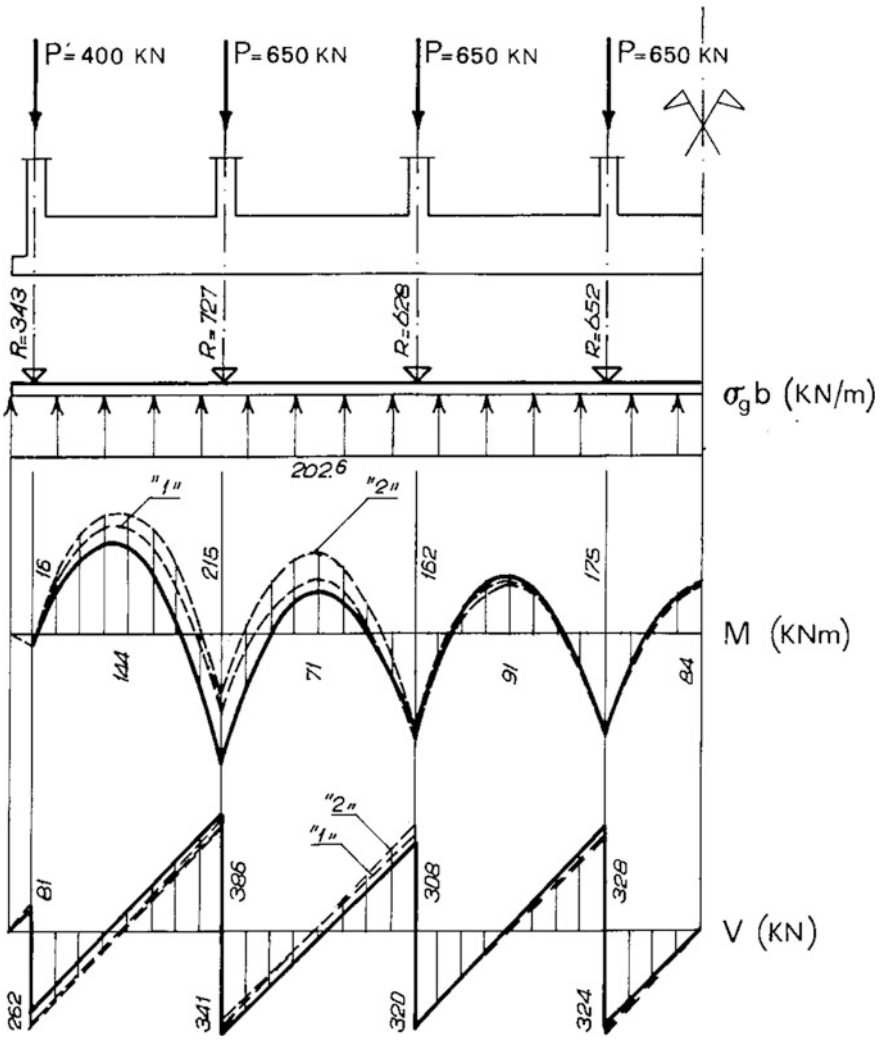


Fig. 9.24 Approximated model and comparison of stress responses

$$\sigma_g b = (2P' + 6P)/23.2 = 202.6\,\text{kN/m}$$

Such pressure can be seen as applied to a *continuous beam* on fixed supports, according to the model presented in Fig. 9.24. Its solution leads to the diagrams of forces shown with a continuous line on the same figure.

It can be immediately noted that the solution does not satisfy equilibrium giving reactions R at the supports that are significantly different from the loads coming from the relative columns. The diagrams of the internal forces M and V are also significantly different from the ones previously calculated with $\beta = 0.40\ \text{m}^{-1}$

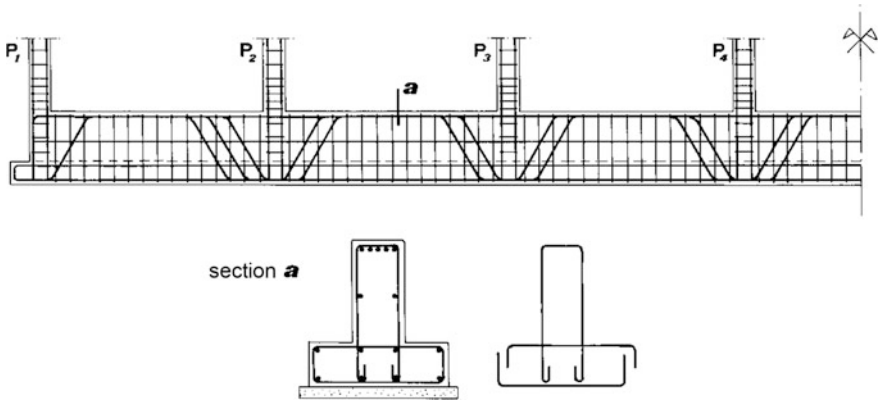


Fig. 9.25 Reinforcement details of the foundation beam

and with $\beta = 0.24\ \mathrm{m}^{-1}$ and shown with a dashed line on the same Fig. 9.23 (respectively with the indexes "1" and "2"). The solution would be much less accurate if the forces were calculated substituting the supports with the forces coming from the columns.

The model is therefore generally not reliable and, if used for the predesign of the foundations, it should be substituted in the final verification with the more accurate model of beam on elastic soil previously presented.

After deriving the diagrams of the internal forces M and V, which are similar and upside-down with respect to those of the common continuous beams at the upper floors of buildings, one can proceed to the proportioning of reinforcement and to the same verifications of typical reinforced concrete beams. A possible reinforcement layout is shown in Fig. 9.25.

9.2.2 Structure–Foundation Interaction

The description in the previous paragraph assumes a constant value of the loads P coming from the structure, which does not depend on the foundation settlements. This is correct if the superstructure is isostatic. For a hyperstatic superstructure, the behaviour of the whole system structure–foundation–soil is interdependent.

For low values of the stiffness of the structure, the solution obtained isolating the superstructure from the foundation and solving the two parts independently one after the other (see Fig. 9.26) is acceptable. Otherwise a global analysis of the entire structure–foundation system should be carried.

The case of a plain frame is shown in Fig. 9.27 with a possible simplified scheme, which neglects, for example, the horizontal flexibility of the foundations.

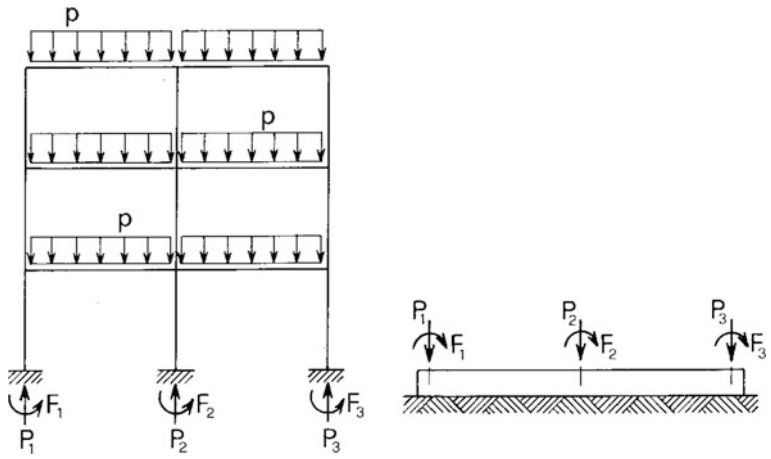


Fig. 9.26 Separate calculation models for superstructure and foundations

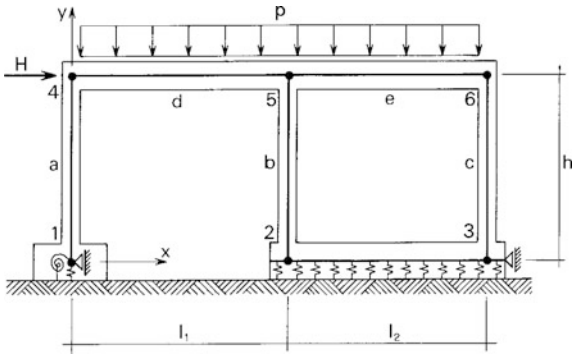


Fig. 9.27 Global calculation model for the structure

It should be mentioned that in general the real foundations of buildings are much more complex being often connected in three-dimensional systems with elements of different shape and dimensions. Problems arise for the definition of correct schemes, such as the ones related to the non-negligible dimensions of the intersection nodes and the consequent eccentricities of the end sections of the elements. Some of those problems will be mentioned in the next section.

Adopting the simple static scheme of Fig. 9.27 and neglecting the axial flexibility of the elements, one can proceed in the following way.

The footing centred on node 1 can be represented with a vertical translational spring with a stiffness K_v and a rotational spring with a stiffness K_ϕ. Assuming a base constant k for the soil, one has

$$K_v = kA$$
$$K_\phi = kI$$

with A and I respectively equal to the area and the moment of inertia of the base of the footing itself.

The equilibrium equation with respect to the rotation of node 1 will therefore be

$$\left(K_\phi + \frac{4EI_a}{h}\right)\phi_1 + \frac{2EI_a}{h}\phi_4 - \frac{6EI_a}{h^2}\xi = 0$$

where ϕ_1 and ϕ_4 are the rotations of the nodes 1 and 4 and ξ is the horizontal translation of the top beam.

The equilibrium equation with respect to the vertical translation of the column a will be

$$\left(K_v + \frac{12EI_d}{l_1^3}\right)\eta_a - \frac{12EI_d}{l_1^3}\eta_b - \frac{6EI_d}{l_1^2}\phi_4 - \frac{6EI_d}{l_1^2}\phi_5 + \frac{pl_1}{2} = 0$$

where η_a and η_b are the vertical translations of the columns a and b.

In order to evaluate the direct and indirect stiffnesses at nodes 2 and 3 of the ground beam, the expression of the elastic line presented at the previous section can be used. The static effects M and V (see Fig. 9.28) are to be evaluated for the unit values of the corresponding geometrical parameters ϕ and η

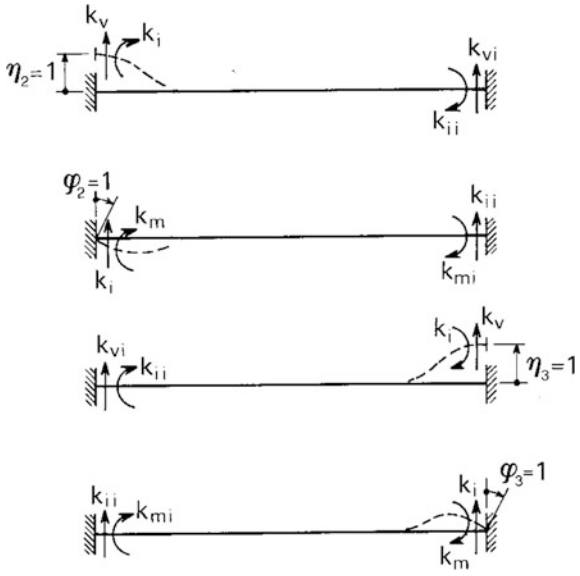


Fig. 9.28 Stiffness parameters of the beam on elastic soil

	η_2	ϕ_2	η_3	ϕ_3
V_2	k_{v}	k_i	$k_{\mathrm{v}i}$	k_{ii}
M_2	k_i	k_{m}	k_{ii}	$k_{\mathrm{m}i}$
V_3	$k_{\mathrm{v}i}$	k_{ii}	k_{v}	k_i
M_3	k_{ii}	$k_{\mathrm{m}i}$	k_i	k_{m}

with the reduction of parameters to be calculated thanks to the equality of the indirect effects ($k_{ij} = k_{ji}$) and the symmetry of the problem.

Given that the position of nodes 2 and 3 of the frame can be assumed to be respectively in the initial and end sections of the ground beam, the constants $\eta_{\mathrm{o}} = -\eta_2$, $\phi_{\mathrm{o}} = +\phi_2$ of the elastic line are immediately defined. For the other two constants, M_{o} and V_o the system $v(l) = -\eta_3$, $\phi(l) = +\phi_3$ is set

$$\begin{cases} \beta g_3(\beta l) M_{\mathrm{o}} + g_4(\beta l) V_{\mathrm{o}} = -\beta^3 EI b_1 \\ \beta g_2(\beta l) M_{\mathrm{o}} + g_3(\beta l) V_{\mathrm{o}} = -\beta^2 EI b_2 \end{cases}$$

with l equal to the length of the ground beam and where the contributions of the constant terms b_1 and b_2 are equal to

$$\begin{array}{ll} \text{for } \eta_2 = 1 & (\eta_{\mathrm{o}} = -1, \phi_{\mathrm{o}} = 0, v(l) = 0, \phi(l) = 0) \\ b_1 = +g_1(\beta l) & b_2 = -4\beta g_4(\beta l) \\ \text{for } \phi_2 = 1 & (\eta_{\mathrm{o}} = 0, \phi_{\mathrm{o}} = +1, v(l) = 0, \phi(l) = 0) \\ b_l = -\frac{1}{b} g_2(\beta l) & b_2 = -g_1(\beta l) \\ \text{for } \eta_3 = 1 & (\eta_{\mathrm{o}} = 0, \phi_{\mathrm{o}} = 0, v(l) = -1, \phi(l) = 0) \\ b_1 = -1 & b_2 = 0 \\ \text{for } \phi_3 = 1 & (\eta_{\mathrm{o}} = 0, \phi_{\mathrm{o}} = 0, v(l) = 0, \phi(l) = +1) \\ b_1 = 0 & b_2 = +1 \end{array}$$

It is consequently obtained

$$\begin{aligned} k_{\mathrm{v}} &= \beta^3 EI \frac{g_1(\beta l) g_2(\beta l) + 4 g_3(\beta l) g_4(\beta l)}{g_3^2(\beta l) - g_2(\beta l) g_4(\beta l)} \\ k_i &= \beta^2 EI \frac{g_1(\beta l) g_3(\beta l) - g_2^2(\beta l)}{g_3^2(\beta l) - g_2(\beta l) g_4(\beta l)} \\ k_{\mathrm{v}i} &= \beta^3 EI \frac{g_2(\beta l)}{g_3^2(\beta l) - g_2(\beta l) g_4(\beta l)} \\ k_{ii} &= \beta^2 EI \frac{g_3(\beta l)}{g_3^2(\beta l) - g_2(\beta l) g_4(\beta l)} \\ k_{\mathrm{m}} &= \beta EI \frac{g_2(\beta l) g_3(\beta l) - g_1(\beta l) g_4(\beta l}{g_3^2(\beta l) - g_2(\beta l) g_4(\beta l)} \\ k_{mi} &= \beta EI \frac{g_4(\beta l)}{g_3^2(\beta l) - g_2(\beta l) g_4(\beta l)} \end{aligned}$$

Such stiffnesses of the beam on elastic soil, as already mentioned, are introduced in the equilibrium system in the same way as those of the common elements of a frame. One should note the complexity of the required calculations and the significant dimensions of the solving systems associated to even simple frames such as the one of Fig. 9.27. For the analysis of the whole foundation–structure system, appropriate procedures of automatic calculations are therefore necessary.

9.2.3 *Foundation Grids and Rafts*

An extract of the layout plan and the section of a foundation grid is shown in Fig. 9.29, consisting of two crossing sets of foundation beams, connecting the vertical structural elements (columns) from which the loads of the building come. The analysis of such type of foundation structure can be carried appropriately adapting the calculation procedures typical of beam grids based on the displacements method, according to which there are three geometrical unknown on each node: the vertical translation and the two rotations on two vertical orthogonal planes.

If the nodes are considered with null dimensionless and the characteristics of the ground beams are extended to the nodes, the soil reactions for the areas corresponding to the intersections of the beams (the ones hatched in Fig. 9.29) are summed twice. Furthermore, the axes of the structural elements (columns and ground beams) often do not converge to a single intersection point.

For these and as well for other reasons (for example, the possibility for the axes of the different beams of the grid not to be on the same plan), the displacements

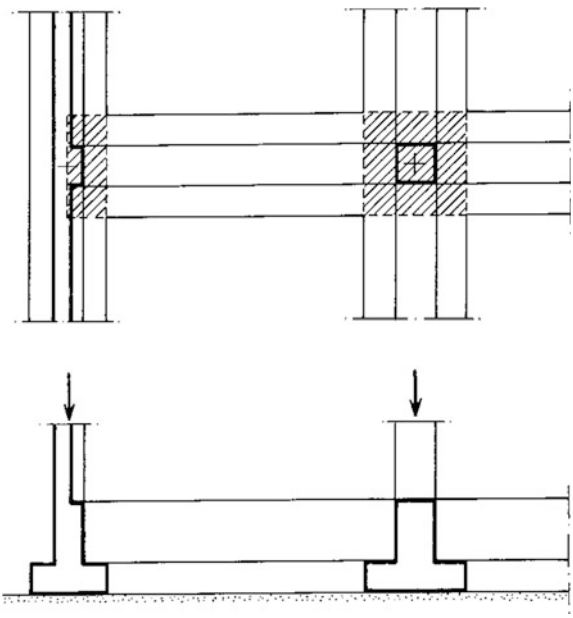


Fig. 9.29 Finite dimensions of nodes

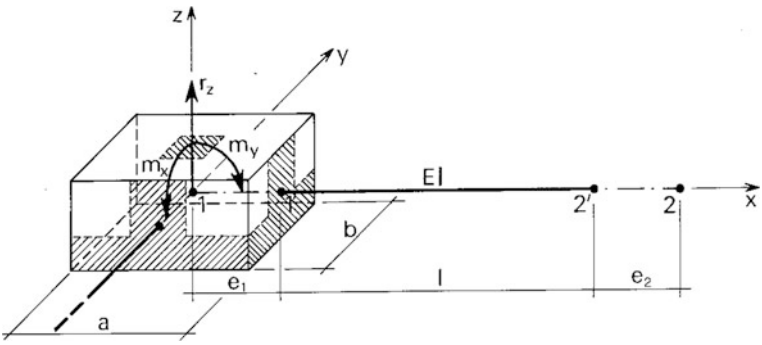


Fig. 9.30 Case of finite dimensions of a node

method should be seen as based on the equilibrium of a set of elements of finite dimensions (the nodes of the intersections of beams) connected to each other by linear elements (the beams themselves), arranged eccentrically with respect to the nodes. The centres of the nodes should be taken, independently from the axes of the beams, as the reference of the respective moments and rotations and they can conveniently correspond to the axis of the column where the forces to be applied to the grid were evaluated.

The general case of analysis of this type of frame should be approached with the matrix methods typical of the *Automated structural analysis* and one should refer to this discipline for further information. A simple case of orthogonal sets of beams is analysed here, with axes converging to the centres, predominantly vertical loads, so to consider only the grid components r_z, m_x and m_y represented in Fig. 9.30 in the equilibrium of the node, neglecting instead the components r_x, r_y and m_z due to the frame behaviour.

The stiffnesses of node 1 of Fig. 9.30, assumed rigid, can be calculated similar to what indicated for the footing of Fig. 9.27 in the previous section

$$\begin{aligned} K_\mathrm{v} &= kA \quad \text{(translational stiffness along } z\text{)} \\ K_x &= kI_x \quad \text{(rotational stiffness about } x\text{)} \\ K_y &= kI_y \quad \text{(rotational stiffness about } y\text{)}, \end{aligned}$$

where k is the subgrade constant and $A = ab$, $I_x = ab^3/12$, $I_y = ba^3/12$. The corresponding stiffnesses of the beams that converge to the node should be summed to these ones.

One can consider, for example, the beam 1–2 characterized by a cross section with a flexural stiffness EI and a base width b. For the internal segment of length l, assumed flexible, the flexural stiffnesses k_v, $k_{\mathrm{v}i}$, k_m, $k_{\mathrm{m}i}$, k_i, k_{ii} can be calculated with reference to its ends 1′ and 2′ with the formulas deduced in the previous paragraph. The torsional stiffnesses associated with the rotations ϕ_{x1} and ϕ_{x2} of the nodes should be added to these ones.

Torsional Stiffnesses

The torsional stiffnesses of the beam on elastic soil are deduced from the equation of the torsional elastic line

$$\frac{\mathrm{d}\phi}{\mathrm{d}x} = \frac{T}{GJ}$$

where ϕ is the rotation of the section about the beam axis and GJ is the torsional stiffness of the section itself. For the equilibrium with the soil reaction due to the rotation ϕ, one has (see Fig. 9.31)

$$\frac{\mathrm{d}T}{\mathrm{d}x} = \frac{kb^3}{12}\phi$$

from which one obtains, without torsional loads distributed along the axis of the beam, the differential equation

$$\phi^{\mathrm{II}} - \beta_{\mathrm{t}}^2 \phi = 0$$

with

$$\beta_{\mathrm{t}}^2 = \frac{kb^3/12}{GJ}$$

The integration of this equation leads to

$$\phi(x) = C_1 ch\beta_{\mathrm{t}} x + C_2 sh\beta_{\mathrm{t}} x$$

which, with the initial conditions

$$\phi_{\mathrm{o}} = \phi(0)$$
$$T_{\mathrm{o}} = GJ\phi^{I}(0)$$

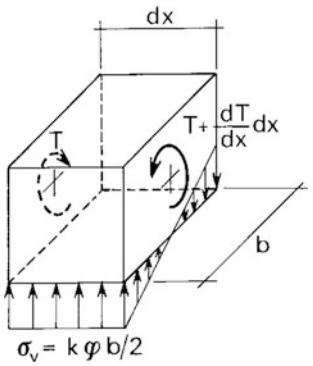


Fig. 9.31 Equilibrium of a beam segment subject to torsion

leads to

$$\phi(x) = \phi_o \, ch\beta_t x + \frac{T_o}{GJ\beta_t} sh\beta_t x$$
$$T(x) = \phi_o \, GJ\beta_t sh\beta_t x + T_o ch\beta_t x$$

Setting $\phi(0) = 1$ *and* $\phi(l) = 0$ the direct and indirect torsional stiffnesses of the beam on elastic soil are obtained

$$k_t = -T_o = + \frac{GJ\beta_t}{th\beta_t l}$$
$$k_{ti} = Tl = -\frac{GJ\beta_t}{sh\beta_t l}$$

Translation of Stiffnesses

In total, one therefore has, at the ends 1′ and 2′ of the beam, the set of stiffnesses organized in the following matrix:

	δ'_{z1}	ϕ'_{x1}	ϕ'_{y1}	δ'_{z2}	ϕ'_{x2}	ϕ'_{y2}
r'_{z1}	k_v	0	k_i	k_{vi}	0	k_{ii}
m'_{x1}	0	k_t	0	0	k_{ti}	0
m'_{y1}	k_i	0	k_m	k_{ii}	0	k_{mi}
r'_{z2}	k_{vi}	0	k_{ii}	k_v	0	k_i
m'_{x2}	0	k_{ti}	0	0	k_t	0
m'_{y2}	k_{ii}	0	k_{mi}	k_i	0	k_m

In order to transfer forces and displacements from the ends 1′ and 2′ of the beams to the centres 1 and 2 of the nodes, it is set (where e_1 and e_2 are the eccentricities indicated in Fig. 9.30):

$$r_{z1} = r'_{z1} \quad r_{z2} = r'_{z2}$$
$$m_{x1} = m'_{x1} \quad m_{x2} = m'_{x2}$$
$$m_{y1} = m'_{y1} - e_1 r'_{z1} \quad m_{y2} = m'_{y2} + e_2 r'_{z2}$$

and also

$$\delta'_{z1} = \delta_{z1} - e_1 \phi_{y1} \quad \delta'_{z2} = \delta_{z2} + e_2 \phi_{y2}$$
$$\phi'_{x1} = \phi_{x1} \quad \phi'_{x2} = \phi_{x2}$$
$$\phi'_{y1} = \phi_{y1} \quad \phi'_{y2} = \phi_{y2}$$

subsequently obtaining, with a double substitution, the new values of the translated stiffnesses

$$
\begin{aligned}
r_{z1} &= r'_{z1} = k_{\mathrm{v}}\delta'_{z1} + k_i\phi'_{y1} + k_{\mathrm{v}i}\delta'_{z2} + k_{ii}\phi'_{y2} = \\
&= k_{\mathrm{v}}\delta_{z1} + (k_i - e_1 k_{\mathrm{v}})\phi_{y1} + k_{\mathrm{v}i}\delta_{z2} + (k_{ii} + k_{\mathrm{v}i}e_2)\phi_{y2} \\
m_{x1} &= m'_{x1} = k_t\phi'_{x1} + k_{\mathrm{t}i}\phi'_{x2} = k_t\phi_{x1} + k_{\mathrm{t}i}\phi_{x2} \\
m_{y1} &= m'_{y1} - e_1 r'_{z1} = (k_i - e_1 k_{\mathrm{v}})\delta'_{z1} + (k_{\mathrm{m}} - e_1 k_i)\phi'_{y1} + \\
&\quad + (k_{ii} - e_1 k_{\mathrm{v}i})\delta'_{z2} + (k_{\mathrm{m}i} - e_1 k_{ii})\phi'_{y2} = \\
&= (k_i - e_1 k_{\mathrm{v}})\delta_{z1} + \left(k_m - 2e_1 k_i + e_1^2 k_{\mathrm{v}}\right)\phi_{y1} + (k_{ii} - e_1 k_{\mathrm{v}i})\delta_{z2} + \\
&\quad + (k_{\mathrm{m}i} - e_1 k_{ii} + e_2 k_{ii} - e_1 e_2 k_{\mathrm{v}i})\phi_{y2}
\end{aligned}
$$

and the same can be done for node 2.

Rafts

To conclude it should be noted how sometimes, in certain situations of very heavy loads, the footing is extended to the entire squares of the structural grid. It is the case of raft foundations, consisting of a continuous plate, usually stiffened by protruding beam ribs connecting the columns.

The equation of the plate on elastic soil is obtained from one of the common elastic plate bending theory adding the linear term that represents the soil reaction

$$
\frac{EI}{1-\nu^2}\left\{\frac{\partial^4 w}{\partial x^4} + 2\frac{\partial^4 w}{\partial x^2 \partial y^2} + \frac{\partial^4 w}{\partial y^4}\right\} + kw = p
$$

with $I = t^3/12$. The appropriate boundary conditions (and the ones of continuity if applicable) of the plate are to be associated to this equation. The difficult formal integration of this equation leads to the adoption of appropriate discretized numerical procedures. Approximate methods can be applied at the proportioning stage, based on the assumption of simplified schemes of the soil reaction (for example: constant distribution on each square of the structural grid) and the subsequent analysis with the classical formulas of plates in bending, appropriately interpreting the effectiveness of the constraints on the perimeter edges.

9.3 Retaining Walls

At this point, it is necessary to recall some additional notions relative to *Soil mechanics* to define the actions applied by the soil to the retaining walls. A model for the calculation of the soil capacity at the foundation bases will also be required, as it is strictly related to the verifications of the global equilibrium of the supported element against overturning.

Lateral Earth Pressure

According to the classical *Rankine's theory,* the action of an embankment against a vertical retaining element can be deduced on the basis of a model according to which a thrust wedge forms, delimited by an inclined sliding plane.

The mechanism of *active pressure* corresponding to the failure of the retaining element is shown in Fig. 9.32a. According to this model, for non-cohesive soils a

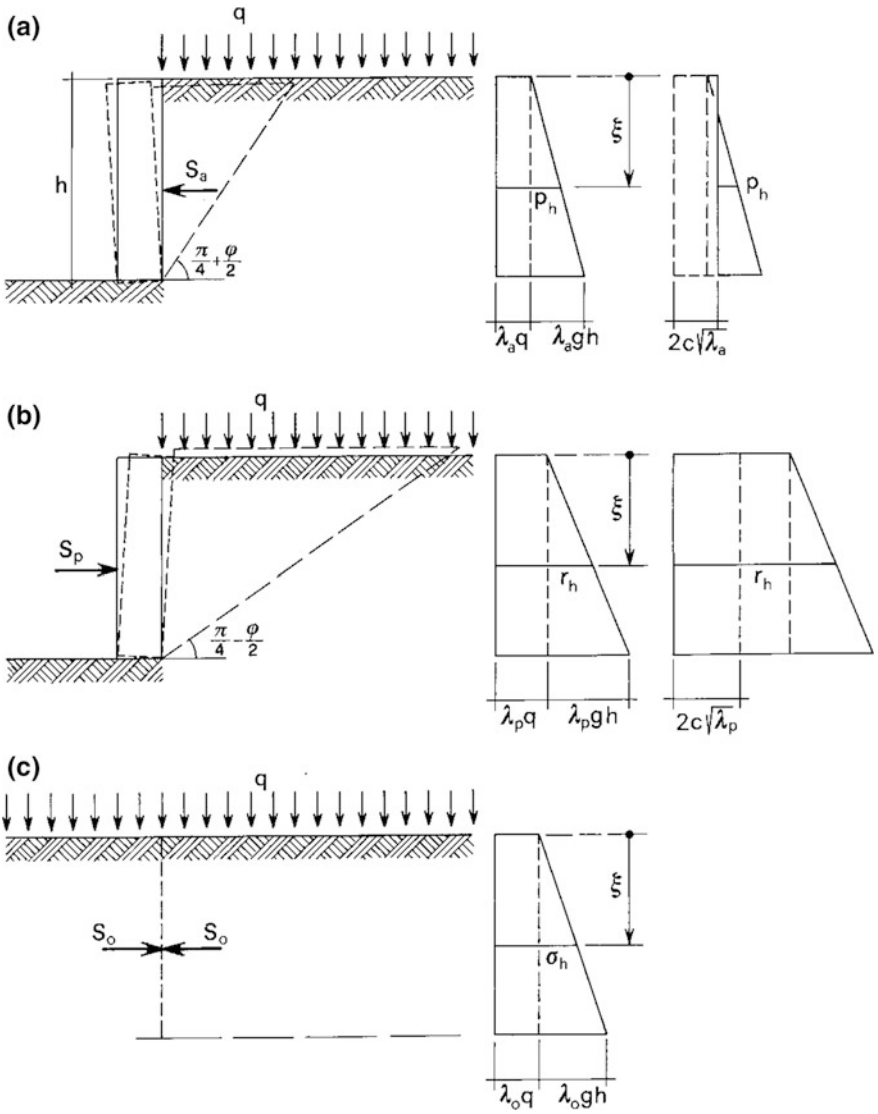


Fig. 9.32 Models of active (**a**), passive (**b**) and at rest (**c**) soil pressure

horizontal pressure can be assumed on the retaining elements varying linearly along the depth ξ

$$p_h = \lambda_a \sigma_v \; (\sigma_v = q + g\xi)$$

proportionally to the vertical pressure σ_v with the coefficient of active pressure

$$\lambda_a = tg^2\left(\frac{\pi}{4} - \frac{\phi}{2}\right),$$

where g is the unit weight of the soil and ϕ is the angle of internal friction. For cohesive soils there is a constant additional term related to the cohesion parameter c

$$p_h = -2c\sqrt{\lambda_a} + \lambda_a \sigma_v \quad (\geq 0)$$

The diagrams of the pressure p_h to be adopted in the verifications of the retaining element are shown in Fig. 9.32 in the two cases.

If instead an action is applied against the retained soil (see Fig. 9.32b), at the ultimate limit state of failure corresponds a *passive resistance* which, according to the same model, is expressed with

$$r_h = \lambda_p \sigma_v$$

or

$$r_h = +2c\sqrt{\lambda_p} + \lambda_p \sigma_v$$

respectively for non-cohesive and cohesive soils.

The coefficient of passive resistance is equal to

$$\lambda_p = \frac{1}{\lambda_a} = tg^2\left(\frac{\pi}{4} + \frac{\phi}{2}\right)$$

Between the two defined above, there is eventually the *pressure at rest*, which corresponds to the horizontal pressure σ_h, transferred on the vertical surface under consideration, in the undisturbed original situation of the soil (see Fig. 9.32c). This lateral pressure can be expressed as

$$\sigma_h = \lambda_o \sigma_v$$

valid for non-cohesive and cohesive soils. The coefficient of pressure at rest λ_o again depends on the angle of internal friction, but it cannot be directly deduced from Rankine's model; it has values between $\lambda_a < \lambda_o < \lambda_p$ which depend on the geological formation process of the soil. It can be conventionally assumed

$$\lambda_o = 1 - \sin \phi$$

Soil Capacity

The resisting pressure r_v at the base of a continuous foundation, whose length a is much greater than its width b, can be deduced from the model of Fig. 9.33, where the failure mechanism by lateral sliding (on one or both sides) of the soil beneath is represented. From the *plastic equilibrium* one obtains

$$r_v = N_q q + N_c c + N_g g b/2 = r_o + r_1 b,$$

where N_q, N_c and N_g depend on the angle of internal friction ϕ.

First it can be noted that the *limit pressure* as defined above does not depend on the soil characteristics only, but also on the width b of the base. The weight g of the soil contributes to the resistance, both from the strata underneath with the coefficient N_g, and with the pressure $q = gh$ of the adjacent top strata with the coefficient N_q. The third contribution is given by cohesion c of the soil with the coefficient N_c.

Globally the capacity of the foundation, expressed in terms of vertical (centred) force per unit length, having added the model coefficient, is equal to

$$P_R = r_v b/\gamma_R$$

When an eccentric vertical load $P_E (< P_R)$ is applied to the foundation, the maximum eccentricity corresponding to the limit of plastic equilibrium is obtained with reference to the section not entirely in compression of Fig. 9.34, substituting the total width b with the one x of the loaded strip in the formula of the capacity

$$\gamma_R P_E = r_v x = r_o x + r_1 x^2$$

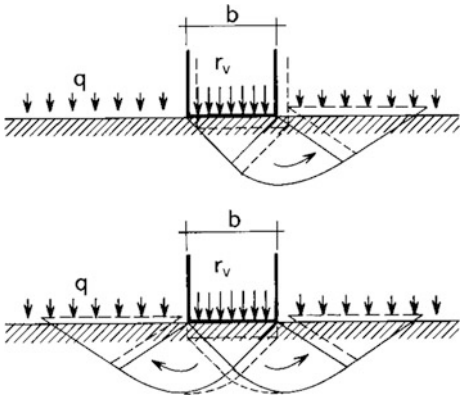


Fig. 9.33 Model of soil failure mechanism

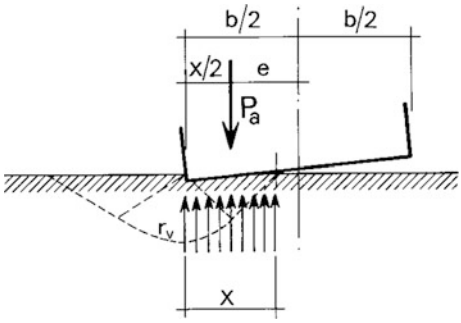


Fig. 9.34 Plastic limit equilibrium of foundation

with

$$r_o = N_q q + N_c c$$
$$r_l = N_g g/2$$

The unknown is subsequently deduced

$$x = \left\{ -r_o + \sqrt{r_o^2 + 4 r_l \gamma_R P_E} \right\} / 2 r_l$$

and the limit eccentricity is calculated

$$e_{lim} = \frac{b}{2} - \frac{x}{2}$$

compatible with the stability of the soil. The same limit can be expressed in terms of resisting moment (function of the applied load P_E):

$$M_{lim} = e_{lim} P_E$$

The verification of the foundation with eccentric load can therefore be set in terms of the moment with

$$M_E = P_E e \leq M_{lim}$$

If the supported element is isolated and maintains its equilibrium thanks to the stability of the soil underneath, the plastic limit situation defined above corresponds also to the one of *overturning* of the same element (see Fig. 9.35). For a given vertical load $P_{E,}$ the interval

$$-e_{lim} < e < +e_{lim}$$

represents the portion of foundation where the resultant of forces shall be located not to have overturning.

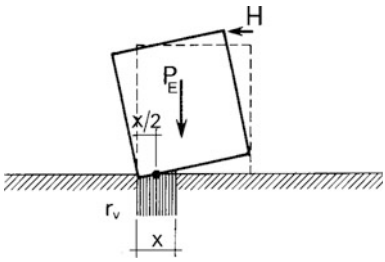


Fig. 9.35 Overturning limit condition

For a foundation with a length a comparable to its width b, the condition of plastic equilibrium becomes

$$r_v = s_q N_q q + s_c N_c c + s_g N_g g b/2 \qquad (\text{with } b \le a),$$

where the shape coefficients depend on the aspect ratio of the sides ($s = s(b/a)$—see Chart 9.2). For a centred load the capacity is therefore calculated with

$$P_R = r_v ab/\gamma_R \qquad (\le P_E)$$

When an eccentric load causing the partial uplift of the base is applied (see Fig. 9.34), the limit equilibrium condition referred to the loaded strip cannot be expressed with a second degree algebraic equation

$$r_{ox} x + r_{lx} x^2 = \gamma_R P_E/a$$

since the coefficients

$$r_{ox} = s_q N_q q + s_c N_c c$$
$$r_{lx} = s_g N_g g/2$$

also depend on the ratio x/a.

For small loads P_E with respect to the capacity for a centred load, expecting a thin loaded strip ($x << a$) at the ultimate limit state, in an approximate way it can be set $s_q = s_c = s_g = 1$ going back to the case of constant coefficients with a solution

$$x \simeq \left\{ -r_o + \sqrt{r_o^2 + 4 r_l \gamma_R P_E/a} \right\} / 2 r_l$$

In the following text, several typical cases of structural elements subject to soil pressures are examined, limiting the analysis to the calculations of resistance and stability of the elements. The problems related to the soil, either local or global, are not considered, such as the one relative to the general stability of the whole wall-soil system with respect to the possible failure by *deep sliding* as indicated in Fig. 9.36.

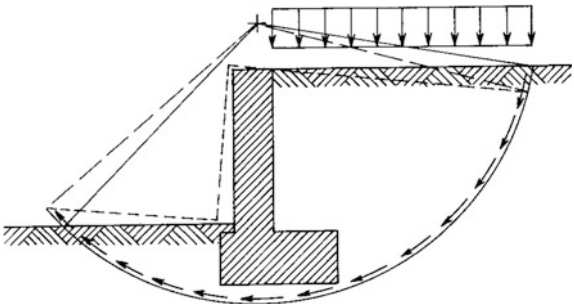


Fig. 9.36 Deep sliding failure mechanism

9.3.1 Gravity Walls

The rigid-body equilibrium verifications of a gravity retaining wall refer to the possible overturning by rotation about the limit eccentricity point defined above, as well as the possible horizontal sliding by exceeding the limit friction at the base.

The forces involved are firstly the self-weight of the structural parts (for example: G_0 and G_1 of Fig. 9.37) and the soil directly over the structural parts (for example: G_2 of Fig. 9.37). The forces coming from the retained soil are then to be evaluated, which consist in the mentioned horizontal pressures (for example: S_0 deriving from the superimposed surface load q and S_1 deriving from the self-weight of the soil). There are finally the soil reactions: the vertical ones at the base that will be evaluated later on; the horizontal ones due to friction at the base, which come into play in the sliding verification. The possible passive soil reaction on the foundation is usually neglected, as it is given by the soft backfill (for example: R of Fig. 9.37).

Having set

$$\sigma_v = q + g\xi,$$

where g is the unit weight of the soil and ξ is the depth of the considered stratum, for a unit length one therefore has the resultants indicated in Fig. 9.37, with

$$S_0 = \lambda_a q h$$

applied at $h_0 = h/2$ from the base of the wall, with

$$S_1 = \lambda_a g h^2/2$$

applied at $h_1 = h/3$ from the base of the wall and where

$$\lambda_a = tg^2\left(\frac{\pi}{4} - \frac{\phi}{2}\right)$$

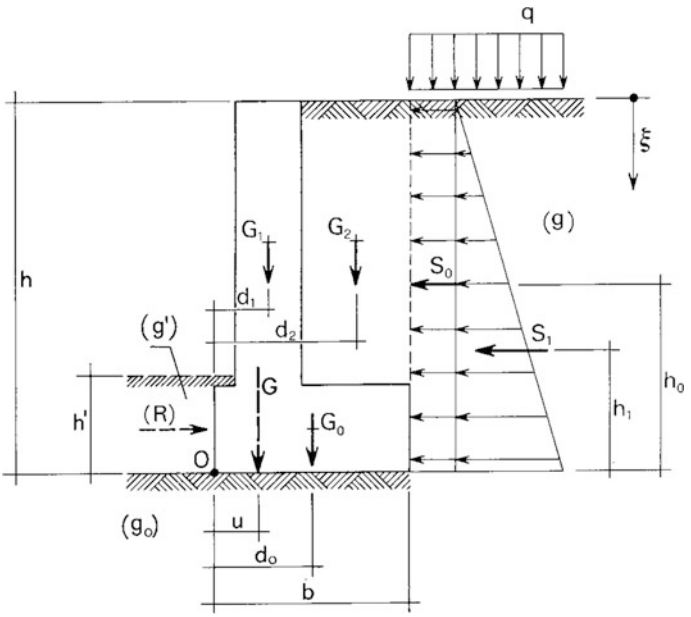


Fig. 9.37 Force components acting on the retaining wall

In the above description no cohesion has been assumed for the backfill, also neglecting its (balancing) vertical component of pressures due to friction on the considered vertical surface.

For the rotational equilibrium about the edge O one has

$$M_a = S_0 h_0 + S_1 h_1$$

as the overturning moment;

$$M_r = G_0 d_0 + G_1 d_1 + G_2 d_2$$

as the moment of the balancing weights. The position of the resultant of weights

$$G = G_0 + G_1 + G_2$$

on the base, measured from the edge O, is

$$u = \frac{M_r - M_a}{G}$$

with an eccentricity

$$e = b/2 - u$$

Verification of Overturning

It is implied that, for the overturning verification, the different components G_i and S_i of the forces are to be calculated adopting the appropriate factors γ_F. Although the overturning forces should always be amplified with the maximum value of the relative factor γ_F, the balancing forces G_i have two opposed effects: the one of balancing effect, increasing the distance u of the resultant from the extreme edge of the support, and the effect of extending the necessary dimension x for the limit reaction r_v of the soil. Therefore, in the general case the verification is to be repeated, once with the maximum value, once with the minimum value of the relative factor γ_F.

For the definition of the loaded strip in the ultimate overturning situation, one should evaluate

$$x = \left\{ -r_o + \sqrt{r_o^2 + 4 r_1 \gamma_R G} \right\} / 2 r_1$$

with

$$r_o = N_q g' h' + N_c c_o$$
$$r_1 = N_g g_o / 2,$$

where

$$N_q = N_q(\phi')$$
$$N_c = N_c(\phi_o)$$
$$N_g = N_g(\phi_o),$$

and where g', ϕ' are referred to the backfill soil ahead of the wall (see Fig. 9.37) and g_o, ϕ_o, c_o to the foundation soil under the base.

It is to be noted that the resisting characteristics of the soil mentioned above are also to be reduced with the appropriate safety factors.

For the stability verification (resistance and overturning) one shall have

$$u > x/2$$

that is, with $e_{lim} = b/2 - x/2$

$$e < e_{lim}$$

Verification of Sliding
Neglecting the reaction R given by the backfilling soft soil (see Fig. 9.37), for the sliding verification, the horizontal force

$$H_{\mathrm{E}} = S_0 + S_1$$

should be compared to the resistance

$$H_{\mathrm{R}} = \mu G$$

with

$$H_{\mathrm{E}} < H_{\mathrm{R}}/\gamma'_{\mathrm{R}},$$

where

$$\mu \leq tg\phi_{\mathrm{o}}$$

is the friction coefficient of the base surface. It is emphasized that, also in this verification, the parameters should be penalized with the respective partial safety factors, being reduced or increased depending on their favourable or unfavourable effect.

Elastics Response of Soil
The response of the soil, to be evaluated with the usual elastic assumptions for the subsequent calculation of the internal forces in the wall, is represented by a linear distributions of pressures applied at the support base. With the formulas presented at Sect. 6.1.1, the following pressures are obtained at the edges

$$\sigma_{\mathrm{g}} = \frac{G}{b}\left(1 \pm \frac{6e}{b}\right)$$

in the case of a surface entirely in compression (with $u \geq b/3$). In the case of surface not entirely in compression (with $0 < u < b/3$), the diagram of pressures is triangular, as indicated in Fig. 9.38; the maximum value is

$$\sigma_{\mathrm{g}} = \frac{2G}{3u}$$

Verification of the Retaining Wall
Regarding the structural element, it can consist of massive walls of stones, blocks or unreinforced concrete, or reinforced concrete thinner walls and toes (cantilever or buttressed wall).

For the definition of the internal forces, in the case of *massive walls* (unreinforced) the calculations similar to the ones presented above for the support base are to be repeated at different levels along the height of the wall (see for example

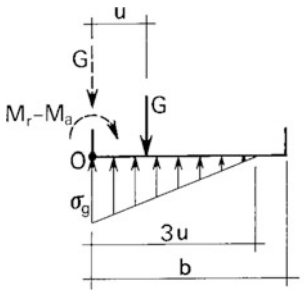


Fig. 9.38 Elastic response of the foundation soil

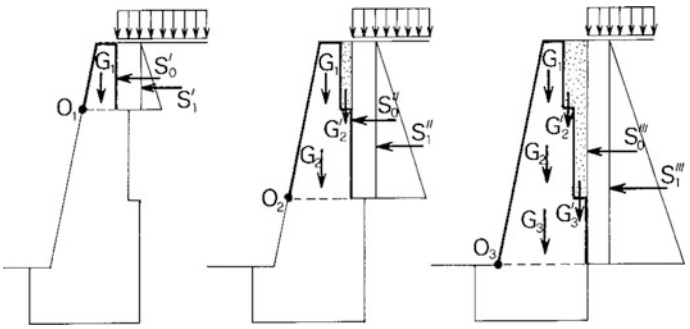


Fig. 9.39 Verification levels of a massive gravity wall

Fig. 9.39), whereas the resistance verifications are carried with formulas shown at Sect 6.1.2.

In the case of *reinforced concrete walls,* the reinforcement should be calculated on the basis of the flexural behaviour of the different parts and the appropriate verifications of the most stressed sections should be carried with the common formulas of reinforced concrete design and with the possible adoption of resisting strut-and-tie schemes for the D-regions.

For the *cantilever wall* of Fig. 9.40a the main reinforcement necessary to the resistance of its parts are indicated. The secondary compression reinforcement and the horizontal distribution bars are to be added.

In the *buttressed wall* of Fig. 9.40b, the cantilever resistance in bending is concentrated in the buttresses, to be reinforced with longitudinal bars and stirrups similar to the common reinforced concrete beams. The soil lateral pressures are brought to the buttresses through the wall panels and the footing thanks to their flexural plate behaviour. The reinforcement of wall and footing are then to be added, and designed similar to the common reinforced concrete slabs.

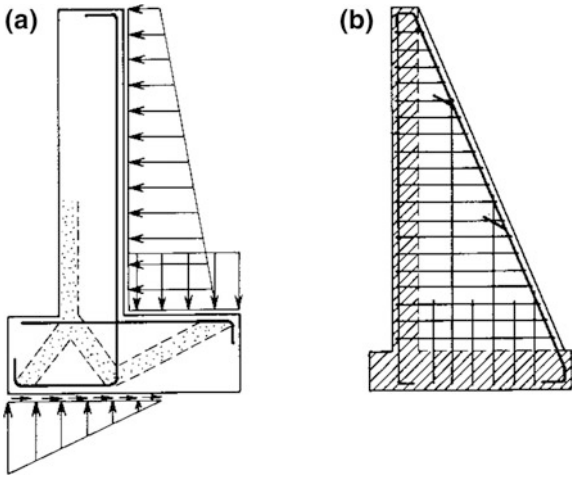


Fig. 9.40 Cantilever (**a**) and buttressed (**b**) retaining walls

9.3.2 Foundation Retaining Walls

The retaining walls of the basement levels of buildings are usually braced with respect to the lateral soil pressures. They are supported by transverse structural elements, horizontal and vertical, that constitute a box system which is very stiff and often subject to balanced forces coming from the opposite perimeter retaining walls. In this case the retaining wall does not behave as a gravity wall, as shown at the previous paragraph, but with schemes of plate in bending with different boundary conditions.

Figure 9.41 shows for example a retaining wall horizontally supported at the top by the floor of the first deck, which is connected to the other walls of the box system that ensures stability. In the same Fig. 9.41 a possible static scheme is shown that

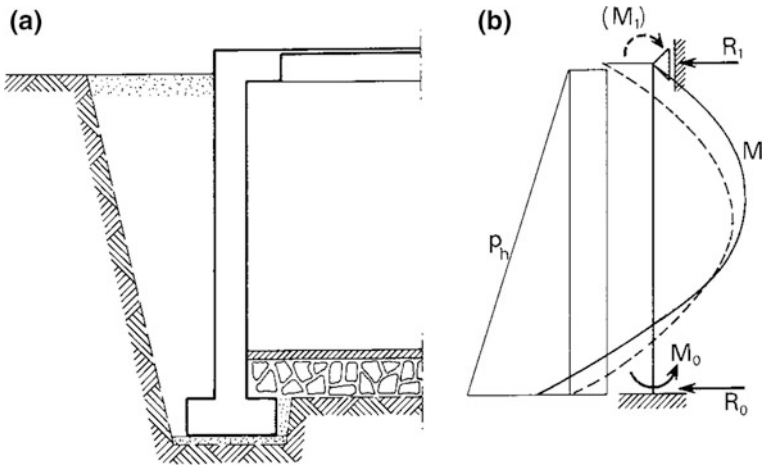


Fig. 9.41 Example of laterally braced retaining wall

interprets the constraints at the top and the bottom as simple support and fixed end, and applies the horizontal load according to the already mentioned model of active pressure. This scheme is more onerous for the evaluation of the moment M_0 at the base, and a different negative moment M_1 due to the continuity with the floor is to be added.

Carrying out the calculations for a wall strip of unit width, one can calculate the internal forces, proportion the reinforcement and perform the competent verifications.

Concerning the evaluation of actions, first it is to be noted that the model of active pressure, deduced from the equilibrium of the wedge of soil isolated by the sliding plane against the retaining wall, is not equally reliable when applied to the case of braced walls with restrained displacements.

In fact, the first transverse action that the wall receives is the one of the loose soil placed to backfill the excavation. This action can be evaluated with the formulas of the pressures of loose silage materials. If we assume that this soft material can settle further to compaction, the wedge of back soil bank can move and generate its higher active pressure.

Other actions are applied on the wall, such as the vertical one coming from the floor and the concentrated loads of the columns from the upper floors. The force of the floor only adds a normal compression component to the bending force indicated in Fig. 9.41b in the verification of the vertical wall strip.

The loads coming from the columns lead to local diffusion phenomena, together with the global in-plane behaviour on the entire foundation wall-beam.

To the one due to the transverse bending, as schematically indicated in Fig. 9.42a, the reinforcement due to the longitudinal behaviour is to be added, leading to a layout as the one shown in Fig. 9.42b.

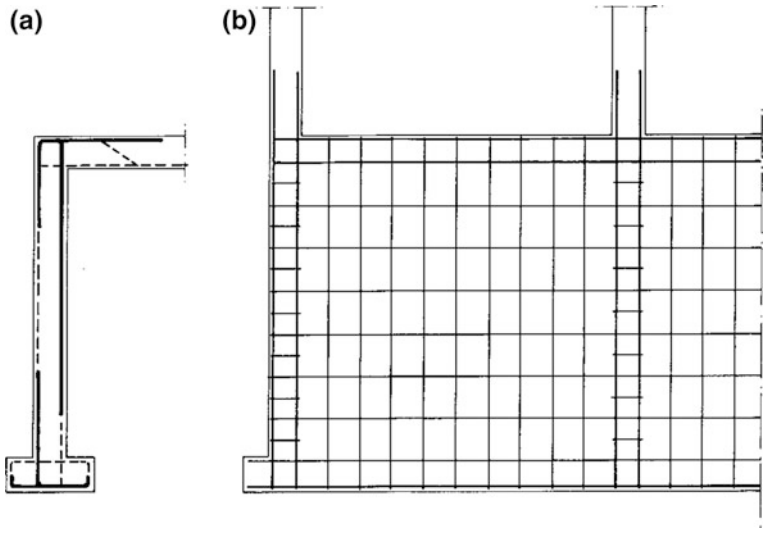


Fig. 9.42 Scheme of flexural (**a**) and general layout (**b**) of reinforcement

Design of the Wall-Beam

To conclude, the diagrams of internal forces of a foundation wall-beam analysed with the same static scheme of the beam on elastic soil of Sect. 9.2.1 (v. Figure 9.21) is shown in Fig. 9.43. Substituting only the value of the moment of inertia of the section, assumed equal to 20 I, one obtains

$$\beta = 0.40/4\sqrt{20} \cong 0.19\,\mathrm{m}^{-1}$$
$$\beta' = 0.24/4\sqrt{20} \cong 0.11\,\mathrm{m}^{-1}$$

From these values, the diagrams of bending moment and shear are obtained. They are significantly different from the ones shown in Fig. 9.23 for the more flexible beam, although the distribution of pressures on the soil is not very different.

The pressures due to uniformly distributed loads, such as the reaction force of the first deck and the self-weight of the wall-beam, are to be added to the pressures σ_v of Fig. 9.43. The transverse fixed-end moment M_0, caused by the soil pressure should be added, which makes the pressures under the foundation toe vary linearly around the average value σ_g deduced from the longitudinal analysis.

The moment diagram that would be obtained under the assumption of *infinitely rigid beam* ($\beta = 0$) is shown with a dashed line in Fig. 9.43: it corresponds to a distribution of pressures σ_g, perfectly linear and, in the symmetric case under consideration, of constant intensity. This assumption allows a simple hand calculation of the internal forces in the foundation beam with the basic equations of statics, but leads to big errors, except for very stocky beams.

Other approximated models will be presented at Sect. 9.4.2 for the design of the longitudinal reinforcement, with reference to their role to ensure the diffusion of concentrated loads coming from the columns.

9.3.3 Diaphragm Walls

Let us consider the diaphragm wall of Fig. 9.44 with a retained soil height h and a related load q. Its stability relies on the fixed end obtained with the deep embedment of the wall in the soil strata below.

Having calculated the forces at level O according to the model of active pressure used in the design of retaining walls, the problem can be referred to the analysis of the scheme of Fig. 9.45a for which one has (with a width $b = 1$ and indicating with g the unit weight of the soil)

$$V_o = \lambda_a q h + \lambda_a g h^2/2$$
$$M_o = \lambda_a q h^2/2 + \lambda_a g h^3/6$$
$$p_o = q + g h$$

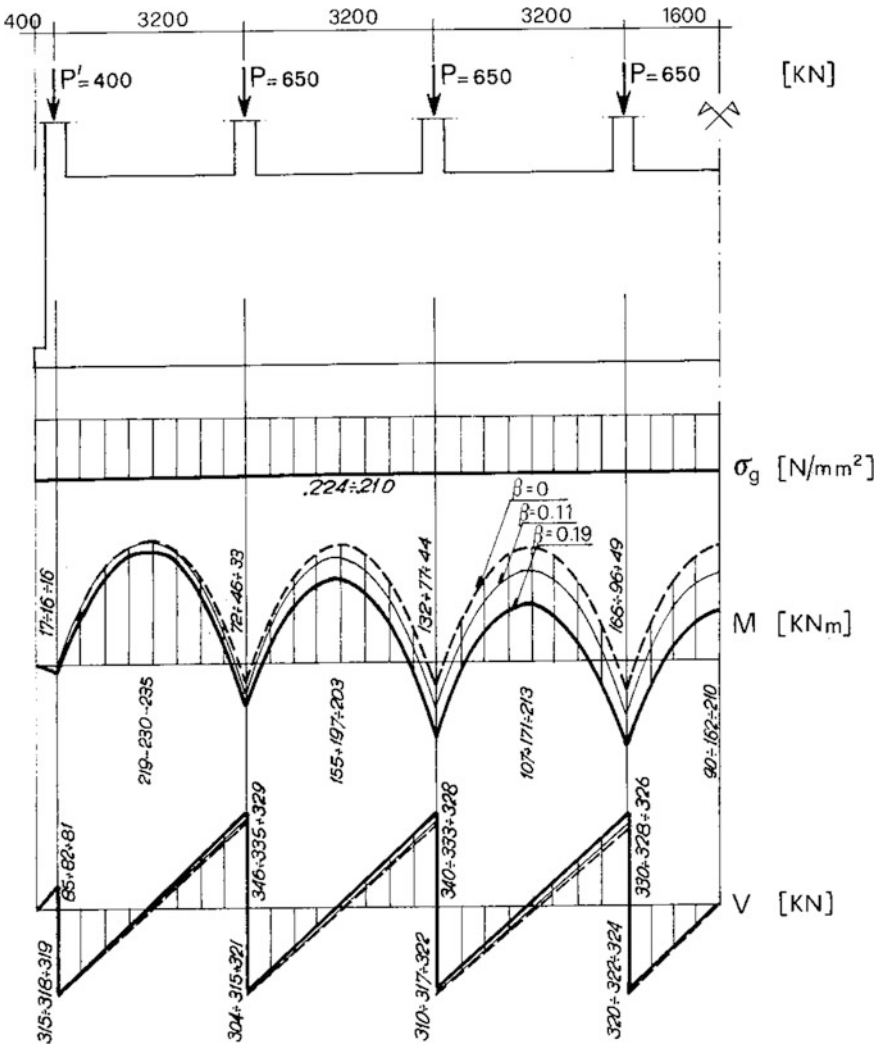


Fig. 9.43 Soil pressure and internal forces on foundation wall-beam

In particular, the axial force N_o due to the self-weight of the wall is neglected, as well as the possible friction between the bank soil bank and the wall, because of its small magnitude. They can be resisted with the same mechanism of lateral friction and end bearing typical of foundation piles.

Assuming that the depth h_o is limited so that the flexibility of the embedded wall segment can be neglected with respect to the much greater flexibility of the surrounding soil, it is possible to analyze the problem with the simplified model of rigid block already discussed at Sect. 9.1. Another simplification can be introduced, derived from the different aspect ratio with respect to the massive foundation

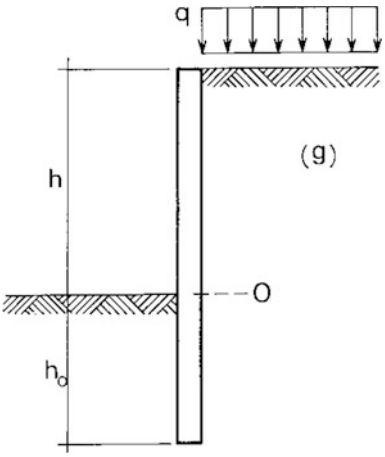


Fig. 9.44 Diaphragm retaining wall

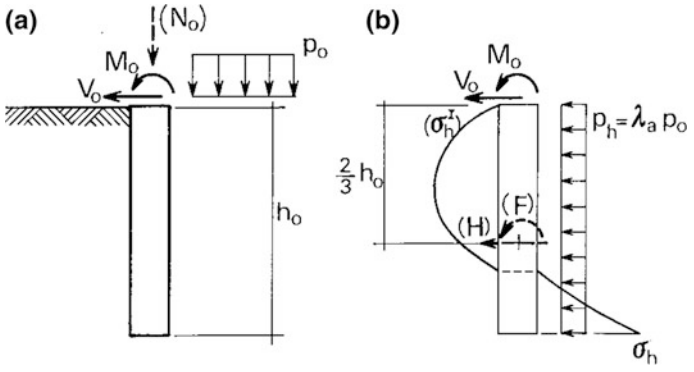


Fig. 9.45 Equilibrium of the embedded wall segment

blocks, neglecting the moment contribution of the possible vertical reaction σ_v at the base, which remains equal to zero when any vertical action on the wall is neglected.

One therefore has, taking into account only the horizontal pressures σ_h on the lateral surfaces of the wall and referring the actions to the point located at two-third of the embedment depth h_o (see Fig. 9.45b)

$$H = V_o + p_h h_o$$

$$F = M_o + \frac{2}{3} V_o h_o + \frac{1}{6} p_h h_o^2$$

The two competent equation of equilibrium between the actions mentioned above and the soil reactions are therefore similar to the ones of Sect. 9.1.1, where the contribution of σ_v is removed from the moments

$$\frac{1}{2}k_1 h_o^2 \delta_h = H$$
$$\frac{1}{36}k_1 h_o^4 \phi = F,$$

where δ_h is the horizontal translation of the wall, ϕ is the rotation about the same point chosen to define the moments, and indicating the constant of the coefficient of horizontal response typical of a non-cohesive soil with k_1.

The solution is

$$\delta_h = \frac{2H}{k_1 h_o^2}$$
$$\phi = \frac{36}{k_1 h_o^4}$$

from which one obtains (see Fig. 9.45b)

$$\sigma_h = k_1 h_o \left(\phi \frac{h_o}{3} - \delta_h\right) = \frac{12F}{h_o^2} - \frac{2F}{h_o}$$
$$\sigma_h^I = \frac{2}{3}k_1 h_o \phi + k_1 \delta_h = \frac{24F}{h_o^3} - \frac{2H}{h_o^2}$$

which are equivalent to the expressions of Sect. 9.1.1, where the aspect ratio is set $\alpha = \infty$ (with $b = 1$).

Assuming a non-cohesive soil characterized by a passive resistance

$$r_h = \lambda_r \xi$$

the verifications can be set as

$$\sigma_h < \lambda_r h_o$$
$$\sigma_h^I < \lambda_r$$

From these, with the appropriate substitutions, one can obtain the minimum value of the embedment depth h_o based on the resistance parameter λ_r of the soil and the components V_o, M_o, p_o of the action on the wall. The following inequalities are in fact obtained:

$$12M_o + 6Vh_o < \lambda_r h_o^3$$
$$24M_o + 14V_o h_o + 2\lambda_a p_o h_o^2 < \lambda_r h_o^3$$

Having noted that the limiting inequality is the second one, that limits the gradient of the horizontal pressure at the superficial level O of the embedment in the soil, the minimum value of h_o is therefore obtained solving the third degree equation

$$-\lambda_r h_o^3 + 2\lambda_a p_o h_o^2 + 14V_o h_o + 24M_o = 0$$

It is to be noted that with the assumption of rigid wall, the superficial gradient σ_h^I of the pressure on the soil is underestimated. The verification formulas shown above should therefore be applied with the appropriate precautions (increased safety factors) and only for embedded segments that are not too slender.

The general case that does not neglect the flexibility of the wall leads to an equation that is formally identical to the one of the beam on elastic soil

$$EIv^{IV} + k_h v = p_h \qquad (b = 1),$$

where $v = v(\xi)$ is the horizontal displacement of the current section at a depth ξ, but with the coefficient

$$k_h = k_1 \xi$$

which is not constant. Its solution requires appropriate discretization numerical techniques.

Within the domain of the approximated solution with rigid diaphragm wall, for the verification in bending of the wall the *embedment depth* $\overline{\zeta}$ is defined so that it results

$$M(\overline{\zeta}) = \overline{M},$$

where $\overline{M}$ is the maximum value of the bending moment. In the same section of peak moment the shear force $V(\overline{\zeta})$ is zero (see Fig. 9.46).

Having set

$$V(\zeta) = V_o + p_h \zeta - \int_0^\zeta \sigma(\xi) \mathrm{d}\xi$$

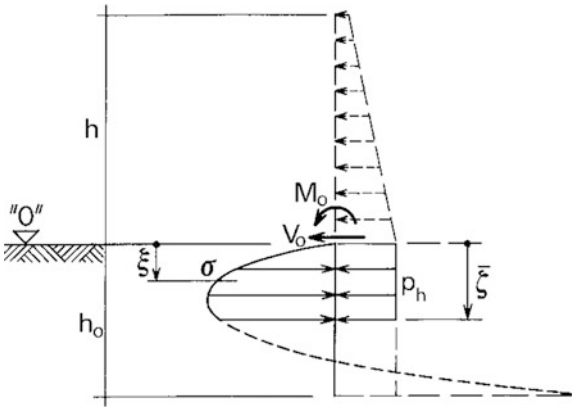


Fig. 9.46 Global equilibrium condition of the diaphragm wall

where, with $k_h = k_1\xi$, one has

$$\sigma(\xi) = k_1\xi\delta_h + k_1\xi\left(\frac{2}{3}h_o - \xi\right)$$

the third-degree equation is eventually obtained from which $\overline{\zeta}$ is to be obtained

$$\frac{12F}{h_o^4}\zeta^3 - \left(\frac{H}{h_o^2} + \frac{12F}{h_o^3}\right)\zeta^2 + p_h\zeta + V_o = 0$$

The maximum moment, with which the section of the wall is to be verified, is therefore

$$M = M_o + V_o\overline{\zeta} + p_h\frac{\overline{\zeta}^2}{2} - \int_0^{\overline{\zeta}}(\overline{\zeta} - \zeta)\sigma(\xi)\mathrm{d}\xi =$$

$$= \frac{3F}{h_o^4}\overline{\zeta}^4 - \left(\frac{H}{3h_o^2} + \frac{4F}{h_o^3}\right)\overline{\zeta}^3 + \frac{p_h}{2}\overline{\zeta}^2 + V_o\overline{\zeta} + M_o$$

Technological Aspects

Diaphragm walls can be used as support structures, other than for the horizontal pressures, also for vertical loads, giving a deep foundation working by skin friction and end bearing (see Fig. 9.47a). In this case, the embedment depth h_o of the wall is given more by vertical capacity requirements than horizontal fixity, for which it is usually more than sufficient.

If the height h of the wall to be supported is too much for the cantilever behaviour of the diaphragm wall, tendons can be used, which are anchored in deep soil strata and are tensioned against the diaphragm wall itself, giving intermediate horizontal supports. The prestressing of the tendons aims at re-establishing in the

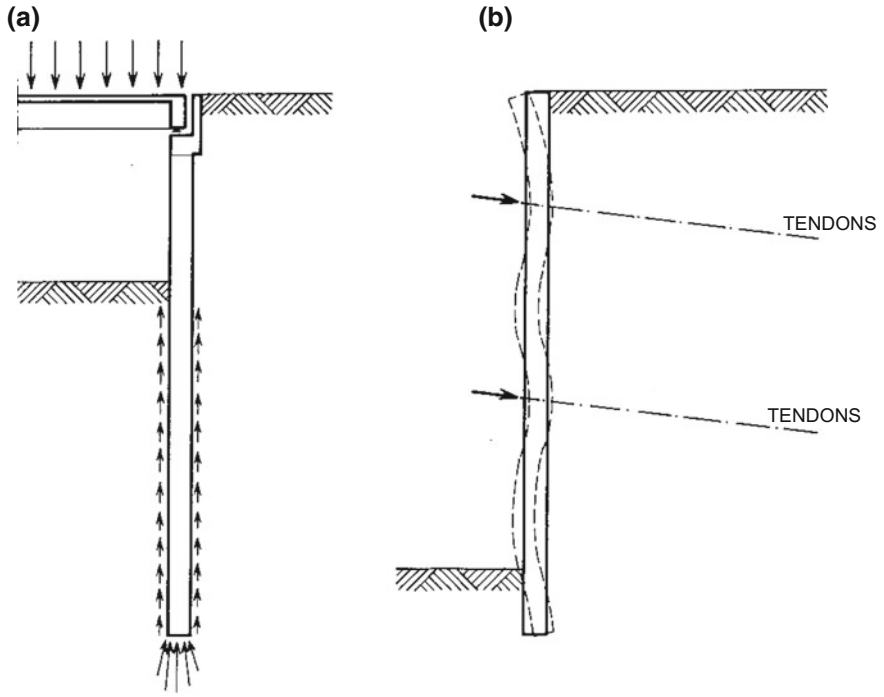


Fig. 9.47 Deep foundation wall (**a**) and diaphragm with prestressed tendons (**b**)

retained soil the stress state at rest before the excavation, therefore limiting the vertical settlements of the lateral soil. The structural scheme of this solution is shown in Fig. 9.47b, where the flexural deformed shape is also shown to visualize the behaviour.

To conclude, it should be noted how what mentioned above refers to diaphragm walls that are cast in situ, performing a to size excavation and then filling it with concrete, after positioning the appropriate reinforcement. Only after the adequate hardening of concrete the general excavation is carried.

There are also prefabricated elements, called *sheet piles*, which are driven one next to the other by hammering, in order to retain the soil with the same cantilever behaviour analysed in the previous pages.

9.4 Case A: Foundation Design

In this section, the design examples of the multi-storey reinforced concrete building presented in Chap. 2 (see figs. 2.19 and 2.20 are concluded. The resistance calculations of several foundation structural elements are shown, adopting for the

foundations the overall arrangement described in the layout plan of fig. 9.50: foundation retaining walls on the entire perimeter of the building, isolated footings for the internal columns and a raft at the bottom of the stairs core.

Several initial notes on the construction details of the structural elements of the foundations are given, first indicating the need for a *minimum reinforcement* in all parts where tensile stresses could arise. Such minimum reinforcement can be quantified with the same criterion of non-brittleness adopted for other structural elements, such as ties and beams.

For continuous foundations where, in addition to the effects of the applied loads, one can have significant stresses due to shrinkage, such criterion leads to a minimum longitudinal reinforcement defined with

$$A_s \geq A_c f_{ctm}/f_{yk}$$

as for *RC* ties (see Sect. 2.3.3). What described above is to be applied to edge beams and other tie elements that are supposed to resist axial forces.

For any element subject to bending, a minimum reinforcement should be provided equal to

$$A_s \geq \frac{1}{2}(h - x) b f_{ctm}/f_{yk}$$

as for RC beams (see Sect. 3.21), where h is the depth of the beam and x indicates the position of the neutral axis in uniaxial bending for the uncracked section ($x \cong h/2$).

With respect to the corrosion protection of the reinforcement the appropriate *increased covers* are specified, with respect to the ones required for the superstructure. A summary of the limit values for such covers is shown in Chart 9.7.

In designing the different parts of a foundation, it is good practice to keep a rather homogeneous pressure on the soil, in order to avoid significant *differential settlements* and subsequent hyperstatic internal forces in the supported structures.

Such rule should be interpreted only as an approximate recommendation. First, in fact, the value of surface pressure is not the only parameter that determines the magnitude of the soil settlement that is also affected by the smaller dimension of the loaded footprint of the foundation, from which the depth of the soil volume involved in the deformation depends (see Fig. 9.48). So larger foundations will have higher settlements under the same surface pressure.

The presence of continuous foundations of significant stiffness, such as the perimeter retaining walls, can allow significant redistributions of stresses, attenuating the effects of possible differences in loads.

Eventually, there can be specific requirements that lead to sizing certain foundation elements so that they are stressed very differently from the rest under the predominant serviceability conditions. It is the case, for example, of the foundations of corewalls of tall buildings, usually overdesigned with respect to the

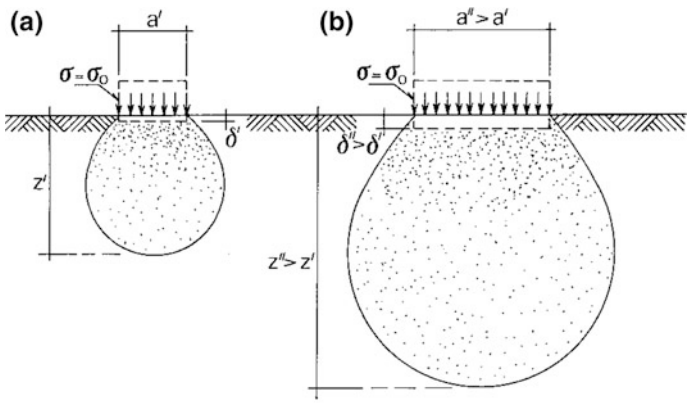


Fig. 9.48 Soil volume involved in settlement

quasi-permanent condition corresponding to vertical loads only, as they are designed for the onerous conditions under horizontal loads of wind or earthquakes.

As already mentioned, the *soil settlements* under loads consist of a short-term component and a delayed component

$$w = w_o + w_t$$

The short-term component can be calculated with the *elastic* formula

$$w_o = \kappa \frac{qB}{E_O}$$

where q is the bearing pressure on the base surface, E_o is the elastic modulus of the soil, B is the characteristic dimension of the base of the foundation which approximately corresponds to the concerned soil depth, whereas κ depends on the global geometry of the problem.

The delayed one is called *consolidation* component, it develops progressively in time and can even reach values significantly higher than the short-term initial one.

9.4.1 Verification of Footings

Only the design of the foundation element of column P14 is shown, for which the analysis of forces has already been carried at Sect. 2.4.1. From this analysis, at the bottom of the lower segment of the column, a characteristic value of the axial force is obtained equal to

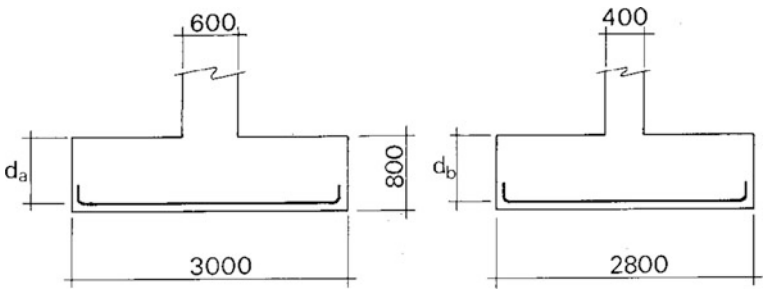


Fig. 9.49 Footing to column P14

$$N_k = 1842.9 \text{ kN}$$

It is reminded that the balanced loads coming from the upper levels lead to the absence of significant bending moments, whereas the horizontal forces on the building are resisted by the stairs core (see Serct. 8.4).

As indicated in Fig. 9.49, the foundation of the 60×40 cm column P14 see Fig. 9.50 is a 300 × 280 cm footing with a depth of 80 cm. Taking into account the self-weight of the footing, the following vertical action is applied on the support base:

From the column	1842.9 kN
−3.00 × 2.80 × 0.80 × 25	=168.0 kN
P	=2010.9 kN

which leads to a pressure

$$\sigma_g = \frac{2010900}{3000 \times 2800} = 0.239 \text{ N/mm}^2$$

Soil Resistance

The partial safety factors of Chart 9.6 are adopted, from which, with $\gamma_{G1} = 1.0$ and $\gamma_{G2} = \gamma_Q = 1.3$, the following average approximate value is obtained for the actions

$$\gamma_F \cong 0.3 \times 1.0 + 0.7 \times 1.3 \cong 1.20$$

The design value of the applied action becomes

$$\sigma_d = \gamma_F \sigma_g = 1.2 \times 0.239 = 0.287 \text{ N/mm}^2$$

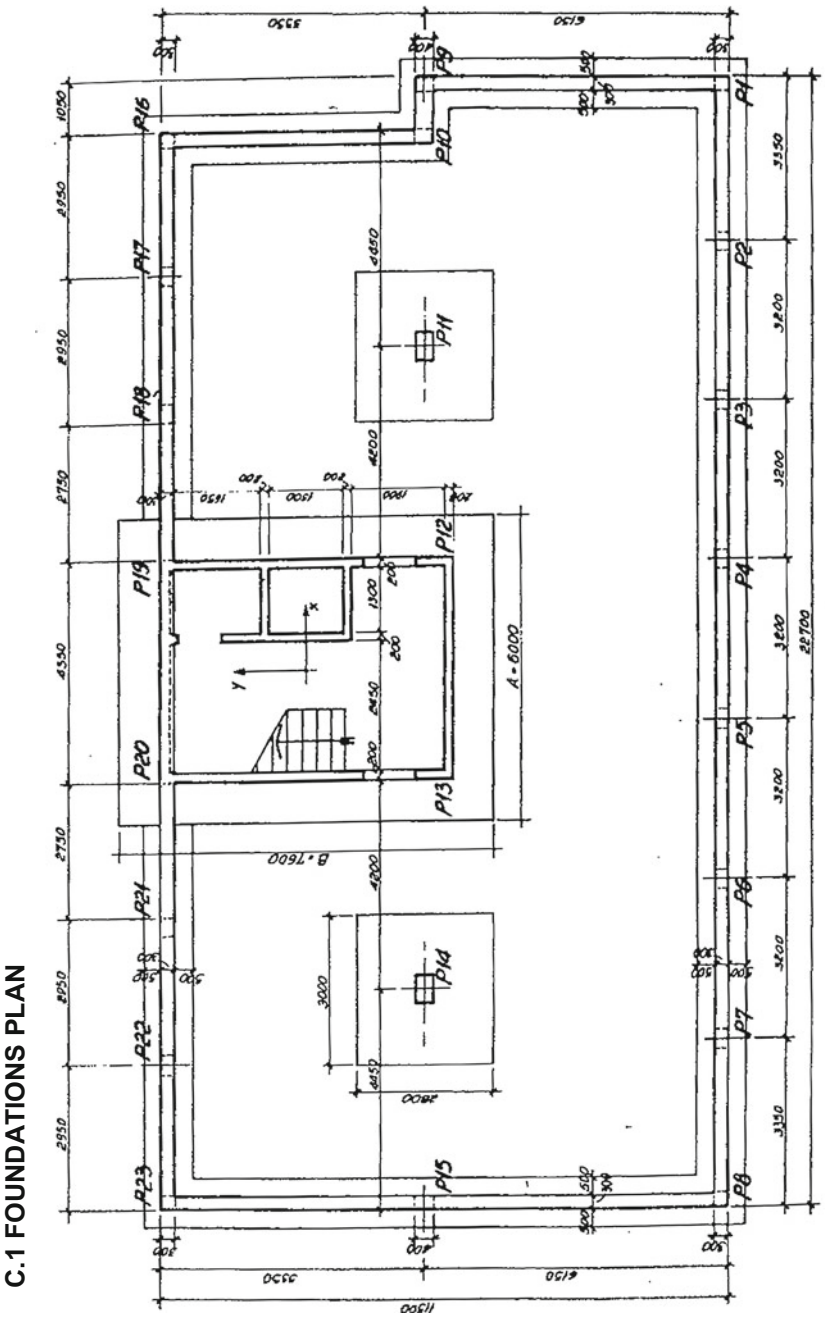


Fig. 9.50 Foundation layout

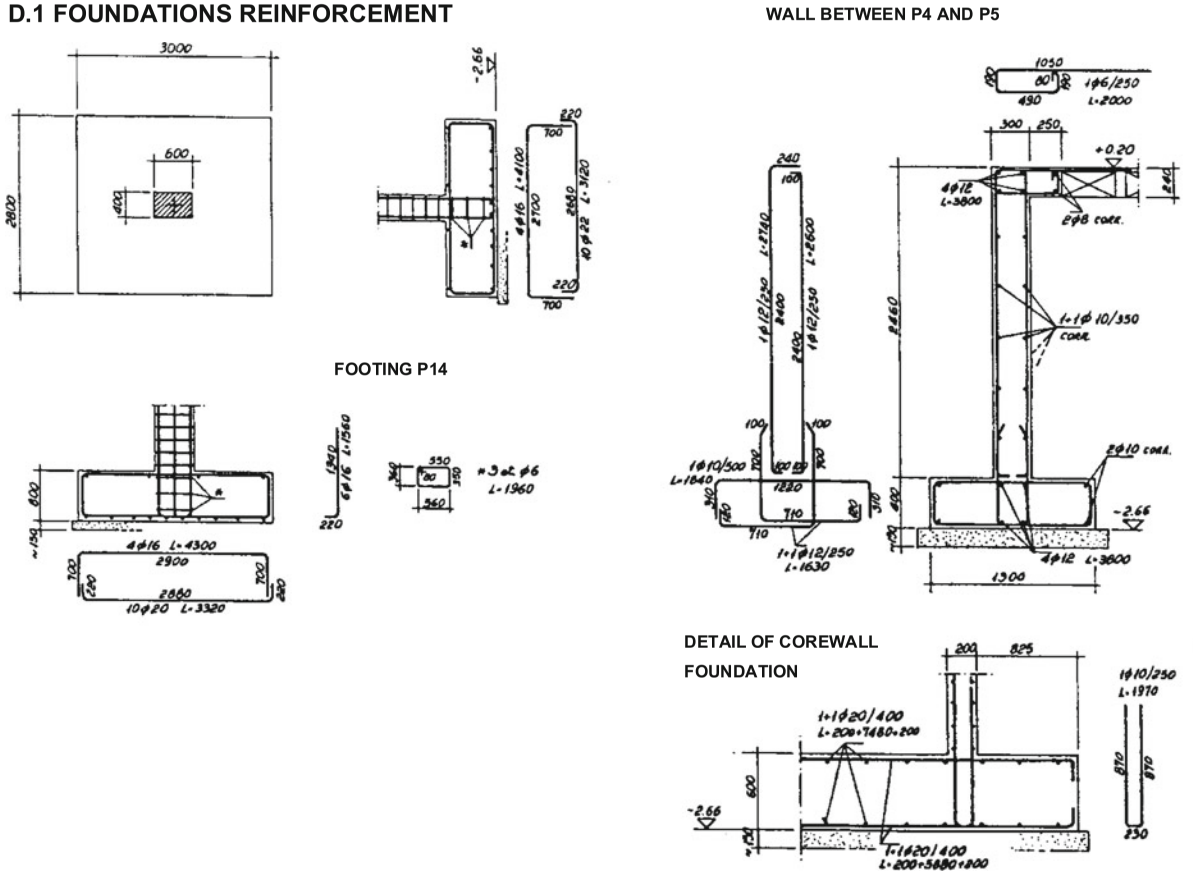


Fig. 9.51 Foundations reinforcement

A compact gravelly soil is assumed with $c = 0$, $\phi = 35°$ and with $g = 18$ kN/m^3. The resistance is therefore calculated, for a depth $h = 0.80$ m of partial excavation with

$$r_V = s_q N_q g h + s_g N_g g b/2$$

where the design value of the resistance parameter is used

$$tg\phi/\gamma_\phi = 0.70/1.25 = 0.56$$

From the table of Chart 9.3 one consequently obtains

$$N_q = 16.91 \quad N_g = 20.06$$

For $b/a \cong 2800/3000 = 0.933$, one has the shape coefficients

$$s_q = 1 + (b/a)tg\varphi = 1.522$$
$$s_g = 1 - 0.4b/a = 0.627$$

which eventually lead to

$$-1.522 \times 16.91 \times 18 \times 0.80/1000 = 0.371 \text{ N/mm}^2$$
$$-0.627 \times 20.06 \times 18 \times 2.80/2000 = \underline{0.317} \text{ N/mm}^2$$
$$r_v = 0.688 \text{ N/mm}^2$$

With the model coefficient $\gamma_R = 1.8$ the design value of the resistance becomes

$$r_V = 0.688/1.8 = 0.382 \text{ N/mm}^2 \quad (> \sigma_d)$$

and the verification remains satisfied.

Design of the Footing

For the design of the reinforcement, with $f_{yd} = 391$ N/mm^2 and $\gamma_F \cong 1.43$, one has the following values.

- *Direction a* ($a = 300$ cm, $a' = 60$ cm, $d_a = 75$ cm)

$$c_a = 60/4 = 15 \text{ cm} \quad (= 0.2 \times 75)$$
$$l_a = \frac{300 - 60}{4} + 15 = 75 \text{ cm}$$
$$\lambda_a = 75/75 = 1.000$$
$$2P_a = \frac{300 - 60}{300} 1842.9 = 1474 \text{ kN}$$
$$A_{sa} \geq \frac{1474 \times 1.000}{2 \times 39.1} 1.43 = 26.95 \text{ cm}^2$$

$10\phi 20$ are chosen with $A_{sa} = 31.42$ cm^2.

- *Direction b* (a = 280 cm, b' = 40 cm, d_b = 73 cm)

$$c_b = 40/4 = 10\,\text{cm} \quad (<0.2 \times 73)$$
$$l_b = \frac{280 - 40}{4} + 10 = 70\,\text{cm}$$
$$\lambda_b = 70/73 = 0.959$$
$$2P_b = \frac{280 - 40}{280} 1842.9 = 1580\,\text{kN}$$
$$A_{sb} \geq \frac{1580 \times 0.959}{2 \times 39.1} 1.43 = 27.71\,\text{cm}^2$$

  10ϕ20 are chosen with A_{sb} = 31.42 cm^2.

- *Concrete capacity* (f_{cd} = 14.2 MPa)

$$\frac{P - P_O}{P} = 1 - \frac{60 \times 40}{300 \times 280} = 0.971$$
$$\left(1 + \lambda_a^2\right) = 1 + 1.000^2 = 2.000$$
$$\left(1 + \lambda_b^2\right) = 1 + 0.959^2 = 1.920$$

$$P_{rc} = 2 \times 0.4 \times d_a b' f_{c1} / \left(1 + \lambda_a^2\right) + 2 \times 0.4 d_b a' f_{cd} / \left(1 + \lambda_b^2\right) =$$
$$= 0.8 \times 75 \times 40 \times 1.42/2.000 + 0.8 \times 73 \times 60 \times 1.42/1.92 =$$
$$= 1704 + 2591 = 4295\,\text{kN}$$

The design value of the applied load is

$$P'_d = 0.971 \times 1842.9 \times 1.43 = 2559\,\text{kN} \quad (<P_{rc})$$

It is to be noted that the self-weight of the footing is not considered in its verifications since, balanced at each point by the corresponding soil reaction, it does not generate internal forces.

The details of the footing are shown in Fig. 9.51. In addition to the main reinforcement (in tension) designed above, several top bars are indicated, which complete the reinforcement cage in compression, as well as the starter bars of the column as already indicated in Fig. 2.24.

9.4.2 Design of the Retaining Wall

Only the foundation wall of columns *P*1, *P*2, …, *P*8 (Fig. 9.52) of the building described in the already mentioned Figs. 2.19 and 2.20 will be analysed, starting

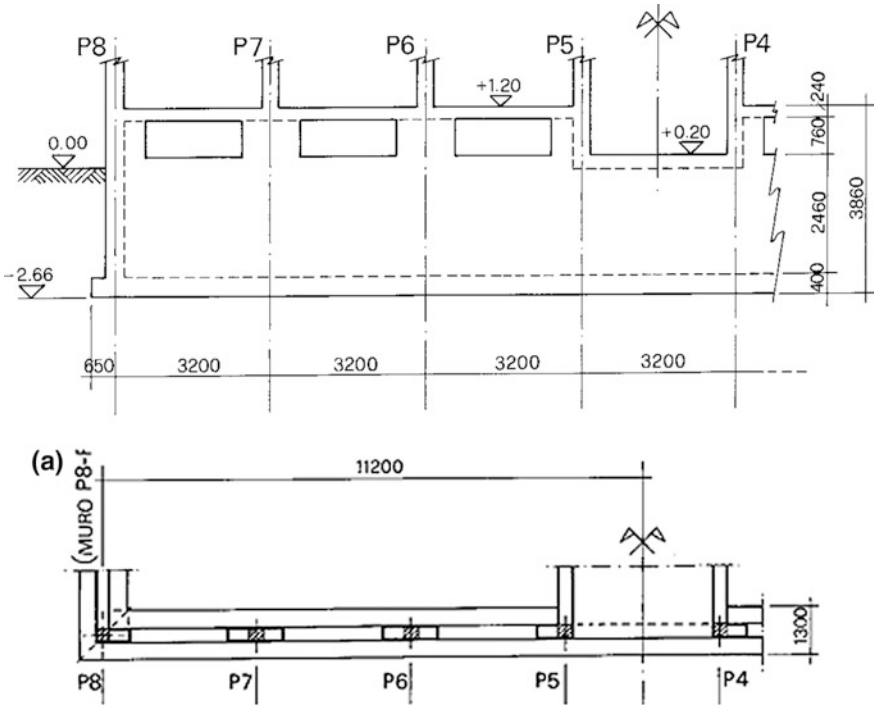


Fig. 9.52 Dimensions of the foundation wall

with the calculation of the vertical actions on the internal columns, for which in Fig. 2.23 a tributary area can be measured equal to

$$0.9 \times 3.20 \times 3.15 = 9.07 \text{ m}^2$$

Analysis of Actions

With the data of Sect. 2.4.1, the analysis of loads leads to the vertical actions calculated below.

Permanent loads			
Floor	9.07×7.00	=	63.5 kN
Column	$2.82 \times 0.30 \times 25$	=	6.3 kN
			69.8 kN
Cladding wall	$1.0 \times 9.00 \times 2.90$	=	26.1 kN
			95.9 kN
Roof			
Live	9.07×1.20	=	10.9 kN
Permanent			69.8 kN
			80.7 kN

(continued)

(continued)

4th floor			
Variable	9.07 × 1.40	=	12.7 kN
Permanent			95.9 kN
			108.6 kN
Lower floors			
Variable	9.07 × 1.40	=	12.7 kN
Permanent			95.9 kN
			108.6 kN

The axial actions in the columns *P*3, *P*4, …, *P*6 under analysis at the different levels of the building are shown in the following table:

	F_k (kN)	N_k (kN)
4°	80.7	80.7
3°	108.6	189.3
2°	108.6	297.9
1°	108.6	406.5
PR	108.6	515.1
SI	108.6	623.7

If the load of the foundation wall (see Fig. 9.53) is added to the load *P* coming from the columns, with some approximations in the calculations one obtains:

$$0.30 \times 2.46 = 0.738 \times 25 = 18.45$$
$$1.00 \times 0.40 = 0.400 \times 25 = \underline{10.00}$$
$$= 28.45\,\text{kN/m}$$

From the column		623.7
Wall self-weight	3.20 × 28.45 =	91.0
		714.7 kN

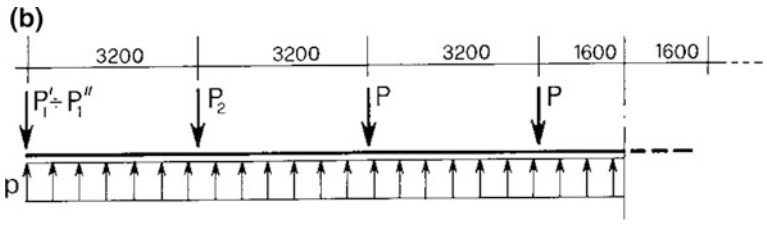


Fig. 9.53 Isolated static scheme of the foundation wall

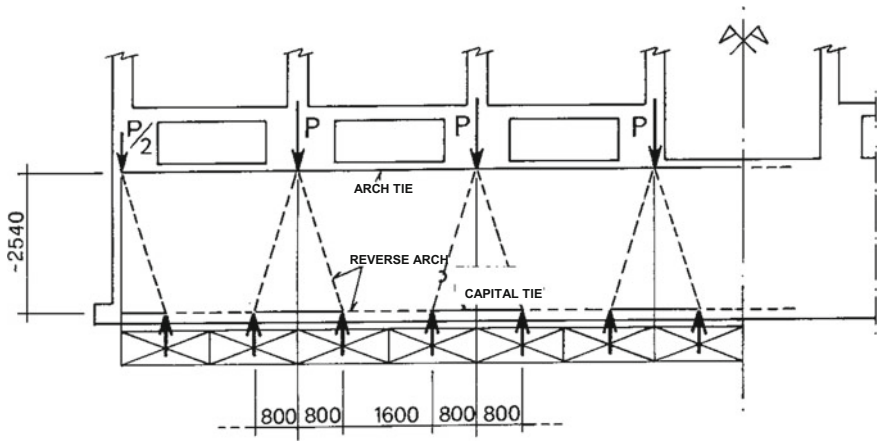


Fig. 9.54 Strut and tie balanced scheme for the foundation wall

Soil Resistance

Therefore, for a support width equal to 1.30 m (see Fig. 9.53), one has an approximate average value of the characteristic pressure on the soil

$$\sigma_g = \frac{714.7}{1.30 \times 3200} = 0.172\,\mathrm{N/mm^2}$$

with a design value

$$\sigma_d = \gamma_F \sigma_g = 1.2 \times 0.172 = 0.206\,\mathrm{N/mm^2}$$

to be compared to the soil capacity ($b << a$)

$$\begin{aligned} 16.91 \times 18 \times 0.80/1000 &= 0.244\,\mathrm{N/mm^2} \\ 20.06 \times 18 \times 2.80/200 &= \underline{0.235\mathrm{N/mm^2}} \\ r_V &= 0.479\,\mathrm{N/mm^2} \end{aligned}$$

for the verification

$$r_{Vd} = r_V/\gamma_R = 0.479/1.8 = 0.266 \quad (> \sigma_d)$$

Wall-Beam

In order to calculate the longitudinal internal forces in the foundation wall, the function of the beam on elastic soil presented at Sect. 9.2.1 should be elaborated. About the distribution of the load coming from the column at the corner between

the two orthogonal foundation walls, (for example the column P8 in the extract of Fig. 9.52), instead of designing the entire foundation as a grid (as described at Sect. 9.2.3), an initial calculation can be carried based on the appropriate flexural stiffnesses of the walls or, more simply, on isolated scheme of Fig. 9.53 can be elaborated twice, first with an upper bound assumption P_1', then with a lower bound assumption P_1'' of the competent portion of the load.

Only the approximate calculations of preliminary sizing are described here, which ensure the equilibrium for each span of the current uniform loads. The global effects of uneven loads can be added later, as the ones usually present at the ends of the wall at the corner columns. An adjustment of the results with an appropriate increase of the reinforcement should eventually be carried, to compensate the limited refinement of the model (for example with $\gamma_R = 2$).

The arch scheme to ensure the local diffusion of current loads coming from the columns P onto the entire support extent of each span is shown in Fig. 9.54. With $P = 623.7$ kN, the equilibrium with the distributed reaction of the soil can be ensured with a force in the tie of the arch equal to

$$Z \cong \frac{80}{254}\frac{P}{2} = 98.2\,\text{kN}$$

Assigning this force to the tie of the reverse capital along the bottom chord, the capacity is doubled, also ensuring the flexural continuity of the wall. This leads, with $f_{yd} = 391$ N/mmq and $\gamma_F \cong 1.43$, to a double longitudinal reinforcement at least equal to

$$A_s = A_s' = \frac{1.43 \times 98.2}{39.1} = 3.59\,\text{cm}^2$$

4ϕ12 are chosen, equal to 4.52 cm^2

Lateral Earth Pressure

To conclude the design of the reinforcement, as described in the cross section of Fig. 9.51, the transverse bending calculation of the wall should be carried under the lateral soil pressure. The static scheme referred to a vertical strip of unit width of the central portion of the wall between the columns P4 and P5 (see Fig. 9.52) is represented in Fig. 9.55. With a conservative approximation, the constraints at top and bottom have been assumed as simple supports, extending however symmetrically on the entire height of the wall the reinforcement calculated in this way.

Of the two contributions p_1 and p_o of the lateral pressure indicated in Fig. 9.55, the triangular one derives from the self-weight g of the soil, and the constant one from the superimposed surface load q. For this it is assumed

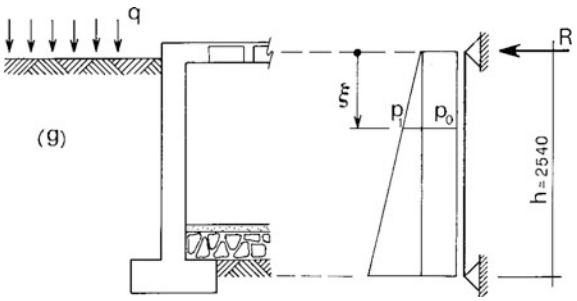


Fig. 9.55 Lateral earth pressure on the foundation wall

$$q = 20\,\mathrm{kN/m^2}$$

which is required even when the building is not adjacent to a traffic road, to allow the passage of the fire truck in case of fire in the building. For the soil, a unit weight g = 18 kN/m^3 and an internal friction angle ϕ = 35° have been assumed. With a design value $tg\phi/\gamma_\phi$ = 0.70/1.25 = 0.56 from Table 9.3 a friction angle reduced to ϕ = 29.2 is obtained.

Subsequently, assuming no cohesion, a coefficient of active pressure is deduced equal to

$$\lambda_a = tg^2\left(\frac{\pi}{4} - \frac{\phi}{2}\right) = 0.344$$

which leads to the two contributions of lateral pressure (see Fig. 9.53)

$$p_o = 0.344 \times 20 = 6.88 \quad \mathrm{kN/m^2\ (constant)}$$
$$p_l = 0.344 \times 18\xi = 6.19\xi \quad \mathrm{kN/m^2\ (linear)}$$

Indicating with R the horizontal reaction given by the top constraint of the floor, one has

$$\mathrm{R} = \frac{6.88 \times 2.54}{2} + \frac{6.19 \times 2.54^2}{6} = 8.74 + 6.66 = 15.40\,\mathrm{kN/m}$$

the internal forces are consequently expressed as

$$V(\xi) = 15.40 - 6.88\xi - 6.19\xi^2/2 = 8.74 - 6.88\xi - 3.095\xi^2$$
$$M(\xi) = 15.40\xi - 6.88\xi^2/2 - 6.19\xi^3/6 = 15.40\xi - 3.44\xi^2 - 1.032\xi^3$$

For $V(\xi) = 0$ one obtains

$$\overline{\xi} = \frac{-6.88 + \sqrt{6.88^2 + 4 \times 3.095 \times 15.40}}{2 \times 3.095} = 1.38\,\text{m}$$

from which the maximum bending moment is obtained

$$\overline{M} = M(\overline{\xi}) = 21.25 - 6.55 - 2.71 = 11.99\,\text{kNm/m}$$

If the axial force N is neglected, which is low in the central zone of the span P4–P5 under analysis, with $\gamma_F = 1.5$ and $d = 26$ cm one obtains

$$A_s \cong \frac{1.5 \times 11.99}{0.9 \times 0.26 \times 39.1} = 1.97\,\text{cm}^2/\text{m}$$

The small height of the wall with respect its thickness leads to little reinforcement. In order to comply with the non-brittleness criterion, this reinforcement should be brought, for the thickness $h = 30$ cm of the wall, to minimum values of

$$A_s \cong \frac{1}{2}\frac{h}{2}\frac{f_{ctm}}{f_{yk}} = 0.25 \times 3000 \times 2.78/450 \cong$$
$$\cong 0.0015 \times 3000 = 4.50\,\text{cm}^2/\text{m}$$

independently from the applied action.

The reinforcement adopted is 4ϕ12/m on each side for a total of 2×4.52 cm^2/m, and the horizontal bars are also added with an appropriate spacing along the height of the wall, as indicated in Fig. 9.51.

Toe Reinforcement

The verification of the reinforcement of the foundation toe is eventually to be carried. Using the formulas of stocky cantilevers, as for the footing of Fig. 9.49, for a width $b = 100$ cm one has (with $d = 35$ cm, $a = 130$ cm and $a' = 30$ cm)

From the column	623.7/3.20	194.91 kN/m
Wall self-weight		18.45 kN/m
		N = 213.36 kN/m

$$c_a = 0.2 \times 35 = 7.0\,\text{cm}(< 30/4)$$
$$l_a = \frac{130 - 30}{4} + 7.0 = 32.0\,\text{cm}$$
$$\lambda_a = \frac{32.0}{35.0} = 0.914$$
$$2P_a = \frac{100}{130}213.36 = 164.1\,\text{kN/m}$$
$$A_{sa} \geq \frac{1641 \times 0.914}{2 \times 391}1.43 = 2.74\,\text{cm}^2/\text{m}$$

In order to adjust the reinforcement of the footing to the vertical reinforcement of the wall above and the criteria of non-brittleness, as shown in the layout of Fig. 9.51, $4\phi 12/m$ are chosen, equal to 4.52 cm^2/m.

The capacity of the concrete remains largely higher

$$P_{\mathrm{Rc}} = 2 \times 04 \times 35 \times 100 \times 1.42/\left(1 + 0.914^2\right) = 2167\,\mathrm{kN}$$
$$P_{\mathrm{Ed}} = 168.7 \times 1.43 = 234.7 \quad (\ll P_{\mathrm{Rc}})$$

9.4.3 Design of the Corewall Foundation

Contrarily to foundation elements mainly subject to vertical loads, for which the moment resistance was not essential for equilibrium, the raft at the base of the stair core is subject to the overturning effects of the horizontal forces. On this raft the stability core of the entire building is founded.

As already described in the diagrams of Fig. 8.25, it can be assumed that the horizontal shear stresses due to shear and torsion are spread on the entire box system of the perimeter retaining walls at the raised ground floor level, thanks to the rigid diaphragm of the floor. The bending moment on the core is transferred down to the raft with the same magnitude, whereas the axial force increases due to the weight of the tributary portion of the floor and the last segment of the walls. The resistance to the significantly eccentric load of this foundation is therefore crucial for the equilibrium of the entire building.

A full analysis of the internal forces in the core has been carried at Sect. 8.2.1. The following characteristic values can be read from the pertinent tables

Axial force	N = 6000 kN
Moment along x	M_y = 3190 kNm
Moment along y	M_x = 4815 kNm

where the two moments M_x and M_y are not simultaneous. The self-weight of the slab (see Figs. 9.50 and 9.51) is also to be added to the axial force N

$$G = 0.60 \times 25 \times 6.00 \times 7.60 = 15 \times 6.00 \times 7.60 = 648\,\mathrm{kN}$$

Several conservative assumptions have been made in the following calculations, such as neglecting the continuity of the slab with the retaining wall towards columns P18 and P21, which is very effective with respect to the moment M_y. With reference to an isolated stair core on its foundation, the following calculations are carried, which contemplate the design of the reinforcement of the raft and the overturning verification.

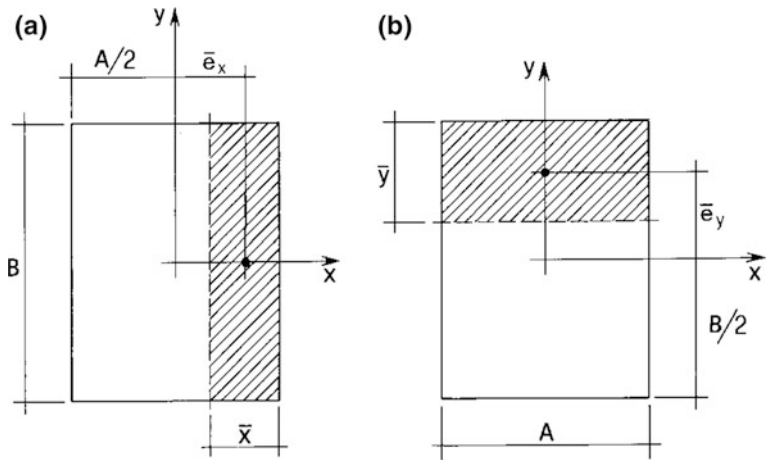


Fig. 9.56 Limit allowable eccentricities for action along x (**a**) and along y (**b**)

Minimum vertical load

The following design actions are assumed (with P_k = 6000 + 648 = 6648 kN):

$$P_d = 1.0 \times 6648 = 6648\,\text{kN}$$
$$M_{yd} = 1.5 \times 3190 = 4785\,\text{kNm}$$
$$M_{xd} = 1.5 \times 4815 = 7222\,\text{kNm}$$

- *Force along x* (A = 6.00 m—see Fig. 9.56)

$$e_x = 4785/6648 = 0.72\,\text{m} \quad (<A/6)$$

Maximum ground bearing pressure (section entirely in compression)

$$7.60 \times 6.00 = 45.6\,\text{m}^2$$
$$7.60 \times 6.00^2/6 = 45.6\,\text{m}^3$$
$$\bar{\sigma}_g = \left\{\frac{6648}{45.6} + \frac{4785}{45.6}\right\}10^{-3} = 0.251\ \text{N/mm}^2$$

- *Reinforcement design* (d_x = 55 cm)
  raft protrusion

$$l_x = 0.825 + 0.20/2 \cong 0.93\,\text{m}$$

pressure under wind (without raft self-weight)

$$p = 251 - 15 = 236 \ \text{kN/m}^2$$

fixed-end moment

$$M \cong 236 \times 0.93^2/2 = 102.1 \ \text{kNm/m}$$

bottom reinforcement ($f_{yd} = 391 \ \text{N/mm}^2$)

$$A_s \geq \frac{102.1}{0.9 \times 0.55 \times 39.1} = 5.28 \ \text{cm}^2/\text{m}$$

1ϕ20/400 is chosen, equal to 7.85 cm^2/m

- *Loaded limit strip* (for $x/A \approx 0.40$)

$$(\phi = 35°, g = 18 \ \text{kN/m}^3, tg\phi/\gamma_\phi = 0.56, \ \text{N}_q = 16.91, N_g = 20.06)$$
$$s_g \cong 1 - 0.4 \times 0.40 = 0.84 \quad s_q \cong 1 + 0.4 \times 0.56 = 1.22$$
$$r_o = s_q N_q g h = 1.22 \times 16.19 \times 18 \times 0.8 = 297.1 \ \text{kN/m}^2$$
$$\text{r}_1 = s_g N_q \text{g}/2 = 0.84 \times 20.06 \times 18/2 = 151.7 \ \text{kN/m}^3$$
$$\overline{x} = \left\{ - r_o + \sqrt{r_o^2 + 4 r_1 \gamma_R P_d / B} \right\} / (2 r_1)$$

with $\gamma_R = 1.8$, $B = 7.6$ m and $P_d = 6648$ kN one obtains

$$\overline{x} = 2.38 \ \text{m} \qquad (2.38/6.00 = 0.397)$$

- *Overturning verification* (see Fig. 9.54a)

$$\bar{e_x} = 3.00 - 2.38/2 = 1.81 \ \text{m} \qquad (> e_x = 0.72 \ \text{m})$$

- *Force along y* (B = 7.60 m—see Fig. 9.56)

$$e_y = 7222/6648 = 1.08 \ \text{m} \qquad (< B/6)$$

maximum ground bearing pressure (section entirely in compression)

$$7.60 \times 6.00 \qquad = 45.6 \ \text{m}^2$$
$$7.60^2 \times 6.00/6 = 57.76 \ \text{m}^3$$
$$\bar{\sigma}_g = \left\{ \frac{6648}{45.6} + \frac{7222}{57.76} \right\} \times 10^{-3} = 0.271 \ \text{N/mm}^2$$

- *Reinforcement design* (d_y = 53 cm)
  raft protrusion

$$l_y = 0.825 + 0.20/2 \cong 0.93\,\text{m}$$

  pressure under wind (without raft self-weight)

$$p = 271 - 15 = 256\,\text{kN/m}^2$$

  fixed-end moment

$$M \cong 256 \times 0.93^2/2 = 110.7\,\text{kNm/m}$$

  bottom reinforcement ($f_{yd} = 391\ \text{N/mm}^2$)

$$A_s \geq \frac{110.7}{0.9 \times 0.53 \times 39.1} = 5.94\,\text{cm}^2/\text{m}$$

  1ϕ20/400 is chosen, equal to 7.85 cm^2/m

- *Overturning verification* (see Fig. 9.54b—assuming $y/B \approx 0.40$)

$$r_o = 297.1\,\text{kN/m}^2$$
$$r_1 = 151.7\,\text{kN/m}^3$$
$$\overline{y} = \left\{-r_o + \sqrt{r_o^2 + 4r_1\gamma_R P_d/A}\right\}/(2r_1)$$

  with γ_R = 1.8, A = 6.0 m and P_d = 6648 kN one obtains

$$\overline{y} = 2.78\,\text{m} \quad (2.78/7.60 = 0.365)$$
$$\overline{e}_y = 3.80 - 2.78/2 = 2.41\,\text{m} \quad \left(> e_y = 1.08\,\text{m}\right)$$

  Maximum vertical load

$$P_d = 1.43 \times 6648 = 9507\,\text{kN}$$
$$M_{yd} = 1.5 \times 3190 = 4785\,\text{kNm}$$
$$M_{xd} = 1.5 \times 4815 = 7222\,\text{kNm}$$

- *Force along x* (A = 6.00 m—see Fig. 9.56)

$$e_x = 4785/9587 = 0.50\,\text{m} \quad (<A/6)$$

maximum earth pressure

$$\overline{\sigma}_{\mathrm{g}} = \left\{\frac{9507}{45.6} + \frac{4785}{45.6}\right\} \times 10^{-3} = 0.313 \ \mathrm{N/mm^2}$$

- *Verification of the raft in bending* (d_x = 55 cm)

$$p = 313 - 15 = 298\,\mathrm{kN/m^2}$$
$$M \cong 298 \times 0.93^2/2 = 128.9\,\mathrm{kNm/m}$$
$$1\phi 20/400 \quad A_{\mathrm{s}} = 7.85\ \mathrm{cm^2/m}$$
$$\overline{x} = \frac{7.85 \times 391}{100 \times 14.2} = 2.16\ \mathrm{cm} \quad (<0.08d_{\mathrm{x}})$$
$$z = 0.96 \times 0.55 = 0.528\,\mathrm{m}$$
$$M_{\mathrm{Rd}} = 7.85 \times 39.1 \times 0.528 = 162.1\,\mathrm{kNm/m} \quad (>M)$$

- *Overturning verification* (assuming $x/A \approx 0.50$)

$$s_g \cong 1 - 0.4 \times 0.5 = 0.80 \quad s_q \cong 1 + 0.4 \times 0.56 = 1.28$$
$$r_o = s_{\mathrm{q}} N_{\mathrm{q}} g h = 1.28 \times 16.91 \times 18 \times 0.8 = 311.7\ \mathrm{kN/m^2}$$
$$r_1 = s_{\mathrm{g}} N_{\mathrm{g}} g/2 = 0.80 \times 20.06 \times 18/2 = 144.4\,\mathrm{kN/m^3}$$
$$\overline{x} = \left\{-r_{\mathrm{o}} + \sqrt{r_{\mathrm{o}}^2 + 4 r_1 \gamma_{\mathrm{R}} P\mathrm{d}/B}\right\}/(2r_1)$$

with $\gamma_{\mathrm{R}} = 1.8$, $B = 7.6$ m and P_{d} = 9507 kN one obtains

- *Force along y* (B = 7.60 m—see Fig. 9.56)

$$e_y = 7222/9507 = 0.76\,\mathrm{m} \qquad (<B/6)$$

maximum earth pressure

$$\overline{\sigma}_{\mathrm{g}} = \left\{\frac{9507}{45.6} + \frac{7222}{57.76}\right\} \times 10^{-3} = 0.334 \ \mathrm{N/mm^2}$$

- *Verification of the raft in bending* (d_y = 53 cm)

$$p = 334 - 15 = 319\,\mathrm{kN/m^2}$$
$$M \cong 319 \times 0.93^2/2 = 138.0\,\mathrm{kNm/m}$$
$$1\phi 20/400 \quad A_{\mathrm{s}} = 7.85\ \mathrm{cm^2/m}$$
$$z = 0.96 \times 0.53 = 0.509\,\mathrm{m}$$
$$M_{\mathrm{Rd}} = 7.85 \times 39.1 \times 0.509 = 156.2\,\mathrm{kNm/m} \quad (>M)$$

- *Overturning verification* (assuming $y/B \approx 0.50$)

$$r_o = 311.7\ \text{kN/m}^2$$
$$r_1 = 144.4\,\text{kN/m}^3$$
$$\overline{y} = \left\{ -r_o + \sqrt{r_o^2 + 4r_1\gamma_R P_d/B} \right\} / (2r_1)$$

with $\gamma_R = 1.8,\ B = 6.0$ m and $P_d = 9507$ kN one obtains

$$\overline{y} = 3.49\,\text{m} \quad (3.49/7.60 = 0.460)$$
$$\overline{e}_y = 3.80 - 3.49/2 = 2.05\,\text{m} \quad \left(> e_y = 0.76\ \text{m} \right)$$

The reinforcement layout of the raft is shown in Fig. 9.51. A double mesh $\phi 20$ 40×40 cm is chosen, which will have to be appropriately verified based on the orthogonal bending moments calculated in different zones of the plate, in addition to the fixed ends of the lateral protrusions already considered above.

Appendix: Data on Soils and Foundations

Table 9.1: Soil Parameters

The following tables give indicative values for the main soil parameters, necessary for the stability calculations:

k subgrade coefficient (expressed in N/mm^3)
g unit weight (expressed in kg/dm^3)
ϕ internal friction angle (expressed in degrees)
c cohesion (expressed in N/mm^2)

a—subgrade coefficient (N/mm^3)

Type of soil	k
Coarse gravel	0.150–0.250
Gravel–sand mixtures	0.100–0.150
Dry clay or silt	0.070–0.100
Compact sand	0.050–0.100
Humid clay or silt	0.030–0.060
Fine or soft sand	0.015–0.020
Recent backfills	0.010–0.020
Organic tillage	0.005–0.015

b—unit weight of soils (kg/dm^3)

Type of soil	g (soft)	g (compact)
Dry gravel[a]	1.5–1.7	1.8–2.0
Humid gravel[a]	1.7–1.9	1.9–2.1
Saturated gravel[a]	1.9–2.1	2.0–2.2
Dry organic[b]	1.4–1.6	1.7–1.9
Humid organic[b]	1.6–1.8	1.8–2.1
Saturated organic[b]	1.8–2.0	2.0–2.2
Clay, silt	1.7–1.9	2.0–2.2

[a]or sand [b]tillage

c—internal friction angle of soils

Type of soil	ϕ
Multi-graded coarse compact gravel	45–50
Multi-graded coarse loose gravel	35–40

(continued)

(continued)

Type of soil	ϕ
Multi-graded round compact gravel	40–45
Mono-graded round compact gravel	35–40
Multi-graded round loose gravel	30–35
Mono-graded round loose gravel	25–30
Compact sand	35–40
Loose sand	25–30
Organic (tillage) sand	15–25
Fat[a] organic (tillage)	0–20
Sandy clay	15–25
Fat[a] clay	0–20
Silt	20–25

[a]Depending on moisture content, or pore water pressures

d—cohesion of soils (N/mm^2)

Type of soil	c
Hard clay	0.100–1.000
Stiff clay	0.050–0.100
Plastic clay	0.020–0.050
Sandy clay	0.010–0.020
Compact silt	0.005–0.010

Chart 9.2: Soil Resistance—Formulas

The following formulas refer to a type of *global failure* with the formation of a sliding surface in the soil from underneath the foundation up to the ground level. They give the capacity of the foundation in terms of distributed pressure on the horizontal support base of the foundation under the effect of the vertical loads. It is implied that such pressure is constant on the entire resisting support surface, centred on the point O where the resultant of forces is located.

Symbols

r_v resisting pressure
ϕ internal friction angle of foundation soil
c cohesion of foundation soil
g unit weight of foundation soil
q pressure acting on adjacent peripheral zones
b characteristic width of foundation

a characteristic length of foundation
A area of resisting surface
P_{Ed} resultant of vertical loads on the base of the foundation

Resistance Verification
(see Table 9.6 for partial safety factors)

$$P_{Rd} = r_v A \geq \gamma_R P_{Ed},$$

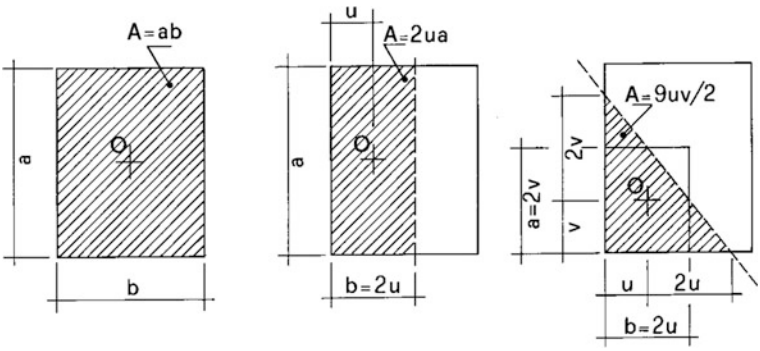
where

$$r_v = s_q N_q q + s_c N_c c + s_g N_g g b/2$$

with

$$q = hg'$$
h = depth of surrounding soil above the base
g' = unit weight of surroundings soil
$$s_q = 1 + (b/a) tg\phi$$
$$s_c = 1 + (b/a)\left(N_q/N_c\right)$$
$$s_g = 1 - 0.4(b/a)$$
γ_R = model coefficient (see Table 9.6)

The characteristic dimensions a, b ($a \geq b$) of the foundation are described in the figure.



The values of N_q, N_c ed N_g are given in Table 9.3 as a function of ϕ.

Table 9.3: Parameters of Resistance Formulas

The following table gives, as a function of the internal friction angle ϕ of soil, the values of the three parameters N_q, N_c and N_g of the formula of Chart 9.2. These values are derived from

$$N_q = e^{\pi tg\phi} tg^2\left(\frac{\pi}{4} + \frac{\phi}{2}\right)$$
$$N_c = (N_q - 1)/tg\phi$$
$$N_g = 2(N_q + 1)tg\phi$$

$tg\phi$	Nq	Nc	Ng	Nq/Nc	ϕ
0.00	1.00	5.14	0.00	0.195	0.0
0.01	1.05	5.28	0.04	0.200	0.6
0.02	1.11	5.42	0.08	0.205	1.1
0.03	1.17	5.56	0.13	0.210	1.7
0.04	1.23	5.71	0.18	0.215	2.3
0.05	1.29	5.86	0.23	0.221	2.9
0.06	1.36	6.02	0.28	0.226	3.4
0.07	1.43	6.19	0.34	0.232	4.0
0.08	1.51	6.36	0.40	0.237	4.6
0.09	1.59	6.53	0.47	0.243	5.1
0.10	1.67	6.72	0.53	0.249	5.7
0.11	1.76	6.91	0.61	0.255	6.3
0.12	1.85	7.10	0.68	0.261	6.8
0.13	1.95	7.31	0.77	0.267	7.4
0.14	2.05	7.52	0.85	0.273	8.0
0.15	2.16	7.73	0.95	0.279	8.5
0.16	2.27	7.96	1.05	0.286	9.1
0.17	2.39	8.19	1.15	0.292	9.6
0.18	2.52	8.43	1.27	0.299	10.2
0.19	2.65	8.69	1.39	0.305	10.8
0.20	2.79	8.95	1.52	0.312	11.3
0.21	2.93	9.21	1.65	0.319	11.9
0.22	3.09	9.49	1.80	0.325	12.4
0.23	3.25	9.78	1.95	0.332	13.0
0.24	3.42	10.08	2.12	0.339	13.5
0.25	3.60	10.39	2.30	0.346	14.0
0.26	3.79	10.71	2.49	0.353	14.6
0.27	3.98	11.05	2.69	0.361	15.1
0.28	4.19	11.39	2.91	0.368	15.6
0.29	4.41	11.75	3.14	0.375	16.2

(continued)

(continued)

$tg\phi$	Nq	Nc	Ng	Nq/Nc	ϕ
0.30	4.64	12.12	3.38	0.383	16.7
0.31	4.88	12.50	3.64	0.390	17.2
0.32	5.13	12.90	3.92	0.398	17.7
0.33	5.39	13.32	4.22	0.405	18.3
0.34	5.67	13.74	4.54	0.413	18.8
0.35	5.97	14.19	4.88	0.420	19.3
0.36	6.27	14.65	5.24	0.428	19.8
0.37	6.60	15.12	5.62	0.436	20.3
0.38	6.94	15.62	6.03	0.444	20.8
0.39	7.29	16.13	6.47	0.452	21.3
0.40	7.67	16.66	6.93	0.460	21.8
0.41	8.06	17.21	7.43	0.468	22.3
0.42	8.47	17.79	7.95	0.476	22.8
0.43	8.90	18.38	8.52	0.484	23.3
0.44	9.36	18.99	9.11	0.493	23.7
0.45	9.83	19.63	9.75	0.501	24.2
0.46	10.33	20.29	10.43	0.509	24.7
0.47	10.86	20.98	11.15	0.518	25.2
0.48	11.41	21.69	11.91	0.526	25.6
0.49	11.99	22.42	12.73	0.535	26.1
0.50	12.59	23.19	13.59	0.543	26.6
0.51	13.23	23.98	14.51	0.552	27.0
0.52	13.90	24.80	15.49	0.560	27.5
0.53	14.60	25.65	16.53	0.569	27.9
0.54	15.33	26.54	17.64	0.578	28.4
0.55	16.10	27.46	18.81	0.586	28.8
0.56	16.91	28.41	20.06	0.595	29.2
0.57	17.75	29.39	21.38	0.604	29.7
0.58	18.64	30.41	22.78	0.613	30.1
0.59	19.57	31.47	24.27	0.622	30.5
0.60	20.54	32.57	25.85	0.631	31.0
0.61	21.57	33.72	27.53	0.640	31.4
0.62	22.64	34.90	29.31	0.649	31.8
0.63	23.76	36.13	31.20	0.658	32.2
0.64	24.93	37.40	33.20	0.667	32.6
0.65	26.17	38.72	35.32	0.676	33.0
0.66	27.46	40.09	37.56	0.685	33.4
0.67	28.81	41.51	39.94	0.694	33.8
0.68	30.23	42.98	42.47	0.703	34.2
0.69	31.71	44.51	45.14	0.712	34.6
0.70	33.26	46.09	47.97	0.722	35.0

(continued)

(continued)

$tg\phi$	Nq	Nc	Ng	Nq/Nc	ϕ
0.71	34.89	47.73	50.96	0.731	35.4
0.72	36.59	49.44	54.14	0.740	35.8
0.73	38.38	51.20	57.49	0.750	36.1
0.74	40.25	53.04	61.05	0.759	36.5
0.75	42.20	54.94	64.80	0.768	36.9
0.76	44.25	56.91	68.78	0.778	37.2
0.77	46.39	58.95	72.99	0.787	37.6
0.78	48.64	61.07	77.43	0.796	38.0
0.79	50.99	63.27	82.14	0.806	38.3
0.80	53.44	65.55	87.11	0.815	38.7
0.81	56.01	67.92	92.36	0.825	39.0
0.82	58.71	70.37	97.92	0.834	39.4
0.83	61.52	72.92	103.78	0.844	39.7
0.84	64.47	75.55	109.98	0.853	40.0
0.85	67.55	78.29	116.53	0.863	40.4
0.86	70.77	81.13	123.45	0.872	40.7
0.87	74.14	84.07	130.75	0.882	41.0
0.88	77.67	87.12	138.46	0.891	41.3
0.89	81.36	90.29	146.60	0.901	41.7
0.90	85.21	93.57	155.19	0.911	42.0
0.91	89.25	96.98	164.25	0.920	42.3
0.92	93.46	100.51	173.81	0.930	42.6
0.93	97.87	104.17	183.91	0.940	42.9
0.94	102.48	107.96	194.55	0.949	43.2
0.95	107.30	111.90	205.78	0.959	43.5
0.96	112.34	115.98	217.61	0.969	43.8
0.97	117.61	120.21	230.10	0.978	44.1
0.98	123.11	124.60	243.26	0.988	44.4
0.99	128.86	129.15	257.13	0.998	44.7
1.00	134.87	133.87	271.75	1.007	45.0
1.01	141.16	138.77	287.15	1.017	45.3
1.02	147.72	143.84	303.39	1.027	45.6
1.03	154.58	149.10	320.49	1.037	45.8
1.04	161.74	154.56	338.51	1.046	46.1
1.05	169.23	160.22	357.48	1.056	46.4
1.06	177.05	166.08	377.46	1.066	46.7
1.07	185.22	172.17	398.51	1.076	46.9
1.08	193.75	178.47	420.66	1.086	47.2
1.09	202.66	185.01	443.98	1.095	47.5
1.10	211.97	191.79	468.53	1.105	47.7
1.11	221.69	198.82	494.37	1.115	48.0

(continued)

(continued)

$tg\phi$	Nq	Nc	Ng	Nq/Nc	ϕ
1.12	231.84	206.11	521.56	1.125	48.2
1.13	242.44	213.66	550.17	1.135	48.5
1.14	253.51	221.50	580.28	1.145	48.7
1.15	265.06	229.62	611.94	1.154	49.0
1.16	277.13	238.04	645.25	1.164	49.2
1.17	289.72	246.77	680.28	1.174	49.5
1.18	302.87	255.82	717.12	1.184	49.7
1.19	316.59	265.20	755.86	1.194	50.0
1.20	330.91	274.93	796.59	1.204	50.2

Chart 9.4: Lateral Earth Pressure

The following formulas refer to the pressures applied on the vertical face of a retaining wall by a horizontal embankment.

Symbols

ξ depth of a stratum from the surface of the retained soil
q superimposed surface load applied on the retained soil
σ_v vertical pressure applied at a depth ξ
p_h horizontal pressure on the wall due to active pressure
r_h horizontal pressure on the wall due to passive resistance

see also Chart 9.2.

Lateral Earth Pressures

$$p_h = -2c\sqrt{\lambda_a} + \lambda_a \sigma_v \quad (\geq 0) \quad \text{active pressure}$$
$$r_h = +2c\sqrt{\lambda_p} + \lambda_p \sigma_v \quad \text{passive resistance}$$

with

$$\sigma_v = q + g\xi$$
$$\lambda_a = tg^2\left(\frac{\pi}{4} - \frac{\phi}{2}\right) \quad \text{active pressure coefficient}$$
$$\lambda_p = tg^2\left(\frac{\pi}{4} + \frac{\phi}{2}\right) = \frac{1}{\lambda_a} \quad \text{passive resistance coefficient}$$

The values of λ_a and λ_p are shown in Table 9.5.

Table 9.5: Active and Passive Pressure Coefficients

For the meaning of symbols see Charts 9.2 and 9.4.

$tg\phi$	λ_a	λ_p	ϕ	$tg\phi$	λ_a	λ_p	ϕ
0.00	1.000	1.000	0.0				
0.01	0.980	1.020	0.6	0.42	0.442	2.264	22.8
0.02	0.961	1.041	1.2	0.44	0.426	2.349	23.8
0.03	0.942	1.062	1.7	0.46	0.411	2.436	24.7
0.04	0.923	1.083	2.3	0.48	0.396	2.526	25.6
0.05	0.905	1.105	2.9	0.50	0.382	2.618	26.6
0.06	0.887	1.127	3.4	0.52	0.369	2.713	27.5
0.07	0.869	1.150	4.0	0.54	0.356	2.811	28.4
0.08	0.852	1.173	4.6	0.56	0.344	2.911	29.3
0.09	0.835	1.197	5.1	0.58	0.332	3.014	30.1
0.10	0.819	1.221	5.7	0.60	0.321	3.119	31.0
0.11	0.803	1.246	6.3	0.62	0.310	3.228	31.8
0.12	0.787	1.271	6.8	0.64	0.299	3.339	32.6
0.13	0.772	1.296	7.4	0.66	0.290	3.453	33.4
0.14	0.756	1.322	8.0	0.68	0.280	3.569	34.2
0.15	0.742	1.348	8.5	0.70	0.271	3.689	35.0
0.16	0.727	1.375	9.1	0.72	0.262	3.811	35.8
0.17	0.713	1.403	9.7	0.74	0.254	3.936	36.5
0.18	0.699	1.431	10.2	0.76	0.246	4.064	37.2
0.19	0.685	1.459	10.8	0.78	0.238	4.195	38.0
0.20	0.672	1.488	11.3	0.80	0.231	4.329	38.7
0.21	0.659	1.517	11.9	0.82	0.224	4.466	39.4
0.22	0.646	1.547	12.4	0.84	0.217	4.605	40.0
0.23	0.634	1.578	13.0	0.86	0.211	4.748	40.7
0.24	0.622	1.609	13.5	0.88	0.204	4.893	41.4
0.25	0.610	1.640	14.0	0.90	0.198	5.042	42.0
0.26	0.598	1.672	14.6	0.92	0.193	5.193	42.6
0.27	0.586	1.705	15.1	0.94	0.187	5.347	43.2
0.28	0.575	1.738	15.6	0.96	0.182	5.505	43.8
0.29	0.564	1.772	16.2	0.98	0.177	5.665	44.4
0.30	0.554	1.806	16.7	1.00	0.172	5.828	45.0
0.31	0.543	1.841	17.2	1.02	0.167	5.995	45.6
0.32	0.533	1.877	17.7	1.04	0.162	6.164	46.1
0.33	0.523	1.913	18.3	1.06	0.158	6.337	46.7
0.34	0.513	1.949	18.8	1.08	0.154	6.512	47.2
0.35	0.503	1.987	19.3	1.10	0.149	6.691	47.7
0.36	0.494	2.024	19.8	1.12	0.146	6.872	48.2

(continued)

(continued)

$tg\phi$	λ_a	λ_p	ϕ	$tg\phi$	λ_a	λ_p	ϕ
0.37	0.485	2.063	20.3	1.14	0.142	7.057	48.7
0.38	0.476	2.102	20.8	1.16	0.138	7.244	49.2
0.39	0.467	2.141	21.3	1.18	0.134	7.435	49.7
0.40	0.458	2.182	21.8	1.20	0.131	7.629	50.2

Table 9.6: Partial Safety Factors

The following table gives the values of the partial safety factors, the ones to be used to amplify forces:

$$\left\{\begin{array}{l} G_{1d} = \gamma_{G1} G1 \quad \text{(structural self-weight)} \\ G_{2d} = \gamma_{G2} G2 \quad \text{(superimposed dead load)} \\ Q_d = \gamma_G Q_k \quad \text{(live loads-variable actions)} \end{array}\right\}$$

and the ones to be used to reduce the soil characteristics

$$\begin{array}{l} (tg\phi)_d = (tg\phi)_k/\gamma_\phi \quad \text{(internal friction)} \\ c_d = c_k/\gamma_c \quad \text{(cohesion)} \\ c_{ud} = c_{uk}/\gamma_{cu} \quad \text{(undrained cohesion)} \\ g_d = g/\gamma_\gamma \quad \text{(weight of soil)} \end{array}$$

There are three types of verifications, referred to three different ultimate limit states of the resisting system

EQU stability verifications against the possible *loss of equilibrium of the structure* as rigid body (with irrelevant mechanical properties of the soil);

STR verifications of *resistance of the foundation element* against the possible failure of its critical zones (with elastic reaction of the soil);

GEO verifications of *stability of the soil* against its possible global failure (see Chart 9.2) or any other type of failure (including the verifications of overturning and sliding)

In particular, the undrained cohesion c_u is used, together with $\phi = 0$, in place of the cohesion c in the formulas of resistance and lateral pressures (see Charts 9.2 and 9.4) for the short-term verification of soft clays.

It is implied that for each couple of values, the lesser or greater is used depending on whether the action is favourable or unfavourable,

The coefficients referred to the soil always reduce its characteristics, with respect to both the possible lower resistance and the possible greater active pressure,

The coefficients shown here are related to the ones of Charts 3.1 and 3.2 for the forces and the ones of Charts 2.2 and 2.3 for the resistance of materials (verifications of the type STR).

		EQU	STR	GEO
Forces–loads				
Structural self-weight	γ_{G1}	0.9 ÷ 1.1	1.0 ÷ 1.3	1.0
Other permanent loads	γ_{G2}	0.0 ÷ 1.5	0.0 ÷ 1.5	0.0 ÷ 1.3
Live loads–variable actions	γ_{Q}	0.0 ÷ 1.5	0.0 ÷ 1.5	0.0 ÷ 1.3
Soil parameters				
Friction angle	γ_{φ}	1.25	1.25	1.25
Cohesion	γ_{c}	1.25	1.25	1.25
Undrained cohesion	γ_{cu}	1.4	1.4	1.4
Weight of soil	γ_{γ}	1.0	1.0	1.0
Model coefficients				
Overturning	γ'_{R}	1.0	–	1.8
Sliding	γ'_{R}	1.1	–	1.1
Soil resistance	γ_{R}	–	–	1.8
Driven piles (tip bearing)	γ_{b}	–	–	1.45
Driven piles (skin friction)	γ_{s}	–	–	1.45
Bored piles (end bearing)	γ'_{b}	–	–	1.7
bored piles (skin friction)	γ'_{s}	–	–	1.45

Chart 9.7: Construction Requirements of Foundations

With reference mainly to the durability requirements, the following minimum measures are recommended.

Reinforcement Cover

In order to take into account the lower construction precision of the foundation works, the reinforcement covers should be appropriately increased with respect to the ones given in Table 2.17.

Bored piles	75 mm
Surface cast against the excavation	75 mm
Surface cast against levelled ground	50 mm
Surface cast against blinding	35 mm
Footings (except the base)	40 mm
Beams (except the base)	40 mm
Walls: surface against retained soil	30 mm

These values should be taken as minimum design values and include the following tolerances:

Footings	± 15 mm
Beams	± 10 mm
Walls	± 5 mm
Bored piles	± 50 mm

For aggressive soils, the minimum values of covers shown above should be increased by 25 mm.

Minimum Reinforcement

If their size is relatively big and the possible cracking due to shrinkage does not compromise the resistance significantly, the foundations can be made of unreinforced or lightly reinforced concrete. In this case, the following prescriptions on minimum reinforcement do not apply.

For *continuous tie beams* and other slender tying elements that resist axial tension forces, when the significant length can lead to early cracking due to shrinkage, a minimum longitudinal reinforcement should be provided equal to

$$A_s \geq A_c f_{ctm}/f_{yk}$$

similar to reinforced concrete ties (see Chart 2.14).

For element predominantly in bending, such as *foundation beams*, a minimum reinforcement on the edge in tension should be provided

$$A_s \geq \frac{1}{2} y'_c b f_{ctm}/f_{yk}$$

similar to uncracked reinforced concrete beams (see Chart 3.19), where y'_c indicates the depth of the portion in tension and b indicates its width.

Chart 9.8: Verifications Against Overturning and Sliding

The following formulas refer to the equilibrium of the isolated foundation as a rigid body, whose stability relies only on the support base.

Symbols

P_{Ed} vertical action on the support base of the foundation
e eccentricity of the vertical action with respect to the centre
a length of the foundation (orthogonal to e)
b width of the foundation (parallel to e)
x width of the loaded limit strip

H_{Ed} horizontal force on the support base of the foundation
μ soil-foundation friction coefficient

see also Charts 9.2 and 9.4.

Overturning Verification
We refer to combined compression and uniaxial bending on a rectangular foundation, whose support base is not entirely in compression, with the dimensions of the resisting footprint $a{\cdot}x$ (Charts 9.2 and 9.3). For a given vertical action P_{Ed}, the limit equilibrium situation is characterized by the value x defined as follows.

The overturning verification is set with

$$e_{lim} > e,$$

where

$$e_{lim} = (b - x)/2$$

Cohesive soil—general case
The width x of the loaded strip is obtained solving the equation:

$$r_l(x)x^2 + r'_o(x)x - \gamma_R p_{Ed} = 0$$

with

$$\begin{aligned}
r_l &= s_g N_g g/2 \\
r_o &= s_q N_q q + s_c N_c c \\
p_{Ed} &= P_{Ed}/a \\
s_g &= 1 - 0.4\beta_x \\
s_q &= 1 + \beta_x tg\phi \\
s_c &= 1 + \beta_x N_q/N_c \\
\beta_x &= x/a \quad se \quad x \le a \\
\beta_x &= a/x \quad se \quad x > a
\end{aligned}$$

Cohesive soil—β_x assigned
For a rectangular foundation, if an assumption is made for the ratio β_x, consequently giving a constant value to the three coefficients s_g, s_q and s_c, the following solution is obtained

$$x \cong \left\{ -r_o + \sqrt{r_o^2 + 4 r_l \gamma_R p_{Ed}} \right\} / (2 r_l)$$

The solution can be refined re-evaluating the three coefficients s_g, s_q and s_c on the basis of the calculated x.

Cohesive soil—strip footing
For a strip footing with $a \gg b$, being $x/a \cong 0$ one has $s_g = s_q = s_c = 1$, therefore one obtains:

$$x = \left\{ -r_o + \sqrt{r_o^2 + 4r_1\gamma_R p_{Ed}} \right\} / (2r_1)$$

Non-cohesive soil—without surrounding pressure
With $c = q = 0$ and with an assumption on β_x for the evaluation of $s_g = 1–0.4\beta_x$, one obtains

$$x \cong \sqrt{2\gamma_R p_{Ed} / s_g N_g g}$$

The solution can be refined re-evaluating s_g on the basis of the calculated x. For a strip footing ($s_g = 1$) the revised solution is obtained directly with

$$x = \sqrt{2\gamma_R p_{Ed} / N_g g}$$

Sliding Verification
When the horizontal translational equilibrium relies on the friction of the support base, it is verified when

$$H_{Ed} < \mu P_{Ed}$$

with $\mu \leq tg\phi$.

Chart 9.9: Reinforced Concrete Footings: Resistance Verifications

We refer to a stocky footing, with a parallelepiped shape, to support a centred column. It is implied that such footing is reinforced with an orthogonal grid of bars at the bottom.

Symbols

P_{Ed}	vertical action transferred from the column to the footing
M_{Ed}	bending moment from the column (along a')
H_{Ed}	shear force from the column (along a')
a', b'	sides of the column
h	footing depth
a, b	sides of the footing (parallel to a′, b′)

G footing self-weight
A_{sa}, A_{sb} footing reinforcement along a and b
d_a, d_b footing effective depths along a and b

see also Charts 2.2 and 2.3.

Verifications of Resistance

The resistance of each part of the footing shall be related to the pressure received back from the soil, distributed on the support base as deduced on the basis of the applied loads, with the assumptions of elastic behaviour of the soil and infinitely rigid footing.

Centred load (e = 0)

$$\sigma_g = \frac{P_{Ed}}{ab} \quad \text{constant pressure (without } G)$$

- reinforcement along a

$$s_a = (a - a')/2 \quad \text{footing protrusion}$$
$$P_{ad} = s_a b \sigma_g = \frac{a - a'}{2a} P_d$$
$$A_{sa} \geq \lambda_a P_{Ed}/f_{yd}$$

with

$$\lambda_a = l_a/d_a \quad l_a = c_a + s_a/2$$
$$c_a = \min(0.2d_a, a'/4)$$

- reinforcement along b

$$s_b = (b - b')/2 \quad \text{footing protrusion}$$
$$P_{bd} = s_b a \sigma_v = \frac{b - b'}{2b} P_{Ed}$$
$$A_{sd} \geq \lambda_b P_{bd}/f_{yd}$$

with

$$\lambda_b = l_b/d_b \quad l_b = c_b + s_b/2$$
$$c_b = \min(0.2d_b, b'/4)$$

- concrete resistance

$$P'_{\mathrm{Ed}} = \left(1 - \frac{a'b'}{ab}\right) P_{\mathrm{Ed}} < P_{\mathrm{rc}}$$

with

$$P_{\mathrm{rc}} = 0.8 f_{\mathrm{cd}} \left(\frac{b' d_{\mathrm{a}}}{1 + \lambda_{\mathrm{a}}^2} + \frac{a' d_{\mathrm{b}}}{1 + \lambda_{\mathrm{b}}^2} \right)$$

Eccentric load (e > 0)

$$N = P_{\mathrm{Ed}} + G$$
$$M = M_{\mathrm{Ed}} + H_{\mathrm{Ed}} h$$
$$e = M/N$$

- *Base entirely in compression* ($e \leq$ a/6)

$$\sigma_{\mathrm{o}} = P_{\mathrm{Ed}}/ab \quad \text{centroidal (without } G\text{)}$$
$$\sigma = 6M/a^2 b \quad \text{due to bending moment}$$
$$\sigma'_{\mathrm{g}} = \sigma_{\mathrm{o}} + (a'/a)\sigma \quad \text{at column edge}$$
$$\sigma''_{\mathrm{g}} = (1 - a'/a)\sigma \quad \text{increment at footing edge}$$

pressures resultant

$$P_{\mathrm{ad}} = s_{\mathrm{a}} b \sigma'_{\mathrm{g}} + s_{\mathrm{a}} b \sigma''_{\mathrm{g}}/2$$

resultant position

$$u = \left(s_{\mathrm{a}}^2 b \sigma'_{\mathrm{g}}/2 + s_{\mathrm{a}}^2 b \sigma''_{\mathrm{g}}/6 \right) / P_{\mathrm{ad}}$$
$$A_{\mathrm{sa}} \geq \lambda_{\mathrm{a}} P_{\mathrm{ad}}/f_{\mathrm{sd}}$$

with

$$\lambda_{\mathrm{a}} = l_{\mathrm{a}}/d_{\mathrm{a}} \quad l_{\mathrm{a}} = c_{\mathrm{a}} + s_{\mathrm{a}} - u$$
$$c_{\mathrm{a}} = \min(0.2d, a'/4)$$

- Base not entirely in compression (e > a/6)

$$x = 3(a/2 - e) \quad \text{zone in compression}$$
$$\sigma_g = 2N/bx \quad \text{maximum at the edge}$$
$$\sigma_o = G/ab \quad \text{pad self-weight}$$

with $x \geq s_a$ one has

$$\sigma'_g = (1 - s_a/x)\sigma_g - \sigma_o \quad \text{column edge (without } G)$$
$$\sigma''_g = (s_a/x)\sigma_g - \sigma_o \quad \text{increment at pad edge}$$

the verification A_{sa} follows as for the previous case.

Chapter 10
Prestressed Beams

Abstract After a historical note about the origin of prestressing and its expected effects on RC elements, this chapter presents the main features of the two technologies, one based on the pretensioning and the other on the postensioning of the steel tendons, including the effects of prestressing losses. A discourse on the tendon profile in the beams is developed to orientate the deign choices. The resistance calculations of the current prestressed sections are eventually presented, concluding with the specific analysis of tendons anchorage and stresses diffusion. In the final section three calculation examples are shown related one to a precast pretensioned floor element, one to a precast post-tensioned beam and the last one to a flanged beam provided with a cast-in situ upper slab.

10.1 Prestressing: Technological Aspects

The concept of precompression initially appeared at the first applications of reinforced concrete, as an expedient "to fully utilize the entire cross section". In a mentality still confined to the elastic behaviour of materials, the possibility of avoiding the cracking of the section was seen as an enhancement of its resistance.

The first texts on prestressed concrete visualized this concept with drawings similar to the one of Fig. 10.1, indicating how most of the concrete did not contribute to the resistance in beam "*a*" without prestressing, whereas with the initial action σ_o induced by the prestressing tendon, in beam "*b*" it was possible to resist the moment M even without the need for specific reinforcement, at least as long as the stress at the lower edge did not go in tension ($\sigma_i \geq 0$).

It was also specified that it was more convenient to move the prestressing tendon towards the lower edge (in tension under the bending moment—see Fig. 10.2a), and some authors, in order to emphasize the concept, represented the beam of Fig. 10.1b as a set of loose bricks, whose resistance in bending was given by prestressing.

At that time it was not noted that the tendon, required to induce the prestressing action, was also a reinforcement, and it was not analyzed how the prestressed section

© Springer International Publishing AG 2017

G. Toniolo and M. di Prisco, *Reinforced Concrete Design to Eurocode 2*,
Springer Tracts in Civil Engineering, DOI 10.1007/978-3-319-52033-9_10

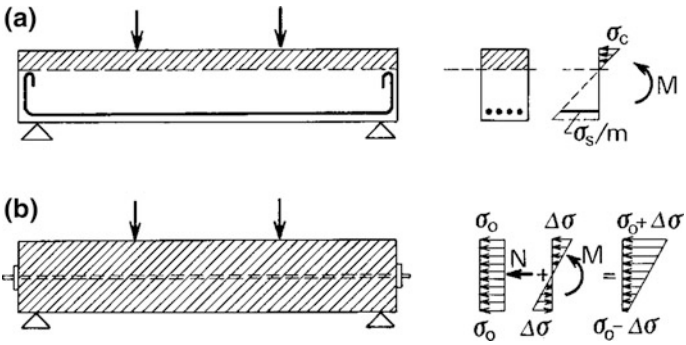


Fig. 10.1 Original concept of "fully utilize the entire section" in bending

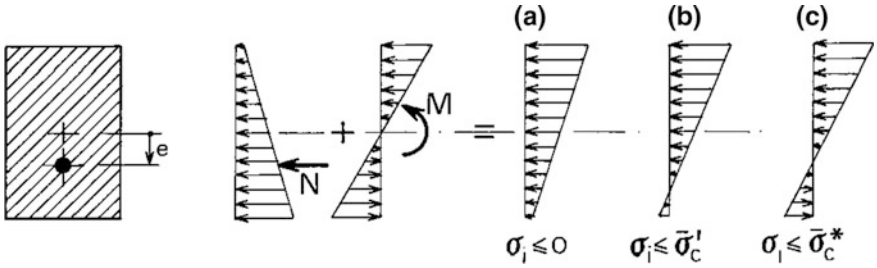


Fig. 10.2 Optimization of the tendon position

could go from the elastic situation (which we would now call serviceability) to rupture (or, as we would now say, at the resistance ultimate limit state).

The concept of prestressing did not have immediate practical applications because of the technological limitations of the production at that time, mainly for steel. Keeping in fact the stresses of the tendons approximately at:

$$\sigma_{po} \cong 155\,\mathrm{N/mm^2}$$

one obtained elongations of

$$\varepsilon_{po} \cong 155/205{,}000 = 0.00075$$

that were largely reduced by the shortening due to the shrinkage of the beams

$$\varepsilon_{cs\infty} \cong 0.00035$$
$$\varepsilon_{cs\infty}/\varepsilon_{po} \cong 0.47$$

Added to relaxation and creep, the effect led to excessive losses of stresses, incompatible with an effective practical use of prestressing.

High-strength steel changed the terms of the problem. With initial stresses almost ten times higher:

$$\sigma_{po} \cong 1350\,\mathrm{N/mm^2} \quad (\varepsilon_{po} \cong 0.00655)$$

as for modern products (in strands for example), the losses due to shrinkage are lower than 6%.

Freyssinet, who is rightfully considered the father of prestressed concrete, arrived to the solution of the use of high-strength steel. After extensive studies on concrete creep, identified as the main cause of stress losses, this French inventor started to produce his patents in 1928 and apply the relative systems in real constructions. He was able to publish the conclusions of his first experiences on the magazine Travaux already in 1933.

Another scholar interested in concrete creep, Dishinger, brought the new prestressing techniques in Germany in 1936, starting the international diffusion of the research on the various aspects of this material.

Other aspects of the technological evolution contributed to the achievement of prestressed concrete, which had a great diffusion in the second half of the past century, thanks mainly to the original French school. With figures such as Freyssinet and his pupil Guyon, this school was the first one to give an organic theoretical–experimental set up to the design problems and their practical evidence in the numerous constructions of that period.

Prestressed reinforced concrete was seen as a new material, autonomous from the ordinary reinforced concrete, with different properties for production technologies and design criteria. In particular they substantially derived from the old concept of uncracked section, adopted also for the emerging problems related to deformation and cracking behaviour of beams and fatigue of steel reinforcement.

The shift of the interest to the aspects of deformation and cracking behaviour in service opened a bridge between the two materials, firstly leading to the concept of partial precompression as intermediate state between ordinary and prestressed reinforced concrete, then to the unitary vision without distinctions, that only defines the functional standards to be respected with the appropriate serviceability verifications.

Already in 1939 the Austrian Emperger proposed the adoption of post-tensioned additional tendons as a technological expedient to enhance the cracking and deformation behaviour of reinforced concrete beams. This initial idea has been progressively developed by different authors and led to the definition of partial precompression as the one related to mixed reinforcement (passive and pretensioned).

Reversing Emperger's initial idea, the interest of this concept remained in the correct evaluation of the contribution offered by the additional passive reinforcement to the cracking behaviour in the prestressed beams, especially with post-tensioned tendons. What mentioned above has been translated into the design standards with some construction requirements concerning the minimum amount of

additional passive reinforcement and its correct distribution in the portion of the beams in tension.

Abeles in 1945 explicitly talks about partial prestressing as an alternative method in the design of prestressed reinforced concrete, proposing to allow limited tensile stresses in the section, still treated as uncracked (see Fig. 10.2b).

From this proposal the significant activity of the English school developed. Despite the categorical opposition of the French school that refused middle ways between reinforced and prestressed concrete, in 1951 the criteria for the use of partial precompression were codified for the first time. Significantly ahead of times, rare, frequent and quasi-permanent serviceability situations were mentioned, to be related to section decompression and cracking verifications.

In the years 1954/67 Abeles presented the results of several applications of such design approach that measured partial precompression starting from the decompression limit of the section.

The criteria of the British school have been officially adopted by the competent British Standards, initially in the 1959 version where the allowable tensile stresses at the tension concrete edge were quantified, then in the 1972 version where a "full prestressing" was defined, distinguishing it from a "limited prestressing" and a "partial prestressing", referred, respectively, to the concrete decompression, crack formation and crack opening width.

The English school therefore leads to the definition that interprets partial prestressing as the one that allows cracking of the section, but reduces the control of crack opening to a conventional verification: that is the section is always assumed as uncracked, assuming for the concrete in tension a "hypothetical tensile stress" as a limit beyond the tensile concrete strength (see Fig. 10.2c).

In the European continent, having overcome the initial French opposition that gained authority from many beautiful constructions in prestressed concrete, the main contribution came from the Swiss school and in particular from its most eminent representative, prof. Rös from Zurich.

In 1968 the SIA-norm 162 marked a significant step forward towards the correct analysis of partial precompression, interpreting the section as cracked (see Fig. 10.3) and moving the verification from concrete to steel. With the limit on tensile stresses in the reinforcement, an implicit control on crack opening was introduced, whereas a verification on the range of stresses in the tendons was added with reference to the important phenomenon of fatigue.

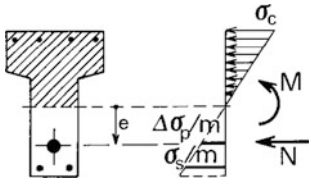


Fig. 10.3 Prestressed section in cracked state

On the other hand, in these norms the definition of the serviceability verifications seems more elementary, only requiring the verification of decompression under permanent loads.

Finally in 1983 at the Waterloo congress, the concept of partial precompression arrived where it had to be naturally completed: Bachmann in fact presented his proposal of a "unified approach", removing any interest for an autonomous definition of partial prestressing.

Further to this new philosophy, to which the documents of C.E.B. now fib (see Model Code) have been conformed, and that has been adopted by the latest versions of the national design standards based on the semi-probabilistic limit states method, the problem concerns reinforced concrete in general. Having defined the serviceability limit states (e.g. decompression, cracking and crack opening width, …) related to the functional and durability aspects of structures, the degree of precompression has to be quantified necessary for the compliance with the related verifications based on the characteristics of the chosen materials.

In particular, the possibility to use high-strength steel as tension reinforcement in reinforced concrete beams is limited by the cracking behaviour of the concrete around. For example, similarly to Sect. 2.3.3, assuming an allowable limit between 0.2 and 0.3 mm for the crack opening and a distance between cracks of 200 mm, a limit for the average strain ε_{sm} in steel between 0.10 and 0.15% is obtained. Such limit corresponds to a stress σ_s between 200 and 300 N/mm^2. These values represent the upper bound in service for non-pretensioned reinforcement.

Therefore, in order to use higher stress levels, corresponding to high-strength steels, a prior elongation has to be induced in them so that its subsequent variation range, measured from concrete decompression, does not exceed the indicative value of 0.10 or 0.15% set by the cracking limit state in service.

10.1.1 Prestressing Systems

Only few fundamental aspects of the technology of prestressed reinforced concrete are described in this chapter, together with few other design aspects strictly related to this technology. The basis of resistance and serviceability calculations remain the ones presented in the previous chapters. Construction problems require more deepened presentations, as they are linked to a very varied technology, often significantly complex and still in rapid evolution. Addressing to specialist disciplines for those problems, the topic is introduced describing the two main execution systems of prestressed concrete, from which the two main products derive, that also differ for certain technical design aspects.

Pretensioning

A first type of product, based on tendons pre-tensioning, is produced in appropriate plants of relevant size. They consist of long prestressing beds with big blocks founded in the ground at their ends (see Fig. 10.4). The anchorage devices are fixed

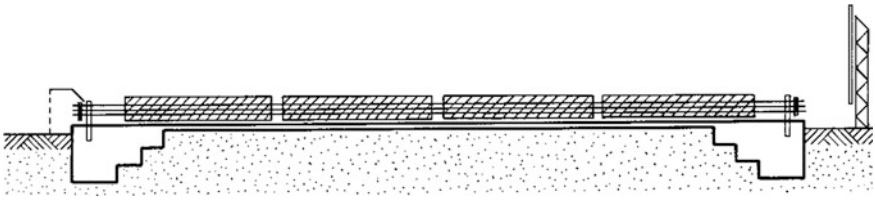


Fig. 10.4 Production line of pre-tensioned precast beams

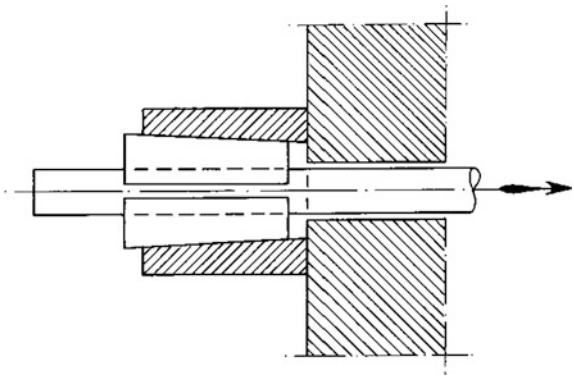


Fig. 10.5 Detail of the end anchorage of a tendon

to the blocks: two robust vertical cantilevers and a thick steel perforated plate between them, in addition to a system of hydraulic jacks that allows a controlled horizontal movement of the plate.

The tendons (wires or strands) are laid along the bed, using a trolley carrying the tendon reels or other systems; they are inserted into the holes of the anchorage plates, the wires are locked on them (see detail of Fig. 10.5) and tensioned with a first moderate force, sufficient to keep them in position during the subsequent operations.

Steel workers then enter the prestressing beds, install the passive reinforcement and eventually position the shutters that complete the formworks where concrete will be cast. Usually, as indicatively shown in Fig. 10.4, several elements aligned along the bed are produced together.

The final tensioning is eventually applied on the tendons. Since forces are very high, this operation represents a hazard if not carried out correctly with the due safety measures: the failure of an anchorage could make a wire snap, with destructive effects on the prestressing bed and the adjacent areas. Having planned the operative cycle so that tensioning occurs in the afternoon, towards the end of the day, the access to the concerned area of the plant is closed with the activation of the specific flashing signals. The specific team for tendon tensioning works at one end of the pre-stressing bed in a protected space, and a protective screen is positioned at the other end.

The cycle is concluded with concrete casting, the bed covering with sheets and the steam injection in the heating circuit for the accelerate curing of concrete. This hardening process continues overnight.

At the beginning of the next working day, after about 14 or 16 h of curing, the elements are uncovered and the formwork opened. The strands are released gradually with the hydraulic jacks that control the displacement of the anchoring plates.

These displacements have significant values: if the wires at tensioning had an elongation of

$$\varepsilon_{po} = \sigma_{po}/E_p = 1350/205{,}000 = 0.00655$$

which, for a bed of 150 m in length, leads to a translation

$$\Delta_o l = l\,\varepsilon_{po} = 15{,}000 \times 0.00655 = 98\,\text{cm}$$

of the ends to be tensioned, assuming an average compression in the concrete, at the bottom edge of the elements, equal to

$$\sigma_i \cong 15\,\text{N/mm}^2$$

and a low elastic modulus due to the early-age, the following value is indicatively obtained

$$\Delta l = l\,\sigma_i/E_c = 15{,}000 \times 15/27{,}000 \cong 8\,\text{cm}$$

for the displacement on the prestressing bed of the element end close to the mobile anchorage, when the tendons are released.

The shortening of the tendons, which remain embedded in the concrete and follow the same deformations thanks to the bond, has the same order of magnitude. Referred to the initial elongation $\Delta_o l$, such shortening indicates the effect of the so called *elastic loss* typical of pre-tensioned tendons: about 8% in the numerical example presented above.

The operations following the release of tendons are mentioned for completeness, that consist of cutting the tendons between different elements, lifting and transporting them in the stock area, waiting for the delivery to site and the final installation.

After the demoulding of the concrete elements, the bed is cleaned and prepared for the subsequent operational cycle, usually following the same daily cycle described above.

Countless variations are obviously possible for the production of this type of prestressed concrete, always based on the tendon pre-tensioning with external anchorages, on the subsequent encasing of the same tendons in the concrete casting and on their final release that activates, through bond, the precompression of the elements.

Post-Tensioning

The other type of product instead uses the same concrete element previously cast and cured, for the necessary contrast to the tensioning of the tendons. This prestressing technology does not require particular plant equipment for its production. Elements can be prefabricated in factories or on site at ground level, but it is possible to prestress structures directly in situ bringing on site hydraulic jacks necessary for the tendons tensioning.

Substantially, this execution technology reproduces the one typical of ordinary reinforced concrete, except of few additional operations. Having fixed the passive reinforcement cage, the metal ducts that host the prestressing tendons are introduced before casting. The ducts follow specific layouts, chosen according to the criteria discussed as follows, and are fixed to the reinforcement cage in order to ensure the stability of their position during casting. This is carried within the relative formwork and concrete is left aging until it has sufficiently hardened.

If no particular techniques of accelerated curing are adopted, few weeks have to pass before tendons can be tensioned, positioning the hydraulic jacks on the active anchorage that exchanges the applied force directly on the concrete element to be prestressed. During this operation the tendon slides inside the duct, exchanging also lateral pressures distributed along its length depending on its layout.

During tensioning, friction forces arise, which prevent the complete transfer of the tensioning force up to the fixed anchorage at the other end of the tendon. In order to control this effect, it is good practice to measure the elongation based on the extracted portion of the tendon, in addition to the applied force read with the hydraulic jack manometer. These *friction losses* are typical of the post-tensioned tendons: their evaluation should be carried out for each case according to the criteria indicated at the following section.

The works are eventually completed with the injection of grout in the ducts, necessary to ensure the bond of the tendons and to protect them against corrosion. Particular precautions are required for this operation, given the negative past experiences (of early oxidation) shown in many structures. For example, appropriate outlet vents are required to allow the penetration of the grout in the voids of the ducts and to show when the ducts are completely filled (see Fig. 10.6).

Countless patents are available for the anchorage details of the tendons. Tendons themselves can consist of big diameter bars, bundles of wires or strands (see Fig. 10.7). Many variations can also occur in the operations with respect to the cycle described above, aimed at post-tensioning of initially unbonded tendons using

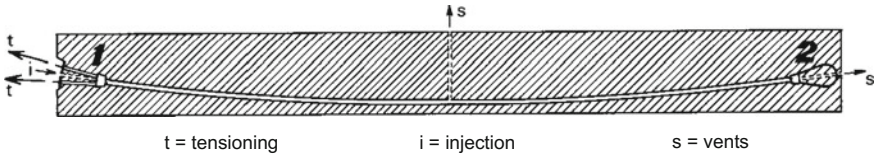


Fig. 10.6 Scheme of the tendon post-tensioning in a beam



Fig. 10.7 Types of tendons for post-tensioning technology

the resistance of the same elements to be prestressed, so that the force read at tensioning is the one that remains as internal co-action, except for long-term losses that will be described at Sect. 10.1.2, but without the elastic loss that occurs in the other type of system when tendons are released.

Stability of Prestressed Elements

It is to be noted how both technologies described above require prestressing with tendons that remain integrated with the prestressed elements once they are completed: they are in fact forced to follow the same deformations. This avoids problems of instability of the elements that can be very slender or curved. Contrary to what shown in Fig. 10.8a, where the external axial force P remains on the same axis generating, with respect to the deformed configuration v, the instability moment Pv that leads to the well-known problems of buckling, the internal action $N = P$ that runs along the tendon of Fig. 10.8b follows the deformed shape without generating any additional moment: this action is exchanged in any section between concrete in compression and steel in tension, without generating second order effects that could lead to instability.

In what follows the symbol E_p will be used to indicate the elastic modulus of the prestressing reinforcement. Actually, the high-strength steel used for this kind of reinforcement has the same elastic modulus of the one of the ordinary reinforcement. For bars and wires, it will always be $E_p = E_s$.

There are, however, products made of groups of spiral wrapped wires (such as strands) for which the applied tension causes, in addition to the elongation of the material, the geometrical straightening of the spires. An apparent elastic modulus is exhibited, referred to the product, lower than the actual one of the material. For the current production, which uses weaving techniques under tensioning, the wire compaction in the bundle limits the phenomenon.

10.1.2 Instantaneous Losses

The two effects mentioned at the previous paragraph are indicated with the name of instantaneous losses: the elastic loss in the prestressing reinforcement at the release of bonded pre-tensioned tendons; the reduction in force of the post-tensioned reinforcement along its length due to friction in the ducts, starting from the active anchorage up to the fixed one.

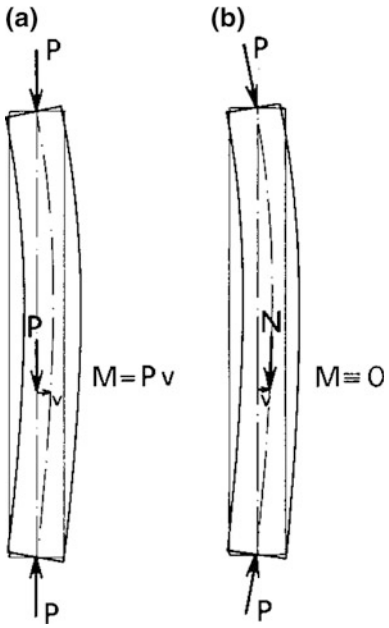


Fig. 10.8 Stability aspects of prestressed slender elements

Elastic Losses

In order to analyse the first effect, one can consider the reinforced concrete element of Fig. 10.9 which has, in addition to a passive reinforcement A_s, a reinforcement A_p, pretensioned with a stress σ_{po}, initially locked to the external anchorage devices. For simplicity one can consider a perfectly centred configuration, but the results can then be extended to the eccentric case, which involve the bending behaviour of the element in addition to the axial one.

First of all it can be observed that, except for the long-term losses that will be discussed at the next section, the situation described above corresponds to the limit of decompression of concrete, with $\sigma_c = \sigma_s = 0$, and therefore the corresponding force

$$N_{po} = A_p \sigma_{po},$$

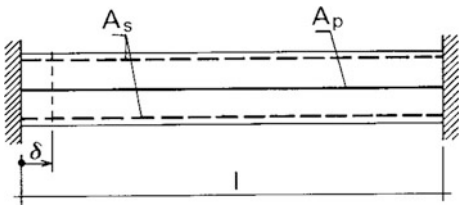


Fig. 10.9 Scheme of a prestressed element

read at the hydraulic jack manometer, coincides with the initial prestressing force on which the verifications should be based, according to the formulas deduced at Sects. 2.2.2, 2.3.3 and 3.1.3.

In order to analyse the situation after the prestressing reinforcement is released, one can take the shortening δ of the element as geometrical unknown in the logic of the Stiffness Method and write the equation of equilibrium for which the external force N_{po}, the one of the anchorage constraints that have been removed, should be equal to zero:

$$\left(\frac{E_c A_c}{l} + \frac{E_s A_s}{l} + \frac{E_p A_p}{l}\right)\delta - N_{po} = 0$$

One immediately obtains a value of the shortening of the element which is inversely proportional to its axial stiffness, including the contributions of concrete, passive reinforcement and active (prestressing) reinforcement:

$$\delta = \frac{N_{po}}{\frac{E_c A_c}{l} + \frac{E_s A_s}{l} + \frac{E_p A_p}{l}} = \frac{N_{po} l}{E_c\left(A_c + \alpha_e A_s + \alpha'_e A_p\right)} = \frac{N_{po} l}{E_c A_i}$$

Therefore, with $\varepsilon = \delta/l$, one obtains the following stresses:

$$\sigma_c = E_c \varepsilon = \frac{N_{po}}{A_i} \quad \text{compression in concrete}$$

$$\sigma_s = \alpha_e \sigma_c = \alpha_e \frac{N_{po}}{A_i} \quad \text{compression in passive reinforcement}$$

$$\sigma_p = \sigma_{po} - \alpha'_e \sigma_c = \sigma_{po} - \alpha'_e \frac{N_{po}}{A_p} \quad \text{tension in the tendon}$$

which represent the state of internal mutual action of the prestressed element according to the formulas discussed in the mentioned Sect. 2.2.2.

In terms of stresses, the effect of the elastic loss is taken into account simply referring the force N_{po} at tensioning, to the equivalent area of the homogenized section equalized to concrete, which includes the contributions of all three materials:

$$A_i = A_c(1 + \alpha_e \rho_s + \alpha'_e \rho_p)$$

In particular, if there are flexural eccentricities, the moment of inertia I_i of such homogenized section will also come into play, to which the flexural component $N_{po}e$ of the prestressing force is to be related, according to the formulas of elastic verification of sections (see Sect. 3.1.3).

For an element prestressed with a post-tensioned tendon instead, the force N'_p at tensioning gives directly the action exchanged between reinforced concrete and the tendon:

$$\sigma_c = \frac{N'_p}{A_c + \alpha_e A_s} = \frac{N'_p}{\bar{A}_i} \qquad \text{compression in concrete}$$

$$\sigma_s = \alpha_e \sigma_c = \alpha_e \frac{N'_p}{\bar{A}_i} \qquad \text{compression in passive reinforcement}$$

$$\sigma_p = \frac{N'_p}{A_p} \qquad \text{tension in the tendon}$$

In order to deduce the prestressing force corresponding to the decompression of concrete (in the final element made integral with end anchorages locked and ducts injected), one should apply an external tensile force such that the stress σ_c is equal to zero, obtaining:

$$\sigma_{po} = \sigma_p + \alpha'_e \sigma_c \quad (\sigma_c < 0)$$

For centred cables one has the prestressing force

$$N_{po} = A_p \sigma_{po} = N'_p + \alpha'_e \sigma_c A_p = \frac{A_i}{\bar{A}_i} N'_p$$

whereas for eccentric cables, the stress on the concrete fibre at the strand level should be assumed for σ_c in the variable diagram of stresses.

For relatively small ratios of prestressing reinforcement, with $A_i/\bar{A}_i \approx 1$, one can approximately set $N_{po} \approx N'_p$.

Friction Losses

In order to analyse the friction losses one can consider an infinitely small cable segment, belonging to a curved portion (see Fig. 10.10). The radius of the curve in the considered point is indicated with r, the tensile force in the strand with N, the normal and tangent pressures transferred along the contact with the duct, respectively, with p_n and p_t. The linear relationship between the two pressures depends on the friction coefficient:

$$p_t = \mu p_n$$

The equilibrium conditions of the examined tendon segment, set, respectively, on the tangent and normal translations, give:

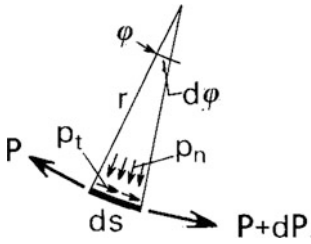


Fig. 10.10 Equilbriun of a tendon elementary segment

$$(P + \mathrm{d}P) - P + p_\mathrm{t}\,\mathrm{d}s = 0$$
$$-P\,\mathrm{d}\varphi + p_\mathrm{n}\,\mathrm{d}s = 0$$

From these two equations with $\mathrm{d}s = r\ \mathrm{d}\varphi$ one obtains, respectively, the two expressions

$$p_\mathrm{t} = -\frac{1}{r}\frac{\mathrm{d}P}{\mathrm{d}\varphi}$$
$$p_\mathrm{n} = \frac{P}{r}$$

which, substituted in the original friction relationship, lead to the differential equation:

$$\frac{\mathrm{d}P}{\mathrm{d}\varphi} + \mu P = 0$$

Its integral

$$P = P_1 e^{-\mu\varphi}$$

shows how, starting from the value P_1 corresponding to the end where the prestressing is applied, the force P decreases exponentially based on the progressive angle φ of angular deviation of the cable, taken as absolute value. The values of the friction coefficient μ range on average between 0.3 and 0.5.

In the straight segments theoretically there should not be any friction effects. However, with respect to the nominal layout, construction tolerances lead to unintentional deviations and accidental contacts of wires and spacers. These spacers are usually introduced in the limited space inside the ducts to avoid tangles of the wires and possible consequent catching of the tendons. Therefore, even in straight segments friction losses occur. Assuming a conventional deviation α per unit length along the developed length s of the tendon, one obtains:

$$P = P_1 e^{-\mu\alpha s}$$

where for α one can assume the value 0.01 rad/m.

In the curved segments the interaction between the two friction losses, the systematic and accidental ones, can be conventionally set with:

$$P_1 e^{-\mu(\varphi + \alpha s)}$$

10.1.3 Long-Term Losses

Starting from its initial value σ_{pi}, the stress in the prestressing tendon undergoes significant decrements $\Delta\sigma_p$, which progressively occur in time until they stabilize on the final value

$$\sigma_{p\infty} = \sigma_{pi} - \Delta\sigma_{p\infty}$$

Of this effect the three main causes are mentioned here in chronological order: The relaxation in the prestressing reinforcement, the shrinkage and the creep of concrete.

Steel Relaxation

Relaxation is a phenomenon that occurs in steel tendons when subject to high stresses and can be investigated with experimental tests similar to the ones described for creep in concrete. For the wire of Fig. 10.11, subject to the force P constant in time, after the initial instantaneous elastic elongation, progressive increments of the deformation occur afterwards that tend to extinguish within a few years. The dual aspect, which concerns the behaviour of elements in prestressed concrete, consists of a progressive loss of stress under an imposed elongation of constant value.

These effects, however, derive from a physical phenomenon which is substantially different from the one of creep in concrete. For steel, it is the tendency of crystals to orient themselves according to the direction of the force. This tendency can be measured with parameters that do not vary in time, such as concrete aging, but that are affected by possible previous loads that may have strained the material making it more stable. No delayed elastic return of the deformation increments occurs after unloading. Eventually the relationship with the initial elastic value cannot be set in a simply linear form. There is also the significant influence on the entity of the phenomenon of thermal treatments which the material in tension may be subject to.

For the evaluation of the effects of the prestressing steel relaxation, an approximated technical procedure can be followed that calculates the relative tension losses $\Delta\sigma_{p\infty}$ as a function of the initial stress σ_{pi} with coefficient deduced experimentally for the individual elements and related to the initial stress based on an appropriate relationship.

The experimental values can be deduced with specific tests. A tension force is applied on a tendon segment and the load is continuously adjusted, with an



Fig. 10.11 Representation of long-term elongation effects

automatic system connected to the measurement of the elongation, so that the deformation is kept constant.

If the test is stopped at 1000 h (see. Figure 10.12) and set from the initial value $\bar{\sigma}_{pi} = 0.70 f_{ptk}$, the measured loss $\Delta\bar{\sigma}_{p1}$ gives the parameter:

$$\bar{\rho}_1 = \Delta\bar{\sigma}_{p1}/\bar{\sigma}_{pi}$$

This value is then adjusted based on the initial stress σ_{pi} actually applied, with its ratio $r = \sigma_{pi}/f_{ptk}$ to the characteristic strength of steel, and joined by a function that expresses the evolution of the phenomenon in time. The curves deduced experimentally for tendons made of ordinary wires (class 1), stabilized wires (class 2) and bars (class 3) are shown in Fig. 10.13. The analytical expressions of the curves are:

$$\rho_1 = \frac{\Delta\sigma_{p1}}{\sigma_{pi}} = \bar{\rho}_1 c(r)$$

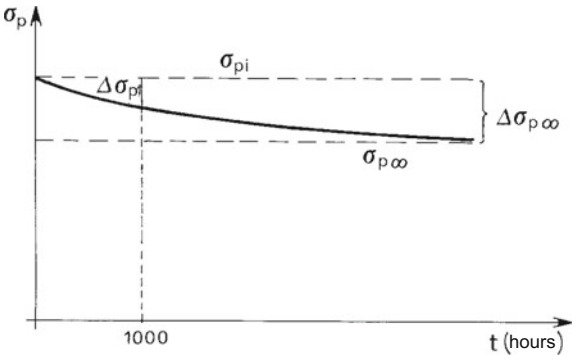


Fig. 10.12 Progressive stress losses due to relaxation

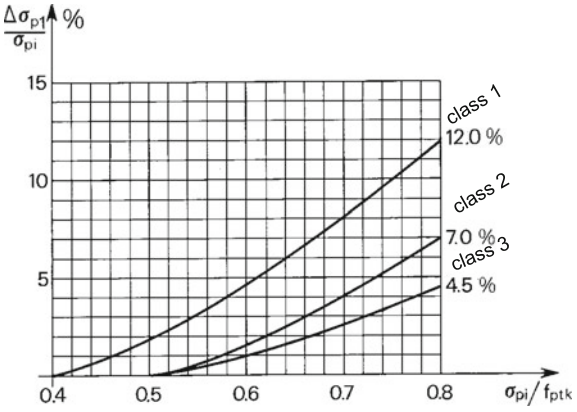


Fig. 10.13 Curves of reference relaxation losses

with

$$c(r) = \left[\frac{r - 0.4}{0.3}\right]^{\frac{4}{3}} \quad \text{for class 1}$$

$$c(r) = \left[\frac{r - 0.5}{0.2}\right]^{\frac{4}{3}} \quad \text{for classes 2 and 3}$$

where

$$\bar{\rho}_1 = 8.0\% \quad \text{for class 1}$$
$$\bar{\rho}_2 = 2.5\% \quad \text{for class 2}$$
$$\bar{\rho}_3 = 4.0\% \quad \text{for class 3}$$

It should be noted that below a given limit value of σ_{pi} (= 0.4 f_{ptk} for class 1, = 0.5 f_{ptk} for classes 2 and 3) there are no losses due to relaxation. The evolution of relaxation in time can be represented by a function of $\tau = t/1000$ with t expressed in hours:

$$\rho(\tau) = \frac{\Delta\sigma_p}{\sigma_{pi}} = \rho_1 \tau^{0.75(1-r)}$$

The final loss due to relaxation can be evaluated with the formulas indicated above for a time t = 500,000 h (57 years).

The initial stress to which this evaluation of the loss $\Delta\sigma_{p\infty}$ due to relaxation should be related is calculated, for post-tensioned tendons, based on the force P'_o exchanged with concrete at tensioning:

$$\sigma_{pi} = \sigma_p = P'_o/A_p$$

For pre-tensioned tendons it is calculated based on the prestressing force P_o measured at tensioning (unloaded concrete):

$$\sigma_{pi} = \sigma_{po} = P_o/A_p$$

For the latter system it can be taken into account that the initial portion of tendons relaxation, before the concrete hardening, already occurs independently from the concrete element, without producing any effect in it.

Losses Due to Shrinkage

Shrinkage has already been discussed at Sect. 2.2.1, showing the effects of the contraction ε_{cs} on a symmetrical centred reinforced element. In the general case, the condition of rotational equilibrium should be added to the one of translational equilibrium, to take into account the flexural effects. However, the technical solution adopted in practice overestimates the deformation of the reinforced element setting it equal to the shrinkage, as if reinforcement did not have any contribution against it:

$$\varepsilon = \varepsilon_{cs}$$

With such simplified assumption one can directly set:

$$\Delta\sigma_{p\infty} = E_p\, \varepsilon_{cs\infty}$$

overestimating the relative tension loss which, with $E_p \cong 200{,}000\ \mathrm{N/mm^2}$ and $\varepsilon_{cs\infty} \cong 0.00035$, corresponds on average to

$$\Delta\sigma_{p\infty} \cong 70\,\mathrm{N/mm^2}$$

For post-tensioned tendons even for shrinkage one can take into account the portion of losses that occurred before locking the tendons and grouting the ducts, and therefore does not cause the tension losses described above.

Losses Due to Creep

A similar technical solution can be proposed for the evaluation of the effects of creep. Neglecting the elastic opposition given by the reinforcement, for this solution it is assumed that each concrete fibre exhibits a viscous contraction proportional to the initial elastic deformation, according to the linear formula valid under constant loads:

$$\varepsilon_{v\infty} \cong \phi_\infty \varepsilon_{ci} = \phi_\infty \frac{\sigma^*_{ci}}{E_c}$$

If the stress at the tendon level is assumed as σ^*_{ci} , one consequently obtains:

$$\Delta\sigma_{p\infty} = E_p \varepsilon_{v\infty}$$

which, with $\alpha'_e = E_p/E_c$, becomes:

$$\Delta\sigma_{p\infty} \cong \phi_\infty \alpha'_e \sigma^*_{ci}$$

A more rigorous solution can be deduced from the constitutive relationship of creep under variable regime according to the procedures presented at Sect. 3.3.

Effects of Losses

If the interaction between different types of losses is neglected, the relative tension losses can be simply summed, with a conservative approximation. Indicating the final loss with $\Delta\sigma_{p\infty}$, which includes the effects of relaxation, shrinkage and creep, considering negligible the possible inclination of the tendon with respect to the beam axis ($P \cong N_p$) it can be set

$$\Delta N_{p\infty} = A_p\, \Delta\sigma_{p\infty}$$

and with this axial force, assumed in tension and applied on the section with the eccentricity e of the tendon, one can proceed with the usual calculation of stresses on the three materials, to be added to the ones already present, to give the final situation from which the verifications for the final phases of the structure in service depend.

10.2 Tendons Profile

As indicated by the title of the chapter, the current section only refers to elements in bending. With reference to the resistance of beams against bending moment, the prestressing reinforcement should be placed as close as possible to the edge in tension, as for the passive reinforcement. In the case of prestressing reinforcement, however, this recommendation, valid for the resistance ultimate limit state of the cross sections in the final states, has limits imposed by both the initial situations and the requirements in service of the beams. The cracking limit states for the parts in tension and the one of maximum compression at the opposite concrete edge limit the position of the tendon to certain eccentricity values, as the resistance verifications in the initial transient stages under minimum loads can do.

Given that, as it will be shown later, the eccentricity limits of the tendon depend, in addition to the characteristics of the section, on the internal forces induced by the external loads along the beam. The position of the tendons can vary consistently with the configuration of the diagrams of the internal forces. The different criteria to be considered for the determination of the tendons profile are presented in this Section.

It should initially be noted how the system with post-tensioned tendons, thanks to the flexibility of the tendons and the ducts, allows significant freedom in their installation: they can have subsequent straight and curved segments in any sequence (see for example Fig. 10.6). For pre-tensioned tendons instead, the natural configuration of the tendon between the two ends remains straight. In this case there are therefore limited possibilities in varying the profile. It is possible to prescribe their deviation, as long as a prestressing bed with the relative complex devices is available, obtaining a layout consisting of successive straight segments (see Fig. 10.14a). It is possible to sheathe the tendons with ducts in certain segments, avoiding bond with the concrete subsequently cast, obtaining a straight layout without deviations with partial segments of parallel wires (see Fig. 10.14b).

The presence of inclined tendons in a prestressed reinforced concrete section gives a significant contribution to the shear resistance. Given that the inclination is appropriately oriented with respect to shear, one has that the transverse component of the prestressing force is subtracted from the effect of the external loads (see Fig. 10.15) reducing the magnitude of the resulting shear force:

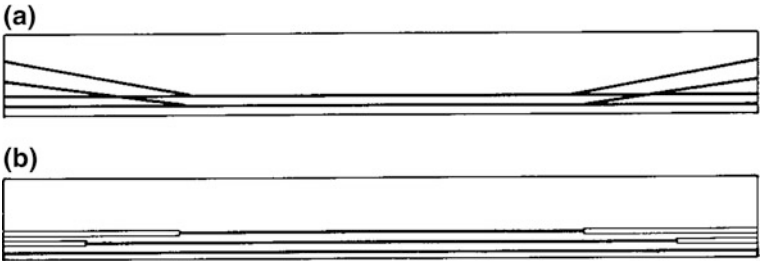


Fig. 10.14 Deviation (**a**) and sheathing (**b**) of pretensioned tendons

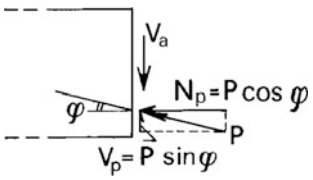


Fig. 10.15 Effects of tendon inclination

$$V = V_a - P \sin \varphi$$

Both the elastic serviceability verifications and the calculation of the ultimate resistance in shear will take into account such favourable effect.

10.2.1 Loads Equivalent to the Tendon

The concept of *loads equivalent* to the tendon is presented here, which can be used to approximately determine the tendon profile in relation to the configuration of the external loads. An elementary segment of a curved portion of a tendon subject to a prestressing force P is shown in Fig. 10.16. Neglecting friction, for the translational equilibrium in the vertical direction one has

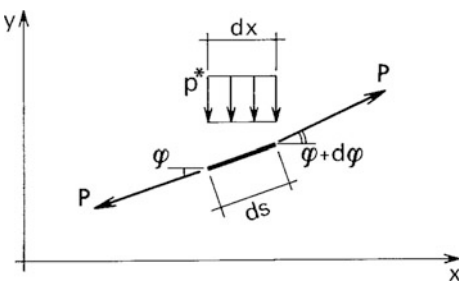


Fig. 10.16 Equilibrium of a tendon elementary segment

$$P\ \sin(\varphi + \mathrm{d}\varphi) - P\ \sin\varphi = p^* \mathrm{d}x$$

For relatively small inclination of the tendon, one has:

$$\varphi \cong \sin\varphi \cong \mathrm{tg}\,\varphi = y^I$$
$$(\cos\varphi \cong 1,\ \mathrm{d}x \cong \mathrm{d}s)$$

and the equation becomes:

$$P\left(y^I + \frac{\mathrm{d}y^I}{\mathrm{d}x}\mathrm{d}x\right) - Py^I = p^*\mathrm{d}x$$

which, appropriately reduced, gives

$$p^* = P\frac{\mathrm{d}^2 y}{\mathrm{d}x^2} \cong P\frac{1}{r}$$

A tendon is therefore statically equivalent, with respect to the internal forces induced in the beam, to a distributed load. The magnitude p^* of this load in particular depends linearly on the curvature $1/r$ through the prestressing force.

This concept is visualized in Fig. 10.17a in the case of a parabolic layout with constant curvature, having neglected the effect of friction. The forces applied by the tendon on the beam are represented, both the ones distributed along its length according to the behaviour described above and the ones concentrated at the ends where the anchorages are positioned (with $N = P\cos\ \varphi_o \cong P$ and with $V = P\sin\varphi_o$).

As these are internal mutual action, in the isostatic configuration of the beam such forces are internally balanced and do not induce reactions of the external constraints in Fig. 10.17a. For an appropriate configuration of the tendon, it is necessary that the opposite system of equivalent loads be as close as possible to the configuration of the external loads in service.

The case of a beam with straight bonded tendons is instead shown in Fig. 10.17b. As there is no curvature, there is no vertical force component of the tendon along its length. The end forces acting on the bonded segments remain: the axial force N in compression, which enhances the flexural behaviour of the sections, and the bending moment Ne, due to the eccentricity, which gives an indirect enhancement, opposed but not coinciding with the configuration of external forces.

The following forces are obtained with the deviation of the tendons (see Fig. 10.17c):

$$V_1 = P\ \sin\alpha_1$$
$$V_2 = P\ \sin\alpha_2$$

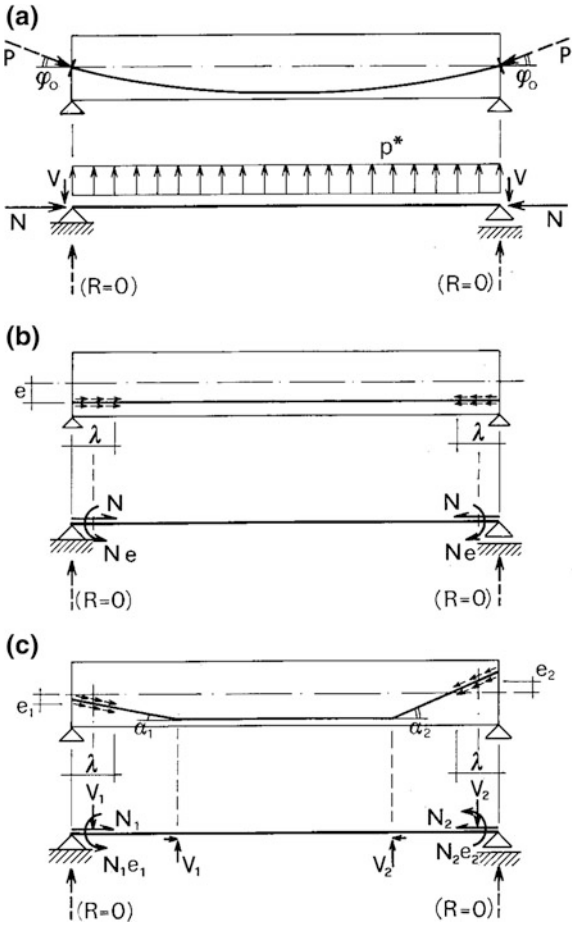


Fig. 10.17 Concept of equivalent loads

which are in opposition to the external forces, with concentrated forces on intermediate positions. There are also the end forces distributed on the bonded segments λ: the horizontal ones N_1 and N_2 ($\cong P$ for small values of the deviations α), the vertical ones that provide a concentrated sustenance contribution V_1 and V_2 and eventually the bending moments due to the possible eccentricities e_1 and e_2 (positive or negative) of the tendon close to the supports.

The equivalent loads give an alternative way to evaluate the internal forces in the beam induced by precompression: not as a force exchanged locally between tendon and cross section, but introduced in the overall arrangement of the beam as forces and moments; the precompression is therefore represented in a similar way to schemes with external forces. The usefulness of such interpretation lies in the more immediate qualitative perception of the type of beneficial effect offered by the layout of the tendons against the effect of external loads as already mentioned, rather than the corresponding alternative calculation algorithms.

10.2.2 Available Moment and Limit Points

The following description refers to the serviceability verifications, as they usually determine the most restrictive limits to the choices of the tendon positioning. The formulas reported below therefore correspond to the elastic behaviour of beams under loads assumed with their characteristic value. The limit state of maximum compression $\bar{\sigma}_c$ in concrete is considered on one side, and on the other, for the cracking verification, the limit state $\bar{\sigma}_{ct}$ that can refer to decompression or the formation of cracks ($\bar{\sigma}_{ct} = 0$ or $\sigma_{ct} = f_{ctk}$).

For the section of Fig. 10.18 let assume A, I, $W = I/y$, $W' = I/y'$ as the geometrical characteristics homogenized to concrete and N_p, e as the parameters of precompression. The variations in time of the concerned parameters are neglected here, both the ones due to concrete aging and the ones consequent to the tension losses in the tendons. The prestressing force N_p in the formulas shown below is assumed positive.

In the situation "a" of minimum loads, assuming that the effect of prestressing prevails on the one of the external action, the verifications of stresses at the two edges of the section are written as:

$$\sigma_{ca} = -\frac{N_p}{A} + \frac{N_p e}{W} - \frac{M_{min}}{W} \leq \bar{\sigma}_{ct} \quad \text{tension positive}$$

$$\sigma'_{ca} = +\frac{N_p}{A} + \frac{N_p e}{W'} - \frac{M'_{min}}{W'} \leq \bar{\sigma}_c \quad \text{compression positive}$$

Using the equalities as limit situations, from the two relationships above one obtains, respectively, for the minimum moment the values

$$M'_{min} = M'_{min}(A,\ W;\ N_p,\ e;\ \bar{\sigma}_{ct})$$
$$M''_{min} = M''_{min}(A,\ W';\ N_p,\ e;\ \bar{\sigma}_c)$$

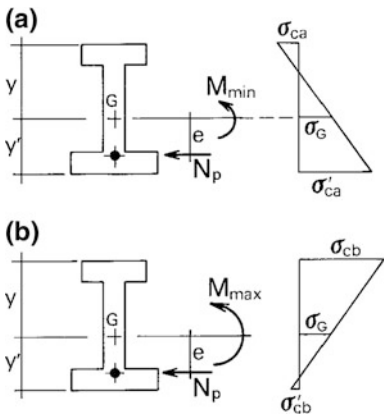


Fig. 10.18 Limit allowable situations under minimum (**a**) and maximum (**b**) loads

the greater of which gives the lower limit

$$M_{\min} = \max\left(M'_{\min}, M''_{\min}\right)$$

of the external action compatible with the fulfilment of the competent serviceability verifications.

The same verifications are proposed now in the situation "b" of maximum loads, for which the effect of the external action prevails on the one of prestressing:

$$\sigma_{cb} = +\frac{N_p}{A} - \frac{N_p\, e}{W} + \frac{M_{\max}}{W} \leq \bar{\sigma}_c \quad \text{compression positive}$$
$$\sigma'_{cb} = -\frac{N_p}{A} - \frac{N_p e}{W'} + \frac{M'_{\max}}{W'} \leq \bar{\sigma}_{ct} \quad \text{tension positive}$$

Using the equalities the two following values are consequently obtained for the maximum moment:

$$M'_{\max} = M'_{\max}(A,\, W;\, N_p,\, e;\, \bar{\sigma}_c)$$
$$M''_{\max} = M''_{\max}(A,\, W';\, N_p,\, e;\, \bar{\sigma}_{ct})$$

the lesser of which gives the upper limit

$$M_{\max} = \min\left(M'_{\max}, M''_{\max}\right)$$

of the external action compatible with the fulfilment of the competent serviceability verifications.

Available Moment

The range

$$\Delta M = M_{\max} - M_{\min}$$

gives the *available moment* of the section related to its capacity. It is a function of the section (A, W, W') under prestressing ($N_p\, e$), in addition to the parameters $\bar{\sigma}_c$, $\bar{\sigma}_{ct}$ related to the resistance of the material.

It is to be noted that, contrary to the sections in ordinary reinforced concrete, for which the absence of external load is always within the allowable limits of the structural behaviour corresponding to zero stresses, for sections in prestressed reinforced concrete there is a lower limit under which the external action cannot go: without any loads the internal actions of prestressing can in fact lead to stresses higher than the allowable limits of the materials.

Usually the minimum load corresponds to the self-weight of the beam. Its effect arises at the same time for the application of prestressing, when the beam tends to bend upwards because of it, remaining supported at the ends. Other than the initial situation, there could be transient phases of lifting and transportation where the beam is suspended or supported on intermediate supports with consequent

reduction of the bending moment due to the self-weight. Once dropped into the final position, the beam usually goes back to a configuration similar to the initial one with supports placed at the ends. From this point all subsequent applied loads, including the effects of prestressing losses, lead towards the situation of maximum loads. What has been described does not take into account the possibility of alternate actions which would cause the inversion of bending moment, as for example occurs in the continuous decks of bridges subject to moving loads.

Therefore, for typical situations similar to the one previously described:

- the maximum prestressing is limited by the initial situations of self-weight only;
- the minimum prestressing is limited by the final situations with all loads applied;
- the design of the cross section is also related to the range of loads between the two extreme situations mentioned above.

Limit Points

The same problem, set before in terms of minimum and maximum moment, can be analyzed in terms of extreme positions of the resultant of the internal forces. In Fig. 10.19 it is shown how, adding the prestressing force N to the moment M due to external loads, the resultant is a force N translated vertically by M/N with respect to the prestressing force. If this vector sum is done on the minimum moment (see Fig. 10.19a), one obtains the extreme position

$$u_{\text{inf}} = e - \frac{M_{\min}}{N_{\text{p}}}$$

under which the resultant cannot go in order to satisfy the serviceability verifications for the minimum loads of the initial situations. If the same sum is done with the maximum moment (see Fig. 10.19b), one obtains the extreme position

$$u_{\text{sup}} = \frac{M_{\max}}{N_p} - e$$

beyond which the resultant cannot go in order to satisfy the serviceability verifications for maximum loads of final situations. Each intermediate position of the resultant is obviously admissible.

These limit positions can be directly deduced from the usual verification formulas written as:

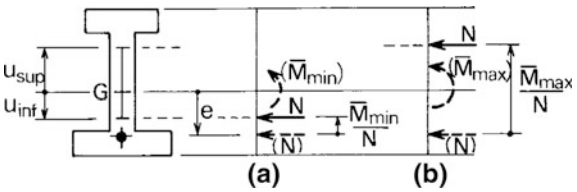


Fig. 10.19 Limit points under minimum (**a**) and maximum (**b**) loads

$$\sigma_{ca} = -\frac{N_p}{A} + \frac{N_p u_{inf}}{W} \leq \bar{\sigma}_{ct}$$
$$\sigma'_{ca} = +\frac{N_p}{A} + \frac{N_p u_{inf}}{W'} \leq \bar{\sigma}_c$$

for the lower limit, or written as:

$$\sigma_{cb} = +\frac{N_p}{A} + \frac{N_p u_{sup}}{W} \leq \bar{\sigma}_c$$
$$\sigma'_{cb} = -\frac{N_p}{A} + \frac{N_p u_{sup}}{W'} \leq \bar{\sigma}_{ct}$$

for the upper limit, assuming the lesser of the two values from the corresponding equations.

The calculated *lower* and *upper bound limit points* are therefore function of:

- the resistance parameters of the materials $\bar{\sigma}_c$, $\bar{\sigma}_{ct}$;
- the geometrical characteristics of the section A, W, W';
- the prestressing force N_p.

The extent of the admissible interval is directly correlated to the available moment with:

$$u_{inf} + u_{sup} = \Delta M / N_p$$

that is the admissible range for external loads.

Guyon's Zone

Let us now consider a given structural arrangement, for example a simply supported beam with constant cross section, under uniformly distributed loads, as shown in Fig. 10.20a. For such configuration one should expect parabolic bending moment diagrams, such as the one represented in the figure, with maximum value $pl^2/8$ at the mid-span.

If the axial force N_p deriving from prestressing is assumed constant along the entire length of the beam, neglecting friction and the inclination of tendons, all the limit points form the straight lines indicated in the same Fig. 10.20a.

For a given eccentricity e of the tendon at the most highly stressed mid-span section, the verifications in this section are satisfied if the two translations

$$M_{min}/N_p$$
$$M_{max}/N_p$$

respectively, under minimum and maximum loads, are within the admissible interval, as assumed in the mentioned Fig. 10.20a. Taking into account that the magnitude of the above translations decreases parabolically along the beam towards the ends according to the variation of bending moment, one could assign a parabolic

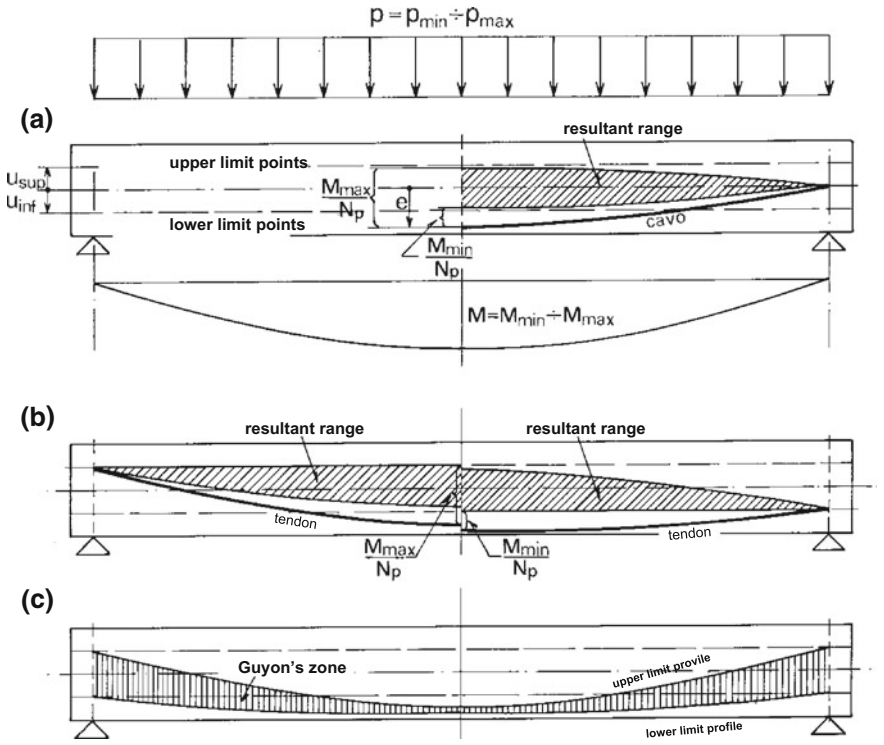


Fig. 10.20 Allowable tendon profile (Guyon's zone)

profile to the tendon, which moves up to the centroid of the end section on the support.

Such profile is represented by the right-hand side of Fig. 10.20a, together with the range of the resultant that derives. In particular under minimum loads the resultant of the force will follow the bottom edge of such zone, under maximum loads it will follow the top edge, under intermediate loads it will follow internal parabolic routes.

The parabolic profile of Fig. 10.20a therefore satisfies the serviceability verifications along the entire beam for the given structural arrangement, with a range of the resultant within the admissible zone.

Other profiles of the tendon around the central one discussed above are possible, provided the corresponding ranges of the resultant are within the allowable zone. For example, the highest possible profile of the tendon is indicated on the left-hand side of the beam of Fig. 10.20b that is the parabolic one for which the translation under maximum loads brings the resultant on the upper limit point in all sections. At the opposite extremity there is the profile of the lowest possible tendon, for which the translation under the minimum loads brings the resultant on the bottom limit point, as described in the right-hand side of the beam of Fig. 10.20b.

These two limit profiles identify the so called *Guyon's zone*, within which the actual tendon profile can be placed, with respect to the competent serviceability verifications for all sections of the beam.

10.2.3 Hyperstatic Beams

So far we have analyzed isostatic beams where prestressing does not induce any reaction of the external supports nor any distribution of hyperstatic internal forces. In each section, the effects of prestressing are calculated based on the local values of the three internal forces:

– axial	$N\mathrm{p} = P \cos \varphi$
– shear	$V\mathrm{p} = P \sin \varphi$
– bending	$M\mathrm{p} = N\mathrm{p}\ e$

In hyperstatic beams instead, there is an additional force which depends on the arrangement of the supports.

In order to show this behaviour, let us consider the simple beam on three supports of Fig. 10.21, assumed with constant section. In the straight tendon, let us assume a prestressing force $N_\mathrm{o} = P$ be applied with an eccentricity e with respect to the centroidal axis of the beam.

Following the flexibility method, the beam can be made isostatic removing the rotational constraint of flexural continuity at the intermediate support and applying the corresponding hyperstatic moment X. In order to find the value of this moment, the compatibility equation can be written with respect to the relative rotation between the contiguous sections of the two spans of the beam, which has to be equal to zero:

$$\phi_l X + \phi_\mathrm{o} = 0$$

where

$$\phi_1 = 2\frac{l}{3\mathrm{EI}} \quad \phi_0 = -2\frac{l}{2\mathrm{EI}} N_\mathrm{O} e$$

The hyperstatic moment is eventually obtained

$$X = \frac{3}{2} N_\mathrm{o} e$$

which leads to the following internal forces in the generic section at the abscissa x of the first span:

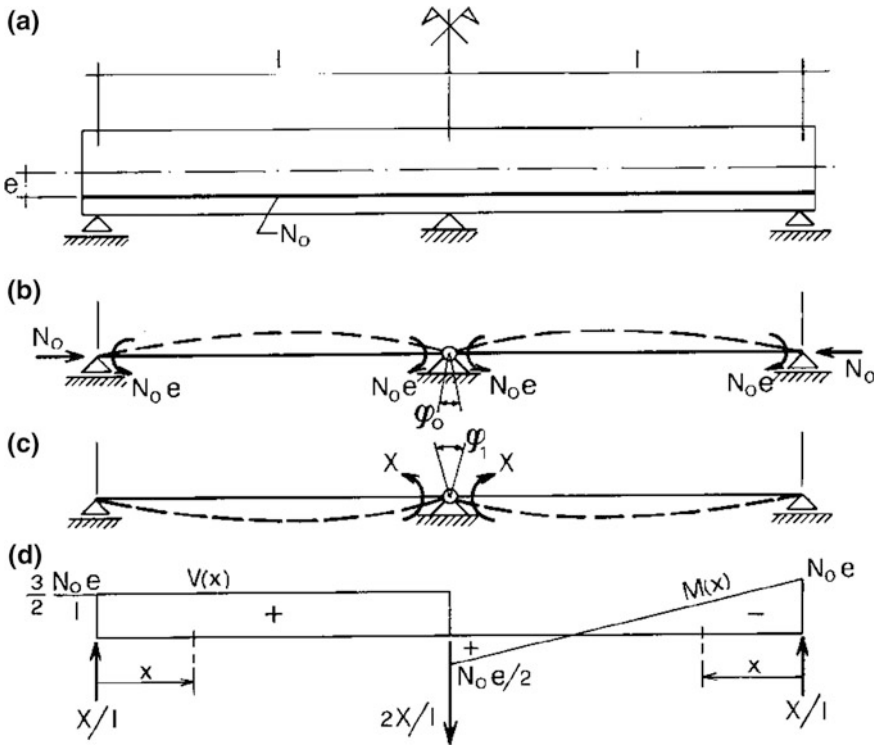


Fig. 10.21 Solution of the hyperstatic beam

$$N(x) = N_o \qquad (= \text{cost.})$$

$$V(x) = \frac{X}{l} = \frac{3}{2}\frac{N_o e}{l} \qquad (= \text{cost.})$$

$$M(x) = -N_o e + \frac{X}{l}x = -N_o e\left(1 - \frac{3x}{2l}\right)$$

and symmetrically in the second span.

From the example analyzed above (see in particular Fig. 10.21d), it can be seen how the hyperstatic effect of prestressing can even predominate, leading to the inversion of the moment in certain segments of the beam. The situation presented in Fig. 10.21 actually contemplates an inconsistent tendon profile in relation to real configurations. The latter contemplate profiles that are more consistent with the structural arrangement, following the concept of equivalent loads presented at Sect. 10.2.1. For example, Fig. 10.22 reproduces a typical layout for the continuous beam, under the usual uniformly distributed load described in the same figure. For these cases the magnitude of the hyperstatic effects is much smaller and usually has an influence of less than 10%.

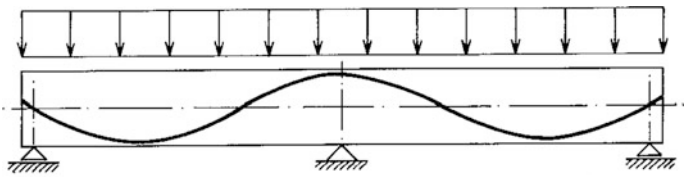


Fig. 10.22 Consistent tendon profile

Complying Tendon

In particular, from the compatibility equation written before it can be noted that, if the tendon profile does not generate any rotation ϕ_o, there is no hyperstatic force, having

$$X = -\phi_o/\phi_1 = 0$$

Such profile is called *complying*; it directly gives a distribution

$$M_o(x) = N_o(x) \cdot e(x)$$

of bending moment consistent with the compatibility of the hyperstatic beam.

If for example friction and tendon inclination are neglected, assuming an axial force N_o = cost along the entire beam, the layout *e(x)* of the tendon coincides with the bending moment, save for the constant N_o

$$M_p(x) = N_o\, e(x)$$

With such premises, a complying tendon can be the one whose profile reproduces, save for a scaling factor, the bending moment diagram of the hyperstatic beam under the given load distribution, as described in Fig. 10.23.

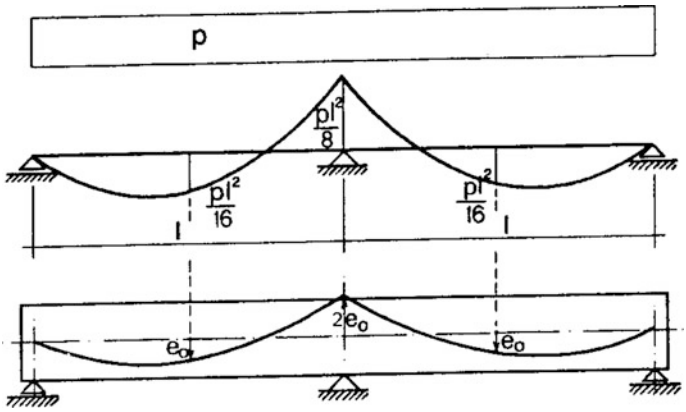


Fig. 10.23 Theoretical complying tendon

Compared to the theoretical configuration that does not induce any hyperstatic internal force, the actual one requires some technological adjustments, such as the introduction of continuous links around the the corner points, the straightening of the end segments corresponding to the rigid anchorage devices, or an increased proximity to the edges of the beam. Added to the effects of friction and the inclination of the tendons, such adjustments of the layout induce hyperstatic internal forces; their magnitude is much smaller than the one of the first example and usually limited to a small percentage of the local precompression effect as already mentioned.

10.3 Resistance Calculations

Firstly, in addition to what mentioned at Sect. 2.4.2, a few construction requirements are given on the positioning of post-tensioned prestressing tendons. For post-tensioned beams, before being grouted the ducts represent a weakening of the resisting section that one should take into account in the verification calculations and in the construction phase in order to ensure an adequate cover of the ducts for their significant dimensions.

The following provisions should not be taken as exact and prescriptive. However, it is necessary to follow them generally to ensure the actual respect of the design assumptions. They will always have to be coordinated with the analogous rules for the passive and prestressing reinforcements presented at Sect. 2.4.2 and integrated with appropriate specific verifications, of which few examples are given later in this section.

Ducts Spacing

For post-tensioned tendons the following minimum dimensions can be indicated, expressed in mm (see Fig. 10.24).

– net horizontal spacing i_{oh}:

$$\begin{array}{llll} 1.6\,d_a & & 1.0\,\phi & 40 \\ 1.6\,d_a & 1.0\,b & 0.7\,a & 40 \end{array}$$

– net vertical spacing i_{ov}:

$$\begin{array}{llll} 1.6\,d_a & & 1.0\,\phi & 50 \\ 1.6\,d_a & 1.0\,b & – & 50 \end{array}$$

– net horizontal cover c_{oh}:

$$\begin{array}{llll} 1.6\,d_a & & 0.7\,\phi & 40 \\ 1.6\,d_a & – & 0.5\,a & 40 \end{array}$$

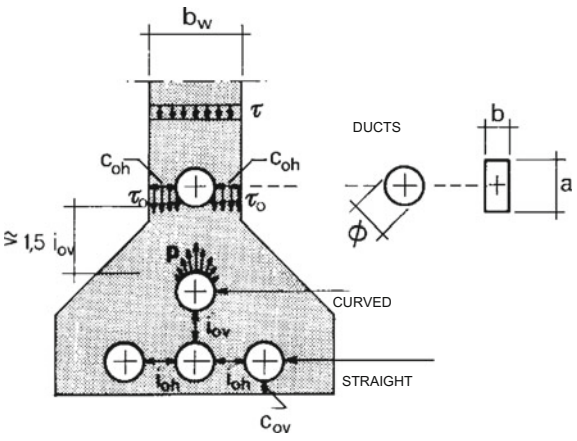


Fig. 10.24 Positioning of ducts for post-tensioned tendons

– net vertical cover c_{ov}:

$1.6\,d_a$		$0.7\,\phi$		30
$1.6\,d_a$	$0.7\,b$		$0.5\,a$	30

Circular (with a diameter ϕ) and rectangular (with vertical a and horizontal b sides) ducts are considered. The maximum aggregate size is indicated with d_a.

In Fig. 10.24 it is also indicated how, *in the curved segments*, the tendon applies a significant transverse pressure p on the inner edge of the duct; in order to ensure the integrity of the separating concrete layer, in such segments the spacing of the contiguous duct towards which pressures act should be increased. More generally the tendons deviations should always be orientated so to direct the transverse pressures due to curvature towards the inner resisting part of the beam, avoiding the external edges as well as the internal voids left by contiguous ducts.

It should also be noted that, for the phases before the grouting of the ducts, the shear verifications of the section should refer to the *net width*, subtracting the holes of the ducts from the width of the section. In the situation of Fig. 10.24 one has for example:

$$b_o = b_w - \phi$$

with

$$\tau_o = \frac{b_w}{b_o}\tau$$

and with the consequent reduction of the resistance of the concrete web.

Bonded Reinforcement

It should be noted that post-tensioned tendons represent a reinforcement that is too concentrated and internal with respect to what is required for an effective cracking control. Prestressed beams with post-tensioned tendons should always have longitudinal integrative passive bonded reinforcement, in a minimum amount with respect to the beam section and appropriately distributed along its perimeter. Appropriate strengthening of this reinforcement should be positioned where tensile stresses are expected in the subsequent lifting, transportation and service phases.

Pre-tensioned tendons instead are quite effective for cracking control. In the beams prestressed with pre-tensioned tendons, the passive reinforcement should be added only in the most distant parts of the sections lacking in active bonded reinforcement.

Considering all types of bonded reinforcement, either passive or pre-tensioned, from the criterion of non-fragility already discussed, the following minimum requirements can be deduced. For the *longitudinal reinforcement*:

$$A_s \geq kA_c f_{ctm}/\sigma_s$$

with $\sigma_s = f_{yk} \leq 500\,\text{N/mm}^2$ and where A_c is the area of concrete in tension of the uncracked section, whereas k takes into account the type of stress distribution on the tension zone itself (k = 1.0 for a constant distribution, k = 0.5 for a triangular distribution on a rectangular tension zone of a section in bending).

Such requirement is consistent with the ones given at Sects. 2.3.3 and 3.2.3, respectively, for tie elements and beams in bending, with the clarification that, for a good cracking control, the stress in the pretensioned tendons should be referred to the decompression of concrete with the nominal limit of σ_s = 500 N/mm^2.

For the *transverse reinforcement* the requirements for the minimum amount of stirrups given at Sect. 4.3.3 are again valid:

$$a_s \geq 0.2 b_w f_{ctm}/\sigma_s$$

with

$$\sigma_s = f_{yk} \leq 500\,\text{N/mm}^2$$

and where b_w is the web thickness.

10.3.1 Verification of Prestressed Concrete Sections

The calculation of the resisting moment of the sections in prestressed reinforced concrete has already been presented at Sect. 3.1.3. Only a few clarifications are to be added with respect to what described in that section.

Firstly, it should be noted that at the mentioned section, in the algorithm of calculation of the resistance, prestressing has been interpreted as a geometrical quantity that is the elongation ε_{po} (see Fig. 3.15) that corresponds to the *internal mutual action* of prestressing. Such interpretation is the closest to the nature of the problem and allows a more precise definition of the ultimate limit state of the section.

Nevertheless, there is an alternative way to represent prestressing that is useful to facilitate several practical calculations. It consists of substituting the tendon with its static effect that is the *prestressing force P* assumed as a constant external force. The approximations of such interpretation are conservative as the stress variations in the tendon from the serviceability to the ultimate resistance situation are neglected.

The first approach allows to take into account fully the steel strength f_{pyd} in the calculation of the positive resisting moment, or to consider the decrease $\sigma_{po} - \sigma_p$ of the stress in steel when in the compression zone for the calculation of the negative resisting moment. The second approach instead assumes a constant value in the tendon, corresponding to the prestressing σ_{po} that underestimates the actual stress at the ultimate limit of the positive resisting moment and overestimates the one at ultimate limit of the negative resisting moment.

In any case, in the definition of the stress σ_{po} or the corresponding elongation $\varepsilon_{po} = \sigma_{po}/E_p$, one has to take into account the long-term losses developed at the considered verification stage. In general in the initial stages, such as the one at prestressing, the initial values σ_{pi} and $\varepsilon_{pi} = \sigma_{pi}/E_p$ will be used (which include the instantaneous losses or the ones due to friction); in the final phases, corresponding to the application of live loads, the values $\sigma_{p\infty}$ and $\varepsilon^*_{p\infty} = \sigma_{p\infty}/E_p$ will be used.

Internal Mutual Action

With reference to the case of a single post-tensioned beam with curved tendons (see for Ex. Fig. 10.6), let us consider the zone of maximum moment where in general the tendons are located close to the edge in tension and approximately parallel to the beam axis. For this situation the rigorous model expressed in Fig. 10.25 can be easily applied, where prestressing is accurately represented by the elongation ε_{po} (= ε_{pi} for the initial stages, = $\varepsilon^*_{p\infty}$ for the final ones), whereas the tendons are correctly assumed as resisting reinforcement.

The resisting moment is calculated with

$$M_{Rd} = A_p f_{pyd} z_p + A_s f_{yd} z + A'_s f_{yd} z' \quad (> M_{Ed})$$

with

$$z_p = d_p - \bar{x}/2 \quad z = d - \bar{x}/2$$
$$z' = \bar{x}/2 - d' \quad \bar{x} = \left(\omega_p + \omega_s - \omega'_s\right) d$$

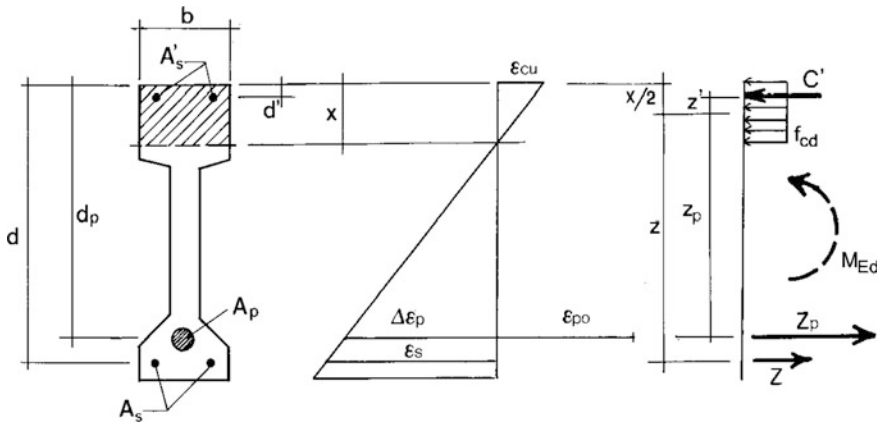


Fig. 10.25 Strain and stress distribution in a post-tensioned section

where

$$\omega_p = \frac{A_p f_{pyd}}{d\, b f_{cd}} \quad \omega_s = \frac{A_s f_{yd}}{d\, b f_{cd}} \quad \omega'_s = \frac{A'_s f_{yd}}{d\, b f_{cd}}$$

adding the appropriate controls of elongations required for the validity of the formula written above:

$$\varepsilon_p = \frac{d_p - x}{x}\varepsilon_{cu} + \varepsilon_{po} \quad \left(\varepsilon^*_{yd} \le \varepsilon_p \le \varepsilon_{pd}\right)$$
$$\varepsilon_s = \frac{d - x}{x}\varepsilon_{cu} \quad \left(\varepsilon_{yd} \le \varepsilon_s \le \varepsilon_{sd}\right)$$
$$\varepsilon'_s = \frac{x - d'}{x}\varepsilon_{cu} \quad \left(\varepsilon_{yd} \le \varepsilon'_s\right)$$

with $x \cong \bar{x}/0.8$ and $\varepsilon_{cu} = 0.35\%$ (see Figs. 1.30 and 1.32).

Prestressing Force

In the end zones of the beam, with low values of bending moment, the tendons are usually shifted upward towards the central axis with significant inclinations. The longitudinal reinforcement of the edge in tension should consist of passive reinforcement, whereas the variations $\Delta\varepsilon_p$ of the elongations in the prestressing steel are smaller and can leave the steel in the elastic range.

For these reasons a simpler approximated model can be assumed, where the tendon is substituted with an external constant force $P_d = \gamma_P P$, appropriately quantified with the partial factor γ_P (decreasing or magnifying depending whether it enhances or not the resistance). The problem therefore goes back to the one of the reinforced concrete section under combined compression and bending of Fig. 10.26.

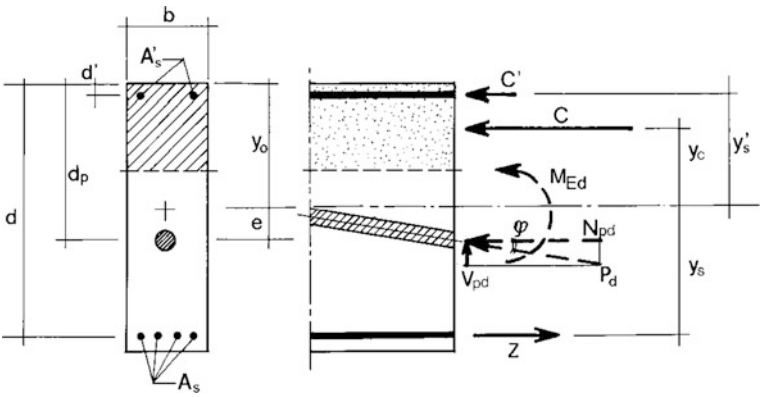


Fig. 10.26 Force representation of the precompression

The resisting moment should be calculated with respect to the design axis with

$$M^*_{\mathrm{Rd}} = b\bar{x}f_{\mathrm{cd}}y_{\mathrm{c}} + A_{\mathrm{s}}f_{\mathrm{yd}}y_{\mathrm{s}} + A'_{\mathrm{s}}f_{\mathrm{yd}}y'_{\mathrm{s}}$$

and should be compared with the reduced moment

$$M^*_{\mathrm{Ed}} = M_{\mathrm{Ed}} - N_{\mathrm{pd}}e \quad \left(< M^*_{\mathrm{Rd}}\right)$$

where

$$N_{\mathrm{pd}} = P_{\mathrm{d}}\cos\varphi$$

In the case of rectangular concrete compression zone, as in Fig. 10.26, its depth is defined by

$$\bar{x} = \frac{N_{\mathrm{pd}}}{bf_{\mathrm{cd}}} + \frac{A_{\mathrm{s}}f_{\mathrm{yd}}}{bf_{\mathrm{cd}}} - \frac{A'_{\mathrm{s}}f_{\mathrm{yd}}}{bf_{\mathrm{cd}}} = \left(v_{\mathrm{p}} + \omega_{\mathrm{s}} - \omega'_{\mathrm{s}}\right)d$$

from which one obtains

$$y_{\mathrm{c}} = y_{\mathrm{o}} - \bar{x}/2 \quad y_{\mathrm{s}} = d - y_{\mathrm{o}} \quad y'_{\mathrm{s}} = y_{\mathrm{o}} - d'$$

and the usual checks should be added (with $x \cong \bar{x}/0.8$):

$$\varepsilon_{\mathrm{s}} = -\frac{d-x}{x}\varepsilon_{\mathrm{cu}} \quad \left(\varepsilon_{\mathrm{yd}} \le \varepsilon_{\mathrm{s}} \le \varepsilon_{\mathrm{sd}}\right)$$

$$\varepsilon'_{\mathrm{s}} = -\frac{x-d'}{x}\varepsilon_{\mathrm{cu}} \quad \left(\varepsilon_{\mathrm{yd}} \le \varepsilon'_{\mathrm{s}}\right)$$

In the formulas above, the effect of the prestressing tendon has been shifted from the resistance to the action, using ν_p instead of ω_p.

Shear Resistance

In the same zone of Fig. 10.26, the inclination of the tendon leads to the resistance contribution in shear

$$V_{pd} = P_d \sin\varphi$$

used to calculate the reduced force

$$V^*_{Ed} = V_{Ed} - V_{pd}$$

according to the same approximated interpretation of the precompression as an external constant force.

The verification is therefore set, assuming the use of vertical stirrups, with:

$$\begin{aligned} V^*_{Rd} &= \min\left(V^*_{sd}, V^*_{cd}\right) > V^*_{Ed} \\ V^*_{sd} &= a_w z^* f_{yd} \lambda_c \\ V^*_{cd} &= z^* b_w f_{c2} \lambda_c / \left(1 + \lambda_c^2\right) \end{aligned}$$

where

$$z^* = d^* - \bar{x}^*/2$$

is the lever arm of the internal moment with respect to the reduced effective depth (see Sect. 6.3.1)

$$d^* = \left(1 - \nu_p + \omega'_s\right) d \quad \bar{x}^* = \omega_s d$$

and where λ_c is bounded within the limits (see Sect. 4.3.2):

$$\lambda_I \le \lambda_c \le \lambda_{max} \quad (\lambda_{max} = \lambda_I + \Delta\lambda)$$

In particular, for high precompression forces, as the effective depth is reduced significantly ($d^* \ll d$) with very low inclination of initial cracking ($\lambda_I = \tau/\sigma_I \gg 1$), the shear resistance is generally limited by compressions in the concrete web ($V^*_{cd} < V^*_{sd}$) with small amounts of stirrups.

Pre-tensioned Tendons

Beams prestressed with pre-tensioned tendons usually have straight tendons close to the edge in tension. With this configuration, for the calculation of the resisting moment one can immediately apply the rigorous model that represents precompression as an internal mutual action, interpreting the pre-tensioned tendons as resisting reinforcement and not as an external force (see Fig. 10.27a).

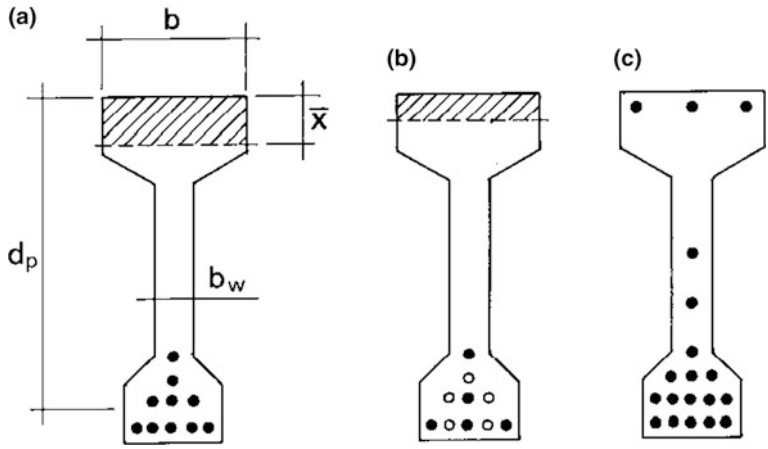


Fig. 10.27 Section prestressed with pretensioned tendons

With respect to the shear verification in the lateral zones, two different cases should be distinguished. The first one refers to a *prestress reduced* with the use of ducts for a certain number of tendons (see Fig. 10.27b). In this case, under the ultimate load the section should be assumed as cracked with yielded tension reinforcement. Prestressing is considered only in the inclination of initial cracking

$$\lambda_{\mathrm{I}} = \tau/\sigma_{\mathrm{I}}$$

and the verification of the resisting shear force (with $\lambda_{\mathrm{I}} \leq \lambda_{\mathrm{c}} \leq \lambda_{\max}$) is again referred to the entire effective depth:

$$\begin{aligned} V_{\mathrm{Rd}} &= \min(V_{\mathrm{sd}}, V_{\mathrm{cd}}) > V_{\mathrm{Ed}} \\ V_{\mathrm{sd}} &= a_{\mathrm{w}} z f_{\mathrm{yd}} \lambda_{\mathrm{c}} \\ V_{\mathrm{cd}} &= z b_{\mathrm{w}} f_{\mathrm{c2}} \lambda_{\mathrm{c}} / \left(1 + \lambda_{\mathrm{c}}^2\right) \end{aligned}$$

with

$$z = d_{\mathrm{p}} - \bar{x}/2 \quad \left(\cong 0.9 d_{\mathrm{p}}\right)$$

A second case is the one of high prestressing force extended to the lateral zones of low bending moment, for which the sections remain *uncracked* under the ultimate load. In this case the shear verification is carried out as indicated at Sect. 6.3.1 for uncracked segments that is calculating the resistance with

$$V_{\mathrm{Rd}} = \bar{z} b_{\mathrm{w}} \sqrt{\bar{\sigma}_{\mathrm{td}} (\bar{\sigma}_{\mathrm{td}} + \sigma_{\mathrm{G}})} \quad (> V_{\mathrm{Ed}})$$

where

$$\begin{aligned} \bar{\sigma}_{td} &= f_{ctd} && \text{per} \quad \sigma_G \leq f_{cd}/3 \\ \bar{\sigma}_{td} &= f_{ctd}\tfrac{3}{2}(1 - \sigma_G/f_{cd}) && \text{per} \quad \sigma_G > f_{cd}/3 \end{aligned}$$

and where $\sigma_G = N_{pd}/A_i$ is the centroidal stress, whereas $\bar{z} = I_i/S'_i$ is the lever arm of the internal moment of the section based on the elastic formulas.

There can be intermediate cases with respect to the limit ones considered above, with *cracked sections* and completely or partially within the elastic range; for these cases the shear verification can also be carried out as indicated at Sect. 6.3.1 for cracked segments and therefore based on a truss model for the web extended to a reduced effective depth appropriately calculated.

In the cases of high precompression there are usually a lot of pre-tensioned tendons distributed along the depth of the section (see Fig. 10.27c). These cases can be analyzed with rigorous procedures that set the equilibrium equations of the prestressed section with iterative procedures and numerical integrations of stresses, based on the appropriate models $\sigma-\varepsilon$ of the resistance of materials and the appropriate assumptions of plane section and compatible deformations.

10.3.2 Resistance Models of Prestressed Beams

The main global models for reinforced concrete beams in bending have already been presented in Sect. 5.1. For beams with no shear reinforcement, one should remember the *tooth model* shown in Fig. 5.2, whose capacity is based on the tensile strength of the concrete of the web, in addition to the resistance of the compression and tension chords. For beams with no transverse reinforcement the *arch model* is also recalled, shown in Fig. 5.6, which transfers the loads with a flux of inclined compressions in the concrete balanced on the supports by the steel tie. For the beams with shear reinforcement, the *truss model* is also recalled, shown in Fig. 5.7, consisting of concrete compression struts and steel ties in tension.

In these *global models* the effect of prestressing now has to be included, integrating the verification formulas already deduced in the mentioned paragraph.

Models for Prestressing

The models to represent prestressing on the overall beam layout derived from the criteria of equivalent loads already discussed at Sect. 10.2.1, integrated by schemes of the elements, straight or curved, that resist the precompression in the longitudinal direction.

The *arch-catenary* model, described in Fig. 10.28a for a tendon with curved profile, represents prestressing with its forces P applied on the end anchorages and with the pressure p^* applied on the duct towards the concavity; the reaction element consists of an arch of compressions inside the concrete that go down towards the anchorages, starting from the centre of pressures of the mid-span section assumed

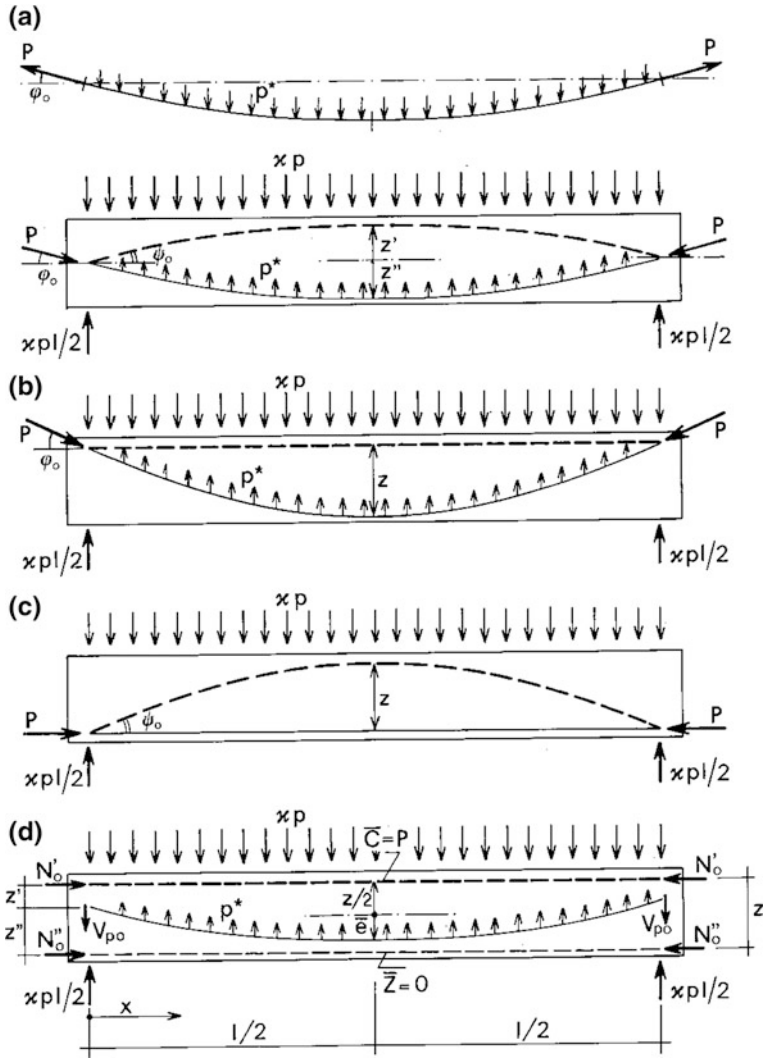


Fig. 10.28 Arch andcatenary models of a prestressed beam

as cracked in bending. The tendon is removed from the model of the resisting mechanism, replaced by its equivalent forces.

For a given prestressing force P, assumed constant along the developed length of the tendon (neglecting the effects of friction and with $\cos\varphi \cong 1$), such model is balanced with a portion κp of the total load p applied on the beam.

For a parabolic shape of compression arch and catenary in tension, defining $1/r'$ and $1/r^*$ the respective curvatures, one has the following equilibrium with the vertical load:

$$\kappa p = p' + p^* = \frac{1}{r'}P + \frac{1}{r^*}P = \left(\frac{8z'}{l^2} + \frac{8z''}{l^2}\right)P$$

which leads, with $z = z' + z''$ (see Fig. 12.28a), to

$$\kappa p = 8Pz/l^2$$

This resisting contribution of the prestressing force P also corresponds to the equilibrium of moments of the section at the mid-span where:

$$\kappa M_{\max} = \frac{\kappa p l^2}{8} = Pz$$

and where the force in the resisting arch (with a sectional area $A_c \cong 0.2\ db$) is equal to:

$$\overline{C} = P$$

At the ends, the vertical resisting contribution of prestressing is given both by arch and catenary

$$\kappa V_o = V'_o + V''_o = P \operatorname{tg} \psi_o + P \operatorname{tg} \varphi_o = P\left(\frac{z'}{l/4} + \frac{z''}{l/4}\right)$$

proportionally to the respective depths z' and z''. In the concrete web, close to the supports, a force proportional to z'/z is transferred, that translates into a flux of compressions included within an area difficult to define.

In the case of catenary only represented in Fig. 10.28b ($z'/z = 0$) there is not any force in the concrete web due to precompression P: this force runs with a constant value in the top chord that reacts to it. In the opposite limit case of arch behaviour only, shown in Fig. 10.28c ($z'/z = 1$), the entire shear force

$$\kappa V_o = \kappa p l/2 = 4Pz/l$$

is deviated in the concrete web; for its verification the resistance formula of the arch behaviour presented at Sect. 5.1.1 applies:

$$V_R \cong 0.4 d b_w f_{cd} / \left(1 + \lambda^2\right)$$

with $\lambda = l/(4z)$. With certain approximations this formula is extended to the intermediate cases of Fig. 10.28a with reference to the competent fraction $\kappa V_o z'/z$ of the force.

Simplified Model

It is to be noted that the bearing effect p^* of the catenary, introduced here in the global model of the beam, is summarized in the single section at the abscissa x by the integral

$$V_\mathrm{p} = V_\mathrm{p}(x) = P \sin \phi$$

(see Fig. 10.15) together with the eccentricity $e = e(x)$ of the contemporary axial force $N_\mathrm{p} = \mathrm{P} \cos \varphi \cong P$. In the schemes that do not have a significant contribution from the arch behaviour, where any contribution of the downward component of compressions (see Sect. 4.3) can be neglected, it is possible to summarize in each section the effect of prestressing with its two components V_p, N_p and the relative eccentricity e, the first one being attributed to the web, the second to the two longitudinal chords in inverse proportion to the respective distance from their centre of pressures.

What described above is reproduced in the *simplified model* of Fig. 10.28d, that ignores the arch behaviour and transfers the precompression in the two resisting straight chords, dividing it at the ends in the two forces N'_o and N''_o . In this model a portion of the shear force remains unbalanced

$$V'_\mathrm{o} = \kappa V_\mathrm{o} z'/z$$

and therefore this portion has to be taken into account in the second resisting mechanism, the one reserved for superimposed loads.

In particular, in the scheme of Fig. 10.28d the depth $d_\mathrm{p} = \bar{e} + a/2$ of the tendon at the mid-span has been separated from the lever arm of the internal moment z, considering the general case of a bottom reinforcement that does not coincide with the bottom of the catenary. In the balanced configuration with the quota κp of the load, the centre of pressures, starting from the depth z' at the ends, moves up to the top chord at the mid-span. Consistently the compression in this chord goes from the value $N'_\mathrm{o} = Pz''/z$ to the value $\bar{C} = P$, with an intermediate variation that can be calculated with

$$C(x) = \frac{P}{2} - \frac{Pe(x)}{z} + \frac{\kappa M(x)}{z}$$

where $\kappa M(x)$ is the bending moment due to the load κp. In a complementary way the compression in the bottom chord varies from $N''_\mathrm{o} = Pz'/z$ to $\overline{Z} = 0$, with an intermediate variation

$$Z(x) = \frac{P}{2} + \frac{Pe(x)}{z} - \frac{\kappa M(x)}{z}$$

For equilibrium, at the mid-span one has:

$$\kappa M_{\max} = P\left(\frac{z}{2} + \bar{e}\right) = Pd_{\mathrm{p}}$$

with

$$d_{\mathrm{p}} = \bar{e} + z/2$$

Models for Superimposed Loads

The remaining quota (1-κ)p of the load, which exceeds the one κp balanced by prestressing, is assumed as applied to a second mechanism which, working in parallel to the previous one, provides to the beam the resistance capacity towards its ultimate limit state.

For a beam without transverse web reinforcement, Fig. 10.29a gives the known *arch model* with tie. For this model one has the following forces:

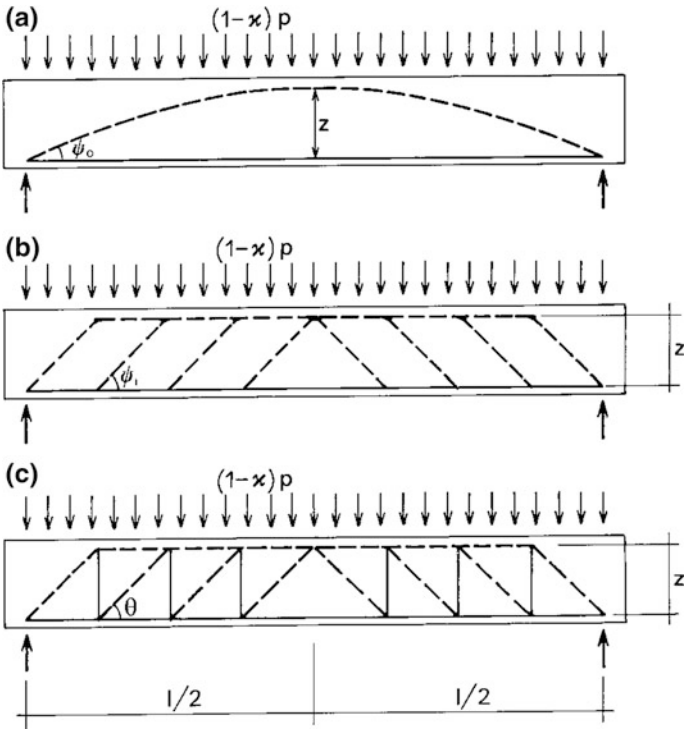


Fig. 10.29 Arch (**a**), tooth (**b**) and truss (**c**) models of the prestressed beam

- *in the tie* (of section A_s)

$$Z = (1-\kappa)\frac{pl^2}{8z} = (1-\kappa)\frac{M_{\max}}{z} \text{ (constant over } \quad 0 \le x \le l)$$

- *at the mid-span of the arch* (with section $\cong 0.2\ db$)

$$\overline{C} = Z = (1-\kappa)\frac{M_{\max}}{z} \quad (\text{per } x = l/2)$$

- *at the end bearings of the arch* (of section $\cong 0.4\ db_w \sin \psi_o$)

$$R_c = (1-\kappa)\frac{pl}{2}\sin\ \psi_o = (1-\kappa)\frac{V_{\max}}{\sin\ \psi_o} \quad (\text{for } x = 0 \text{ and } x = l)$$

Again for a beam without shear reinforcement, Fig. 10.29b shows the *tooth model*, for which one has the following forces (varying with the abscissa x):

- *in the tension chord* (of section A_s)

$$Z = (1-\kappa)\left[\frac{M}{z} + \mathrm{V}\ \mathrm{ctg}\,\psi_I\right] \quad \left(\le (1-\kappa)\frac{M_{\max}}{z}\right)$$

- *in the compression chord* (of section $\cong 0.2\ db$)

$$C = (1-\kappa)\frac{M}{z}$$

- *in the concrete web* (of width b_w)

$$q = (1-\kappa)\frac{V}{z} \quad (\text{longitudinal shear})$$

Eventually, for a beam with vertical stirrups, Fig. 10.29c shows the *truss model*, for which one has the following forces (varying with the abscissa x):

- *in the tension chord* (of section A_s)

$$Z = (1-\kappa)\left[\frac{M}{z} + \frac{V}{2}\mathrm{ctg}\,\theta\right] \quad \left(\le (1-\kappa)\frac{M_{\max}}{z}\right)$$

- *in the compression chord* (of section $\cong 0.2\ db$)

$$C = (1-\kappa)\left[\frac{M}{z} - \frac{V}{2}\mathrm{ctg}\,\theta\right] \quad (\text{compressions})$$

- *in the transverse stirrups* (of section $a_w = A_w/s$)

$$q' = (1-\kappa)\frac{V}{z}\frac{1}{\operatorname{ctg}\theta} \quad \text{(tensions)}$$

- *in the concrete web* (of width b_w)

$$q'' = (1-\kappa)\frac{V}{z}\frac{1}{\cos\theta} \quad \text{(compressions)}$$

Global Arch Model

Superimposing the resistance effects of both models, the one for prestressing and the one for superimposed loads, the verification formulas referred to the global model are obtained. If the simplified model of Fig. 10.28d is initially assumed and superimposed to the scheme of Fig. 10.29a, the formulas shown below are obtained. In particular, in the formulas related to shear, the missing contribution $\kappa V' z'/z$ of the first simplified model is added, which means that, with respect to the one V of the total load, it has been taken into account that only the contribution $P\sin\varphi$ of the catenary has been neglected.

- *Verification of the tie* (with $\kappa M_{max} = Pd_p$)

$$Z = 0 + (1-\kappa)\frac{M_{max}}{z} = \frac{M_{max}}{z} - \frac{Pd_p}{z} < A_s f_{yd}$$

- *Verification of the arch at the mid-span* ($d_p = \bar{e} + z/2$)

$$\overline{C} = P + (1-\kappa)\frac{M_{max}}{z} = \frac{M_{max}}{z} + \left(1 - \frac{d_p}{z}\right)P < 0.2bdf_{cd}$$

- *Verification of the arch at the end bearings* (with $\lambda = l/4z$)

$$V_o^* = V_o - P\sin\varphi_o < 0.4db_w f_{cd}/(1+\lambda^2)$$

Global Tooth Model

In an analogous way, if the scheme of Fig. 10.28d is superimposed to the one of Fig. 10.29b, the formulas shown below are obtained.

- *Verification of tension chord* (with $\kappa M_{max} = Pd_p$)

$$Z = -\left[\frac{P}{2} + \frac{Pe}{z} - \frac{\kappa M}{z}\right] + (1-\kappa)\left[\frac{M}{z} + V^* \operatorname{ctg}\psi_I\right] =$$
$$= -\left[\frac{P}{2} + \frac{Pe}{z}\right] + \frac{M}{z} + (1-\kappa)[V - P\sin\varphi]\operatorname{ctg}\psi_I < A_s f_{yd}$$

where the sum of the three contribution can be noted, the one of prestressing, the one of bending moments and the one of the shifting of moments. In particular in the mid-span section with no shear one has

$$\overline{Z} = (1-\kappa)\frac{M_{\max}}{z} < A_s f_{yd}$$

- Verification of compression chord

$$C = \left[\frac{P}{2} - \frac{Pe}{z} + \frac{\kappa M}{z}\right] + (1-\kappa)\frac{M}{z} = \left[\frac{P}{2} - \frac{Pe}{z}\right] + \frac{M}{z} < 0.2bdf_{cd}$$

- *Verification of concrete web*

$$q = \frac{V^*}{z} = \frac{V - P\ \sin\ \varphi}{z} < 0.28 b_w f_{ctd} c$$

where the coefficient c includes the enhancing effects of the shear resistance of the tooth model (see Sect. 4.2).

Global Truss Model

Superimposing the scheme of Fig. 10.28d with the one of Fig. 10.29c, the verification formulas of the global model of the beam with orthogonal stirrups are obtained.

- *Tension chord verification*

$$\begin{aligned} Z &= -\left[\frac{P}{2} + \frac{Pe}{z} - \frac{\kappa M}{z}\right] + (1-\kappa)\left[\frac{M}{z} + \frac{V^*}{2}\mathrm{ctg}\,\theta\right] = \\ &= -\left[\frac{P}{2} + \frac{Pe}{z}\right] + \frac{M}{z} + (1-\kappa)\frac{V - P\ \sin\ \varphi}{2}\mathrm{ctg}\,\psi < A_s f_{yd} \end{aligned}$$

where one can note the sum of the three contributions of prestressing, bending moment and moment shifting. At the mid-span with no shear force one has

$$\overline{Z} = (1-\kappa)\frac{M_{\max}}{z} < A_s f_{yd}$$

- *Verification of compression chord*

$$\begin{aligned} C &= \left[\frac{P}{2} - \frac{Pe}{z} + \frac{\kappa M}{z}\right] + (1-\kappa)\left[\frac{M}{z} - \frac{V^*}{2}\mathrm{ctg}\,\theta\right] = \\ &= \left[\frac{P}{2} - \frac{Pe}{z}\right] + \frac{M}{z} - (1-\kappa)\frac{V - P\ \sin\ \varphi}{2}\mathrm{ctg}\,\theta < 0.2\mathrm{bdf}_{cd} \end{aligned}$$

- *Verification of transverse stirrups*

$$q' = \frac{V^*}{z}\frac{1}{\operatorname{ctg}\theta} = \frac{V - P\sin\varphi}{z\operatorname{ctg}\theta} < a_w f_{yd}$$

- *Verification of concrete*

$$q'' = \frac{V^*}{z}\frac{1}{\operatorname{ctg}\theta} = \frac{V - P\sin\varphi}{z\operatorname{ctg}\theta} < b_w f_{c2}\sin\theta$$

where the inclination $\lambda_c = \operatorname{ctg}\theta$ of compressions should be comprised within

$$\lambda_I < \lambda_c < \lambda_{max}$$

where $\lambda_I = \tau/\sigma_I$ is the inclination of first cracking and $\lambda_{max} = \lambda_I + \Delta\lambda$ is increased based on the ductility of the shear reinforcement.

It should be noted that the resistance of the compression chord can be written in more general terms as

$$C_r = A'_c f_{cd} + A'_s f_{yd}$$

indicating with A'_c the concrete area in compression, not necessarily rectangular, and adding the contribution of the possible longitudinal reinforcement within such area, whereas the resistance of the tension chord becomes

$$Z_r = A_s f_{yd} + A_p f^*_p$$

adding the possible contribution of the tendons within such area, which is evaluated with reference to the *residual strength*

$$f^*_p = f_{pyd} - \sigma_{po}$$

beyond the level of precompression which is already taken into account in the corresponding model.

However, the models presented here do not have a practical interest, as they are used to formulate a clear synthesis of the equilibrium conditions on which the resistance capacity is based. Referred to schemes of simplified isostaticity they are not very accurate as the ones of the more rigorous verification formulas of cross sections previously presented.

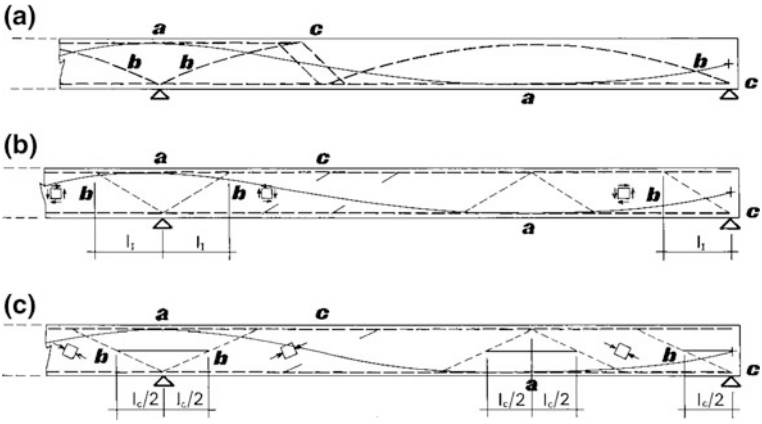


Fig. 10.30 Critical sections of the calculation procedure

Procedure

Recalling what has already been mentioned at Sect. 5.1.3 and with reference to the three models presented here, the sequence of calculations in practical design applications can be summarized as follows (see Fig. 10.30):

- *sections "a"*
  of maximum moment for the common verifications of bending moment (based on the longitudinal reinforcement and the consistency of the concrete chord in compression)
- *sections "b"*
  of maximum shear for the appropriate verifications of:
  - compressions in the web in the arch model (see Fig. 10.30a),
  - tensions in the web in the tooth model (see Fig. 10.30b),
  - tensions and compressions in the truss model (see Fig. 10.30c);
- *sections "c"*
  of zero moment for the superposition of opposing reinforcements, the bars anchorage at the support ends and the hangers of the internal arches;
- *sections "d"*
  of discontinuity of shape or reinforcement for the necessary repetition of the appropriate verifications.

It should be noted that the arch model works very well in the case of solid rectangular sections, as the ones of slabs in bending; in the case of slender sections, T-shaped or similar, with thin webs with respect to the flanges, the more reliable tooth model is preferred because of the uncertainties related to the diffusion of compressions from the web towards the collaborating flange width. This is true as long as stirrups are not required, at least in the minimum amount recalled at the beginning of the current Chapter.

10.3.3 Anchorage and Diffusion of Precompression

Other than the verifications of critical sections in the current segments of prestressed concrete beams, as presented at the previous section, the ones of tendon anchorage and the relative end zones of the beams concerned by the phenomena of the diffusion of prestressing are of fundamental importance. They are "D" zones *of discontinuity and transition*, as defined in Sect. 5.2, and can be treated with balanced strut and tie schemes. In such zones, the appropriate devices should be introduced to resist the prestressing force, in addition to the ones already discussed at Sect. 5.2.1 for the supports of ordinary beams.

End Anchorage of Tendons

The typical detail of an end anchorage (to be tensioned) of a post-tensioned tendon is shown in Fig. 10.31, assumed isolated and at the centroid position. The device consists of a steel plate thick enough to distribute uniformly the prestressing force on the area, with sides a', b', small with respect to the dimensions a, b of the entire section.

If P is the force read at tensioning, the pressure applied on the concrete under the plate is equal to

$$\sigma_c' = \frac{P}{a'b'}$$

referred to the gross area of the plate itself.

The diffusion of stresses from the contact bearing area to the entire section is also shown on Fig. 10.31 with indicated the lines of compression and tension. After a small segment approximately equal to the greater transverse dimension, the compressions stabilize on the value

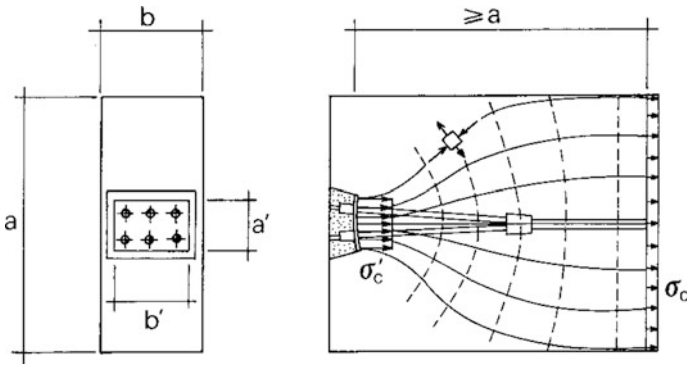


Fig. 10.31 End anchorage of a post-tensioned tendon and stress diffusion

$$\sigma_c = \frac{P}{ab}$$

constant on the entire section.

The analysis of the stress field would require the integration of complex algorithms of three-dimensional elasticity. Associating the competent assumption of rupture of the material, one would deduce the critical point where failure is triggered off. Because of the transverse confinement offered by the plate itself through friction, such point is located towards the inside. Correlating this limit situation with the corresponding value of the pressure under the plate, the strength σ'_{cr} is obtained, to be compared with the applied stress σ'_c. With the appropriate safety factor, for the verification one therefore has

$$\sigma'_c < \sigma'_{cr}/\gamma = f^*_c$$

where f^*_c is the design value of the resisting contact pressure localized under the plate.

The resistance f^*_c, for pressures localized on partial areas (see Fig. 10.32), in addition to the concrete strength, depends on:

- the ratio between the dimensions of the contact area and the total area of the element;
- the position of the contact area with respect to the edges of the section;
- the interferences with the adjacent contact areas.

Small contact areas with respect to the global dimensions and in central position exhibit higher resistance values (see situation "1" of Fig. 10.32a); the resistance decreases with the proximity to an edge and even more towards the corners (see situations "2" and "3" of Fig. 10.32a); the resistance levels are lower if one of the dimensions is close to the corresponding global dimension (see situations "4" and "5" of Fig. 10.32b); if eventually the contact area extends on the entire global area

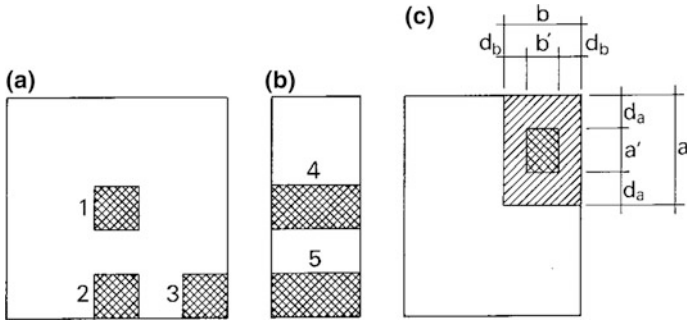


Fig. 10.32 Localised pressure—posisions of the poaded print

the situation coincides with the one of current sections, which are verified with the common prismatic resistance f_c of the material.

The *resistance verification* can rely on a conventional procedure which compares the applied design value

$$P_d = \gamma_P P$$

to the resisting one

$$P_{Rd} = f^*_{cd} A_o$$

where $A_o = a' b'$ is the gross contact area (see Fig. 10.32c) and f^*_{cd} is a resistance value deduced approximately from the formula

$$f^*_{cd} = f_{cdj} \sqrt{A_1 / A_o}$$

where $f_{cdj} = f_{ckj}/\gamma_C$ indicates the design strength of concrete at the day j of load application, whereas $A_1 = ab$ indicates the involved surface (see Fig. 10.32c), defined by the margins d_a, d_b of the contact area with respect to the closest edges of the entire global area with

$$a = a' + 2d_a \leq 3a'$$
$$b = b' + 2d_b \leq 3b'$$

In order to locally increase the concrete resistance, a confining reinforcement can be used similarly to the ones of confined columns. Their effect has already been described at Sect. 2.1.2. Such solution is shown in Fig. 10.33, where in particular on the right-hand side a loop-shaped fixed anchorage cast inside the concrete is shown, as a very common solution.

Bursting Reinforcement

The diffusion of stresses described in Fig. 10.31 occurs thanks to the dragging of the lateral fibres not directly loaded, towards which part of the central flux of compressions is deviated up to its complete and uniform diffusion. There is therefore a lateral exchange of shear stresses to which the principal stresses shown

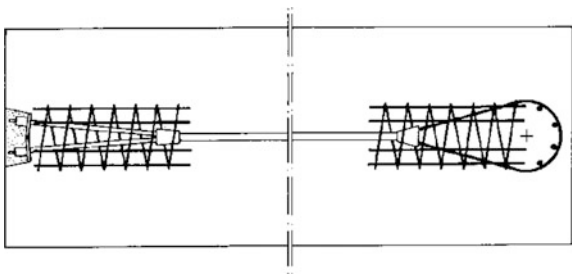


Fig. 10.33 Confinining reinforcement of the end anchorages

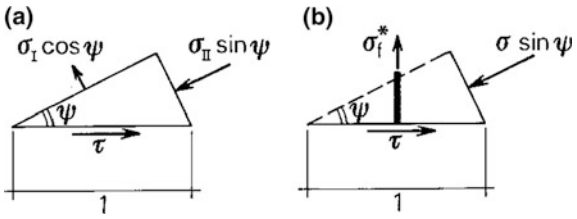


Fig. 10.34 Local equilibrium of stresses

in Fig. 10.34a correspond. The presence of transverse tensile stresses can therefore be noted, which increases in magnitude beyond a certain depth $\bar{x}$, and disappears when the diffusion is completed. For isolated load footprints with a small dimension a' with respect to the depth a of the beam, these transverse tensile stresses can lead to rupture by longitudinal splitting, analogous (although less evident) to the one typical of the indirect tension test (see Sect. 1.1.2).

In order to ensure a diffusion of stresses without relying on the concrete tensile strength, it is possible to introduce a transverse reinforcement, thanks to which the resisting mechanism described in Fig. 10.34b develops. In this case the equilibrium with the shear stress τ is given by an increased compression σ in concrete and the (equivalent) transverse tension σ_f^* in the reinforcement.

For this resisting mechanism, the beam portion concerned by the stress diffusion is represented in Fig. 10.35a. This diffusion is indicated with a dashed line with the schematic trajectory of the two semi-resultants of compressions. The transverse forces N_y are shown, which allow the double deviation of the fluxes of compressions. Close to the anchorage plate, the transverse action is also in compression and enhances the local resistance of the material. The point of possible failure moves inwards, at the tip of the confined wedge that tends to penetrate inducing the mentioned transverse tension action.

The detail (b) of the same Fig. 10.35 shows the continuous curve along which the flux n_y varies, of which the concentrated action N_y of scheme (a) represents the competent semi-resultant. The one in tension refers to the portion comprised between $\bar{x}$ and a, where the longitudinal crack can form (see the track marked on the x axis of Fig. 10.35a).

The configuration of the diagram n_y, as the one of the contemporary diagram of longitudinal flux n_x, also measured along the central axis x of the beam, depends on the arrangement of the anchorage plates and can vary significantly. Every individual case therefore requires an appropriate analysis, mainly aimed at identifying the location and magnitude of the transverse stresses.

The scheme of Fig. 10.35a shows a simplified design model for a simple case. A portion of tensile stresses is indicated, where the transverse reinforcement is to be placed. This could consist of *bursting meshes* or more simply stirrups similar to the ones represented in the detail on the left-hand side of Fig. 10.35, in addition to the current transverse reinforcement of the beam and designed for the force

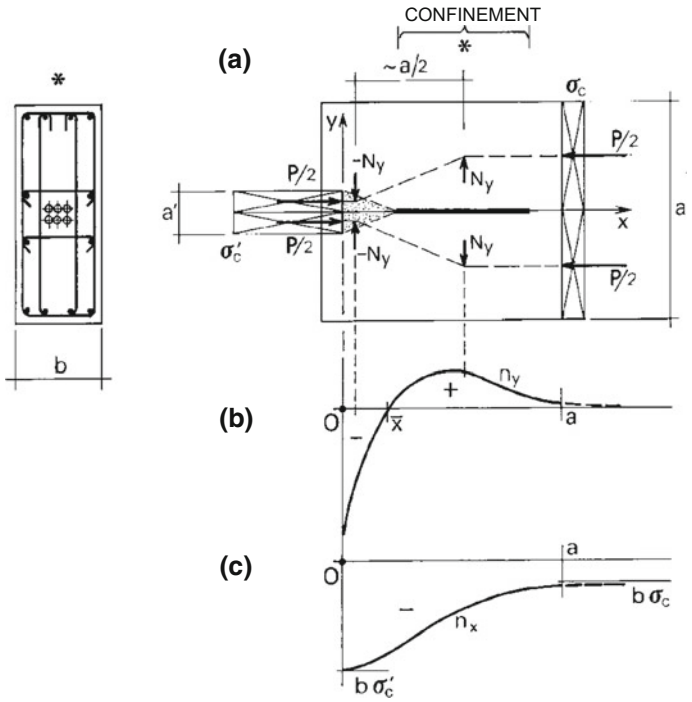


Fig. 10.35 Transverse splitting action due to stress diffusion

$$N_y \cong \frac{a - a'}{4a} P$$

that is deduced from the equilibrium of the assumed model.

Tendon Bond

The detail of the end anchorage of a pre-tensioned tendon is shown in Fig. 10.36. When released, the tendon tends to shorten, resisted by the bond that simultaneously arise at its ends. Bond is enhanced by the phenomenon of self-anchorage that has been mentioned at Sect. 1.4.3. Because of the high-strength steel, a significant anchorage length is necessary before the tendon can reach its full capacity. For example, for a strand with f_{yk} = 1500 N/mm^2 and a concrete with f_{ckj} = 35 N/mm^2 (f_{ctk} = 2.3 N/mm^2), one obtains

$$f_{pd} = 1500/1.15 = 1304\,\mathrm{N/mm^2}$$
$$f_{ctd} = 2.3/1.5 = 1.53\,\mathrm{N/mm^2}$$
$$f_{bd} \cong 3.0 \times 1.53 = 4.59\,\mathrm{N/mm^2}$$
$$l_b = \frac{\phi}{4}\frac{1304}{4.59} \cong 71\phi$$

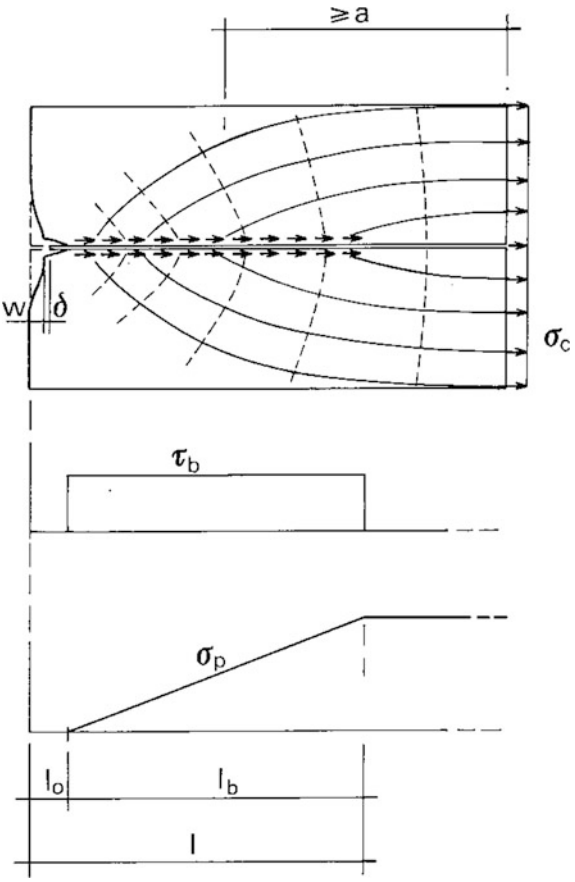


Fig. 10.36 Detail of end bond anchorage of a pretensioned tendon

If the strand is suddenly cut instead of being slowly released, the anchorage length would have to be appropriately increased in order to take into account the damages on the bonded concrete surface. The ineffective end portion would have to be added to the length l_b, equal to

$$l_o \cong 7\,\phi$$

for a total of

$$l = l_o + l_b \cong 78\,\phi$$

The products made of wire eventually require greater anchorage lengths because of the lower bond strength.

The detail of Fig. 10.36 shows the effect of a pre-tensioned tendon at its end segment where bond is active. The warping of the end section of the beam and the penetration of the tendon can be noted. This is due to two contributions: the first

one w related to the local deformation of the element, the second one δ partially due to the slip necessary for the activation of the effective contacts, partially due to the debonding of the last portion of the tendon that remains ineffective.

Excessively high values of the slip δ that occur when the tendon is released or progressively later on, indicate the bond failure. The phenomenon can have limited effects that stabilize further to a translation deeper in the bonded segment; it can lead to the progressive failure of the bond between the two materials, with drastic consequences on the capacity of the beam.

If a constant distribution of the bond stresses τ_b is assumed on the segment l_b, a linear variation of stresses σ_p in the tendon follows; such model can be assumed to evaluate the level of effectiveness reached by the tendon for the competent local resistance verifications.

Local Verification of Stresses

In order to ensure good bond, a concrete layer of sufficient thickness and adequate strength should be provided around the tendon. The interference of stresses with the other active segments of contiguous tendons should also be taken into account, which could lead to slip of the entire group due to the failure of the surface around them. For a first approximate verification related to these aspects of bond, the conventional procedure described below can be followed.

This procedure consists of evaluating the order of magnitude of stresses transferred from the tendon on the competent portion of concrete around it along the bonded length, and comparing such conventional value with an allowable limit sufficiently conservative.

First of all, based on the distance c from the closest edge (see Fig. 10.37), a tributary area A_i is defined for the tendon i. For an isolated tendon (see case "1" of Fig. 10.37) one has:

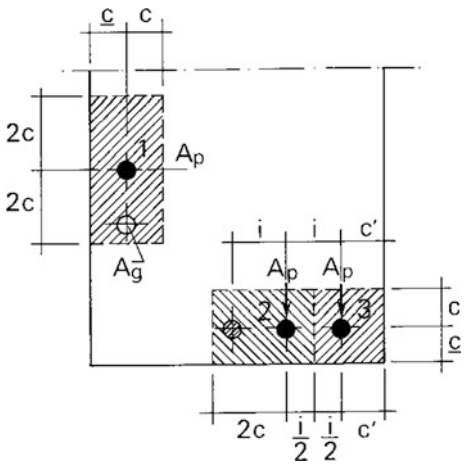


Fig. 10.37 Tributary areas of local compression stresses

$$A_1 = 2c \times 4c \quad (\text{case } ''1'')$$

The proximity Active segments of other strands requires to limit the competent semi-dimension of the area in relation to their spacing, for example with

$$A_2 = 2c \times (2c + i/2) \quad (\text{case } ''2'')$$

A similar limitation should be fixed with reference to the lateral cover c' ($> c$) for edge locations, with

$$A_3 = 2c \times (c' + i/2) \quad (\text{case } ''3'')$$

In the calculation of these areas, the section A_p of the related active tendon, as well as the one of possible inert (sheathed) tendons A_g included in the competent area should be subtracted. With reference to the cases of Fig. 10.37, one has for example:

$$A_{b1} = A_1 - A_p - A_g$$
$$A_{b2} = A_2 - A_p$$
$$A_{b3} = A_3 - A_p$$

The presence of typical reinforcement, such as rebar, does not decreases the resistance of the areas (see dashed bar of case "2" in Fig. 10.37).

The progressive application of the load along the bonded length and the contemporary diffusion of stresses towards the entire section of the beam are taken into account in an approximated way assuming a reduced value of the force transferred from the tendon:

$$P' = P/2.5$$

With this residual force, a conventional value of the compression on the concerned net area is calculated

$$\sigma'_c = P'/A_{bi}$$

to be compared with the allowable stress

$$\sigma'_c < f_{ckj}$$

The criteria exposed here are explained in Fig. 10.38 with reference to the typical situation of the end portion of a prestressed beam with pre-tensioned tendons. In the section (a) for the strand "1" one would have:

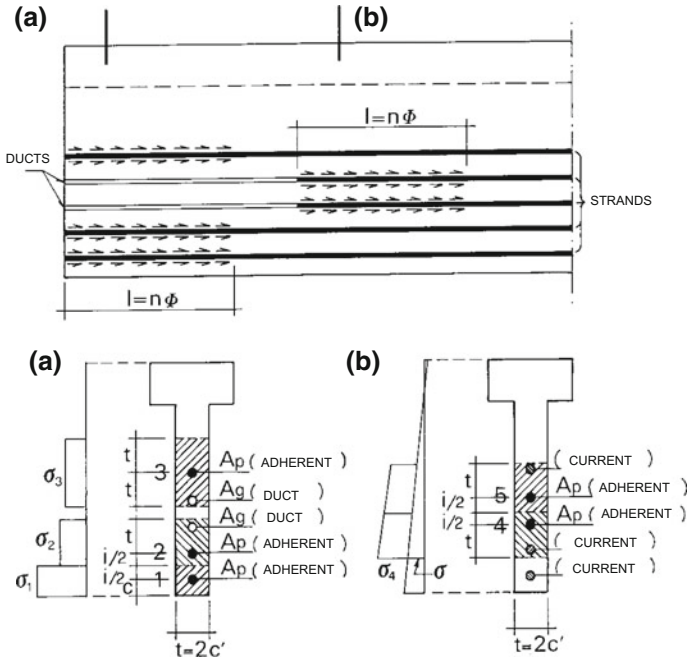


Fig. 10.38 Application example of the conventional procedure

$$A_{b1} = t \times (c + i/2) - A_p$$
$$P'_1 = \sigma_p A_p / 2.5$$
$$\sigma'_c = \sigma_1 = P'_1 / A_{b1} \quad (\leq \sigma'_c)$$

In the same figure it is indicated how, for the inner section (b), the value of the current stress already diffused on the beam section is added to the one of the compression due to the local bond (for example: $\sigma'_c = \sigma_4 + \sigma$). The conventional procedure should be intended as referred to a verification in service of the integrity of the concrete around the tendons in the bonded segments, and remains largely approximate. No precise information can be deduced about the limit of local resistance, for which much more complex calculations would be required.

The great effectiveness of the transverse confining reinforcement for the enhancement of the bond mechanism should be noted (see Sect. 1.4.3). A good shear reinforcement should be eventually provided to well connect the portion where the prestressed reinforcement is concentrated to the rest of the beam, in the bonded portions. These stirrups, related to the diffusion of stresses, have a behaviour analogous to the bursting reinforcement located under the anchorage plates of unbonded tendons, even though for pre-tensioned tendons the longitudinal splitting forces are mitigated by the gradual application of the load along the bonded

portions and by the consequent greater beam length where the transverse tensile stresses are distributed.

Diffusion of Prestressing

The diffusion mechanism of prestressing from the end anchorage of the tendons leaves out the end segments of the beam. In these segments the effects of prestressing are reduced and the appropriate reinforcement described as follows is required to meet with the consequent reduction in performance. This strengthening should be extended until it is joined with the current part of the beam with full prestressing (Fig. 10.39).

For the diffusion angle β, measured with reference to the line of application of the prestressing force on the anchorage (initial tangent of the tendon axis), a value of about 34° (ctg $\beta \cong 1.5$) can be assumed.

An analogous diffusion scheme can be assumed for a bond anchorage of pre-tensioned tendons (see Fig. 10.40), locating the apex of the diffusion angle halfway along the bonded segment.

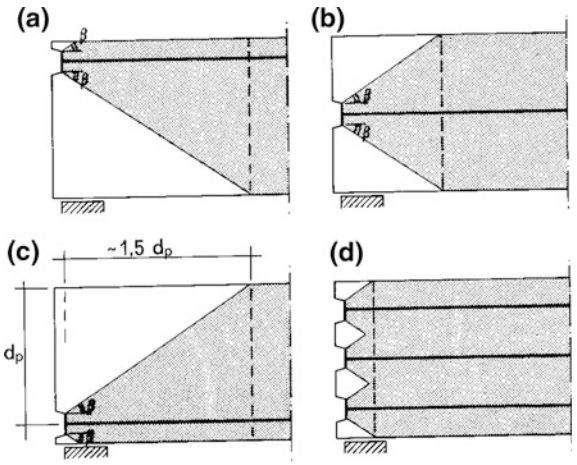


Fig. 10.39 Post-tensioned tendons—model of prestressing diffusion

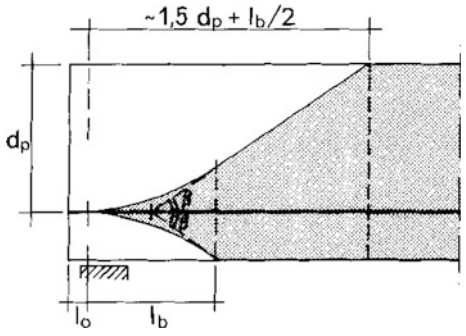


Fig. 10.40 Pretensioned tendon—model of prestressing diffusion

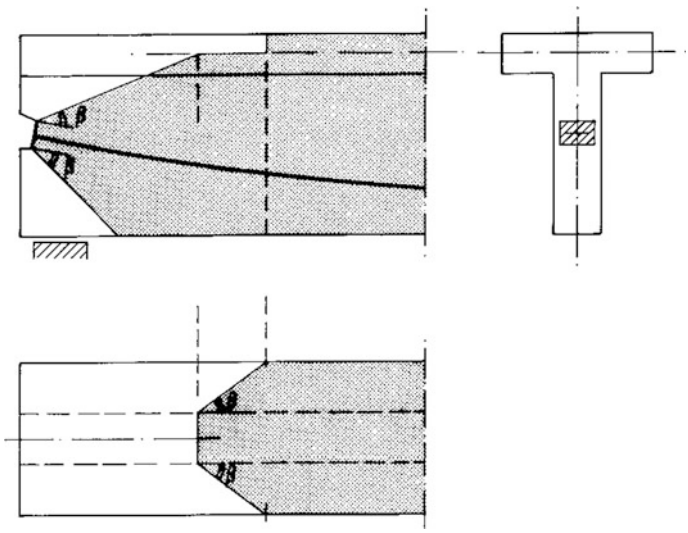


Fig. 10.41 Post-tensioned tendon—model of prestressing diffusion

The case of a T-shaped section is eventually shown in Fig. 10.41, where the horizontal angle on the flange that leads to the first section of complete prestressing should be added to the one of vertical diffusion on the beam web.

Bearing Details

The technical solution adopted in practice for the dimensioning of the support ends of prestressed beams neglects the effects of prestressing in all segments of its partial diffusion. These segments are therefore to be designed as ordinary reinforced concrete.

A typical detail of reinforcement at the support end of a prestressed beam with post-tensioned tendons is shown in Fig. 10.42a. The fluxes of compressions in concrete related to the adopted design schemes are also indicated, according to what has been largely discussed at Sect. 5.2.1 (see Figs. 5.17, 5.19 and 5.20). It should be noted that the position of the tendons is too far from the bottom edge of the beam to rely on a significant local contribution to the local tensile resistance from them, even if inserted in the ducts beyond the end device connected to the plate. The resisting schemes therefore, for the equilibrium with the support reaction, rely on the longitudinal bars added along the bottom edge, on the bent bars possibly added in the web and on the contribution of stirrups that enhance the concrete resistance also towards the localized pressures under the anchorage plates.

An analogous detail of a prestressed beam with pre-tensioned tendons is shown in Fig. 10.42b. The prestressing tendons in this case can contribute to the resisting mechanism, at least the ones close to the bottom edge of the beam. However, their effectiveness should be limited based on the bond of the anchored portion beyond the support. For example it can be set (see also Fig. 10.42b):

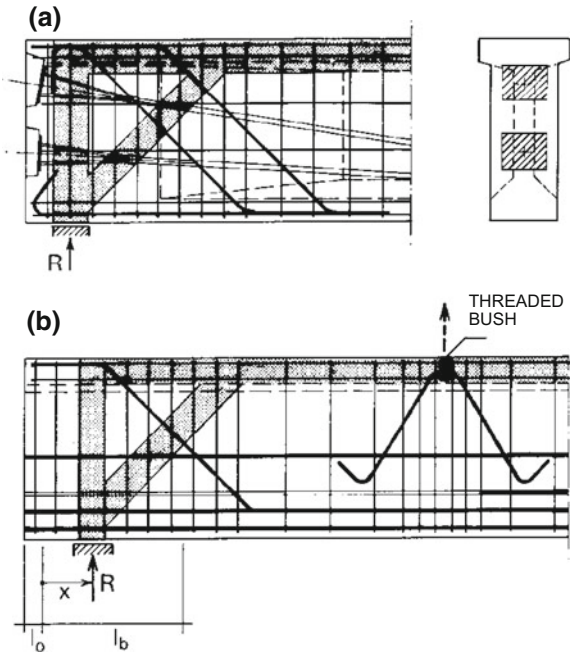


Fig. 10.42 Details of reinforcement at the beam ends

$$f_{\mathrm{xd}} = f_{\mathrm{pd}} x / l_{\mathrm{b}}$$

to obtain the resistance contribution

$$R_{\mathrm{pd}} = A'_{\mathrm{p}} f_{\mathrm{xd}} / \lambda_{\mathrm{o}}$$

having indicated with A'_{p} the total area of the portion of the pre-tensioned tendons close to the bottom edge and with $\lambda_{\mathrm{o}} = \lambda_{\mathrm{c}}/2$ the average inclination of the compressions in the web.

Additional passive reinforcement can be added if required, such as bent bars on the support, that give a contribution to the resistance equal to:

$$R_{\mathrm{sd}} = A_{\mathrm{s}} f_{\mathrm{yd}} \sin \alpha$$

having indicated with α the bending angle of the bars with respect to the beam axis, whereas the straight bars, if the geometry allows their insertion along the bottom beam edge, give a contribution equal to:

$$R_l \mathrm{d} = A_l f_{\mathrm{yd}} / \lambda_{\mathrm{o}}$$

The sum of the three contributions gives the overall resistance of the support, referred to the reinforcement, to be compared to the external reaction. In addition,

the verification of the concrete in compression should be carried according to the same criteria described at Sect. 5.2.1.

For completeness, the detail of the lifting device with which the beam is transported is included in Fig. 10.42b.

It should be noted that it is necessary to provide other restraints to the beam when placed in the structure for the stability of its overall behaviour, such as the lateral ones on the supports against overturning, the transverse horizontal ones along the span for the necessary lateral stability and the ones against horizontal longitudinal sliding of the supports when friction is not sufficient. For these specific aspects that concern more generally the installation of the components in precast constructions, one should refer to the competent specific discipline.

10.4 Design Examples

The following examples are outside the general scope of "Case A" to which the ones of the previous Chapters belong. Without explicit reference to a complete building, several typical prestressed elements in flexure are considered, analyzed on an independent simply supported static scheme.

The first example concerns a typical pre-tensioned long span element for roofs (or decks); the second shows the design of a typical post-tensioned beam; the last one refers to a rib of a deck obtained by connecting the pre-tensioned precast element with a cast-in situ reinforced concrete upper slab.

The range of possible applications of prestressing is very extensive and in continuous expansion. Just a very limited part is therefore covered by the examples presented here, which are developed in the simplest way and show only few main verifications for service and resistance limit states.

It is emphasized how important a careful design of the construction details is, which is only marginally shown in the following section. The actual design calculations are therefore generally broader and more detailed. The examples in this section only show an application of the main design criteria, aiming at keeping the description to a limited length for an easier comprehension.

10.4.1 Pretensioned Concrete Element

The design of a TT roof element is developed as follows, made of prestressed reinforced concrete with pre-tensioned strands, to be used as simply supported on a span $l = 15$ m. Only few main verifications are carried, adopting several simplifications, such as neglecting the reinforcement in the calculation of the geometrical characteristics of the section and neglecting the weight of the extreme segments of the beam beyond the supports. The lateral view of the element is shown in Fig. 10.43 where the verification sections are indicated: "a" of maximum moment,

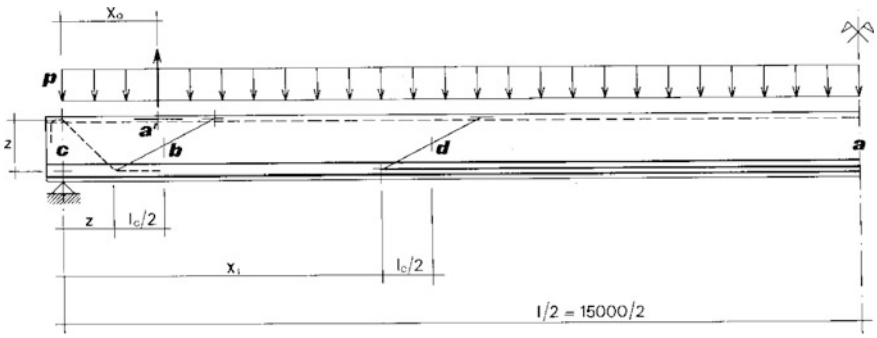


Fig. 10.43 Lateral view of the pretensioned element

"b" of maximum shear, "c" at the support (with no moment) and "d" of change of reinforcement. The tendons layout is shown in the same figure, where the effective (not unbonded) segments are indicated.

A more complete description of the element is given on Fig. 10.45.

In particular, not having an adequate anchorage length for the strands at the supports, the bent bars have been positioned at 45° which, picking up the reaction from above, bring the first bottom node of the web truss at a distance z from the support.

The section a' is also closely located, where the maximum negative moment displays in the transient lifting situation.

Analysis of Forces

- *Loads*

– self-weight	$g_1 = 5.90\,\text{kN/m}$
– other permanent loads	$g_2 = 3.00\,\text{kN/m}$
– variable loads	$q = 3.60\,\text{kN/m}$

- *Design sections*
  (abscissa x from the support)
  - *a*—of maximum moment

$$x_a = 7.50\,\text{m}$$

  - *b*—of maximum shear
    with $d \cong 0.52\,\text{m}$

$$z \cong 0.9 \times 0.52 \cong 0.47\,\text{m}$$

and with $\lambda_c = 2$ one has

$$x_b \cong z + \lambda_c z/2 = 0.47 + 0.47 = 0.94\,\text{m}$$

– *c*—at the support

$$x_c = 0.00$$

– *d*—at the change in reinforcement

$$x_d = x_1 + \lambda_c z/2 = 3.00 + 0.47 = 3.47\,\text{m}$$

– *a′*—of maximum negative moment (lifting hook)

$$x_o = 0.90\,\text{m}$$

- *Initial stage*
  (l = 15.0 *m* − x_b = 0.94 m − x_d = 3.47 m)

$$\begin{aligned} R' &= g_1 l/2 = 44.25\,\text{kN} \\ M'_a &= g_1 l^2/8 = 165.94\,\text{kNm} \\ V'_b &= R' - g_1 x_b = 38.70\,\text{kN} \\ M'_d &= R' x_d - g_1 x_d^2/2 = 118.03\,\text{kNm} \end{aligned}$$

- *Transient stage*
  (Lifting: x_o = 0.90 m − l_b = 1.37 m anchorage length of strands)

$$\begin{aligned} R' &= g_1 l/2 = 44.25\,\text{kN} \\ M_o &= -g_1 x_o^2/2 = -2.38\,\text{kNm} \\ x &= x_d + l_b = 4.84\,\text{m} \\ M_d^+ &= R'(x - x_o) - g_1 x^2/2 = 105.24\,\text{kNm} \end{aligned}$$

- *Other permanent loads*

$$\begin{aligned} R'' &= g_2 l/2 = 22.50\,\text{kN} \\ M''_a &= g_2 l^2/8 = 84.37\,\text{kNm} \\ V''_b &= R'' - g_2 x_b = 19.68\,\text{kN} \\ M''_d &= R'' x_d - g_2 x_d^2/2 = 60.01\,\text{kNm} \end{aligned}$$

- *Variable loads*

$$R = ql/2 = 27.00\,\text{kN}$$
$$M_a = ql^2/8 = 101.25\,\text{kNm}$$
$$V_b = R - qx_b = 23.62\,\text{kNm}$$
$$M_d = Rx_d - qx_d^2/2 = 72.02\,\text{kNm}$$

Characteristics of Materials
(controlled production)
Concrete

- maximum aggregate size d_a = 20 mm
- resistance class C50/C60
(see Table 1.1, 1.2, 1.8 and 1.16)

$$f_{ck} = 50.0\,\text{N/mm}^2 \qquad f_{cm} = 55.0\,\text{N/mm}^2$$
$$f_{ctk} = 3.1\,\text{N/mm}^2 \qquad f_{ctm} = 3.9\,\text{N/mm}^2$$
$$f_{ckj} = 30.0\,\text{N/mm}^2$$
$$f_{ctkj} = 1.9\,\text{N/mm}^2$$
$$E_c = 37{,}000\,\text{N/mm}^2$$
$$\varepsilon_{cs\infty} \cong 0.00032 \qquad \varphi_\infty \cong 2.7$$

- design values (γ_C = 1.40)
(see Chart 2.2)

$$f_{cd} = 0.85 f_{ck}/\gamma_C = 30.4\,\text{N/mm}^2$$
$$f_{cdj} = 0.85 f_{ckj}/\gamma_C = 18.2\,\text{N/mm}^2$$
$$f_{c2} = 0.50 f_{cd} = 15.2\,\text{N/mm}^2$$
$$f_{c2j} = 0.50 f_{cdj} = 9.1\,\text{N/mm}^2$$

- allowable stresses
(see Chart 2.2)

$$\bar{\sigma}_c = 0.45 f_{ck} = 22.5\,\text{N/mm}^2 \quad \text{(compressions in service)}$$
$$\bar{\sigma}_{cj} = 0.70 f_{ckj} = 21.0\,\text{N/mm}^2 \quad \text{(initial compressions)}$$
$$\bar{\sigma}'_{ct} = 1.3 f_{ctk} = 4.03\,\text{N/mm}^2 \quad \text{(tensions in service)}$$
$$\bar{\sigma}'_{ctj} = 1.3 f_{ctkj} = 2.47\,\text{N/mm}^2 \quad \text{(initial tensions)}$$

Ordinary reinforcement
(ribbed bars)

- steel type B450C
(see Table 1.17)

$$f_{yk} = 450\,\text{N/mm}^2 \qquad f_{tk} = 540\,\text{N/mm}^2$$
$$E_s = 205{,}000\,\text{N/mm}^2 \qquad \varepsilon_{uk} = 0.075$$

- design values (γ_S = 1.15)

$$f_{yd} = f_{yk}/\gamma_S = 391\,\text{N/mm}^2$$
$$\varepsilon_{yd} = 0.19\%$$

Prestressing steel

- strands 7 W ϕ = 15.2 mm (= 0.6″)
(see Table 1.21)

$$f_{ptk} = 1860\,\text{N/mm}^2 \qquad f_{p0.1k} = 1580\,\text{N/mm}^2$$
$$E_p = 19{,}500\,\text{N/mm}^2 \qquad \varepsilon_{uk} = 0.05$$

- design values

$$f_{pd} = 0.9 \times 1860/1.15 = 1456\,\text{N/mm}^2$$
$$\varepsilon_{yd} \cong 0.75\%$$

- allowable stresses

$$\bar{\sigma}_p = 0.80 f_{p0.1k} = 1264\,\text{N/mm}^2$$
$$\bar{\sigma}_{pi} = 0.90 f_{p0.1k} = 1422\,\text{N/mm}^2$$

- relaxation (class 2—stabilized)

$$\rho_{1000} \simeq 2.5\% \text{ at } \sigma_{pi} = 0.7 f_{ptk}$$

Bond

$$f_{ctdj} = f_{ctkj}/\gamma_C = 1.9/1.40 = 1.36\,\text{N/mm}^2$$
$$f_{bd} \cong 3.0 \times 1.36 = 4.07\,\text{N/mm}^2$$
$$l_b = \frac{\phi}{4}\frac{1456}{4.07} \cong 90\phi \quad (= 137\,\text{cm})$$

Tendons tensioning
(at 14 h of accelerated concrete curing)

- initial overstress

$$\sigma'_{pi} = 1400\,\mathrm{N/mm^2} \quad \left(< \bar{\sigma}_{pi} = 1422\,\mathrm{N/mm^2}\right)$$

- tension loss due to heat
(accelerated concrete curing)

$$\Delta\theta = 70 - 20 = 50\,^{\circ}\mathrm{C}$$
$$\Delta\sigma_p = E_p \alpha_T \Delta\theta = 19{,}500 \times 10^{-5} \times 50 \simeq 100\,\mathrm{N/mm^2}$$

- initial stress

$$\sigma_{pi} = \sigma'_{pi} - \Delta\sigma_p = 1300\,\mathrm{N/mm^2}$$
$$A_p = 2 \times 139 = 278\,\mathrm{mm^2} \qquad \text{for each level}$$
$$P'_o = 278 \times 1.30 = 361\,\mathrm{kN} \qquad \text{for each level}$$

Verification of Stresses

• *Characteristics of section*
(see Fig. 10.44)
Area and static moment

$240 \times 5 = 1200 \times 2.5 = 3000$
$18 \times 55 = 990 \times 32.5 = 32{,}175$
$3 \times 55 = 165 \times 23.3 = 3845$
$A = 2355\ \mathrm{cm^2} \quad S = 39{,}020\ \mathrm{cm^3}$

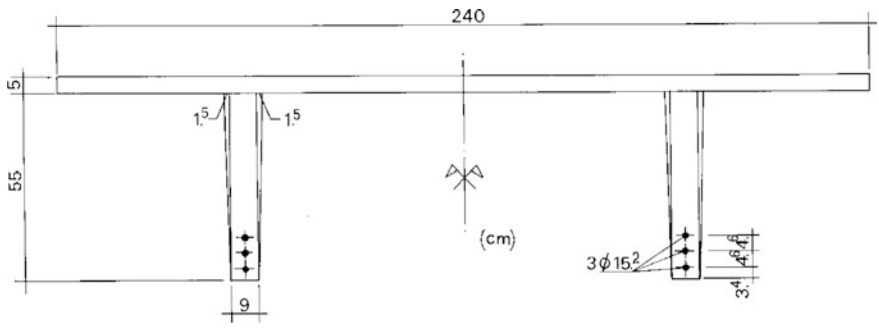


Fig. 10.44 Cross section of the element

Weight

$$g_1 = 0.2355 \times 25 \cong 5.90\,\text{kN/m}$$

Centroid

$$y'_o = 39{,}020/2355 = 16.6\,\text{cm}$$
$$y''_o = 60.0 - 16.6 = 43.4\,\text{cm}$$

Moment of inertia

$$\begin{aligned} 1200(5^2/12 + 14.1^2) &= 241{,}072 \\ 990(55^2/12 + 15.9^2) &= 499{,}844 \\ 165(55^2/18 + 6.7^2) &= 35{,}136 \\ &\underline{\qquad\qquad} \\ &776{,}052\,\text{cm}^4 \end{aligned}$$

Resisting moduli of the edges

$$W' = 776{,}052/16.6 = 46{,}750\,\text{cm}^3$$
$$W'' = 776{,}052/43.4 = 17{,}881\,\text{cm}^3$$

Resisting moduli on the strands

$$y_1 = 43.4 - 12.6 = 30.8\,\text{cm}$$
$$y_2 = 43.4 - 8.0 = 35.4\,\text{cm}$$
$$y_3 = 43.4 - 3.4 = 40.0\,\text{cm}$$
$$W_1 = 776{,}052/30.8 = 25{,}196\,\text{cm}^3$$
$$W_2 = 776{,}052/35.4 = 21{,}922\,\text{cm}^3$$
$$W_3 = 776{,}052/40.0 = 19{,}401\,\text{cm}^3$$

Centroidal static moment
($3 \times 43.4/55 = 2.4\,\text{cm}$ increased width of centroidal chord)

$$\begin{aligned} 18 \times 43.4 \times 21.7 = &\quad 16{,}952 \\ 2.4 \times 43.4 \times 14.5 = &\quad \underline{\quad 1510} \\ &18{,}462\,\text{cm}^3 \end{aligned}$$

Lever arm of internal moment

$$z = 776{,}052/18{,}462 = 42.0\,\text{cm}$$

Section a
(with 2×3 strands)
- Prestressing
(with self-weight)

$$\begin{array}{lll} 361 \times & 0.308 & = 111.2 \\ 361 \times & 0.354 & = 127.8 \\ \underline{361} \times & 0.400 & = \underline{144.4} \end{array}$$
$$N_p = 1083 \text{ kN} \qquad M_p = 383.4 \text{ kNm}$$

$$\sigma_c' = 1083/235.5 - (383.4 - 165.9)/46.75 = 4.60 - 4.65 = -0.05\,\text{N/mm}^2$$
$$\sigma_c'' = 1083/235.5 + 217.5/17.88 = 4.60 + 12.16 = 16.76\,\text{N/mm}^2$$
$$\sigma_{c1} = 4.60 + 217.5/25.20 = 13.23\,\text{N/mm}^2$$
$$\sigma_{c2} = 4.60 + 217.5/21.92 = 14.52\,\text{N/mm}^2$$
$$\sigma_{c3} = 4.60 + 217.5/19.40 = 15.81\,\text{N/mm}^2$$

- Losses

relaxation

$$r = \sigma_{pi}/f_{ptk} = 1300/1860 = 0.70$$
$$c(r) = 1 \qquad \rho_1 = 2.5 \quad (\text{class } 2)$$
$$\tau^{0.75(1-r)} = 4 \qquad \text{for } \tau = 500$$
$$\Delta\sigma_{p\infty}/\sigma_{pi} = 4 \times 2.5 = 10\%$$
$$\Delta N_{p1} = \Delta N_{p2} = \Delta N_{p3} = 0.10 \times 361 = 36.1\,\text{kN}$$

shrinkage

$$\Delta N_{p1} = \Delta N_{p2} = \Delta N_{p3} = 0.00032 \times 195 \times 278 = 17.3\,\text{kN}$$

creep

$$\alpha_e = 195{,}000/37{,}000 = 5.3$$
$$\Delta N_{p1} = 5.3 \times 2.7 \times 13.23 \times 0.278 = 52.6\,\text{kN}$$
$$\Delta N_{p2} = 5.3 \times 2.7 \times 14.52 \times 0.278 = 57.8\,\text{kN}$$
$$\Delta N_{p3} = 5.3 \times 2.7 \times 15.81 \times 0.278 = 62.9\,\text{kN}$$

total

$$\Delta N_{p1} = 36.1 + 17.3 + 52.6 = 106.0 \quad (\cong 29\%)$$
$$\Delta N_{p2} = 36.1 + 17.3 + 57.8 = 111.2 \quad (\cong 31\%)$$
$$\Delta N_{p3} = 36.1 + 17.3 + 62.9 = 116.3 \quad (\cong 32\%)$$

in the section

$$\begin{array}{rcl} 106.0 \times 0.308 & = & 32.65 \\ 111.2 \times 0.354 & = & 39.36 \\ \underline{116.3 \times 0.400} & = & \underline{46.52} \\ \Delta N_p = 333.5 \text{ kN} & & \Delta M_p = 118.53 \text{ kNm} \end{array}$$

$$\Delta\sigma'_c = -333.5/235.5 + 118.53/46.75 = -1.42 + 2.54 = +1.12\,\text{N/mm}^2$$
$$\Delta\sigma''_c = -1.42 - 118.53/17.88 = -1.42 - 6.63 = -8.05\,\text{N/mm}^2$$
$$\sigma'_c = -0.05 + 1.12 = +1.07\,\text{N/mm}^2$$
$$\sigma''_c = +16.76 - 8.05 = +8.71\,\text{N/mm}^2$$

- Permanent loads

$$\Delta\sigma'_c = 84.4/46.75 = +1.80\,\text{N/mm}^2$$
$$\Delta\sigma''_c = -84.4/17.88 = -4.72\,\text{N/mm}^2$$
$$\sigma'_c = +1.07 + 1.80 = +2.87\,\text{N/mm}^2$$
$$\sigma''_c = +8.71 - 4.72 = +3.99\,\text{N/mm}^2$$

- Total loads

$$\Delta\sigma'_c = 101.2/46.75 = +2.16\,\text{N/mm}^2$$
$$\Delta\sigma''_c = 101.2/17.88 = -5.66\,\text{N/mm}^2$$
$$\sigma'_c = +2.87 + 2.16 = +5.03\,\text{N/mm}^2$$
$$\sigma''_c = +3.99 - 5.66 = -1.67\,\text{N/mm}^2$$

Verifications

$$\sigma'_c < \bar{\sigma}_c = 22.5\,\mathrm{N/mm^2}$$
$$-\sigma''_c < \bar{\sigma}'_{ct} = 4.03\,\mathrm{N/mm^2}$$

Section d′
(*a x* = $x_b + l_b$—with 2 × 3 strands)

- Lifting

(dynamic effect ± 0.15)

$$\sigma'_c = 4.60 - (383.4 - 0.85 \times 105.2)/46.75 = 4.60 - 6.29 = -2.18\,\mathrm{N/mm^2}$$
$$\sigma''_c = 4.60 + 294.0/17.88 = 4.60 + 16.44 = 21.04\,\mathrm{N/mm^2}$$

verifications

$$-\sigma'_c < \bar{\sigma}''_{ctj} = 2.47\,\mathrm{N/mm^2}$$
$$\sigma''_c \cong \bar{\sigma}_{cj} = 21.0$$

Section d
(with 2 × 2 strands)
• Prestressing (with self-weight)

$$\begin{array}{rrl} 361 \times & 0.308 & = 111.2 \\ \underline{361 \times} & \underline{0.400} & = \underline{144.4} \\ N_p = 722\ \mathrm{kN} & & M_p = 255.6\ \mathrm{kNm} \end{array}$$

$$\sigma'_c = 722/235.5 - (255.6 - 118.0)/46.75 = 3.07 - 2.94 = +0.13\,\mathrm{N/mm^2}$$
$$\sigma''_c = 3.07 + 137.6/17.88 = 3.07 + 7.70 = +10.77\,\mathrm{N/mm^2}$$
$$\sigma_{c1} = 3.07 + 137.6/25.20 = 8.53\,\mathrm{N/mm^2}$$
$$\sigma_{c3} = 3.07 + 137.6/19.40 = 10.16\,\mathrm{N/mm^2}$$

- Losses
creep

$$\Delta N_{p1} = 5.3 \times 2.7 \times 8.53 \times 0.278 = 33.9\,\mathrm{kN}$$
$$\Delta N_{p3} = 5.3 \times 2.7 \times 10.16 \times 0.278 = 40.4\,\mathrm{kN}$$

total

$$\Delta N_{p1} = 36.1 + 17.3 + 33.9 = 87.3\,\text{kN} \quad (\cong 0.25\%)$$
$$\Delta N_{p3} = 36.1 + 17.3 + 40.4 = 93.8\,\text{kN} \quad (\cong 0.28\%)$$

in the section

87.3×0.308	$= 27.89$
93.8×0.400	$= 37.52$
$\Delta N_p = 181.1$ kN	$\Delta M_p = 65.41$ kNm

$$\Delta\sigma'_c = -181.1/235.5 + 65.41/46.75 = -0.77 + 1.40 = +0.63\,\text{N/mm}^2$$
$$\Delta\sigma''_c = -0.77 - 65.41/17.88 = -0.77 - 3.66 = -4.43\,\text{N/mm}^2$$
$$\sigma'_c = +0.13 + 0.63 = +0.76\,\text{N/mm}^2$$
$$\sigma''_c = +10.77 - 4.43 = +6.34\,\text{N/mm}^2$$

- Permanent loads

$$\Delta\sigma'_c = +60.01/46.75 = +1.28\ \text{N/mm}^2$$
$$\Delta\sigma''_c = -60.01/17.88 = -3.36\ \text{N/mm}^2$$
$$\sigma'_c = +0.76 + 1.28 = +2.04\ \text{N/mm}^2$$
$$\sigma''_c = +6.34 - 3.36 = +2.98\ \text{N/mm}^2$$

- Total loads

$$\Delta\sigma'_c = +72.02/46.76 = +1.54$$
$$\Delta\sigma''_c = -72.02/17.88 = -4.03$$
$$\sigma'_c = +2.04 + 1.54 = +3.58\ \text{N/mm}^2$$
$$\sigma''_c = +2.98 - 4.03 = -1.05\ \text{N/mm}^2$$

verifications

$$\sigma'_c < \bar{\sigma}_c = 22.5\ \text{N/mm}^2$$
$$-\sigma''_c < \bar{\sigma}'_{ct} = +4.03\ \text{N/mm}^2$$

Section a'
(with 2×2 strands)

- Prestressing

$$\sigma'_c = 722/235.5 - 255.6/46.75 = 3.07 - 5.47 = -2.40 \text{ N/mm}^2$$
$$\sigma''_c = 3.07 + 255.6/17.88 = 3.07 + 14.30 = +17.37 \text{ N/mm}^2$$

- lifting (with dynamic effect)

$$\Delta\sigma'_c = -1.15 \times 2.4/46.76 = -0.06$$
$$\Delta\sigma'_c = +1.15 \times 2.4/17.88 = +0.15$$
$$\sigma'_c = -2.40 - 0.06 = -2.46 \text{ N/mm}^2$$
$$\sigma''_c = 17.37 + 0.15 = +17.52 \text{ N/mm}^2$$

Verifications

$$-\sigma'_c < \bar{\sigma}'_{ctj} = 2.47 \text{ N/mm}^2$$
$$\sigma''_c < \bar{\sigma}'_{cj} = 21.0 \text{ N/mm}^2$$

Resistance Verifications
Section a

- prestressed reinforcement ($n\phi$ − A_p − d_p)

$$\begin{aligned} 2\phi 15.2 \quad & 2.78\,\text{cm}^2 \quad 56.6\,\text{cm} \\ 2\phi 15.2 \quad & 2.78\,\text{cm}^2 \quad 52.0\,\text{cm} \\ 2\phi 15.2 \quad & \underline{2.78\,\text{cm}^2} \quad 47.4\,\text{cm} \\ A_p = \quad & 8.34\,\text{cm}^2 \end{aligned}$$

- resistance of compression flange (t = 5 cm)

$$f^*_{cd} \cong (0.5 + 0.1t/d_a) f_{cd} = 0.75 \times 30.4 = 22.8 \text{ N/mm}^2$$

- compression zone depth

$$\bar{x} = \frac{f_{cd} A_p}{b f^*_{cd}} = \frac{8.34 \times 1456}{240 \times 22.8} = 2.2 \text{ cm}$$

with d = 52 it is assumed

$$\bar{x} = 0.08 \times 52 = 4.2 \text{ cm} \quad \left(\sigma_c < f^*_{cd}\right)$$

- resisting moment

$$z = 52.0 - 4.2/2 = 49.9 \text{ cm}$$
$$M_{\text{Rd}} = A_{\text{p}} f_{\text{pd}} z = 8.34 \times 145.6 \times 0.499 = 605.9 \text{ kNm}$$

- applied moment

$$\begin{aligned} 1.30 \times 165.94 &= 215.7 \\ 1.50 \times 84.37 &= 126.6 \\ 1.50 \times 101.25 &= 151.9 \\ M_{\text{ed}} &= 494.2 \text{ kNm } (< M_{\text{Rd}}) \end{aligned}$$

Section d

- prestressed reinforcement ($n\phi - A_p - d_p$)

$$\begin{aligned} 2\phi\ 15.2 \quad & 2.78 \text{ cm}^2 \quad 56.6 \text{ cm} \\ 2\phi\ 15.2 \quad & 2.78 \text{ cm}^2 \quad 47.4 \text{ cm} \\ A_{\text{p}} &= 5.56 \text{ cm}^2 \end{aligned}$$

- it is assumed

$$\bar{x} = 4.2 \text{ cm} \quad \left(\sigma_{\text{c}} < f^*_{\text{cd}}\right)$$
$$z = 52.0 - 4.2/2 = 49.9 \text{ cm}$$

- resisting moment

$$M_{\text{Rd}} = 5.56 \times 145.6 \times 0.499 = 404.0 \text{ kNm}$$

- applied moment

$$\begin{aligned} 1.30 \times 118.03 &= 153.4 \\ 1.50 \times 60.01 &= 90.0 \\ 1.50 \times 72.02 &= 108.0 \\ M_{\text{ed}} &= 351.4 \text{ kNm } (< M_{\text{Rd}}) \end{aligned}$$

Section b

- applied shear

$1.30 \times 38.70 = 50.3$
$1.50 \times 19.68 = 29.5$
$1.50 \times 23.62 = 35.4$
$V_{ed} = 115.2$ kN

$$\tau_G = \frac{V_{Ed}}{z_o b_w} = \frac{1152}{42.0 \times 18.0} = 1.45 \text{ N/mm}^2$$

- applied prestressing ($\gamma_P = 1.00$)
(partial diffusion of prestressing)

$$x_b/l_b = 0.94/1.37 = 0.69$$
$$\text{losses} \cong 0,70$$
$$N_P = 2 \times 361 = 722\,\text{kN} \quad (2 \times 2 \text{ strands})$$
$$N_{Ed} = 1.00 \times 722 \times 0.69 \times 0.70 = 342\,\text{kN}$$
$$\sigma_G = \frac{N_{Ed}}{A} = \frac{3400}{2355} = 1.48 \text{ N/mm}^2$$
$$\sigma_I = \frac{1}{2}\left(-1.33 + \sqrt{1.48^2 + 4 \times 1.45^2}\right) = 0.89\,\text{N/mm}^2$$
$$\lambda_I = \tau_G/\sigma_I = 1.45/0.89 = 1.63$$

- minimum stirrups

$$\bar{a}_w = 0.2 b_w f_{ctm}/f_{yk} = 0.2 \times 1800 \times 3.9/450 = 3.12 \text{ cm}^2/\text{m}$$
2 U-shaped mesh ϕ 6/200 (see Table 10.18)
$$a_w = 4 \times 1.41 = 5.64 \text{ cm}^2/\text{m} \quad (> \bar{a}_w)$$
$$\omega_w = \frac{a_w f_{yd}}{a_w f_{c2}} = \frac{5.64 \times 391}{1800 \times 15.2} = 0.0806$$
$$\lambda_r = \sqrt{(1 - \omega_w)/\omega_w} = 3.38 \quad (> \lambda_{max} = \lambda_I + 1)$$
it is assumed $\lambda_c = 2 \quad (\lambda_I < \lambda_c < \lambda_{max})$
$$V_{Rd} = 0.9 d a_w f_{yd} \lambda_c = 0.9 \times 0.52 \times 5.64 \times 39.1 \times 2 = 206 \text{ kN} \quad (> V_{ed})$$

Support
(2 + 2ϕ14 bent - $\alpha = 45°$)

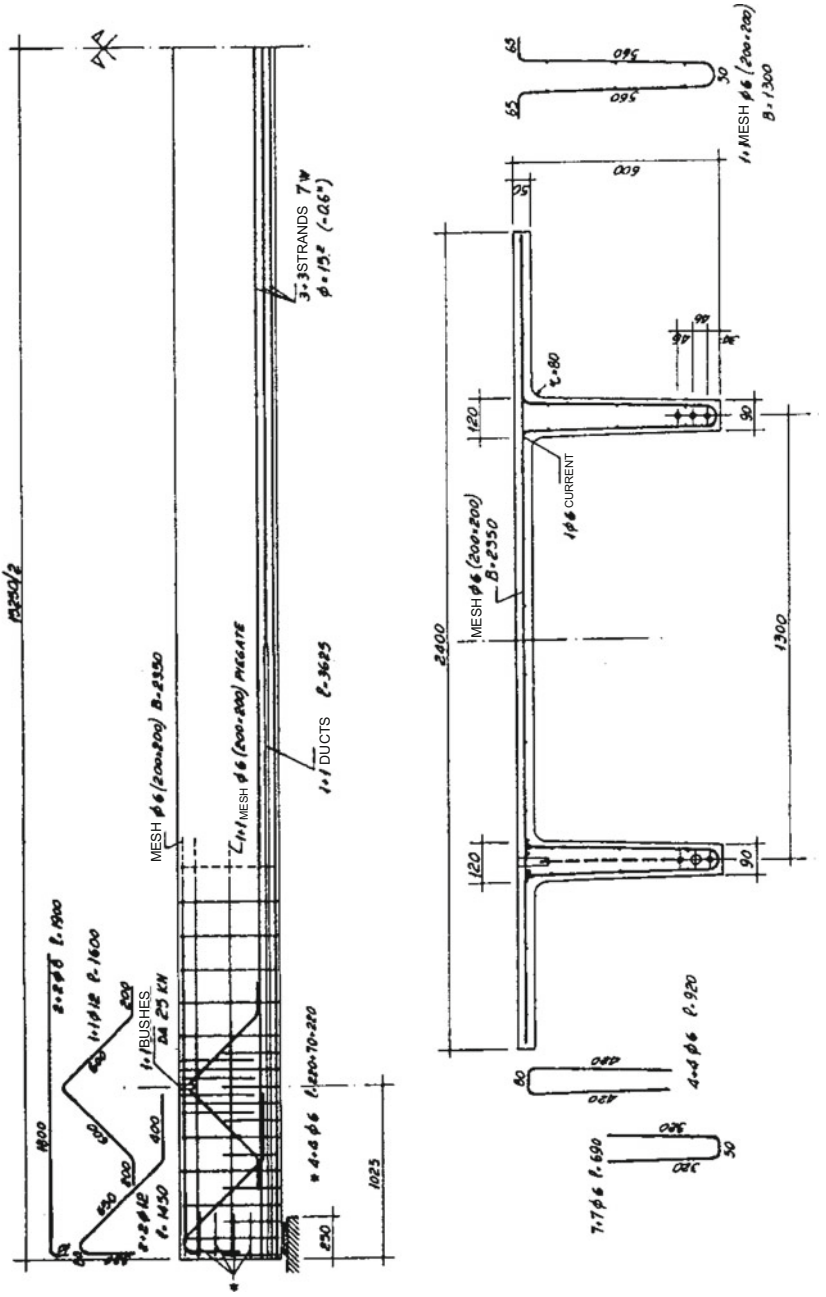


Fig. 10.45 Reinforcement details of the floor element

$$
\begin{aligned}
1.30 \times 44.25 &= 57.5 \\
1.50 \times 22.50 &= 33.8 \\
1.50 \times 27.00 &= \underline{40.5} \\
R_{ed} &= 131.8 \text{ kN}
\end{aligned}
$$

$$A_s = 6.16 \text{ cm}^2 \quad (\lambda_S = 1, \lambda_o = \lambda_c/2 = 1)$$

$$R_{sd} = A_S f_{yd}/\sqrt{2} = 6.16 \times 39.1/\sqrt{2} = 170 \text{ kN} \quad (> R_{ed})$$

at the bottom node

$$l = 12.5 + 47.0 \cong 59 \text{ cm} \quad \text{from the beam edge}$$

$$R_{ld} = \frac{A_p f_{pd}}{\lambda_S + \lambda_o} \frac{l}{l_b} = \frac{5.56 \times 145.6 \times 59}{2 \times 137} = 174 \text{ kN} \quad (> R_{ed})$$

The construction drawings are shown in Fig. 10.45.

10.4.2 Post-tensioned Concrete Beam

The design of a simply supported beam in prestressed post-tensioned reinforced concrete is developed below, for which only few main verifications are carried out, with several simplifications such as the one of neglecting the tendon holes and the reinforcing bars in the calculating the characteristics of the section. The view of the beam of Fig. 10.46 shows on the left-hand side the marks of the verification sections: "a" of maximum bending moment, "b" of maximum shear force, "c" at the support (with zero moment). On the right-hand side the tendons profile is eventually shown, with straight segments connected by parabolic portions. The overall profile is symmetric, except for prestressing losses due to friction that leave a tension force at the fixed end of the tendons lower than the one at the active end.

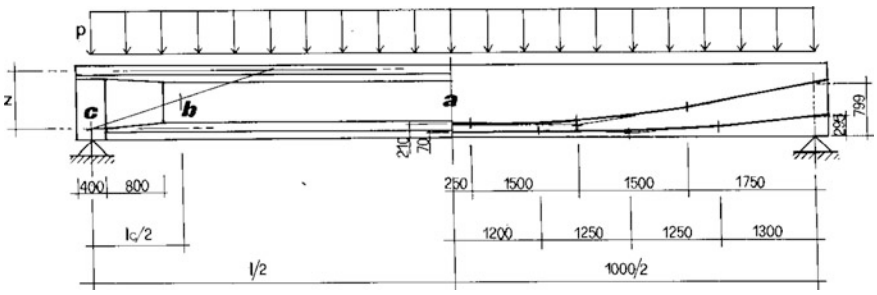


Fig. 10.46 Post-tensioned concrete beam

A more complete description of the beam is given in Fig. 10.48.

Analysis of Forces

- *Loads*
  - self weight $g_1 + 7.0$ kN/m
  - other permanent loads $g_2 + 45.0$ kN/m
  - variable loads $q = 50.0$ kN/m
- *Design sections*
  (abscissa x from the support on the left-hand side)
  - a—of maximum bending moment

$$x_a = 5.00\,\text{m}$$

  - b—of maximum shear force

$$d = 1.05\,\text{m}$$
$$z \cong 0.9 \times 1.05 \cong 0.94\,\text{m}$$

  with $\lambda_c = 2$ one has

$$x'_b = \lambda_c\, z/2 = 0.94\,\text{m}$$
$$x''_b = 10.00 - 0.94 = 9.06\,\text{m}$$

  - c—at the support

$$x'_c = 0.00\,\text{m}$$
$$x''_c = 10.00\,\text{m}$$

- *Initial stage*

$$R = g_1 l/2 = 35.0\,\text{kN} \quad (\cong V_c)$$
$$M'_a = g_1 l^2/8 = 87.5\,\text{kNm}$$
$$V'_b = R - g_1 x_b = 28.4\,\text{kN}$$
$$M'_b = R x_b - g_1\, x_b^2/2 = 29.8\,\text{kNm}$$

- *Other permanent loads*

$$R = g_2 l/2 = 225.0\,\text{kN}$$
$$M''_a = g_2 l^2/8 = 562.5\,\text{kNm}$$
$$V''_b = R - g_2 x_b = 183.0\,\text{kN}$$
$$M''_b = R x_b - g_2 x_b^2/2 = 191.6\,\text{kNm}$$

- *Variable loads*

$$R = ql/2 = 250.0\,\text{kN}$$
$$M_a = q\,l^2/8 = 625.0\,\text{kNm}$$
$$V_b = R - qx = 203.0\,\text{kN}$$
$$M_b = R x_b - q\,x_b^2/2 = 212.9\,\text{kNm}$$

Characteristics of Materials

Concrete

- maximum aggregate size d_a = 20 mm
- resistance class C45/55
  (see Tables 1.1, 1.2, 1.8 and 1.16)

$$f_{ck} = 45.0\,\text{N/mm}^2 \qquad f_{cm} = 53.0\,\text{N/mm}^2$$
$$f_{ctk} = 2.7\,\text{N/mm}^2 \qquad f_{ctm} = 3.8\,\text{N/mm}^2$$
$$f_{ckj} = f_{ck} \qquad \text{(pre-stressed after 28 days)}$$
$$E_c = 36{,}000\,\text{N/mm}^2$$
$$\varepsilon_{cs\infty} \cong 0.00028 \qquad \varphi_\infty \cong 1.9$$

- design values (γ_C = 1.50)

$$f_{cd} = 0.85 f_{ck}/\gamma_C = 25.5\,\text{N/mm}^2$$
$$f_{c2} = 0.50 f_{cd} = 12.7\,\text{N/mm}^2$$

- permissible stresses

$$\bar{\sigma}_c = 0.45 f_{ck} = 20.2\,\text{N/mm}^2 \quad \text{(compressions in operation)}$$
$$\bar{\sigma}_{cj} = 0.60 f_{ck} = 27.0\,\text{N/mm}^2 \quad \text{(initial compression)}$$
$$\bar{\sigma}'_{ct} = 1.3 f_{ctk} = 3.51\,\text{N/mm}^2 \quad \text{(limit tensile)}$$

Ordinary reinforcement

- ribbed bars
- steel type B450C (see Table 1.17)

$$f_{yk} = 450\,\mathrm{N/mm^2} \qquad f_{tk} = 540\,\mathrm{N/mm^2}$$
$$E_s = 205{,}000\,\mathrm{N/mm^2} \qquad \varepsilon_{uk} = 0.75$$

- design values (γ_S = 1.15)

$$f_{yd} = f_{yk}/\gamma_S = 391\,\mathrm{N/mm^2}$$
$$\varepsilon_{yd} = 0.19\%$$

Prestressing steel

- strands 7 W ϕ = 15.2 mm (= 0.6″)
(see Table 1.21)

$$f_{ptk} = 1860\,\mathrm{N/mm^2} \qquad f_{p0.1k} = 1580\,\mathrm{N/mm^2}$$
$$E_p = 19{,}500\,\mathrm{N/mm^2} \qquad \varepsilon_{uk} = 0.05$$

- design values (γ_S = 1.15)

$$f_{pd} = 0.9 \times 1860/1.15 = 1456\,\mathrm{N/mm^2}$$
$$\varepsilon_{yd} \cong 0.75\%$$

- permissible stresses

$$\bar{\sigma}_p = 0.80 f_{p0.1k} = 1264\,\mathrm{N/mm^2}$$
$$\bar{\sigma}_{pi} = 0.85 f_{p0.1k} = 1343\,\mathrm{N/mm^2}$$

- relaxation (class 2—stabilized)
(see Table 10.2)

$$\rho_{1000} = 2.5\% \; at \; \sigma_{pi} = 0.7 f_{ptk}$$

Prestressing
Tendons profile

- n° 2 tendons made of 6 strands each
(see Tables 1.21)

$$A_p = 2 \times 6 \times 139 = 2 \times 834\,\text{mm}^2$$

- ducts $\phi 60$

$$\mu = 0.20 \quad \alpha = 0.01\,\text{rad/m}$$

- profile (in mm)
  upper tendon (symmetric)—α_{po} = 0.1793

$x = 0$	$y = 799$		
		straight	$\text{tg}\,\alpha_p = 0.1812$
$x = 1750$	$y = 482$		
		parabolic	$\text{tg}\,\alpha_p = \text{var.}$
$x = 4750$	$y = 210$		
		straight	$\text{tg}\,\alpha_p = 0.0000$
$x = 5000$	$y = 210$		

  lower tendon (symmetric)—α_{po} = 0.0880

$x = 0$	$y = 295$		
		straight	$\text{tg}\,\alpha_p = 0.0882$
$x = 1300$	$y = 180$		
		parabolic	$\text{tg}\,\alpha_p = \text{var.}$
$x = 3800$	$y = 70$		
		straight	$\text{tg}\,\alpha_p = 0.0000$
$x = 5000$	$y = 70$		

  design sections

section b' $x = 0.94\,\text{m}$

– upper tendon y = 629 mm $\text{tg}\,\alpha_p = 0.1812$ $\alpha_p = 0.1793$
$\sin\alpha_p = 0.1783$ $\cos\alpha_p = 0.9840$ $\Delta\alpha_p = 0.0000$

friction reduction coefficient

$$0.20 \times 0.01 \times 0.94 = 0.00188$$
$$e^{-0.00188} = 0.998$$

– lower tendon $y = 212\,\text{mm}$ $tg\,\alpha_p = 0.0882$ $\alpha_p = 0.088$
$\sin\alpha_p = 0.0879$ $\cos\alpha_p = 0.9961$ $\Delta\alpha_p = 0.0000$

friction reduction coefficient

$$0.20 \times 0.01 \times 0.94 = 0.00188$$
$$e^{-0.0188} = 0.998$$

section a $x = 5.00\,\text{m}$
– upper tendon $y = 210\,\text{mm}$ $\text{tg}\,\alpha_\text{p} = 0.0000$ $\alpha_\text{p} = 0.0000$
$\sin\alpha_\text{p} = 0.0000$ $\cos\alpha_\text{p} = 1.0000$ $\Delta\alpha_\text{p} = 0.1793$

friction reduction coefficient

$$0.20 \times (0.1793 + 0.01 \times 5.00) = 0.04586$$
$$e^{-0.04586} = 0.955$$

– lower tendon $y = 70\,\text{mm}$ $\text{tg}\,\alpha_\text{p} = 0.0000$ $\alpha_\text{p} = 0.0000$
$\sin\alpha_\text{p} = 0.0000$ $\cos\alpha_\text{p} = 1.0000$ $\Delta\alpha_\text{p} = 0.0880$

friction reduction coefficient

$$0.20 \times (0.0880 + 0.01 \times 5.00) = 0.02760$$
$$e^{-0.02760} = 0.973$$

section b'' $x = 9.06\,\text{m}$
– upper tendon $y = 629\,\text{mm}$ $\text{tg}\,\alpha_\text{p} = 0.1812$ $\alpha_\text{p} = 0.1793$
$\sin\alpha_\text{p} = 0.1783$ $\cos\alpha_\text{p} = 0.9840$ $\Delta\alpha_\text{p} = 0.3586$

friction reduction coefficient

$$0.20 \times (0.3586 + 0.01 \times 9.06) = 0.08984$$
$$e^{-0.08984} = 0.914$$

– lower tendon $y = 212\,\text{mm}$ $\text{tg}\,\alpha_\text{p} = 0.0882$ $\alpha_\text{p} = 0.0880$
$\sin\alpha_\text{p} = 0.0879$ $\cos\alpha_\text{p} = 0.9961$ $\Delta\alpha_\text{p} = 0.1760$

friction reduction coefficient

$$0.20 \times (0.176 + 0.01 \times 9.06) = 0.05332$$
$$e^{-0.05332} = 0.948$$

Tendons tensioning
(at 28 days of natural concrete aging)

$$\sigma_{pi} = 1300\,\mathrm{N/mm^2} \qquad \left(\bar{\sigma}_{pi} = 1343\,\mathrm{N/mm^2}\right)$$
$$P_o = 834 \times 1.300 = 1084\,\mathrm{kN}$$

section b′

- upper tendon

$$N_p = 0.9840 \times 0.998 \times 1084 = 1065\,\mathrm{kN}$$
$$V_p = 0.1783 \times 0.998 \times 1084 = 193\,\mathrm{kN}$$

- lower tendon

$$N_p = 0.9961 \times 0.998 \times 1084 = 1078\,\mathrm{kN}$$
$$V_p = 0.0879 \times 0.998 \times 1084 = 95\,\mathrm{kN}$$

section a

- upper tendon

$$N_p = 1.0000 \times 0.955 \times 1084 = 1035\,\mathrm{kN}$$
$$V_p = 0$$

- lower tendon

$$N_p = 1.0000 \times 0.973 \times 1084 = 1055\,\mathrm{kN}$$
$$V_p = 0$$

section b″

- upper tendon

$$N_p = 0.9840 \times 0.914 \times 1084 = 975\,\mathrm{kN}$$
$$-V_p = 0.1783 \times 0.914 \times 1084 = 177\,\mathrm{kN}$$

- lower tendon

$$N_p = 0.9961 \times 0.948 \times 1084 = 1024\,\mathrm{kN}$$
$$-V_p = 0.0879 \times 0.948 \times 1084 = 90\,\mathrm{kN}$$

Verification of Stresses

(concrete compressions positive)

Section characteristics

(symmetric, see Fig. 10.47)

Area

$$\begin{aligned} 2 \times 50 \times 14 &= 1400 \\ 2 \times 18 \times 6 &= 216 \\ 14 \times 84 &= \underline{1176} \\ A &= 2792\,\text{cm}^2 \end{aligned}$$

Moment of inertia

$$\begin{aligned} 1400\left(14^2/12 + 49^2\right) &= 3{,}384{,}267 \\ 216\left(6^2/18 + 40^2\right) &= 346{,}032 \\ 1176\left(84^2/12\right) &= \underline{691{,}488} \\ I &= 4{,}421{,}787\,\text{cm}^4 \end{aligned}$$

Resisting modulus

$$W = 4{,}421{,}787/56 = 78{,}960\,\text{cm}^3$$

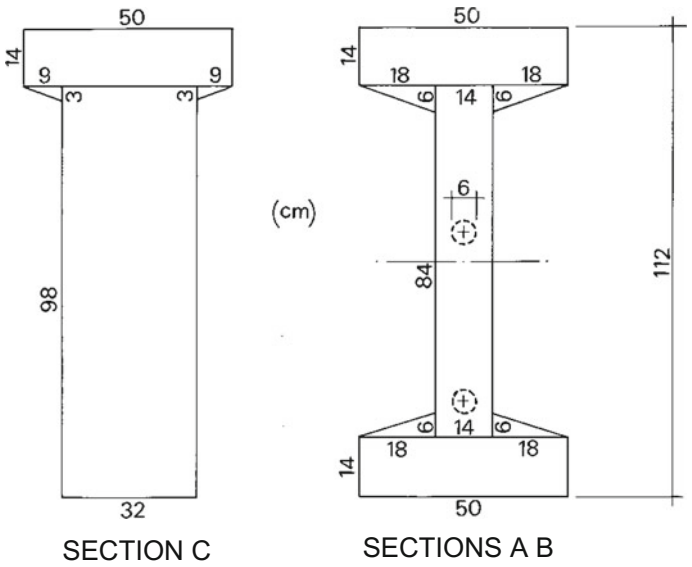


Fig. 10.47 Geometric dimensions of the sections

Centroidal static moment

$$\begin{aligned} 700 \times 49 &= 34{,}300 \\ 108 \times 40 &= 4320 \\ 14 \times 42 \times 21 &= \underline{12{,}348} \\ A &= 50{,}968\,\text{cm}^3 \end{aligned}$$

Lever arm

$$z = 4{,}421{,}787/50{,}968 = 86.75\,\text{cm}$$

Section a

- Prestressing

$$\begin{aligned} 1035 \times 0.350 &= 362.2 \\ \underline{1055} \times 0.490 &= \underline{516.9} \\ N_\text{p} = 2090\,\text{kN} \quad M_\text{p} &= 879.1\,\text{kNm} \end{aligned}$$

$$\sigma'_\text{c} = 2090/279.2 - (879.1 - 87.5)/78.96 = 7.46 - 10.03 = -2.57\,\text{N/mm}^2$$
$$\sigma''_\text{c} = 7.46 + 10.03 = +17.49\,\text{N/mm}^2$$
$$\sigma_{\text{c}1} = 7.46 + (879.1 - 87.5)35/4422 = 13.7\,\text{N/mm}^2$$
$$\sigma_{\text{c}2} = 7.46 + (879.1 - 87.5)49/4422 = 16.2\,\text{N/mm}^2$$

- Lifting
(vertical at the ends)
dynamic effect

$$\Delta M'_\text{g} = 0.15 \times 87.5 = 13.1\,\text{kNm}$$
$$\Delta\sigma = \pm 13.1/78.96 = \pm 0.17\,\text{N/mm}^2$$
$$\sigma'_\text{c} = -2.57 - 0.17 = -2.74\,\text{N/mm}^2$$
$$\sigma''_\text{c} = 17.49 + 0.17 = 17.66\,\text{N/mm}^2$$

verifications

$$-\sigma'_\text{c} < \bar{\sigma}'_\text{ct} = 3.51\,\text{N/mm}^2$$
$$\sigma''_\text{c} < \bar{\sigma}_\text{cj} = 27.0\,\text{N/mm}^2$$

- Losses
  relaxation

$$r = \sigma_{pi}/f_{ptk} = 1300/1860 = 0.70$$
$$c(r) = 1 \qquad \rho_1 = 2.5 \quad (\text{class } 2)$$
$$\tau^{0.75(1-r)} = 4 \qquad \text{for } \tau = 500$$
$$\Delta\sigma_{p\infty}/\sigma_{pi} = 4 \times 2.5 = 10\%$$
$$\Delta N_{p1} = 0.10 \times 1035 = 103.5\,\text{kN}$$
$$\Delta N_{p2} = 0.10 \times 1055 = 105.5\,\text{kN}$$

  shrinkage

$$\Delta N'_{p1} = \Delta N_{p2} \cong 0.00028 \times 195 \times 834 = 45.5\,\text{kN}$$

  creep

$$\alpha_e = 195{,}000/36{,}000 = 5.4$$
$$\Delta N_{p1} \cong 5.4 \times 1.9 \times 13.7 \times 0.834 = 117.2\,\text{kN}$$
$$\Delta N_{p2} \cong 5.4 \times 1.9 \times 16.2 \times 0.834 = 138.6\,\text{kN}$$

  total

$$\Delta N_{p1} = 103.5 + 45.5 + 117.2 = 266.2\,\text{kN} \quad (\cong 26\%)$$
$$\Delta N_{p2} = 105.5 + 45.5 + 138.6 = 289.6\,\text{kN} \quad (\cong 27\%)$$

  in the section

$$\begin{aligned} 266.2 \times \quad 0.350 \quad &= \quad 93.2 \\ \underline{289.6} \times \quad 0.490 \quad &= \underline{141.9} \\ \Delta N_p = 555.8 \qquad &\Delta M_p = 235.1\,\text{kNm} \end{aligned}$$

$$\Delta\sigma'_c = -555.8/279.2 + 235.1/78.96 = -1.99 + 2.98 = +0.99\ \text{N/mm}^2$$

$$\Delta\sigma''_c = -1.99 - 2.98 = -4.97\ \text{N/mm}^2$$
$$\sigma'_c = -2.57 + 0.99 = -1.58\ \text{N/mm}^2$$
$$\sigma''_c = +17.49 - 4.97 = +12.52\ \text{N/mm}^2$$

- Permanent loads

$$\Delta\sigma = \pm\, 562.5/78.96 = \pm\, 7.12 \text{ N/mm}^2$$
$$\sigma'_c = -1.58 + 7.12 = 5.54 \text{ N/mm}^2$$
$$\sigma''_c = 12.52 - 7.12 = 5.40 \text{ N/mm}^2$$

- Total loads
(rare combination)

$$\Delta\sigma = \pm 625/78.96 = \pm\, 7.92 \text{ N/mm}^2$$
$$\sigma'_c = +5.54 + 7.92 = \pm\, 13.46 \text{ N/mm}^2$$
$$\sigma''_c = 5.40 - 7.92 = -\,2.52 \text{ N/mm}^2$$

Verifications

$$\sigma'_c < \bar{\sigma}_c = 20.2 \text{ N/mm}^2$$
$$-\sigma''_c < \bar{\sigma}'_{ct} = 3.51 \text{ N/mm}^2$$

Sections b′/b″
net web width

$$b_o = 14 - 6 = 8 \text{ cm}$$

- Lifting (side b′)

$$N_p = 1065 + 1078 = 2143 \text{ kN}$$
$$V_p = -193 - 95 = 288 \text{ kN}$$

dynamic effect

$$(1 - \alpha_d)V'_g = 0.85 \times 28.4 = 24.1 \text{ kN}$$
$$V = 24.1 - 288 = -263.9 \text{ kN}$$

stresses at centroid

$$\sigma_G = 21{,}430/2792 = 7.68 \text{ N/mm}^2$$
$$\tau_G = V/zb_o = -2639/(86.75 \times 8) = -3.80 \text{ N/mm}^2$$

principal stresses

$$\sigma_{\mathrm{I}} = \frac{1}{2}\left(\sigma_{\mathrm{c}} - \sqrt{\sigma_{\mathrm{c}}^2 + 4\tau_{\mathrm{c}}^2}\right) = -1.56\ \mathrm{N/mm^2}$$
$$\sigma_{\mathrm{II}} = \frac{1}{2}\left(\sigma_{\mathrm{c}} + \sqrt{\sigma_{\mathrm{c}}^2 + 4\tau_{\mathrm{c}}^2}\right) = +9.24\ \mathrm{N/mm^2}$$

Verifications

$$-\sigma_{\mathrm{I}} < \bar{\sigma}'_{\mathrm{ct}} = 3.51\ \mathrm{N/mm^2}$$
$$\sigma_{\mathrm{II}} < \bar{\sigma}'_{\mathrm{cj}} = 27.0\ \mathrm{N/mm^2}$$

- Prestressing (side b″)

$$\begin{aligned} 975 \times \quad & (-0.350) = -67.3 \\ \underline{1024} \times \quad & 0.348 \ = \ \underline{356.4} \\ N_{\mathrm{p}} = 1999\,kN \quad & M_p = 289.1 \end{aligned}$$

$$M = M'_{\mathrm{g}} - M_{\mathrm{p}} = 29.8 - 289.1 = -259.3\ \mathrm{kNm}$$
$$V_{\mathrm{p}} = 179 + 90 = 267\ \mathrm{kN}$$
$$V = V'_{\mathrm{g}} - V_{\mathrm{p}} = 28.4 - 267 = -238.6\ \mathrm{kN}$$

stresses at centroid

$$\sigma_{\mathrm{G}} = 19{,}990/2792 = 7.16\ \mathrm{N/mm^2}$$
$$\tau_{\mathrm{G}} = V/zb_{\mathrm{o}} = -2386/(86.75 \times 8) = -3.44\ \mathrm{N/mm^2}$$

tendons stresses

$$\sigma_{\mathrm{c1}} = 7.16 - 259.3 \times 6.9/4422 = 6.76\ \mathrm{N/mm^2}$$
$$\sigma_{\mathrm{c2}} = 7.16 + 259.3 \times 34.8/4422 = 9.20\ \mathrm{N/mm^2}$$

- Losses
relaxation

$$\Delta N_{\mathrm{p1}} = 0.010 \times 975 = 97.5\ \mathrm{kN}$$
$$\Delta N_{\mathrm{p2}} = 0.010 \times 1024 = 102.4\ \mathrm{kN}$$

shrinkage

$$\Delta N'_{p1} = \Delta N_{p2} \cong 0.00028 \times 195 \times 834 = 45.5 \text{ kN}$$

creep

$$\Delta N_{p1} \cong 5.4 \times 1.9 \times 6.76 \times 0.834 = 57.8 \text{ kN}$$
$$\Delta N_{p2} \cong 5.4 \times 1.9 \times 9.20 \times 0.834 = 78.7 \text{ kN}$$

total

$$\Delta N_{p1} = 97.5 \times 54.5 \times 57.8 = 209.8 \text{ kN} \quad (\cong 22\%)$$
$$\Delta N_{p2} = 97.5 \times 54.5 \times 78.7 = 230.7 \text{ kN} \quad (\cong 23\%)$$

in the section

$$209.8 \times 0.1783 = 37.4$$
$$\underline{230.7} \times 0.0879 = \underline{18.2}$$
$$N_p = 440.5\,\text{kN} \quad V_p = 55.6\,\text{kN}$$

$$\Delta\sigma = -4405/2792 = 1.58 \text{ N/mm}^2$$
$$\Delta\tau = +556/(86.75 \times 8) = +0.80 \text{ N/mm}^2$$
$$\sigma_G = +7.16 - 1.58 = +5.58 \text{ N/mm}^2$$
$$\tau_G = -3.44 + 0.80 = -2.64 \text{ N/mm}^2$$

- Permanent loads

$$\Delta\tau = 1830/(86.75 \times 8) = +2.64 \text{ N/mm}^2$$
$$\tau_G = -2.64 + 2.64 = 0.00 \text{ N/mm}^2$$

- Total loads
(rare combination)

$$\Delta\tau = 2030/(86.75 \times 8) = +2.93 \text{ N/mm}^2$$
$$\tau_G = +0.00 + 2.93 = +2.93 \text{ N/mm}^2$$
$$\sigma_I = \frac{1}{2}\left(\sigma_G - \sqrt{\sigma_G^2 + 4\tau_G^2}\right) = -1.26 \text{ N/mm}^2$$
$$\sigma_{II} = \frac{1}{2}\left(\sigma_G + \sqrt{\sigma_G^2 + 4\tau_G^2}\right) = +6.84 \text{ N/mm}^2$$

Verifications

$$-\sigma_{\mathrm{I}} < \bar{\sigma}'_{\mathrm{ct}} = 3.51\ \mathrm{N/mm^2}$$
$$\sigma_{\mathrm{II}} < \bar{\sigma}_{\mathrm{c}} = 20.2\ \mathrm{N/mm^2}$$

Resistance Verifications
Section a

- Maximum loads
  (A_{s}, A'_{S} neglected)
  prestressed reinforcement ($n\phi$ - A_{p} - d_{p})

$$\begin{aligned} &6\phi 15.2 \quad 8.34\,\mathrm{cm^2} \quad 91\,\mathrm{cm} \\ &6\phi 15.2 \quad \underline{8.34\,\mathrm{cm^2} \quad 105\,\mathrm{cm}} \\ &A_p = \quad 16.68\,\mathrm{cm^2} \end{aligned}$$

concrete in compression

$$A_{\mathrm{c}} = A_{\mathrm{p}} f_{\mathrm{pd}} / f_{\mathrm{cd}} = 16.78 \times 1456/25.5 = 958\ \mathrm{cm^2}$$

bulb area

$$\begin{aligned} &50 \times 14 = 700 \times 7 = 4900 \\ &18 \times 6 = 108 \times 16 = 1728 \\ &14 \times 6 = \ \underline{84 \times 17 = 1428} \\ &A_{\mathrm{o}} = \quad 892\,\mathrm{cm^2} \qquad S_{\mathrm{o}} = 8056\,\mathrm{cm^3} \end{aligned}$$

web protrusion

$$\begin{aligned} &\Delta A = A_{\mathrm{c}} - A_{\mathrm{o}} = 958 - 892 = 66\ \mathrm{cm^2} \\ &\Delta \bar{x} = \Delta A / b_{\mathrm{w}} = 66/14 = 4.7\ \mathrm{cm} \\ &\bar{x} = 20.0 + 4.7 = 24.7\ \mathrm{cm} \\ &S = 8056 + 66(20.0 + 4.7/2) = 9531\ \mathrm{cm^3} \\ &d_{\mathrm{c}} = 9531/958 = 9.9\ \mathrm{cm} \end{aligned}$$

elongation of upper tendon (after losses)

$$\begin{aligned} &x \cong \bar{x}/0.8 = 30.1\ \mathrm{cm} \\ &\Delta\varepsilon_{\mathrm{p}} = 0.35(91.0 - 30.1)/30.1 = 0.708 \\ &\varepsilon^*_{\mathrm{po}} \cong 0.74 \times 0.955 \times 1300/1950 = 0.471\% \\ &\varepsilon_{\mathrm{p}} \cong 0.708 \times 0.471 = 1.18\% \quad \left(> \varepsilon_{\mathrm{yd}}\right) \end{aligned}$$

resisting moment

$$\begin{aligned} 8.34 \times 145.6 \times (0.910 - 0.099) &= 985 \\ 8.34 \times 145.6 \times (1.050 - 0.099) &= \underline{1155} \\ M_{\mathrm{Rd}} &= 2130\,\mathrm{kNm} \end{aligned}$$

Verification

$$\begin{aligned} 1.30 \times 87.5 &= 113.8 \\ 1.50 \times 562.5 &= 843.8 \\ 1.50 \times 625.0 &= \underline{937.5} \\ M_{\mathrm{Ed}} &= +1895.1\,\mathrm{kNm}\ (< M_{\mathrm{Rd}}) \end{aligned}$$

Sections b′/b″

$$\begin{aligned} &a_{\mathrm{w}} \geq 0.2 b_{\mathrm{w}} f_{\mathrm{ctm}}/f_{\mathrm{yk}} = 0.2 \times 1400 \times 3.8/450 = 2.36\ \mathrm{cm}^2/\mathrm{m} \\ &z = M_{\mathrm{Rd}}/\left(A_{\mathrm{p}} f_{\mathrm{pd}}\right) = 2140/(2 \times 8.34 \times 145.6) = 0.88\ \mathrm{m} \\ &1\phi 8/20\ \mathrm{cm} \rightarrow A_{\mathrm{s}} = 5.02\ \mathrm{cm}^2/\mathrm{m} \\ &f_{\mathrm{yd}}/f_{\mathrm{c2}} = 391/12.7 = 31 \end{aligned}$$

- Lifting (side b′)

$$\begin{aligned} &b_{\mathrm{o}} = 14 - 6 = 8\ \mathrm{cm} \\ &\omega_{\mathrm{W}} = (5.02 \times 31)/(8 \times 100) = 0.195 \quad (< 0.2) \\ &\lambda_{\mathrm{c}} = \sqrt{(1 - \omega_{\mathrm{W}})/\omega_{\mathrm{W}}} = 2.03 \text{ assumed } \lambda_c = 2 \\ &V_{\mathrm{Rd}} = V_{\mathrm{sd}} = z A_{\mathrm{s}} f_{\mathrm{yd}} \lambda_{\mathrm{c}} = 0.88 \times 5.02 \times 39.1 \times 2.0 = 345\,\mathrm{kN} \\ &\left(V_{\mathrm{cd}} = 8 \times 1.27 \times 88 \times 2.0/\left(1 + 2.0^2\right) = 358\ \mathrm{kN}\right) \end{aligned}$$

verification

$$\begin{aligned} 1.20 \times 288 &= +345.6 \quad \text{from prestressing} \\ -0.85 \times 28.4 &= \underline{-24.1} \quad \text{self weight with dynamic effect} \\ V_{\mathrm{Ed}} &= +321.5\,\mathrm{kN} \quad (< V_{\mathrm{Rd}}) \end{aligned}$$

- Maximum loads (side b'')

$$b_o = 14 - 0.5 \times 6 = 11 \text{ cm}$$
$$\omega_W = (5.02 \times 31)/(11 \times 100) = 0.141 \quad (< 0.2)$$
$$\lambda_c = 2$$
$$V_{Rd} = V_{sd} = 0.88 \times 5.02 \times 39.1 \times 2 = 345 \text{ kN}$$
$$\left(V_{cd} = 11 \times 1.27 \times 88 \times 2/\left(1 + 2^2\right) = 492 \text{ kN}\right)$$

Verification

$$\begin{aligned} -1.00 \times 267 &= -267.0 \\ 1.30 \times 28.4 &= +36.9 \\ 1.50 \times 183 &= +274.5 \\ 1.50 \times 203 &= \underline{+304.5} \\ V_{Ed} &= +348.9 \text{ kN} \quad (< V_{Rd} = 345 \text{ kN}) \end{aligned}$$

Section c
with $P = 0 \quad \lambda_o = \lambda_c/2 = 1 \quad d \cong 107$ cm $\quad b_w = 32$ cm

- Longitudinal reinforcement

$$2\phi 10 + 6\phi 20 \quad A_s = 1.57 + 18.85 = 20.42 \text{ cm}^2$$

resistance at the support

$$R_{Rd} = R_{RS} = A_S f_{yd}/\lambda_o = 20.42 \times 39.1/1 = 798 \text{ kN}$$
$$R_{Rc} = 0.6 d b f_{c2}/\left(1 + \lambda_o^2\right) = 0.6 \times 107 \times 32 \times 1.27/\left(1 + 1^2\right) = 1305 \text{ kN}$$

verification

$$\begin{aligned} 1.30 \times 35.0 &= 45 \\ 1.50 \times 225.0 &= 338 \\ 1.50 \times 250.0 &= \underline{375} \\ R_{Ed} &= 748 \text{ kN} \quad (< R_{Rd}) \end{aligned}$$

The construction drawings of the beam with the necessary reinforcement detailing are shown in Fig. 10.48.

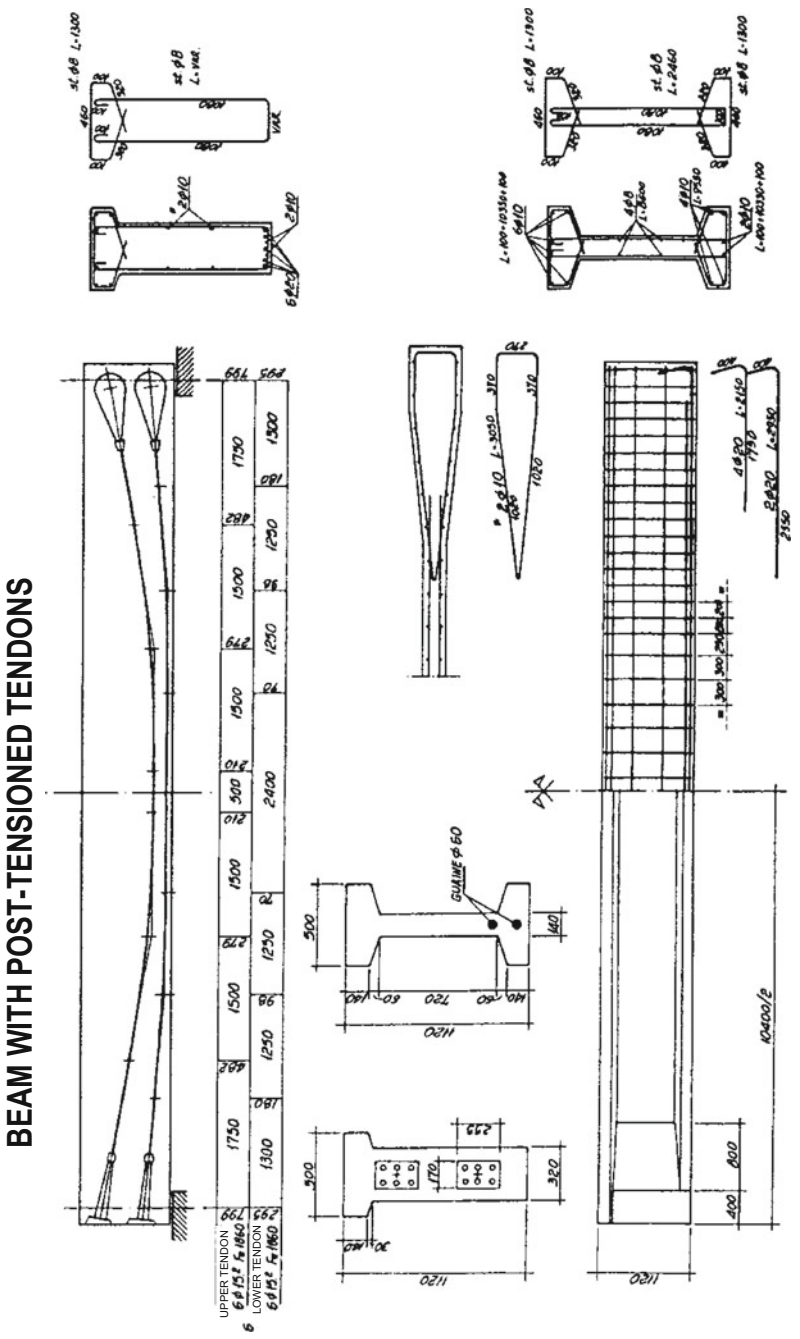


Fig. 10.48 Reinforcement details of the beam

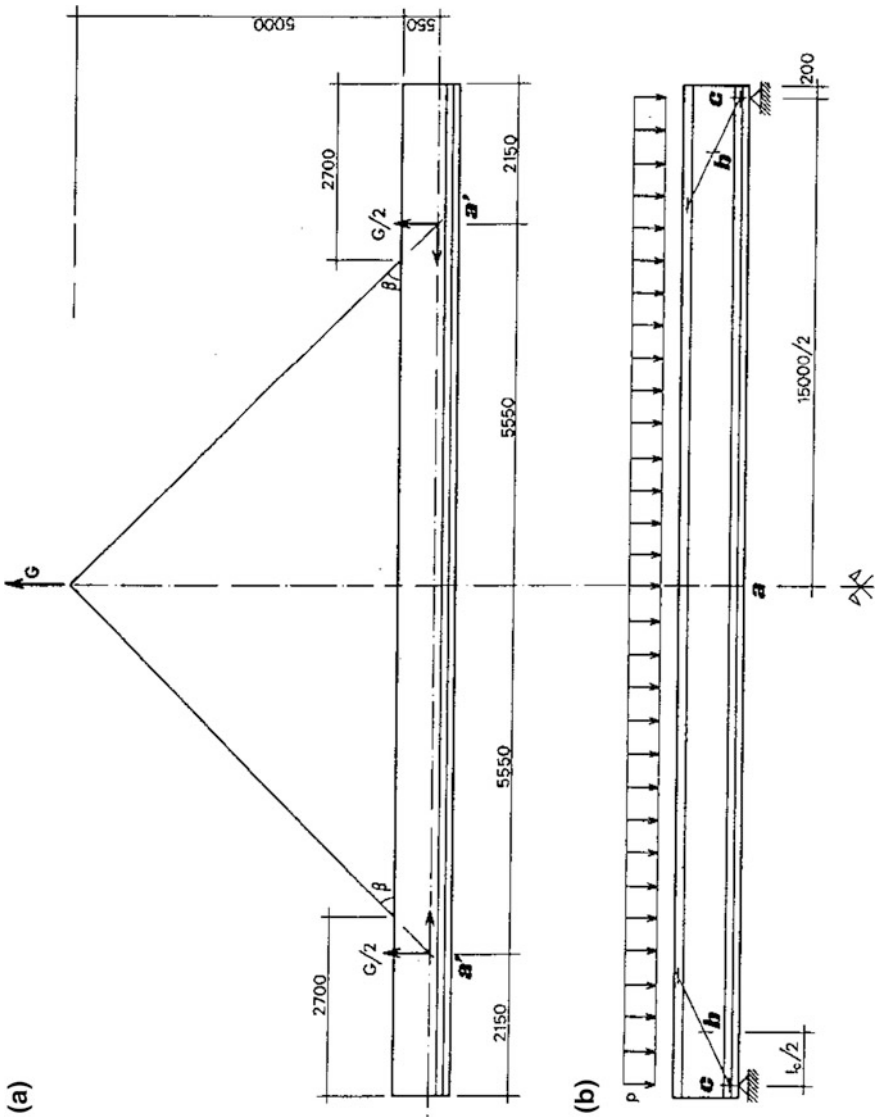


Fig. 10.49 Precast pretensioned beam—lifting stage (**a**) and service arrangement (**b**)

10.4.3 Prestressed Concrete Flanged Beam

The design of one rib of a deck made of precast prestressed concrete beams with pre-tensioned tendons and a cast-in situ upper slab. The effective width b of the slab corresponds to the spacing between ribs. The deck is simply supported on a span l of 15 m.

The configuration of the finished deck is shown in Fig. 10.49b, whereas the lifting scheme of the precast beam is shown in Fig. 10.49a. Figure 10.50 shows the current cross section of a rib. The construction drawings of the element are eventually shown on Fig. 10.53 and 10.54. Two cast-in situ transverse beams at the end supports of the deck are added for the lateral stability of the ribs and another one is positioned at the mid-span, necessary for the transverse distribution of loads.

Only few verifications are shown below, omitting others such as the ones relative to the local bending of the slab. Among the omitted verifications there is the very important one against flexural-torsional buckling of the precast beam during lifting; this type of instability can be particularly dangerous for the type of beam of concern, because of the limited torsional stiffness of its section with an inverted T-shape and the axial compression force induced by the inclination of the lifting cables.

The example shows the case of a structure with variable configuration, for which the verification stages follow the construction sequence. In particular the precast beam is supposed to resist the weight of the cast-in situ concrete of the top slab and transverse beam, other than its self-weight; the additional permanent and the variable loads are instead resisted by a much stronger structure, thanks to the collaboration with the compression upper slab after its hardening.

For simplicity, in the calculations it has been assumed that all prestressing losses occur in the beam without top slab. A more accurate evaluation is obviously possible, to take into account that a significant portion of the losses occurs on the stiffer composite beam, with effects smaller than the ones deduced with the above simplified assumption.

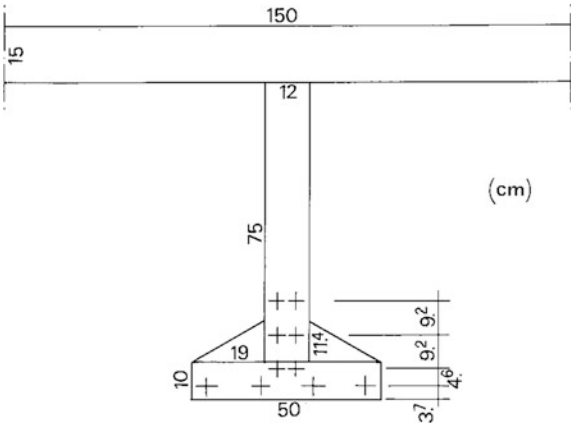


Fig. 10.50 Geometric dimensions of the flanged element

Stress analysis

- *Loads*

– beam self-weight	g = 4.0 kN/m
– slab self-weight	g_1 = 5.6 kN/m
– middle transverse beam	G = 4.5 kN
– other permanent loads	g_2 = 4.5 kN/m
– variable loads	q = 15.0 kN/m

- *Design sections*
(abscissa x from the support on the left-hand side)
  - *a*—of maximum bending moment

$$x_a = 7.50 \text{ m}$$

  - *a′*—lifting point

$$x_o = 1.95 \text{ m}$$

  - *b*—of maximum shear force: with $d \approx 0.90$ m $\lambda_c = 2$ one has

$$z \cong 0.9d \cong 0.81 \text{ m}$$
$$x_b \cong \lambda_c z/2 = 0.81 \text{ m}$$

  - *c*—at the support

$$x_c = 0.00 \text{ m}$$

- *Initial stage*
(l = 15.0 m − x_b = 0.81 m)

$$R_o = gl/2 = 30.00 \text{ kN}$$
$$M_a = gl^2/8 = 112.50 \text{ kNm}$$
$$V_b = R - gx_b = 26.76 \text{ kN}$$

- *Transient stage*
(Lifting: x_o = 1.95 m − β = 45°)

$$R_o = gl/2 = 30.00 \text{ kN}$$
$$N_o = R_o \text{ctg}\,\beta = 30.00 \text{ kN}$$
$$M_o = -gx_o^2/2 = -7.60 \text{ kNm}$$

- *Completion of the structure*
  (casting of slab and transverse beams)

$$R' = g_1 l/2 + G/2 = 42.00 + 2.25 = 44.25 \text{ kN}$$
$$M'_a = g_l 1^2/8 + Gl/4 = 157.50 + 16.88 = 174.38 \text{ kNm}$$
$$V'_b = R' - g_1 x_b = 39.71 \text{ kNm}$$

- *Other permanent loads*

$$R'' = g_2 l/2 = 33.75 \text{ kN}$$
$$M''_a = g_2 l^2/8 = 125.56 \text{ kNm}$$
$$V''_b = R'' - g_2 x_b = 30.11 \text{ kN}$$

- *Variable loads*

$$R = ql/2 = 112.50 \text{ kN}$$
$$M_a = ql^2/8 = 421.88 \text{ kNm}$$
$$V_b = R - qx_b = 100.35 \text{ kN}$$

Characteristics of Materials
(controlled production)
Precast concrete

- max aggregate size d_a = 20 mm
- strength class C50/60
  (see Tables 1.1, 1.2, 1.8 and 1.16)

$$f_{ck} = 50.0 \text{ N/mm}^2 \qquad f_{ctm} = 55.0 \text{ N/mm}^2$$
$$f_{ctk} = 3.1 \text{ N/mm}^2 \qquad f_{ctm} = 3.9 \text{ N/mm}^2$$
$$f_{ckj} = 30.0 \text{ N/mm}^2$$
$$f_{ctkj} = 1.9 \text{ N/mm}^2$$
$$E_c = 37{,}000 \text{ N/mm}^2$$
$$\varepsilon_{CS\infty} \cong -0.00032 \qquad \varphi_\infty \cong 2.7$$

- design values (γ_C = 1.40)
  (see Chart 2.2)

$$f_{cd} = 0.85 f_{ck}/\gamma_C = 30.4 \text{ N/mm}^2$$
$$f_{cdj} = 0.85 f_{ckj}/\gamma_C = 18.2 \text{ N/mm}^2$$
$$f_{c2} \cong 0.50 f_{cd} = 15.2 \text{ N/mm}^2$$
$$f_{c2j} = 0.50 f_{cdj} = 9.1 \text{ N/mm}^2$$

- allowable stresses

$$\begin{aligned}
&\bar{\sigma}_c = 0.45 f_{ck} = 22.5\ \text{N/mm}^2 && \text{(compressions in service)}\\
&\bar{\sigma}_{cj} = 0.70 f_{ckj} = 21.0\ \text{N/mm}^2 && \text{(initial compressions)}\\
&\bar{\sigma}'_{ct} = 1.3 f_{ctk} = 4.03\ \text{N/mm}^2 && \text{(tensions in service)}\\
&\bar{\sigma}'_{ctj} = 1.3 f_{ctkj} = 2.47\ \text{N/mm}^2 && \text{(initial tensions)}
\end{aligned}$$

In situ *concrete*
(ordinary production)

- max aggregate size d_a = 25 mm
- strength class C25/30
(see Table 1.2)

$$\begin{aligned}
&f_{ck} = 25.0\ \text{N/mm}^2 \quad f_{cm} = 33.0\ \text{N/mm}^2\\
&f_{ctk} = 1.90\ \text{N/mm}^2 \quad f_{ctm} = 2.80\ \text{N/mm}^2\\
&E'_c = 31.0\ \text{GPa}
\end{aligned}$$

- design values (γ_C = 1.5)

$$f_{cd} = 0.85 f_{ck}/\gamma_C = 14.2\ \text{N/mm}^2$$

- allowable stress

$$\bar{\sigma}_c = 0.45 f_{ck} = 11.2\ \text{N/mm}^2$$

Passive reinforcement

- ribbed bars
- steel type B450C
(see Table 1.17)

$$\begin{aligned}
&f_{yk} = 450\ \text{N/mm}^2 \quad f_{tk} = 540\ \text{N/mm}^2\\
&E_S = 205{,}000\ \text{N/mm}^2 \quad \varepsilon_{uk} \geq 0.75
\end{aligned}$$

- design values (γ_S = 1.15)

$$\begin{aligned}
&f_{yd} = f_{yk}/\gamma_S = 391\ \text{N/mm}^2\\
&\varepsilon_{yd} = 0.19\%
\end{aligned}$$

Prestressing reinforcement

- strands 7 W ϕ = 15.2 mm (= 0.6″)
(see Table 1.21)

$$f_{ptk} = 1860\ \text{N/mm}^2 \quad f_{p0.1k} = 1580\ \text{N/mm}^2$$
$$E_p = 19{,}500\ \text{N/mm}^2 \quad \varepsilon_{uk} = 0.05$$

- design values (γ_S = 1.15)

$$f_{pd} = 0.9 \times 1860/1.15 = 1456\ \text{N/mm}^2$$
$$\varepsilon_{yd} = 0.75\%$$

- allowable stresses

$$\bar{\sigma}_p = 0.80 f_{p0.1k} = 1264\ \text{N/mm}^2$$
$$\bar{\sigma}_{pi} = 0.90 f_{p0.1k} = 1422\ \text{N/mm}^2$$

- relaxation (class 2—stabilized)

$$\rho_{1000} = 2.5\%\ at\ \sigma_{pi} = 0.7 f_{ptk}$$

Bond

$$f_{ctdj} = f_{ctkj}/\gamma_C = 1.9/1.40 = 1.36\ \text{N/mm}^2$$
$$f_{bd} \cong 3.0 \times 1.36 = 4.07\ \text{N/mm}^2$$
$$l_b = \frac{\phi}{4}\frac{1456}{4.07} \cong 90\phi \quad (= 137\ \text{cm})$$

Tendons tensioning
(at 14 h of accelerated aging of concrete)

$$\sigma_{pi} = 1300\ \text{N/mm}^2 \quad \left(< 0.9 f_{p0.1k}\right)$$

- initial overstress

$$\sigma'_{pi} = 1400\ \text{N/mm}^2 \quad \left(< \bar{\sigma}_{pi} = 1422\ \text{N/mm}^2\right)$$

- tension loss due to heating
(accelerated aging of concrete)

$$\Delta\theta = 70 - 20 = 50\,^{\circ}\text{C}$$
$$\Delta\sigma_p = E_p \alpha_T \Delta\theta = 19{,}500 \times 10^{-5} \times 50 = 100\text{N/mm}^2$$

- initial stress

$$\sigma_{pi} = \sigma'_{pi} - \Delta\sigma_p = 1300\ \text{N/mm}^2$$

- level 1, 2 and 3

$$A_p = 2 \times 139 = 278\ \text{mm}^2 \quad \text{for level}$$
$$P'_O = 278 \times 1.300 = 361\ \text{kN} \quad \text{for level}$$

- level 4

$$A_p = 4 \times 139 = 556\ \text{mm}^2$$
$$P'_o = 556 \times 1.300 = 723\ \text{kN}$$

Verification of Stresses
(compressions in concrete positive)

- *Characteristics of section*
- precast portion

Area	Static moment
$12 \times 75 = 900$	$\times\ 37.5 = 33{,}750$
$19 \times 11.4 = 217$	$\times\ 71.2 = 15{,}422$
$50 \times 10 = \underline{500}$	$\times\ 80.0 = \underline{40{,}000}$
$A = 1617\,\text{cm}^2$	$S = 89{,}172\,\text{cm}^3$

Centroid

$$y'_c = 89{,}172/1617 = 55.1\ \text{cm} \quad \text{upper edge}$$
$$y''_c = 85.0 - 55.1 = 29.9\,\text{cm} \quad \text{upper edge}$$

Moment of inertia

$$900\left(75^2/12 + 17.6^2\right) = 700{,}659$$
$$217\left(11.4^2/18 + 16.1^2\right) = 57{,}815$$
$$500\left(10^2/12 + 24.9^2\right) = \underline{314{,}172}$$
$$I = 1{,}072{,}646\,\text{cm}^4$$

Beam self weight

$$g = 0.1617 \times 25 \cong 4.0\ \text{kN/m}$$

Resisting modules

$W' = 1{,}072{,}646/55.1 = 19{,}467\ \text{cm}^3$ upper edge
$W'' = 1{,}072{,}646/29.9 = 35{,}874\ \text{cm}^3$ upper edge
$y_1 = 29.9 - 26.7 = 3.2\ \text{cm}$
$y_2 = 29.9 - 17.5 = 12.4\ \text{cm}$
$y_3 = 29.9 - 8.3 = 21.6\ \text{cm}$
$y_4 = 29.9 - 3.7 = 26.2\ \text{cm}$
$W_1 = 1{,}072{,}646/3.2 = 335{,}202\ \text{cm}^3$ tendons level 1
$W_2 = 1{,}072{,}646/12.4 = 86{,}504\ \text{cm}^3$ tendons level 2
$W_3 = 1{,}072{,}646/21.6 = 49{,}660\ \text{cm}^3$ tendons level 3
$W_4 = 1{,}072{,}646/26.2 = 40{,}941\ \text{cm}^3$ tendons level 4

Centroidal static moment

$$55.1^2 \times 12/2 = 18{,}216\ \text{cm}^3$$

Internal lever arm

$$z = 1{,}072{,}646/18{,}216 = 58.88\ \text{cm}$$

- with upper slab

$$E'_{\text{cm}}/E_{\text{cm}} = 31.0/37.0 = 0.838$$
$$A_{\text{c}} = 150 \times 15 = 2250\ \text{cm}^2$$

Slab self weight

$$g' = 0.2250 \times 25 = 5.6\ \text{kN/m}$$

characteristics

$$\begin{array}{rr} 0.838 \times 2250 = 1885 \times (-7.5) = -14{,}137 & \\ \underline{1617} \qquad\qquad \underline{+89{,}172} & \\ A = 3502\,\text{cm}^2 \qquad S = 75{,}034\,\text{cm}^3 & \end{array}$$

$y'_{\text{c}} = 75{,}034/3502 = 21.4\,\text{cm}$ top beam edge
$y''_{\text{c}} = 85.0 - 21.4 = 63.6\,\text{cm}$ bottom beam edge
$y_{\text{c}} = 15.0 + 21.4 = 36.6\,\text{cm}$ top slab edge

$$1885\left(15^2/12 + 28.9^2\right) = 1{,}609{,}715$$
$$1617 \times 33.7^2 = 1{,}836{,}411$$
$$\underline{1{,}072{,}646}$$
$$I = 4{,}518{,}772\,\text{cm}^4$$

Resisting modules

$$W' = 4{,}518{,}772/21.4 = 211{,}158\,\text{cm}^3$$
$$W'' = 4{,}518{,}772/63.6 = 71{,}050\,\text{cm}^3$$
$$W' = 4{,}518{,}772/36.4 = 124{,}142\,\text{cm}^3$$

Centroidal static moment

$$1885 \times 28.9 = 54{,}476$$
$$21.4^2 \times 12/2 = \underline{\ 2748}$$
$$57{,}224\,\text{cm}^3$$

Internal lever arm

$$z = 4{,}518{,}772/57{,}224 = 78.97\,\text{cm}$$

Section a

– Prestressing

$$361 \times 0.032 = 11.5$$
$$361 \times 0.124 = 44.8$$
$$361 \times 0.216 = 78.0$$
$$\underline{723} \times 0.262 = \underline{189.4}$$
$$N_\text{p} = 1806\,\text{kN} \quad M_\text{p} = 323.7\,\text{kNm}$$

$$\sigma'_\text{c} = 1806/161.7 - 323.7/19.47 = 11.2 - 16.6 = -5.4\,\text{N/mm}^2$$
$$\sigma''_\text{c} = 1806/161.7 + 323.7/35.87 = 11.2 + 9.0 = +20.2\,\text{N/mm}^2$$
$$\sigma_{\text{c}1} = 11.2 + 323.7/335.2 = 12.2\,\text{N/mm}^2$$
$$\sigma_{\text{c}2} = 11.2 + 323.7/86.5 = 14.9\,\text{N/mm}^2$$
$$\sigma_{\text{c}3} = 11.2 + 323.7/49.7 = 17.7\,\text{N/mm}^2$$
$$\sigma_{\text{c}4} = 11.2 + 323.7/40.9 = 19.1\,\text{N/mm}^2$$

with self-weight

$$\sigma'_c = -5.4 + 112.5/19.47 = +1.1\,\mathrm{N/mm^2}$$
$$\sigma''_c = +20.2 - 112.5/35.87 = +17.1\,\mathrm{N/mm^2}$$
$$\sigma_{c1} = +12.2 - 112.5/335.2 = +11.9\,\mathrm{N/mm^2}$$
$$\sigma_{c2} = +14.9 - 112.5/86.5 = +13.6\,\mathrm{N/mm^2}$$
$$\sigma_{c3} = +17.7 - 112.5/49.7 = +15.4\,\mathrm{N/mm^2}$$
$$\sigma_{c4} = +19.1 - 112.5/40.9 = +16.3\,\mathrm{N/mm^2}$$

– Losses
relaxation

$$r = \sigma_{pi} + f_{ptk} = 1300/1860 = 0.70$$
$$c(r) = 1 \qquad \rho_1 = 2.5 \quad (\text{class } 2)$$
$$\tau^{0.75(1-r)} = 4 \qquad \text{for } \tau = 500$$
$$\Delta\sigma_{p\infty}/\sigma_{pi} = 4 \times 2.5 = 10\%$$
$$\Delta N_{p1} = \Delta N_{p2} = \Delta N_{p3} = 0.10 \times 361 = 36.1\mathrm{kN}$$
$$\Delta N_{p4} = 0.010 \times 723 = 72.3\mathrm{kN}$$

shrinkage

$$\Delta N_{p1} = \Delta N_{p2} = \Delta N_{p3} = 0.00032 \times 195 \times 278 = 17.3\,\mathrm{kN}$$
$$\Delta N_{p4} = 0.00032 \times 195 \times 556 = 34.7\,\mathrm{kN}$$

creep

$$\alpha_e = 195{,}000/37{,}000 = 5.3$$
$$\Delta N_{p1} = 5.3 \times 2.7 \times 11.9 \times 0.278 = 47.3\,\mathrm{kN}$$
$$\Delta N_{p2} = 5.3 \times 2.7 \times 13.6 \times 0.278 = 54.1\,\mathrm{kN}$$
$$\Delta N_{p3} = 5.3 \times 2.7 \times 15.4 \times 0.278 = 61.3\,\mathrm{kN}$$
$$\Delta N_{p4} = 5.3 \times 2.7 \times 16.3 \times 0.556 = 129.7\,\mathrm{kN}$$

total

$$\Delta N_{p1} = 36.1 + 17.3 + 47.3 = 100.7 \quad (\cong 28\%)$$
$$\Delta N_{p2} = 36.1 + 17.3 + 54.1 = 107.5 \quad (\cong 30\%)$$
$$\Delta N_{p3} = 36.1 + 17.3 + 61.3 = 114.7 \quad (\cong 32\%)$$
$$\Delta N_{p4} = 72.3 + 34.7 + 129.7 = 236.7 \quad (\cong 33\%)$$

in the section

$$\begin{aligned} 100.7 \times 0.032 &= 3.2 \\ 107.5 \times 0.124 &= 13.3 \\ 114.7 \times 0.216 &= 24.8 \\ \underline{236.7} \times 0.262 &= \underline{62.0} \end{aligned}$$

$$\Delta N_p = 559.6\,\text{kN} \quad \Delta M_p = 103.3\,\text{kNm}$$

$$\Delta\sigma_c' = -559.6/161.7 + 103.3/19.47 = -3.5 + 5.3 = +1.8\,\text{N/mm}^2$$
$$\Delta\sigma_c'' = -559.6/161.7 - 103.3/35.87 = -3.5 - 2.9 = -6.4\,\text{N/mm}^2$$
$$\sigma_c' = +1.1 + 1.8 = +2.9\,\text{N/mm}^2$$
$$\sigma_c'' = +17.1 - 6.4 = +10.7\,\text{N/mm}^2$$

– Slab and transverse beam self weight

$$\Delta\sigma_c' = 174.4/19.47 = +9.0\,\text{N/mm}^2$$
$$\Delta\sigma_c'' = -174.4/35.87 = -4.9\,\text{N/mm}^2$$
$$\sigma_c' = +2.9 + 9.0 = +11.9\,\text{N/mm}^2$$
$$\sigma_c'' = +10.7 - 4.9 = +5.8\,\text{N/mm}^2$$

– Permanent loads

$$\Delta\sigma_c' = +125.6/211.16 = +0.6\,\text{N/mm}^2$$
$$\Delta\sigma_c'' = -125.6/71.50 = -1.8\,\text{N/mm}^2$$
$$\sigma_{co} = 0.838 \times 0.6 = 0.5\,\text{N/mm}^2 \quad \text{(slab bottom)}$$
$$\sigma_c = 0.838 \times 125.6/124.14 = +0.8\,\text{N/mm}^2 \quad \text{(slab top)}$$
$$\sigma_c' = +11.9 + 0.6 = +12.5\,\text{N/mm}^2$$
$$\sigma_c'' = +5.8 - 1.8 = +4.0\,\text{N/mm}^2$$

– Total loads

$$\Delta\sigma_c' = 421.9/211.16 = +2.0\,\text{N/mm}^2$$
$$\Delta\sigma_c'' = -421.9/71.50 = -5.9\,\text{N/mm}^2$$
$$\Delta\sigma_{co} = 0.838 \times 2.0 = +1.7\,\text{N/mm}^2$$
$$\Delta\sigma_c = 0.838 \times 421.9/124.14 = +2.8\,\text{N/mm}^2$$
$$\sigma_c' = +12.5 + 2.0 = +14.5\,\text{N/mm}^2$$
$$\sigma_c'' = +4.0 - 5.9 = -1.9\,\text{N/mm}^2$$
$$\sigma_{co} = 0.5 + 1.7 = +2.2\,\text{N/mm}^2 \quad \text{(slab bottom)}$$
$$\sigma_c = 0.8 + 2.8 = 3.6\,\text{N/mm}^2 \quad \text{(slab top)}$$

Verifications

$$\begin{aligned} &\sigma'_c < \bar{\sigma}_c = 22.5\,\mathrm{N/mm^2} && \text{(beam top)} \\ &-\sigma''_c < \bar{\sigma}'_{ct} = 4.03\,\mathrm{N/mm^2} && \text{(beam bottom)} \\ &\sigma_c < \bar{\sigma}'_c = 11.2\,\mathrm{N/mm^2} && \text{(slab top)} \end{aligned}$$

The diagrams of stresses in section *a* during the different stages are shown in Fig. 10.51.

Section a′

- Prestressing

$$-\sigma'_c = 5.4 > \bar{\sigma}'_{ctj} = 2.47\,\mathrm{N/mm^2}$$

cracked section (see Fig. 10.52)

$$\begin{aligned} &b = 50.0\,\mathrm{cm} && b_w = 12.0\,\mathrm{cm} \\ &\beta = b_w/b = 0.24 && \alpha = 1-\beta = 0.76 \\ &t \cong 15.0\,\mathrm{cm} && a = b - b_w = 38.0\,\mathrm{cm} \end{aligned}$$

resulting tendon $A'_s = A_p(10\phi 15.2)$:

$$\begin{aligned} &d' = d_p = [4 \times 3.7 + 2(8.3 + 17.6 + 26.8)]/10 = 12.0\,\mathrm{cm} \\ &d = 81.0\,\mathrm{cm} \end{aligned}$$

- Lifting
(with dynamic effect)

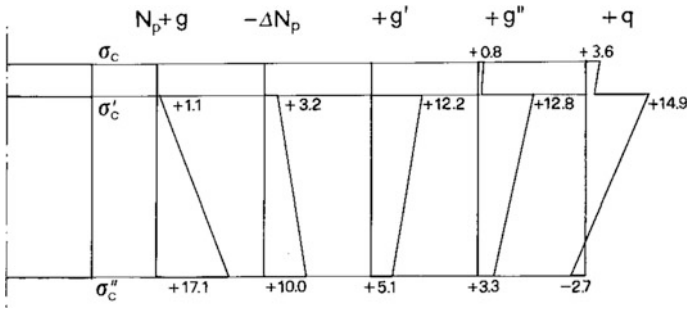


Fig. 10.51 Stress distribution at the different construction stages

$$
\begin{aligned}
&M_o = 1.15 \times 7.60 = 8.74\,\text{kNm}\\
&N_p = 1806\,\text{kN}\\
&-d_o = 12.0 - 874/1806 = 11.5\,\text{cm}\\
&d_s = d + d_o = 69.5\,\text{cm} \quad d'_s = d' + d_o = 0.5\,\text{cm}\\
&E_{cj} \cong 0.87E_c \qquad\qquad (\text{see Table 1.1})\\
&\alpha_{ej} = \alpha_e/0.87 = 5.3/0.87 \cong 6.1\\
&A_s = 6.28\,\text{cm}^2 \quad (2\phi 20)\\
&A'_s = 13.90\,\text{cm}^2 \quad (10\phi 15.2)\\
&\psi_s = 6.28 \times 6.1/(50 \times 81) = 0.00946\\
&\psi'_s = 13.90 \times 6.1/(50 \times 81) = 0.02094
\end{aligned}
$$

The neutral axis is obtained from the equation (see Chart 6.1):

$$
x^3 + 3d_o x^2 + \frac{3}{\beta}\left[\alpha t(2d_o + t) + 2(\psi_s d_s + \psi'_s d'_s)d\right]x +
$$
$$
-\frac{1}{\beta}\left[\alpha t^2(3d_o + 2t) + 6(\psi_s d_s d + \psi'_s d'_s d')d\right] = 0
$$

that is

$$
x^3 - 34.5x^2 + 213x - 108{,}085 = 0
$$

which gives

$$
x \cong 60.5\,\text{cm}
$$

from which one obtains (see Fig. 10.52)

$$
\begin{aligned}
12.0 \times 60.5 &= 726 \times 30.25 &&= 21{,}984\\
38.0 \times 15.0 &= 570 \times \ \ 7.5 &&= 4275\\
6.1 \times 6.28 &= \ \ 38 \times 81.0 &&= 3078\\
6.1 \times 13.9 &= \ \ \underline{85} \times 12.0 &&= \underline{1020}\\
A_i &= 1419\,\text{cm}^2 \quad S_i &&= 30{,}357\,\text{cm}^3
\end{aligned}
$$

$$
\begin{aligned}
y_c &= 30{,}357/1419 = 21.4\,\text{cm}\\
y_s &= 81.0 - 21.4 = 59.6\,\text{cm}
\end{aligned}
$$

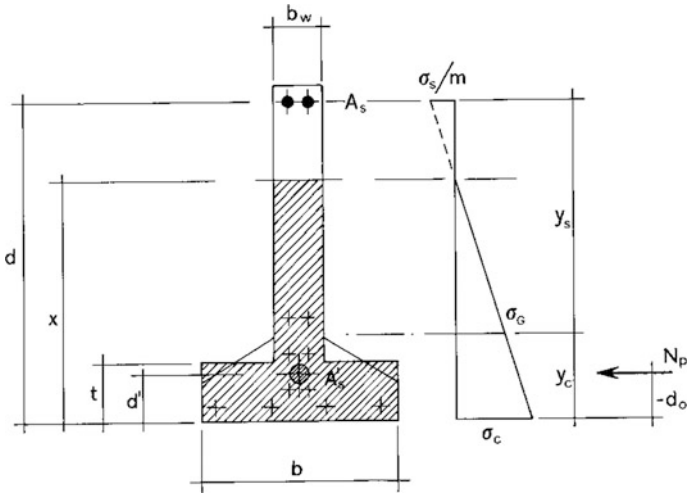


Fig. 10.52 Cracked resisting section in lifting stage

$$\begin{aligned} 726\left(60.5^2/12 + 8.85^2\right) &= 278{,}307 \\ 570\left(15.0^2/12 + 13.9^2\right) &= 120{,}817 \\ 38 \times 59.6^2 &= 134{,}982 \\ 118 \times 9.4^2 &= \underline{10{,}426} \\ I_i &= 544{,}532\,\text{cm}^4 \end{aligned}$$

$$W_c = 544{,}532/21.4 = 25{,}445\,\text{cm}^3$$

$$W_s = 544{,}532/59.6 = 9136\,\text{cm}^3$$

$$M'_{Ek} = 1806(21.4 - 11.5)/100 = 178.8\,\text{kNm}$$

$$\sigma_c = \frac{1806}{147.3} + \frac{178.8}{25.44} = +12.3 + 7.0 = +19.3\,\text{N/mm}^2$$

$$\sigma_s = 6.1\left(-12.3 + \frac{178.8}{9.14}\right) = 8.5 \times 5.7 = 44.3\,\text{N/mm}^2$$

verifications

$$\sigma_c < \bar{\sigma}_{cj} = 21.0\,\text{N/mm}^2$$

$$\sigma_s \ll \bar{\sigma}_s$$

Resistance Verifications

Section a

(with top slab)

prestressed reinforcement ($n\phi - A_p - d_p$)

$$\begin{aligned} 2\phi 15.2 \quad & 2.78\,\text{cm}^2 \quad 73,3\,\text{cm} \\ 2\phi 15.2 \quad & 2.78\,\text{cm}^2 \quad 82.5\,\text{cm} \\ 2\phi 15.2 \quad & 2.78\,\text{cm}^2 \quad 91.7\,\text{cm} \\ 4\phi 15.2 \quad & \underline{5.56\,\text{cm}^2} \quad 96.3\,\text{cm} \\ A_p &= 13.90\,\text{cm}^2 \end{aligned}$$

depth of compression zone

$$\bar{x} = \frac{13.90 \times 1456}{150 \times 14.2} = 9.5\,\text{cm} \quad (con\, d = 88\,\text{cm}\, \bar{x}/d \cong 0.11)$$

resisting moment

$$\begin{aligned} 2.78 \times 145.6 = 404.8 \times (73.3 - 9.5/2)/100 &= 277 \\ 404.8 \times (82.5 - 9.5/2)/100 &= 315 \\ 404.8 \times (91.7 - 9.5/2)/100 &= 352 \\ 5.56 \times 145.6 = 809.5 \times (96.3 - 9.5/2)/100 &= \underline{741} \\ M_{Rd} &= 1685\,\text{kNm} \end{aligned}$$

applied moment

$$\begin{aligned} 1.30 \times 112.5 &= 146.2 \\ 1.30 \times 174.4 &= 226.7 \\ 1.50 \times 125.6 &= 188.4 \\ 1.50 \times 421.9 &= \underline{632.8} \\ M_{Ed} &= 1194.1\ \text{kNm} \quad (< M_{Rd}) \end{aligned}$$

Section b

applied shear

$$\begin{aligned} 1.30 \times 26.76 &= 34.79 \\ 1.30 \times 39.71 &= \underline{51.62} \\ V'_{Ed} &= 86.41\ \text{kN} \end{aligned}$$

$$1.50 \times 30.11 = 45.16$$
$$1.50 \times 100.35 = \underline{150.53}$$
$$V''_{\mathrm{Ed}} = 195.69 \text{ kN}$$

$$\tau_{\mathrm{G}} = \frac{864.1}{12.0 \times 58.9} + \frac{1956.9}{12.0 \times 79.1} = 1.22 + 2.06 = 3.28\,\mathrm{N/mm^2}$$

applied precompression ($\gamma_{\mathrm{P}} = 1.00$)

$$x'_{\mathrm{b}}/l_{\mathrm{b}} = 1.01/1.37 = 0.74$$

losses $\cong 0.69$

$$N_{\mathrm{Ed}} = 1.00 \times 1806 \times 0.74 \times 0.69 = 922\,\mathrm{kN}$$
$$\sigma_{\mathrm{G}} = \frac{9220}{1617} = 5.70/\mathrm{mm^2}$$
$$\sigma_{\mathrm{I}} = \frac{1}{2}\left(-5.70 + \sqrt{5.70^2 + 4 \times 3.28^2}\right) = 1.49\,\mathrm{N/mm^2}$$
$$\sigma_{\mathrm{II}} = \frac{1}{2}\left(+5.70 + \sqrt{5.70^2 + 4 \times 3.28^2}\right) = 7.20\,\mathrm{N/mm^2}$$

verification (with $\sigma_{\mathrm{II}} < f_{\mathrm{cd}}/3 = 10.1$ N/mm^2)

$$\sigma_{\mathrm{I}} < f_{\mathrm{ctd}} = 3.1/1.4 = 2.21\mathrm{N/mm^2}$$
$$\lambda_{\mathrm{I}} = 3.28/1.49 = 2.20$$
$$\lambda_{\max} = \lambda_{\mathrm{I}} + 1.5 = 3.70$$

applied precompression ($\gamma_{\mathrm{P}} = 1.2$)
$x'_{\mathrm{b}}/l_{\mathrm{b}} \cong 1.0$ and without losses

$$N_{\mathrm{Ed}} = 1.20 \times 1806 = 2167\mathrm{kN}$$
$$\sigma_{\mathrm{G}} = \frac{21{,}670}{1617} = 13.4\,\mathrm{N/mm^2}$$
$$\sigma_{\mathrm{I}} = \frac{1}{2}(-13.4 + \sqrt{13.4^2 + 4 \times 3.28^2}) = 0.76\,\mathrm{N/mm^2}$$
$$\sigma_{\mathrm{II}} = \frac{1}{2}\left(+13.4 + \sqrt{13.4^2 + 4 \times 3.28^2}\right) = 14.16\,\mathrm{N/mm^2}$$

verification (with $\sigma_{\mathrm{II}} > f_{\mathrm{cd}}/3 = 10.1$ N/mm^2)

$$\sigma_{\mathrm{I}} < f_{\mathrm{ctd}}\frac{3}{2}\left(1 - \frac{\sigma_{\mathrm{II}}}{f_{\mathrm{cd}}}\right) = 2.21 \times 0.801 = 1.77\,\mathrm{N/mm^2}$$

Assuming $\lambda_c = 2.5$ ($\lambda_I < \lambda_c < \lambda_{max}$) one obtains

$$V_{Ed} = 84.41 + 195.69 = 280.10\,\text{kN}$$
$$a_w = \frac{V_{Ed}}{0.9 d f_{yd} \lambda_c} = \frac{280.1}{0.9 \times 0.82 \times 39.1 \times 2.5} = 3.88\,\text{cm}^2/\text{m}$$

with 1ϕ8/250 for $a_w = 4.04$ cm^2/m

$$\omega_w = \frac{a_w f_{yd}}{b_w f_{c2}} = \frac{4.04 \times 391}{1200 \times 15.2} = 0.0868$$
$$\lambda_r = \sqrt{(1 - \omega_w)/\omega_w} = 3.24 \quad (< \lambda_{max})$$

and assuming $\lambda_c = 2.5$ ($\lambda_I < \lambda_c < \lambda_{max}$) one has

$$V_{Rd} = 0.9 \times 0.82 \times 4.04 \times 39.1 \times 2.5 = 291.4\text{kN} \quad (> V_{Ed})$$

– *Beam-slab longitudinal shear*

(section b)

$$S_i^* = 1885 \times 28.9 = 54{,}476\,\text{cm}^3$$
$$I_i/S_i^* = 4{,}518{,}772/54{,}476 = 82.9\,\text{cm}$$

Actions with integrated upper slab

$$V_{Ed}^* = 195.7\,\text{kN}$$
$$q_{Ed}^* = V_{Ed}^*/z = 195.7/0.829 = 236.1\,kN/m$$

The longitudinal shear resistance of the connection between beam and slab can be calculated with:

$$q_{Rd}^* = 0.62 k b^* f_{ctd} + \mu p + \mu a_s f_{yd}$$

where

$0.62 f_{ctd}$	adhesion resistance of castings
f_{ctd}	referred to the concrete with lower strength
b^*	contact width between beam and slab
k	roughness index of surface
	0.72 for hammered/sandblasted surface
	0.56 for rough surface
	0.00 for smooth surface
μ	friction coefficient between pours

0.70 for hammered/sandblasted surface
0.60 for rough surface
0.50 for smooth surface

P vertical load on the joint

a_s transverse reinforcement area per unit length at the joint

With rough joint and with

$$f_{ctd} = f_{ctk}/\gamma_C = 1.90/1.50 = 1.27\,\text{N/mm}^2$$
$$p = 5.6 + 4.5 + 15.0 = 25.1\,\text{kN/m}$$
$$a_s = 8.08\,\text{cm}^2/\text{m} \quad (1\,\text{staffa}\,\phi 8/125)$$

one obtains

$$0.62 \times 0.56 \times 120 \times 1.27 = 52.9$$
$$0.6 \times 25.1 = 15.1$$
$$0.6 \times 808 \times 391 = \underline{189.6}$$
$$q^*_{Rd} = 281.9\ \text{kN/m} \quad (> q^*_{Ed})$$

Supports
(3ϕ14 added—A_{so} = 4.62 cm^2)

$$1.30 \times 30.0 = 39.0$$
$$1.30 \times 44.2 = 57.5$$
$$1.50 \times 33.8 = 50.7$$
$$1.50 \times 112.5 = \underline{168.8}$$
$$R_{Ed} = 316.0\ \text{kN}$$

Neglecting the two lateral strands (A_p = 8×1.39 = 11.1 cm^2), at the centre of the support (l/l_b = 20/137 = 0.15) one has:

$$0.15 A_p f_{pd} = 0.15 \times 11.1 \times 145.6 = 242.4\ \text{kN}$$
$$A_s f_{yd} = 4.62 \times 39.1 = \underline{180.6\,\text{kN}}$$
$$Z_r = 423.0\,\text{kN}$$

and with $\lambda_o = \lambda_c/2$ = 1.25 the verification becomes:

$$R_{Rs} = Z_r/\lambda_o = 338.4\,\text{kN} \quad (> R_{Ed})$$
$$R_{rc} = \frac{0.6 b_w d f_{cd}}{1 + \lambda_o^2} = 0.234 \times 12 \times 82 \times 3.04 = 700\,\text{kN} \quad (\gg R_{Ed})$$

The construction drawings are shown in Figs. 10.53 and 10.54.

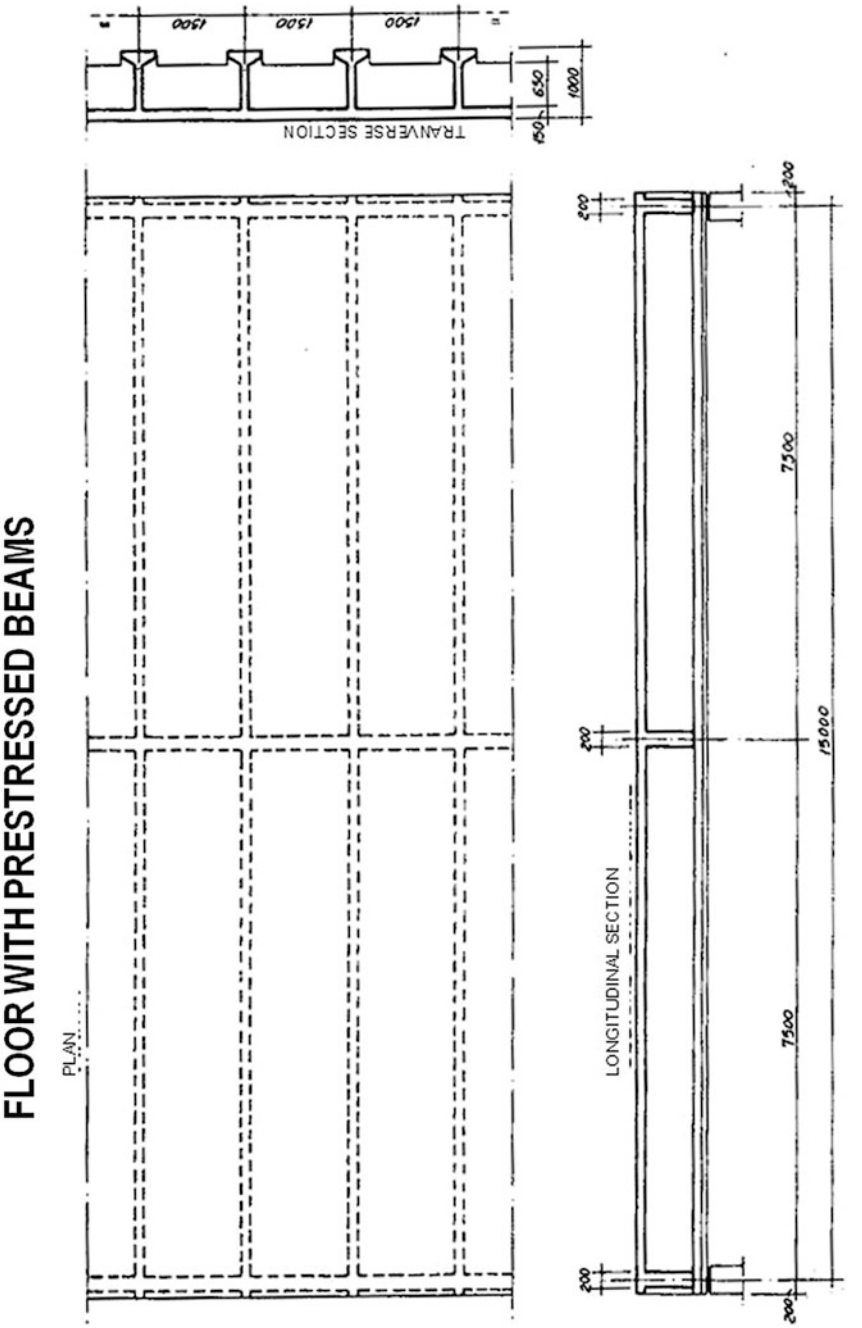


Fig. 10.53 Plan and sections of the floor deck

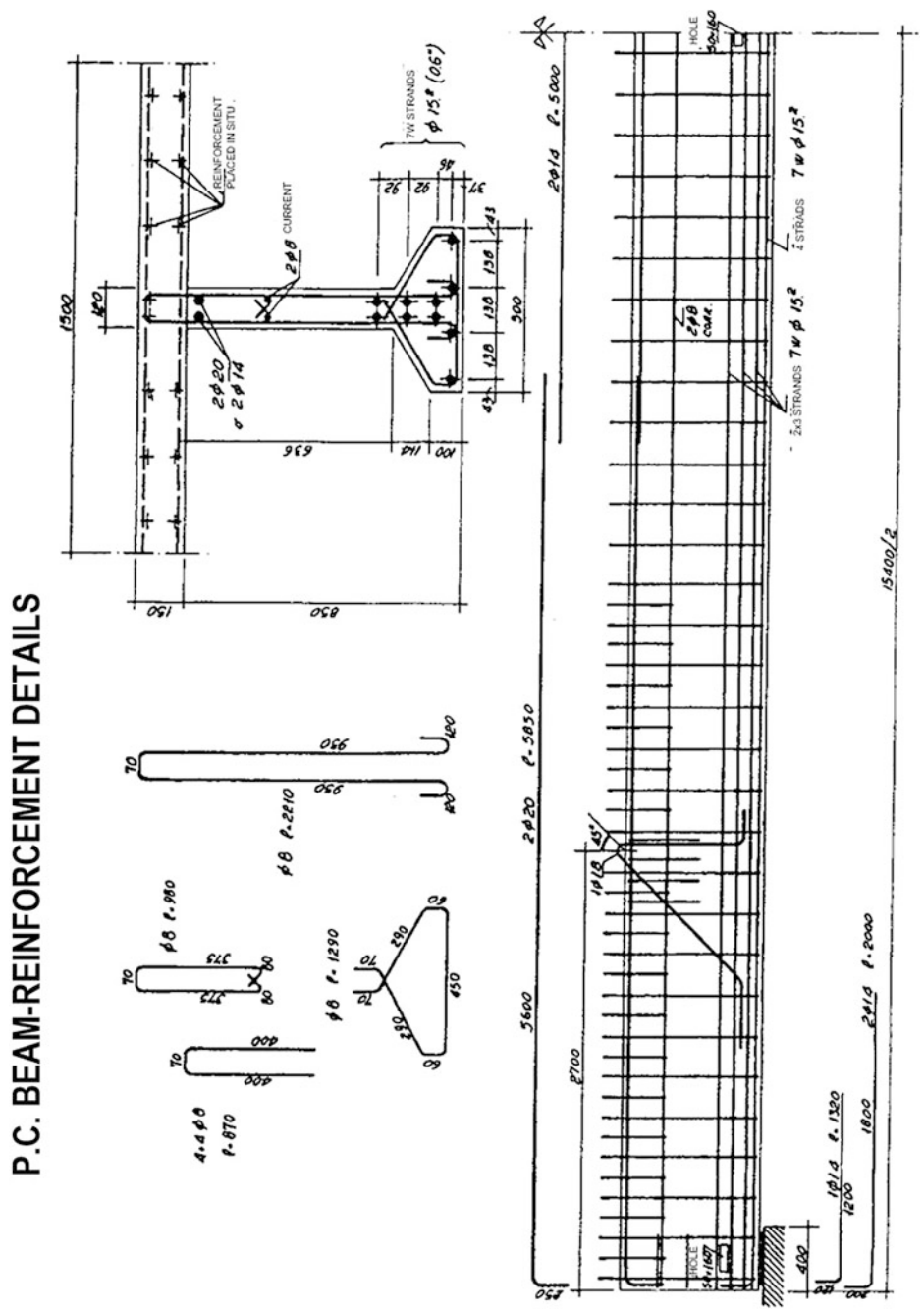


Fig. 10.54 Reinforcement details of the element

Appendix: Data on Prestressing

Chart 10.1: Prestressing and Instantaneous Losses

Beams in pressed reinforced concrete.

Symbols

P_o	initial prestressing (at concrete decompression)
$N_{po} = P_o \cos \phi$	axial component of P_o
$V_{po} = P_o \sin \phi$	transverse component of P_o
P'_o	prestressing at tendons tensioning
$N'_{po} = P'_o \cos \phi$	axial component of P'_o
$V'_{po} = P'_o \sin \phi$	transverse component of P'_o
ϕ	angle of the tendon on the beam axis
e	tendon eccentricity (positive towards the bottom)
M'_g	bending moment due to self-weight
V'_g	shear due to self-weigth
A_p	area of prestressing reinforcement
E_p	elastic modulus of prestressing reinforcement

see also Charts 3.4 and 6.1.

Initial Stresses "*i*"
(post-tensioned tendons)

$$\sigma_{ci} = -\frac{N'_{po}}{\bar{A}_i} - \frac{M'_g - N'_{po}\bar{e}}{\bar{I}_i}\bar{y}_c \qquad \text{upper edge}$$

$$\sigma_{\overline{G}i} = -\frac{N'_{po}}{\bar{A}_i} \qquad \tau_{\overline{G}} = \frac{V'_g - V'_{po}\bar{e}}{\bar{z}b_{\overline{G}}} \qquad \text{centroid}$$

$$\sigma^*_{ci} = -\frac{N'_{po}}{\bar{A}_i} + \frac{M'_g - N'_{po}\bar{e}}{\bar{I}_i}\bar{e} \qquad \text{tendon level}$$

$$\sigma'_{ci} = -\frac{N'_{po}}{\bar{A}_i} + \frac{M'_g - N'_{po}\bar{e}}{\bar{I}_i}\bar{y}'_c \qquad \text{lower edge}$$

$$\sigma_{pi} = \frac{P'_o}{A_p} \qquad \text{tendon}$$

with positive tensile stresses where

$$\bar{A}_i = A_c + \alpha_e A_s \quad \alpha_e = E_s/E_c$$

and with $\bar{I}_i$, $\bar{y}_c$, $\bar{y}'_c$, … calculated similarly to the homogenized concrete section with passive reinforcement.

The allowable stresses for the verification in service can be deduced from Charts 2.2 and 2.3.

Losses Due to Friction
(post-tensioned tendons)

$$P = P_1 e^{-\mu(\psi + \alpha s)}$$

with

P_1 tension applied at end 1 (active side)
P force in the tendon at the abscissa s from end 1
s abscissa of the considered section (in m)
ψ progressive angle in rad between 1 and s (absolute value)
μ friction coefficient in the duct
α unintentional unit angular deviation

Without more accurate data, for tendons against metallic ducts without rust one can assume:

$\mu = 0.20$ for wires or strands
$\mu = 0.35$ for smooth bars
$\mu = 0.65$ for ribbed bars
$\alpha = 0.01$ rad/m

Elastic Losses
(pre-tensioned tendons)

$$\sigma_{ci} = -\frac{N_{po}}{A_i} - \frac{M'_g - N_{po}e}{I_i} y_c \quad \text{upper edge}$$

$$\sigma_{Gi} = -\frac{N_{po}}{A_i} \quad \tau_G = \frac{V'_g - V_{po}}{z b_G} \quad \text{centroid}$$

$$\sigma^*_{ci} = -\frac{N_{po}}{A_i} + \frac{M'_g - N_{po}e}{I_i} e \quad \text{tendon level}$$

$$\sigma'_{ci} = -\frac{N_{po}}{A_i} + \frac{M_g - N_{po}e}{I_i} y'_c \quad \text{lower edge}$$

$$\sigma'_{pi} = \sigma_{po} + \alpha'_e \sigma^*_{ci} \quad \text{tendon} (\sigma_{po} = P_o / A_p)$$

with

$$A_i = A_c + \alpha_e A_s + \alpha'_e A_p \quad \alpha'_e = E_p / E_c$$

and with I_i, y_c, y'_c, … calculated similarly to the homogenized concrete section. With passive and active reinforcement (with $\cos \phi \cong 1$, $N_{po} \cong P_o$).

Chart 10.2: Losses Due to Steel Relaxation

The tension loss due to steel relaxation, calculated after t hours from the load application in relation to the initial stress σ_{pi}, is given by

$$\rho_\tau = \rho(\tau) = \frac{\Delta\sigma_{p\tau}}{\sigma_{pi}} = \rho_1 \tau^{0.75(1-r)}$$

with τ = t/1000 and $r = \sigma_{pi}/f_{ptk}$. The loss at 1000 h ($\tau = 1$) is given by

$$\rho_1 = \bar{\rho}_1 c(r)$$

Where $\bar{\rho}_1$ is the loss measured at the time above for an initial stress corresponding to $r = 0.7$ and an average temperature of 20 °C. For the following product classes

Class 1—Ordinary wires and strands
Class 2—Stabilized wires and strands
Class 3—Prestressing bars

In the absence of test results, one can assume

$$\overline{\rho}_1 = 8.0\% \quad \text{for class 1}$$
$$\overline{\rho}_1 = 2.5\% \quad \text{for class 2}$$
$$\overline{\rho}_1 = 4.0\% \quad \text{for class 3}$$

and

$$c(r) = \left[\frac{r-0.4}{0.3}\right]^{\frac{4}{3}} \quad \text{for class 1}$$
$$c(r) = \left[\frac{r-0.5}{0.2}\right]^{\frac{4}{3}} \quad \text{for classes 2 and 3}$$

The final value of the loss $\rho_\infty = \Delta\sigma_{p\infty}/\sigma_{pi}$ can be calculated with $\tau = 500$ (≈57 years). The table gives the final loss for the different values of the initial stress.

$\frac{\sigma_{pi}}{f_{ptk}}$	$100\Delta\sigma_{p\infty}/\sigma_{pi}$			$\frac{\sigma_{pi}}{f_{ptk}}$	$100\Delta\sigma_{p\infty}/\sigma_{pi}$		
	Class 1	Class 2	Class 3		Class 1	Class 2	Class 3
0.40	0.00						
0.42	3.23			0.66	32.25	9.06	14.49
0.44	7.41			0.67	32.36	9.37	15.00
0.46	11.59			0.68	32.43	9.65	15.45
0.48	15.50			0.69	32.43	9.90	15.84
0.50	19.01	0.00	0.00	0.70	32.39	10.12	16.19
0.52	22.09	1.09	1.74	0.71	32.29	10.31	16.49
0.54	24.71	2.50	3.99	0.72	32.15	10.47	16.75
0.56	26.90	3.90	6.25	0.73	31.98	10.60	16.96
0.58	28.67	5.22	8.35	0.74	31.76	10.71	17.14
0.60	30.06	6.40	10.24	0.75	31.51	10.79	17.27

(continued)

(continued)

$\frac{\sigma_{pi}}{f_{ptk}}$	$100\Delta\sigma_{p\infty}/\sigma_{pi}$			$\frac{\sigma_{pi}}{f_{ptk}}$	$100\Delta\sigma_{p\infty}/\sigma_{pi}$		
	Class 1	Class 2	Class 3		Class 1	Class 2	Class 3
0.61	30.62	6.94	11.10	0.76	31.22	10.86	17.37
0.62	31.10	7.44	11.90	0.77	30.91	10.90	17.43
0.63	31.49	7.90	12.64	0.78	30.57	10.92	17.47
0.64	31.81	8.32	13.31	0.79	30.21	10.92	17.47
0.65	32.06	8.71	13.93	0.80	29.82	10.90	17.45

Chart 10.3: Experimental Evaluation of Relaxation

If the experimental value ρ_{1exp} of the tension loss due to relaxation is available, measured at 1000 h from the load application for an initial stress $\Delta\sigma_{i\,exp} = r_{exp}f_{ptk}$, the final loss $\Delta\sigma_{p\infty} = \rho_{\infty}\sigma_{pi}$ can be evaluated with

$$\rho_{\infty} = \kappa\bar{\rho}_1$$

where

$$\kappa = c(r)500^{0.75(1-r)}$$
$$\bar{\rho}_1 = \rho_{1\,exp}/c(r_{exp})$$

(see Chart 10.2 for the expression c(r)).

The following tables give the values of the factors $\kappa(r)$ and $1/c(r_{exp})$, respectively, for the different product classes as defined Chart 10.2.

$\kappa = \kappa(r)$	$r = \sigma_{pi}/f_{ptk}$				
	0.60	0.65	0.70	0.75	0.80
Class 1	2.962	3.175	4.048	3.938	3.728
Class 2 and 3	2.561	3.482	4.048	4.350	4.361

$1/c(r_{exp})$	$r_{exp} = \sigma_{pi\,exp}/f_{ptk}$				
	0.60	0.65	0.70	0.75	0.80
Class 1	1.717	1.275	1.000	0.814	0.681
Class 2 and 3	2.519	1.467	1.000	0.743	0.582

Chart 10.4: Total Prestressing Losses

With respect to the initial values calculated with the formulas of Chart 10.1, the stresses in the materials are subject to the following long-term losses.

Symbols

ΔP_ρ	loss due to steel relaxation
ΔP_s	loss due to concrete shrinkage
ΔP_v	loss due to concrete creep
ΔP	total prestressing loss
$\Delta N_p = \Delta P \cos \phi$	axial component of ΔP
$\Delta V_p = \Delta P \sin \phi$	transverse component of ΔP

see also Chart 10.1.

Long-Term Losses

(with $\cos \phi \cong 1$, $\Delta N_p \cong \Delta P$)

Without more precise data, the following final values can be assumed.

$\Delta P_\rho = A_p \Delta \sigma_{\rho\infty}$	loss due toi relaxation (Chart 10.2)
$\Delta P_s = A_p \Delta \sigma'_p = A_p E_p \varepsilon_{cs\infty}$	loss due to shrinkage (Chart 1.5)
$\Delta P_v = A_p \Delta \sigma''_p = A_p \alpha'_e \phi_\infty \sigma^*_{ci}$	loss due to creep (Chart 1.14)

Total loss

$$\Delta P = \Delta P_\rho + \Delta P_s + \Delta P_v = A_p \Delta \sigma_p$$

In order to take into account the interaction with the losses due to shrinkage and creep, the one due to relaxation can be reduced with the coefficient 0.8.

Variations of stresses (positive in tension)

$$\Delta\sigma_c = +\frac{\Delta N_p}{A_i} - \frac{\Delta N_p e}{I_i} y_c \qquad \text{upper edge}$$

$$\Delta\sigma_G = +\frac{\Delta N_p}{A_i} \qquad \Delta\tau_G = +\frac{\Delta V_p}{z b_G} \qquad \text{centroid}$$

$$\Delta\sigma'_c = +\frac{\Delta N_p}{A_i} + \frac{\Delta N_p e}{I_i} y'_c \qquad \text{lower edge}$$

$$\Delta\sigma^*_c = +\frac{\Delta N_p}{A_i} + \frac{\Delta N_p e^2}{I_i} \qquad \text{tendon level}$$

$$\Delta\sigma'_p = -\Delta\sigma_p + \alpha'_e \Delta\sigma^*_c \qquad \text{tendon}$$

Chart 10.5: Stages of Verification of Stresses

The main stages of verification of stresses in the materials of a beam prestressed off-site and then transported to its final position are listed below. The verification in particular concern:

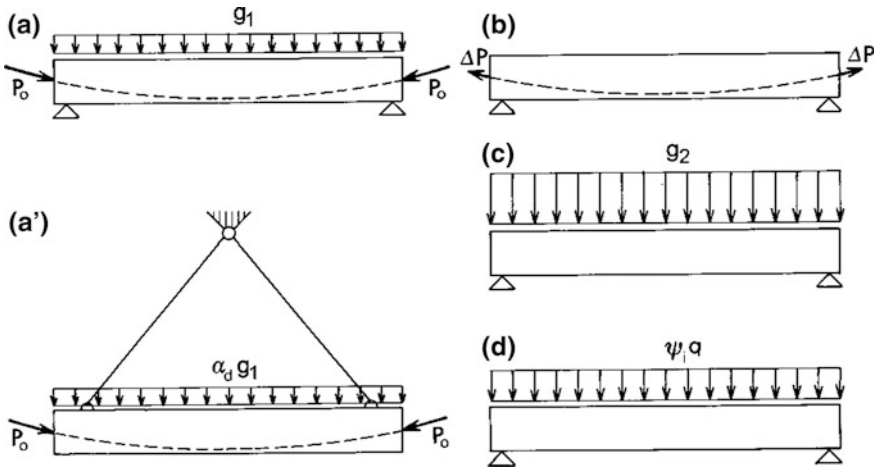
- the *maximum compressions in concrete* to avoid an excessive propagation of microcracking (see Chart 2.2);
- the *maximum tensions in steel*, both passive and prestressed to avoid yielding (see Chart 2.3);
- the *maximum tensions in concrete* for the verification of decompression and formation of cracks (see Chart 2.2);
- the *range of tensions in steel* measured from decompression of concrete for the verifications of cracks opening (see Chart 2.16)

The verifications related to cracking refer to the criteria of Chart 2.15. For the stresses due to shear see Charts 4.1, 4.5 and 4.6. The stresses in the section of the beam are assumed to be calculated with the load combinations related to the serviceability limit states (see Chart 3.2).

The stages of verification of stresses can be articulated in various ways, depending of the type of structure, the construction methods and the refinement of the calculation itself. The main ones, listed below, are illustrated with the schemes of the following figure and represent the incremental actions to be progressively cumulated to the previous ones. A separate case is the transient condition (a′) of lifting that ends with no further developments.

Initial Stage (a): "Precompression"
(with self-weight g_1)

The initial stresses σ_{ci}, … are calculated with the formulas of Chart 10.1; the prestressing losses of the scheme (b) will then be evaluated based on these values.



Transient Stage (a′): "Lifting"
(change of supports and dynamic effects)

Stresses are calculated with the same formulas of Chart 10.1 where the internal forces M'_g and V'_g due to the self-weight refer to the new configuration of supports with the action $\alpha_d g_1$. Without more accurate calculations, the dynamic effects can be calculated in the most unfavourable way with the coefficient

$$\alpha_d = 1 \pm 0.15$$

The *verifications under minimum loads* are usually carried on this stage.

Incremental stage (b): "Losses"
The stress losses with respect to the initial values are calculated with the formulas of Chart 10.4.

Incremental Stage (c): "Permanent"
The effects of permanent loads g_2 are calculated with

$$\begin{aligned}
\Delta\sigma_c &= -\frac{M''_g}{I_i} y_c && \text{upper edge} \\
\Delta\tau_G &= \frac{V''_g}{z b_G} && \text{centroid} \\
\Delta\sigma_p &= \alpha_e \frac{M''_g}{I_i} e && \text{tendon} \\
\Delta\sigma'_c &= +\frac{M''_g}{I_i} y'_c && \text{lower edge}
\end{aligned}$$

The combination (a) + (b) + (c) for the *verification under permanent loads* is deduced at this point.

Incremental Stage (d): "Serviceability"
The effects of variable loads $\psi_i q$ are calculated with

$$\begin{aligned}
\Delta\sigma_c &= -\frac{M_q}{I_i} y_c && \text{upper edge} \\
\Delta\tau_G &= \frac{V_q}{z b_G} && \text{centroid} \\
\Delta\sigma_p &= \alpha'_e \frac{M_q}{I_i} e && \text{tendon} \\
\Delta\sigma'_c &= +\frac{M_q}{I_i} y'_c && \text{lower edge}
\end{aligned}$$

The combination (a) + (b) + (c) + (d) for the verifications under serviceability loads is deduced at this point, with the combination coefficient ψ_i deduced from Chart 3.2 depending on the requirements (frequent or rare combination).

Tensile stresses have been assumed positive in what mentioned above.

Chart 10.6: Verification of Resistance in Bending

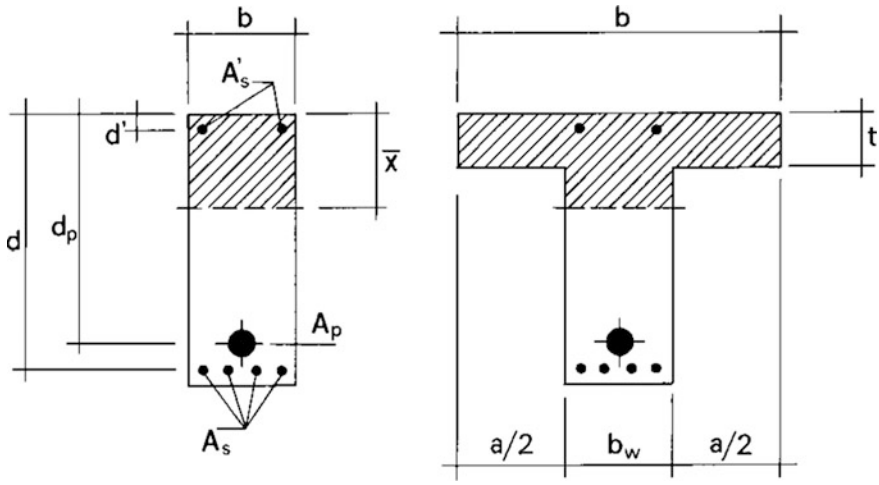
Section in prestressed concrete subject to uniaxial bending.

Symbols

M_{Ed}	design value of applied bending moment
M_{Rd}	design value of the resisting bending moment
A_s, A'_s	areas of passive reinforcement in tension and compression
d, d'	distance of reinforcement from the edge in compression (see figure)
A_p	area of prestressing reinforcement
d_p	distance of tendon from the edge in compression (see figura)
b	width of the edge in compression (see figure)
b_w	web width (see figure)
t	flange thickness (see figure)
ε_{po}	initial strain of prestressing reinforcement

see also Charts 2.2, 2.3 and 10.1.

Verifications with Resisting Tendon
(longitudinal tendon with initial strain ε_{po})



Rectangular section
(or T-shaped with $\bar{x} \leq t$)

$$M_{Rd} = A_p f_{pd}(d_p - \bar{x}/2) + A_s f_{yd}(d - \bar{x}/2) + A'_s f_{yd}(\bar{x}/2 - d') \geq M_{Ed}$$

with

$$\bar{x} = \left(A_p f_{pd} + A_s f_{yd} - A'_s f_{yd}\right)/b f_{cd}$$

and with the limits

$$\varepsilon_p = \frac{d_p - x}{x}\varepsilon_{cu} + \varepsilon_{po} \quad \left(\varepsilon^*_{yd} \le \varepsilon_p \le \varepsilon_{pd}\right)$$
$$\varepsilon_s = \frac{d - x}{x}\varepsilon_{cu} \quad \left(\varepsilon_{yd} \le \varepsilon_s \le \varepsilon_{sd}\right)$$
$$\varepsilon'_s = \frac{x - d'}{x}\varepsilon_{cu} \quad \left(\varepsilon_{yd} \le \varepsilon'_s\right)$$

where

$$x \cong \bar{x}/0.8 \quad \varepsilon_{cu} = 0.35\% \,(up\,to\,\text{class}\,C50/60)$$

T-shaped
(with $\bar{x} > t$)

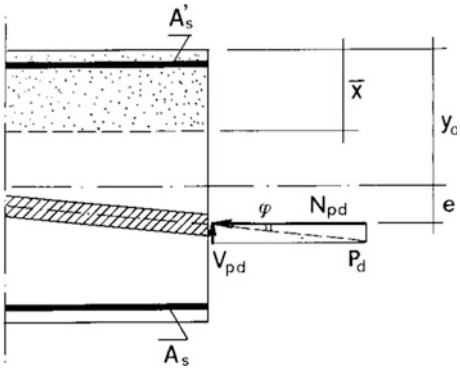
$$M_{Rd} = atf_{cd}\left(d_p - t/2\right) + b_w \bar{x} f_{cd}\left(d_p - \bar{x}/2\right) + \\ + A_s f_{yd}\left(d - d_p\right) + A'_s f_{yd}\left(d_p - d'\right) \ge M_{Ed}$$

with

$$\bar{x} = \left(A_p f_{yd} + A_s f_{yd} - A'_s f_{yd} - \text{atf}_{cd}\right)/b_w f_{cd}$$
$$a = b - b_w$$

and with the same limits of the rectangular section.

Verifications with Prestressing Force
(constant force $P_o = E_p\ \varepsilon_{po}$ in place of the tendon)



Rectangular section
(or T-shaped with $\bar{x} \le t$)

$$M^*_{\mathrm{Rd}} = b\bar{x}f_{\mathrm{cd}}(y_{\mathrm{o}} - \bar{x}/2) + A_{\mathrm{s}}f_{\mathrm{yd}}(d - y_{\mathrm{o}}) + A'_{\mathrm{s}}f_{\mathrm{yd}}(y_{\mathrm{o}} - d') \geq M^*_{\mathrm{Ed}}$$

where

$$M^*_{\mathrm{Ed}} = M_{\mathrm{Ed}} - N_{\mathrm{pd}}e$$
$$N_{\mathrm{pd}} = P_{\mathrm{d}}\cos\phi \quad P_{\mathrm{d}} = \gamma_{\mathrm{P}}P_{\mathrm{O}}$$

with

$$\bar{x} = \left(N_{\mathrm{pd}} + A_{\mathrm{s}}f_{\mathrm{yd}} - A'_{\mathrm{s}}f_{\mathrm{yd}}\right)/bf_{\mathrm{cd}}$$

and with the limits

$$\varepsilon_{\mathrm{s}} = \frac{d - x}{x}\varepsilon_{\mathrm{cu}} \quad \left(\varepsilon_{\mathrm{yd}} \leq \varepsilon_{\mathrm{s}} \leq \varepsilon_{\mathrm{sd}}\right)$$
$$\varepsilon'_{\mathrm{s}} = \frac{x - d'}{x}\varepsilon_{\mathrm{cu}} \quad \left(\varepsilon_{\mathrm{yd}} \leq \varepsilon'_{\mathrm{s}}\right)$$

where

$$x \cong \bar{x}/0.8 \quad \varepsilon_{\mathrm{cu}} = 0.35\% \,(\text{up to class C50/60})$$

T-shaped section
(with $\bar{x} > t$)

$$M^*_{\mathrm{Rd}} = atf_{cd}(y_{\mathrm{o}} - t/2) + b_{\mathrm{w}}\bar{x}f_{\mathrm{cd}}(y_{\mathrm{o}} - \bar{x}/2) + \\ + A_{\mathrm{s}}f_{\mathrm{yd}}(d - y_{\mathrm{o}}) + A'_{\mathrm{s}}f_{\mathrm{yd}}(y_{\mathrm{o}} - d') \geq M^*_{\mathrm{Ed}}$$

where

$$M^*_{\mathrm{Ed}} = M_{\mathrm{Ed}} - N_{\mathrm{pd}}e$$
$$N_{\mathrm{pd}} = P_{\mathrm{d}}\cos\phi \quad P_{\mathrm{d}} = \gamma_{\mathrm{P}}P_{\mathrm{O}}$$

with

$$\bar{x} = \left(N_{\mathrm{pd}} + A_{\mathrm{s}}f_{\mathrm{yd}} - A'_{\mathrm{s}}f_{\mathrm{yd}} - atf_{cd}\right)/b_{\mathrm{w}}f_{\mathrm{cd}}$$
$$a = b - b_{\mathrm{w}}$$

and with the same limits of the rectangular section.

Chart 10.7: Anchorage of Tendons

End anchorages of unbonded post-tensioned or bonded pre-tensioned tendons.

Verification of Anchors of Post-Tensioned Tendons
The verification of concrete bearing can be set with

$$P_{\mathrm{d}} = \gamma_{\mathrm{P}} P \leq P_{\mathrm{Rd}}$$

where the resisting value of prestressing force is given by

$$P_{\mathrm{Rd}} = f^{*}_{\mathrm{cd}} A_{\mathrm{o}}$$

with

$A_{\mathrm{o}} = a'b'$ gross area of loaded print
a', b' sides of the anchorage plate

and where

$$f^{*}_{\mathrm{cd}} = f_{\mathrm{cdj}} \sqrt{A_1 / A_{\mathrm{o}}}$$

with

$f_{\mathrm{cdj}} = f_{\mathrm{ckj}} / \gamma_{\mathrm{C}}$ design resistance at tensioning
$A_1 = ab$ involved loaded surface

The sides a, b are calculated with

$$a = a' + 2d_{\mathrm{a}} \leq 3a' \quad b = b' + 2d_{\mathrm{b}} \leq 3b'$$

based on the margins d_{a}, d_{b} of the loaded print with respect to the closest edges of the section. In any case, the surfaces involved are to be cut halfway to the closest adjacent plates.

Anchorage Length of Bonded Tendons
The end anchorage length of bonded pre-tensioned strand is calculated with

$$l_{\mathrm{b}} = \frac{\phi}{4} \frac{f_{\mathrm{pd}}}{f_{\mathrm{bd}}}$$

where ϕ is the diameter of the bar, wire or strand, $f_{\mathrm{pd}} = 0.9\, f_{\mathrm{ptk}} / \gamma_{\mathrm{S}}$ is its design resistance, $f_{\mathrm{bd}} = \beta_{\mathrm{b}} f_{\mathrm{ctk}} / \gamma_{\mathrm{C}}$ the design value of the bond resistance. Without more accurate measurements, it can be assumed

$$\beta_b = 2.25 \quad \text{for wires and ribbed bars}$$
$$\beta_b = 3.00 \quad \text{for strands}$$

If the tendon is cut without a previous slow release, an uneffective end segment should be added, equal to

$$l_o \cong 7\phi$$

It can be assumed that the effectiveness of the strand vary linearly within the bonded segment $0 \leq x \leq l_b$:

$$f_{pd} x / l_b$$

Chart 10.8: Additional Data

Prestressed elements in bending with or without shear reinforcement.

Verifications in Shear with Resisting Tendons
(bonded pre-tensioned strands along the edge in tension)

What given in Charts 4.1, 4.2, 4.5 and 4.6, respectively, for elements without shear reinforcement and for resistance, serviceability and cracking of beams with stirrups is valid.

Verifications in Shear with Prestressing Force
(Constant force in place of tendons)

What given in Chart 6.21 is valid, provided $N_o = P_d \cos \phi$ is assumed and V_{Ed} is substituted with $V^*_{Ed} = V_{Ed} - P_d \sin \phi$.

Construction Rules and Support Details
What given in Chart 4.5 for shifting of moments, spacing and minimum shear reinforcement is valid, as well as what given in Chart 5.2 for support details, and what mentioned in Chart 6.22 for minimum longitudinal bonded reinforcement.

References

General Books

1. T. Y. Lin, N. H. Burns: Design of Prestressed Concrete Structures, Wiley, 2004.
2. P. M. Ferguson, J. E Breen, J. O. Jirsa: Reinforced Concrete Fundamentals, Wiley, 1988.
3. M. K. Hurst: Prestressed Concrete Design, Spon, 2007.
4. J. R. Libby: Modern Prestressed Concrete, CBS Publishers, 2007.
5. P Bhatt, T. J. MacGinley, B. S. Choo: Reinforced Concrete Design to Eurocodes: Design Theory and Examples, CRC Press, 2013.
6. R. Favre, J. P. Jaccoud, O. Burdet, H. Charif: Dimensionnement de structures en béton, Presses Plytech. et Univ. Romandes, 1990.
7. R. I. Gilbert, N. C. Mickleborough, G. Ranzi: Design of Prestressed Concrete to AS3600-2009, CRC Press, 2015.
8. R. Favre, J. P. Jaccoud, M. Koprna, A. Radojicic: Dimensionnement des structures en béton, Presses polytechniques universitaires et romandes, 1990.
9. R. Chaussin, A. Fuentes, R. Lacroix, J. Perchat: La précontrainte, Ponts et chaussées, 1992.
10. R. Walther, M. Miehlbradt: Dimensionnement des structures en béton: Bases et technologie, Presses Plytech. et Univ. Romandes, 1990.
11. E. O'Brien, A. Dixon, E. Sheils: Reinforced and Prestressed Concrete Design to EC2, CRC Press, 2012.
12. M. P. Collins, D. Mitchell: Prestressed Concrete Structures, Prentice-Hall, 1997.
13. B. G. Gerwick: Construction of Prestressed Concrete Structures, Wiley, 1997.
14. E. G. Nawy: Reinforced Concrete: a Fundamental Approach, Pearson, 2008.
15. M. G. Richardson: Fundamentals of Durable Reinforced Concrete, Taylor and Francis, 2002.
16. J. McCormac, J. H. Brown: Design of Reinforced Concrete, Wiley, 2013.
17. S. Teng, F. K. Kong: Reinforced and Prestressed Concrete, Taylor & Francis 2007.
18. R. Park, T. Paulay: Reinforced Concrete Structures, Wiley on line, 2009.
19. fib: Structural concrete – Textbook on behaviour, design and performance, bull. nn. 51/52/53/54 & 62 (voll. 1, 2, 3, 4 & 5), 2009 to 2012.
20. fib: Model Code 2010, bull. nn. 65/66 (voll. 1 & 2), 2012.
21. W.H. Mosley, R. Hulse, J.H. Bungey,: Reinforced Concrete Design to Eurocode 2, Palgrave, 2012.
22. A.E. Naaman: Prestressed Concrete Analysis and Design, Techno Press 3000, 2012.
23. H. Bachmann, A. Steinle: Precast Concrete Structures, Ernst & Sohn, 2012.
24. G. F. Limbrunner: Reinforced Concrete Design, Pearson, 2014.
25. P. Bhatt, T. J. MacGinley, B. S. Choo: Reinforced Concrete Design to Eurocodes: Design Theory and Examples, CRC Press, 2014.
26. J. K. Wight: Reinforced Concrete: Mechanics and Design, Pearson, 2016.

© Springer International Publishing AG 2017

G. Toniolo and M. di Prisco, *Reinforced Concrete Design to Eurocode 2*,
Springer Tracts in Civil Engineering, DOI 10.1007/978-3-319-52033-9

Specific Books

27. A. C. Liebenberg: Concrete Bridges: Design and Construction, Longman, 1992.
28. J. Moehle: Seismic Design of Reinforced Concrete Buildings, McGraw-Hill, 2014.
29. T. C. Hsu, Y.-L. Mo: Unified Theory of Concrete Structures, Wiley, 2010.
30. J. E. Bowles: Foundation Analysis and Design, McGraw-Hill, 2001.
31. R. Park, W. L. Gamble: Reinforced Concrete Slabs, Wiley, 1999.
32. E. G. Nawy: Fundamentals of High-Performance Concrete, Wiley 2001.
33. P. Mondorf: Concrete Bridges, Taylor & Francis, 2006.
34. A. Bentur, S. Mindess, Routledge: Fibre Reinforced Cementitious Composites, CRC Press, 2006.
35. A. Peled, A. Bentur, B. Mobasher: Textile Reinforced Concrete, CRC Press, 2017.

Handbooks

36. J. Eibl (Ed.): Concrete Structures Euro-design Handbook, Ernst & Sohn 1995.
37. C. E. Reynolds, J. C. Steedman: Reinforced Concrete Designer's Handbook, CRC Press, 2007.
38. T. Threlfall: Reinforced Concrete Designer Handbook, Taylor & Francis, 2007.
39. C. Sigmund: Cemento armato. Manuale di calcolo agli stati limite – Handbook delle strutture, Flaccovio, 2008.
40. SP-017(14): The Reinforced Concrete Design Handbook Volumes 1 & 2 Package.

European CEN Standards

– EN 1992-1-1:2015 Eurocode 2 – Design of concrete structures – Part 1-1: General rules and rules for buildings.
– EN 1992-1-2:2011 Eurocode 2 – Design of concrete structures – Part 1-2: Structural fire design.
– EN 1992-2:2013 Eurocode 2 – Design of concrete structures – Part 2: Concrete bridges – Design and detailing rules.
– EN 1992-3:2011 Eurocode 2 – Design of concrete structures – part 3: Liquid retaining and containment structures.
– EN 206: 2014 Concrete – Specification, performance, production and conformity.
– EN 10080: 2006 Steel for the reinforcement of concrete – Weldable reinforcing steel – General.
– EN 10138-1: * Prestressing steel – Part 1: General requirements.
– EN 10138-2: * Prestressing steel – Part 2: Wire.
– EN 10138-3: * Prestressing steel – Part 3: Strand.
– EN 10138-4: * Prestressing steel – Part 4: Bars.
– EN 13670: 2013 Execution of concrete structures.
**to be published, existing draft is dated 2000.*